

WL-TR-94-4079

PROCEEDINGS OF THE 1993 USAF STRUCTURAL
INTEGRITY PROGRAM CONFERENCE

AD-A285 684



EDITORS:

Thomas D. Cooper
WL/Materials Directorate
Wright-Patterson AFB, Ohio

John W. Lincoln
ASC/Deputy for Engineering
Wright-Patterson AFB, Ohio

James L. Rudd
WL/Flight Dynamics Directorate
Wright-Patterson AFB, Ohio

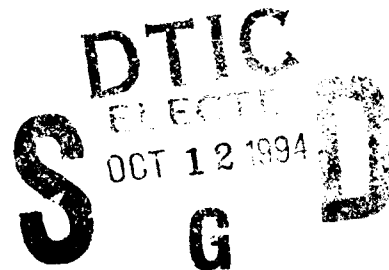
USAF Structural Integrity Program Conference
Hyatt Regency
San Antonio, Texas

Final Report for Period 30 November - 2 December 1993

August 1994

Approved for public release; distribution is unlimited

MATERIALS DIRECTORATE
WRIGHT LABORATORY
AIR FORCE MATERIEL COMMAND
WRIGHT-PATTERSON AFB, OHIO 45433-7718



DTIC QUALITY INSPECTED 8

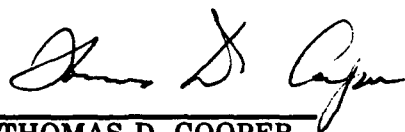
6468 94-32022

NOTICE

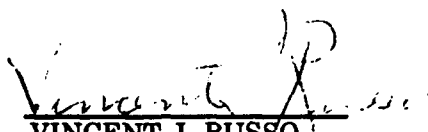
When government drawings, specifications, or other data are used for any purpose other than in connection with a definitely related government procurement operation, the United States Government thereby incurs no responsibility or any obligation whatsoever; and the fact that the government may have formulated, furnished, or in any way supplied the said drawings, specifications, or other data, is not to be regarded by implication or otherwise as in any manner licensing the holder or any other person or corporation, or conveying any rights or permission to manufacture use, or sell any patented invention that may in any way be related thereto.

This report has been reviewed by the Office of Public Affairs (ASC/PA) and is releasable to the National Technical Information Service (NTIS). At NTIS, it will be available to the general public, including foreign nationals.

This technical report has been reviewed and is approved for publication.



THOMAS D. COOPER
Chief
Systems Support Division



VINCENT J. RUSSO
Director
Materials Directorate

If your address has changed, if you wish to be removed from our mailing list, or if the addressee is no longer employed by your organization, please notify WL/MLS Bldg 652, 2179 Twelfth St Ste 1, Wright-Patterson AFB, Ohio 45433-7718 to help us maintain a current mailing list.

Copies of this report should not be returned unless return is required by security considerations, contractual obligations, or notice on a specific document.

REPORT DOCUMENTATION PAGE

Form Approved
OMB No. 0704-0188

Public reporting burden for this collection of information is estimated to average 1 hour per response, including the time for reviewing instructions, searching existing data sources, gathering and maintaining the data needed, and completing and reviewing the collection of information. Send comments regarding this burden estimate or any other aspect of this collection of information, including suggestions for reducing this burden, to Washington Headquarters Services, Directorate for Information Operations and Reports, 1215 Jefferson Davis Highway, Suite 1204, Arlington, VA 22202-4302, and to the Office of Management and Budget, Paperwork Reduction Project (0704-0188), Washington, DC 20503.

1. AGENCY USE ONLY (Leave blank)		2. REPORT DATE August 1994	3. REPORT TYPE AND DATES COVERED Final, 30 November-2 December 1993	
4. TITLE AND SUBTITLE Proceedings of the 1993 USAF Structural Integrity Program Conference			5. FUNDING NUMBERS PE 62101F PR 2418 TA 07 WU 04	
6. AUTHOR(S) 1-Thomas D. Cooper, Compiler & Editor; 2-John W. Lincoln, ASC/ENF; and 3-James L. Rudd, WL/FIB, Editors.				
7. PERFORMING ORGANIZATION NAME(S) AND ADDRESS(ES) 1-Materials Directorate; 2-Aeronautical Systems Center, 3-Flight Dynamics Directorate Deputy for Engineering Wright Laboratory Air Force Materiel Command Wright-Patterson AFB OH 45433			8. PERFORMING ORGANIZATION REPORT NUMBER WL-TR-94-4079	
9. SPONSORING/MONITORING AGENCY NAME(S) AND ADDRESS(ES) Materials Directorate Wright Laboratory Air Force Materiel Command Wright-Patterson AFB OH 45433-7718			10. SPONSORING/MONITORING AGENCY REPORT NUMBER WL-TR-94-4079	
11. SUPPLEMENTARY NOTES				
12a. DISTRIBUTION/AVAILABILITY STATEMENT Approved for public release; distribution is unlimited.			12b. DISTRIBUTION CODE	
13. ABSTRACT (Maximum 200 words) This report is a compilation of the papers presented at the 1993 USAF Structural Integrity Program Conference held at the Hyatt Regency, San Antonio, Texas on 30 November - 2 December 1993.				
			<input checked="" type="checkbox"/> Unannounced <input type="checkbox"/> Justification	
			By _____ Distribution/	
			Availability Codes	
			Dist Avail and/or Special	
			A-1	
14. SUBJECT TERMS			15. NUMBER OF PAGES 861	
			16. PRICE CODE	
17. SECURITY CLASSIFICATION OF REPORT UNCLASSIFIED	18. SECURITY CLASSIFICATION OF THIS PAGE UNCLASSIFIED	19. SECURITY CLASSIFICATION OF ABSTRACT UNCLASSIFIED	20. LIMITATION OF ABSTRACT UNLIMITED	

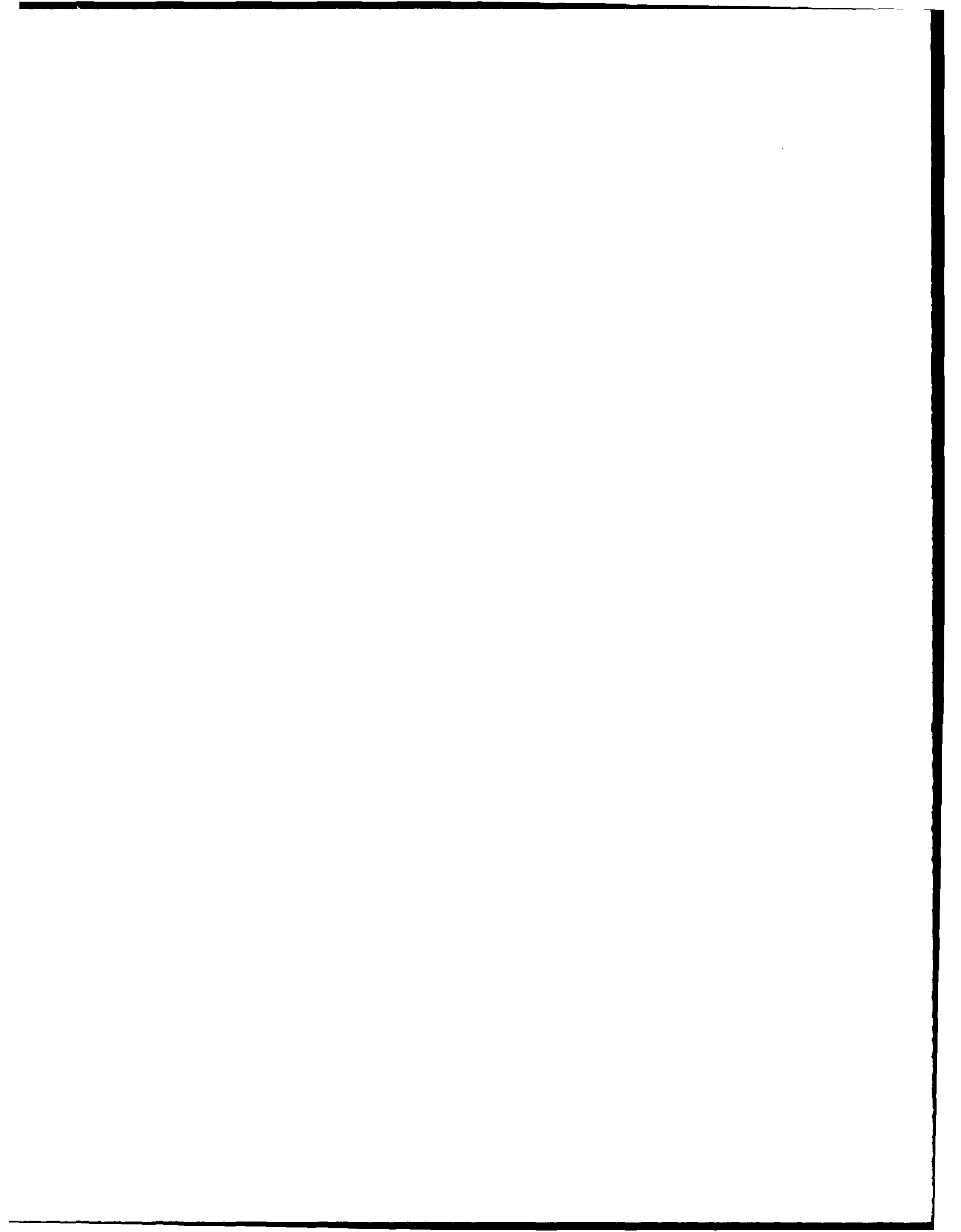


TABLE OF CONTENTS

	Page
FOREWARD	vi
AGENDA	vii
INTRODUCTION	xiv
 <u>SESSION I - OVERVIEWS</u>	
MSD, Where We Are and Where We Should Go	1
An Aircraft Structural Integrity Program - FAA Flight Inspection Beech 300 Fleet -	34
A Probabilistic Strategy for Aircraft Fleet Inspection Considering Unanticipated Environments	67
Probabilistic Design System Development at Pratt & Whitney	97
The Cost Effectiveness of Aircraft Structural Integrity Program	115
 <u>SESSION II - STRUCTURAL ANALYSIS</u>	
Non-Linear Fatigue Crack Growth Analysis for Problems with Small-Scale Yielding	142
Results-To-Date on Fatigue Test of Combined F-15 A and C Article Subjected To Actual Usage Spectrum	165
The 90/95 Crack Length Revisited	180
Aircraft Fatigue and Crack Growth Considering Loads By Structural Component	201
Pitting Corrosion Fatigue of Aircraft Materials - A Review	219
 <u>SESSION III - STRUCTURAL ANALYSIS AND MATERIALS</u>	
Progressive Fracture of Polymer Matrix Composite Structures: A New Approach	233
The Influence of Initial Quality on the Durability of 7050-T7451	255
Maintaining Structural Integrity By Prevention of Surface Initiating Failure Modes ...	268
Effect of Corrosion on Fatigue Crack Propagation in Aluminum Alloy 2024-T3	276
A Comparison of Fracture Criteria for Crack Coalescence and Other Observations Based on Residual Strength Calculations	290

Destructive Teardown of a C-141B Lower Surface Inner Wing 321

SESSION IV - NONDESTRUCTIVE AND DESTRUCTIVE EVALUATION

Holistic Life Prediction Methodology for Powder Metal Engine Components..... 364

Engine Life Measurement and Diagnostics - The Future Direction for the Air Force 378

**Hollow Fan Blade Damage Tolerance Capability/Benefits for an Advanced
Technology Engine..... 410**

Effect of Peak Loads on Dwell Crack Growth in Inconel 718 at 600°C..... 442

**Damage Assessment in Composites Using Thermoelastic Stress Analysis (TSA)
Techniques 507**

The Influence of NDE in Assessing Aging Aircraft 529

Probabilistic Structural Analysis Methods for Engine Components 554

SESSION V - STRUCTURAL TESTING, ANALYSIS, AND FORCE MANAGEMENT

Fracture Analysis of C-141 Weepole Cracks 580

**Cold Expansion Rework of Weep Holes in the Lower Wing Structure of C-141B
Aircraft..... 600**

**Split Mandrel Coldworking - A Manufacturing Solution Automating a Critical
Process 613**

Review of Boron Epoxy Reinforcement of Aging Metallic Aircraft Structures..... 622

**An Integrated Design, Fabrication, Testing and Analysis for the Fatigue
Performance Evaluation of Composite Patch Re-paired Aluminum Aircraft
Structure Samples..... 634**

**Soft Patches for Damage Tolerant Riveted Repair of Aluminum Fuselage
Structures 672**

B-1B Shoulder Longeron Repair..... 689

SESSION VI - STRUCTURAL ANALYSIS AND FORCE MANAGEMENT

Aircraft Accident/Incident Analysis Using Animation Techniques..... 699

**The Challenges Associated with the Operation of Loads Monitoring Equipment for
Efficient Structural Life Management..... 721**

An Improved G-Tracking Method for Large Transport Aircraft 741

Naval aircraft Approach and Landing Data Acquisition Systems (NAALDAS)
Acceptance Test Results.....714

Structural Upgrade of the F-16 C/D and Results of the Loads Flight Test.....795

**Integration of Smart Structures Concepts for Improved Structural Integrity
Monitoring of the T-38 Aircraft**835

Accession For	
NTIS	CRA&I
DTIC	TAB
Unannounced Justification	
By	
Distribution	
Availability Codes	
Dist. Avail. and/or Special	

FOREWORD

This report was compiled by the Systems Support Division, Materials Directorate, Wright Laboratory, Wright-Patterson Air Force Base, Ohio. It was initiated under Task 24180704 "Corrosion Control & Failure Analysis" with Thomas D. Cooper as the Project Engineer.

This technical report was submitted by the editors.

The purpose of this 1993 Conference was to bring together technical personnel in DOD and the aerospace industry who are involved in the various technologies required to ensure the structural integrity of aircraft gas turbine engines, airframes and other mechanical systems. It provided a forum to exchange ideas and share new information relating to the critical aspects of durability and damage tolerance technology for aircraft systems. The conference was sponsored by the Air Force Materiel Command (AFMC), Aeronautical Systems Center, Deputy for Engineering and Materials and Flight Dynamics Directorates of the Wright Laboratory, Wright-Patterson Air Force Base, Ohio. It was hosted by AFMC's San Antonio Air Logistics Center.

AGENDA

1993 USAF STRUCTURAL INTEGRITY PROGRAM

30 NOVEMBER - 2 DECEMBER 1993

**Hyatt Regency
San Antonio, Texas**

SPONSORED BY:

ASC/Aeronautical Systems Center

ASC/EN Deputy for Engineering

WL/Flight Dynamics Directorate

WL/Materials Directorate

HOSTED BY:

**San Antonio Air Logistics Center
Aircraft Directorate**

**Aircraft Structural Integrity Branch
(SA-ALC/LADD)**

AGENDA

MONDAY, 29 NOVEMBER 1993

1800-2000 **Pre-Registration**

TUESDAY, 30 NOVEMBER 1993

0730-0830 **Registration/Continental Breakfast**

SESSION I - OVERVIEWS

Chairman - H. Wood, ASC/ENF

- 0830-0900** **MSD, Where We Are and Where We Should Go**
E. B. de la Motte
Swedish Defence Materiel Administration, Stockholm, Sweden
Capt F. A. Opalski
WL/FIBEC
- 0900-0930** **An Aircraft Structural Integrity Program - FAA Flight Inspection**
Beech 300 Fleet -
P. Gould
Beech Aircraft Corp.
- 0930-1000** **Ten Years with Calspan's Variability Stability Learjet**
J. Ball
Arvin-Calspan Co.
J. Roesch
Consultant
(PAPER NOT PUBLISHED)
- 1000-1030** **REFRESHMENT BREAK**
- 1030-1100** **A Probabilistic Strategy for Aircraft Fleet Inspection Considering**
Unanticipated Environments
E. J. Tugel, C. L. Brooks, and D. L. Rich
McDonnell Douglas Aerospace-East
- 1100-1130** **Probabilistic Design System Development at Pratt & Whitney**
J. D. Adamson
Pratt & Whitney
- 1130-1200** **The Cost Effectiveness of Aircraft Structural Integrity Programs**
Capt A. J. Appels
Canadian Armed Forces
- 1200-1330** **LUNCH and PRESENTATION**
C-17A Aircraft Structural Integrity Program Update
R. Eastin and B. Zimmerman
McDonnell Douglas Aerospace
(PAPER NOT PUBLISHED)

SESSION II - ANALYSIS AND TESTING

Chairman - J. Rudd, WL/FIB

- 1330-1400** **Non-Linear Fatigue Crack Growth Analysis for Problems with Small Scale Yielding**
D. L. Ball
Lockheed Fort Worth Co.
- 1400-1430** **D Sight Corrosion Detection In Aircraft Structures**
J. P. Komorowski, K. Shankar, and R. W. Gould
National Research Council, Canada
O. L. Hageniers
Diffrauto Ltd.
(PAPER NOT PUBLISHED)
- 1430-1500** **Determination of Structural Loads Using Holometric Analysis**
L. Pllum
Kaman Aerospace Corp.
A. Ghannadan
ESPRIT Technology Inc.
(PAPER NOT PUBLISHED)
- 1500-1530** **REFRESHMENT BREAK**
- 1530-1600** **Results-To-Date on Fatigue Test of Combined F-15 A and C Article Subjected to Actual Usage Spectrum**
R. Foster and R. Milliere
McDonnell Douglas Aerospace-East
- 1600-1630** **The 90/95 Crack Length Revisited**
A. P. Berens
University of Dayton Research Institute
S. I. Vukelick
ASC/ENFSF
- 1630-1700** **Aircraft Fatigue and Crack Growth Considering Loads by Structural Component**
J. D. Yost
DPRO-BHT
- 1700-1730** **Pitting Corrosion Fatigue of Aircraft Materials - A review**
D. W. Hoepfner, T. Goswami and C. Elliot
University of Utah
- 1800-1930** **RECEPTION**

WEDNESDAY 1 DECEMBER 1993

SESSION III - STRUCTURAL MATERIALS

Chairman - T. Cooper, WL/MLS

- 0800-0830** **Registration/Continental Breakfast**
- 0830-0900** **Progressive Fracture of Polymer Matrix Composite Structures: A New Approach**
C. C. Chamis and P. L. N. Murthy
NASA Lewis Research Center
L. Minnetyan
Clarkson University
- 0900-0930** **The Influence of Initial Quality on the Durability of 7050-T7451 Aluminum Plate**
A. F. Grandt, Jr., C. Zezula, and J. Elsner
Purdue University
A. J. Hinkle
Alcoa Technical Center
- 0930-1000** **Maintaining Structural Integrity By Prevention of Surface Initiation Failure Modes**
J. Harrison
Metal Improvement Co.
- 1000-1030** **REFRESHMENT BREAK**
- 1030-1100** **Effect of Corrosion on Fatigue crack Propagation**
G. H. Koch
Cortest Columbus Technologies
J. G. Burns
WL/FIBE
- 1100-1130** **A New Method for Conducting Short Crack Fatigue Tests**
R. L. Carlson
Georgia Institute of Technology
(PAPER NOT PUBLISHED)
- 1130-1200** **A Comparison of Fracture Criteria for Crack Coalescence and Other Observations Based on Residual Strength Calculations**
J. P. Gallagher, S. Dhar, and A. P. Berens
University of Dayton Research Institute
J. G. Burns
WL/FIBE
- 1200-1330** **LUNCH and PRESENTATION**
Destructive Teardown of a C-141B Lower Surface Inner Wing
R. E. Alford
WR-ALC/LJLE
G. M. Weitz
Lockheed Aeronautical Systems Co.
(PAPER PUBLISHED)

SESSION IV - ENGINE STRUCTURAL INTEGRITY

Chairman - W. Taylor, ASC/ENFP

- 1330-1400** **Holistic Life Prediction Methodology for Powder Metal Engine Components**
P. A. Domas
G. E. Aircraft Engines
- 1400-1430** **Engine Life Measurement and Diagnostics - The Future Direction for the Air Force**
Squadron Leader C. Pomfret
Royal Air Force
WL/POTC
- 1430-1500** **Hollow Fan Blade Damage Tolerance for an Advanced Technology Engine**
T. T. King, J. M. Delvaux, and M. J. Duffy
Pratt & Whitney
- 1500-1530** **REFRESHMENT BREAK**
- 1530-1600** **Effect of Peak Loads on Dwell Crack Growth in Inconel 718 at 600°C**
R. J. H. Wanhill
National Aerospace Laboratory NLR, The Netherlands
- 1600-1630** **Damage Assessment in Composites Using Thermoelastic Stress Analysis (TSA) Techniques**
D. H. Nethaway
Pratt & Whitney
- 1630-1700** **The Influence of NDE in Assessing Aging Aircraft**
C. Annis
Pratt & Whitney
- 1700-1730** **Probabilistic Structural Analysis Methods for Engine Components**
H. R. Millwater, Y.-T. Wu, and O. H. Burnside
Southwest Research Institute

THURSDAY, 2 DECEMBER 1993

SESSION V - STRUCTURAL REPAIR

Chairman - C. Petrin, ASC/ENF

- 0800-0830** **Registration/Continental Breakfast**

- 0830-0900** Fracture analysis of C-141 Weepole Cracks
S. N. Atluri
Georgia Institute of Technology
D. C. Register
WR-ALC/TIED
D. S. Pipkins and E. F. Punch
Knowledge Systems Inc.
- 0900-0930** Cold Expansion Rework of Weep Holes in the Lower Wing Structure of C-141B Aircraft
L. Reid, A. C. Rufin, D. W. Glenn, and E. Easterbrook
Fatigue Technology Inc.
R. Jansen and D. Register
WR-ALC/TIED
- 0930-1000** Split Mandrel Coldworking - A Manufacturing Solution for Automating a Critical Process
G. A. Rodman
West Coast Industries
M. Creager
Structural Integrity Engineering
- 1000-1030** REFRESHMENT BREAK
- 1030-1100** Review of Boron Epoxy Reinforcement of Aging Metallic Aircraft Structures
S. J. Whicher
Textron Specialty Materials
- 1100-1130** An Integrated Design, Fabrication, Testing and Analysis for the Fatigue Performance Evaluation of Composite Patch Repaired Aluminum Aircraft Structure Samples
T. P. Sivam and T. Behrens
Chrysler Technologies Airbourne Systems, Inc.
A. Fancett and O. Ochoa
Texas A&M University
- 1130-1200** Soft Patches for Damage Tolerant Riveted Repair of Aluminum fuselage Structures
R. Fredell and M. F. Heerschap
Delft University of Technology
B. van Wimersma
Structural Laminates Co., The Netherlands
- 1200-1330** LUNCH AND PRESENTATION
B-1B Shoulder Longeron Repair L. G. Hansen
Rockwell International NAAD
(PAPER PUBLISHED)

SESSION VI - FORCE MANAGEMENT

Chairman - J. Turner, SA-ALC/LADD

- 1330-1400** **Aircraft Accident/Incident Analysis Using Animation Techniques**
R. Kerr
MASIIS, Tinker AFB, OK
M. Poole
Canadian Transportation Safety Board
- 1400-1430** **The Challenges Associated with the Operation of Loads Monitoring**
Equipment for Efficient Structural Life Management
Major M. B. Zgela
Canadian Armed Forces
- 1430-1500** **An Improved G-Tracking Method for Large Transport Aircraft**
B. Martin
Lockheed Aeronautical Systems Co.
R. E. Alford
WR-ALC/LJLE
- 1500-1530** **REFRESHMENT BREAK**
- 1530-1600** **Naval Aircraft Approach and Landing Data Acquisition System**
((NAALDAS) Acceptance Test Results
R. P. Micklos
Naval Air Warfare Center, Aircraft Division
- 1600-1630** **Structural Upgrade of the F-16 C/D and Results of the Loads Flight Test**
2Lt D. R. Mack
ASC/YPEF
- 1630-1700** **Integration of Smart Structures Concepts for Improved Structural**
Integrity Monitoring of the T-38 Aircraft
C. B. Van Way, J. N. Kudva, and C. Marantidis
Northrop Corporation, Aircraft Division
- 1700-1730** **The Life Management of Aging Systems; an M&P Prospective**
T. Cordell
WL/MLLP
(PAPER NOT PUBLISHED)

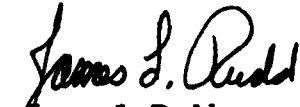
INTRODUCTION

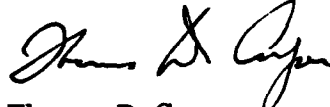
This report contains the proceedings of the 1993 USAF Structural Integrity Program Conference held at the Hyatt Regency Hotel in San Antonio, Texas from 30 November - 2 December 1993. The conference, which was sponsored by the ASC Deputy for Engineering and the Wright Laboratory Flight Dynamics and Materials Directorates, was hosted by the San Antonio Air Logistics Center Aircraft Directorate, Aircraft Structural Integrity Branch (SA-ALC/LADD).

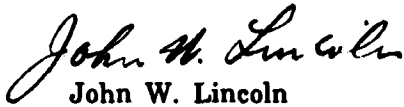
This conference, as in previous years, was held to permit experts in the field of structural integrity to communicate with each other and to exchange views on how to improve the structural integrity of military weapon systems. In addition, a new session on structural repair was included to reflect the increasing emphasis on this topic in light of our aging aircraft fleet. This year our friends from outside the U.S. borders continued to provide the audience with outstanding presentations on activities within their countries. It is anticipated that this conference will include their contributions in the agenda of future meetings.

The sponsors are indebted to their hosts for their support of the conference. The sponsors are also indebted to the speakers for their contributions. In particular, thanks are due to the three luncheon speakers for their informative presentations. They are R. Eastin and B. Zimmerman of McDonnell Douglas Aerospace; R.E. Alford of WR-ALC/LJLE and G.M. Weitz of Lockheed Aeronautical Systems Co.; and L.G. Hansen of Rockwell International NAAD.

Much of the success of the conference is due to the efforts of Lori Mantia and her team of Denise Abernathy and Esther Burnett from Universal Technology Corporation. Their cooperation is greatly appreciated. We are also very grateful to Rita Scholes of WL/MLS for assisting us during the conference, compiling the Proceedings and preparing this publication.


James L. Rudd
WL/FIB


Thomas D. Cooper
WL/MLS


John W. Lincoln
ASC/ENF

1993 USAF Structural Integrity Conference
30 November - 2 December 1993, San Antonio, Texas

MSD: WHERE WE ARE AND WHERE WE SHOULD GO

Mr. Eddy B. de la Motte	Capt Frank A. Opalski
Swedish Exchange Engineer	Flight Dynamics Directorate
Swedish Defence Material Adm.	Wright Laboratory
Stockholm, Sweden	WPAFB, OH

I. Summary

At Wright Laboratory our goal is to develop technologies that can be directly transferred to the user. Since the 1988 Aloha Airlines Boeing 737 incident, a renewed emphasis has been placed on the area of aging aircraft and, more specifically, multiple-site damage and corrosion. What we've tried to do is determine who's doing what in these areas and where we need to concentrate additional efforts. We performed a literature search under the subjects of multiple-site damage, fatigue, and corrosion as they relate to aircraft and came up with several hundred articles satisfying these criteria.

We then reviewed these papers to get a feel of what areas have been receiving significant attention and any noteworthy results that have occurred. The objective of this report is to give a general overview of the level of knowledge regarding MSD and corrosion as they appear in the performed literature survey. It also summarizes some of the general trends we've seen regarding MSD and corrosion and concludes with recommendations for future research efforts to pursue.

II Table of Contents

- I. Summary
- II. Table of Contents
- III. Introduction
- IV. Ways to handle MSD
- V. Predicting MSD
 - V.a. Initiation
 - V.b. Crack growth
 - V.c. Link up
- VI. Corrosion
- VII. Conclusions/Recommendations
- VIII. List of references

III. Introduction

MSD (Multiple-Site-Damage) typically consists of a large number of small cracks, originating mostly at the edges of several adjacent and collinear fastener holes, lap joints, etc. MSD usually occurs in longitudinal lap-joints of pressurized fuselage structures. It is less likely to occur in wings as a more or less uniform stress field is required to develop an MSD situation (2). During recent years the research community has focused on lap joints in pressurized fuselages but there are, however, examples where widespread cracking has occurred in wing structures, like in the original Air Force KC-135 and C-5A. This implies that MSD has the potential to appear anywhere in the older fleets (1).

There are, nevertheless, several differences between MSD in riveted fuselage lap joints and wings. For MSD to occur in a fuselage lap joint the following must be present:

- * Numerous, closely spaced rivets are in the same rivet row
- * The sheet thickness is low
- * The stress field is close to uniform
- * The spectrum loading is close to constant amplitude.

In an MSD situation subcritical cracks, where the individual crack can be very small and usually very difficult to detect with visual inspection (naked eye), can link up before detection and go to unstable cracking at a load below limit load. With MSD the crack growth and failure characteristics are significantly different from those of an isolated crack which the current damage tolerant requirements are based on. The fatigue lifetime becomes shorter than that of a single crack with a similar length and the fail-safe capability of the structure may be affected. For example the fuselage may not leak before burst or tear straps may not stop or alter the direction of the crack in the presence of MSD.

MSD in fuselage lap joints is almost always influenced by corrosion and fretting or a combination of the two. Fretting usually shortens the time to initiate a crack while corrosion both can shorten the initiation time and accelerate the crack growth.

Let us now define MSD. A number of different definitions have been noted in the literature. In order to define MSD more precisely, a three part definition was proposed (1) as follows:

1. MSD is the occurrence of independent cracks which may linkup to cause greater damage or partial fracture, for which the residual strength is less than it would be if such greater damage developed as a consequence of growth of a single crack.
2. This linkup may become unstoppable due to further interaction with otherwise subcritical cracks ahead of the partial fracture.

3. A change in inspection procedure or interval from that for a single crack is needed.

Under the present definition the occurrence of multiple cracks is not MSD if no linkup occurs or the linkup of these cracks does not result in the reduction of residual strength below the limit load which defines plastic collapse.

How big of a problem is MSD?

The damage tolerance philosophy assumes a rogue flaw in the most critical point and it also assumes that adjacent members in a fail safe structure can have cracks grown from an initial flaw, representative of the initial fatigue quality of that article. The problem is that it doesn't take into account MSD. That is small cracks in front of the lead (rogue flaw) crack. This means that the inspection interval based on the propagation of the rogue flaw crack can be unconservative. In the research community there appears to be an overemphasis on unrealistic MSD situations where numerous small cracks, with equal size, interact and finally lead to failure.

Nevertheless, it would be incorrect not to pay attention to the problem knowing that at least three aircraft accidents are said to have been caused by MSD:

- * AVRO 748 in Argentina, April 1976.
- * Boeing 747, JAL, 1983
- * Boeing 737, Aloha, April 1988.

Furthermore in (4) it is shown that MSD can play a major role in the life management program for wing structures in addition to other components of an aircraft, for example C-141, KC-135 and C-5.

Since these problems were discovered, numerous fatigue tests have been carried out in many laboratories. In (3) it is reported that Shutz tested lap joints until 50% of the average life indicated by other specimens. After pulling to failure it could be established that small part-thru cracks could be observed on the fracture surface. On a review of a large number of specimens tested by students at Delft it was found that crack nuclei could be found at almost all holes. Furthermore Schive postulates that "if the fatigue life of a riveted lap joint is limited cracks will occur at many rivets in the same row, and a potential MSD problem is present". Most lap joints in pressurized fuselage are strength designed and, therefore, have a limited fatigue life. This implies that most lap joints will develop an MSD situation. It is just a question of time.

IV. Ways to Deal with MSD

So how can we deal with MSD? There are two principally different ways to maintain an adequate level of safety: use a "safe life" approach or an "inspections" approach.

The "safe life" approach is based on retiring the aircraft when its original crack-free design life has been reached or modifying the actual structural element when the original crack-free life has been reached. The "inspections" approach is based on reducing the inspection interval, improving the inspection methods, finding an alternative way to detect the crack, and finally performing repairs and/or modifications.

To retire an aircraft after its original crack free design life seems to be a straight forward and obvious method to avoid MSD. The drawback, of course, is that it's not economically sound to retire an aircraft in good condition. If retirement is used we again lean on the safe life philosophy that the authorities around the world have been trying to get away from.

If one wants to handle the problem with the "safe life" approach one has to answer question No. 1 below. On the other hand, if the "inspection" approach is chosen, one has to answer all questions below:

1. At what age of the aircraft should the cracks be expected?
2. What size of cracks will be consistently located?
3. How fast will the cracks grow?
4. How long is the crack when it starts growing unstable?
5. What is the failure load?
6. Do (2 - 5) give sufficient time to find the crack with economically acceptable inspection periods?
7. How long does it take before a dangerous situation occurs if cracks are overlooked during inspections?

There are several ways to obtain the answers:

- a. Component testing
- b. Testing of substructural parts
- c. Full scale fatigue tests
- d. Tear down inspections
- e. Theoretical models
- f. Nondestructive inspection

These are the standard tools to ensure structural integrity. Items (c) and (d) have been used extensively successfully to assure that MSD does not develop in aging structures, for instance 737, 747-400, KC-135 and C-141. The following will discuss methods found in the literature to answer the above questions.

V. Methods to Predict MSD

MSD can be divided in three different phases. These phases differ mainly by the mechanism driving the crack (5). These phases are:

1. Local stage.
2. Crack growth.
3. Linkup and Failure.

Phases 1 and 2 determine the life of the structure and, therefore, the inspection interval. Phase 3 has a minor influence on the lifetime but is essential for the failure load. Several papers report that after the first linkup the test went to failure after less than 3% of the total life.

V.a. Local Stage/Initiation

The local stage is the period when cracks are too small to influence adjacent cracks and thus the development of each crack is dominated by the influence of its local structural details. Approximately 80% of the total life is spent in this stage (8). If we want to predict MSD we have to be able to predict the initiation phase. This stage starts with initiation and ends when the crack has reached some length L when the interaction effects are becoming essential. Different values of L have been given in the literature. In (6) the initial crack length is taken from a method proposed by Dowling

$$a_t = r / [(1.12 * K_t)^2 - 1] \quad [1]$$

Where: r is the radius of the hole
 a_t is the transition crack length
 K_t is the stress concentration factor

In other papers (7) the initial crack length is chosen more arbitrarily as the length when the crack becomes visible under the rivet head. What is important is that the crack is long enough to be detected and not being influenced by local and short crack effects (see below). On the other hand it should not be long enough to interact with other cracks and holes.

The initiation of cracks in a riveted lap joint is certainly a very complicated phenomena due to the many factors that influence the initiation time:

1. Gross stress
2. Lap joint dimensions
3. Type of rivet
4. Use of anti-fretting seal
5. Riveting procedure/quality
6. Environment/environment protection
7. Scatter in material fatigue properties
8. Influence of other damage (another crack)

Some comments on the problem of modelling the initiation phase are appropriate. Most of the discussion is taken from (3). Load transmission by a rivet implies a bearing pressure on the rivet hole (pin-loaded hole). It causes a local stress concentration at the edge of the hole, that is rivet row 1. Load transmission also occurs at row 2, which leads to a by-pass load for row 1. Apart from that the sheet bending induced by eccentricities of the joint has its maximum at these rows. Secondary bending is a non-linear function of the applied load and is dependent on the joint design, especially the length of the joint.

The pin loaded hole case is problematic in view of the bearing distribution on the hole, friction between the pin and hole, and more the unknown load transmission by friction between the sheets. The friction is certainly not constant but increases during fatigue cycling and decreases if a crack develops at the hole. The stress concentration of the by-pass load also offers a problem because the rivet hole is filled. Furthermore, the load transmission is a 3-dimensional problem. The bearing stress is not distributed homogeneously over the sheet thickness.

Another complicating factor is that the fit of the rivet can vary. The fatigue life has been shown to vary with the clamping force (riveting intensity) by as much as a factor of 3 (8). The clamping force affects the amount of load transferred by friction and, therefore, the amount of fretting that can be expected. Fretting also alters the initiation points and has been very hard to predict theoretically. The effects of corrosion on initiation will be discussed under that section.

A large scatter is expected in the initiation period due to the complex nature of the joint. However, the riveted lap joint is a poor joint. Whatever the complexity of the load transmission, cracks will initiate. Another factor to reduce the scatter is that there are many critical holes. Tests show (7) that the scatter is dependent on the stress for constant amplitude loading, as shown in Fig 1. An interesting observation for variable amplitude loading is that the scatter seems to be approximately constant. Scatter in two test series of 20 riveted joints is shown in fig 2. Both the log-normal distribution and the Weibull 3-parameter agree rather well. Apparently, 20 results is an insufficient number to express a preference for the Weibull distribution which is preferred on physical grounds.

Some papers (3 & 4) report observations of relatively uniform MSD in older aircraft fuselages. This suggests low scatter in initiation and/or a mechanism for shorter cracks to catch up with longer cracks or an equivalent mechanism that keeps longer cracks from running away from the shorter. This basic mechanism has not yet been identified.

The above discussion clearly implies that fatigue initiation in riveted lap joints is a complex phenomenon. Accurate predictions cannot be expected. The fact that the scatter is less than can be expected by the complexity of the joint implies that empirical methods can be used. A model for predicting initiation in lap joints must be able to describe the statistics involved.

Very few investigations focusing on initiation have been seen in the literature. That is probably because of the difficulties involved in describing this process. Furthermore, very few tests on riveted joints regarding initiation have been found. That might be explained by this kind of information remaining corporate secrets within the industry.

In the academic world the work on MSD seems to have been focused on the crack growth phase and the link up phase. The initiation phase has either been omitted by using precracked specimens or predicted from unloaded holes. Calculations (6) using Palmgren-Miner's rule while simultaneously solving a version of Neubers rule, the hysteresis curve equation and the stress-strain equation seem to give reasonable results of initiation of unloaded holes influenced by a nearby crack.

The initiation times in riveted joints are dependent on so many factors that we can't theoretically model. However, reasonable predictions can be made by semi-empirical methods. The initiation times and initiation scatter must be found by tests. As crack initiation of riveted lap joints is so strongly affected by local effects close to the rivet and often induced by fretting, the literature recommends that the specimen configuration used to obtain the data should be as close to the real structure as possible, preferably identical.

To use wide specimens to find the distribution of initiation times can cause problems like not all hole perimeters will crack or local stress risers due to other damage may exclude data points.

Some of these problems can be avoided if specimens are used with only one column of rivets, see Fig 3. Influence of a crack on one hole side on the local stress level on the other hole side still remains if you have initiation close to each other in time. The interaction effects between cracks in this kind of specimen are described in (13). Other questions still remain about using smaller specimens like theoretical stress concentration factors, clamping and secondary bending (6). This should be investigated further.

One empirical method was found in the literature (8) to predict initiation in lap joints. That is to use scatter curves (time to crack initiation) combined with Palmgren-Miners rule. In this method every hole side is assigned a fixed cumulative probability randomly based on initiation scatter curves, see Fig 3. Influence of other cracks, already initiated, is accounted for by using linear-elastic stress concentration factors. The initiation tests have been related to gross stress so an equivalent gross stress is used representing an equivalent undamaged situation for which the initiation curve is known. This value is determined by:

$$\sigma_{\text{gross, equivalent}} = \sigma_{\text{gross}} * K_t / K_t^* \quad [2]$$

Where, K_t^* is the stress concentration factor for the undamaged riveted lap joint (tested configuration) and K_t is the actual stress concentration factor of the cracked configuration. In this way a function $F(K_t/K_t^*)$ is created, which is one for the undamaged situation and increases as soon as a crack is present at the opposite side of the hole or at one of the neighboring rivets. This linear elastic "scaling" is not only allowed as long as the peak stress is less than $\sigma_{0.2}$ but also for situations with small scale yielding. The argument for this statement can be found in

(8). The stress concentration factors K_t and K_t^* are found using superposition, see (8) for details. The changing geometry, that is crack growth, will change the value of σ used in the initiation curve. Palmgren-Miner's cumulative damage rule is used to account for accumulated damage after each increment of cycles. When $\sum n/N=1$, the crack is initiated and the crack growth calculation starts.

Instead of using Palmgren-Miner's cumulative damage rule to account for the influence of nearby cracks on a not-yet-initiated hole, one of the two approaches proposed by Manning and Yang (9 & 10) could probably be used. These are:

1. Stochastic crack growth from a single initial flaw.
2. Deterministic crack growth from an Equivalent Initial Flaw Size Distribution (EIFSD).

See Fig 5. These approaches have not been used in an MSD situation but would probably work as they have been shown to give reasonable results for joints with load transfer. As these methods are based on tests of the actual local geometry (rivet, clamping force, etc.) and the principal of growing cracks forward and backward in the same way, one avoids the problem with local effects and "short crack behavior". Each hole side could randomly be assigned either an Equivalent Flaw Size or, in case 1, a crack growth rate. The elevated stresses, due to nearby cracks, could be found by using the linear elastic "scaling" method, mentioned above. That equivalent gross stress would then be used to change the deterministic crack growth rate in 2 above or change the median crack growth rate in 1. See (10) for details.

NASA reports in (11) that a FE-code was used to obtain stress concentration factors for a wide range in hole size and countersink depth. Stress analysis of countersunk holes has not been reported in the literature previously. Different kinds of loading were considered for both the straight-shank hole and the countersunk. This is reported in (12) (not read in this survey). Also in (11) it is reported that NASA treats initiation by predicting the growth of micron-size cracks initiating at inclusion particles in the subgrain boundary microstructure. This has been made possible with the coupling of the closure methodology with the small crack growth data base. How this method works in reality, especially in view of the complex stress field near the rivet, has not been found during this literature search.

V.b. Crack Growth

The crack growth stage is the stage where the cracks are long enough to interact with each other. To be able to model cracks in this stage, one has to consider both crack interactions as well as local geometry. Most work found in the literature deals with this stage. To be able to predict crack growth, one must determine the stress intensity factor. There are different ways to obtain that. A summary of different approaches was found in (6) and is repeated here except for the paragraph regarding hybrid FEM which was taken from (1).

FEM with alternating techniques

FEM with alternating techniques are based on the principle of superposition of stresses associated with cracks and free boundaries. The stresses in the uncracked body are analyzed first by using finite element or boundary element methods. The effects of the cracks are assessed by erasing the traction at the crack location in the otherwise uncracked body. To accomplish this, the finite body is replaced by an infinite one, with the stresses going to zero at infinity. This infinite body problem has an analytical solution, but the far field stresses do not satisfy the boundary conditions. To account for this, the residual tractions at the boundaries are erased, first by solving an uncracked infinite body with the residual boundary tractions, and then by erasing the crack tractions in the uncracked body. This iterating loop is repeated until the analytical solution for this infinite body also satisfies the zero traction condition of the finite body. Once the solution has converged, the stress intensity factor may be obtained.

The alternating technique has been employed by Dawicke and Newman (5), Tong/Atluri and Park/Atluri. Dawicke and Newman used boundary elements to analyze different types of MSD specimens with open holes and uniaxial loading. They report agreement within 20% of the experimental lives for all crack configurations considered (5).

The hybrid finite element method

The hybrid finite element method is based on a variational formulation in which relevant field variables in the element need not satisfy a priori the requirements of inter-element displacement compatibility and inter-element traction reciprocity. The constraint condition can then be included in the functional by the use of Lagrange multipliers, which are the additional variables at the element boundary. The method can provide directly the solution for the strength singularities (such as stress intensity factors at the tips of a crack). Hybrid elements are reported (1) to have been extensively developed and used and are said to be extremely accurate and efficient in comparison to the standard finite element method.

Finite element analysis with super-convergent methods

Actis and Szabo used finite element analyses with super-convergent methods to solve for the stress intensity factors at MSD crack tips. The solution was obtained using the p-version program "PEGASYS" which allows extraction of the stress integral on an arbitrary circular path around the crack tip. Similar work was presented at ICAF by Andersson et al with the adaptive FE-code STRIPE. The development in computational speed lets us use more complicated codes. These methods will probably be used more in the future.

Compound methods

For an array of collinear cracks in structural components the common approach currently being used in the aircraft industry is the compounding solution method. The principle of the compounding method is to obtain a solution for the stress intensity factor of

a complex geometric configuration by superimposing a set of appropriate assisting solutions, usually associated with simple configurations of cracks and component boundaries and having known solutions. An assisting configuration usually contains only one boundary which interacts with the crack. Combining the effects of each boundary on individual cracks is subject to the principle of superposition with the addition of an interaction effect between the separate boundaries. The resultant stress intensity factor with all boundaries present is then expressed in terms of (2):

$$K_r = K_o + \sum (K_n - K_o) + K_e \quad [3]$$

Where K_o is the stress intensity factor (SIF) in the absence of all boundaries, K_n is the SIF with only the nth boundary present and K_e is the contribution which may be present due to boundary-boundary interaction. In plane-sheet problems the factor K_e is small (few percent) and therefore can be ignored. However, the contribution of K_e to the resultant may become important if the growing crack approaches some boundary.

Often (2 & 6), a more simple engineering approach is applied. The contribution from each ancillary configuration to the resultant stress intensity factor can be compounded in the terms of:

$$K_r = K_o * \sum_{\text{all } x} f_x \quad [4]$$

Where the f_x -values are the geometry correction factors associated with the ancillary solutions. According to (2) the difference between equation [3] and [4] is negligible as long as the f_x values are close to one. If f_x factors are not small compared to one, Eq [4] will give conservative results.

The compound method has been used by numerous scientists. In (2) this technique was used on a panel having a collinear row of open holes with the center three cracked. They report agreement within 14% of experimental results. Although this is a simplified case their results show that simple compounding techniques based on superposition produce very acceptable results for MSD analysis. Also in (6) good agreement was reported. Fig 6 shows a comparison between predicted versus actual fatigue lives, with and without interactions, for two different type of specimens. Type A specimens had nearly uniform MSD at all holes and type B had a lead crack.

One interesting question is how important are the interaction effects? The interaction between cracks is the significant problem with predicting MSD. Schive reports in (2) that the interaction effects were relatively small for the major part of the life. Significant interaction effects were observed when the ligament between cracks became smaller than half the pitch between the holes, see Fig 7, but then the remaining life is relatively short. Others (6) that tested panels with extensive MSD report that the interaction effects significantly increase the rate of growth even with the cracks as short as .05 to .1 inches. The difference in

these two conclusions is probably caused by the fact that Schive used 40 mm between each hole and Moukawsher used 1 inch (25.4 mm).

Schive draws the conclusion that the MSD problem in aging aircraft will not benefit a great deal from more sophisticated crack growth prediction techniques. This conclusion is supported by (6) even though the interaction effects are more dominant due to the closer spacing of the rivets. These kind of analyses with rivet holes have not been found in the literature. If the initiation crack length is chosen with care, the fact that hole is riveted shouldn't affect the prediction significantly.

To account for scatter in the crack growth process one can assign each crack crack-growth properties before the analysis start. Paris' law with a Weibull distribution for the crack growth coefficient C is proposed in the literature (6).

Tear Straps and MSD

The role of tear straps in an airplane fuselage is to arrest an axial crack which is propagating either subcritically under fatigue loading or dynamically after reaching criticality. The crack arrest can occur by the lower stresses due to the reinforcing effect of the tear strap or by crack curving due to the complex crack tip stress field generated by the crack flap and the tear strap. Although the tear strap is the last defense of an axially rupturing fuselage, little is known about its effectiveness in arresting an axial crack and much of its design is based on empirical rules derived from sub- and full-scale tests of pressurized fuselages. Two papers were found that deal with tear straps in the presence of MSD. In (28) Kosai et al developed a crack extension criteria and a crack kinking criterion where the effects of MSD can be incorporated by artificially increasing K_I by a magnification factor. The analysis made did not address how MSD affected the effectiveness of the tear strap. One can argue that the tear strap should be treated as a hidden margin and, therefore, doesn't have to be considered in an MSD analysis. This may, however, lead to unnecessary conservative inspection intervals for some aging aircraft. This complicated problem needs to be investigated further.

V.c. Linkup and failure

The linkup and failure criteria is obviously paramount. It determines when and at what load the cracks cause failure. Structural safety, maintained through a damage tolerance philosophy, depends on an inspection program, as already mentioned in Section III. The inspection interval is determined by growing a crack from the initial detectable size to the critical size, that is when limit load causes unstable fracture. The critical damage size can be influenced by the condition of the surrounding structure. For instance if the structure is operated beyond the life substantiated by tests there is a possibility that MSD might affect the residual strength of that crack. The inspection interval based on critical crack size without taking other cracks into account may be unconservative.

Three different failure criteria have been noted, in the literature, for predicting linkup/failure in an MSD situation.

1. Fracture mechanics method. $K \geq K_c$
2. Net ligament loss. $\sigma_{ns} \geq \sigma_{cr}$
3. Swift's residual strength method.

Also, an additional criteria has been noted (8). Here the distance between crack tips is used as a criterion. If the distance between the crack tips is smaller than a certain value they are regarded as linked together. A brief description of these criteria will be given.

1. Fracture mechanics method (6):

The theory of linear elastic fracture mechanics states that there is a critical stress intensity value after which unstable cracking occurs. This value, the fracture toughness, varies with the specimen thickness, until a limiting value is reached K_{Ic} (plain strain). In thin sheets, a valid test for this value is difficult to obtain, so K_c (plane stress) is usually determined for the given condition. In (6) Moukawsher used K_{app} to approximate K_c . K_{app} is based on the crack length the specimen had when the fracture toughness test starts, which is easier to test. K_{app} is not only a material property (as K_c is) but depends on geometry and crack configuration.

2. Net ligament loss:

When the cracks grow in a collinear row of rivets, the area of material that can carry the load is reduced. When the stress reaches the yield strength the panel will fail. The net section stress can be approximated by dividing the remote applied load with the remaining material area. This is a failure criteria more than a link up.

3. Swift's residual strength method:

Swift has proposed a criteria (14) based on the gross stress level which will cause the lead crack plastic zone to touch the MSD crack plastic zone, see fig 14. That is:

$$R_1 + R_2 = (P-d/2-a_1) \quad [5]$$

The plastic zone sizes can be expressed as:

$R_i = (K_i/\sigma_y)^2/(2\pi)$ $i=1,2$; K_i can be found according to earlier sections in this chapter. Swift derives the following expression for the residual strength:

$$\sigma_R = \{2\sigma_y^2(P-d/2-a_1)/[\beta_n\beta_{11}^2a_1 + \beta_s^2\beta_{12}^2a_2]\}^{1/2} \quad [6]$$

Where β_i are correction factors for K_i based on the compounding technique mentioned earlier. This criteria which was proposed as a linkup criteria can be used to modify the net ligament loss criteria as the net ligament criteria tends to overestimate the

strength. The plastic zones should be subtracted from the total ligament when computing the residual strength of the panel.

The only paper found in the literature that has evaluated different fracture criteria, by tests, is (8). The three criteria mentioned above were evaluated using specimens with a lead crack and with and without MSD cracks. The failure load obtained experimentally was compared with the predicted failure loads made by the three methods, see Table 1. The Swift method was the most accurate for panels with MSD while the Fracture Mechanics method closely predicted the failure loads when no MSD was present. Note that the Swift criterion was not tested without MSD. The average error was:

For Panels with MSD		For Panels without MSD	
Swift method	9.7 %	Swift method	n/a
Fracture Mechanics	28.8 %	Fracture Mechanics	3.9 %
Net Ligament Loss	22.4 %	Net Ligament Loss	11.2 %

Specimen RS-04, Table 1, was the only case where the Swift criterion did not closely predict the failure load. This specimen did not have uniform MSD. The holes to the left of the lead crack had relatively large cracks about 0.147 inches, while the holes to the right had much smaller cracks averaging 0.055 inches.

Dahr, Gallagher and Berens made a comparison of three fracture criteria: R-curve analysis, Swift's method, and Fracture Mechanics method (14). Based on analysis they conclude that;

- * These three criteria imply that crack coalescence is influenced by the distance between the adjacent crack tips.
- * Crack coalescence is independent of the largest crack size and its ratio to the crack with which it coalesces.
- * Effect of fracture toughness on the residual strength and the crack coalescence is more severe than the yield strength of the material.
- * The lower bound for the residual strength is decided by the Fracture Mechanics method or R-curve criterion for large distances between the crack tips. As that distance approaches zero, Swift criterion dominates. See Fig 8.

All the criteria seen in the literature can show unconservative results which is unsatisfactory. Only one investigation dealing with linkup and failure was found. However, failure load predictions within 10% seem possible which should be accurate enough. Further studies of the possibilities to use the distance between the cracks as a link up/failure criteria is recommended.

VI. Corrosion

It is well known that high strength aluminum alloys are highly susceptible to environmental degradation. Corrosion observed on aging airframes falls, according to de Luccia (16), into the three categories shown below. The speed with which these corrosion failures occur are also indicated.

Corrosion

Time Dependent

General Attack
Pitting
Exfoliation
Crevice Corrosion
Filiform Corrosion
Intergranular

Time Independent

Stress Corrosion Cracking
Environmental Embrittlement
* Hydrogen
* Liquid Metals

Time Related Corrosion Fatigue

Slow Failure ----- Catastrophic Failure

The events labelled "time dependent" are the common forms of corrosion and continue to occur on a real time basis as long as the three following principal criteria are present:

1. A metal that is susceptible to electrochemical corrosion
2. A corrosive environment
3. A continuous electric path within the metal and the environment

Time dependent corrosion, such as pitting, exfoliation and crevice corrosion will, if not prevented or controlled, accumulate to potentially unsafe proportions. These events may act as precursors to the more damaging time related event of corrosion fatigue when the part is under cyclic loading or the time "independent" event of stress corrosion cracking. Corrosion fatigue is said to occur when the conjoint action of corrosion acting during fatigue produces considerably more damage than either acting alone.

In this investigation we will focus on the types of corrosion that can influence the time to initiation and the crack growth rate in a fuselage lap joint.

Pitting

Pitting is a form of corrosion that occurs locally and thus results in the consumption of metal in a non-uniform fashion. Metals which naturally form protective passive oxides are particularly vulnerable to pitting corrosion. Most of the commonly used metals for aerospace application are susceptible to pitting. The environment at the base of the pit can become more aggressive with time. This means that the local environment at the base of the pit will accelerate the growth of the pit so that the process is autocatalytic. Additionally, the negative geometrical aspect of

pits is obvious. They can initiate a fatigue crack when cyclic stresses are superimposed on the part.

Intergranular/exfoliation

When corrosion occurs preferentially along the boundaries of grains, the metal is said to experience intergranular corrosion. If the intergranular corrosion occurs in an elongated grain structure it is called exfoliation. Exfoliation usually occurs on aluminum alloy aircraft parts that have exposed edges to a corrosive environment, for instance, countersunk rivet holes.

Crevice corrosion

If a stagnant area in the form of a crevice or debris deposit occurs on the surface of a metal exposed to an aqueous environment, accelerated corrosion can be expected to occur within the crevice or under the debris deposit. A classic example of crevice corrosion is that which occurs at lap joints that allow ingress to the environment. Crevice corrosion as well as the previously mentioned pitting corrosion will form a more aggressive environment with time.

Most researchers agree that corrosion fatigue involves the mechanism of hydrogen embrittlement. There are several arguments which support the hydrogen embrittlement process, see for example (17). The most significant observation is that water vapor alone can produce increases in crack propagation rates, which are equivalent to rates obtained in distilled H₂O alone. Pre-corrosion experiments in NaCl followed by tests in laboratory air result in significant decreases in fatigue resistance. However, this effect is at least partially reversible. Post exposure heat treatment prior to fatigue testing increases fatigue resistance with larger increases observed as heat treatment times are extended. See table 2. This partial reversibility of damage when tested in air after exposure to pre-corrosion is strongly indicative of a dissolved species rather than an absorbed species which is responsible for embrittlement. This also means that it is possible to first corrode the specimen and then fatigue test it.

Figs 9 & 10 show the degrading effects of corrosion to 7075-T651 (18). The stress level was 210 Mpa in Fig 9 and 144 Mpa in Fig 10. Some important conclusions supported by other papers can be drawn from these figures.

1. Environmental effects on fatigue lives are significant. Factors exceed two for the worst environment compared to fatigue in air.
2. Environmental effects are relatively greater for the higher σ_{max} , which is in contrast to many other data found in the literature. The specimens used in this test were designed to simulate a structural joint, see Fig 9, in contrast to most environmental testing that used simple dogbone specimens. Correct assessment of the environmental effects requires realistic specimens. The

reason is that corrosion not only changes the crack growth rate but can change the initiation site also.

3. These figures indicate that pre-exposure + fatigue in air can be as severe as fatigue in salt spray. In the FACT programme (The Fatigue in Aircraft Corrosion Testing, 18) it was also indicated that alternate immersion in distilled water was as severe for 7075-T76 as continuous fatigue testing in salt-spray. This might be used to simplify the testing procedure. However the stress level seems to influence this, and other materials could have other relations between the two environments. Tests supporting the above statement for 2024 have not been found.

Most of the reviewed papers regarding corrosion have done tests on how the environment affects either the crack growth rate or the fatigue life. This has been done for several different environments. In (19) Krupp et al found that for commonly used aluminum alloys 2024 and 7075, the accelerated cracking due to a corrosive environment occurs only during the early stages of crack development. During later stages, at high ΔK levels, the cracking rates in dry air, humid air and in salt water tend to become similar. See Figs 11 and 12. This suggests that the initiation phase is more affected by the environment than the crack growth phase.

Only one paper (20) was found that addresses the question of how much the time to initiation is changed. Fig 13 shows how long time it takes to initiate a 0.4 mm long crack and it also shows the crack propagation life for different aluminum alloys. The specimen had realistic stress concentrations but is not believed to simulate a riveted joint. The figure supports the statement that corrosion mainly effects the early stages in crack growth. It is evident that the initiation phase is very important also in a corrosive environment.

Two papers have been found that present mechanistically based models of pitting corrosion combined with crack propagation from those pits (21 and 22). These models basically use pitting rate theory to predict the numbers of cycles required to generate a pit that is large enough for a mode I fatigue crack to develop at the pit. The size of the pit, at a given stress condition, at which a mode I crack will form is determined from the fatigue crack growth threshold. The crack is propagated by using fatigue crack growth methodology. These models use different models for the growth of the pit. In the fatigue crack growth model a Weibull cumulative damage function is used for the crack growth coefficient. The Weibull parameters are found by tests.

None of these models have been applied to a fuselage joint geometry. In (23) Miller and Meyer propose a corrosion model to take into account the environmental effects on:

1. Corrosion fatigue
2. Stress corrosion cracking
3. General corrosion (including exfoliation and pitting)
4. Coating degradation.

For corrosion fatigue a corrosive factor was included in the Forman equation. This factor was determined by plotting da/dN data vs ΔK for specific aircraft alloys in dry air, distilled water, and in 3.5% NaCl in the same plot. By assuming an average ΔK (10 ksi-in^{1/2}), the values of da/dN for each environment were read off and converted to corrosivity factors using:

$$CF = (da/dN)^1 / (da/dN)^2$$

1=in actual environment
2=obtained at 100% humidity

Based on Dr Summit's data for Air Force bases (not read in this survey), each base was assigned a set of Corrosivity Factors corresponding to its environmental conditions. In the case of general corrosion a damage function for metals in contaminated environments was used

$$M = AT^B$$

Where M is metal loss by corrosion (either penetration depth or weight loss), T is exposure time, and A and B are empirical constants determined by the environmental conditions, the metal involved and the type of corrosion product on the metal. Tests were conducted for different metals and different environments like nitric and sulfuric acid solutions. The constants which were developed for the major aircraft alloys in mild, moderate, severe and very severe environments are summarized in Tab 3. It is not known how well this model works.

None of the models found in the literature seems suitable for modeling initiation in a corrosive environment. To test initiation in a corrosive environment and develop scatter curves seems to be the best way. Initiation is shortened by a corrosive environment. It is not known how the scatter is affected. Perhaps it is possible to find a transfer function that, depending on the environment, can transform the scatter curves developed for fatigue in air to fatigue in a corrosive environment. In the crack growth phase a change of the crack growth coefficient depending on the environment seems to be the best way. A stochastic treatment is recommended also for corrosive environment.

Two papers have been found that address the development of a laboratory testing protocol that replicates, in an accelerated timeframe, corrosion damage to representative structural assemblies associated with in-service experience.

In (24) Alcoa exposed painted 2024-T3 riveted lap joint assemblies to laboratory accelerating and seacost environment. The environments used were EXCO ASTM G34 (7 days), 3.5% NaCl solution

by alternate immersion ASTM G44 (90 days) and seacost atmosphere at Point Judith, RI (8 months). Alcoa reports that in general, the most severe corrosion occurred on samples exposed in EXCO followed by 3.5% NaCl and then the seacost atmosphere. The EXCO and the 3.5% NaCl tests were both effective in meeting the objective of producing corrosion in the lap joints. The alternate immersion test was the protocol of choice since it more accurately replicated observed aircraft corrosion in lap splices. How long a time-in-service the 90 days, 3.5% alternate immersion would simulate is not known.

Battelle made a similar investigation in (25) to simulate pitting and exfoliation corrosion as recommended by ASTM. The specimens consisted of a collinear row of open fastener holes and table 4 shows a summary of the different environments used. The specimen that was corroded by the exfoliation (EXCO) procedure was fatigue tested. The gross-area stress was 82.58 Mpa (12 ksi, R=0 and a cyclic frequency of 3 Hz. The results are shown in Table 5. The conclusions drawn were:

1. The copper-acidified-salt-fog test was most suitable for producing accelerated pitting corrosion. It produces realistic pit depths and densities in short time periods.
2. Exfoliation corrosion is best simulated using the EXCO test. This procedure can produce varying levels of corrosion, which according to aircraft experts, are realistic in terms of actual aircraft component degradation.
3. The effects of prior corrosion on fatigue crack initiation was found to greatly reduce fatigue crack life in both aluminum alloys.

The best source of data on pitting of the alloys 7075-T6 and 2024-T3 are, according to Battelle, outdoor exposure tests conducted by ASTM (26. Not read during this survey). For seacoast exposure up to seven years, pit depths of 0.1-0.15 mm (4-6 mils) are expected. Such data on exfoliation corrosion has not been compiled according to Battelle.

It certainly seems possible to simulate corrosion that can be seen in aging aircraft. The question of how to translate a certain usage to a corrosion state still remains. Nothing has been found regarding this in the literature. The literature does not suggest that the linkup/failure criteria needs to be modified due to a corrosive environment. Several papers report that corrosion influences mainly initiation and the early stages of crack growth. General corrosion that consumes material can, of course, change the thickness of the sheet and thereby influence the failure load.

VI. Conclusions/Recommendations

The damage tolerance philosophy assumes a rogue flaw in the most critical point and also assumes that adjacent members in a fail safe structure can have cracks grown from an initial flaw, representative of the initial fatigue quality of that article. The problem is that it doesn't take into account Multi Site Damage, MSD. That is, small cracks ahead of the lead (rogue flaw) crack. This means that the inspection interval based on the propagation of the rogue flaw crack can be unconservative. In addition, the synergistic effects of MSD along with the long-term effects of corrosion can reduce the inspection interval even further.

In the research community there has been an overemphasis on unrealistic MSD situations where numerous small cracks with equal sizes interact and finally fail. We need to develop methods that can predict the inspection interval of the rogue flaw crack in presence of MSD and a corrosive environment. We believe that it is possible to develop such models that will give reasonable accuracy.

Based on the performed literature search the following recommendation/conclusion can be made:

- * Component-level testing rather than coupon level should be increased. The ability to predict actual behavior can be significantly reduced when based on a portion of the component only.
- * These component-level tests should simulate real world environment. While tests have been accomplished to study MSD and corrosion, no studies were identified which included both at the same time.
- * The initiation stage needs to be explored further.
Initiation of cracks in riveted lap joints is a very complicated phenomena. Local effects, like type of rivet, riveting procedures, and lap joint dimensions can influence the fatigue life by a factor of 3-4. The best way to address this issue seems to be to develop initiation scatter curves by testing specimens that locally, around the rivet, describe reality as well as possible. This could be done on specimens with only one column of rivets.
- * Fretting, the "rubbing" of two surfaces, needs to be pursued. While we as engineers may "assume" two joined surfaces are rigid, realism dictates that over time, this rubbing will produce fatigue problems.
- * Corrosion environments seem to mainly affect the time to initiate a crack (early stages in crack growth). The change in crack growth, in later stages, contributes less although the crack growth rate is higher.

- * To evaluate initiation times in a corrosive environment realistic specimens should be used to simulate the local geometry and environment. Corrosion not only changes the crack growth rate, it also can change the initiation site. Similar specimens that were mentioned above could be used.
- * It seems that the MSD problem in aging aircraft will not benefit a great deal from more sophisticated crack growth prediction techniques. There are enough theories so get more data to prove/validate the existing ones. The compound method seems accurate enough and fast and easy to use. To account for scatter in the crack growth process a Weibull distribution for the crack growth coefficient C is proposed.
- * Little is known about the effectiveness of tear straps in the presence of MSD. Although tear straps are the last defense of an axially rupturing fuselage very conservative inspection intervals could be predicted if the tear strap is not accounted for in the analysis. A test program on realistically large specimens is proposed as a base to gain knowledge in this field.
- * All three failure criteria found in the literature can show unconservative results, which is unsatisfactory. For panels with MSD, Swift's residual strength method predicts the link up/failure most accurately. Failure load predictions within 10% seem possible which should be accurate enough. Further studies of the possibilities to use the distance between the cracks as a linkup/failure criteria is recommended.
- * The literature does not suggest that the linkup/failure criteria need to be modified due to a corrosive environment. General corrosion that consumes material can, of course, change the thickness of the sheet and thereby influence the failure load.
- * Two different laboratory testing protocol that, in an accelerated time frame, replicate corrosion damage in the form of pitting and exfoliation were found. Alternate immersion testing, with 3.5% NaCl solution, is said to accurately replicate observed corrosion in aging aircraft.
- * Several papers have been found that have investigated the change in crack growth rate for different corrosive environments, but no answer was found to the question of how one translates a certain usage to a corrosion test environment. This definitely requires additional study.

While this concludes the overall discussion regarding MSD and corrosion, one noteworthy point observed during this literature search is that while there is a large amount of information available regarding these topics, there is no specific location to access it all. If two different organizations were to perform data searches, they would probably come up with significantly different

lists. The Fatigue, Fracture, and Reliability Section is exploring the possibility of bringing together the many organizations performing work in this area in order to maximize resources and avoid duplication of studies.

It appears that efforts in these areas are increasing but on an independent basis such that various organizations are performing research that has actually been accomplished in some form already by another agency.

Initially, what we're suggesting is almost a "laundry list" of who's doing what and what other plans they have as well as what they've completed so far, focusing on the United States only for the time being. In addition, it would be nice to have one "depository" for any studies accomplished so that every interested organization could have access to a brief summary of the types of tests run and the results.

Given the enormous size of this task, what we're looking for now are just some comments on whether this is a feasible and worthwhile task to pursue. Any suggestions as to approaches, additional addressees, lead agencies, etc., would be appreciated. Lead contact for this project is Capt Frank Opalski. You can also talk to Capt Karl Hart or Mr Joe Burns. Our phone number is (513) 255-6104 (DSN 785-6104) and fax number is (513) 476-4999. Mailing address is

WL/FIBEC Building 45
2130 Eighth St Suite 11
WPAFB, OH 45433-7552

VII. References

- 1 Tong, P.; Arin, K.; Jeong, D.Y.; Greif, R.; Brewer, J.C.; and Bobo, S.N.; "Current DOT Research on the Effect of Multiple Site Damage on Structural Integrity," in 1991 International Conference on Aging Aircraft and Structural Airworthiness, 19 - 21 Nov 1991.
- 2 Partl, O. and Schijve, J., "Multiple-Site-Damage in 2024-T3 Alloy Sheet," Delft University of Technology, Report LR-660, January 1992.
- 3 Schijve, J., "Multiple-Site Damage Fatigue of Riveted Joints," Delft University of Technology, Report LR-679, presented at International Workshop on Structural Integrity of Aging Airplanes, Atlanta, 31 Mar - 2 Apr 1992.
- 4 Lincoln, John W., "Life Management Approach for USAF Aircraft," in AGARD, Fatigue Management, December 1991.
- 5 Dawicke, D.S. and Newman, J.C. Jr., "Analysis and Prediction of Multiple-Site Damage (MSD) Fatigue Crack Growth," NASA Technical Paper 3231, 1992.

6 Moukawsher, Elias James, "Fatigue Life and Residual Strength of Panels with Multiple Site Damage," Master of Science Thesis, Purdue University, 1282 Grissom Hall, West Lafayette, Indiana, 47907-1282, May 1993.

7 Schijve, J., "The fatigue life of unnotched and notched 2024-T3 Alclad sheet materials from different manufacturers," National Aerospace Laboratory NLR, TR 68093, 1968.

8 Wit, G.P., "MSD in fuselage lap joints - Requirements for inspection intervals for typical fuselage lap joint panels with Multiple Site Damage," Master thesis at the Technical University of Delft, The Netherlands, July 1992, Report LR-697.

9 Manning, S.D., and Yang, J.N., "Advanced Durability Analysis, Volumes I - IV, AFWAL-TR 86-3017, 31 Jul 1987.

10 Manning, S.D. and Yang, J.N., "Demonstration of probabilistic based durability analysis method for metallic airframes," in Journal of Aircraft, Volume 27, Number 2, Feb 1990, pp 169-175.

11 Harris, Charles E., and Heyman, Joseph S., "An Overview of NASA Research Related to the Aging Commercial Transport Fleet," pp 1661-1666.

12 Newman, J.C. and Shivakumar, K.N., "Stress Concentrations for Straight-Shank and Countersunk Holes in Plates Subjected to Tension, Bending, and Pin Loading," Technical Report NASA-TP-3192, June 1992.

13 Hsu, T.M. and Markham, J.W., "Interaction Effects of Multiple Cracks," AIAA Journal, Vol. 15, No. 3, March 1977.

14 Swift, T., "Damage Tolerance Capability," presented at Specialists' Conference on Fatigue of Aircraft Materials, Delft University of Technology, Delft - The Netherlands, 14 - 15 October, 1992.

15 Dhar, Subrato; Gallagher, Joseph P.; and Berens, Alan P., "A Comparison of Fracture Criteria for Crack Coalescence", University of Dayton Research Institute, 3 Aug 93.

16 DeLuccia, J.J., "The Corrosion of Aging Aircraft and its Consequences," Naval Air Development Center, AIAA-91-0953-CP.

17 Duquette, D.J., "Mechanisms of Corrosion Fatigue of Aluminum Alloys," AGARD Conference Proceedings No 316 on Corrosion Fatigue.

18 "The Fatigue in Aircraft Corrosion Testing (FACT) Programme," AGARD Report No 713, 1989.

19 Krupp, W.E., Hoepfner, D.W., and Walker, E.K., "Crack Propagation of Aluminum in Corrosive Environments," International Conference on Corrosion Fatigue, June 14 - 18, 1971.

20 Wanhill, R.J.H., "Environmental Effects on Fatigue of Aluminum and Titanium Alloys," in AGARD Report No. 659 on Corrosion Fatigue of Aircraft Materials, presented at the 44th Meeting of the Structures and Materials Panel of AGARD, April 1977.

21 Hoepfner, David W., "Corrosion Fatigue and Fatigue Crack Growth in Aircraft Structural Materials," University of Toronto, prepared for AFOSR, Bolling AFB, D.C., 20332, Contract No. AFOSR 77-3178, June 1979.

22 Wei, Robert P. and Harlow, D. Gary, "A Mechanistically Based Probability Approach for Predicting Corrosion and Corrosion Fatigue Life," Lehigh University.

23 Miller, Robert N., "Predictive Corrosion Modeling," Contract F33615-85-C-5058, performed by Lockheed-Georgia Co., Nov 87.

24 Liput, J.J. Jr., "Aging Aircraft Research Program - Effects of Corrosion on Structural Integrity," Report No. 56-XA-397, 15 December 1992, Subcontract to DOT Contract No. DTRS-57-89-C-00007.

25 Smith, S.H., Christman, T.K., Brust, F.W., and Oliver, M.L., "Accelerated Corrosion Fatigue Test Methods for Aging Aircraft," presented at the 1991 Conference on Experimental Mechanics.

26 F. L. McGaery. T. J. Summerson and W. H. Ailor. ASTM STP 435, pp 141-174, Atmospheric Exposure of Nonferrous Metals and Alloys - Aluminum, Metal Corrosion in the Atmosphere.

27 Kosai, M. and Kobayashi, Albert S., "Axial Crack Propagation and Arrest in Pressurized Fuselage," Office of the Chief of Naval Research, Contract N00014-89-J-1276, Technical Report No. UWA/DME/TR-90/86, April 1990.

28 Kosai, M., Kobayashi, A.S., and Ramulu, M., "Tear Straps in Airplane Fuselage," Office of Naval Research, Contract N00014-89-J-1276, Technical Report No. UWA/DME/TR92/68, March 1992.

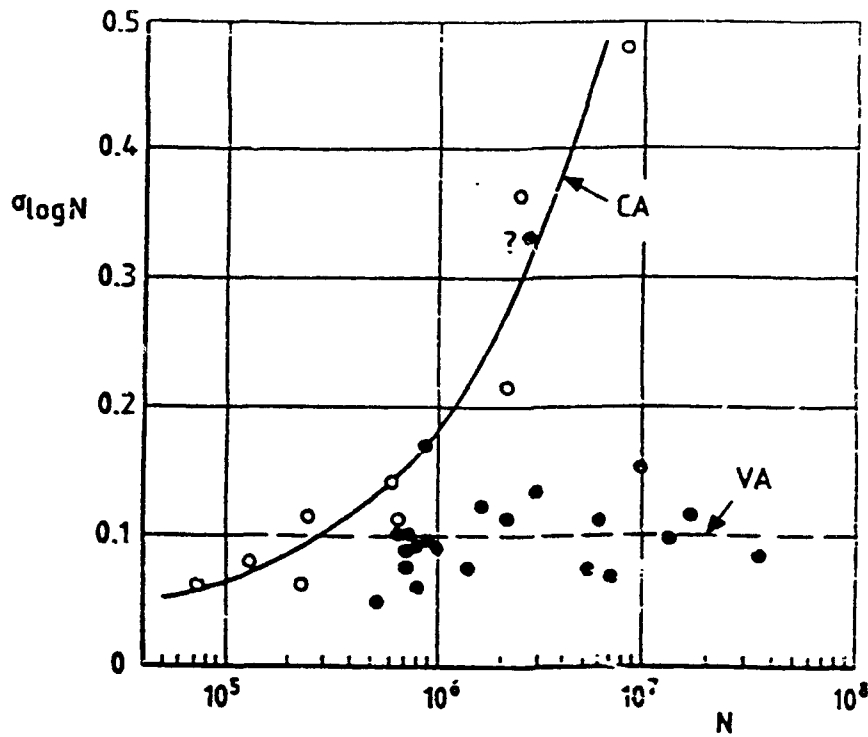


Fig 1: Results of fatigue test on riveted lap joints, 2024-T3 Alclad and 7075-T6 Clad sheets. Standard deviation ($\sigma_{\log N}$) for constant-amplitude (CA) loading (10 specimens for each ∇) and for variable-amplitude (VA) loading (7 specimens for each ∇). (7)

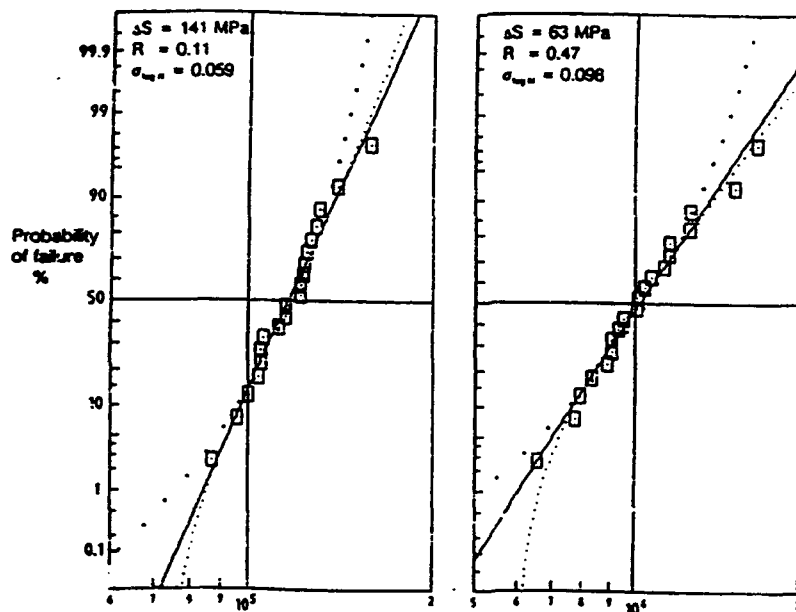


Fig 2: Scatter in two test series of 20 riveted lap joints. Comparison between the log-normal distribution (full line), the Weibull 3-parameter distribution (small dots) and the Weibull 2-parameter distribution with zero location parameter (larger dots). (7)

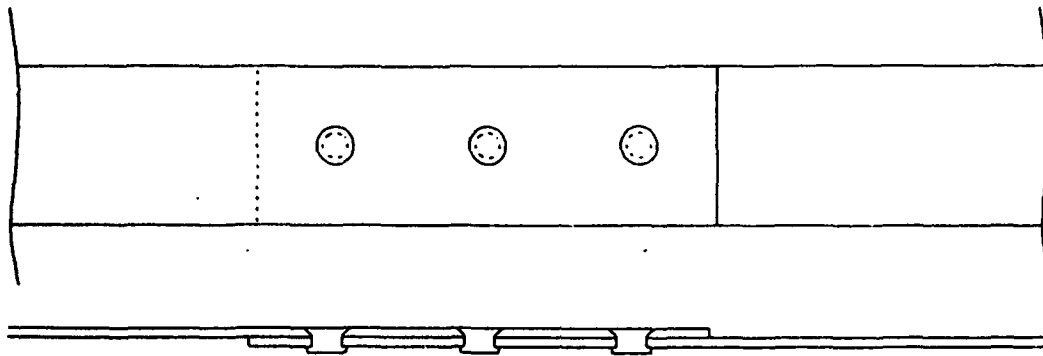


Fig 3: Specimens with a single column of rivets (8).

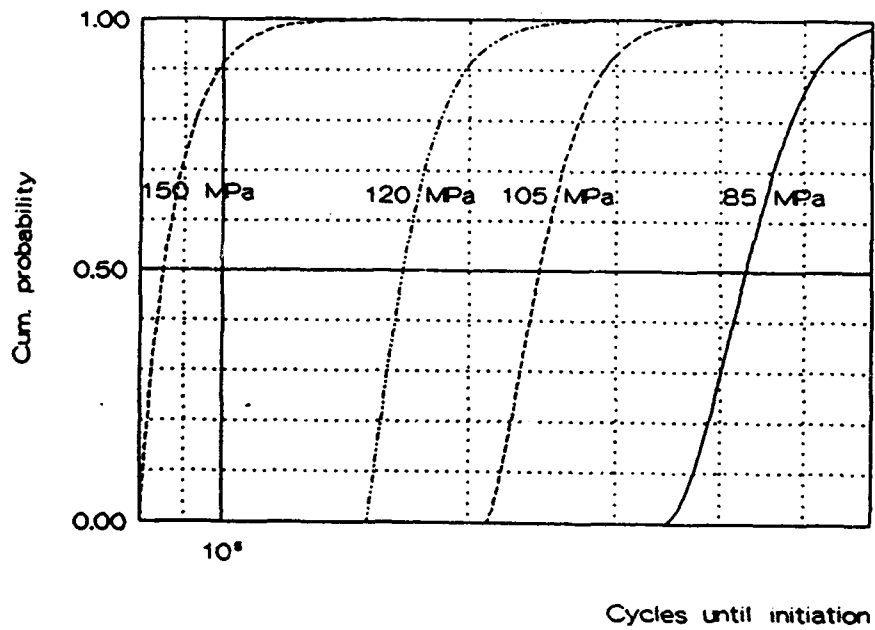


Fig 4: Initiation scatter curves (8).

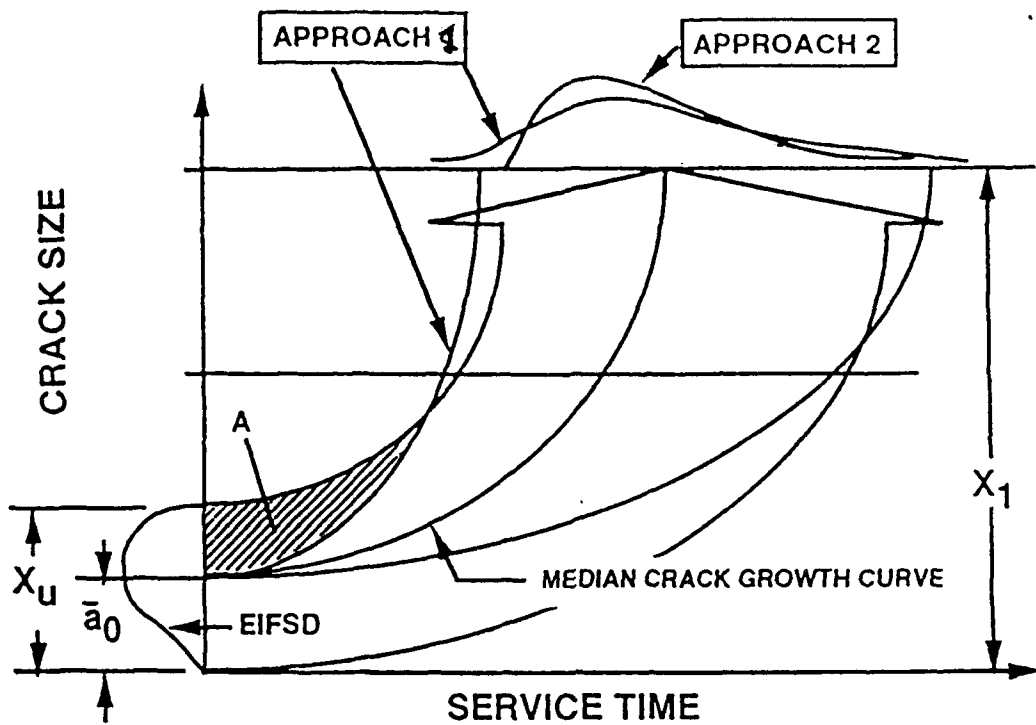


Fig 5: Stochastic crack growth from a single initial flaw, approach 1.
 Deterministic crack growth from Equivalent Initial Flaw Size Distribution (EIFSD), approach 2. (10)

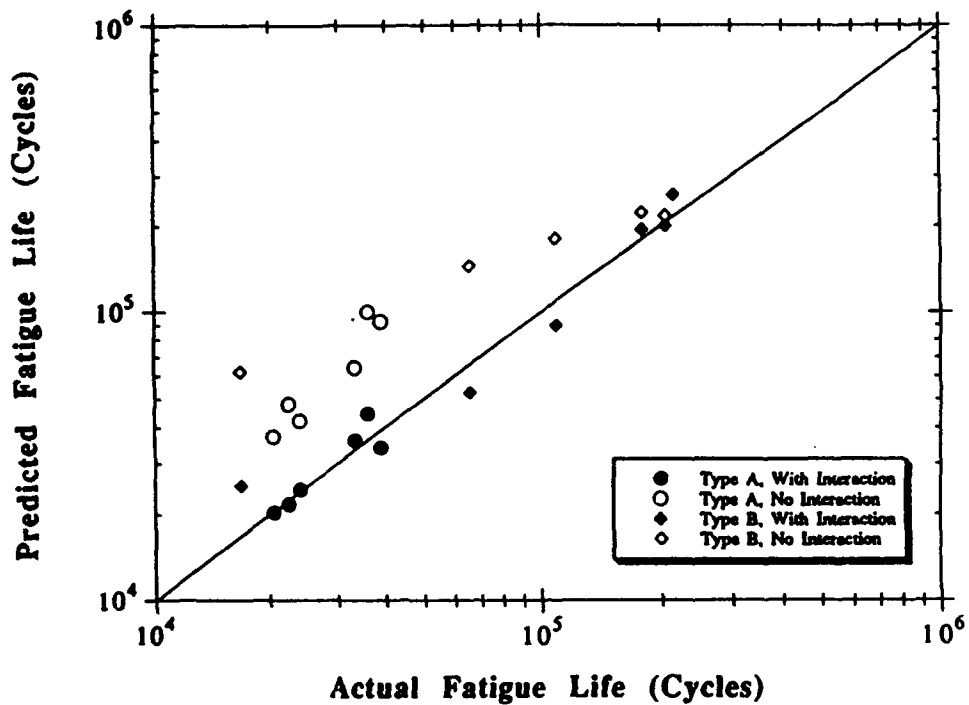


Fig 6: Predicted versus actual fatigue lives for all MSD specimens. (6)

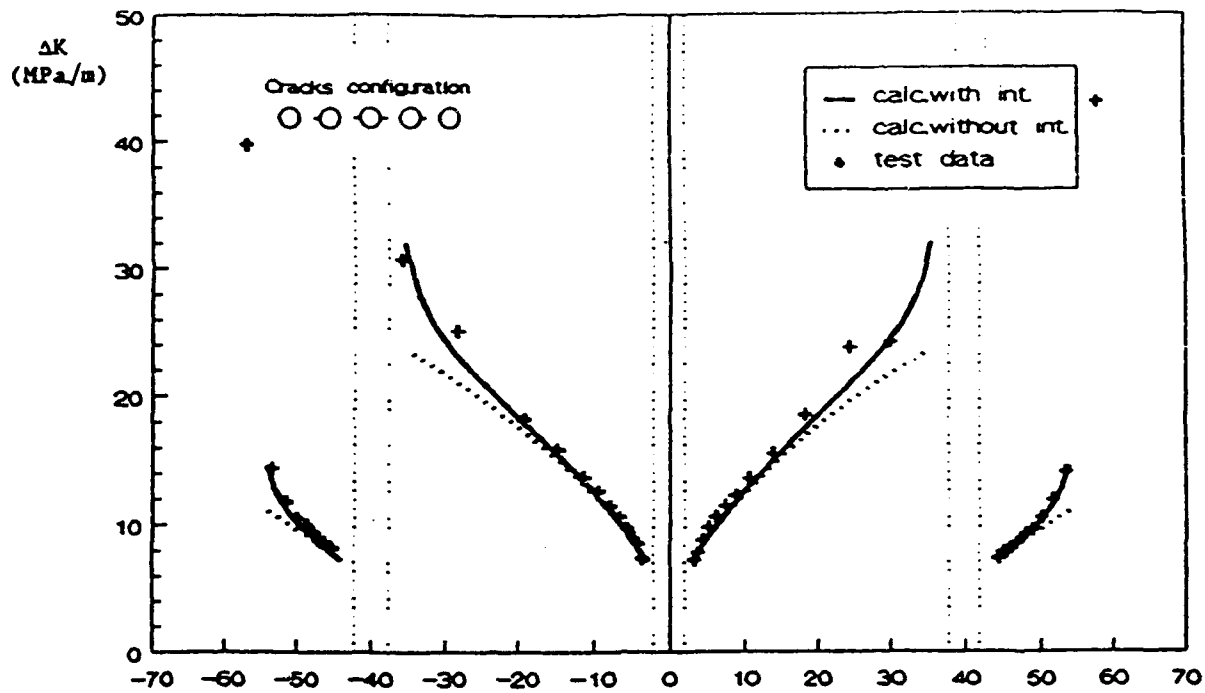


Fig 7: Comparison of predicted (ΔK vs a) curves with results obtained with the shown crack configuration. (2)

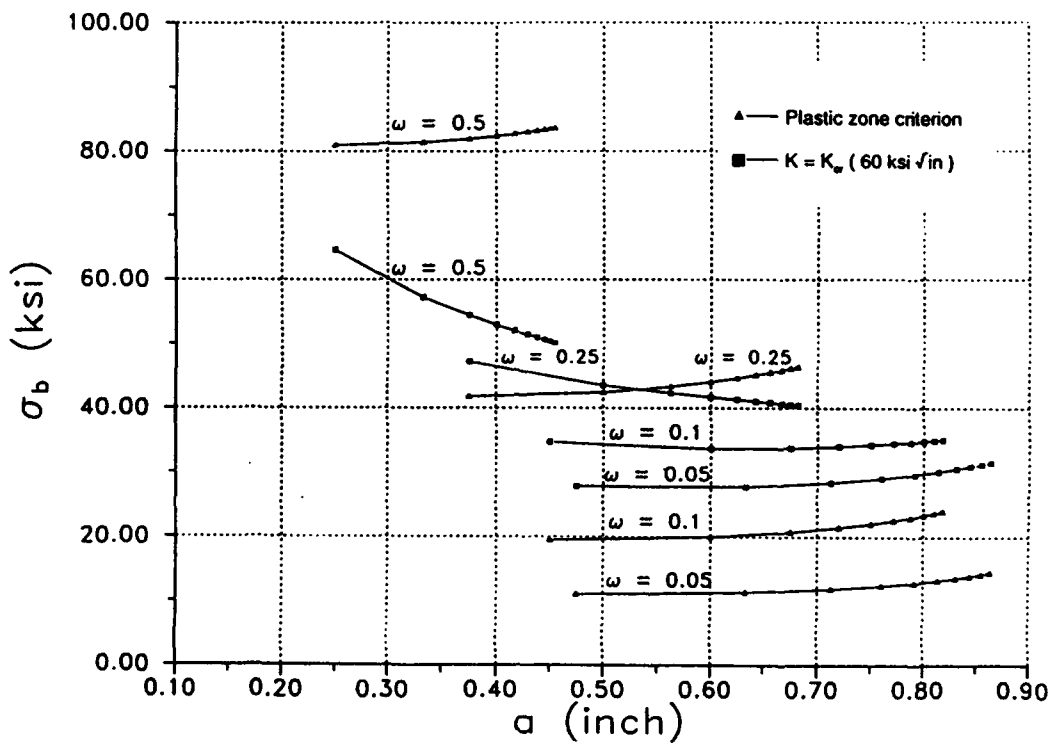


Fig 8: Comparison of residual stress levels between plastic zone and critical stress intensity factor criteria for two unequal collinear cracks. (15)

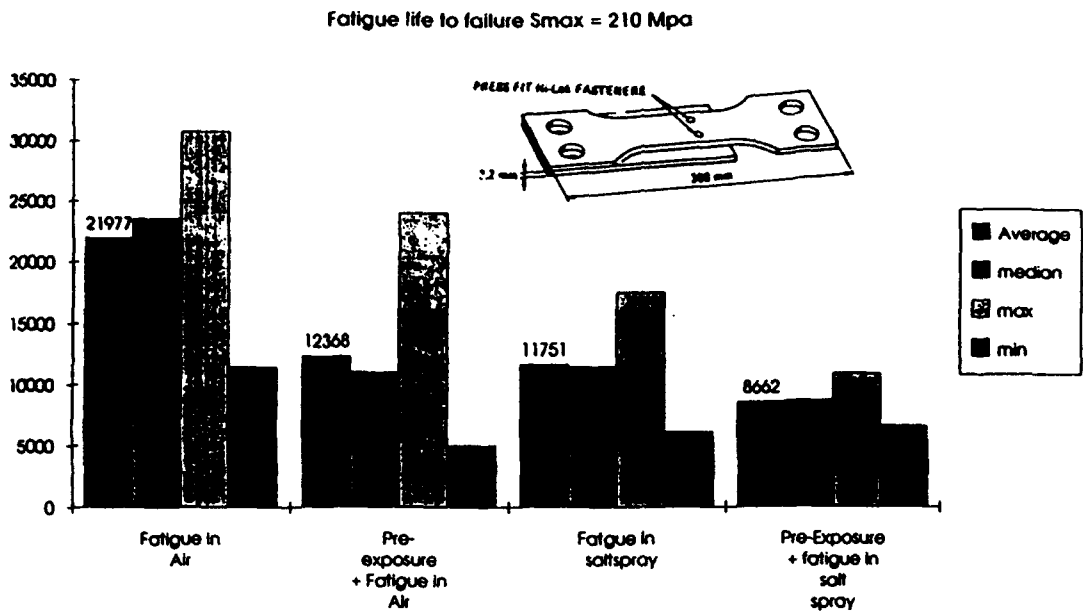


Fig 9: Degrading effect of corrosion on 7075-T651. (18)

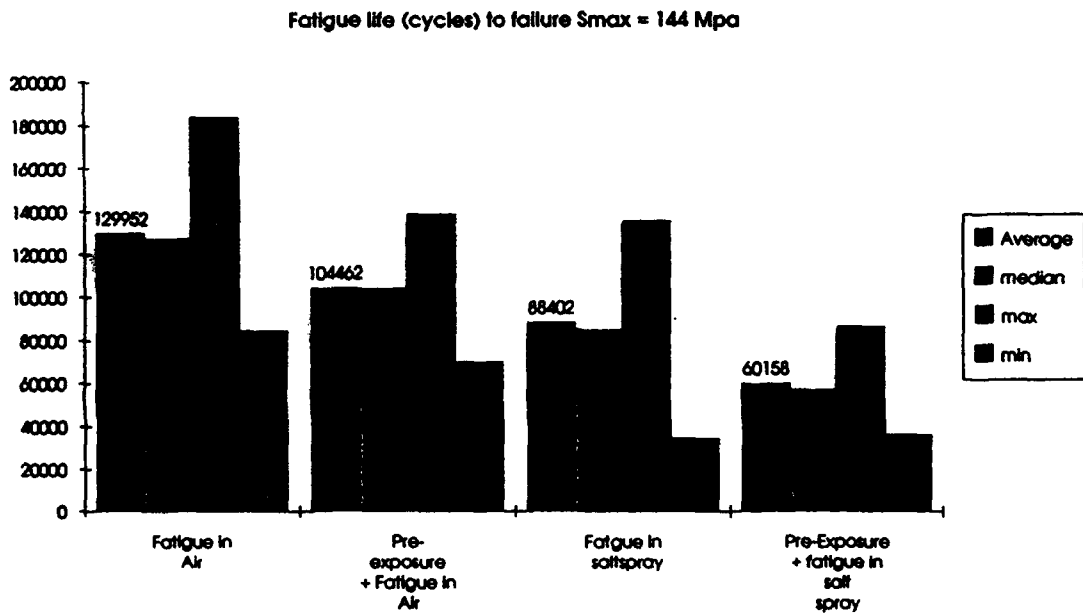


Fig 10: Degrading effect of corrosion on 7075-T651. (18)

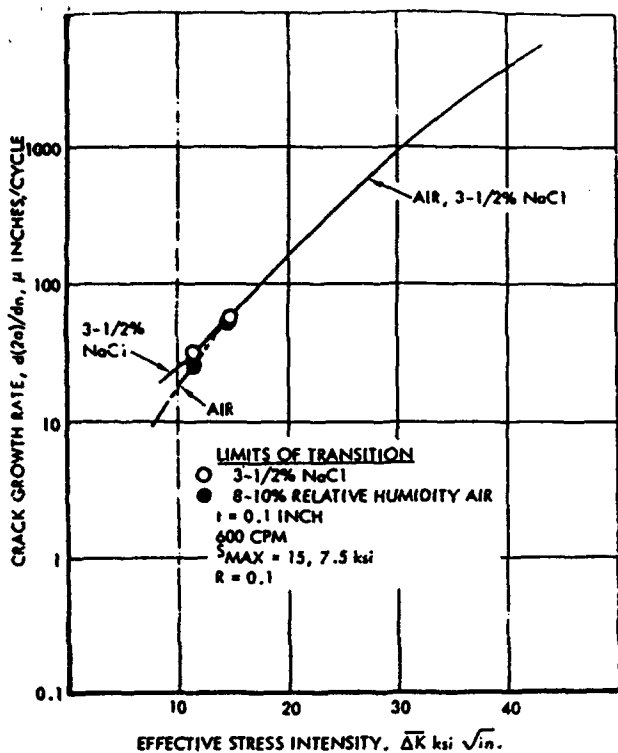


Fig 11: Crack growth in 2024-T3 aluminum. (19)

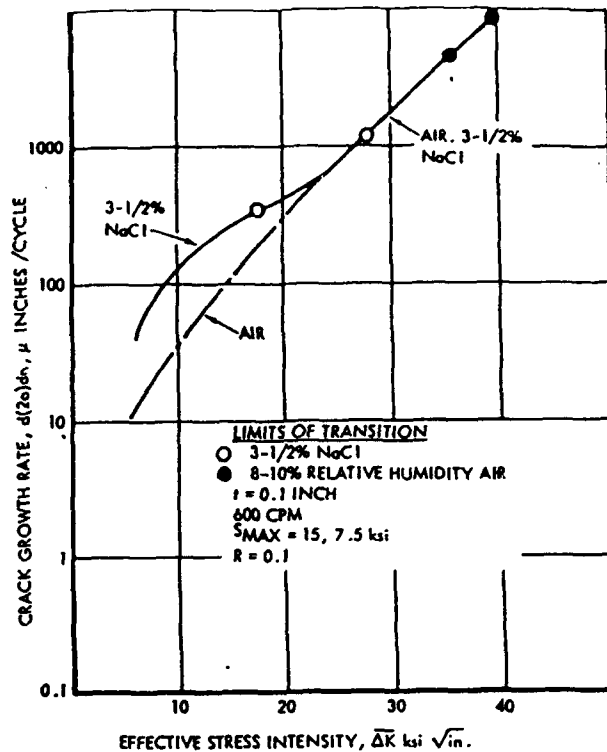


Fig 12: Crack growth in 7075-T6 aluminum. (19)

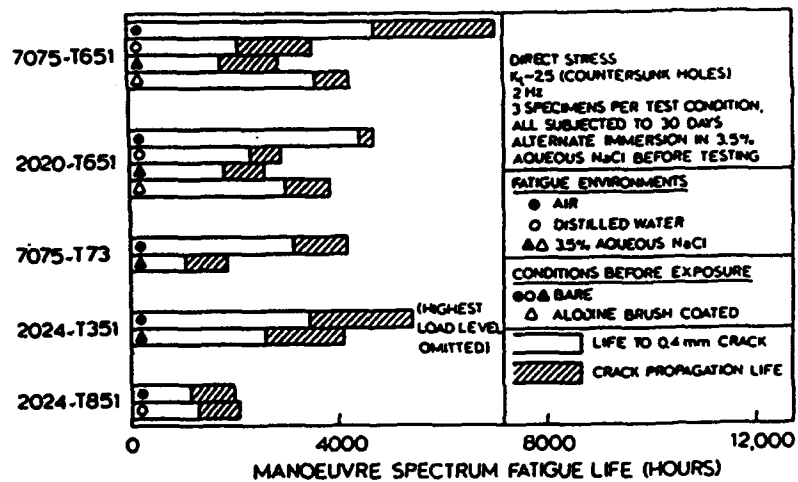
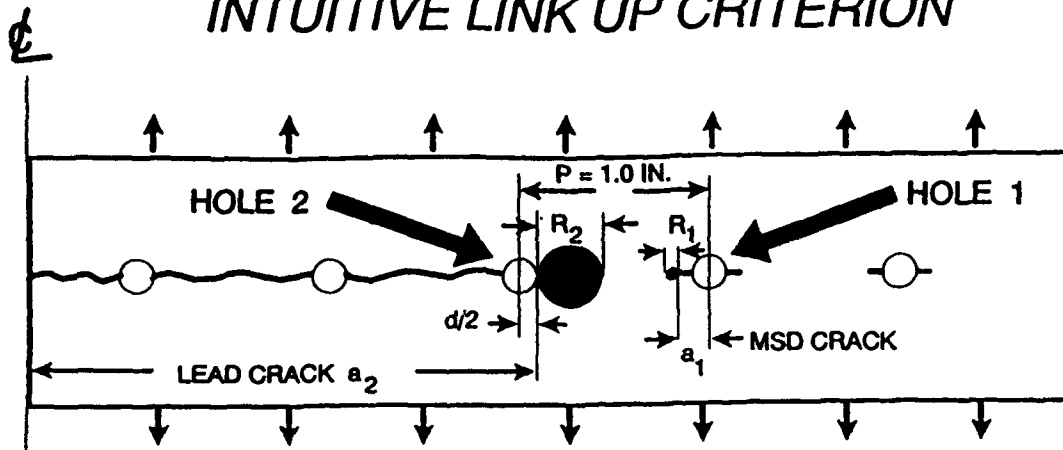


Fig 13: Time to initiate a 0.4mm long crack for various alloys and environments. (20)

INTUITIVE LINK UP CRITERION



CRITERION FOR LINK - UP
 WHEN PLASTIC ZONES
 FROM LEAD CRACK AND MSD
 CRACK TOUCH
 $R_1 + R_2 = [P - d/2 - a_1]$

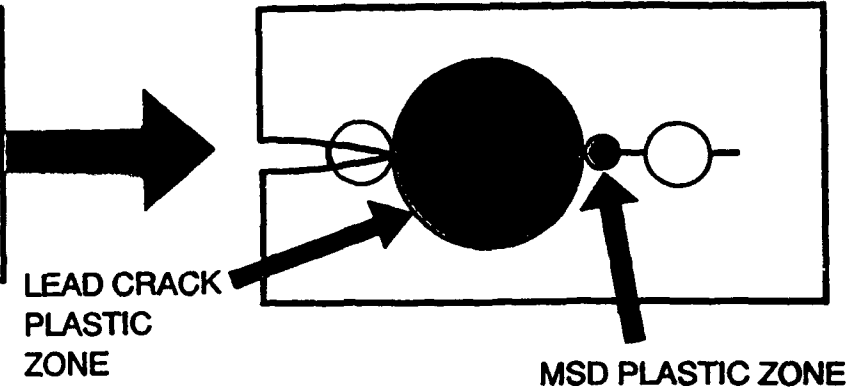


Fig 14: Swift Link-up Criterion. (14)

SPECIMEN	MSD and HOLES	LEAD- CRACK LENGTH (2a) (inches)	MEASURED (kips)	CALCULATED (kips)			ERROR (%)		
			P _{Cactual}	P _{Cnet}	P _{Cswift}	P _{CKapp}	P _{Cnet}	P _{Cswift}	P _{CKapp}
RS-01a	MSD	2.4	20.20	25.22	21.34	25.0	24.8	5.7	23.8
RS-01b	MSD	2.4	23.25	26.37	23.36	25.6	13.4	0.5	10.2
RS-01c	MSD	2.4	19.82	23.01	21.00	25.2	16.1	6.0	27.1
RS-02a	No MSD	2.4	25.55	27.67	n/a	25.9	8.3	n/a	1.5
RS-03a	No Holes	2.4	27.95	30.82	n/a	26.4	10.3	n/a	-5.5
RS-03b	No Holes	2.4	28.46	31.94	n/a	26.5	12.2	n/a	-7.0
RS-04a	MSD	3.2	12.91	18.11	17.36	21.2	40.3	34.5	64.5
RS-04b	MSD	3.2	17.15	19.92	17.81	21.2	16.2	3.8	23.7
RS-04c	MSD	3.2	16.26	19.78	18.066	20.4	21.6	11.1	25.4
RS-04d	MSD	3.3	15.59	19.41	16.52	19.8	24.5	6.0	27.0
RS-05a	No MSD	3.3	21.73	23.57	n/a	21.6	8.5	n/a	-0.4
RS-05b	No MSD	3.2	21.81	22.97	n/a	21.6	5.3	n/a	-0.7
RS-06a	No Holes	3.2	23.64	28.26	n/a	22.4	19.5	n/a	-5.4
RS-06b	No Holes	3.2	23.95	27.32	n/a	22.4	14.1	n/a	-6.7

Note: Error is calculated by subtracting the actual failure load from the predicted and dividing by the actual. The term "no holes" means no holes or cracks are present other than at the central lead crack.

Table 1: Actual and predicted failure loads for the tested specimens. (6)

Table 2
The effect of a Re-Heat Treatment Duration on Subsequent Fatigue Properties in Air (17)

Pre-Corrosion: 24 hour in aerated 0.5 NaCl

Re-Heat treat: Solutionize at 470 deg C for x hours.
Age at 121 deg C for 24 hours.

Fatigue in air: Mean stress 276 Mpa, cyclic stress 96 Mpa

<u>Time at 470 deg C</u>	<u>Numbers of cycles</u>
0 hours	30000
3 hours	85000
6 hours	101000
24 hours	> 13 00 000

Environmental Constants for Corrosion Equations

Alloy	Corrosion Index							
	Mild		Moderate		Severe		Very Severe	
	A	B	A	B	A	B	A	B
7075-T6 Al	3.0E-5	.46	2.95E-5	.59	2.9E-5	.72	1.78E-3	.12
2024-T3 (CLAD)	3.6E-6	.70	4.9E-6	.77	6.3E-6	.85	1.48E-5	.70
7079-T6	1.9E-6	.89	2.05E-6	.94	2.2E-6	1.00	5.4E-9	2.00
7075-T73	3.0E-5	.46	3.6E-5	.50	9.0E-4	.50	9.3E-4	.50

Environmental Constants for Corrosion Equations (Cont'd)

Alloy	Corrosion Index							
	Mild		Moderate		Severe		Very Severe	
	A	B	A	B	A	B	A	B
AZ31B-H24	4.0E-4	.77	2.8E-4	.87	1.6E-4	.97	1.2E-4	1.30
2024-T3	5.0E-4	.30	5.3E-3	.11	1.43E-2	-.05	1.1E-3	.30
4340 Steel	3.5E-11	2.52	2.6E-8	1.40	4.11E-5	1.00	6.9E-5	1.00
300M Steel	3.5E-11	2.52	6.3E-9	2.00	7.3E-5	1.00	5.7E-4	1.00

Table 3 (23)

Method of Corrosive Environment	Aluminum Alloys Evaluated	Result of Corrosion Damage*
PITTING TESTS		
Salt Fog up to 7 days exposure, ASTM B-117-90	7075-T6	Mean 1.0 - 1.5 mils Max 2.5 mils Lognormal Distribution
Copper Acidified Salt Fog up to 6 days exposure, ASTM B-368-85	7075-T6, T651 2024-T3, T351	Mean 2 mils Max 8 mils Lognormal Distribution
Alternate Immersion Test 10 minutes wet - 50 minutes dry, up to 7 days, Uses chemical solution from ASTM B-368-85	7075-T6	Mean 2 mils Max 7 mils Lognormal Distribution
EXFOLIATION TESTS		
EXCO Acid-Chloride Bath up to 5 days immersion, ASTM G-34-90	7075-T6, T651 2024-T3, T351	Mean 5 mils Max 20 mils Max depth increases with log of time

* Method of evaluation was microscopic examination and measurement of pitting and exfoliation penetration

Table 4: Accelerated corrosion procedures. (24)

Specimen	First Crack Initiation	Failure	Cycles Between Initiation and Failure
7075-T651 Base	78	108	30
7075-T651 Corroded	20	37	17
2024-T351 Base	208	252	44
2024-T351 Corroded	46	74	28

Table 5: Results of fatigue tests on corroded and uncorroded specimen (data in kilo cycles). (24)

AN AIRCRAFT STRUCTURAL INTEGRITY PROGRAM

- FAA FLIGHT INSPECTION BEECH 300 FLEET -

Presented to:
1993 USAF STRUCTURAL INTEGRITY PROGRAM CONFERENCE

November 30th - December 2nd 1993

Peter Gould
Beech Aircraft Corporation
Wichita, Kansas

Introduction

This paper will introduce you to an aircraft structural integrity program that is currently underway for the FAA involving the flight inspection fleet of Beech model 300's. These aircraft are flown in a flight inspection/airways calibration role.

The need for a flight inspection role is well documented. The United States Standard Flight Inspection Manual quotes: "The phenomenal growth of air traffic operations has dictated the establishment of a common system of all-weather air navigation to enable large numbers of aircraft to move quickly and safely to destinations. Safety of flight and effective control of aircraft movements necessitates that the components of this air navigation system be accurate, adequate and reliable". Hence the need for a fleet such as the Beech model 300's operated by the FAA.

The Beech model 300 is an aircraft of gross weight 14,000 lb which, when flown in an executive configuration, carries up to 9 passengers and in the high density configuration carries 13 passengers. It is certified to FAR 23 and SFAR 41C requirements as a pressurized executive transport aircraft (figure 1).

Analytical Tools

The flight inspection role (figure 2) calls for an aircraft to be flown at low altitudes for significant amounts of time. It is therefore flown in a more severe environment than the typical commuter airline or executive aircraft. If measured load spectra data are not available for the missions being flown, use can be made of published material such as FAA document AFS 120-73-2, ESDU 69023 or LR516 (figure 3). These are three references used at Beech to derive maneuver and gust spectra as a function of

altitude. Figure 4 is an extract from AFS 120 and shows the increase in gust exceedances with decrease in altitude. These data were collected and reduced from VGH recorders installed on about 100 aircraft operating in the general aviation category. The data base was collected through the NASA VGH General Aviation program which began in 1961.

A general comparison of these load spectra to measured data for particular aircraft has indicated AFS 120 to be conservative (see figure 5). These data are from a military model 90, the T44, used in a training role by the Navy.

Conservatism may lead to low replacement lives or frequent inspections that cause an economic burden to operators. A viable on-going aircraft structural integrity program is essential to assure continued long term structural integrity and airworthiness and will also remove some of the conservatism that are inherent in the analysis of data.

All branches of the aviation community are concerned with aging aircraft with its emphasis on structural deterioration as flight hours accumulate and corrosion becomes an increasingly significant factor. However, there is a need to also consider special mission roles including flight inspection where, structural deterioration may not be due to high cumulative flight hours, but the more severe environment of flight hours at low altitudes.

FAA Fleet

The FAA operates a fleet of 19 King Air model 300's in such a role (figure 6). A role in which for 67% of flight time the aircraft is operated at or below 2000 feet altitude. These are conditions for significant increases in gust and maneuver occurrences from that of the original design criteria. This environment goes beyond the normal design analysis of current executive aircraft and a state-of-the art structural integrity program is required. With timely, efficient data reduction, the appropriate maintenance practices for continued airworthiness can be assured.

Accordingly, as part of the acquisition of Beech model 300 aircraft for use in the flight inspection program, an agreement was reached between the Secretary of Transportation and the FAA to install stress/load recorder systems in the FAA fleet.

This requirement, in conjunction with an FAA policy to install flight data recorders and engine trend monitoring systems, has resulted in the development of this program.

Flight Data Recorder System

The program goal is to provide visibility of the structural status of the FAA flight inspection fleet. The structural integrity/engine monitoring recording system consists of installing a solid state flight recorder supplied by Smiths Industries in each aircraft (figure 7). The system will allow for engine condition monitoring, serve as a crash recorder by protecting and retaining the last 8 hours of flight data as well as being an airframe structural monitor. The data collected will provide the basis for management decisions covering parts replacement, special inspections, modifications that may be required, possible usage changes, or rotation of aircraft between bases.

All FAA flight inspection fleet aircraft will have vertical acceleration sensors at the aircraft center of gravity and 5 aircraft - one at each of the operating bases, will have strain gages installed. Therefore, one can consider this program to be made up of a Loads/Environment Spectra Survey and an Individual Aircraft Tracking Program as well as engine trend monitoring.

The recorder system hardware (figure 8) consists of 4 major components, a signal data recorder or acquisition unit, a flight data panel which allows basic information to be entered such as gross weight, fuel weight, base # and serial # of aircraft and engine, a flight data memory unit also known as a crash survivable memory unit and a data transfer interface unit which records the data into a module with 1 megabyte of memory.

The primary mission of the flight data recorder is to acquire raw parameter data from the aircraft ARINC 429 busses and from the analogue sensors and other discrete sources (figure 9). The data will be processed and compressed onboard in the Signal Acquisition Unit and recorded as Mishap, Structural or Engine data into non-volatile memory. The data will be downloaded at periodic intervals via the data transfer module to a PC at each bBase and forwarded to Oklahoma City where it will be copied and sent by modem to Beech Aircraft for decompression, validity checking and storing prior to semi-annual data reduction, evaluation and reporting (figures 10,11).

Parameters

The flight data recorder is to meet or exceed the requirements as shown in figure 12. Consequently, the parameter list is quite comprehensive.

Mishap parameters are shown in figure 13. They are recorded using time history techniques into the crash survivable memory unit. Data are recorded when values change by a specified amount.

Snapshot data are also taken at a 2 minute time hack or when the event switch is activated. Eight hours of data can be recorded after which time over-writing occurs. However, the last eight hours of flight data is always available.

The engine data parameter list is shown in figure 14. Data snapshots are recorded in response to a parameter exceeding a specific limit, at weight-on-wheels transition, or when the event switch is activated. Some events which will cause a trigger of engine parameters are shown in figure 15.

The structural data parameter list is shown in figure 16 and considers the installation of 12 strain gages in a total of 5 of the aircraft. All aircraft will have accelerometers installed so there will be a correlation between aircraft with gages and those without. The strain and accelerometer data are stored as peaks and valleys in a time sequence format. Data snapshots are also taken at weight-on-wheels transition and whenever the event switch is activated.

The locations of the strain gages have been carefully chosen to reflect the critical areas of the primary structure (figure 17). Where space permits, encapsulated gages are installed to ease installation (for this program, the Columbia 2684-1 1000 ohm full bridge gages are used). Other locations make use of conventional gages with suitable temperature compensation (for this program, Micromeasurements WK13-125-350 350 ohm full bridge gages are used).

There are 2 gages installed on the wing in the wheel well area on the lower main spar. This is an area known for its high stress from previously performed in-flight strain surveys and ground test data. Stresses for other locations along the spar are known from these data and consequently, a relationship can be developed between the flight data recorder wing strain and other locations on the wing.

Four gages are installed at the root of the vertical stabilizer and four at the root of the horizontal stabilizer. These are installed on the front and rear spars in areas of highest stress determined from previous in-flight strain surveys.

There are also two gages installed in the fuselage - one on a stringer primarily loaded by fuselage bending and one on a frame primarily loaded by cabin pressurization. These two locations were chosen by review of data from over 100 gages during a ground test where combinations of fuselage bending and pressurization loads were applied.

Data Reduction

Strains and load factor are recorded in a time history sequence of peaks and valleys (figure 18). The choice of threshold and gate values is very important. It is a balancing act where too fine a value will fill the memory too quickly leading to frequent downloads; too coarse a value could lead to the elimination of stress or load cycles which contribute to the overall damage.

Following installation of the strain gages, a preset value reflecting an on-ground condition is required. This information is determined from the previous flight survey where the effects of structure and fuel inertia are known. Other programs not having the benefit of this information would use conventional analysis to determine strain magnitude due to inertia.

This preset value is accounted for by building each unique value for each aircraft into the individual system. As each peak and valley is detected, either the Operational Flight Program can adjust them on-board prior to storage, as is the case for this program, or the ground processing software can make the adjustment prior to evaluation.

Because of engine trend monitoring, data will be downloaded every 3 to 5 days, hence the likelihood of module overflow for this program is remote. For aircraft having downloads much less frequently, a more efficient method of compressing and storing data is required. One such method is storing in a matrix format as shown in figure 19. This form of data collection loses the load sequencing but if stored on a flight-by-flight basis one can use a low to high sequence and still correlate well with random loading since the block size is small. Figure 20 shows the effects of sequencing for various block sizes and is from the USAF Damage Tolerance Design Handbook.

Data will be sent to Beech by modem for decompression and validity checking 2 to 3 times per week. Any parameter problems will be noted and FAA informed so that maintenance action to remedy the situation can be taken. Valid data will be stored for semi-annual data reduction.

The reduction phase will present stress and load factor exceedance plots (figure 21). The previous 6 months data can be compared to the total to date to reveal changes in severity for that particular aircraft. Comparisons between the 5 strain gaged aircraft can indicate degrees of severity between each base. Comparison of load exceedance data (figure 22) for all aircraft allows correlation of an aircraft from the last six months data to its total on an individual basis, on a per base basis and across all bases.

The data reduction evaluation will consist of calculating the fatigue life expended for each major assembly - wing, fuselage, and empennage using the strain recorded from the 5 strain-gaged aircraft. A factored life based on the mission mix to date will be determined (figure 23) and a projected time to reach this value will be established. The current contract calls for the use of the Palmgren-Miner Cumulative Damage Hypothesis for the determination of fatigue damage thereby eliminating the need to pursue load sequencing effects. It is however, probable that damage tolerant concepts will be adopted in the near future and therefore, data will be stored in a format to suit both processes.

Based on a safelife approach, a replacement time for components is obtained. A damage tolerance approach will allow an inspection program to be established and components only replaced "on condition".

The data evaluation phase will make use of full scale test results whenever possible. This will allow reduced scatter factors to be used because of test correlation and validated material properties based on S-N curves or fracture mechanics.

The program calls for prototype installation in June of 1994. Following installation of all gages and sensors a comprehensive flight checkout phase will be conducted where "fine tuning" of the parameters will take place (figure 24). Unique flights will be completed where strain and load factor magnitude and occurrences can be confirmed, and engine parameter exceedances can be checked. Typical flight profiles for the flight inspection role will be flown to verify the amount of memory used.

Schedule and Status

Figure 25 summarizes the program tasks and their status. Contract award occurred April 1993. Design work is complete, manufacturing of kits and development of software are in progress. Prototype installation will commence June of 1994 with the first data reduction report scheduled for December 1994.

In summary (figure 26), when aircraft are known to be flying in a severe environment, an effort should be made to identify and measure the fatigue impact on the aircraft. Tools do exist that allow some consideration of the environment such as the FAA document AFS 120 and ESDU 69023, where data collection has occurred, been reduced and presented as generic information for public use; but it is no substitute for measured data from the specific role.

Special mission roles are a way-of-life for many operators. The FAA, through this program, will assure continued airworthiness of the model 300 flight inspection fleet.

The program is on schedule and by the end of 1994, data will be forthcoming which will identify the structural status of the fleet. This will allow decisions to be made concerning replacement time for components, special inspections, modifications, or possible usage changes.

The means will be available to ensure efficient, cost-effective and safe usage of the FAA model 300 flight inspection fleet when flown in such extreme conditions.

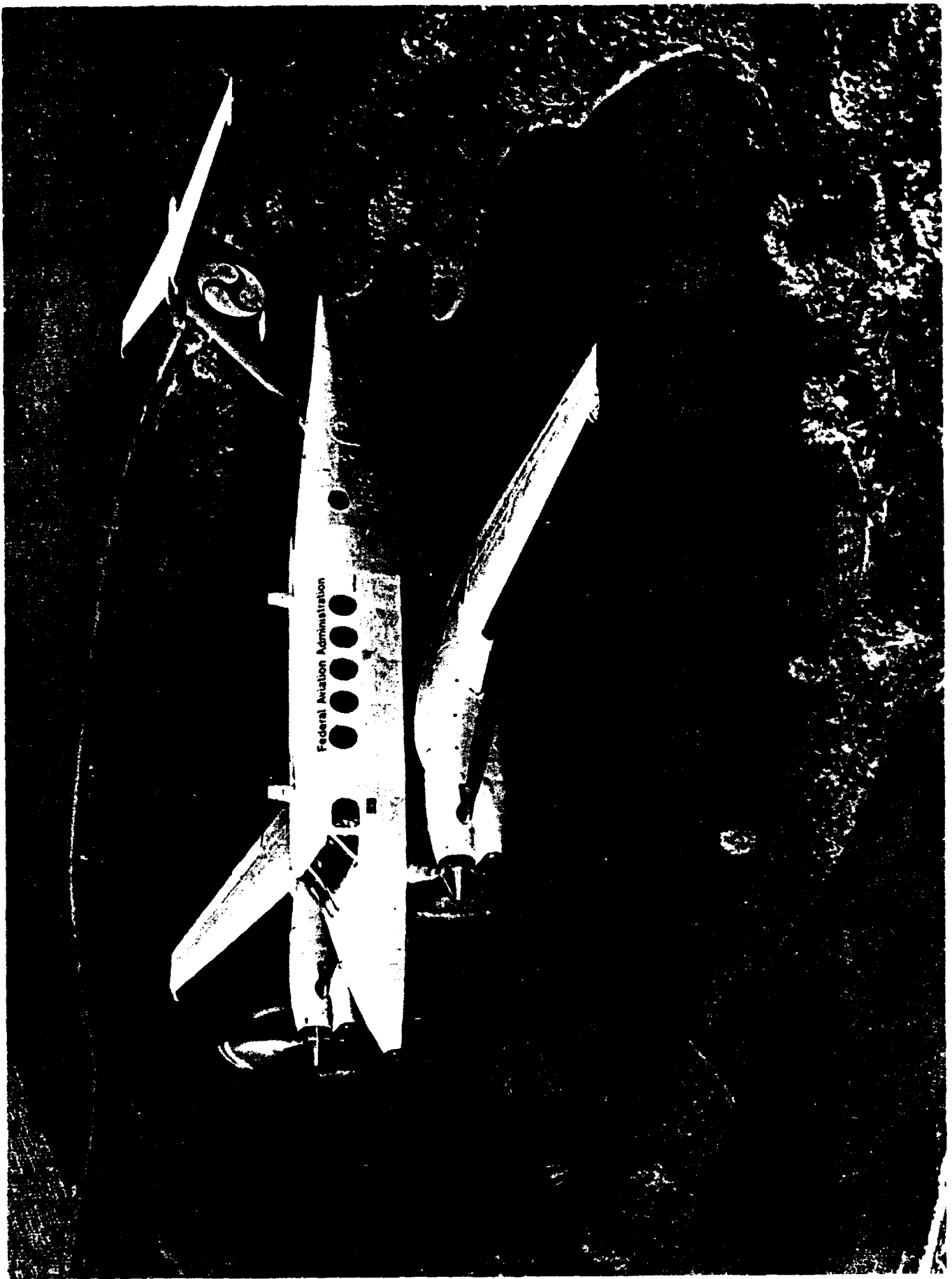


Figure 1

ASIP - FAA FLIGHT INSPECTION FLEET



Typical Flight Inspection Profile

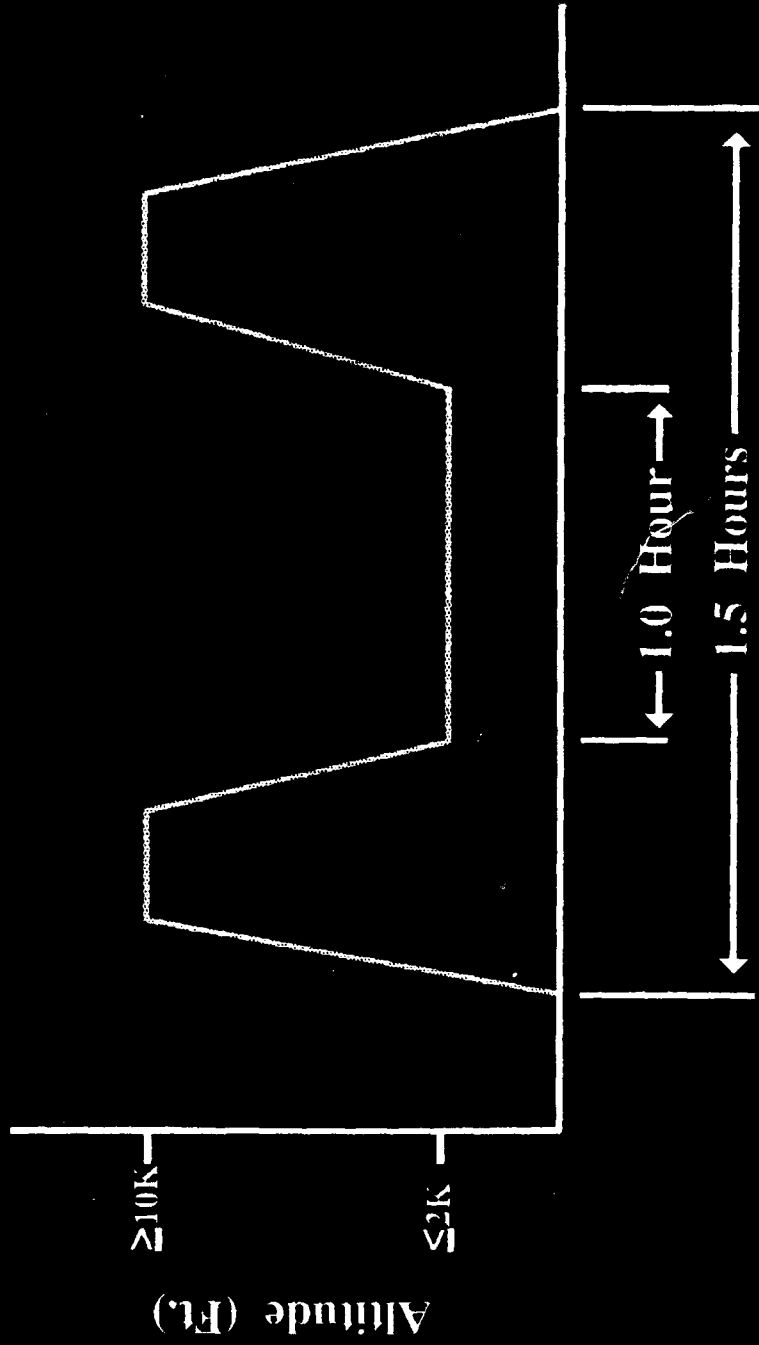


Figure 2

ASIP - FAA FLIGHT INSPECTION FLEET



Available Spectra Sources

Fatigue Evaluation Of Wing
& Associated Structure On
Small Airplanes

AFS 120-73-2

Average Gust Frequencies,
Subsonic Transport Aircraft

ESDU69023

Analysis Of Flight Loads
During Low-Altitude Pipeline
Patrol Operations




LR-516

Figure 3

ASJP - FAA FLIGHT INSPECTION FLEET



Spectra Comparison Based On Altitude

-  > 10,000 Feet
-  5001 - 10,000 Feet
-  1001 - 5000 Feet

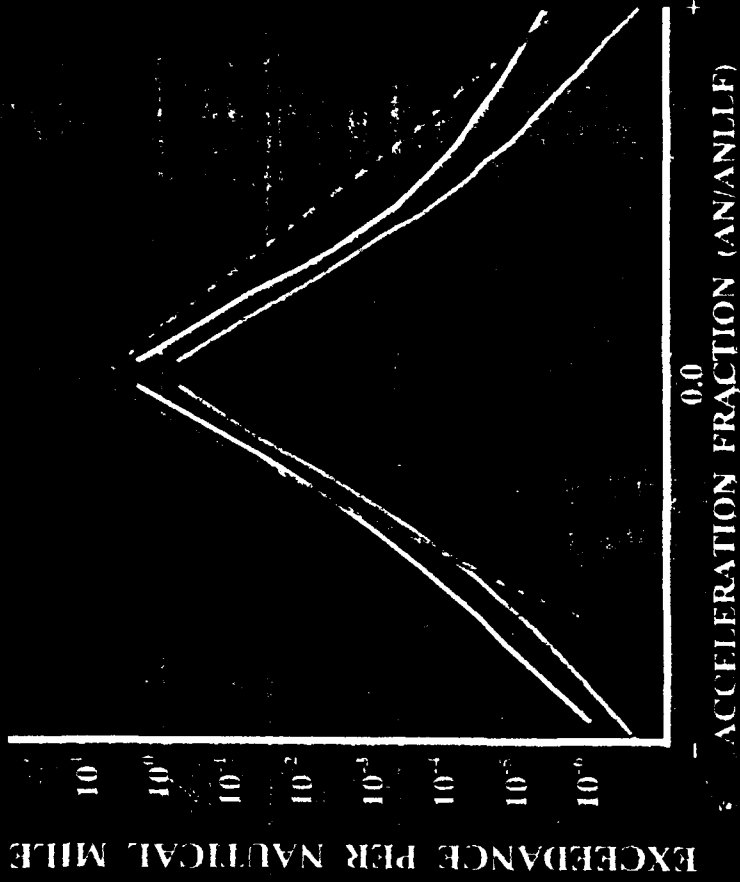


Figure 4

ASJP - FAA FLIGHT INSPECTION FLEET



G Load History Comparison

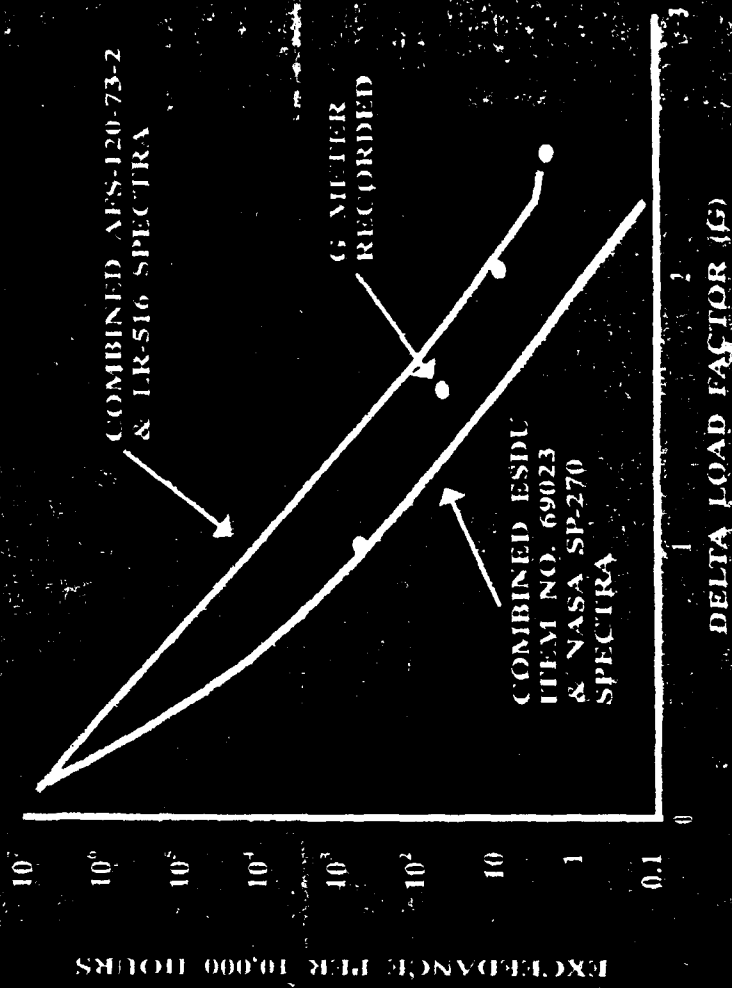


Figure 5

ASIP - FAA FLIGHT INSPECTION FLEET



19 Beech King Air Model 300's

5 Operating Bases

67% Flight Time Spent \leq 2000 Ft.

Significant Pattern Work

Figure 6

ASIP - FAA FLIGHT INSPECTION FLEET



19 Aircraft

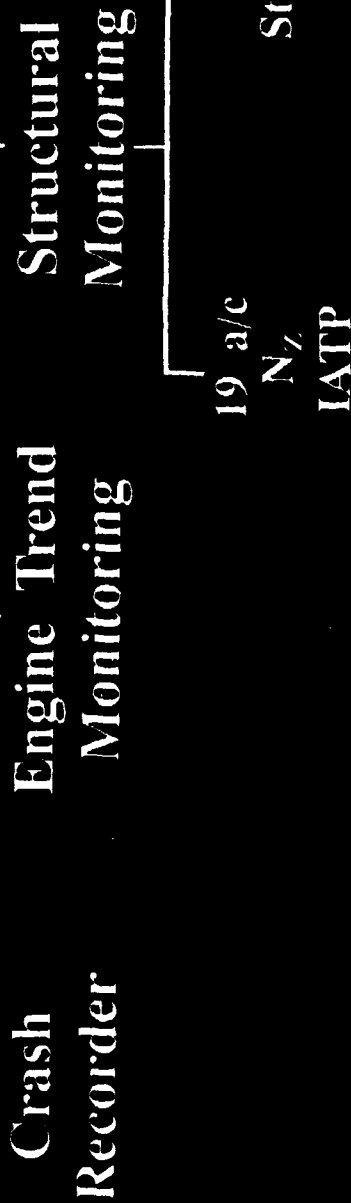
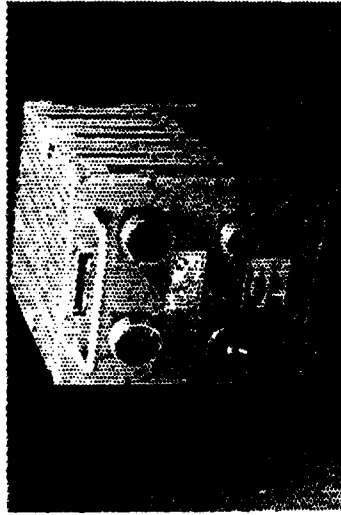


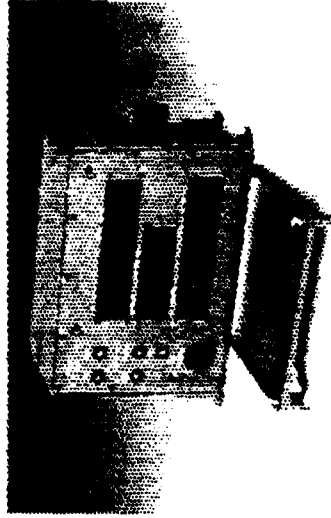
Figure 7



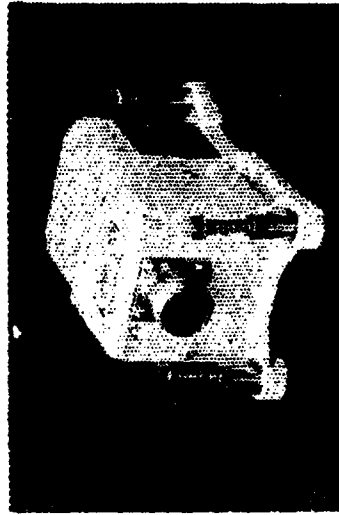
Discussion of recorder system design
Recorder System Hardware Overview



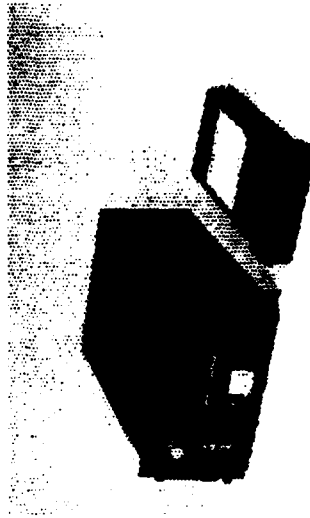
Signal Data Recorder, Reproducer



Flight Data Panel



Flight Data Memory Unit



Data Transfer Interface Unit

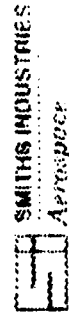
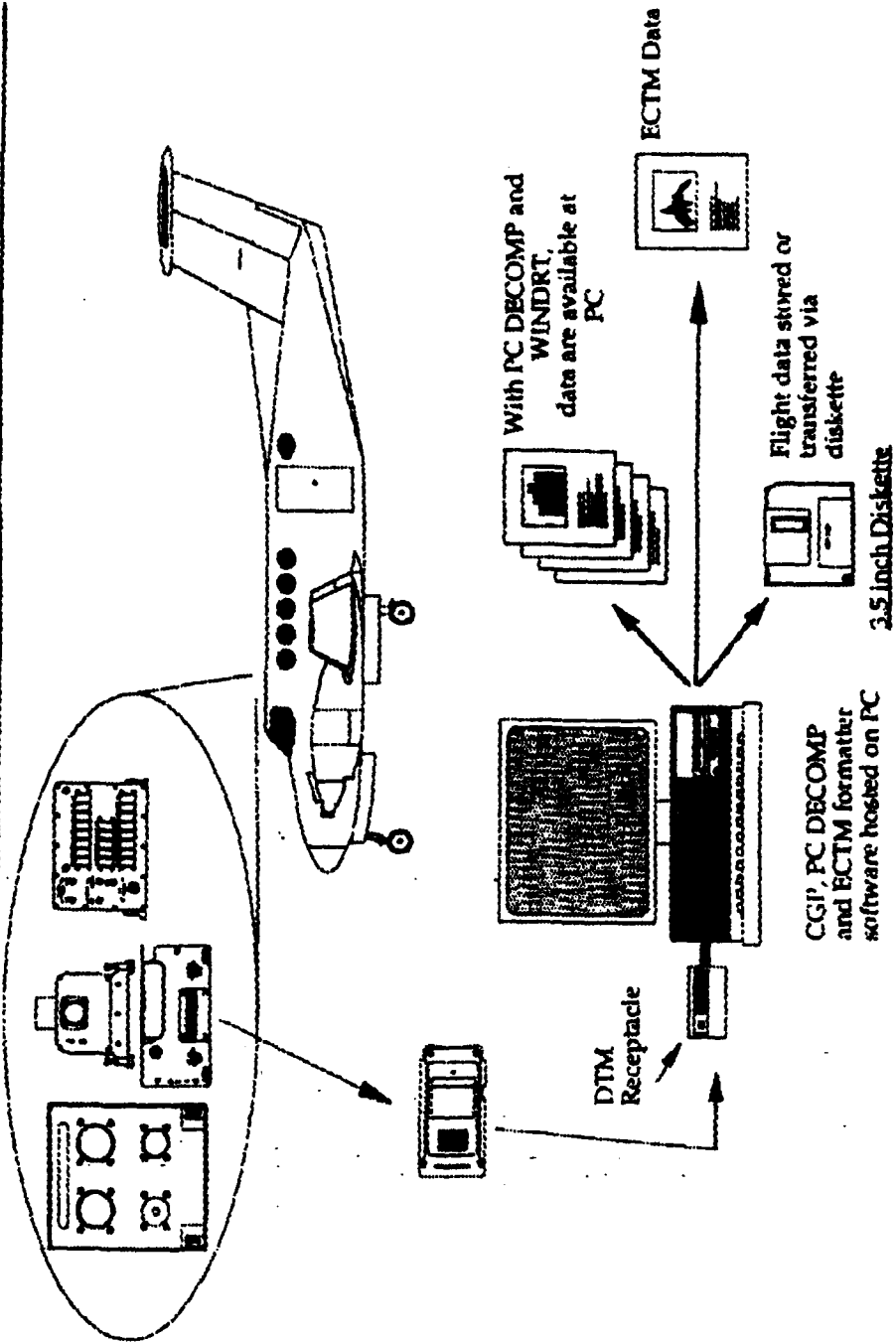


Figure 8

Discussion of recorder system design
System Operation Flowchart



SMITHS INDUSTRIES
 Aerospace

Figure 9

SOFTWARE FLOW CHART

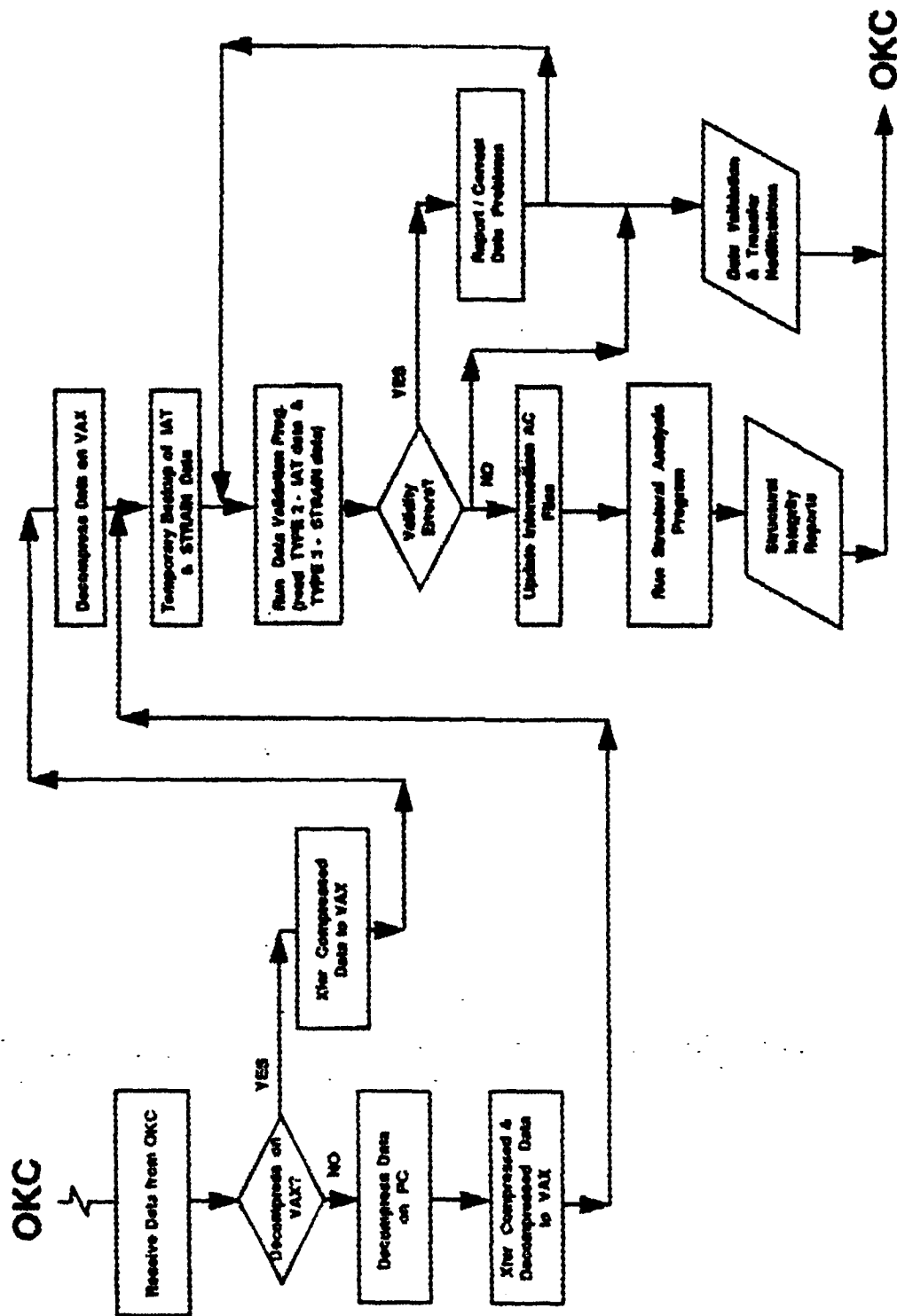


Figure 10

ASIP - FAA FLIGHT INSPECTION FLEET



Fielded System Data Collection

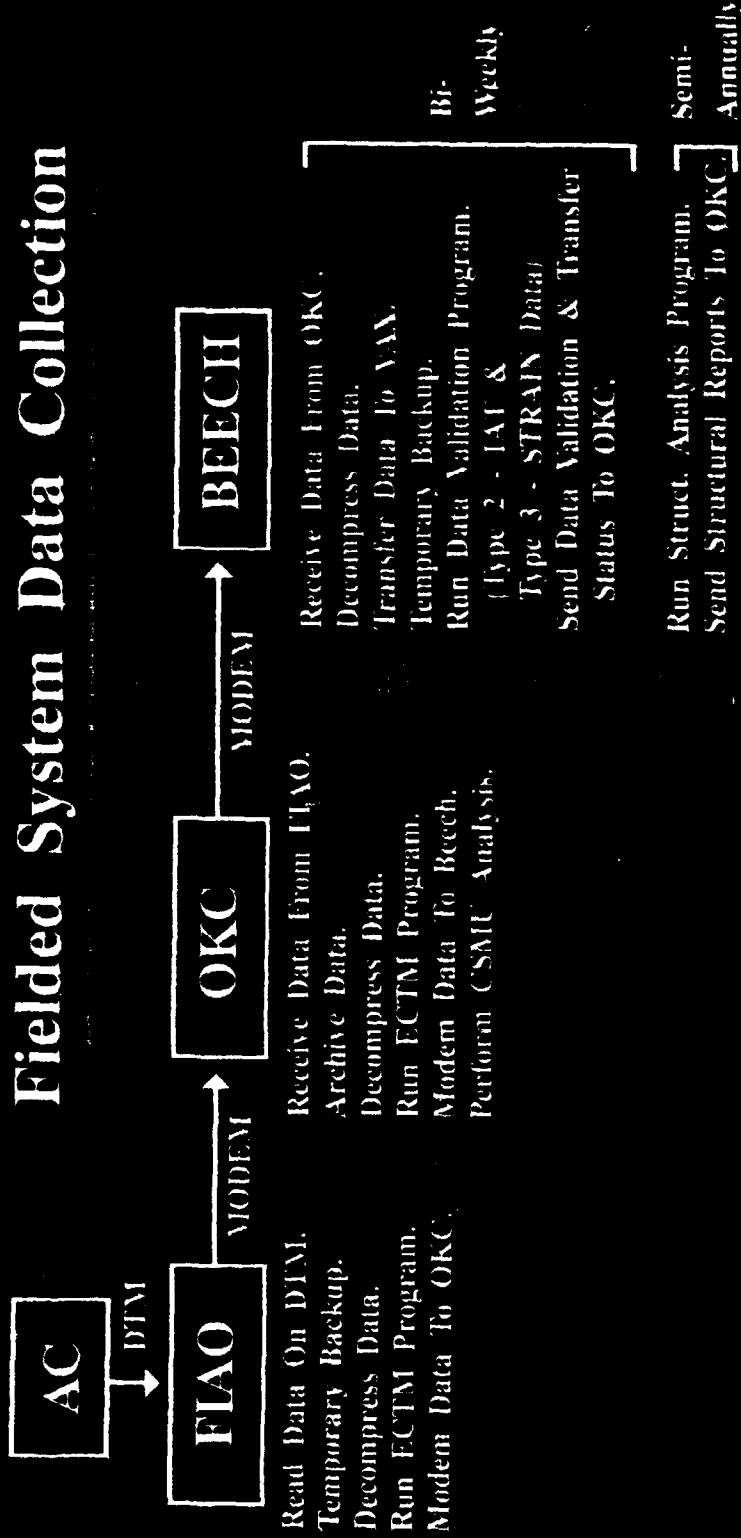


Figure 11

ASIP - FAA FLIGHT INSPECTION FLEET



The System Is To Meet Or Exceed

TSO - C51a

TSO - C124

RTCA/DO-160C

RTCA/DO-178-A

FAR 135 (App. B)

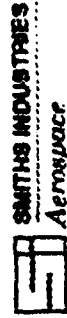
FAR 21

FAR 23

EURO CAE ED-55

Figure 12

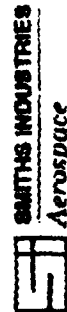
Discussion of recorder system design
Mishap Parameter List



TTEO ID.#	Parameter	Source	Rate
1	Indicated Airspeed (IAS)	ARINC #1	1 HZ
2	Pressure Altitude (HP)	ARINC #1	1 HZ
3	Outside Air Temperature (OAT)	ARINC #1	1 HZ
4 a	Right Trailing Edge Flap Up (RPUT)	OPEN/28V #7	1 HZ
4 b	Right TEF Down (RFDWN)	OPEN/28V #8	1 HZ
4 c	Right TEF App (RFAPP)	OPEN/28V #9	1 HZ
4 d	Left TEF Up (LFUP)	OPEN/28V #1	1 HZ
4 e	Left TEF Down (LFDWN)	OPEN/28V #5	1 HZ
5	Left TEF App (LFAPP)	OPEN/28V #6	1 HZ
6	Normal Accel (NZ)	DC DIF #1	16 HZ
7 L	Left Interurbine Temp (ITTL)	DC DIF #2	1 HZ
7 R	Right ITT (ITTR)	DC DIF #3	1 HZ
8 L	Left Engine Torque (NgL)	AC/DC DIF #1	1 HZ
8 R	Right Engine Torque (NgR)	AC/DC DIF #2	1 HZ
9 L	Left Propeller Speed (NpL)	AC/DC DIF #8	1 HZ
9 R	Right Propeller Speed (NpR)	AC/DC DIF #9	1 HZ
10 L	Left Gas Generator Speed (NgL)	AC/DC DIF #10	1 HZ
10 R	Right Gas Generator Speed (NgR)	AC/DC DIF #11	1 HZ
11 L	Left Engine Fuel Flow (WFL)	DC DIF #4	1 HZ
11 R	Right Engine Fuel Flow (WFR)	DC DIF #5	1 HZ
17	Heading, MAG (MHDC)	ARINC #2	1 HZ
18	Pitch Attitude (PITCH)	ARINC #2	4 HZ
19	Roll Attitude (ROLL)	ARINC #2	2 HZ
20	Radio Transmitting Key - Pilot (RKEYP)	OPEN/CND #1	1 HZ
20	Radio Transmitting Key - Co-Pilot (RKEYCP)	OPEN/CND #2	1 HZ
21	Long Accel (RX)	ARINC #2	4 HZ
22	Pitch Position (PITPOS)	TBD	1 HZ
23	Autopilot Engage (AUTOP)	OPEN/28V #2	1 HZ
24	Main Gear Squat Switch #1 (WOW)	OPEN/CND #3	1 HZ
	Pitch Trim Position (PTRPOS)	TBD	1 HZ
	Event Switch	OPEN/CND #4	1 HZ
	Lateral Accel (NY)	ARINC #2	4 HZ
	Radio Altitude (RALT)	AC/D.C. DIF #12	1 HZ
	Gross Weight	RS 422 channel A	1 HZ
	Fuel Weight	RS 422 channel A	1 HZ
	Base Number	RS 422 channel A	1 HZ
	Date	RS 422 channel A	1 HZ

Figure 13

Discussion of recorder system design
Engine Data Parameter List



TTEO ID.#	Parameter	Source	Rate
1	Indicated Airspeed (IAS2)	ARINC #1	1 HZ
2	Pressure Altitude (HP2)	ARINC #1	1 HZ
3	Outside Air Temperature (OAT)	ARINC #1	1 HZ
7 L	Left ITT (ITTL2)	DC DIFF #2	1 HZ
7 R	Right ITT (ITTR2)	DC DIFF #3	1 HZ
8 L	Left Engine Torque (NGL)	AC/DC DIFF #1	1 HZ
8 R	Right Engine Torque (NGR)	AC/DC DIFF #2	1 HZ
9 L	Left Propeller Speed (NpL2)	AC/DC DIFF #8	1 HZ
9 R	Right Propeller Speed (NpR2)	AC/DC DIFF #9	1 HZ
10 L	Left Gas Generator Speed (NGL2)	AC/DC DIFF #10	1 HZ
10 R	Right Gas Generator Speed (NGR2)	AC/DC DIFF #11	1 HZ
11 L	Left Engine Fuel Flow (WFL)	DC DIFF #4	1 HZ
11 R	Right Engine Fuel Flow (WFR)	DC DIFF #5	1 HZ
12 L	Left Engine Oil Pressure (OILPL)	DC DIFF #6	1 HZ
12 R	Right Engine Oil Pressure (OILPR)	DC DIFF #7	1 HZ
13 L	Left Engine Oil Temp (OILTL)	DC DIFF #8	1 HZ
13 R	Right Engine Oil Temp (OILTR)	AC/DC DIFF #7	1 HZ
14 L	Left Engine Nacelle Bleed Valve POS (NACL)	OPEN/28V #3	1 HZ
14 R	Right Engine Nacelle Bleed Valve POS (NACR)	OPEN/28V #4	1 HZ
15 L	Left Engine Cycles	Calculated	
15 R	Right Engine Cycles	Calculated	
16 L	Left Engine Total Time	Calculated	
16 R	Right Engine Total Time	Calculated	
	Event Switch	OPBN/CNID #4	1 HZ
	Base Number	RS 422 channel A	1 HZ
	Date	RS 422 channel A	1 HZ
	Fuel Weight	RS 422 channel A	1 HZ
	Cross Weight	RS 422 channel A	1 HZ

Figure 14

ASIP - FAA FLIGHT INSPECTION FLEET

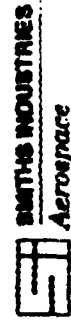


Engine Usage Recording Requirements

REASON FOR RECORDING	PARAMETERS TO RECORD	TRIGGER ID
Recording Start	All	1
Recording Stop	All	2
Baseline Event	All	3
Event Switch Set	All	4
Steady-State Trigger	All	5
ITT _L or ITT _R > 820	Parameters That Exceed MCTR	NA
N _{pL} Or N _{pR} > 104	Parameters That Exceed MCTR	NA
N _{qL} Or N _{qR} > 1700	Parameters That Exceed MCTR	NA
Torq L Or Torq R > 100%	Parameters That Exceed MCTR	NA
Peak Of N _{pL} Or N _{pR} When > 104	Value Of Peak	6
Valley Of N _{pL} Or N _{pR} When > 104	Value Of Valley	6
Peak Of N _{qL} Or N _{qR} When > 1700	Value Of Peak	7
Valley Of N _{qL} Or N _{qR} When > 1700	Value Of Valley	7
Peak Of ITT _L Or ITT _R When > 820	Value Of Peak	8
Valley Of ITT _L Or ITT _R When > 820	Value Of Valley	8
Valley Of Torq L Or Torq R When > 100%	Value Of Valley	9
Peak Of Torq L Or Torq R When > 100%	Parameters That Exceed MCTR	9

Figure 15

Discussion of recorder system design Structural Data Parameter List

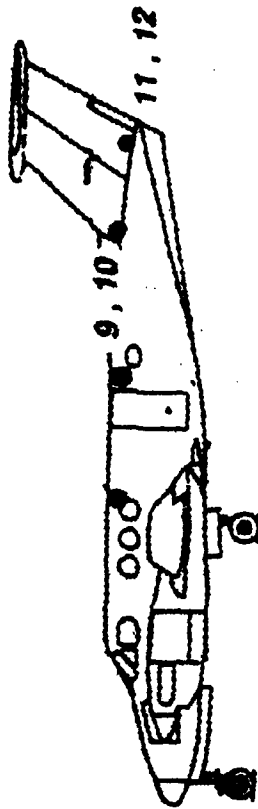
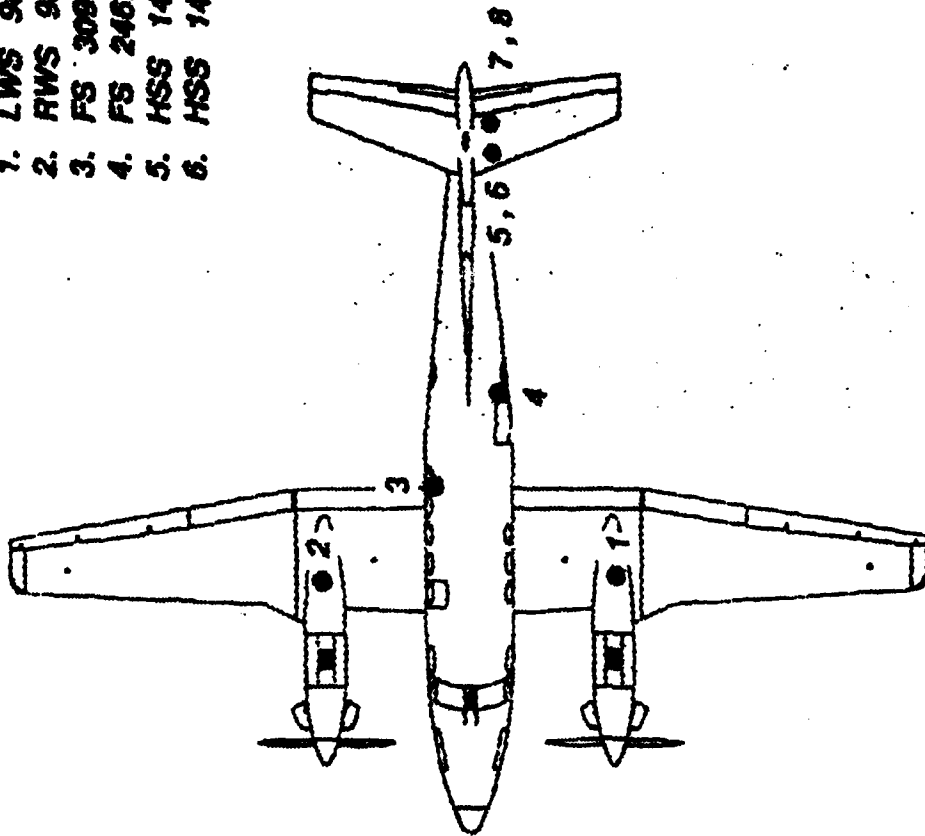


TIBO ID #	Parameter	Source	Rate
1	Indicated Airspeed (IAS)	ARINC #1	1 HZ
1	Indicated Airspeed (IAS2)	ARINC #1	1 HZ
2	Pressure Altitude (HPZ)	ARINC #1	1 HZ
3	Outside Air Temperature (OAT)	ARINC #1	16 HZ
5	Noxnal Accel (NZ)	DC Diff #1	1 HZ
24	Main Gear Squat Switch #1 (AVON)	OPEN/GND #3	1 HZ
	Radio Altitude (RALT2)	AC/DC DIFF #12	1 HZ
6 a	Strain Gage Input #1 (WL)	LL DC Diff #1	32 HZ
6 b	Strain Gage Input #2 (WK)	LL DC Diff #2	32 HZ
6 c	Strain Gage Input #3 (HSAU)	LL DC Diff #3	32 HZ
6 d	Strain Gage Input #4 (HSAU)	LL DC Diff #4	32 HZ
6 e	Strain Gage Input #5 (HSFL)	LL DC Diff #5	32 HZ
6 f	Strain Gage Input #6 (HSAL)	LL DC Diff #6	32 HZ
6 g	Strain Gage Input #7 (VSFL)	LL DC Diff #7	32 HZ
6 h	Strain Gage Input #8 (VSAR)	LL DC Diff #8	32 HZ
6 i	Strain Gage Input #9 (VSAR)	LL DC Diff #9	32 HZ
6 j	Strain Gage Input #10 (VSAL)	LL DC Diff #10	32 HZ
6 k	Strain Gage Input #11 (RF)	LL DC Diff #11	32 HZ
6 l	Strain Gage Input #12 (FA)	LL DC Diff #12	32 HZ
	Event Switch	OPEN/GND #4	1 HZ
	Avionics on switch (AVON)	OPEN/28V #10	1 HZ
	Base Number	RS 422 channel A	1 HZ
	Date	RS 422 channel A	1 HZ
	Fuel Weight	RS 422 channel A	1 HZ
	Gross Weight	RS 422 channel A	1 HZ

Strain Gage
Equipped Aircraft

Figure 16

1. LWS 98.8 - Lwr Spar Cap
2. RWS 98.8 - Lwr Spar Cap
3. FS 309.8 - Stringer 4L
4. FS 246.0 - Tiestrap
5. HSS 14.0 - Upper Fwd Spar Cap
6. HSS 14.0 - Lwr Fwd Spar Cap



7. HSS 14.0 - Upper Rear Spar Cap
8. HSS 14.0 - Lwr Rear Spar Cap
9. Left CVSS -3.12 - Front Spar Cap
10. Right CVSS -3.12 - Front Spar Cap
11. Left VSS 10.1 - Rear Spar Cap
12. Right VSS 10.1 - Rear Spar Cap

Figure 17



ASIP - FAA FLIGHT INSPECTION FLEET

Raw Valley/Peak Detection

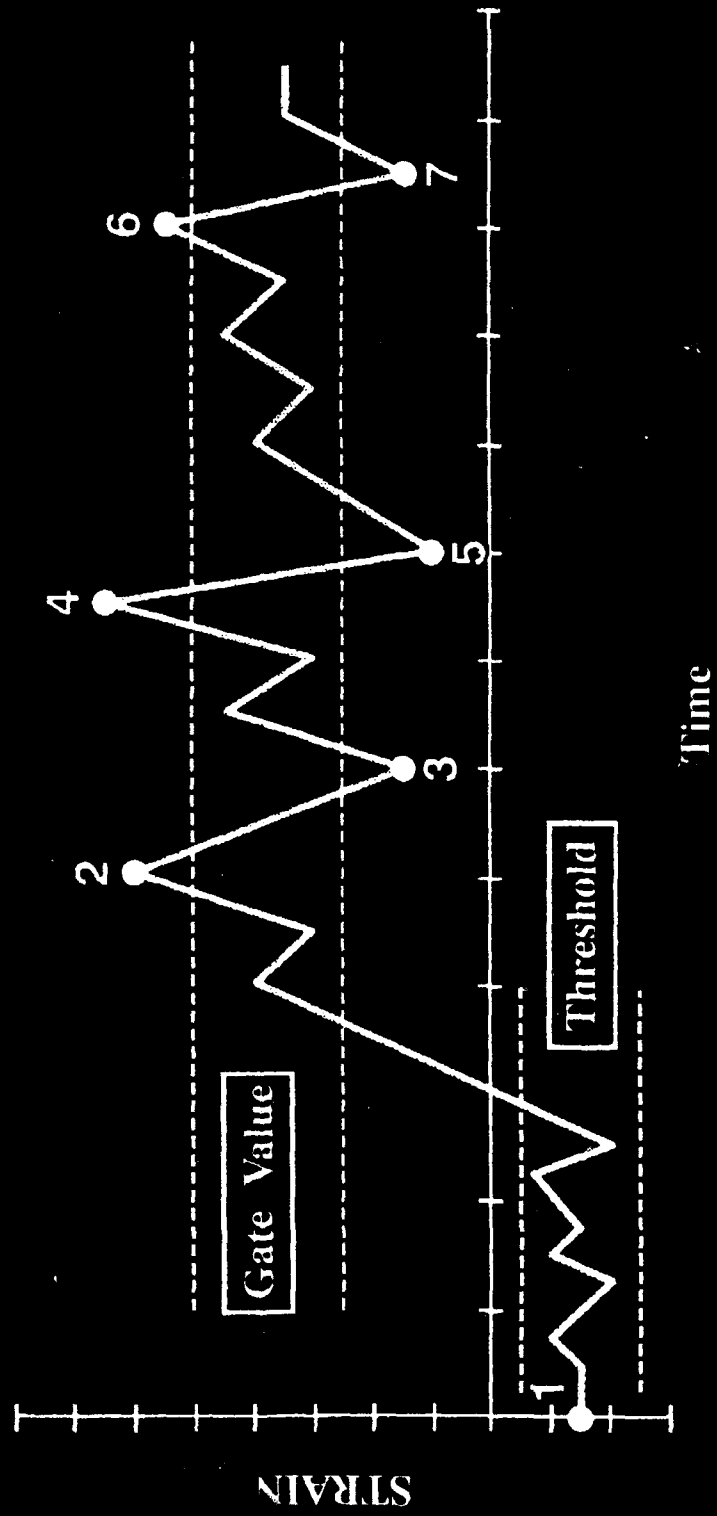


Figure 18

ASIP - FAA FLIGHT INSPECTION FLEET



		PEAK STRAIN (μ in/in)							
		-9999	-800	---	-200	---	701	801	
		-801	-701		200		800	9999	
-9999									
-801	0	0	0	0	0	0	0	0	
-800									
-701	0	0	0	0	0	0	0	0	
--									
--				0	0	0	0	0	
-200									
200				0	0	0	0	0	
--									
--						0	0	0	
701									
800							0	0	
801									
9999								0	

VALLEY STRAIN μ in/in

Figure 19

ASIP - FAA FLIGHT INSPECTION FLEET



Effect of Block Programming
and Block Size On Crack Growth
Life (All Histories Have Same
Cycle Content) Alloy: 2024-T3
Aluminum

SOURCE:
AFWAL-TR-82-3073
USAF Damage Tolerant
Design Handbook

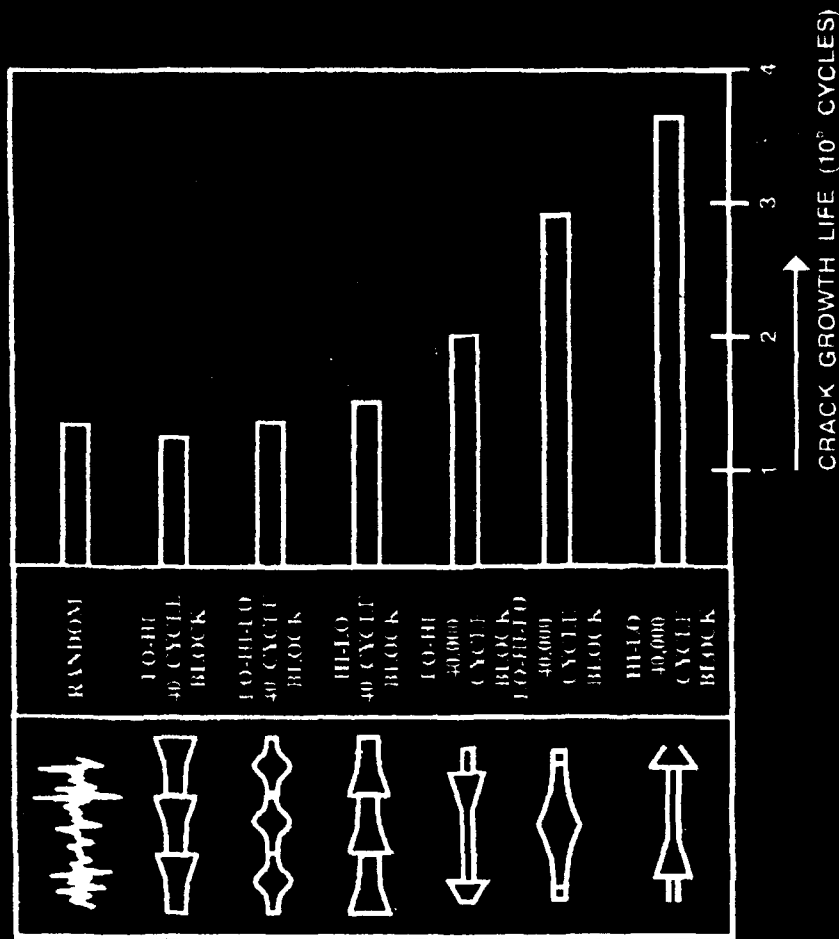


Figure 20



ASIP - FAA FLIGHT INSPECTION FLEET

Typical Stress Plot

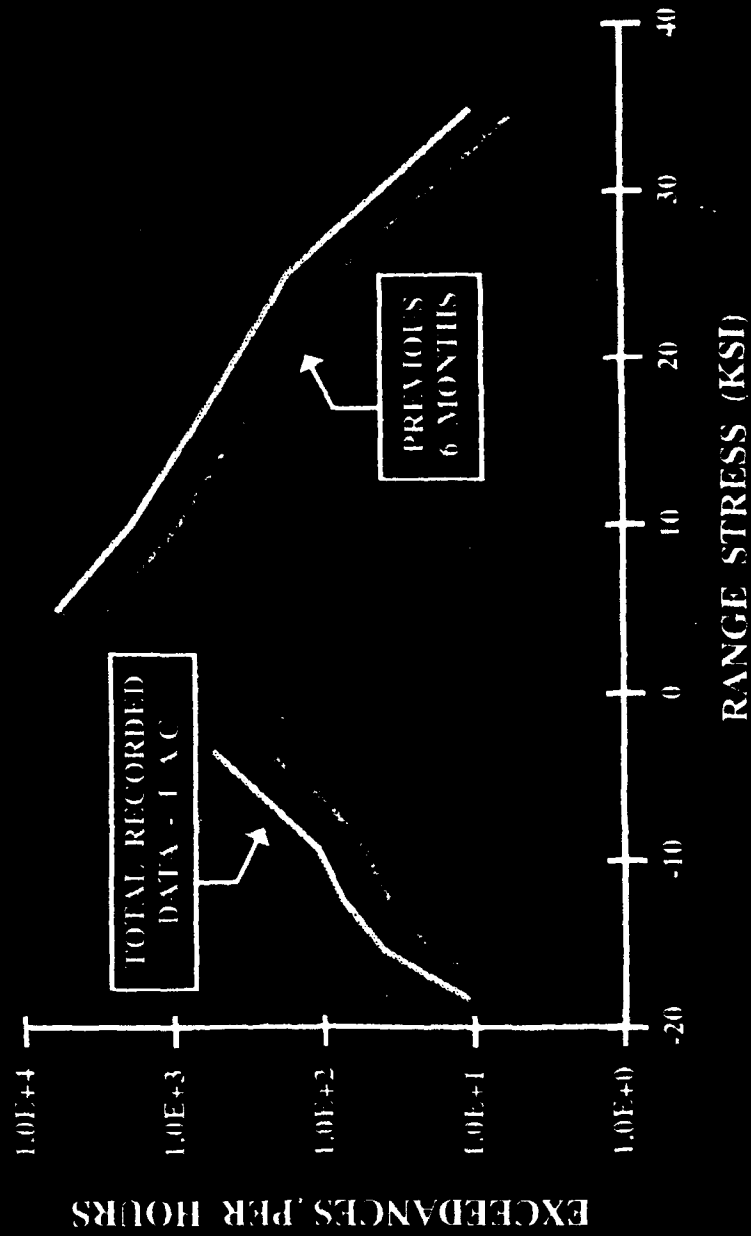


Figure 21



ASIP - FAA FLIGHT INSPECTION FLEET Typical N_z Plot

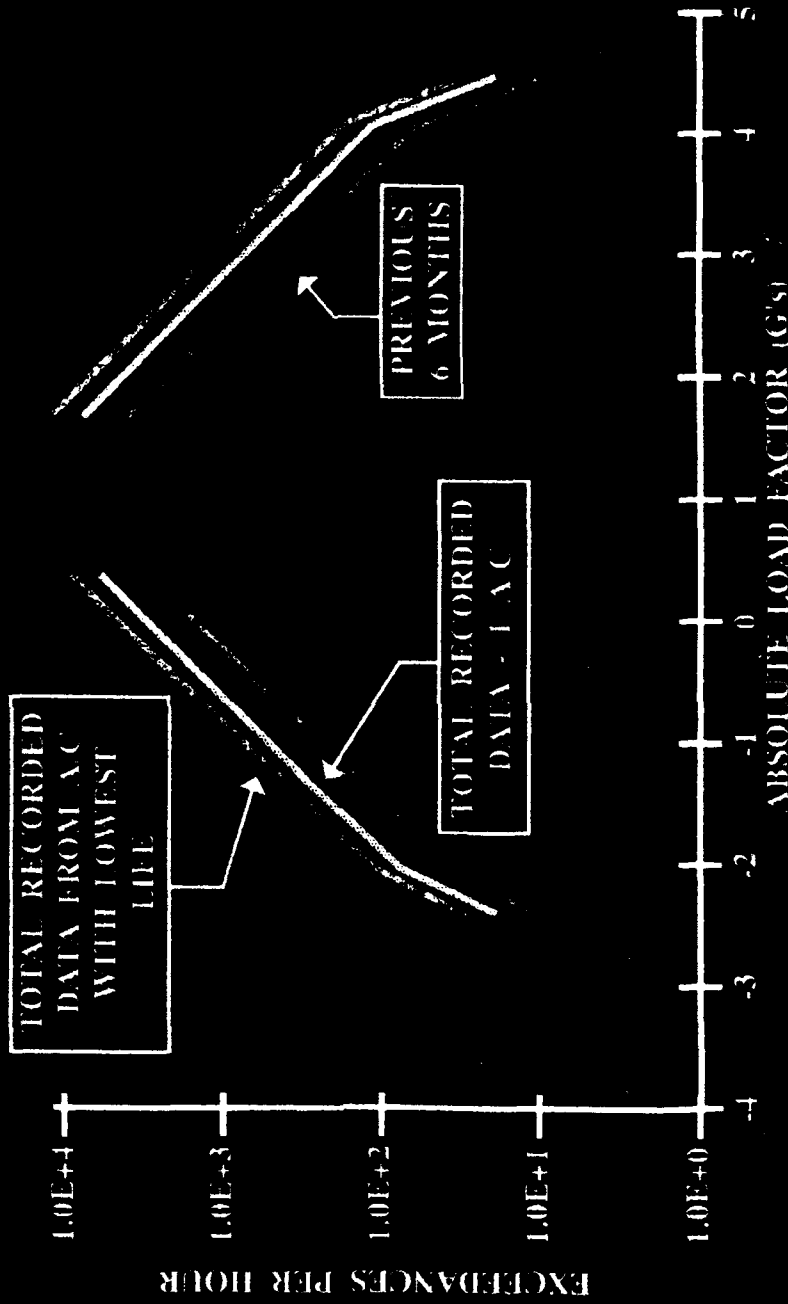


Figure 22

ASIP - FAA FLIGHT INSPECTION FLEET



Location Analyzed	Aircraft Serial No.	Factored Life (Hrs) (1st Inspection)	Projected FILE Data
Wing	FF-xx	xx,xxx	2Q2001
Fuselage			
Horizontal Stabilizer			
Vertical Stabilizer			

Figure 23

ASIP - FAA FLIGHT INSPECTION FLEET



Flight

- Comparison Of Strain Magnitude Data With Previous Flight Strain Survey
- Confirmation Of Occurrences By Performing Simple Maneuvers
- Confirm Memory Used

Engine

- Verify The Exceedence Occurrence Recorded With Flight Log Data
- Confirm Memory Used

Crash Data

- Confirm Valid Data

ASIP - FAA FLIGHT INSPECTION FLEET



Program Status

System Design	Complete
Kit Manufacture	In Progress
Software Development	In Progress
Prototype Installation	June '94
Flight Checkout	June '94
Training FAA Personnel	Sept '94
Fleet Installation	Sept '94 - Aug. '96
Decompression & Analysis	Dec '94 - Dec '97

ASIP - FAA FLIGHT INSPECTION FLEET



Summary

Special Missions → Severe Environment

Existing Tool → Measure Actual Data

FAA FIAC → IAT + L/ESS + Engine Trend

Program On Schedule

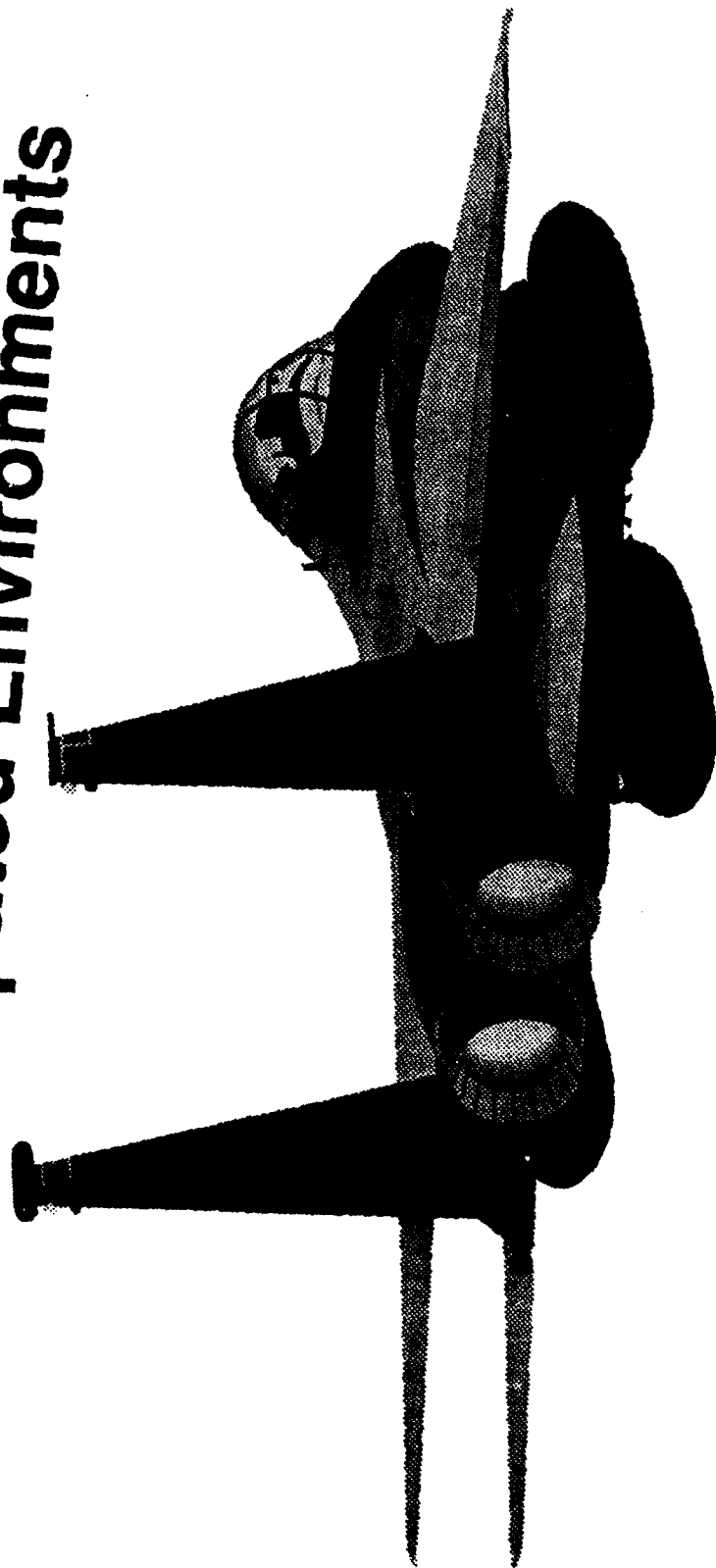
Data Available End Of 1994

Provides Structural Status Of Fleet

Figure 26

Probabilistic Inspection

A Probabilistic Strategy For Aircraft Fleet Inspection Considering Unanticipated Environments



**E.J. Tuegel, C.L. Brooks, and D.L. Rich
McDonnell Douglas Aerospace
St. Louis, Mo**

McDonnell Douglas Corporation

CP-2000-001-VC

OBJECTIVE

The objective of this paper is to present some ideas on how to develop a fleet inspection program to provide early detection of fatigue cracking as a result of environments and loading conditions which may not have been accurately identified during the design of the aircraft or tested in the full-scale fatigue test. The environments that are of primary concern are low amplitude, high frequency loading such as those created by vibratory fatigue interaction with primary loading; high amplitude fatigue created by acoustic or resonant responses of panels; and corrosion-temperature-fatigue interactions affecting many aircraft components that are subjected to hostile environments such as salt, sump tank water, or elevated temperatures.

Objective

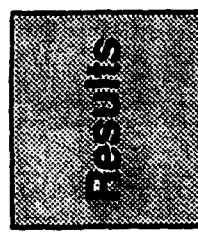
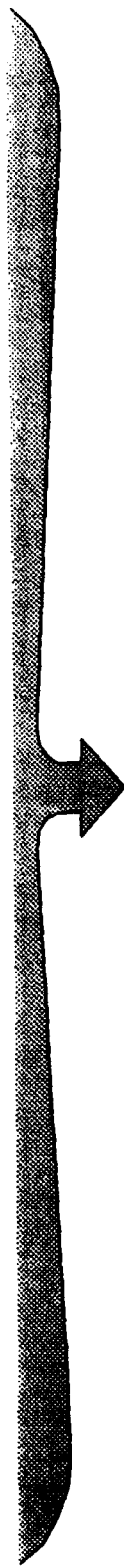
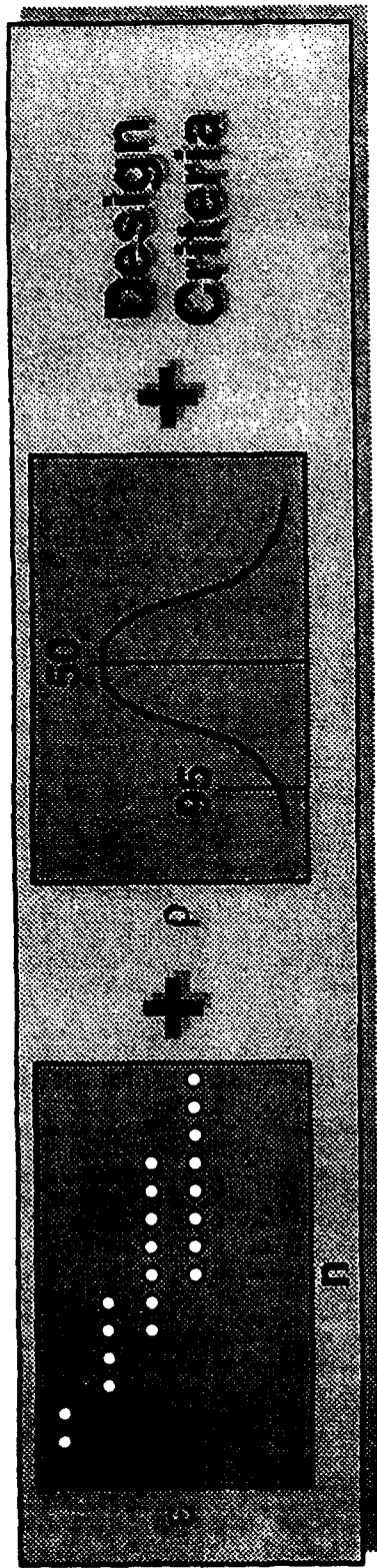
- **Develop a technique for determining Fleet Inspection Programs that provide early crack detection due to unanticipated environments:**
 - Low amplitude, high frequency fatigue (Buffet and vibratory fatigue interaction)
 - High amplitude fatigue (Acoustic or resonant fatigue)
 - Environmental effects (Corrosion-time-temperature fatigue interactions)

APPROACH

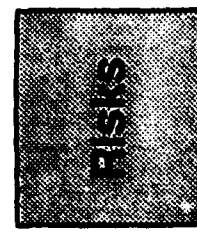
This inspection plan uses probability distributions developed from coupon fatigue test data to assess the risk of cracks developing in the fleet. A phased-sampling inspection program is used along with 95% confidence bounds to establish where in the fatigue distributions the fleet is at any given time. The 95% confidence bound is also used to optimize the number of aircraft inspected in order to reduce support costs while ensuring safety. The results of the inspections in relation to the number of aircraft and locations inspected provide the assessment of the level of risk for the entire fleet.

Probabilistic Inspection

Approach



Sample Inspection



Action Plan

- Optimize A/C Inspected
- Reduce Support Cost
- Risk Assessment
- Fleet Protection

McDonnell Douglas Aerospace

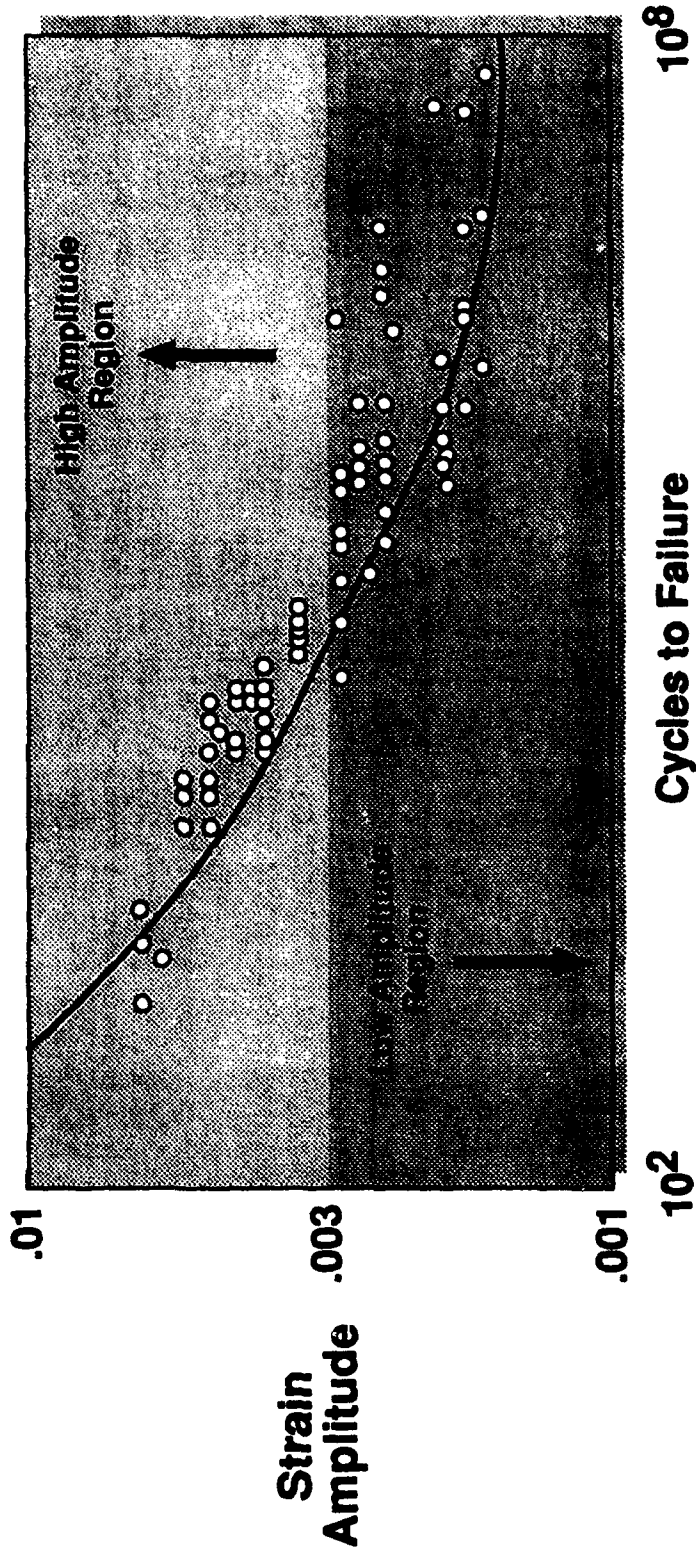
CP-30-001-001-1/C

CORRELATION BETWEEN ANALYSIS AND COUPON DATA SCATTER PROVIDE FOUNDATION

For 7075-T6 sheet, the analytical curve representing the number of applied cycles to fatigue crack initiation (approx. 0.01 in.) relative to the strain amplitude is plotted. In this case, the curve used for analytical predictions represents an approximate lower bound on the number of cycles at each strain level.

To illustrate the approach of this paper, the data is divided into two regions. The division was taken at the strain-level where the data scatter becomes larger; a strain of 0.003. The region above 0.003 is identified as High ϵ -Amplitude and below 0.003 is the Low ϵ -Amplitude. Each region is examined to obtain its characteristic distribution. Typically, the low amplitude fatigue data has a larger scatter band than the high amplitude fatigue data. This data for 7075-T6 sheet shows a distinct change in the data scatter at a strain amplitude of 0.003 as shown in subsequent slides.

Correlation Between Analysis and Coupon Data Scatter Provide Foundation 7075-T6 Sheet, R=1, Smooth Specimens



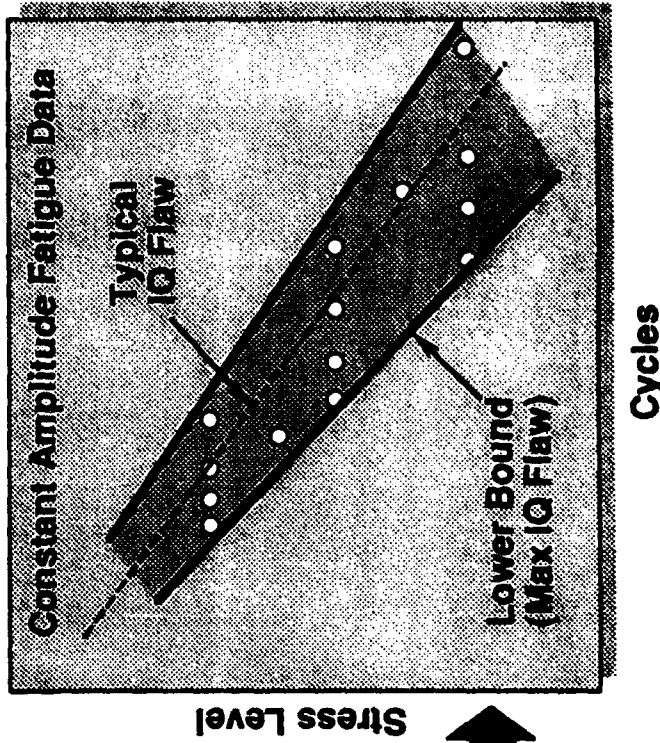
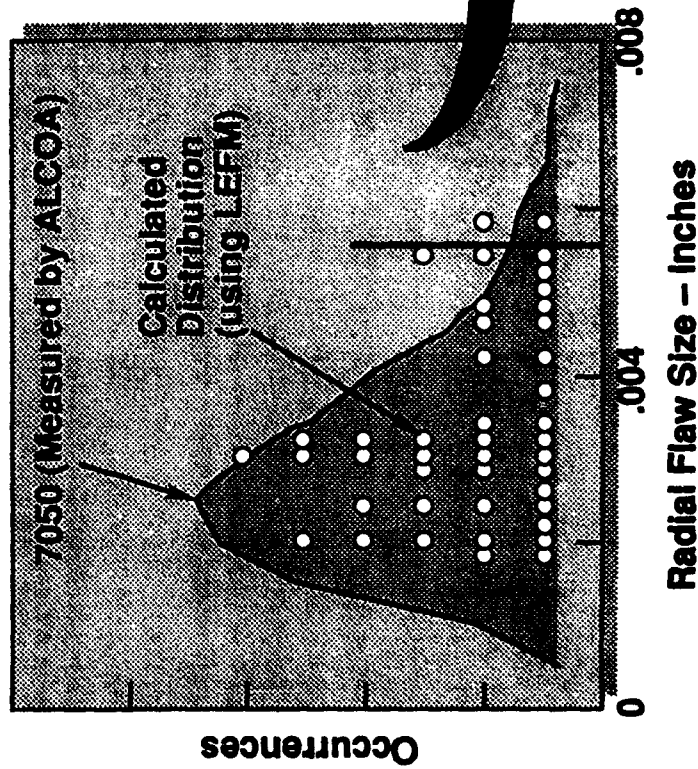
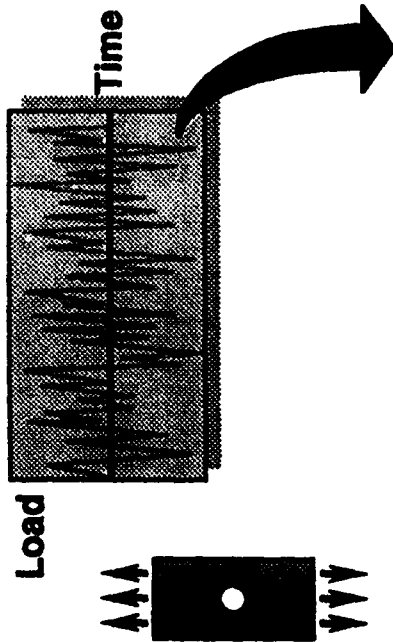
CORRELATION OF EQUIVALENT INITIAL FLAW TO INITIAL QUALITY CHARACTERISTIC SCATTER

The scatter or distribution of fatigue data may be associated with inherent material variables characterizing the initial quality of the material such as the size of microporosity, or non-metallic inclusions, etc. Variable amplitude spectrum tests have been monitored to determine crack initiation to approx. 0.01 in. flaws. Crack growth calculations were then performed to determine the equivalent initial flaw that would grow, assuming conventional linear elastic fracture mechanics, to the 0.01 in. flaw size. The back calculated flaw distribution for 2024 correlated well with SEM data for 7050 microporosity sizes measured by ALCOA[1]†. Using the distribution of flaw sizes and the same crack growth algorithms, constant amplitude fatigue crack initiation data up to 0.01 inch were predicted. These predictions demonstrated the same relative scatter as a function of strain/stress amplitude as the fatigue data. As a result, the assumption of using the characteristic scatter of basic coupon data may be appropriate for representing crack initiation probabilities.

† Numbers in brackets, [...], denote references.

Probabilistic Inspection

Correlation of Equivalent Initial Flaw to Initial Quality Characteristic Scatter



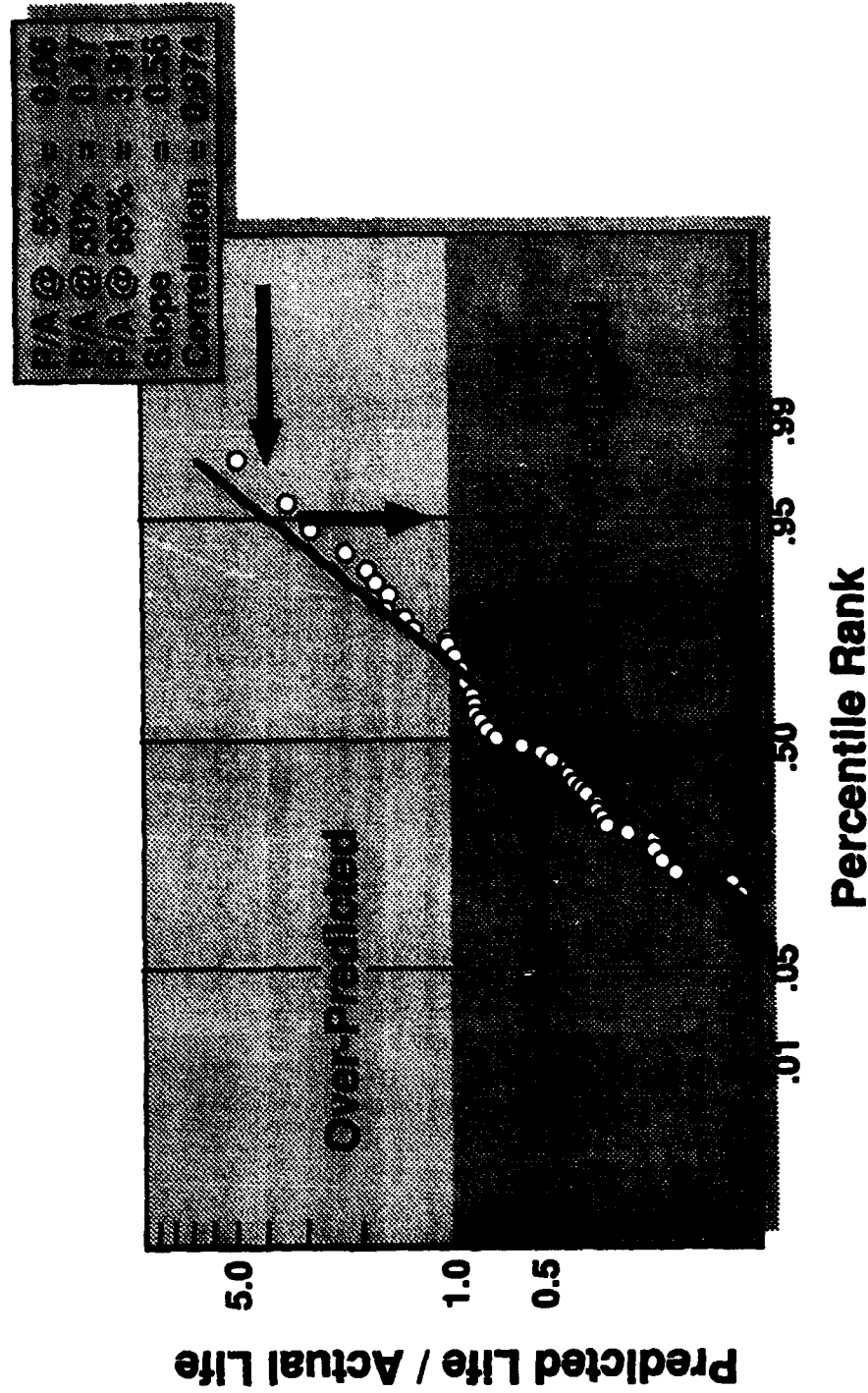
CHARACTERISTIC LOG-NORMAL DISTRIBUTION OF LOW-AMPLITUDE FATIGUE REGION

The ratios of the analytical life (hereafter referred to as the predicted life) to the actual test lives is fit with a distribution; a log-normal distribution was used for this example. The plot shown is for the low amplitude region defined in a previous chart as strain amplitudes less than 0.003. Data for which the predicted to actual life ratio was less than 0.1 are not shown to provide clarity in the chart. The standard deviation of this distribution is the slope of the line fit to the data by the least squares method. The validity of assuming a log-normal distribution for the data can be judged by the correlation coefficient of the linear fit. For this data the qualified measure of fit was considered good. Had the log-normal distribution not fit well, a Weibull or other appropriate distribution could have been used. For low amplitude fatigue data, a normal distribution would amplify the significance of over-predicting the life emphasizing the data for $P/A > 1.0$ to produce a lower slope in the area of interest in subsequent analyses. Using the log-normal plot the following observations can be made:

- 50% of the data is under-predicted by more than 50% of the actual lives. The typical behavior correlation is conservative by a factor of 2.
- 28% of the data is over-predicted.
- Only 5% of the data is over-predicted by a factor of 4 or more.

Probabilistic Inspection

Characteristic Log-Normal Distribution of Low-Amplitude Fatigue Region



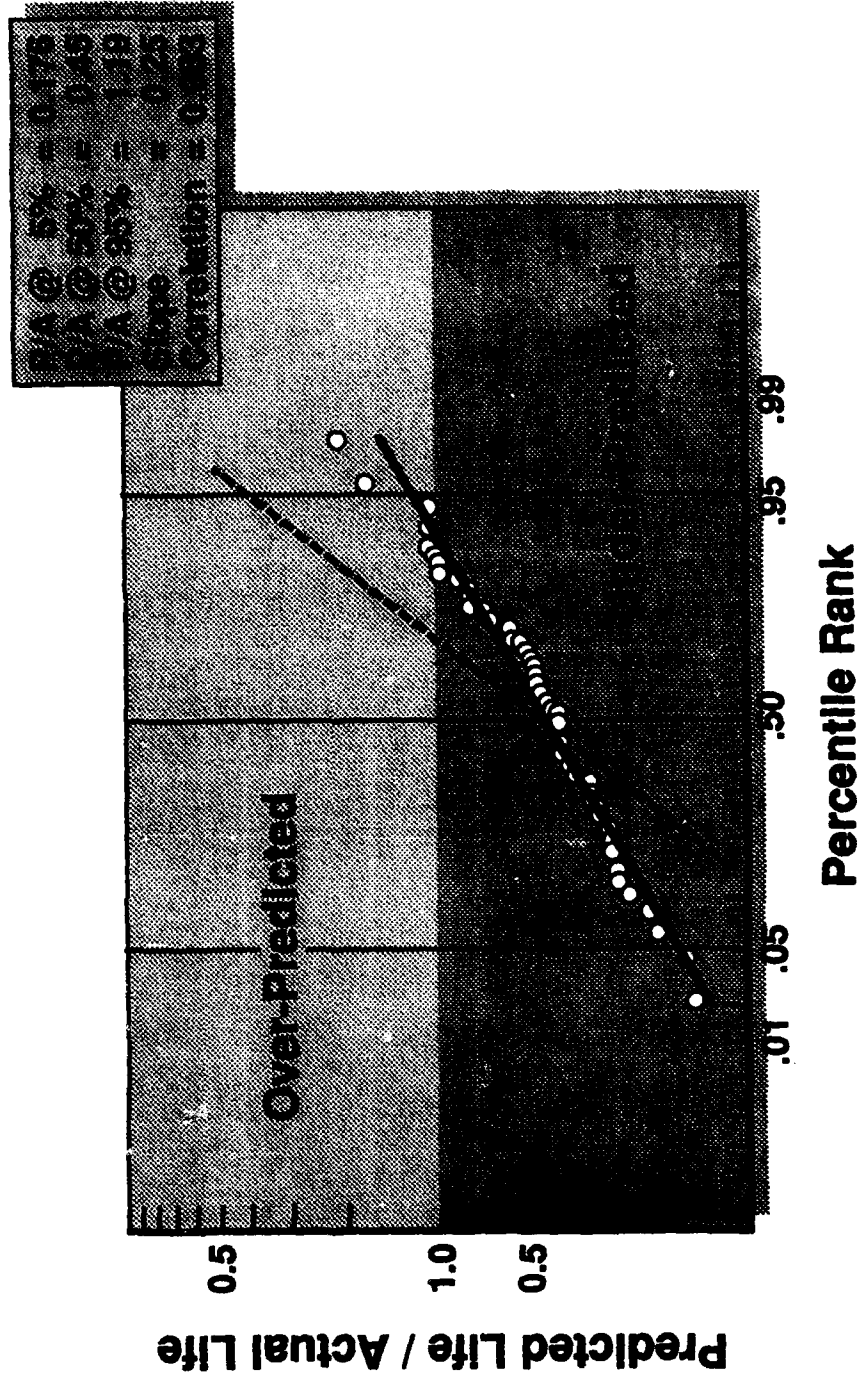
CHARACTERISTIC LOG-NORMAL DISTRIBUTION OF HIGH AMPLITUDE FATIGUE REGION

Similarly, a log-normal distribution was fit to the ratios of predicted to actual lives in the high amplitude region with good agreement. The standard deviation of this distribution, i.e., the slope of the solid line fit to the data using least-squares, is less than half the standard deviation for the low amplitude region, the dashed line.

From this plot, the following observations can be made:

- 50% of the data is under-predicted by more than 50% of the actual lives. The typical behavior correlation is conservative by a factor of 2.
- 10% of the data is over-predicted.
- Only 1% of the data is over-predicted by more than a factor of 2.

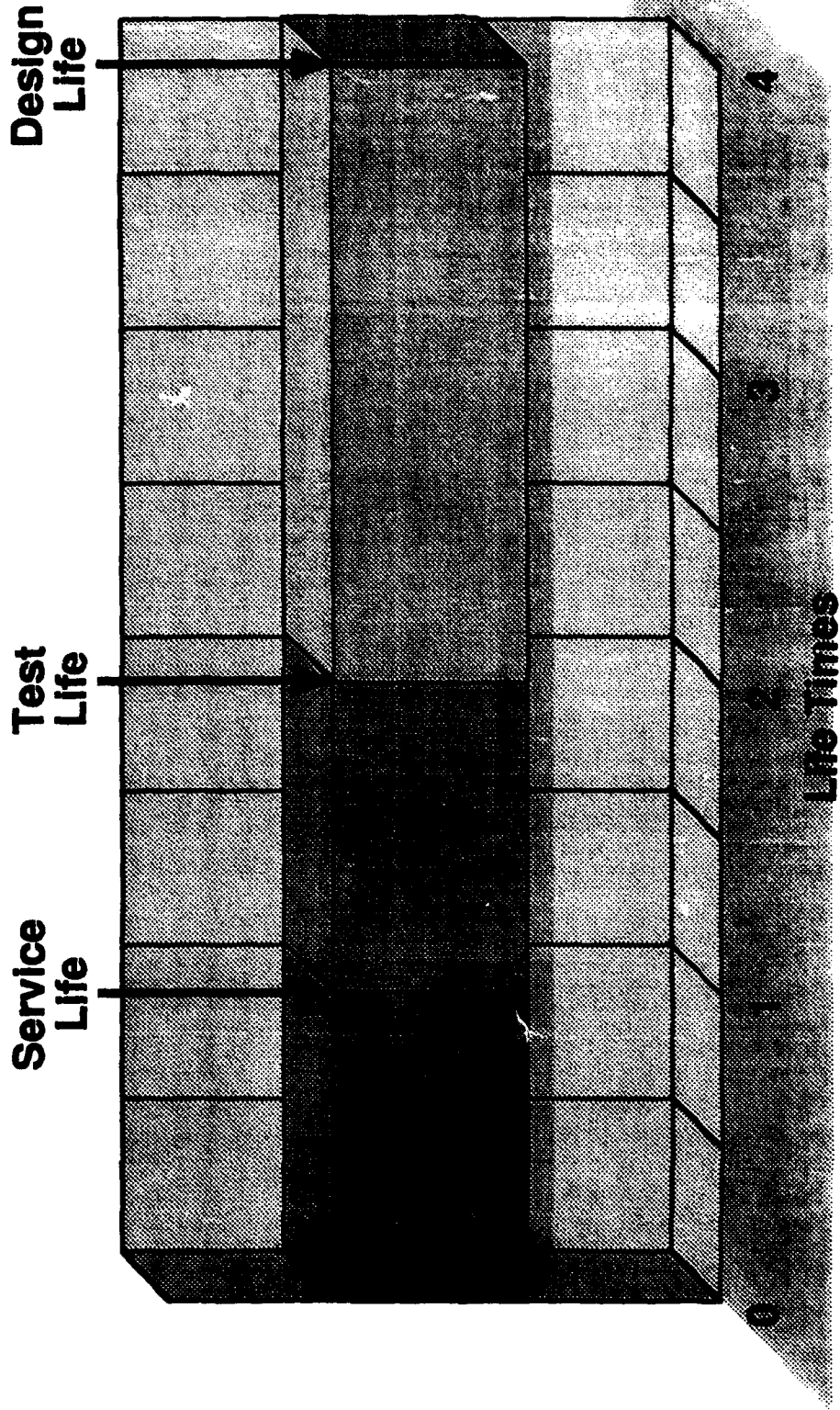
Characteristic Log-Normal Distribution of High-Amplitude Fatigue Region



FATIGUE DESIGN PHILOSOPHY

The most important USAF and USN requirement for ensuring that aircraft and systems are designed with due consideration for the structural integrity is that the aircraft and system must pass two lifetimes of fatigue testing to a specified usage. To ensure success in meeting the fatigue test requirement, many aircraft systems are designed to a crack initiation life of 4 lifetimes of the specified usage. This gives an extra margin of protection against unanticipated usage.

Fatigue Design Philosophy



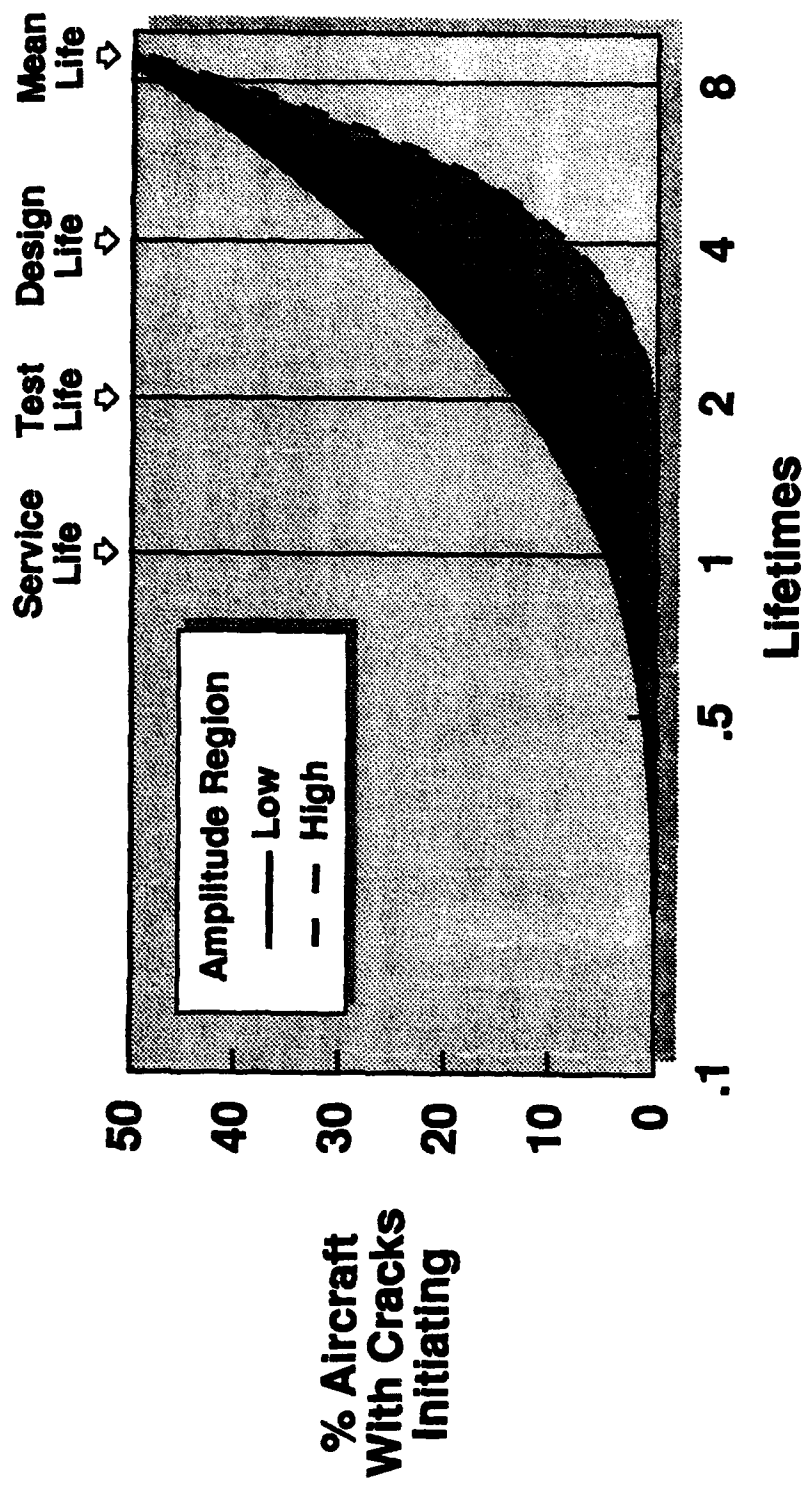
CRACKING PREDICTED IN THE FLEET USING THESE DISTRIBUTIONS

Assuming the structure is designed to the analytical predictions and all other design parameters are accurate (stress analysis, loads, spectra, etc.), the log-normal distributions for Predicted/Actual Life can be used to estimate the percentage of fleet aircraft that have cracks initiated as a function of the service life. This is accomplished using the analytical design life of 4 lifetimes in the numerator of the predicted to actual life ratio. A plot of the resulting cumulative distributions versus service life reveals the following:

- The mean life of the fleet is 8.5 to 9 lifetimes for all strain amplitudes at each location. (Mean life is when 50% of the aircraft will have cracks at this location.)
- At the design life of 4 lifetimes:
 - 8% of the aircraft would have initiated cracks under high amplitude fatigue;
 - 28% of the aircraft would have initiated cracks under low amplitude fatigue.
- For the 2 lifetimes of Full-Scale Fatigue Testing, the number of aircraft can be referred to the number of locations with cracks. So,
 - Less than 1% of the locations would have initiated cracks under high amplitude fatigue;
 - 14% of the locations would have initiated cracks under low amplitude fatigue.
- For service of 1 Lifetime:
 - No aircraft would be cracked due to high amplitude fatigue;
 - 5% of the aircraft would be cracked due to low amplitude fatigue.

Note that the basic assumptions are that the locations and aircraft are coincident in their relative cracking scenarios, whereas the probabilities will not distinguish themselves by aircraft but by location.

Cracking Predicted in Fleet From These Distributions



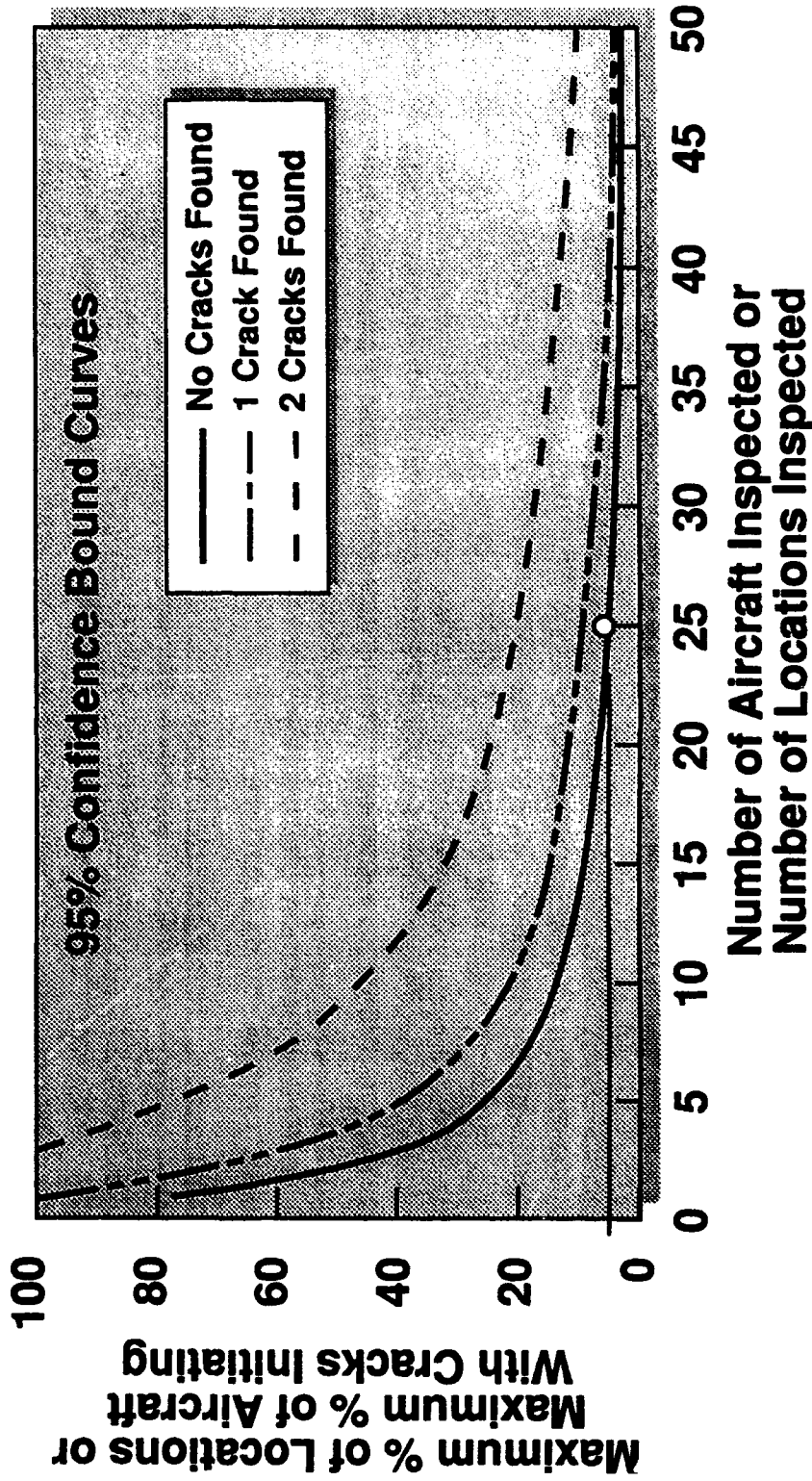
CONSIDERING AN INSPECTION PHILOSOPHY THAT ADDRESSES PROBABILITY

At present, aircraft receive Program Depot Maintenance at 20-25% of the service life. This approach economizes costs by phasing in the detailed inspection for components of concern at this time through careful inspection of a select number of lead-the-fleet aircraft. The goal of these inspections is to find cracks that have initiated as a result of unanticipated usage or environments.

95% confidence upper bound curves are generated using tables in [2] in order to select the number of aircraft in the fleet which need to be inspected. In generating these curves, it was assumed that the aircraft are symmetric for the locations of interest. So if a sample of 20 aircraft were inspected, 40 locations would actually be looked at.

The number of aircraft and locations to be inspected should be selected to minimize the risk and/or the number of locations, and to provide a reasonably accurate estimate of the number of aircraft in the entire fleet that could have cracks initiating. In general, it is desirable to be on the relatively horizontal portions of the confidence band curves; inspecting one aircraft more or less does not dramatically affect the confidence limit. There is also little benefit to moving out on the horizontal part of the curves; the cost of inspecting additional aircraft does not significantly improve the estimate of the percent of aircraft with cracks. For 0 to 5 cracks found in the sample, the optimum number of aircraft to inspect is between 20 and 30.

Considering an Inspection Philosophy That Addresses Probability



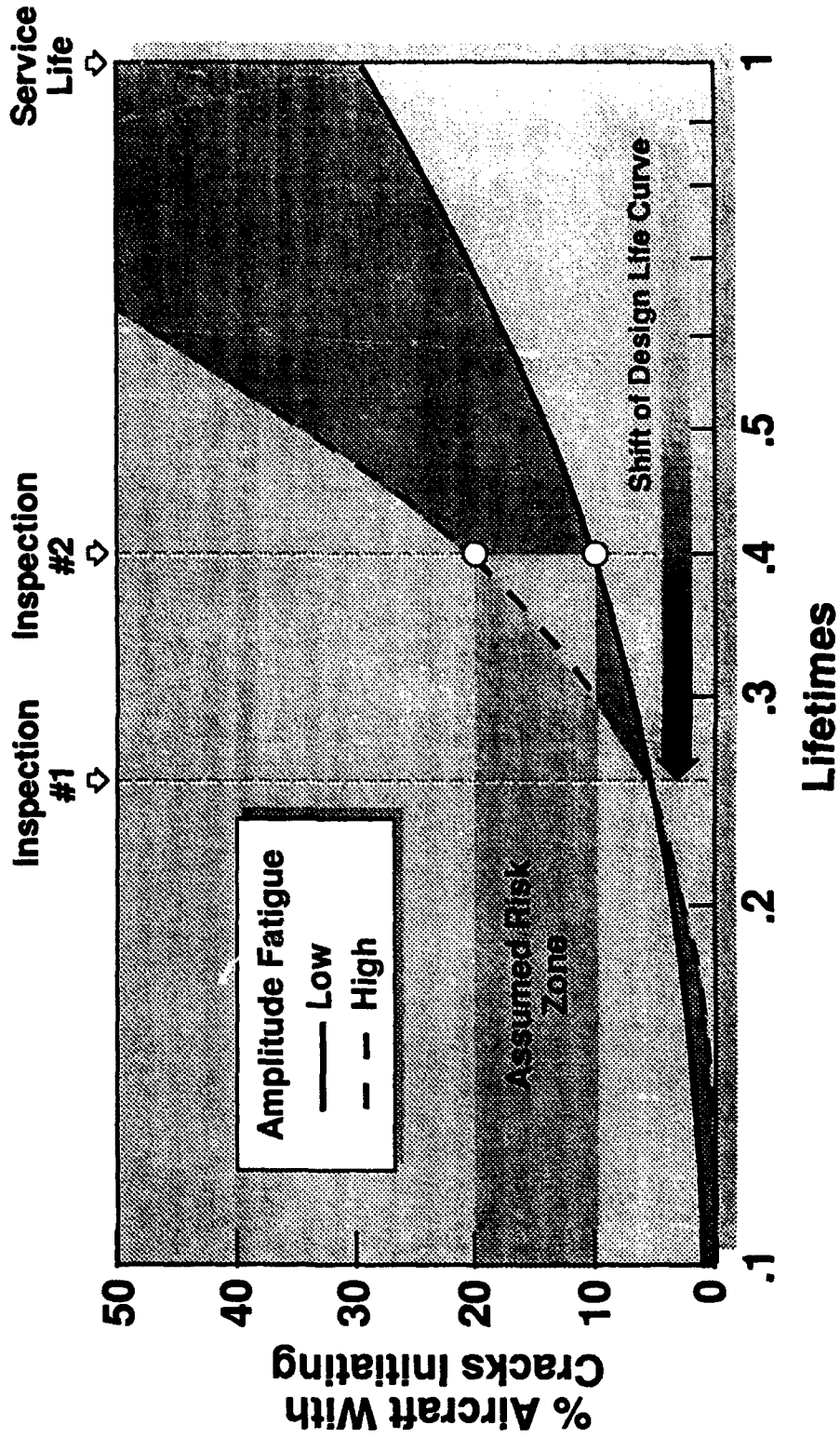
INSPECTION PLAN

Assume the first inspection occurs at approximately 0.25 lifetimes when the aircraft are brought into the depot. Detailed inspections are performed on 25 high time aircraft. If no cracks are found in the representative sample, then the actual percentage of aircraft in the fleet which are at risk of initiating cracks at 0.25 lifetimes is no more than 5% based upon the 95% confidence upper bound curve. So we move the cumulative fatigue distributions for low amplitude and high amplitude fatigue to the left along the lifetime axis until 5% on the curves lies at 0.25 lifetimes. This is the worst case scenario which accounts for our uncertainty about the other aircraft in the fleet. This approach is similar to the damage tolerance inspection philosophy that assumes a flaw just below the inspectable flaw size exists in the structure.

These distributions can now be used to set the interval for the next inspection based upon the risk that the fleet manager is willing to accept. For illustration purposes, we chose the next inspection to occur when the adjusted fatigue distributions reach the level where 10% - 20% of the aircraft are at risk of having initiated cracks, about 0.4 lifetimes. Remember that these probabilities represent the worst case, the fleet could readily pass 5 to 10 inspection intervals without any cracks being found if most of the environments are accounted for during design. The objective of this approach is to provide early detection of potential problems due to cracking from unanticipated environments.

Upon performing the second inspection and finding no cracks, the curves would shift to the right so that 5% lies at 0.40 lifetimes. Once the inspections start to find cracks initiating, the curves shift up as shown in the previous charts according to the number of cracks found.

Inspection Plan



MAINTENANCE PLAN

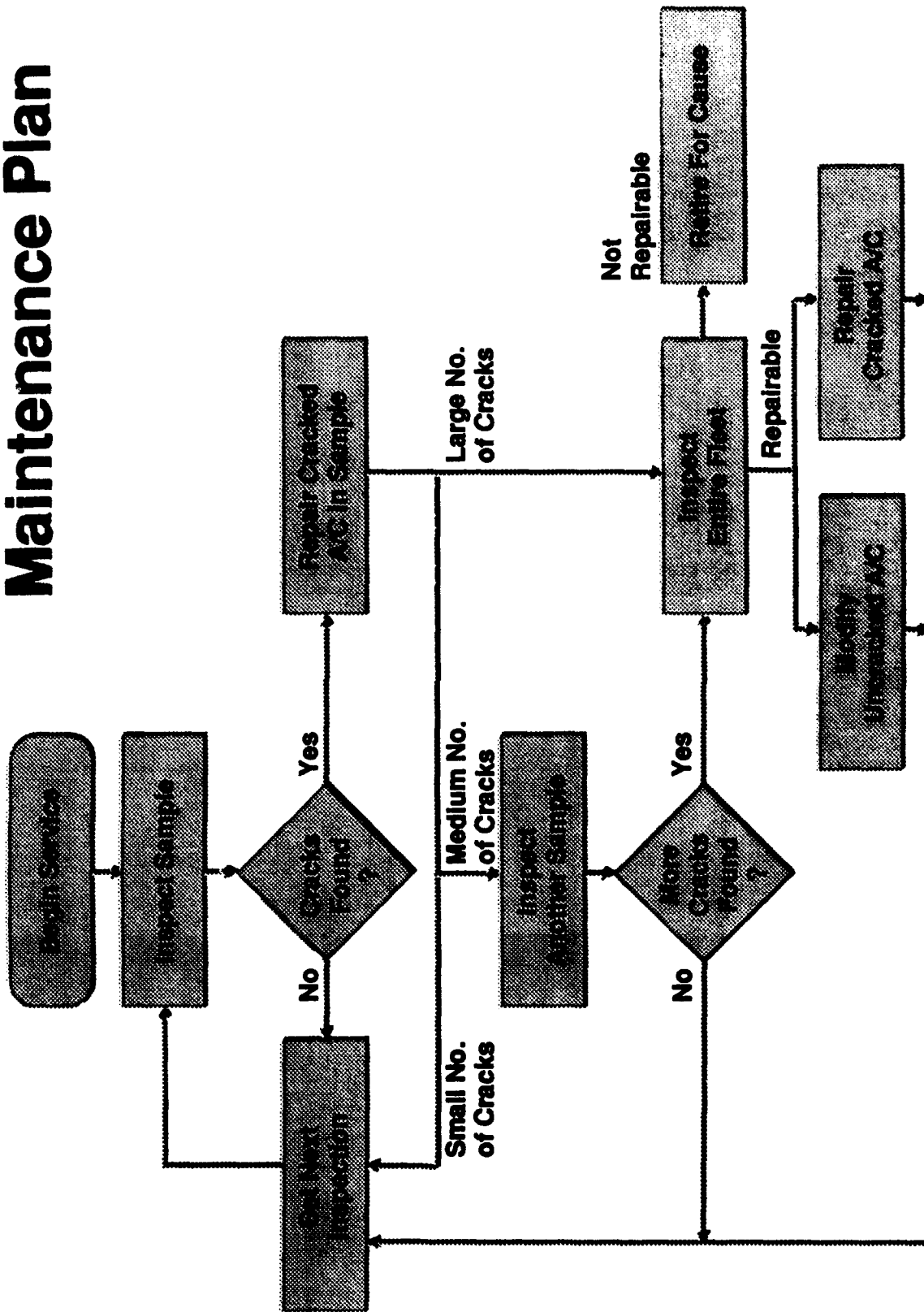
Consider how this inspection plan leads into an overall fleet maintenance plan. If no cracks are found in the inspection sample, the next inspection interval is set using the distributions as shown on the previous slide. Suppose during a subsequent inspection that cracks are found after inspecting 25 aircraft. If only 1 crack is found in the sample, only 9% of the fleet would be at risk of developing cracks. For a 250 aircraft fleet, this means that fewer than 25 aircraft could potentially develop similar cracks. It is probably not cost effective to inspect all 250 aircraft to be sure that all the aircraft with cracks are found unless there is an overriding safety issue. So, this one aircraft should be repaired and the next inspection interval set. It will be a shorter interval than if no cracks had been found because of the higher value of the 95% confidence bound.

If 5 cracks were found in the sample, the 95% confidence bound curve indicates that the fleet has less than 20% of the aircraft at risk of developing cracks. For a 250 aircraft fleet, this is fewer than 50 aircraft that could potentially develop cracks. For this number of aircraft, it may not be cost effective to inspect the entire fleet looking for the few aircraft with cracks. There are two alternatives depending upon the size of the cracks and the risk involved. If the damage tolerance aspects of the structure indicate that the risk is low, the next inspection can be scheduled based upon the adjusted fatigue distribution. If the risk is considered high, 25 more aircraft can be inspected at the particular location of concern. If no more cracks are found then the percentage of aircraft at risk of developing cracks drops to 10% and it is reasonable to just schedule the next inspection. If more cracks are found, it may be advisable to inspect the entire fleet repairing those aircraft with cracks, modifying the remaining ones, and implementing appropriate fleet precautions as necessary.

This inspection plan coupled with damage tolerance concepts would assist in detecting the interaction of conditions that were not incorporated in the product design. The results of the inspections with the probability based on data scatter establishes a quantitative way to assess risk, economic repair limits and retirement for cause.

Probabilistic Inspection

Maintenance Plan



COST BENEFITS

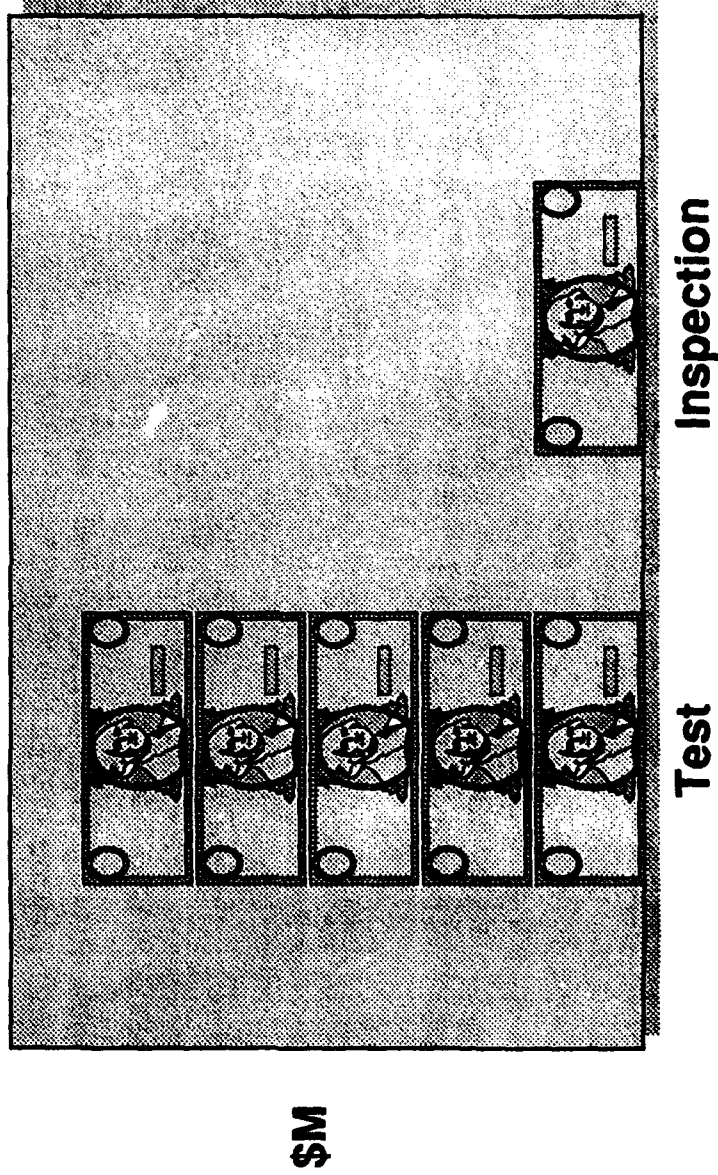
The benefits of this inspection approach are illustrated by considering how it can be used in a structural life extension program. Often questions exist as to whether certain areas of the airframe, particularly buffet prone areas, need to be modified in order to meet an extended life requirement.

One approach to answering this question is to conduct a test program. The program would consist of defining the environment followed by a full-scale fatigue test. The test results would provide the basis for modification of these additional areas.

A second approach would be to inspect several high-time airframes looking for unanticipated cracking in the buffet-prone areas. The results of this inspection are then used with the fatigue distributions to predict the likelihood that the structure will meet the extended life requirements.

A comparison of the estimated costs of these two approaches shows that the inspection approach is about 20% the cost of the test program.

Cost Benefits



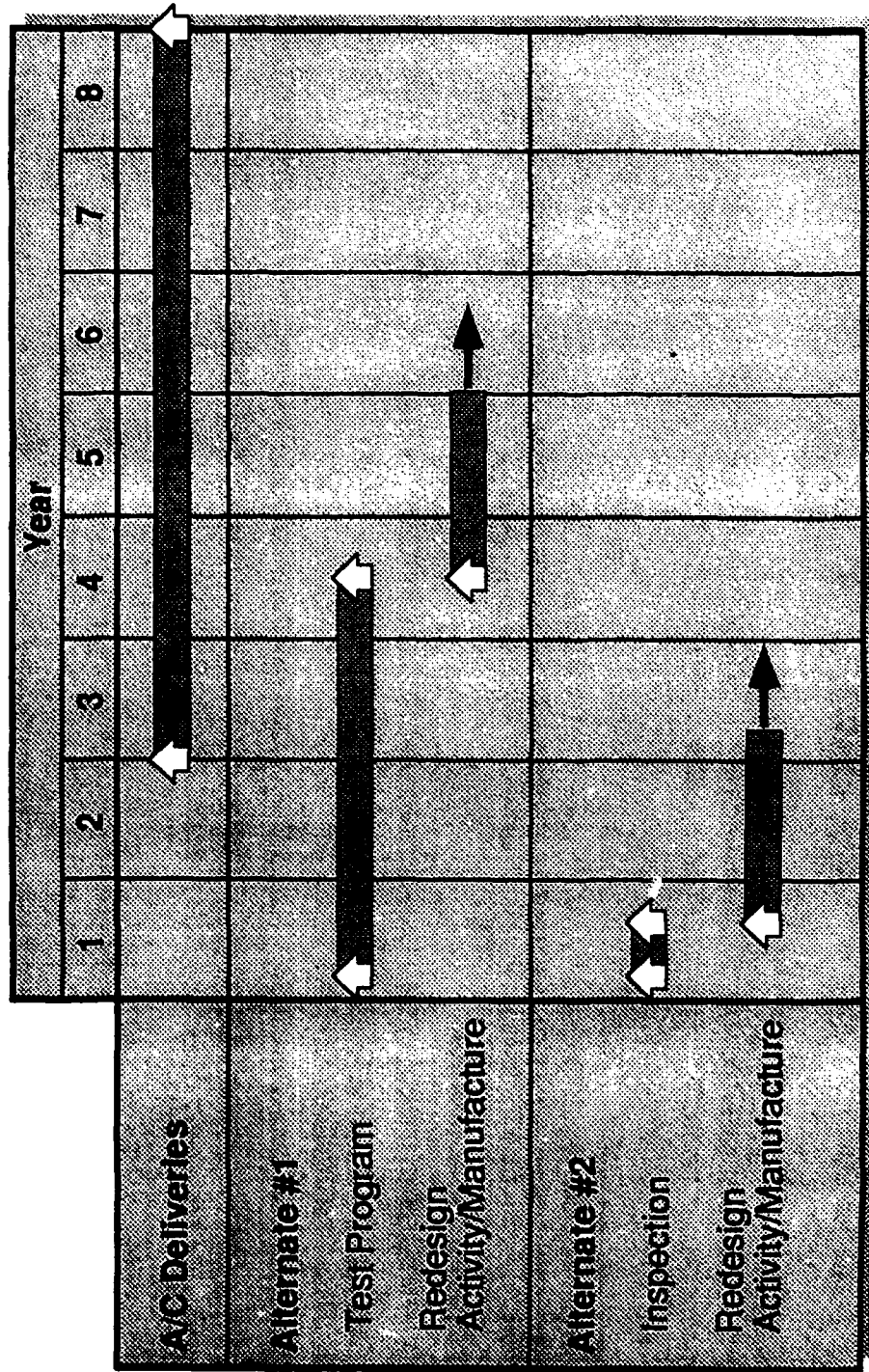
SCHEDULE BENEFITS

It is also estimated that under the test program the result from the full scale fatigue test would not be available for 4 years after the start date. Aircraft deliveries would start after the second year of an 8 year program. If redesign of the structure in question is necessary it is estimated that new structure for installation on aircraft would be available during the sixth year of the program. The aircraft which had been delivered during years 3, 4 and 5 would have to be brought back for further modification.

In the inspection option, all the inspections are completed during the first year and the decision whether to redesign is made at this time. During this first year, flight test data on the environment is gathered to assist in the redesign decision. The redesigned structure, if necessary, would be available during year 3 of the program, shortly after aircraft deliveries started. A small number of aircraft would have to be brought back. This is a more desirable situation.

Similar benefits are possible in a new aircraft production program by limiting the scope of the full scale fatigue test to those environments which are readily identified. The purpose of the full scale fatigue test is then to verify the overall adequacy of the airframe. An inspection program is implemented to identify fatigue hot-spots resulting from unanticipated environments. Modifications to the aircraft can then be implemented early in the life of the program.

Schedule Benefits



SUMMARY

A technique has been proposed for developing an aircraft fleet inspection program to protect the aircraft against fatigue failures resulting from unanticipated use and environments. Probability distributions from coupon fatigue test data are used to estimate the risk of cracks developing in the fleet. A phased-sampling inspection program is used to find the developing cracks. Upper 95% confidence bounds are used to optimize the number of aircraft inspected at each interval as well as to provide worst-case estimates for the number of aircraft in the fleet at risk of developing cracks.

The inspection plan was shown to have significant benefits in terms of cost and schedule for a life extension program. This approach could provide similar benefits for new aircraft.

This concept could be readily applied to Mechanical Equipment Systems and Avionics Systems. Damage Tolerance concepts could readily be integrated into this approach to improve Maintenance Programs.

Summary

- **An inspection plan for unanticipated environments and usage**
- **Basic fatigue data provide characteristic distributions**
- **Statistics and inspection results provide 95% confidence**
- **Decisions based on level of risk assessments**
- **Optimization of maintenance and repair phasing**
- **Cost and schedule benefits**

REFERENCES

1. Magnusen, P.E., Hinkle, A.J., and Bucci, R.J., "Methodology for the Assessment of Material Quality Effects on Airframe Fatigue Durability," Fatigue '90, July 15-20, 1990, Honolulu, Hawaii.
2. Natrella, M.G., Experimental Statistics, National Bureau of Standards Handbook 91, October 1966.

Case: 93-S-4200

Export Authority ITAR Exemption 125.4(b)(13) Applies

McDonnell Douglas Aerospace

PROBABILISTIC DESIGN SYSTEM DEVELOPMENT at PRATT and WHITNEY

**1993 USAF Structural
Integrity Program Conference**

**J. D. Adamson
Pratt and Whitney
Government Engines and Space Propulsion
November 30, 1993**



PROBABILISTIC DESIGN SYSTEM DEVELOPMENT at PRATT and WHITNEY
Probabilistic Design System (PDS)

Contract Awarded by WL/POTC - F33615-92-C-2219

United States Air Force Monitor:

Squadron Leader Chris Pomfret

Chris Lykins

Ted Fecke

The Focus of the P&W PDS Contract is to Develop the Tools for Probabilistic Design of Gas Turbine Disks

Six Program Phases - 5 Year Program

• **Data Acquisition**

• **Methods Development**

• **Validation**

• **Application**

• **Application Test**

• **Method Extension**

PROBABILISTIC DESIGN SYSTEM DEVELOPMENT at PRATT and WHITNEY

Probabilistic Design Determines Risk of Failure

	<u>DETERMINISTIC</u>	<u>PROBABILISTIC</u>
--	----------------------	----------------------

Input	Single Valued, Worst Case	Statistical Distribution
Output	Life/Margin	Probability of Failure
Risk Assessment	Not Possible	Built In
Conservatism	Usually Significant But Not Calculable	Calculable

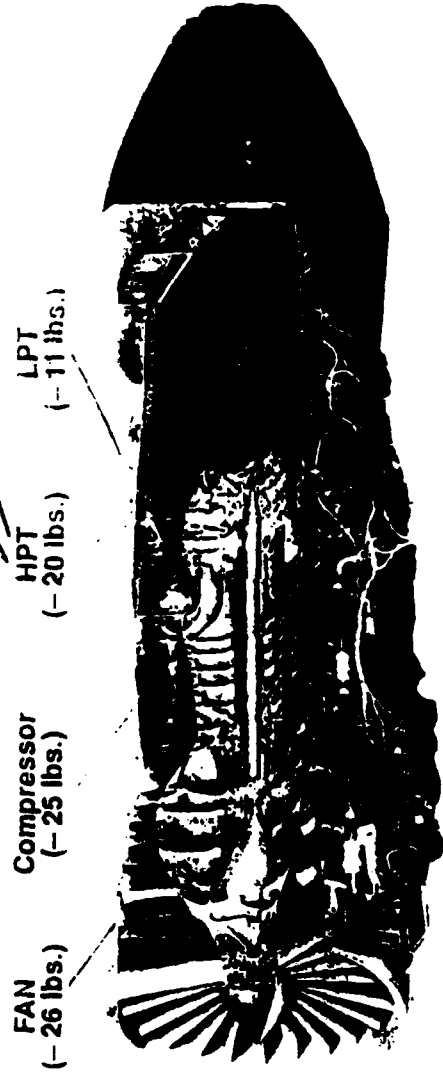
PROBABILISTIC DESIGN SYSTEM DEVELOPMENT at PRATT and WHITNEY

The Payoffs of the Probabilistic Design Process

The anticipated benefits that can be realized from the application of statistical methods to the gas turbine engine design process are:

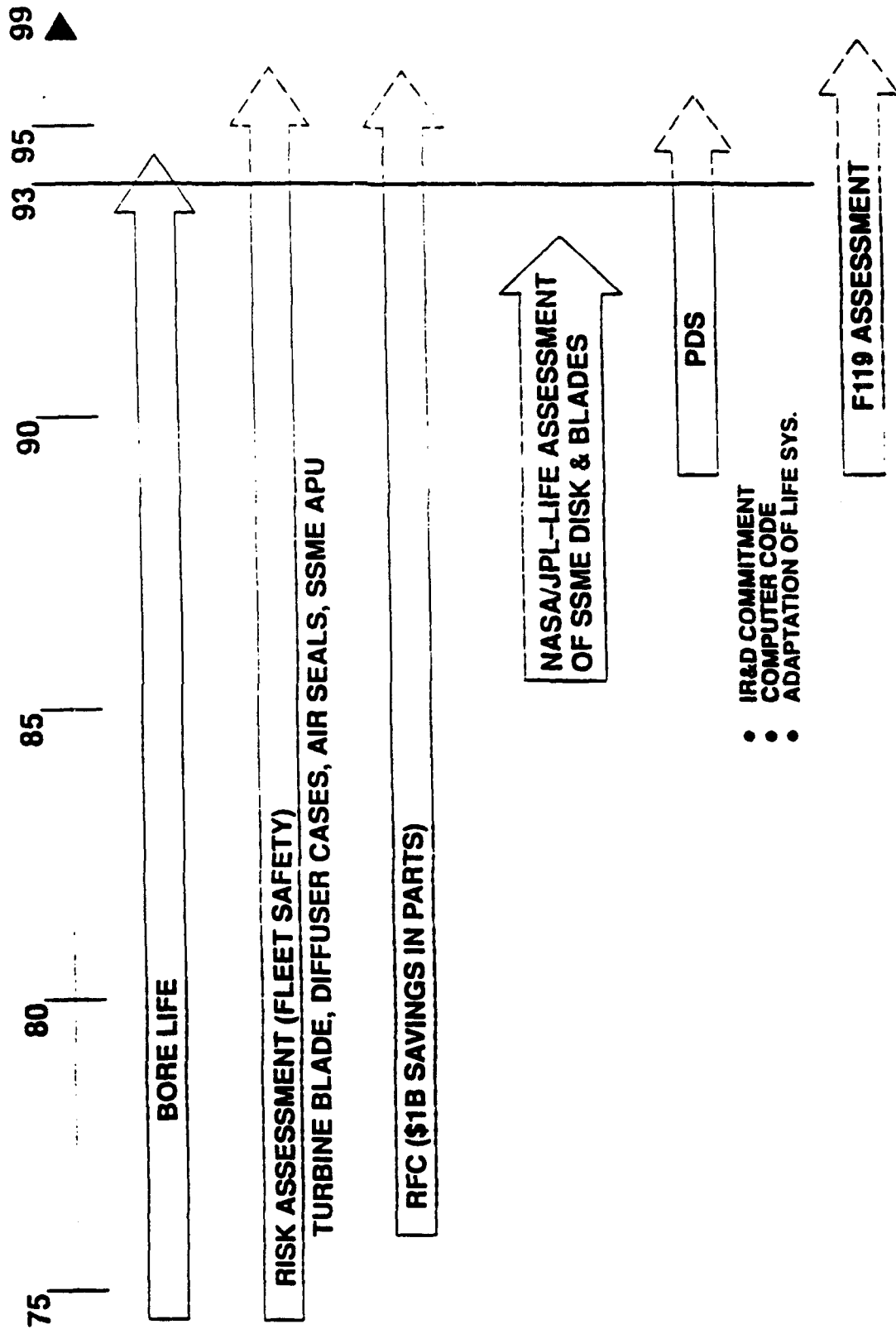
- Reduced Rotor Weight
- Increased Component Design Life
- Increased Rotor Speeds
- Quantified Risk for Components
- Evaluated Effects of Production and NDE Methods on Component Durability
- Establish Frame Work for Composite Life Systems
- Rapid Design Sensitivity/Parametric Analysis

Life Cycle Cost Savings \$69M



PROBABILISTIC DESIGN SYSTEM DEVELOPMENT at PRATT and WHITNEY

P&W has Extensive Experience with Probabilistic Methods



- IR&D COMMITMENT
- COMPUTER CODE
- ADAPTATION OF LIFE SYS.

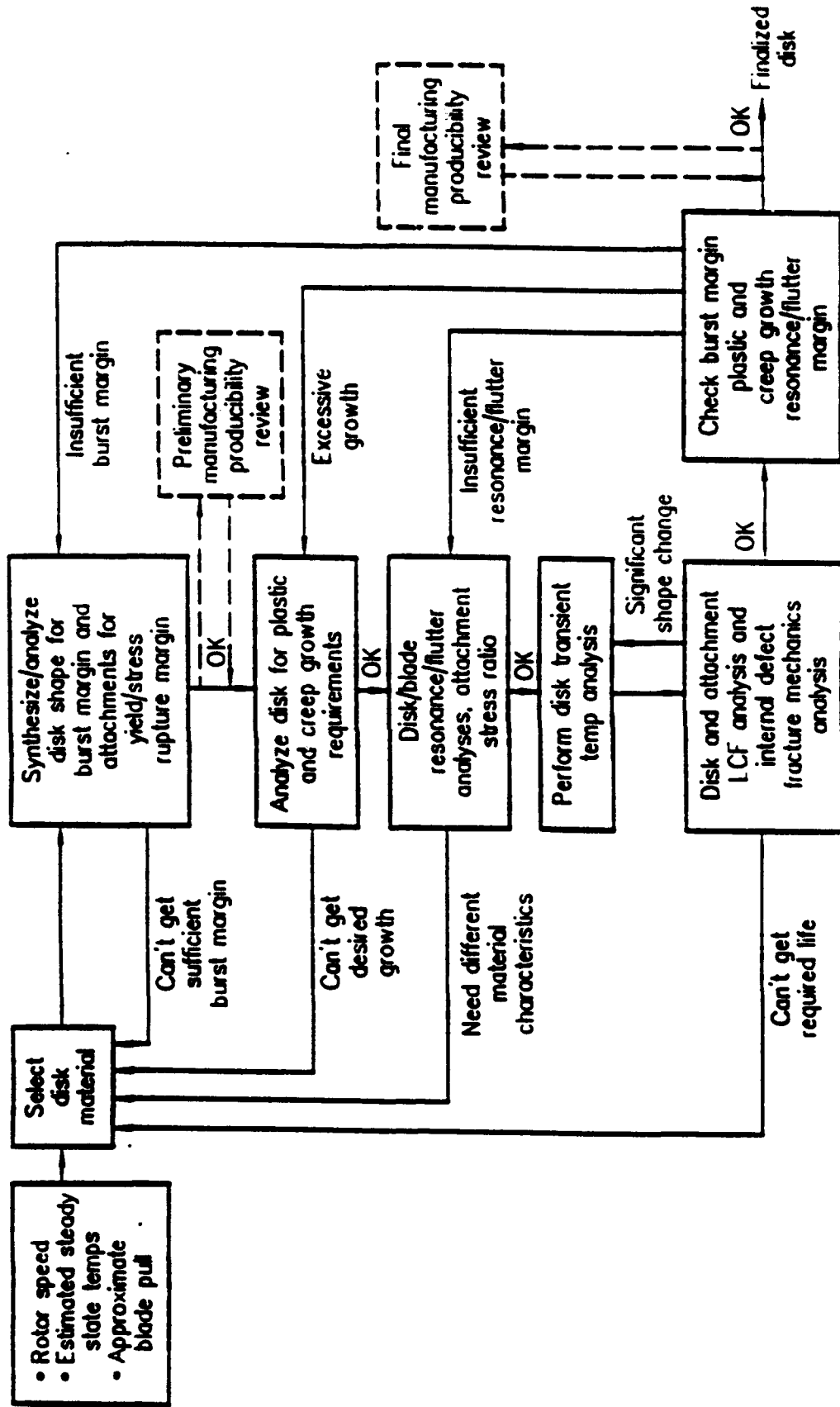
PROBABILISTIC DESIGN SYSTEM DEVELOPMENT at PRATT and WHITNEY

Elements of Constructing a PDS

- 1. Establish the process, design drivers, and failure modes**
- 2. Acquire data (field, laboratory, manufacturing, etc.)**
- 3. Establish distributions for design inputs**
- 4. Modify design criteria for probabilistic process**
- 5. Determine how to combine failure modes**
- 6. Develop "Appropriate Risk" criteria**
- 7. Develop probabilistic computer methods**
- 8. Validate design system**
- 9. Evaluate probabilistic design system potential by redesigning components**

PROBABILISTIC DESIGN SYSTEM DEVELOPMENT at PRATT and WHITNEY

Establish the Design Process, Drivers, and Significant Failure Modes

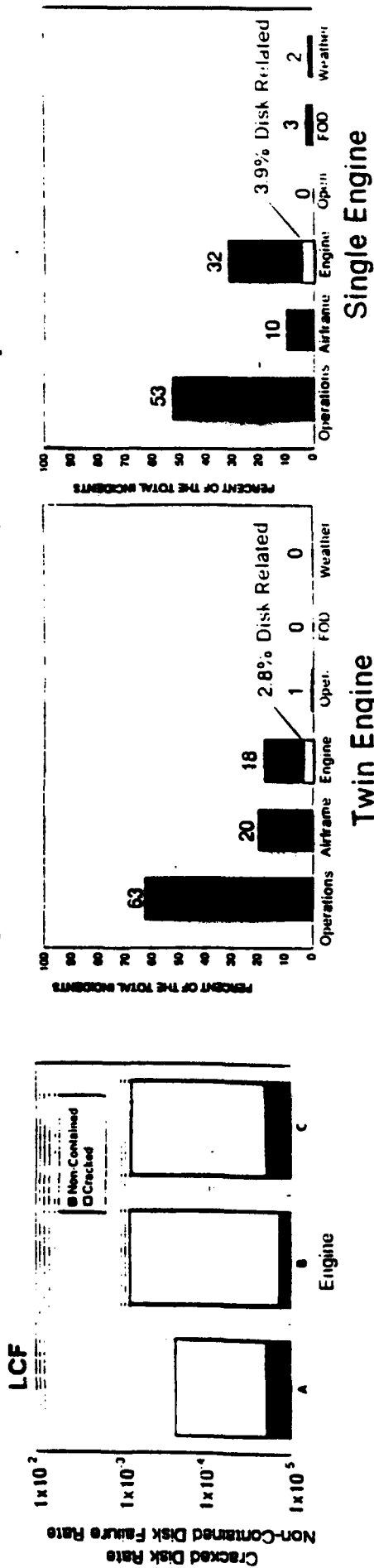


Deterministic Disk Design Process

PROBABILISTIC DESIGN SYSTEM DEVELOPMENT at PRATT and WHITNEY

Data Acquisition

- Sources: Manufacturing, laboratory data, Air Force records, failure reports



104

- How Good are Deterministic Systems

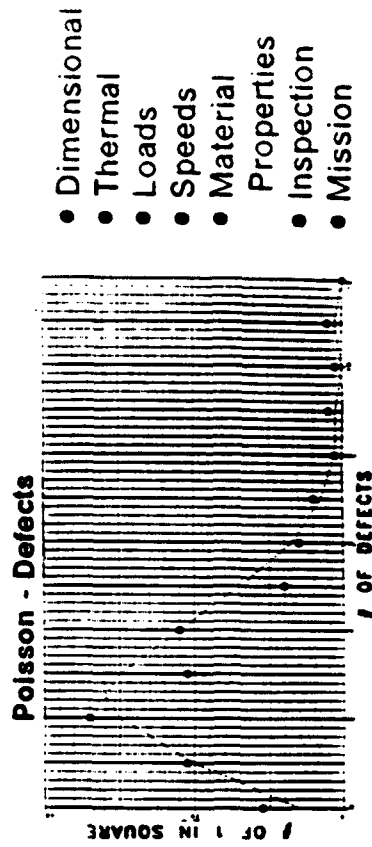
- Establish Appropriate Risk

HPC Inspection Rejection Rates vs. Probabilistic Predictions

DISK STAGE	PREDICTED % REJECT RATE	NUMBER INSPECTED	NUMBER REJECTED	ACTUAL % REJECT RATE
4th	0.8-5.0	687	21	3.1
5th	3.5	763	21	2.8
7th	11.8	736	88	12.1
8th	2.9	736	20	2.7
9th	11.4-16.0	841	91	10.8
10th	2.0	871	19	2.2
11th	4.2-10.8	678	51	7.5
12th	7.8	1005	48	4.8
13th	12.3-20.7	987	120	12.4
Aggregate	6.7-9.7	7094	460	6.5

- Validation

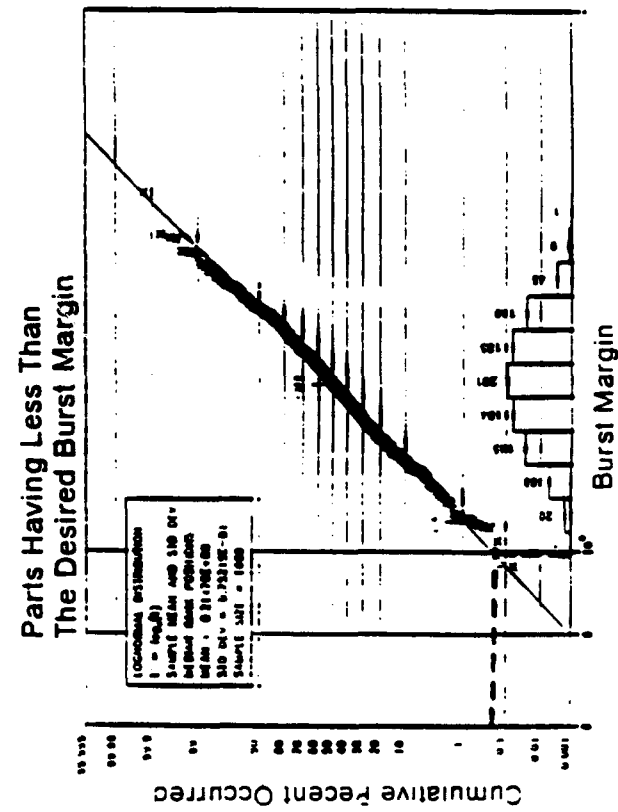
- Establish - Distribution for Important Life Drivers



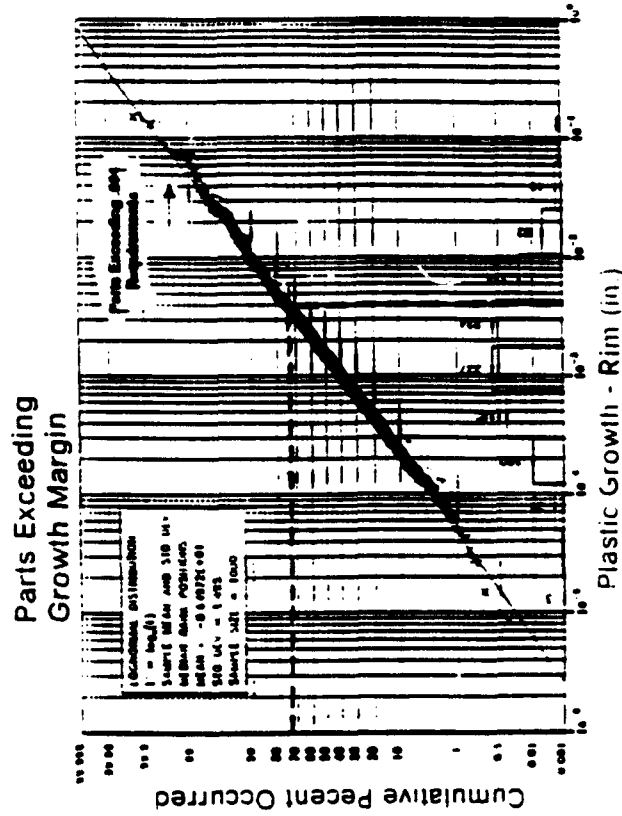
PROBABILISTIC DESIGN SYSTEM DEVELOPMENT at PRATT and WHITNEY

Design Criteria - Criteria Must Be Modified to Reflect Distributional Approach to Probabilistic Analysis

- Burst
 - Growth
 - Yield
 - LCF
 - Fracture Mechanics - Surface
 - Fracture Mechanics - Buried
 - Creep
 - HCF
- Based on existing criteria/design experience
 - Field experience



Probabilistic = 0.2%
Deterministic = 1.2

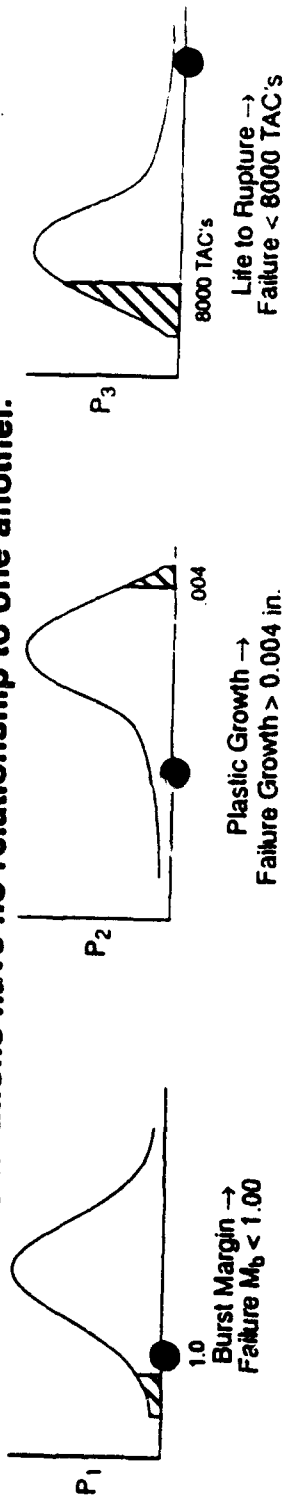


Probabilistic = 28%
Deterministic
Growth \leq 0.004 in

PROBABILISTIC DESIGN SYSTEM DEVELOPMENT at PRATT and WHITNEY

Accumulating Risk From Failure Modes - What is the Best Method? Are Distributions Related or is Random Sampling Best?

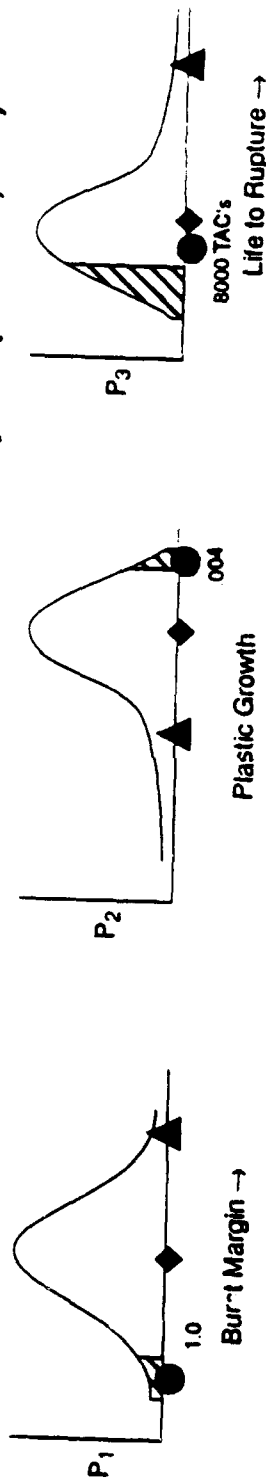
- Un-correlated - Distributions have no relationship to one another.



$$\text{Probability of Failure} = 1 - P \text{ (no failure)}$$

$$= 1 - (1 - P_1)(1 - P_2)(1 - P_3) \dots (1 - P_n)$$

- Correlated - Distributions are related through (speed, geometry, temperature, etc.)



CASE 1 ● 2 "Failures" - failures
 CASE 2 ▲ 0 "Failures" - no failures
 CASE 3 ◆ 0 "Failures" - no failures
 ⋮
 CASE n ⋮ ⋮ ⋮ ⋮

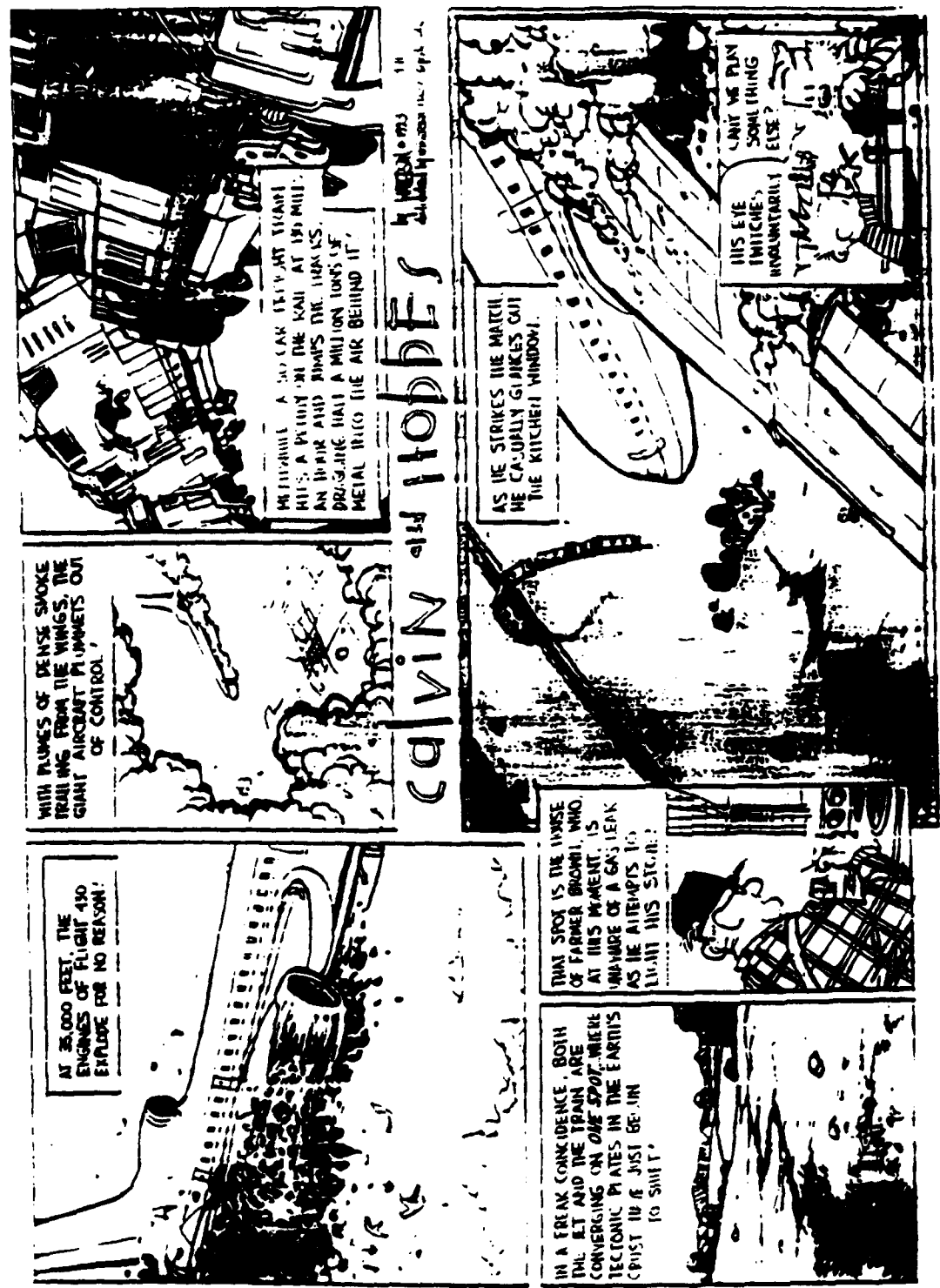
Total number of Failures

$$\text{Probability of Failure} = \frac{\text{Total Failure}}{n}$$

- P&W recommends considering correlation when accumulating risk.

PROBABILISTIC DESIGN SYSTEM DEVELOPMENT at PRATT and WHITNEY

What is Appropriate Risk?



PROBABILISTIC DESIGN SYSTEM DEVELOPMENT at PRATT and WHITNEY

- Probabilistic Analysis will Design Based on Risk of Rupture
- Appropriate Risk - Historically Based and Anchored by Everyday Risk Levels and Existing Specifications

SPEC.'S

- ENSIP 1783 -- $1/10,000$ DISKS
- AFGS - 87221A - 1×10^{-7} occur / flight

108

HISTORY

Disk Non - Containment Rates

Category	C	A	B	Average
By engine	3.4×10^{-3}	3.7×10^{-3}	2.4×10^{-3}	3.4×10^{-3}
By disk	2.0×10^{-4}	2.1×10^{-4}	1.1×10^{-4}	1.9×10^{-4}
By hour	2.1×10^{-6}	1.2×10^{-6}	7.0×10^{-6}	1.4×10^{-7}
By cycle	1.1×10^{-6}	1.4×10^{-6}	2.8×10^{-7}	2.0×10^{-7}

EVERYDAY RISKS

Cause	Mortality Rate per 100,000 population	
	25-44 year Males	Total Population
All Causes	243.1	882
Accident/Public (All Causes)	56.0	39.5
Motor Vehicle	31.8	20.0
Poisoning	6.7	2.2
Drowning	3.5	2.0
Falls	2.3	4.9
Fire and Burns	1.8	2.0
Air transport (1990/Commercial general aviation, military)	0.4*	0.3
Water transport (1990)	0.3*	0.3
Railroads (1990)	0.3*	0.2
Cancer	24.1	187.3
Heart Disease	29.4	311.3

* - include male and female

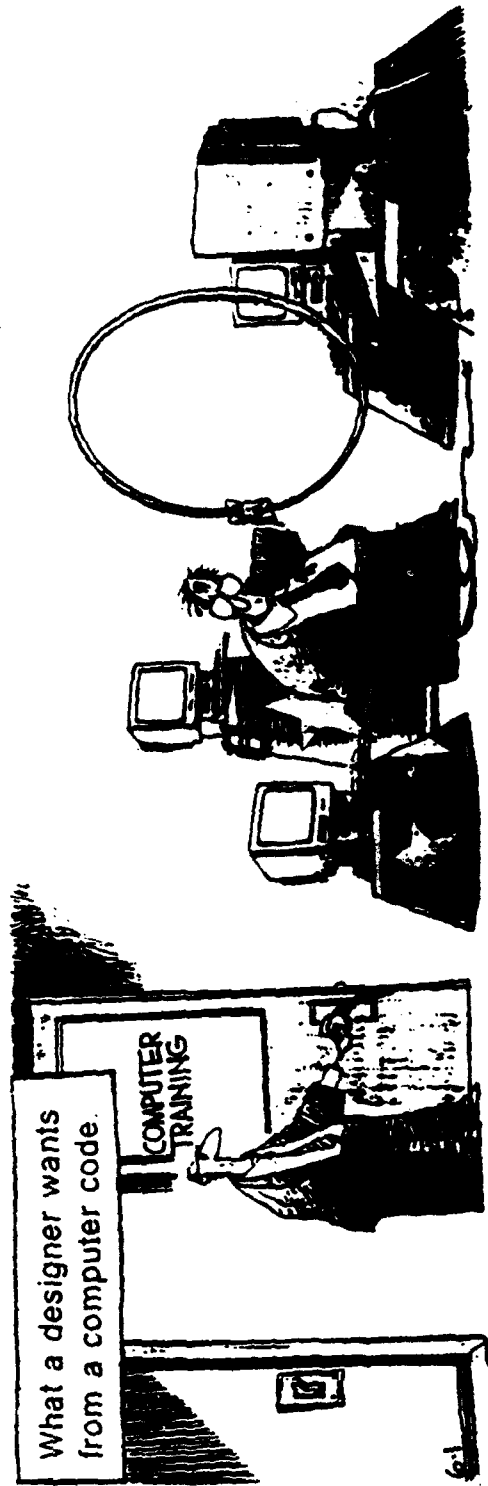
PDS Appropriate Risk Levels for Non-contained Disks

Category	Appropriate Risk Level
By engine	3.4×10^{-3}
By disk	1.9×10^{-4}
By hour	1.4×10^{-7}
By cycle	2.0×10^{-7}

PROBABILISTIC DESIGN SYSTEM DEVELOPMENT at PRATT and WHITNEY

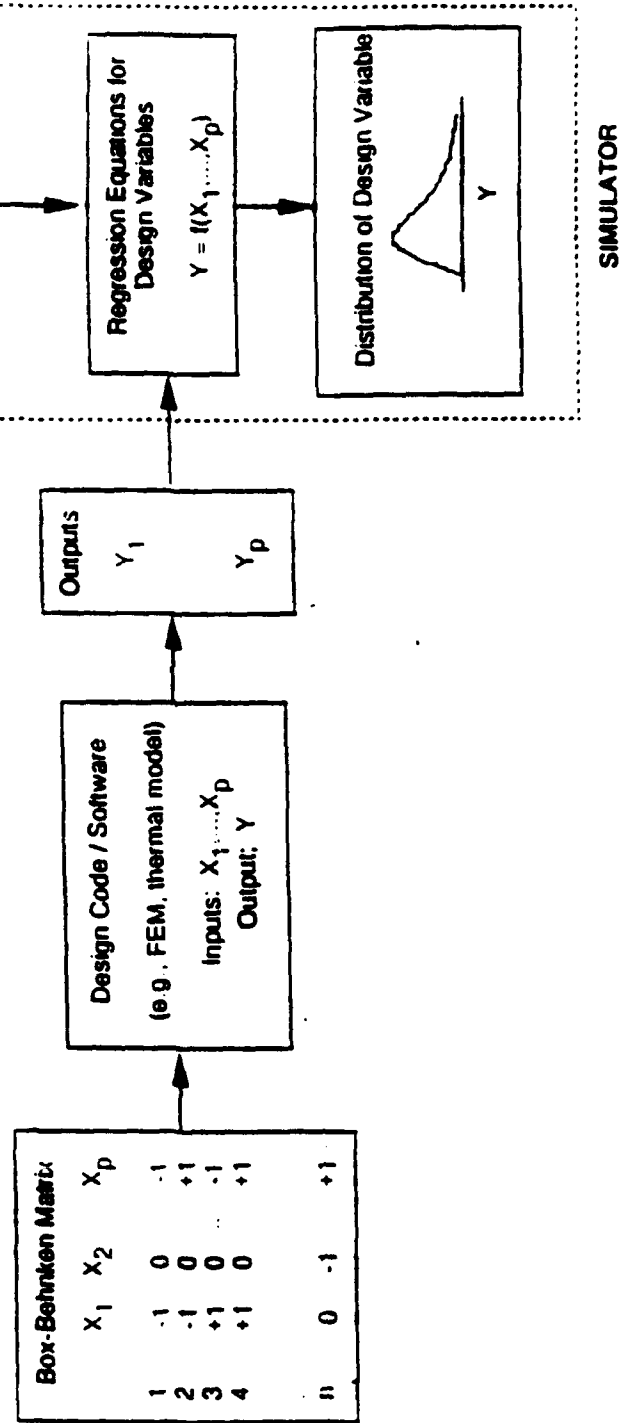
Probabilistic Design System (PDS) - Computer Code

- Based on common codes the designer is use to using
- Easy to use
 - Graphic user interface/panel driven approach
 - Property and distributional description readily available
 - Flexible graphics capability
- Speedy to use
- Distributed network operating system
- Ideal for parametric and sensitivity studies



PROBABILISTIC DESIGN SYSTEM DEVELOPMENT at PRATT and WHITNEY

Use of Regression Equation in Probabilistic Design System (PDS) Simulator



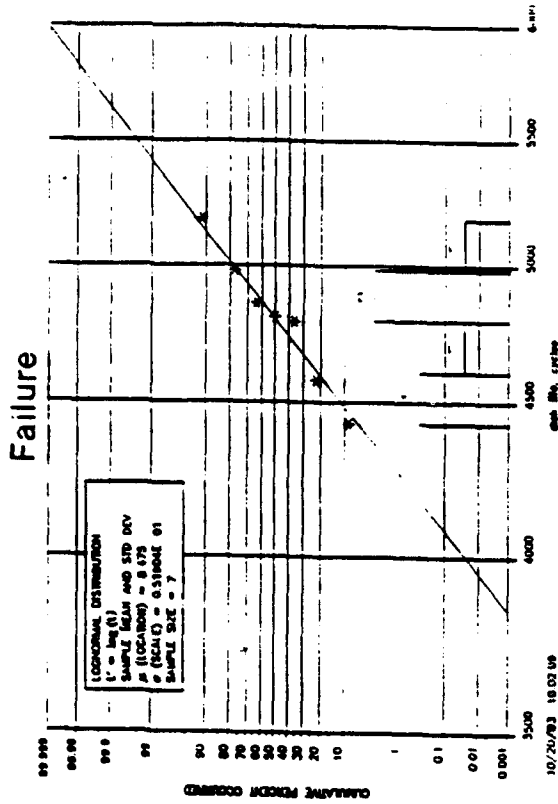
Structure of Probabilistic Design System Simulator

PROBABILISTIC DESIGN SYSTEM DEVELOPED AT PRATT and WHITNEY

Validation Procedures Being Employed to Calibrate PDS

DISK STAGE	PREDICTED % REJECT RATE	NUMBER INSPECTED	NUMBER REJECTED	ACTUAL % REJECT RATE
4th	0.8-5.0	687	21	3.1
5th	3.5	763	21	2.8
7th	11.8	736	89	12.1
8th	2.9	738	20	2.7
9th	11.4-18.0	841	91	10.8
10th	2.0	671	19	2.8
11th	4.2-10.8	678	51	7.5
12th	7.8	1003	46	4.8
13th	12.3-20.7	967	120	12.4
Aggregate	6.7-9.7	7084	480	6.8

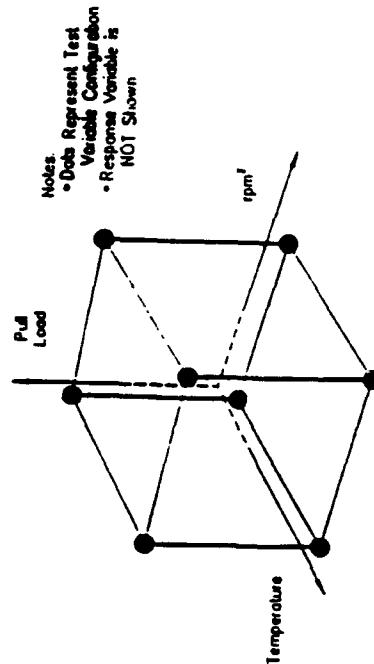
Inspection/Rejection Records



Field Incidents

2³ Actual Test Matrix

Run No	Temperature	Load	RPM?
1	Low	Low	Low
2	Low	Low	High
3	Low	High	Low
4	Low	High	High
5	High	Low	Low
6	High	Low	High
7	High	High	Low
8	High	High	High



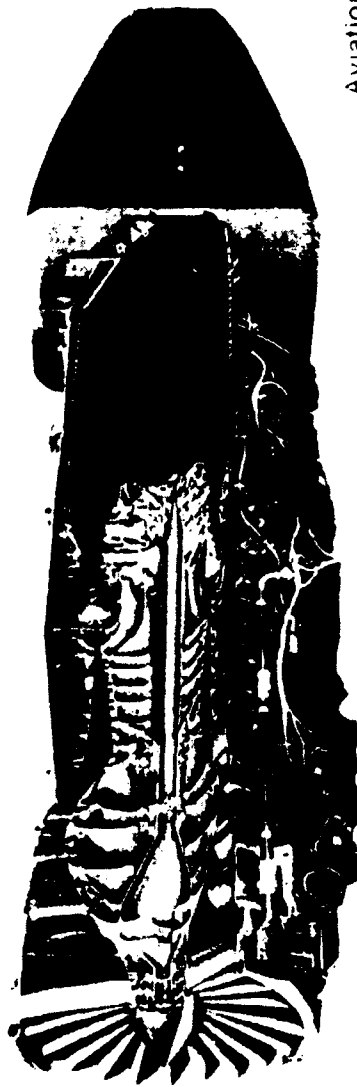
Subscale Rotor Testing

JDA
428W13

PROBABILISTIC DESIGN SYSTEM DEVELOPMENT at PRATT and WHITNEY

Evaluation

- An F119 fan, compressor and turbine stage will be redesigned with probabilistic methods to assess weight savings
- A turbine disk will then be fabricated and tested in ATEGG XTC-66/SC



Aviation Week and Space Technology
August 2, 1993, p.26

F119

PROBABILISTIC DESIGN SYSTEM DEVELOPMENT at PRATT and WHITNEY

Probabilistic Design has Yet to be Embraced by the Industry or Government as a Replacement for Deterministic Design

- **Recommendations:**
 - **Strong participation in the SAE G-11 committee is recommended to develop standards for probabilistic design for both industry and government use.**
 - **More comparisons/experience should be gained with competing probabilistic design systems**
 - **Air Force/P&W/NASA-LeRC/Navy - subscale rotor test program**
 - **Mil-STD-1783 should be modified to include probabilistic design method**

PROBABILISTIC DESIGN SYSTEM DEVELOPMENT at PRATT and WHITNEY

Summary

- 1. The payoffs of the Probabilistic Design Process include reduced weight, reduced inspection requirements, and increased component life through reduced design system conservatism.**
- 2. Probabilistic design methods developed at P&W are based on long experience with probabilistic analysis and risk assessment techniques.**
- 3. A methodical process has been followed to produce the P&W PDS process which could be used by others to develop similar systems.**
- 4. Government and industry need to establish standards for probabilistic design systems.**

THE COST EFFECTIVENESS OF
AIRCRAFT STRUCTURAL INTEGRITY PROGRAMS

Captain A.J.A. Appels
CF-18 Aircraft Structures Engineer
Directorate of Aerospace Support Engineering
National Defence Headquarters,
Ottawa, Canada
November, 1993

1.0 BACKGROUND

The effectiveness of a military force depends in part on the operational readiness of its weapon systems. Similarly, the operational readiness of an airborne weapon system is largely dependant on the condition of the airframe structure. In order to minimize any adverse impact on airworthiness and operational readiness, potential structural and/or material problems must be identified and addressed early in the life cycle of the aircraft.

The Aircraft Structural Integrity Program (ASIP) is the mechanism by which the Canadian Forces (CF) ensure the structural airworthiness of its aircraft fleets. The objective of this paper is to discuss the ASIP philosophy in the context of CF operations and assess the impact of the ASIP on airworthiness, operational readiness, and operations and maintenance (O&M) costs. In light of the continuing climate of fiscal restraint, particular emphasis is given to characterizing the ASIP as a tool for controlling the life cycle costs of military aircraft fleets.

2.0 ASIP REQUIREMENTS AND OBJECTIVES

2.1 General Philosophy and Objectives

The Aircraft Structural Integrity Program is the engineering vehicle by which the structural integrity of CF aircraft fleets are assured and forms an integral part of our airworthiness policy^[1,17]. In general terms the ASIP can be defined as the proper definition, integration, and scheduling of engineering, maintenance, and logistics activities necessary to ensure that the risk of catastrophic structural failure due to accidental damage, corrosion, fatigue, wear, or other structural/material degradation is maintained at an acceptable level throughout the operational life of the aircraft.

The basic objectives which evolve from this definition are as follows:

- a. to establish, evaluate, and substantiate the structural integrity (airframe strength, rigidity, damage tolerance, and durability) of the aircraft structure;
- b. to acquire, evaluate, and utilize operational usage and structural condition monitoring data to provide an ongoing assessment of in-service structural integrity;
- c. to provide a basis for determining logistics and planning requirements for airframe maintenance activities (inspections, modifications, spares, repair and overhaul (R&O), equipment rotation, and system phase-out);
- d. to provide a basis for determining the engineering, logistics, modification, and maintenance requirements to facilitate service life extensions; and
- e. to provide feedback regarding structural problems, operational usage, maintenance, and logistics to improve structural design/evaluation criteria for future aircraft.

2.2 General ASIP Requirements

The philosophy which evolves from the basic ASIP objectives follows a cradle-to-grave approach starting from conceptual design to fleet retirement (Figure 1). The ASIP encompasses a very broad range of engineering, maintenance, and logistics activities throughout the entire life cycle, and these activities can be grouped into five distinct and interrelated functional tasks:

- a. Task I - Design Information
- b. Task II - Design Analysis and Development Tests
- c. Task III - Full Scale Certification Testing
- d. Task IV - In-Service Usage Data Management
- e. Task V - In-Service Management.

The implementation of specific elements and activities associated with each of these tasks (Figure 2) is governed by the ASIP Master Plan which defines the engineering activities required to satisfy general ASIP objectives for each aircraft fleet. The end product of the ASIP is the Force Structural Maintenance Plan (FSMP). This is a dynamic plan which continually integrates design and certification data with in-service usage and structural condition monitoring data to define and rationalize fleet structural maintenance requirements. For the purposes of this paper we will consider ASIP as a "black box" process which addresses these general areas of concern.

2.3 Structural Maintenance Costs and ASIP

While cost effectiveness is not a stated ASIP requirement, the program can prove to be a very effective means to control airframe support costs. As shown by Figures 3 and 4, maintenance, engineering, and logistics costs related to airframe structural integrity can constitute over 20% of the total life cycle costs for a fighter aircraft¹, which is typically comparable to the original aircraft procurement cost. It is obvious that even a marginal reduction in recurring structural maintenance and post-production modification/repair requirements can yield substantial savings over the life cycle of a weapon system.

The opportunities to optimize structural efficiency and hence reduce the total life cycle costs are obviously maximized early in the development of an aircraft (Figure 5). The use of post-production modifications to rectify structural deficiencies generally proves to be very inefficient and costly for the following reasons:

- a. the design of modifications is physically restricted by the configuration of surrounding structure, hence there is very little design flexibility. In some cases retrofit may not be practical or feasible, and component replacement is the only viable alternative;
- b. limited physical access can make modification embodiment difficult and expensive;

1. 60% of total life cycle costs due to maintenance, engineering and logistics support, with 30% of this cost directly attributable to the airframe structure.

- c. the incorporation of post-production modifications generally results in an increase in airframe weight with possible CG problems and operational performance penalties; and
- d. the design, fabrication, and embodiment costs for modification kits are a substantial incremental cost not normally included in weapon system procurement and O&M estimates.

In the operational context, ASIP must also maintain the delicate balance between safety and operational demands and can be viewed as the balance point of a "cost fulcrum" (Figure 6). To illustrate this point, consider the implications of a significant change in the operational role of a fighter aircraft. While the ASIP engineering effort required to modify and validate structural maintenance plans in light of new operational usage can be seen as a direct cost, an effective ASIP can rationalize necessary changes to the FSMP so as to minimize adverse impact on total life cycle costs. As will be demonstrated by subsequent case studies, the net savings can be substantial.

2.4 ASIP - The Cost of Failure

While the objective of this paper is to characterize the ASIP as a potential tool for controlling the life cycle costs, the true cost effectiveness of an ASIP cannot be based solely on its impact on incremental life cycle costs. It must take into account the inherent value associated with ensuring the structural airworthiness of the fleet, which is the primary objective of the program. The impact of failing to meet this objective is very difficult to quantify as it encompasses economic, operational, and human "costs", many of which are largely subjective in nature:

- a. potential loss of life (both aircrew and persons on the ground);
- b. direct economic costs associated with a major in-service structural failure, specifically:
 - (1) the cost of the flight safety investigation;
 - (2) the cost to clean-up the crash site and dispose of explosive and/or hazardous materials;
 - (3) the potential cost of litigation due to secondary injury, death, and property damage;
 - (4) the value of the lost aircraft.

- c. adverse impact on continued weapon system operations due to reactive groundings, subsequent inspections, mods, and repairs, and possible loss of operator confidence in the airworthiness of the aircraft.

3.0 ASIP IN THE CANADIAN CONTEXT

To maximize its effectiveness the ASIP must be implemented as an integral part of the development, acquisition, and operation of an aircraft weapon system, and priority must be given to the early identification and resolution of potential structural problems. Due primarily to political considerations discussed below, Canadian Forces implementation of ASIP requirements is generally restricted to Tasks III, IV, and V.

3.1 Off-The-Shelf Procurement

The Canadian tendency to make "off-the-shelf" procurements generally precludes the definition and implementation of unique ASIP requirements until well after the aircraft is in production. In fact, most CF ASIPs are not rigorously implemented until after initial aircraft delivery and typically do not give adequate emphasis to the integration of ASIP requirements into the evaluation, selection, and procurement process. Given the typical "budget squeezing" associated with major equipment acquisitions, long-term engineering requirements (such as those arising from the ASIP) are often deferred or eliminated in order to control initial capital expenditures. As a result, the benefits of early identification and rectification of potential structural problems are never fully realized. However, the subsequent impact on life cycle costs can be substantially greater than any short term savings realized, particularly as structural O&M costs over the life cycle can be comparable to the initial procurement costs.

A case in point is the issue of the early production CF-18 Hornet aircraft. Eleven aircraft with a structurally deficient centre fuselage configuration were delivered to the CF, and these aircraft currently have a safe operating service life only half that of the remainder of the fleet⁽¹¹⁾. This shortfall constitutes a capital cost of \$190M to the CF, a cost which could have been minimized or even avoided had the engineering concerns related to these early structural configurations been identified and addressed earlier in the procurement process.

3.2 Mission Profile Variations and Role Changes

The CF have historically been forced to employ aircraft in a multi-role capacity or in an unconventional operational environment which is inconsistent with the original procurement and/or design specifications. Specific cases which merit consideration include:

- a. conversion of the CF-104 Starfighter from a tactical nuclear strike role to a conventional air-ground role;
- b. increased emphasis on aerobatic training using the CT-134 (Beech) Musketeer;
- c. use of the CT-114 Tutor jet trainer in the dedicated air demonstration role (431 Squadron Snowbirds);
- d. increased use of the CC-130 Hercules for low level tactical transport;
- e. use of the CC-144 Challenger in the Electronic Warfare Training (EWT) and coastal patrol roles; and
- f. unexpectedly severe early usage of the CF-18 Hornet.

All of these examples constitute aircraft usage of a nature and/or severity not envisaged by the designers or defined in the procurement specifications and will have an obvious impact on structural maintenance requirements. Any subsequent rationalization of the FSMP must be based on a logical analysis of changes to the Baseline Operational Spectrum (BOS), which can only be accurately quantified through a Loads/Environment Spectra Survey (LESS) or by analysis of detailed Individual Aircraft Tracking (IAT) data.

3.3 Service Life Requirements

In light of past and present budget constraints, it is safe to say that the CF history of extending the service lives of military aircraft will continue into the foreseeable future. The estimated life expectancy (ELE) of the CF-116 Freedom Fighter has recently been extended from 1995 to 2005 (with the possibility of further extensions), and the ELE of the CT-114 Tutor has been extended to 2005. It is also anticipated that the ELE of the CF-18 Hornet will be extended from 2003 to 2010 based on the results of an aggressive Fatigue Life Management Program (FLMP), full scale Durability and Damage Tolerance Testing (DADTT), and an extensive avionics update being implemented by the CF.

4.0 CF-18 HORNET ASIP - COST/BENEFIT CASE STUDY

4.1 General

The CF-18 Hornet is Canada's primary fighter aircraft and is employed in both the air-air and air-ground roles by the Canadian Forces. The CF purchased 138 CF-18 aircraft with initial deliveries starting in the fall of 1982, initial operational capability established in early 1984, and a projected operational ELE of 2003. In light of the tremendous costs associated with operating fighter aircraft² and ongoing pressures to defer the replacement of major weapon systems, it is anticipated that efforts will be made to sustain CF-18 operations out to 2010 (Section 3.3 refers).

4.2 CF-18 Structural Integrity Costs

Figure 9 details the estimated costs (non-recurring and recurring) for CF-18 ASIP engineering activities and provide a projected total cost of \$115M over the service life of the fleet. While this undoubtedly a significant sum, it must be viewed in the context of total life cycle costs. Based on departmental cost projections (Figures 10 and 11), the cost of ASIP core engineering activities represents less than 1% of the projected \$13.4B life cycle cost of the fleet. In contrast it is projected that total maintenance/engineering/logistics costs related to airframe structural integrity could cost in excess of \$2.5B over the full life cycle, representing almost 19% of the total projected life cycle costs of the fleet.

4.3 CF-18 ASIP Benefits

The specifics of CF-18 ASIP⁽⁷⁾ are beyond the scope of this paper, however a listing of selected engineering activities is provided at Figure 7 to give the reader a sense of the scope of this program. Despite the fact that the CF-18 ASIP was implemented as a post procurement engineering activity and is subject to the limitations discussed in Section 3, it has proven to be very effective. Specific benefits include the following:

-
2. CF-18 operating, engineering, maintenance, and logistics costs were \$316M for fiscal year 92/93 and constituted 25% of all expenditures in support of Air Command Operations. Combined fighter ops (CF-5 and CF-18) represented 30% of total air operations expenditures.

- a. Sustained Fleet Airworthiness. Fleet airworthiness is the primary objective of the CF-18 ASIP, and its value cannot be understated. As discussed in Section 2.4, the costs (both tangible and intangible) associated with a catastrophic in-service structural failure can be substantial, and far outweigh the projected \$115M investment in ASIP;
- b. Proactive Structural Maintenance. Through the effective use of IAT data, structural test data, aircraft sampling inspections, in-service failure data, and engineering analyses, CF-18 structural maintenance activities are becoming much less reactive. This yields obvious (though largely unquantifiable) benefits related to recurring O&M costs and aircraft availability;
- c. Rationalized Logistics. As a result of the recent Landing Gear Sampling Inspection and the reassessment of MLG fatigue lives using the CF-18 BOS, it will be possible to re-assess the service lives of landing gear components and set up a rationalized depot level R&O program;
- d. Enhanced Operational Flexibility. The ASIP provides valuable engineering data/tools which have greatly increased operational flexibility through:
 - 1) rationalization of airframe bulletins and special inspections based on unique CF operations and requirements;
 - 2) rationalization of modifications proposed by the Original Equipment Manufacturer (OEM) based on unique CF operations and requirements;
 - 3) development of CF unique modifications and repairs independent of the OEM.
- e. Individual Aircraft Tracking (IAT) Capabilities. The CF-18 IAT capabilities facilitate a number of important fleet management activities including the Fatigue Life Management Program, optimized modification/inspection scheduling, and BOS development/validation; and
- f. Risk Management Capabilities. ASIP provides the necessary tools for the fleet manager to make informed risk management decisions.

In addition to the obvious benefits detailed above, the CF-18 ASIP is also proving to be a very effective tool for controlling and reducing overall O&M costs. The following sections of this paper provide a cost-benefit assessment for selected CF-18 ASIP activities based on Department of National Defence financial data^(8,9,10) using the governing assumptions detailed in Figure 8.

4.4 CF-18 Fatigue Life Management Program (FLMP)

4.4.1 Background

Analysis of CF-18 usage data in 1987 indicated that the fleet was being operated in a much more severe manner³ than was originally accounted for during design and certification testing (Figure 12). Fleet attrition projections indicated that the ELE of 2003 could not be met, and that a credible operational capability could not be maintained beyond 1998. To address this problem an aggressive Fatigue Life Management Program (FLMP) was implemented with the objective of controlling and tailoring aircraft usage such that the economic life of the fleet could be maximized while satisfying training objectives and maintaining full operational effectiveness.

4.4.2 The Elements of Fatigue Life Management

The CF-18 FLMP consists of three fundamental elements: fatigue awareness training, usage characterization, and guidance and control⁽⁶⁾:

- a. Fatigue Awareness Training. The objective of fatigue awareness training is to provide aircrew and maintenance personnel with a basic understanding of the causes and consequences of fatigue and the steps that can be taken to minimize these consequences. Such training has been formalized as part of aircrew operational training and maintenance management training courses and is reinforced by annual status review briefings provided to all operational squadrons;

3. The 95th percentile fatigue rate anticipated by McAir was 0.167 WRFLE/1000 FH, while average CF-18A usage peaked at 0.181 in 1987.

b. Usage Characterization. Usage characterization consists of the gathering, processing, analysis, and interpretation of continuously monitored structural and flight parameters provided by the Maintenance Signal Data Recording System (MSDRS). Of primary interest are direct strain histories tracked at seven different airframe locations, with the critical location being the lower centre wing attachment lug (Figure 13). Using MSDRS data, Fatigue Life Expended (FLE) indices and usage rates are calculated for individual aircraft, and corresponding usage information is generated in a variety of formats, including:

- (1) usage rates by aircraft/squadron/wing/fleet,
- (2) usage rates by mission type,
- (3) usage rates by pilot, and
- (4) flight specific usage/tactical information.

Accurate and timely fleet and aircraft usage data provides the feedback essential to monitor fleet usage trends and assess the ongoing effectiveness of guidance and control measures; and

c. Guidance and Control. Control of fleet usage is exercised by the operational community based on IAT data provided through the ASIP. Typical control measures include the optimization/tailoring of mission profiles, control of aircraft external stores configurations, aircraft operational scheduling based on mission severities, rotation of aircraft between squadrons, and other discrete damage control measures detailed in Figure 14.

4.4.3 IAT System Technical Issues

Over the past 3 years, significant engineering efforts have been made to address documented technical problems with the F/A-18 IAT system^[15]. While it is beyond the scope of this paper to discuss the specifics of these issues, a brief summary is provided at Figure 15. Resolution of these problems is being addressed through an aggressive collaborative effort involving McDonnell Douglas Aerospace (MDA), the United States Navy (USN), the Canadian Forces (CF), and the Royal Australian Air Force (RAAF).

While substantial financial commitments have been made by the CF to address these problems⁴, tremendous progress has been made to correct system deficiencies and maximize the accuracy of IAT data. From the CF perspective, confidence in the IAT system as a fleet tracking tool is currently extremely high, and resolution of the remaining technical issues and reprocessing of historical IAT data should ensure the accuracy of individual aircraft fatigue status.

4.4.4 The Benefits of FLMP

The most obvious tangible benefit of FLMP has been a 42% reduction in the average fleet fatigue rate since the introduction of the FLMP in 1988 (Figure 12). Based on statistical attrition projections⁽⁴⁾, this fatigue rate reduction combined with a recent 20% reduction in the yearly flying rate (YFR) represents a 5 year increase in the sustainable ELE of the fleet. Engineering efforts to enhance the accuracy of IAT data will serve to further increase operator confidence in the FLMP and are expected to yield further improvements to the sustainable ELE of the fleet.

The projected total cost (non-recurring and recurring) of the CF-18 FLMP is estimated at \$14.8M, which represents an effective annual cost of \$550K (Figures 16 through 18). Based on the 5 year increase in the sustainable ELE of the fleet, the incremental life cycle costs of extended CF-18 operations have been compared to those associated with the premature procurement of a New Fighter Aircraft (NFA). The results of this assessment are summarized in Figure 19 and confirm the following:

- a. life cycle cost savings in excess of \$490M will be realized as a direct result of the FLMP. This represents a net reduction of 3.7% in the projected total life cycle costs to 2003; and
- b. a 5 year deferral of procurement activities for a replacement fighter infers significant capital cost avoidance in times of severe budgetary constraint as well as an indirect saving due to deferred interest payments on capital acquisitions accomplished through deficit financing.

4. CF expenditures to address IAT system technical concerns are expected to exceed \$1.9M by the end of fiscal year 95/96. This will include complete reprocessing of historical IAT data at a cost of \$800K.

In addition, the CF-18 IAT capability makes it possible to optimize modification embodiment times based on strain-based FLE indices, which despite documented technical limitations (Section 4.4.3) are considered to be a very accurate indicator of fatigue damage accumulation. A comparison to more conventional (and less accurate) NzW tracking⁽¹⁴⁾ yields the following:

- a. the current structural modification program has been forecast as a 10 year effort at an estimated cost of \$80M. Induction based on NzW tracking infers the requirement for an accelerated 7 year program to account for inherent conservatism and statistical uncertainty in NzW usage data (Figure 20); and
- b. while the overall cost of the modification effort is fixed, the strain-based IAT capability offers the opportunity to extend the time line which yields:
 - 1) a net reduction of \$3.4M in the annual O&M funding baseline due to extended cash phasing;
 - 2) an extended stable workload for the depot level contractor. This facilitates the establishment and maintenance of depot level cognisance and experience which is a tangible benefit to the CF.

4.5 Modification Rationalization

The CF-18 ASIP also provides the basis for rationalizing of OEM structural modifications based on unique CF operations and requirements. The following sections detail two such modification reviews which will yield substantial savings to the CF.

4.5.1 ECP 319/428 MLG Trunnion and Bulkhead Rework

Engineering Change Proposal (ECP) 319 is a McAir developed structural modification which addresses the depot level rework of fatigue critical areas on the main landing gear trunnions. ECP 428 is a related rework of the Y470 bulkhead at the trunnion attachment lug. The direct cost of these modifications to the CF has been estimated at \$2.4M. As these modifications are driven primarily by the severity of US Navy carrier operations, the CF requirement for embodiment is currently being reassessed based on a Canadian unique landing spectrum. The engineering costs associated with spectrum development are estimated at \$200K, yielding a net savings to DND of \$2.2M.

4.5.2 Y574 Former Modification/Repair

In-service inspections by the US Navy identified fatigue cracking in the speedbrake pocket of the Y574 former. The OEM recommended modification/repair involved the manufacture and installation of complex bathtub fittings (a depot level effort) at an estimated cost of \$22K per aircraft. Based on a CF evaluation of the problem a Canadian unique mod/repair was developed with an estimated embodiment cost of only \$4K per aircraft, resulting in a net saving of \$2.2M. In addition, the repair was within base level capabilities resulting in reduced Mobile Repair Party (MRP) and Fly-In repair costs and minimal aircraft downtime.

4.6 International Follow On Structural Test Project

4.6.1 Background

The F/A-18 airframe was originally designed to a US Navy Specification with a safe service life of 6000 hours under representative carrier-based operations. This service life was certified through a series of full scale and component fatigue tests conducted by McAir, however the CF have concerns regarding the validity and applicability of these test results for the CF-18 fleet, specifically:

- a. there have been numerous premature test and in-service structural failures resulting in ECPs (both production and retrofit) which were not adequately addressed during the certification process;
- b. the configuration of McAir fatigue test articles was often inconsistent with the structural configuration of many CF-18 aircraft;
- c. CF usage is significantly different and typically more severe than originally accounted for during design and certification testing;
- d. CF flight test data indicates that fatigue test loading of critical centre fuselage structural components was unconservative; and
- e. most major structural ECPs (production and retrofit) resulting from premature fatigue failures were never certified by follow-on testing.

In order to address these serious airworthiness concerns, the International Follow-On Structural Test Project (IFOSTP) is being implemented⁽¹³⁾. This project is a joint Canadian/Australian effort to undertake full scale fatigue testing of the CF-18 centre fuselage, aft fuselage, and wing, with the following key objectives:

- a. determine and certify the safe life of the CF-18 airframe under a representative CF/RAAF usage spectrum;
- b. validate structural repairs and modifications currently being carried out on the CF-18 fleet;
- c. determine the economic life potential of the airframe and identify future structural modification requirements associated with service life extensions; and
- d. obtain crack growth data to support increased management on a safety by inspection basis consistent with CF airworthiness policy⁽¹¹⁾.

4.6.2 IFOSTP Cost-Benefit Assessment

Direct costs related to the IFOSTP are currently estimated at \$65.6M with the breakdown detailed in Figure 21. While it is impossible to accurately quantify the potential life cycle cost savings which may evolve from IFOSTP, a reasonable estimate can be made given the following assumptions and conditions:

- a. governing assumptions detailed in Figure 8 apply;
- b. estimates are based on a target increase in airframe service life of 2000 hours⁽¹⁶⁾. Statistical fleet attrition projections⁽⁴⁾ indicate this would correspond to a 7 year increase in the sustainable ELE of the CF-188 fleet; and
- c. the cost of additional structural modifications arising from IFOSTP are conservatively estimated at \$65M⁽⁸⁾, which represents 80% of the current structural retrofit effort. Provision has also been made for an additional \$35M to address unique modifications/repairs for the life limited early production aircraft.

The incremental life cycle costs of extended CF-18 operations to 2010 have been compared to those associated with the procurement of a New Fighter Aircraft (NFA) with initial operational capability by the year 2004. The results of this assessment are summarized in Figure 22 and confirm that net life cycle cost savings in excess of \$930M could be realized as a result of IFOSTP.

4.7 Estimated Life Cycle Cost Savings Due to ASIP

Based on this limited assessment of selected CF-18 ASIP activities, total projected life cycle cost savings in excess of \$1.4B have been identified. This represents a 10% reduction in the projected total life cycle cost of the CF-18 fleet and is a tremendous return for the nominal \$115M investment in the ASIP.

While it is recognized that this case study has focussed on high visibility and "high yield" ASIP activities, the results clearly indicate that an aggressive and focussed ASIP can yield life cycle cost reductions which far outweigh the direct costs of the supporting engineering activities.

5.0 CONCLUSIONS

The success of any ASIP must ultimately be measured in terms of achieving its primary objective -- to prevent catastrophic in-service structural failures. As a result, the true effectiveness of an ASIP cannot be verified until the fleet in question is phased out, particularly as the risk of structural failures generally increases towards the end of the fleet service life. Despite this obvious caveat, an aggressive and focussed ASIP can provide numerous tangible benefits including:

- a. reduced risk of catastrophic in-service structural failures. This infers the potential to avoid both indirect (human) and direct (economic) costs, which can be substantial;
- b. increased emphasis on proactive vice reactive structural maintenance and logistics support. Through proactive rationalization of maintenance, sparing, and R&O requirements it is possible to reduce the overall O&M costs as well as prevent large fluctuations in funding requirements which are typical of reactive maintenance;

- c. improved risk management capabilities for fleet managers;
- d. the capability to undertake rationalized and cost effective Service Life Extension Programs (SLEP); and
- e. operational usage and maintenance feedback for subsequent aircraft design/procurement activities.

The CF-18 case study confirms that the rational application of ASIP concepts can also result in significant life cycle cost savings. Potential cost savings in excess of \$1.4B have been identified as a direct result of ASIP engineering activities, which represents a 10% reduction in the projected total life cycle costs of the fleet. Of particular note are the benefits of Individual Aircraft Tracking (IAT) activities and an aggressive Fatigue Life Management Program (FLMP). The FLMP has yielded quantifiable life cycle cost savings in excess of \$490M for a nominal \$550K annual investment.

In conclusion, a well planned and rationalized ASIP will by its very nature be cost effective in achieving its primary objective - an airworthy fleet. Application of a judicious mix of engineering, logistics, and operational input can also make the ASIP a very effective tool for controlling the overall life cycle costs of airborne weapon systems.

List of References

1. D-12-010-013/SG-000, "Canadian Forces Aircraft Structural Integrity Program"
2. MIL-STD-1530, "Aircraft Structural Integrity Program Requirements"
3. AFR 173-13, "Aircraft Operational Cost Summary"
4. 3550-1(AIRCOM DCOS Op Rsch), "CF-18 Sustainment Study", dated 07 Apr 93
5. 11500MD-508(DAS Eng 6-3-2), "CF-18 Fleet Usage Review", dated 10 Mar 93
6. SES DI 1095, "CF-18 Statement of Operational Usage and Fatigue Management", dated 18 Dec 92
7. SES DI 0503, "CF-18 ASIP Master Plan (Rev C)", dated 21 Aug 92
8. 3210-55(DG Proc S), "CF-18 National Procurement Estimates", dated Jan 93
9. Department of National Defence Cost Factors Manual (D Cost S), 1988-1993
10. CF-18 System Engineering Support Contract
11. 11500MD-507(DAS Eng 6-3-6), "Requirements for a Fatigue Life Management Program", dated 25 May 88
12. CF-18 Weapon System Development Plan (WSDP), dated 30 Jun 90
13. Durability and Damage Tolerance Testing and Fatigue Life Management - A CF-18 Experience, M.B. Zgela and W.B. Madley, 1991
14. SES DI 0989, "CF-18 IAT Damage Fill-In Verification", dated 16 Mar 92
15. 1500MD-508(DAS Eng 6-3-2), "Rationalization of the CF-18 Fatigue Life Management Program", dated 24 Aug 93
16. 11500MD-507(DAS Eng 6-3-2), "CF-18 Fleet Service Life Potential" dated Nov 93.
17. C-05-005-001/AG-000, "Airworthiness Policy for Canadian Forces Aircraft"

List of Abbreviations and Acronyms

ASIP	Aircraft Structural Integrity Program
CF	Canadian Forces
DADTT	Durability and Damage Tolerance Test
DOC	Direct Operating Cost
ELE	Estimated Life Expectancy
EW	Electronic Warfare
FLE	Fatigue Life Expended
FLMP	Fatigue Life Management Program
IAT	Individual Aircraft Tracking
IFOSTP	International Follow-On Structural Test Project
IOC	Initial Operational Capability
LESS	Load and Environmental Spectrum Survey
MDA	McDonnell Douglas Aerospace
MRP	Mobile Repair Party
MSDRS	Maintenance Signal Data Recording Set
NFA	New Fighter Aircraft
NzW	Vertical Acceleration multiplied by Aircraft Weight
OEM	Original Equipment Manufacturer
O&M	Operations and Maintenance
RAAF	Royal Australian Air Force
R&O	Repair and Overhaul
USN	United States Navy

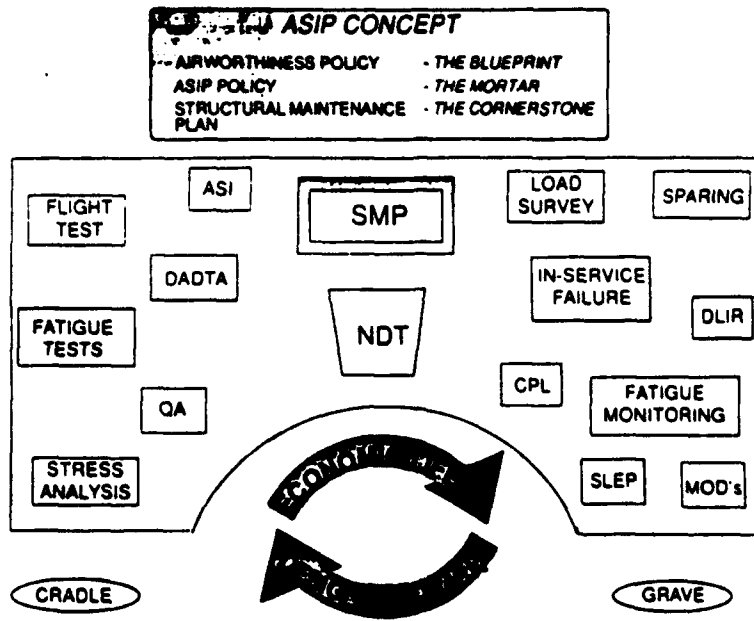


Figure 1 - The ASIP Concept

TASK I	TASK II	TASK III	TASK IV	TASK V
Design Information	Design Analysis and Development Tests	Full-Scale Testing	In-Service Management Data Package	In-Service Management
ASIP Master Plan Structural Design Criteria Damage Tolerance & Durability Control Plans Selection of Mat'ls, Processes & Joining Methods Design Service Life and Design Usage	Material and Joint Allowables Load Analysis Design Service Loads Spectra Design Chemical/Thermal/Environmental Spectra Stress Analysis Damage Tolerance Analysis Durability Analysis Semic Analysis Vibration Analysis Flutter Analysis Nuclear Weapons Effects Analysis Non-Nuclear Weapons Effects Analysis Design Development Tests	Static Tests Durability Tests Damage Tolerance Tests Flight & Ground Operations Tests Semic Tests Flight Vibration Tests Flutter Tests Interpretation & Evaluation of Test Results	Final Analysis Strength Summary In Service Structural Maintenance Plan Loads/Environment Spectra Survey Individual Aircraft Tracking Programs	Loads/Environment Spectra Survey Individual Aircraft Tracking Data Individual Aircraft Maintenance Times Structural Maintenance Records Economic Operational Usage Fatigue Management

Figure 2 - ASIP Tasks and Activities

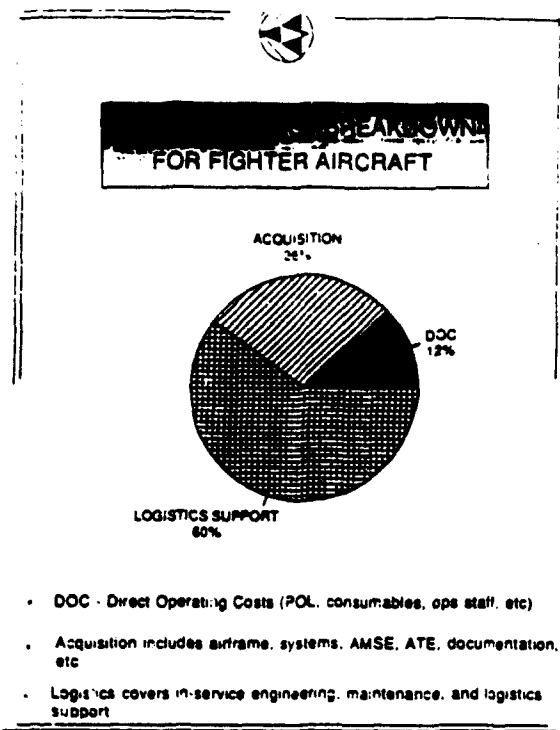


Figure 3 - Life Cycle Costs

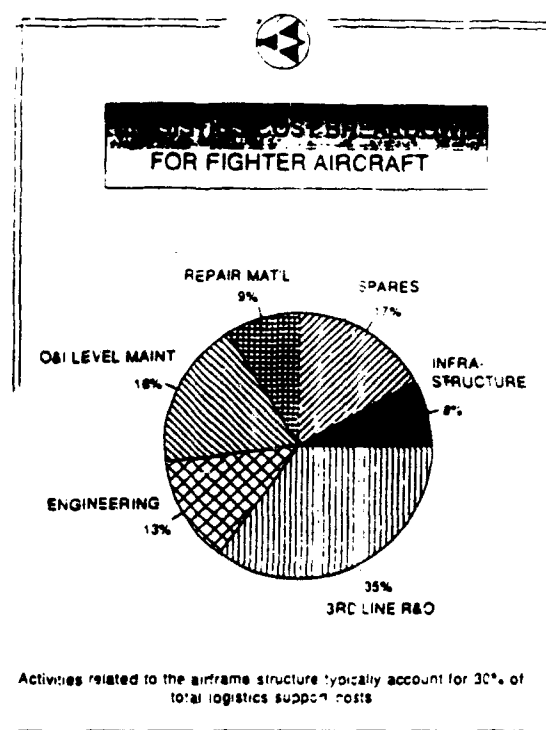


Figure 4 - Logistics Costs

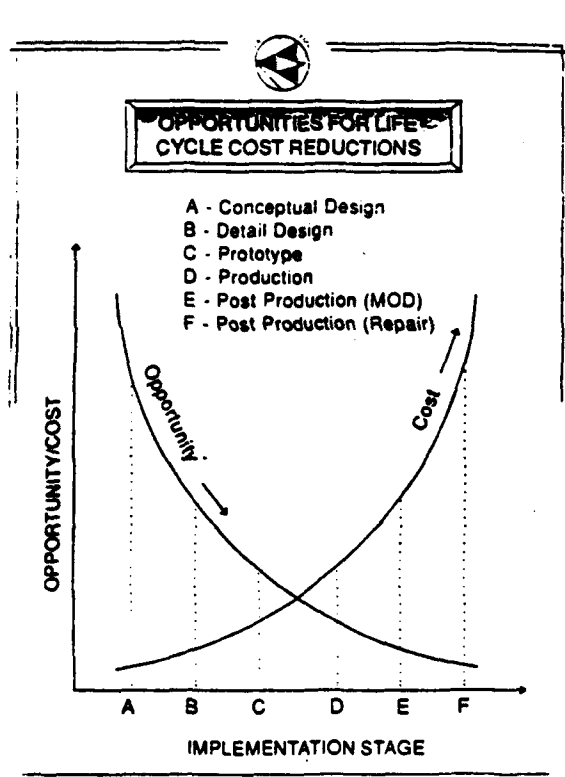


Figure 5 - Opportunities for Life Cycle Cost Reductions

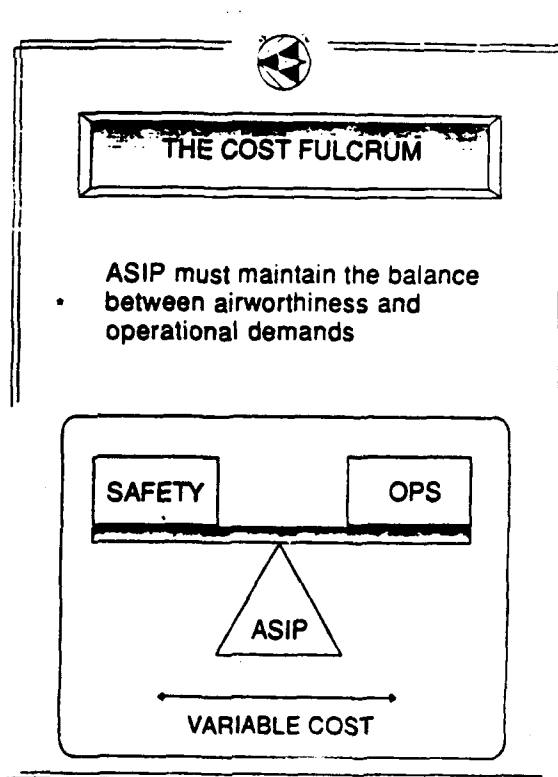


Figure 6 - The Cost Fulcrum



COMPLETED ACTIVITIES

- ASIP Master Plan
- Durability and Damage Tolerance Control Plan
- FEM Model Baseline
- Fatigue Analysis Baseline
- IFOSTP Centre Fuselage Spectrum
- Landing Gear Baseline Operational Spectrum
- Individual Aircraft Tracking Capability
- Fatigue Life Management Tools
- Statement of Operational Usage and Fatigue Management
- Life Limited Components Automated Tracking System
- Aircraft Sampling Inspection (ASI)
- Landing Gear Sampling Inspection (LGS)

ONGOING ACTIVITIES

- McAir Test Results Review
- In-Service Failure Review
- Fuselage Load Analysis
- Stress Analysis of ECPs
- MLG Service Life Assessment
- MLG Maintenance Rationalization
- Preliminary Damage Tolerance Analyses
- Evaluation of Fatigue Enhancements
- Aft Fuselage Dynamic Load Analysis
- Aft Fuselage Fatigue Tracking
- Y488 Bulkhead Fatigue Life Assessment
- Life Limited Parts Tracking Data
- Aircraft Sampling Inspection Rationalization
- Enhanced Fatigue Tracking Capabilities
- Damage/Repair Tracking and Monitoring
- Fatigue Life Management Program Reporting
- Preliminary FSMP
- Full Scale Durability and Damage Tolerance Testing

FUTURE ACTIVITIES

- Damage Tolerance Analysis
- FLMP Enhancements
- Spectrum Sensitivity Studies
- Final FSMP
- Inspection Rationalization
- Early Production Aircraft Life Extension Study
- Structural Life Extension Program (SLEP)

FIGURE 7 - REPRESENTATIVE CP-18 ASIP ACTIVITIES



Cost-benefit assessments for several specific ASIP activities based on Department of National Defence (DND) financial data (references 8, 9, 10, and 12) using the following governing assumptions:

- a. all costs in current year (CY) Canadian dollars. Inflation adjustments for historical data based on the economic model;
- b. immediate savings calculated based on cost avoidance for structural modifications/repairs;
- c. cost of ownership based on the initial capital expenditure amortized over the service life of the fleet. This "smeared" cost of ownership does not reflect overlapping capital costs to phase in/phase out successive weapon systems;
- d. Direct Operating Costs (DOC) based on cost of consumables (POL armament, etc) and operational infrastructure (aircrew, airfield/facilities maintenance, air traffic control, etc).
- e. life cycle cost savings estimated based on comparison of combined O&M costs and smeared ownership costs (capital cost) for the CF-18 and a New Fighter Aircraft (NFA);
- f. CF-18 procurement cost (CY\$) = \$4.8B. Projected NFA procurement costs based on Weapon System Development Plan (WSDP) estimates are \$6.6B (CY\$) for NFA IOC in 2003 and \$7.8B (CY\$) for NFA IOC in 2010;
- g. comparable CF-18/NFA reliability and direct operating costs, with a 10% increase in NFA O&M costs (new technology);
- h. 20 year baseline service life expectancy with three year operational overlap with previous and subsequent weapon systems during phase in/phase out; and
- i. real O&M cost growth trends based on historical data:
 - (1) ramp-up to steady state during first 3 years of service. Combined with overlapping phase-out costs, total O&M costs for first 3 years are assumed to be stable.
 - (2) stable O&M costs during subsequent 7 years of service;
 - (3) subsequent real O&M growth of 3% annually to the target 20 year service life, and
 - (4) real O&M cost growth of 7% annually for service life extensions beyond 20 years.

FIGURE 8 - COST ANALYSIS GOVERNING ASSUMPTIONS

CF-188 ASIP COSTS (CYS)	
SET-UP COSTS (NON-RECURRING)	\$9.600K
- Capability Buildup	
- Facilities/ADP	
- McAir Licence Agreement	
- Training	
- Baselining Activities	
SPECIAL PROJECTS (NON-RECURRING)	
- Early Production A/C SLEP	\$1,200K
- IAT Data Reprocessing	\$1,180K
- Aircraft Sampling Inspection	\$8,580K
- Landing Gear Sampling Inspection	\$1,400K
- DADTT (Centre Fuse/Wing)	\$65,600K
- Misc Projects	\$2,250K
CORE ENGINEERING (RECURRING)	
- Fatigue Life Management	\$622K
- Structural Engineering	\$750K
- Loads/Flight Sciences	\$330K
TOTAL NON-RECURRING COSTS	\$89,800K
TOTAL PROJECTED RECURRING COST	\$26,600K
TOTAL PROJECTED ASIP COST	\$116,400K

Figure 9 - CF-18 ASIP Costs

CF-18 - PROJECTED LIFE CYCLE COSTS (CYS)						
SCALE YEAR	COST DRIVER					TOTAL
	DOC	AIRFRAME O&M	OTHER O&M	COST OF OWNERSHIP	OTHER COSTS	
TOTAL TO FY92/93	\$300M	\$632M	\$1,347M	\$1,770M		\$4,449M
83/94	\$50M	\$89M	\$182M	\$178M		\$499M
94/95	\$50M	\$91M	\$182M	\$178M		\$501M
95/96	\$50M	\$94M	\$182M	\$178M		\$504M
96/97	\$50M	\$103M	\$182M	\$178M		\$513M
97/98	\$50M	\$108M	\$182M	\$178M	\$30M	\$518M
98/99	\$50M	\$108M	\$182M	\$178M	\$30M	\$519M
99/00	\$50M	\$112M	\$182M	\$178M	\$30M	\$522M
00/01	\$50M	\$131M	\$201M	\$178M	\$30M	\$540M
01/02	\$50M	\$133M	\$201M	\$178M	\$30M	\$542M
02/03	\$50M	\$141M	\$201M	\$178M	\$30M	\$570M
03/04	\$50M	\$160M	\$201M	\$178M	\$30M	\$578M
04/05	\$50M	\$160M	\$201M	\$178M		\$580M
05/06	\$50M	\$160M	\$201M	\$178M		\$578M
06/07	\$50M	\$159M	\$200M	\$178M		\$567M
07/08	\$36M	\$121M	\$153M	\$178M		\$480M
08/09	\$28M	\$64M	\$106M	\$178M		\$366M
09/10	\$14M	\$47M	\$60M	\$178M		\$300M
TOTAL	\$1,278M	\$2,612M	\$4,346M	\$4,800M	\$210M	\$13,446M

Figure 10 - CF-18 Life Cycle Costs

CF-18 COST OF STRUCTURAL MAINTENANCE			
CF-18 ANNUAL O&M COSTS (FY 92/93)			
Item	Total Cost	Airframe Cost	
		Cost	% Total
D.O.C.	\$50.0M		
O&I LEVEL MAINT	\$35.0M	\$14.3M	41%
LOGISTICS	\$10.0M	\$3.5M	35%
ENGINEERING SVCS	\$12.5M	\$4.0M	32%
ENGINE SPARES	\$31.4M		
AVIONICS SPARES	\$7.0M		
AIRFRAME SPARES	\$9.3M	\$3.2M	34%
COLOG SPARES	\$13.0M	\$7.0M	54%
DADTT	\$6.8M	\$6.8M	100%
S/W SUPPORT	\$4.9M		
ENGINE R&O	\$25.2M		
AVIONICS R&O	\$11.2M		
SYSTEMS R&O	\$2.6M		
AIRFRAME R&O	\$17.7M	\$17.7M	100%
MISC R&O	\$21.0M	\$9.3M	44%
DEPOT MAINT/ENG	\$59.3M	\$18.9M	32%
TOTAL OPERATIONS	\$50.0M	0	0
TOTAL LOGISTICS	\$266.9M	\$84.7M	32%
TOTAL COSTS	\$316.9M	\$84.7M	27%

Figure 11 - Structural Maintenance Costs for CF-18

RESULTS TO OCTOBER 1993

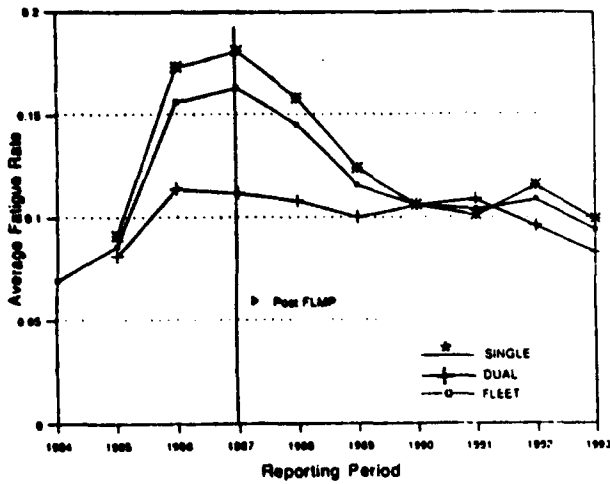


Figure 12 - CF-18 FLMP Results to October 1993

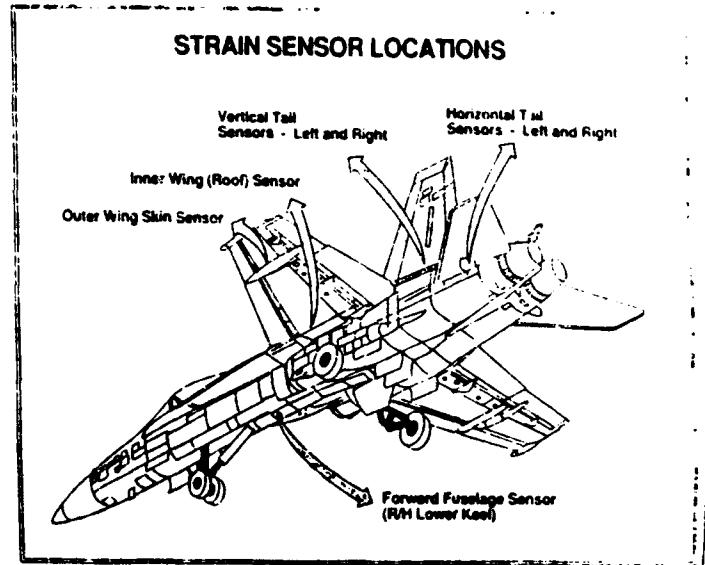


Figure 13 - CF-18 IAT System Strain Sensor Locations

MISSION PLANNING ISSUES

- AVOID HIGH FATIGUE EXTERNAL STORE CONFIGURATIONS WHENEVER POSSIBLE
- SCHEDULE HIGH FATIGUE AIRCRAFT INTO LOW FATIGUE SORTIES WHENEVER POSSIBLE
- PLAN MISSIONS TO REDUCE WEIGHT PRIOR TO HIGH "G" MANOEUVRING
- MAXIMIZE TRANSIT ALTITUDES EN-ROUTE TO AND FROM TRAINING AREAS
- MINIMIZE THE NUMBER OF CLOSED AIRFIELD PATTERNS TO BE FLOWN COMMENSURATE WITH TRAINING REQUIREMENTS/OBJECTIVES

MISSION PROFILE ISSUES

- FOR AIR COMBAT MANOEUVRING AND AIR INTERCEPT MISSIONS, MAXIMIZE ENGAGEMENT ALTITUDES COMMENSURATE WITH TRAINING OBJECTIVES
- LIMIT AIR COMBAT MANOEUVRING (ACH) TO ONLY THAT REQUIRED TO MEET THE TRAINING OBJECTIVES
- KNOCK-OFF AIR COMBAT ENGAGEMENTS WHEN STAGNATION OCCURS OR TRAINING OBJECTIVES HAVE BEEN MET
- EMPHASIZE OPTIMUM DELIVERY AND RECOVERY TECHNIQUES FOR AIR-GROUND RANGE MISSIONS
- USE CIRCULAR VICE BOX-ENDED RANGE PATTERNS FOR AIR-GROUND MISSIONS

ATTITUDE ISSUES

- MINIMIZE "G" DURING PRE-ENGAGEMENT SET-UPS
- INCREASED EMPHASIS ON SMOOTH APPLICATION OF CONTROLS AND ENERGY CONSERVATION
- AVOID UNNECESSARY FLYING AT HIGH ANGLES OF ATTACK
- MAXIMUM 3"G" IN OVERHEAD BREAKS
- MAXIMUM 4"G" IN ALL NON-COMBAT PHASES OF MISSION
- NO UNNECESSARY AEROBATICS EXCEPT FOR APPROVED AIRSHOW DISPLAYS AND ANNUAL PROFICIENCY TRAINING/CHECK RIDES.

Figure 14 - CF-18 FLMP Damage Control Measures



The scope of technical improvements being made to the CF-18 IAT system is detailed in reference [15]. The key issues which have been/are being addressed are summarized below:

- a. correction of strain sensor connectivity identification (primary and backup sensors).
- b. introduction of strain sensor replacement policies/procedures aimed at maximizing availability of accurate strain data.
- c. introduction of wing root strain sensor calibration flights.
- d. development of calibration manoeuvres for horizontal stab sensors.
- e. improved correlation of logged flight hours and data hours.
- f. characterization/correction of wing root strain sensor drift.
- g. introduction of improved damage fill-in algorithms.
- h. investigation/resolution of wing root sensor triggering issues
- i. improved bad sensor checks and spike rejection checks
- j. validation/enhancement of aft fuselage tracking methodology.
- k. improved characterization of sensor reference strains
- l. characterization of outer wing buffet problems, particularly as they relate to wing fold and control surface tracking.
- m. incorporation of enhanced crack initiation routines.
- n. characterization of system sensitivity to spectrum truncation and blocking.
- o. improved characterization of local overstrains.
- p. incorporation of transfer functions to track other critical airframe locations.
- q. processing software efficiency modifications.
- r. reprocessing of accumulated IAT data to correct known historical errors.
- s. rationalization of MSDRS data requirements.

FIGURE 15 - IAT SYSTEM TECHNICAL CONCERNS

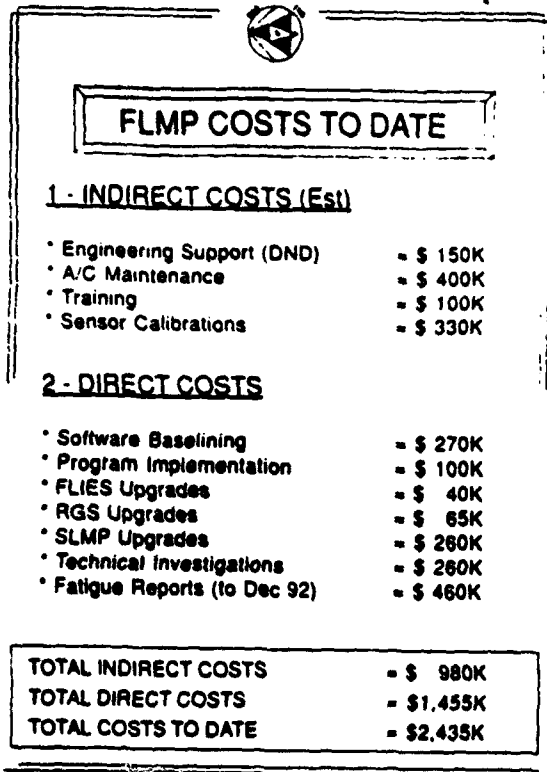


Figure 16 - FLMP Costs to Date

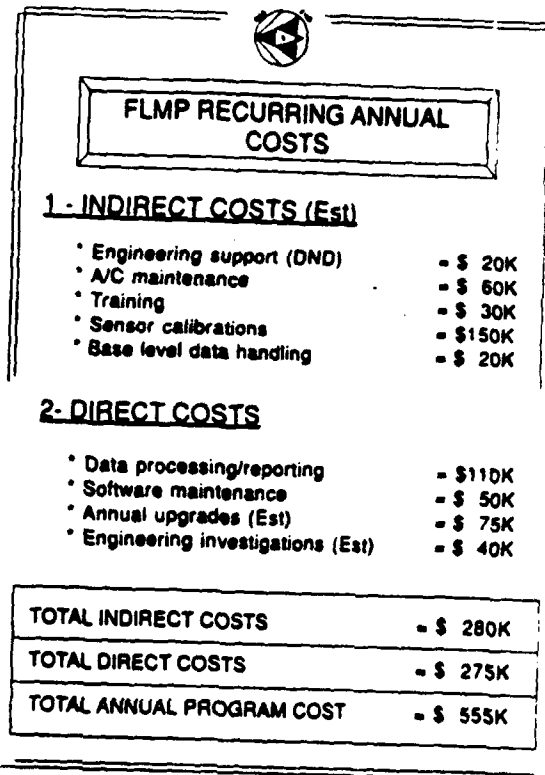


Figure 17 - FLMP Annual Recurring Costs

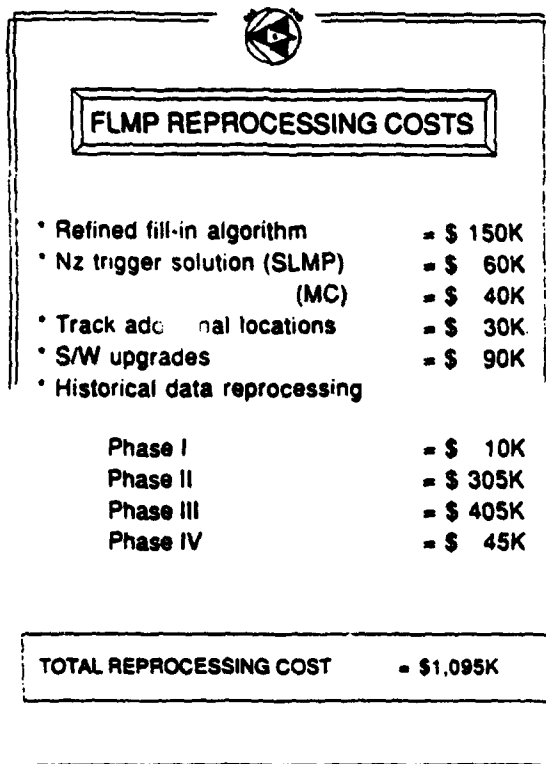


Figure 18 - FLMP Data Reprocessing Costs (Est)

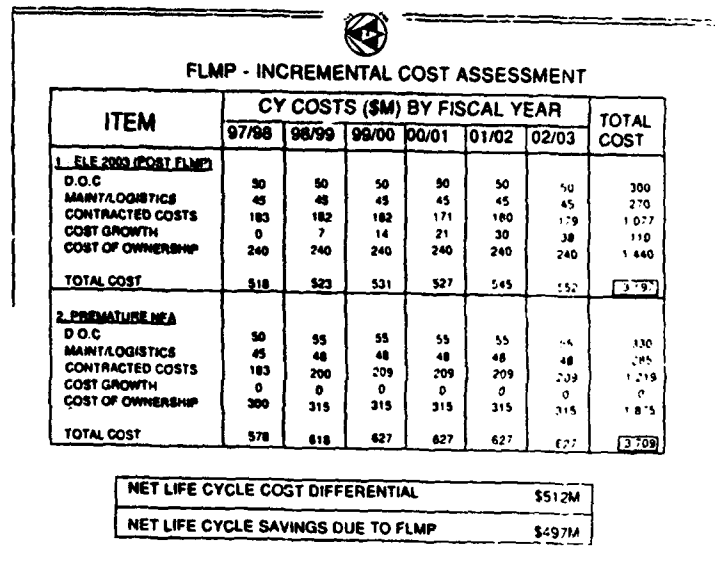


Figure 19 - Cost Savings Due to Fatigue Life Management

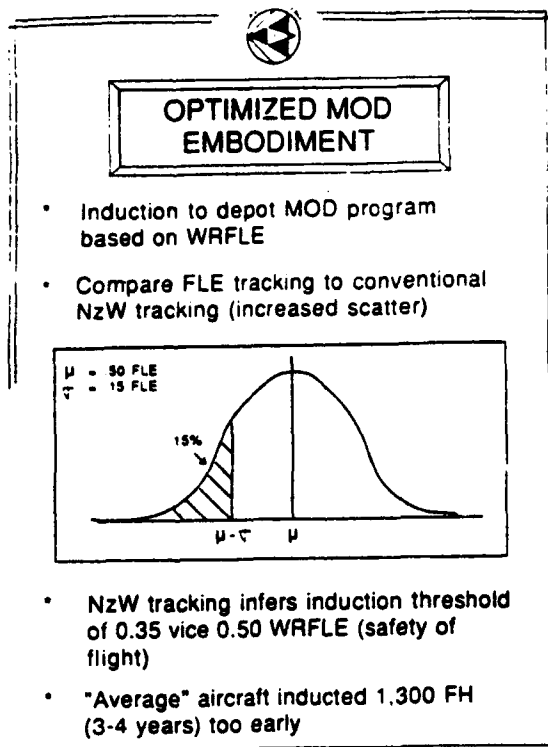


Figure 20 - Optimized Mod Embodiment

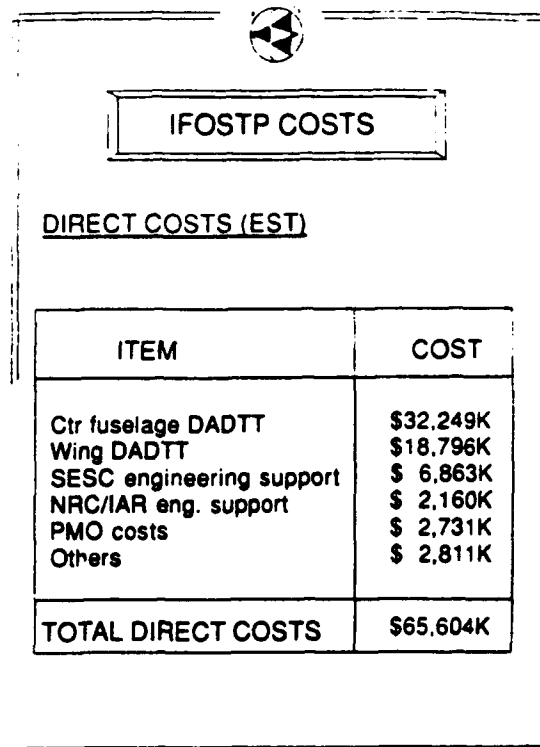


Figure 21 - IFOSTP Costs

IFOSTP POTENTIAL SAVINGS

ITEM	CY COSTS (\$M) BY FISCAL YEAR								TOTAL COST
	02/03	03/04	04/05	05/06	06/07	07/08	08/09	09/10	
1 - ELE 2010									
D.O.C	50	50	50	50	50	50	50	50	400
MAINT/LOGISTICS	45	45	45	45	45	45	45	45	360
CONTRACTED O&M	179	179	177	178	181	175	175	175	1,425
BASLINE ADJUST	38	38	38	38	38	38	38	38	304
COST GROWTH	0	8	18	28	39	58	59	71	275
SLEP MODS	43	22	22	10	0	0	0	0	87
COST OF OWNERSHIP	178	178	178	178	178	178	178	178	1,424
TOTAL	533	521	528	527	531	542	545	557	4,283
2 - ELE 2003									
D.O.C	50	55	55	55	55	55	55	55	435
MAINT/LOGISTICS	45	48	48	48	48	48	48	48	381
CONTRACTED O&M	180	208	208	208	208	208	208	208	1,647
BASLINE ADJUST	38	0	0	0	0	0	0	0	38
COST GROWTH	0	0	0	0	0	0	0	0	0
SLEP MODS	240	373	373	373	373	373	373	373	2,851
COST OF OWNERSHIP	178	178	178	178	178	178	178	178	1,424
TOTAL	563	680	678	678	679	679	679	679	5,314
NET LIFE CYCLE COST DIFFERENTIAL							\$1,030M		
NET PROJECTED LIFE CYCLE COST SAVINGS							\$965M		

Figure 22 - Projected Cost Savings Due to IFOSTP

NON-LINEAR FATIGUE CRACK GROWTH ANALYSIS FOR PROBLEMS WITH SMALL-SCALE YIELDING

D.L. Ball
Lockheed Fort Worth Company

ABSTRACT

An engineering model for the estimation of fatigue crack growth in components which experience small-scale or localized yielding is presented. The model uses a modified Neuber's rule approach for the estimation of non-linear response stress distributions on a given uncracked section on a cyclic basis. Stress intensity factors are calculated for cracks growing in these stress distributions using the Green's function approach. These stress intensity factors are then used in a standard, cycle by cycle crack growth analysis algorithm which increments crack size until failure. Example calculations ranging from predicted response stress distributions for simplified geometries up to fatigue crack growth life predictions for two in-service aircraft are presented.

NOMENCLATURE

a	crack depth
A	area
c	half crack length
C_z	elastic constraint factor
E	modulus of elasticity
E_s	secant modulus
J_2	second invariant of the stress deviator tensor
K_I	mode I stress intensity factor
LEFM	Linear Elastic Fracture Mechanics
N	number of elements
p	applied load
β	normalized stress intensity factor
ϵ_i	i'th component of strain (Voigt notation)
ν	Poisson's ratio
σ_e	equivalent stress
σ_i	i'th component of stress (Voigt notation)

INTRODUCTION

The occurrence of fatigue crack growth in components which experience local yielding one or more times during their design lifetime is quite common in many cyclically loaded structures. Some of the assumptions inherent in 'traditional' Linear Elastic Fracture Mechanics (LEFM) based fatigue crack growth analysis may be inappropriate for a variety of such problems. For example, the assumption that the stress distribution in the critical region for all applied loads may be found by linearly scaling a single,

elastic distribution becomes incorrect when one or more of the applied loads causes plastic deformation and introduces or alters a residual stress field in this region.

Typical problems which involve an initial residual stress field include inadvertent structural overload, coldworking of surfaces and fastener holes, welding and structural and fastener interference. The usual approach taken in such problems is to determine a residual stress intensity factor based on the initial (static) residual stress field and then superimpose that with the appropriate applied (cyclic) stress intensity factor. The methods discussed in references [1] through [9] are typical. This 'effective' stress intensity factor is then used to estimate the crack growth rate which in turn is integrated to find crack growth life. As such, it fits neatly into existing LEFM based damage tolerance analysis methodology.

However, none of these studies have addressed problems in which one or more of the spectrum load cycles are of such magnitude as to cause repeated yielding (and hence redefinition of residual stress fields) in the region of interest. This, on the other hand, is precisely what notch strain analysis [10] does, since it 'tracks' material hysteresis behavior caused by plastic straining. These effects can be accounted for to a limited extent by using the one dimensional analog of hysteresis loop tracking [11]: range pair or rain-flow counting [12]. But both loop tracking and cycle counting techniques track the cyclic variation of stress at a single point only; they provide no information about the rest of the stress distribution in the area. Normally finite element or boundary element techniques are required for determination of complete response stress fields; but these are not practical for application in fatigue analyses involving potentially large numbers of cycles. And yet there exists a class of problems in which LEFM based fatigue crack growth analysis may be successfully applied if modeling of small scale yielding due to structural configuration is introduced.

TECHNICAL APPROACH

CHARACTERIZATION OF APPLIED STRESSES

Applied, elastic stresses are characterized by defining a rectangular array of grid points on the cross-section which is coincident with the anticipated plane of crack growth. Grid point arrays for three typical geometries are shown in Figure 1. The applied stresses (which are assumed to be known from hand analysis, FE analysis, BE analysis etc.) are specified at each of these grid points. The array of grid points is then used to define rectangular elements, each of which carries a constant stress which is defined as the average of the four corner grid point stresses. This is shown schematically in Figure 2. Large stress gradients are accommodated by refining the mesh as required.

The following is a discussion of the further development of an integrated notch strain and cycle-by-cycle fatigue crack growth analysis technique that was first proposed in [13].

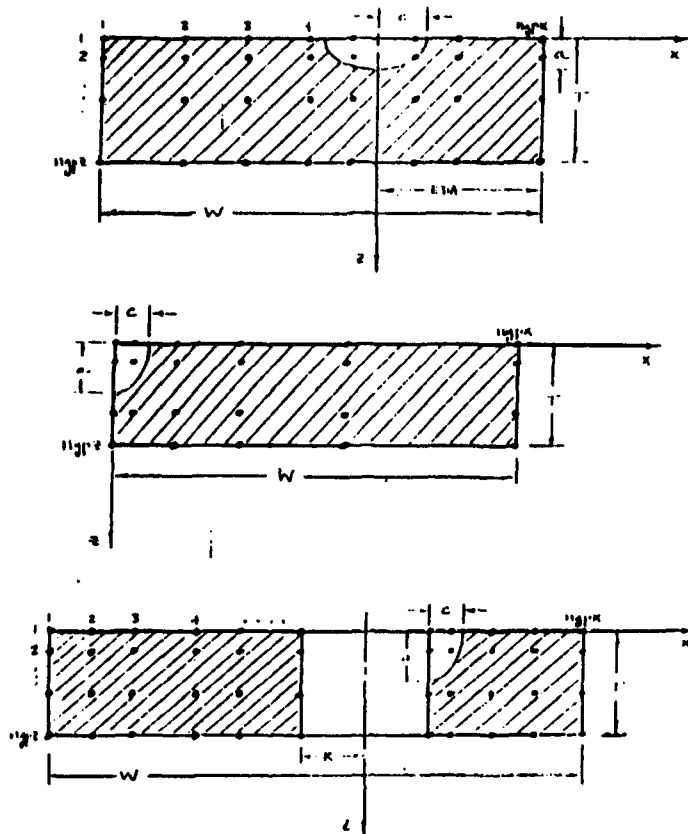


Figure 1. Example Grid Point Configurations for Typical Geometries.

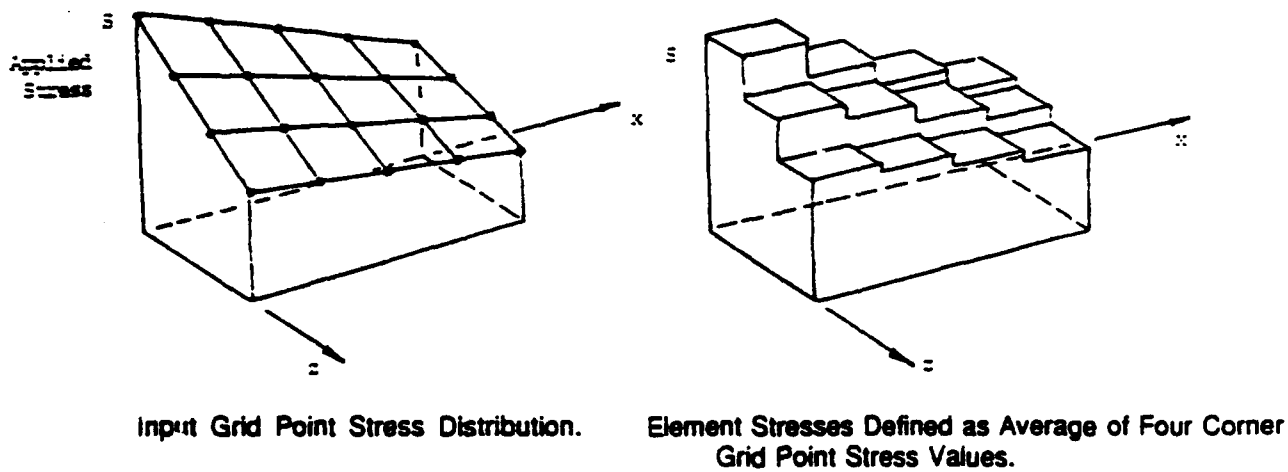


Figure 2. Schematic of Constant Stress Element Definition.

In addition to the applied stresses, consideration is given to potential induced stresses which are the result of elastic constraint. With the coordinate system defined such that the applied stresses act in the y-direction, normal constraint stresses may be generated in both the in-plane transverse (x-direction) and the transverse (z-direction) directions [14-15]. See Figure 3.

Under conditions of plane stress the transverse components of stress and strain are

$$\sigma_z = 0 \quad (1)$$

$$\epsilon_z = \frac{-\nu}{E}(\sigma_x + \sigma_y) \quad (2)$$

while under plane strain they are given as

$$\epsilon_z^E = 0 \quad (3)$$

$$\sigma_z = \nu(\sigma_x + \sigma_y) \quad (4)$$

It is convenient to define a constraint index as follows

$$C_z = 0, \text{ plane stress} \quad (5)$$

$$C_z = 1, \text{ plane strain} \quad (6)$$

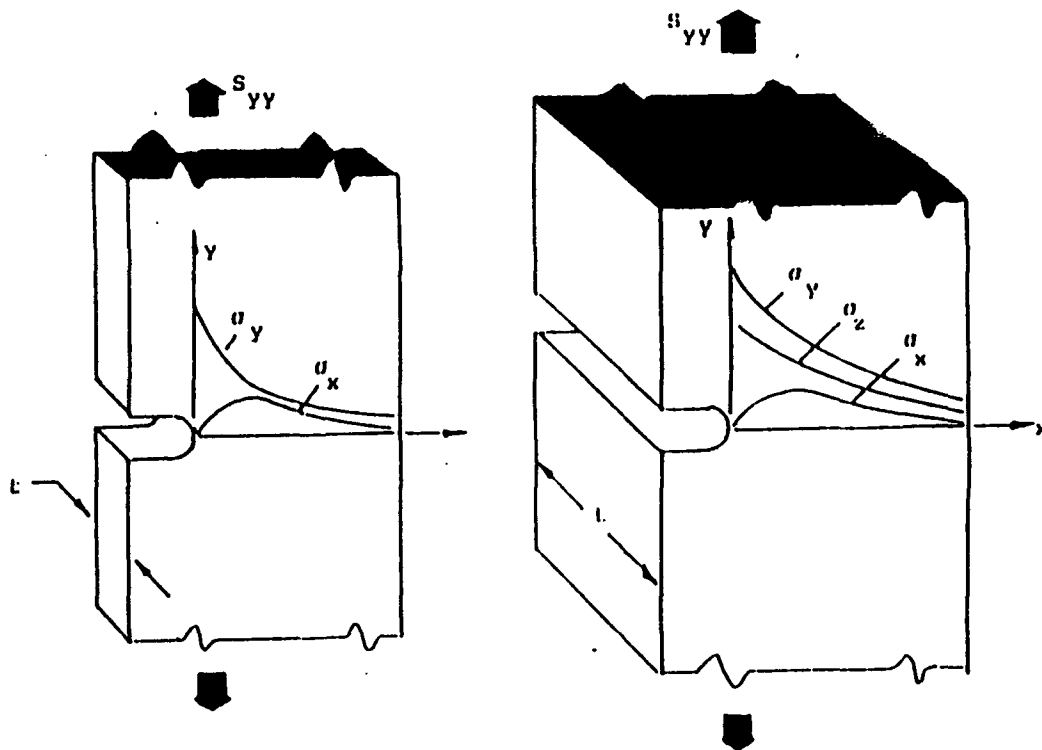


Figure 3. Stress Distributions at a Notch Under Plane Stress and Plane Strain Conditions.

With this definition, the estimated transverse normal stresses and strains (due to the Poisson effect) are

$$\sigma_z = C_z \nu (\sigma_x + \sigma_y) \quad (7)$$

$$\epsilon_z^E = (C_z - 1) \frac{\nu}{E} (\sigma_x + \sigma_y) \quad (8)$$

ESTIMATED ELASTIC-PLASTIC RESPONSE

Given the applied and any induced stresses for each element, an equivalent stress is defined as follows

$$\sigma_*^E = \sqrt{3 J_2} \quad (9)$$

where J_2 is the second invariant of the stress deviator tensor [16] and the superscript E indicates an elastic quantity. We then assume a generalized form of Neuber's rule [17] to find a response equivalent stress and strain as

$$\sigma_* \epsilon_* = \frac{(\sigma_*^E)^2}{E} \quad (10)$$

As shown in Figure 4, if the applied stress state is outside the yield surface, then the response stress state is taken as the vector sum of the applied stress vector, σ^E , and a differential stress vector, $\delta\sigma$

$$\sigma_i = \sigma_i^E + \delta\sigma_i \quad (11)$$

By definition the response stress state lies on the yield surface. The response strains are taken to be the sum of elastic and plastic components

$$\epsilon_i^T = \epsilon_i^E + \epsilon_i^P \quad (12)$$

where the elastic component is

$$\epsilon_y^E = \frac{1}{E} [\sigma_y - \nu(\sigma_x + \sigma_z)] \quad (13)$$

and the plastic component is given by

$$\epsilon_y^P = \left(\frac{1}{E_s} - \frac{1}{E} \right) [\sigma_y - \nu^P(\sigma_x + \sigma_z)] \quad (14)$$

E_s is the secant modulus defined at the point ϵ_0, σ_0 on the uniaxial stress-strain curve.

When plastic straining occurs in any given element, the load increment in the y-direction (the applied load direction), which is shed due to yielding is found as

$$(\delta p_y)_i = (\sigma_y^E - \sigma_y) dA_i \quad (15)$$

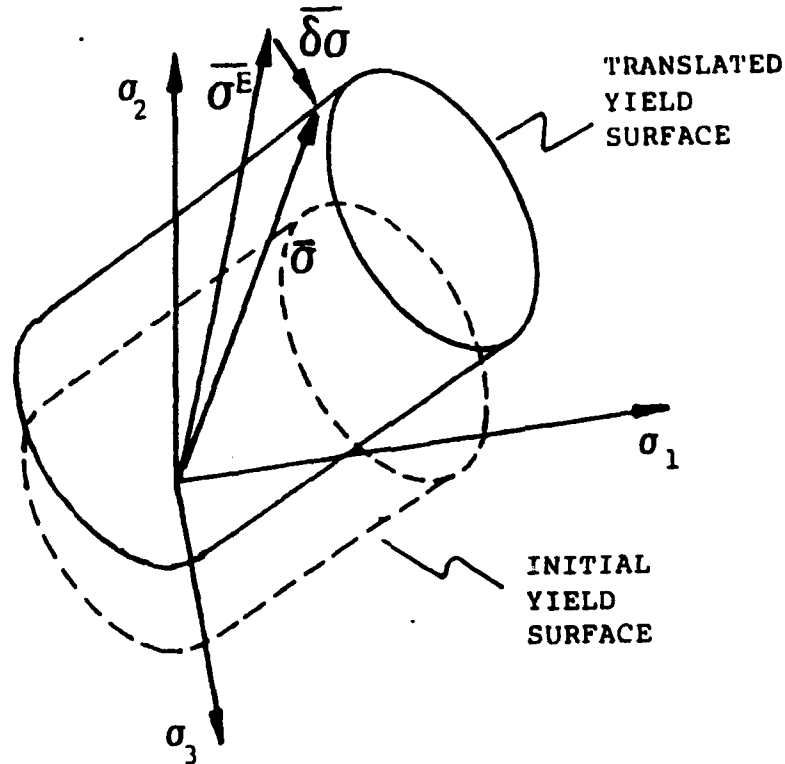


Figure 4. Motion of Cylindrical Yield Surface in Principal Stress Space.

and it is distributed over all of the elements of the cross-section according to

$$(\delta p_y)_j = \omega_j (\delta p_y)_i \quad (16)$$

where ω_j is a weight function defined such that

$$\sum_{j=1}^N \omega_j = 1 \quad (17)$$

Similar calculations are made for the x- and z-directions and for the xy and zy shears, with the exception that the load increments in these cases are transmitted only to adjacent elements.

CYCLIC STRESS-STRAIN RESPONSE

Response calculations are made for each element in the uncracked section, for each load point in the applied spectrum. These calculations are carried out on a point-to-point basis with the response stress and strain at any given load point in the applied load sequence (n) serving as the effective origin for the response to the next load point (n+1).

$$\sigma_i^{n+1} = \Delta\sigma_i + \sigma_i^n \quad (18)$$

$$\epsilon_i^{n+1} = \Delta\epsilon_i^E + \Delta\epsilon_i^P + \epsilon_i^n \quad (19)$$

For point stress analyses, this results in the hysteresis loop tracking which is typical for notch strain analysis [10]. This is shown schematically in Figure 5.

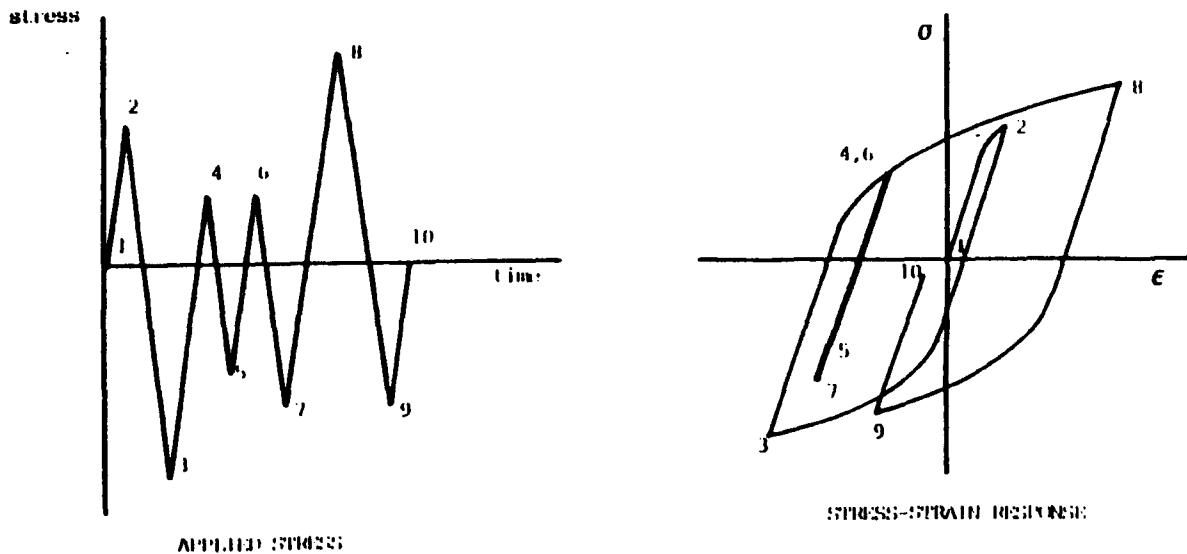


Figure 5. Schematic Applied Stress vs Time Sequence and Corresponding Stress-Strain Response.

For analyses of full stress distributions, results of the type shown in Figure 7 are found. The results shown are for an idealized problem in which a triangular stress distribution is applied to a finite width strip as shown in Figure 6. This simplified geometry and loading were employed to allow a clearer picture of the potential difference between applied and response stress distributions and the manner in which those distributions are effected by prior yielding. The predicted response stress distributions for a sequence of six applied, peak stresses: 0 ksi, 20 ksi, -80 ksi, 10 ksi, -10 ksi and 0 ksi, are shown in Figures 7a-7f. The plate material was taken to be 2124-T851 Aluminum. Figure 7c shows the predicted response to a large compressive underload: significant yielding has occurred in the peak stress region. In Figure 7d, the prior yielding is shown to significantly alter the small applied (elastic) stress distribution. In particular,

the response stress is considerably more tensile than the applied stress. The effect of this type of behavior on fatigue crack growth can be significant. In reality, the calculations shown in Figure 7 violate the small-scale yielding requirement recommended for this technique. The problem was intentionally run in this manner, however, to demonstrate two significant features of this approach: that the predicted stresses and strains are history dependent, and that at each load point, complete stress and strain distributions (as opposed to just point values) are determined.

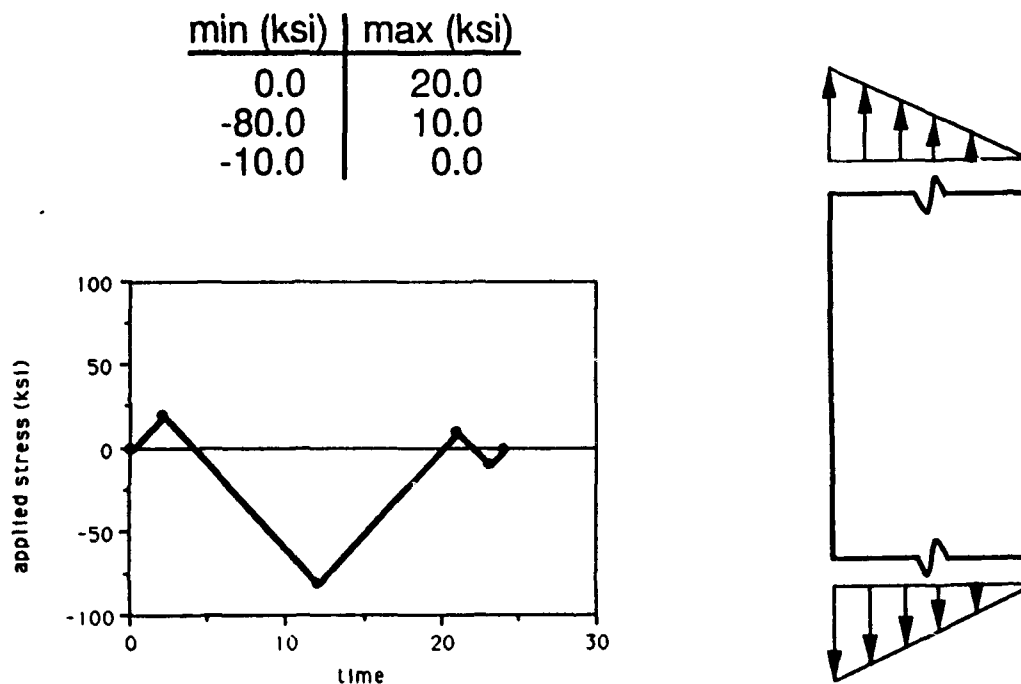


Figure 6. Geometry and Loading Definition for Linear Stress Distribution on Finite Width Strip.

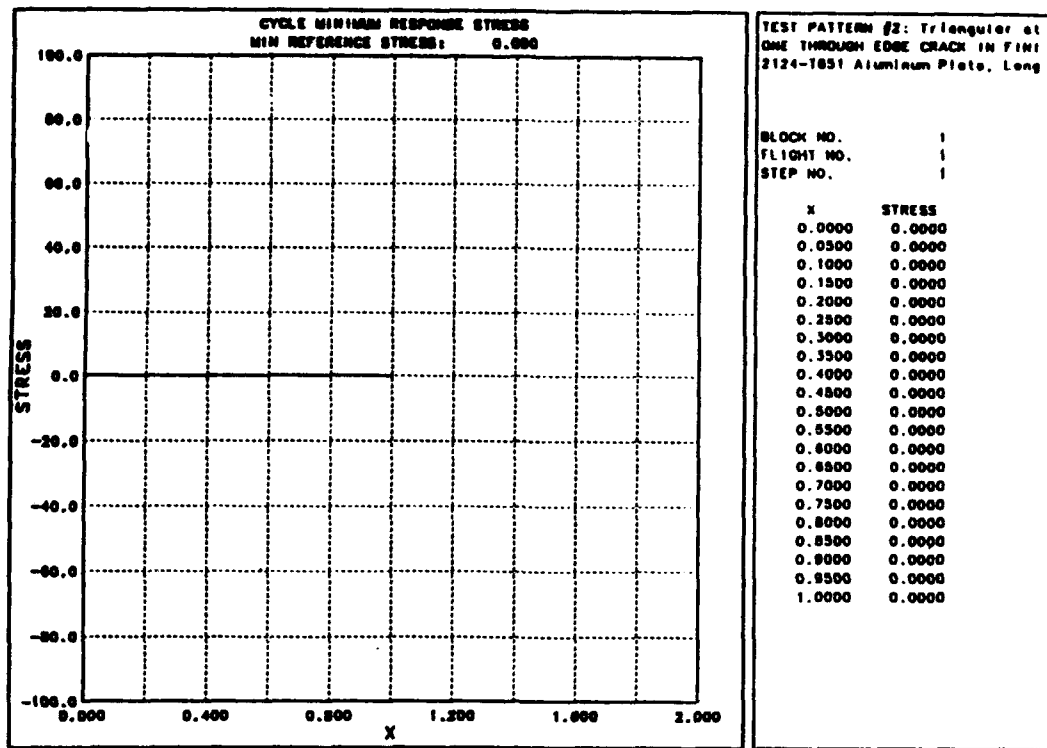


Figure 7a. Predicted Response Stress Distribution at Load Point 1: Applied Peak Stress=0 ksi.

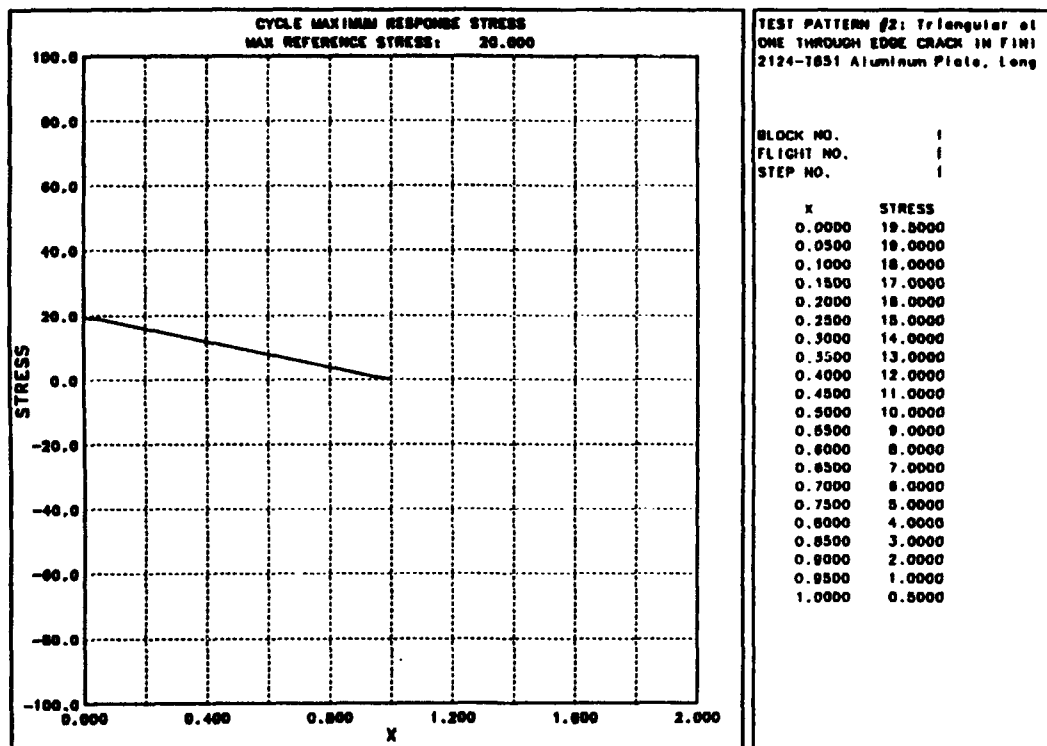


Figure 7b. Predicted Response Stress Distribution at Load Point 2: Applied Peak Stress=20 ksi.

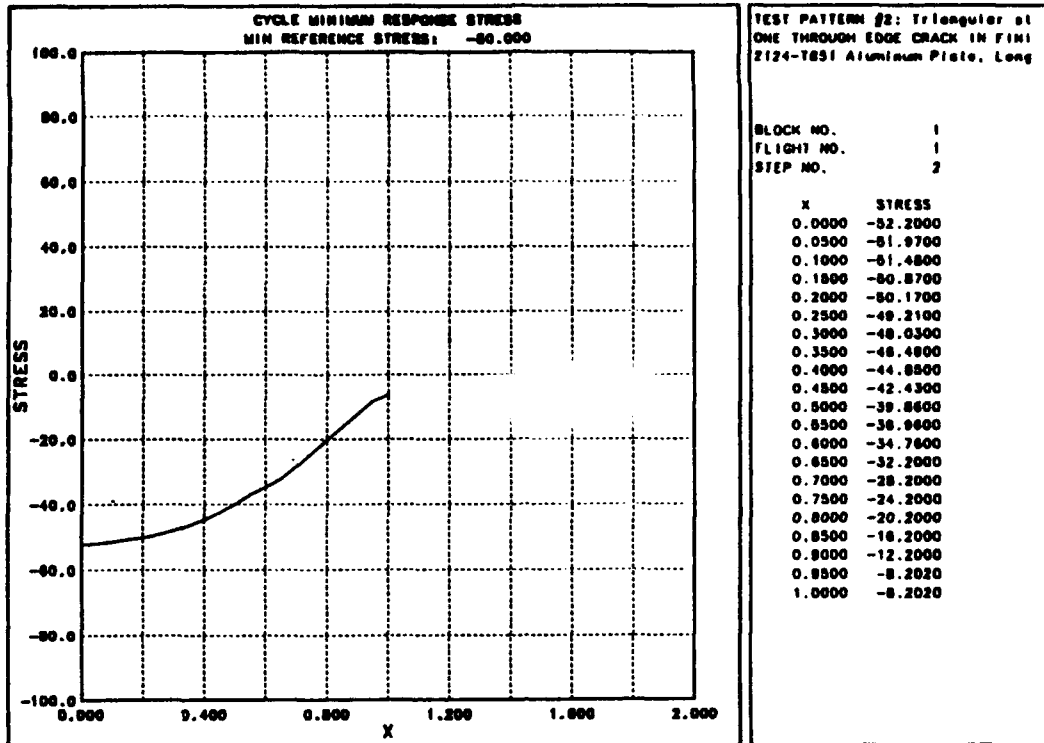


Figure 7c. Predicted Response Stress Distribution at Load Point 3: Applied Peak Stress=-80 ksi.

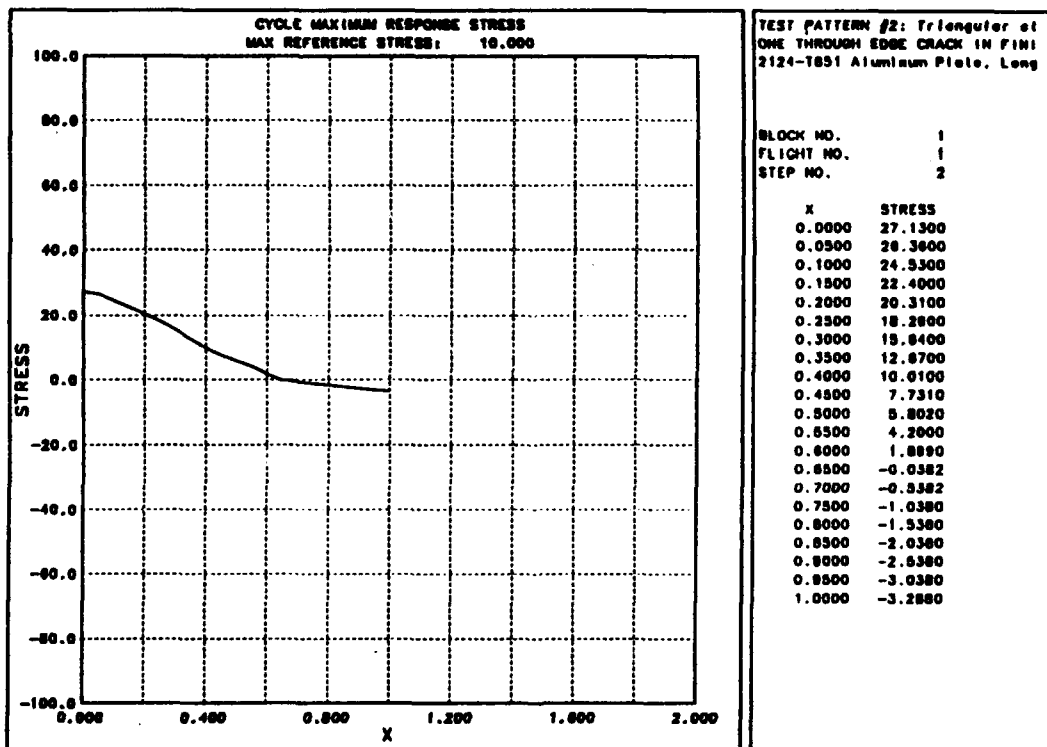


Figure 7d. Predicted Response Stress Distribution at Load Point 4: Applied Peak Stress=10 ksi.

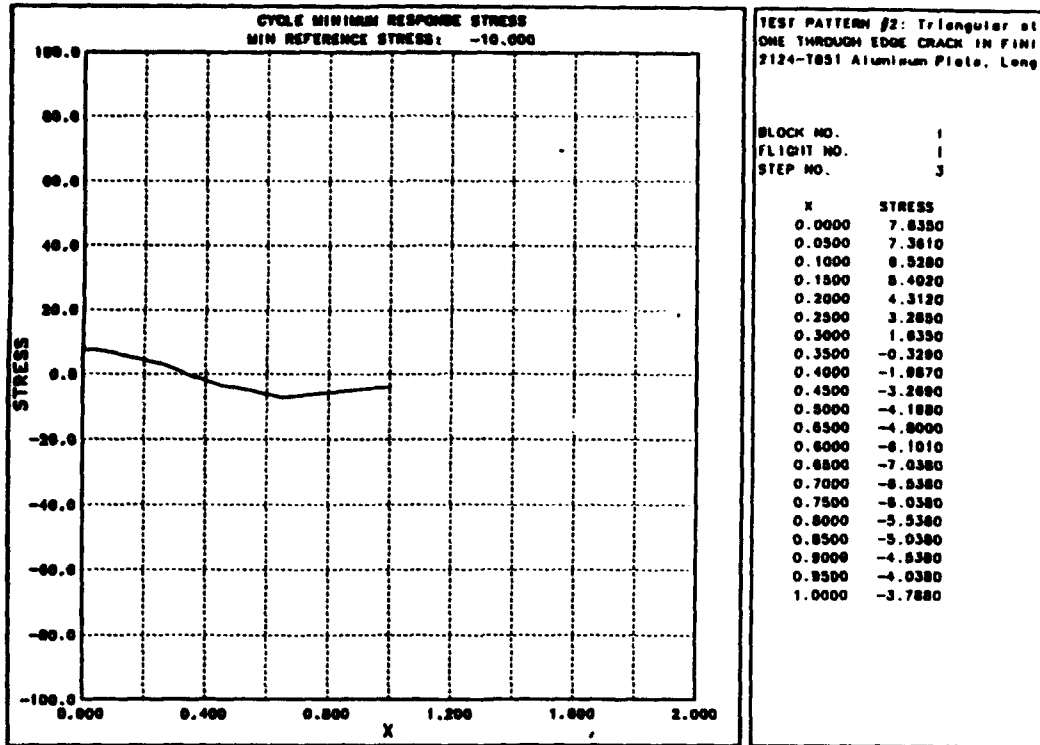


Figure 7e. Predicted Response Stress Distribution at Load Point 5: Applied Peak Stress=-10 ksi.

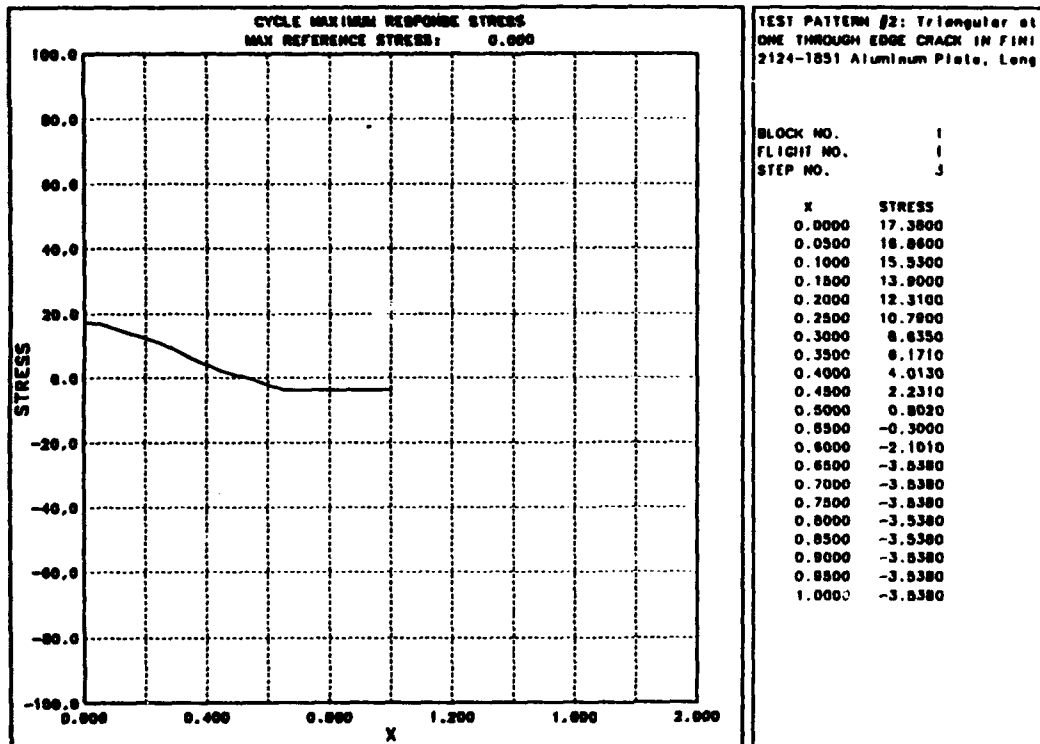


Figure 7f. Predicted Response Stress Distribution at Load Point 6: Applied Peak Stress=0 ksi.

STRESS INTENSITY FACTOR CALCULATION

Given these response stress distributions which evolve with time, a stress intensity factor solution technique which is not based on the assumption of uniform applied stress is required. The Green's function approach [18-20] was selected for use here

$$K_I = \int_0^c \bar{\sigma} G dx \quad (20)$$

where

- $\bar{\sigma}$ - normalized distribution of stress over the crack plane
- G - Green's function for given loading/boundary conditions

FATIGUE CRACK GROWTH ANALYSIS

With the stress intensity factor known, the remainder of the problem is carried out in the manner of traditional, LEFM based fatigue crack growth analysis [21-22]. Specifically, the procedure is as follows: 1) apply the stress due to load point 'n' in load history to the model, 2) estimated the elastic-plastic response as discussed above, 3) calculate the stress intensity factor based on that response, 4) calculate crack growth increment based on DK between sequential min and max, 5) increment crack size, 6) check for failure and 7) assuming failure has not occurred, repeat the process for load point 'n+1'. This process is shown schematically in Figure 8.

The only data over and above that normally required for a traditional fatigue crack growth analysis is the cyclic stress-strain curve [23-24] for the material being analyzed.

EXAMPLE CALCULATIONS

STRESS DISTRIBUTION AT CIRCULAR HOLE IN FINITE WIDTH STRIP

The first example to be considered is that of a centered circular hole in a finite width strip. In this case the elastic stress distribution due to applied tension is available in the literature. The estimated elastic-plastic response is shown compared with results from a non-linear finite element analysis [25] of the same problem.

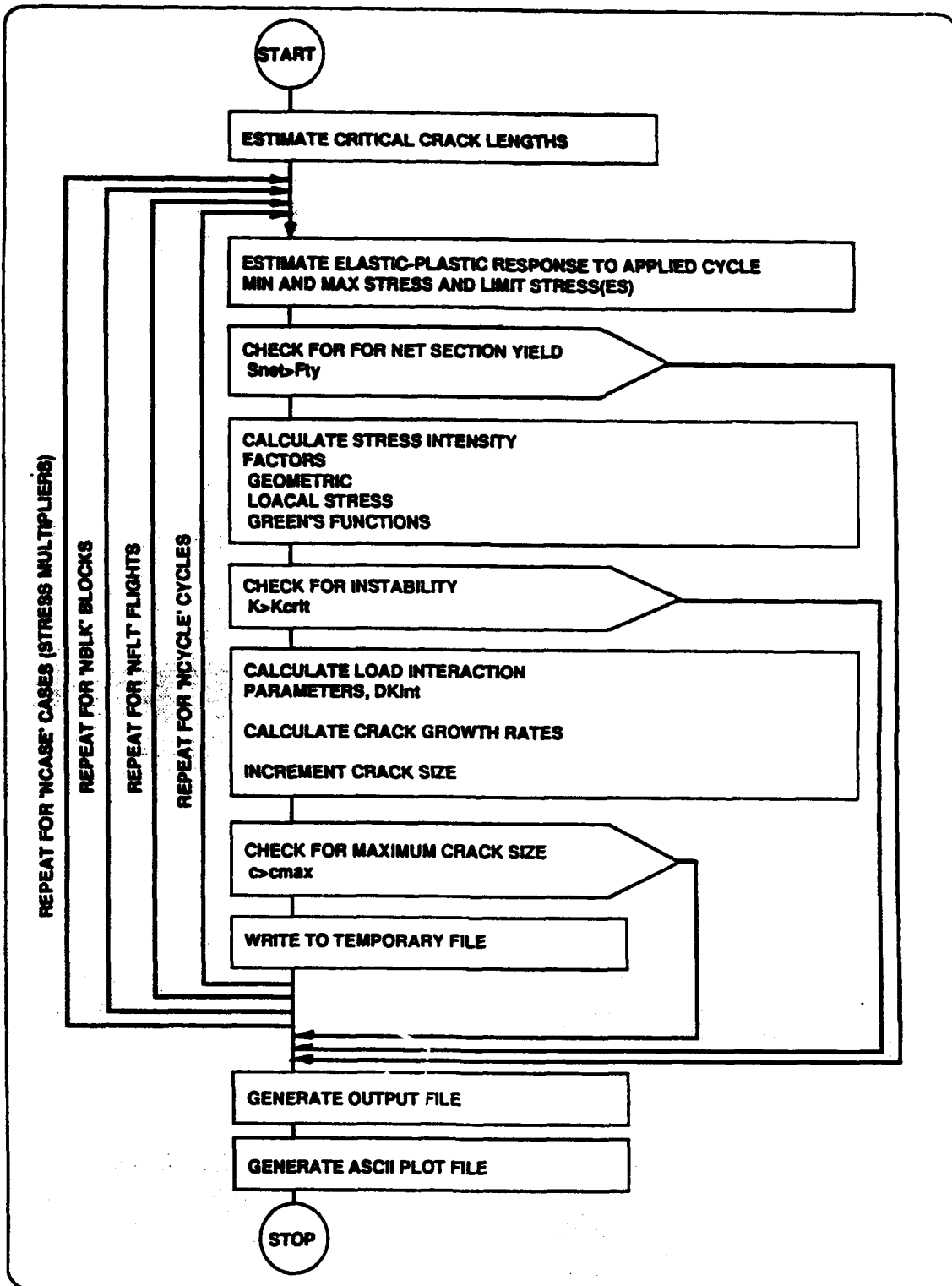


Figure 8. Procedure for Non-Linear Fatigue Crack Growth Analysis.

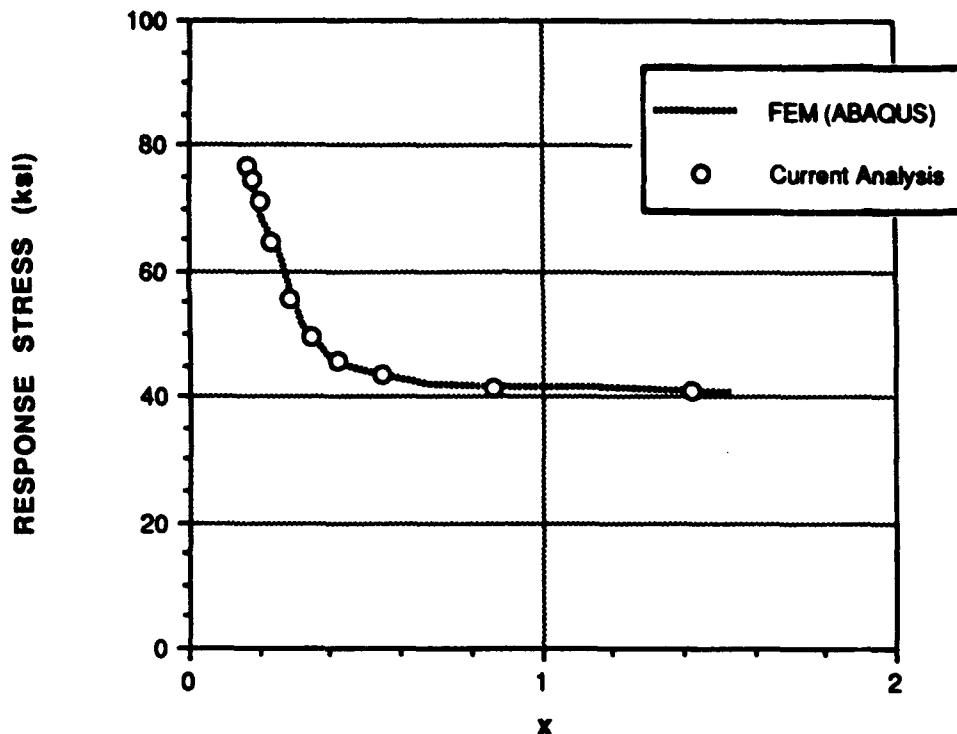


Figure 9. Comparison of Calculated Elastic-Plastic Response Stress Distributions at a Centered Circular Hole in a Finite Width Strip.

FIGHTER-BOMBER AIRCRAFT UPPER WING FUEL VENT HOLE

One of the first applications of this technique was for the analysis of fatigue cracking in the upper wing substructure a fighter-bomber aircraft. To insure flight safety, this aircraft is periodically subjected to a cold proof test in which the wings are statically loaded to both maximum and minimum limit loads. These high applied wing bending moments are sufficient to cause local yielding in areas of moderate to high stress concentration within the pivot fitting. As a result, any fatigue crack growth which may occur at such locations is dependent on both the residual stresses due to the cold proof test, and the subsequent service load history. The problem presented here is further complicated in that the control location is near the wing upper surface, resulting in an applied fatigue spectrum which is compression dominated. The crack initiation site in this case is at the lower, inboard radius of fuel vent hole (FVH) #13. The general placement of the FVH within the center stiffener and the pertinent dimensions are shown in Figure 10. The cracked stiffener was modeled as a through-the-thickness edge crack in a finite width strip.

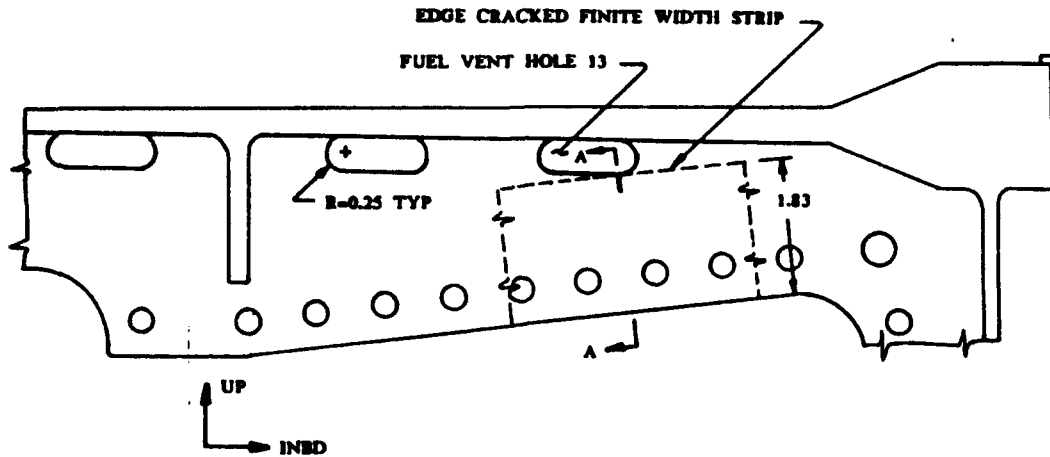


Figure 10. Fighter-Bomber Aircraft Wing Pivot Fitting, Fuel Vent Hole 13.

For this problem, results from a fine grid, elastic finite element analysis of the center stiffener in the area of FVH-13 [26] were used to define the elastic (applied) stress distribution. The cyclic stress-strain curve for the pivot fitting material, 220-240 HT D6AC steel [27], is shown in Figure 11.

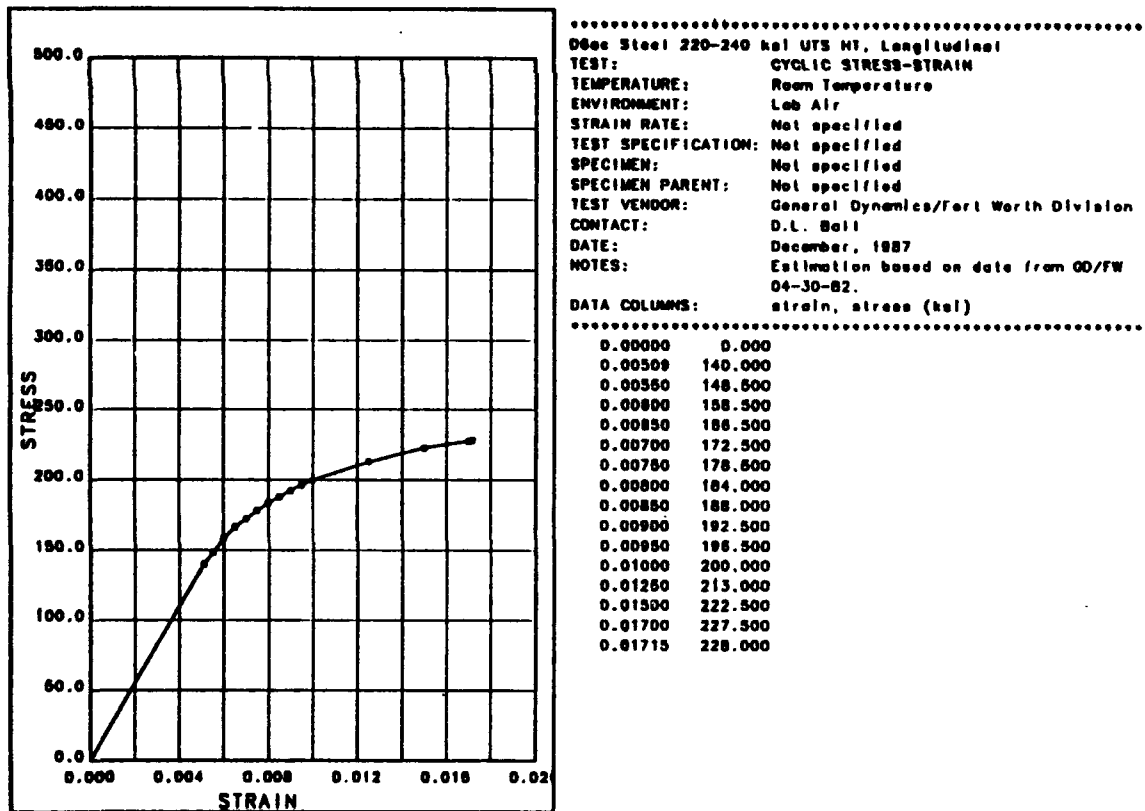


Figure 11. Cyclic Stress-Strain data for D6AC, 220-240 HT Steel [28].

The predicted residual stress distribution in the critical region (y-component of stress vs depth into the stiffener) at the conclusion of the cold proof test is shown in Figure 12.

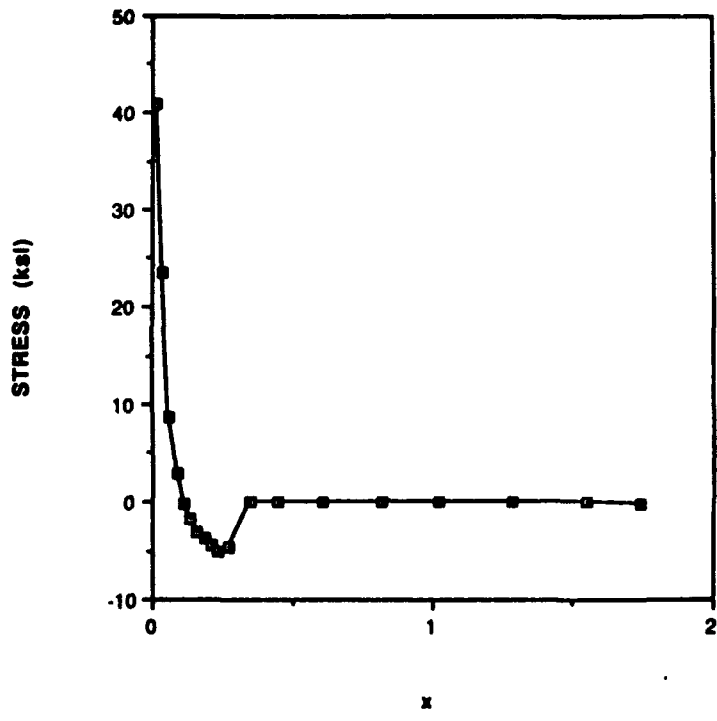


Figure 12. Residual Stresses Through Depth of Stiffener After Cold Proof Test, Zero Applied Load.

As indicated in Figure 13, a traditional LEFM based fatigue crack growth analysis of the FVH-13 cracking problem indicated essentially no crack growth. In contrast however, the non-linear technique predicted significant growth; the results of this analysis are compared with fleet cracking data [28] in Figure 13.

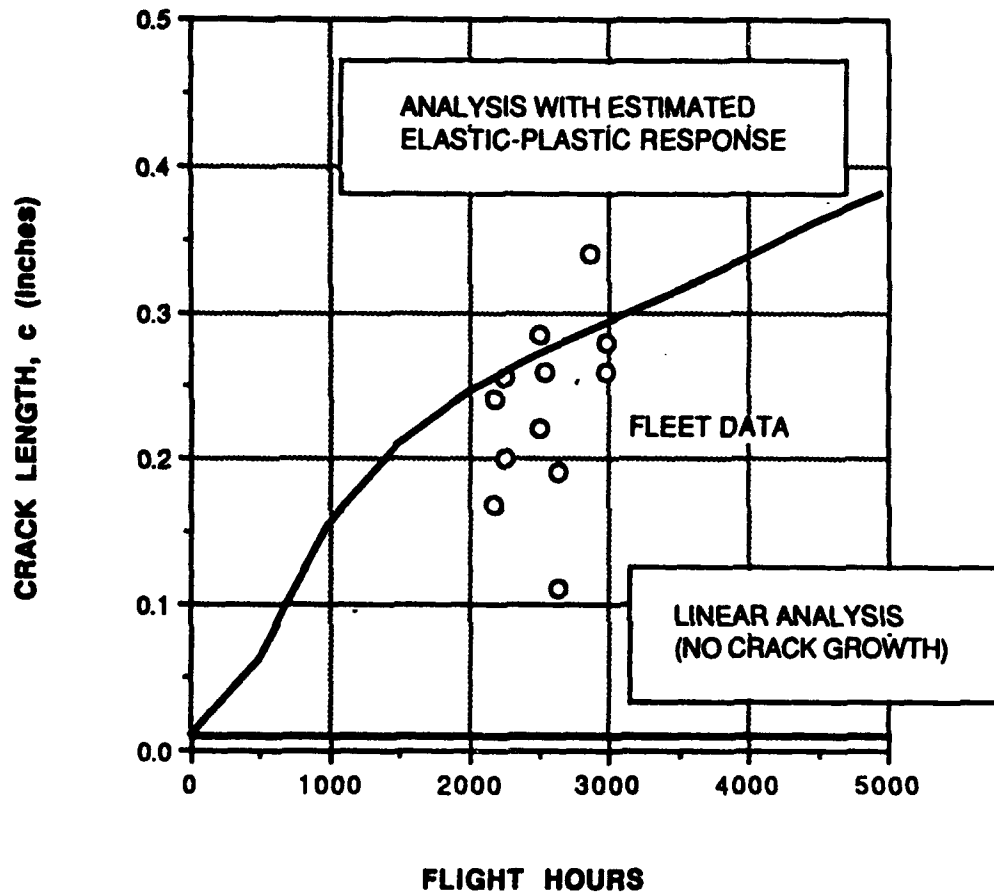


Figure 13. Correlation of Non-Linear Fatigue Crack Growth Analysis Results With Fleet Cracking Data.

FIGHTER AIRCRAFT VERTICAL TAIL ATTACH PAD RADIUS

Another problem for which this approach has been effective is that of fatigue cracking in the radius at the intersection of the vertical stabilizer attach pad and an aft fuselage bulkhead of a fighter aircraft. See Figure 14.

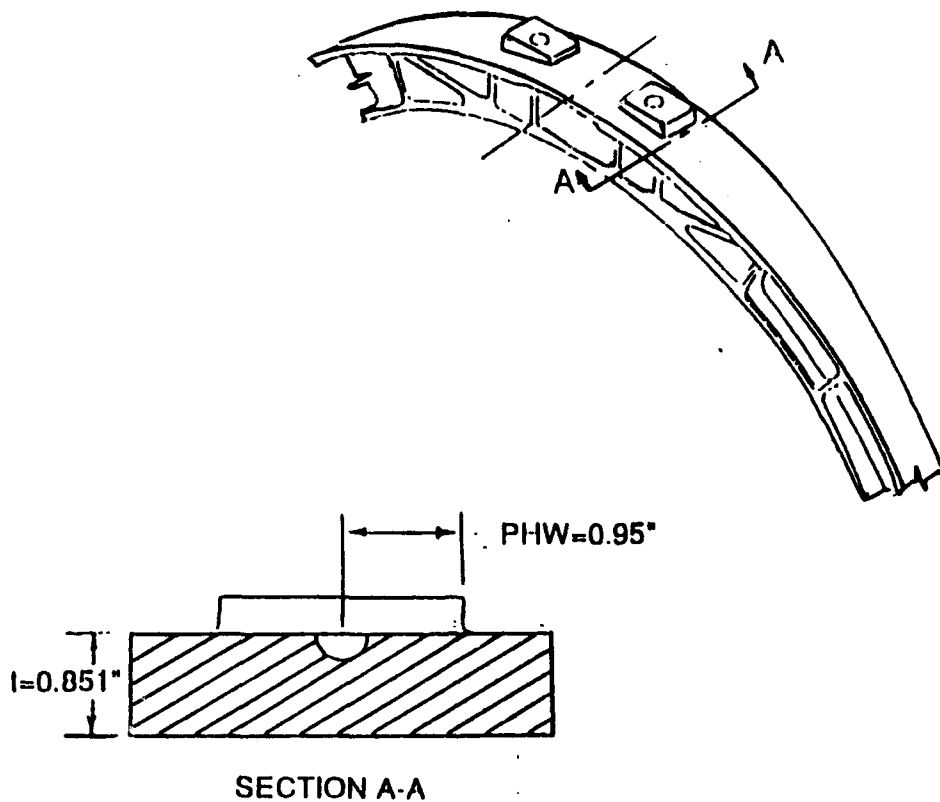


Figure 14. Vertical Tail Attach Pad on an Aft Fuselage Bulkhead of a Fighter Aircraft.

As with the previous problem, results from a fine grid, elastic finite element analysis of the bulkhead in the region of the attach pad [29] were used to define the elastic (applied) stress distribution. The cyclic stress-strain curve for the bulkhead material, 2124-T851 Aluminum plate [30], is shown in Figure 15.

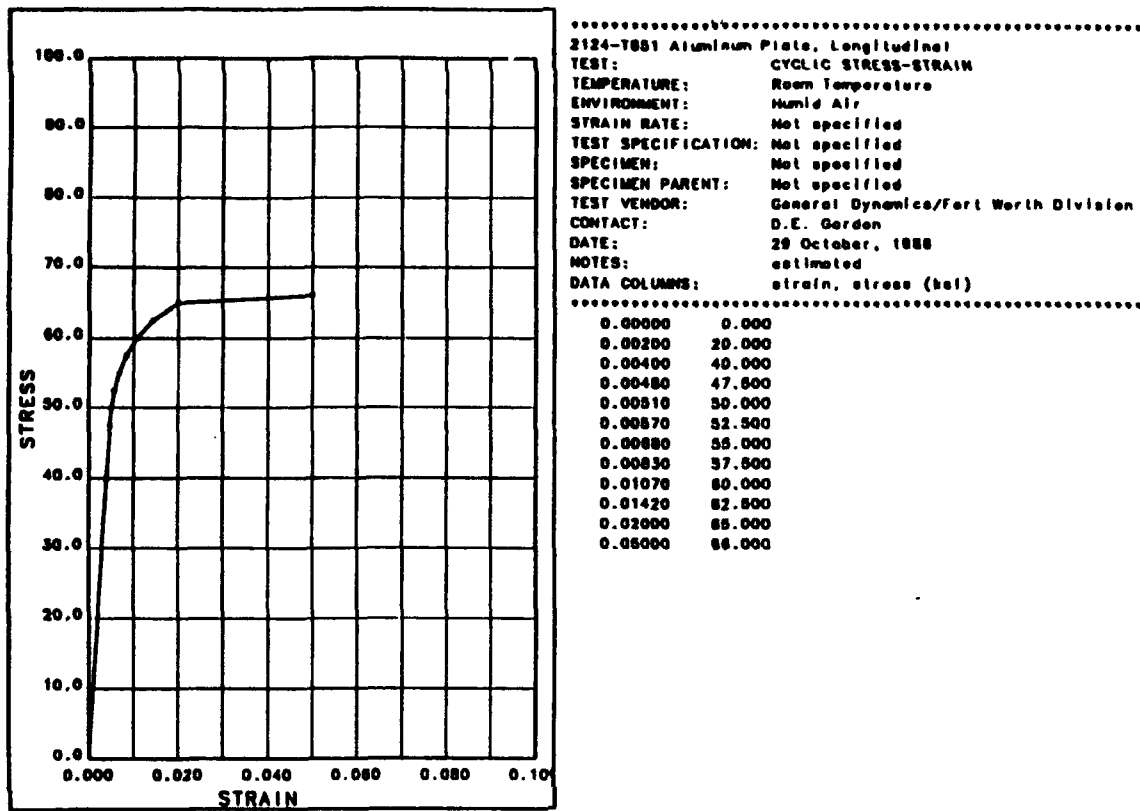


Figure 15. Cyclic Stress-Strain data for 2124-T851 Aluminum Plate [30].

The results of the non-linear analysis of the bulkhead cracking problem are compared with fleet cracking data [29] in Figure 16. In this case, as indicated in the figure, the traditional LFM based fatigue crack growth analysis proved to be much too conservative; the applied stresses were so high that immediate failure of the part was predicted.

SUMMARY

The proposed non-linear fatigue crack growth analysis technique offers the following benefits:

- o It predicts the creation and evolution of both tensile and compressive residual stress fields due to compressive or tensile overloads respectively.
- o Stress intensity factors are based on response, not applied, stress distributions.
- o It models cyclic hysteresis behavior with kinematic material hardening.

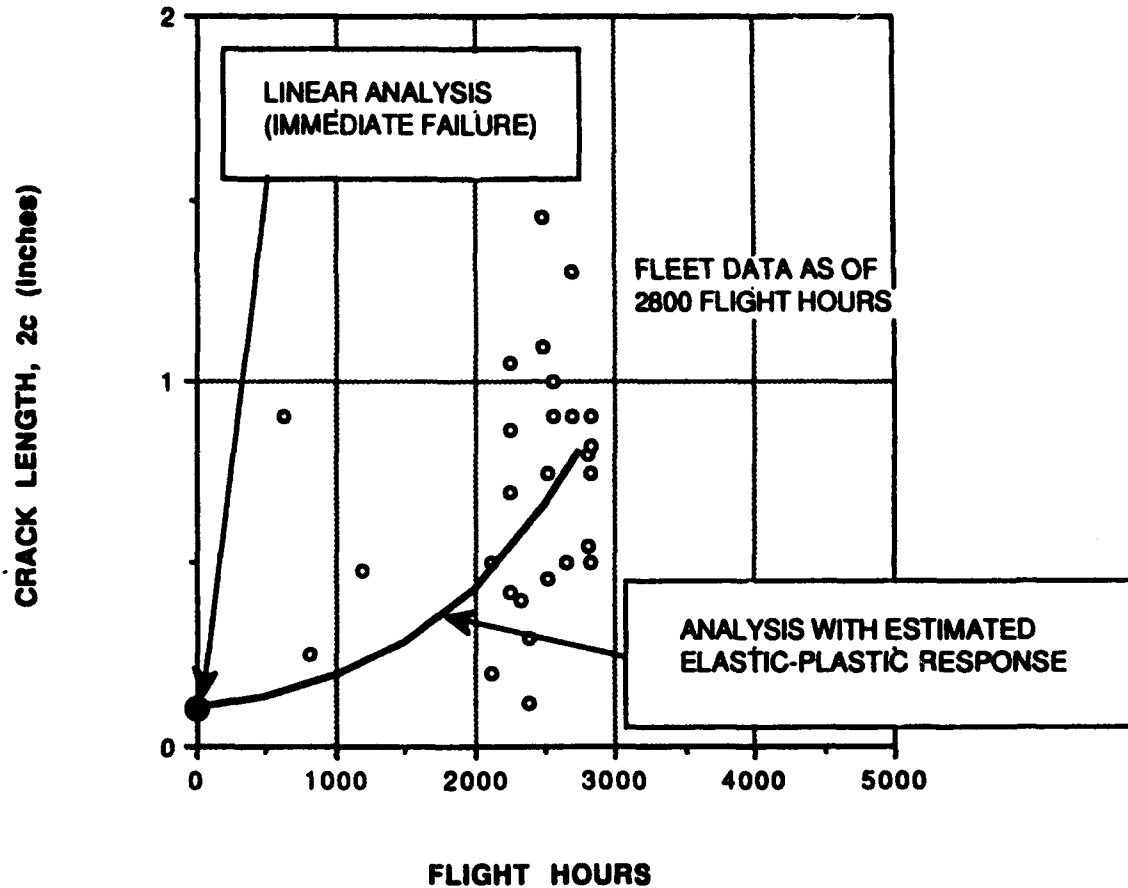


Figure 16. Correlation of Non-Linear Fatigue Crack Growth Analysis Results With Fleet Cracking Data.

The most significant limitations to this method include

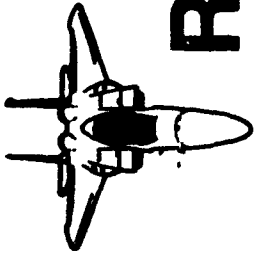
- o Crack sizes must be small (with respect to body dimensions) for the estimated response calculation to remain valid; load redistribution due to the presence of the crack is not considered
- o Elastic predominance is required for the validity of the LEFM based fatigue crack growth analysis
- o Current capability is limited to simple geometries.

REFERENCES

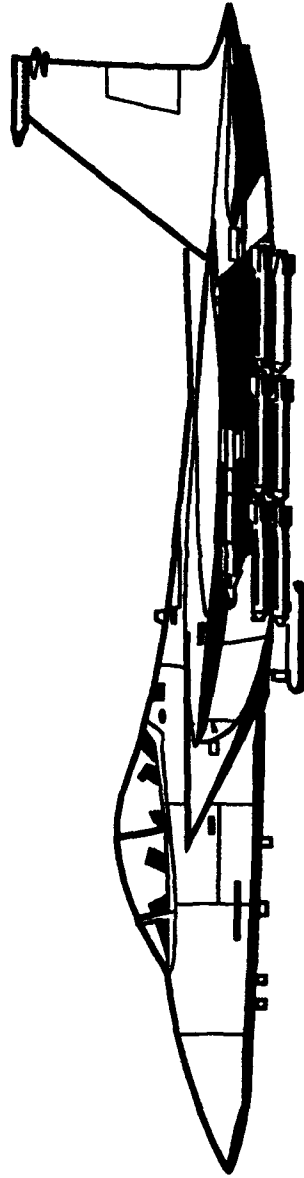
- [1] Hall, L.R., Shah, R.C. and Engstrom, W.L., "Fracture and Fatigue Crack Growth Behavior of Surface Flaws and Flaws Originating at Fastener Holes, Vol. I," Air Force Flight Dynamics Laboratory, AFFDL-TR-74-47, May 1974.
- [2] Shah, R.C., "On Through Cracks at Interference Fit Fasteners," Trans. ASME, J. Pressure Vessel Technology, Feb. 1977, pp. 75-82.
- [3] Chang, J.B., "Prediction of Fatigue Crack Growth at Coldworked Fastener Holes," J. Aircraft, Vol. 14, No. 9, Sept. 1977, pp. 903-908.
- [4] Hsu, T.M., McGee, W.M. and Aberson, J.A., "Extended Study of Flaw Growth at Fastener Holes, Vol. I," Air Force Flight Dynamics Laboratory, AFFDL-TR-77-83, Apr. 1978.
- [5] Glinka, G., "Effect of Residual Stress on Fatigue Crack Growth in Steel Weldments Under Constant and Variable Amplitude Loads," Fracture Mechanics, ASTM STP 677, American Society for Testing and Materials, 1979, pp. 198-214.
- [6] Parker, A.P., "Stress Intensity Factors, Crack Profiles, and Fatigue Crack Growth Rates in Residual Stress Fields," Residual Stress Effects in Fatigue, ASTM STP 776, American Society for Testing and Materials, 1982, pp. 13-31.
- [7] Nelson, D.V., "Effects of Residual Stress on Fatigue Crack Propagation," Residual Stress Effects in Fatigue, ASTM STP 776, American Society for Testing and Materials, 1982, pp. 172-194.
- [8] Kim, C., Diesburg, D.E., and Ellis, G.T., "Effect of Residual Stress on Fatigue Fracture of Case-Hardened Steels -- An Analytical Model," Residual Stress Effects in Fatigue, ASTM STP 776, American Society for Testing and Materials, 1982, pp. 224-234.
- [9] Armen, H., Levy, A. and Eidinoff, H.L., "Elastic-Plastic Behavior of Coldworked Holes," J. Aircraft, Vol. 21, No. 3, Mar. 1984, pp. 193-201.
- [10] Morrow, J., Martin, J.F. and Dowling, N.E., "Local Stress-Strain Approach to Cumulative Fatigue Damage Analysis," Dept. of Theoretical and Applied Mechanics, University of Illinois, T.&A.M. Report No. 379, Jan. 1974.
- [11] Ball, D.L. and Neff, D.R., "Fatigue Load Spectrum Cycle Counting Methods," SDM-1001, LTV Aerospace and Defense, Nov. 1985.
- [12] Dowling, N.E., "Fatigue Failure Predictions for Complicated Stress-Strain Histories," Journal of Materials, JMLSA, Vol. 7, No. 1, March 1972, pp. 71-87.

- [13] Ball, D.L., "Proposed Integration of Notch Strain and Fatigue Crack Growth Analyses," *J. Aircraft*, Vol. 27, No. 3, April 1990, pp. 358-367.
- [14] Dieter, G.R., "Notch Effects," Mechanical Metallurgy, 2ed., McGraw-Hill Book Co., New York, 1976, pp. 280-284.
- [15] Fuchs, H.O. and Stephens, R.I., "Self Stresses and Notch Strain Analysis," Metal Fatigue in Engineering, Wiley, New York, 1980, pp. 125-146.
- [16] Mendelson, A., "Criteria For Yielding," Plasticity: Theory and Application, Krieger Publishing Co., Malabar FL, 1983, pp. 70-97.
- [17] Neuber, H., "Theory of Stress Concentration for Shear-Strained Prismatical Bodies with Arbitrary Nonlinear Stress-Strain Law," *Transaction ASME, J. Applied Mechanics*, Vol. 8, Dec. 1961, pp. 544-550.
- [18] Gallagher, J.P., Giessler, F.J., Berens, A.P. and Engle, R.M. Jr., "USAF Damage Tolerant Design Handbook," AFWAL-TR-82-3073, Air Force Wright Aeronautical Labs, Wright-Patterson AFB, OH, May 1984.
- [19] Cartwright, D.J. and Rooke, D.P., "Green's Functions in Fracture Mechanics," Fracture Mechanics-Current Status, Future Prospects, R.A. Smith, ed., Pergamon, Toronto, 1979, pp. 91-123.
- [20] Bueckner, H.F., "The Propagation of Cracks and Energy of Elastic Deformation," *Trans. ASME*, Vol. 80, Series E, 1958, pp. 1225-1229.
- [21] Chang, J.B., Hiyama, R.M. and Szamosi, M., "Improved Methods For Predicting Spectrum Loading Effects," USAF Wright Aeronautical Laboratories, AFWAL-TR-81-3092, Nov. 1981.
- [22] Chang, J.B., Szamosi, M. and Liu, K-W, "A User's Manual for a Detailed Level Fatigue Crack Growth Analysis Computer Code, Vol. I - The CRKGRO Program," USAF Wright Aeronautical Laboratories, AFWAL-TR-81-3093, Nov. 1981.
- [23] Endo, T., and Morrow, JoDean, "Cyclic Stress-Strain and Fatigue Behavior of Representative Aircraft Metals," *Journal of Materials, JMLSA*, Vol.4, No. 1, March 1969, pp. 159-175.
- [24] Landgraf, R.W., Morrow, JoDean and Endo, T., "Determination of the Cyclic Stress-Strain Curve," *Journal of Materials, JMLSA*, Vol.4, No. 1, March 1969, pp. 176-188.
- [25] Hibbit, H.D., Karlsson, B.I. and Sorensen, E.P., "ABAQUS, Structural and Heat Transfer Analysis Program, Version 5.2," Hibbit, Karlsson & Sorensen, Inc., Pawtucket RI, 1992.

- [26] Altstaeter, G.P., FZS-12-531, General Dynamics/Fott Worth Division, March, 1987.
- [27] Logan, B.J. and LaBar, B.G., FZS-12-454, General Dynamics/Fort Worth Division, April 1982.
- [28] Patin, R.M., FZS-12-533, General Dynamics/Fort Worth Division, August 1987.
- [29] Hadley, S.A, et.al., 16PR11666, Vol. I, Lockheed Fort Worth Company, August 1993.
- [30] Gordon, D.E., "2124-T851 Aluminum Cyclic Stress-Strain Data," Unpublished, General Dynamics/Fort Worth Division, October 1986.



Results - To - Date on Fatigue Test of Combined F-15 A and C Article Subjected to Actual Usage Spectrum

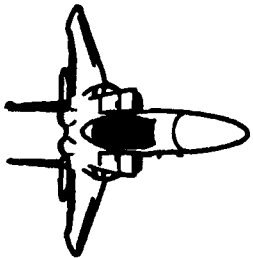


**Rick Foster
Ron Melliore**

McDonnell Douglas Aerospace

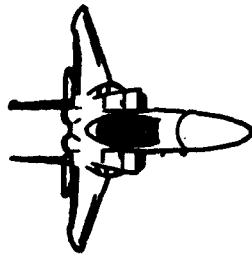
MCDONNELL DOUGLAS

30 Nov 1993



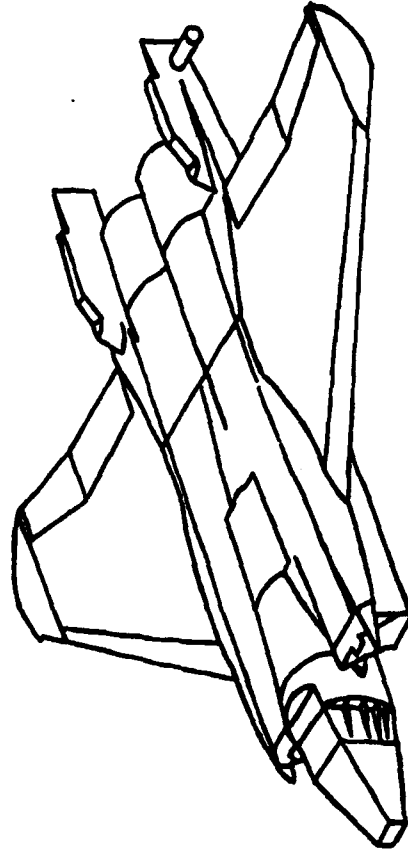
Summary

- **Original Test Was Conducted in 1973**
- **DTA in 1981 Indicated Need For Additional Testing**
- **Teardown of Original Article in 1988 Was Too Late**
- **New Test of Wing/Center Fuselage Began in 1988**
- **Only Minor (Repairable) Wing Cracking Has Occurred to Date**

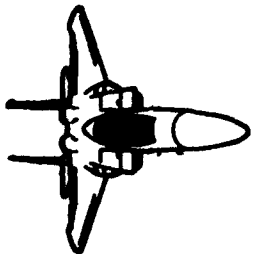


Original Test of F-15A Was Conducted in 1973

- Durability Test of Wing/Center Fuselage
- 1000 Hour Repeating Design Spectrum
 - * Max Peak of 105% Design Limit Load Every 1,000 Hours
 - * One Time Application of 125% Design Limit Load at 8,000 Hours
- Completed 16,000 Hours With Only Minor Cracking
- Article Was Stored for Potential Test Continuation

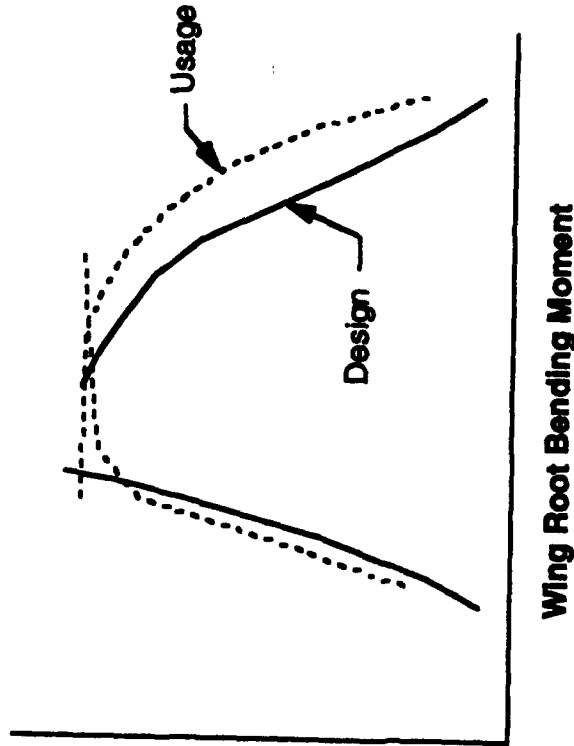


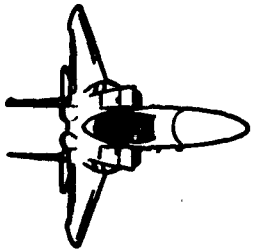
FTA-1 Wing/Center Fuselage
Fatigue Test Article



Actual Usage is More Severe Than Design

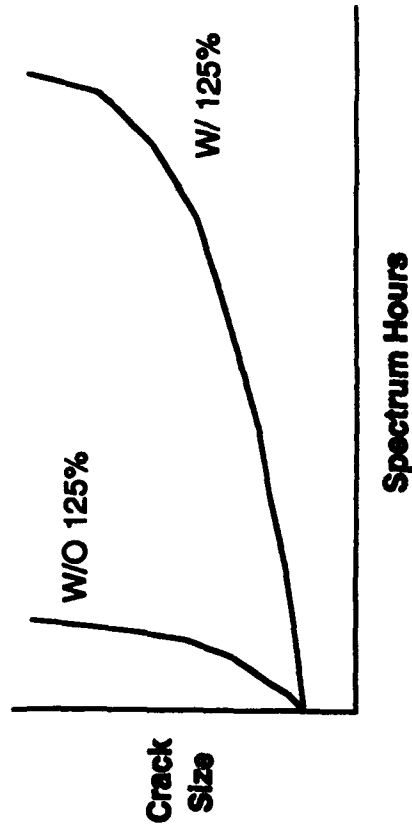
- DTA Was Conducted in 1981
- Actual Wing Usage Found to Be 4 Times as Severe as Design
- Severity Was Due to Two Factors
 - * Usage Contained 85% Air-To-Air Missions vs. 48% for Design
 - More Severe Nz Occurrence Rate
 - More Severe Point-in-the-Sky
 - * Air-To-Air Combat Weight Was 5,000 lbs Heavier Than Design
 - Higher Wing Load for Same Nz



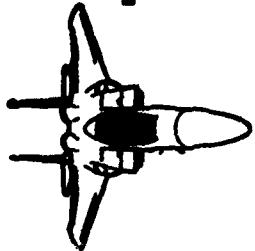


Additional Fatigue Testing Was Needed

- Original Test Article Was Considered for Restart
- Element Tests Indicated That 125% Load Applied at 8,000 Hours Made It Unfit for Continuation
- * Beneficial Residual Stresses Retarded Crack Growth and Could Delay Crack Initiation



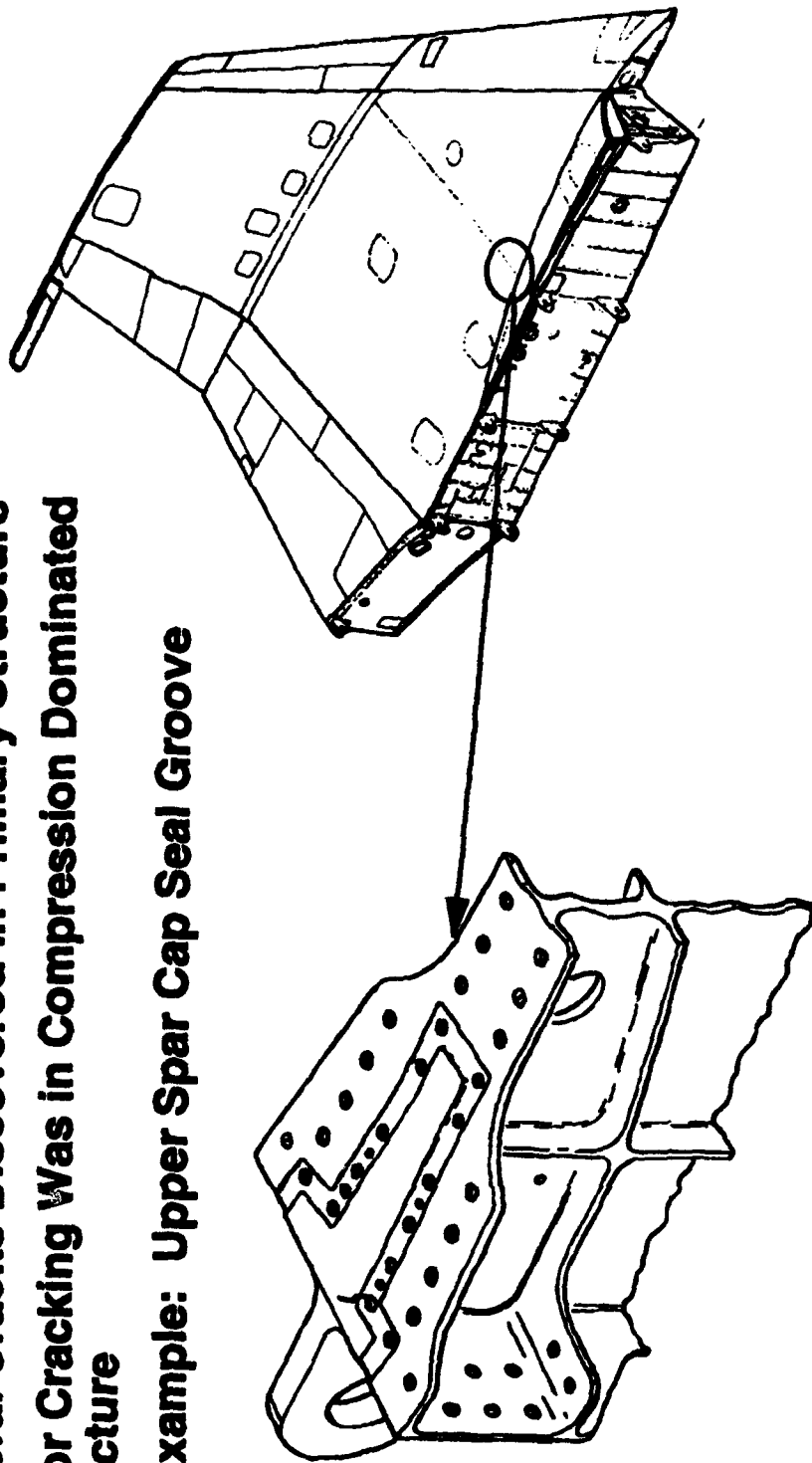
- Conclusions:**
1. Restart Test With Virgin Test Article
 2. Teardown Original Article



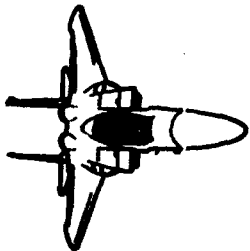
Teardown of Original Test Article Yielded Useful Data Too Late

- Several Cracks Discovered in Primary Structure
- Major Cracking Was in Compression Dominated Structure

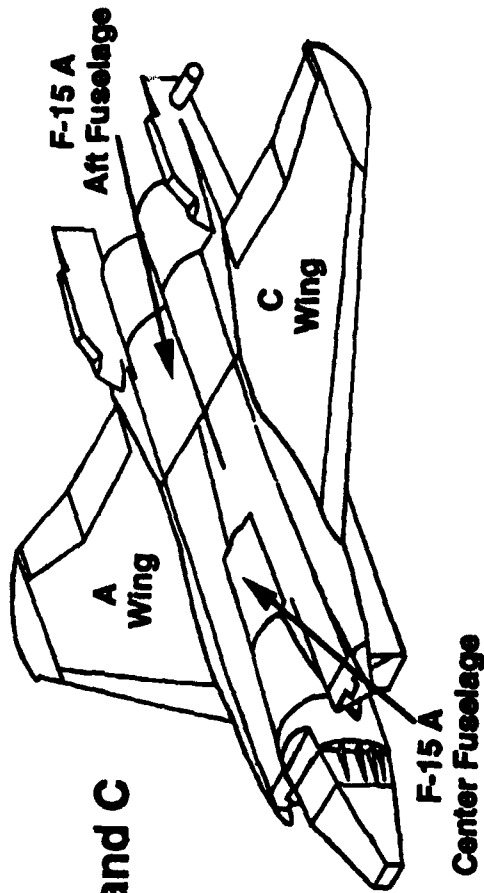
Example: Upper Spar Cap Seal Groove



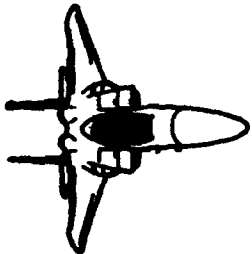
- Data Was Too Late to Avoid USAF Maintenance Cost



New Durability Fatigue Test Began in 1988



- **Wing / Center Fuselage Spectrum Representative of Average F-15 A and C**
 - * **1,000 Hour Repeating Block**
 - * **Max Peak = 115% DLL Every Block**
- **Test Plan - Achieve 24,000 Hours or Economic Life, Whichever is First**
- **Goals:**
 - 1) **Determine Critical Locations**
 - 2) **Determine Fatigue Lives and Crack Growth Characteristics at Critical Locations**
 - 3) **Define Economic Life of the Airframe**

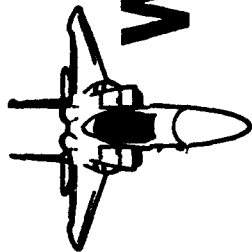


Testing is in Progress at AFWAL

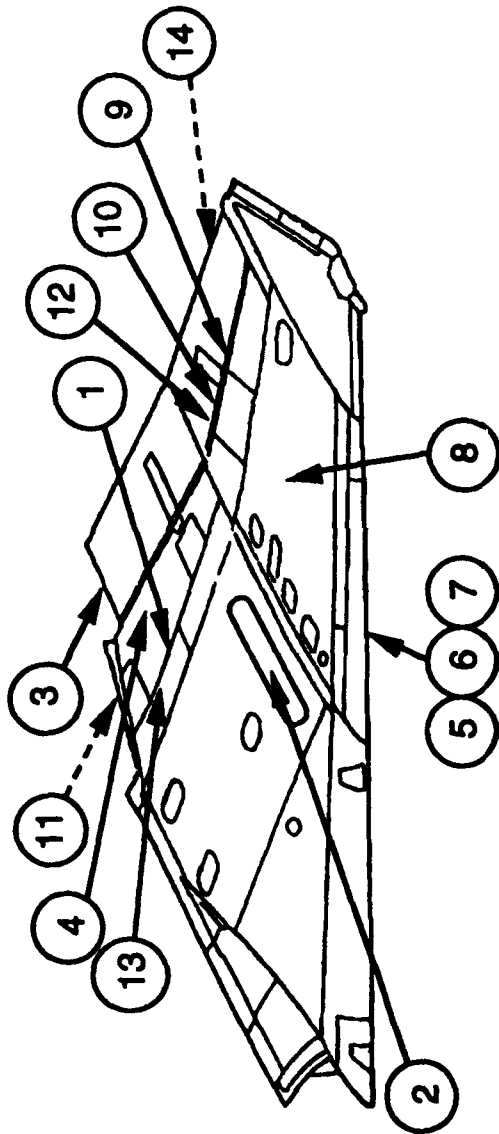
- **Article Has Achieved 13,600 Flight Hours**



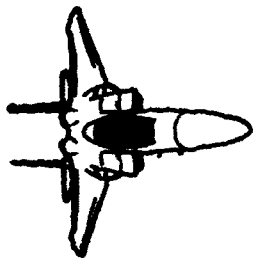
- **Several Cracks Have Occurred on Wings**
- *** None Have Been Life Limiting - Depot Repairs Installed**
- *** Most Cracks Had Already Been Experienced by Service Aircraft, But Were More Extensive on the Test Article**
- **Virtually No Cracking Discovered in Fuselage**



Wing Cracking Has Been Repairable

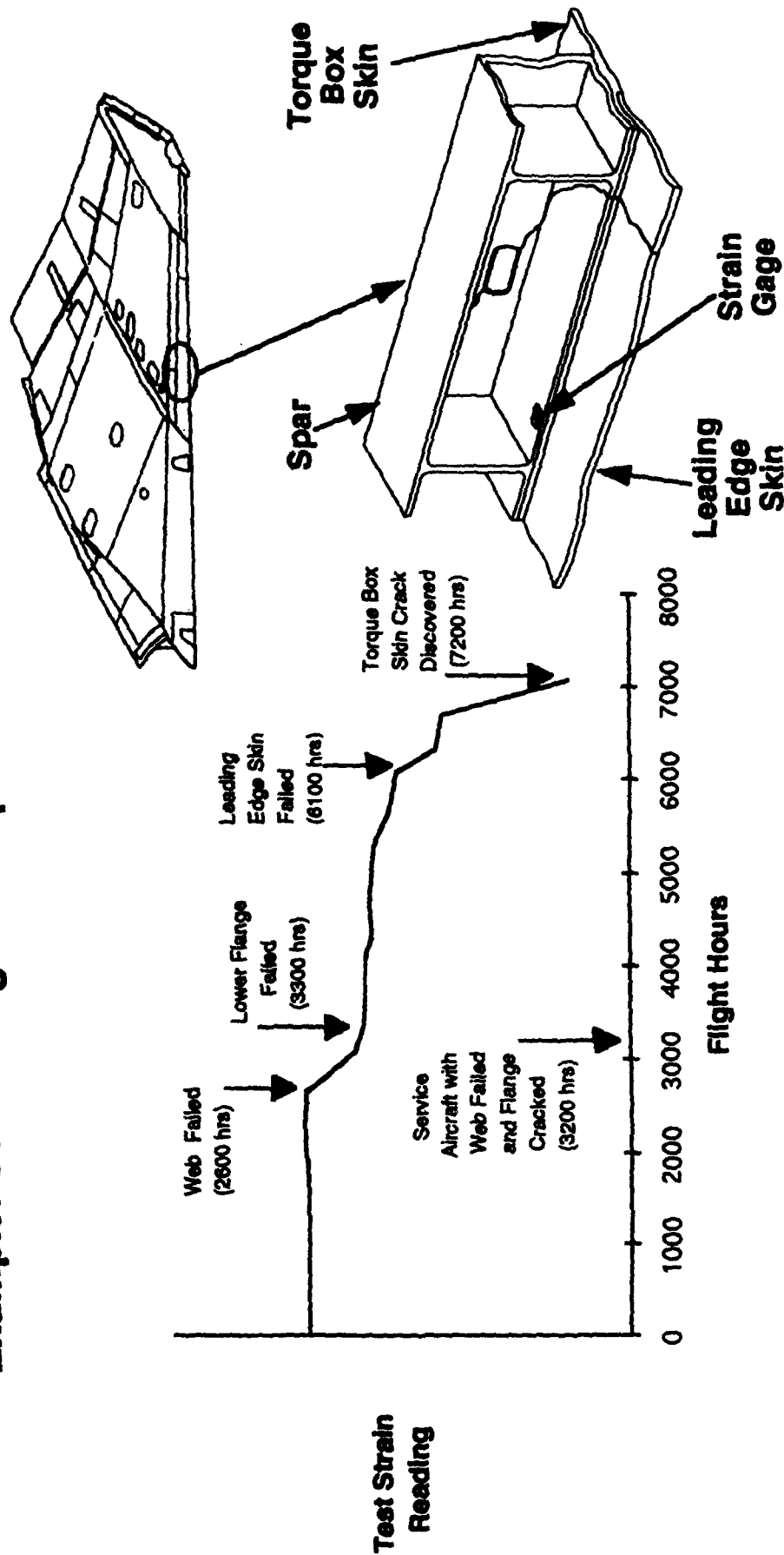


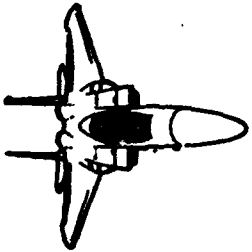
Cracking Area	Spectrum Hours	Disposition
1 Trailing Edge Door Sill	5500	Replaced
2 Upper Skin Stringers	5500	Repaired
3 Flap Upstop	6600	Replaced
4 Flap Inboard Hinge	6600	Replaced
5 Front Spar	7200	Repaired
6 Lower Skin	7200	Repaired
7 Leading Edge Skin	7200	Repaired
8 Upper Rib Caps	7200	Replaced
9 Closure Spar Actuator Cutout	7200	Repaired
10 Closure Spar Transducer Hole	9200	Repaired
11 Lower Trailing Edge Skin	9700	Repaired
12 Aileron Hinge	9700	Repaired
13 Fuel Beam	12000	Repaired
14 Lower Trailing Edge Skin	13600	Repaired



Test Cracking Correlates With Service Experience

Example: Outer Wing Front Spar on F-15A

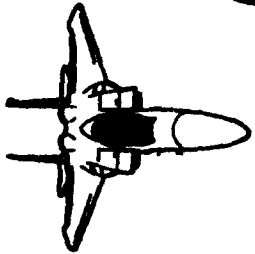




Service Hours Demonstrated to Date Exceed High Time Aircraft

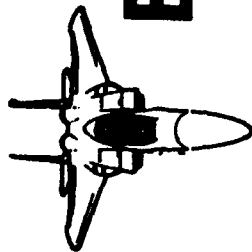
- Test Hours Completed = 13,600
- High Time Service Aircraft Are at 4,800 Flight Hours
- Equivalent Service Hours Demonstrated to Date -

	Usage Severity Relative to Test	Demonstrated Hours
Average F-15A	0.92	14,800
Average F-15C	1.16	11,700
Severe F-15A	1.46	9,300
Severe F-15C	2.39	5,700



Teardown Inspection Will Be Conducted at Conclusion of Test

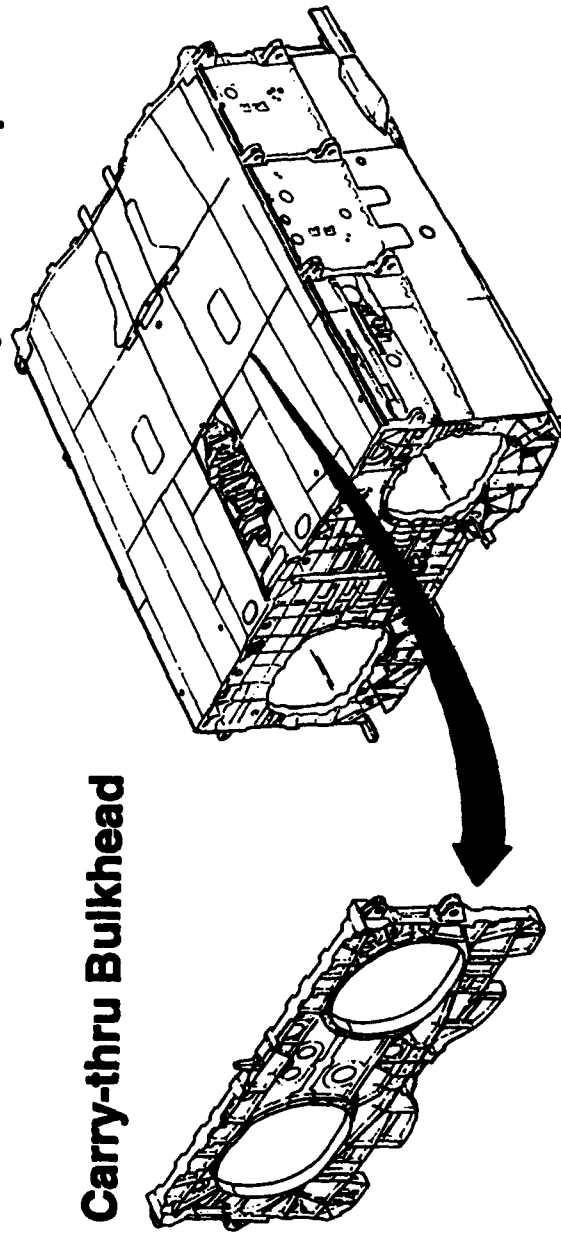
- **Test Article Will Be Disassembled and Cracks/Failures Located**
- **Cracks and Failures Will Be Analyzed to Determine Economic Life**
- **Life Limiting Failure Areas Will Be Candidates for:**
 - * **Preventive Maintenance**
 - * **Safety Inspections**



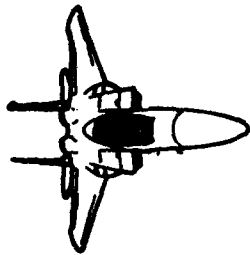
Economic Life is Likely to Exceed 8,000 Hours

- USAF Has Determined That the Wing Will Not Define Economic Life
 - * All Components Are Economical to Repair or Replace
- Fuselage Will Define Economic Life
 - * Major Load Paths Are Not Economical to Repair or Replace

e.g. Carry-thru Bulkhead

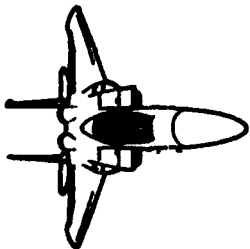


- No Indication of Impending Fuselage Failure (or Cracking) Yet



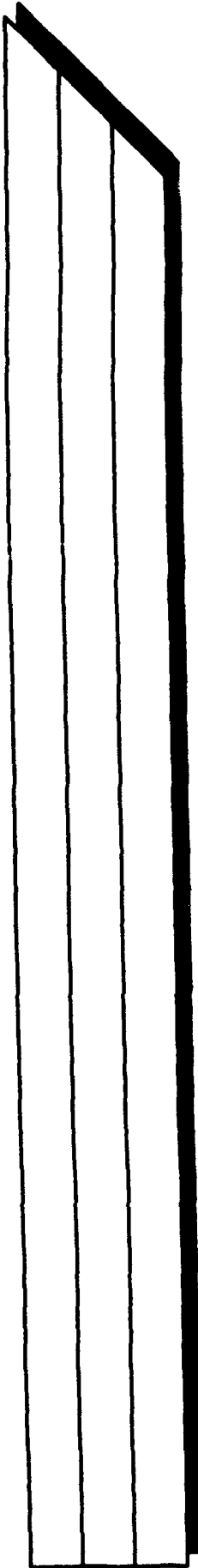
Conclusions to Date Relative to Service Aircraft

- **Cracking Prior to 8,000 Hours Will Occur Primarily in Repairable Wing Structure**
- **No Significant Fuselage Cracking Expected Prior to 8,000 Hours**
- **Economic Life Will Likely Exceed 8,000 Hours**



Lessons Learned / Recommendations

- **Durability Fatigue Test Well Beyond 2 Lifetimes of Design Usage, Preferably Until Economic Life is Reached**
- **Conduct Teardown Inspection Immediately After Test Completion**
- **Do Not Include "Beneficial" Load Cycles Occurring Less Frequently Than Every 1,000 Flight Hours**
- **Do Not Ignore Fatigue Details in Compression Dominated Structure**



THE 90/95 CRACK LENGTH REVISITED

Alan P. Berens
University of Dayton Research Institute

Sharon I. Vukelich
ASC/ENFSF

**1993 USAF Structural Integrity
Program Conference
San Antonio, Texas**

Agenda

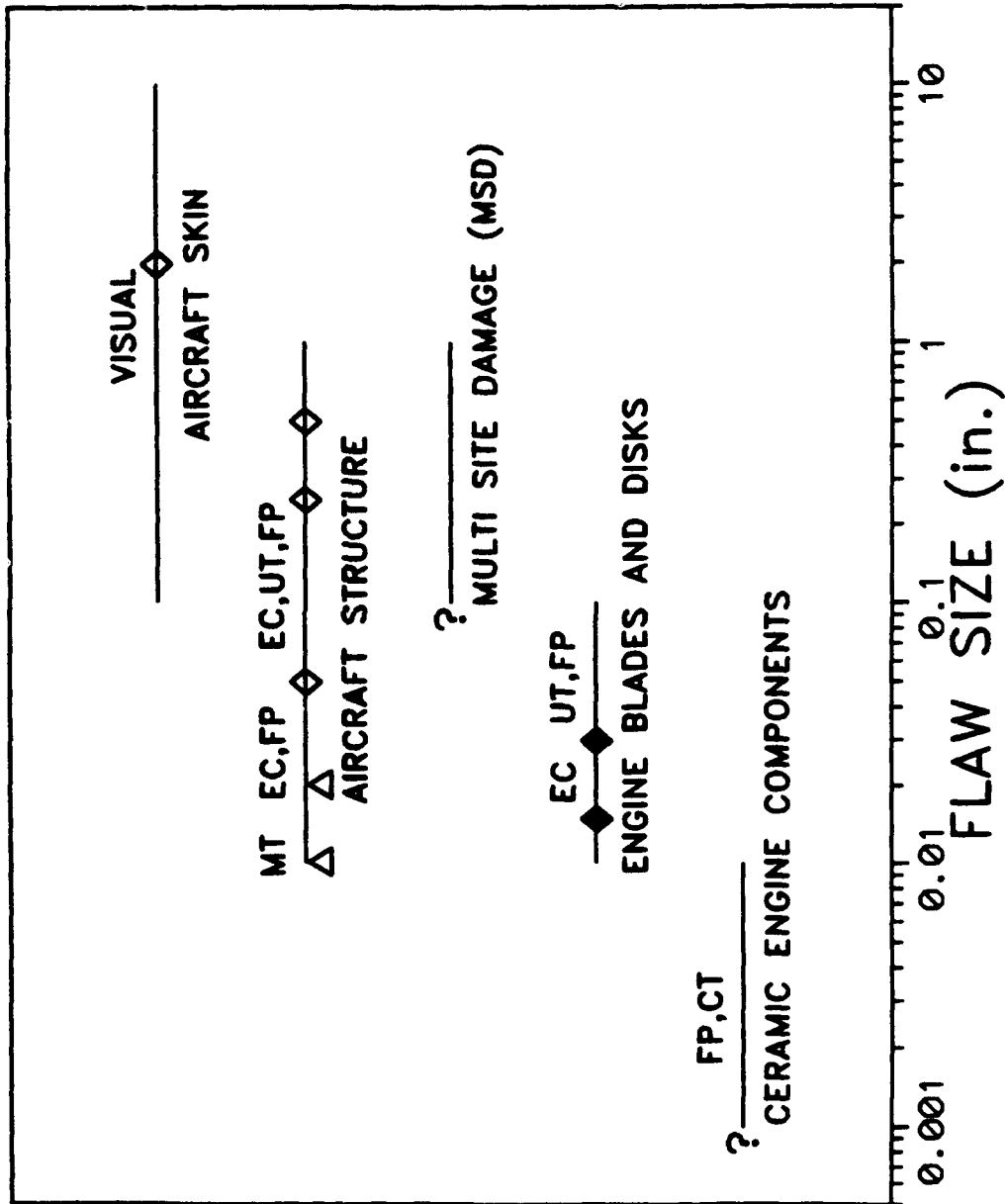
- **Basics**
 - *Uncertain Nature of Process*
 - *What is POD(a)*
- **Demonstration Programs**
- **Analysis Methods**
 - *Parametric vs Binomial*
- **MIL-STD-XXX**

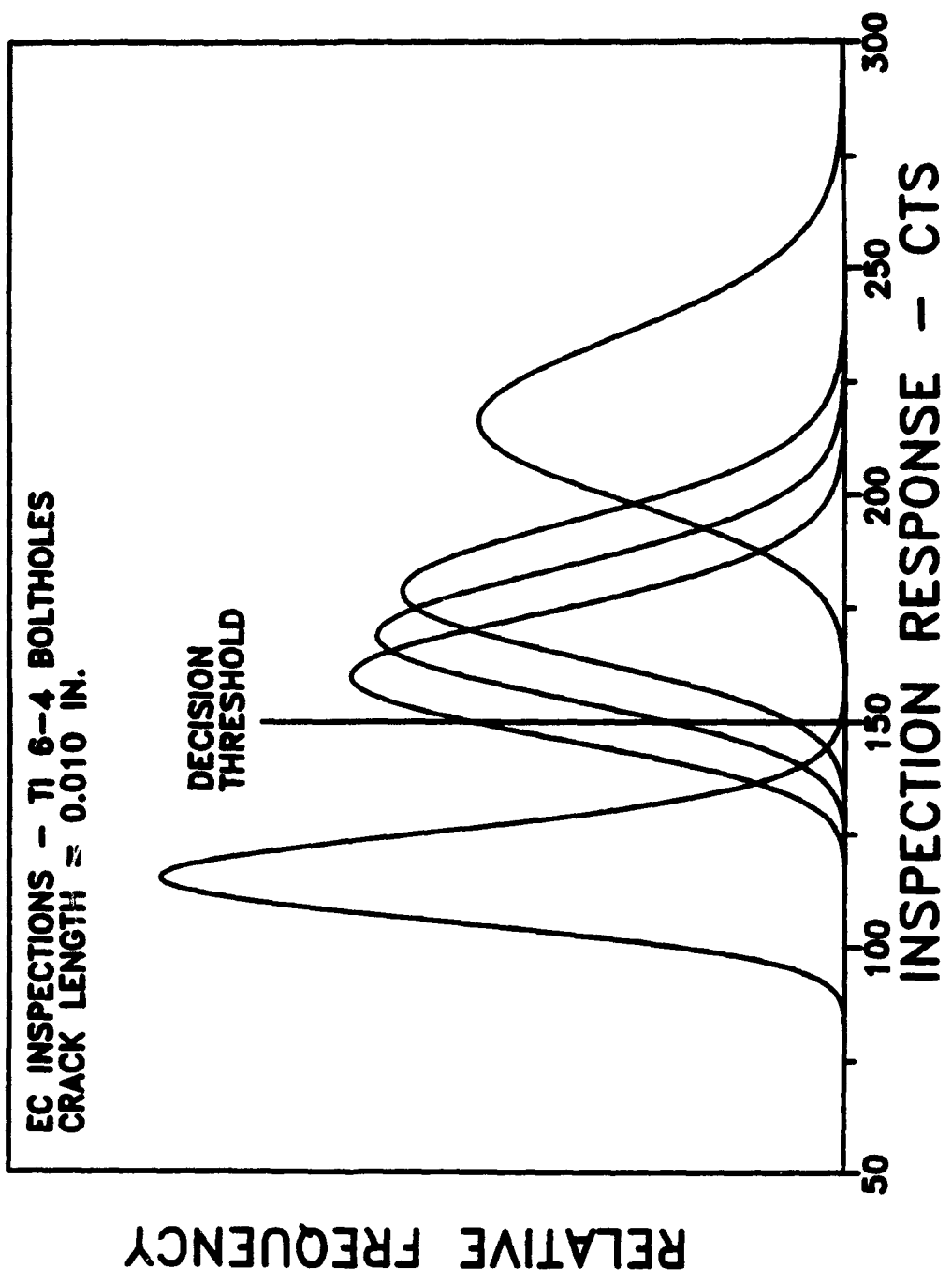
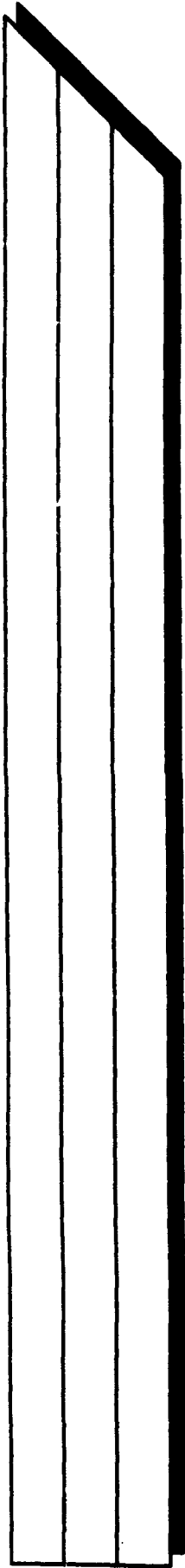
Assessment Objectives

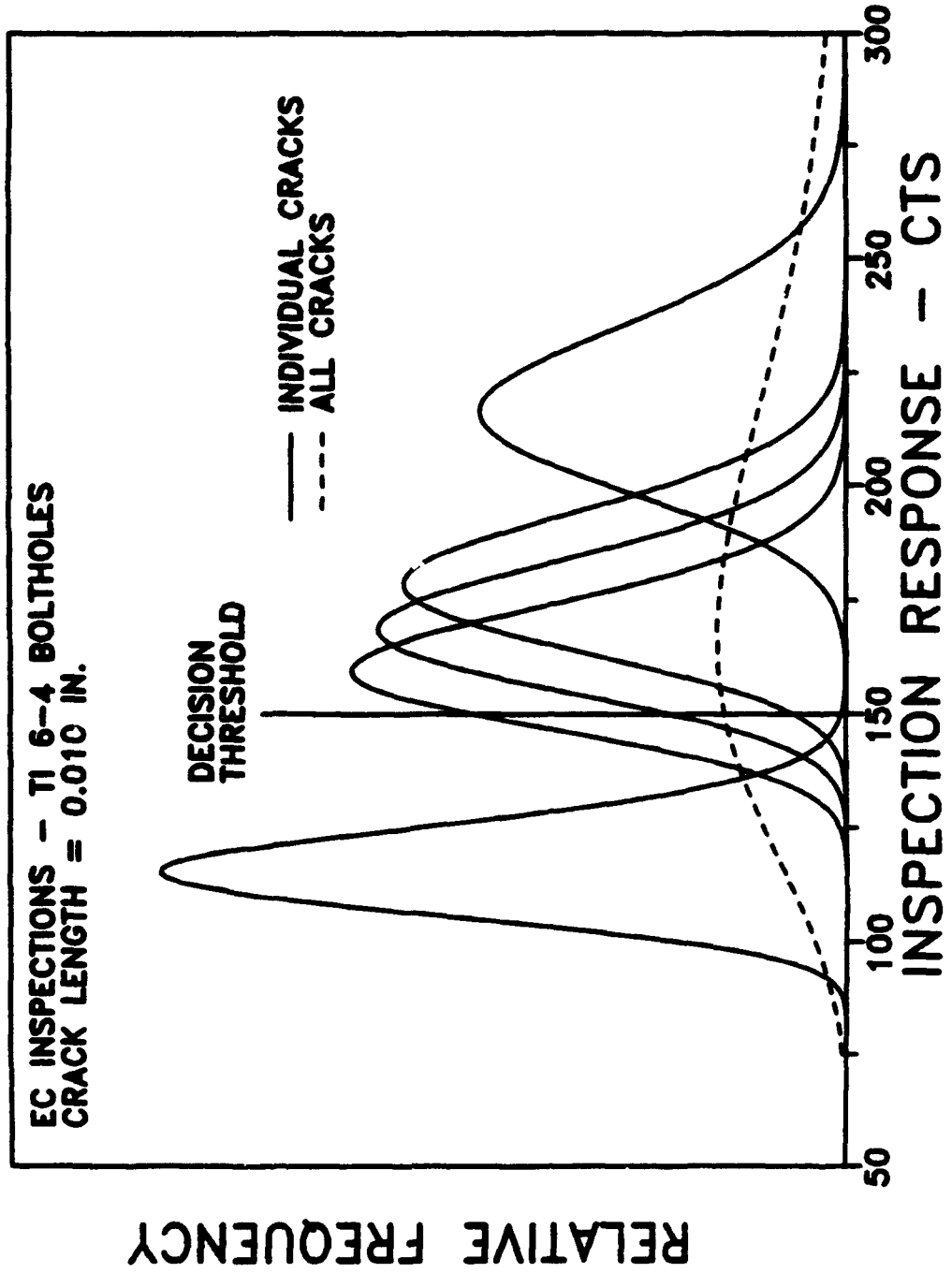
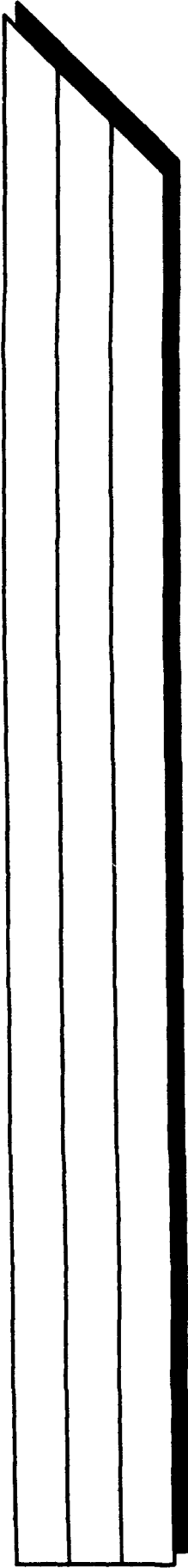
- **NDI Technologists**
 - *Design/Develop/Apply Methods*
- **Inspectors**
 - *Evaluate/Compare Individuals*
- **Inspection Shops**
 - *Production Rates*
- **Safety**
 - *Repair/Replace Damaged Structure*
 - *DTA for Period of Safe Operation*
 - » *Size Detected Flaws*
 - » *Potential Flaw Sizes After Inspection*

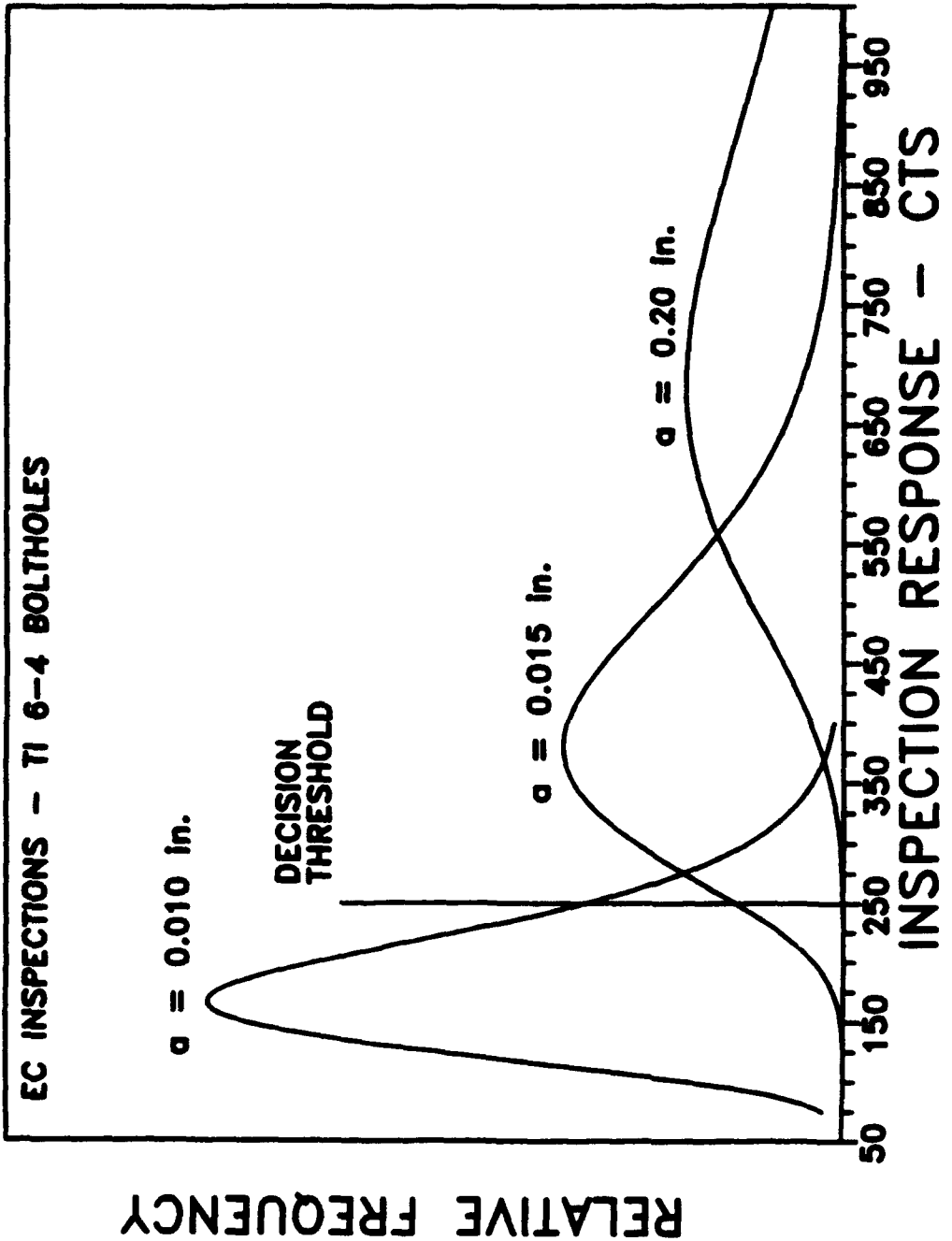
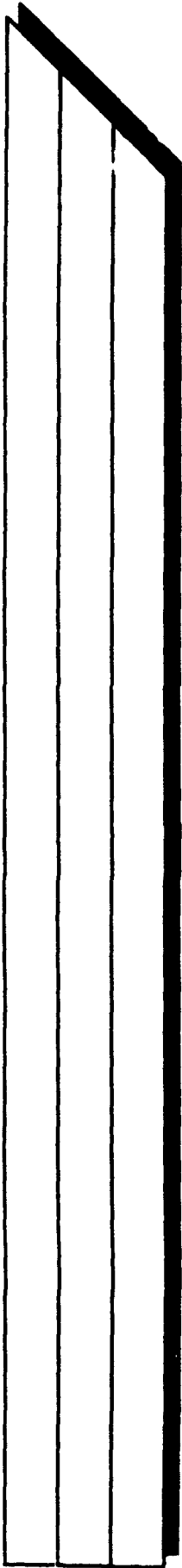
Reliably Detected Crack Size

- **What is a_{NDE}**
- **a_{NDE} From Historical Inspection Records**
 - **Includes Human Factors**
 - **Real Inspection Scenarios**
 - **Adjust Detected Crack Size**
- **a_{NDE} From Demonstration Experiments**









What is $POD(a)$?

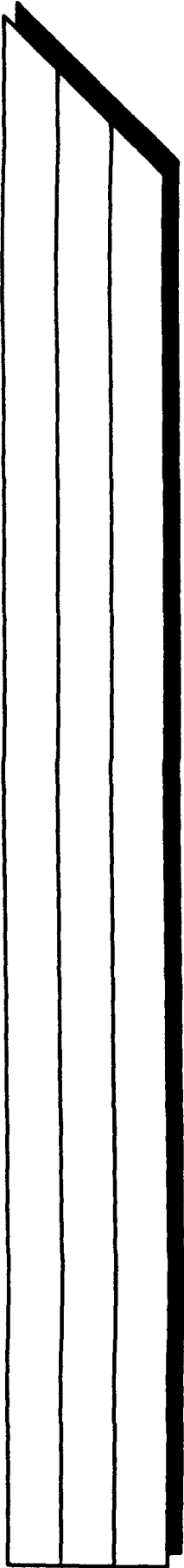
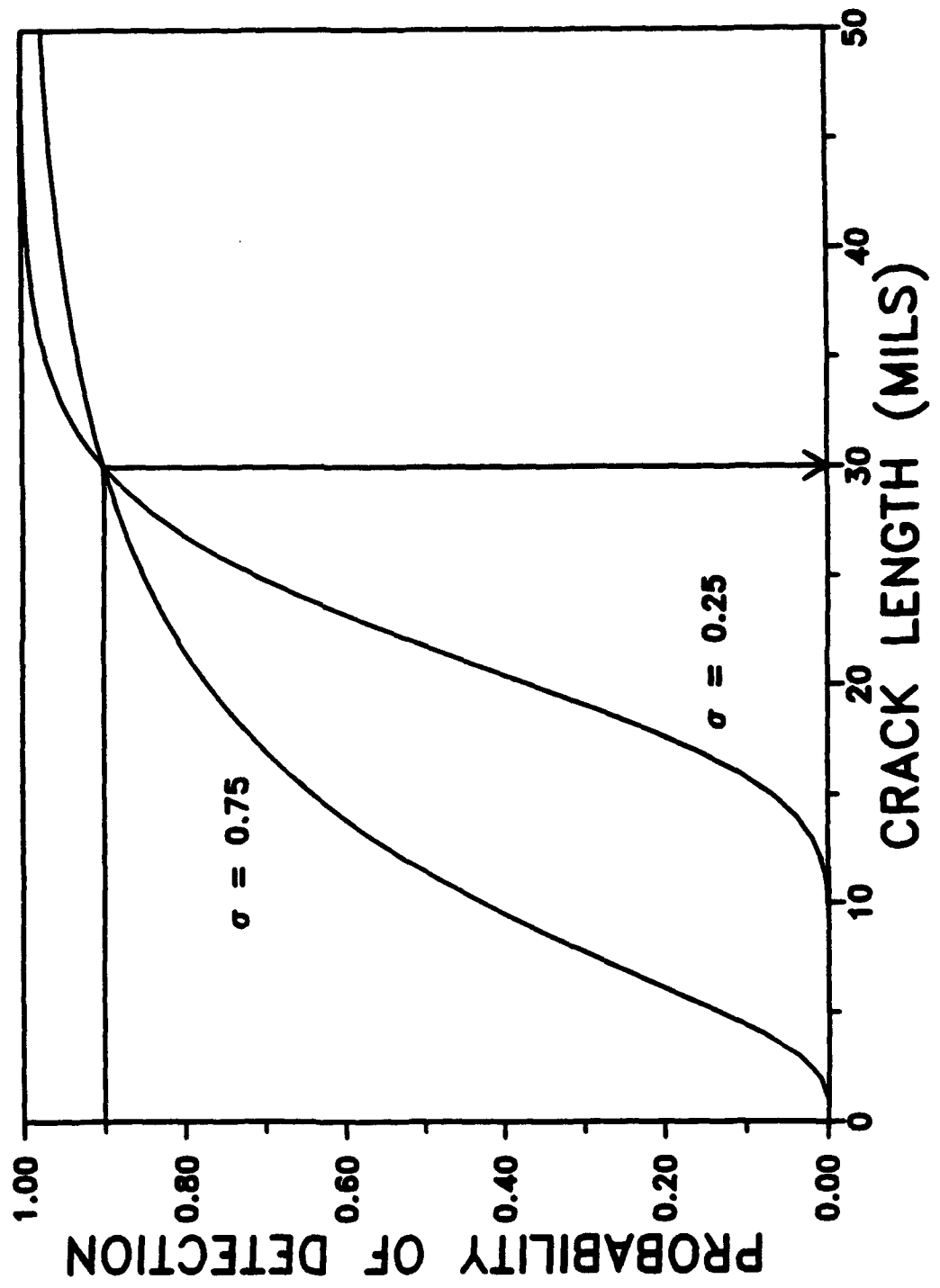
- ***Given a Population of Cracks of Size a***
 - ***Given a Defined Inspection System***
 - ***$POD(a)$ = Probability that Randomly Selected Cracks from the Population will be Detected***
- $POD(a)$ = Proportion of all Cracks from the Population that Would be Detected***

What is a_{NDE} ?

- **Crack Size with High Pod**
 - $P(a_{NDE}) \geq 0.9$
- **But $POD(a)$ can Only be Estimated**
 - Statistical Variation in Estimate
- **Quantify Uncertainty with Confidence Bound**
 - 95% Confident that $POD(a_{NDE}) \geq 0.9$ (The 90/95 Crack Size)
- **N.B. 90/95 Crack Size is not a Constant (i.e., Not a Fixed Property of Inspection System)**

Demonstrate or Estimate?

- **Simulate Inspections**
 - **Defined Inspection System**
 - **Representative Cracks**
- **Demonstrate - One Crack Size**
 - **Observe Proportion of Finds**
 - **Lower Confidence Limit**
- **Estimate - Entire POD(a) Function**
 - **Model for POD(a)**
 - **Fit Parameters from Data**
 - **Lower Confidence Bound**



Binomial Analysis to Demonstrate 90/95 Capability for a_{NDE}

- **Specimen Set With Many Cracks of Size a_{NDE}**
- **95% Confidence That at Least 90% of Cracks
of Size a_{NDE} will be Detected**
 - 29 Finds in a Set Containing 29 Cracks
 - 45 Finds in a Set Containing 46 Cracks
 - 59 Finds in a Set Containing 61 Cracks
 - etc.
- **Cannot use Multiple Inspections of Same
Cracks**

Binomial Analysis to Demonstrate 90/95 Capability for a_{NDE} (Cont'd)

- **Many More Specimens Needed for More Confidence or Greater Pod**

e.g., 95% Confidence that at Least 95% of Cracks of Size a_{NDE} will be Detected

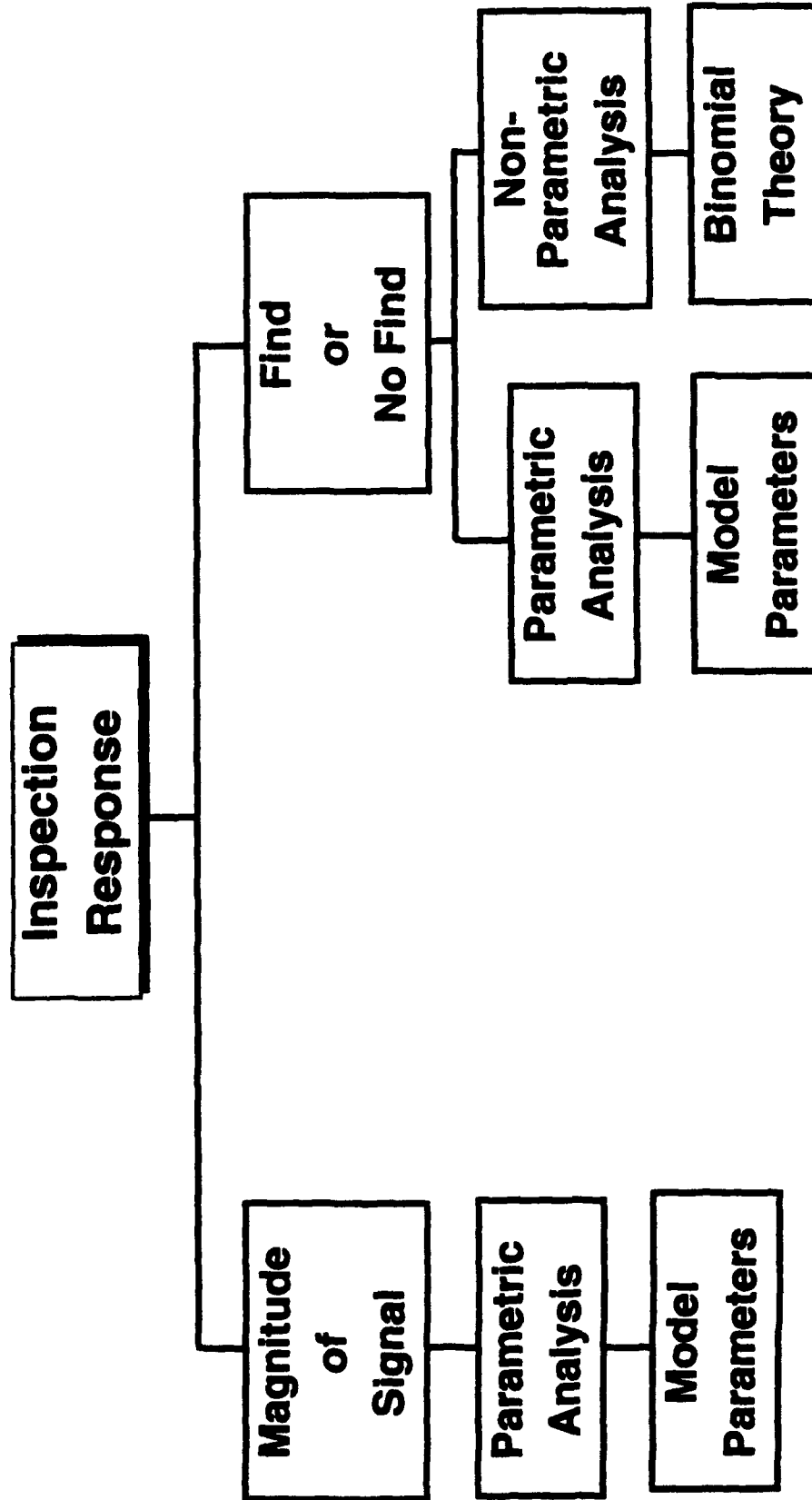
» **59 Finds in a Set Containing 59 Cracks**

- **Human Factors Problem**
- **No Information at Other Crack Sizes**
 - **Changing Requirements**

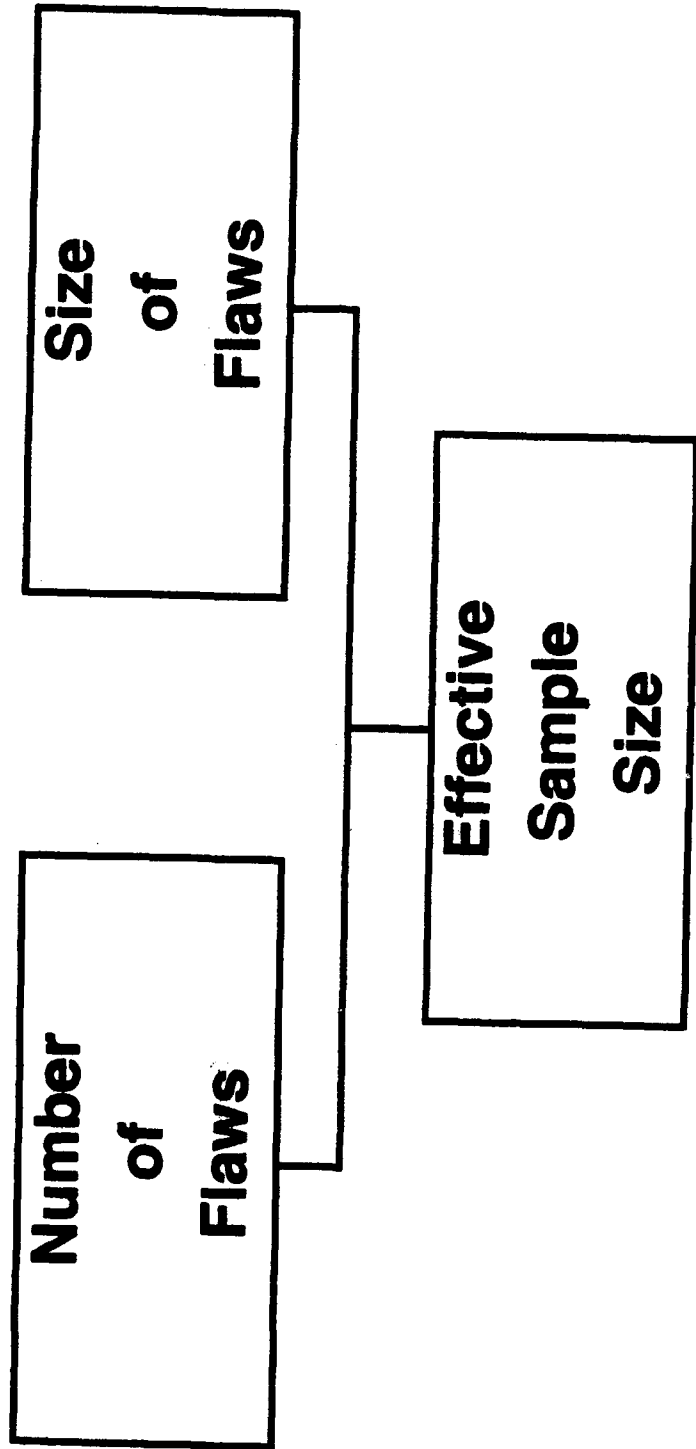
Maximum Likelihood Analysis to Estimate $POD(a)$ and Confidence Bound

- **Quantitative Comparisons of Inspection Systems**
- **Evaluations of Inspection System Factors**
- **Many Cracks of Many Sizes**
 - *Range of Increase of the $POD(a)$ Function*
- **Analysis can Account for Multiple Inspections of Cracks**

Nature of Inspection Result



Sample Size



- *At Least 40-60 Flawed Inspection Sites for $\hat{\alpha}$ Data*
- *At Least 60-80 Flawed Inspection Sites for Hit/Miss Data*
- *At Least Three Times as Many Unflawed Inspection Sites*

Maximum Likelihood Estimation - \hat{a}

- *Inspection Result - \hat{a}_i :*

$$\hat{a}_i \sim N(\beta_0 + \beta_1 \ln a, \sigma^2)$$

- *POD(a) is Cumulative Log Normal*
- $L(\beta_0, \beta_1, \sigma) = \prod f(a_i; \beta_0, \beta_1, \sigma)$
- *Determine $\hat{\beta}_0$, $\hat{\beta}_1$, and $\hat{\sigma}$ to Maximize L*
- *Known Asymptotic Statistical Properties*

Maximum Likelihood Estimation - Hit/Miss

- *Inspection Result - Hit (1) or Miss (0)*

$$POD(\mathbf{a}_i) = \Phi(\mathbf{a}_i, \mu, \sigma), \text{ say } P_i$$

- $L(\mu, \sigma) = \prod P_i^{z_i} (1 - P_i)^{1 - z_i}$

- $Z_i = 1$ (Find) or 0 (Miss)

- Determine $\hat{\mu}, \hat{\sigma}$ to Maximize L

- Known Asymptotic Statistical Properties

MIL-STD for USAF NDE System Reliability Assessment

- **General Requirements**
 - *Responsibilities*
 - *System Definition and Control*
 - *Demonstration Design*
 - *Demonstration Tests*
 - *Data Analysis*
 - *Presentation of Results*
 - *Retesting*
 - *Process Control Plan*
- **Specific Requirements for EC, FP, UT, MT**
- **Appendices**

Summary

- ***NDE Reliability Must be Quantified***
- ***90/95 Crack Size for a Defined Inspection System is not a Constant***
- ***Demonstration Program Simulates Inspections***
 - ***Number of Cracks (Not Inspections) Determines Sample Size***
 - ***Binomial Analysis - Limited Inferences***
 - ***POD(a) Model - More General Characterization***
- ***Military Standard for NDE System Reliability Assessment***



**AIRCRAFT FATIGUE AND CRACK GROWTH
CONSIDERING LOADS BY STRUCTURAL COMPONENT**

**James D. Yost
DPRO -
Bell Helicopter Textron, Inc.
Fort Worth, Texas**

**1993 USAF Structural Integrity Program Conference
30 November - 2 December, 1993
San Antonio, Texas**

AIRCRAFT FATIGUE AND CRACK GROWTH CONSIDERING LOADS BY STRUCTURAL COMPONENT

J. D. Yost*

The indisputable 1968 C-130 fatigue/crack growth data is reviewed to obtain additional useful information on fatigue and crack growth. The proven Load Environment Model concept derived empirically from F-105D multi-channel recorder data is refined to a simpler method by going from 8 to 5 variables in the spectra without a decrease in accuracy. This approach provides the true fatigue/crack growth and load environment by structural component for both fatigue and strength design. Methods are presented for defining fatigue scatter and damage at crack initiation. These design tools and criteria may be used for both metal and composite aircraft structure.

INTRODUCTION

The main objective is to provide the best methods for fatigue/crack growth and load environment prediction. In most cases only one full scale fatigue test is conducted per aircraft type. The local loading on component elements can not be simulated even though shear, torsion and bending moment at a station may be in good agreement with theoretical or flight test values.

In 1967 many C-130 aircraft were flying in Southeast Asia with fatigue cracks (Yost (1)) at low risk due to their damage tolerant structural design. Aircraft were sent to be repaired when the cumulative cracks' length at a surface wing station was 10 inches or more. In about 1970 the aluminum 7075T6 center wing sections on the C-130s were replaced with a new structure due to many fatigue cracks in fleet aircraft. Wing station (WS) 120 center section crack data are used to give a better understanding of structural fatigue in aircraft.

*DPRO-BHTI, P.O. Box 1605, Fort Worth, Tx 76101-1605

The primary elements of the load environment may be broken down into ground-air-ground (GAG), gust, maneuver, buffet, taxi, jump takeoff and landing. Buffet loads may be superimposed on gust or maneuver and sometimes on both. Load spectra of most concern for fighter aircraft (Yost and Johnson (2)) is maneuver loads. Both gust and maneuver are very important for transport design for the flight domain. Current civil transport aircraft fly at higher speeds than earlier prop aircraft thus they respond to a lower frequency portion of the gust Power Spectral Density or longer wavelength higher magnitude gusts (Yost et al. (3)). Comparison of current versus past NASA VGH data shows this trend. Also, severe turbulence is avoided and the normal load factor (N_z) spectra contains buffet, gust and maneuver. Military Specifications in the MIL-A-8860 series have been updated as new data became available from test programs and fleet aircraft load recorder programs. Even though these data are N_z spectra which include buffet, gust and maneuver, the breakdown to mission segment is of great value.

Ground operations are centered on landing gear design for sink rate, taxi response for usage and gear dynamic magnification factor (DMF). DMF for spin-up and spring-back loads may be greater in the Drop-Tower certification than during aircraft landings so fatigue and strength design is conservative. Fatigue is accumulated on other aircraft components besides the landing gear and backup structure during ground operations.

A new method is presented for defining scatter in fatigue failures (Yost (4)). It is believed that the methods for prediction of loads ((2), Yost (5)) and fatigue failures in metal structure is the same for composite structure.

C-130 CRACK GROWTH DATA BASE

The C-130 data (1) from 1967 and 1968 is the best most complete large statistical sample source for fatigue and crack growth by mission of documented data for upper and lower wing surface. The in flight fatigue test data cover nine different missions. These included a mild load environment long range cargo mission. One of the most severe load environment missions was low altitude with gust loads superimposed on the maneuvers. A very high percentage of these fleet aircraft had fatigue cracks as shown in Table 1.

The crack growth was monitored by measuring the crack length every two weeks. Accumulated crack growth data was added to the data base. The past history of individual aircraft was defined by taking records

of missions flown per base and the flight hours accumulated at assigned bases.

TABLE 1 - C-130 fleet aircraft cracks in 1968.

Total aircraft	619
Aircraft with fatigue cracks	345
Aircraft with fatigue cracks at WS 120	289
Aircraft repaired	81

A crack growth curve was derived from documented data with crack length on the ordinate and fatigue damage on the abscissa. This crack growth curve was used to convert the total crack length per upper or lower surface at WS 120 to fatigue damage on the left or right side. A new crack growth curve was obtained by least squares curve fit of fleet crack growth data and is presented in Figure 1 for upper and lower surface.

The actual fatigue damage on individual aircraft was obtained by taking the crack growth curve in Figure 1 and cumulative crack length per surface for converting to actual damage. Next a regression analysis was conducted using actual damage as the dependent variable and flight hours for each of the nine missions as independent variables. These analyses produced coefficients that were damage per flight hour for upper and lower surfaces at WS 120 for each of the nine missions. Validation of these coefficients was accomplished by using crack growth data from aircraft which had most or all of their usage on only one mission.

The actual damage per mission flight hour was used as a dependent variable to interrogate the fleet data with regression analysis for the damage source. Statistical sound parameters were used as independent variables in this analysis. These variables were: (% time in turbulence) (gust intensity factor)/ (mission/hour) for gust, (GAG/mission/hour) for GAG, (ratio of paved to unpaved runway roughness standard deviation) (number of landings/mission/hour) for taxi. To define maneuver damage per hour, the missions having very low time in turbulence gave maneuver contribution as the equation constant, so this one unknown resulted in some iteration.

These empirical relations allow a definitive look at aircraft structural fatigue that is not available for any other aircraft.

AIRCRAFT FATIGUE LIFE

In order to define what portion of the aircraft life that is available after crack initiation we selected a 0.5-inch crack as the actual total life for our analysis. The two crack growth equations in Figure 1 were used in computing the actual damage per 0.03-inch and 0.5-inch crack lengths for the crack growth portion. This produces a crack growth portion of 26.7% for lower surface and 18.6% for upper surface. The average portion of fatigue life that is crack growth is about 23%. Since this statistical sample is so large, this information provides a better understanding of structural fatigue. One point we must make is that these aircraft had flaws which required the use of stress concentration factors (Kt) in fatigue analysis of 8 and 10.

C-130 SCATTER FACTORS

The Long Range Cargo was selected as the mildest and Sky-Hook as one of the most severe load environment missions to study scatter. Data was available on these two missions for crack initiation where the aircraft were almost single mission usage aircraft. Then 10,000 flight hours were computed as the mean flight hours to crack initiation from Figure 1 and the damage per flight hour, for the Long Range Cargo mission at WS 120 on the lower surface. The first crack initiations were about 5,000 flight hours, which allowed the calculation of 2 for the scatter factor. Using this same procedure on Sky-Hook the mean flight hours to crack initiation was 1,400 and first crack initiation was about 950 flight hours, so the computed scatter factor is 1.47. The crack initiation and crack growth curve for the first aircraft on each of these two missions is shown in Figure 2.

The more severe load/stress cyclic environment has less scatter, which is the same trend in stress versus cycles (S/N) curve raw data points. In an earlier paper (4), we derived an equation to represent the scatter in S/N raw data points as a function of stress amplitude, mean stress and stress concentration factors. The natural log of the variation coefficient ($\ln V$) as the dependent variable in Equation 1 represents the scatter.

$$\ln V = 1.56 + \frac{9.57}{S_a} + \frac{2.53}{Kt} - 0.0255Sm \quad (1)$$

Data for this equation derivation was a very large number of 2024T3 and 7075T6 aluminum specimens. This coefficient is computed from Miner's Damage Equation ($\text{SUM} [n/N] = 1.0$) values.

THEORETICAL FATIGUE SCATTER ($\Sigma[n/N]$)

To help keep scatter to a minimum relative to the S/N curve effects, it is suggested that good statistical coverage of mean stress (S_m), stress amplitude (S_a) and stress concentration factors is needed for small specimens. The next step we propose is to derive an equation for these type data to represent the complete family of S/N curves for each material, as we have done. Other variables should be added to the equation for component specimens, loading complexity and specimen size. Thus six component specimens per helicopter S/N curve and a large scatter factor would not be needed. Accurate load spectra are needed to reduce scatter in fatigue predictions. These spectra should be per mission segment for structural component location.

For each analysis location, the design stress concentration factor must be defined from use of finite element model and/or detailed stress analysis.

THEORETICAL CRACK GROWTH ANALYSIS SCATTER

The same accurate load spectra for fatigue analysis is needed for crack growth analysis predictions. The design stress concentration factors are also needed with detailed information about the analysis locations. Structural inspection of fleet aircraft are required to validate the crack growth predictions.

AIRCRAFT FATIGUE PREDICTIONS

Some of the many parameters to be considered for fatigue analysis are listed in Table 2. A scatter factor of about 40 is common for helicopter parts and 4 is used on most airplanes. The main objective is to keep the scatter to a minimum. Critical crack length is the best selection for fatigue to avoid high risk. Miner's damage equation is the best fatigue damage method to define crack initiation when corrections are included for scatter. The selection of the most severe mission for fatigue life calculations allows adequate life on any mission.

TABLE 2 - Aircraft fatigue predictions.

Scatter range:

<i>S/N</i> curves	-	1 to 40
Loads	-	1 to 3
Design <i>Kt</i>	-	1 to 10

Define Fatigue Life:

Select crack length
Critical crack length
Crack initiation

Method of fatigue prediction:

Miner's Damage Equation $SUM(n/N)$
Crack growth analysis

Select load environment:

Most severe mission
Mission mix

LOAD ENVIRONMENT MODEL

A method is desired that provides the positive and negative load peaks for any selected location on the aircraft for design strength or fatigue analysis. The Load Environment Model (2) concept is capable of doing these things and has been computer programmed for the F-106, F-111 and A-7D aircraft. The initial model was eight variables and was derived with F-105D multichannel recorder data. The new method uses all the proven features of the above model minus the aircraft angular velocities and without any decrease in accuracy.

This new model has five variables and may need to go to six variables if the longitudinal load factor is important for the aircraft being analyzed. A step-by-step description of model derivation starts with a good statistical normal load factor spectra per mission segment that the model aircraft is expected to be flying during its usage life. The next requirement is multichannel recorder data from a similar type of aircraft,

which includes angular acceleration about each of the three axes, plus N_z and lateral load factor (N_y). Then derive probability curves for N_y , roll acceleration (A_x), pitch acceleration (A_y), and yaw acceleration (A_z) versus N_z . These probability curves are used to expand the N_z spectra per mission segment to a five-variable Load Environment Model per mission segment. Table 3 is taken from MIL-A-8866A (USAF) to show an example of N_z spectra per mission segment.

TABLE 3 - Maneuver-Load-Factor Spectra A, F, TF classes, cumulative occurrences per 1,000 flight hours by mission segment.

N_z	Cruise	Air-Ground	Air-Air
			Positive
2.0	10,000	175,000	300,000
3.0	2,500	100,000	150,000
4.0	400	40,000	50,000
5.0	1	10,000	13,000
6.0		1,500	2,500
7.0		200	900
8.0		15	180
9.0		1	60
10.0			15
			Negative
0.5			44,000
-0.5			1,200
-1.5			60
-2.5			1

To make use of the model, regression equations are needed for control surface positions and load/stress regression equations for selected structural component locations. Next, use the most severe mission to compute load spectra with the load equations and the Load Environment Model. These location spectra are to be used to compute strength required and fatigue analysis for design. Each component spectrum will be different and will allow the minimum structural weight to be defined for

strength and fatigue. Strength design limit loads are the maximum values for one life on the spectra. The flowchart in Figure 3 shows how the Load Environment Model fits in with other tasks.

LOAD REGRESSION EQUATIONS

Load equations are required to go from a Load Environment Model to a structural component location spectrum. Load equations for the F-111 were complex due to the wing variable sweep, but were high-quality since they were derived from recorded flight test data. The tiltrotor on the V-22 presented a different set of problems in obtaining valid load equations even before flight test. Data for the F-106 equations were very limited. Equations for the A-7D were very good, but consideration of Buffet was not included.

Detailed stress analysis and finite element models (FEM) must be validated, plus all critical control points for strength and fatigue must be correctly selected.

The independent variables must be logical for the component analysis locations selected. Goodness of fit for the computed equations is best measured with the standard error and correlation coefficient. Two independent variables which have high correlation with each other should not be used in the same equation. The maximum number of variables per equation should be about ten. As variables enter an equation, the standard error decreases and the correlation coefficient increases to approach 1. The point in equation derivation where the correlation coefficient does not increase when a new variable is added may be the stopping place for that equation. Also, another stopping point is when the standard error does not decrease when a new variable is added to the equation.

A short list of independent variables is as follows: N_z , N_y , A_x , A_y , A_z , Q , W , I_{yy} , I_{zz} , I_{xx} , STW , FW , AC , and CG . A list of control surface equations and other dependent variables with their crossproduct variables are listed in Table 4.

A minimum of thirty theoretical conditions are needed to cover the edges of the aircraft operational envelope and have a good statistical base for regression analysis.

TABLE 4 - Key regression equation variables.

Dependent Variable	Independent Variable			
	1	2	3	4
Aileron position (<i>Da</i>)	N_yW/Q	$I_{xx}A_x/Q$	$I_{zz}A_z/Q$	
Rudder position (<i>Dr</i>)	$I_{xx}A_x/Q$	B	$I_{zz}A_z/Q$	N_yW/Q
Elevator position (<i>De</i>)	$I_{yy}A_y/Q$	$N_zW(AC - CG)/Q$	N_zW/Q	
Sideslip angle (<i>B</i>)	N_yW/Q	$I_{zz}A_z/Q$		
Angle of attack (<i>Aa</i>)	N_zW/Q	$N_zW(AC - CG)$		
Wing stress	N_zW	N_zSTW	N_zFW	
Vertical stab. stress	BQ	DrQ	A_x	
Horizontal stab. stress	AaQ	DeQ	A_y	
Wing/fuselage lug stress	DaQ	BQ	N_zW	A_y

COMPUTING WEIGHTED SCATTER FACTORS

It was shown earlier that scatter increases as *N* goes to the higher values on an *S/N* curve. So the scatter should be multiplied by damage at *N* values as a weighting consideration. This process is shown best by Equation 2.

$$V_t = \frac{\sum \left[\left(\frac{n}{N_j} \right) v_j \right]}{\sum \left(\frac{n}{N_j} \right)} \quad (2)$$

The total weighted variation coefficient (*Vt*) is computed for the analysis locations on the *S/N* curve at *j* values.

FATIGUE LIFE EQUATION

The fatigue life damage at crack initiation (D_i) is defined with Equation 3.

$$D_i = \sum \left(\frac{n}{N} \right) - \frac{3Vt}{100} \quad (3)$$

An adjustment factor for crack initiation should be obtained from the full-scale cyclic test and is identified as F_c . When cracks start showing up in fleet aircraft, F_c should be replaced with F_f , which represents the adjustment factor for crack initiation in the fleet.

For all locations or elements with no alternate load path, not damage tolerant, noninspectable joints, critical crack length is so short it cannot be seen by visible inspection and helicopter rotor system parts, then use a safety factor ($F_s = 2$) for these designs. In addition, a safety factor of 1.5 should be used for the complete aircraft when using a low-confidence load environment, to help prevent fatigue modifications.

Weight reductions during design could affect fatigue life. The most common problem is an aircraft which is operated in a more severe load environment than that for which it was designed. In computing upper surface damage for flight, change the mean stress from negative to positive to agree with C-130 fleet damage data and to allow use of current S/N curves. Fatigue prediction correction factors are presented in References (1) and (4).

CRACK GROWTH ANALYSIS

Any fleet aircraft with cracks should be inspected periodically to validate crack growth predictions and define its location on the damage versus crack growth plot. The damage versus crack growth plot is the best way to define where individual aircraft are in the scatter distribution and their F_f . Residual strength for cracked structure is very important and analysis/test at the end of the full-scale cyclic test is required to define risk of aircraft flight with cracks. Crack growth analysis should begin on a fleet airplane when cracks are found during inspection.

The Kt of a crack is about 18, so crack growth is predictable and high loads cause retardation as they do in fatigue. Critical crack length is defined as the length at which theoretical failure will occur when limit load is applied. The crack growth analysis and fatigue analysis can be used as tools to define inspection requirements. Repair of areas which have

cracks approaching critical length and their total number is basic data for defining the aircraft economic life. These methods provide a direct path for updating design criteria for strength and fatigue.

CONCLUSIONS

In review of the interrogation of the C-130 fleet damage sources, ground-air-ground was almost twice as great for the lower surface as it was for the upper surface. Taxi damage was high for only the upper surface on the Shuttle mission, which included operations on unpaved runways. Gust damage was about the same for upper and lower surfaces for all nine missions. Missions with a high percentage of maneuver damage were Sky-Hook, Support, and Proficiency Training where the upper surface damage was a little higher than the lower surface damage. However, the damage rate per flight hour on the Support mission was low, thus the evasive maneuvers for missiles and ground fire would account for this maneuver damage.

The most extreme case is finding the 2-4g maneuvers on the Air Drop mission caused a small percentage of maneuver negative damage for the lower surface. Keep in mind the C-130 has a 2.5g design limit load factor. Extremely high loads such as C-130 air drops changed the shape of flaws and reduced the Kt only in the lower surface.

Compression load cycles on the wing upper surface must be considered during design. Actual damage in the C-130 fleet was linear and had low scatter.

The methods for design loads in this paper are needed to prevent pilots from taking their airplanes to nearly twice the design limit load, as occurred with the F-86's in Korea. Thus the load limiter concept may put the pilot in great danger in air-to-air combat.

Strength and fatigue design for composite structure can make use of these methods with consideration that flaws exist and in some cases they can be removed. In addition, the damaged hot wet specimens represent the worst case for structural conditions in the fleet. Risk of adhesive and resins to debond with age, temperature, and humidity effects is another problem designers must face.

Most of the NASA-airplane large statistical samples of normal load factor data include maneuvers with gust cycles superimposed on them. USAF recording programs for aircraft response also do not separate gust from maneuver, but do have a wider range of aircraft types.

There are many advantages for deriving one equation per material type and its family of S/N curves. First, the scatter and error due to interpolation are cut to a minimum. Also, high-cycle conditions such as buffet and helicopter rotor loads can be easily handled.

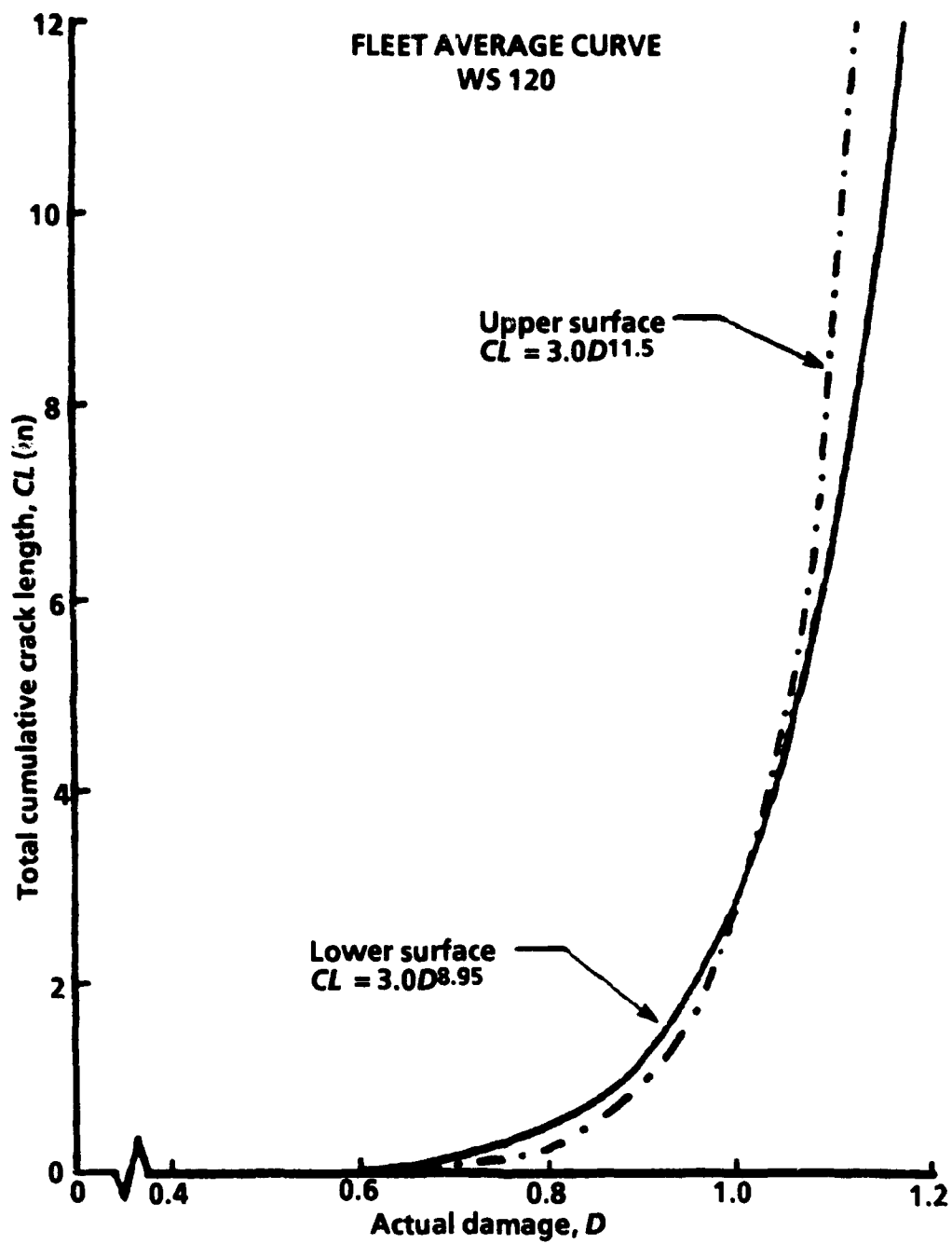
SYMBOLS USED

<i>Aa</i>	=	angle of attack (deg)
<i>AC</i>	=	aerodynamic center (in)
<i>Ax</i>	=	roll acceleration (deg/s ²)
<i>Ay</i>	=	pitch acceleration (deg/s ²)
<i>Az</i>	=	yaw acceleration (deg/s ²)
<i>B</i>	=	sideslip angle (deg)
<i>CG</i>	=	center of gravity (in)
<i>CL</i>	=	crack length (in)
<i>D</i>	=	Miner's damage equation: $\Sigma(n/N) = 1$
<i>Da</i>	=	aileron position (deg)
<i>De</i>	=	elevator position (deg)
<i>Di</i>	=	damage at crack initiation
<i>Dr</i>	=	rudder position (deg)
<i>FW</i>	=	fuel weight (lb)
<i>g</i>	=	acceleration due to gravity (ft/s ²)
<i>Ixx</i>	=	roll moment of inertia (lb-s ² -ft)
<i>Iyy</i>	=	pitch moment of inertia (lb-s ² -ft)
<i>Izz</i>	=	yaw moment of inertia (lb-s ² -ft)
<i>Kt</i>	=	stress concentration factor
<i>n</i>	=	structure stress cycles
<i>N</i>	=	cycles read on <i>S/N</i> curve

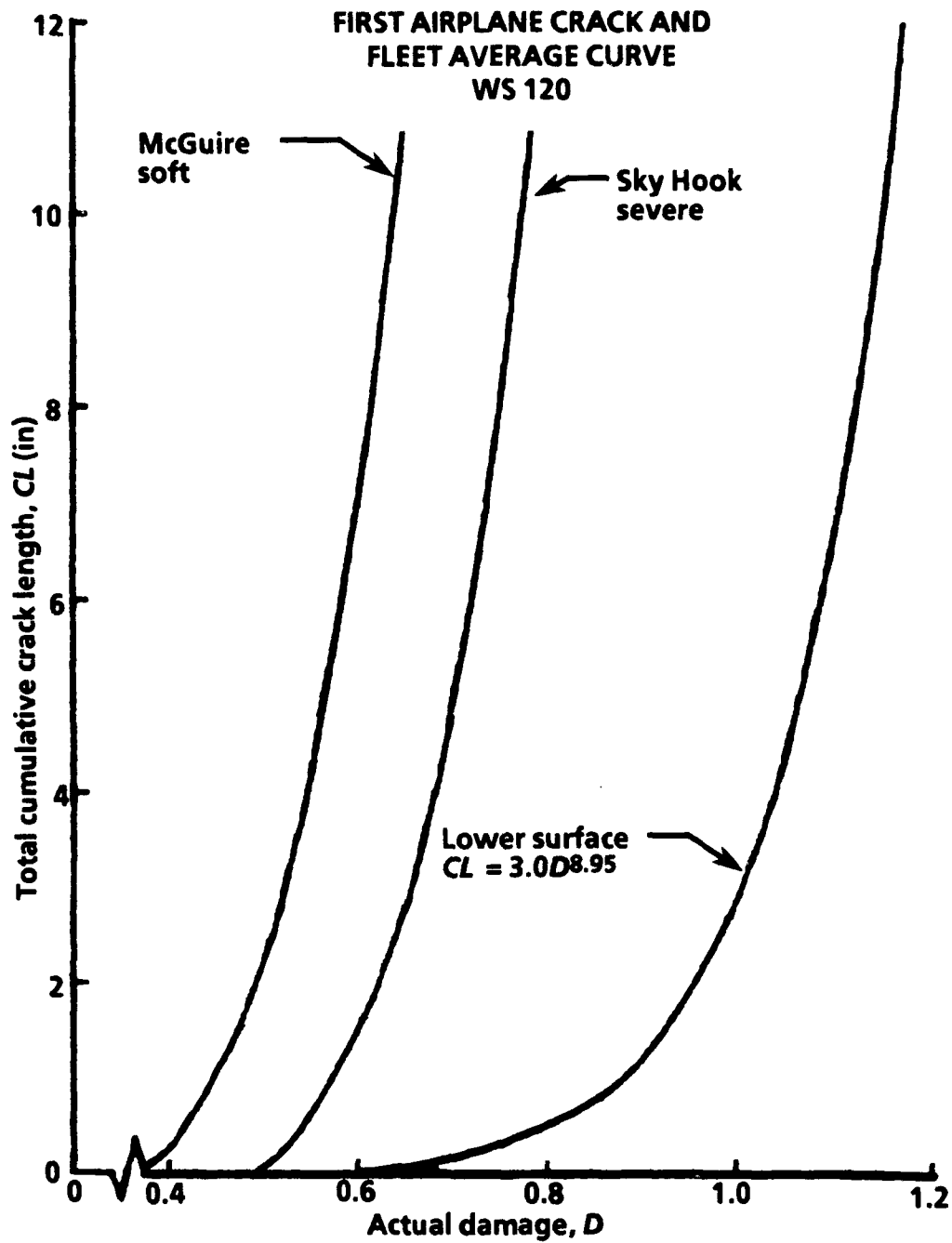
- N_y* = lateral load factor (g)
- N_z* = normal load factor (g)
- Q* = dynamic pressure (psf)
- S_a* = stress amplitude (ksi)
- S_m* = mean stress (ksi)
- S/N* = stress versus cycles curve
- STW* = store weight (lb)
- V* = variation coefficient
- VGH* = velocity, g, altitude
- W* = gross weight (lb)

REFERENCES

- (1) Yost, J. D., "Correction Factors for Miner's Fatigue Damage Equation Derived From C-130 Fleet Aircraft Fatigue Cracks," AIAA-86-2684, U. S. A., Oct. 1986.
- (2) Yost, James D. and Johnson, Guinn S., "Strength and Fatigue Loads Computed with a Load Environment Model," AIAA J. of Aircraft, Vol. 9, No. 3, U. S. A., March 1972.
- (3) Yost, James D., Jackson, Wayne B., and Salter, L. Wayne, "Improved Methods of Atmospheric Turbulence Prediction for Aircraft Design and Operation," AIAA J. of Aircraft, Vol. 9, No. 4, U. S. A., April 1972.
- (4) Yost, James D., "Parameters Affecting Structural Fatigue Scatter Factors with Fatigue Life Defined as Critical Crack Length," copyright James D. Yost, U. S. A., February 1972.
- (5) Yost, James D., "Reduction of Pressure Survey Date with Regression Analysis," SAE 760451, U. S. A., April 1976.



30757
Figure 1. C-130 fatigue crack propagation



3N637
Figure 2. C-130 fatigue crack propagation: 1st aircraft on two missions

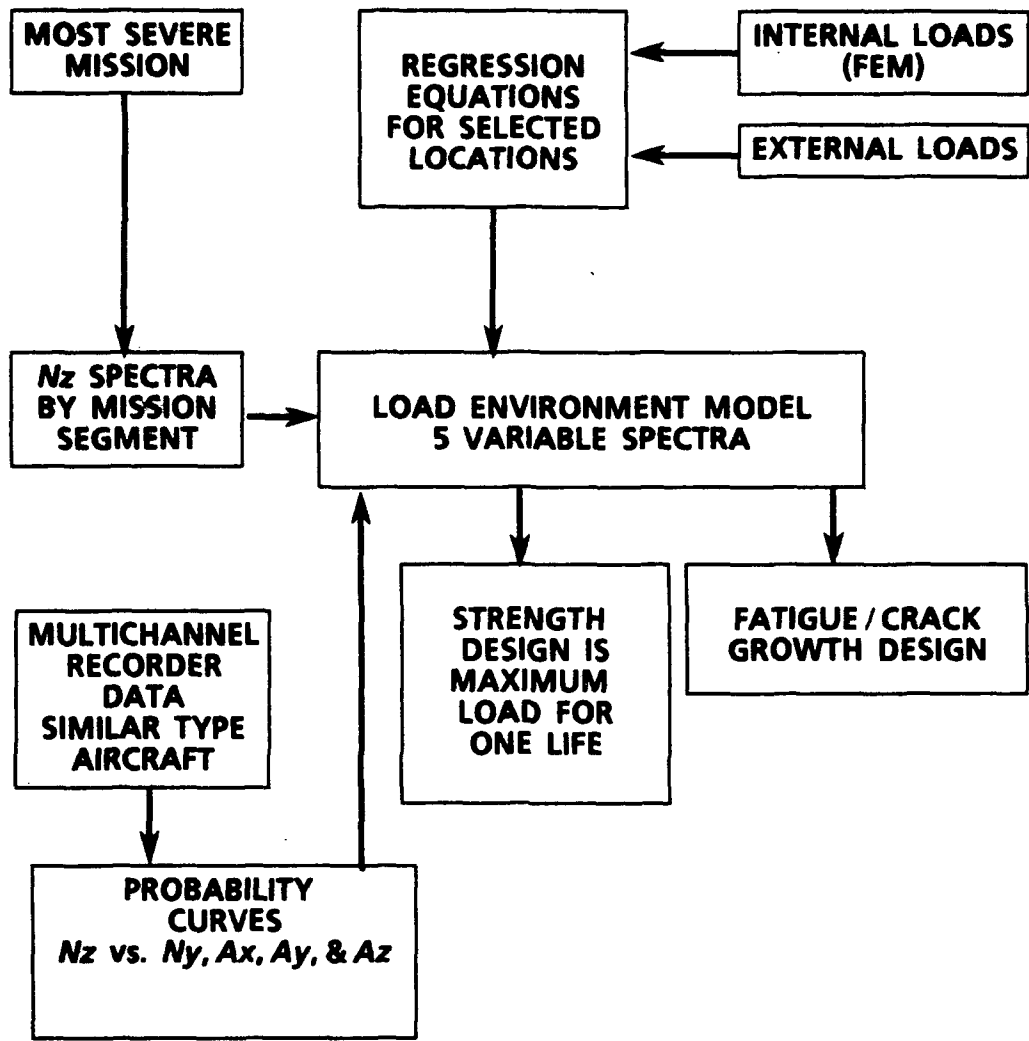


Figure 3. Design loads per structural component

PITTING CORROSION FATIGUE OF AIRCRAFT MATERIALS - A REVIEW

**Hoepfner, D.W. and Goswami, T.
Professor and Research Assistant Professor, Respectively.
Quality and Integrity Design Engineering Center
Department of Mechanical Engineering
University of Utah
Salt Lake City, 84112, UT.**

ABSTRACT:

Aircraft structural materials accrue time dependent deterioration by corrosion. Pitting is one of the major localized corrosion mechanisms of aircraft structural materials, yet very little research has been done on the nucleation, growth and pitting corrosion fatigue of these materials.

Electrochemical aspects of the generation of pits are reviewed in this paper. Aircraft corrosion fatigue has been separated into localized corrosion and corrosion fatigue. Various theories proposed on pit nucleation, growth, and pit transformation into corrosion fatigue cracks and their growth also are reviewed. A pitting corrosion fatigue crack growth model is discussed and a review of recent attempts to model the process are presented.

INTRODUCTION:

Corrosion occurs in many parts of our lives. Corrosion is a "slow", time dependent process by which metals and alloys reverse to a more stable structure. The cost of corrosion has been studied all over the world. It is estimated that industrial nations are paying the price in a range of 4 to 4.5% of their GNP every year. In the USA alone the cost of corrosion per year has been estimated to be approximately \$126 billion. These details are summarized in Fig. 1.

Corrosion also is blamed for loss of many human lives. There are several examples where corrosion resulted in the premature failures of bridges, airplanes, pipelines, and industrial equipment. Figure 2 describes a few examples where human lives were claimed by corrosion.

Engineering artifacts are likely to corrode and thus corrosion poses a risk in their utilization. Hence, there is a growing need to understand the different types of corrosion, their growth and how that it be controlled. This paper is focused on discussion of some points with particular emphasis on aircraft structural materials.

ELECTROCHEMICAL ASPECTS IN CORROSION:

Luigi Galvani (1) first published a discussion of the electrochemical action of two electrical conductors in 1791. Galvanic reaction became more widely known after his work. However, for more than 100 years the pace of his research was not maintained. Then in 1904 Tafel (2), presented "the Tafel equation", which described the variation in the rate of reaction with overpotential. Pilling and Bedworth (3) showed a breakaway oxidation that resulted in localized corrosion attack. It is known in the literature as Pilling and Bedworth ratio.

Combining Tafel's work and the charge transfer overpotential, Evans (4) presented a linear relationship that represented the rate of corrosion by corrosion current density.

Wagner and Traud (5) studied the electrode kinetics and Pourbaix (6) presented potential versus pH diagram. This diagram is well known and it describes the onset of passive film formation and also is known as the isothermal phase diagram. Several other milestones (7-14) occurred in furthering the understanding of the kinetics of localized corrosion are summarized in the "Time Scale" of Fig. 3.

Lessons learned from these investigations help us understand that for localized corrosion attack to take place two different electrode potentials are needed. Microstructures of alloys used in aircraft have several phases that include localized discontinuities. Oxide film is uneven as a result of this. Hence dependent upon the microstructure, localized corrosion damage may take place if all conditions are met.

AIRCRAFT CORROSION FATIGUE:

Some corrosion fatigue studies were conducted in the late 1960's. Fracture mechanics modeling methods in the corrosion fatigue were first proposed by Brown (15). Later Wei and Landes (16), as well as others, proposed a superposition model (linear summation of crack growth by plasticity driven fatigue and crack growth by chemical reaction) below:

$$\frac{da}{dN_e} = \left\{ \frac{da}{dN_m} \right\} + \left\{ \frac{da}{dN_r} \right\} \quad (1)$$

where subscripts e, m and cf represent total crack growth rate (CGR) in aggressive environment, plasticity driven CGR in an inert environment, and incremental difference on the CGR plot and represents the effect of interacting cyclic plastic deformation and chemical reaction respectively. Austin and Walker (17) argued the superposition model and suggested that the two processes are competing with one another and are not superposition, instead, competition mechanisms. Several defense and civil aircraft operators formulated a discussion of corrosion problems at this time (18) and the first international conference on corrosion fatigue held in 1971.

The role of localized corrosion in the acceleration of fatigue crack growth (FCG) was conceptually presented by Hoepfner (19-21) and corrosion fatigue crack growth studies were conducted on a series of aircraft structural materials. A parallel effort in the corrosion fatigue crack growth rate (CFCGR) determination was made by Hall et al (22). Several review articles (23) were written during this time as shown in the "Time Scale" of Fig. 4. This work was a major undertaking by the USAF in the late 1960's and early 1970's to increase our understanding of environmental effects on fatigue crack growth.

Several attempts were made by the Advisory Group for Aerospace Research and Development, Structures and Materials Panel in a NATO effort to investigate corrosion fatigue and in terms of a Round Robin Testing program as shown in Fig. 4. In recent years more and more concerns were expressed by aircraft operators who either experienced premature failures or want to extend the design life of their fleet. Several such interests are reflected in references (24-35).

When the areas of aircraft corrosion fatigue (CF) and CFCG were developing, practically no attempts were made to address the effect of localized corrosion such as pitting and its transformation into CF or fatigue cracks. Hence, there is a need of further research for the localized corrosion mechanisms such as pit nucleation and growth. Once these mechanisms are understood, they can be combined with the fatigue and crack growth concepts to either eliminate or minimize the insidious effects of

corrosion. These data can be synthesized and used further in the development of probabilistic models that can be used in the design, maintenance and setting of inspection intervals of the existing fleets. Also corrosion fatigue considerations can be included in the Aircraft Structural Integrity Programs once the modeling and data requirements are formulated.

PIT NUCLEATION MECHANISMS:

The mechanisms of pit nucleation can be divided into the three frameworks, below:

1) Adsorption and Adsorption Induced Mechanisms: Most mechanisms of pit nucleation consider the adsorption of aggressive anions at energetically preferred "sites". Developments (36-43) made chronologically in this area of research are shown in the "Time Scale" of Fig. 5, where concepts based on either competitive adsorption or surface complex ion formation are included. In this framework, continuous Cl⁻ anions and passivating agents are adsorbed. Above a critical potential Cl adsorption is favored and breakdown of passivity results.

2) Ion Migration or Penetration Theories: Theoretical models (44-46) in this framework require either penetration of damaging anions from the oxide/electrolyte interface to the metal /oxide interface, or migration of cations as a decisive process.

3) Mechanical Film Breakdown Theories: Mechanical breakdown (47-48) of the passive films is an independent as well as combined phenomenon with the above two frameworks. Breakdown of the passive films provides the electrolyte direct access to the base metal. Localized corrosion occurs.

PIT GROWTH MECHANISMS:

Three mechanisms by which a pit grows, shown in Fig. 6, are as follow:

1) Charge Transfer Based Pit Growth: The early stage of pitting occurs due to the high current density present at the bottom of a pit. However, validating this experimentally has proved to be very complex. As a result constant current potentials within pits is a widely accepted idea in the literature (49-51).

2) Diffusion Related Mechanisms: The presence of a salt layer on the surface of passive materials results in the breakdown of the passive film (52-54). Solubility of salt in metals (aluminum alloys) is quite high, salt precipitates in the metal surface. Aircraft structural materials are expected to deteriorate by this mode as active salt powder (white powder) has been observed in the tear down corrosion investigation of a C/KC 135 for example.

3) Ohmic Resistance Controlled Pit Growth : Pitting in titanium and aluminum alloys occurs because of high Ohmic -limited current densities (55-56). The rate of pit growth also depends upon the time of exposure and applied potential. These models are shown in Fig. 6.

PITTING CORROSION FATIGUE MODELING:

Pit nucleation and growth mechanisms are very important in the development of localized corrosion fatigue concepts. Since this is a time dependent process, where the pit growth rate is accelerated by several factors, such as microstructure, discontinuities present, film composition (coherence and mechanical properties of the film), previous plastic deformation, etc., the exact growth rate in aluminum alloys is a very complex

process. Pit shapes also are very important with respect to pit transformation into either a fatigue or CF crack. Much work needs to be done in the development of pitting CFCG models. Earlier works in modeling crack growth numerically and with Weibull parameters approaches are summarized in references (57-59).

Hoepfner (60), proposed a pitting CFCG model of aluminum alloys in the early 1970's. As the pit growth kinetics are not yet understood properly, when to consider a pit a crack is still a point of great concern. Hoepfner, used a power law pit growth model where the exponent described the linear, parabolic and cubic growth rates respectively. A four parameter Weibull analysis was used to fit the CG data. The equation employed in ref. (60) has the following form:

$$1 - \frac{\Delta K}{K_{Ib}} = \exp. \left[- \left\{ \frac{\log_e \left(\frac{da}{dN} + 1 \right) - e}{v - e} \right\}^k \right] \quad (2)$$

For a decade no other model was put forward in the pitting CFCG modeling. Figure 7 compiles the models (57-69) that have been developed in the two decades. Recently Kondo (68) used a pit transition to a crack criterion and crack growth modeling within the linear elastic fracture mechanics. However, conventional pit shapes (hemispherical) have been assumed so modeling with actual pit shapes requires much research. In recent years several Japanese investigators have made significant strides in developing pitting models. As well, recent work in our laboratories funded by Boeing Seattle, has resulted in significant progress. This work will be reported in the literature soon.

SUMMARY:

This paper has briefly reviewed corrosion pitting fatigue over the last 200 years. Recent interest in the extensive detection of corrosion and corrosion induced fatigue cracks has increased the concern of the community related to our ability to model the pitting corrosion fatigue process to incorporate life prediction into structural integrity assurance procedures. Models proposed in the early 1970's allow these predictions to be made. However, additional developments are needed to allow greater confidence in the applicability of the models to assure residual strength of structure will not be jeopardized. The greatest needs are related to the following:

1. Continued development of pitting corrosion prevention systems with verification of their validity.
2. Consideration of pit size, shape, density and interaction on structural integrity.
3. Evaluation of need to identify structurally significant items (SSI) related to pitting corrosion fatigue.
4. Development of understanding of pit growth kinetics, link up potentials of MPS (multiple pitting sources) and conversion of pits to cracks modelable by fracture mechanics.
5. Crack growth data in the structurally dependent regime and LEFM regimes -expand data base.

ACKNOWLEDGEMENTS:

The authors wish to acknowledge Ms. Shauna Forbes for assistance in preparation of the manuscript and presentation. Mr. Tom Mills, graduate student in QIDEC, provided assistance with photography. The University of Utah and the State of Utah provided support by provision of facilities.

The Lockheed Corporation and Office of Naval Research provided support for the development of the pitting corrosion fatigue models. Boeing Commercial Airplane Co. and Boeing Defense and Space Group have provided support for additional development of recent revisions to the corrosion fatigue models. Individuals that continue to interact with us and provide insights and encouragement are:

Dr. Charles Elliott, University of Utah.

Mr. Alan Emerson, Australian CAA.

Mr. R. Jeal, Hawker deHavilland, Sydney, Australia.

Dr. J. deLuccia, NAWC, Warminster.

Dr. W. Wallace, NRC-IAR, Ottawa, Canada.

REFERENCES:

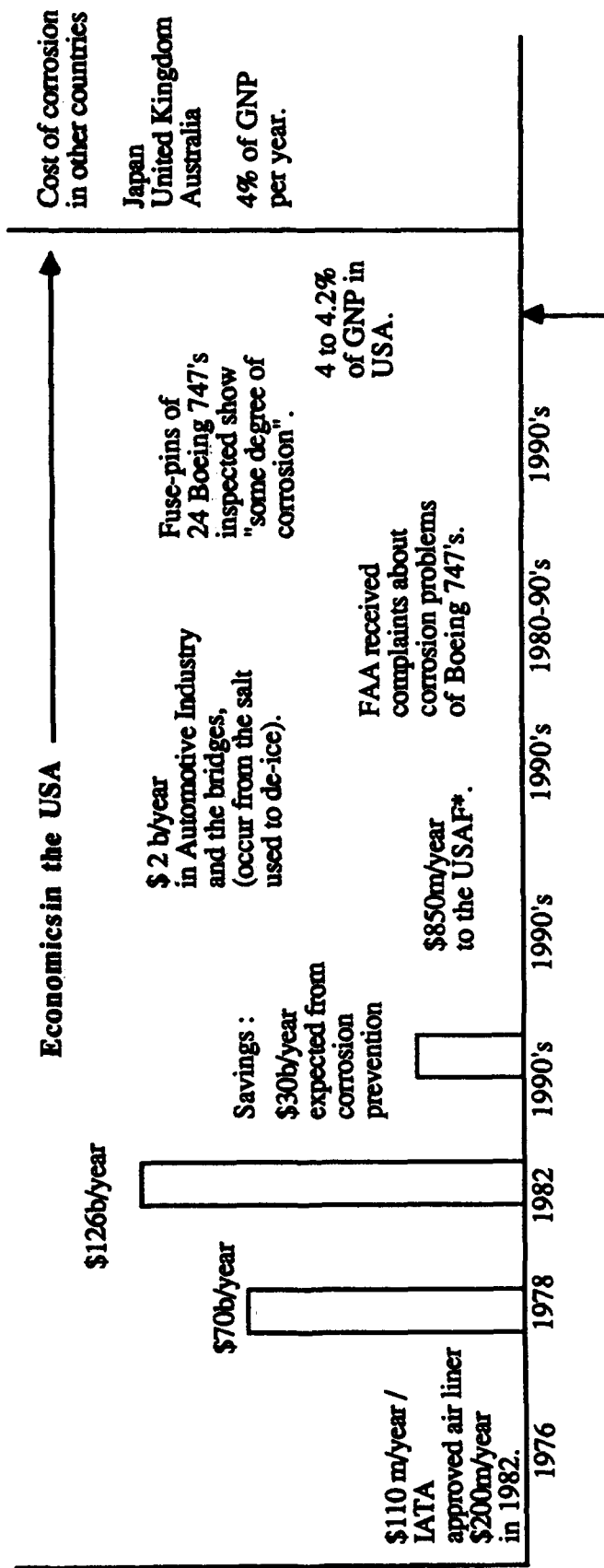
- 1) Galvani, L. (1791) Published electrochemical action of two electrical conductors in Italy.
- 2) Tafel, J. (1904) Z. Phys. Chem., 50 pp. 641.
- 3) Pilling, N. and Bedworth, R. (1923) J. Inst. Metals, 29, pp. 534.
- 4) Evans, U.R. (1929) J. Franklin Inst. 208 pp. 45.
- 5) Wagner, C. and Traud, W. (1938) Z. Electrochem, 44 pp. 391.
- 6) Pourbaix, M. (1938) Thermodynamique des solutions aqueuses Diluees. Potentiel D'oxydo-Reduction (resume de conference) Bull. Soc. Chim. Belgique, Vol. 48.
- 7) Roiter, W.A., Juza, W.A. and Poluyan, E.S. (1939) Acta Physiochim, URSS 10: pp. 389.
- 8) Kabanov, B.N. and Leikis, D.I. (1946) Zh. Fiz. Khim. 20, pp. 995.
- 9) Uhlig, H.H. (1950) J. Electrochemical Soc. 97, pp. 215c.
- 10) Hoar, T.P. and Hurlen, T. (1958) CITCE VIII, London, pp. 445.
- 11) Heusler, K.E. (1958) Z. Electrochem. Ber. Bunsenges. Phys. Chem., 62. pp. 582.
- 12) Bockris, J. O'M and Drazic, D. (1962) Electrochim. Acta 7, pp. 293.
- 13) Lorenz, W.J. and Eichkorn, G. (1965) J. Electrochemical Society, 112, pp. 1255.
- 14) Hilbert, F., Miyoshi, Y., Eichkorn, G. and Lorenz, W.J. (1971) J. Electrochemical Society, 118, pp. 1919 and pp. 1927.
- 15) Brown, B.F. (1968) Met. Rev. 129, pp.171.
- 16) Wei, R.P. and Landes, J.D. (1969) Mater. Res. Stds. 9, pp.25.
- 17) Austin, I.M. and Walker, E.F. Proc. of International Conference on Influence of environment on fatigue, pp. 1.
- 18) Cohen, B. (1972) in NACE -2 pp. 65.
- 19) Hoepfner, D.W. (1972) Corrosion Fatigue, NACE -2, pp. 3.
- 20) Pettit, D.E., Ryder, J.T., Krupp, W.E. and Hoepfner, D.W. (1974) AFML Report, AFML-TR -74.
- 21) Pettit, D.E., Ryder, J.T., Krupp, W.E. and Hoepfner, D.W. (1974) Technical Report AFML TR 74 183-Vol. 1.
- 22) Hall, L.R., Finger, R.W. and Spurr, W.F. (1973) Final Technical Report, AFML TR 73-204.
- 23) Laird, C. and Duquette, D.J. (1972) in NACE-2, pp.88.
- 24) Schijve, J. (1977) I. Mech. Eng., Nominated Lecture.
- 25) AGARD NATO (1981) Report No. 315, on "Aircraft Corrosion".
- 26) AGARD NATO (1981) Report No. CP-316, on "Corrosion Fatigue".
- 27) AGARD NATO (1982) Report R-695, Coordinated Corrosion Fatigue Co-operative testing program.
- 28) Examination of steam generator tube sample from Millstone Point -2, Babcox and Wilcox, Nov. 1982.

- 29) AGARD NATO (1985) AG 278 Vol. 1, AGARDograph No. 278 on "Aircraft corrosion: causes and case histories".
- 30) Gangloff, R.P. (1988) NACE-10, pp. 55.
- 31) Marceau, J.A. and Caton, R.G. (1989) NADC-SIRL AB -1089 pp.7.
- 32) AGARD NATO (1989) Report -713, on "The fatigue in aircraft corrosion testing (FACT) programme".
- 33) Komai, K., Minoshima, K. and Kim, G. (1989) JSME International J. Series I, Vol. 32, No.2, pp. 282.
- 34) McGuire, J.F. and Goranson, U.G. (1991) AGARD meeting, Bath, U.K..
- 35) DeLuccia, J.J. (1991) AIAA 32nd Structures, Structural and Dynamics and Materials Conference.
- 36) Kolotyркиn, Y.M. (1961) J. Electrochem. Soc. 108, pp. 209.
- 37) Hoar, T.P. and Jacob, W.R. (1967) Nature 126, pp.1299.
- 38) Leckie, H.P. and Uhlig, H.H. (1966) J. Electrochemical Soc. 113, pp.1262.
- 39) Galvele, J.R. (1976) J. Electrochemical Soc. 123, pp. 464.
- 40) Vetter, K.J. (1965) Ber. Bunsen. Phys. Chem. 69, pp. 589.
- 41) Janik-Czachor, M., Szummer, A. and Szklarska-Smialowska, Z. (1975) Corrosion Sci. 15, pp.775.
- 42) Heusler, K.E. and Fischer, L. (1976) Werkst. Korros. 27, pp. 788 and 551.
- 43) Strehblow, H.H., Titze, B. and Lochel, B.P. (1979) Corrosion Sci. 19, pp.1047.
- 44) Hoar, T.P., Mears, D.C. and Rothwell, G.P. (1965) Corrosion Sci. 5, pp. 279.
- 45) Galvele, J.R., de De Micheli, S.M., Muller, I.L., de Wexler, S.B. and Alanis, I.L. (1974) Localized Corrosion NACE pp. 580.
- 46) Chao, C.Y., Lin, L.F. and Macdonald, D.D. (1981) J. Electrochemical Soc. 128, pp. 1187.
- 47) Sato, N. (1971) Electrochim Acta, 16, pp. 1683.
- 48) Videm, K. (1974) Kjeller Rept. 149. Institut for Atomenergi, Kjeller, Norway.
- 49) Engell, H.J. and Stolica, N.D. (1959) Z. Phys. Chem. 20, pp. 113.
- 50) Vetter, K.J. and Strehblow, H.H. (1970) Ber. Bunsenges. Phys. Chem. 74, pp. 1024 and 75, pp. 449.
- 51) Popov, Yu. A., Alekseev, Yu. V. and Kolotyркиn, Ya. M. (1978) Elektrokhimiya, 14, pp. 1447.
- 52) Engell, H.J. (1977) Electrochim, Acta, 22, pp. 987.
- 53) Alkire, R., Ernsberger, D. and Beck, T.R. (1978) J. Electrochem. Soc.125, pp. 1382.
- 54) Hunkeler, F. (1980) Dissertation No. 6663 ETH Zurich.
- 55) Beck, T.R. (1977) Corrosion 33, pp. 9.
- 56) Hunkeler, F. and Bohni, H. (1981) Corrosion, 37, pp. 645.
- 57) Bowie, G.E. and Hoepfner, D.W. (1976) in Proc. of the 1976 International Conference on Computer Simulation for materials applications, Ed., Arsenault, R.J., Beeler, J.R. jr. and Simmons, J.A., pp. 1171.
- 58) Reeves, R.K. and Hoepfner, D.W. (1978), Eng. Fracture Mechanics, vol. 10, pp. 571.
- 59) Newman, J.C. jr., and Raju, I.S.. (1978) NASA Technical Paper, 1578.
- 60) Hoepfner, D.W. (1979) Fatigue Mechanisms, proc. of ASTM STP 675 pp.841.
- 61) Wei, R.P. (1979) Fatigue Mechanisms ASTM STP 675 ed., Fong, J.T., pp. 816.
- 62) Matsuda, S., Okazaki, K., Hasegawa, H., Ono, H. and Nihei, K. (1984) JSMS vol.33, no. 374 pp. 1414.
- 63) Elsander, A. and Batte, A.D. (1982) ASME 82- JPGC-Pwr.-19.
- 64) Lindley, T.C., McIntyre, P. and Trant, P.J. (1982) Metals Tech. Vol.9, pp.135.
- 65) Kawai, S. and Kasai, K. (1985) Fatigue Fract. Engng. Mater. Struct. Vol.8, no. 2, pp. 115.

- 66) Kondo, Y. and Endo, T. (1985) Proc. of Current Research on Fatigue Cracks, Materials Research Series 1, The Society of Materials Science, Japan.
- 67) Kondo, Y. (1989) Corrosion Science, vol.45, No. 1, pp. 7.
- 68) Kondo, Y. and Wei, R.P. (1989) in proc. of International Conference on Evaluation of Materials Performance in severe environments - towards the development of materials for marine and other uses, EVALMAT 89, , Japan, pp. 135.
- 69) Ford, F.P. (1989) Status of research on environmentally assisted cracking in LWR pressure vessel steels, ASME.

Fig.1.

CORROSION STATISTICS



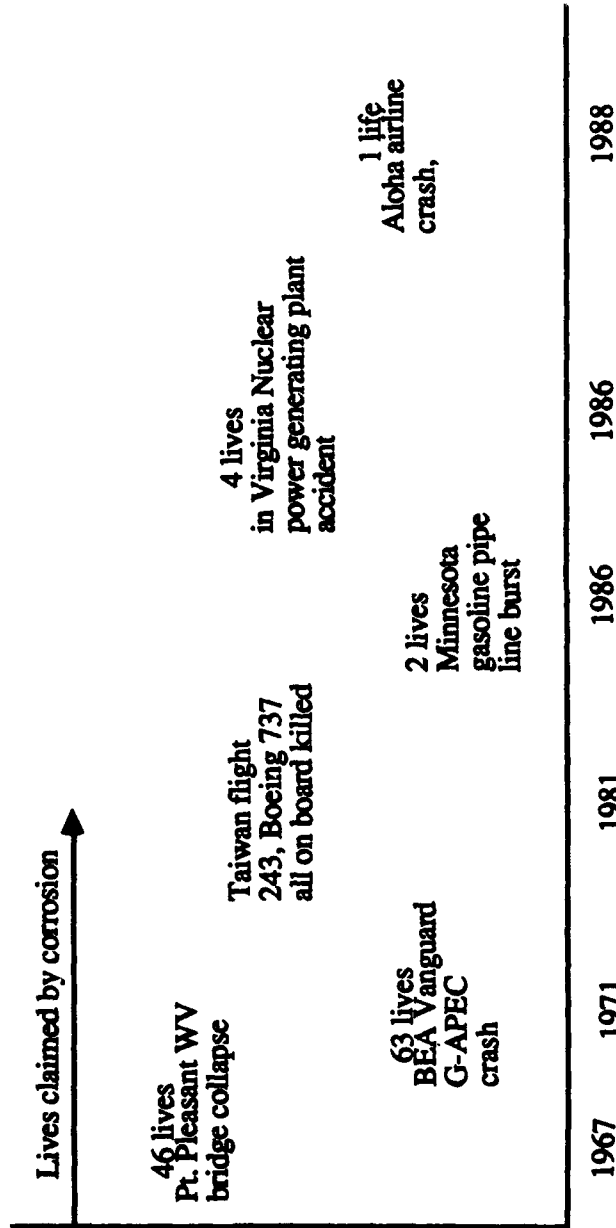
*: An approximate estimate, this figure may be higher.

**QIDEC
U of U**

Hoepfner, D.W. and Goswami, T., USAF, SI Conference, San Antonio, 11/93.

Fig.2.

LIVES CLAIMED BY CORROSION

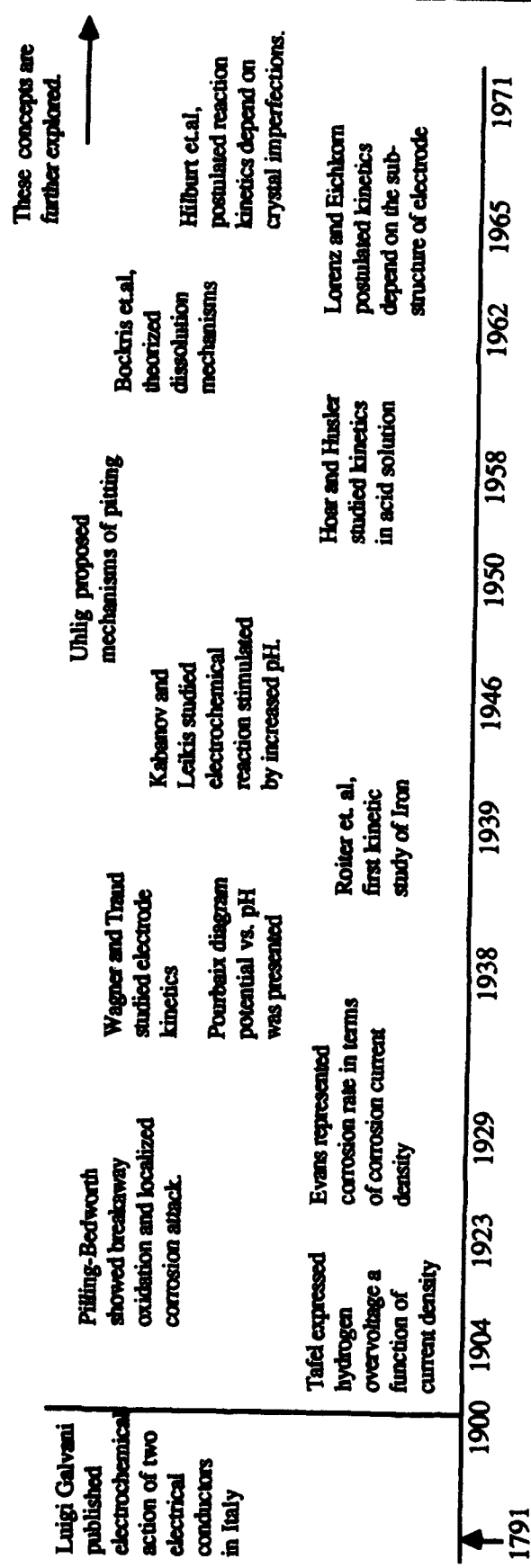


QIDEC
U of U

Hoepfner, D.W. and Goswami, T., USAF, SI Conference, San Antonio, 11/93.

Fig.3.

ELECTROCHEMICAL ASPECTS IN CORROSION

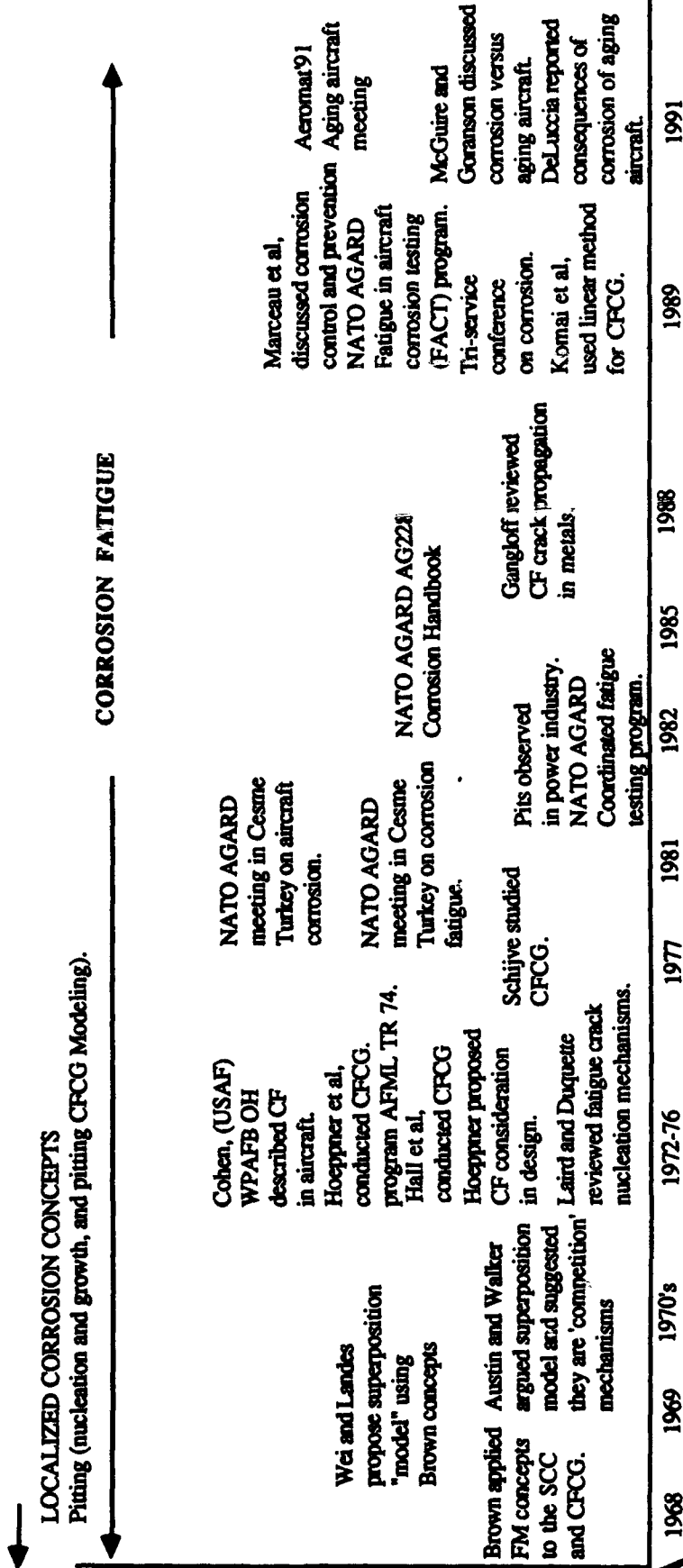


QIDEC
U of U

Hoepfner, D.W. and Goswami, T., USAF, SI Conference, San Antonio, 11/93.

Fig.4.

AIRCRAFT CORROSION FATIGUE

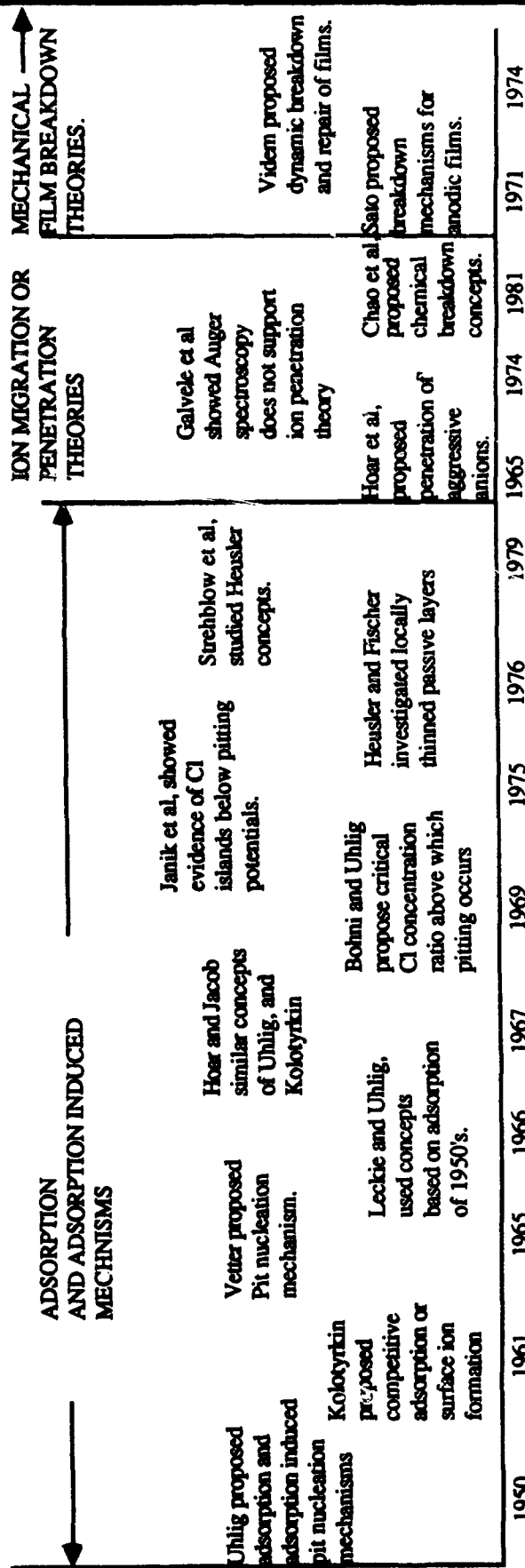


QIDEC
U of U

Hoepfner, D.W. and Goswami, T., USAF, SI Conference, San Antonio, 11/93.

Fig.5.

PIT NUCLEATION MECHANISMS

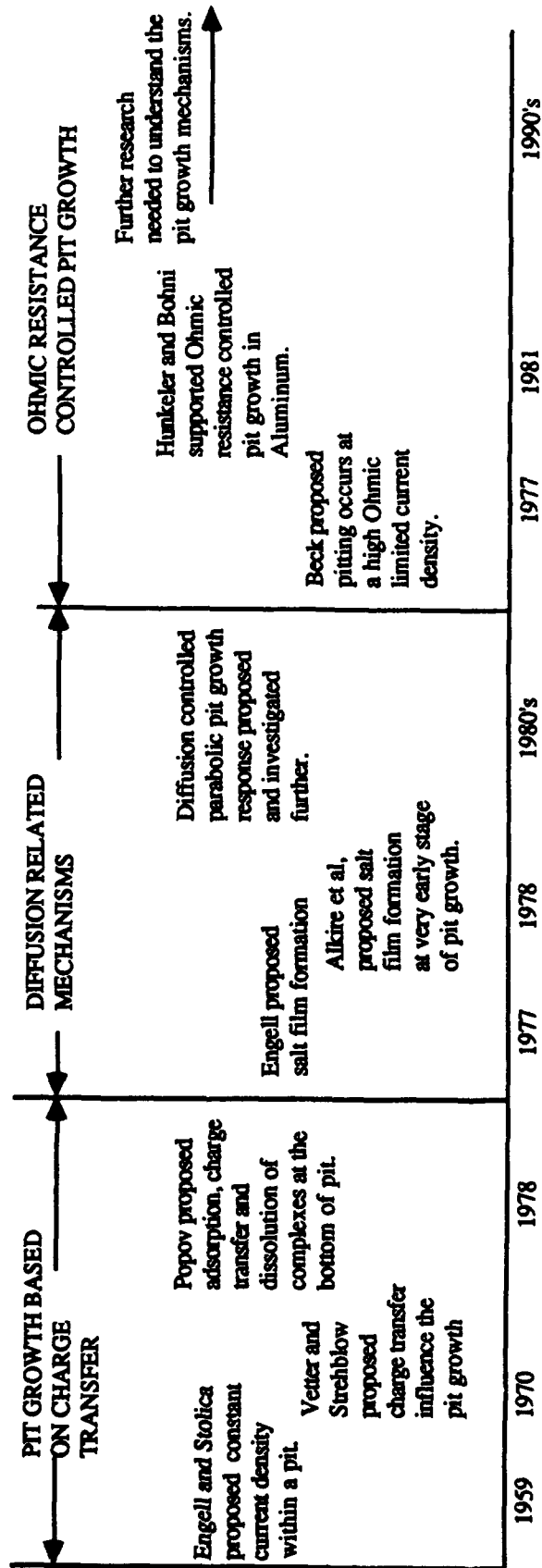


QIDEC
U of U

Hoepfner, D.W. and Goswami, T., USAF, SI Conference, San Antonio, 11/93.

Fig.6.

PIT GROWTH MECHANISMS

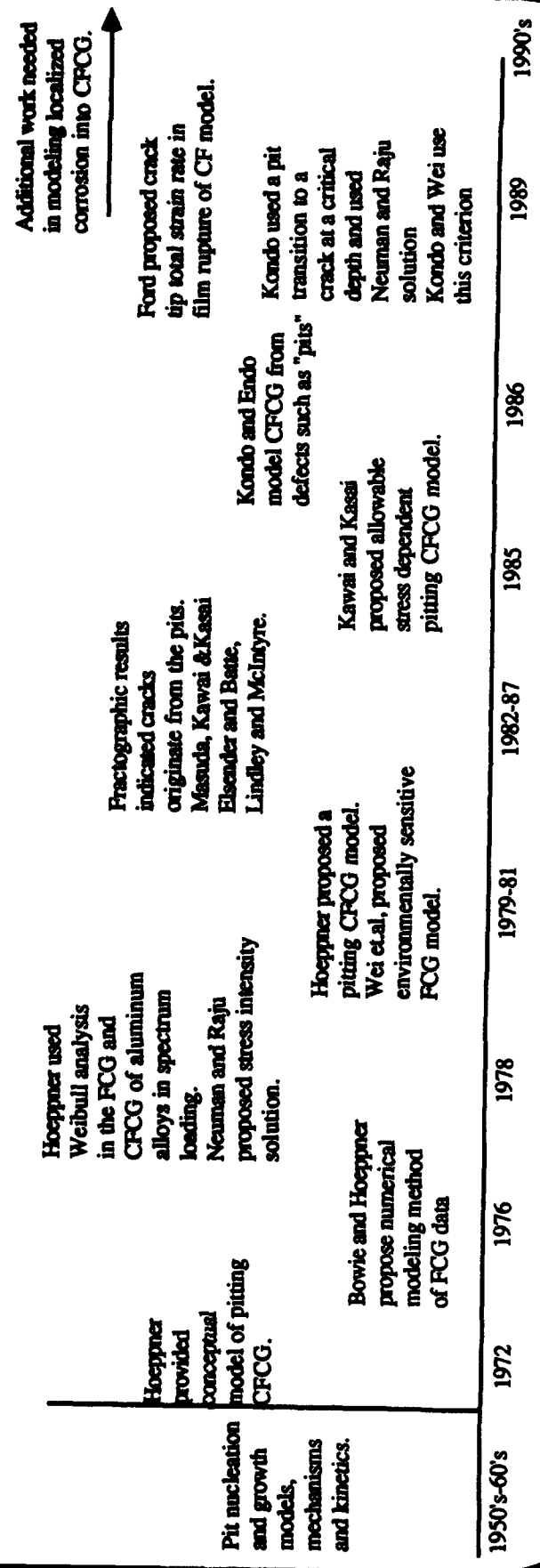


QIDEC
U of U

Hoepfner, D.W. and Goswami, T., USAF, SI Conference, San Antonio, 11/93.

Fig.7.

PITTING CORROSION FATIGUE MODELING



QIDEC
U of U

Hoepfner, D.W. and Goswami, T., USAF, SI Conference, San Antonio, 11/93.

Progressive Fracture of Polymer Matrix Composite Structures: A New Approach

Christos C. Chamis* and Pappu L. N. Murthy†
National Aeronautics and Space Administration
Lewis Research Center, Cleveland, Ohio 44135

Levon Minnetyan‡
Clarkson University, Potsdam, New York 13699-5710

SUMMARY

A new approach independent of stress intensity factors and fracture toughness parameters has been developed and is described for the computational simulation of progressive fracture of polymer matrix composite structures. The damage stages are quantified based on physics via composite mechanics while the degradation of the structural behavior is quantified via the finite element method. The approach accounts for all types of composite behavior, structures, load conditions, and fracture processes starting from damage initiation, to unstable propagation and to global structural collapse. Results of structural fracture in composite beams, panels, plates, and shells are presented to demonstrate the effectiveness and versatility of this new approach. Parameters and guidelines are identified which can be used as criteria for structural fracture, inspection intervals and retirement for cause. Generalization to structures made of monolithic metallic materials are outlined and lessons learned in undertaking the development of new approaches, in general, are summarized.

INTRODUCTION

It is generally accepted that flawed structures fail when the flaws grow or coalesce to a critical dimension such that (1) the structure cannot safely perform as designed and qualified or (2) catastrophic global fracture is imminent. This is true for structures made from traditional homogeneous materials as well as fiber composites. The difference between fiber composites and traditional materials is that composites have multiple fracture modes that initiate local flaws compared to only a few for traditional materials. Any predictive approach for simulating structural fracture in fiber composites needs to formally quantify: (1) all possible fracture modes, (2) the types of flaws they initiate, and (3) the coalescing and propagation of these flaws to critical dimensions for imminent structural fracture.

One of the ongoing research activities at NASA Lewis Research Center is directed toward the development of a methodology for the "Computational Simulation of Structural Fracture in Fiber

*Senior Aerospace Scientist, Structures Division.

†Senior Aerospace Engineer, Structures Division.

‡Associate Professor, Dept Civil and Environmental Engrg.

Composites." A part of this methodology consists of step-by-step procedures to simulate individual and mixed mode fracture in a variety of generic composite components (refs. 1 to 3). Another part has been to incorporate these methodologies into an integrated computer code identified as CODSTRAN for Composite Durability Structural Analysis (refs. 4 and 5). The objective of this report is to describe the fundamental aspects of this new approach and to illustrate its application to a variety of generic composite structures.

The generic types of composite structural fracture illustrated in this report are: (1) single and combined mode fracture in beams, (2) laminate free-edge delamination fracture, (3) laminate center flaw progressive fracture, (4) plate and shell structural fractures, and (5) bolted composite fracture. Structural fracture is assessed by one or all of the following indicators: (1) the displacements increase very rapidly, (2) the frequencies decrease very rapidly, (3) the buckling loads decrease very rapidly, or (4) the strain energy release rates increase very rapidly. These rapid changes are herein assumed to denote imminent global structural fracture. Based on these rapid changes, parameters and guidelines are identified which can be used as criteria for (1) structural fracture, (2) inspection intervals, and (3) retirement for cause.

In the present approach, computational simulation is defined in a specific way. Also general remarks are included with respect to (1) application of this new approach to large structures and/or structural systems and (2) lessons learned about conducting such a long duration research activity, with regard to increasing computational efficiency, gaining confidence, and expediting its application. Sample case results are included for composite beams, panels, plates, and shells to illustrate the effectiveness and versatility of this new approach.

FUNDAMENTALS

This new approach to structural fracture is based on the following concepts.

1. Any structure or structural component can sustain a certain amount of damage prior to structural fracture (collapse).
2. During damage propagation, the structure exhibits progressive degradation of structural integrity as measured by global structural behavior variables such as loss in frequency, loss in buckling resistance, or excessive displacements.
3. The critical damage can be characterized as the amount of damage beyond which a small additional damage or loading increase will cause a rapid degradation in the structural integrity.
4. Structural damage is characterized by the following five sequential stages: (1) initiation, (2) growth, (3) accumulation, (4) stable or slow propagation (up to critical amount), and (5) unstable or very rapid propagation (beyond the critical amount) to collapse.

These concepts are fundamental to developing formal procedures to (1) identify the five different stages of damage, (2) quantify the amount of damage at each stage, and (3) relate the degradation of global structural behavior to the amount of damage at each stage.

The formal procedures included in this new approach are as follows:

Damage-stage identification. - (1) Damage initiates when the local stress state exceeds the corresponding material resistance. (2) Initial damage grows when the stress exceeds the corresponding

material resistance on the damaged periphery for every possible failure mode. (3) Damage accumulates when multiple sites of damage coalesce. (4) Damage propagation is stable or slow when small increases, in either the damage propagation or loading condition, produce insignificant or relatively small degradation in the structural behavior (frequencies, buckling resistance, and displacements). (5) Damage propagation is unstable or very rapid when small increases in the damage propagation or in loading conditions produce significant or very large changes in the global structural behavior variables (frequencies, buckling resistance, and displacements).

Damage quantification. - The amount of damage is formally quantified by modeling the physics, in the periphery of the damaged region, to keep the structure in equilibrium for the specified loading conditions, structural configuration and boundary conditions. This part of the procedure is most conveniently handled by using computational simulation in conjunction with incremental/iterative methods as will be described later.

Structural behavior degradation. - This part of the procedure is quantified by using composite mechanics in conjunction with the finite element analysis. The damage stages are quantified by the use of composite mechanics while degradation of the structural behavior is quantified by the finite element method where the damaged part of the structure does not contribute to the resistance but is carried along as a parasitic material. It is very important to note that nowhere in this approach mention of either stress intensity factors or fracture toughness parameters was made. This new approach bypasses both of them. However, use is made of the structural fracture toughness in terms of global Strain Energy Release Rate (SERR) because it is a convenient parameter to identify the "critical damage amount." The critical global SERR in the context of present approach is described subsequently.

The fundamental concepts described previously are concisely summarized in figure 1. The steps are few and simple and the parameters for "critical damage" are readily identifiable.

The combination of composite mechanics with the finite element method to permit formal description of local conditions to global structural behavior is normally handled through an integrated computer code as shown schematically in figure 2. The bottom of this figure describes the conditions of the material (microstress versus resistance) and where the criteria for damage initiation, growth, accumulation, and propagation are examined. The left part integrates (synthesizes) local damage conditions to global structural behavior (response). The right part of the figure tracks (decomposes) the effects of global changes (loading conditions for example) on the local (micro) material stress/resistance. Increases in damage are induced at the micro level while increases in the load conditions are applied at the global structural model. Overall structural equilibrium is maintained by iterations around this simulation (cart-wheel type) cycle until a specified convergence is reached. Implementation of the new approach to track the various stages of damage is illustrated schematically in figure 3. The final result in terms of load versus global displacement is shown in figure 4. The schematics in figures 1 to 4 collectively summarize the fundamentals and implementation of this new approach to composite structural fracture and also to structural fracture in general. Applications to specific structures and components are described in subsequent sections.

BEAMS

The new approach has been applied to three different types of beams: (1) double cantilever for opening mode delamination, (2) end-notch-shear for shear mode delamination, and (3) mixed mode

delamination. Typical results obtained are summarized below. The details are described in the references cited for each specific application.

Double cantilever. - A typical result from applying this new approach to a double cantilever for opening mode delamination is shown in figure 4 (ref. 1). For this simulation, a preexisting damage (1 in. long) was assumed across the beam width. A small amount of damage growth/accumulation (about 0.05 in) had severe effect on the strain energy release rate (SERR-G). Rapid damage occurred to about 1.12 in., beyond which the SERR increased very rapidly indicating unstable damage propagation to complete delamination. Referring to figure 1, the critical damage for this beam is less than 1.0 in. long (a) and less than 1.0 psi-in. structural fracture toughness (G). These values are in the range of those experimentally measured by using the double cantilever test method (about 0.8 psi-in. at 1-in. crack length).

End-notch-shear. - Typical results for shear-mode delamination in a beam, as can be measured by end-notch-flexure, are shown in figure 5 (ref. 1). A preexisting damage of 1 in. across the width was assumed for the simulation. A rapid damage growth/accumulation took place to about 1.1 in. followed by a stable damage propagation to about 1.18 in. Beyond this point, the damage propagation became unstable. Note that the range of measured data is indicated by the horizontal dashed lines. Note also that the local crack closure technique, which is commonly used, is also shown as a dashed curve. Applying the criteria in figure 1, the critical fracture toughness parameters are from the global curve about 1.18 in. for "a" and about 3.5 psi-in. for "G". Those from the local curve are about 1.2 in. for "a" and 2.5 psi-in. for "G". This example illustrates the difference between local and global quantities. It is worth noting that the local method requires about three times the computer time compared to the global.

Mixed mode delamination. - Two types can be simulated: (1) Shear mode (Mode II) combined with opening mode (Mode I) and (2) opening mode (Mode I) combined with shear mode (Mode II) and with tearing mode (Mode III). A typical result for the first type is shown in figure 7 (ref. 1). This figure illustrates that the global method does not distinguish how much each mode contributes. It is necessary to use the local closure technique to quantify the simultaneous contribution of each mode. An interesting observation is that the opening mode drives the delamination to beam splitting while the shear mode reaches a stable propagation state and remains there. Referring to figure 1, the critical structural fracture parameters are about 1.18 in. for "a" and about 3.3 psi-in. for "G." These are about 5 and 8 percent smaller, respectively, compared to shear mode (Mode II) fracture.

A typical result for the second type of mixed mode delamination is shown in figure 8 (ref. 2). The curves plotted in this figure are for critical values obtained from figure 1, that is, when the damage propagation state becomes unstable. The individual mode contributions were obtained by the local "crack closure" technique. A few interesting observations are: (1) the tearing mode (Mode III) is insignificant compared to the other two; (2) Mode I contributes the most; and (3) superposition of the three modes does not equal that of the total. This again indicates that the global fracture parameters appear to be more representative indicators of structural fracture. The other important observation is that the unsymmetric laminate configuration can be used in the end-notch mixed mode beam to measure the tearing mode. This is a simple test method indeed. The authors are not aware of any measured results obtained by using this test method. Collectively, the results from the different beams demonstrate that the new approach is readily applicable to these types of composite structures. Through-the-thickness damage and embedded damage can be simulated just as readily.

PANELS

The new approach has been applied to computationally simulate structural fracture of composite panels subjected to in-plane loads. Typical results for three types of delamination are described to demonstrate application of the procedure (ref. 3).

Edge delamination. - The physics and stress state of edge delamination in composite laminates are schematically illustrated in figure 9. The delamination processes and their quantification using global parameters is shown in the schematic in figure 10. Typical results obtained for laminates from three different composite systems are shown in figure 11. This type of delamination grows and accumulates rapidly to about 6 percent of the area and then reaches a stable state. This stable state implies: (1) that a specific composite laminate will have a unique critical delamination parameter and (2) edge delamination, induced by predominantly tensile in-plane stress, will not lead to panel collapse or disintegration.

Referring to figure 11, the parameters for stable damage state are about 7 percent area delamination for all composite systems and about 35, 50 and 70 psi-in. for S-G/IMHS, AS/HMHS, and AS/IMHS composites, respectively. Additional observations from figure 11 are that the structure fracture toughness depends on fiber type (difference in S-G and AS for the same matrix IMHS) and matrix (HMHS and IMHS for the same fiber AS). An important conclusion is that this new approach provides a relatively simple formal procedure to evaluate and/or identify fiber/matrix combinations for specified structural fracture toughness.

Edge-pocket-delamination. - Edge delamination is usually preceded by transply cracks which can occur in several locations simultaneously thus forming pocket-type delaminations along the edge. These types of delaminations can be simulated the same way as described previously except that they represent a form of multisite damage initiation, growth, accumulation, and propagation. Typical results for structural fracture toughness are shown in figure 12 for three different composite systems. Several interesting aspects of fracture progression can be observed in this figure. (1) Pocket delaminations grow rapidly inward to about 5 percent in delaminated area. (2) Stable delamination occurs inward to about 20 percent in delaminated area. (3) The pocket delaminations coalesce as indicated by the jump in "G." (4) The accumulated delamination grows with a decreasing rate to a stable level of about 45 percent in delaminated area. (5) The propagation exhibits stable behavior beyond this elaminated area. The structural fracture toughness value after stabilization is the same as that for stable edge delamination. The important conclusions are: (1) this new approach provides sufficient information to identify and quantify the fracture process from initiation to structure/component collapse and (2) it is readily adaptable to multiple site fracture initiation.

Internal or embedded delamination. - This type of delamination is a result of the fabrication process or damage sustained by inadvertent normal impact. In either case the damage growth, accumulation, and propagation can be simulated by using this new approach. Typical results are shown in figure 13 for the three different composite systems. An important observation is that substantial internal damage (up to 55 percent in delaminated area) occurs with negligible increase in the global SERR. Keep in mind that this panel and delamination results are for tensile in-plane load which does not cause local buckling.

The results from the panel clearly demonstrate that the new approach for structural fracture is readily adaptable to these types of delamination fractures including those initiated at internal

hidden sites.

Through-the-thickness defects. - The previous examples were special cases of structural fracture. A panel with through-the-thickness defects is a more general case because 14 different failure modes are possible including fiber fractures. Three specific cases are simulated using the computer code CODSTRAN (fig. 2). These specific cases are selected to illustrate the similarities in fracture growth accumulation and propagation. Schematics of the three different cases (no defect (a), crack-like-defect (b), and hole-like defect(c)) are shown in figure 14 with respective schematics depicting the damage propagation extent by element annihilation (ref. 6).

The damage extent for all three cases is approximately the same. The load that induced the damage is not the same. That, for the crack-like and hole-like initial defects are about the same (figs. 14(b) and (c)). However, the load for the case without initial defects (fig. 14(a)) is about twice as high as that for the defective laminates. The failure modes for each panel with different angle ply laminates are summarized in figure 15. As can be seen, the failure modes for all defect (notch) types are practically identical. The important observation is that irrespective of the initial defect shape, the damage growth, damage accumulation, and propagation appear to remain constant at least for uniform tensile load. An important conclusion is that this new approach to composite structural fracture simulates all aspects of the fracture process.

PLATES

This case is selected to illustrate the effects of damage propagation on vibration frequencies and buckling resistance as well as the effects of hygrothermal environments. Typical results obtained by using CODSTRAN (fig. 2) are shown in figures 16 and 17 (refs. 7 to 9) where the schematics of the plate and the various hygrothermal environments are also shown. The important observations are: (1) the reference case, at room temperature and without moisture, exhibits the least amount of damage accumulation to fracture compared to the other cases; (2) moisture alone has a negligible effect on fracture load but increases the damage extent to fracture (fig. 16(b)); (3) combined temperature and moisture (hygrothermal) decrease the load to fracture but permit substantial damage accumulation to fracture (fig. 16(b)); (4) both the vibration frequency and the buckling resistance decrease very rapidly as the fracture load (structural collapse) is approached (fig. 16(c)); (5) the hygrothermal environments degrade the structural behavior of the plate (figs. 17(b), (c), and (d)); and (6) the buckling resistance is the most discriminating structural behavior for hygrothermal degradation (fig. 17(d)).

The important conclusion is that this new approach provides the formalism to simulate complex environmental effects from the micromechanics to structural behavior. That is, the temperature and moisture affect the matrix locally while the composite mechanics and the finite element method integrate these local effects to structural behavior (buckling resistance in this case).

SHELLS

CODSTRAN is used to simulate the damage initiation, growth accumulation, and propagation to fracture in a composite shell with through-the-thickness as well as partial initial defects and subjected to internal pressure with hygrothermal environment.

Through-the-thickness defect. - Typical results for a through-the-thickness initial defect are shown

in figure 18 (ref. 9). The results in this figure show that: (1) shells subjected to internal pressure sustain relatively low damage accumulation to fracture compared to other structural components (fig. 18(b)); (2) shells are less tolerant to hygrothermal effects compared to other structural components (fig. 18(c)); (3) the vibration frequencies of the shell do not degrade rapidly as the fracture pressure is approached (fig. 18(c)), and (4) hygrothermal environments have a significant effect on the higher vibration frequencies of the shell (Fig. 18(c)). The effects on frequencies depends on specific shell/defect combination. An important observation is that composite shells with through-the-thickness defects subjected to internal pressure, exhibit a brittle type behavior to fracture. This explains, in part, the successful application of Linear Elastic Fracture Mechanics to these types of structures.

Partial-thickness defects.- The composite shell shown in figure 19 is investigated with initial fiber defects in two adjacent hoop plies occurring as (1) surface ply defects and (2) internal ply defects, as depicted in figure 20 (ref. 10). Computational simulation results for these two cases are summarized in figure 21. Case (2) exhibits results in a gradual damage growth and propagation with local degradation. There is sufficient local distortion of the shell geometry during the damage propagation to serve as a warning of approaching structural fracture. On the other hand, in case (1) damage propagation to structural fracture occurs without warning as a sudden catastrophic fracture of the shell. Figure 22 summarizes damage initiation and structural fracture pressures for the two cases with reference to the fracture pressure of a defect-free shell. It is noteworthy that surface ply defects reduce the ultimate fracture pressure by 15 percent whereas interior or midthickness ply defects reduce the ultimate fracture pressure by 23 percent. The important conclusion is that the complex structural behavior of shells with damage accumulation can be computationally simulated for any type of defects as well as for defect-free shells.

BOLTED COMPOSITE

A composite panel of 4.0 in. width, 8.0 in. length and 0.25 in. thickness is fastened by a 1.0 in. diameter fastener at 2.0 in. from one of its ends and is subjected to a uniformly distributed loading at the other end as shown in figure 23. The composite system is made of AS-4 graphite fibers in a high-modulus high-strength epoxy matrix (AS-4/HMHS). The fiber volume ratio is 0.60 and the void volume ratio is two percent. The laminate consists of forty eight 0.132 mm (0.00521 in.) plies. The laminate configuration is $[90/\pm 45/0]_{12}$. The 90° plies are perpendicular to the load direction and the 0° plies are oriented in the loading direction of the specimen as shown in figure 23. A cure temperature of 350°F is assumed for residual stresses. The bolt is modelled using high strength steel properties. The finite element model of the combined composite specimen and bolt contains 67 nodes and 48 elements as shown in figure 23. The bolt is fixed with respect to all displacement and rotational degrees of freedom at its center. The composite specimen is subjected to a gradually increasing load until it is fractured and torn off the bolt.

Figure 24 shows the simulated damage progression with increasing load on the specimen. During the first load increment of 800 lbs, finite element connectivities between the bolt and the composite are released at the bolt-laminate boundary where generalized membrane stresses N_x and N_y are both tensile. Under a 6.8 kip load damage is initiated at nodes adjacent to the bolt by matrix cracking in the 90° plies. After damage initiation by σ_{11C} failures, the damaged plies also undergo σ_{11C} failures during the next iteration. Damage grows to the -45° and $+45^\circ$ plies under the same load. When the load is increased to 10 kips the damaged region grows larger. Gradual damage

accumulation in selective plies continues until a 32.8 kip load is reached when fracture begins. Fracture is rapidly propagated to cause the ultimate break of the connection due to the fracture line that started at one side of the fastener. Figure 25 shows the primary, secondary, and ultimate fracture lines, as well as remote damage locations. Figure 26 shows the strain energy release rate (SERR) that is minimum under a 12.8 kip loading but recovers to higher levels as damage progression continues. Figure 27 shows the end displacement with applied loading, indicating that initial damage stages will not be apparent from the observation of a test.

GENERALIZATION AND LESSONS LEARNED

The discussion of this new approach focussed on its application to composite structures which are far more complex than conventional metallic structures. However, the approach is readily adaptable to structures made from any material or any combination of materials. Based on the experience and success to date, it can be readily generalized as is outlined in figure 28. The steps in the outline are the same for any structure. The difference is only in the description and history-tracking of the material behavior.

The important lessons learned in developing this new approach are generic and should be instructive for undertaking the development of new approaches in general. These lessons are summarized in figure 29. The authors firmly believe (they are convinced) that all the items in this summary are necessary for the successful development of new approaches. The authors are also convinced that the development of any new approach is not and should not be a short term activity because the developers increase their knowledge with continuous feedback and mature with the accumulation of experience during the development stage.

SUMMARY

A new approach independent of stress intensity factors and fracture toughness parameters has been developed and described for the computational simulation of the fracture of composite structures. This approach is inclusive in that it integrates composite mechanics (for composite behavior) with finite element analysis (for global structural response). The integration of these two disciplines permits: (1) quantification of the fracture progression from local damage initiation to structural fracture (collapse), (2) accommodation of any loading conditions including temperature and moisture, and (3) the effects of material degradation due to hygrothermal environments. The versatility of the approach is demonstrated by using it to computationally simulate fracture in typical structures (beams, panels, plates, and shells) in a variety of fracture conditions. Parameters and guidelines are identified which can be used as criteria for structural fracture, inspection intervals, and retirement for cause. Generalization to structural systems and structures made from other components is outlined. Important lessons learned from undertaking the development of new approaches are summarized.

References

- [1] Murthy, P.L.N., and Chamis, C.C., 1985, "Interlaminar Fracture Toughness: Three-Dimensional Finite Element Modeling for End-Notch and Mixed-Mode Flexure," NASA TM 87138.
- [2] Murthy, P.L.N., and Chamis, C.C., 1986, "Composite Interlaminar Fracture Toughness: 3-D Finite Element Modeling for Mixed Mode I, II and III Fracture," NASA TM-88872.
- [3] Wilt, T.A., Murthy, P.L.N., and Chamis, C.C., 1988, "Fracture Toughness, Computational Simulation of General Delamination in Fiber Composites," NASA TM-101415.
- [4] Chamis, C.C., and Smith, G.T., 1978, "CODSTRAN: Composite Durability Structural Analysis," NASA TM-79070.
- [5] Chamis, C.C., 1986, "Computational Simulation of Progressive Fracture in Fiber Composites," NASA-TM 87341.
- [6] Irvine, T.B., and Ginty, C.A., 1986, "Progressive Fracture of Fiber Composites," Journal of Composite Materials, Vol. 20, pp. 166-184.
- [7] Minnetyan, L., and Chamis, C.C., and Murthy, P.L.N., 1990, "Structural Behavior of Composites with Progressive Fracture," NASA TM-102370.
- [8] Minnetyan, L., Murthy, P.L.N., and Chamis, C.C., 1990, "Composite Structure Global Fracture Toughness via Computational Simulation," Computers and Structures, Vol. 37, pp. 175-180.
- [9] Minnetyan, L., Murthy, P.L.N., and Chamis, C.C., 1991, "Progressive Fracture in Composites Subjected to Hygrothermal Environment," AIAA/ASME/ASCE/AMS/ASC Thirty-Second Structures, Structural Dynamics and Materials Conference, Pt. 1, pp. 867-877.
- [10] Minnetyan, L., Chamis, C.C., and Murthy, P.L.N., 1991, "Damage and Fracture in Composite Thin Shells," NASA TM-105289.

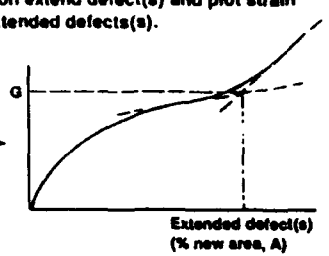
- o Determine requisite properties at desired conditions using composite mechanics.
 - o Run 3-D finite element analysis for an arbitrary loading condition.
 - o Scale loading condition to match ply stress (or microstresses) at the maximum stress element(s) adjacent to defect(s).
 - o With scaled loading condition extend defect(s) and plot strain energy release rate vs extended defects(s).
- 
- o Method is versatile/general.

Figure 1.- General procedure for predicting fracture toughness in composite structures with defects.

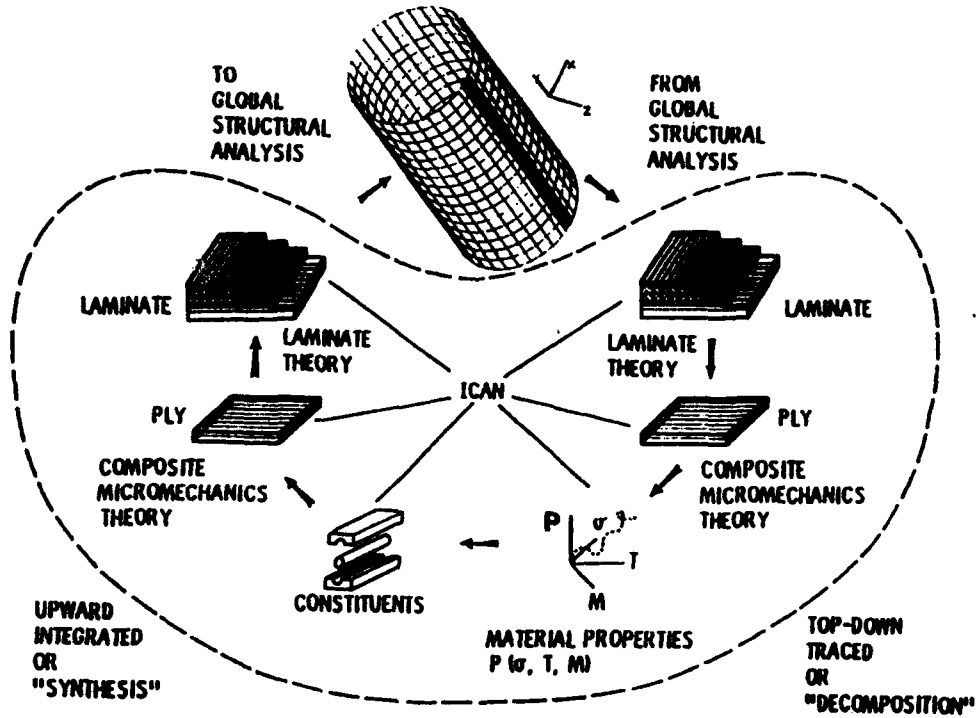


Figure 2.- CODSTRAN analysis Cycle.

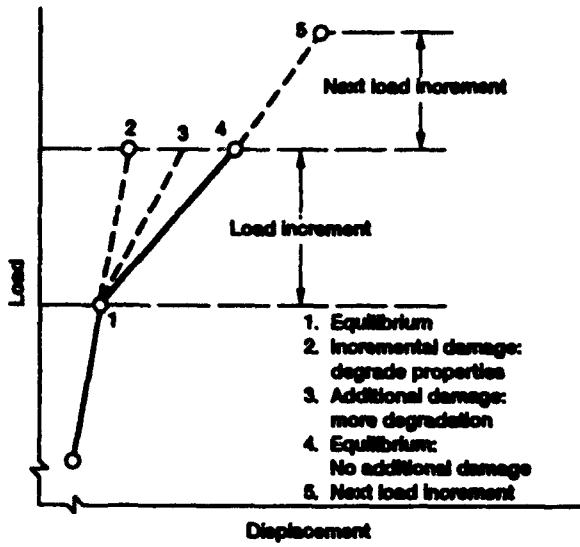


Figure 3.- CODSTRAN load incrementation.

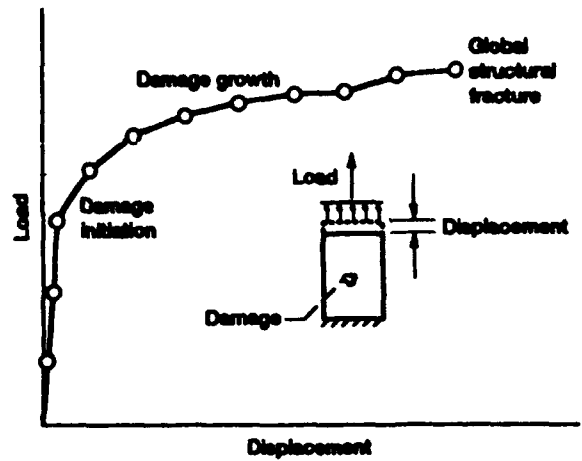


Figure 4.- Overall CODSTRAN simulation.

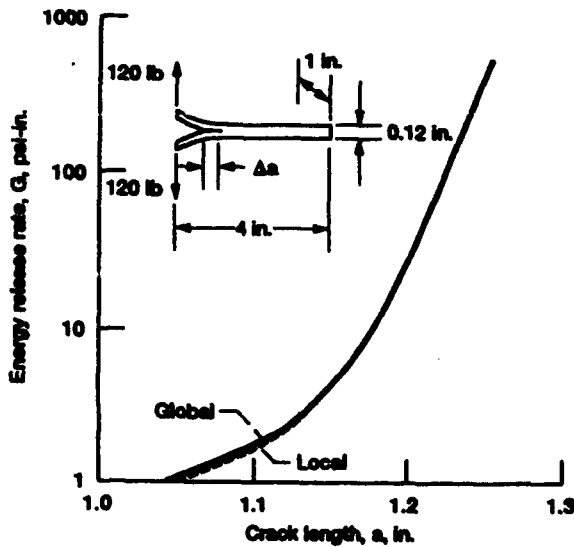


Figure 5.- Double-cantilever energy release rate comparisons (AS/E).

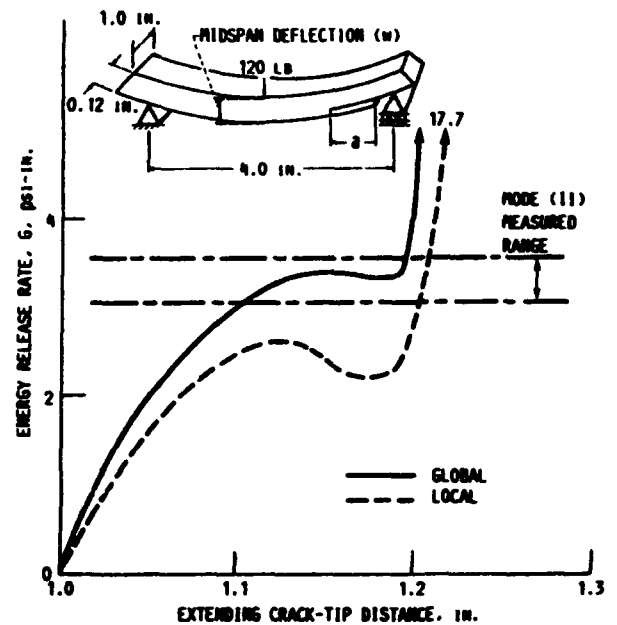


Figure 6.- End-notch-flexure energy release rate comparisons.

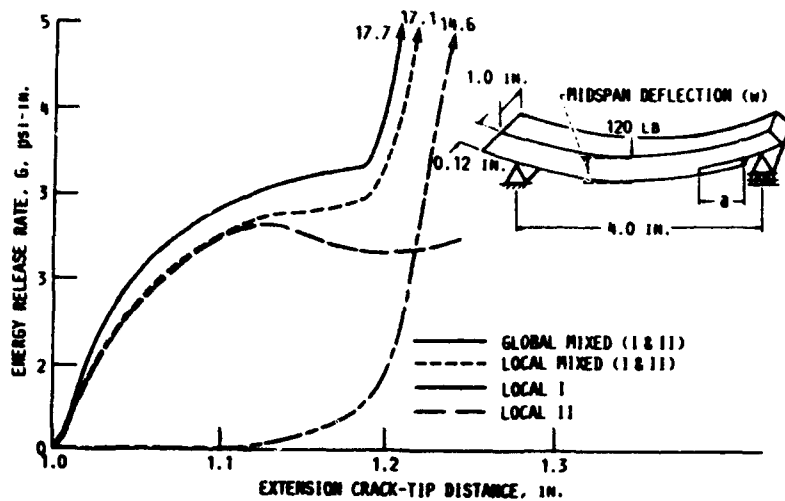


Figure 7.- Mixed-mode-flexure energy release rate and components (AS/E) (single point constrained (Lewis) method).

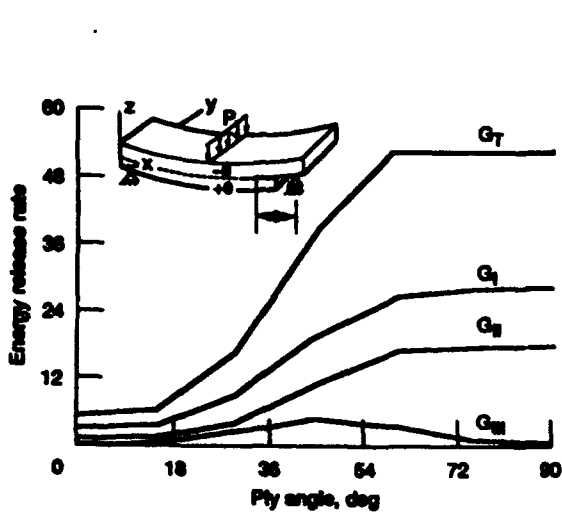


Figure 8.- Ply orientation effects on maximum strain energy release rates (in.-lb/in.²) for constant load $[-\theta_{36}/+\theta_{12}]$.

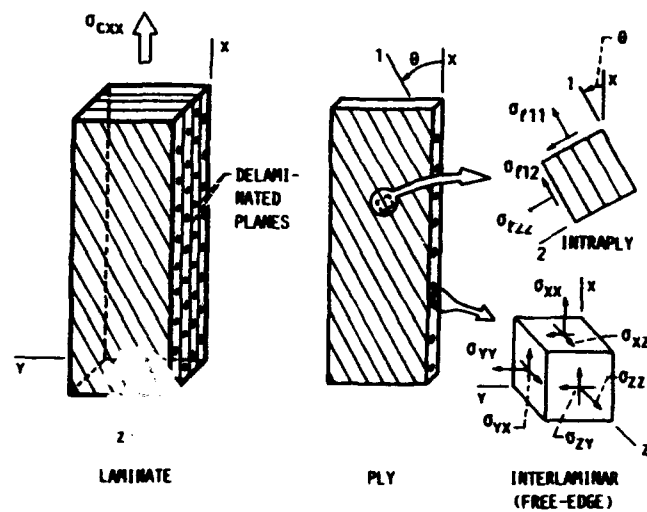


Figure 9.- Lamination decomposition for free-edge interlaminar stresses.

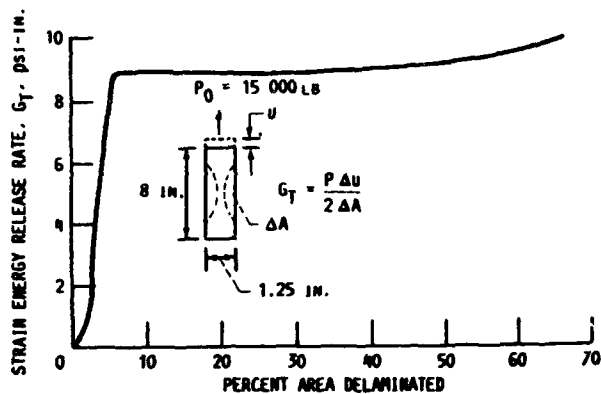


Figure 10.— Strain energy release rate for a "typical" lab specimen (AS/E [$\pm 30/90$], 0.6 FVR composite).

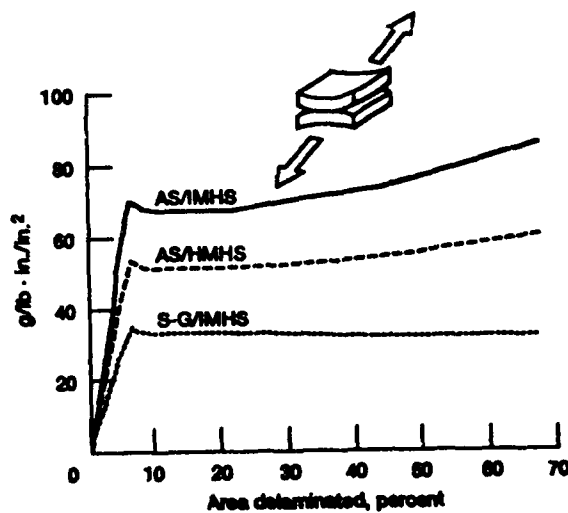


Figure 11.— Strain energy release rate. 6-ply center delamination.

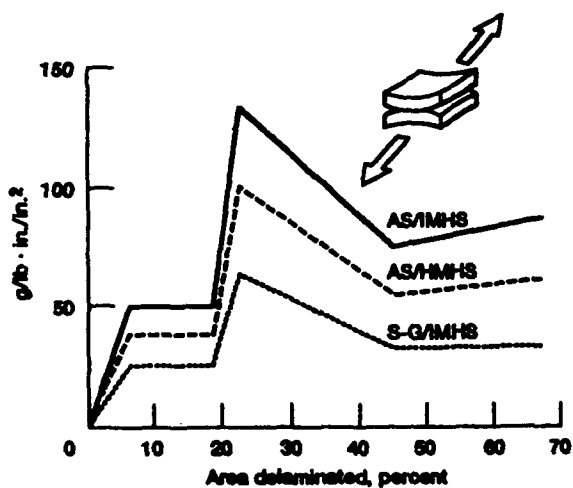


Figure 12.— Strain energy release rate. 6-ply center/pocket delamination.

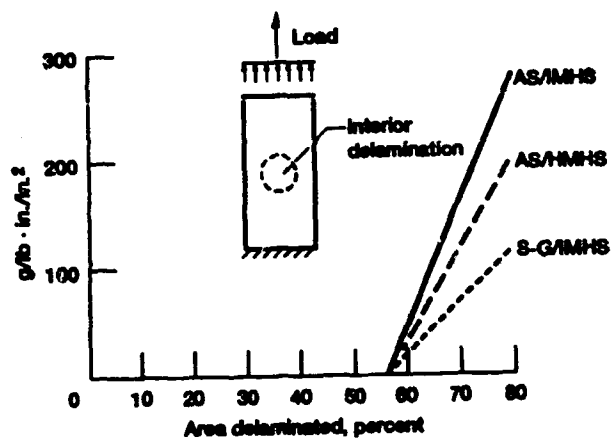


Figure 13.— Strain energy release rate. 6-ply interior/center delamination.

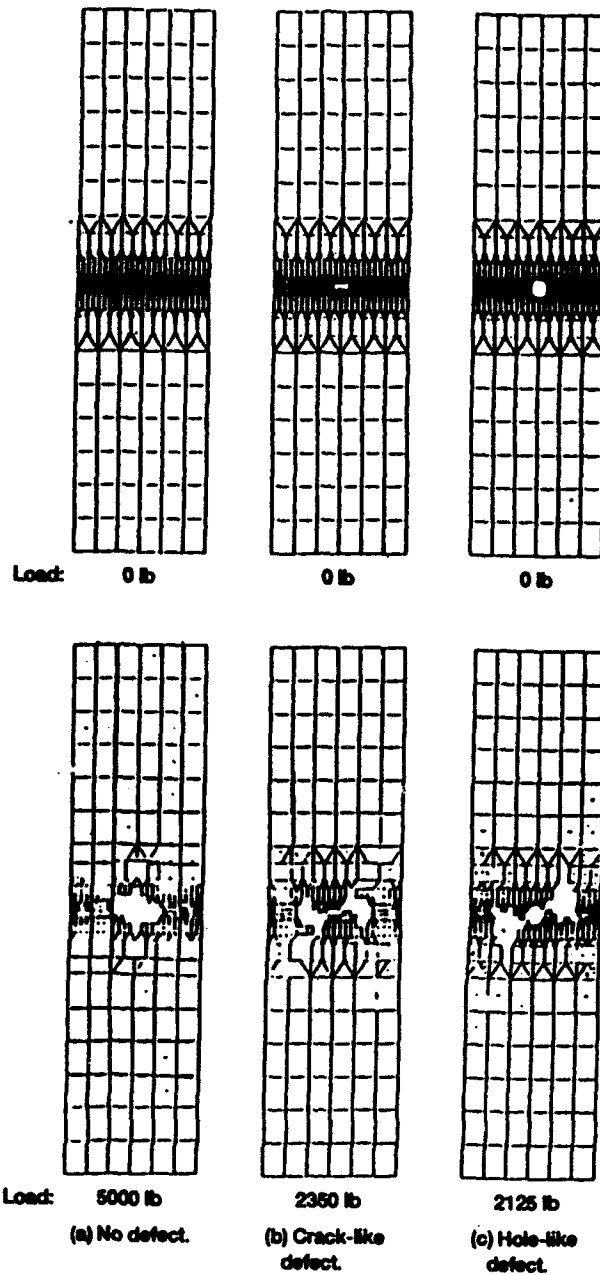


Figure 14.- Computationally simulated progressive fracture of laminates with different types of defects ($G_r/E [\pm 15]_s$) and subjected to in-plane tensile loading.

Notch type	Ply orientation; $[\pm\theta]_n$; θ in degrees									
	0	3	5	10	15	30	45	60	75	90
Unnotched-- solid	LT	LT S ²	LT S ²	LT S ²	I S	S	I S	TT	TT	TT
Notched-- thru slit	S ¹ LT	S ¹ LT	S ¹ LT	S	S	I ⁴ S	I ⁴ S	I ⁴ TT S ²	TT	TT
Notched-- thru hole	S ¹ LT	S ¹ LT	S ¹ LT	S	S LT	I ⁴ S	I ⁴ S TT	I ⁴ TT	TT	TT

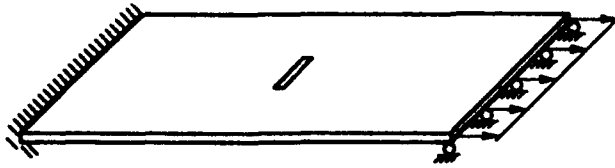
* LT = Longitudinal Tension

TT = Transverse Tension

S = Interply Shear: 1) Initial fracture due to intraply shear in the notch tip zone
2) Minimal intraply shearing during fracture
3) Some intraply shear occurring near constraints (grips)
4) Delaminations occur in notch tip zone prior to any intraply damage

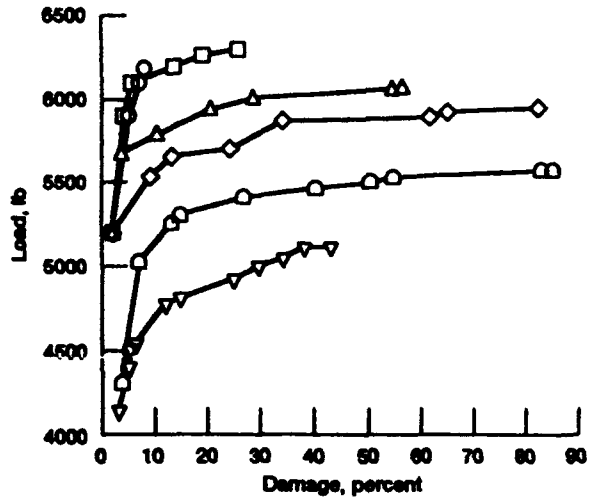
I = Interply Delamination

Figure 15.- Fracture modes* of $[\pm\theta]_n$ G/E laminates (predicted by CODSTRAN).

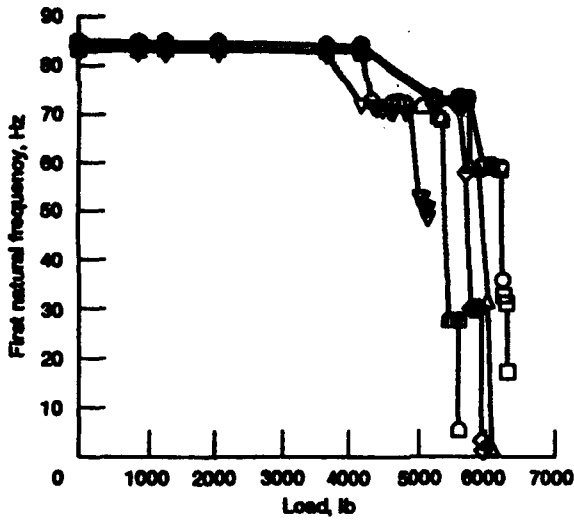


	$T_{\%}$	$M_{\%}$
○	70	0
□	70	1
△	200	0
◇	200	1
◻	300	0
▽	300	1

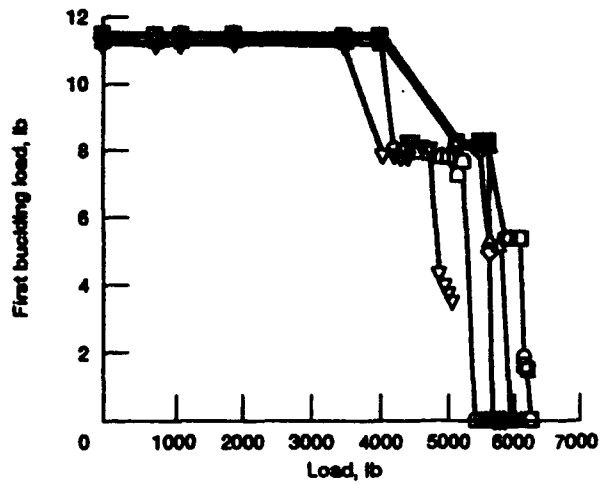
(a) Geometry and environment.



(b) In-plane displacement.

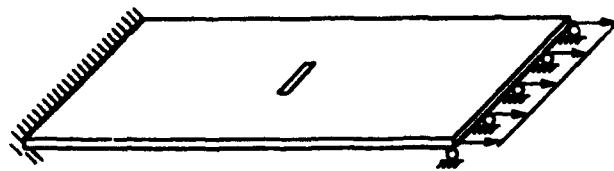


(c) Vibration frequency.



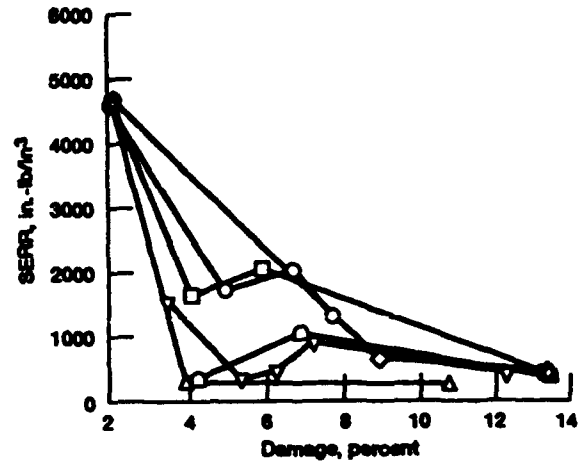
(d) Buckling load.

Figure 16.-- Load induced progressive damage and effects on composite (T300/EP $[\pm 15]_2$) plate structural response including hygrothermal environment.

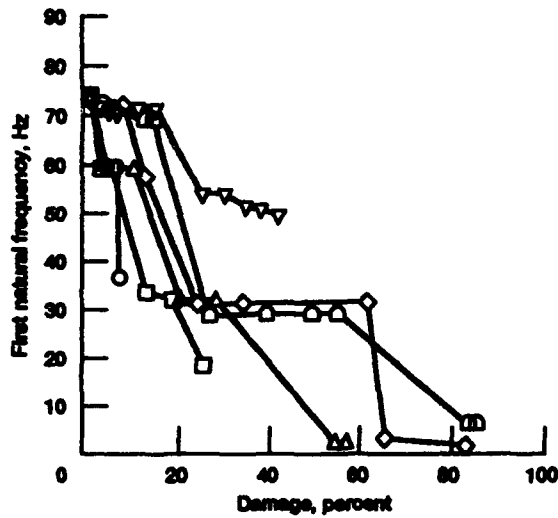


	T_c °F	M, %
○	70	0
□	70	1
△	200	0
◇	200	1
◇	300	0
▽	300	1

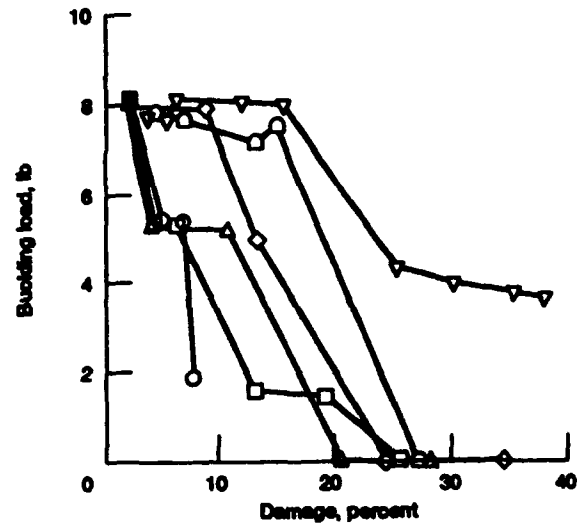
(a) Geometry and environment.



(b) Global strain energy release rate (SERR).

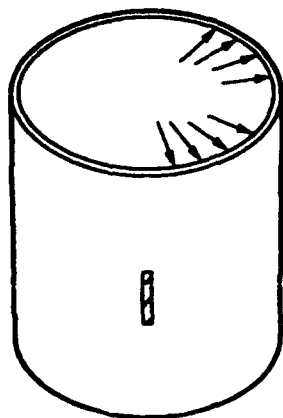


(c) Vibration frequency.



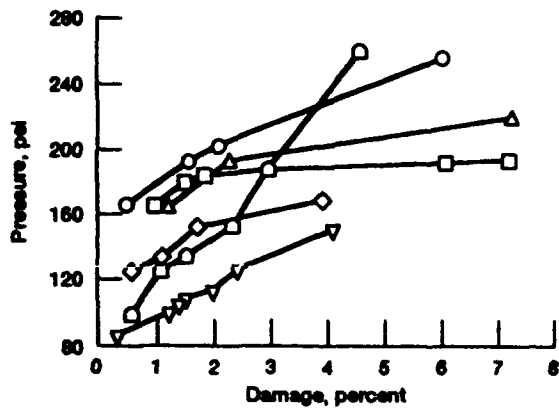
(d) Buckling load.

Figure 17.- Progressive damage degradation effects on composite plate (T300/EP $[\pm 15]_2$) structural behavior including hygrothermal environment.

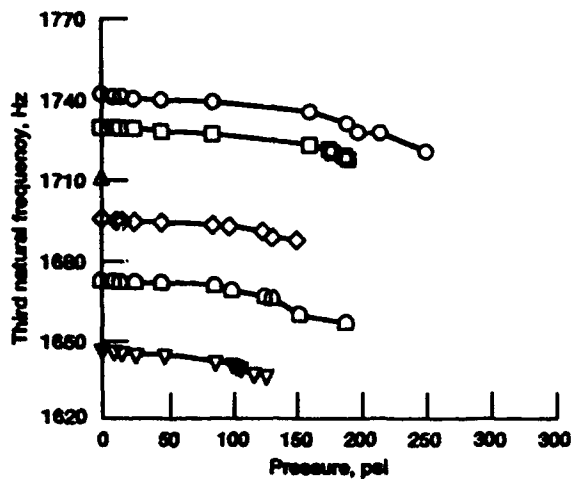


	T_{L_1}	M, %
○	70	0
□	70	1
△	200	0
◇	200	1
◻	300	0
▽	300	1

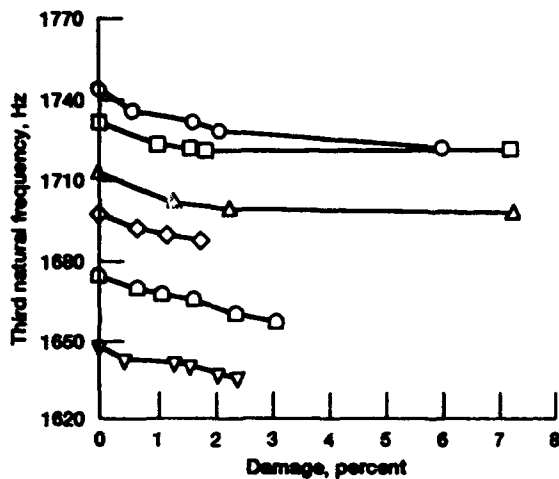
(a) Geometry and environment.



(b) Pressure.

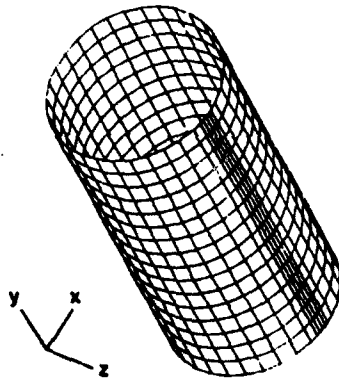


(c) Vibration frequency.



(d) Buckling load.

Figure 18.- Load induced progressive damage and effects on composite shell (T300/EP $[90_2/\pm 15/90_2/\pm 15/90_2]$) structural behavior including hygrothermal environment.



Composite Shell T300/Epoxy $[90_2/\pm 15/90_2/\pm 15/90_2/\pm 15/90_2]$
 Shell diameter = 40 in., Length = 80 in.
 612 nodes, 576 quadrilateral elements
 Initial fiber defect in 2 adjacent hoop piles
 Defect extends 5 in. along axial direction of shell

Figure 19.- Shell structure evaluated.

Pre-existing defect before loading assumed

Cases considered:

- Surface defect (plies 1 and 2 or plies 13 and 14)
- Mid-thickness defect (plies 9 and 10)

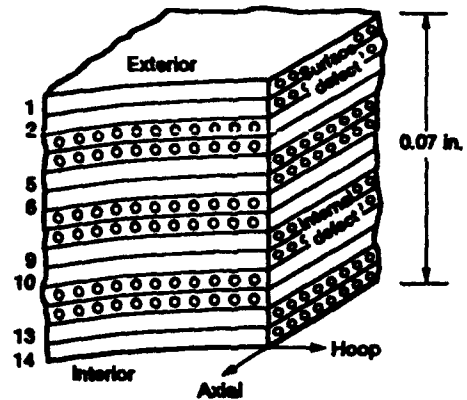


Figure 20.- Shell laminate structure schematic indicating initial defects. T300/EP $[90_2/\pm 15/90_2/\pm 15/90_2]$.

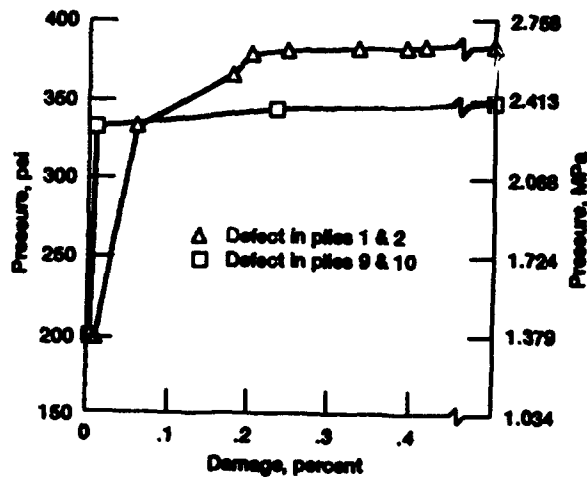


Figure 21.- Damage propagation with pressure. Composite shell T300/EP $[90_2/\pm 15/90_2/\pm 15/90_2]$.

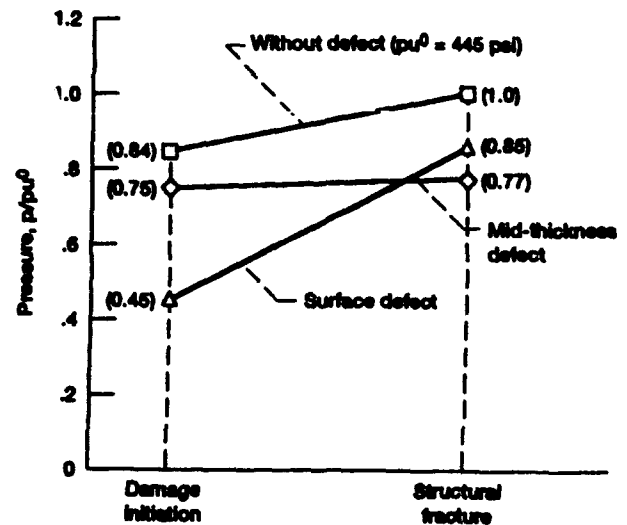


Figure 22.- Summary of results, Composite shell T300/EP $[90_2/\pm 15/90_2/\pm 15/90_2]$.

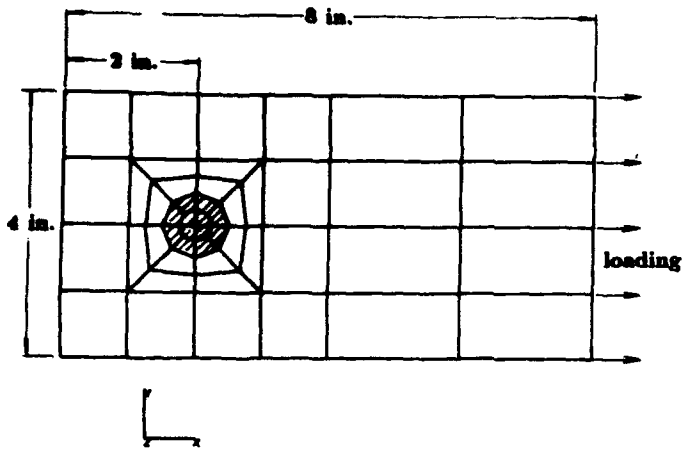


Figure 23.- Bolted laminate finite element model

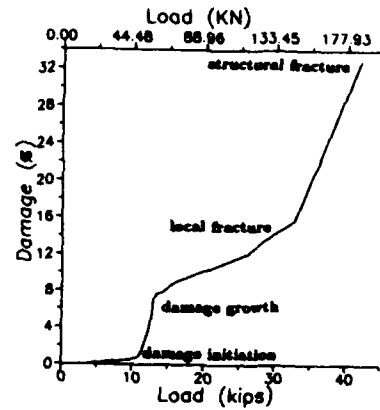


Figure 24.- Damage progression for bolted AS-4/HMHS laminate
48 Plies $[0/90/\pm 45]_{12}$

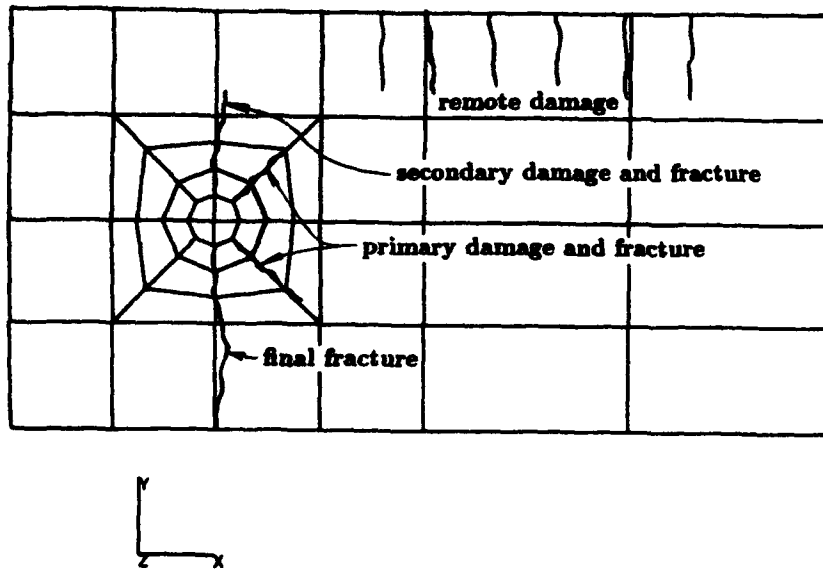


Figure 25.- Damage and fracture locations for bolted laminate
AS-4/HMHS Composite System:
48 Plies $[0/90/\pm 45]_{12}$

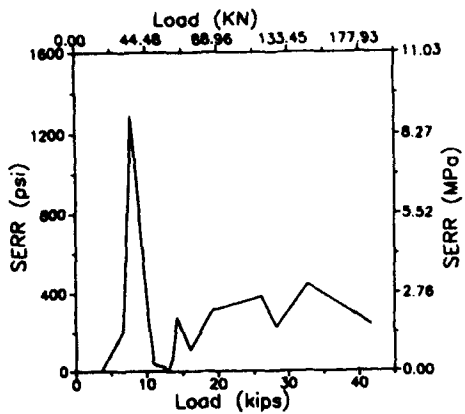


Figure 26 Strain energy release rates for bolted AS-4/HMHS laminate 48 Plies $[0/90/\pm 45]_{12}$

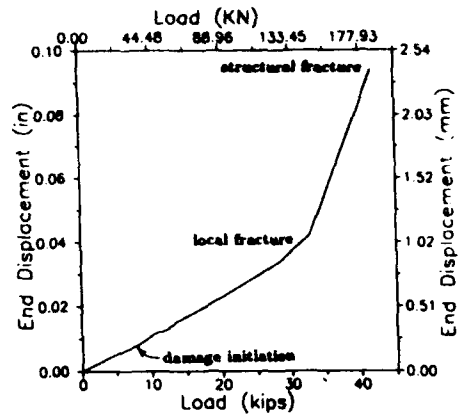
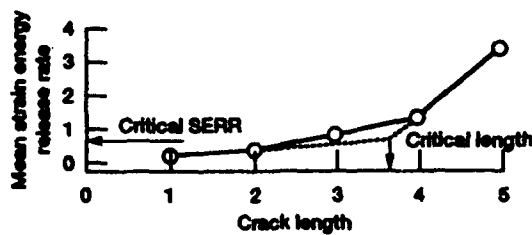
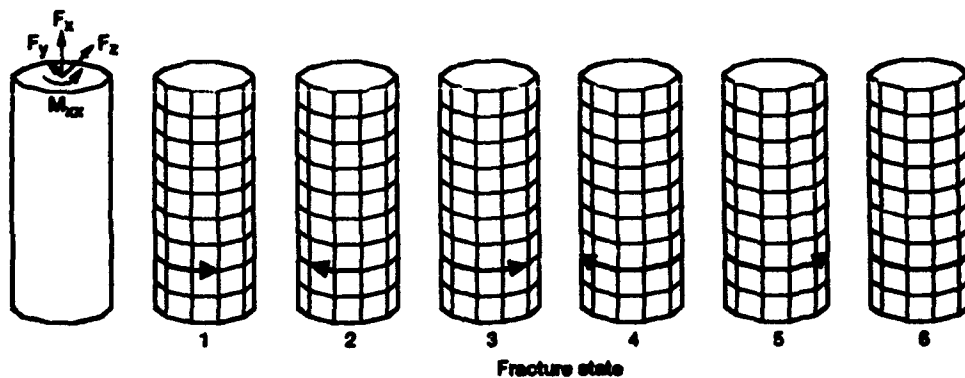


Figure 27 End displacement with loading for bolted AS-4/HMHS laminate 48 Plies $[0/90/\pm 45]_{12}$



- Computational simulation of structural fracture
- Develop global finite element structural/stress analysis model
 - Apply spectra loads
 - Identify hot spots for spectra loads
 - Introduce flaws
 - With spectra loads on structure grow flaws
 - Monitor structural performance degradation versus flaw growth
 - Identify flaw size for unacceptable performance degradation
 - Set qualification, inspection, and retirement-for-cause criteria

Figure 28 Generalization.

- Continuity in research activity
- Participants' composite knowledge:
 - Structural mechanics principles
 - Finite element analysis
 - Composite mechanics
 - Fracture mechanics concepts
 - Software development
- Participants willing to question traditional approaches adopt/invent new ones
- Management support
- Availability of computer facilities and support

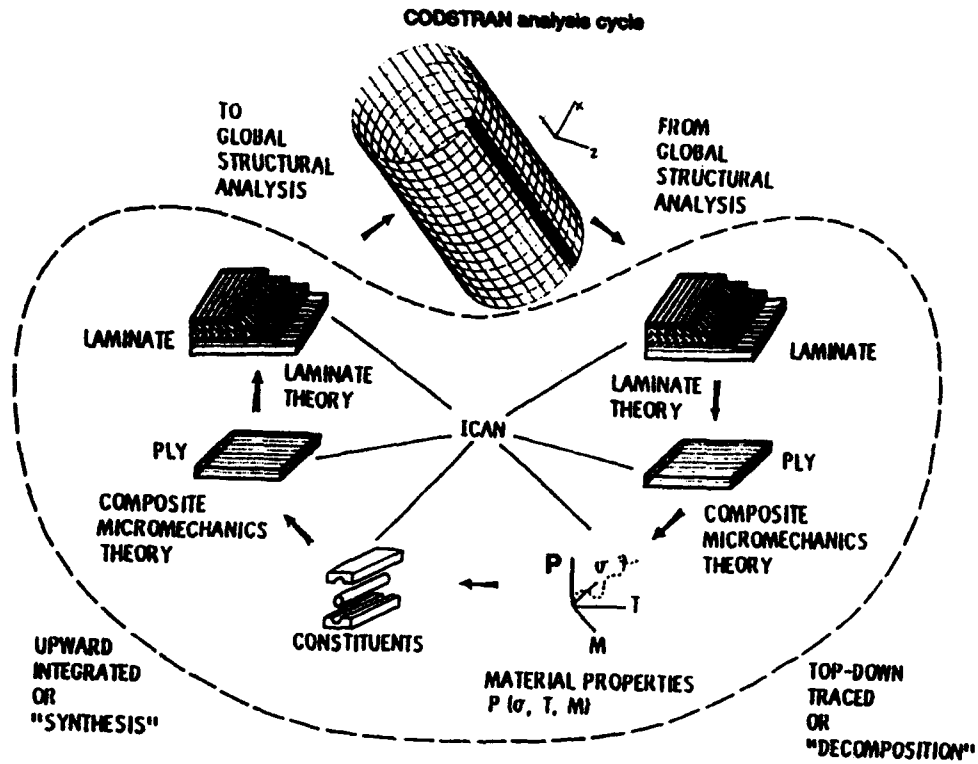


Figure 29 Lessons learned.

**The Influence of Initial Quality on the
Durability of 7050-T7451 Aluminum Plate**

by

A. F. Grandt, Jr.,* A. J. Hinkle, C. E. Zezula,* and J. H. Elsner*****

**(Prepared for Presentation at 1993 USAF Structural Integrity Program Conference,
San Antonio, Texas 30 November - 2 December, 1993)**

ABSTRACT

This paper describes research directed at quantifying improvements in component durability which may be achieved with an improved quality 7050-T7451 aluminum plate. Fatigue tests are described for thick plate materials produced to different initial qualities as reflected by the initial size and number of inhomogeneities. The results indicate that the "crack initiation" life (time to develop a crack larger than 0.005 in. = 0.127 mm) is significantly longer for notched specimens made from the higher quality plate, although fatigue crack growth properties are similar for all quality levels. It is suggested that the improved material would be especially useful for long life structures which need to avoid multiple-site cracking which degrades the load crack residual strength of primary structure. Since the initial quality improvements significantly impede crack initiation, widespread fatigue cracking would be delayed in structures made from the improved quality material, resulting in a longer service life.

*Professor and graduate student, respectively, School of Aeronautics and Astronautics, Purdue University, W. Lafayette, IN 47907-1282.

**Technical Specialist, Product Design & Mechanics Division, Alcoa Technical Center, Alcoa Center, PA 15069-0001.

***Graduate Student, School of Materials Engineering, Purdue University, W. Lafayette, IN 47907-1289.

EXPERIMENTAL PROGRAM

Alcoa has developed process control procedures to reduce the size and frequency of inhomogeneities present in 7050 thick aluminum plate [1]. This shift to smaller and less frequent inhomogeneities, such as the microporosity quantified in Table 1 [2], causes a significant increase in the total fatigue life of both smooth and notched specimens [3-4] while keeping the good mechanical properties of standard 7050 thick product (Table 2). This paper examines the initiation and growth of small fatigue cracks emanating from these inhomogeneities, and discusses how the improved crack initiation behavior (time to develop a 0.005 in. = 0.127 mm crack) is valuable for structures designed to damage tolerant criteria.

Samples of 7050-T7451 aluminum plate which had been processed to yield three different initial distributions of inhomogeneities were examined. Two of the material pedigrees represent "old" and "new" versions of six-inch (15 cm) thick plate, where the "old" pedigree is representative of pre-1984 material, and the "new" pedigree is today's standard material. The pedigrees differ primarily in the degree of microporosity which is present following rolling of the plate. The third material pedigree consists of three-inch (8 cm) thick plate, which has less severe inhomogeneities due to additional mechanical work required to reduce the thickness to 3 inches (8 cm). The initiation and growth of small fatigue cracks were measured in notched specimens at three different constant amplitude ($R = 0.1$) stress levels. Figure 1 shows the specimen geometry employed for the current tests, while Table 3 summarizes the test matrix. The stresses given in Table 3 are the maximum net area stresses in the notched specimen per cycle.

A replicating tape technique [5-6] was used to determine the cyclic life required to develop fatigue crack sizes of 0.001 in. (25 μm), 0.003 in. (76 μm), and 0.005 in. (127 μm). The notch bore locations of various crack initiation sites were recorded on the replicating tapes along with the growth and coalescence of the small fatigue cracks. The replicating tapes were subsequently examined under a microscope which allowed detection of crack sizes as small as 0.0006 inch (15 μm). Individual crack tip coordinates were measured from the replicating tapes, providing a digitized description of the initiation, growth, and coalescence of multiple cracks along the bore of the notch. Figure 2 shows a typical reconstruction of multiple cracks which developed along the bore of the notch in one of the "old" quality specimens, while Fig. 3 presents crack growth curves for the small fatigue cracks which developed in that specimen.

Table 3 summarizes the total fatigue lives for the 26 specimens examined here, along with the cycles required to develop the first crack exceeding 0.001, 0.003, or 0.005 inches (0.025, 0.076 or 0.127 mm) in a given specimen. The total number of cracks to develop in a given notch are also recorded in Table 3. The number of cracks in the notches decreases as one goes from "old" to "new" to "3-inch plate" material. The "old" material specimens averaged 4.67 cracks per notch, for example, while the "new" and "3-inch plate" material yielded 2 and 1.2 cracks per specimen notch, respectively. This crack initiation observation is consistent with the distribution of initial inhomogeneities in the three materials.

Figure 4 compares the "initiation," crack propagation, and total fatigue lives for the three material qualities. "Crack initiation life" is defined here as the number of cycles to develop the first specimen crack whose surface length exceeds 0.005 inch (0.127 mm), total fatigue life is the time to specimen failure, and the "crack propagation life" is the difference between total and initiation lives. Note that although the total specimen life varies with initial material pedigree, Fig. 4 indicates that the crack propagation life is relatively independent of material. The total notch fatigue life in this material is, thus, governed by the initiation lives for the three material pedigrees.

This point is further demonstrated by examining the fatigue crack growth properties of the three materials. The "small" fatigue crack growth behavior was examined here to determine how $da/dN - \Delta K$ for "small cracks" (crack size < 0.01 inch = 0.25 mm) varied with material quality. To avoid potential interaction effects while computing the stress intensity factors, only cracks which were well separated along the notch were used to establish the $da/dN - \Delta K$ properties. Since only the crack surface dimension was measured by the replication procedure, it was necessary to assume a crack shape here for the stress intensity factor calculations. The empirical relationship between crack shape and size given in Ref. 6 was used along with the Newman stress intensity factor solutions [7] for corner and surface cracks in a semicircular edge notch to determine the $da/dN - \Delta K$ relationship shown in Fig. 5. Note that the small crack growth rates are similar for all three materials. A linear regression has been performed on these data to give the following small crack growth equation:

$$da/dN = 7.41 \times 10^{-9} (\Delta K)^{2.738} \quad [1]$$

Here da/dN is measured in inch/cycle and ΔK is in ksi-in^{1/2}. The "large" crack equation shown in Fig. 5 was taken from Ref. 8, which also reported that initial material pedigree does not influence the "large" crack da/dN behavior in the 7050-T7451 plate. These data demonstrate the well known "small crack" phenomenon, where physically short cracks grow faster than large cracks at similar ΔK values [6,7]. Although the cause for this "small crack effect" has not been studied in the present materials, it has been attributed to crack closure phenomena in other materials.

DISCUSSION

The results of the notch fatigue tests described here indicate that process controls that limit intrinsic microstructural inhomogeneity populations do offer significant life extension potential in high strength aerospace materials through delay in the development of small cracks. This improvement in crack initiation life is achieved while also maintaining the alloy's strength and crack growth properties. Since many current aircraft design criteria are based on damage tolerant philosophies which assume pre-existent cracks, and may not readily discriminate between the three material conditions, it is important to discuss how the high quality plate offers substantial improvements in structural safety and durability.

Consider, for example, the Multiple-Site Damage (MSD) issue which is one of the symptoms of the "aging aircraft" problem [9]. Coalescence of many "small" cracks with a

large "lead crack" can lead to sudden fracture at loads which are significantly below those which would be expected from considering the lead crack alone. The MSD phenomenon was the cause of the well known Aloha Airlines incident of April 28, 1988, in which a 15 foot (4.5 m) long section of fuselage structure "peeled open" in flight, resulting in one death and near loss of the 737 aircraft [10]. This accident dramatically demonstrated that small cracks, acting together, can significantly reduce the ability of aircraft structure to resist large lead cracks.

The key to avoiding MSD, and thus to achieving the longest possible service life with a high degree of safety, is to delay development of multiple site damage. The single crack assumption, while appropriate for a new structure, does not protect against multiple fatigue cracks which develop in the later stages of an aircraft's life. As an aircraft ages, crack initiation can develop at any of the stress concentrations in the aircraft (literally millions of fastener holes in a large transport). Potential manufacturing induced cracks (i.e. "rogue" flaws) will have developed (and hopefully been detected and repaired), leaving the material microstructure to control the later stages of structural life.

The current research results indicate two properties which delay the development of MSD in the new pedigree materials: fewer small cracks develop at a notch, and the time required to develop a crack larger than 0.005 in. (0.127 mm) is longer. The development of fewer cracks is associated with reducing the frequency of the intrinsic material inhomogeneities, while the longer "initiation" time is associated with reducing the sizes of the inhomogeneities. Limited testing of 24 hole specimens on a joint Alcoa/Air Force program [4], have indicated that under spectrum loading the "new" pedigree material showed an average fatigue life increase of 70%. Clearly the "new" quality 7050-T7451 aluminum plate tested here, which maintains excellent strength and crack growth properties with improved resistance to crack initiation, offers significant advantages for long life structures.

Another issue in aging aircraft is the planning of inspection intervals. Current inspection intervals are based on a single crack analysis which may not be conservative when multiple-site damage is present. Reducing the occurrence of MSD should make the single crack analysis for inspection intervals conservative. In addition, a probabilistic based planning method could be used to set intervals based on a high degree of structural safety [11]. Improvement in microstructural features (such as type and size of inhomogeneity, frequency of inhomogeneity, and time to develop a small crack) would lengthen the time needed between inspections.

CONCLUSIONS

As shown in Fig. 4, the time to initiation of a given "small" crack size has been extended by the improved quality material. Once a crack has developed, however, all three materials yield similar fatigue crack growth rates (both in the "small" and "large" crack regimes). Although a damage tolerant structural design based on the growth of relatively large flaws (e.g. cracks > 0.05 in. = 1.27 mm) may not discriminate between the three material conditions, the material with smaller inhomogeneity distributions does offer substantial improvements in structural durability. These improvements would be especially important in "aging aircraft," where one is concerned with how multiple-site

cracking which develops late in life can degrade the lead crack residual strength of primary structure. Since initial material quality improvements can significantly impede crack initiation, widespread fatigue cracking would be delayed in structures made from the improved initial quality material, resulting in a longer service life. Additionally, with the use of probabilistic inspection planning, the structure should be safer during that time.

It is suggested here that it is possible to take advantage of changes in a material's microstructure in the design of structural components, and to improve the long term structural integrity and durability by delaying the occurrence of multiple-site damage. While the microstructural variants evaluated on this program were all derivatives of standard 7050-T7451 product fabricated on a commercial plant scale, the paradigm of improving the fatigue durability of a material by identifying and changing microstructural features is being applied to other metallic alloy systems. The authors also believe that this paradigm should be applicable to other durability limit states such as corrosion.

ACKNOWLEDGEMENTS

The authors wish to acknowledge other concurrent projects in this area: ONR Contract N00014-91-C0128 under Program Manager A. K. Vasudevan, an Alcoa/USAF Wright Laboratories cooperative program with J. Burns and J. Rudd, and various internal Alcoa programs. In addition the authors would like to thank J. R. Brockenbrough, R. J. Bucci, J. Liu, P. E. Magnusen and S. M. Miyasato for their input into this project. Portions of this research conducted by Purdue University were sponsored by The Alcoa Technical Center. The first author is also pleased to acknowledge the support of National Science Foundation Grant No. MSS-9213769 which allowed him to spend a Faculty Internship at the Alcoa Technical Center during the first half of 1993.

REFERENCES

1. Owen, C. R., Bucci, R. J., Kegarise, R. J., "Aluminum Quality Breakthrough for Aircraft Structural Reliability," *Journal of Aircraft*, Vol 26, No. 2, Feb. 1989, pp 178-184.
2. Magnusen, P. E., Hinkle, A. J., Rolf, R. L. Bucci, R. J. Lukasak, D. A., (1990), "Methodology for the Assessment of Material Quality Effects on Airframe Fatigue Durability", *Proceedings of Fatigue 90*, Honolulu, HA, July 15-20.
3. Hinkle, A. J., Magnusen, P. E., Rolf, R. L., Bucci, R. J., (1989), "Effect of microporosity on Notched Specimen Fatigue Life", *Structural Safety and Reliability, Volume 2*, pp. 1467-1474, Edited by A. H-S Ang, M. Shinozuka, G. I. Schueller, American Society of Civil Engineers, New York, NY, Proceedings of ICOSSAR '89, The 5th International Conference on Structural Safety and Reliability, San Francisco, CA 1989, Aug 7-11.
4. Magnusen, P.E., Bucci, R. J., Hinkle, A. J., Burns, J. G., Rudd, J. L., (1992), "Effect of Microporosity on Fatigue Durability of Thick 7050 Aluminum Plate", presented at 1992 USAF Structural Integrity Program Conference, Dec. 1-3, 1992, San Antonio, Texas.

5. Forsyth, E. N., "Initiation, Growth, and Coalescence of Small Fatigue Cracks at Notches," M.S. Thesis, School of Aeronautics and Astronautics, Purdue University, May 1993.
6. Swain, M. H. and Newman, J.C., Jr, "On the Use of Marker Loads and Replicas for Measuring Growth Rates for Small Cracks," *Fatigue Crack Topography*, AGARD Conference Proceedings No. 376, 1984, pp 12.1-12.17.
7. Newman, J. C., Jr., "Fracture Mechanics Parameters for Small Fatigue Cracks," *ASTM Symposium on Small Crack Test Methods*, San Antonio, Texas, November 14, 1990, pp 35-39.
8. Magnusen, P. E., Hinkle, A. J., Kaiser, W., Bucci, R. J., Rolf, R. L., (1990), "Durability Assessment Based on Initial Material Quality", *ASTM Journal of Testing and Evaluation*, Nov. 1990, p. 439-445.
9. Moukawsher, E. J., Neussl, M. A., and Grandt, A. F., Jr., "A Fatigue Analysis of Panels With Multiple Site Damage," presented at *1992 USAF Structural Integrity Program Conference*, December 1992, San Antonio, Texas.
10. Hendricks, W. R., "The Aloha Airlines Accident - A New Era for Aging Aircraft," *Structural Integrity of Aging Airplanes*, S. N. Atluri, S. G. Sampath, P. Tong, Editors, Springer-Verlag, Berlin, Heidelberg, 1991.
11. Sigurdsson, G., Cramer, E. H., Hinkle, A. J., Skjong, R., "Probabilistic Methods for Durability and Damage Tolerance Analysis," presented at the *1992 USAF Structural Integrity Program Conference*, Dec. 1-3, 1992, San Antonio, Texas.

Table 1

**Quantitative Microporosity Measurement at
Mid-Thickness Plane in Old and
New Quality 7050-T7451 Plate (145 mm = 5.7 inch thick).
Data from Ref. 2.**

Material	Area Percent Porosity	Mean Pore Area	
		inch ²	(μm^2)
Old Quality	0.030	2.22×10^{-5}	(143.0)
New Quality	0.007	1.05×10^{-5}	(67.6)

Table 2

Mechanical Properties of "old" and "new" qualities of 7050-T7451 plate (5.7 inch = 14.5 cm thickness) compared with specification AMS4050D (data from Ref. 2).

Quality pedigree	Lot number	Longitudinal						Long Transverse				Short Transverse			
		Tensile strength (ksi)	Yield strength (ksi)	Elong. (%)	L-T K_{IC} (ksi \sqrt{in})	Tensile strength (ksi)	Yield strength (ksi)	Elong. (%)	Tensile strength (ksi)	Yield strength (ksi)	Elong. (%)	Tensile strength (ksi)	Yield strength (ksi)	Elong. (%)	
Old	416961	74.7	67.1	10.0	30.7	75.1	65.3	7.0	71.5	61.7	3.5				
		74.3	66.5	10.5		74.7	65.1	6.5	70.5	60.9	3.5				
Old	416971	74.5	66.4	10.0	31.3	74.6	63.9	7.0	70.4	60.1	2.7				
		74.4	66.1	10.0		75.0	64.5	7.0	69.4	60.2	2.7				
New	417001	75.0	66.9	9.0	29.0	75.5	64.7	7.0	72.4	60.3	4.5				
		74.9	65.6	9.0		76.2	65.6	8.5	73.4	61.6	5.0				
New	417011	74.4	65.5	11.0	29.7	75.1	63.8	9.0	72.1	60.9	4.4				
		74.0	65.4	11.0		77.0	66.4	9.5	71.8	60.5	5.2				
AMS4050D		70.0	60.0	8.0	24.0	70.0	60.0	4.0	67.0	57.0	2.0				

Table 3: Specimen Data Table for Project Number TC919697TC

Specimen ID	Net Area Peak Stress (ksi)	Number of Cracks in notch**		Cycles to 1st crack (same notch)			Cycles to Specimen Failure
		front	back	2a > 0.001" .025mm	2a > 0.003" .076mm	2a > 0.005" .127mm	
"Old" Material:							
6612-b21	16	0	1	0	10,001	20,002	76,952
6611-a11	16	0	15	0	0	5,001	56,741
6612-b22	16	9	7	(0)*	2,001	8,001	104,296
6611-a12	16	10	3	0	2,501	5,001	75,066
6611-a21	18	4	2	(10,002)*	20,004	20,004	84,154
6611-a22	18	0	4	(-1)*	15,003	20,004	72,892
6713-a21	18	3	4	35,010	35,010	35,010	109,170
6612-a11	20	9	7	-1	-1	8,000	47,330
6711-a11	20	2	4	4,000	13,000	13,000	50,190
"New" Material:							
7111-b12	16	0	2	162,511	192,503	200,004	243,912
7012-a21	16	10	2	0	0	10,001	95,341
7012-a22	16	4	4	0	0	27,501	125,262
7011-b21	18	0	1	46,008	51,000	66,002	122,687
7112-a21	18	0	3	(-1)*	38,008	45,009	102,597
7111-b21	18	2	0	(-1)*	40,020	50,020	115,640
7112-a22	20	2	0	(-1)*	12,000	12,000	73,730
7111-b22	20	3	2	45,000	55,000	62,010	110,630
3" Plate Material:							
8T3	16	1	0	120,708	128,209	128,209	245,771
8B3	16	6	1	(0)*	15,001	22,502	77,798
8B2	16	0	1	(0)*	15,002	22,503	86,962
8T1	18	0	5	0	20,002	25,003	93,902
8T2	18	0	1	187,504	195,005	195,005	255,410
8B4	18	0	1	220,000	220,000	230,000	282,010
8T4	20	0	1	12,000	30,000	35,000	69,650
8T5	20	1	1	400,000	430,000	430,000	451,520
8B6	20	0	3	15,000	21,000	27,000	71,710
TOTAL:		66	75				

Note: -1 cycles indicates the period before any loading was done on the MTS machine

(*) - 2a is taken as width of inhomogeneity, not crack length

** - front and back notch refers to orientation to the testing machine

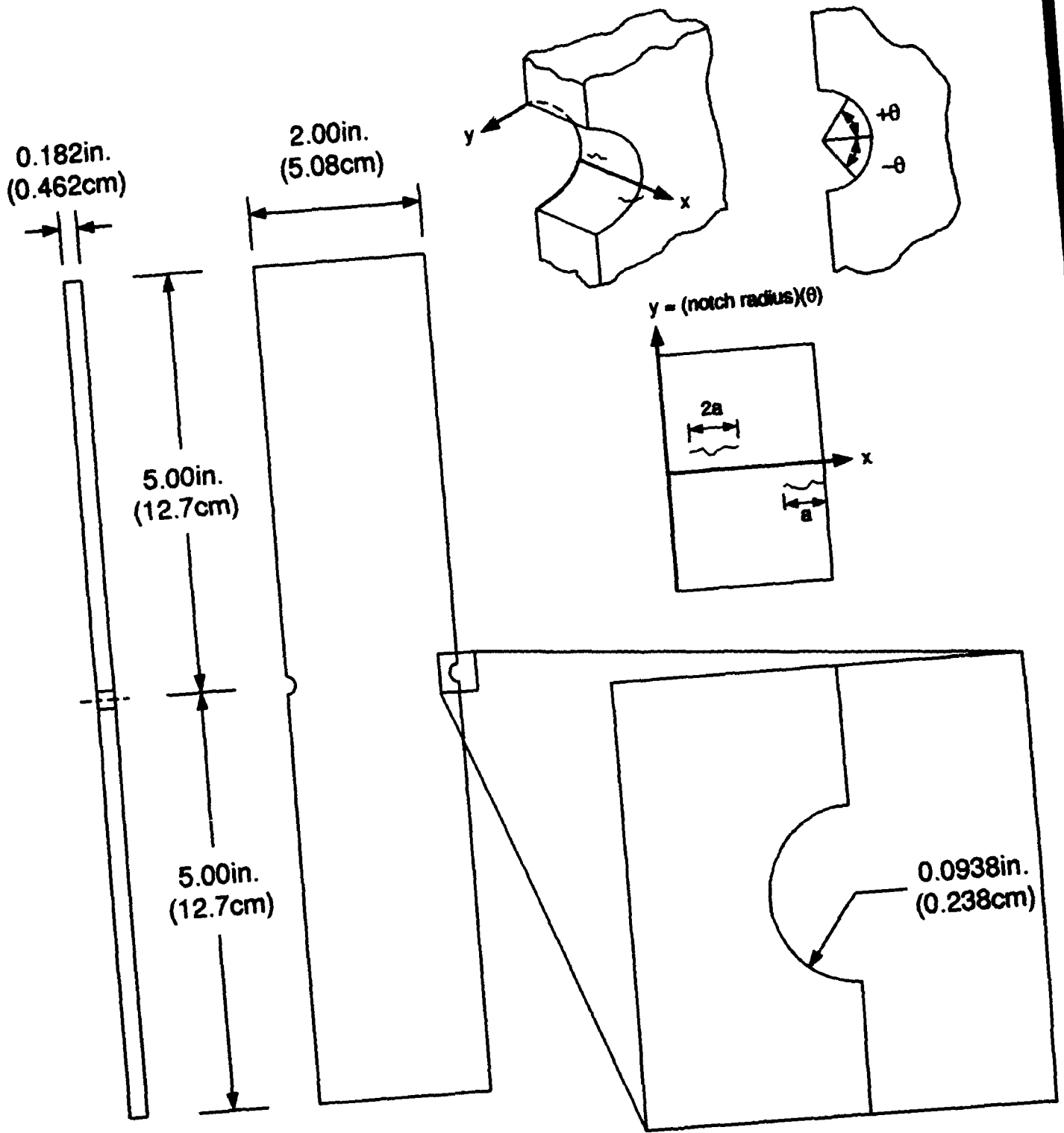
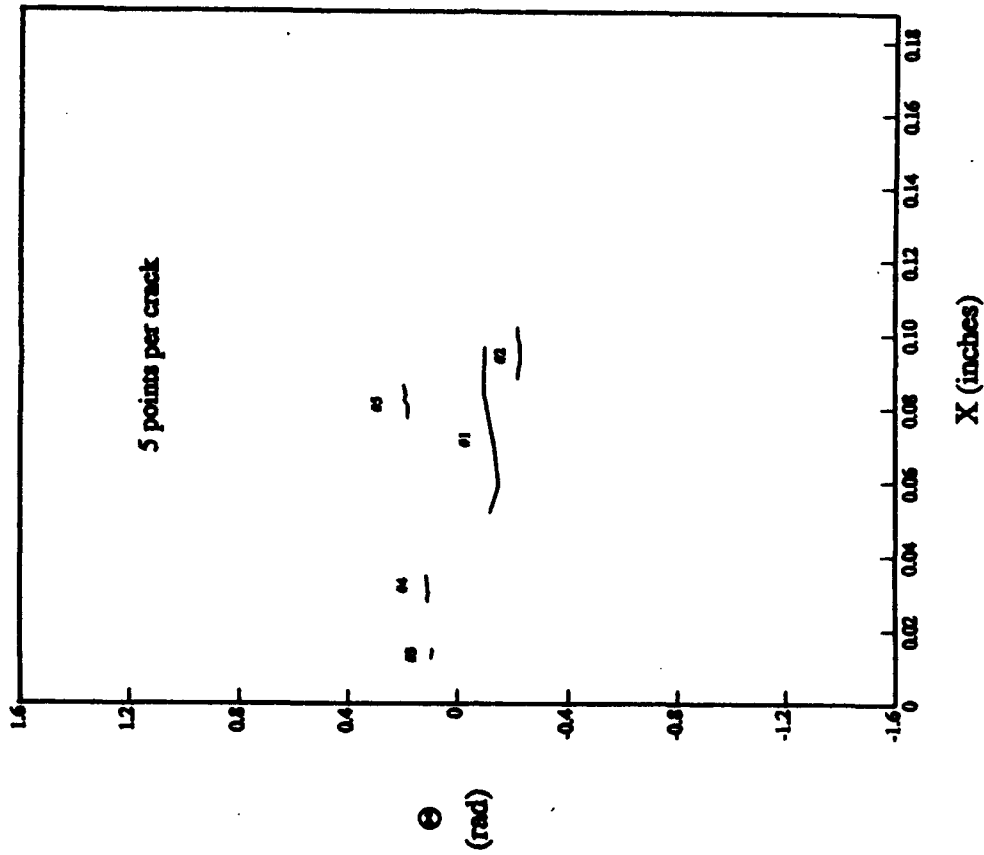


Figure 1: Al 7050-T7451 Semicircular Edge Notch Specimen Geometry and Coordinate Definition Used for Testing

b. Specimen 6612-a11, Bech Notch
22,000 cycles



a. Specimen 6612-a11, Bech Notch
24,000 cycles

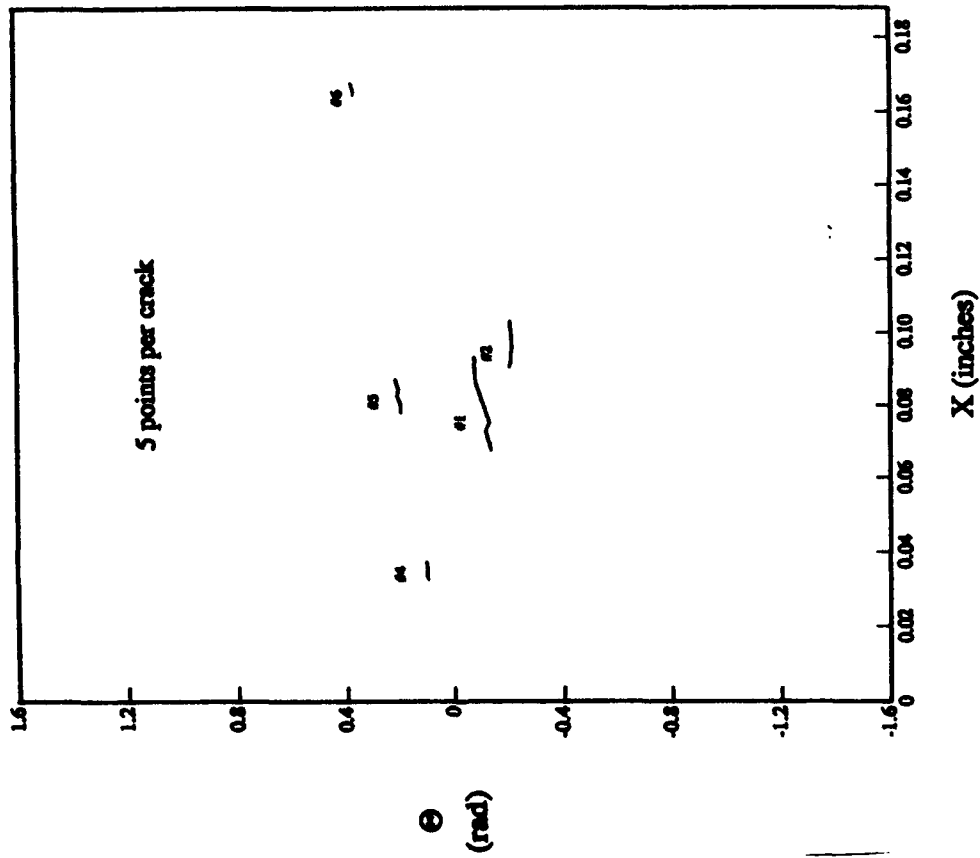
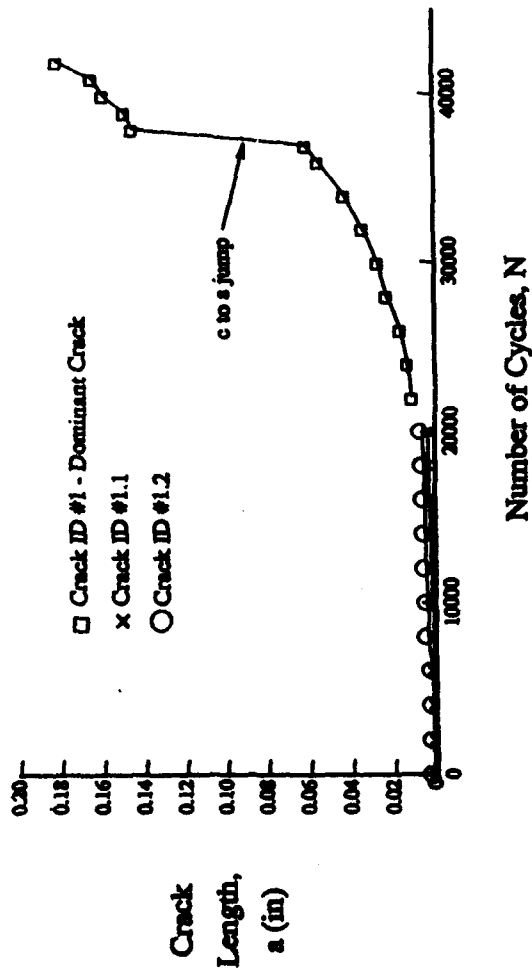


Figure 2: Digitized Reconstruction of Crack Initiation Along Hole Bore in "Old" Material Specimen 6612-a11, Cycled at 20 ksi (138 MPa) Net Area Maximum Stress with R = 0.1

a. Specimen 6612-a11, Beck Notch



b. Specimen 6612-a11, Beck Notch

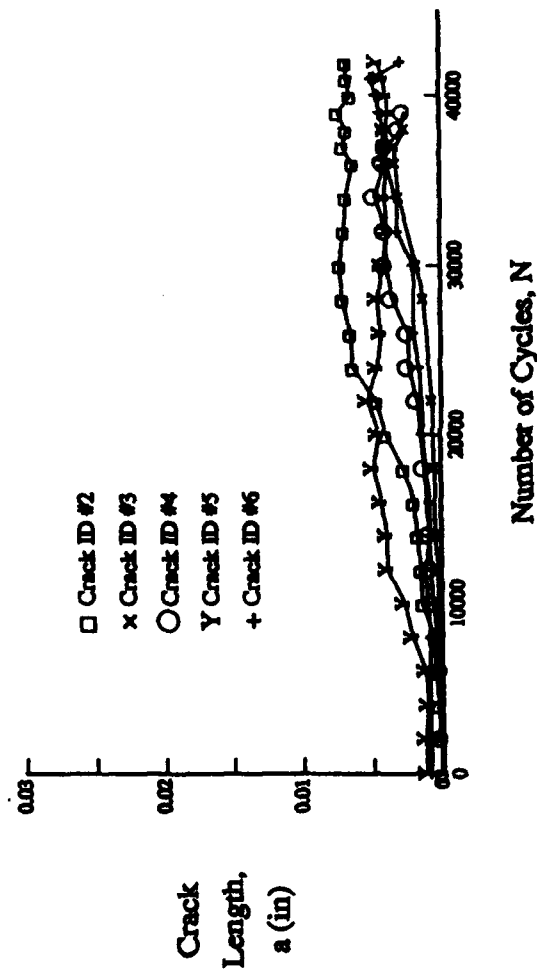
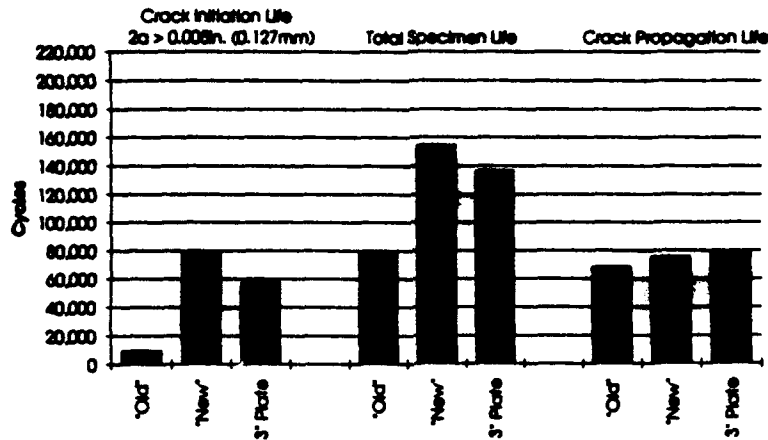
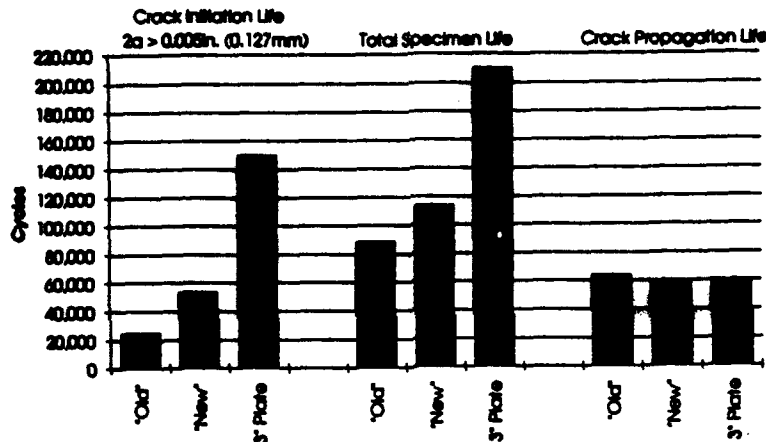


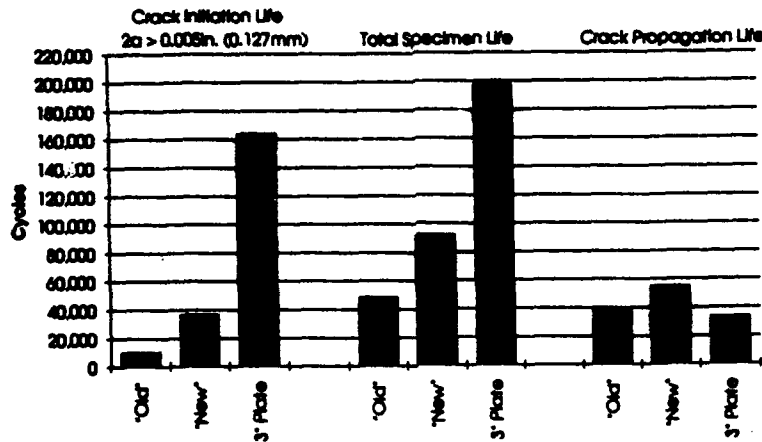
Figure 3: Fatigue Crack Growth Curves for Multiple Cracks which Developed in "Old" Material Specimen 6612-a11, Cycled at 20 ksi (138 MPa) Net Area Maximum Stress with $R = 0.1$



a. 16 ksi (110 MPa) tests



b. 18 ksi (124 MPa) tests



c. 20 ksi (138 MPa) tests

Figure 4: Summary of Initiation, Propagation, and Total Fatigue Lives for Three Material Qualities. Indicated Stresses are Maximum Net Area Stresses with R = 0.1

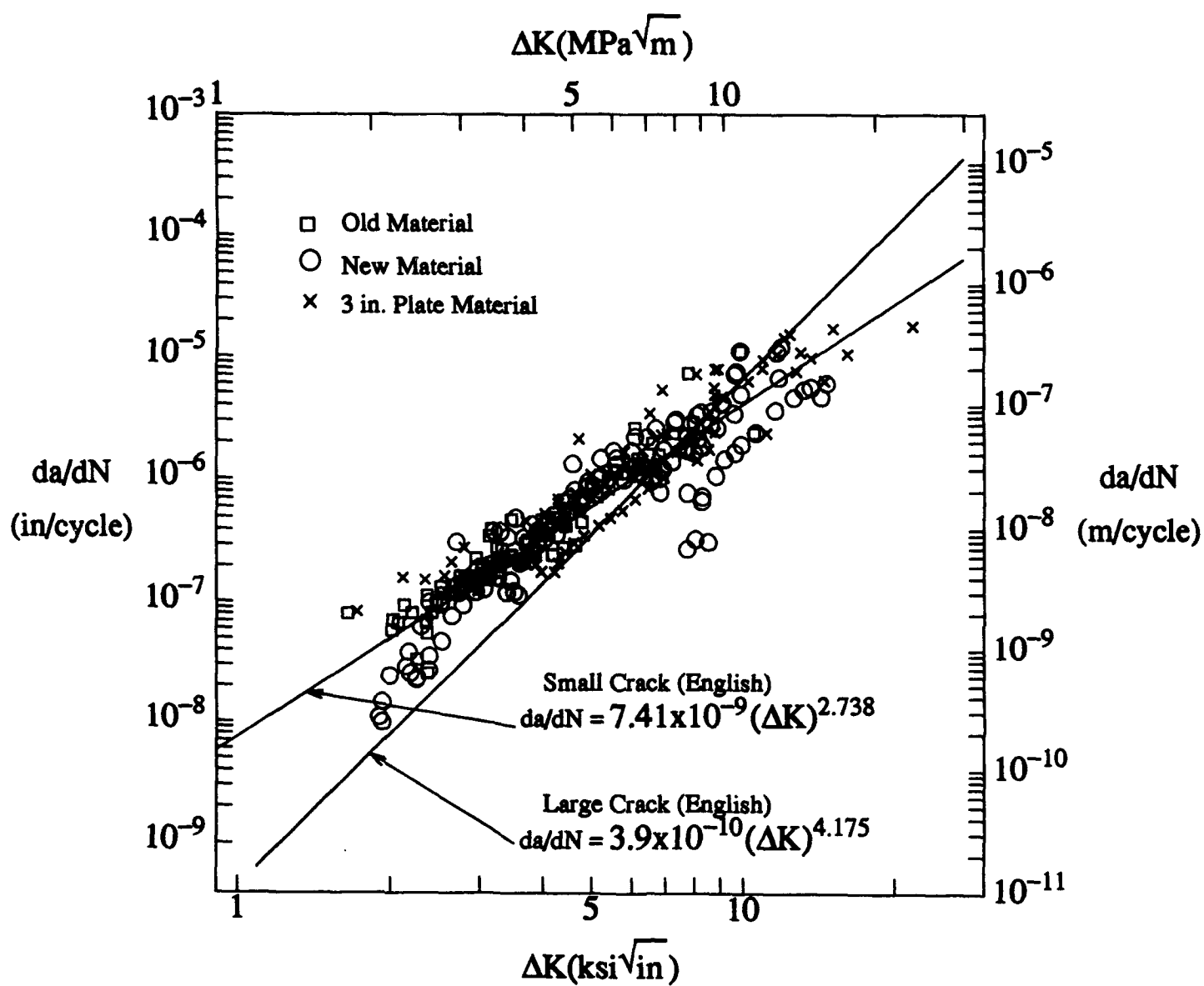


Figure 5: Small Crack Growth Rate Data for Al 7050-T7451 Plate Material.

MAINTAINING STRUCTURAL INTEGRITY BY
PREVENTION OF SURFACE INITIATING FAILURE MODES

BY

JAMES R. HARRISON
MANAGER, TECHNICAL SERVICES
METAL IMPROVEMENT COMPANY
WICHITA, KANSAS

A presentation for the
1993 U. S. A. F. Structural
Integrity Program Conference

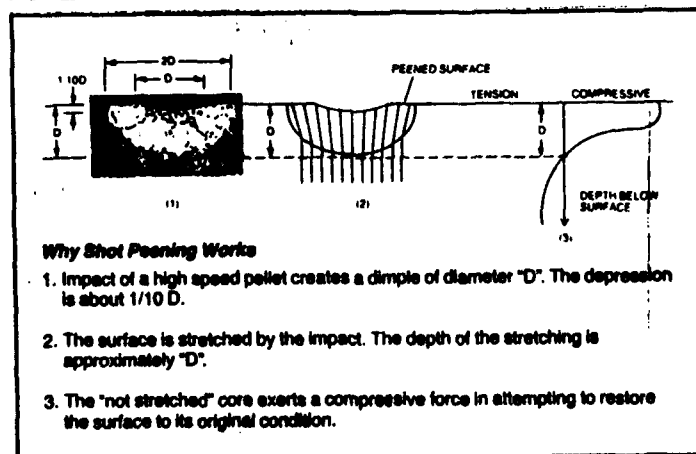
Introduction

Military and commercial aircraft are being called upon to fill ever increasing missions with today's new technological payloads. It is becoming commonplace for these load demands on the structure of the aircraft to be far greater than those originally calculated by the designer. Aircraft are flying for two and three times their original design life, with few replacements in the foreseeable future. Tensile stress related metal failures are commonplace and many of the repairs made to structures today can create new areas of tensile stress and stress raisers that later become sources for crack initiation. Corrosion of all types requires removal without compromising the structural integrity of the entire system. The subsequent replacement of the compressive stresses induced in the surface as a requirement of the original design is of paramount importance.

The Role Compressive Stress Plays In Prevention of Tensile Stress Related Failures

Shot peening as an industrial process began on valve springs for the engines of General Motors vehicles back in the 1920's. The process spread to the aerospace industry in the 1940's as the role of compressive stress in preventing fatigue and corrosion-related cracking became better understood. Shot peening is a cold working process that relies on the bombardment of metal surfaces by millions of tiny, spherical particles of steel, glass, or ceramic. The media is normally propelled by a centrifugal wheel or by air blast nozzles. This process has the ability to impact small radii, holes with diameters as small as .080 inch, as well as large surfaces, in a totally random non-directional pattern, to induce a uniform layer of compressive residual stress, which is the reason for the effectiveness of shot peening in the prevention of surface initiating failure modes. (Ref. 1)

The photomicrograph (Fig. 1) shows the hemisphere of Fig. 1, Ref. 2

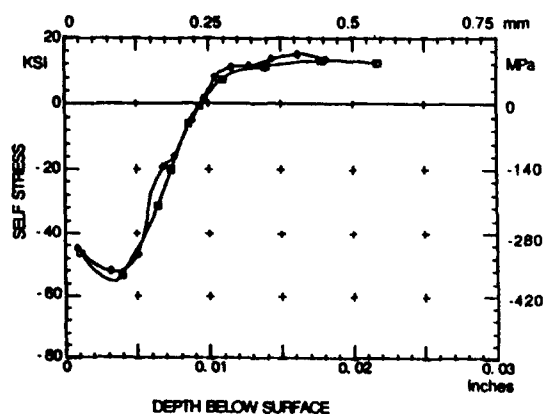


cold worked metal under a dimple caused by the impact of a single piece of shot. The surface fibers have yielded in tension. Just below the surface, the fibers try to restore the dimple to its original shape, creating a zone of compressive stress. The magnitude of this sub-surface compressive stress is at least 50% of the tensile strength of the material peened. (Ref. 2)

Figure 2 illustrates the stress profile of a specimen of 7075-T6 aluminum with an ultimate tensile strength of 80 KSI. The maximum compressive stress from peening is 55 KSI just below the surface and the total depth, at an Almen intensity of 11A, is approximately .010 inch.

Residual Stress Profiles of Two Shot Peened Materials

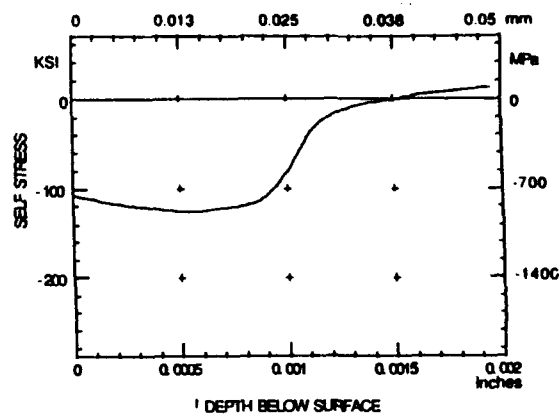
Fig. 2, Ref. 3



Material: 7075-T6 aluminum alloy
 Tensile strength: 80 ksi (550 MPa) (handbook data)
 Yield strength: 70 ksi (485 MPa) (handbook data)
 Specimen: Sheet 0.104 in (2.64 mm) thick
 Intensity: 11 A
 Shot: P 19 (0.019 in 0.5 mm nominal dia)

Reference: Walsman, J.L., Report from Technical Service Co. to Metal Improvement Co. 1982

Fig. 3, Ref. 3



Material: Titanium alloy Ti-6Al-4V

Tensile strength: 183 ksi (1275 MPa)
 Yield strength: 151 ksi (1040 MPa)

Specimen: 0.048x1.5x1.5 in (1.2x38x38 mm)
 peened on one side

Intensity: 80 psi 3/16 nozzle (4.8 N expected)
 Coverage: 5 seconds peening time

Shot: GP 25 glass (0.08 mm nominal diameter)

Reference: Grant, D.N. and Royter, D.M. "X-Ray Measurement of Residual Stress in Titanium Alloy Sheet." In J.R. Mottishaw and G.R. Mottishaw, editors, *Advances in X-Ray Analysis*, Vol. 10 (1968) pp 285-310

The offsetting tensile stress in the core of the material balances the surface layer of compressive stress so that the forces within the part remain in equilibrium. It is important to note that the magnitude of the core stress, at approximately 15 KSI, is considerably less than the compressive stress, and only very rarely contributes to subsurface crack initiation.

In Figure 3, titanium alloy Ti-6Al-4V was peened very lightly, because of the thin cross section, to an

Almen intensity of 4-6N. Results show a compressive stress that equals 74% of the ultimate tensile strength while the core tensile stresses are less than 10%. (Ref. 3)

The damage tolerance discipline has given rise to unnecessary concern about the core tensile stress caused by shot peening. Concern that a surface defect 0.050 inch deep will propagate faster because of peening is unfounded. In an article published in the Journal of Mechanical Working Technology, S. A. Meguid and E. B. Chee found that "Once a crack has propagated beyond the compressed layer into the bulk material, its rate of propagation approaches that of an unpeened specimen." (Ref. 4) Damage extending through the compressive stress layer, caused by a defect, will relieve the compressive stress, and because the core tensile stress is present only as the result of the compressive stress, once the compression is removed, the core tensile stress disappears also. A recent study by an aircraft company showed no difference in the rate of crack propagation between smooth and shot peened specimens tested with an EDM-induced defect deliberately deeper than the compressive layer.

Why New and Used Aircraft Components Are Shot Peened

The shot peening of rotating jet engine components when new and at every overhaul is standard practice and is used for several reasons. The primary problems in a jet engine are bending fatigue and fretting fatigue, but may include, among others, vibration, corrosion, torsional and thermal fatigue. Just about every part is peened to prevent surface initiating failures. During overhaul these same parts are required to be re-shot peened in exactly the same manner, to the same specification, as when new, to restore the compressive stress to its original magnitude. Parts such as blades, disks, main shafts and other rotating hardware, as well as engine casings and shrouds, are peened on overhaul to the original manufacturer's stringent specifications.

Many structural components of today's aircraft were also shot peened in a highly controlled process to achieve maximum and predictable fatigue strength. Unfortunately, not all operators have taken advantage of the benefits of this economical process. It has been shown that "tests conducted on initially un-peened and subsequently peened specimens at various stages of their estimated fatigue life, generally revealed a substantial life improvement." (Ref. 4)

Aircraft landing gear are shot peened when new and again shot peened at overhaul. These parts often have areas that are machined, or repaired at overhaul, necessitating the restoration of the compressive stresses. More importantly, tests have shown that "previously peened,

Fig. 4, Ref. 3

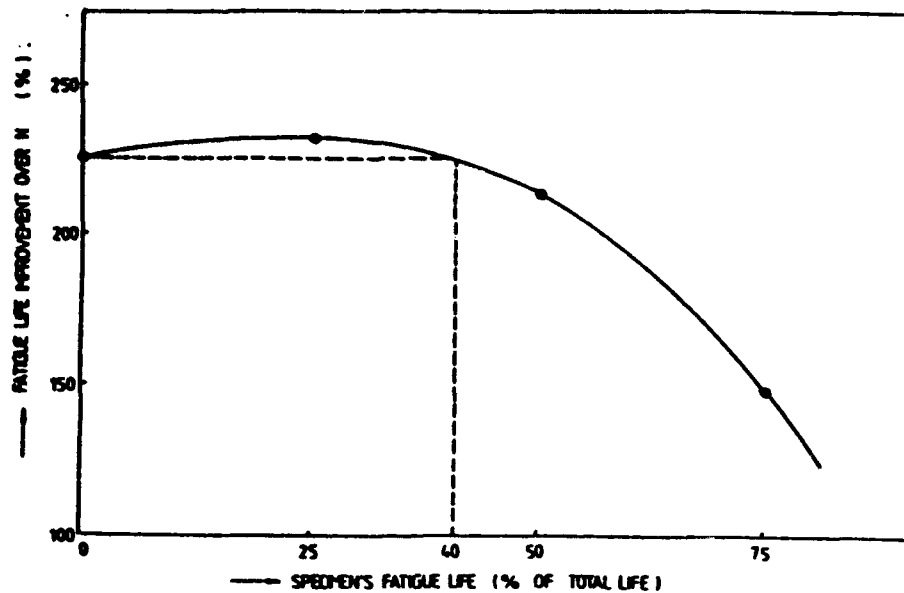


Fig. 6. Fatigue life improvement (over N) due to the shot-peening of partially fatigued un-peened specimens.

Note: N = Total fatigue life of an un-peened specimen.

partially fatigued and subsequently re-peened specimens," tested in rotating bending fatigue machines, "indicated complete recovery, even when the parts had been partially fatigued by as much as 75% of their estimated fatigue life." (Ref. 4)

Shot peening applications to prevent surface initiating failure modes go beyond fatigue cracking. In the corrosion list, there is stress corrosion cracking, corrosion fatigue and exfoliation corrosion. Replacement aircraft skins can be formed to fit without fixtures and shimming by the use of peen forming on the aircraft.

Stress corrosion cracking by definition can be eliminated by the reversal of the tensile stress needed for this phenomenon. (Ref. 5) Many materials, especially those used in older aircraft, are susceptible to SCC. Shot peening replaces residual tensile stress and leaves the surface in compression which is retained even under an applied load of over 50% of the ultimate strength.

Surface corrosion removal, even by gentle grinding or sanding, may induce tensile stresses which coupled with the reduction in section thickness will produce a stress raiser. Again shot peening is the best process to overcome this weakening of the part. Flapper peening quite often is used in an attempt to induce compressive stresses into a repair area on an aircraft. Although simple in theory, in practice

this process cannot get into critical radii and is very directional making a 100% covered, randomly uniform layer of compressive stress very difficult to achieve. Shot peening has not been used as often because of fear that steel particles will somehow get past the masking and enter the structure causing later corrosion problems. Advances in masking techniques and, more importantly, the approved use of totally inert ceramic media has removed these fears.

Exfoliation corrosion usually initiates adjacent to fastener heads when the sacrificial coating, such as cad plating, begins to break down and galvanic corrosion starts between the aluminum skin and the fastener. White corrosion products form so that the skin starts blistering. A Metal Improvement Company process first uses plastic media blasting (PMB) to remove the paint and coating, exposing the corrosion. A light shot peening stretches the surface and causes the laminations to blister. Controlled light sanding to remove the blistered surface is followed by a re-peening to restore fatigue strength in the dressed area that would be thinner and therefore weaker than before. We call this process "search peening." (Ref. 1)

Quality Control on Site

Metal Improvement Company has applied for a patent on a machine, known as the Wing Walker, to automate this process and ensure quality and repeatability that is so essential and to make this search peening an economical process. By using four suction cups on the frame and four more on the peening enclosure, this machine can travel along the rivet lines automatically, while containing and recovering the peening media.

The shot peening of parts on the airplane requires special equipment that can be delivered on site with a trained crew in short notice. All operations that can be automated will be done so. Most specifications allow for some manual peening because of the difficulty of automating some of the operations when it comes to peening on the aircraft. Paragraph C of MIL-S-13165 states that "manually controlled peening may be used for surface of holes, edges, cutouts, etc." (Ref. 6) It is critical that exact planning, detailing every variable in the repair, be laid out and that technicians are certified. The media must be essentially rounded. Broken, sharp-cornered shapes are totally unacceptable because they can cause stress raisers. (Ref. 6)

Intensity is measured by the Almen strip in the shop and at the job site. Almen intensity is a measure of kinetic energy being transferred to the parts, which ties directly to the depth of compression. A saturation curve is built to calibrate the energy of the shot stream. The most

critical consideration of shot peening is coverage, and because on-site peening is usually not just for a safety margin, but necessary to ensure the fatigue life of a component, a fluorescent tracer liquid per MIL-S-13165C, is used to measure uniformity and coverage on a shot peened part. (Ref. 6 & 7)

Aging Aircraft Applications

Numerous on site repairs requiring shot peening have been performed and a partial listing follows:

- DC8, Removing corrosion on steel fastener heads.
- DC9, Shot peening of landing gear attach fittings to prevent stress corrosion cracking.
- Concorde, Shot peening of rudder cradles and aileron attachment fittings.
- B-737, Shot peening the tail fin attachment lugs and the startruss assembly lugs. Search peening on a significant number of older aircraft for exfoliation corrosion, followed by shot peening.
- B-747, Shot peening after corrosion removal in the wing center sections. Shot peening of landing gear during overhaul before chrome plating.
"Search peening," then saturation peening of upper and lower wing planks along fastener lines.
- B-757, "Search peening" of the wing access ports, where the cover plates fit, followed by shot peening.
- L-1011, "Search peening" of center torque box, wing box sections, and along wingskin rivet lines.

On Site Peen Forming

- B-737, Boeing Service Bulletin 737-57A1081 covers the repair of the left and right front wing chords. To access the cords, it is necessary to remove a wing skin panel that is approximately 10 inches wide by 120 inches long. The replacement panel is essentially flat, so it is shot peen formed to bring spring-up values to less than 0.10 inch so that no shimming is required. (Ref. 1)

Conclusion

The cost of shot peening an aircraft part when new is generally less than 5% of the cost of the part, or comparable to the cost of heat treating. The charges to shot peen, "search peen," or peen form on site, although much higher than in house, are still a much less expensive alternative than replacing a part of the complete assembly. Metal Improvement Company has trained crews located in more than 20 FAA approved locations in the U.S., Canada, and Europe capable of providing these services world-wide.



MIC field crew prepares topeen form B-737 replacement wing panel.

BIBLIOGRAPHY

1. Eckersley, J. "The Aging Aircraft Fleet," Impact, Fall, 1991.
2. Shot Peening Applications. Seventh Edition, Metal Improvement Company.
3. Fuchs, H. O. Shot Peening Stress Profiles available from Metal Improvement Company.
4. Meguid, S. A. and E. B. Chee, "The Effect of Peening and Re-peening upon Partially Fatigued Components," Journal of Mechanical Working Technology, 8(1983), 129-146.
5. MIL-S-13165C "Shot Peening of Metal Parts" U. S. Military Specification, June, 1989.
6. Milo, J. H. "Shot Peening Prevents Stress Corrosion Cracking In Aircraft Equipment," Materials Protection (NACE) September, 1968.
7. O'Hara, P. "DYESCAN Tracers as a Quality Control Tool for Coverage Determination in Controlled Shot Peening," SAE Technical Paper Series 850708, February, 1985.

EFFECT OF CORROSION ON FATIGUE CRACK PROPAGATION IN ALUMINUM ALLOY 2024-T3

**G.H. Koch and T.H. Bieri
Cortest Columbus Technologies**

and

**J. G. Burns
WL/FIBE**

Abstract

Corrosion of aging aircraft components has become a major factor in determining their structural integrity and life expectancy. For example it is anticipated that the KC-135 fleet will not reach its fatigue life limit, but that rather corrosion will be life limiting. Corrosion can have a detrimental effect on the integrity of aircraft structures by promoting fatigue crack initiation and growth, and by decreasing the residual strength of a critical component. Although the interaction between fatigue damage and corrosion from a quantitative point of view is not well understood, fatigue propagation data from high strength aluminum alloys strongly suggests that fatigue cracks propagate differently in new structures than in aged or corroded structures. This paper describes the results of ongoing work to determine the effect of corrosion on fatigue cracking in aircraft aluminum alloys.

Introduction

Crack growth in high strength aluminum alloys has been studied extensively in the past, and its understanding has contributed to the development of damage tolerance concepts for aircraft structures. Fracture control in aircraft structures has become an integral part of aircraft safety, from the design to the operational phase. Although initially the most attention was given to fatigue cracking behavior in laboratory or shop environments, design engineers have come to appreciate the detrimental effects of actual operating environments which manifests itself as corrosion. Corrosion typically initiates in localized areas in the form of pitting, crevice corrosion, and exfoliation corrosion. It has been established that the local environments inside pits, crevices, and exfoliated areas are acidic¹, and are therefore much more aggressive than the bulk environment. These areas often form initiation sites for environmentally assisted cracking such as stress-corrosion cracking, hydrogen induced cracking, and corrosion fatigue.

Localized corrosion may affect fatigue cracking in different ways. First, areas of localized corrosion can function as stress concentrators and promote the initiation of cracks. Once initiated, the small cracks may coalesce and form longer fatigue cracks. Secondly, when corrosion progresses, material thinning takes place which may also accelerate fatigue crack propagation. Moreover, as a result of the reduced cross section, the residual strength of a particular component may be reduced. Thirdly, because of the presence of an acidic localized environment created by pitting, crevice corrosion, and exfoliation corrosion, hydrogen may be formed and diffuse into the alloy. When hydrogen diffuses into the alloy, it could alter the material properties and have a detrimental effect on the fracture mode. Hydrogen has been shown by several authors²⁻⁵ to cause embrittlement of high strength aluminum alloys and contribute to stress corrosion and corrosion fatigue cracking. Thus, it is reasonable to speculate that if hydrogen is introduced into the alloy lattice through the corrosion process, fatigue cracking may be accelerated. Furthermore, since hydrogen is very mobile, it can, once introduced into the lattice, diffuse towards highly stressed regions such as tips of propagating fatigue cracks, accelerating crack propagation. The rate of hydrogen diffusion towards the crack tip is likely to be a function of crack tip condition, load amplitude, and frequency.

The interaction between corrosion and fatigue damage is not well understood from a quantitative point of view, because corrosion damage does not lend itself to simple quantitative analysis. The results of fatigue crack propagation studies in corroded aluminum alloys reported by previous authors⁶, strongly suggest that fatigue cracks propagate differently in new structures than in aged or corroded structures. In order to assess the life of fatigue cracks in corroded structures and to determine the structural integrity of such structures, it is necessary to understand the mechanism that controls the propagation of these cracks. Only then can a reliable damage tolerance program be developed for corroded airframe components.

Experimental Procedure

The material used to study the effect of precorrosion on fatigue crack propagation is approximately 10-15 years old aluminum alloy 2024-T3. In order to be able to monitor a long fatigue crack over a broad range of ΔK values, it was decided to use a modified compact tension (CT) specimen such as shown schematically in Figure 1. The relationship between stress intensity (K) and the crack length (a) was produced with an experimental compliance calibration:

$$K = P \sqrt{\frac{E(-2 \times 10^{-6} + 8.462 \times 10^{-6} \cdot a - 3.72 \times 10^{-6} \cdot a^2)}{2B}}$$

where K is the stress intensity, P is the load, B is the sheet thickness and E is the elastic modulus.

The modified CT specimen allows for crack growth over a range of approximately 4 inches, while different areas of corrosion can be created in the path of the propagating crack. Because of the size of the specimen, antibuckling plates are attached to both sides of the specimen.

Prior to starting the crack growth studies, corrosion studies were conducted to characterize and reproduce various degrees of corrosion which are typical in aircraft structures. It was decided to apply the copper acidified salt spray (CASS ASTM 386-B85)⁷ and exfoliation (EXCO ASTM G34)⁸ tests. The compositions of the CASS environment which is used to induce pitting corrosion, and the EXCO environment which is used to induce exfoliation corrosion, are given in Tables 1 and 2. Following the corrosion studies, the modified CT specimens were machined and precorroded in the CASS and EXCO environment for 6 days. The precorroded specimens were then fatigued in laboratory air at a frequency of 1 Hz and R-ratio of 0.1. The crack propagation was monitored using the crack opening displacement method.

Results and Discussion

Corrosion Studies

After exposure to the CASS saltspray environment, the aluminum 2024-T3 test coupons, 1 inch x 1 inch exposed area, were metallographically cross sectioned and polished. The pit depth and width of each pit along the cross section was measured and recorded. After the measurements, the pit depths, widths and areas (depth x width) were ordered and statistically analyzed. Pitting initiation is a statistical process, and the number of pits formed on the surface occurs in a random fashion and can be described by a Poisson function. Thus, the above mentioned corrosion parameters can be described by lognormal distributions in which the logarithms of the respective parameters are distributed according to a Gaussian normal distribution. The probability distribution function of the lognormal distribution is given by the following equation:

$$P(x) = \frac{1}{zx(2\pi)^{1/2}} \exp\left\{-\frac{(\ln x - \lambda)^2}{2z^2}\right\}$$

where x is the corrosion parameter and z and λ are parameters with the following definitions:

$$z^2 = \ln \left(1 + \frac{\sigma^2}{\mu^2} \right)$$

$$\lambda = \ln \mu - \frac{z^2}{2}$$

where μ = the sample mean and σ = the sample standard deviation.

The cumulative distribution function is the probability that a pit cross sectional area lies between two values x_1 and x_2 , and can be obtained by integrating the probability distribution function between those values. After the pit areas are measured, the logarithms of their values are taken and their mean and standard deviation are calculated. The probability distribution of pit cross sectional areas at exposure times of 1, 4, 7, and 21 days is shown in Figure 2.

In addition to the CASS exposure tests, the 2024-T3 aluminum alloy was exposed to an EXCO (ASTM-G34) solution for 1, 2, 4, and 6 days, respectively. This standard test was conducted to determine the susceptibility and extend of exfoliation corrosion. The degree of corrosion in this test is more severe than that in the CASS. To determine the extend of exfoliation corrosion the five deepest penetrations after 1, 2, 4 and 6 days were measured and their averages plotted as a function of time, see Figure 3.

Fatigue Crack Propagation Studies

Following the corrosion characterization studies, specimens were machined and precorroded in the CASS and EXCO environments for 6 days. The results of the constant amplitude fatigue tests on the precorroded modified CT specimens are presented as da/dN vs. a and as da/dN vs. ΔK . Figures 4 and 5 show typical fatigue crack propagation results for specimens exposed to the CASS and EXCO solutions for 6 days. The figures show fatigue crack propagation through 2 distinct areas (1.5 inches long) of corrosion at different crack lengths.

Comparison of the data in Figure 6, indicated that a 6 day exposure to the CASS environment which resulted in relatively shallow pitting attack, had no effect on fatigue crack propagation in the 2024-T3 alloy. However, exfoliation corrosion which resulted from a 6 day exposure to the EXCO solution was found to have a significant effect on the fatigue crack propagation of the aluminum alloy. The results show that crack propagation becomes irregular once it reaches an exfoliated region, which may be the result of various competing processes such as environmental, mechanical and crack blocking due to corrosion products at the crack tip.

A strong indication of hydrogen induced cracking is given Figure 6, which shows that the crack in the exfoliated specimens propagates at a much higher rate in the region ahead of and between the corroded regions than in the same regions of the non-corroded base line specimen. This observation suggests that a diffusible species, such as hydrogen generated at the corrosion sites, may have changed the physical properties of the aluminum alloy away from the corroded area. The concept of hydrogen induced cracking is further supported by fractography with scanning electron microscopy (SEM). Fractographs such as shown in Figure 7 show the presence of mud cracking features which are characteristic for stress corrosion cracking and hydrogen cracking where hydrogen has been reported to play a dominant role in the cracking process.

Summary and Conclusions

The results of the fatigue crack propagation tests on precorroded modified CT specimens strongly suggest that hydrogen generated during the corrosion process plays a predominant role in the acceleration of the rate of cracking. Additional experiments are being conducted to more quantitatively define the role of hydrogen in the cracking process. If indeed the suggestion that hydrogen plays a predominant role in fatigue cracking as indicated in this paper, this will have serious implications, and will have significant effect on damage tolerance considerations. In addition to affecting fatigue crack propagation, hydrogen generated by corrosion may also affect fatigue crack initiation and residual strength of aircraft components.

Acknowledgement

This work is jointly sponsored by the FAA-Technical Center and the Air Force (WL/FIBE) under Contract F33615-C-3201.

References

1. A. Turnbull, "Chemistry Within Localized Corrosion Cavities" Advanced Localized Corrosion NACE-9 Ed. H. Isaacs, U. Bertocci, J. Kruger and S. Smialowski, Orlando, Florida, 1987, p. 359.
2. R.J. Jacko and D.J. Duquette. "Hydrogen Embrittlement of a Cyclically Deformed High Strength Aluminum Alloy" Metallurgical Transactions A, Volume 8A, November, 1977, p. 1821.
3. E.F. Smith III and D.J. Duquette, "The Corrosion Fatigue Behavior of a High Purity Al-Zn-Mg-Cu Alloy" Technical Report to the Office of Naval Research Project No. N00014-75-C-0466, November, 1979, (NTIS-AD-A077-461).
4. W. Gruhl, Z. Metallkunde, Volume 75, No. 11, 1984, p. 819.
5. T.D. Burleigh, "The Postulated Mechanisms for Stress-corrosion Cracking of Aluminum Alloys - A Review of the Literature 1980-1989" Corrosion Volume 47, no. 2, February 1991, p. 89.
6. J.P. Chubb, T.A. Morad, B.S. Hockenhill and J.W. Bristow, "The Effect of Exfoliation Corrosion on the Fatigue Behavior of Structural Aluminum Alloys" Structural Integrity of Aging Airplanes Ed. S.N. Atluri, S.G. Sampath and P. Tong, Atlanta, Georgia, 1990, p. 87.
7. "Copper Accelerated Acetic Acid Salt Spray (Fog) Testing (CASS Test)", ASTM-368-B-85. American Society for Testing and Materials, 1985.
8. "Exfoliation Corrosion Susceptibility in 2XXX and 7XXX Series Aluminum Alloys (EXCO Tests), ASTM G34-90, American Society for Testing and Materials, 1992.

Table 1. CASS Solution Composition (ASTM-368) for Corrosion Pitting Exposure Specimens

Chemical Compound	Molarity	Weights & Volumes
NaCl	0.90	5 gm/95 gm distilled H ₂ O (5.0 weight percent)
CuCl ₂	0.0014	0.197 gm/l of solution
Acetic acid	0.025	21.45 cc/l of solution*

* pH = 3.0 to 3.1

Table 2. EXCO Solution Composition (ASTM G-34) for Exposed Fatigue Specimens

Chemical Compound	Molarity	Weights and Volumes per liter distilled H ₂ O
NaCl	4.0	234 gm
KNO ₃	0.5	50 gm
HNO ₃	0.1	6.3 ml*

* pH = 0.4 (Initial), 4.0 (After 5 Days)

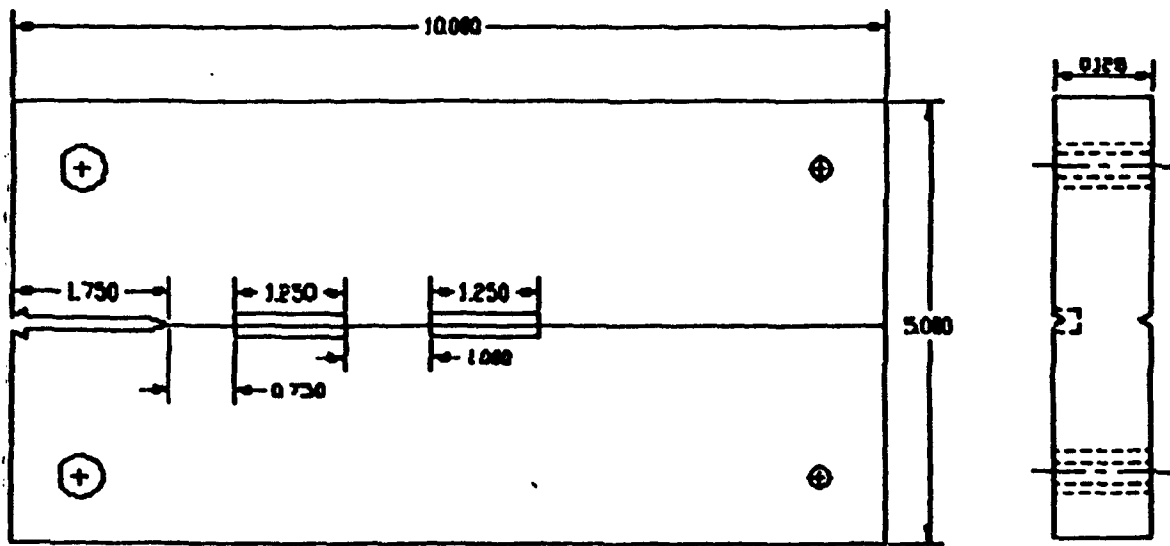


Figure 1. Schematic Drawing of Modified Compact Tension Specimen

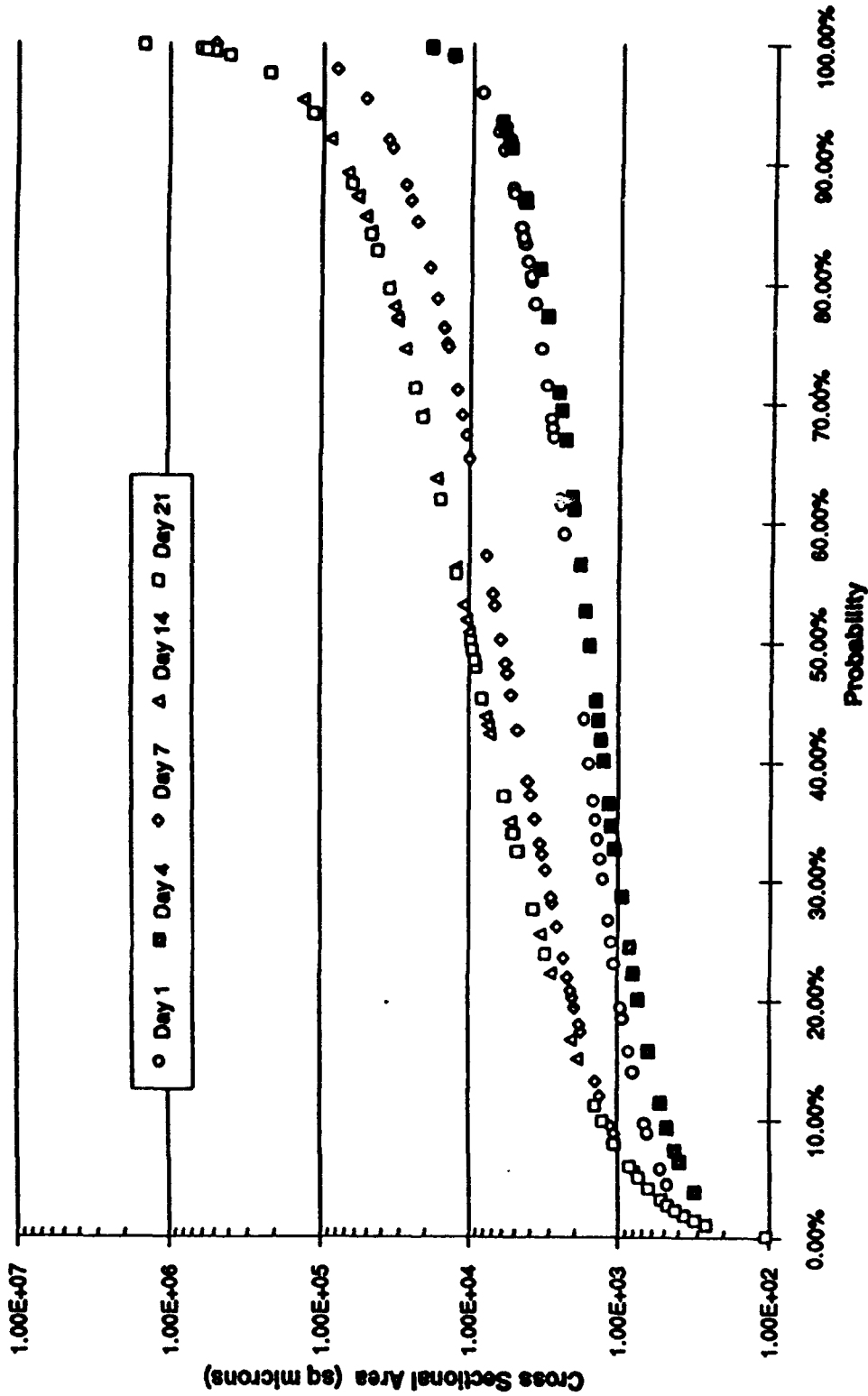


Figure 2. Pit Size Distribution for Aluminum Alloy 2024-T3 Exposed to the CASS Environment for 1, 4, 7, 14 and 21 days, respectively.

2024-T3 Average Exfoliation

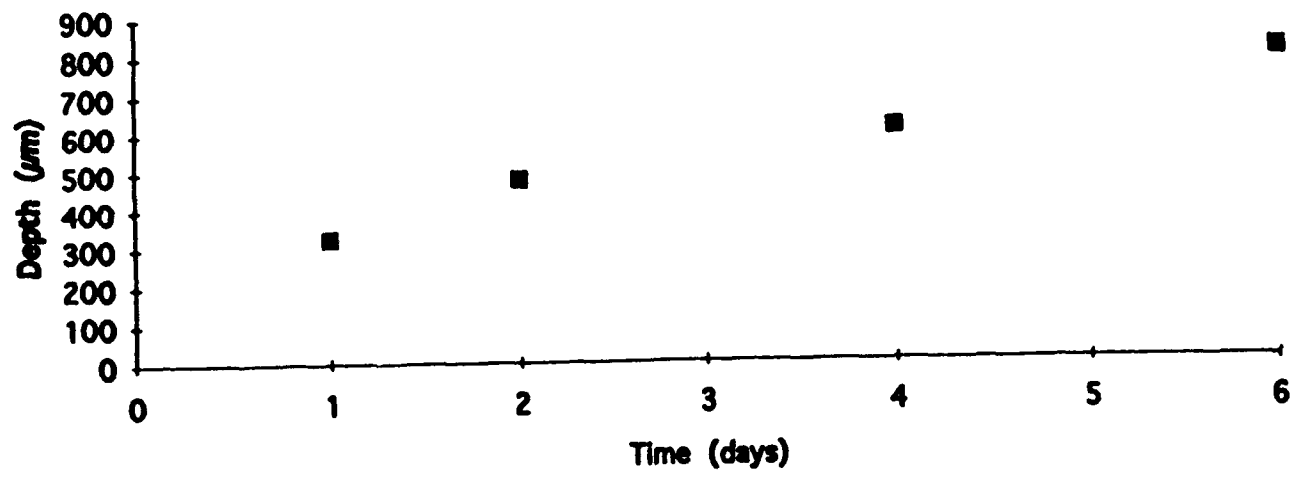


Figure 3. Exfoliation Depth of Aluminum Alloy 2024-T3 as a Function of Exposure Time in the ASTM G34 EXCO Solution

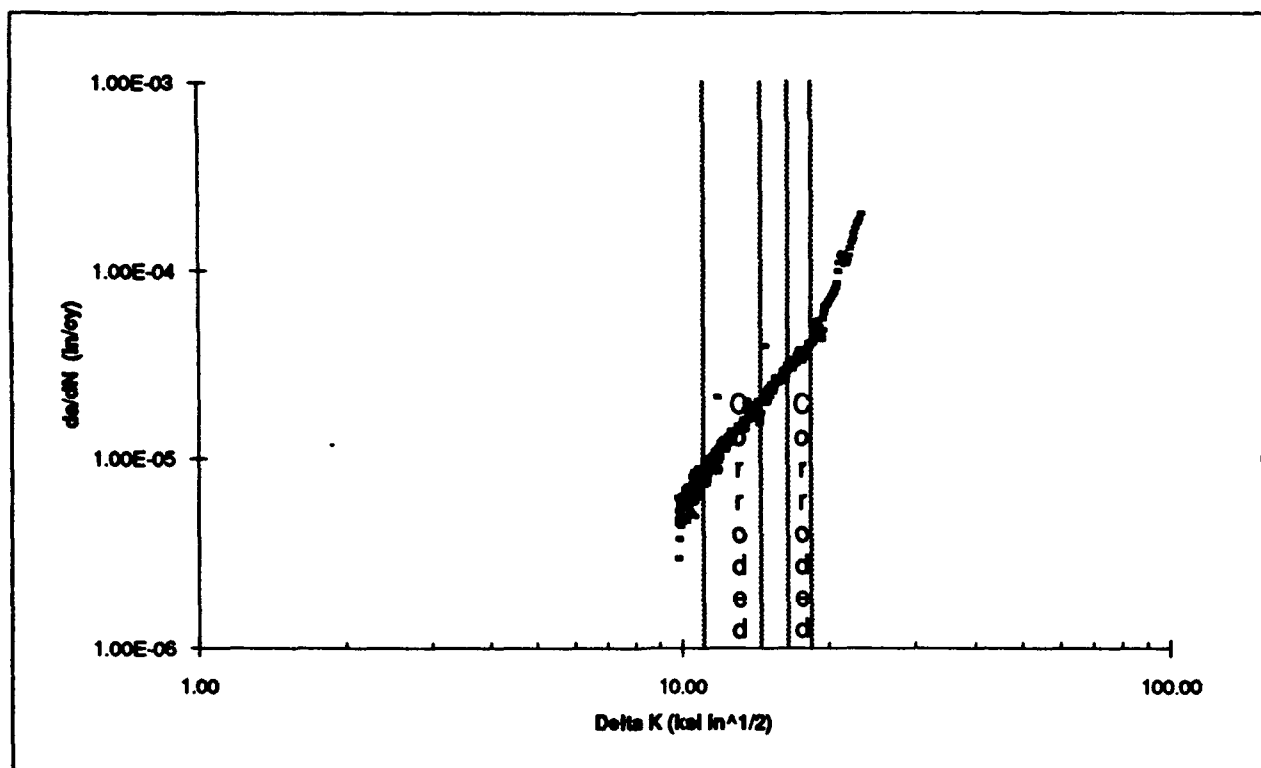
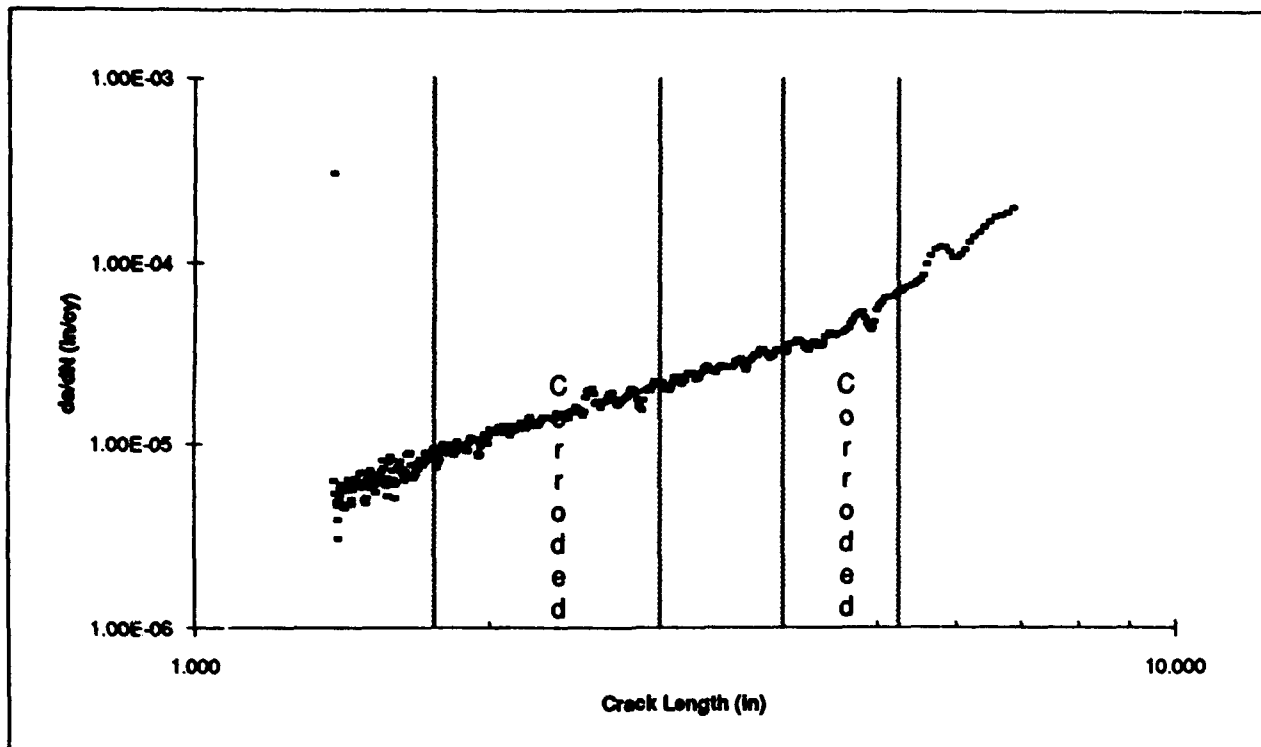


Figure 4. Fatigue Crack Velocity da/dN as a Function of Crack Length (a) and ΔK for Modified CT Specimens Precorroded in CASS Environment for 6 Days.

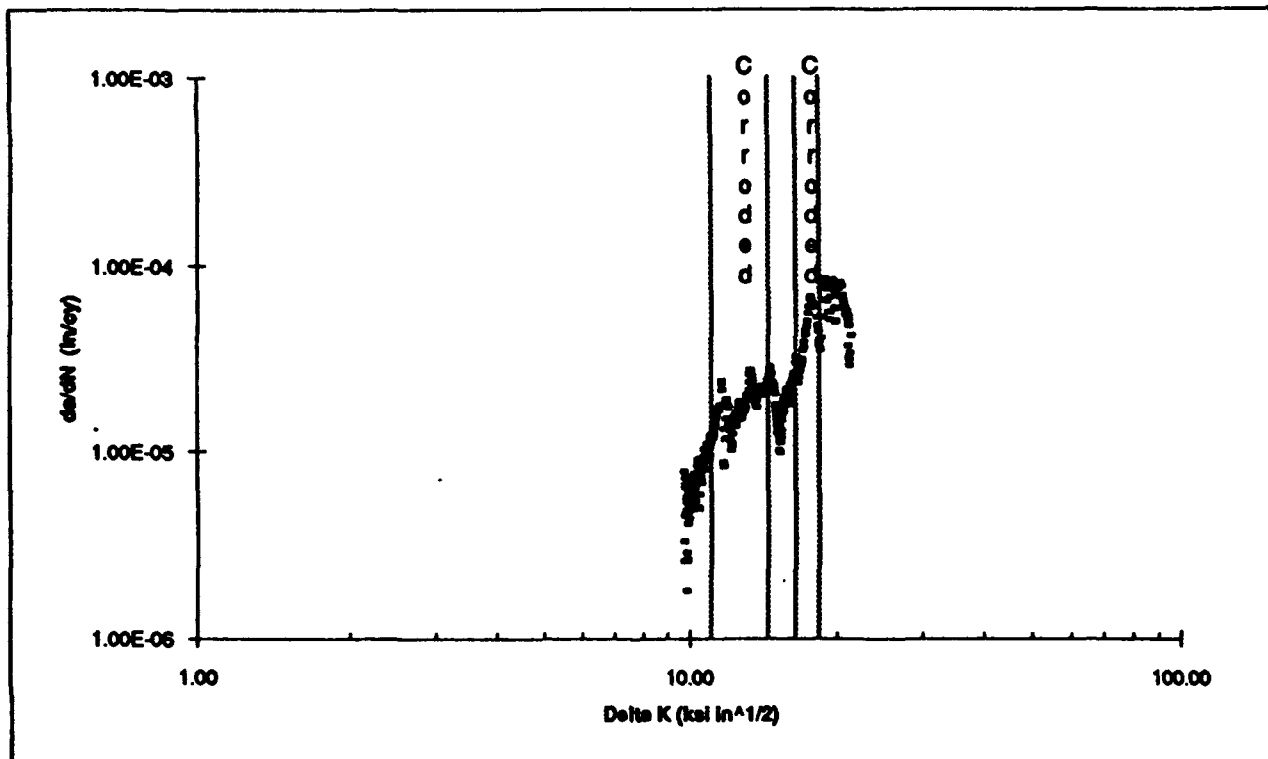
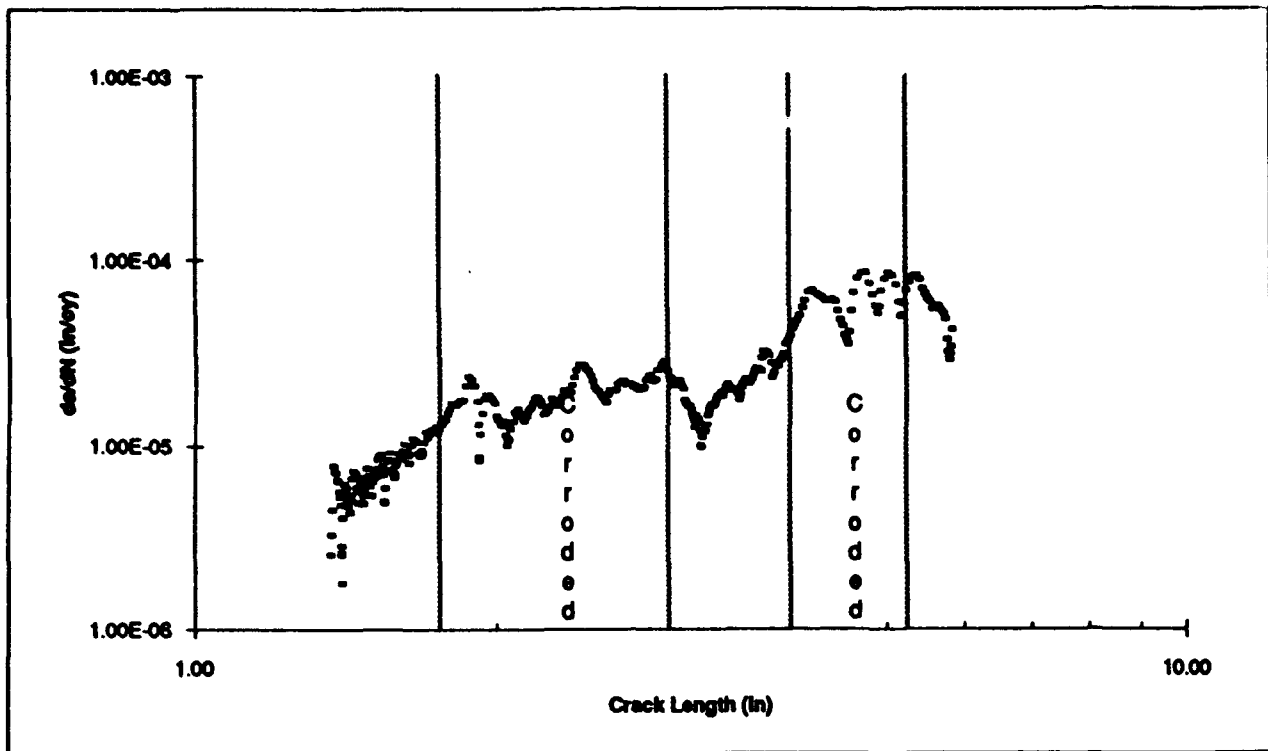


Figure 5. Fatigue Crack Velocity (da/dN) as a Function of Crack Length (a) and ΔK for Modified CT Specimen Precorroded in EXCO Solution for 6 Days

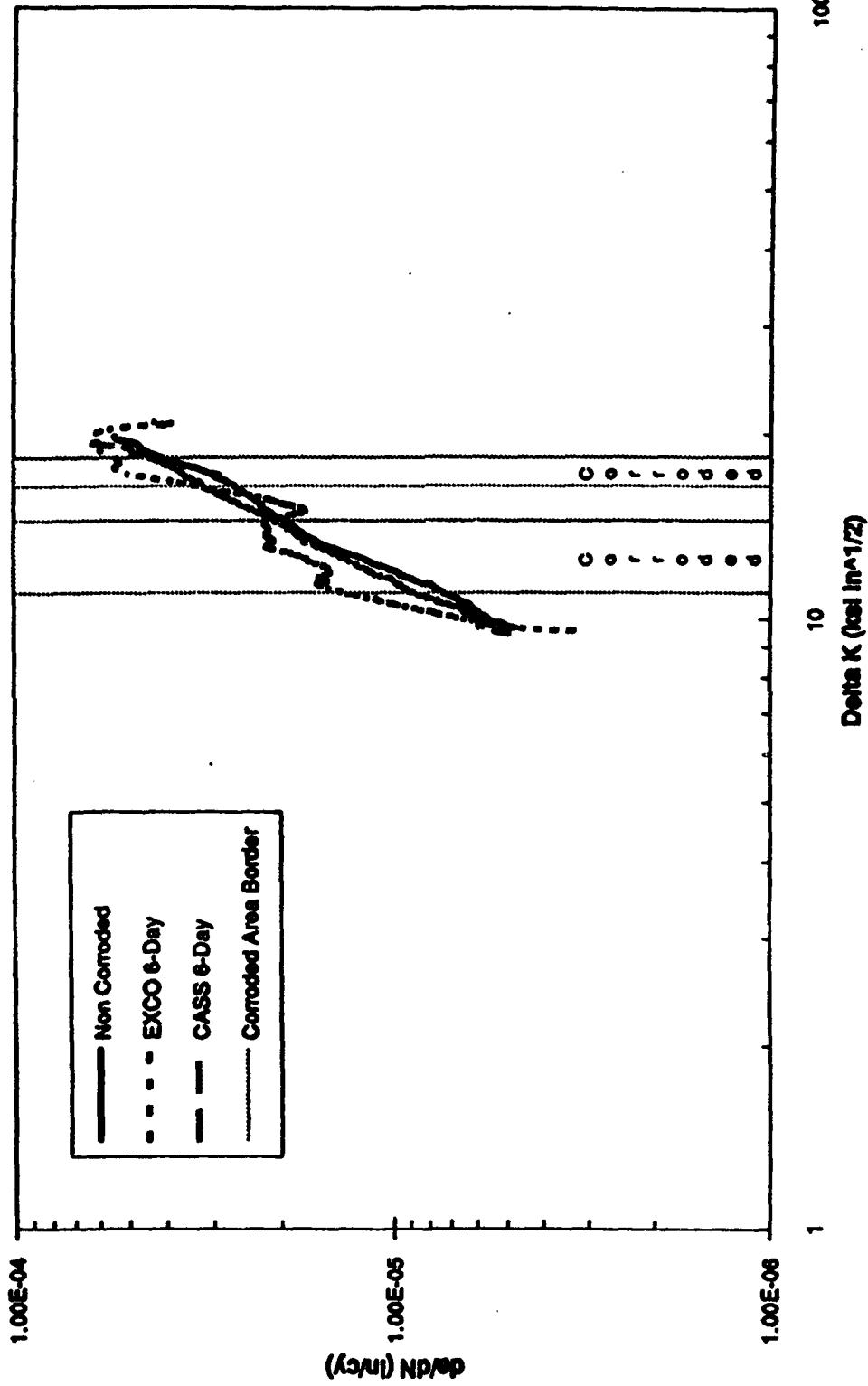


Figure 6. Fatigue Crack Velocity as a Function of ΔK for Non-Corroded Modified CT Specimens and Modified CT Specimens Corroded in the EXCO and CASS Solution, respectively.



Figure 7. Scanning Electron Fractograph of Fatigue Fracture Surface of Modified CT Specimen After a 6 Day EXCO Exposure

A COMPARISON OF FRACTURE CRITERIA FOR CRACK COALESCENCE AND OTHER OBSERVATIONS BASED ON RESIDUAL STRENGTH CALCULATIONS

J. P. Gallagher, Subrato Dhar, and A. P. Berens
Structural Integrity Division
University of Dayton Research Institute
300 College Park
Dayton, OH 45469

and

Joseph G. Burns
Fatigue, Fracture and Reliability Section
Flight Dynamics Directorate - Wright Laboratory
Wright-Patterson Air Force Base, OH 45433

ABSTRACT

The residual strength levels associated with crack coalescence are calculated and compared as a function of three different fracture criteria. These criteria are based on (a) the Irwin fracture hypothesis or critical stress intensity factor K_c approach, (b) the Swift plastic zone interaction model, and (c) a two parameter R-curve analysis. As expected, the choice of criterion and their associated material properties (fracture toughness, yield strength, and R-curve power law coefficients) affect the predicted levels of residual strength of coalescence. One important observation from this study is that, as two crack tips approach each other, the dominant criterion becomes the Swift plastic zone interaction criterion. One of the more interesting observations from the study is based on residual strength comparisons between several different crack geometries. These comparisons show that the distance ω between the adjacent crack tips, i.e. the uncracked ligament, is a more important variable than the physical size of the cracks or other geometric features. Comparisons are also made between the residual strength for the various crack configurations before and after crack coalescence. For the crack sizes and configurations considered, observations are made relative to the potential for immediate impending failure after coalescence. The results are summarized in figures and tables.

INTRODUCTION

Multi-site damage (MSD) is generally associated with many neighboring cracks along a row of rivets (fastener holes) in the fuselage or wing structure and has been widely discussed over the last several years [1-6]. Summaries of the damage tolerance approach to this problem are discussed by Lincoln [7] for commuter aircraft and by Swift [8] for commercial aircraft. Early evaluations of the effect of multiply cracked structures were conducted by Brussat and coworkers [9,10], Broek [11], Karlsson and Backlund [12], and Burck and Rau [13] for single and multi-site cracks. Brussat introduced the use of the compounding method, whereby known solutions are combined using the product of the different geometrical factors, to obtain approximate solutions. In general, the early investigators [9-13] reported stress intensity factor results primarily for multiple-site cracks emanating from fastener holes in infinite plate configurations. More recently, Nishimura, Noguchi and Uchimoto [14] discussed their compounding method for estimating stress intensity factors for multiple-site cracks emanating from a row of fastener holes located perpendicular to the loading direction in a finite plate. The finite element and boundary element techniques also have been used to estimate the stress intensity factor for complex structures. Overviews of finite element and analytical methods are given by Atluri [15] and Actis and Szabo [16]. A number of investigators [17-19] have used the finite element method to solve multi-site damage problems. Recently, Dawicke and Newman [20] have discussed an alternating indirect boundary element (AIBE) technique, which can be incorporated into a fatigue growth prediction code.

The objective of this paper is to determine (i) the influence of crack sizes on the predicted strength levels for link-up i.e., the coalescence strength, (ii) the influence of the spacing between adjacent crack tips, (iii) the influence of the fracture criterion and material properties, and (iv) a suitable design criteria for predicting structural failure after coalescence.

This paper first addresses the crack coalescence process using various fracture criteria (Irwin Fracture Hypothesis [21], Swift Plastic Zone Interaction Model [22] and R-Curve analysis [21]) and by considering different types of crack configurations in an infinite sheet subjected to uniform, uniaxial tensile stress. The crack configurations considered are:

- (a) single crack,
- (b) two unequal length collinear cracks,
- (c) three collinear cracks,
- (d) periodic array of collinear cracks,

with the geometric parameters illustrated in Figure 1. The single crack results provide a bound on the crack coalescence process of a multiple crack system, since the initial multiple crack problem will eventually become a single crack problem after the cracks coalesce.

GEOMETRIC PARAMETERS

In the analysis of a multiple crack system (see Figure 1 a,c,d), the geometric parameters are (a) a/b , the ratio of long crack size to short crack size and (b) ω/d , the ratio of the distance between adjacent crack tips to the periodic spacing of the cracks. Table 1 lists the values of these parameters chosen for the different crack configurations employed in this study.

The foundation for all analysis conducted in the study was the linear elastic fracture mechanics parameter K , i.e., the stress intensity factor. The stress intensity factor can in general be described using

$$K = \sigma\beta\sqrt{\pi a} \quad (1)$$

where σ is the remotely applied stress, β is the geometry factor and a is the crack length. For a single crack in an infinite sheet $\beta = 1$ (see Figure 1b). The expressions for β corresponding to two collinear cracks, three collinear crack and periodic array of collinear cracks, in an infinite sheet are given by Rooke and Cartwright [23]. Using the values for K for each of the crack tips shown in Figure 1, we determined the crack tip location where the driving force was highest; these locations are indicated in Table 1.

Initial studies evaluated the influence of the fracture criteria, material properties, and crack sizes on residual strength levels for the multiple crack configurations identified in Figure 1. To evaluate the effect of other geometric variables, the periodic spacing parameter d was set equal to 1 inch, a typical fastener spacing. The size of the uncracked ligament ω , i.e., the distance between the adjacent crack tips, was varied from 0.05 inch to 0.95 inch. The crack size parameter a/b was varied from 1 to 10, so that the crack size a varied from 0.025 to a maximum of 0.475 inch.

To determine the influence of the longer crack length a on the residual strength, the size of the short crack b in Figures 1 c and d was fixed to 0.25 inch. The crack length a was varied from 0.025 inch to 48 inches.

FRACTURE CRITERIA

(a) Irwin Fracture Hypothesis: The residual strength based on thin sheet abrupt fracture can be written in the form

$$K = K_{cr} \quad (2)$$

where K is obtained from Eq. 1 for a given crack configuration and K_{cr} is determined from standard laboratory tests. For a thin sheet, the fracture toughness K_{cr} can be a function of sheet thickness. The criterion for crack coalescence is the highest K for

adjacent crack tips.

(b) Swift Plastic Zone Interaction Model: Net section yielding stresses for the presence of multiple cracks are calculated based on the asymptotic formula for the stress near a crack tip,

$$r_p = 1/2\pi (K/\sigma_{ys})^2 \quad (3)$$

where σ_{ys} is the yield strength, r_p is the plastic zone radius and K is the stress intensity factor at the crack tip. Swift's criterion for two crack tips approaching each other in terms of the distance ω between the adjacent crack tips is (see Figure 2):

$$\omega = r_{yB} + r_{yC} \quad (4)$$

where r_{yB} and r_{yC} are the radii of the plastic zones at location B and C, respectively. Using Eqs. 3 and 4, Swift's criterion becomes:

$$\omega = 1/2\pi [(K_B/\sigma_{ys})^2 + (K_C/\sigma_{ys})^2] \quad (5)$$

where K_B and K_C are the stress intensity factors at the coalescing crack tips located at points B and C, respectively. For the crack configuration shown in Figure 2, $a > b$, $2a$ represents the length of the long crack (AB) and $2b$ represents the length of the short crack (CD); and d defines the crack spacing parameter. In terms of yield strength σ_{ys} , distance ω between adjacent crack tips, crack sizes a and b , and geometry factors β_B and β_C , one can estimate the coalescence strength σ_{cs} ,

$$\sigma_{cs} = \sigma_{ys} [2\omega/(a \beta_B + b \beta_C)]^{1/2} \quad (6)$$

The geometry factors β_B and β_C are associated with the points shown in Figure 2 and are given in [23] for the various crack geometries.

(c) Two Parameter R-Curve Criterion: The two parameter R-curve criterion

$$K = K_R \quad (7a)$$

$$dK/da \geq dK_R/da \quad (7b)$$

is satisfied by equating the crack tip stress intensity factor K for each stress level to the resistance curve. Crack instability occurs when the rate of change of applied stress intensity (dK/da) equals the rate of change of resistance curve (dK_R/da).

In Figure 3, the σ curve represents the variation of K with the crack length for a fixed value of the applied stress σ and accounts for the effect of adjacent (growing) cracks when necessary. The relationship between the crack size and the stress intensity factor is

$$a = 1/\pi (K/\sigma \beta_B)^2 \quad (8)$$

The R curve is obtained by varying the applied stress σ for a fixed value of ω . The power-law relationship between the resistance stress intensity and increment in crack size is obtained from a curve-fit of the CTOA analytical data.

$$K_R = C (\Delta a)^n \quad (9)$$

The material properties C and n are given Table 2.

The intersection point in Figure 3 is obtained by iterating on Δa to maintain equality between K and K_R until Eq. 7b (the dual criterion) is satisfied. The value of the final crack length a_f in terms of initial crack size a_i and crack growth increment Δa is

$$a_f = a_i + \Delta a. \quad (10)$$

The expression for the residual strength is given by,

$$\sigma_B = K/(\beta_B \sqrt{\pi a_f}) \quad (11)$$

INFLUENCE OF CRACK SIZE

Figure 4 presents the variation of residual strength level as a function of crack size for two extremely different crack geometries. These results are based on the Irwin fracture hypothesis and assume a plane stress fracture toughness (K_{IC}) of 60 ksi $\sqrt{\text{in}}$. In the figure, the link-up process for the infinite collinear array of cracks (with $d=1$) is shown to reduce the residual strength drastically when compared to the residual strength of a single crack of the same size. Note that comparisons are only valid for strength levels below the yield strength and that when the crack size in the periodic array is 0.5 inch, the cracks are linked. For the periodic array configuration, when the cracks coalesce, the structure fails, so the coalescence strength is equal to the residual strength.

Figure 5 compares the coalescence strength behavior for all multiple crack geometries where the distance between cracks is $d (= 1 \text{ inch})$. The curves for single and infinite collinear crack configurations were taken from Figure 4. In Figure 5, the points on the curves associated with the two and three collinear crack geometries are based on constant values of the uncracked ligament parameter ω . These curves represent ratios between the crack sizes (a/b) that range from 1 to 10. For $a/b = 1$, the crack sizes are all equal, and for the two and three collinear crack curves, the ($a/b = 1$) points are located on the left.

In Figure 5, the coalescence strength level for any number (> 2) of equal size collinear cracks, is bounded between the two equal collinear cracks and the infinite collinear crack configuration. For values of $\omega > 0.1$ inch, the coalescence strength decreases with increase in a/b ratio and for values of $\omega < 0.1$ inch, the coalescence strength remains essentially constant. The interaction between a long crack and a short crack in terms of the coalescence strength levels (increase/decrease) is decided by the value of the size of the uncracked ligament ω .

The importance of physical crack size in explaining the link-up of a short crack with the long crack has been addressed previously [17,18]. Our analyses (see Figure 5) show that the distance ω between the adjacent crack tips is a more important variable than the physical size of the individual cracks as the cracks approach each other.

INFLUENCE OF THE LONGEST CRACK SIZE

In this subsection, the shorter crack size b in the two and three crack configurations is kept fixed ($=0.25$ inch) and the larger crack size a is varied for several fixed values of ω . The analytical results are based on Irwin fracture hypothesis, taking $K_{IC} = 60$ ksi $\sqrt{\text{in}}$. The coalescence strength, σ_{cs} , is associated with the stress intensity factor at location B, the tip of the longest crack in the multi-crack system.

Two Crack Configuration

Figure 6 presents the ratio of the coalescence strength (σ_B) to the strength level (σ_A) associated with extending crack tip A for a two crack configuration. The following observations are made from Figure 6 with regard to the strength ratios plotted which describe the relative strength levels required to extend the cracks at positions A, B, and D. Before crack coalescence, the strength ratio level (σ_A or σ_B) required to extend the tips of the longest crack is not affected by increasing the crack size $a > 1$ inch.

The ratio between the coalescence strength and the residual strength at location A (σ_B/σ_A) is greater than the ratio between the coalescence strength and the residual strength at location D (σ_B/σ_D) (see Figure 7); and, the strength, σ_D , is higher than the strengths σ_A or σ_B . This dictates that the critical location for crack link-up or failure is at location B ($\sigma_B < \sigma_A < \sigma_D$), as indicated in Table 3. Increasing the long crack size, a , for a fixed short crack size, b , the residual strength σ_D remains fairly constant, but the strength ratio (σ_B/σ_A or σ_B/σ_D) levels is a function of uncracked ligament size ω . The decreasing effect of ω decreases the strength ratio, σ_B/σ_A , because the coalescence strength decreases by 40 to 50% of the strength corresponding to the crack tip at location A. This shows that ω is the parameter which establishes the strength ratio.

During coalescence the crack tips B and C merge. The residual strength σ_A after

coalescence is now a square root function of the crack spacing d . Figure 8 describes the ratio of coalescence strength to the residual strength after crack link-up. The figure shows that for $0.05 < \omega < 0.5$, the residual strength σ_A after coalescence for $a = 8$ inch is approximately 13% higher than for $a = 1$ inch. When σ_B (before)/ σ_A (after) > 1 , complete fracture of the plate occurs after coalescence. However, for $\omega \leq 0.1$ inch and for any values of $a > 6$ inch the strength ratio, σ_B (before)/ σ_A (after), remains fairly constant. This means that increasing (or decreasing) the value of ω by 15%, the value of the crack size a must be decreased by 1% to make the strength ratio, σ_B (before)/ σ_A (after), remain constant. This analysis shows that the size of the long crack a does not significantly influence the decrease in the coalescence strength σ_B . If $\omega < 0.1$ inch, then after coalescence, the crack will not extend to failure. However, if $\omega > 0.1$ inch, coalescence leads to catastrophic failure.

Figure 9, illustrates the effect of the largest crack size on the residual strength ratio (before/after) for crack tip A. When a short crack is interacting with another short crack, the reduction in the residual strength is much greater than a long crack interacting with a short crack. For example, the strength before coalescence is approximately 1% higher than that after coalescence for $a > 10$ inch.

Three Crack Configuration

Analyses similar to the above are accomplished for the three crack configuration. In Figure 10, the coalescence strength, σ_C , is associated with the stress intensity factor at locations A and B, the tip on either side of the longest crack in a three crack system (see Figure 1d). The following observations are made from Figure 10 with regard to the strength ratios plotted which describe the relative strength levels required to extend the cracks at positions B, and D. Before crack coalescence, the strength levels (σ_A or σ_B) required to extend the tips of the longest crack and the strength level required to extend the crack tip D (σ_D) are not affected by increasing the crack size for $a > 2$ inch. The ratio between the coalescence strength and the residual strength at location D (σ_B/σ_D) is greater than the ratio between the coalescence strengths at location B or C; and, the strength, σ_D , is higher than the strengths σ_B or σ_C . This dictates that the critical location for crack link-up or failure is at location B ($\sigma_B = \sigma_A < \sigma_C < \sigma_D$), as indicated in Table 3.

During coalescence the crack tips B and C merge. The residual strength, σ_D , is now a square root function of $d+b$. Note that the residual strength, σ_B , before and after coalescence remain fairly constant for $a > 3$ inch, whereas the residual strength, σ_D , after coalescence shows a strong decreasing dependence on the periodic spacing parameter d . Because of this the strength ratio, σ_B/σ_D , is an increasing function of crack size a for $\omega < 0.5$ inch, shown in Figure 10. Also, from Figure 11, the residual strength, σ_D , before coalescence is approximately 10% higher than after coalescence for $a > 10$ inch.

Summary

Before crack coalescence (refer to Figures 7 and 10), the residual strength at the crack tip B (σ_B) is not affected by increasing the largest crack size $a > 3$ inch. Figures 9 and 12 infer that the coalescence strength is a function of the number of cracks that are present and does not depend on the crack size a or the spacing ($a > 3$ inch), but shows a strong dependence on the value of the uncracked ligament size ω . For a large number of collinear cracks, the total failure of the structure will be immediate following crack link-up.

INFLUENCE OF FRACTURE CRITERIA AND MATERIAL PROPERTIES

The residual strength levels associated with crack coalescence for infinite collinear cracks, shown in Figure 13 are calculated and compared as a function of three different fracture criteria: (a) Irwin fracture hypothesis, (b) Swift plastic zone interaction model and (c) R-Curve analysis. The lower bound for the residual strength is decided by the Irwin fracture hypothesis or two parameter R-curve criterion for large values of the uncracked ligament, ω . As two crack tips approach each other, the dominant criterion becomes the Swift plastic zone interaction criterion.

In Irwin's model, decreasing the fracture toughness from 60 ksi/in to 30 ksi/in decreases the residual strength by half as shown in Figure 14. In the Swift plastic zone interaction model, the yield strength influences the crack coalescence which is shown in Figure 15. Comparing Figures 14 and 15, the effect of fracture toughness on the residual strength and the crack coalescence is more severe than the yield strength of the material.

The residual strength levels associated with crack coalescence for the two crack configuration are calculated and compared as a function of three different fracture criterion in Figures 16 and 17. In Figure 16, as two adjacent crack tips approach each other, the dominant criterion is based on R-curve analysis as compared to Irwin's fracture hypothesis. Similarly, in Figure 17, as two adjacent crack tips approach each other, the dominant criterion is the Swift plastic zone interaction criterion as compared to the R-curve analysis criterion. A summary of the above results are given in Table 3.

CONCLUSIONS

- (1) For nearby cracks, the crack coalescence strength is largely independent of the largest crack size and its ratio to the crack with which it coalesces.
- (2) By adding a small crack ($2b = 0.5$ inch) ahead of a larger crack of size $2a$, the reduction in the residual strength is greater than 10% for $a < 2$ inch, and the reduction in the residual strength is less than 5% for $a > 10$ inch.
- (3) The potential exists for immediate failure after coalescence occurs.

(4) The effect of variation in fracture toughness on crack coalescence and residual strength levels is more severe than that of the yield strength of the material.

(5) The lower bound for the residual strength is decided by fracture toughness or R-curve criterion for large values of the uncracked ligament, ω . As the value of ω approaches zero, the plastic zone criterion dominates.

(6) The observations for crack coalescence using three fracture criteria (a) Irwin fracture hypothesis, (b) Swift plastic zone interaction model and (c) two parameter R-curve analysis imply that crack coalescence is most heavily influenced by the distance ω between the adjacent crack tips.

REFERENCES

[1] Orringer, O., "How Likely is Multiple Site Damage?," Structural Integrity of Aging Airplanes, ed. by Atluri, S. N., Sampath, S. G. and Tong, P., Springer-Verlag, 1990.

[2] Tong, P., Arin, D. Y., Jeong, R. and Greif, R., "Current DOT Research on The Effect of Multiple Site Damage on Structural Integrity," Proceedings of 1991 International Conference on Aging Aircraft and Structural Airworthiness, Washington, D. C., pp. 111-157, November 19-21, 1991.

[3] Tong, P., Grief, R. and Chen, L., "Residual Strength of Aircraft Panels with Multiple Site Damage," Proceedings of the International Workshop on Structural Integrity of Aging Airplanes, atlantia, pp.200-216, March 31-April 2, 1992.

[4] Tong, P., Sampath, S. C. and Broek, D., "Aging Aircraft, Detection of MSD, and the Risk of Failure," ICAF Conference, pp. , Japan, 1991.

[5] Newman, J. C. and Harris, C. E., "Fracture Mechanics Research at NASA Related to the Aging Commercial Transport Fleet," Aging Aircraft and Structural Airworthiness, Washington, D. C., pp. 75-91, November 19-21, 1991.

[6] Harris, C. E. and Heyman, J. S., "Overview of NASA Research Related to the Aging Commercial Transport Fleet," Journal of Aircraft, Vol. 30(1), 1993.

[7] Lincoln, J. W., "Damage Tolerance for Commuter Aircraft," Proceedings of 1991 International Conference on Aging Aircraft and Structural Airworthiness, Washington, D. C., pp. 187-196, November 19-21, 1991.

[8] Swift, T. "Important Considerations in Commercial Aircraft Damage Tolerance," Int. J. of Vehicle Design, Vol. 7(3-4), pp. 264-287, 1986.

- [9] Brussat, T. R., Chiu, S. T. and Creager, M., "Flaw Growth in Complex Structure," AFFDL-TR-77-79, Vol. 1, December, 1977.
- [10] Brussat, T. R., Chiu, S. T. and Rudd, J. L., and Creager, M., " , " J. Engineering Fracture Mechanics, Vol. 14(4), pp. 665-683, 1981.
- [11] Broek, D., "Cracks at Structural Holes," MCCIC-75-25, Metals and Ceramics Information Center, Columbus, Ohio, March 1975.
- [12] Karlsson, A. and Backlund, J., " , " Int'l J. of Fracture, Vol. 14(6), pp. 585-596, 1978.
- [13] Burck, L. H. and Rau, C. A., " , " Int'l J. of Fracture, Vol. 9(1), pp. 43-51, 1973.
- [14] Nishimura, T., Noguchi, Y. and Uchimoto, T., "Damage Tolerance Analysis of Multiple-Site Cracks Emanating From Hole Array," Journal of Testing and Evaluation, JTEVA, Vol. 18 (6), pp.401-407, 1990.
- [15] Atluri, S. N., "Simplified Computational Methods for Elastic and Elastic-Plastic Fracture Problems," Proceedings of 1991 International Conference on Aging Aircraft and Structural Airworthiness, Washington, D. C., pp. 407-453, November 19-21, 1991.
- [16] Actis, R. L. and Szabo, B. A., "Computation of Stress intensity Factors for Panels with Multi-site Damage," Technical Note WU/CCM-92/3, December, 1992.
- [17] Beuth Jr., J. L. and Hutchinson, J. W., "Fracture Analysis of Multi-site Cracking in Fuselage Lap Joints," Proceedings of the International Workshop on Structural Integrity of Aging Airplanes, Atlanta, pp. 47-60, March 31-April 2, 1992.
- [18] Park, J. H. and Atluri, S. N., " Fatigue Frowth of Multiple-Cracks Near a row of Fastener -Holes in a Fuselage lap-Joints," report No. 92-1, December, 1992.
- [19] Newman Jr., J. C., Dawicke, D. S. and Bigelow, C. A., "Finite-Element Analysis and Fracture Simulation in Thin-Sheet Aluminum Alloy," Proceedings of the International Workshop on Structural Integrity of Aging Airplanes, Atlanta, pp. 47-60, March 31-April 2, 1992.
- [20] Dawicke, D. S. and Newman Jr., J. C., "Analysis and Prediction of Multiple-Site Damage (MSD) Fatigue Crack Growth," NASA Technical Paper 3231, August 1992.
- [21] Gallagher, J.P., Giessler, F.J., Berens, A.P., and Engle, R.M., "USAF Damage Tolerant Design Handbook: Guidelines for the Analysis and Design of Damage Tolerant Aircraft Structures," AFWAL-TR-82-3073, Flight Dynamics Laboratory, Wright-Patterson AFB, OH , May, 1984.
- [22] Swift, T. "Damage Tolerance Capability," FAA, Presented at Specialists

Conference on Fatigue of Aircraft Materials, Delft University of Technology, Delft-The Netherlands, October 14-15, pp. 15, 1992.

[23] Rooke, D. P. and Cartwright, D. J., "Compendium of stress Intensity Factors," Her Majesty's Stationary Office, London, 1976.

Table 1. Geometric Parameters for Different Crack Configurations

Crack System	Figure 1	Critical location for failure	ω (inch)	d (inch)	a/b	a (inch)	b (inch)
Periodic array of Collinear Cracks	a	A = B	0.05 0.10 0.25 0.50	1	1	0→0.5	0→0.5
Single Crack	b	A = B	-----	-----	-----	0→0.5	-----
Two Collinear Cracks	c	B	0.05 0.10 0.25 0.50	1 ----- 1→50	1→10 ----- **	0→0.5 ----- 0→48	0→0.05 ----- 0.25
Three Collinear Cracks	d	B	0.05 0.10 0.25 0.50	1 ----- 1→50	1→10 ----- **	0→0.5 ----- 0→48	0→0.05 ----- 0.25

** a/b ratio is not a variable

Table 2. Material Properties

Properties	Simulated 2024-T3 Aluminum
Yield Strength, σ_{ys}	60±10 (ksi)
Plane Strain Fracture Toughness, K_{Ic}	30 (ksi√in)
Plane Stress Fracture Toughness, K_{Ic}	60 (ksi√in)
Resistance Curve, K_{R}	124 $(\Delta a)^{0.224}$ (ksi√in)

Table 3. A Summary of Critical Crack Location and Coalescence Strength

Crack System	Figure 1	Critical crack tip location for link-up	Next most critical crack tip location for residual strength	Remarks	Residual strength levels
Infinite Series of Cracks	a	$A = B$	---	Coalesce strength \leq Residual strength	Lower Bound
Single Crack	b	$A = B$	---	No coalescence	Upper Bound
Two Collinear Cracks	c	B for $a > b$	A for $a > b$	Coalesce strength \leq Residual strength for $\omega \leq 0.1$ inch	refer remarks
Three Collinear Cracks	d	B for $a > b$	D for $a > b$	Coalesce strength \leq Residual strength for $\omega \leq 0.1$ inch	refer remarks

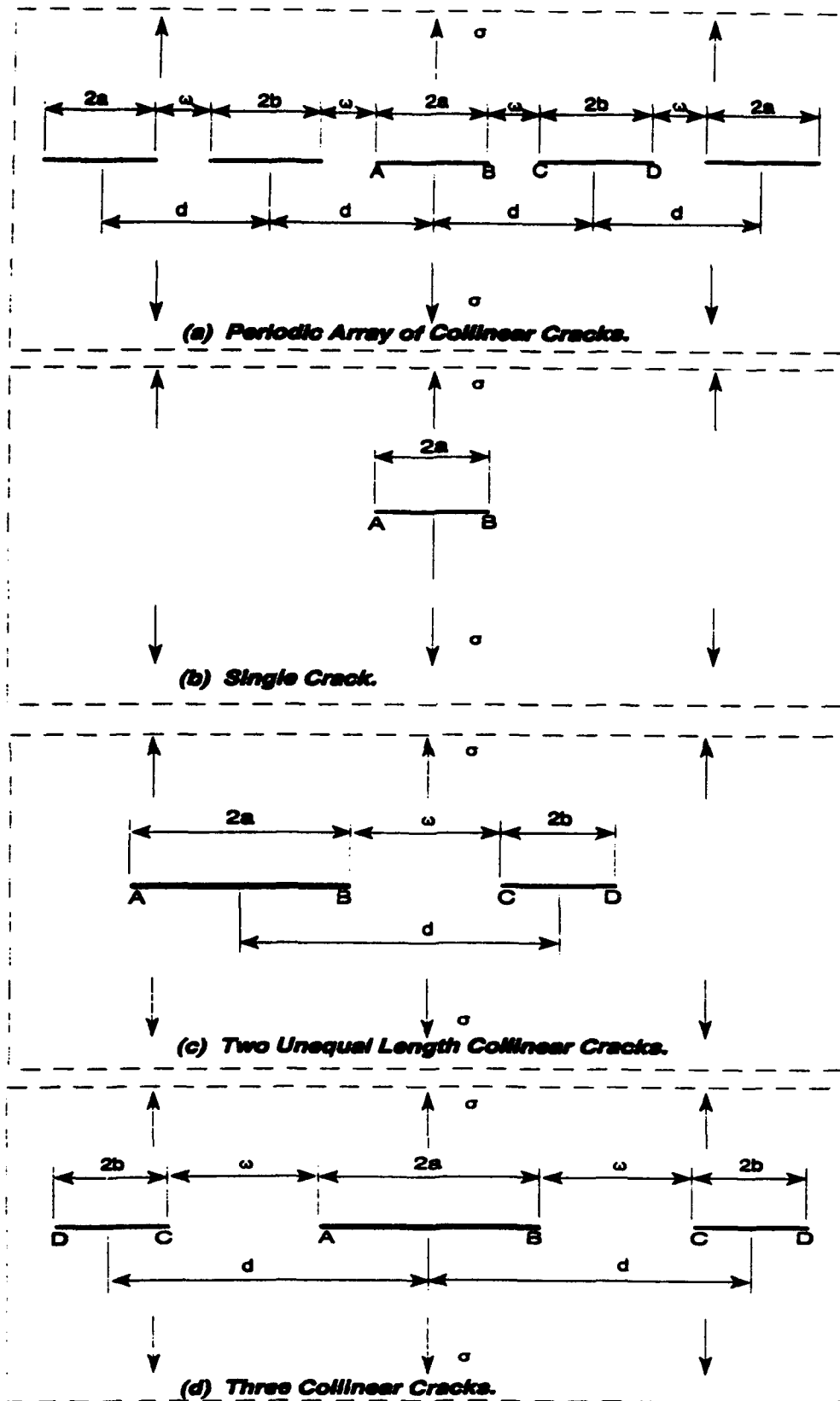


Figure 1. Crack Configurations

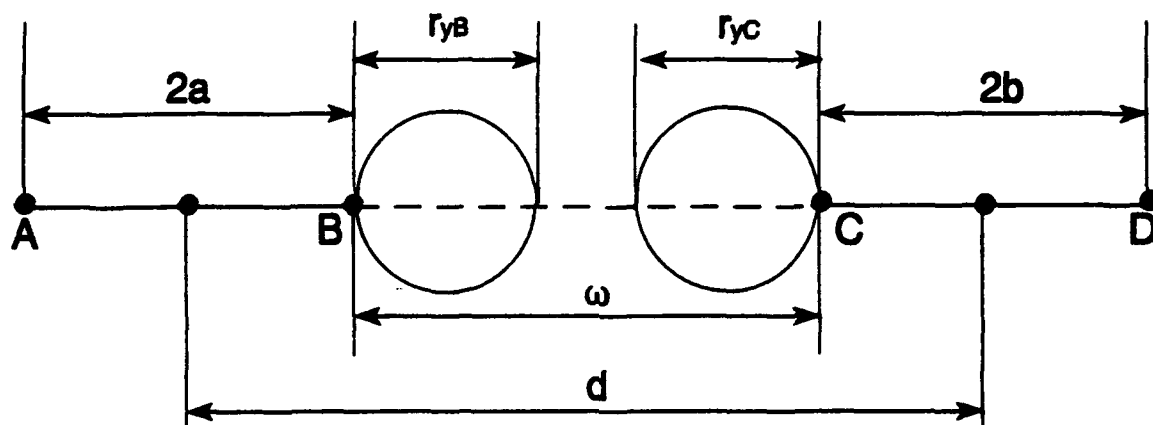


Figure 2. Swift Plastic Zone Interaction Model [22]

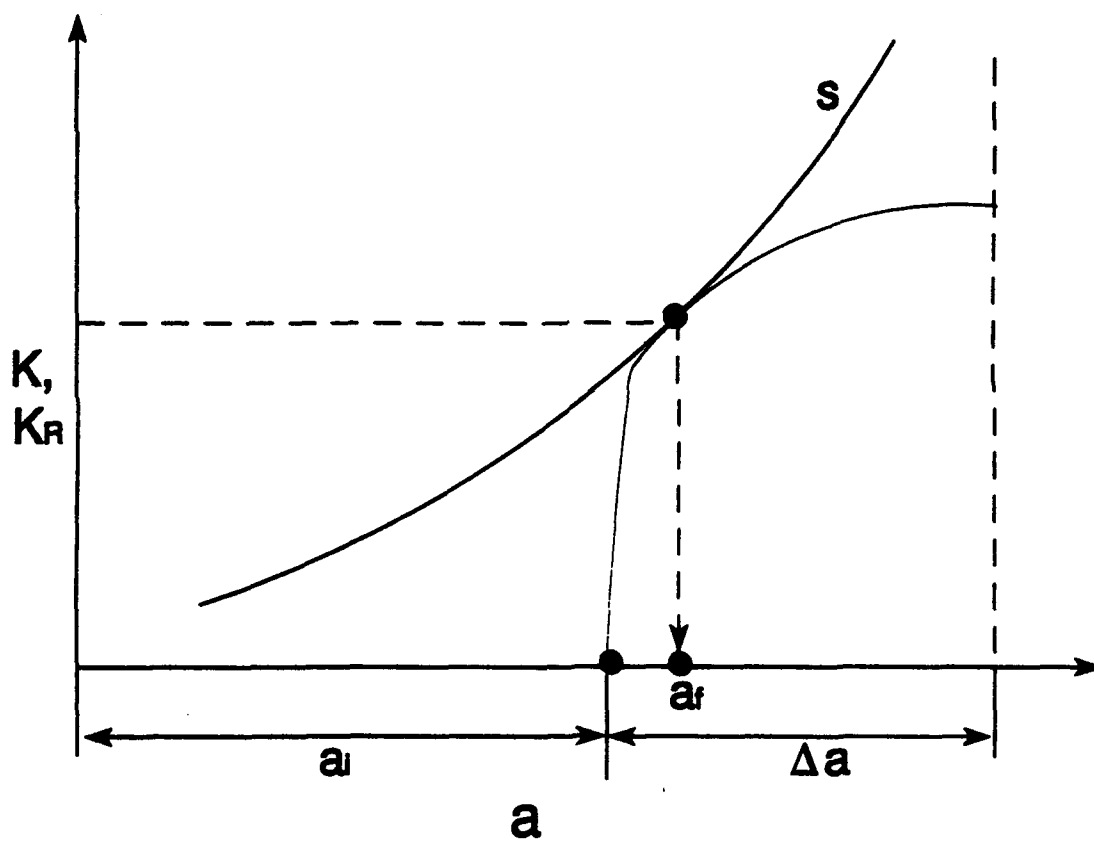


Figure 3. K-R Curve [21]

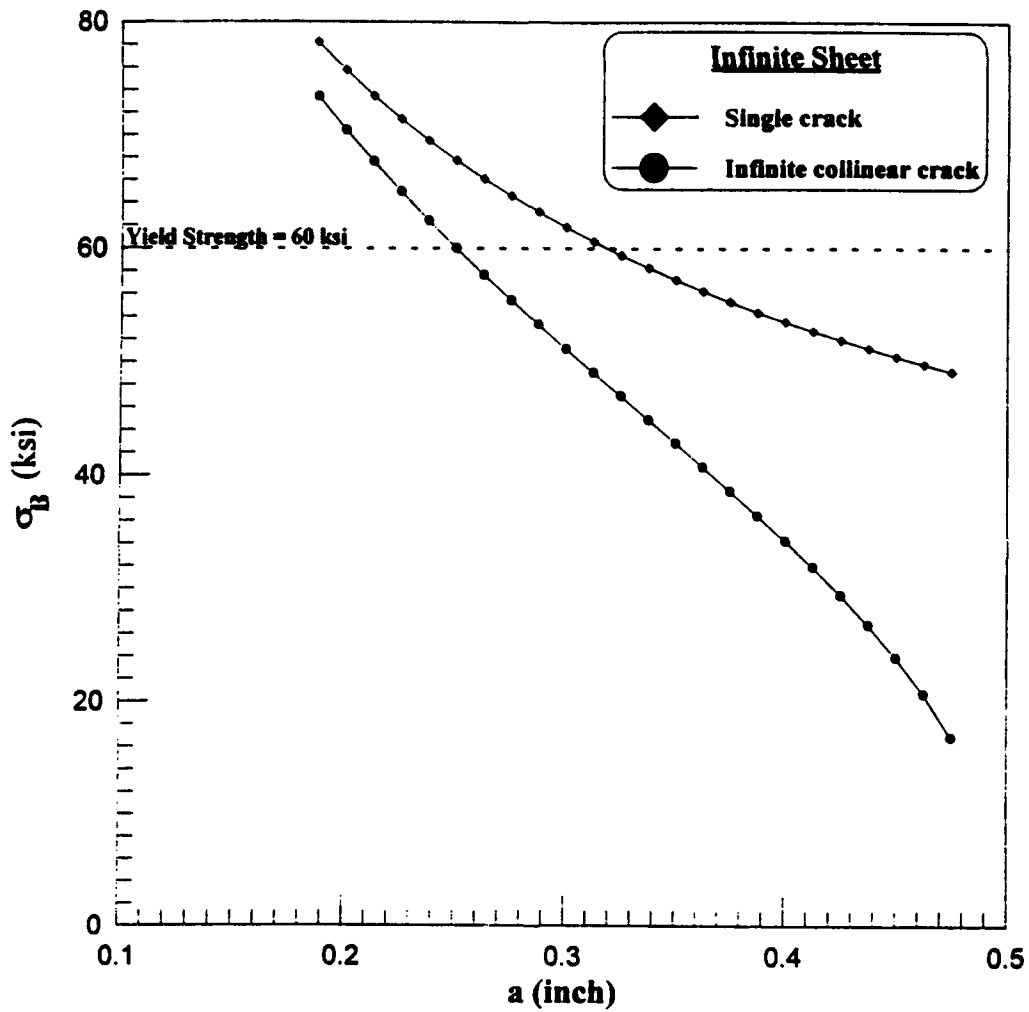


Figure 4. Comparison of residual strength levels between infinite collinear cracks and single crack in an infinite sheet based on critical stress intensity factor criterion.

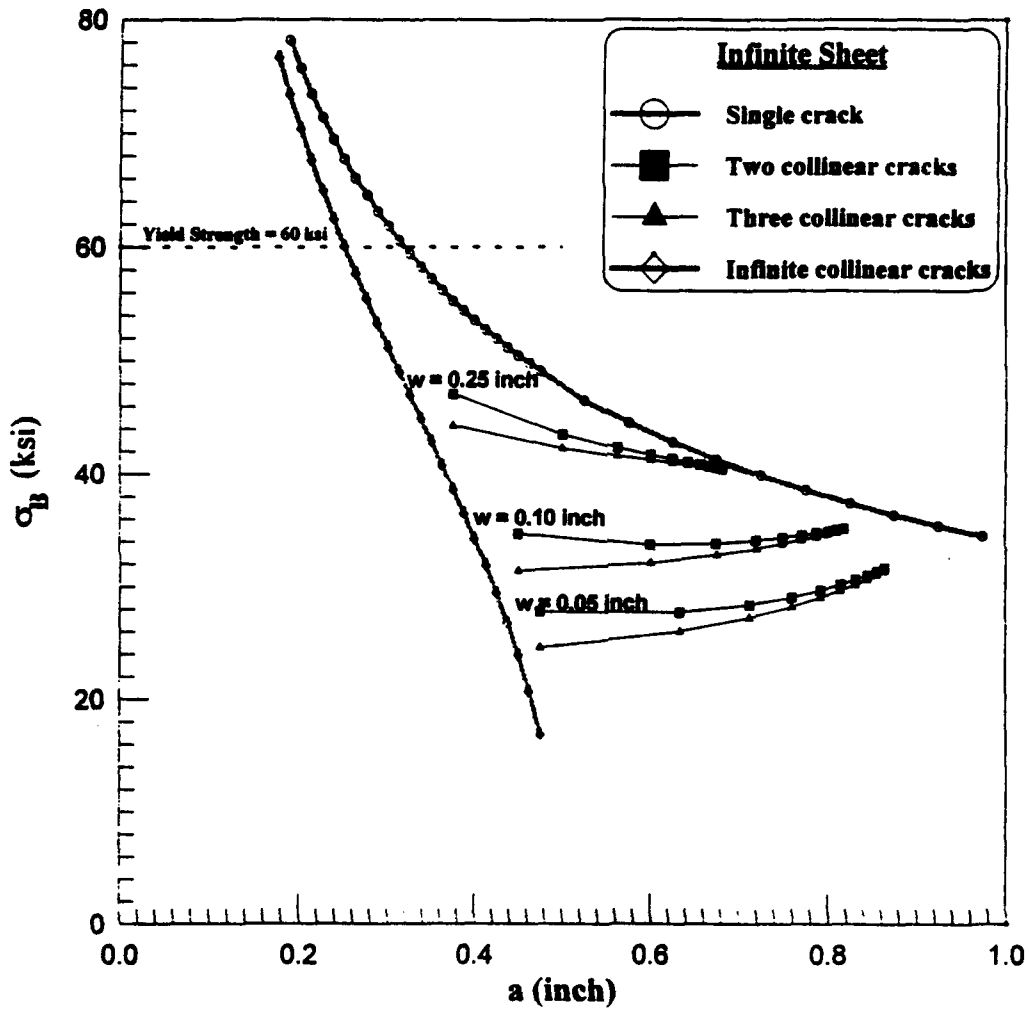


Figure 5. Comparison of residual strength levels among (a) single crack, (b) two collinear cracks, (c) three collinear cracks and (d) infinite collinear cracks, in an infinite sheet based on critical stress intensity factor criterion.

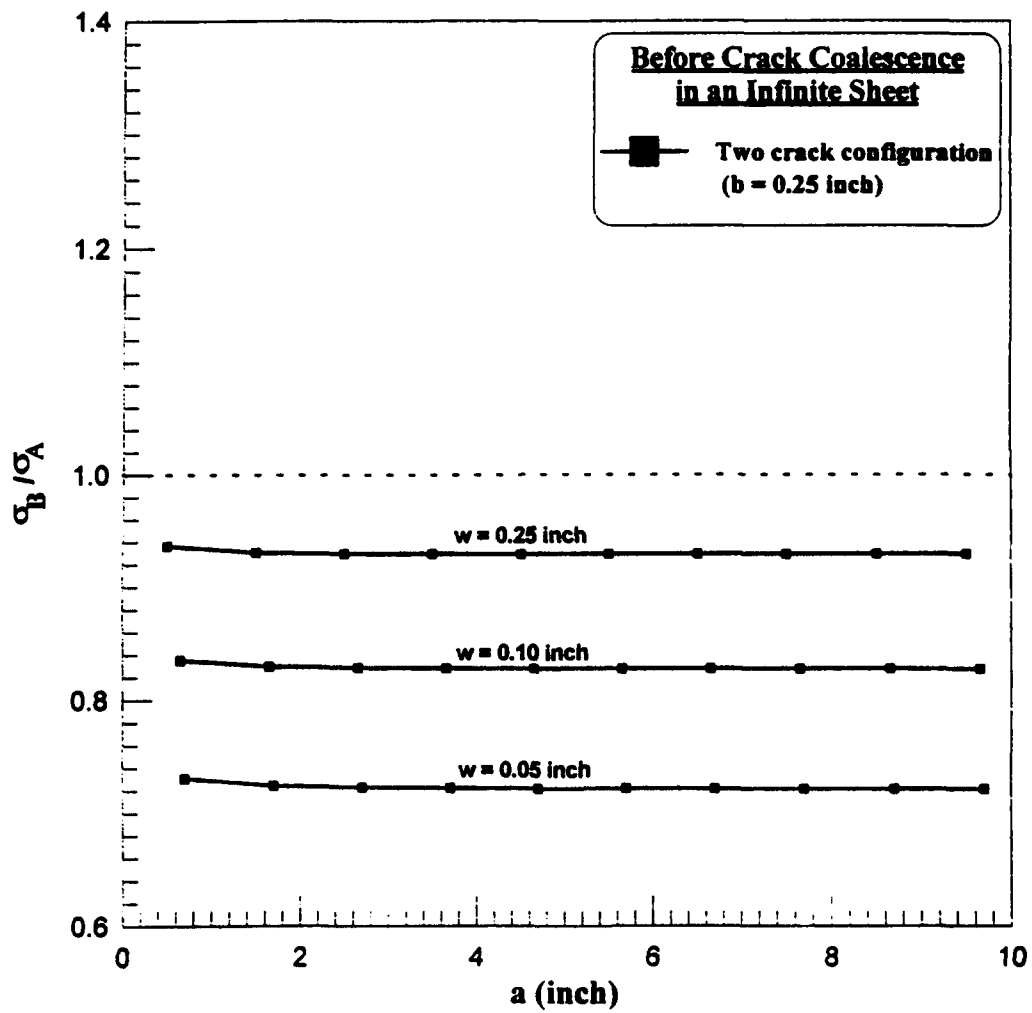


Figure 6. Ratio of strength levels for extending crack tips B and A before coalescence in two collinear crack configuration in an infinite sheet.

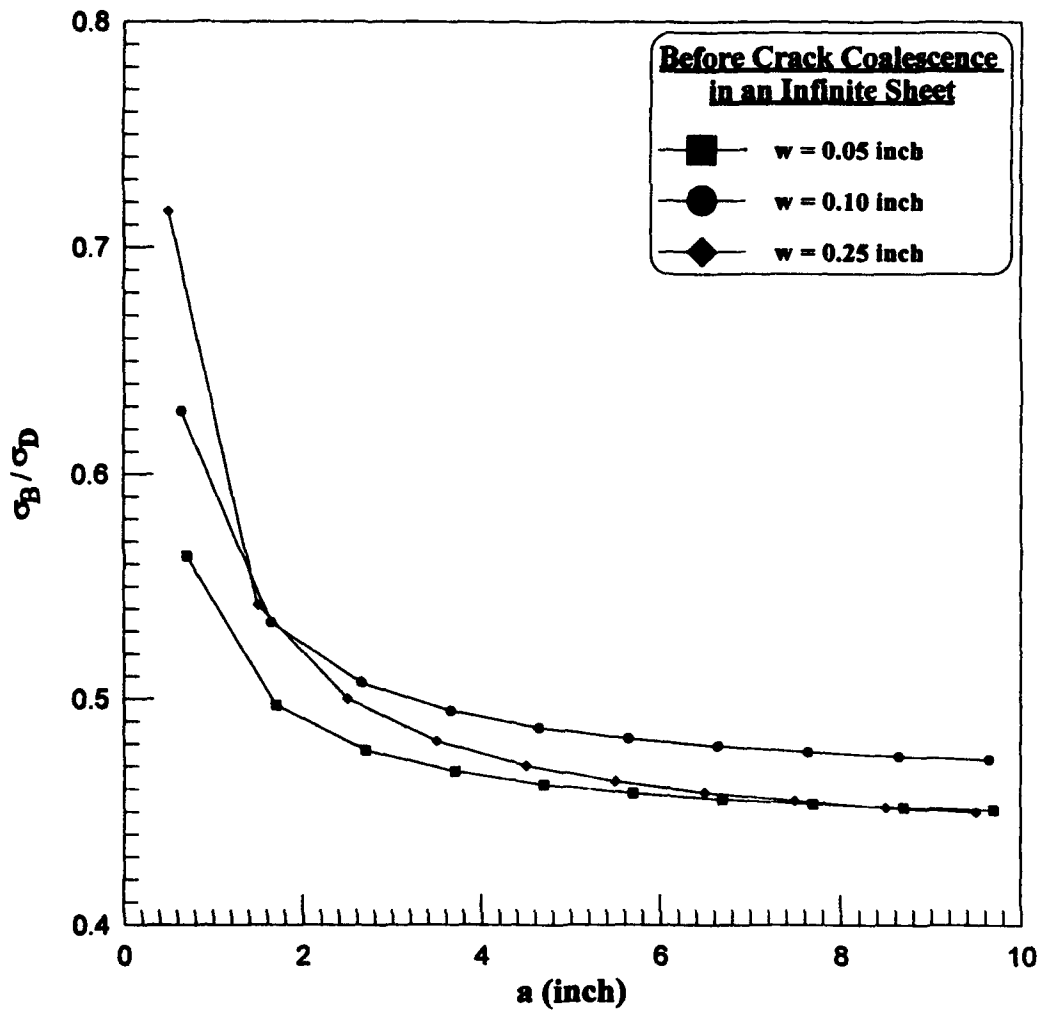


Figure 7. Ratio of strength levels for extending crack tips B and D before coalescence in two collinear crack configuration in an infinite sheet

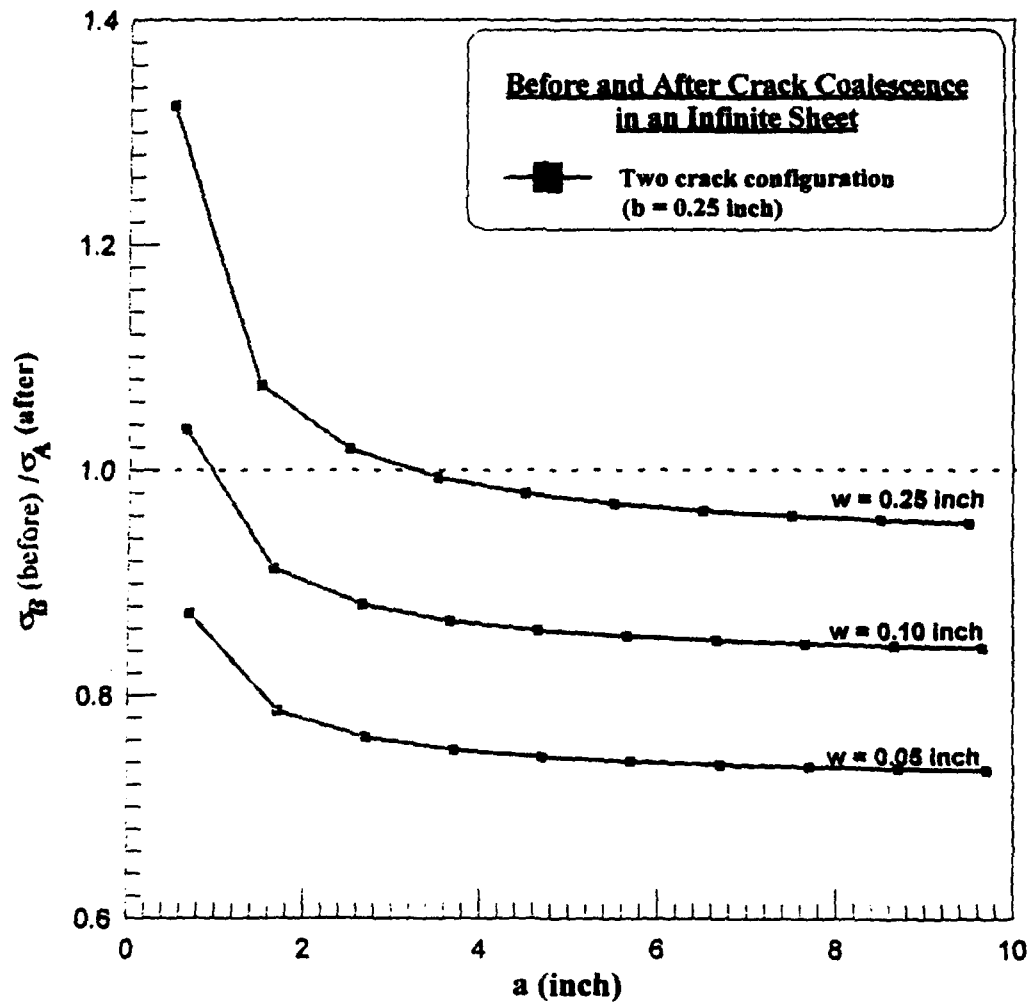


Figure 8. Effect of largest crack size a on coalescence strength at crack tip B in two collinear crack configuration in an infinite sheet.

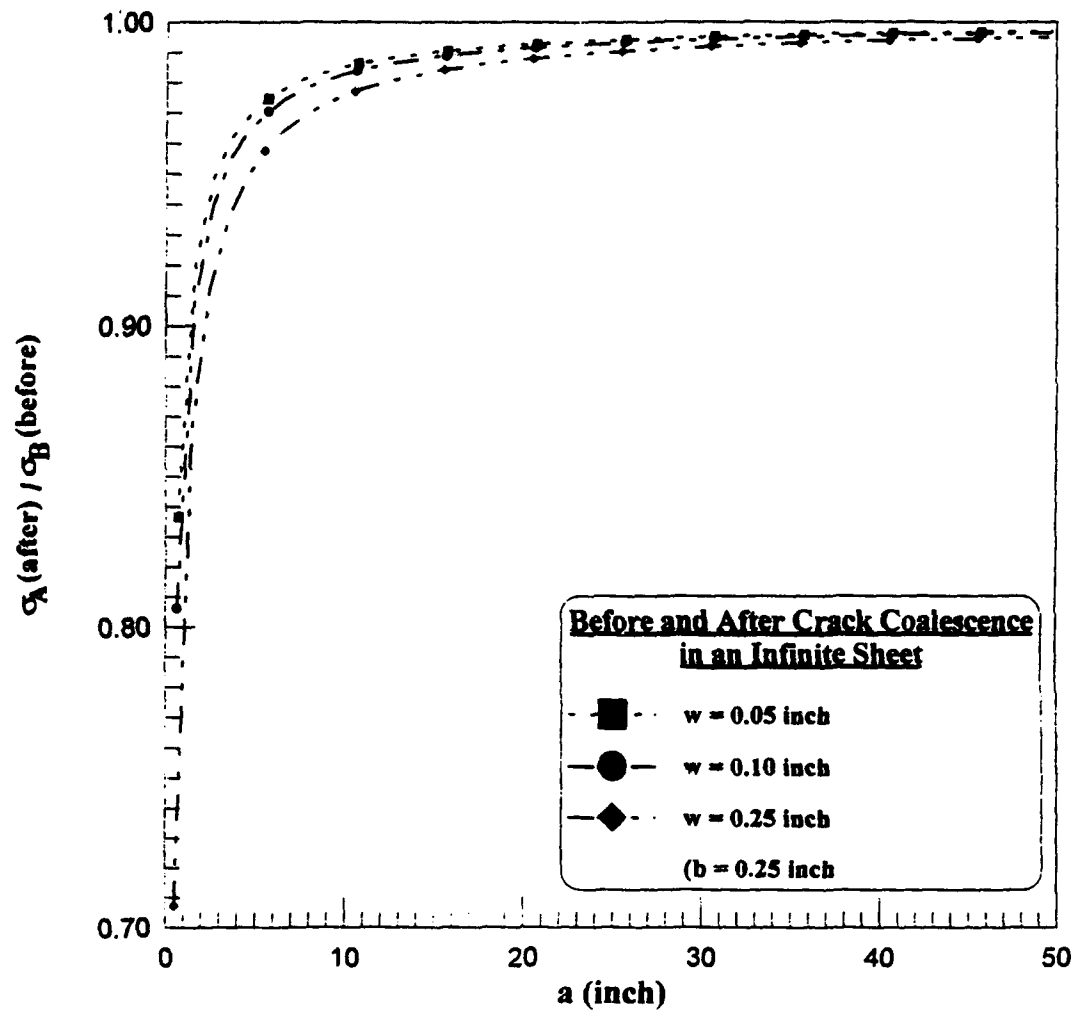


Figure 9. Effect of the largest crack size a on coalescence strength ratio (after/before) at crack tip A in two collinear crack configuration in an infinite sheet.

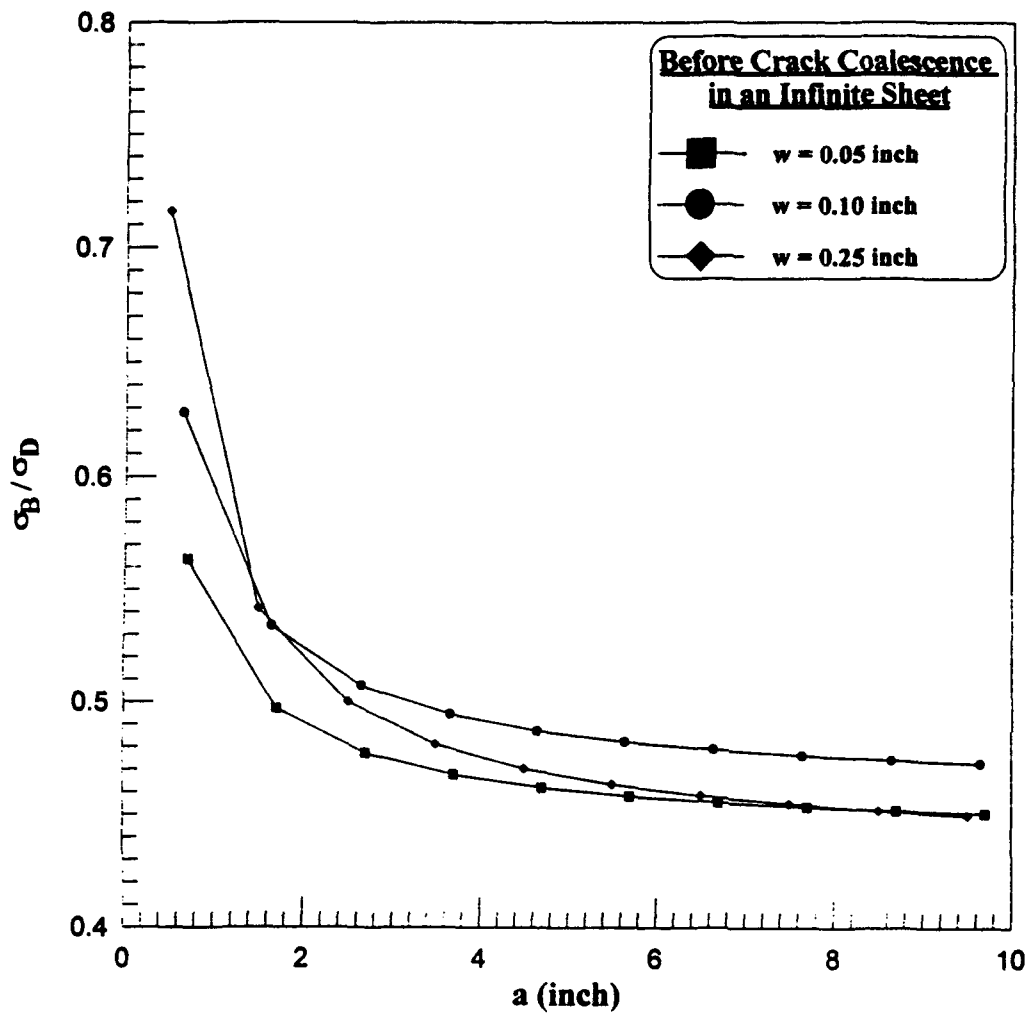


Figure 10. Ratio of strength levels for extending crack tips B and D before coalescence in three collinear crack configuration in an infinite sheet.

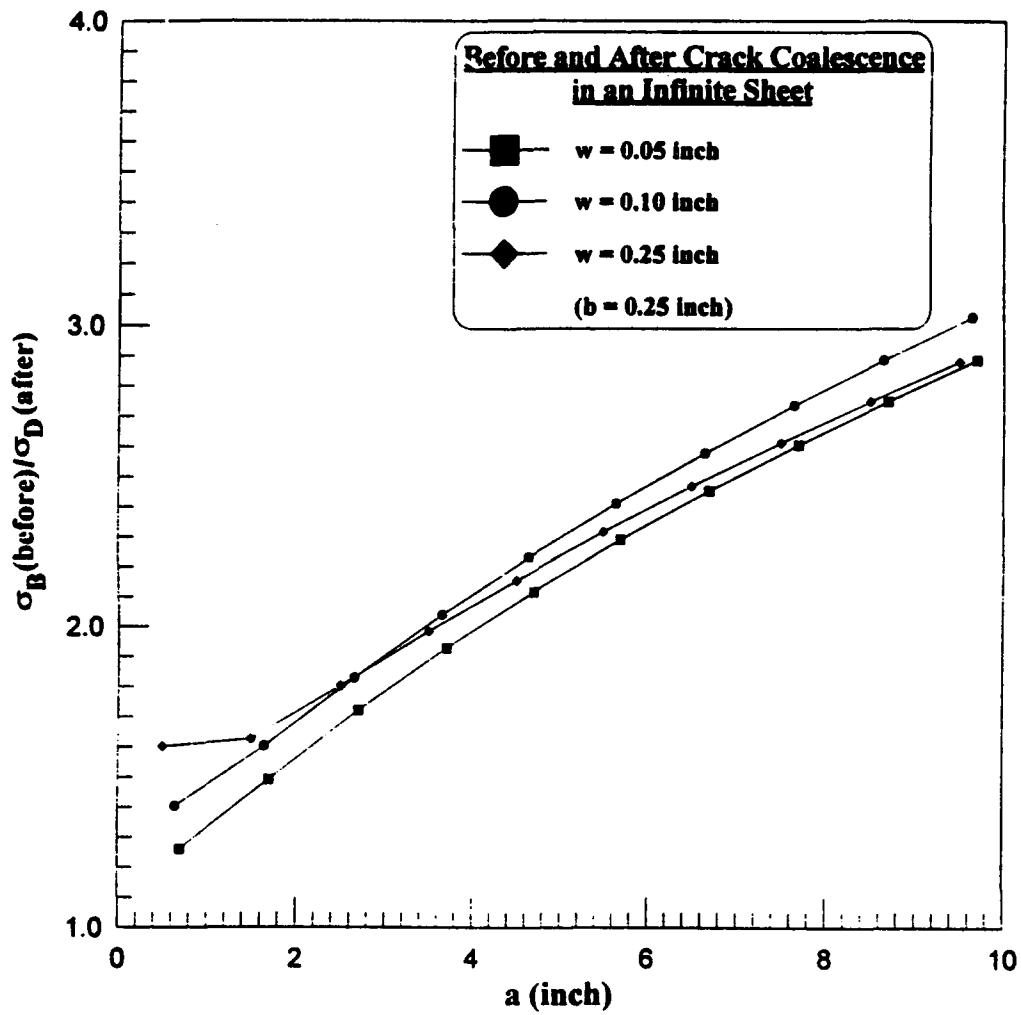


Figure 11. Effect of the largest crack size a on coalescence strength at crack tip B in three collinear crack configuration in an infinite sheet.

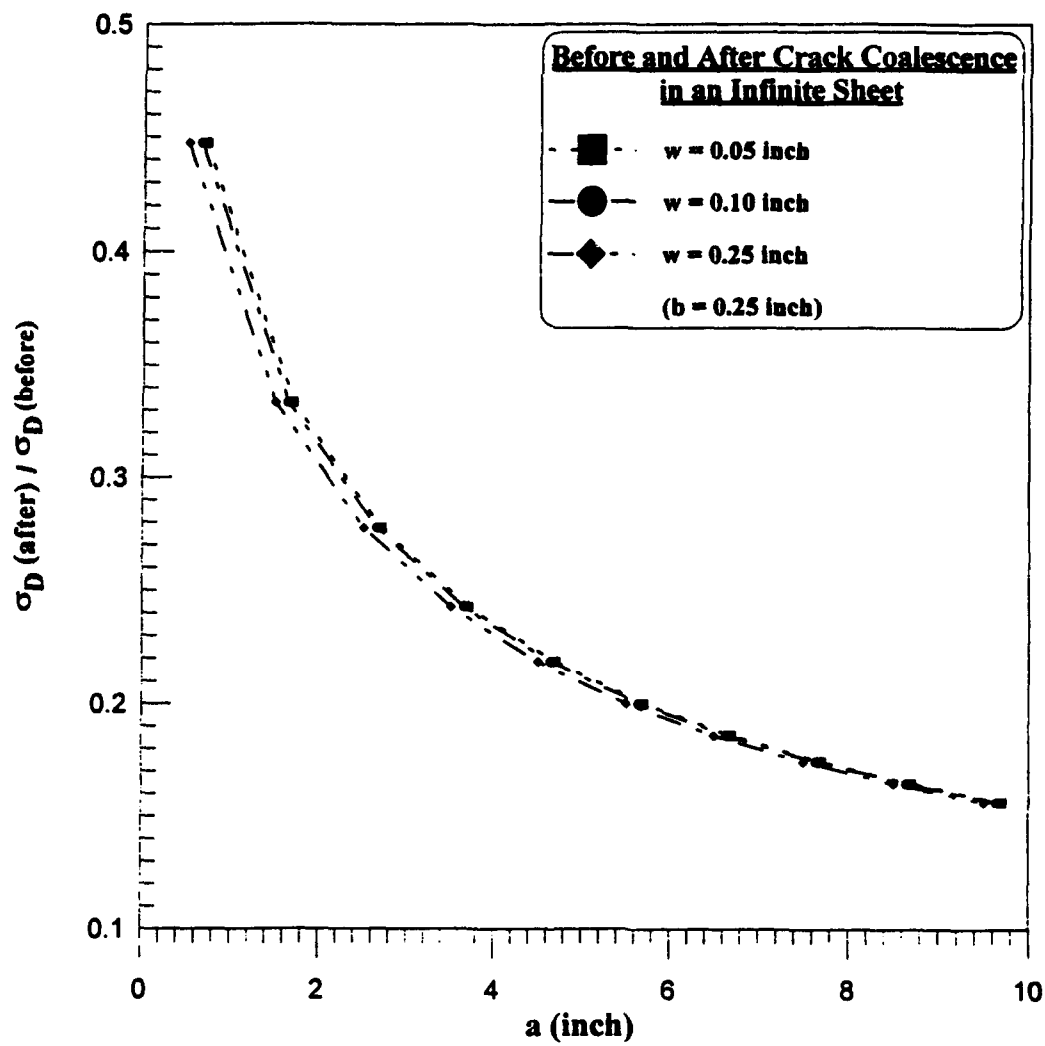


Figure 12. Effect of the largest crack size a on coalescence strength ratio (after/before) at crack tip A in three collinear crack configuration in an infinite sheet.

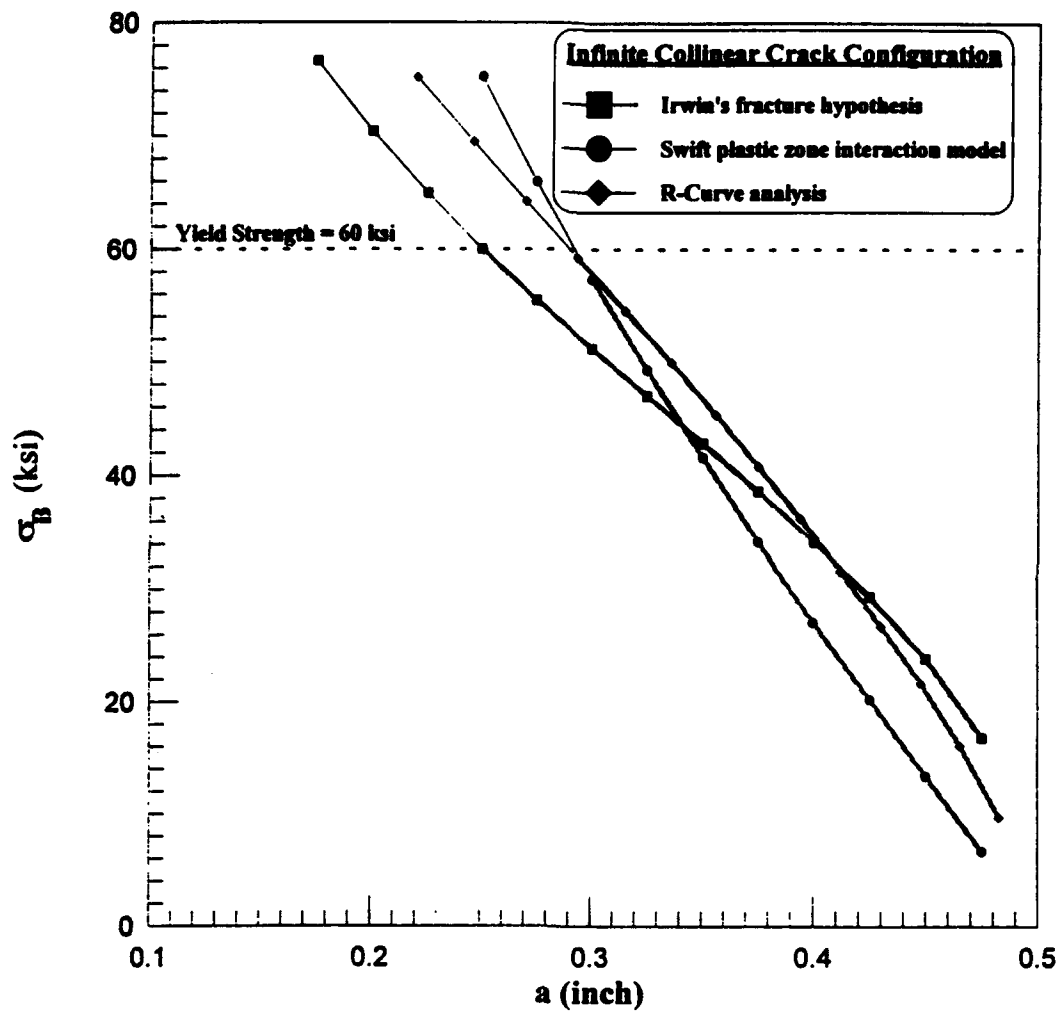


Figure 13. Effect of fracture criteria on the residual strength level in an infinite collinear cracks configuration.

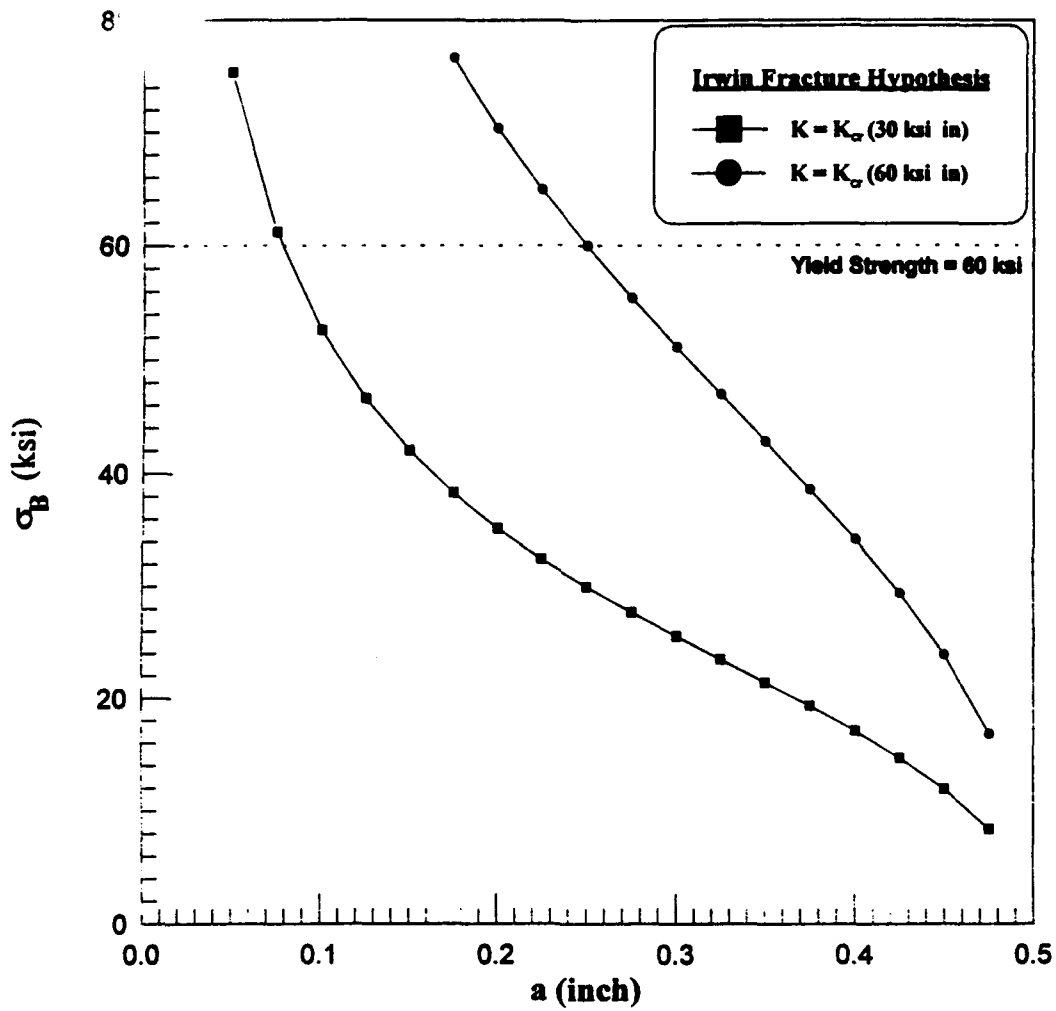


Figure 14. Effect of fracture toughness level on residual strength level in an infinite collinear cracks configuration.

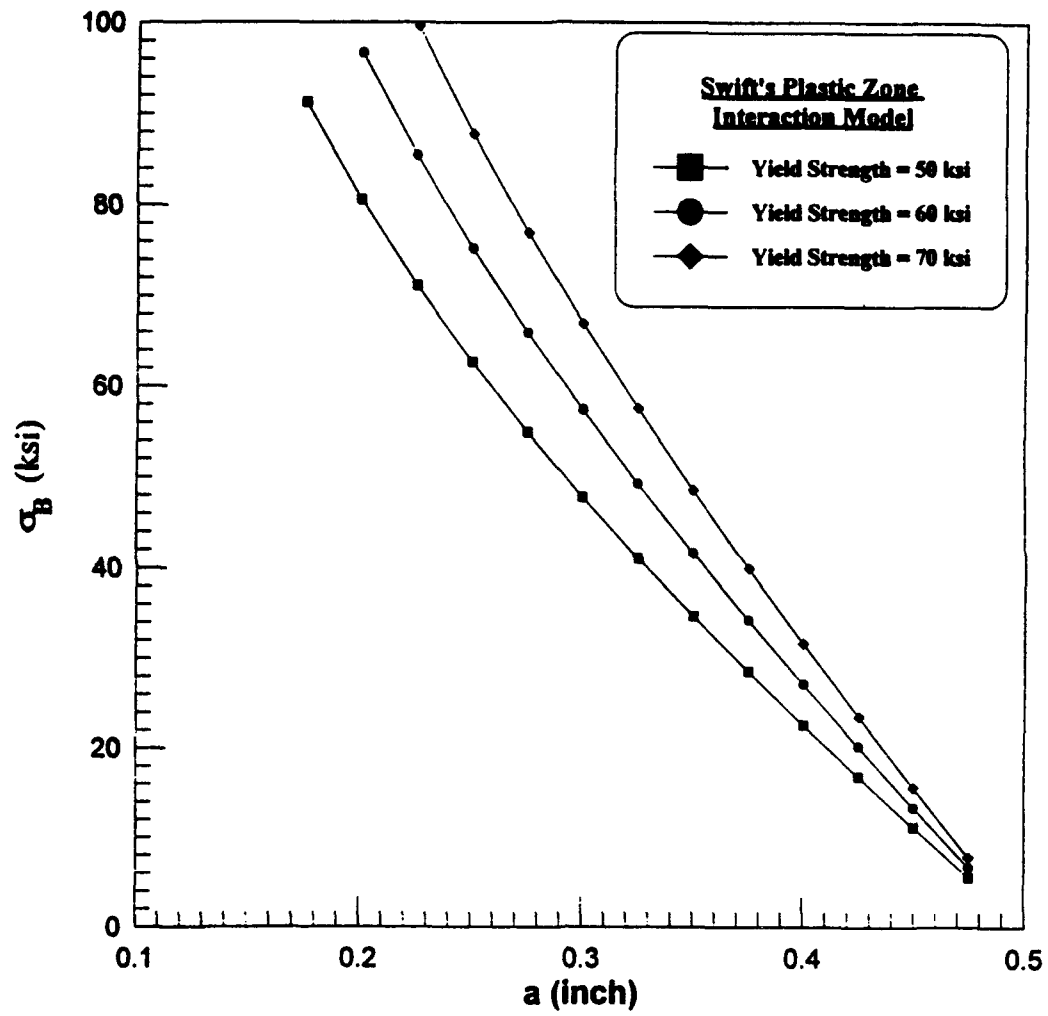


Figure 15. Effect of yield strength level on residual strength level in an infinite collinear cracks configuration.

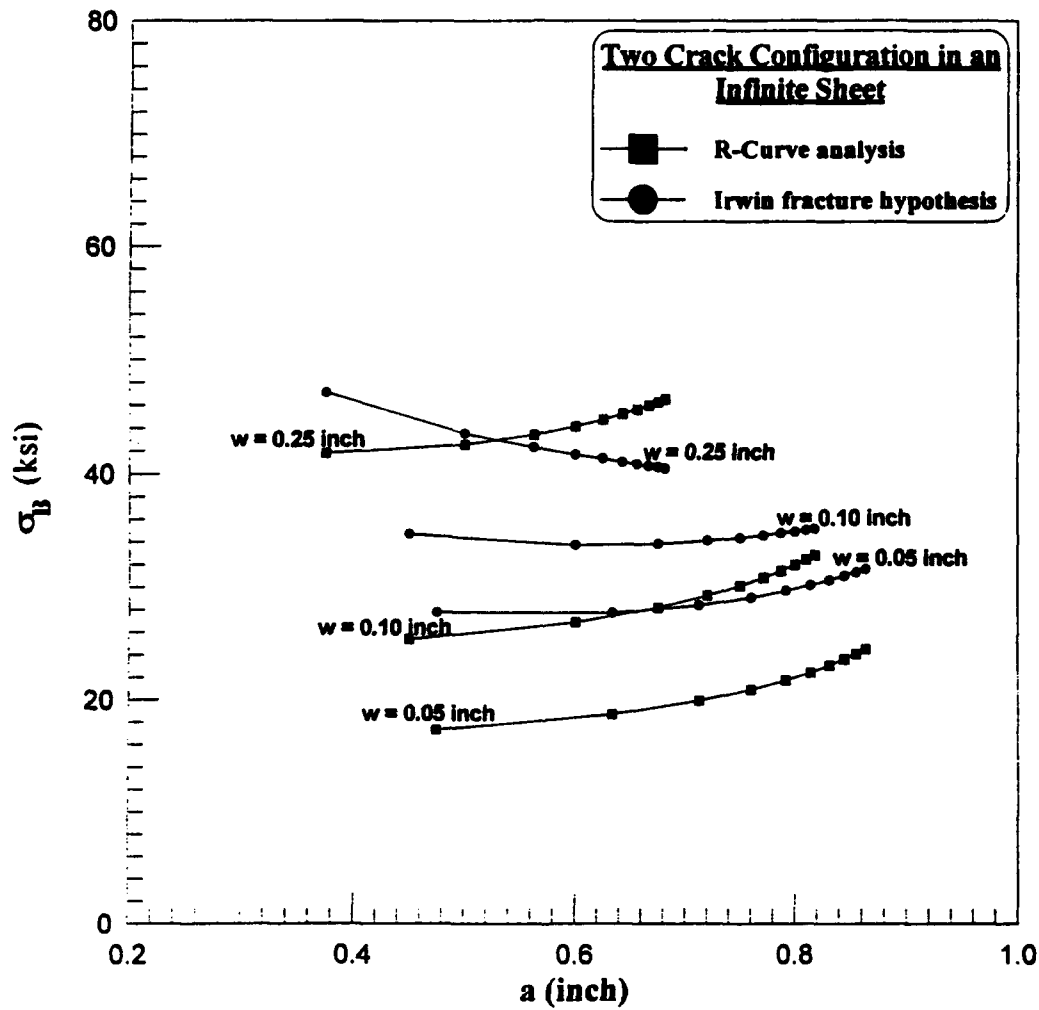


Figure 16. Comparison between R-curve and stress intensity factor criteria to identify the lower bound for the residual strength level in the two collinear crack configuration.

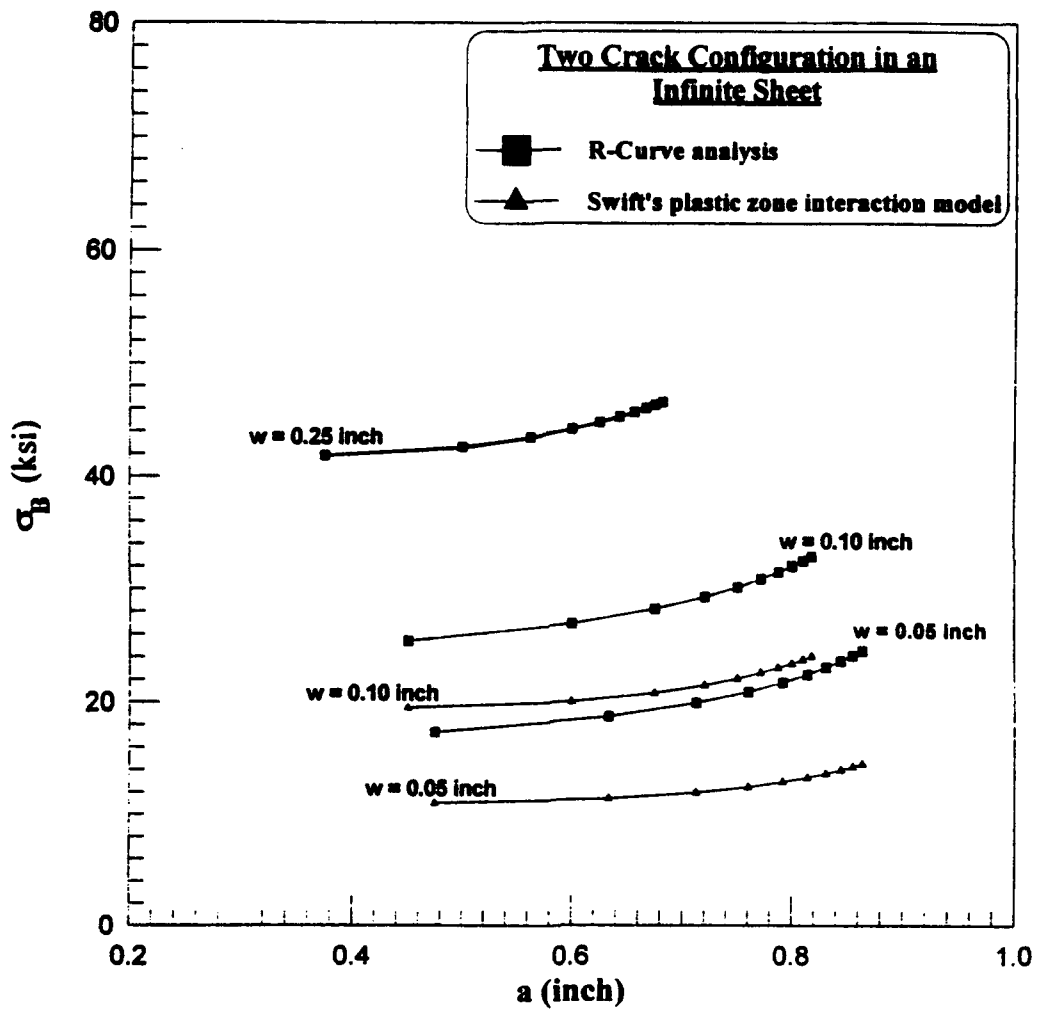
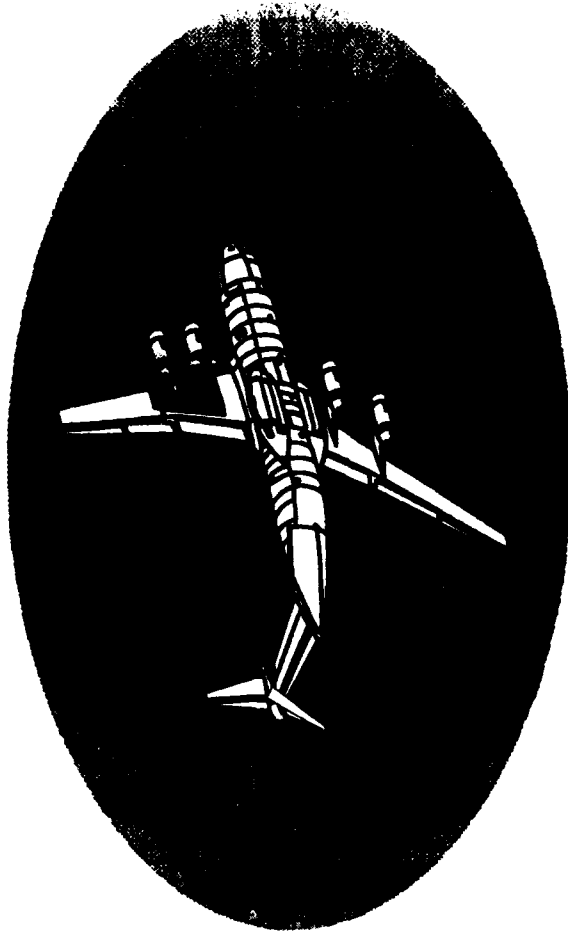


Figure 17. Comparison between R-curve and Swift plastic zone criteria to identify the lower bound for the residual strength level in two collinear crack configuration.

**Destructive Teardown
of
A C-141B Lower Surface Inner Wing**



**1993 USAF Structural Integrity
Program Conference
San Antonio, Texas
30 November - 2 December 1993**

R.E. Alford - WR-ALC

G.M. Weitz - LASC

TITLE PAGE

THIS PAPER WILL DESCRIBE THE TEARDOWN INSPECTION OF A C-141 INNER WING LOWER SURFACE, PERFORMED AT LOCKHEED AERONAUTICAL SYSTEM COMPANY (LASC), MARIETTA GA., 1993. THANKS TO RUSS ALFORD OF WR-ALC ENGINEERING, WITHOUT HIS HELP AND FUNDING FROM WR-ALC THIS WORK WOULD NOT HAVE BEEN POSSIBLE.

Overview

Why Did We Perform
the Teardown ?

Conditions of Aircraft
Before Teardown

How We Did
the Teardown

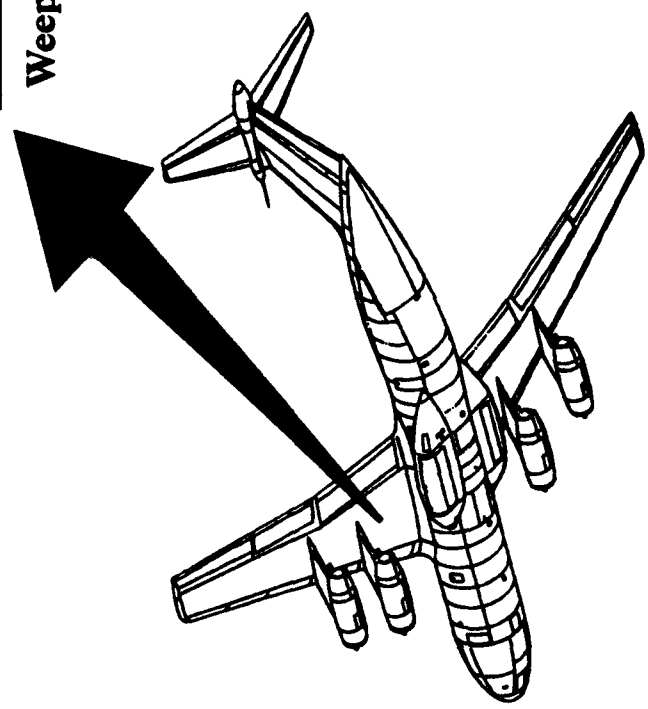
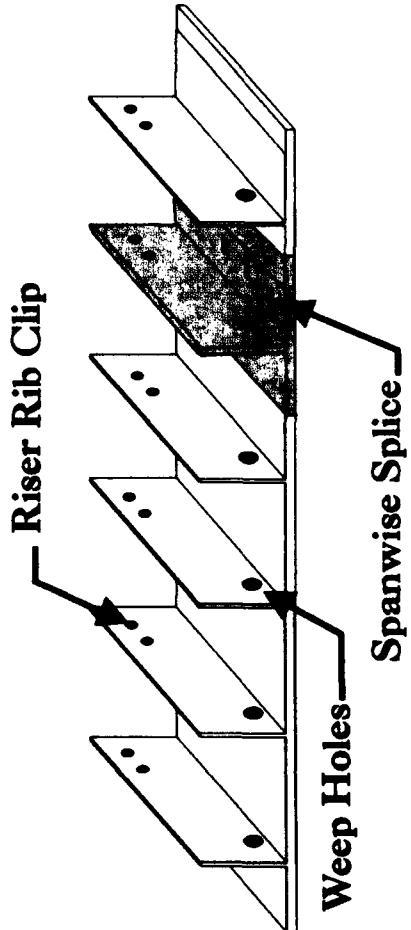
The Results and
How We Used Them

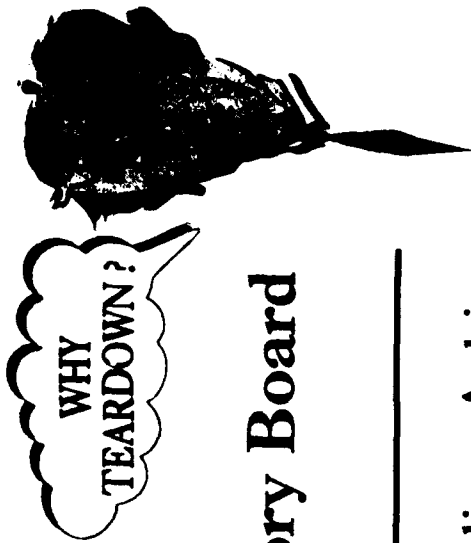
))

OVERVIEW

WHAT YOU WILL SEE IN THIS PRESENTATION ARE THE STEPS TAKEN IN A TEARDOWN INSPECTION.
FIRST, WHY ARE WE DOING THE TEARDOWN? WHAT WAS THE CONDITION OF THE AIRCRAFT BEFORE IT WAS
RETIRED? HOW IS A TEARDOWN PERFORMED? ONCE WE GATHERED THE DATA, WHAT DID WE DO WITH IT?
EACH OF THESE QUESTIONS WILL BE ANSWERED IN THIS PRESENTATION.

Typical Lower Surface Panel Structure





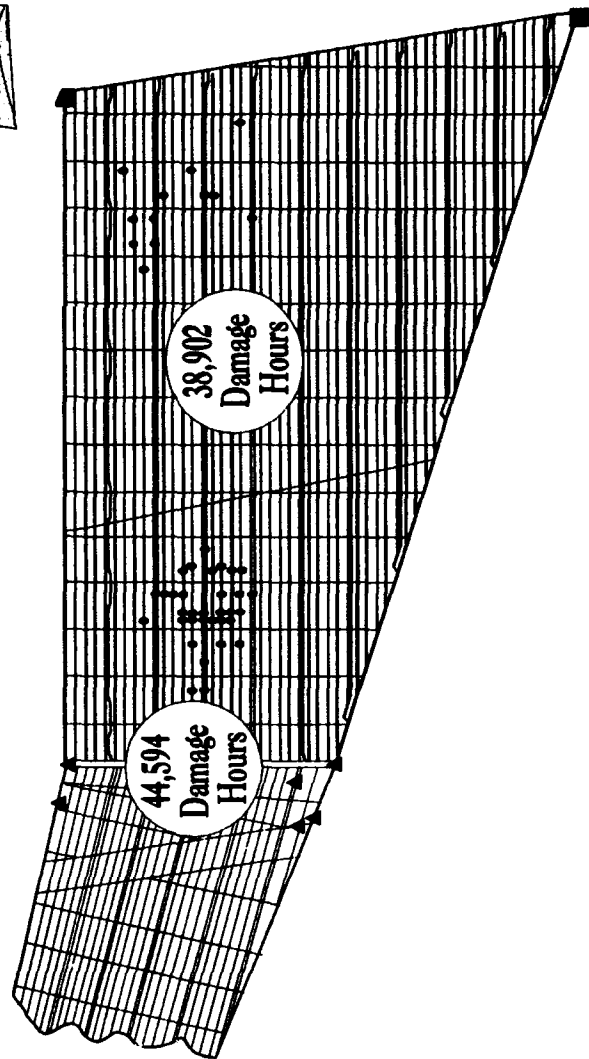
Directed By Scientific Advisory Board January 1993

- Can Lower Surface Spanwise Splices Achieve 45000 Damage Hours ?
- What is The Extent of Weep Hole Damage ?
- Are There Riser Rib Clip Cracks ?

WHY TEARDOWN

THE SCIENTIFIC ADVISORY BOARD (SAB) REQUESTED A TEARDOWN BE PERFORMED ON A C-141 INNER WING LOWER SURFACE. DUE TO NUMEROUS WEEP HOLE CRACKS FOUND IN SERVICE, IT WAS NECESSARY TO DETERMINE THE EXTENT OF WEEP HOLE CRACKING AND ITS EFFECT ON THE STRUCTURAL INTEGRITY OF THE WING. DURABILITY AND DAMAGE TOLERANCE ANALYSIS (DATA) OF THE LATE 1970'S PREDICTED THE LOWER SURFACE OF THE WING WOULD LAST 45,000 DAMAGE HOURS AS LONG AS RECOMMENDED MODIFICATIONS WERE PERFORMED. THIS PREDICTION WAS BASED ON CRACK GROWTH ANALYSIS OF THE LOWER SURFACE SPANWISE SPLICES. MOST MODIFICATIONS HAVE BEEN PERFORMED. HOWEVER, THE WEEP HOLE REAM AND COLD WORK MOD, RECOMMENDED IN 1983, HAS NOT BEEN ACCOMPLISHED. IN VIEW OF WEEP HOLE CRACKS, THIS RAISED THE QUESTION OF WHAT NOW WAS THE LIFE OF THE WING. THE CONDITION OF THE RISER RIB CLIP ATTACHMENT HOLES NEEDED TO BE EVALUATED ALSO. COMBINED WITH WEEP HOLE AND SPANWISE SPLICE CRACKS, THEY COULD CAUSE FAILURE OF THE WING LOWER SURFACE.

Condition of the Aircraft Before Teardown



(

(

CONDITION OF AIRCRAFT BEFORE TEARDOWN

AIRCRAFT 66-0186 WAS AT LASC FOR WS 405 DROP IN MAINTENANCE DURING 1992 AND 1993. INSPECTIONS HAD BEEN COMPLETED AND REPAIR WORK WAS IN PROGRESS, WHEN THE STOP WORK ORDER CAME FEBRUARY 2, 1993. CRACKS WERE FOUND IN 99 WEEP HOLES ON THE INNER WINGS: 48 ON THE RIGHT WING AND 51 ON THE LEFT WING. SEVERAL WS 405 REPAIRS WERE IN WORK. THE LOWER SURFACE HAD FIVE BEAM CAP, THREE WING PANEL AND THREE INNER/OUTER SPLICE FITTING REPAIRS. ALTHOUGH THE AIRCRAFT HAD EXPERIENCED ONLY 23,824 FLIGHT HOURS, DUE TO SEVERE USAGE, THE DAMAGE HOURS ON THE LOWER SURFACE WERE GREATER. THE INNER/OUTER WING TRANSITION AREA HAS 44,594 DAMAGE HOURS, THE GENERAL AREA HAS 38,902 DAMAGE HOURS. SIMILAR DAMAGE WAS ALSO BEING FOUND ON OTHER AIRCRAFT IN THE FLEET.

How We Did The Teardown



(

(

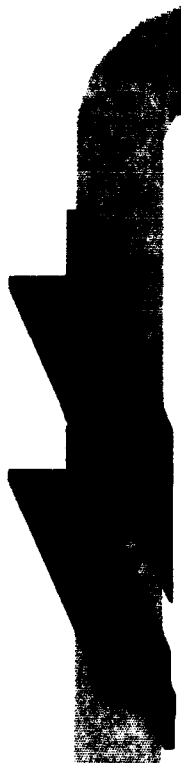
HOW WE DID THE TEARDOWN

SINCE THERE WAS AN URGENT NEED FOR THE TEARDOWN INFORMATION, THE WHOLE PROCESS, INCLUDING THE REPORT, WAS COMPLETED IN SIX MONTHS. THE PREPARATION BEGAN IN MARCH, WITH THE INSPECTIONS STARTING AT THE END OF APRIL. THE RESULTS OF THE NDI WERE CONSTANTLY BEING UPDATED AS THE INSPECTION PROGRESSED. WR-ALC AND MEMBERS OF THE SAB WERE UPDATED PERIODICALLY AS NEW INFORMATION WAS DISCOVERED. THE MOST TIME CONSUMING PORTION WAS THE ENHANCED VISUAL INSPECTIONS PERFORMED BY THE METALLURGICAL LABORATORY. THE REPORT WAS COMPLETED SEPTEMBER 2, 1993.

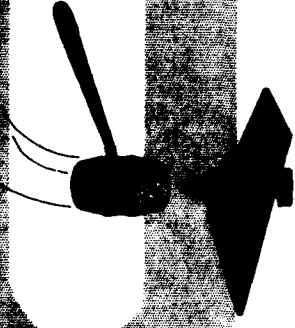
Teardown Sequence



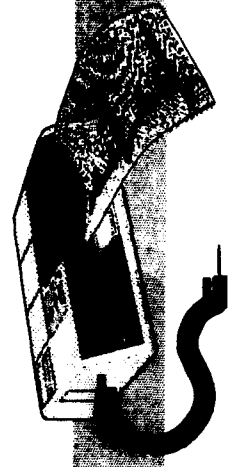
Remove Inner Wing



Spanwise Splices Removed And
Cut Into Sections

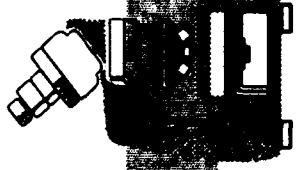


Remove Fastener
and Clean Holes



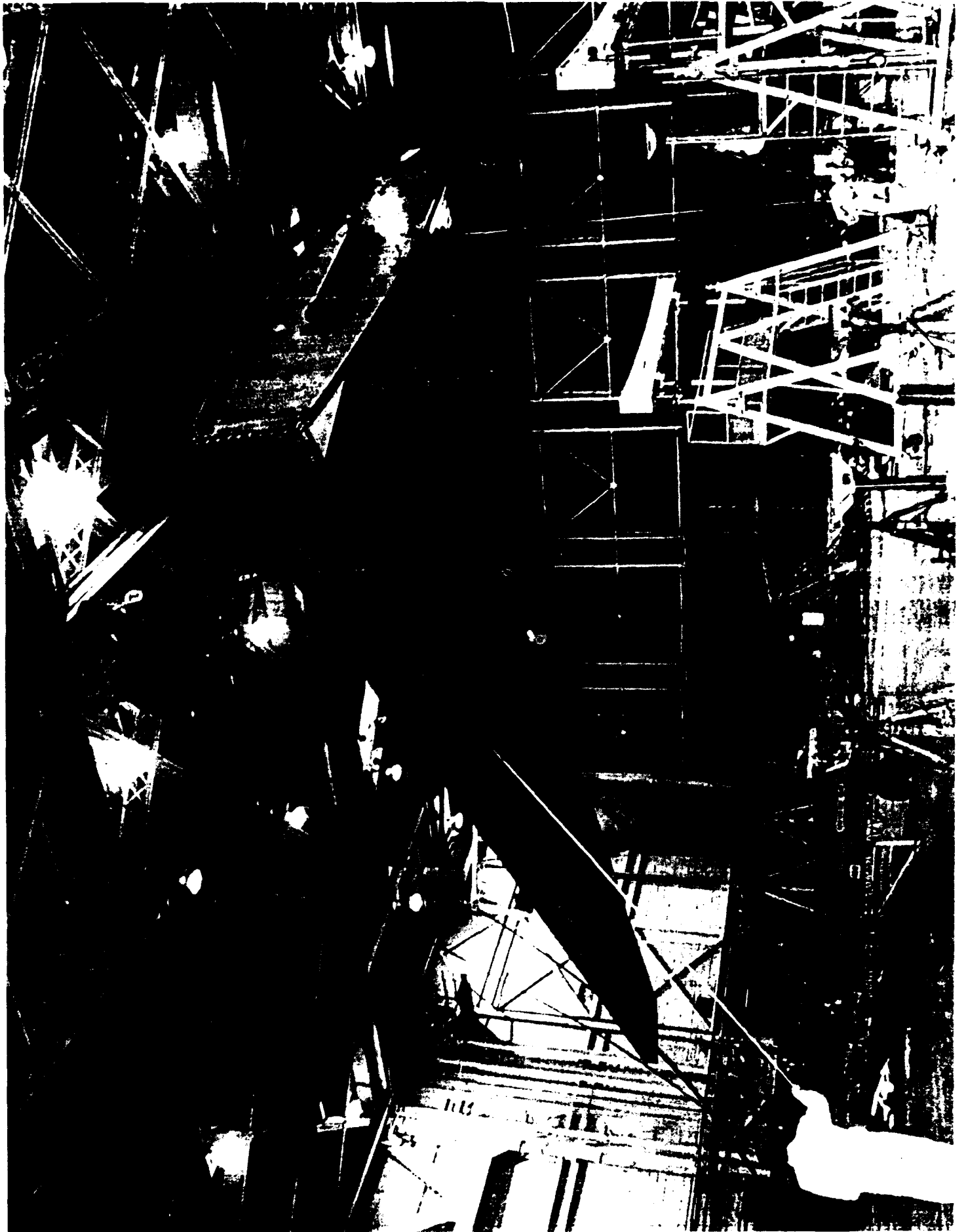
NDI - ABHEC

Metallurgical Lab For
Enhanced Visual Inspection



TEARDOWN SEQUENCE

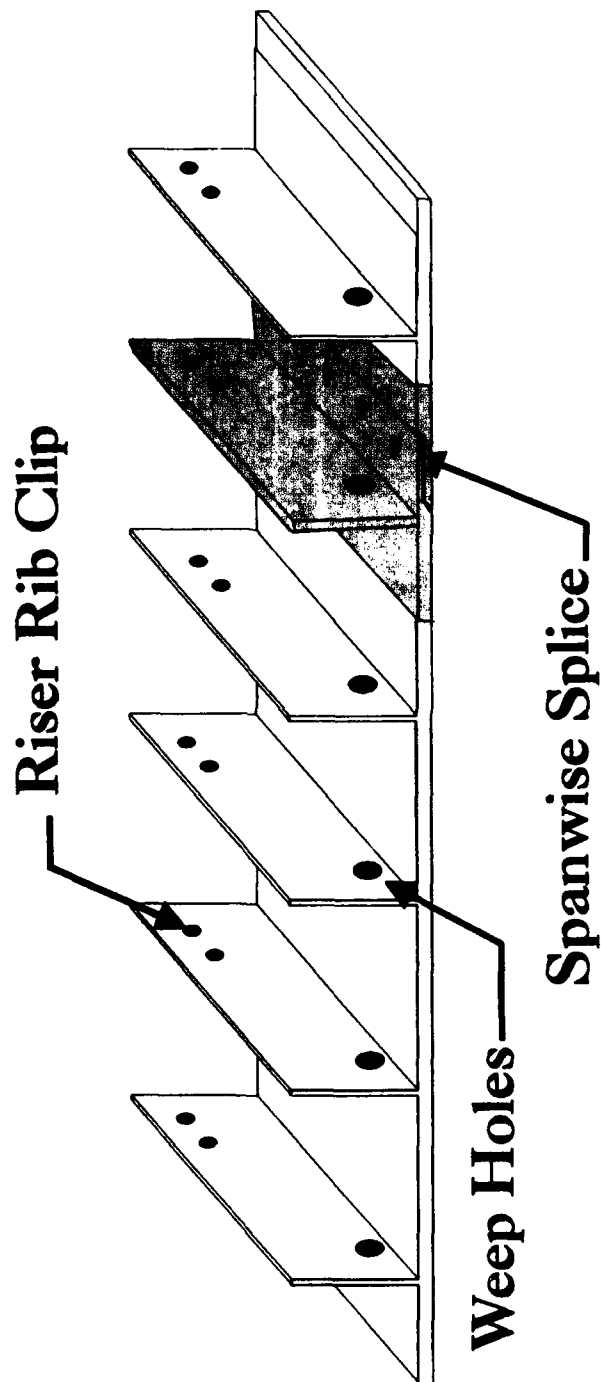
LEFT AND RIGHT WINGS WERE UNBOLTED AT THE CENTER/INNER WING JOINT. THE RIGHT INNER WING PANELS WERE UNBOLTED AT THE INNER/OUTER WING JOINT, AND CUT AT FRONT AND REAR BEAMS INBOARD OF THE JOINT. THE HOLES WERE NUMBERED AND SECTIONS MARKED FOR CUTTING ON THE RIGHT INNER WING LOWER SURFACE. THE SECTIONS WERE THEN CUT OUT. NDI STARTED AS SOON AS FASTENERS WERE REMOVED AND HOLES CLEANED IN EACH SECTION. WHEN NDI OF A SPLICE WAS COMPLETE, THE SPLICE WAS SENT TO THE METALLURGICAL LAB.



RIGHT WING BOX

THE RIGHT WING WAS REMOVED AND PLACED ON SUPPORTS, IN A STABLE POSITION SO THE INNER WING COULD BE REMOVED. ONCE THE INNER WING WAS REMOVED, IT WAS TURNED OVER SO THE LOWER SURFACE WAS UP. THE WING BOX WAS PUT ON A MOVABLE DOLLY AND TRANSPORTED TO THE TEST LAB FOR DISASSEMBLY AND INSPECTION.

Typical Lower Surface Panel Splice Section Removed



TYPICAL LOWER SURFACE PANEL

THE WING PANELS ON THE C-141, CONTAIN FIVE INTEGRALLY STIFFENED RISERS. THE MAIN EMPHASIS OF THE TEARDOWN WAS ON THE SPANWISE SPLICE AND RISER HOLES. IN EACH SPLICE SECTION ARE TWO PANELS FORMING A LAP JOINT AND A RISER. THE SHADED AREA SHOWS THE PANEL SECTION THAT RECEIVED NDI AND ENHANCED VISUAL INSPECTION.



SPANWISE SPLICE SECTIONS REMOVED

SEVEN SPANWISE SPLICES WERE MARKED AND DIVIDED INTO EIGHT SECTIONS EACH. THE SECTIONS STARTED AT EVERY OTHER BOX RIB. HOLE NUMBERS AND ORIENTATION WERE SCRIBED ON THE PANELS BEFORE ANY PARTS WERE CUT. THIS WAS DONE SO THAT WHEN THE PARTS WERE STRIPPED AND ETCHED THEY COULD STILL BE IDENTIFIED. THE SPANWISE SPLICES PLUS THE REAR BEAM WERE THEN CUT FROM THE RIGHT WING LOWER SURFACE. ONCE THE SPLICES WERE REMOVED, THEY WERE CUT INTO EIGHT SECTIONS. THIS PHOTOGRAPH SHOWS THE SEVEN SPLICES REMOVED, AND THE REAR BEAM BEING PREPARED FOR REMOVAL. THE REMAINING PANEL SECTIONS WERE LATER REMOVED FOR WEEP HOLE AND RISER RIB CLIP ATTACHMENT HOLE NDI.



SAMPLE SPANWISE SPLICE SECTION

THE SPLICES WERE CUT INTO EASILY HANDLED 48" SECTIONS. NDI STARTED AS SOON AS FASTENERS WERE REMOVED AND HOLES CLEANED IN A SECTION. WHEN A CRACK INDICATION WAS FOUND THE HOLE WAS MARKED AND A PHOTOGRAPH OF THE SECTION TAKEN. ALL OPEN HOLES IN THE SPLICE SECTION WERE INSPECTED.



FASTENER REMOVAL

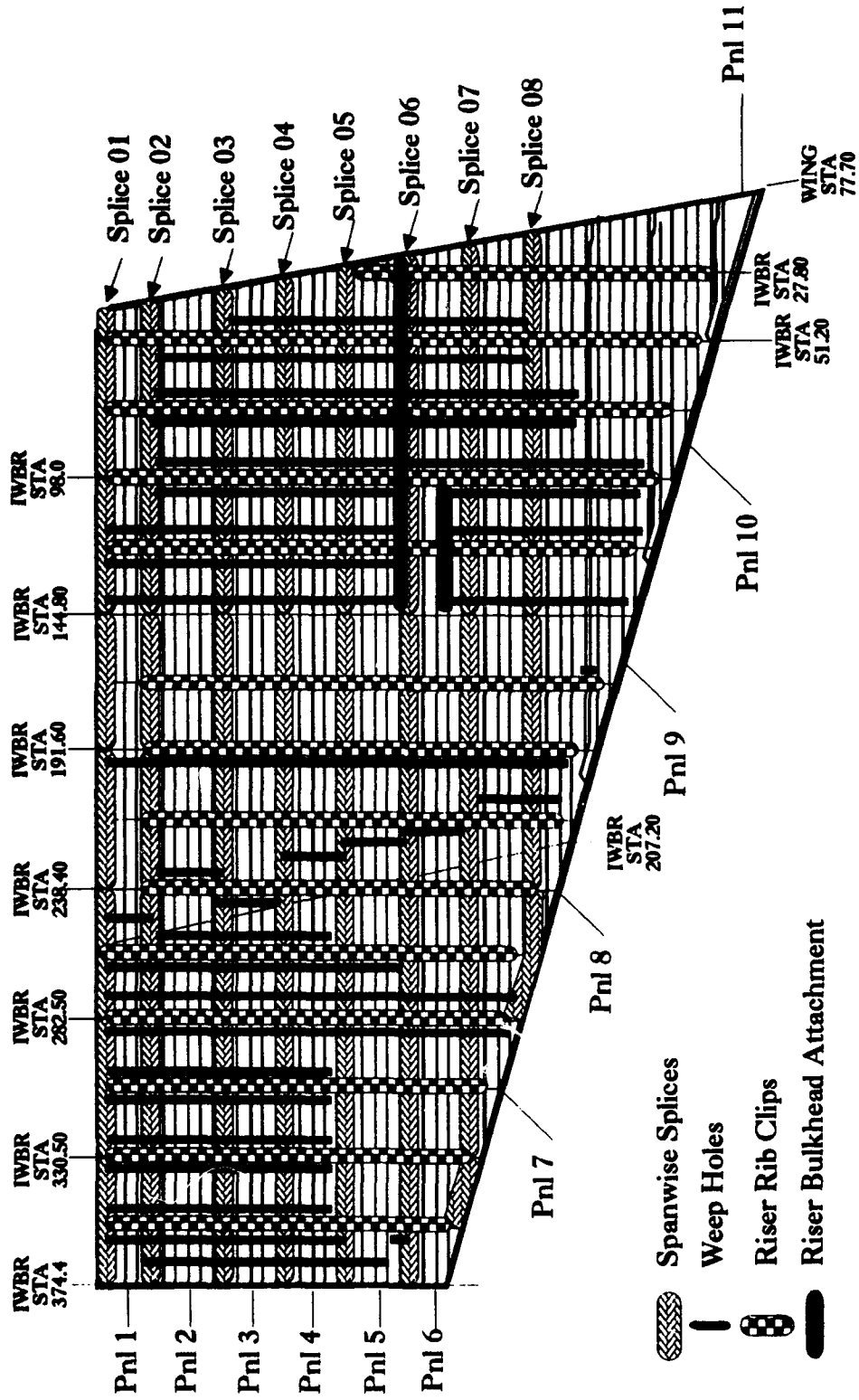
THE TAPER LOCK FASTENER IS AN INTERFERENCE FIT FASTENER AND MUST BE REMOVED BY KNOCKING OUT WITH A Mallet. SPECIAL CARE MUST BE USED SO THAT THE FASTENER HOLE IS NOT DAMAGED WHEN THE FASTENER IS REMOVED. IF THE HOLE IS DAMAGED, FLAW DATA COULD BE LOST. IN ORDER NOT TO DAMAGE THE HOLE, A TOOL WAS SCREWED ON TO THE THREADED END OF THE FASTENER. THIS PREVENTS THE TAIL OF THE FASTENER FROM BEING DEFORMED, SO THAT IT WILL PASS THROUGH THE HOLE WITHOUT SCORING THE HOLE WALL. THE HOLES WERE THEN CLEANED WITH A NONABRASIVE BRISTLE BRUSH.



AUTOMATIC BOLT HOLE EDDY CURRENT

ALL HOLES WERE INSPECTED BY LOCKHEED AUTOMATIC BOLT HOLE EDDY CURRENT (ABHEC). AN ED-530 MANUAL EDDY CURRENT MACHINE WAS USED FOR DETERMINING THE SURFACE CRACK LENGTHS. THE PANEL SEGMENTS WERE CUT SO THERE WAS EASY ACCESS TO ALL RISER HOLES AND SPANWISE SPLICE HOLES. EDDY CURRENT SURFACE SCAN WAS PERFORMED AROUND HOLES WITH RIVETS, THE RIVETS WERE NOT REMOVED.

NDI Inspection Areas - Right Wing Lower Surface

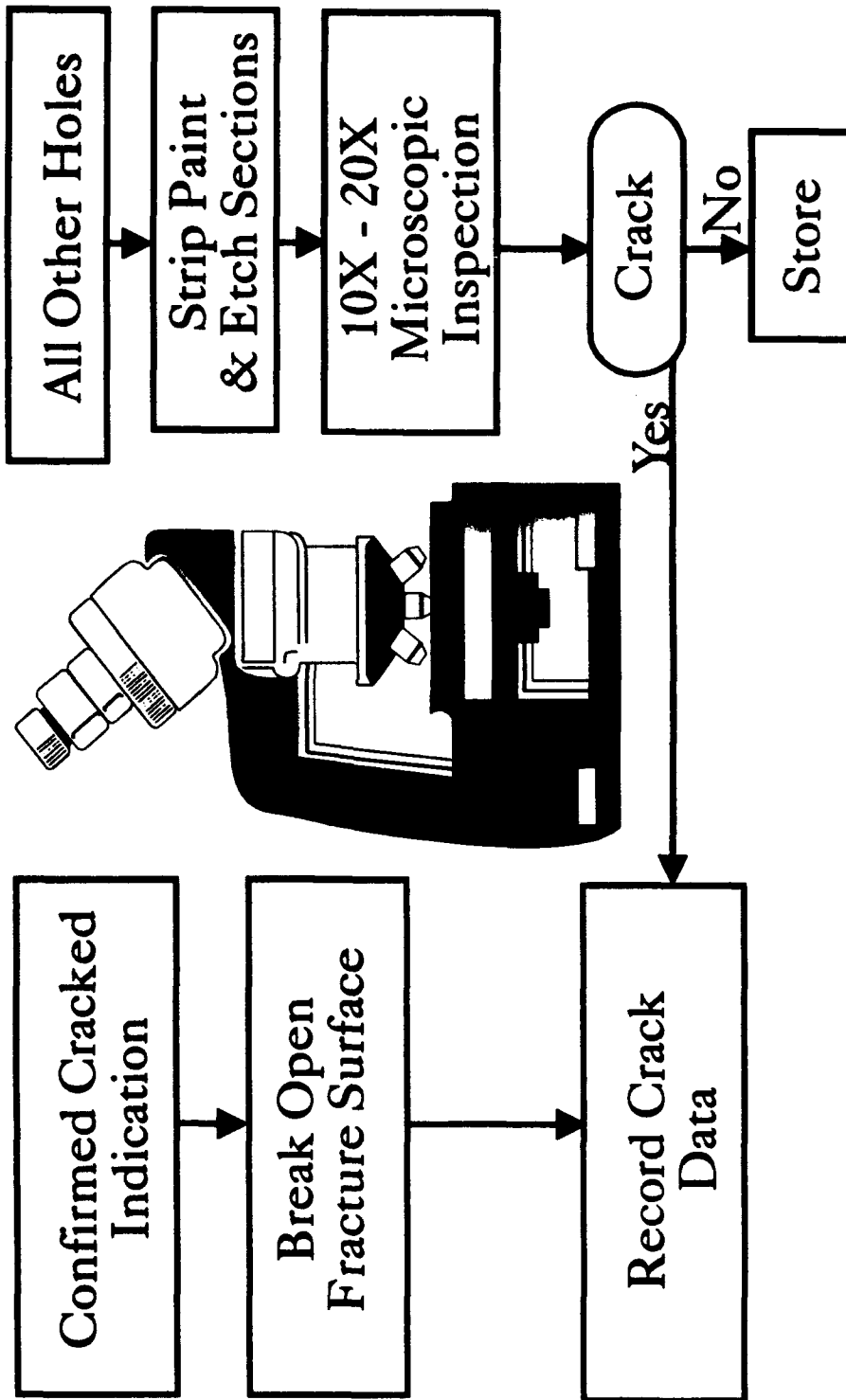


NDI INSPECTION AREAS - RIGHT WING LOWER SURFACE

THESE WERE THE AREAS ABHEC INSPECTION WAS PERFORMED ON THE RIGHT WING:

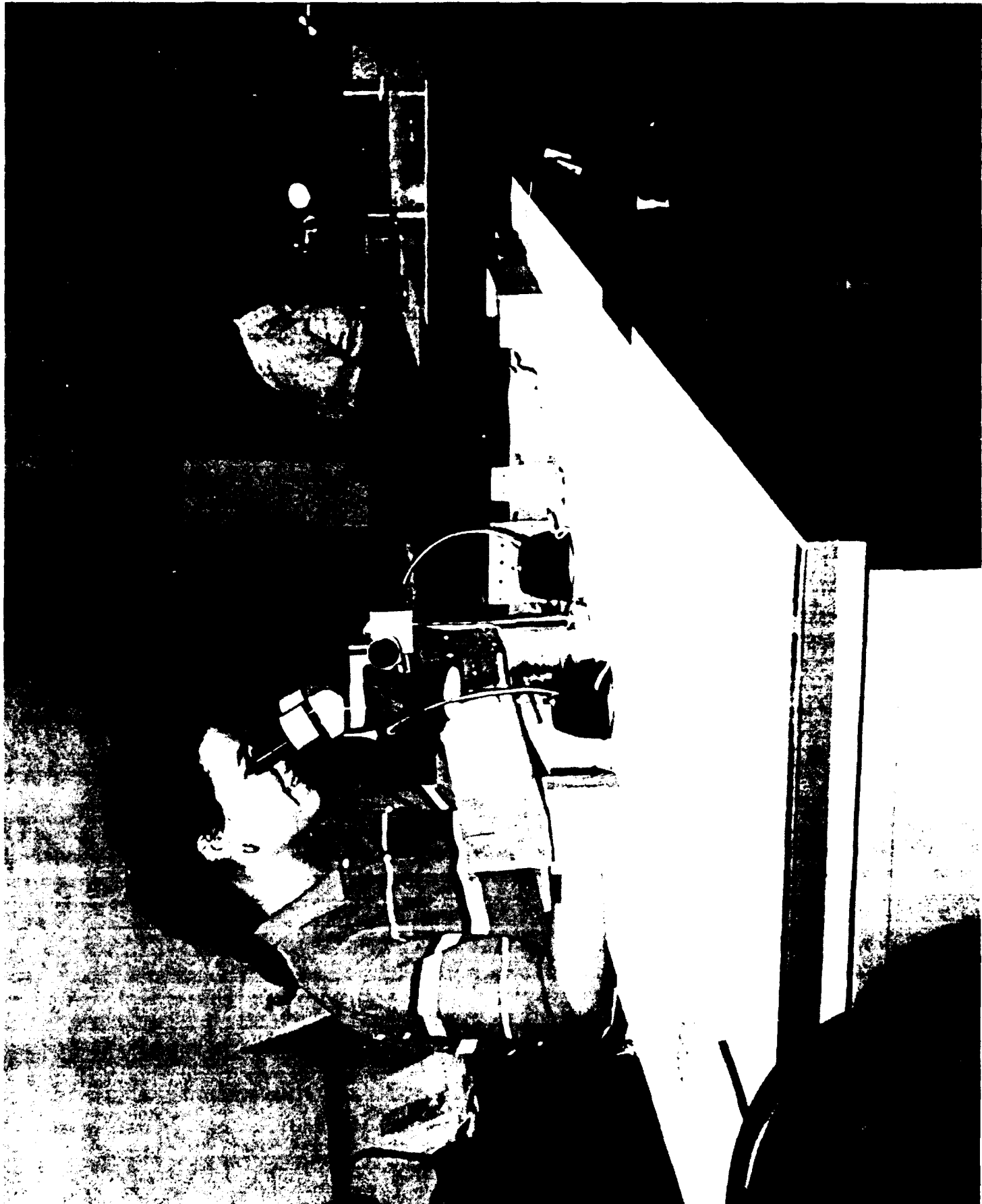
1. SEVEN SPANWISE SPLICES (SPLICE 02 - 08)
2. ALL HOLES COMMON TO THE REAR BEAM (SPLICE 01)
3. ALL RISER WEEP HOLES
4. ALL RISER RIB CLIP ATTACHMENT HOLES
5. ALL RISER BULKHEAD ATTACHMENT HOLES

Enhanced Visual Inspection



ENHANCED VISUAL INSPECTION

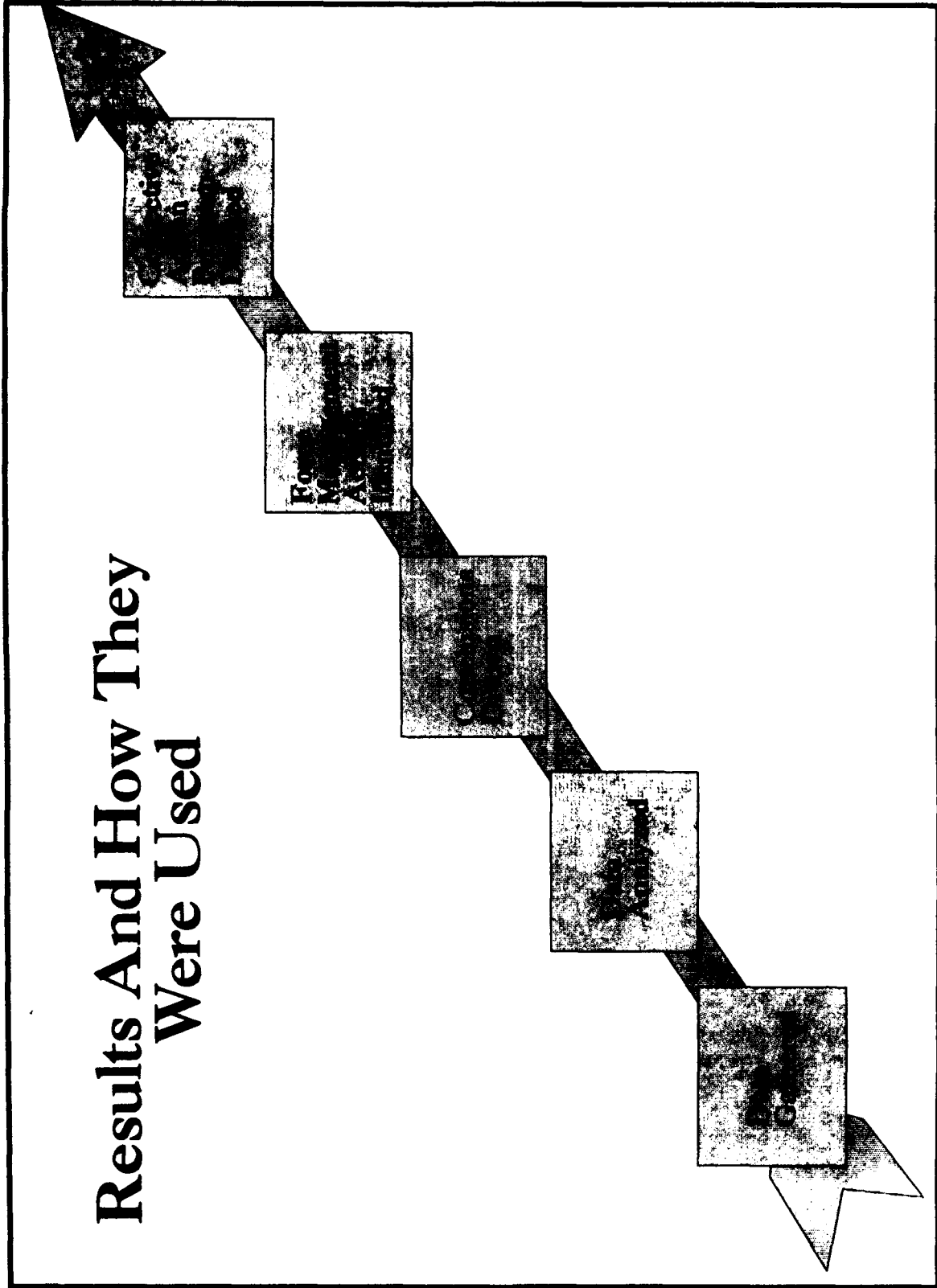
AFTER NDI COMPLETED A SPLICE , AND ALL CRACK INDICATIONS WERE CUT OUT, THE SPLICE WAS SENT TO THE METALLURGICAL LAB. IF THE CRACK INDICATIONS WERE CONFIRMED BY TWO METALLURGIST, THE FRACTURE SURFACES WERE BROKEN OPEN AND CRACK CODES AND LENGTHS RECORDED. THE REMAINING PARTS IN THE SECTIONS WERE SENT TO BE STRIPPED OF PAINT AND ACID ETCHED. THE ETCHING REMOVES THE ANODIZE LAYER AND BRINGS OUT THE CRACKS



MICROSCOPIC EXAMINE

ONCE THE PARTS WERE ETCHED, EVERY HOLE WAS INSPECTED USING A MICROSCOPE WITH MAGNIFICATION OF 10 TO 20 POWER. BOTH SURFACES OF THE PART AROUND THE HOLE, AS WELL AS THE HOLE WALL WERE INSPECTED. MIRRORS MOUNTED ON DOWELS AT 45°, WERE USED TO AID IN THE INSPECTION OF THE HOLE WALLS. WHILE VIEWING THE HOLE THROUGH THE MICROSCOPE, DOWELS OF THE APPROPRIATE DIAMETER WERE INSERTED IN THE HOLES AND ROTATED. WHEN A SUSPECTED CRACK WAS FOUND A SECOND METALLURGIST WOULD CONFIRM OR DENY IT'S EXISTENCE. ALL CONDITIONS OBSERVED WERE THEN RECORDED. THIS WOULD INCLUDE CRACK LENGTH, CRACK TYPE AND ANY OTHER PERTINENT DATA ABOUT THE HOLE.

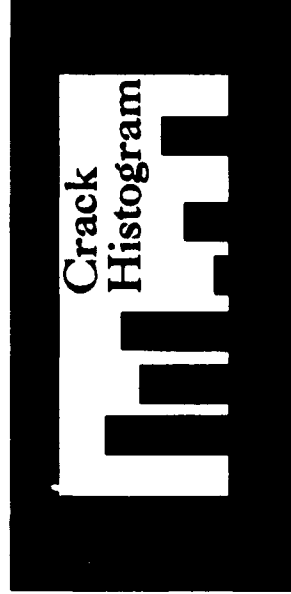
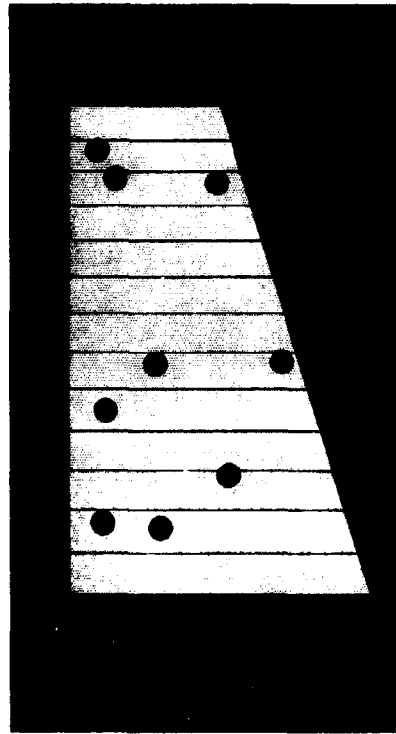
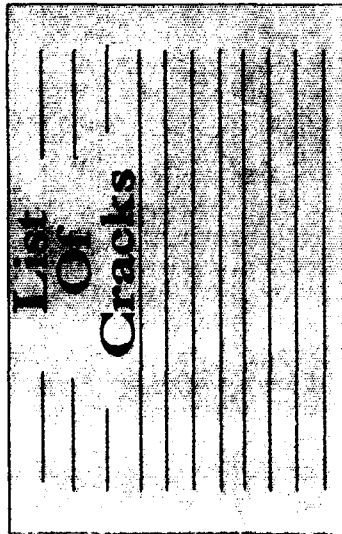
Results And How They Were Used



RESULTS AND HOW THEY WERE USED

ONCE THE DATA WAS GATHERED AND ORGANIZED, THE ANALYSIS BEGAN. BASED ON THIS ANALYSES, CONCLUSIONS WERE DRAWN, ACTION ITEMS WERE IDENTIFIED AND A CORRECTIVE ACTION PROGRAM WAS DEFINED.

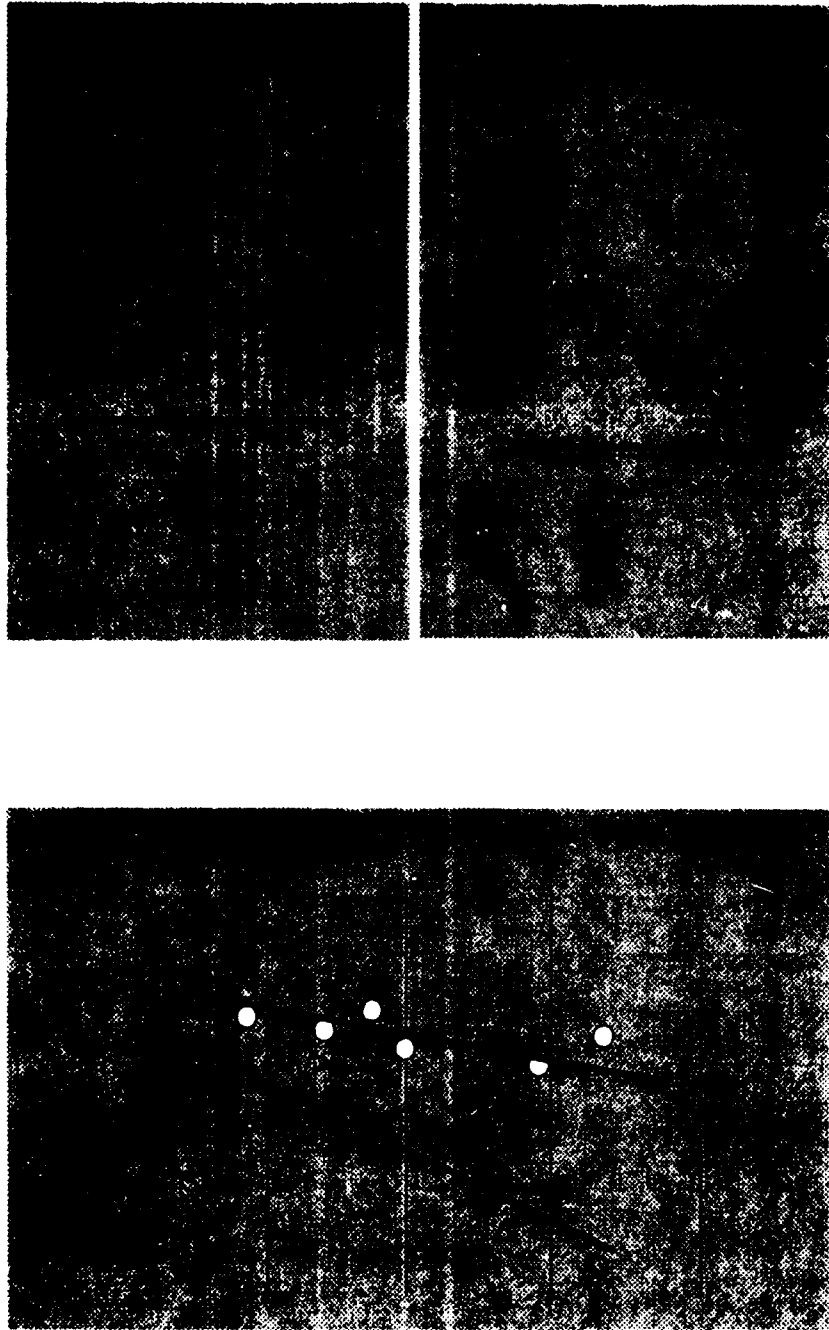
Data Gathered



DATA GATHERED

THERE WAS A TREMENDOUS AMOUNT OF DATA GATHERED FROM THE APPROXIMATELY EIGHT THOUSAND HOLES INSPECTED . IN ORDER FOR THIS FLAW DATA TO BE ORGANIZED IN A USEABLE MANNER, IT WAS ENTERED INTO COMPUTER FILES. THE DATA COULD THEN BE EASILY BROKEN DOWN INTO DIFFERENT TYPES OF CRACKS (WEEP HOLES, SPANWISE SPLICE HOLES, RIB CLIP ATTACHMENT HOLES, ETC.). SUMMARIES OF EACH TYPE OF CRACK WERE THEN COMPILED. FROM THIS LIST THE CRACK LOCATIONS WERE PLOTTED BY COMPUTER ON A PLAN VIEW OF THE WING. COMPUTER GENERATED PLOTS WERE MADE OF EACH CRACK TYPE FOR ANY CONDITION SELECTED. FINALLY HISTOGRAMS OF THE NUMBER OF CRACKS VERSUS CRACK LENGTHS WERE MADE FOR EACH TYPE OF CRACK TO PICTORIALLY PRESENT THIS DATA.

Data Analyzed



DATA ANALYZED

THE THREE AREAS OF INTEREST ANALYZED WERE; WEEP HOLES, SPANWISE SPLICE HOLES AND RISER RIB CLIP ATTACHMENT HOLES. USING THE COMPILED CRACK DATA, STATISTICAL CRACK DISTRIBUTIONS AND CRACK GROWTH ANALYSIS WERE PERFORMED ON THE THREE CRACK TYPES. THIS INFORMATION WAS THEN USED TO PERFORM STANDARD RISK CALCULATIONS. THIS PRODUCED THE PROBABILITY OF FAILURE VERSUS ACCUMULATED DAMAGE HOURS FOR THE THREE CRACK TYPES.

Conclusions Drawn

- **Objectives Of Teardown Satisfied ?**
- **Service Life Limits Identified ?**
- **Multi-Site And/Or Multi-Element Damage Observed ?**
- **Statistical Correlations Made With Force Aircraft ?**

CONCLUSIONS DRAWN

ALL OBJECTIVES OF THE TEARDOWN WERE MET AND NO SURPRISES DISCOVERED. THE SERVICE LIFE LIMIT WAS IDENTIFIED. AS ANTICIPATED THERE WAS MULTI-SITE AND MULTI-ELEMENT DAMAGE OBSERVED IN THE WEEP HOLES. TEARDOWN AIRCRAFT 66-0186 WAS CORRELATED WITH THE FORCE AND THE STATISTICAL AND RISK ANALYSIS CAN BE USED FOR PROJECTING DAMAGE IN THE REST OF THE FORCE.

Force Management Actions Identified

- **Selected Aircraft Removed From Service For Immediate Inspections**
- **Remaining Aircraft Scheduled For Inspections Over A Period Of 90 Days**

These Actions Required Development Of Special NDI Procedures & Equipment

FORCE MANAGEMENT ACTIONS IDENTIFIED

HIGH DAMAGE HOUR AIRCRAFT WERE REMOVED FROM SERVICE DUE TO THE HIGH PROBABILITY OF FAILURE BECAUSE OF WEEP HOLE CRACKS. THE REMAINING AIRCRAFT (NOT RETIRED) ARE TO BE INSPECTED WITH IN A PERIOD OF NINETY DAYS. WR-ALC DEVELOPED A NEW NDI PROCEDURE TO INSPECT THE WEEP HOLES INSIDE THE WING TANKS. THIS PROCEDURE REQUIRED MODIFIED EQUIPMENT AND PRODUCTION OF A NEW TOOL. THIS WAS NECESSARY TO FIND THE SMALL CRACKS THAT DEGRADE THE FAIL SAFE CAPABILITY OF THE STRUCTURE.

Corrective Action Program Defined

- **Repair Actions Categorized**
 - ▶ **Hole Ream (And/Or Coldwork)**
 - ▶ **Composite Patches**
 - ▶ **Panel Segment (Whole Panel If Required)**

- **Repair Sites Selected -- Repair Activity Initiated**

CORRECTIVE ACTION PROGRAM DEFINED

ENGINEERING (WR-ALC AND LASC) DEFINED THREE REPAIR METHODS FOR WEEP HOLE CRACKS. FOR SMALL CRACKS, HOLES WILL BE REAMED UNTIL THE CRACK IS REMOVED AND COLD WORKED TO RETARD ANY FURTHER CRACK INITIATION. FOR ISOLATED LARGE CRACKS COMPOSITE PATCHES WILL BE INSTALLED. LARGE MULTIPLE CRACKS WOULD REQUIRE PANEL SEGMENTS OR WHOLE PANEL REPLACEMENTS. WR-ALC HAS SELECTED REPAIR SITES AND REPAIR ACTIVITY HAS BEEN INITIATED.

THIS TEARDOWN PROVIDED VALUABLE INFORMATION WHICH WAS USED TO MAKE CRITICAL SAFETY OF FLIGHT DECISIONS FOR THE C-141B. THIS PLAN WAS A JOINT EFFORT OF LASC AND AIRFORCE ENGINEERS FOR MANAGING THE FORCE. SPECIFIC DETAILS OF THE TEARDOWN AND SUBSEQUENT FORCE MANAGEMENT INITIATIVES ARE OBTAINABLE FROM WARNER ROBINS C-141 ENGINEERING BRANCH (LJLE).



Holistic Life Prediction Methodology for Powder Metal Engine Components

364

1993 USAF Structural Integrity Conference
30 November - 2 December, 1993
San Antonio, TX

P.A. Domas
GE Aircraft Engines



Overview

Powder metal turbine disk alloy fatigue life prediction

- Must recognize multiple fatigue crack initiation modes
 - Grain facet ("classic") fatigue
 - Ceramic inclusions
 - Processing induced or other surface anomalies
- Necessitates
 - New methods (probabilistic fracture mechanics)
 - New criteria (probability of fracture)
 - Heightened awareness of material processing life influence

Alternate life prediction methods emerge

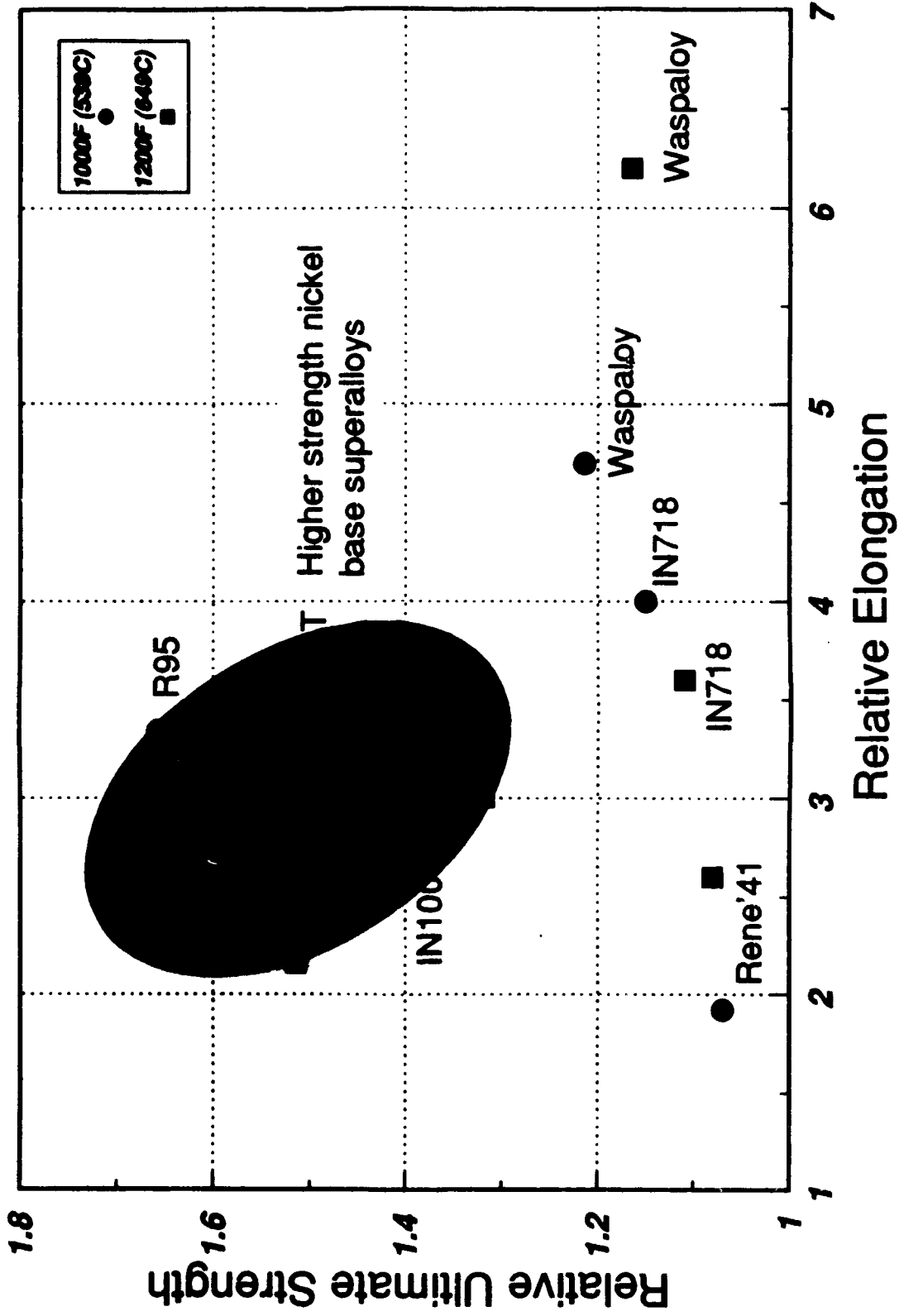


Powder Alloy Characteristics

- **Clear superiority in high temperature capability**
 - **High Strength and Creep resistance**
 - **1200-1300F (649-704C) operating temperature**
- **PM alloys exhibit:**
 - **Uniform grain size**
 - **Freedom from chemical segregation**
 - **High cleanliness**
 - **Excellent ultrasonic inspectability**
- **Fatigue behavior influenced by grain size, compositions, frequency and size of inherent inclusions, and surface condition**



Recognizing material characteristics





Ceramic inclusions can influence fatigue life

Seeded PM alloy low cycle fatigue
1200F (650C)

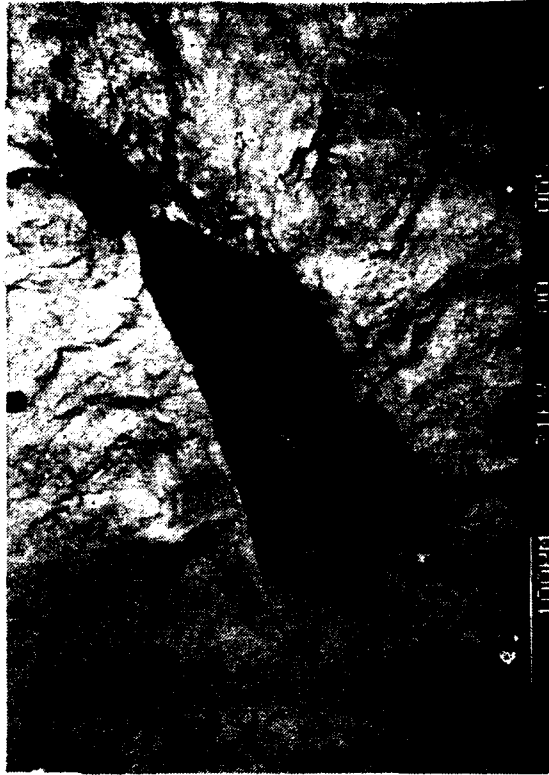
Surface initiation
41 mils² area
6,701 cycles to failure



200X

No shot peened

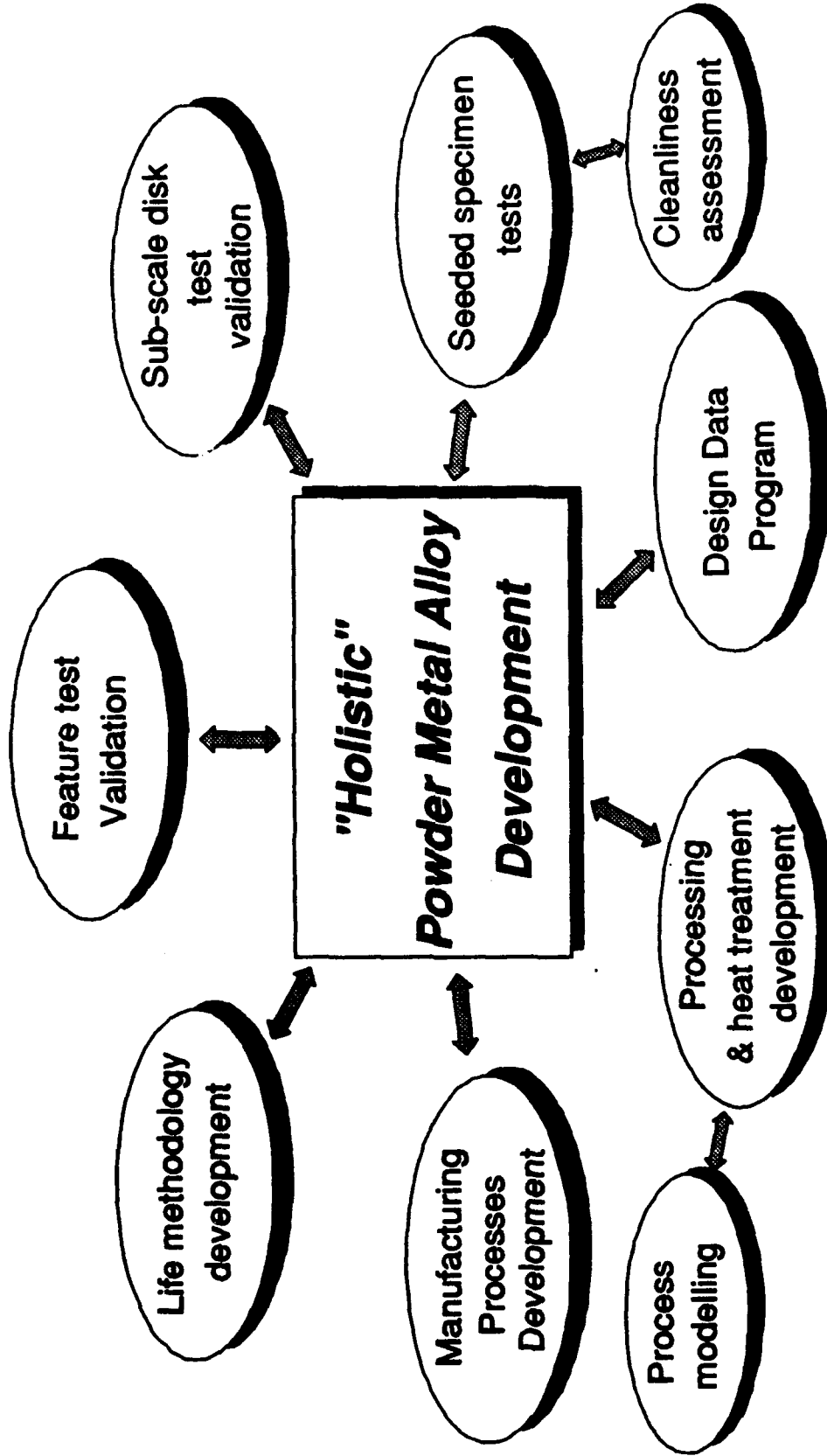
Internal initiation
89 mils² area
33,740 cycles to failure



200X

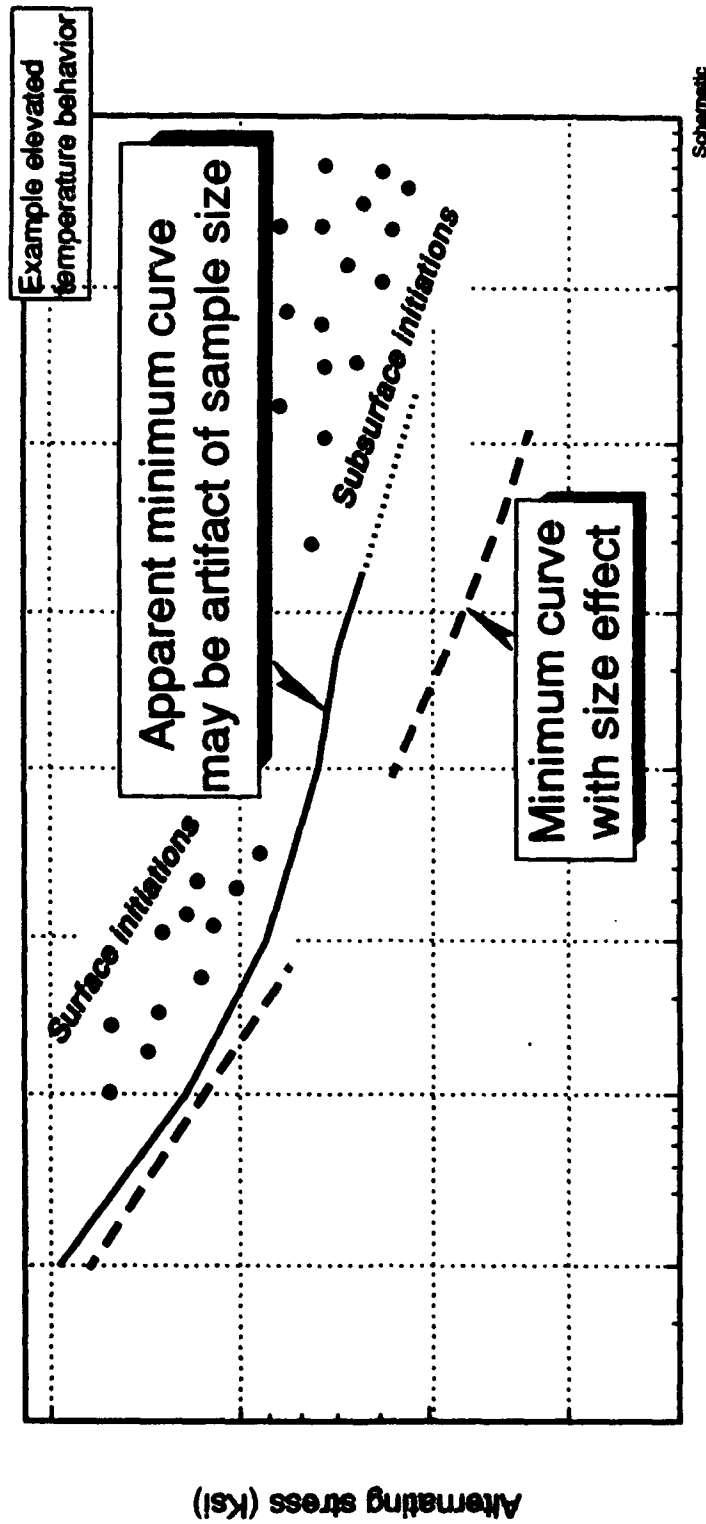
Shot peened

Smaller surface inclusion has shorter life





Probabilistic nature of inclusion occurrence distorts smooth bar test observations



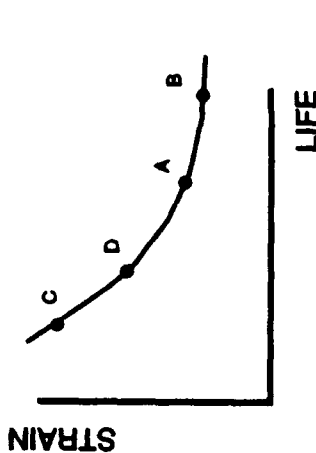
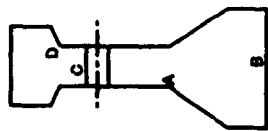
Necessitates probabilistic life prediction



Criteria are different for different mechanisms

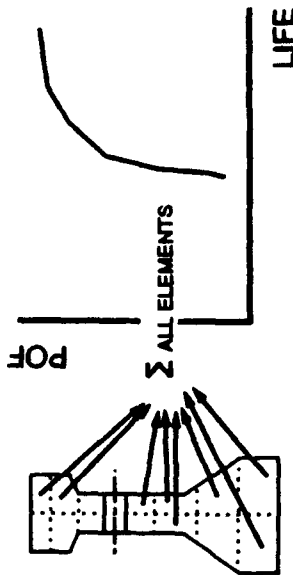
Deformation/slip fatigue mechanism

- All elemental volumes the same
- Life limit - weakest link
- Cycles to crack initiation at limiting location
- (or inspection intervals for crack growth from assumed initial flaw)



Inclusion crack nucleation/growth fatigue

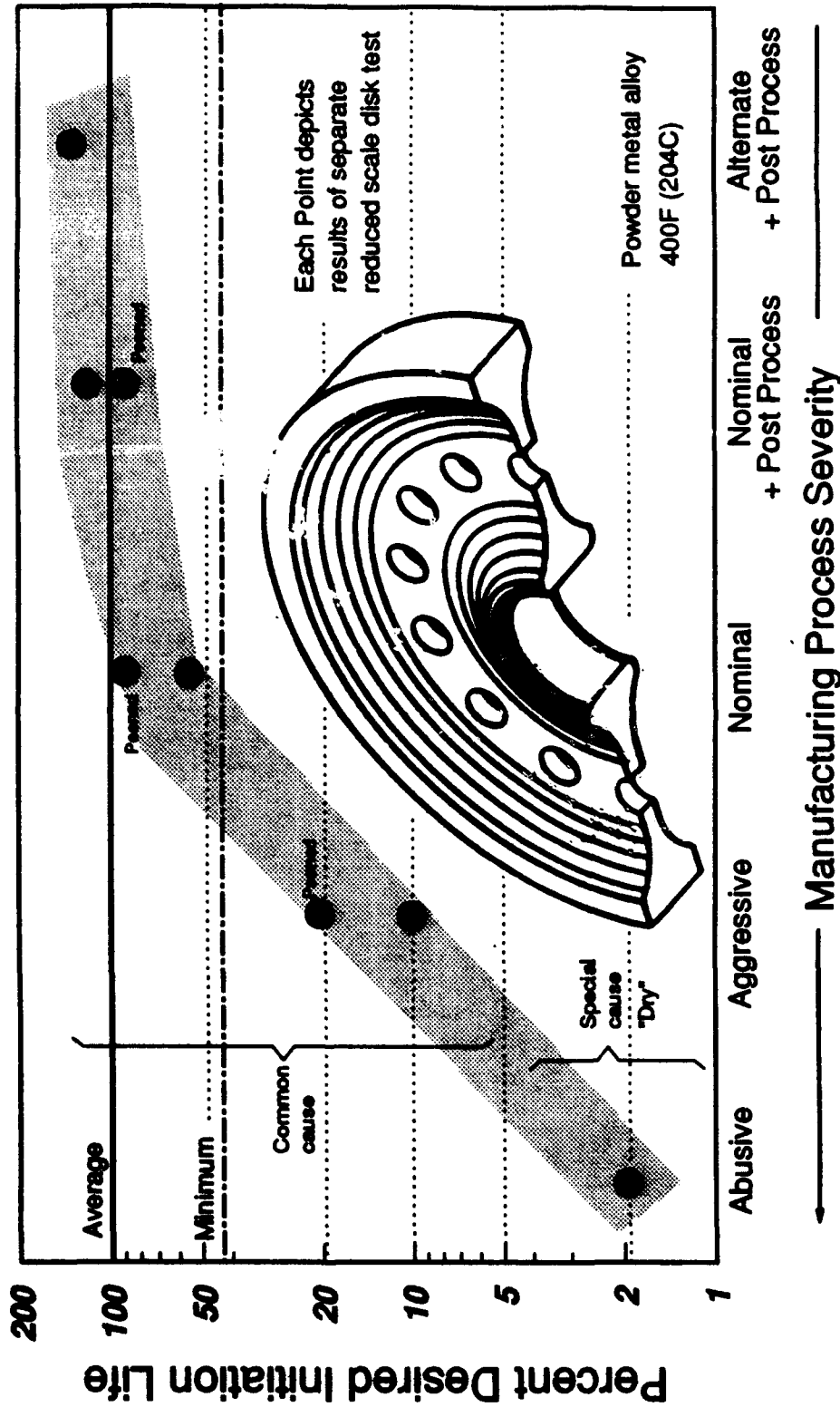
- Elemental volume behavior depends on presence and behavior (size, incubation) of inclusion
- Life limit - probabilistic
- Cycles to fracture (or % full life) for entire component



Component life set at lowest limit



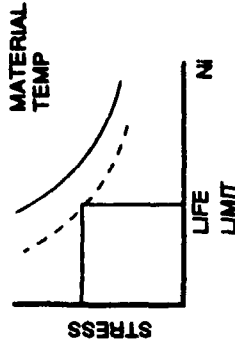
Hole making process has major influence on LCF life
Controlled process necessary to achieve design intent



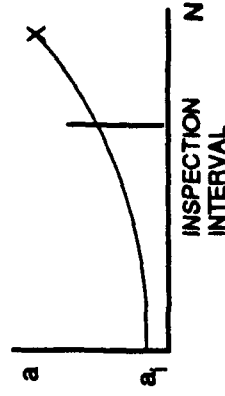


Life Prediction Concepts - Conventional

- Grain Facets (always present)
 - Initiation: Correlate with lab LCF tests
 - Propagation: F/M crack growth from "initiated" crack (Margin)



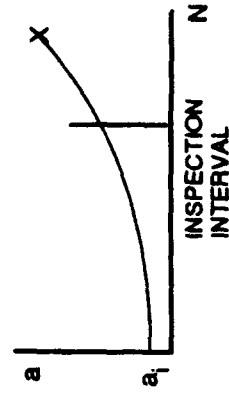
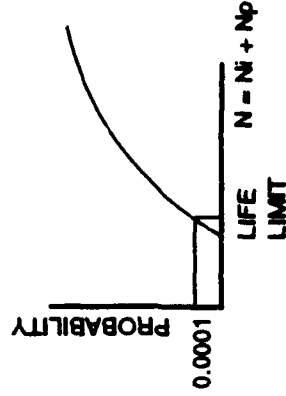
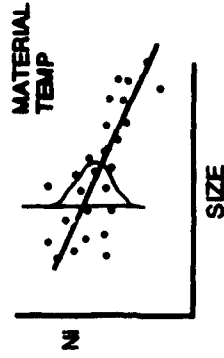
- Surface Damage (may be present - assume unknown)
 - Initiation: Assume no initiation (acts as crack)
 - Propagation: F/M crack growth from surface crack a
 - Inspection interval: Fraction of residual life





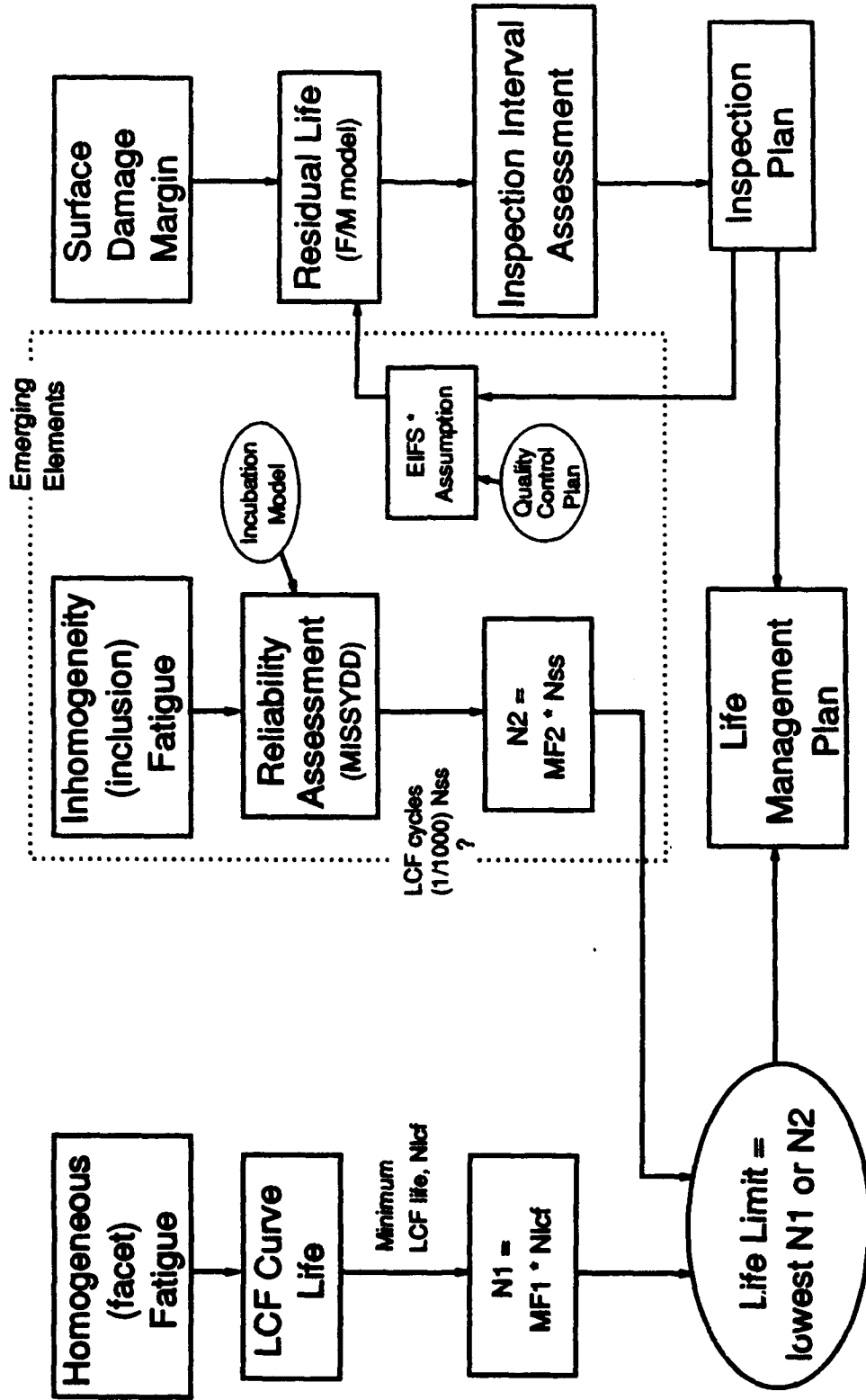
Powder Metal Alloy Additions

- Inclusions (may be present - assume quantifiable)
 - Incubation: Correlate with seeded lab LCF tests
 - Propagation: F/M crack growth from inclusion (Margin?)
 - Reliability Assessment: F(stress, vol, cleanliness, size distribution)
- Surface Damage (may be present - assume unknown)
 - Initiation: Assume no initiation (acts as crack)
 - Propagation: F/M crack growth from surface crack
 - Inspection interval: Fraction of residual life
 - Damage may be subtle (deformation, cold work)





Prototype life assessment methodology framework



MF1 & MF2 = margin factors
 * Effective Initial Flaw Size



Complications being addressed

- **Difficult to obtain inclusion size distributions**
 - **Mechanical tests (tensile, fatigue)**
 - **Raw powder survey**
- **Inclusion severity (crack-like?)**
 - **Seeded bar tests**
 - **Peened and unpeened**
 - **Size, stress, temperature dependent**
- **Manufacturing process optimization and control**



Summary

- **Holistic approach to Powder Metal alloy development**
- **Integrated life method and manufacturing assessments:**
 - **Influence of inclusions can be significant**
 - **Manufacturing process influence can be significant**
- **Implications for ENSIP durability and damage tolerance:**
 - **Durability assessment should address inclusions**
 - **Damage tolerance should place emphasis on evaluation and control of component surface processing**

ENGINE LIFE MEASUREMENT AND DIAGNOSTICS: THE FUTURE DIRECTION FOR THE AIR FORCE

Squadron Leader Chris J Pomfret, Royal Air Force
Wright Laboratory
Wright Patterson AFB OH 45433-7251

INTRODUCTION

The facilities in the Air Force for engine life measurement and diagnostics lag the capabilities of current technology. The emphasis is still on data capture during flight with analysis and diagnosis being carried out after-the-fact. However, recent advances in neural network technology and artificial intelligence provides the opportunity to significantly enhance trending and diagnostic facilities including the on-board real-time analysis of data. Similarly, engine life *prediction*, using probabilistic analysis will become more sophisticated and hopefully more accurate but life usage *measurement* is still centered on Total Accumulated Cycles (TAC) which, whilst better than running hours, only accounts for low cycle fatigue (LCF) considerations and does not directly allow for thermal or vibratory (HCF) effects. With the arrival of 2-level maintenance and the drive for technology which impacts reliability and maintainability, the opportunity now exists to seek significant enhancements to current engine trend analysis and diagnostic capabilities. Prompt and correct diagnosis will have great financial and manpower savings and increase fleet availability; more accurate life measurement will increase engine life usage with a significant financial saving. This paper outlines a direction of developmental effort and the challenge presented to engine designers to achieve the goals outlined and thus provide a major impact on engine management and maintenance in the future.

CURRENT SYSTEMS AND THEIR SHORTCOMINGS

There have been a plethora of engine data recording systems in use in the Air Force for many years. A selection of the systems in use on some of the current aircraft are shown in figure 1. The most widespread is the Comprehensive Engine Management System (CEMS). All these systems were founded on the premise of data collection during flight so that the information could be downloaded after flight and analyzed by a desk-top computer. Analysis consisted of trend plotting the data so that a historical record of various parameters was compiled. Output in graphical or tabular format enabled maintenance personnel or fleet managers to notice trends more easily or to call up and examine the trend if some engine system fault was detected on the aircraft. Figure 2 shows the typical flow and analysis of captured data and the interfaces involved. Whilst these management systems were modern, futuristic even, at their outset they are now dated and technological advances have fast outpaced any in-service enhancements to these systems.

<u>Engine</u>	<u>Aircraft</u>	<u>Airborne Recording System</u>	<u>Trending System</u>
F100	F-16C/D	EMS/DEEC	CEMS IV/CEDS
F101	B-1B	CTTS	EDGE/CEMS IV
F108	KC-135R	TEMS	CEMS IV
F110	F-16C/D	EMS/DEC	GSS/CEMS IV
F117	C-17A	EMS	CEMS IV
TF 30	E-F/111	TEMS	CEMS IV
TF 34	A-10	TEMS	CEMS IV
TF 39	C-5	MADARS	MADARS/GPS/CDB

Figure 1. Engine Recording and Trending Systems

EMS = Engine Monitoring System. DEC = Digital Engine Control. TEMS = Turbine Engine Monitoring System.
 DEEC = Digital Electronic Engine Control. CEDS = Comprehensive Engine Diagnostic System
 CITS = Central Integrated Test System. MADARS = Malfunction Detection Analysis and Recording System
 EDGE = Engine Diagnostic Ground Environment. GPS/CDB = Ground Processing System/ Central Data Base
 CEM^c = Comprehensive Engine Management System. GSS = Ground Station Software.

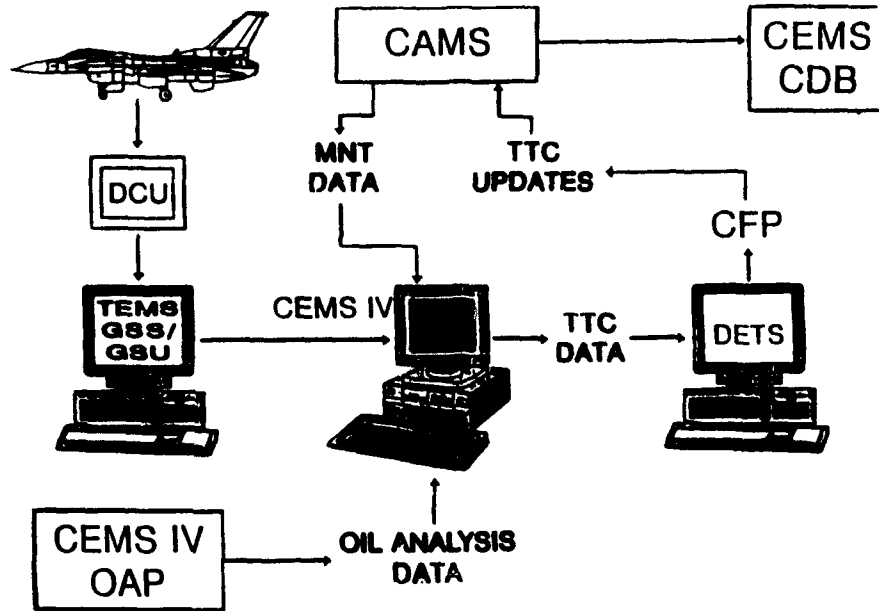


Figure 2. Current Monitoring Systems Require Several Interfaces.

The first shortcoming of current monitoring systems is their labor intensity. Maintenance crews still need to manually download the data at the end of every sortie. Frustrating configuration problems between aircraft and downloading device can prevent data being satisfactorily downloaded or, at worst, cause the data to be lost altogether. For instance, on B-1 aircraft, changes to the CIS processor over time have caused hardware compatibility problems; thus, depending on the modification level of the aircraft, downloading switches need to be set in a specific configuration otherwise the downloaded data is scrambled. When retrieved from the aircraft, the data has then to be loaded into a desk top computer and the historical records for each engine updated. The maintenance personnel then need the time, inclination and expertise to study the analyzed data be it to conscientiously monitor the health of the engines or to specifically diagnose a fault, detected perhaps by the pilot during the sortie. The monitoring system may present an obvious trend or pattern to the viewer but it does not offer a diagnosis to correct the trend. To determine the reason for the trend requires a thorough understanding not only of the other parameters and their interconnection with each other but also of the monitoring system being operated. Mobility of military personnel, the different monitoring systems operated for different engine types within the Air force, insufficient engine health monitoring training courses or time to attend them and the variety of hardware to download or process engine data all conspire to make the day to day operation of the current engine trend monitoring and analysis systems tedious and user unfriendly. Therefore when times are busy on the flight line or the hardware is incompatible or not available, data downloading and/or analysis is likely to be side stepped. Historically, data capture is easy; by contrast, manipulation and analysis of the captured data is an altogether more skillful discipline.

Some of the difficulties mentioned above lead to another serious shortcoming of current systems. If historical data is incomplete, then plots of trends will be like a jigsaw with missing pieces; thus, any attempt to analyze and diagnose faults from the incomplete picture is likely to be more difficult and less accurate. Human confidence in the monitoring facility and the desire to use it for its intended purpose are also likely to diminish. Next, there are discernability shortcomings. Firstly, the recorded parameters tend to be a maximum or minimum value achieved or a snapshot at take off or cruise during the sortie rather than a profile of the parameter throughout the particular sortie. Again, this information, while useful, is of limited value for after the fact diagnosis.

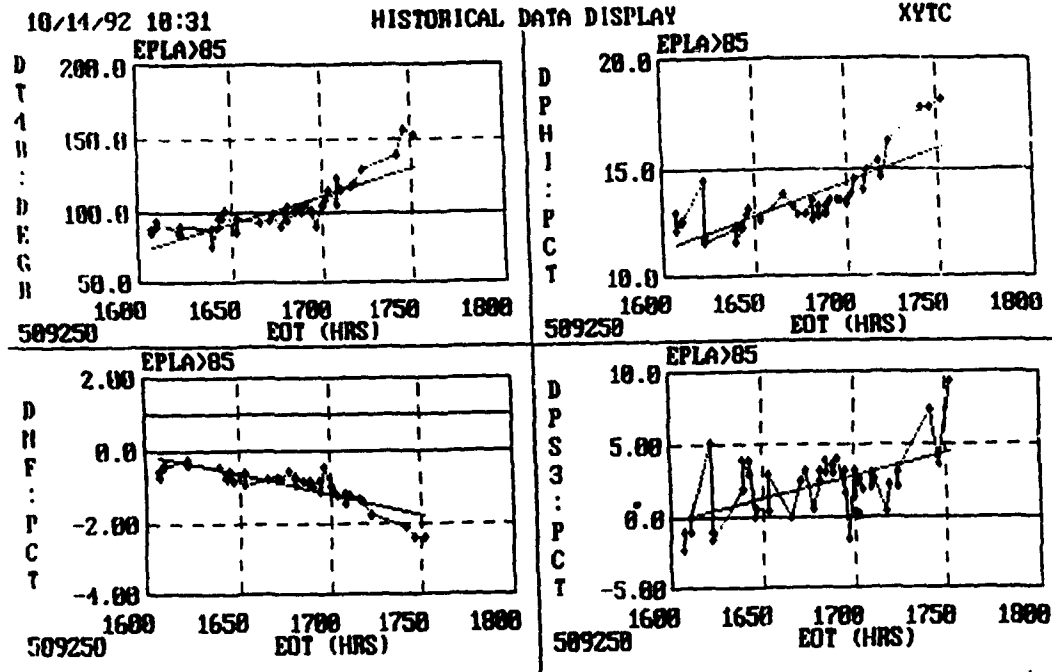


Figure 4. CEMS IV Provides the Trends, but Deciding Which Ones to Compare Requires Expertise.

WHY A CHANGE IS TIMELY AND NECESSARY

While attractive reasons can almost always be fabricated to support a change or improvement, it is sensing the real value or depth of the proposal which is usually the decisive factor. In the case of engine data recorders and trend analyzers, it is undisputed that their capabilities, for whatever reason, have not been significantly upgraded since inception. It might be that there has not been sufficient priority to warrant a change or that no-one has had the desire to pursue identified enhancements. In 1993, however, there are a set of circumstances prevailing which create, and arguably force, the case for wholesale changes in this field.

Possibly the greatest change rippling through all tiers of the Air Force at the moment is the introduction of 2 level maintenance. This concept is, to most people, awesome and extremely courageous. Many do not know the underlying rationale for its introduction, but whatever reasons are cited, 2 level maintenance is here to stay for the foreseeable future. For the past 30 years, engines have been designed with 3 level maintenance in mind; now engine manufacturers are going to have to optimize designs for 2 levels only. Perhaps split half compressor casings will become a thing of the past. Similarly, the way the engine is handled and maintained on the flight line will need to undergo radical and expeditious rethought. Removal of an engine is now an expensive activity because, by definition, the engine will transit to a depot some thousands of miles away and be out of productive service for longer than hitherto. Therefore, there is a greater priority on minimizing engine removals. Consequently we require more reliable engines. That has always been a priority but, without attendant increases in diagnostic reliability, then greater ruggedness and endurance of engines is of limited value. Therefore, efforts now need to be concentrated on ensuring that when an installed engine develops a fault then it is correctly diagnosed and only removed if really necessary. The merits of 2 level maintenance will then be maximized.

Secondly, changes in the world in the last 5 years have necessitated the most significant downsizing of the Air Force for over 45 years. Coupled with this major change is the constant efficiency drive to do more with less. The effects of these 2 factors will be reduced manpower and trimmed manning levels. On the operating bases, the withdrawal of the Intermediate level of maintenance will create a double loss in that, as well as more stringent manning levels, on-hand expertise will decline sharply. Shortages of time, inclination and expertise already tend

to contribute to incomplete data capture, monitoring and analysis; these 3 factors can only increase with reduced manning and less on-hand support.

Next, in the cycle of technological evolution of any product, there tends to be a period of technology advancement followed by a period of consolidation. Currently the Research and Development efforts for gas-turbine engines is focused on an extensive enhancement of propulsive capability. Known as the Integrated High Performance Turbine Engine Technology Initiative (IHPTET) the goal is to double thrust to weight ratios in the next 10 years. Through IHPTET, gas turbine engines in the 21st Century will:

- a. Run at much higher temperatures while using less cooling air.
- b. Operate at higher tip speeds.
- c. Utilize an array of new materials.
- d. Incorporate significant changes in design philosophy.

Once this IHPTET technology is in productive service, there will follow a period during which the youthful technology and philosophies will be consolidated and optimized because, while IHPTET is focused on performance, reliability is indisputably of equal rank. Preparation for that period of consolidation needs to start now so that by identifying the likely requirements and developing them so that they are available when the time comes for their implementation. Efforts to develop non intrusive sensors¹ such as thermo phosphors for turbine metal temperature measurement, embedded fiber optic sensors for detecting nonlinearities within composite structures and blade tip deflection sensors are being actively pursued to meet the post technology introduction requirements. The challenge in this respect is to sense more parameters than hitherto but with minimum or zero increases in intrusion, weight addition and system complexity. The success of these efforts have a direct read across to any health monitoring and life measurement initiatives and it is likely that, within the next 10 years, we will have direct access to an additional suite of operating parameters which have always previously eluded us. The anticipated advances in parameter sensing will only improve the comprehensiveness and value of engine health monitoring in the future. Part of the IHPTET program is to design and life engine rotating components on a more scientific baseline than hitherto. Probabilistics is in use for many civil engineering constructions and the concept can, we believe, be satisfactorily transitioned to gas turbine engines thus extracting more of the safe useful life from major assemblies than has been enjoyed hitherto. Alternatively, the concept can be used to remove some of the conservatism built in to the robustness of, for example, turbine disks so that weight savings as opposed to life increases are achieved. The concept is depicted in Fig. 5. Probabilistics will hopefully be the design cornerstone of future gas turbine engines but, unless there is a life measurement tool which reflects probabilistic principles and can measure life consumption as sophisticatedly and as realistically as the design algorithm predicts design life, then the value of this major step forward in engine design philosophy will be markedly diminished.

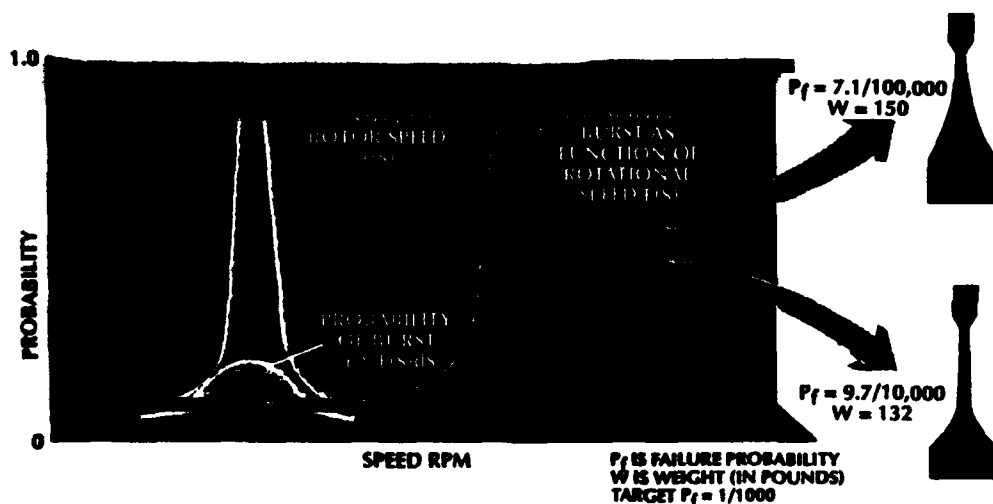


Figure 5. Probabilistics will Optimize Design with Life yet still Maintain Current Safety Levels

Finally, there is the underlying bedrock factor of pursuing technological advancements and improvements. In the health monitoring and structural integrity fields for rotating gas turbine components, the Air Force has been active in trying to extract the maximum operational life from engines without jeopardizing safety. We have advanced from retiring a component because it has reached a safe life threshold to the "Retirement For Cause" (RFC) concept which reissues components if, after reaching a threshold life, they are inspected and found to be defect free. Additionally, "Damage Tolerance" recognizes that not all cracks are bad and that some materials can operate satisfactorily and safely with flaws present. Good though these concepts are, they still rely on regular inspections of essentially serviceable components. The vast majority of disks returned to ALCs for inspection under RFC are found to be fit for reissue without any rework or reinspection. Figure 6 shows a typical breakdown of a large sample size over a period of 5 years².

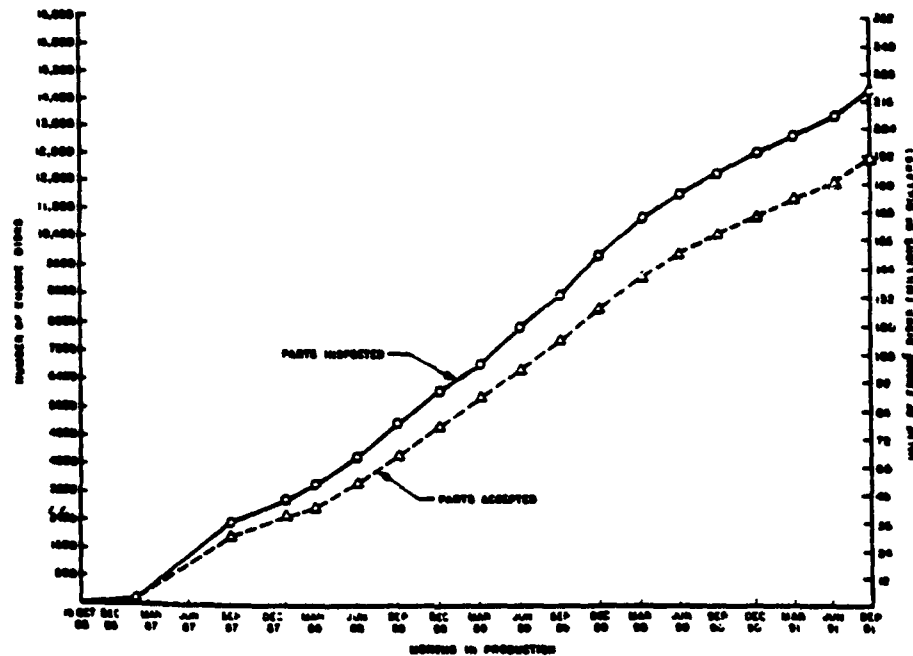


Figure 6. Most Components Inspected under RFC Philosophy are Re-released²

Because the maintenance effort and cost involved to inspect engine disks, the vast majority of which are defect free, we now need to build on the foundation that Damage Tolerance and RFC provide and focus on reducing the number of components which, with hindsight, we unnecessarily remove from service and inspect.

ENGINE HEALTH MONITORING IN THE FUTURE

Having identified the limitations with the current data recording and trending systems, the challenge is to produce a faultless replacement. Fortunately recent technological advancements will contribute greatly to the desired aim. Additionally, fundamental changes to data collection methods is not envisaged; instead the focus would be directed to how collected data is manipulated and analyzed.

Data capture is not generally a problem. Sensors are widely distributed on engines and if a particular parameter cannot be sensed, then it can usually be calculated from other sensed data. While there is a move, as discussed earlier to introduce new sensor technology, there is a counter move, in the interests of system simplicity and weight reduction, to remove sensors that are not absolutely necessary to engine operation or flight safety; the advent of model based concepts for engine control also support this move. Whichever way engine operating data is simulated, sensed or calculated, there will continue to be a strong requirement for such data in the future. Engine operating values will play a fundamental and dual role in future engine life monitoring and diagnostic capabilities.

Fault Detection, Diagnosis and Trend Plotting

Real-time monitoring of the parameters in flight will provide the assurance to aircrew and maintenance crews that the engine is operating as advertised. If one or more parameters are not within acceptable limits with respect to the other parameters then a future on board system will begin to "hunt" for the reason by direct comparison with all the sensed data available. If the parameter is flight safety critical, then the pilot will receive a warning in the cockpit in the same way as occurs currently. The difference would be that the apparent fault will have been "checked out" first to ascertain its genuineness before alerting the pilot. Thus for the first time, full on-board diagnosis would be taking place.

For minor or "routine" faults the diagnoser will start to detect the reason for the fault. Using neural networks, the system will recognize "harmonious" patterns and will know what the value of each of the sensed parameters should be for the given flight conditions. It will thus find the "odd one out" and then try to determine why it is the odd parameter. For instance, an incorrect hot end temperature signal could signify a real fault or it could be spurious because of a sensor problem. If it is real, then either fuel flow delivery is incorrect for the air mass flow being delivered through the engine, or an air bleed valve is open when it should not be etc. Alternatively, if the sensor has adopted a shift or a short circuit then all the other parameters should be in harmony with each other. In the latter scenario, the diagnoser could quickly diagnose a faulty thermocouple or pyrometer and then cancel any overtemperature caution illuminated in the cockpit and thus avoid unnecessary mission abort or diversion procedures. Finally, there are performance trends which can reveal incipient faults or just very slow performance degradation. For such circumstances, the neural nets would be given threshold values for the parameters being monitored so that a diagnostic function would be triggered off if a parameter, *with respect to other associated parameters*, was detected as being out of limits. In this case, analysis and diagnosis of trends would be taking place with better visibility of all the relevant information than can be achieved with current systems and the output would be prompter.

There have been many initiatives within the USA to produce on-board diagnostic reasoners using neural networks⁷ with efforts especially focused on the main engine of the NASA Space Shuttle.^{4,5,6,7} Additionally, models to determine actual engine condition in flight by estimating component performance deviations from a reference model or a predictor model have been demonstrated.^{8,9,10} Unfortunately, and despite positive results from these initiatives, none of them has been progressed further for military application.

Engine Life Measurement

The same data currently captured in flight for in flight monitoring and diagnosis could also be used for life measurement. Currently, engine life is measured somewhat crudely by counting throttle excursions in flight. Engine start up and shut down is deemed to be one cycle and excursions during flight between idle rpm and max rpm are various fractions of a cycle depending on the rpm range excursioned. This technique of measuring low cycle fatigue (LCF), is known as the Total Accumulated Cycle (TAC) and replaced the even more basic life measurement of engine running hours. In the current day, it is generally accepted that LCF measurement does not depict the full picture and whilst allowances for other life influencing parameters such as vibration (high cycle fatigue) and temperature are made in TAC counts and design lives, the approximations are too approximate and probably too conservative. In the current day we could take a step closer to measuring life consumption more accurately, more representatively and in real-time. To measure life usage as it is consumed in flight will require a comprehensive damage accumulation algorithm. The complexity of this task makes it extremely challenging but it should nevertheless be undertaken.

Engine designers and stress engineers already understand as much as possible the properties and characterizations of the material chosen for a given gas turbine engine component. Additionally, they know the environment that the material will be exposed to during its life. Based on this data, they are obligated to define a release to Service or design life for the component. Significant conservatism is afforded to the quoted figure because they know that each individual component will, during its service life, experience a different and unique set of circumstances which will not be recorded nor attributed to the component. Figure 7 shows the reality of two engines flying on the same sortie in formation but it is clear that the difference in engine life will be significantly different. Because these differences have not been measurable in the past, each component is deemed to experience a standard, average, typical life which has been previously defined. However, the resulting conservatism introduced in order to preserve safety across the fleet of components could be significantly reduced if the life of each component was individually tracked and recorded. With the existing knowledge base, and the technology now available, creation of an expert system to measure life as it is consumed should be achievable. The sensitivity

of the material to temperature changes needs to be defined as a comparison to a base reference. For instance, if the material temperature is 5°F greater than the base reference, then what is the penalty on life usage? If the material experiences a sudden temperature surge then how robust is it to the rate of change of temperature experienced and over the time period? Much of this information is known but is probably not in a usable format for algorithmic purposes. It has to be known for engine designers to be able predict and design for a required or declared operational life. Indeed, many efforts have been made and papers written covering this philosophy but few have been directed at military gas turbine engines. Previous efforts that have focused on military applications do not appear to have been progressed. One particular study¹² some 13 years ago devised a Life Utilization Criteria Identification in Design (LUCID) program which quantified the trade offs between life and performance in gas turbine engines. The study was predicated on the belief that life limited parts have failure modes resulting from long-term exposure to the entire range of normal operating events and that creep, erosion and LCF with slow crack growth ideally occur after many years of operation. The installed life capability, in terms of total operating hours, of life limiting parts is dependent on utilization. The cyclic lives of fatigue limited parts are determined by the number and magnitude of stress cycles whereas the lives of creep/erosion limited parts are determined by time at a

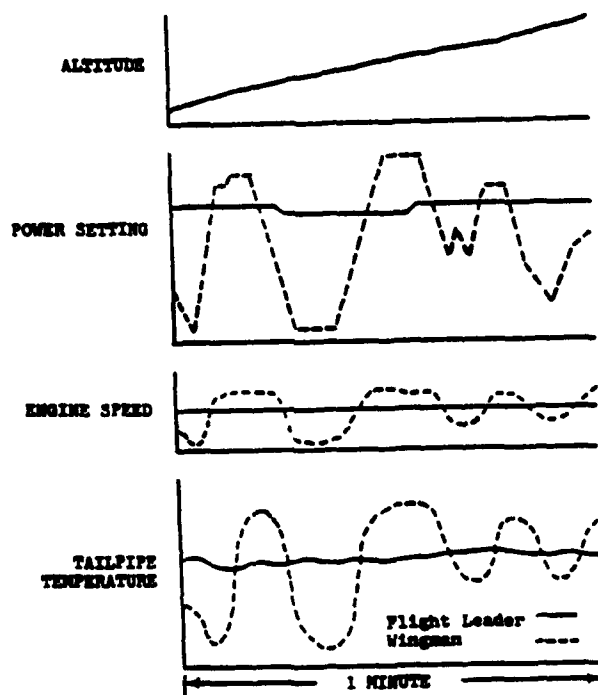


Figure 7. Aircraft on the Same Missions can Consume Significantly Different Usage¹¹

temperature (usually power setting related). The study also showed the large differences which can occur between engine expected (design) usage and actuality. Fig. 8 shows some differences detected for the F100 engine. While the conclusions of this study still hold today, we have been slow to incorporate them in our day-to-day military operations. More recently, fatigue life neural networks¹³ have been developed specifically for the Space Shuttle Main Engine. Additionally, youthful technology such as Synchronous X-Ray Sinography,¹⁴ which has demonstrated an ability to detect cracks in rotating turbine disks, will augment structural integrity programs and provide a new dimension of engine health monitoring in the field. These, and other related efforts, indicate that the foundation technology is available for adaptation to military engines; moreover, the US needs to initiate the further development of this technology now if it is to maintain its position as the world leader in technology advancement.

	Design and Development Utilization	F-15 Field Utilization
Mission Run Time	4,000	4,000
Major Cycles (Shut-off to Intermediate and Above)	3,530	2,360
Partial Cycles (Idle to Intermediate and Above)	0	21,630
Augmented Cycles	2,970	15,200
Supersonic Time, (hours)	10	35
Augmented Time, (hours)	106	104
Total Time at Intermediate to Maximum Power, (hours)	1,050	472

Figure 8. Engine Usage can Vary Greatly from that Originally Expected¹²

Health Monitoring Advancements in the UK.

The UK is particularly active in pursuing real-time life consumption. The Engine Usage Condition and Maintenance Management System (EUCAMS) was established by the RAF in 1974 with additional members drawn from the Navy, Army, the Defense Research Agency (DRA), engine manufacturers and the Procurement Executive Branch of the Ministry of Defense (MOD PE). The aims of the system were threefold:

- a. To promote use of new and existing health and usage monitoring techniques as broadly as possible across all 3 Armed Services wherever there was a perceived cost benefit or operational advantage.
- b. To ensure that the equipments demonstrated were compatible with the overall servicing and management policies of the user services.
- c. To assist project offices in deciding which equipments or functions are appropriate to their particular needs.

Under this umbrella, 4 working groups are established:

- a. Usage. Focus on algorithms for monitoring fatigue consumption.
- b. Mechanical Condition. Vibration, oil, gas path aspects.
- c. Performance. Trending, thrust monitoring.
- d. Maintenance Information Management. Determine data needed and standardizing methods of recording.

In the pursuance of optimizing component life usage, the UK has 2 objectives. First, they aim to reduce the cost of ownership through maximizing the take up of available component safe life and minimizing the number of unscheduled removals and repairs. Second, they aim to ensure that, as new materials and advanced component designs enter service, sufficient data is gathered to ensure safety standards are maintained.

To achieve these objectives the approach is to define the parameters which could lead to component failure, and develop fatigue accumulation algorithms to sum the rate at which lives of critical engine components are consumed during service usage. They believe that this can only be done if the entire fleet is monitored; samples destroy the intended benefits because an assumption that the weakest component in the fleet is not being monitored would otherwise have to be made. The variability in material properties in the fleet is a life prediction problem which concepts such as probabilistics would, it is hoped, accurately incorporate. A particular application of the UK's focus on life consumption is the Harrier Information Management System (HIMS)¹³ which stemmed from the desire to measure life based on LCF, Thermal Fatigue and Creep Counts. While the calculations are not performed on board, the system is nevertheless a step forward to measuring and recording more parameters which influence life than hitherto. The results are fed back to design assumptions so that declared component lives can be adjusted as necessary. The system is therefore deriving a more representative and accurate measurement of life consumption which can only give aircrew and fleet managers more confidence whilst at the same time making better use of the lifed components. HIMS has revealed some interesting facts:

- a. 18% of all start-ups/runs are for ground runs
- b. Tie-down runs consume life at the same rate as flying hours (these runs were unmonitored under the traditional method).
- c. Pilots record, on average, 9% higher hours than the Engine Monitoring Unit records (yet the pilot's figures have, in the past been used for lifing records of the *whole airframe* as well as its sub-systems).
- d. The Taxi time per sortie averages 20 minutes.
- e. The average usage rate for fracture critical components is significantly different (both greater and smaller) from the rates authorized by the engine manufacturers/designers.
- f. There is a poor correlation between sortie duration and life consumption; short duration sorties consume life at a greater rate than longer length sorties. Additionally, landing and take offs are more significant factors than sortie length.
- g. There is a poor correlation between sortie profile code as recorded by the pilot and the life consumed. (either the pilots are less than conscientious in selecting the correct sortie code or the codes are a poor representation of the sortie).
- h. Payload has an insignificant effect on engine life.

The UK's findings are as relevant to the US Air Force as they are to themselves. They illustrate some of the massive savings and the significant impact that accurate life measurement has on available component life, maintenance effort and life cycle costs. The underlying message is that just small usage differences between theory and actuality magnify into enormous differences when applied across the life of an engine or across a fleet of engines. Minimizing the initial discrepancies is therefore the most important priority in engine life management.

CONCLUSION

The importance of in flight monitoring of engine operating parameters will increase as quantum leaps in technology are introduced into the next generation of gas turbine engines. Captured data will not only continue to assist statistical analysis and understanding of material behavior but also play a key role in measuring, more accurately than hitherto, the life consumption of fracture critical components and will, for the first time, provide a real-time diagnostic capability. This increase in importance can be matched by an already improved capability to meet the future requirement. Having been utilized already in NASA's space shuttle main engine, neural network and expert system technology is now sufficiently mature to apply, with confidence, to military aircraft gas-turbine engines for diagnosing faults, monitoring health and life measurement.

Current monitoring systems lack the latest technology and, while they capture data for after the fact manipulation and analysis, they are labor intensive, heavily dependent on human expertise and limited in their output. The current systems are also varied in hardware, operation and capabilities and so standardization within the Air Force and across the Armed Services is sorely required. The introduction of two level maintenance and a whole suite of new technology under IHPTET further strengthen the arguments for radical improvements in the capabilities of health monitoring.

The most cost effective and professionally correct approach is to formulate a joint program which meets the anticipated requirements of users and pools together expertise from the Government and Industry. While the next generation of aircraft will be the primary beneficiary of the technology, existing engine fleets will also benefit greatly where retrospective embodiment is cost effective. Because reliability and performance are impossible to segregate, collaboration under the IHPTET banner is the logical way ahead.

REFERENCES

1. Non Invasive Sensing Techniques for Advanced Turbine Engine Structures. Stange W. A. Wright Laboratory. Gas Turbine and Aeroengine Congress 1990 Brussels.
2. Manufacturing Technology for Non Destructive Evaluation (NDE) System to Implement Retirement for Cause (RFC) Procedures for Gas Turbine Engine Components, Part 2. Angel J. Systems Research Laboratories Inc. Dayton OH. June 92. Report WL-TR-92-8011.
3. A Diagnostic Reasoning Technology Demonstrator for Gas Turbine Engines. Reibling L. A., Bublin S. C. and Stutz J. A. 1992 USAF Structural Integrity Program Conference.
4. Failure Diagnosis System Based on Neural Network Classifier for the Space Shuttle Main Engine. Dwyer A. and Merrill W. C. NASA Tech Memorandum 103607, 29th Conference on Decision and Control, Dec 90.
5. A Distributed Fault Detection and Diagnosis System using on-line Parameter Estimation.. Guo T. H. and Merrill W. IFAC DIS '91. Aug 91.
6. Sensor Failure Detection and Recovery by Neural Networks. Guo T. H. and Nurrew T. International Joint Conference on Neural Networks 91. Jul 91.
7. Real Time Fault Diagnosis for Propulsion Systems. Merrill W. C., Guo T. H., DeLaat J. C. and Dwyer A. Safe Process '91. Sep 91.
8. In Flight Performance Diagnostic Capability of an Adaptive Engine Mode. Bushmann M. A., and Gallops G. W. 28th AIAA SAE ASME ASEE Joint Propulsion Conference, Jul 92.
9. On Board Condition management for Aircraft Gas Turbines. Gallops G. W., Gass F. D., Kennedy M. H. International Gas Turbine and Aero Engine Congress, Germany 1992.
10. Performance Benefits of Adaptive In Flight Propulsion System of Optimization
11. The Role of Advanced Technology on Turbine Engine Life Cycle Costs. Panella R. F., Barga M. A., and McNally R. G. AGARD Conference #289, 1978.
12. Life and Utilization Criteria in Design for Balanced Life and Performance. Osmer J., and Blevins G. 1980 SAE
13. A Real-Time Neural Net Estimator of Fatigue Life. Troudet T. and Merrill W. International Joint Conference on Neural Networks, San Diego California, 17-21 Jun 1990.
14. Synchronous X-Ray Sinography for Nondestructive Imaging of Turbine Engines Under Load. Kirchner T., Burstein P., Youngberg J., Waters D. AIAA Joint Propulsion Conference, 1993.
15. Service Experience of the Harrier Information Management System (HIMS). Bookham R. P. Proceedings of the 5th Meeting of The Technical Cooperation Program, Sub Group H, Technical Panel HTP-7, Melbourne Australia and Auckland New Zealand 29 Apr-8 May 1991.

**ENGINE LIFE MEASUREMENT
AND DIAGNOSTICS -
THE FUTURE DIRECTION FOR
THE AIR FORCE**

**SQUADRON LEADER CHRIS J POMFRET,
ROYAL AIR FORCE
AERO PROPULSION AND POWER DIRECTORATE
WRIGHT LABORATORY
WRIGHT PATTERSON AFB OH
513-255-2351**

OUTLINE

- **Current Data Recording/Analysis Systems**
 - **Strengths**
 - **Limitations**
- **The Need For Upgrade**
 - **2-Level Maintenance**
 - **IHPDET**
 - **Downsizing/Rightsizing**
 - **Technology Advancement to Support R&M**
 - **Further Enhance RFC/Damage Tolerance**
 - **COST EFFECTIVENESS**
- **Engine Health Monitoring in the Future**
 - **Fault Detection**
 - **Fault Diagnosis**
 - **Life Measurement**

CURRENT SYSTEMS

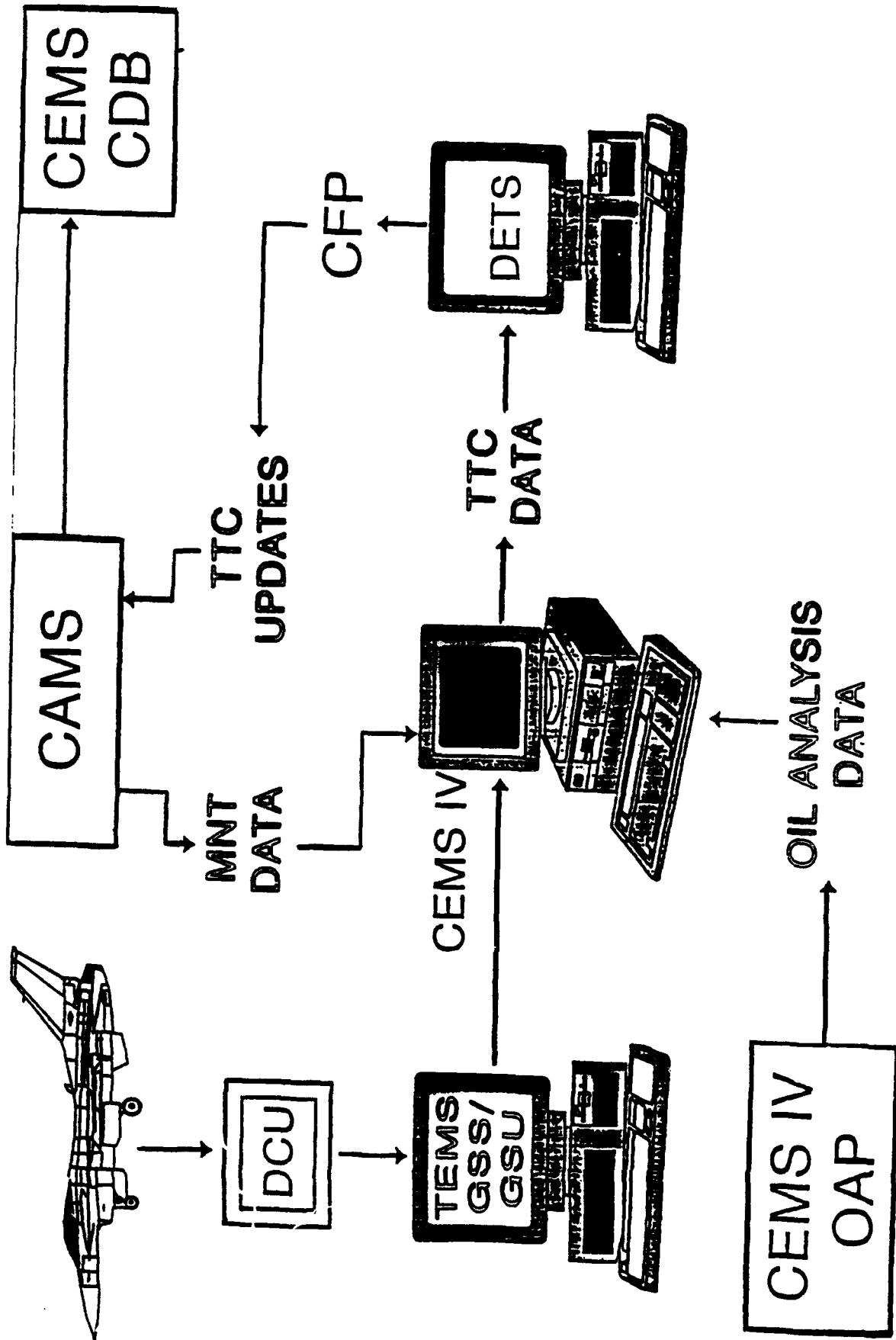
- **Capabilities**
 - Record data and trend it for human analysis/interpretation
- **Limitations**
 - Too many variants e.g.
 - » MADARS, EDGE, CEDS, GSS, SDC, CEMS
 - Too many Interfaces e.g.
 - » DEEC, EMS, DEC, CITS, TEMS
 - User Unfriendly
 - Labor Intensive
 - No Diagnostic Capability
 - Undiscerning
 - Technologically outdated
 - Poorly Supported

ENGINE RECORDING and TRENDING SYSTEMS

<u>Engine</u>	<u>Aircraft</u>	<u>Airborne Recording System</u>	<u>Trending System</u>
F100	F-16C/D	EMS/DEEC	CEMS IV/CEDS
F101	B-1B	CITS	EDGE/CEMS IV
F108	KC-135R	TEMS	CEMS IV
F110	F-16C/D	EMS/DEC	GSS/CEMS IV
F117	C-17A	EMS	CEMS IV
TF 30	E-F/111	TEMS	CEMS IV
TF 34	A-10	TEMS	CEMS IV
TF 39	C-5	MADARS	MADARS/CDB

TRANSLATING THE TERMINOLOGY

- **CEMS = Comprehensive Engine Management System**
- **CEDS = Comprehensive Engine Diagnostic System**
- **SDC = Structural Data Collector (ac & engine data)**
- **CITS = Central Integrated Test System (1 per engine)**
- **EDGE = Engine Diagnostic Ground Enhancement**
- **GSS = Ground Station Software**
- **DEEC = Digital Electronic Engine Control**
- **EMS = Engine Monitoring System**
- **TEMS = Turbine Engine Monitoring System**
- **GPS = Ground Processing System**
- **CDB = Central Data Base**
- **MADARS = Malfunction, Detection, Analysis and Recording System**



10/14/92 09:57

RANK

XYTC

NAME: T4DL.AVG

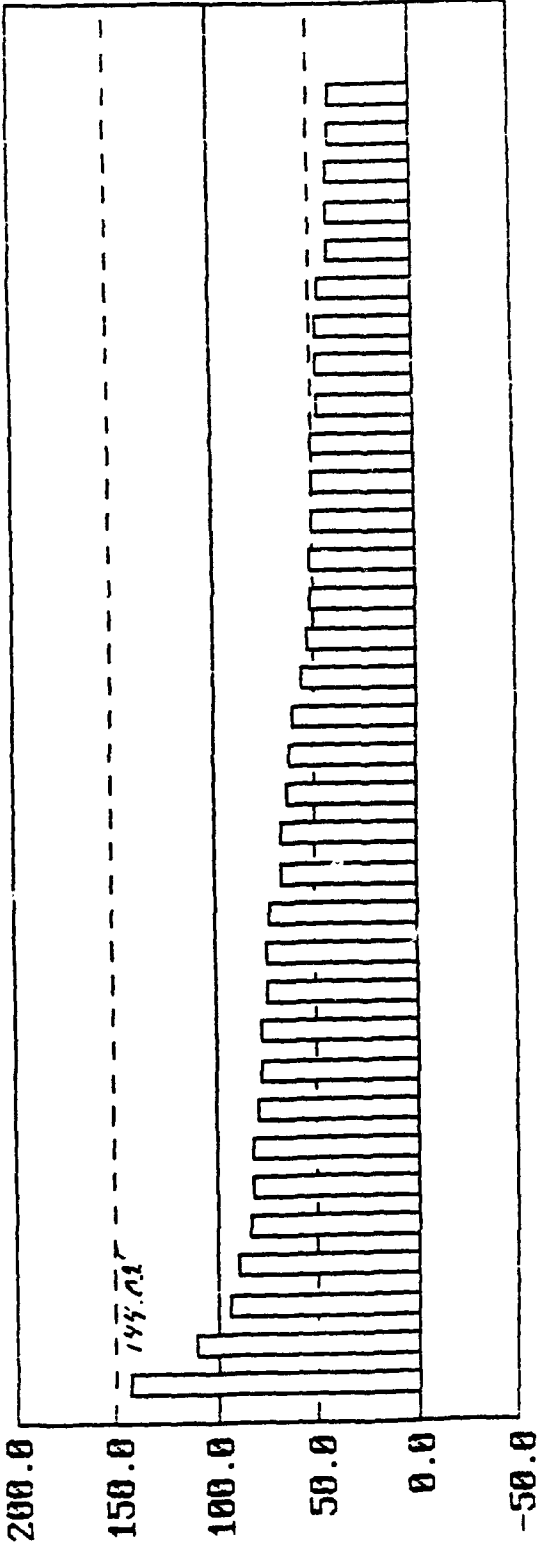
UNITS: DEGR

LIMIT: 100.00

MIN : -40.26

MAX : 144.02

AVG : 38.04

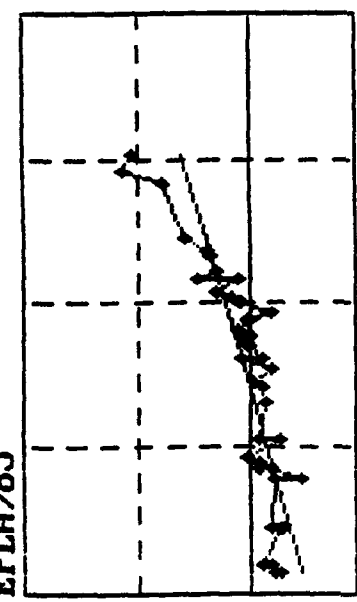


555555555555555555555555555555
000400099999999999999999999999
999599999999999999999999999999
2481218517223239866288657214812559
5841605047500254131652649591555182
0572036252198494121473484080019091

10/14/92 10:31

HISTORICAL DATA DISPLAY

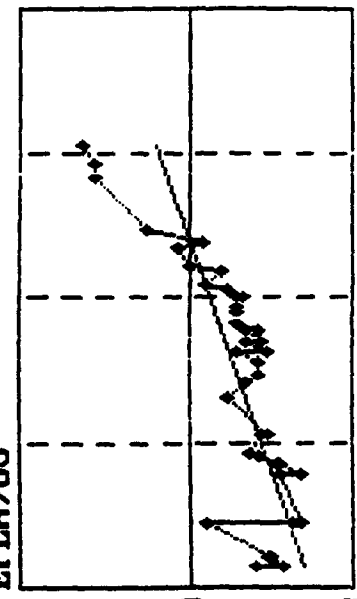
EPLA>85



D T 4 B : D E G R
 200.0
 150.0
 100.0
 50.0
 1600 1650 1700 1750 1800
 EOT (HRS)
 509250

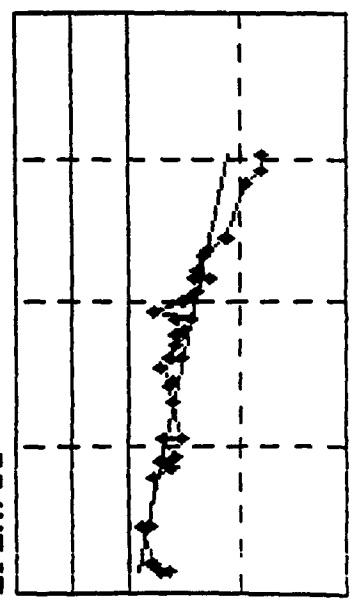
XYTC

EPLA>85



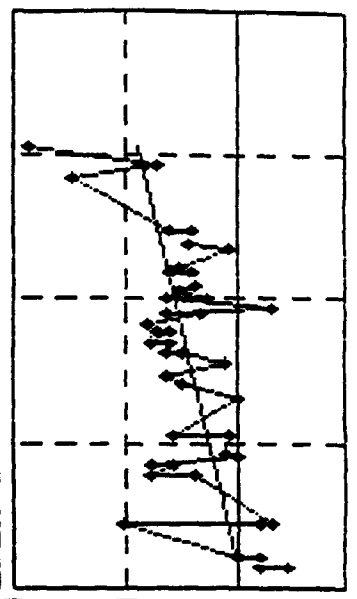
D P H I : P C T
 20.0
 15.0
 10.0
 1600 1650 1700 1750 1800
 EOT (HRS)
 509250

EPLA>85



D H F : P C T
 2.00
 0.0
 -2.00
 -4.00
 1600 1650 1700 1750 1800
 EOT (HRS)
 509250

EPLA>85



D P S 3 : P C T
 10.0
 5.00
 0.0
 -5.00
 1600 1650 1700 1750 1800
 EOT (HRS)
 509250

WHY WE NEED TO IMPROVE

• TWO-LEVEL MAINTENANCE

- Reduce unnecessary engine removals**
- Less Expertise Available**

• DOWNSIZING/RIGHTSIZING

- Do more, or the same, with less**
- Automate to**
 - » Save time, money, manhours**
 - » Increase engine installed life**
 - » Get a quicker, more accurate decision**
 - » Reduce inventory and usage**
 - » Improve ac availability = Force Multiplier**
 - » Enables more to be done with less!**

WHY WE NEED TO IMPROVE

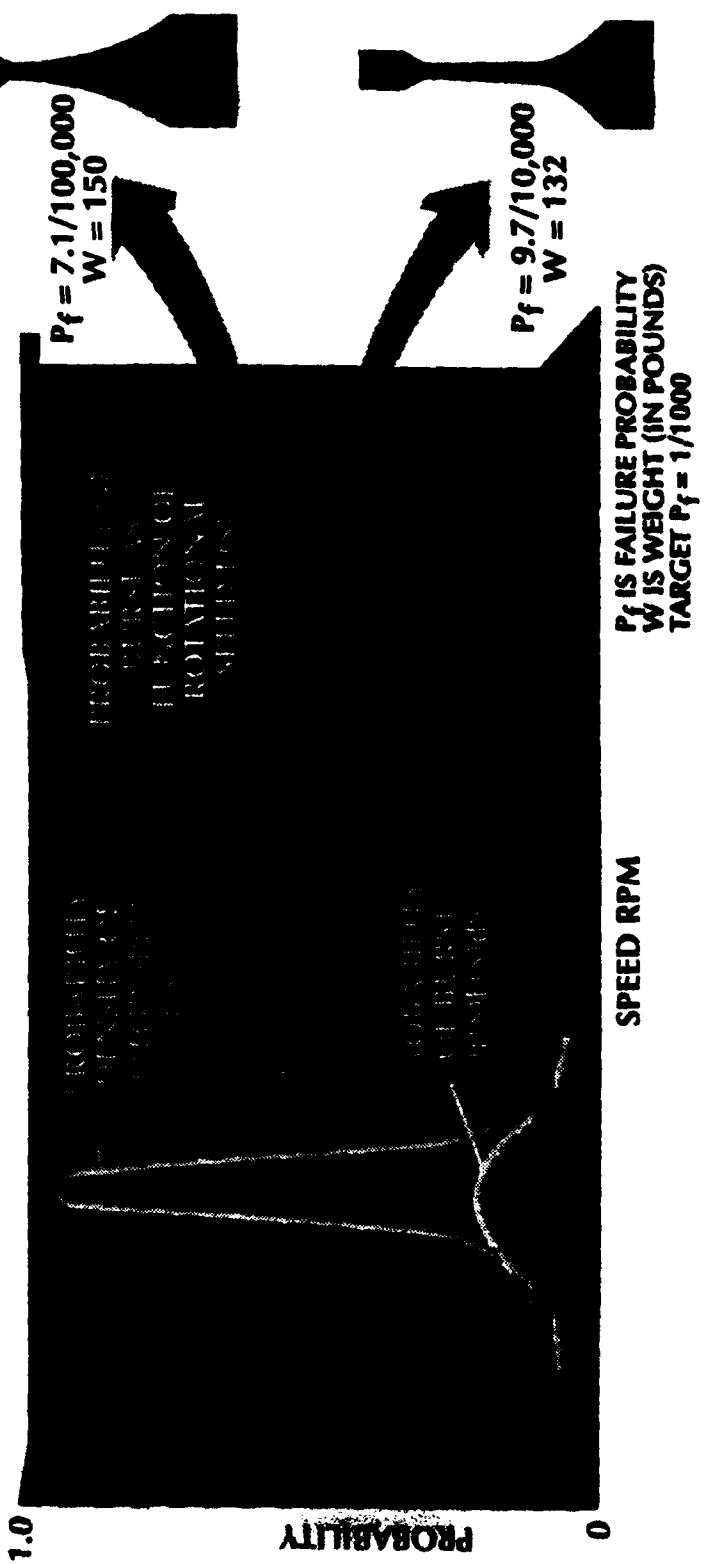
•IHP/TET

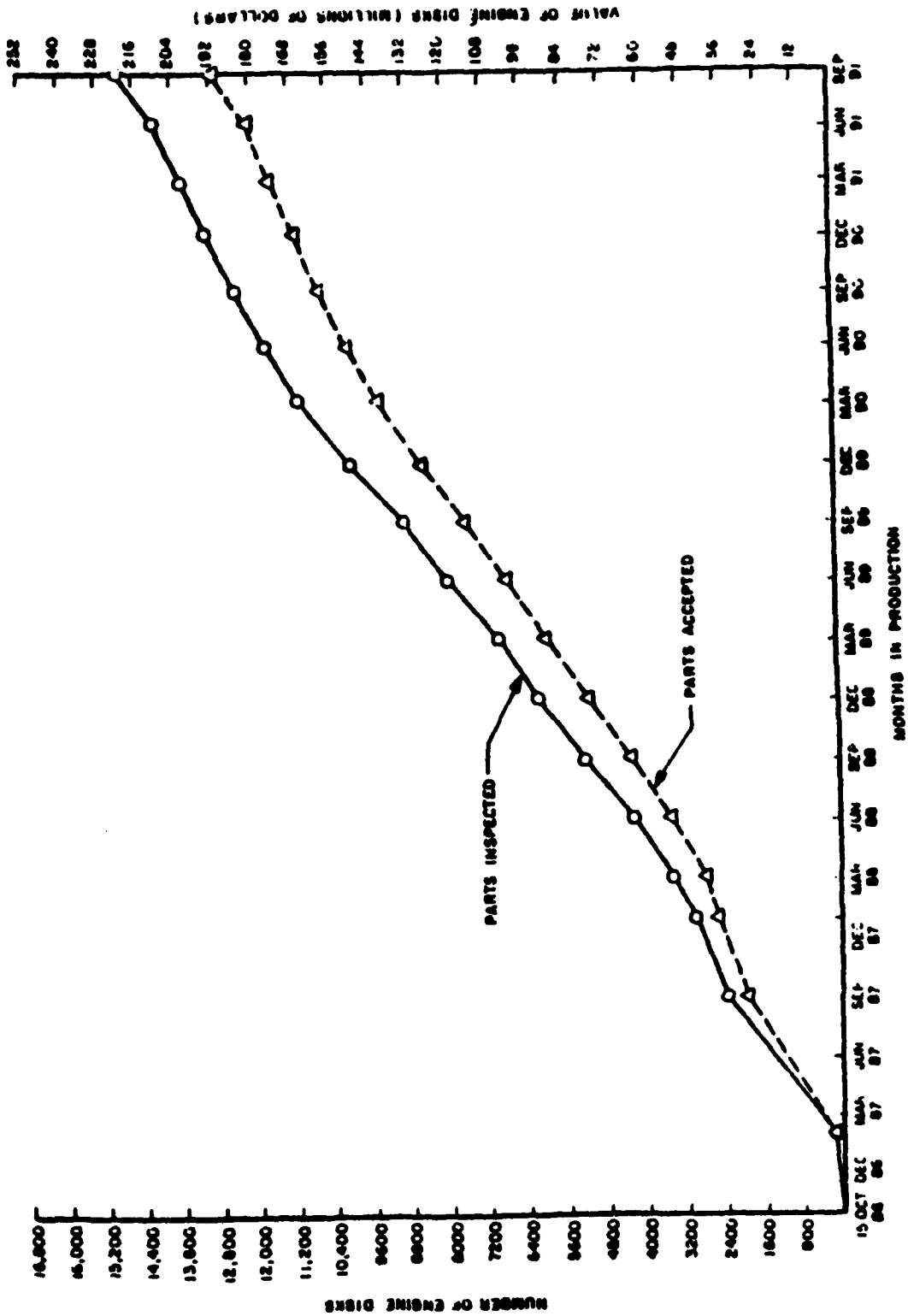
–Technology Revolution

- »Will warrant and need comprehensive monitoring**
- »Probabilistics needs a comprehensive life counter**

•TECHNOLOGICAL ADVANCEMENT

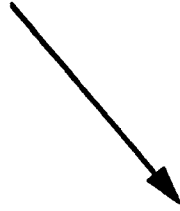
- Obligation to enhance R&M**
- Build on foundations of RFC/Damage Tolerance**





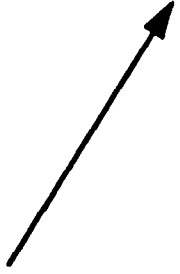
THE IMPLEMENTATION

DATA SENSING/RECORDING/CALCULATION



PERFORMANCE MONITORING

- * Collate Data
- * Trend Data
- * X-refer relevant parameters
- * Identify rogue/inconsistent values
- * Determine reason for inconsistencies
- * Offer a solution/fix



LIFE MEASUREMENT

- * Monitor Engine Parameters
- * Clock-up Life Accumulation
- * Give print out of Life Usage
- * Life corrected by Diagnostics
- * Done for major components

THE CHALLENGES

- **STOP GUESSING LIFE CONSUMPTION**
 - A/C fly the same proportion of sortie types **WRONG !**
 - A/C consume the same life on a given sortie profile **WRONG !**
 - Design is as close to actual as we can get **WRONG !**
- **WRITE A CATCH-ALL LIFING ALGORITHM**
 - Include all parameters which influence life consumption
 - Understand the interaction of life influencing parameters
 - Assume as little as possible
 - Record actualities
- **BUILD A FAULT DETECTOR/DIAGNOSER**
 - Detect Faults
 - Provide Diagnosis
 - Offer or Execute a Remedy

“EVERY AIRCRAFT MISSION

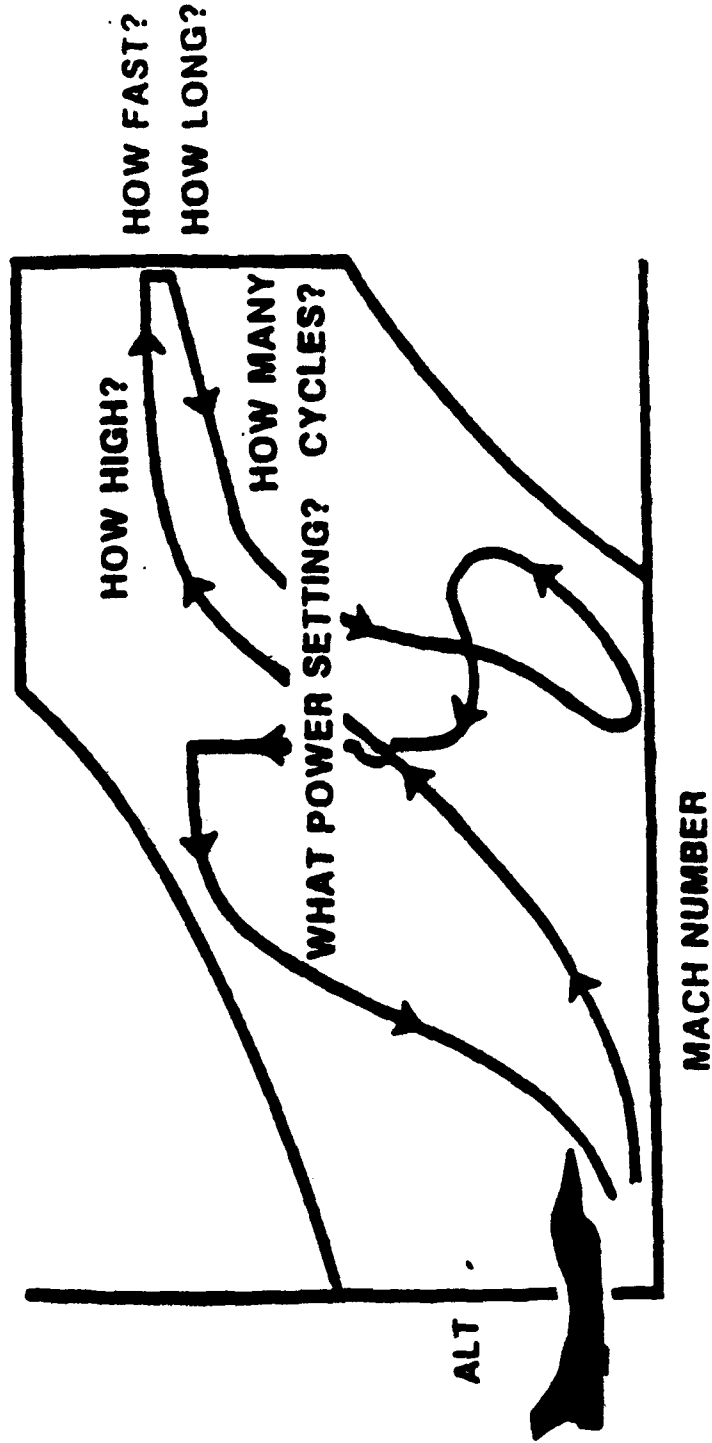
IS AS INDIVIDUAL

AS A FINGERPRINT”

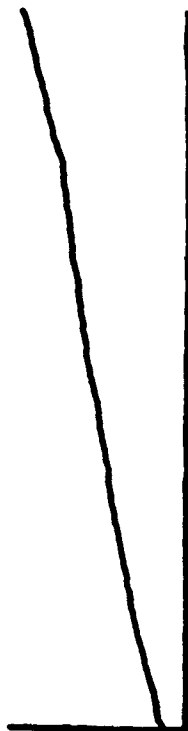
**WE CAN DISTINGUISH BETWEEN FINGERPRINTS,
THEREFORE.....**

**CHRIS POMFRET
DEC 1993**

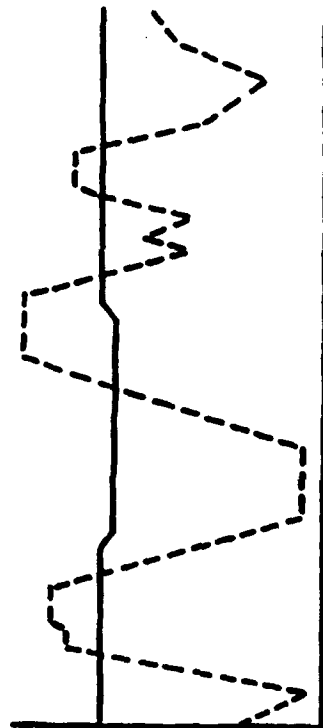
THE MISSION "FINGERPRINT"



MISSION REQUIREMENTS - ENGINE USAGE VARIABLES



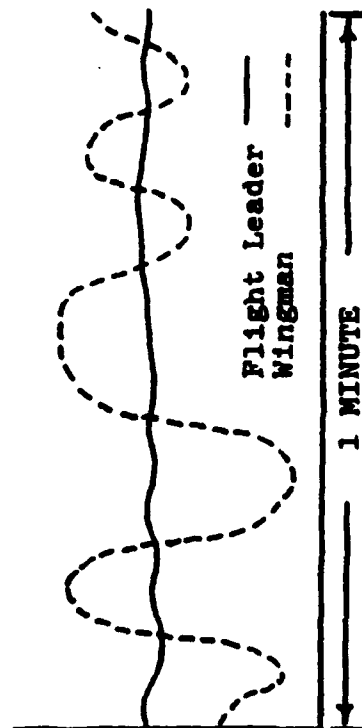
ALTITUDE



POWER SETTING



ENGINE SPEED

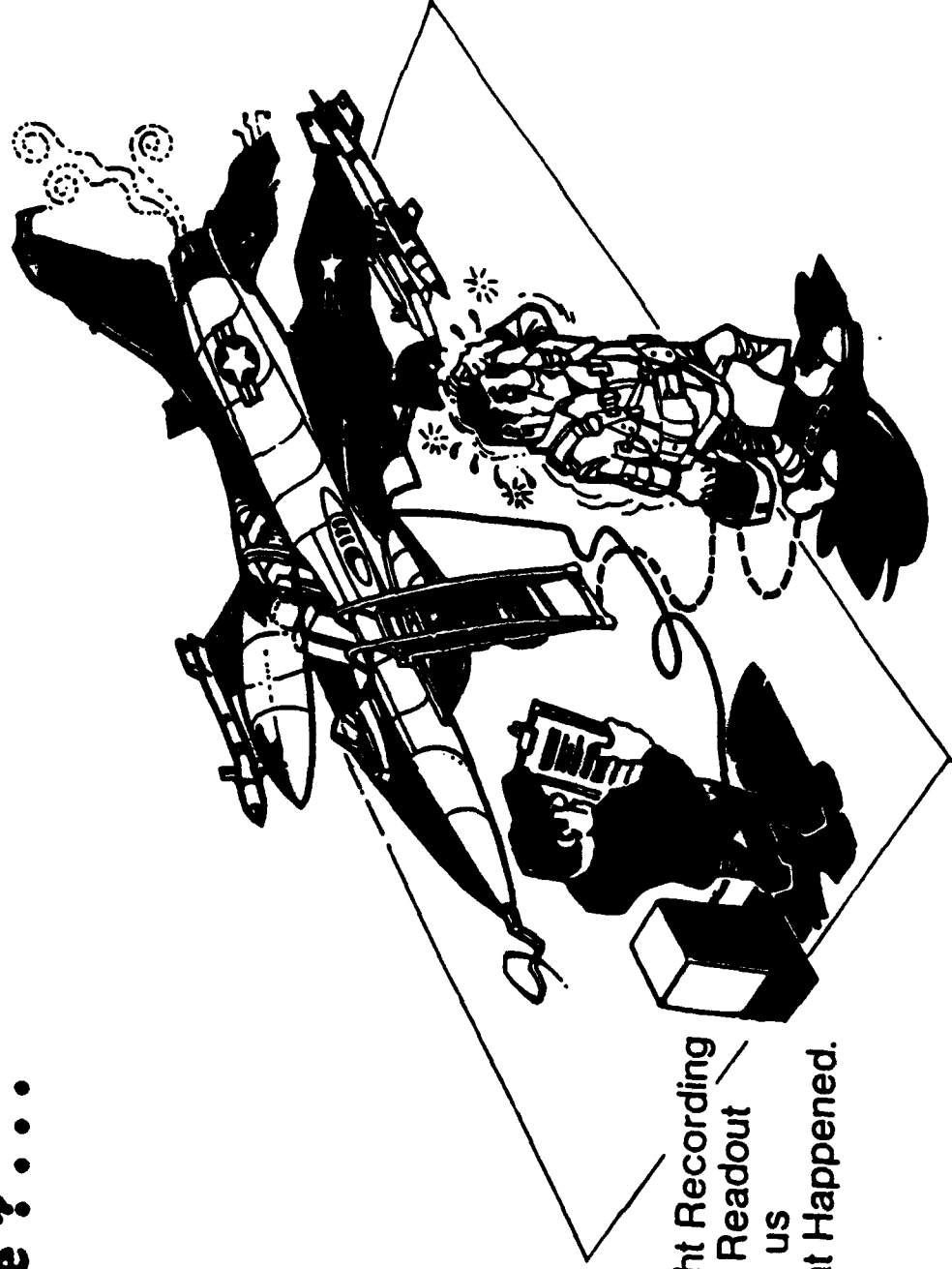


TAILPIPE
TEMPERATURE

Flight Leader
Wingman

1 MINUTE

What Happened Up There ? . . .



Flight Recording
and Readout
tells us
What Happened.

COMPARISON OF F100-PW-100 ENGINE DESIGN AND ACTUAL UTILIZATION

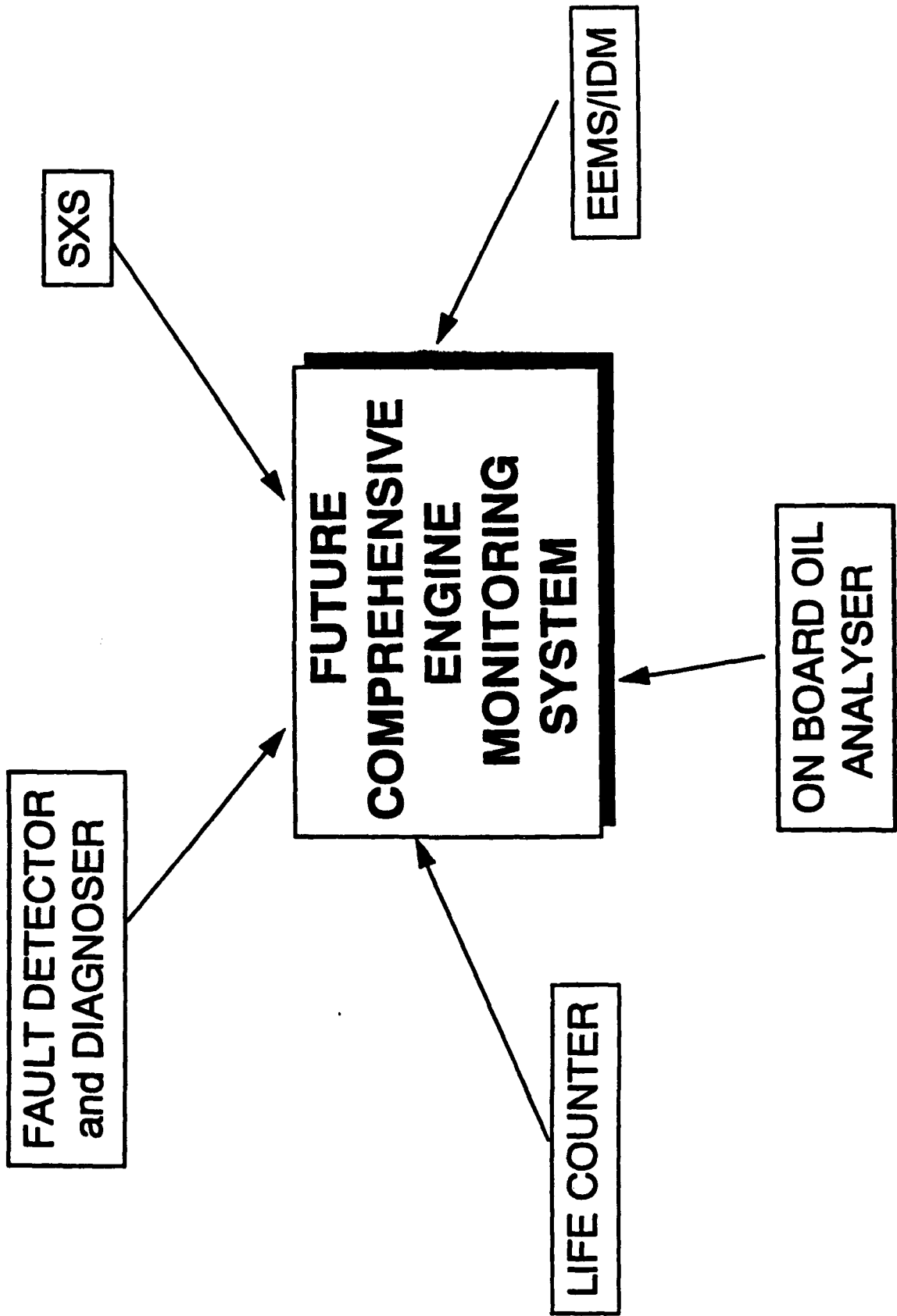
	<u>Design</u>	<u>Field</u>
Mission Run Time, hours	4,000	4,000
Major Cycles (Shut off to Intermediate and Above)	3,530	2,360
Partial Cycles (Idle to Intermediate and Above)	0	21,630
Augmented Cycles	2,970	15,200
Supersonic Time, hours	10	35
Augmented Time, hours	106	104
Total Time at Intermediate to Max Power, hours	1.050	472

QUANTIFYING THE APPROXIMATIONS

- 18% of start-ups are for ground runs
- Tie-down runs consume same life as flying hours
- Pilots log 9% more flying hours than actual
- Taxi time averages 20 minutes per sortie/hop
- Actual use of fracture crit comps \neq expected use
- Poor correlation between life usage rate and time
- Landings and TO's are more significant than hop length
- Poor correlation between sortie code and life usage
- Payload has minimum effect on life usage

CONCLUSION:

MEASURE LIFE AS IT IS CONSUMED



HOLLOW FAN BLADE DAMAGE TOLERANCE
CAPABILITY/BENEFITS FOR AN ADVANCED
TECHNOLOGY ENGINE



John M. Delvaux
Michael J. Duffy
Troy T. King

CHART 1 (TITLE)

THE ANALYSIS SUMMARIZED HERE WAS CONDUCTED BY THE F119 STRUCTURES GROUP IN SUPPORT OF THE STUDY ON HOLLOW FAN BLADE (HFB) DAMAGE TOLERANCE. THE TOTAL STUDY INCLUDED A MANUFACTURING PROCESS REVIEW, HFB EXPERIENCE ON OTHER ENGINES, FLIGHT LINE INSPECTION CAPABILITY/PLANS AND A WEAPON SYSTEMS SAFETY ANALYSIS.

LIFE MANAGEMENT OF THE HFB BY DAMAGE TOLERANCE WITH REDUCED CONTAINMENT IS AN OPTION FOR THE F119 ENGINE.

DAMAGE TOLERANCE OF HOLLOW FAN BLADE

OVERVIEW

- **PURPOSE**
- **FAILURE MODE ANALYSIS**
 - **BIRD INGESTION**
 - **VIBRATORY RESPONSE**
 - **FOD/DOD RESPONSE**
 - **INITIAL FLAW DAMAGE TOLERANCE**
- **MISSION ANALYSIS**
- **SUMMARY**

CHART 2 (OVERVIEW)

FIRST, A FEW WORDS ON THE PURPOSE OF THIS STUDY. IT WAS MORE THAN TO REDUCE WEIGHT, ALTHOUGH THAT IS AN EVER PRESENT CHALLENGE. ATTENTION IS BEING PLACED ON THE USE OF FRACTURE MECHANICS FOR LIFE MANAGEMENT OF DYNAMICALLY LOADED COMPONENTS.

THE VARIOUS FAILURE MODES THAT MIGHT LEAD TO FAILURE/LOSS OF THE HFB HAVE BEEN STUDIED. THESE ARE THE FAILURE MODES THAT ENGINE EXPERIENCE SHOWS TO BE IMPORTANT.

VIBRATORY STRESS IS AN ESPECIALLY CRITICAL FAILURE MODE. AT LOCATIONS OF MAXIMUM VIBRATORY STRESS FOR AIRFOILS, IT IS OFTEN IMPOSSIBLE TO SHOW ANY APPRECIABLE RESIDUAL LIFE FROM A RELIABLY DETECTABLE FLAW SIZE DUE TO THE SMALL THRESHOLD FLAW SIZE. THE SOLUTION IS TO CONTROL VIBRATORY RESPONSE SO THAT HCF INITIATIONS DO NOT OCCUR AND TO PROVIDE CONTAINMENT FOR PORTIONS OF THE BLADE THAT WOULD BE RELEASED. MORE ON THE VIBRATORY STRESS LATER.

A MISSION ANALYSIS SHOWS THAT LOSS OF 100% OF THE BLADE WILL BE CONTAINED A HIGH PERCENTAGE OF THE TIME EVEN WITHOUT FULL CONTAINMENT SINCE THE ENGINE OPERATES AT LESS THAN MAXIMUM CONDITIONS FOR MUCH OF ITS LIFE.

LAST, NATURALLY, IS THE SUMMARY.

DAMAGE TOLERANCE OF HOLLOW FAN BLADE
PURPOSE OF STUDY

- CONTINUE RESPONSE TO RECOMMENDATION OF USAF SAB AD HOC COMMITTEE REPORT ¹
- PROVIDE FOR SAFETY OF HFB BY DAMAGE TOLERANCE RATHER THAN CONTAINMENT FOR LOWER WEIGHT APPROACH

1. Air Force Aircraft Jet Engine Manufacturing and Production Processes, July 1992.

CHART 3 (PURPOSE)

AS SOME OF YOU ARE AWARE, AN SAB AD HOC COMMITTEE HAS RECOMMENDED THE USE OF FRACTURE MECHANICS TO PREVENT STRUCTURAL PROBLEMS ARISING FROM HIGH CYCLE FATIGUE (HCF). THIS RECOMMENDATION FOLLOWS FROM THEIR CONCLUSION THAT HIGH CYCLE FATIGUE HAS BEEN THE PRIMARY CAUSE OF FAILURE IN ENGINE TITANIUM COMPONENTS. THE REPORT ALSO STATES THAT THE GOODMAN DIAGRAM HAS OUTLIVED ITS USEFULNESS FOR THE DESIGN OF JET ENGINES TO RESIST HCF.

I BELIEVE THE GOODMAN DIAGRAM APPROACH FOR AEROMECHANICAL STRESS EVALUATION MUST BE RETAINED, BUT I ALSO BELIEVE THAT FRACTURE MECHANICS MUST ALSO BE USED DURING DESIGN/DEVELOPMENT. THE NEED IS TO DEFINE A DESIGN PROCESS. PRATT & WHITNEY IS WORKING TO DEVELOP SUCH A DESIGN PROCESS.

IN THE MEANTIME, WE ARE USING FRACTURE MECHANICS TO ASSESS THE BLADING IN OUR CURRENT DEVELOPMENT AND OPERATIONAL ENGINE PROGRAMS.

IN THE F119 ENGINE WE ARE EVALUATING THE TURBINE BLADES AS WELL AS THE COMPONENT COVERED IN THIS SUBJECT: THE FAN ROTOR 1 HFB. SO P&W AND THE CUSTOMER TEAM ARE RESPONDING TO THE SAB RECOMMENDATION.

AS A RESIDUAL BENEFIT, LIFE MANAGEMENT OF SAFETY OF THE HFB BY DAMAGE TOLERANCE INSTEAD OF FULL CONTAINMENT RESULTS IN A LOWER WEIGHT FOR THE ENGINE.

FAILURE MODE ANALYSIS - BIRD INGESTION
MOST PROBABLE PORTION OF BLADE LOSS DUE TO BIRD INGESTION IS LESS THAN 50%

- **PREDICTED DAMAGE FOR SMALL AND MEDIUM SIZE BIRDS IS DENT WITHOUT FRACTURE.**
- **PREDICTED DAMAGE FOR LARGE BIRD IS LARGE DENT WITH POSSIBLE HOLLOW CAVITY CRACK/ FRACTURE.**
- **MAX STRAIN IS PERPENDICULAR TO RADIAL PLANE, ORIENTED TOWARDS LEADING EDGE AND IS OUTBOARD OF 50% SPAN.**
- **POSSIBLE BLADE LIBERATION WITH BIRD IMPACT ON UNBLENDED BLADES AFTER FOD DAMAGE.**
- **PROBABILITY OF FOD INCIDENT FOLLOWED BY BIRD STRIKE ON SAME BLADE ON SAME FLIGHT IS REMOTE; CONSIDERED IN SAFETY ANALYSIS.**

HOLLOW FAN MEDIUM BIRD IMPACT RESULTS

Predicted Response from 2.5 lb Bird, 300 ft/sec, 70% span



HOLLOW FAN MEDIUM BIRD IMPACT RESULTS

Strains Below Crack Threshold - > No Cracks or Material Loss



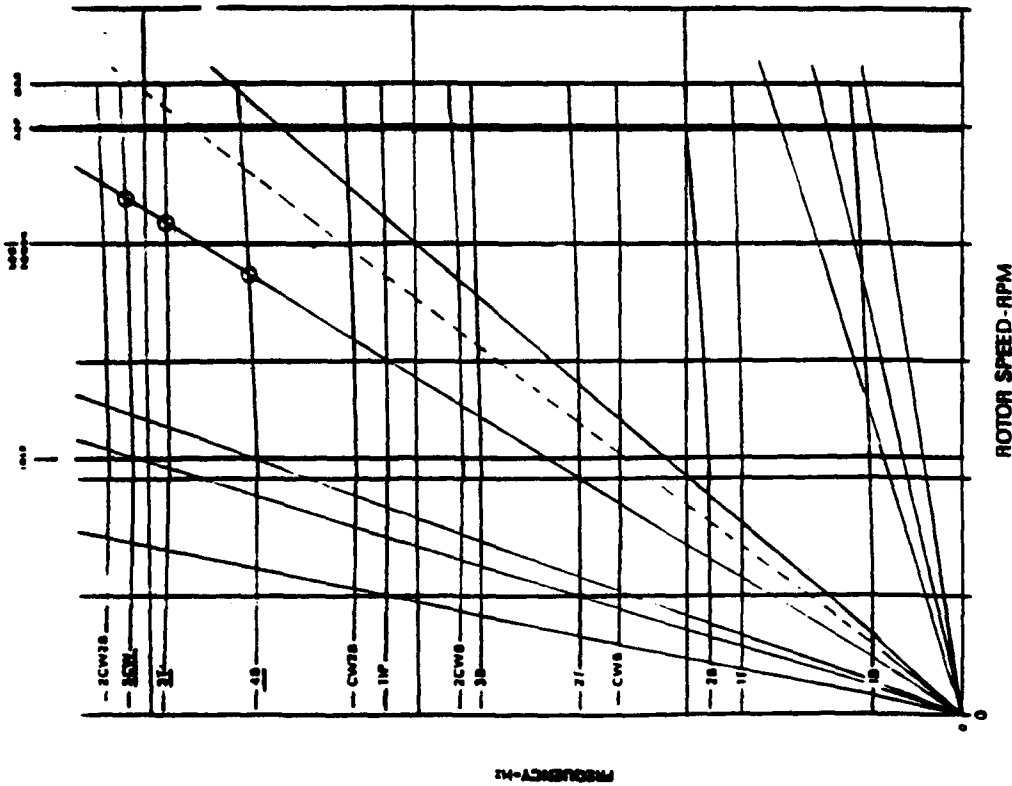
CHART 4, 5, AND 6

1ST STAGE FAN BLADES DO ENCOUNTER BIRDS FROM TIME TO TIME AND BLADE LOSS HAS RESULTED. BIRD INGESTION CAPABILITY IS A REQUIREMENT FOR ENGINES AND THE HFB HAS BEEN DESIGNED TO MEET THESE REQUIREMENTS.

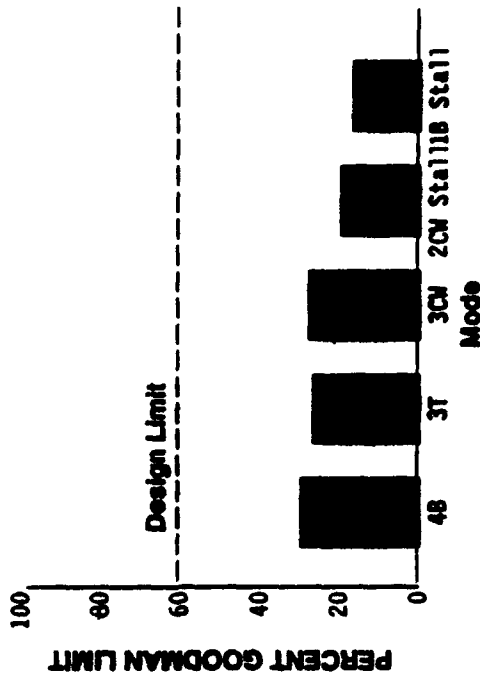
A NON-LINEAR FINITE ELEMENT ANALYSIS HAS BEEN USED THAT GIVES DEFLECTED SHAPE AND STRAIN LEVELS THAT OCCUR DURING BIRD STRIKE. THIS MODEL IS CALIBRATED WITH COMPONENT AND ENGINE TEST RESULTS AND IS A PROVEN, VALUABLE DESIGN TOOL. TYPICAL MODEL OUTPUT IS SHOWN IN CHARTS 5 AND 6. BASED ON THE KNOWLEDGE OF THE LOCATION AND ORIENTATION OF MAXIMUM STRAIN, IT IS JUDGED THAT BIRD STRIKE WILL NOT RESULT IN LOSS OF THE TOTAL BLADE, ALTHOUGH SOME PORTION LESS THAN 50% OF THE TOTAL BLADE MAY SEPARATE. DEVELOPMENT ENGINE TEST WILL BE CONDUCTED FOR CALIBRATION WITH ANALYSIS.

FAILURE MODE ANALYSIS - VIBRATORY RESPONSE CONSERVATIVE ASSUMPTIONS USED PENDING COMPLETION OF AEROMECHANICAL STRESS DEFINITION BY ENGINE TEST

Campbell Diagram



Measured Responses



- Assumed Responses
- 60% of Smooth Capability
 - 100% of $Kt=3$ Capability for LE and TE

CHART 7

LOW ASPECT RATIO (LAR) WIDE CHORD AIRFOILS ARE A CHALLENGE FROM THE DESIGN STANDPOINT. STANDARD CRITERIA IS TO MAINTAIN A MARGIN BETWEEN CRITICAL EXCITATIONS AND MODES AT MAXIMUM SPEED. ALSO DESIRABLE, BUT OFTEN NOT OBTAINABLE DUE TO WEIGHT, IS TO AVOID CROSSING OF THE FUNDAMENTAL BENDING MODE WITH LOW ORDERS OF VIBRATION ($1E-4E$) IN THE OPERATING SPEED RANGE. THIS HFB HAS NUMEROUS CHORDWISE MODES THAT INTERSECT POSSIBLE ENGINE ORDER DRIVERS IN THE OPERATING SPEED RANGE. NUMEROUS OPPORTUNITIES FOR RESONANCE.

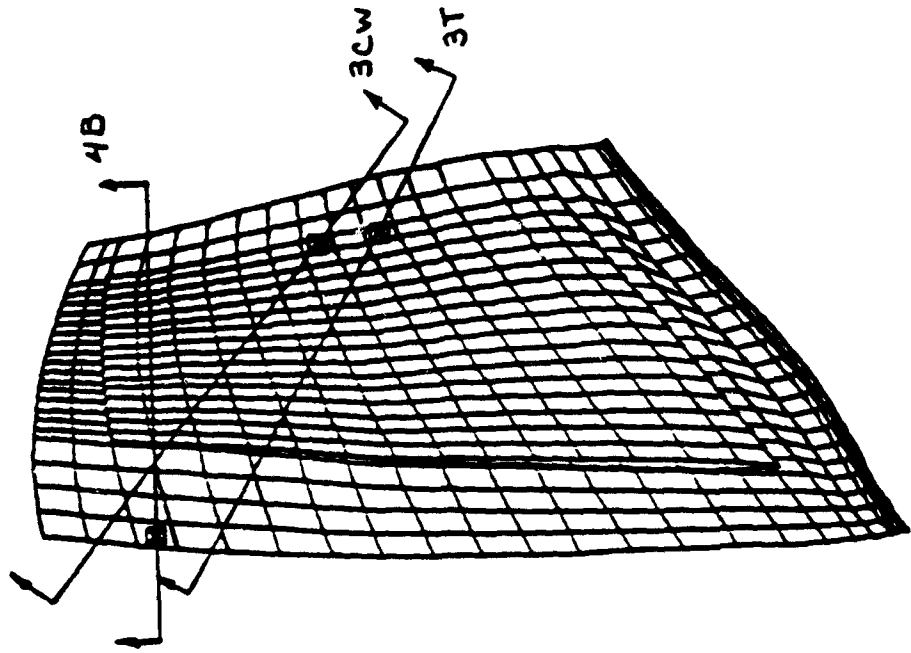
AS SHOWN ON THE CAMPBELL PLOT, THIS 1ST STAGE HFB IS PRIMARILY EXCITED BY THE INLET GUIDE VANE (IGV).

THE BAR CHART SHOWS THE VIBRATORY STRESS AMPLITUDES THAT HAVE BEEN MEASURED TO DATE BY ENGINE TESTS. RESPONSES ARE IN GENERAL LOW, BUT THE STRESS SURVEY TO THE MOST SEVERE ENVELOPE CONDITIONS HAS NOT BEEN COMPLETED. INITIAL DATA DOES NOT SHOW A SIGNIFICANT INCREASE IN STRESS WITH INCREASING INLET PRESSURE AND TEMPERATURE.

HOWEVER, IN OUR ANALYSIS, IT HAS BEEN ASSUMED THAT THE VIBRATORY STRESS AMPLITUDES ARE 60% OF THE GOODMAN DIAGRAM LIMIT IN SMOOTH AREAS, AND 100% OF THE LIMIT IN STRESS CONCENTRATION AREAS. THIS ASSUMPTION IS WELL ABOVE WHAT HAS BEEN MEASURED TO DATE, BUT IT IS THE MAXIMUM ALLOWED BY SPECIFICATION.

FAILURE MODE ANALYSIS - VIBRATION RESPONSE MAXIMUM STRESS (MINIMUM MARGIN) LOCATIONS USED TO ESTIMATE MOST PROBABLE PORTION OF BLADE LOSS

Maximum principal
stress plane assumed
as crack propagation
path (conservative)



↑ Estimated crack growth path.
⊠ - Probable initiation site.

CHART 8

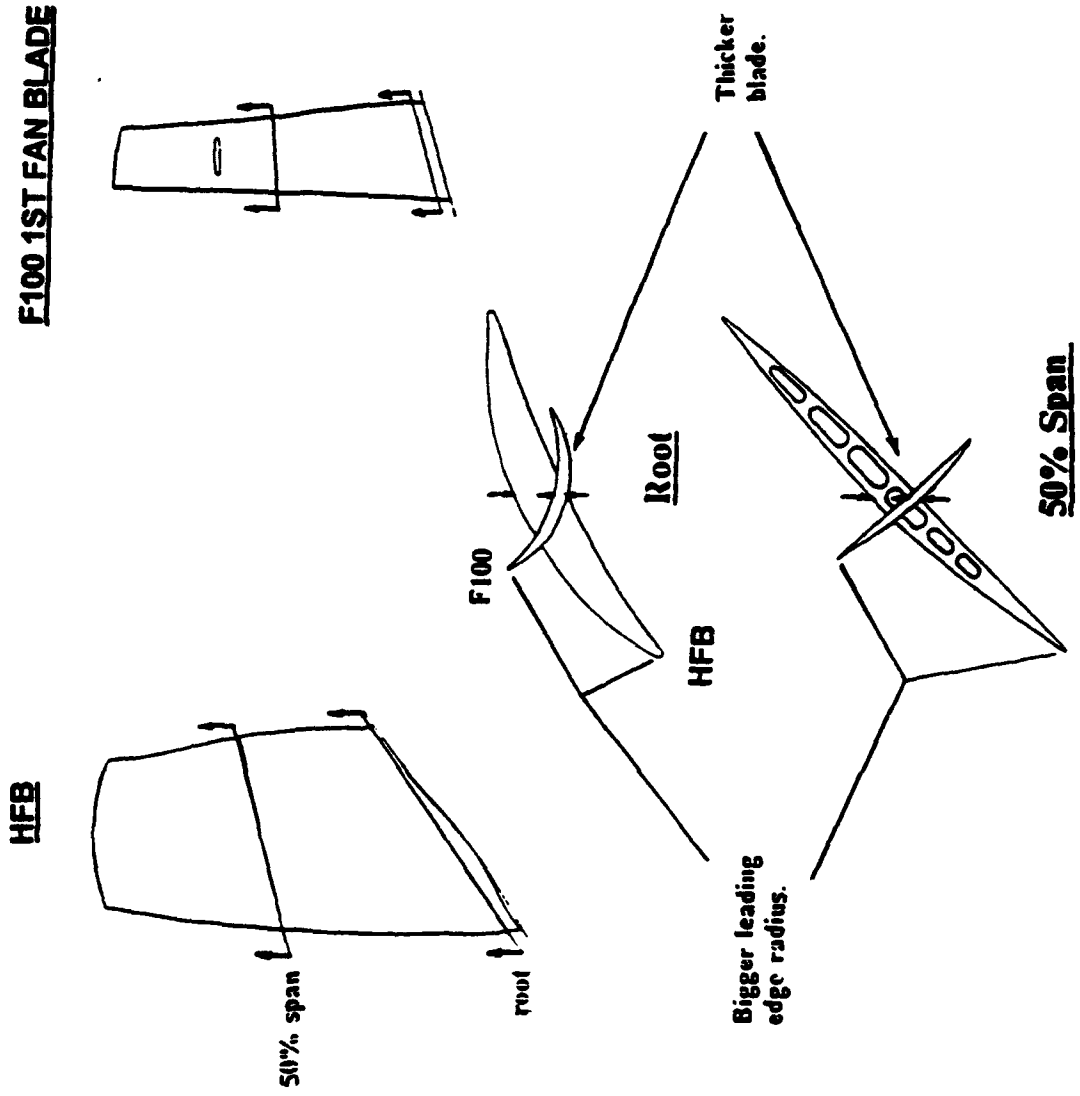
A FINITE ELEMENT ANALYSIS FOR STEADY STRESS AND VIBRATORY MODE SHAPES HAS BEEN CONDUCTED. THIS ANALYSIS GIVES US THE LOCATIONS AND DIRECTIONS OF VIBRATORY STRESS FOR THE MODES OF INTEREST AS WELL AS THE DIRECTION OF THE PRINCIPAL STRESS PLANE OF THESE LOCATIONS.

THE VIBRATORY STRESS PLANES FOR THESE RESPONSE MODES ARE ORIENTED RADIALLY WHERE AS THE PRINCIPAL STRESS PLANES ARE ORIENTED MORE AXIALLY. THE ASSUMPTION MADE HERE IS THAT IF A CRACK INITIATES DUE TO VIBRATORY RESPONSE, IT WILL GROW ALONG THE PRINCIPAL STRESS PLANE. IF THE BLADE SEPARATES DUE TO A PROGRESSING CRACK, THIS ASSUMED PATH RESULTS IN THE LARGEST PORTION OF BLADE LOSS. CONTAINMENT WILL BE PROVIDED FOR THE EQUIVALENT MASSES.

SO, AT LOCATIONS OF MAXIMUM VIBRATORY STRESS FOR THE RESPONSIVE MODES, IT IS ASSUMED THAT BLADE LOSS WILL OCCUR. CONSERVATIVE LEVELS FOR AMOUNT OF BLADE LOSS ARE USED. FAN CASE THICKNESS IS SET TO PROVIDE CONTAINMENT.

NO CRACK GROWTH ANALYSIS HAS EVOLVED YET.

FAILURE MODE ANALYSIS - FOD HFB IS A MORE RUGGED DESIGN



HFB

F100 1ST FAN BLADE

CHART 9

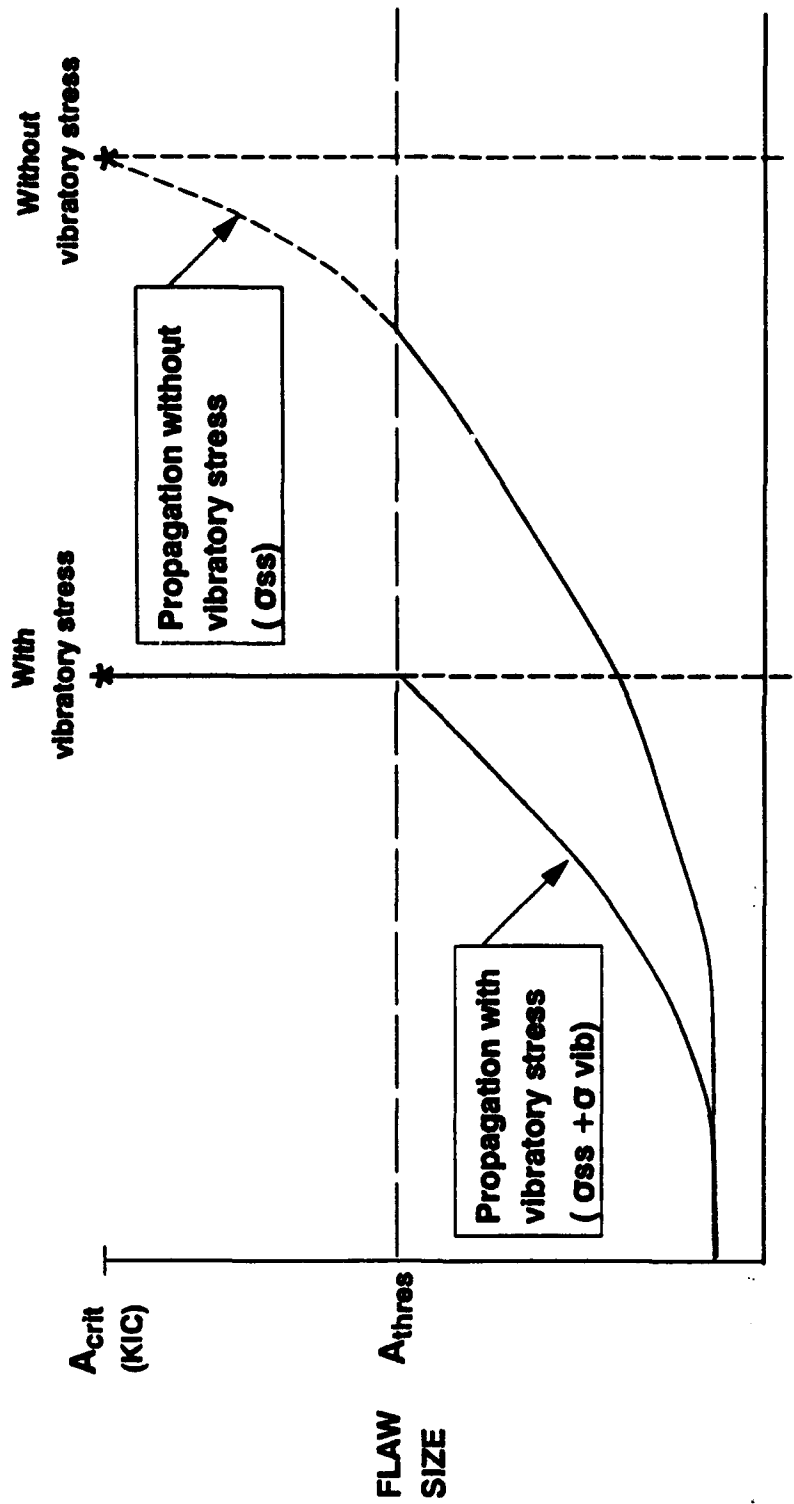
FOREIGN OBJECT DAMAGE (FOD) REPRESENTS THE MAJOR CAUSE OF AIRFOIL LOSS DURING ENGINE OPERATION. FOD OCCURS ON LEADING AND TRAILING EDGES AND CAN LEAD TO CRACK INITIATION AND GROWTH IF THE DAMAGE IS NOT DETECTED AND REMOVED (BLENDING OR REMOVAL).

THE HFB IS A RUGGED DESIGN FOR RESISTING FOD. SHOWN HERE IS A COMPARISON WITH THE 1ST FAN BLADE FROM OUR F100 ENGINE WHICH HAS HAD GOOD SERVICE EXPERIENCE.

COMPARISON AT A LOCATION 1.5" INCHES FROM THE TIP AND 10% CHORD BACK FROM THE LEADING EDGE SHOWS THICKNESS OF .095 INCHES VS. .047 INCHES, AND LEADING EDGE RADIUS OF .020 INCHES VS. .006 INCHES. SO, ON A QUALITATIVE BASIS, THE HFB IS MORE RESISTANT TO THE AMOUNT OF DAMAGE THAT IS INCURRED DUE TO FOD. ACUITY, TEARING, OR OTHER UNDESIRABLE CHARACTERISTICS CAUSED BY FOD WILL BE LESS FOR THE HFB.

FAILURE MODE ANALYSIS - VIBRATORY RESPONSE

Vibratory Stress Reduces Residual Life



RESIDUAL LIFE - CYCLES

- $A_{thres} \leq A_{crit}$ (KIC) ; Can be 1-2 orders less depending on vibratory stress

CHART 10

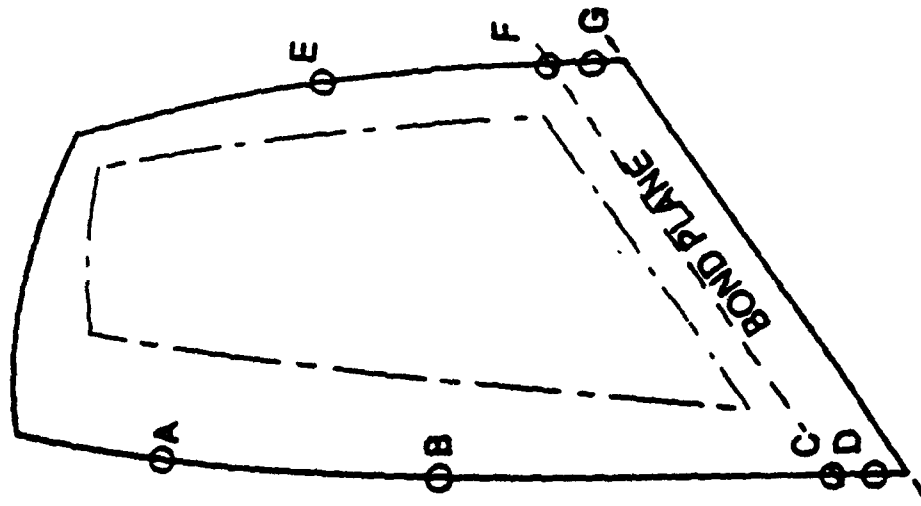
BEFORE I SHOW RESULTS OF CRACK GROWTH ANALYSIS, I WANT TO GIVE A BRIEF DESCRIPTION OF THE SEVERE IMPACT ON FINAL FLAW SIZE LIMITS AND RESIDUAL LIFE THAT OCCURS IN THE PRESENCE OF VIBRATORY STRESS.

WITHOUT VIBRATORY STRESS, CRACKS PROGRESS FROM SOME INITIAL SIZE TO THE CRITICAL SIZE GOVERNED BY THE FRACTURE TOUGHNESS OF THE MATERIAL. THE NUMBER OF CYCLES OF STRESS REQUIRED TO REACH THIS CRITICAL FLAW SIZE IS THE RESIDUAL LIFE. WITH VIBRATORY STRESS PRESENT, THE CRACK SIZE AT WHICH UNSTABLE CRACK GROWTH OCCURS IS REFERRED TO AS THE THRESHOLD FLAW SIZE AND CAN BE ORDERS OF MAGNITUDE LESS THAN THE CRITICAL CRACK SIZE ASSOCIATED WITH FRACTURE TOUGHNESS. WHEN THE CRACK IS BELOW THE THRESHOLD SIZE, IT WILL GROW VERY SLOWLY DUE TO STRESS CYCLES AND WILL NOT GROW IF ENGINE OPERATION IS SUSTAINED AT THE RESONANCE. ABOVE THE THRESHOLD SIZE, THE CRACK WILL GROW VERY RAPIDLY AT THE RESONANCE CONDITION.

WITH VIBRATORY STRESS PRESENT ON EACH ENGINE STRESS CYCLE, THE CRACK GROWTH IS MORE RAPID SINCE THE MAXIMUM STRESS IN THE CYCLE IS INCREASED BY THE AMPLITUDE OF VIBRATORY STRESS. THIS INCREASED MAXIMUM STRESS CYCLE CAUSES THE CRACK TO REACH THE THRESHOLD SIZE MORE RAPIDLY, WHICH, IN TURN, REDUCES THE RESIDUAL LIFE. THIS IS IN GENERAL A SECOND ORDER EFFECT, BUT BECOMES MORE SIGNIFICANT AS VIBRATORY STRESS AMPLITUDE INCREASES. BOTTOMLINE: VIBRATORY STRESS IS AN "ACHILLES HEEL" FOR RESIDUAL LIFE.

FAILURE MODE ANALYSIS - FOD
FOD RESULTING IN .005" DEEP CRACK HAS GOOD CRACK
GROWTH LIFE EXCEPT FOR TIP MODE

<u>LOCATION</u>	<u>a_{th}</u>	<u>REMAINING LIFE</u>
A	.006"	0
B	.014"	> 20,000 TAC'S
C	.047"	> 20,000 TAC'S
D	.140"	> 20,000 TAC'S
E	.012"	> 20,000 TAC'S
F	.019"	> 20,000 TAC'S
G	.250"	> 20,000 TAC'S



Experience established that $a_{th} > .010$ resulted in acceptable service experience

- FOD will be detected at the end of flight inspection prior to blade failure.

CHART 11

AT FIRST BLUSH, THE STARTING AND ENDING FLAW SIZES DO NOT APPEAR TO BE VERY ROBUST. THE ASSUMPTION FOR AI IS .005 INCHES DEEP, AND THE "A" THRESHOLD VALUES OFTEN HAVE A ZERO AS THE FIRST DIGIT TO THE RIGHT OF THE DECIMAL POINT. HOWEVER, A CHARACTERISTIC OF AIRFOILS IS THAT THE RESIDUAL LIFE IS LARGE IF THE STARTING AND ENDING FLAW SIZE ASSUMPTIONS HAVE SOME SEPARATION.

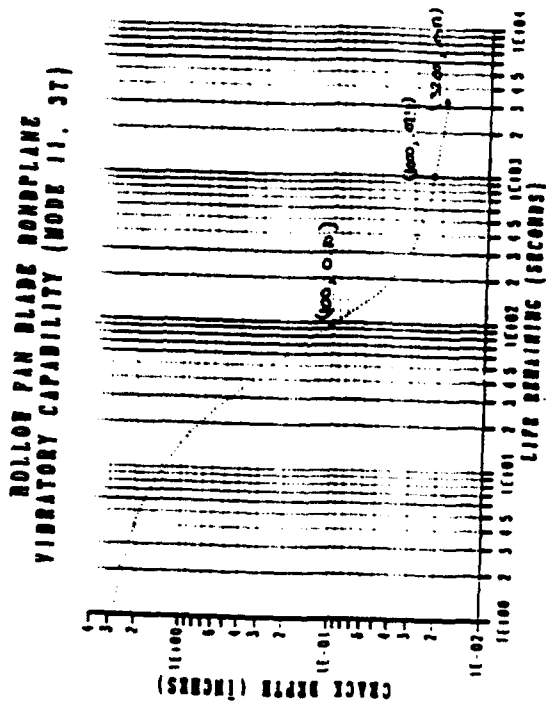
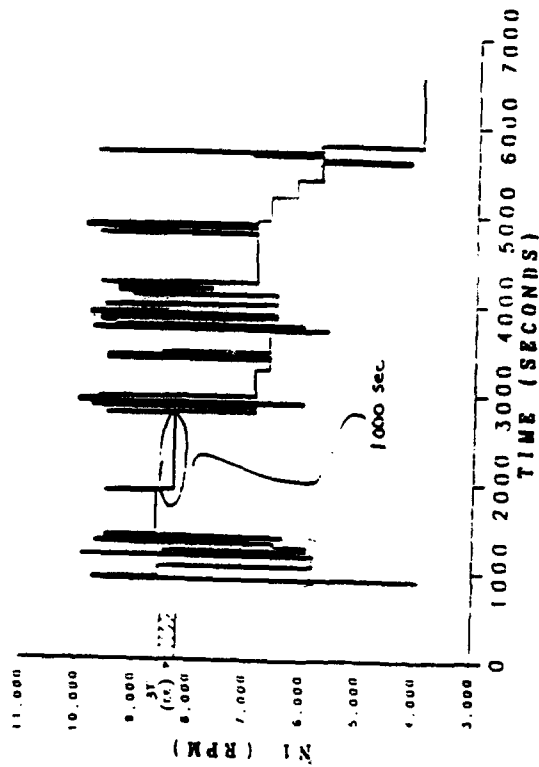
F100 ENGINE EXPERIENCE HAS BEEN GOOD WHEN THE THRESHOLD FLAW SIZE IS ABOVE .010 INCHES DEEP. F100 ENGINE EXPERIENCE HAS BEEN THAT BLADES ARE SENSITIVE TO FOD WHEN THIS THRESHOLD FLAW SIZE APPROACHES .005" INCHES DEEP.

THE ASSERTION IS THAT LE OR TE FOD WILL BE DETECTED BY THE END OF FLIGHT INSPECTIONS PRIOR TO BLADE FAILURE.

AN IMPORTANT NOTE IS THAT THESE INSPECTIONS ARE LOOKING FOR FOD THAT IS VISUALLY DETECTABLE, NOT A 5 MIL CRACK.

FAILURE MODE ANALYSIS - FOD
FOD RESULTING IN ACTIVE CRACK EQUAL TO THE THRESHOLD FLAW
SIZE WILL BE DETECTED BY POST FLIGHT INSPECTION

- LIMITED CRACK GROWTH CAPABILITY SINCE CURRENT DUTY CYCLE IDLE/CRUISE SPEED AND RESONANT SPEEDS CAN COINCIDE.
- TIME IN RESONANCE FOR 1 MISSION ESTIMATED TO BE 1000 SECONDS.
- TIME IN RESONANCE UNTIL BLADE FAILS IN HCF ESTIMATED TO BE 3200 SECONDS.



FOR CRITICAL LOCATION "F", T.E.

CHART 12

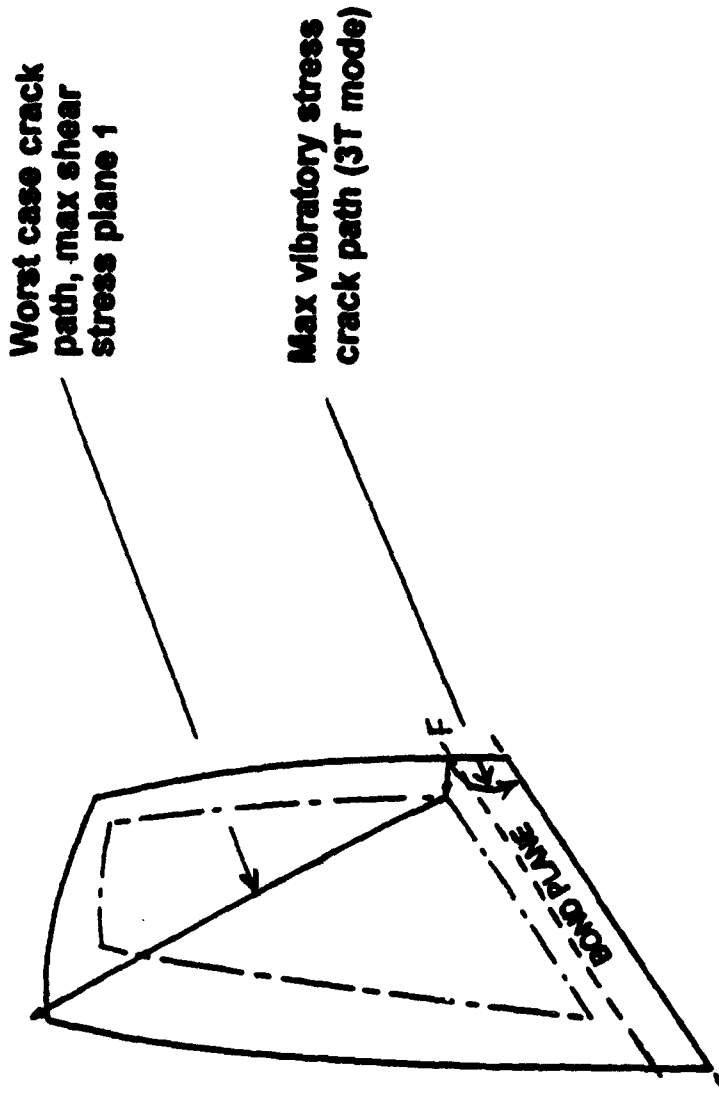
THE QUESTION HAS BEEN ASKED: "WILL THE FOD BE DETECTED PRIOR TO BLADE FAILURE IF THE DAMAGE ACTS AS A SHARP FLAW AND THE SIZE IS EQUAL TO THE THRESHOLD FLAW SIZE?"

FOR THIS ASSUMPTION, CRACK GROWTH CAPABILITY CAN BE VERY LIMITED. RESONANT FREQUENCIES FOR THESE PANEL MODES ARE ~ 2000 HZ AND IN SOME CASES CAN BE 20,000 HZ. STEADY STATE SPEED OPERATION AT THE RESONANCE CONDITION WILL RAPIDLY GROW THE CRACK FROM THE THRESHOLD FLAW SIZE TO THE CRITICAL SIZE ASSOCIATED WITH THE FRACTURE TOUGHNESS. EVEN WITH THIS ASSUMPTION, MISSION ANALYSIS SHOWS THAT THERE ARE MULTIPLE OPPORTUNITIES TO DETECT THE FOD PRIOR TO FAILURE.

TIME TO FAILURE IS EXTREMELY SENSITIVE TO IDLE/CRUISE AND RESONANT SPEEDS THOUGH.

SIMILAR ANALYSIS FOR LEADING EDGE LOCATION "C" SHOWS IT TO BE MUCH LESS CRITICAL: 24000 SECONDS IN RESONANCE UNTIL BLADE FAILURE OCCURS AND, AGAIN, 1000 SECONDS IN RESONANCE PER MISSION.

FAILURE MODE ANALYSIS - FOD
CONTAINMENT IS PROVIDED FOR THE WORST CASE
ASSUMPTION OF BLADE LOSS FOR THE MOST CRITICAL
LOCATION/MODE



1. Additional finite element/fracture analysis and component test required to confirm crack growth path in hollow cavities.

CHART 13

ANOTHER QUESTION HAS BEEN ASKED RELATIVE TO FOD: "WILL THE PORTION OF BLADE LOSS BE CONTAINED UNDER THE WORST CASE ASSUMPTION OF BLADE FAILURE PRIOR TO DETECTION?"

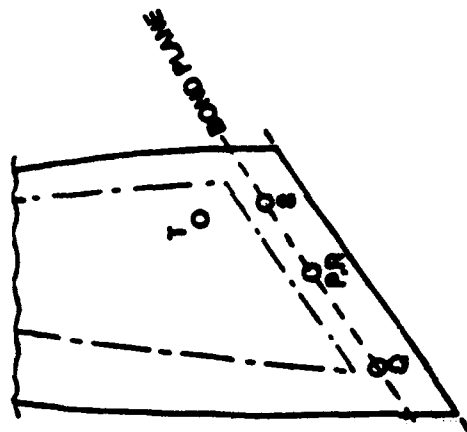
ANALYSIS OF CRITICAL LOCATION "F" INDICATES "YES". IF THE CRACK FOLLOWS THE PLANE OF MAXIMUM VIBRATORY STRESS, THE MOST PROBABLE AMOUNT OF BLADE LOSS IS A SMALL CORNER OF THE ROOT TRAILING EDGE. IF THE CRACK GROWS ALONG THE PLANE OF PRINCIPAL STRESS, IT WILL INTERSECT THE INBOARD AFT PORTION OF THE HOLLOW CAVITY.

A COMPARISON OF THE MARGIN BETWEEN STRESS AND ALLOWABLE SHOWS THE MAXIMUM SHEAR STRESS TO BE LESS THAN THE MAXIMUM TENSILE STRESS WHEN THE CRACK INTERSECTS THE HOLLOW CAVITY. THE ASSUMPTION IS THAT THE CRACK WILL GROW ALONG THE PLANE OF MAXIMUM SHEAR STRESS.

WHILE THE HFB IS VERY RESISTANT TO CRACK GROWTH DUE TO THE PRESENCE OF MULTIPLE LOAD PATHS (SEPARATE THICK SKINS FOR PRESSURE SIDE AND SUCTION SIDE) AND CRACK ARREST FEATURES (MULTIPLE RADIALLY ORIENTED RIBS - NOT SHOWN ON THE SKETCH), CRACK GROWTH PATHS HAVE NOT BEEN VERIFIED. ADDITIONAL ANALYSIS AND COMPONENT TEST IS PLANNED. FOR THE ASSUMED CRACK GROWTH PATH, THE PORTION OF BLADE LOSS WILL BE LESS THAN 50% OF THE TOTAL MASS. BLADE LOSS IS HIGHLY UNLIKELY.

FAILURE MODE ANALYSIS - INITIAL FLAW DAMAGE TOLERANCE

FOR ASSUMED INITIAL DEFECTS, RESIDUAL LIFE IS SUFFICIENT TO MAINTAIN SAFETY BY PRODUCTION AND DEPOT INSPECTION



LOCATION	NDT METHOD	MAX ASSUMED a _i	CRACK GROWTH LIFE, TAC'S	INSPECTION INTERVAL
PURGE HOLE				
P	X-RAY	.250" DIA	> 20,000	NONE
SURFACE FLAW	Q	.020" x .040"	> 20,000	4340 TAC'S
	R	.020" x .040"	> 20,000	4340 TAC'S
	S	.020" x .040"	> 20,000	4340 TAC'S
	T	.005" x .010"	> 20,000	NON-INSPECTABLE
		.010" x .020"	10,500	NON-INSPECTABLE
	.020" x .040"	5,700	NON-INSPECTABLE	

1. Internal location "T": Slow crack growth non-inspectable can be achieved by qualifying FPI to .010" x .020" or by lowering vibratory stress.

CHART 14

THE HFB WAS ALSO EXAMINED FOR DAMAGE TOLERANCE FROM THE CONVENTIONAL STANDPOINT. RESIDUAL LIFE CAPABILITY IN THE PRESENCE OF SHARP CRACKS WITH LIMITED CAPABILITY OF DETECTION - THE ROGUE FLAW CONSIDERATION.

THE LIMITING LOCATIONS/CONDITIONS HERE ARE RELATIVELY HIGH ROTOR SPEED RELATED MAXIMUM STEADY STRESS AND LOW VIBRATORY STRESS. RESIDUAL LIFE FROM RELIABLY DETECTABLE FLAW SIZES IS GOOD FOR THE HFB.

IN FACT, ALL LOCATIONS CAN BE QUALIFIED AS SLOW CRACK GROWTH NON-INSPECTABLE EXCEPT FOR LOCATION "T" WHICH IS ON THE INTERNAL SKIN. OPTIONS HERE INCLUDE QUALIFYING FPI TO .010 INCH BY .020 INCH BY THE 21ST CENTURY OR RE-ANALYSIS OF THIS LOCATION FOR A LOWER VIBRATORY STRESS PENDING COMPLETION OF THE AEROMECHANICAL STRESS SURVEY.

MISSION ANALYSIS

DESIGNING FOR CONTAINMENT OF 50% BLADE LOSS AT MAX CONDITIONS PROVIDES ADDED CAPABILITY FOR MOST OF THE FLIGHT ENVELOPE.

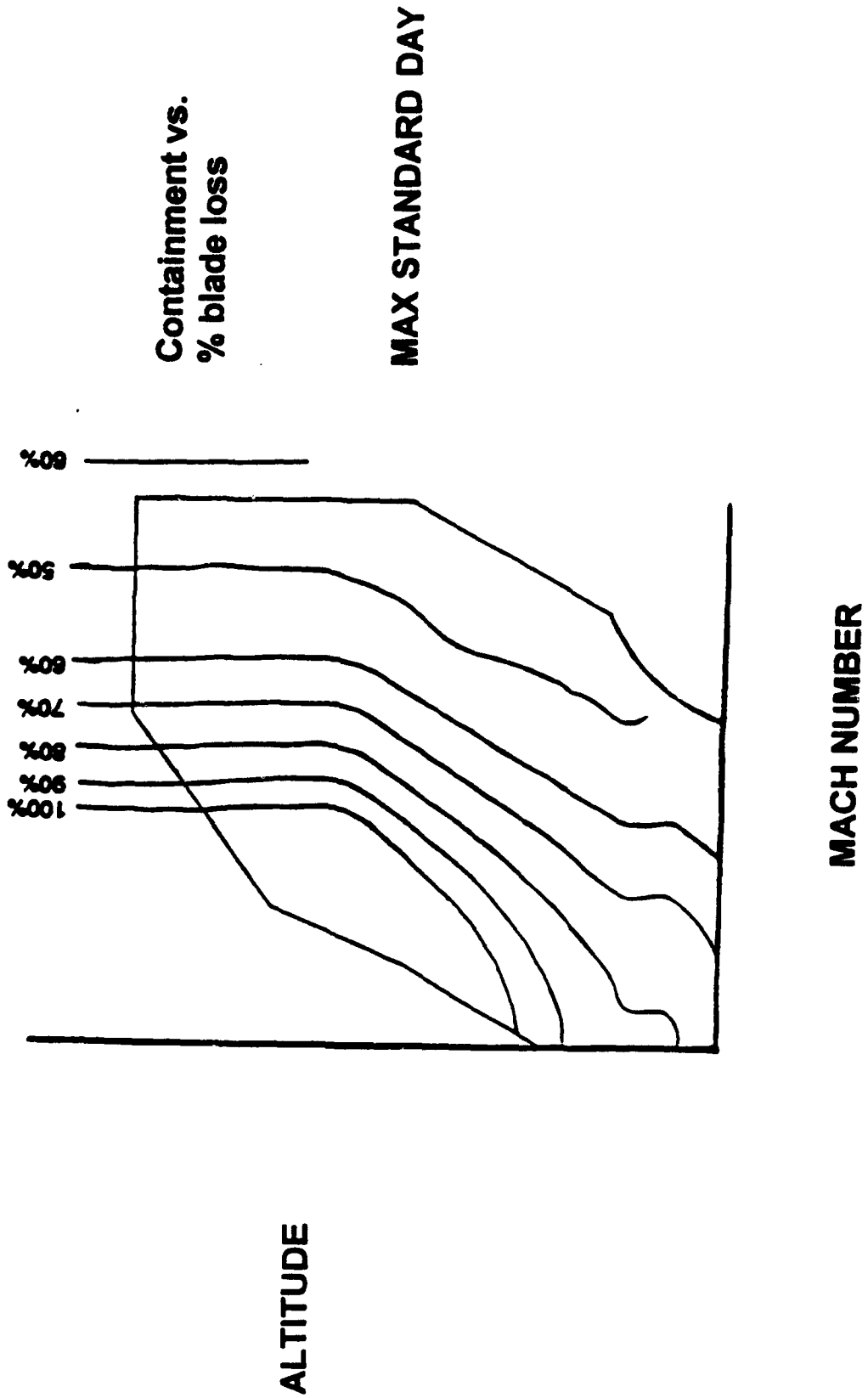


CHART 15

MISSION ANALYSIS PROVIDES SOME QUASI-STATISTICAL PERSPECTIVE ON THE IMPLICATION OF REDUCING CONTAINMENT FROM FULL BLADE TO ONE-HALF BLADE.

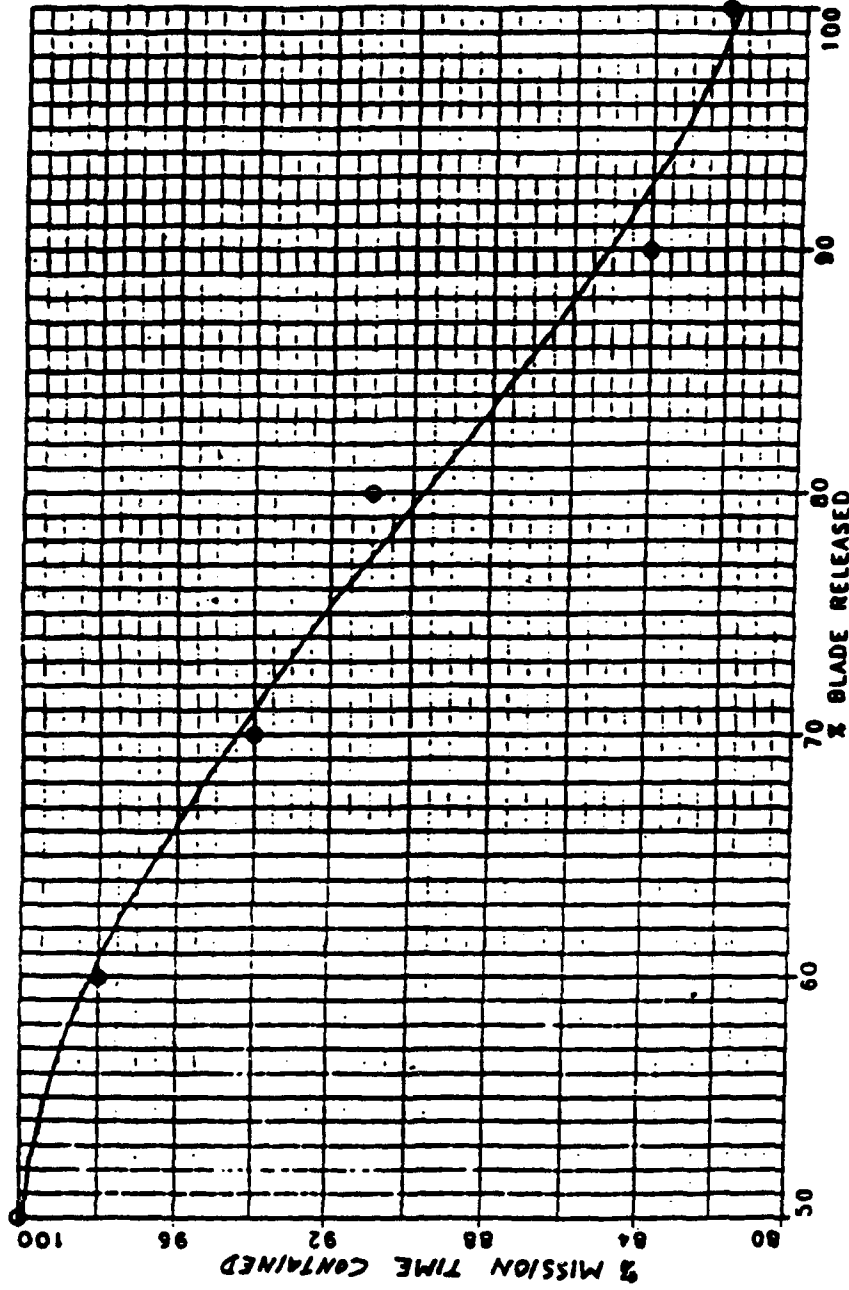
CONTAINMENT CAPABILITY AS A FUNCTION OF FULL POWER INTERMEDIATE ROTOR SPEED, PRESSURE AND TEMPERATURE IS SHOWN ON THE FLIGHT ENVELOPE.

CONTAINMENT VARIES FROM 50% OF THE BLADE (ASSUMED DESIGN CONDITION) AT MAXIMUM CONDITIONS TO 100% BLADE CONTAINMENT AT THE UPPER LEFT-HAND CORNER.

SO, DESIGNING FOR HALF BLADE CONTAINMENT AT MAX CONDITIONS PROVIDES CONTAINMENT UP TO FULL BLADE AT OTHER POINTS IN THE FLIGHT ENVELOPE.

MISSION ANALYSIS

Time at less severe mission points reduces the risk of uncontained failure.



- SAFETY ANALYSIS INDICATES PROBABILITY OF UNCONTAINED EVENT IS VERY LOW ($P = .00043/100K$ EFH)

CHART 16

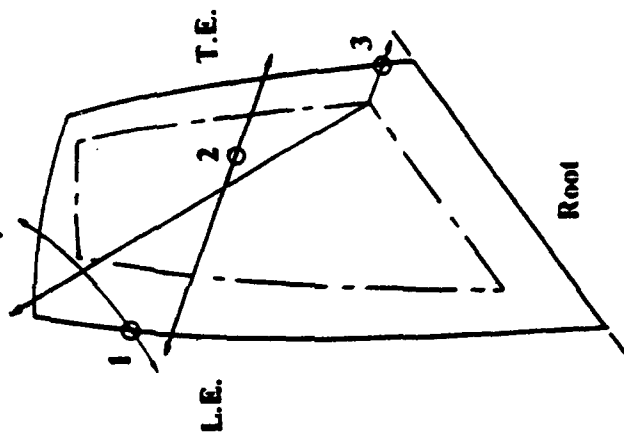
NEXT, THE STATISTICS ON FLIGHT TIME SPENT IN THE VARIOUS REGIONS OF THE FLIGHT ENVELOPE HAS BEEN FACTORED IN. THE MISSION DUTY CYCLE REVEALS THAT VERY LITTLE TIME IS PROJECTED FOR MAX CONDITION FLIGHT POINTS.

AS SHOWN ON THE CHART, CONTAINMENT PROBABILITY RANGES FROM 100% FOR 50% BLADE LOSS TO 82% FOR 100% BLADE LOSS.

TIME AT LESS SEVERE MISSION POINTS REDUCES THE RISK OF UNCONTAINED FAILURE.

DAMAGE TOLERANCE OF HOLLOW FAN BLADE SUMMARY-ANALYSIS IDENTIFIES MOST EFFECTIVE APPROACH

• MOST PROBABLE FAILURE MODES RESULTS IN LESS THAN 1/2 BLADE LOSS



Crack Initiation At:

- (1) The most limiting leading edge location.
- (2) The most limiting vibratory location.
- (3) The most limiting trailing edge location.

- PROVIDE CASE CONTAINMENT FOR MASS EQUAL TO OUTER 1/2 OF THE BLADE (PROVIDES MARGIN).
- MAINTAIN SAFETY FOR INBOARD PORTION OF BLADE BY DAMAGE TOLERANCE.
 - ANALYSIS & TEST VERIFICATION OF CRACK GROWTH
 - PRODUCTION, NORMAL FLIGHT LINE & DEPOT INSPECTIONS

CHART 17 (SUMMARY)

THE STUDY RESULTS INDICATE THAT THE MOST EFFECTIVE APPROACH IS TO PROVIDE CONTAINMENT FOR ONE HALF HFB LOSS AND TO MAINTAIN SAFETY OF THE INBOARD PORTION OF THE BLADE BY DAMAGE TOLERANCE. ONE-HALF BLADE LOSS ASSUMPTION REPRESENTS A FACTOR OF SAFETY OF 1.5 FOR MOST PROBABLE PORTION OF BLADE LOSS.

IMPLEMENTATION OF THIS OPTION WOULD RESULT IN A 9 - 12 LB. WEIGHT SAVINGS FOR THE FAN CASE.

ADDITIONAL ANALYSIS AND COMPONENT/ENGINE TEST IS PLANNED TO QUALIFY THE INBOARD PORTION OF THE BLADE AS FRACTURE CRITICAL.

EFFECT OF PEAK LOADS ON DWELL CRACK GROWTH
IN INCONEL 718 AT 600°C

R.J.H. Wanhill

National Aerospace Laboratory NLR, Amsterdam, The Netherlands

ABSTRACT

An investigation was made of dwell crack growth, including the effect of peak loads, in Inconel 718 disc material at 600°C in an air environment. This investigation is part of the European collaborative project IEPG TA 31: Lifing Concepts for Military Aero-Engine Components. The intention of this work was to determine the usefulness of developing crack growth prediction methods that combine creep and creep crack growth with fatigue crack growth.

It was found that the application of peak loads representative for military aircraft gas turbine discs strongly inhibits dwell crack growth, even when peak loads are immediately followed by underloads. From detailed consideration of this result it is shown that in all probability dwell cracking will not contribute to service crack growth problems for Inconel 718 at 600°C or less. Furthermore, the balance of evidence from this and previous investigations shows that dwell cracking in Inconel 718 occurs under small-scale yielding conditions at temperatures up to 650°C, is environmentally controlled and takes place by grain boundary oxidation and fracture. Any creep deformation in the crack tip region must be limited and may actually hinder dwell cracking.

In view of these results and their interpretation, it is concluded that it is not useful to develop crack growth prediction methods combining creep and creep crack growth with fatigue crack growth for Inconel 718 at 600°C or less. Nor is it likely that dwell crack growth need be included in life predictions. This will be checked by fatigue crack growth tests using the European-developed HOT TURBISTAN load sequence both with and without dwell periods.

CONTENTS

	Page
NOMENCLATURE	3
1 INTRODUCTION	5
2 MATERIAL AND SPECIMENS	5
3 TEST PROGRAMME AND EXPERIMENTAL PROCEDURE	6
4 DATA ANALYSIS PROCEDURE	7
4.1 The Fracture Mechanics Parameters K_I , J and C^*	7
4.2 Load-Line Compliance	9
4.3 Characteristic Time	9
5 MECHANICAL TESTING RESULTS	10
5.1 Dwell Crack Growth Curves	10
5.2 Correlation of Dwell Crack Growth Rates	10
5.2.1 Differences in Correlations by K_I , J and C^*	11
5.2.2 Bilinear Approximations to Crack Growth Rate Curves	11
5.2.3 Comparisons with Previous Results	12
5.3 Load-Line Compliance	13
5.4 Characteristic Time	13
6 METALLOGRAPHY AND MICROSTRUCTURE	13
7 FRACTOGRAPHY	14
7.1 Macrofractography	14
7.2 Microfractography	14
7.2.1 Dwell Crack Growth	14
7.2.2 Dwell Crack Growth + Peak Loads and Underloads	15
8 DISCUSSION	16
8.1 Effect of Peak Loads on Dwell Crack Growth	16
8.1.1 Service-Related Factors Extraneous to Laboratory Testing	17
8.1.2 Crack Growth Regimes: Long and Short Cracks	18
8.1.3 Implications for Crack Growth Prediction Methods	19
8.1.4 Implications for Crack Growth Testing	19
8.2 Dwell Crack Growth	20
8.2.1 Mechanism of Dwell Crack Growth and the Usefulness of Fracture Mechanics Crack Growth Parameters	21
8.2.2 Mechanism of Dwell Crack Growth and the Bilinear Approximations to Crack Growth Rate Curves	23
8.3 Mechanism of Dwell Crack Growth Inhibition by Peak Loads	25
9 CONCLUSIONS	25
10 ACKNOWLEDGEMENTS	26
11 REFERENCES	26

NOMENCLATURE

a	: crack length, from load line in Compact Tension (CT) specimen
a₁, a_f	: initial and final crack lengths, from load line in Compact Tension (CT) specimen
A	: constant in the Norton creep law $\dot{\epsilon} = A\sigma^n$
α	: crack length/ligament length, $a/(W-a)$
B	: specimen thickness
C*	: path-independent time-dependent contour integral
C_T*	: value of C* at transition in dwell crack growth rate dependence on C*
da/dt	: dwell crack growth rate
(da/dt)_T	: values of da/dt at transitions in dwell crack growth rate dependences on K _I and C*
E	: Young's modulus
EPFM	: Elastic-Plastic Fracture Mechanics
$\dot{\epsilon}$: strain rate
η	: crack length/ligament length parameter that is defined by $\eta = [4\alpha^2 + 4\alpha + 2]^{1/2} - 2\alpha - 1$
Γ	: line contour of a cracked body
h₁, h₃	: parameters depending only on a/W and n
IEPG	: Independent European Programme Group
J	: path-independent contour integral
K_I	: mode I stress intensity factor
K_{I,th}	: threshold value of K _I for the beginning of dwell crack growth
K_{I,T}	: value of K _I at transition in dwell crack growth rate dependence on K _I
LEFM	: Linear Elastic Fracture Mechanics
LVDT	: Linear Variable Displacement Transducer
m	: exponent in power law relations between da/dt and K _I or C*
m₁, m₂	: hypotransitional and hypertransitional values of m
n	: exponent in the Norton creep law $\dot{\epsilon} = A\sigma^n$
n_j	: outward normal along Γ
ν	: Poisson's ratio
P, P_{dwell}, P_{max}	: load, dwell load, maximum load
PD	: Potential Drop
r_{c,y}	: maximum extent of the crack tip creep zone in plane strain
r_{p,y}	: maximum extent of the crack tip plastic zone in plane strain

NOMENCLATURE (continued)

R	: stress ratio, $\sigma_{\min}/\sigma_{\max}$
R_f	: linear roughness parameter for fracture surfaces
R.T.	: room temperature
s	: arc length along Γ
SNECMA	: Societé Nationale d'Étude et de Construction de Moteurs d'Aviation
$\sigma, \sigma_{\max}, \sigma_{\min}$: stress, maximum stress, minimum stress
σ_{ij}	: biaxial stress tensor
σ_y	: yield stress, 0.2 % offset
σ_{TS}	: tensile strength
t	: time, testing time
t_c	: characteristic time for distinguishing between small-scale yielding and extensive creep: for plane strain this time is $t_c = [K_I^2(1-\nu^2)]/[(n+1)EC^*]$
t_p	: oxide passivation time
TA	: Technical Area
u_i, \dot{u}_i	: displacement and displacement rate vectors
U, \dot{U}	: strain energy, strain energy rate
v, \dot{v}	: displacement and displacement rate, at load line in Compact Tension (CT) specimen
V_{ref}	: reference potential for the direct current potential drop (PD) method of crack measurement
W	: characterizing width of the Compact Tension (CT) specimen: also strain energy density
W^*	: strain energy rate density
x, y	: crack tip coordinate system: x parallel to crack growth direction, y normal to crack surface
X_1, X_2	: depths of oxygen penetration into metal substrate

1 INTRODUCTION

The NLR is one of eight participants in the Independent European Programme Group cooperative technology project Technical Area 31 (IEPG TA 31) entitled "Lifing Concepts for Military Aero-Engine Components". The overall objectives of this programme are greater operational reliability, lower life cycle costs, and more informed decisions on current and future design concepts. The main technological objectives are:

- (1) Obtaining design data for a widely-used turbine disc material, forged Inconel 718.
- (2) Development and evaluation of life prediction methods.
- (3) Assessment of design lifing concepts.

The present investigation is a contribution to objective (2), and is concerned with determining the usefulness of developing crack growth prediction methods that combine creep and creep crack growth with fatigue crack growth. For this purpose several *dwelt* crack growth tests were done. Some of these tests included peak loads and underloads representative of load histories for military aircraft gas turbine discs, as exemplified by the standard isothermalized load history HOT TURBISTAN [1], which is being used in the design data part of the IEPG TA 31 project. A typical segment of HOT TURBISTAN is shown in figure 1 and illustrates the occurrence of dwells, peak loads and underloads: note the considerable time compression, since real flights usually last about an hour.

2 MATERIAL AND SPECIMENS

The material was a 440 mm diameter X 66 mm thick forged pancake of Inconel 718 supplied by SNECMA. Table 1 gives the material heat treatment, mechanical properties and grain size. The heat treatment is a common one for optimum creep resistance. Compact tension (CT) specimens were machined to the configuration shown in figure 2.

The specimens were fatigue precracked in an AMSLER vibrophore fitted with a 20 kN dynamometer. The fatigue loading was constant amplitude, $R = 0.1$, at cycle frequencies of 104-115 Hz and with maximum loads P_{max} between 6-8 kN.

The fatigue precracks were grown to between 2-4 mm from the notch root. Table 2 lists the specimen codes and the combined notch + precrack length, a_1 , measured from the load line after dwell crack growth testing and final fracture.

3 TEST PROGRAMME AND EXPERIMENTAL PROCEDURE

Table 3 gives an overview of the test programme. Seven specimens were subjected to dwell testing, i.e. constant load crack growth tests, and three specimens were subjected to dwell tests with peak loads and underloads. The peak loads were immediately followed by underloads, as is often the case for military aircraft gas turbine discs, for example figure 1. Furthermore, the immediate succession of peak loads by underloads is conservative, since this is most likely to minimise the retarding or inhibiting effect of peak loads on subsequent dwell crack growth.

The tests were done in a high temperature (600°C) air environment and in a 30 kN AMSLER creep frame. Figure 3 shows the measurement circuitry. During testing the specimen temperature was controlled to $600 \pm 2^\circ\text{C}$ by a thermocouple inserted in a hole drilled in the specimen back face. This location gives the same temperature as that in the plane of cracking [3].

Specimen crack lengths were measured using the direct current potential drop (PD) method, figures 3 and 4. This method is fully described in [4], but it is nevertheless important to note that the specimens were insulated from the load frame by a 0.3 mm thick Al_2O_3 ceramic coating on the loading pins, and that a companion specimen within the furnace was used to obtain a reference voltage V_{ref} .

Crack opening displacements at the load line were measured with two SCHAEVITZ linear variable displacement transducers (LVDTs). These transducers were connected to beams attached to the upper and lower surfaces of the specimens. The beams were shaped such that the load line was contained in the plane made by the transducers' axes [5].

After testing all specimens were broken open to measure the final dwell crack length a_f in the same way as the initial crack length a_1 , see table 2. In addition, for specimens CT49, CT50 and CT51 measurements were made of the intermediate dwell crack lengths at which peak loads and underloads were

applied. The measurements of a_i , a_f and intermediate dwell crack lengths from the specimen fracture surfaces enabled the derivation of average instantaneous dwell crack lengths from the PD measurements made during testing.

4 DATA ANALYSIS PROCEDURE

The PD measurement data were processed to provide average instantaneous crack lengths, a , in terms of testing time t . For the dwell crack growth tests these data and the LVDT load-line displacement data were further processed to provide:

- (1) Correlations between dwell crack growth rates, da/dt , and the fracture mechanics parameters K_I , J and C^* .
- (2) Comparisons between the experimental and analytical load-line compliances.
- (3) Values of the characteristic time t_c for distinguishing between small-scale yielding and extensive creep.

4.1 The Fracture Mechanics Parameters K_I , J and C^*

For the CT specimen the Linear Elastic Fracture Mechanics (LEFM) parameter K_I is given by [6]:

$$K_I = \frac{P}{B\sqrt{W}} \cdot f(a/W) \quad (1)$$

where:

$$f(a/W) = \frac{2+a/W}{(1-a/W)^{3/2}} [0.886 + 4.64a/W - 13.32(a/W)^2 + 14.72(a/W)^3 - 5.6(a/W)^4] \quad (2)$$

The Elastic-Plastic Fracture Mechanics (EPFM) parameters J and C^* can be determined by several methods. In the present work this was done in two ways. First, the procedure of Kumar *et al* [7] was used as the main method of determining J and C^* , in order to correlate dwell crack growth rates. This method uses energy and energy rate interpretations of J and C^* , respectively,

and experimental measurements of displacements and displacement rates. In this method the operating definitions of J and C^* are:

$$J = - \frac{1}{B} \cdot \frac{dU}{da} \Big|_v \quad (3)$$

$$C^* = - \frac{1}{B} \cdot \frac{d\dot{U}}{da} \Big|_{\dot{v}} \quad (4)$$

where U is the strain energy, \dot{U} is the strain energy rate dU/dt , v is the load-line displacement, and \dot{v} is the load-line displacement rate dv/dt . For the CT specimen in plane strain,

$$J = \frac{h_1}{h_3} \cdot \left(\frac{W}{a} - 1 \right) \cdot \frac{1}{1.455 \eta} \cdot \frac{P}{B(W-a)} \cdot v \quad (5)$$

$$C^* = \frac{h_1}{h_3} \cdot \left(\frac{W}{a} - 1 \right) \cdot \frac{1}{1.455 \eta} \cdot \frac{P}{B(W-a)} \cdot \dot{v} \quad (6)$$

where h_1 and h_3 are tabulated by Kumar *et al* [7] as functions of n , the exponent in the Norton creep law $\dot{\epsilon} = A\sigma^n$; and η is given by

$$\eta = [4\alpha^2 + 4\alpha + 2]^{1/2} - 2\alpha - 1 \quad (7)$$

$$\alpha = a/(W - a) \quad (8)$$

and v and \dot{v} are obtained from the dwell crack growth tests. The Norton creep law was derived from figure 5: these data give the following values of A and n (only n is necessary for the method of Kumar *et al*):

$$A = 6.34 \times 10^{-66} \text{ MPa}^{-n}/\text{s}$$

$$n = 19.6$$

Secondly, a few selected values of the contour integrals J and C^* , defined by

$$J = \int_{\Gamma} W dy - \sigma_{ij} n_j \left(\frac{\partial u_i}{\partial x} \right) ds \quad (9)$$

$$C^* = \int_{\Gamma} W^* dy - \sigma_{ij} n_j \left(\frac{\partial \dot{u}_i}{\partial x} \right) ds \quad (10)$$

were obtained by finite element analysis using MARC [9] and a post-processor program developed by Bakker [10]. In this method the determination of C^*

involved a creep analysis using the entire Norton law and hence values of n and A . The finite element analysis also required an approximate description of the tensile properties of Inconel 718 at 600°C and values of Poisson's ratio ν and Young's modulus E . At 600°C these values are $\nu = 0.276$ and $E = 167$ GPa [8].

The two methods of J and C^* determination are very different, and may be expected to give dissimilar values of J and C^* owing to differences between actual material behaviour and analytical assumptions. It is most interesting to determine these dissimilarities, in order to assess the suitability of J and C^* as characterizing parameters for dwell crack growth rates and their use for life predictions.

4.2 Load-Line Compliance

Saxena and Hudak [11] derived the following analytical expression for the CT specimen elastic load-line compliance over the range $0.2 \leq a/W \leq 0.975$:

$$\frac{EB\nu}{P} = \left(\frac{1 + a/W}{1 - a/W} \right)^2 [2.163 + 12.219a/W - 20.065(a/W)^2 - 0.9925(a/W)^3 + 20.609(a/W)^4 - 9.9314(a/W)^5] \quad (11)$$

This expression was compared with experimental compliance values derived from the dwell crack growth tests. To do this, use was made of the experimental values of B , P_{dwell} and ν , and the 600°C value of Young's modulus $E = 167$ GPa [8].

4.3 Characteristic Time

Riedel and Rice [12] derived an analytical expression for the characteristic time t_c representing the transition from small-scale yielding to extensive creep of the whole specimen:

$$t_c = \frac{K_I^2(1 - \nu^2)}{(n + 1)EC^*} \quad (12)$$

Provided the actual deformation behaviour of the specimen is elastic - power law viscous (i.e. in the latter case governed by the Norton creep law $\dot{\epsilon} = A\sigma^n$) then comparison of experimentally derived values of t_c with the actual testing time t should enable a distinction between small-scale yielding and extensive

creep: small-scale yielding prevails when t_c is much larger than t , and extensive creep prevails when t_c is much smaller than t .

5 MECHANICAL TESTING RESULTS

During testing the crack lengths and load-line displacements were continuously monitored with time, resulting in hundreds of measurements for each specimen. These measurements were reduced to reasonable increments of crack growth and displacement. Crack growth rates da/dt and displacement rates dv/dt were calculated by the incremental method:

$$da/dt = (a_{j+1} - a_j)/(t_{j+1} - t_j) \quad (13)$$

$$dv/dt = (v_{j+1} - v_j)/(t_{j+1} - t_j) \quad (14)$$

Values of K_I , J and C^* were derived using the means of the crack growth increments, i.e. $a = (a_{j+1} + a_j)/2$.

5.1 Dwell Crack Growth Curves

Figure 6 compares the dwell crack length versus time data normalised to $t = 0$ at $a = 10$ mm. There is a strong effect of P_{dwell} , but the spread between specimens tested at the same P_{dwell} level is also significant.

Figures 7-9 show the dwell crack growth curves for specimens subjected to peak loads and underloads. The peak loads strongly suppressed dwell crack growth, even at a P_{max}/P_{dwell} ratio as low as 1.25, and even though immediately followed by underloads. For example, the *minimum* delay due to a peak load was about 3 hours, see figure 7. These results are consistent with, but much more pronounced than, those of Weerasooriya and Nicholas [13], who tested Inconel 718 in air at 649°C under fatigue cycling with dwells below P_{max} . They observed that P_{max}/P_{dwell} ratios ≥ 1.25 resulted in almost complete retardation of crack growth during dwell times up to 200 seconds.

5.2 Correlation of Dwell Crack Growth Rates

Figures 10-12 present correlations of dwell crack growth rates for specimens without peak loads and underloads by the fracture mechanics parameters K_I , J and C^* , whereby the method of Kumar et al [7] was used to determine the EPFM parameters. Comparison of these figures shows the following trends:

- (1) C^* provides a generally better correlation of the data than either K_I or J . Nevertheless, the correlations by K_I and J are good.
- (2) The crack growth rate curves have fairly distinct changes in slope near the mid-position of each data set.

5.2.1 Differences in Correlations by K_I , J and C^*

Figure 10 shows that K_I correlated dwell crack growth rates better at lower K_I values. On the other hand, figures 11 and 12 show that J and C^* correlated dwell crack growth rates better at higher J and C^* values. Figure 10 also shows that despite a significant spread in the data there is a general shift of the crack growth rate curves to the right as P_{dwell} is increased. This trend is the same as that for dwell crack growth tests on Inconel 718 at 538°C and 649°C [14].

5.2.2 Bilinear Approximations to Crack Growth Rate Curves

The da/dt versus K_I and C^* curves were analysed in more detail with respect to the changes in slope. Figures 13 and 14 show bilinear approximations to the complete sets of dwell crack growth rate curves, and table 4 lists the transition data corresponding to the intersection of the two linear approximations for each curve.

Figures 13 and 14 show that each complete set of dwell crack growth rate curves can be simply represented by two power law relations. These relations are as follows:

(1) da/dt versus K_I

- hypotransitional relation : $da/dt = 2.45 \times 10^{-15} (K_I)^5$ (15)

- hypertransitional relation: $da/dt = 1.04 \times 10^{-10} (K_I)^2$ (16)

with hypotransitional exponent $m_1 = 5$ and hypertransitional exponent $m_2 = 2$.

(2) da/dt versus C^* calculated by the method of Kumar et al [7]

- hypotransitional relation : $da/dt = 3.19 \times 10^{-7} (C^*)^{0.8}$ (17)

- hypertransitional relation: $da/dt = 2.03 \times 10^{-7} (C^*)^{0.4}$ (18)

with hypotransitional exponent $m_1 = 0.8$ and hypertransitional exponent $m_2 = 0.4$.

With respect to the da/dt versus K_I data, the m_1 and m_2 values are similar to those found by Sadananda and Shahinian [14] for dwell crack growth tests in air at 538°C and 649°C. The m values are significant because $m = n$ would be expected if crack extension occurred by the well-known creep crack growth mechanism involving coalescence of the crack tip with grain boundary voids whose growth rate is controlled by power law creep [15,16]. For the present work it is known that the m values are much less than n , which was found to be 19.6 at 593°C, see section 4.1. Thus the observed dependences of da/dt on K_I do not support a mechanism of crack growth controlled by power law creep.

With respect to the da/dt versus C^* data, a power law creep crack growth mechanism would be expected to result in $m = n/(n+1)$ [15]. For $n = 19.6$ this means $m = 0.95$, but equations (17) and (18) have m values corresponding to $n \leq 4$, which is too low to support a creep crack growth mechanism.

Lastly, table 4 shows that as P_{dwell} is increased there is a general trend of increasing K_{I_T} , the stress intensity factor at the transition between bilinear approximations to each dwell crack growth rate curve. However, there is no trend for C_T^* . Note though that for each specimen the $(da/dt)_T$ values are reasonably constant irrespective of the correlating fracture mechanics parameter, K_I or C^* . This gives confidence that the transitions are not arbitrary.

5.2.3 Comparisons with Previous Results

Figure 15 compares da/dt versus K_I data envelopes for Inconel 718 plate [14], square bar [17], and the forged pancake material in the present investigation, all with similar heat treatments and tested in a high temperature air environment. The data agree well with respect to the general trends of increasing crack growth rates with increasing test temperature and distinct changes in slope. Sadananda and Shahinian [14] and Liu et al [17] determined threshold values of the mode I stress intensity factor, $K_{I_{th}}$, for the commencement of dwell crack growth. These values are 21.5 MPa \sqrt{m} at 538°C and 14 MPa \sqrt{m} at 649°C [14], and 18.7 MPa \sqrt{m} at 650°C [17]. From the relative positions of the data envelopes in figure 15 these threshold values suggest a $K_{I_{th}}$ of 16-17 MPa \sqrt{m} for the forged pancake material.

Figure 16 compares da/dt versus C^* data envelopes for Inconel 718 plate [14] and the forged pancake material in the present investigation. The heat treatment and testing conditions were the same except for the test

temperatures. Comparison of figure 16 with figure 15 suggests that the method of obtaining C^* strongly influences the relative positions of the data envelopes. This is an important disadvantage with respect to the straightforward correlation of data by K_I . This problem is discussed further in sub-section 8.2.1.

5.3 Load-Line Compliance

Figure 17 compares the load-line compliances from the dwell crack growth tests with the analytical elastic load-line compliance given by equation (11). The experimental data show a considerable spread which, however, is due mainly to two specimens. The general trend is to follow the analytical curve, as was also found at 650°C [17]. In other words, the specimen deformation is predominantly elastic during dwell crack growth at temperatures up to 650°C.

5.4 Characteristic Time

Figure 18 compares the dwell crack growth specimen lives with the characteristic times t_c according to equation (12) and using C^* values derived by the method of Kumar *et al* [7]. The t_c values are much smaller than the specimen lives and show that if the actual deformation behaviour of the specimens were to be governed by power law creep, then extensive creep would have occurred and not only small-scale yielding. However, extensive creep is incompatible with the load-line compliance measurements discussed in section 5.3. Thus it may be concluded that the actual deformation behaviour of the specimens was not governed by power law creep.

6 METALLOGRAPHY AND MICROSTRUCTURE

The heat treatment given to the forged pancake material used in the present investigation is a common one for optimum creep resistance, as mentioned in section 2, and may be expected to result in the following microstructural features [19]:

- (1) A fine grain size, with grains containing annealing twins.
- (2) A high volume fraction of γ'' matrix precipitates, visible only by electron microscopy.

- (3) Limited precipitation of δ needles, primarily at grain boundaries.
- (4) Heterogeneously distributed NbC carbides.

Metallographic sections were made in the macroscopic plane of fracture of the dwell crack growth specimens. The sections were ground and polished by standard techniques and etched using Bereha's tint etch [20]. Figure 19 is a representative example of the microstructure, showing the fine grain size, annealing twins, δ precipitates and NbC carbides. The δ needles lay mainly - but not exclusively - along grain boundaries, and the NbC carbides were generally small and isolated.

7 FRACTOGRAPHY

7.1 Macrofractography

Fracture surfaces of the dwell crack growth specimens were examined at low magnification to determine whether transitions in the crack growth rate curves corresponded to a distinct change in fracture topography. No such change was found, but there was a gradual increase in fracture surface roughness, also observed by Sadananda and Shahinian [14].

7.2 Microfractography

7.2.1 Dwell Crack Growth

The fracture surfaces of specimens CT39 and CT47 were examined in detail at medium and high K_I values by scanning electron microscopy. Cross-sections through the fracture surfaces were made at the same locations and examined by optical and scanning electron metallography. These cross-sections were also used for two-dimensional measurements of fracture surface roughness using a digital image analysis system.

Table 5 summarises the results: note that the medium K_I values correspond to the hypotransitional crack growth rate curves, and the high K_I values correspond to near the ends of the hypertransitional crack growth rate curves. The fracture paths were essentially intergranular, as observed by Sadananda and Shahinian [14] and others [21, 22]. However, this was by no means obvious from direct observation of the fracture surfaces, since there

were few - if any - "clean" grain boundary facets. In fact, the cross-sections through the fracture surfaces were necessary to demonstrate the intergranular fracture path.

Figures 20-23 illustrate the fracture characteristics at low and intermediate magnifications. These figures demonstrate the increasing roughness and larger secondary cracks at higher K_I values, and also show that the fracture surface details were unaffected by much longer exposure times (14 hours versus 1 hour) at the 600°C test temperature. Example cross-sections are shown in figures 24-27. These demonstrate the intergranular fracture paths, as well as the increasing roughness and larger secondary cracks at higher K_I values.

Figures 28-30 illustrate specific features, namely the formation of ligaments and ligament breakage between secondary cracks, and grooving at grain boundaries as a probable precursor to cracking. The ligaments are a consequence of crack yawning, and are therefore evidence of local deformation. Note also that fracture surface oxidation is evident at these higher magnifications, and that the amount of oxidation is virtually independent of exposure time at the 600°C test temperature. (However, the ligament breakage shown in figure 29 is brittle, and may well have been caused by slight - but highly localised - oxidation for some time after the main crack passed by.)

7.2.2 Dwell Crack Growth + Peak Loads and Underloads

The fracture surfaces of specimens CT50 and CT51 were examined by scanning electron microscopy at the positions of the peak load and underload combinations imposed on dwell crack growth. Specimen CT51 was also examined at a dwell crack growth length $a \sim 11$ mm, in order to show the fracture characteristics after exposure for about 65 hours at the 600°C test temperature.

Apart from differential heat tinting (visible optically but not by scanning electron microscopy) the imposition of peak load and underload combinations had no effect on the fracture characteristics of dwell crack growth. This is illustrated by figures 31 and 32, which show a series of fractographs of increasing magnification at the position of the peak load + underload combination for specimen CT51.

Figure 33 shows the dwell crack growth characteristics of specimen CT51 after about 65 hours exposure at the 600°C test temperature. Comparison of figure 33 with figures 20-23 demonstrates that there is no loss of detail owing to exposure times much longer than 1 hour.

8 DISCUSSION

8.1 Effect of Peak Loads on Dwell Crack Growth

The most significant result of the present investigation is the strong inhibiting effect of peak loads, even though followed immediately by underloads, on dwell crack growth in Inconel 718 forged pancake disc material at 600°C. The minimum delay in dwell crack growth was about 3 hours, which is much longer than dwell periods in real flights, let alone accelerated test load histories like HOT TURBISTAN [1]. One may therefore conclude the following:

- (1) Unless there are *service-related factors*, extraneous to the present laboratory test conditions, that greatly accelerate dwell crack growth after peak loads, then dwell cracking in the *long crack regime* will not contribute to service crack growth problems for Inconel 718 discs operating at 600°C. This conclusion is also most likely valid for operating temperatures below 600°C, since dwell cracking is considerably slower at lower temperatures, see figure 15.
- (2) Subject to the two italicised caveats in conclusion (1), and taking into account that the strong inhibiting effect of peak loads on dwell crack growth implies negligible or very slow changes in the crack tip stress-strain field owing to creep, it does not appear useful to develop crack growth prediction methods combining creep and creep crack growth with fatigue crack growth for Inconel 718 discs at temperatures of 600°C or less.
- (3) The inclusion of dwell periods during *long fatigue crack growth tests* c. Inconel 718 at 600°C and less, notably tests with the standard load history HOT TURBISTAN, most probably serves no practical purpose. This conclusion may also be inferred from the work of Weerasooriya and Nicholas [13].

The two italicised caveats in conclusion (1) will be addressed in sub-sections 8.1.1 and 8.1.2 respectively. This leads to generalisations of conclusions (2) and (3) in sub-sections 8.1.3 and 8.1.4.

8.1.1 *Service-Related Factors Extraneous to Laboratory Testing*

About the only service-related factor that could conceivably accelerate dwell crack growth is the pressure of cooling air tapped from the compressor and passing over the turbine discs. The reason for this possibility is that dwell crack growth in Inconel 718 is - or can be - controlled by the environment [22-25]. Under the conditions of low slip density and inhomogeneous plastic deformation at the crack tip, which typically means dwell crack growth under small-scale yielding, the crack tip damage is characterized by grain boundary oxidation and subsequent intergranular fracture [25].

The grain boundary oxidation mechanism is a two-stage process, figure 34, that depends on the oxygen partial pressure at the crack tip [26]. Initially, when the *environmental* oxygen partial pressure is available to the crack tip, the oxides formed are selective oxides of FeO and NiO and their spinels. These oxides are porous and cannot act as a barrier to oxygen diffusion, but they do lower the oxygen partial pressure at the oxide/metal interface. This effect provides the reaction kinetics required for formation of a denser sub-layer of Cr_2O_3 . This sub-layer is thermodynamically stable at high temperatures and may be considered protective in the sense that it limits oxygen diffusion to the grain boundary material, thus decreasing the reaction rate with time. At the oxidation passivation time t_p , the build-up of the Cr_2O_3 sub-layer is complete and no further oxygen penetration of the base metal occurs [26].

This oxidation mechanism has been verified [26] and it explains why in the present work the amount of fracture surface oxidation was limited and virtually independent of exposure time at 600°C. This mechanism also enables considering the possible effect of cooling air pressure on dwell crack growth rates. Although high pressures are achieved in the compressors of modern military aircraft gas turbines, leading to cooling air pressures initially - 2.5 MPa (25 atm), the important point is that the oxygen partial pressure remains the same. Thus there is no reason to expect any difference in dwell crack growth rates with respect to laboratory test conditions.

8.1.2 Crack Growth Regimes: Long and Short Cracks

From the discussion in section 8.1 and sub-section 8.1.1, one may conclude that dwell cracking in the *long crack regime* will not contribute to service crack growth problems for Inconel 718 discs operating at temperatures up to 600°C. However, between crack initiation and *long crack growth*, which means essentially that only the crack tip stress-strain field provides the driving force for crack growth and that the crack length is large compared to relevant microstructural dimensions, there is a *short crack regime*.

For a typical turbine disc the significance of the *short crack regime* is twofold. This is illustrated by figure 35, which is a schematic of the very different stress-strain conditions pertaining to *short crack growth* at bore and rim slot locations. At the disc bore a crack may initiate and will then grow in an elastic bulk stress-strain field. In this situation *short crack growth* refers solely to the inapplicability of continuum mechanics when the crack is small compared to characteristic microstructural dimensions such as the grain size. On the other hand, at rim slots cracks may initiate and will then grow in the slot plastic and elastic fields before reaching the bulk stress-strain field. In this situation *short crack growth* refers to the crack being small compared to characteristic microstructural dimensions and/or the scale of local plasticity.

Assuming that cracking under service loading initiates by fatigue, the question arises whether dwell cracking can contribute in the *short crack regime*, unlike the situation for *long crack growth*. For cracks initiating at the disc bore the occurrence of dwell cracking depends in the first instance on K_I exceeding K_{Ith} . A reasonably conservative estimate of the crack size necessary for exceedance of K_{Ith} at 600°C may be obtained from the following expression for the maximum stress intensity factor of a semi-circular crack at the bore surface:

$$K_I = \frac{2\sigma\sqrt{\pi a}}{\pi} \quad (19)$$

where $K_I = K_{Ith} = 16 \text{ MPa}\sqrt{\text{m}}$, see sub-section 5.2.3, and $\sigma = 537 \text{ MPa}$ [27]. Substitution of these values into equation (19) gives $a = 0.7 \text{ mm}$, which is more than thirty times the grain size of the forged pancake disc material, see table 1. This means that cracks initiating at the disc bore cannot grow by dwell cracking in the *short crack regime*.

For cracks initiating at rim slots the slot plastic zones will control at least the first part of *short crack* growth and possibly all of it, since in microstructural terms the crack size in fine grained materials has only to exceed 0.25 - 0.5 mm [28, 29] before reaching the *long crack regime*. The slot plastic zones will promote the conditions of high slip density and homogeneous plastic deformation at *short crack* tips, especially under fatigue loading. This means that environmentally-induced dwell crack growth will be limited or absent [25] and that crack growth will be essentially due to fatigue.

8.1.3 *Implications for Crack Growth Prediction Methods*

The present results and their discussion in section 8.1 and sub-sections 8.1.1 and 8.1.2 strongly suggest that it is not useful to develop crack growth prediction methods combining creep and creep crack growth with fatigue crack growth for Inconel 718 discs at temperatures of 600°C or less. There are two clear reasons for this: firstly, the strong inhibiting effect of peak loads on dwell crack growth, which also implies negligible or very slow changes in the crack tip stress-strain field owing to creep; and secondly the evidence, considered again in section 8.2, that dwell cracking in an air environment at 600°C is an environmentally-controlled process and not due to creep.

8.1.4 *Implications for Crack Growth Testing*

The present results and their discussion in section 8.1 and sub-sections 8.1.1 and 8.1.2 indicate that the inclusion of dwell periods during fatigue crack growth tests of Inconel 718 at temperatures of 600°C or less most probably serves no practical purpose. Note that this conclusion holds even for tests with dwells at maximum load, since although such tests show dwell crack growth during short dwell periods [13, 24, 30] the load histories are unrealistic in not including peak loads significantly above the dwell loads.

The foregoing conclusion will be checked in the design data part of the IEPG TA 31 project, which includes fatigue crack growth tests using the HOT TURBISTAN load sequence with and without dwell periods.

8.2 Dwell Crack Growth

The general characteristics of dwell crack growth in Inconel 718 forged pancake disc material in an air environment at 600°C are:

- (1) The dwell load level P_{dwell} has a strong effect on crack growth lives and rates, figure 6.
- (2) LEFM and EPFM parameters (K_I, J, C^*) provide good correlations of crack growth rates, figures 10-12. (However, for the EPFM parameters this has been shown only for J and C^* calculated by the method of Kumar *et al* [7].)
- (3) The crack growth rate curves have distinct changes in slope that are well represented by two power law relations, figures 13 and 14. The exponents m_1 and m_2 in these relations, see also equations (15) - (18), are too low to support a mechanism of crack growth controlled by power law creep.
- (4) Compliance measurements indicate predominantly elastic deformation during dwell crack growth, figure 17. This also does not support a creep crack growth mechanism.
- (5) The characteristic times t_c obtained using C^* values derived by the method of Kumar *et al* [7], and hence based on measured values of load-line displacement rates, are much smaller than the specimen crack growth lives, figure 18. This suggests that extensive creep should have occurred during dwell crack growth.
- (6) The fracture paths are essentially intergranular. The cracks grow with increasing roughness and increasingly large secondary cracks, and ligaments between secondary cracks indicate local deformation. However, fracture surface oxidation is limited and virtually independent of crack length and the exposure time at 600°C.

Most of these characteristics are interrelated through the mechanism of dwell crack growth, as will be discussed in sub-sections 8.2.1 and 8.2.2.

8.2.1 Mechanism of Dwell Crack Growth and the Usefulness of Fracture Mechanics Crack Growth Parameters

As discussed in sections 5.3 and 5.4, the load-line compliance measurements indicate small-scale yielding while the t_c data in figure 18 suggest that extensive creep should have occurred. These results are incompatible and lead to the conclusion that the t_c data have no meaning for distinguishing between small-scale yielding and extensive creep, and that therefore the actual deformation behaviour of the specimens was not governed by power law creep. On the other hand, if dwell crack growth is not due to power law creep, then one would not expect C^* to provide good correlations of dwell crack growth rates.

An explanation for this apparent anomaly, at least for creep crack growth, has been provided by Saxena [31], who considered the applicability of C^* for different creep crack growth conditions. He pointed out that if measured values of load-line displacement rates are used to calculate C^* , then the values obtained are comparable irrespective of whether crack tip deformation is in the small-scale, transition (non-steady-state) or extensive steady-state creep regimes. In other words, C^* derivations based on formulations like equation (6), see section 4.1, are very forgiving of their more or less indiscriminate use to correlate creep crack growth rates. The present work shows that this is also true for dwell crack growth rates, figure 12.

However, Saxena [31] also pointed out that there is a real problem when load-line displacements cannot be measured and C^* must be calculated analytically. Then it is essential that the actual deformation behaviour at the crack tip corresponds with the analytical assumptions. In the present investigation this problem has been examined by carrying out fully analytical determinations of selected values of J and C^* . As mentioned in section 4.1, these analytical determinations were done as an adjunct to the experiment-based method of Kumar *et al* [7] in order to determine the dissimilarities between J and C^* values calculated by very different methods, and also to assess the suitability of J and C^* as characterizing parameters for dwell crack growth rates and their use for life predictions.

Table 6 gives the analytical values of J and C^* as functions of P_{dwell} and crack length, and figures 36 and 37 compare these selected data with the experiment-based J and C^* versus crack length values. Figure 36 shows that the analytical J values were 2-3 times smaller than the equivalent experiment-

based J values. This is already a serious discrepancy, but figure 37 shows that the situation for C^* is much worse. The analytical C^* values were between 3×10^4 and 3×10^7 times smaller than the equivalent experiment-based C^* values.

The enormous dissimilarities in C^* values must be due to the inappropriateness of the Norton creep law $\dot{\epsilon} = A\sigma^n$ for describing dwell crack growth: in particular the influence of the value of A, which has to be used in the analytical derivation of C^* but is not required for the experiment-based method of Kumar *et al* [7], see also section 4.1. Furthermore, substitution of the much smaller analytical values of C^* for the experiment-based values in equation (12), see section 4.3, gives characteristic times longer than the specimen crack growth lives. This result is consistent with small-scale yielding during the tests, i.e. it is consistent with the load-line compliance measurements, and therefore reinforces the conclusion that the actual deformation behaviour of the specimens was not governed by power law creep.

The foregoing comparison of analytical and experiment-based J and C^* values also leads to the following additional conclusions:

- (1) The EPFM parameters J and C^* are not suitable as characterizing parameters for dwell crack growth rates, since the dissimilarities in values obtained by different methods are too large. (Note that in the case of C^* some evidence for this conclusion was also presented in section 5.2.3.)
- (2) J and C^* cannot be used to predict dwell crack growth behaviour in engineering components. This is because only analytical values of J and C^* can be derived for engineering components, and there is no certainty that these values can be reliably related to the J and C^* values used to correlate experimental dwell crack growth rates.

This leaves only the LFM parameter K_I , which provides good correlations of dwell crack growth rates and also correlates data from different investigations in a logical and consistent manner, for example figure 15. Thus experimental data may be used to predict dwell crack growth behaviour in engineering components provided that accurate K_I values can be determined for these components. In view of the state-of-the-art, this should not be a major problem.

8.2.2 Mechanism of Dwell Crack Growth and the Bilinear Approximations to Crack Growth Rate Curves

As discussed in sub-section 5.2.2, the exponents of the bilinear approximations to the dwell crack growth rate curves are too low to support a mechanism of crack growth controlled by power law creep. This is also true for other investigations of Inconel 718 dwell crack growth in air [14,17]. However, da/dt versus K_I data for Inconel 718 at 540°C in vacuo [23] give a hypotransitional exponent $m_1 \sim 20-23$. This range is what one would expect for the value of the Norton creep law exponent n , and therefore indicates that crack growth occurred by a power law creep mechanism in the absence of an air environment. In other words, one may conclude that dwell crack growth is controlled - or at least strongly influenced - by the high temperature air environment.

The question arises as to why the dwell crack growth rate curves have distinct changes in slope. The most likely explanation is that there is some change in the crack growth mechanism. Sadananda and Shahinian [14] were the first to consider this problem. They argued that crack growth occurs as a balance of two competing processes: a diffusion process in which point defects move along grain boundaries towards the crack tip and assist intergranular creep crack growth, and more general creep deformation which interferes with the diffusion process and relaxes the crack tip stress field.

One part of Sadananda and Shahinian's argument may be discounted, since the balance of evidence from the present and previous investigations strongly suggests that dwell crack growth in Inconel 718 occurs under small-scale yielding conditions at temperatures up to 650°C. As discussed in sub-section 8.1.1, this means that dwell crack growth is environmentally controlled (which is also the conclusion from the present sub-section's discussion of data from tests in air and in vacuo) and takes place by grain boundary oxidation and subsequent intergranular fracture.

On the other hand, it is certainly feasible that creep deformation could hinder the dwell cracking process. Sadananda and Shahinian [14] proposed that more widespread creep deformation could be responsible for the general shift of da/dt versus K_I curves to the right as P_{dwell} is increased, see also sub-section 5.2.1 and figure 10. This proposal must be modified, since the balance of evidence shows that any creep deformation is confined to the crack tip region. However, with this modification Sadananda and Shahinian's

proposal might also explain the changes in slope of the dwell crack growth rate curves. It is possible that the changes in slope, and hence the transition values of the stress intensity factor, K_{I_T} , are the consequences of crack tip deformation zones exceeding a characteristic microstructural dimension such as the grain size. To check this possibility the plane strain plastic and creep zone sizes at the transitions in the da/dt versus K_I plots were calculated using the plastic zone formulae of Hahn *et al* [32,33] and Clavel *et al* [34], and Hui's creep zone formula [16]. The transition zone size equations are as follows:

PLASTIC ZONE SIZE

- Hahn *et al* [32, 33] $r_{p,y} = 0.13 (K_{I_T}/\sigma_y)^2$ (20)

- Clavel *et al* [34] $r_{p,y} = 0.06 - 0.09 (K_{I_T}/\sigma_y)^2$ (21)

CREEP ZONE SIZE

- Hui [16] $r_{c,y} = \frac{1}{4} \left(\frac{1}{2\pi} \right)^{\frac{n-1}{n-3}} \left(\frac{EAK_{I_T}^{n-1}}{(da/dt)_T} \right)^{\frac{2}{n-3}}$ (22)

where A and n are obtained from the Norton creep law $\dot{\epsilon} = A\sigma^n$ and $E = 167$ GPa for Inconel 718 at 600°C [8].

Table 7 gives the results, which in comparison with the grain size information in table 1 show that the crack tip deformation zone sizes corresponding to the transitions in the da/dt versus K_I plots are much larger than the nominal grain diameter. Nevertheless, the creep zone sizes at the transitions are much closer to the nominal grain diameter than the plastic zone sizes, and one may hypothesize that it could be necessary for the creep zone size to reach about 2-3 grain diameters before creep deformation noticeably alters the crack growth rate dependence on K_I .

8.3 Mechanism of Dwell Crack Growth Inhibition by Peak Loads

From sections 8.1 and 8.2 and the balance of evidence from previous investigations [14,17,23,25,26] it may be concluded that dwell crack growth in Inconel 718 occurs under small-scale yielding conditions at temperatures up to 650°C, is environmentally controlled and takes place by grain boundary oxidation and subsequent intergranular fracture. Creep deformation in the crack tip region must be limited and must generally occur at a much slower rate.

These conclusions and the mechanism of grain boundary oxidation [26] described in sub-section 8.1.1 provide an explanation of the strong inhibiting effect of peak loads on dwell crack growth. The plastic zone due to a peak load will result in residual compressive stresses at - or very close to - the crack tip. These compressive stresses will prevent the fracture of oxidised grain boundaries, including fracture of the protective Cr₂O₃ sub-layer (see figure 34). This means that the process of grain boundary oxidation and fracture, i.e. dwell crack growth, will stop until the much slower process of creep deformation relaxes the peak load plastic zone, thereby removing the residual compressive stresses and also enabling the dwell load to result in tensile stresses at the crack tip.

9 CONCLUSIONS

An investigation was made of dwell crack growth, including the effect of peak loads, in Inconel 718 forged pancake disc material at 600°C in an air environment. This investigation is part of the European collaborative project IEPG TA 31: Lifting Concepts for Military Aero-Engine Components. The results of the investigation lead to the following conclusions:

- (1) The application of peak loads representative for military aircraft gas turbine discs strongly inhibits dwell crack growth, even when peak loads are immediately followed by underloads. Discussion of this effect showed that in all probability dwell cracking will not contribute to service crack growth problems for Inconel 718 at temperatures of 600°C or less.
- (2) The balance of evidence from the present and previous investigations shows that dwell crack growth in Inconel 718 occurs under small-scale

yielding conditions at temperatures up to 650°C, is environmentally controlled and takes place by grain boundary oxidation and subsequent intergranular fracture. Any creep deformation in the crack tip region must be limited and may actually hinder the dwell cracking process.

- (3) In view of the evidence for conclusions (1) and (2), it is not useful to develop crack growth prediction methods combining creep and creep crack growth with fatigue crack growth for Inconel 718 at temperatures of 600°C or less. Nor is it likely that dwell crack growth need be incorporated in life predictions.

The last part of conclusion (3) will be checked in the design data part of the IEPG TA 31 project, which includes fatigue crack growth tests using the HOT TURBISTAN load sequence with and without dwell periods.

10 ACKNOWLEDGEMENTS

This investigation was monitored by the Netherlands Agency for Aerospace Programs (NIVR) acting on behalf of the Ministry of Defence of the Netherlands. Many NLR colleagues contributed to this investigation. Particular thanks go to J.A.M. Boogers, L. Schra, H.H. Ottens, C.J. Lof, A.U. de Koning, A. Oldersma and T. Hattenberg.

11 REFERENCES

1. H.-G. Köbler, K. Amelung and S. Durwen, "HOT TURBISTAN : LBF contributions to the experimental part of the international research programme - Final report", LBF Report No. 5092/6533, Fraunhofer-Institut für Betriebsfestigkeit Darmstadt, April 1990.
2. Y. Honnorat, SNECMA Letter YKOM1 no. 68772, Société Nationale d'Étude et de Construction de Moteurs d'Aviation, Evry, 30 May 1989.
3. H.P. van Leeuwen and L. Schra, "Fracture mechanics and creep crack growth of 1%Cr-4%Mo steel with and without prior exposure to creep conditions", Engineering Fracture Mechanics, Vol. 27, pp. 483-499 (1987).

4. A.J.A. Mom and M.D. Raizenne, "AGARD engine disc cooperative test programme", AGARD Report No. 766, Advisory Group for Aerospace Research and Development, Neuilly-sur-Seine, August 1988.
5. H.P. van Leeuwen, F.F. Groep, L. Schra and N. Dam, "Automated measurement of crack length and load line displacement at elevated temperature", AGARD Report No. 751, Advisory Group for Aerospace Research and Development, Neuilly-sur-Seine, February 1988.
6. Standard Test Method for Plane-Strain Fracture Toughness of Metallic Materials, ASTM Standard E399-83, American Society for Testing and Materials 1990 Annual Book of ASTM Standards Section 3 : Metals Test Methods and Analytical Procedures Vol. 03.01, pp. 488-512 (1990).
7. V. Kumar, M.D. German and C.F. Shih, "An engineering approach for elastic-plastic fracture analysis", EPRI Report NP-1931. Electric Power Research Institute, Palo Alto, July 1981.
8. INCONEL alloy 718, Inco Alloys International Brochure 4M6-89IAI-19, Fourth Edition, 1985.
9. MARC, MARC Analysis Research Corporation, Palo Alto.
10. A. Bakker, Virtual Crack Extension (VCE) Post Processor Input Description, Version 2.3, Delft University of Technology, Delft, October 1991.
11. A. Saxena and S.J. Hudak, Jr., "Review and extension of compliance information for common crack growth specimens", International Journal of Fracture, Vol. 14, pp. 453-468 (1978).
12. H. Riedel and J.R. Rice, "Tensile cracks in creeping solids", Fracture Mechanics: Twelfth Conference, ASTM STP 700, American Society for Testing and Materials, pp. 112-130 (1980).
13. T. Weerasooriya and T. Nicholas, "Overload effects in sustained-load crack growth in Inconel 718", Fracture Mechanics: Eighteenth Symposium, ASTM STP 945, American Society for Testing and Materials, pp. 181-191 (1988).

14. K. Sadananda and P. Shahinian, "Creep crack growth in alloy 718", *Metallurgical Transactions A*, Vol. 8A, pp. 439-449 (1977).
15. H. Riedel and W. Wagner, "Creep crack growth in Nimonic 80A and in a 1Cr- $\frac{1}{2}$ Mo steel", *Advances in Fracture Research (Fracture 84)*, Pergamon Press, Vol. 3, pp. 2199-2206 (1984).
16. C.Y. Hui, "Steady-state crack growth in elastic power-law creeping materials", *Elastic-Plastic Fracture: Second Symposium, Volume I - Inelastic Crack Analysis*, ASTM STP 803, American Society for Testing and Materials, pp. I-573-I-593 (1983).
17. C.D. Liu, Y.F. Han and M.G. Yan, "Small-scale creep crack growth", *Engineering Fracture Mechanics*, Vol. 41, pp. 229-239 (1992).
18. J.D. Landes and J.A. Begley, "A fracture mechanics approach to creep crack growth", *Mechanics of Crack Growth*, ASTM STP 590, American Society for Testing and Materials, pp. 128-148 (1976).
19. E.E. Brown and D.R. Muzyka, "Nickel-iron alloys", *Superalloys II*, John Wiley & Sons, pp. 165-188 (1987).
20. *Metals Handbook Ninth Edition, Volume 9 Metallography and Microstructures*, American Society for Metals, p. 308 (1985).
21. S. Floreen, "The creep fracture characteristics of nickel-base superalloy sheet samples", *Engineering Fracture Mechanics*, Vol. 11, pp. 55-60 (1979).
22. S. Floreen and R.H. Kane, "An investigation of the creep-fatigue-environment interaction in a Ni-base superalloy", *Fatigue of Engineering Materials and Structures*, Vol. 2, pp. 401-412 (1980).
23. K. Sadananda and P. Shahinian, "The effect of environment on the creep crack growth behaviour of several structural alloys", *Materials Science and Engineering*, Vol. 43, pp. 159-168 (1980).
24. P. Shahinian and K. Sadananda, "Creep-fatigue-environment interactions on crack propagation in alloy 718", *Engineering Aspects of Creep*, The Institution of Mechanical Engineers, Vol. 2, pp. 1-7 (1980).

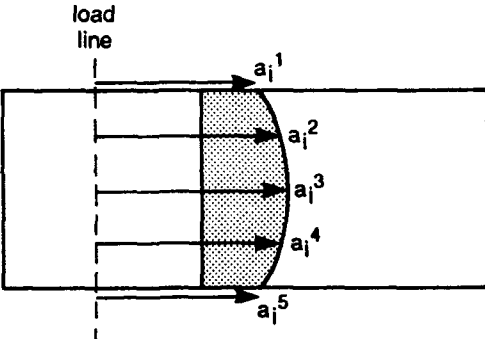
25. H. Ghonem, T. Nicholas and A. Pineau, "Analysis of elevated temperature fatigue crack growth mechanisms in alloy 718", Creep-Fatigue Interaction at High Temperature, AD-Vol. 21, The American Society of Mechanical Engineers, pp. 1-18 (1991).
26. E. Andrieu, H. Ghonem and A. Pineau, "Two-stage crack tip oxidation mechanism in alloy 718", Elevated Temperature Crack Growth, MD-Vol. 18, The American Society of Mechanical Engineers, pp. 25-29 (1990).
27. K. Höschler, "Stress analysis of the modified IEPG-TA 31 model disc and drive assembly", RWTH Report FB 92-07, Rheinisch-Westfälische Technische Hochschule, Aachen, November 1992.
28. R.A. Smith, "On the short crack limitations of fracture mechanics", International Journal of Fracture, Vol. 13, pp. 717-720 (1977).
29. R.F.W. Anstee, "An assessment of the importance of small crack growth to aircraft design", Behaviour of Short Cracks in Airframe Components, AGARD Conference Proceedings No. 328, Advisory Group for Aerospace Research and Development, pp. 3-1 - 3-9 (1983).
30. K. Sadananda and P. Shahinian, "Elastic-plastic fracture mechanics for high-temperature fatigue crack growth", Fracture Mechanics: Twelfth Conference, ASTM STP 700, American Society for Testing and Materials, pp. 152-163 (1980).
31. A. Saxena, "Creep crack growth in high temperature ductile materials", Engineering Fracture Mechanics, Vol. 40, pp. 721-736 (1991).
32. G.T. Hahn, M. Sarrate and A.R. Rosenfield, "Plastic zones in Fe-3Si steel double-cantilever-beam specimens", International Journal of Fracture Mechanics, Vol. 7, pp. 435-446 (1971).
33. G.T. Hahn, R.G. Hoagland and A.R. Rosenfield, "Local yielding attending fatigue crack growth", Metallurgical Transactions, Vol. 3, pp. 1189-1202 (1972).
34. M. Clavel, D. Fournier and A. Pineau, "Plastic zone sizes in fatigued specimens of INCO 718", Metallurgical Transactions A, Vol. 6A, pp. 2305-2307 (1975).

Table 1: Heat treatment, mechanical properties and grain size of the Inconel 718 forged pancake [2]

<ul style="list-style-type: none"> ● ANNEALING: 955°C for 1 hour, air cool ● AGEING : 720°C for 8 hours, furnace cool to 620°C; 620°C for 8 hours, air cool 					
0.2% σ_y (MPa)		σ_{TS} (MPa)		ELONGATION (%)	
R.T.	600°C	R.T.	600°C	R.T.	600°C
1195	1030	1440	1230	18	17
● ASTM GRAIN SIZE: 8 or finer, i.e. nominal grain diameter $\leq 22 \mu\text{m}$					

Table 2: Specimen codes and the initial crack lengths a_i

CODE	a_i (mm)	CODE	a_i (mm)	CODE	a_i (mm)	CODE	a_i (mm)	CODE	a_i (mm)
CT39	9.68	CT42	9.75	CT47	8.85	CT49	11.86	CT51	9.33
CT40	9.57	CT43	9.77	CT48	9.04	CT50	9.09	CT52	8.98



$$a_i = (a_i^1 + a_i^2 + a_i^3 + a_i^4 + a_i^5) / 5$$

Table 3: The test programme

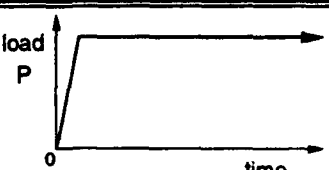
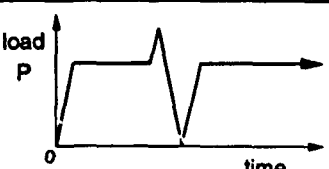
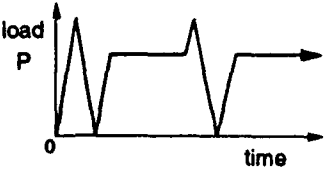
TEST TYPE	LOAD HISTORY AT 600°C	CODE	P_{dwell} (kN)	P_{max} (kN)
Dwell crack growth		CT43	6	6
		CT40	7	7
		CT39, CT42	8	8
		CT47, CT48, CT52	10	10
Dwell crack growth + peak loads and underloads		CT51	7	10
		CT49	8	10
Dwell crack growth + peak loads and underloads		CT50	7	10

Table 4: Transition data from bilinear approximations to each dwell crack growth rate versus K_I or C^* curve

CODE	P_{dwell} (kN)	da/dt versus K_I		da/dt versus C^* (C^* calculated by the method of Kumar et al [7])	
		K_{I_T} (MPa \sqrt{m})	$(da/dt)_T$ (m/s)	C_T^* (W/m ²)	$(da/dt)_T$ (m/s)
CT43	6	32	1.38E-07	0.36	1.42E-07
CT40	7	36	2.12E-07	1.32	2.49E-07
CT39	8	40	1.66E-07	0.75	1.75E-07
CT42	8	40	2.28E-07	1.12	2.39E-07
CT47	10	42	1.41E-07	0.23	1.17E-07
CT48	10	44	2.15E-07	0.76	2.22E-07
CT52	10	40	2.28E-07	1.16	2.38E-07

Table 5: Microfractographic results for dwell crack growth specimens CT39 and CT47

DWELL CRACK GROWTH FRACTURE CHARACTERISTICS	MEDIUM STRESS INTENSITY FACTORS	HIGH STRESS INTENSITY FACTORS
		<ul style="list-style-type: none"> • $K_I = 29-34$ MPa\sqrt{m} • Time at 600°C = 13-14 hours
<ul style="list-style-type: none"> • Fracture path • Specific features • Oxidation • Roughness • Secondary cracks 	<p>Complex-looking intergranular fracture: few, if any, "clean" grain boundary facets</p> <p>(1) Ligaments and ligament breakage (oxide fracture) between secondary cracks (2) Grooving at grain boundaries as probable precursor to cracking</p> <p>Limited: obvious only at magnifications > 2000X, and not dependent on exposure time</p> <p>• Moderate: $R_f = 1.45-1.64$ • Severe: $R_f = 1.82-2.28$</p> <p>• Small and isolated • Larger and more numerous</p>	

Table 6: Analytical determinations of J and C*, using MARC [9] and a post-processor program developed by Bakker [10], for selected values of P_{dwell} and crack length

P _{dwell} (kN)	a=(a _{j+1} +a _j)/2 (mm)	J (kJ/m ²)	C* (W/m ²)
6	9.5	1.63	< 2.8E-09
	13.0	3.68	< 4.7E-09
	19.5	32.3	9.0E-05
8	9.5	2.90	< 5.1E-08
	13.0	6.60	6.0E-07
	19.5	59.3	5.0E-04
10	9.5	4.57	5.0E-07
	13.0	10.4	1.7E-06
	19.5	102.0	1.6E-03

Table 7: Crack tip deformation zone sizes corresponding to transitions in the dwell crack growth rate curves

CODE	P _{dwell} (kN)	K _{I,T} (MPa√m)	(da/dt) _T (m/s)	CRACK TIP DEFORMATION ZONE SIZES (μm)		
				[32,33] r _{p,y}	[34] r _{p,y}	[16] r _{c,y}
CT43	6	32	1.38E-07	125	58-87	30
CT40	7	36	2.12E-07	159	73-110	37
CT39	8	40	1.66E-07	196	90-136	48
CT42	8	40	2.28E-07	196	90-136	47
CT47	10	42	1.41E-07	216	100-150	55
CT48	10	44	2.15E-07	237	109-164	58
CT52	10	40	2.28E-07	196	90-136	47
AVERAGE		35	1.28E-07	152	70-105	37

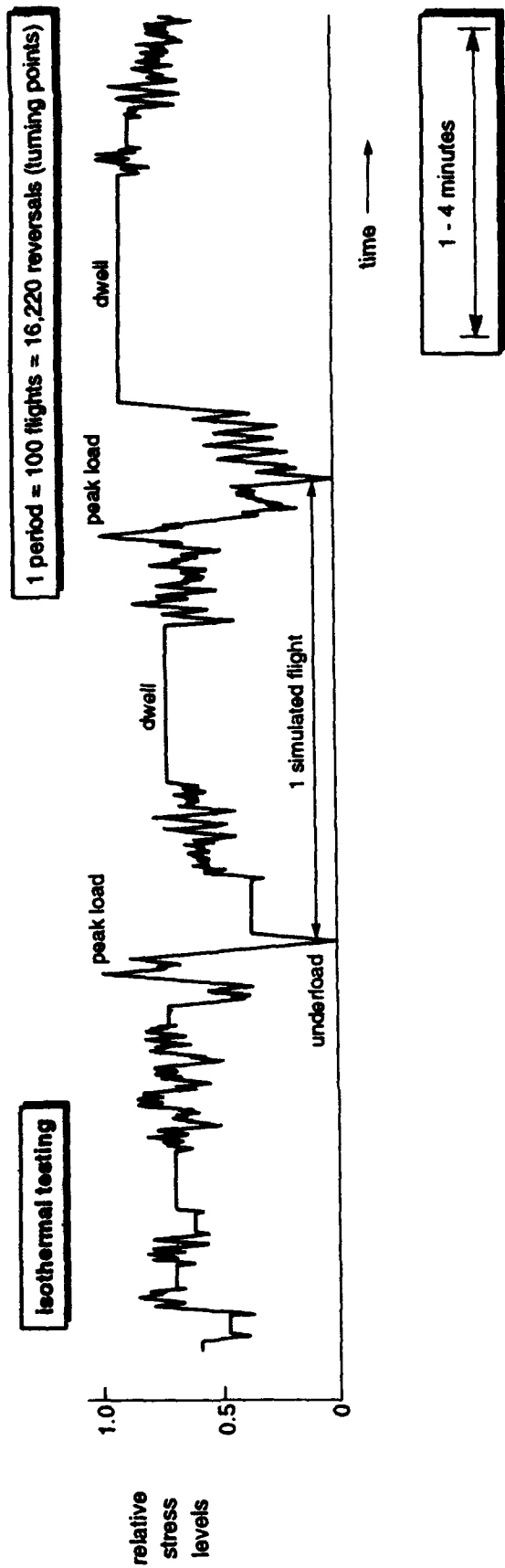


Fig. 1 Typical segment of the European-developed standard load history for military aircraft gas turbine discs, HOT TURBISTAN

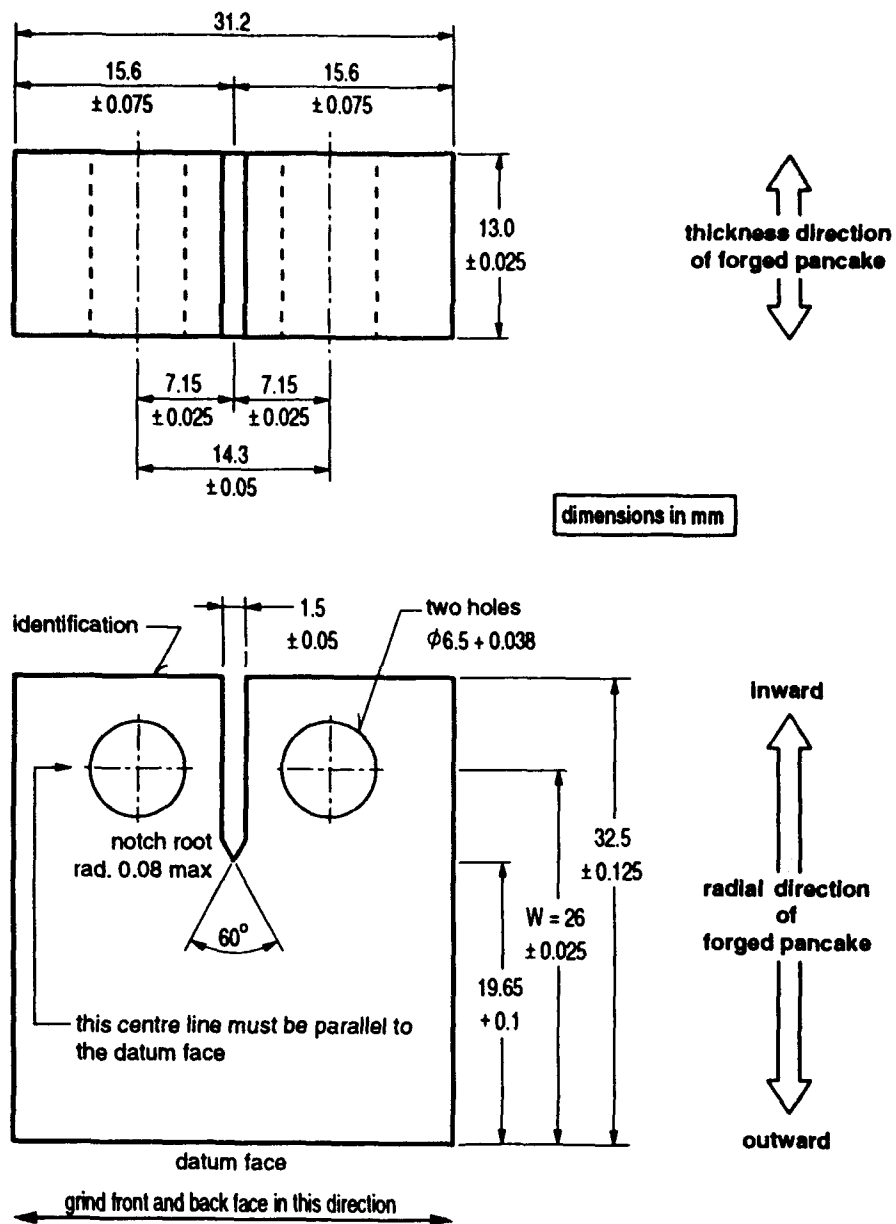


Fig. 2 Compact tension (CT) specimen configuration used for dwell crack growth testing

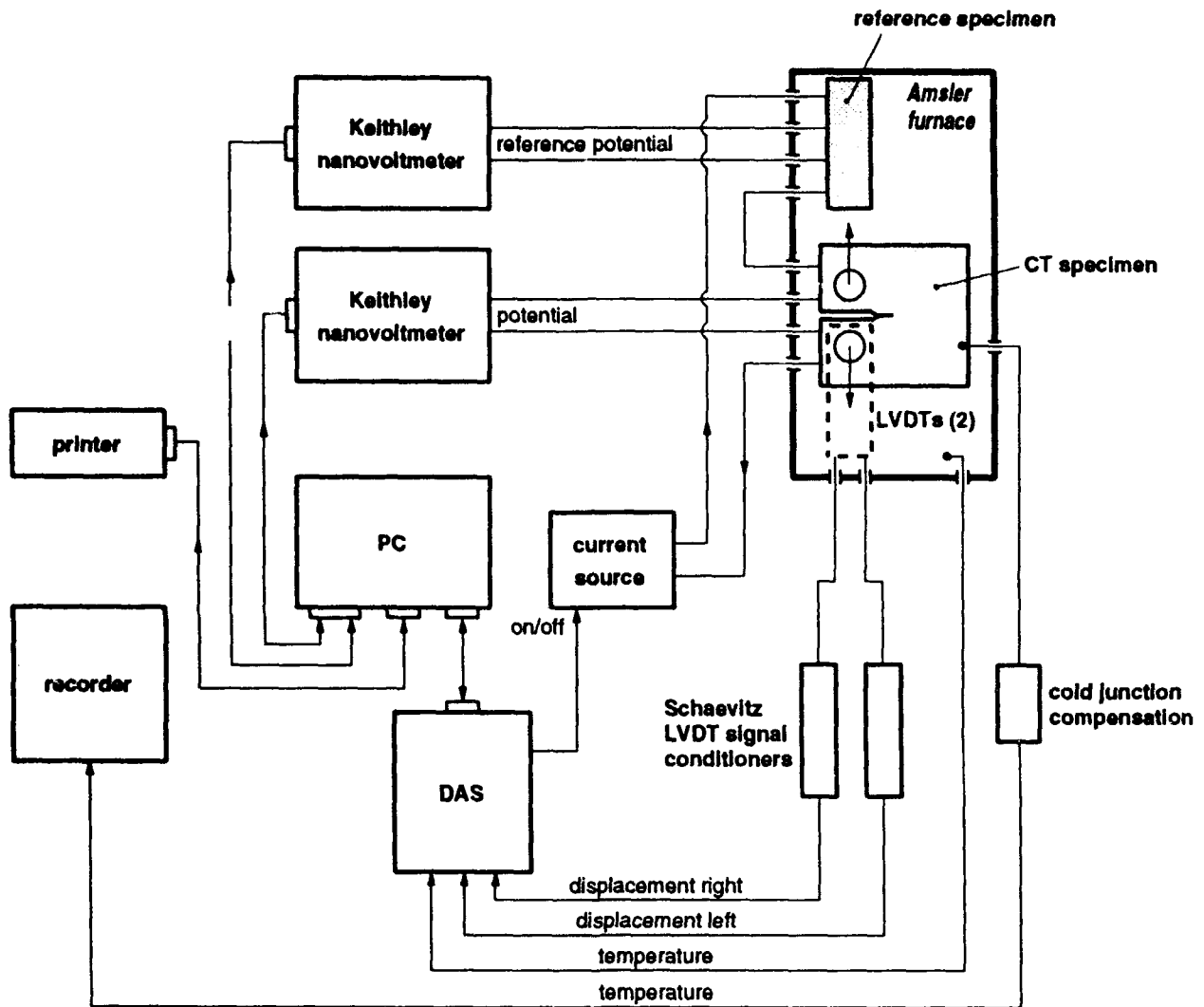


Fig. 3 Measurement circuitry for the test programme: DAS = Keithley Data Acquisition System; LVDT = Linear Variable Displacement Transducer

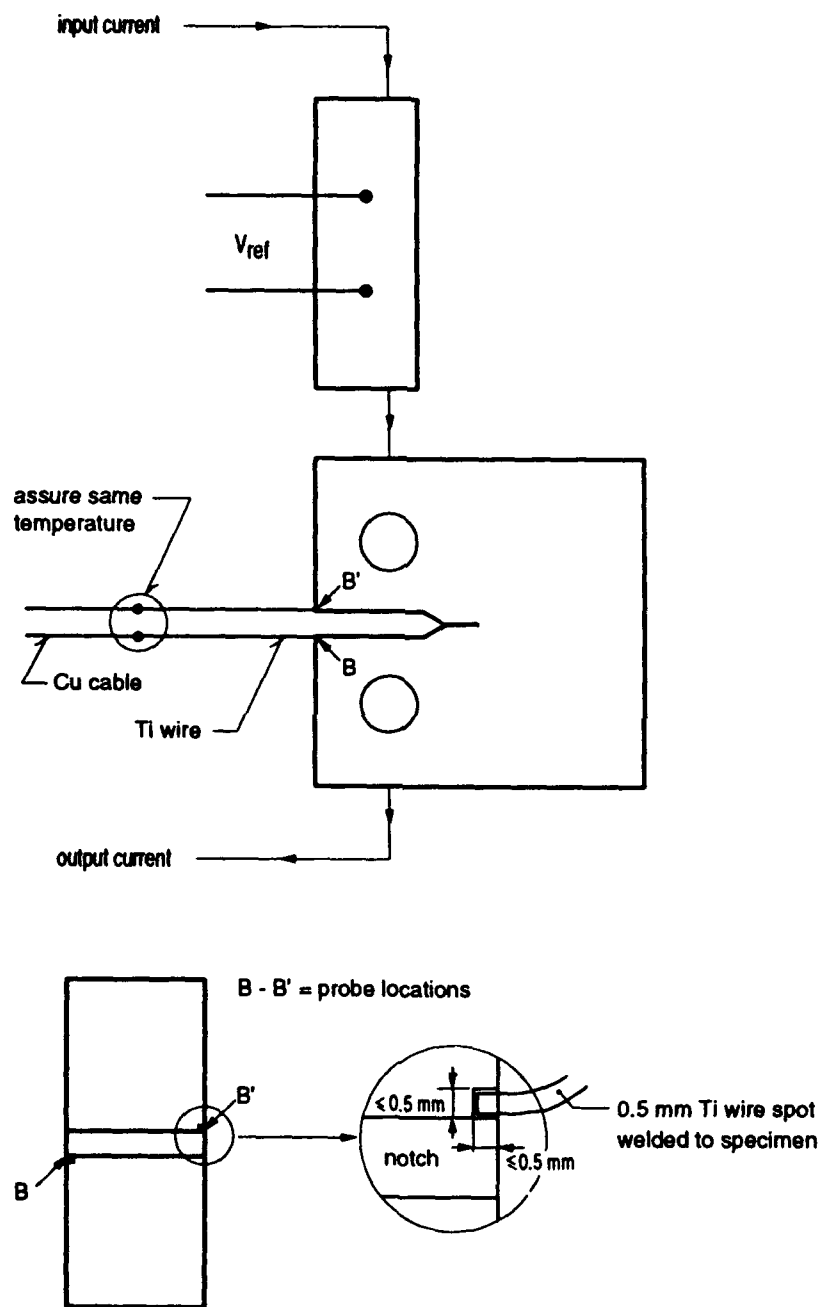


Fig. 4 Direct current potential drop (PD) set-up for measurements of crack lengths in the CT specimens

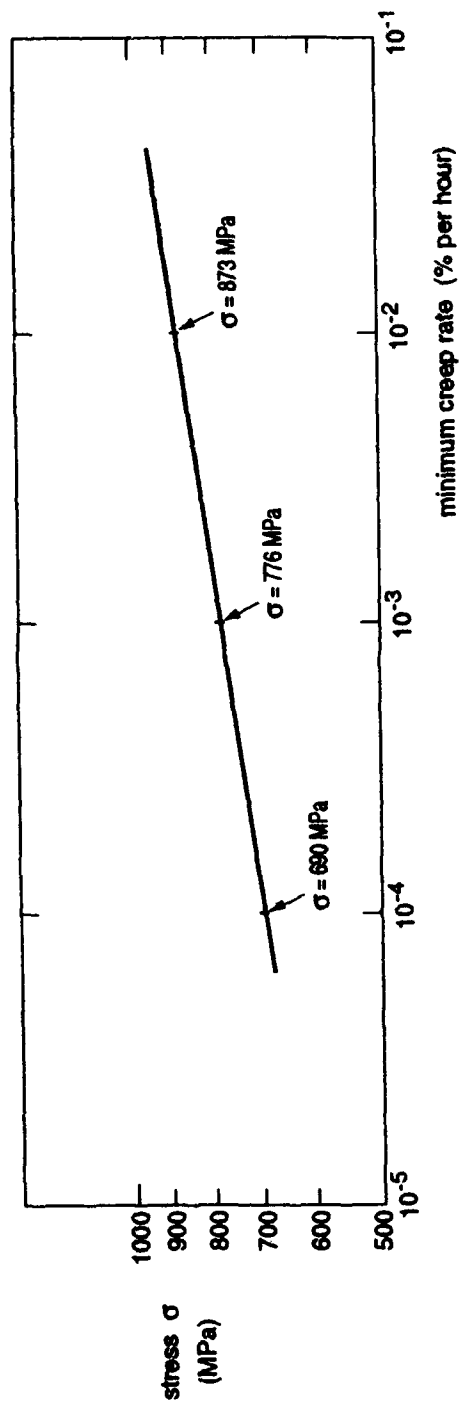


Fig. 5 Creep strength of hot rolled Inconel 718 bar tested at 593 °C [8]. Heat treatment: 982 °C for 1 hour, water quench; age 718 °C for 8 hours, furnace cool to 621 °C; hold at 621 °C for total ageing time of 18 hours

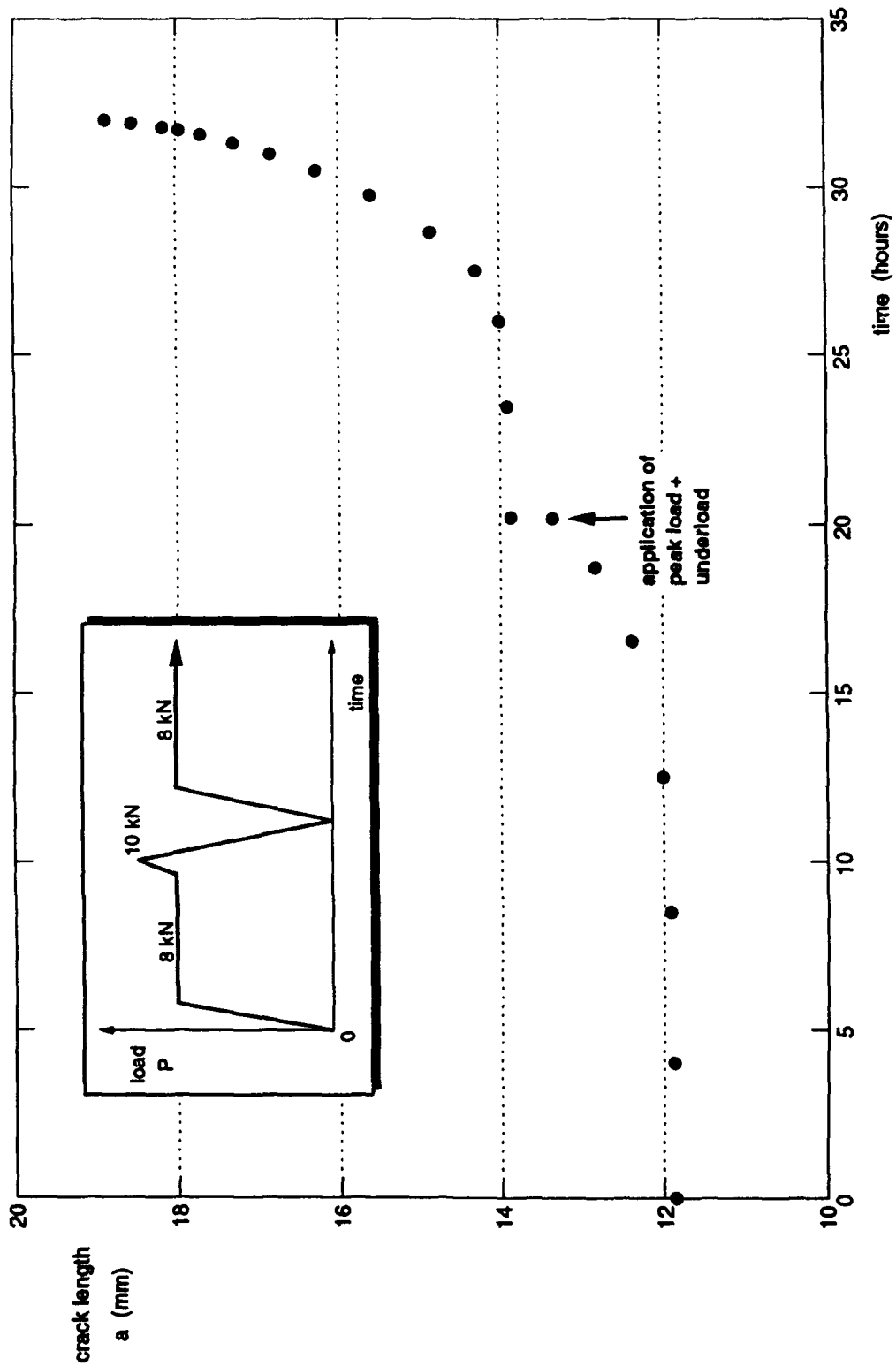


Fig. 7 Dwell crack growth curve for specimen CT49. $P_{max}/P_{dwell} = 1.25$

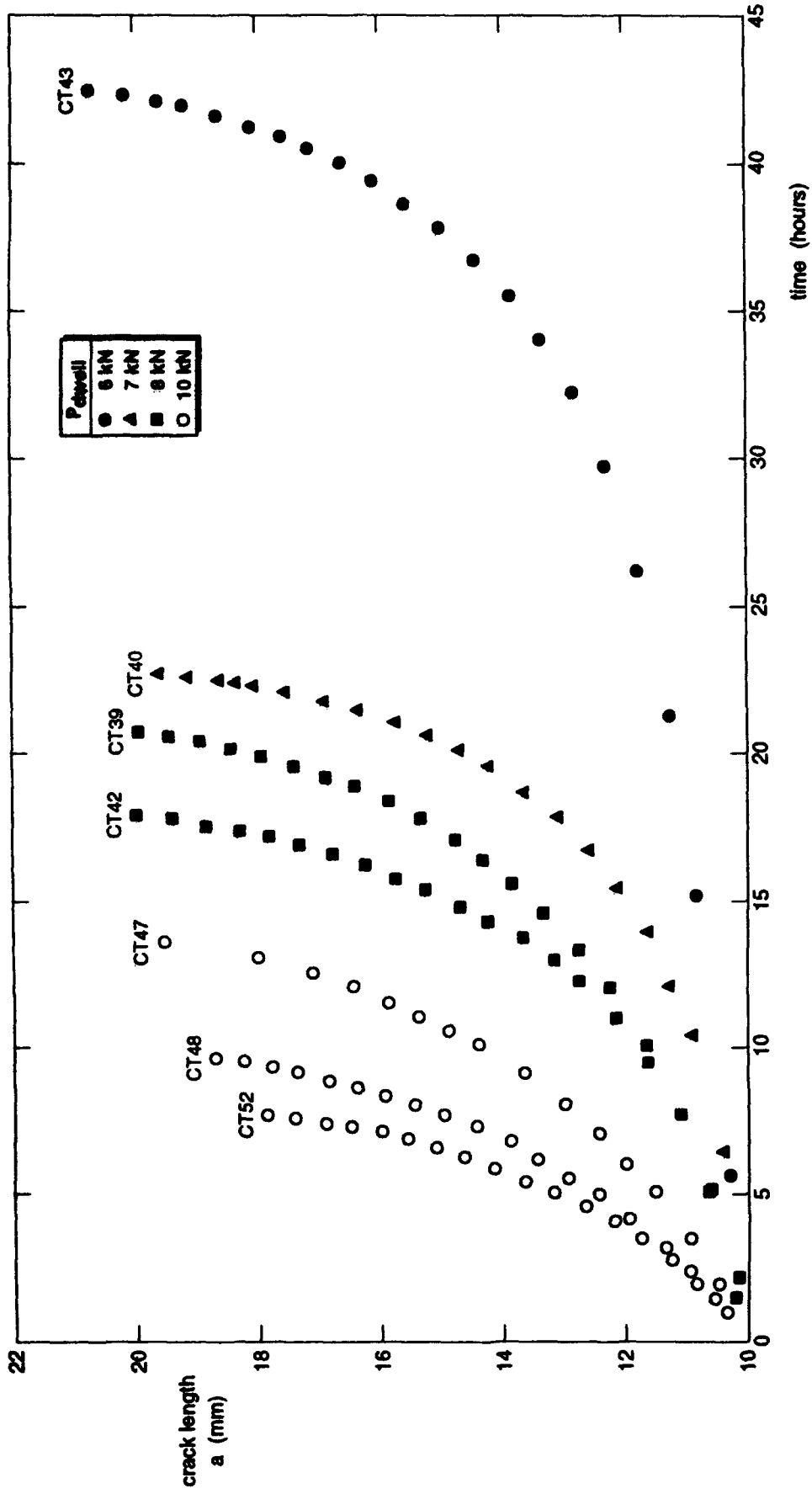


Fig. 6 Dwell crack growth curves

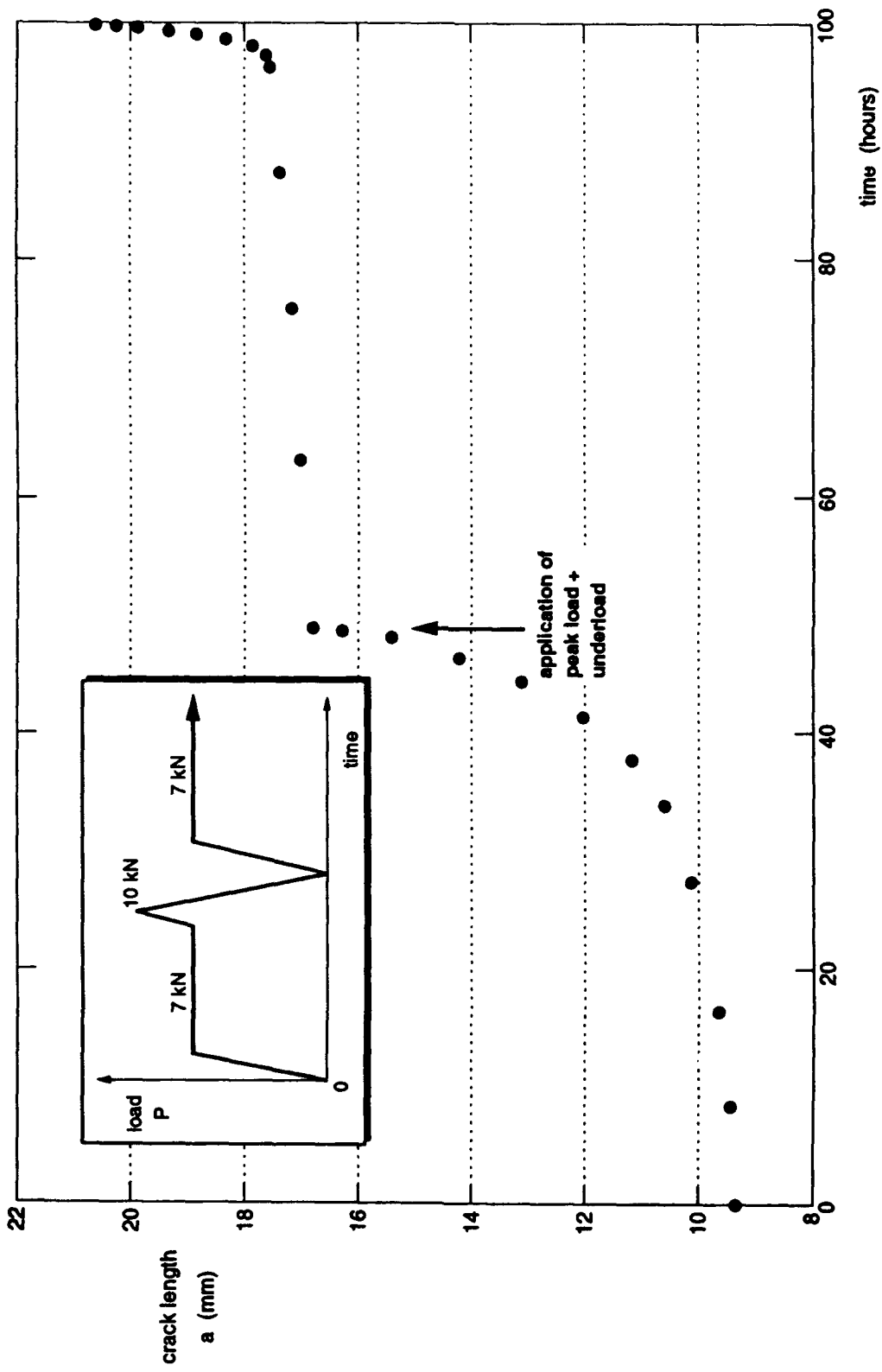


Fig. 8 Dwell crack growth curve for specimen CT51. $P_{max}/P_{dwell} = 1.43$

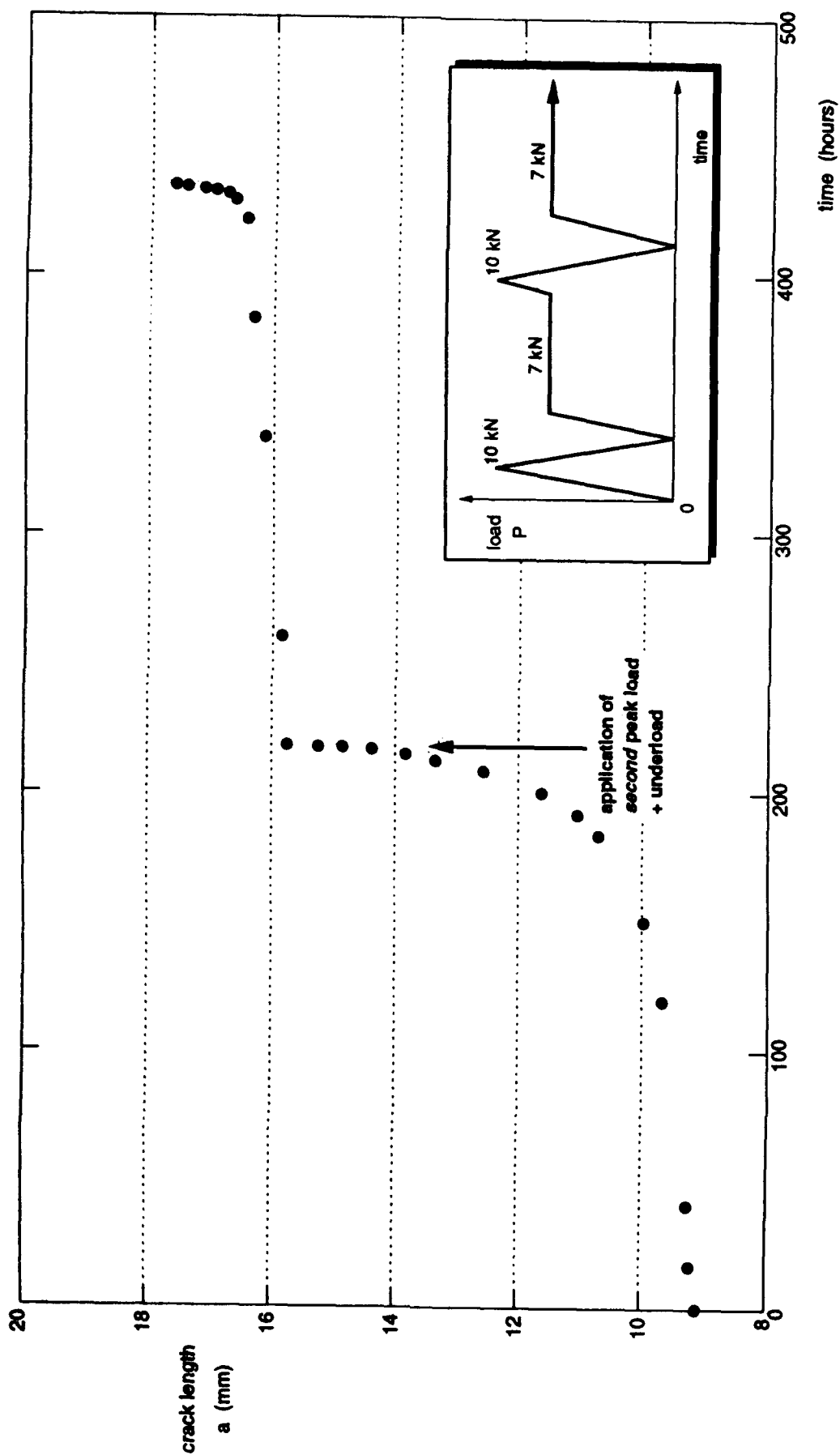


Fig. 9 Dwell crack growth curve for specimen CT50. $P_{max}/P_{dwell} = 1.43$

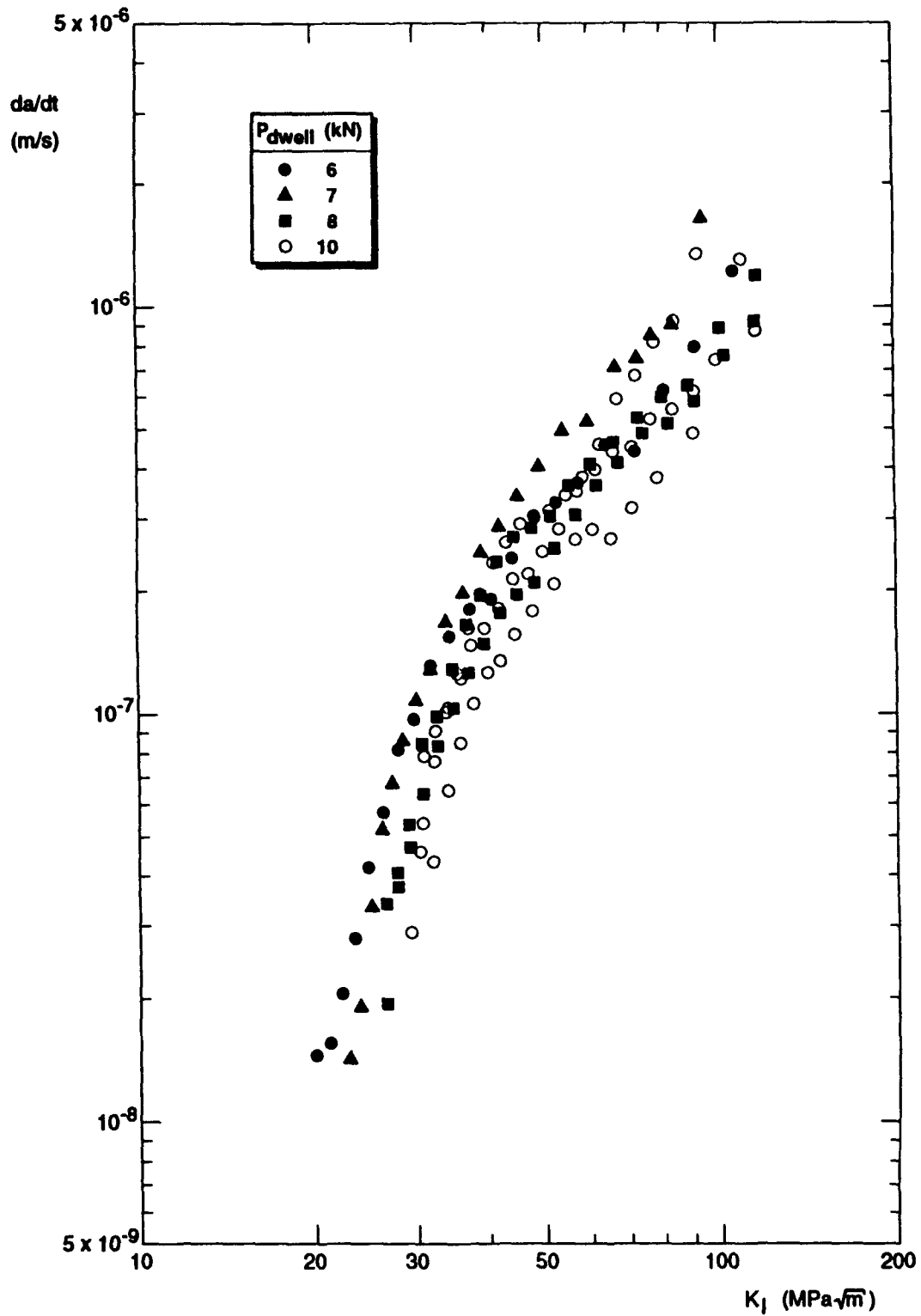


Fig. 10 Correlation of dwell crack growth rates by the LFM mode I stress intensity factor K_I

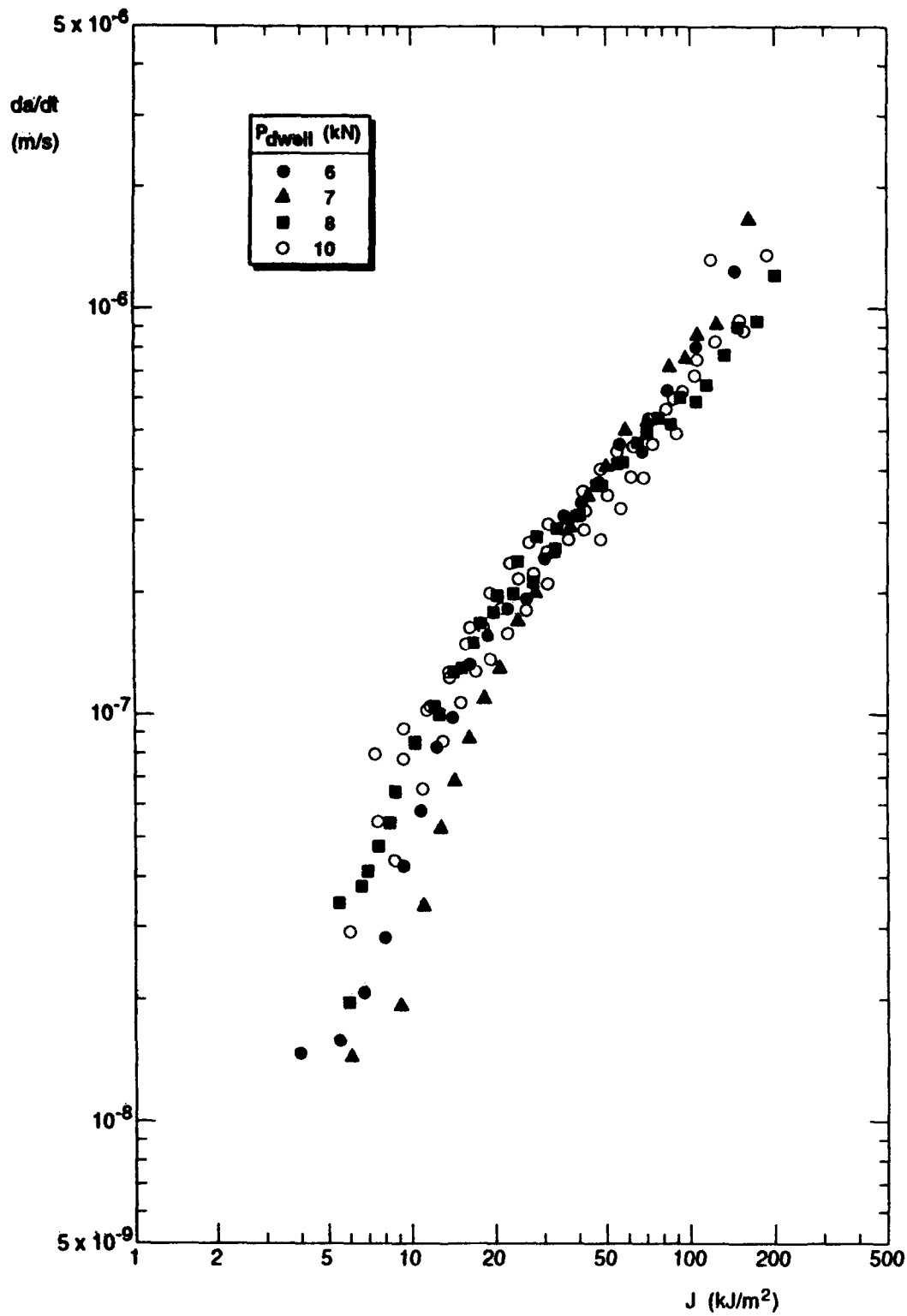


Fig. 11 Correlation of dwell crack growth rates by the EPFM path-independent contour integral J calculated by the method of Kumar et al [7]

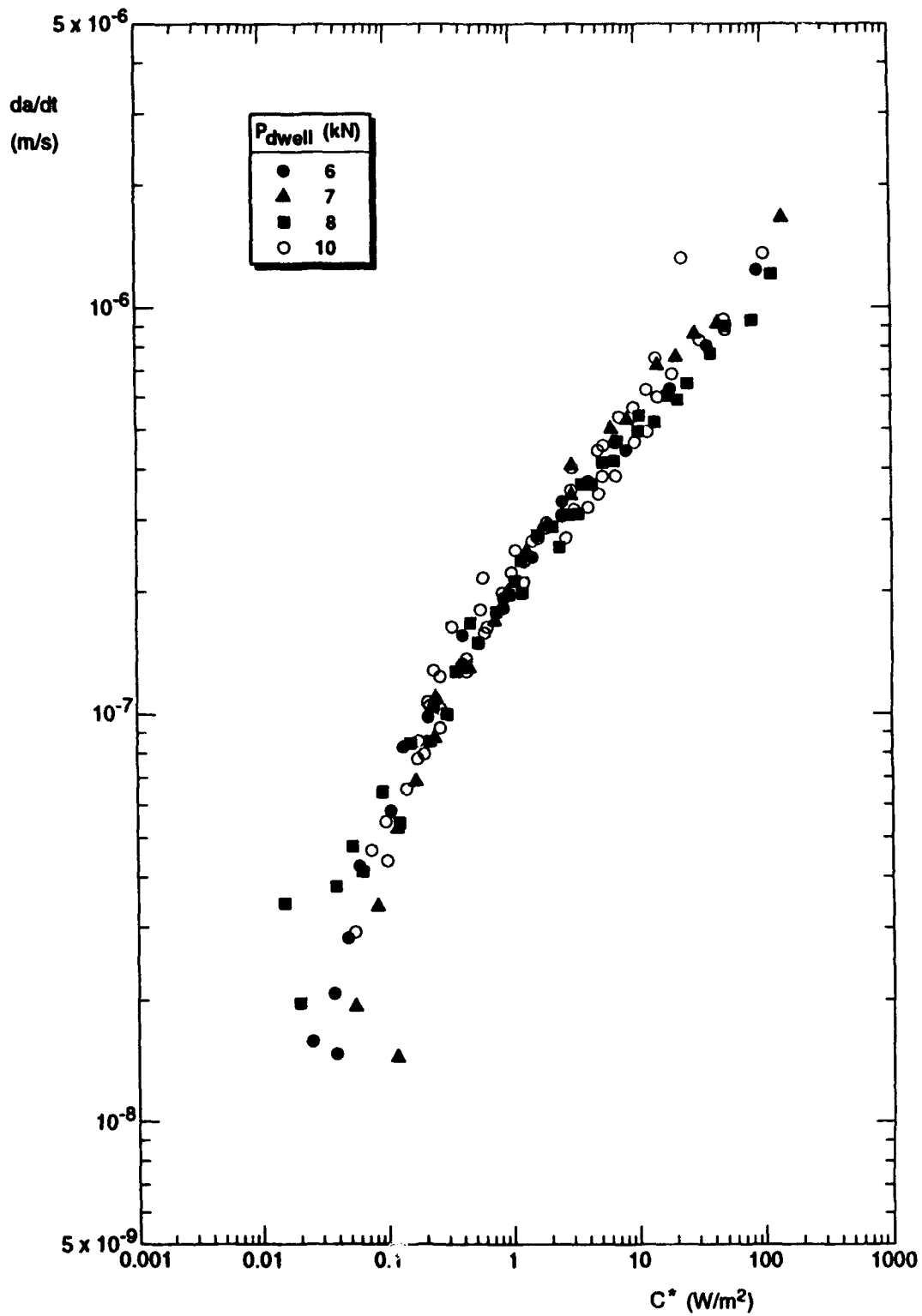


Fig. 12 Correlation of dwell crack growth rates by the EPFM path-independent time-dependent contour integral C^* calculated by the method of Kumar et al [7]

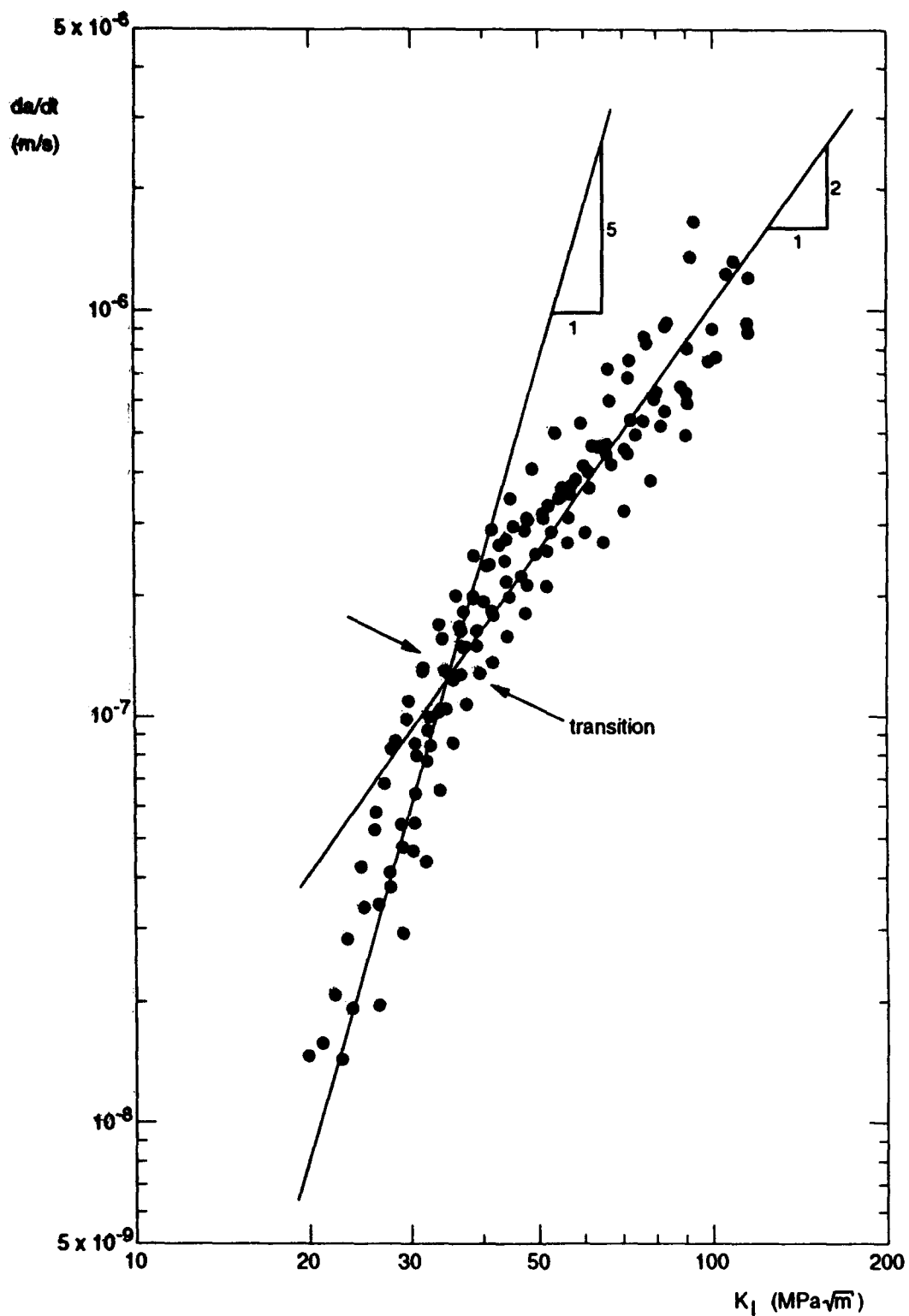


Fig. 13 Bilinear approximation to the dwell crack growth rate versus mode I stress intensity factor data for specimens CT39, CT40, CT42, CT43, CT47, CT48 and CT52

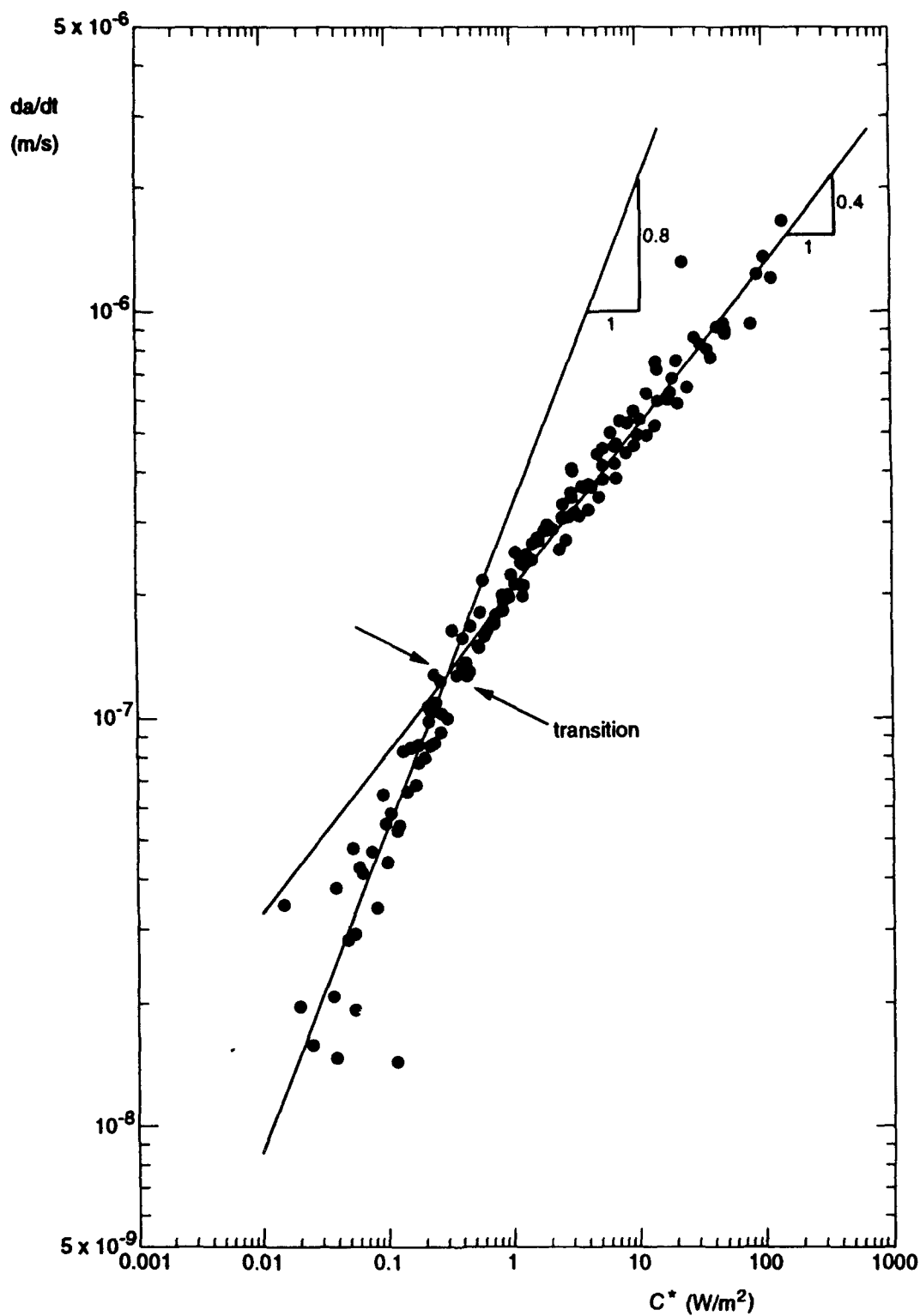


Fig. 14 Bilinear approximation to the dwell crack growth rate data versus C^* calculated by the method of Kumar et al [7] for specimens CT39, CT40, CT42, CT43, CT47, CT48 and CT52

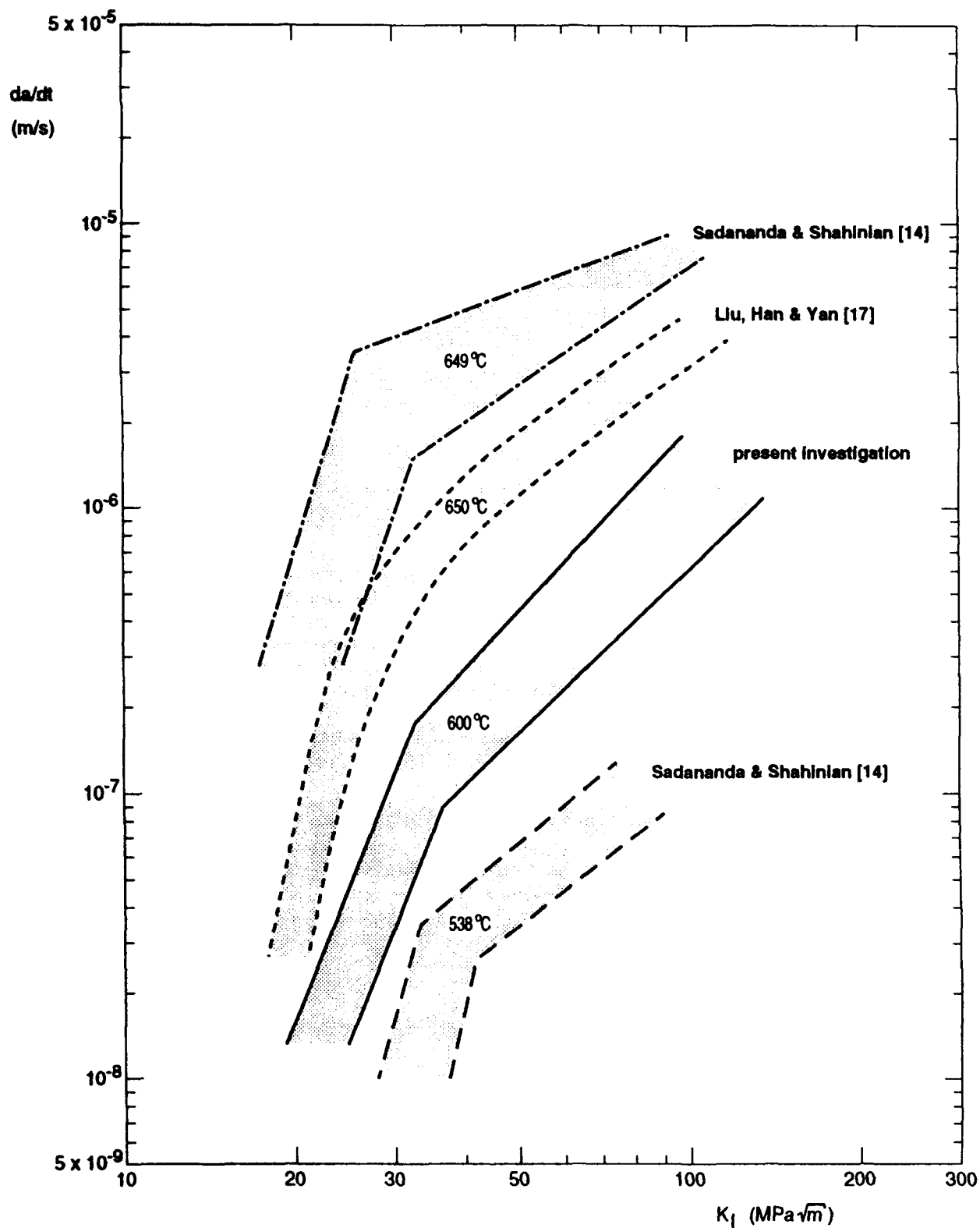


Fig. 15 Comparison of dwell crack growth rate versus mode I stress intensity factor data envelopes for Inconel 718 plate [14], square bar [17], and forged pancake (present investigation). The material heat treatments were similar and designed to provide optimum creep resistance. All tests were done in air

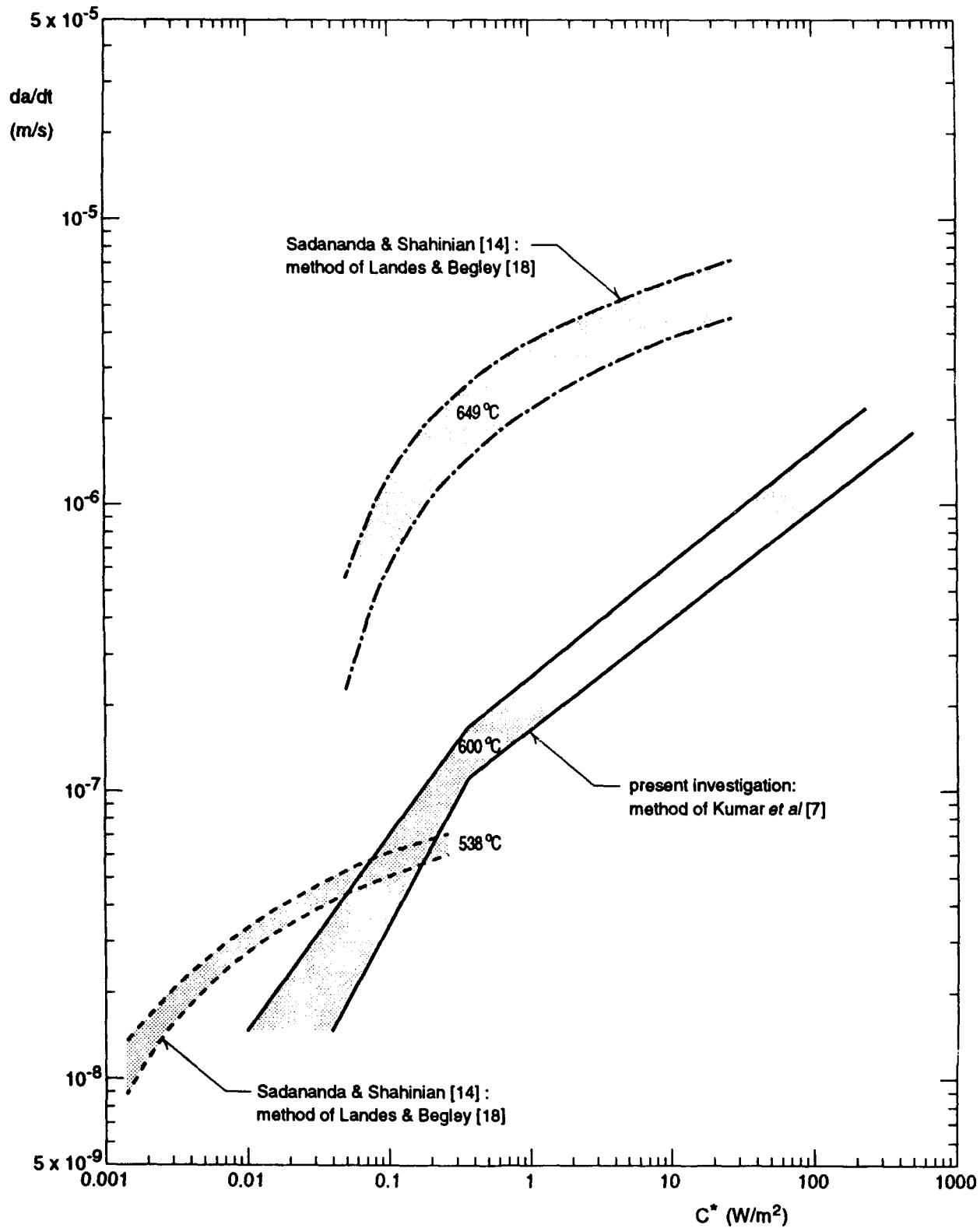


Fig. 16 Comparison of dwell crack growth rate versus C^* data envelopes for Inconel 718 plate [14] and forged pancake (present investigation). The material heat treatments were similar and designed to provide optimum creep resistance. All tests were done in air

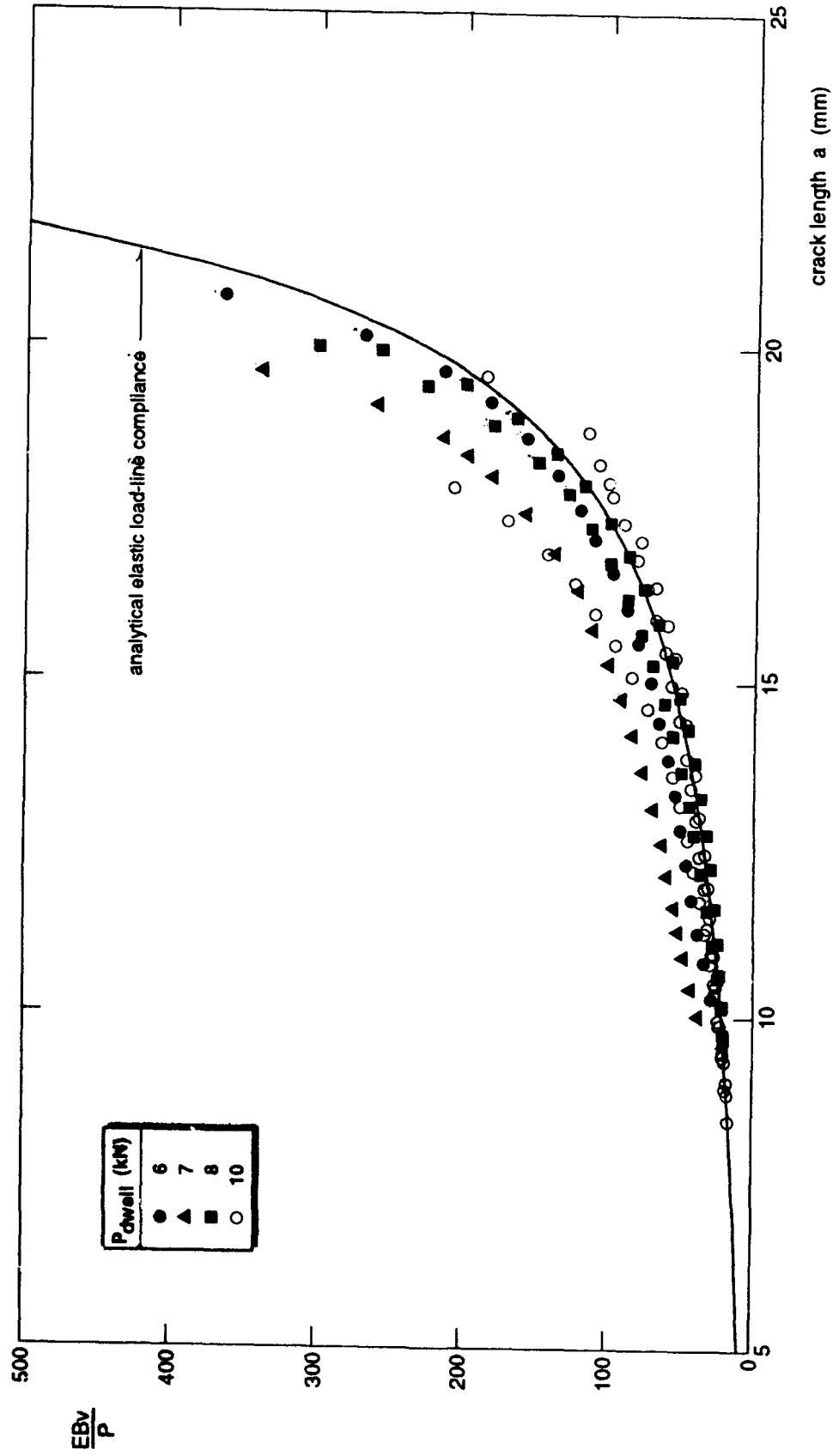


Fig. 17 Comparison of experimental and analytical load-line compliances for the dwell crack growth CT specimens

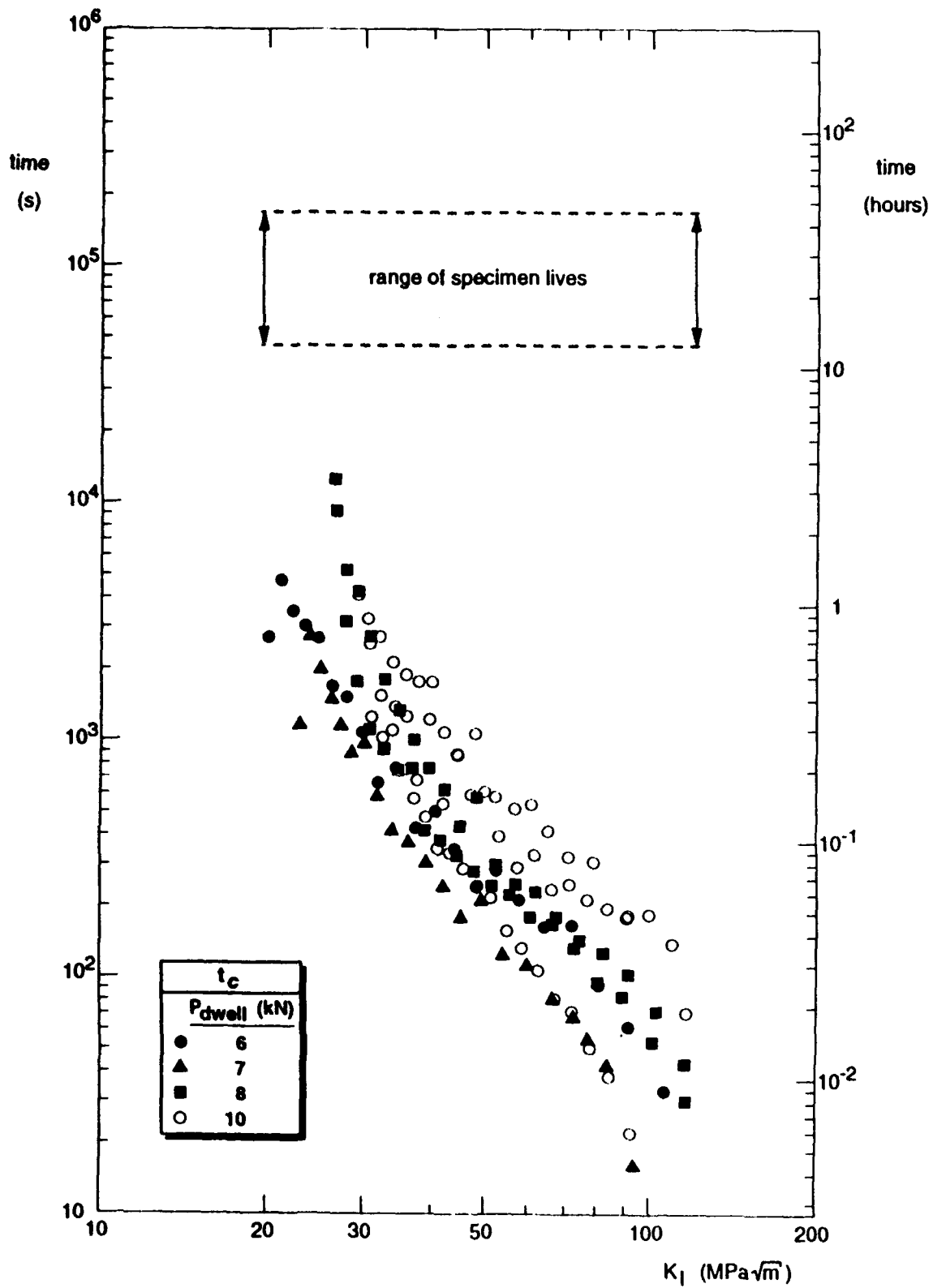


Fig. 18 Comparison of dwell crack growth specimen lives with the characteristic times, t_c , calculated with C^* values derived by the method of Kumar et al (Ref. 7)



Fig. 19 Representative microstructure of the Inconel 718 forged pancake material in the macroscopic plane of dwell crack growth



Fig. 20 Overview of dwell crack growth fracture characteristics at medium stress intensity factors: specimen CT39, $K_I \sim 29.5 \text{ MPa}\sqrt{\text{m}}$. Exposure time at 600°C approximately 14 hours



Fig. 21 Detail of dwell crack growth fracture characteristics at medium stress intensity factors: specimen CT39, $K_I \sim 29.5 \text{ MPa}\sqrt{\text{m}}$. Exposure time at 600°C approximately 14 hours



Fig. 22 Overview of dwell crack growth fracture characteristics at high stress intensity factors: specimen CT47, $K_I \sim 82 \text{ MPa}\sqrt{\text{m}}$. Exposure time at 600°C approximately 1 hour

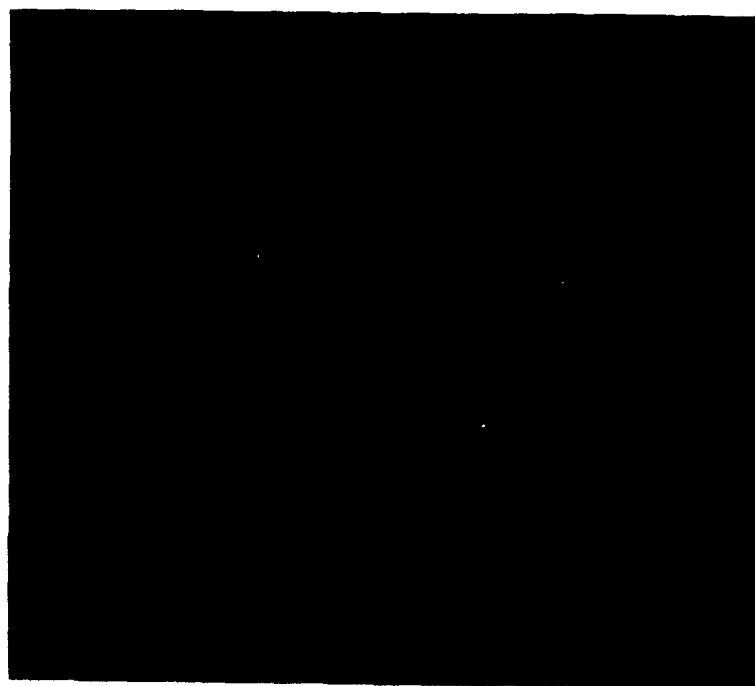


Fig. 23 Detail of dwell crack growth fracture characteristics at high stress intensity factors: specimen CT39, $K_I \sim 79 \text{ MPa}\sqrt{\text{m}}$. Exposure time at 600°C approximately 1 hour

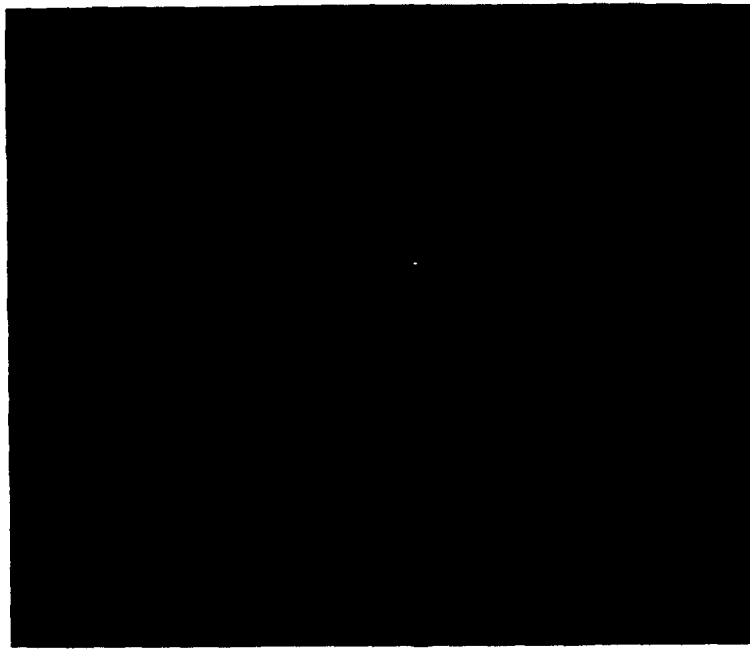


Fig. 24 Example cross-section of dwell crack growth fracture surfaces at medium stress intensity factors: specimen CT47, $K_I \sim 34 \text{ MPa}\sqrt{\text{m}}$

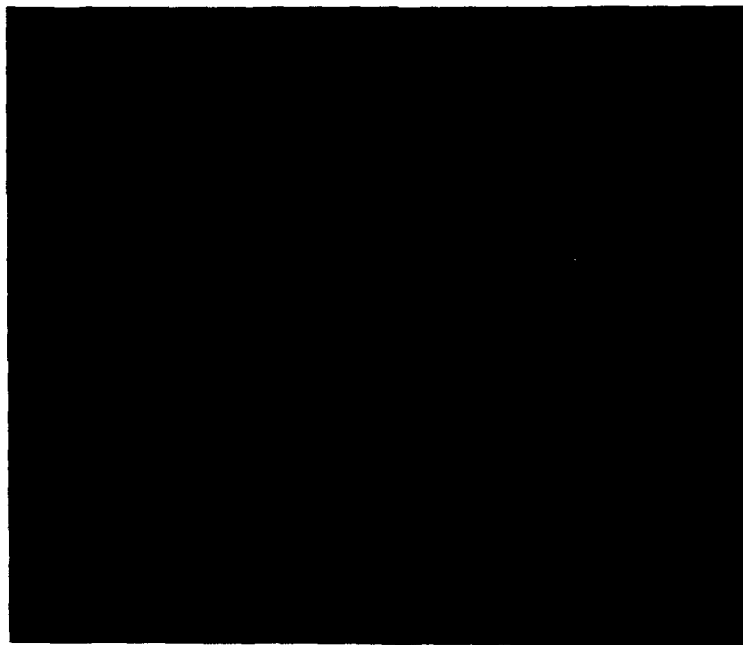


Fig. 25 Detail of secondary cracking during dwell crack growth at medium stress intensity factors: specimen CT47, $K_I \sim 34 \text{ MPa}\sqrt{\text{m}}$; back-scattered electron image from the scanning electron microscope



Fig. 26 Example cross-section of dwell crack growth fracture surfaces at high stress intensity factors: specimen CT39, $K_I \sim 79 \text{ MPa}\sqrt{\text{m}}$



Fig. 27 Detail of secondary cracking during dwell crack growth at high stress intensity factors: specimen CT39, $K_I \sim 79 \text{ MPa}\sqrt{\text{m}}$

a)

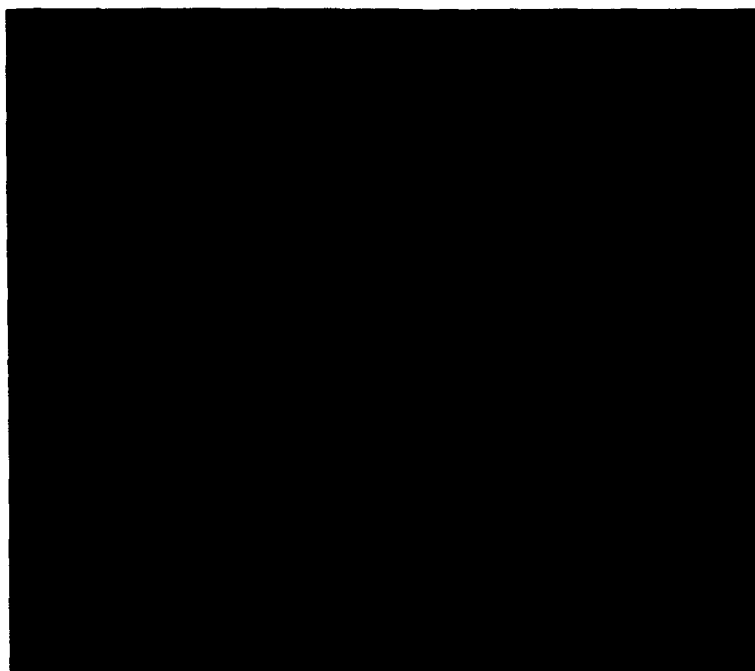


b)



Fig. 28 Example of ligament formation between secondary cracks intersecting the dwell crack growth fracture surface at high stress intensity factors: specimen CT39, $K_I \sim 79 \text{ MPa}\sqrt{\text{m}}$. Exposure time at 600°C approximately 1 hour

a)



b)

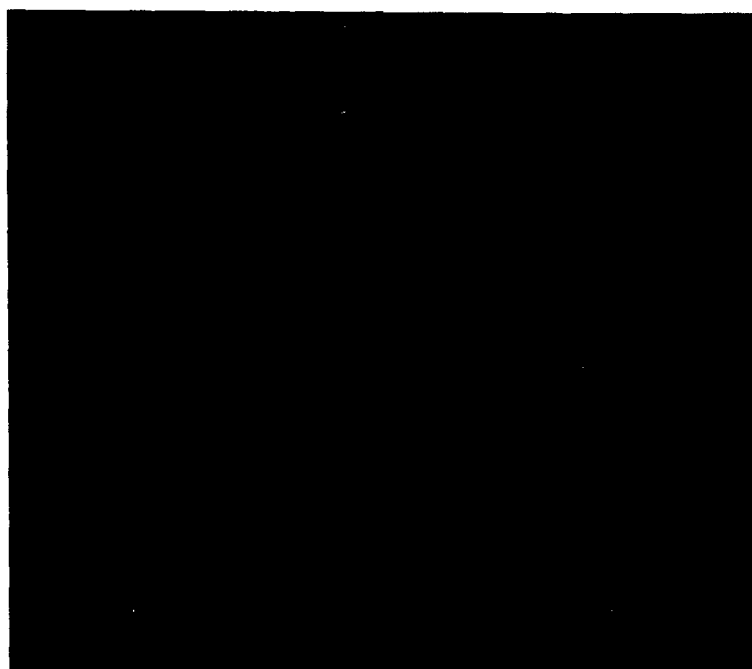
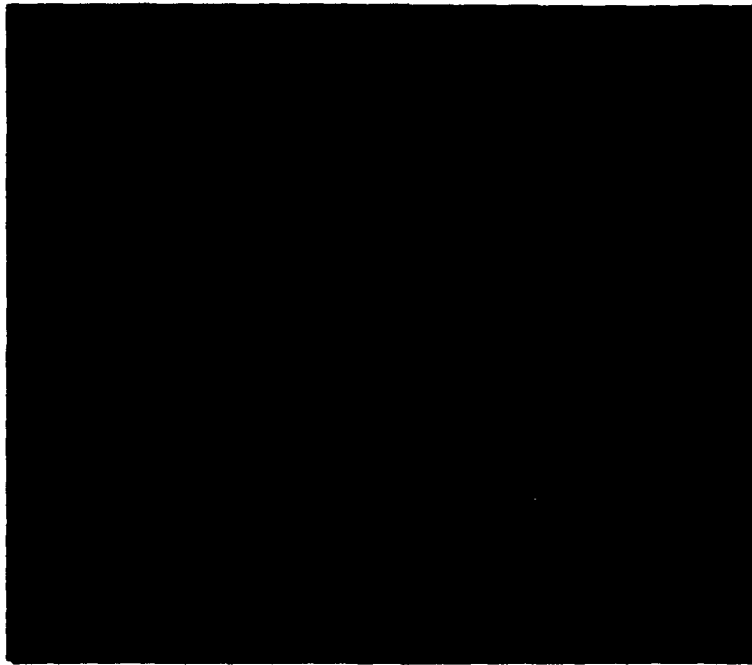


Fig. 29 Example of ligament formation and breakage (oxide fracture) between secondary cracks intersecting the dwell crack growth fracture surface at medium stress intensity factors: specimen CT39, $K_I \sim 29.5 \text{ MPa}\sqrt{\text{m}}$. Exposure time at 600 °C approximately 14 hours

a)



b)

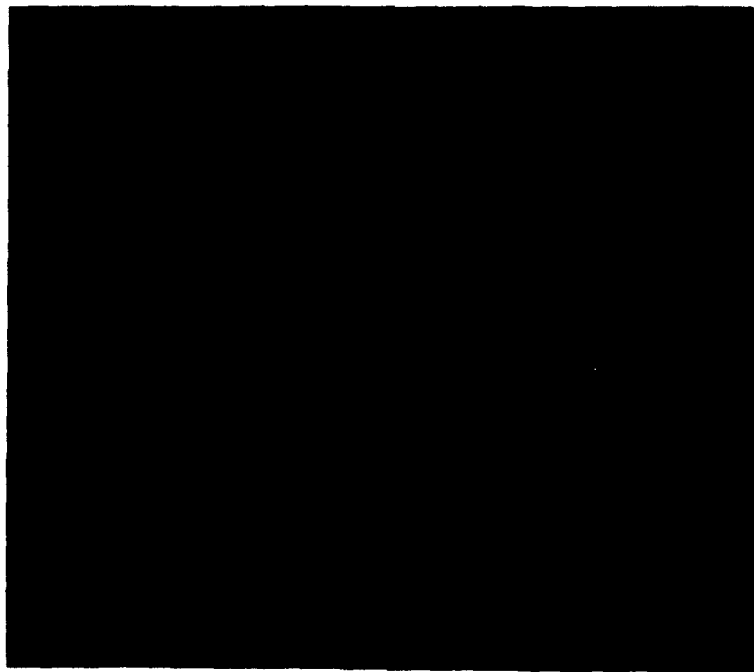
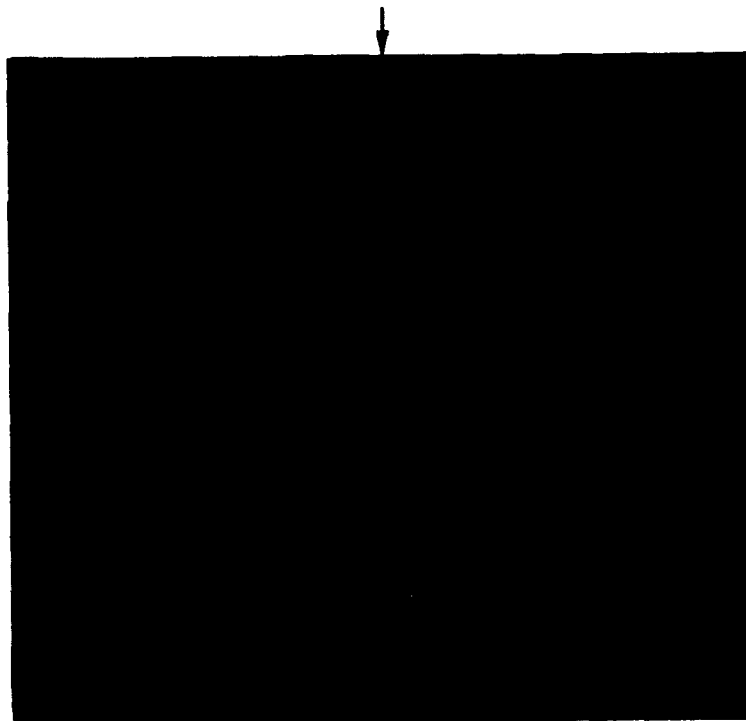


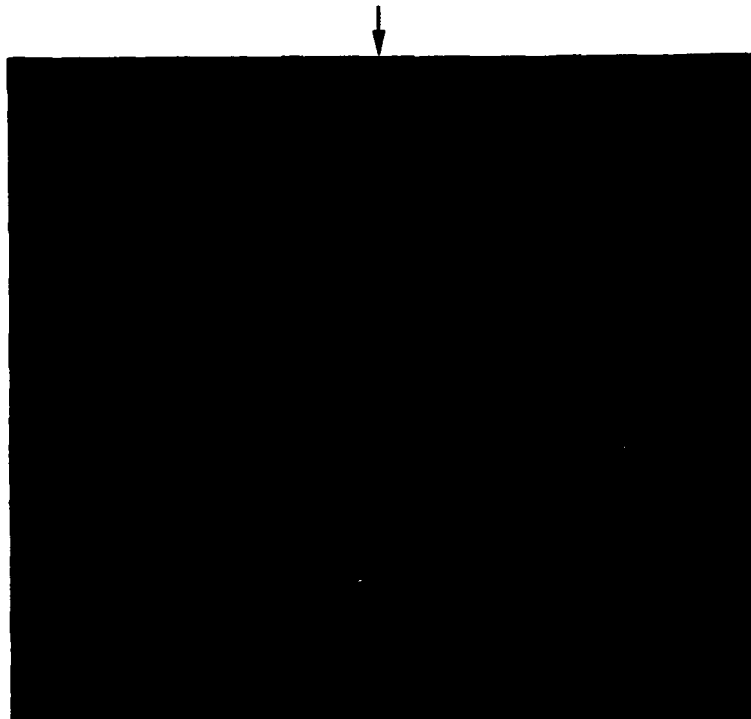
Fig. 30 Example of grooving at grain boundaries on dwell crack growth fracture surfaces: specimen CT39, $K_I \sim 79 \text{ MPa}\sqrt{\text{m}}$. Exposure time at 600°C approximately 1 hour

a)



peak load and underload

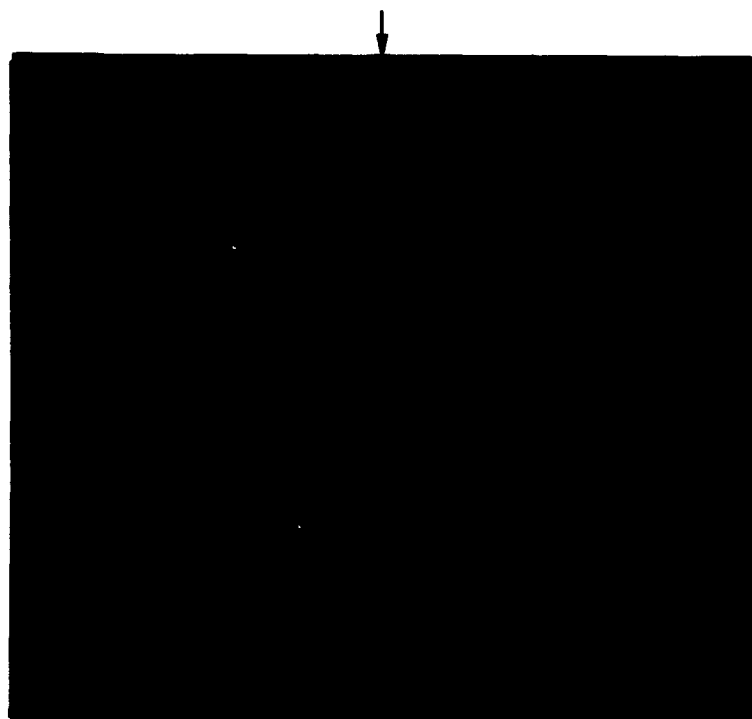
b)



peak load and underload

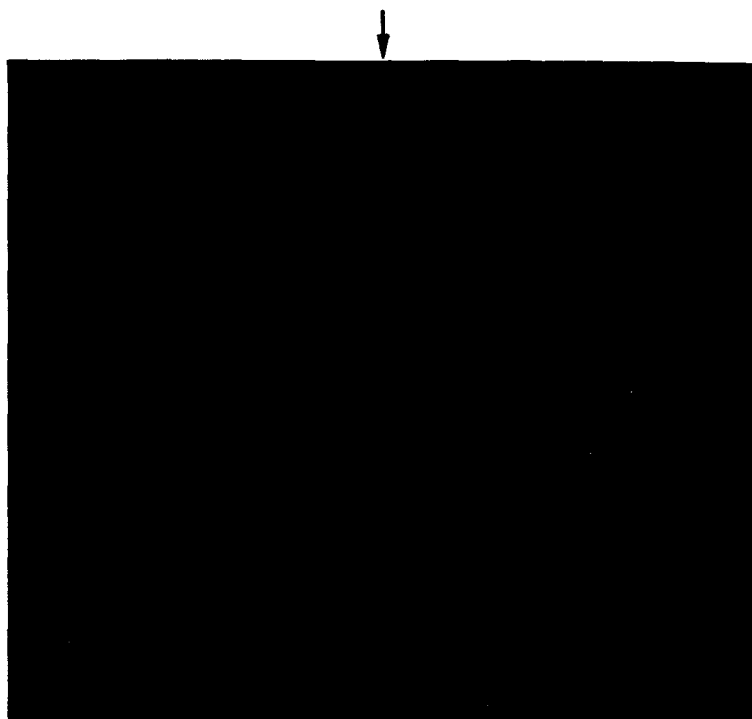
Fig. 31 Low magnification scanning electron fractographs at the position of the peak load and underload combination imposed on dwell crack growth in specimen CT51

a)



peak load and underload

b)



peak load and underload

Fig. 32 Intermediate and high magnification scanning electron fractographs at the position of the peak load and underload combination imposed on dwell crack growth in specimen CT51

a)



b)

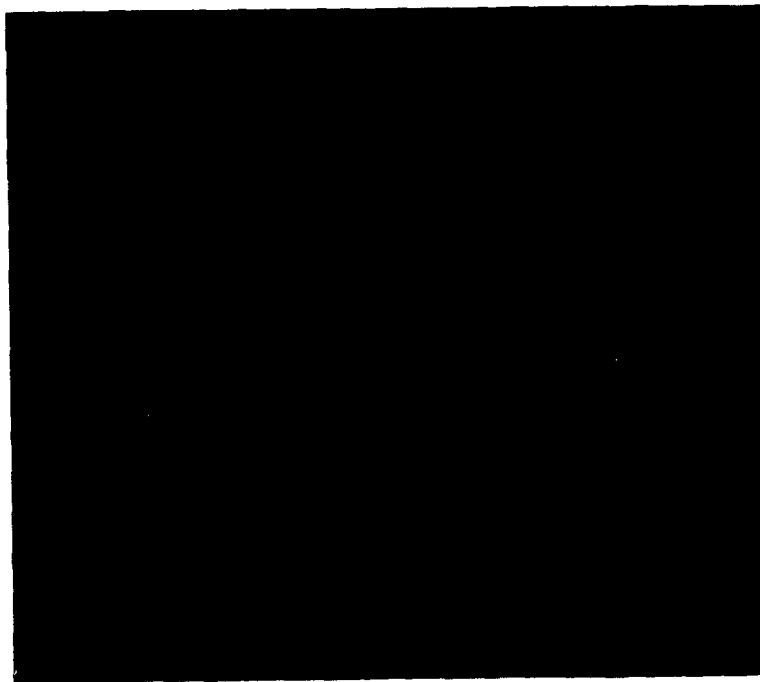


Fig. 33 Overview and detail of dwell crack growth fracture characteristics for specimen CT51: a ~ 11 mm, $K_I \sim 26 \text{ MPa}\sqrt{\text{m}}$. Exposure time at 600 °C approximately 65 hours

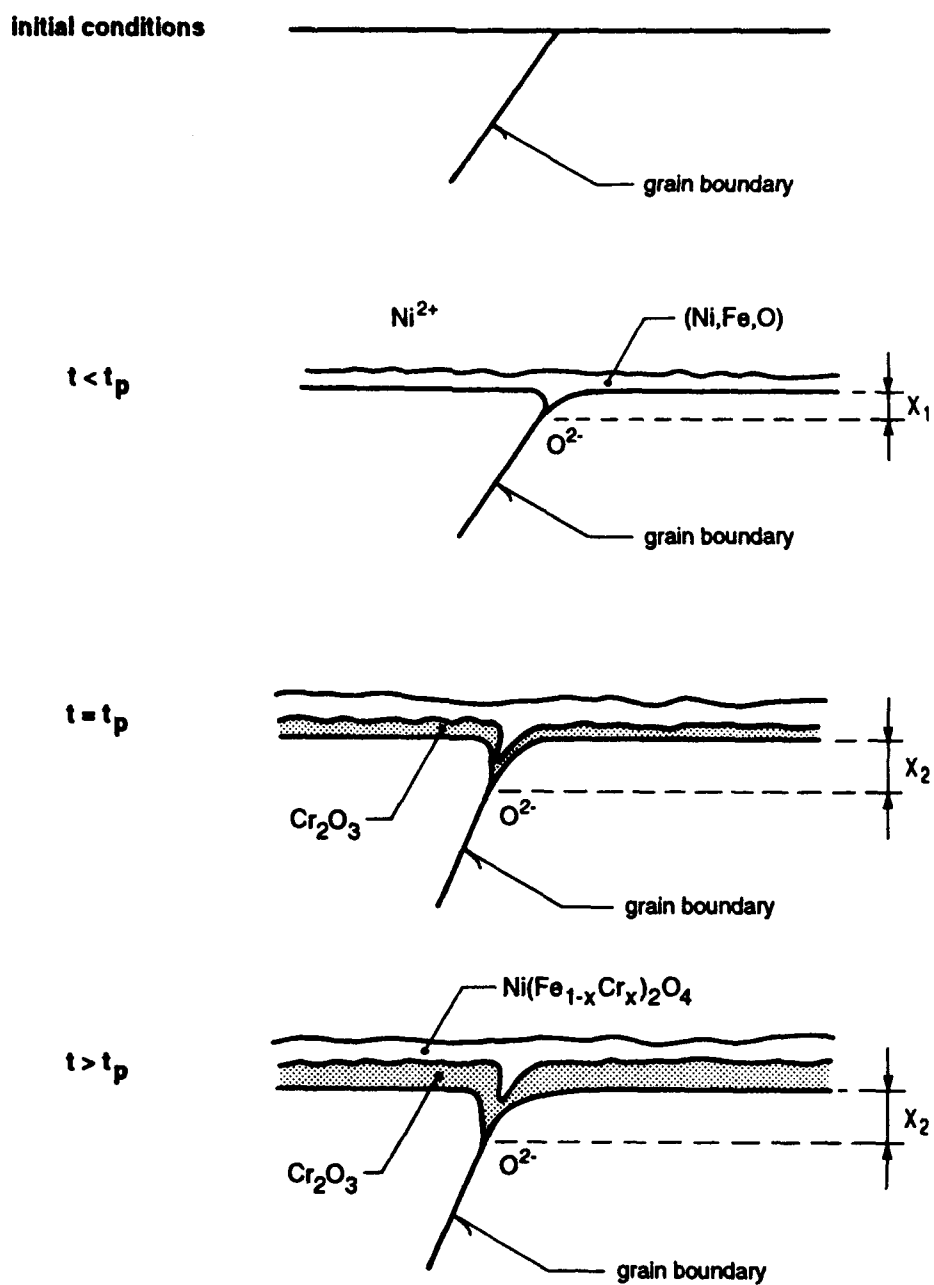


Fig. 34 Two-stage oxidation mechanism for Inconel 718 [26]

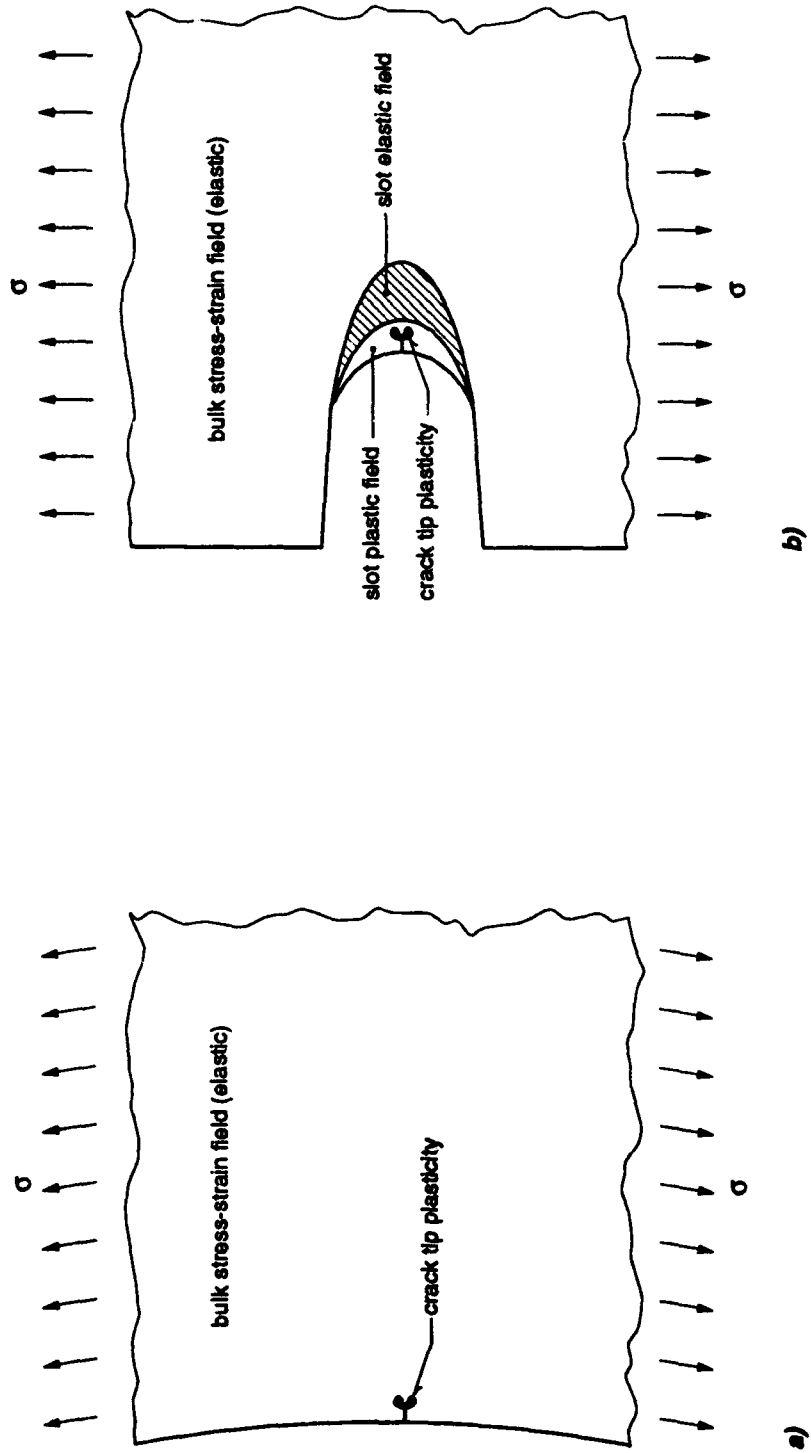


Fig. 35 Schematic of short crack growth at a) bore and b) rim slot locations in a turbine disc

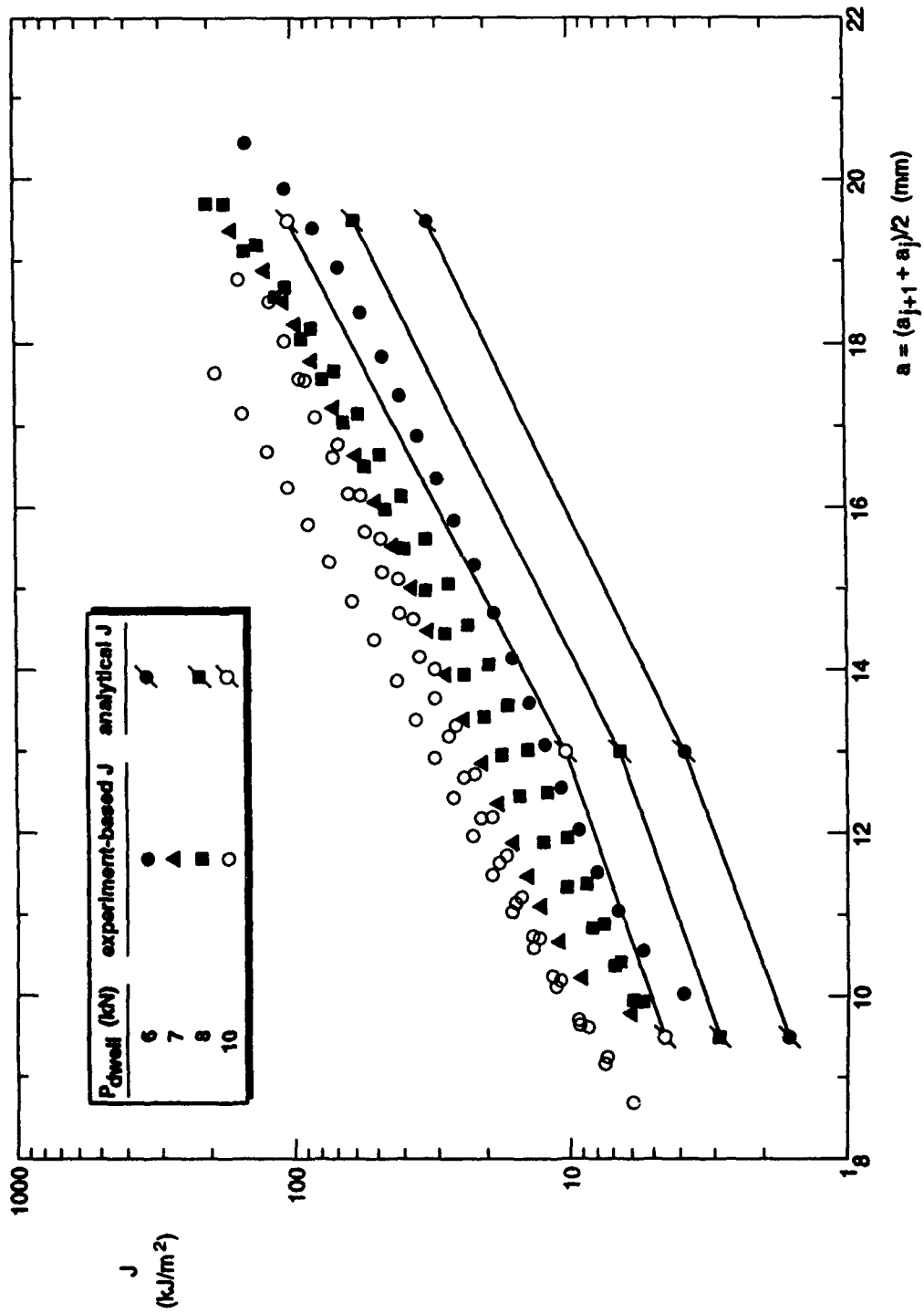


Fig. 36 Comparison of analytical and experiment-based J values as functions of P_{dwell} and crack length

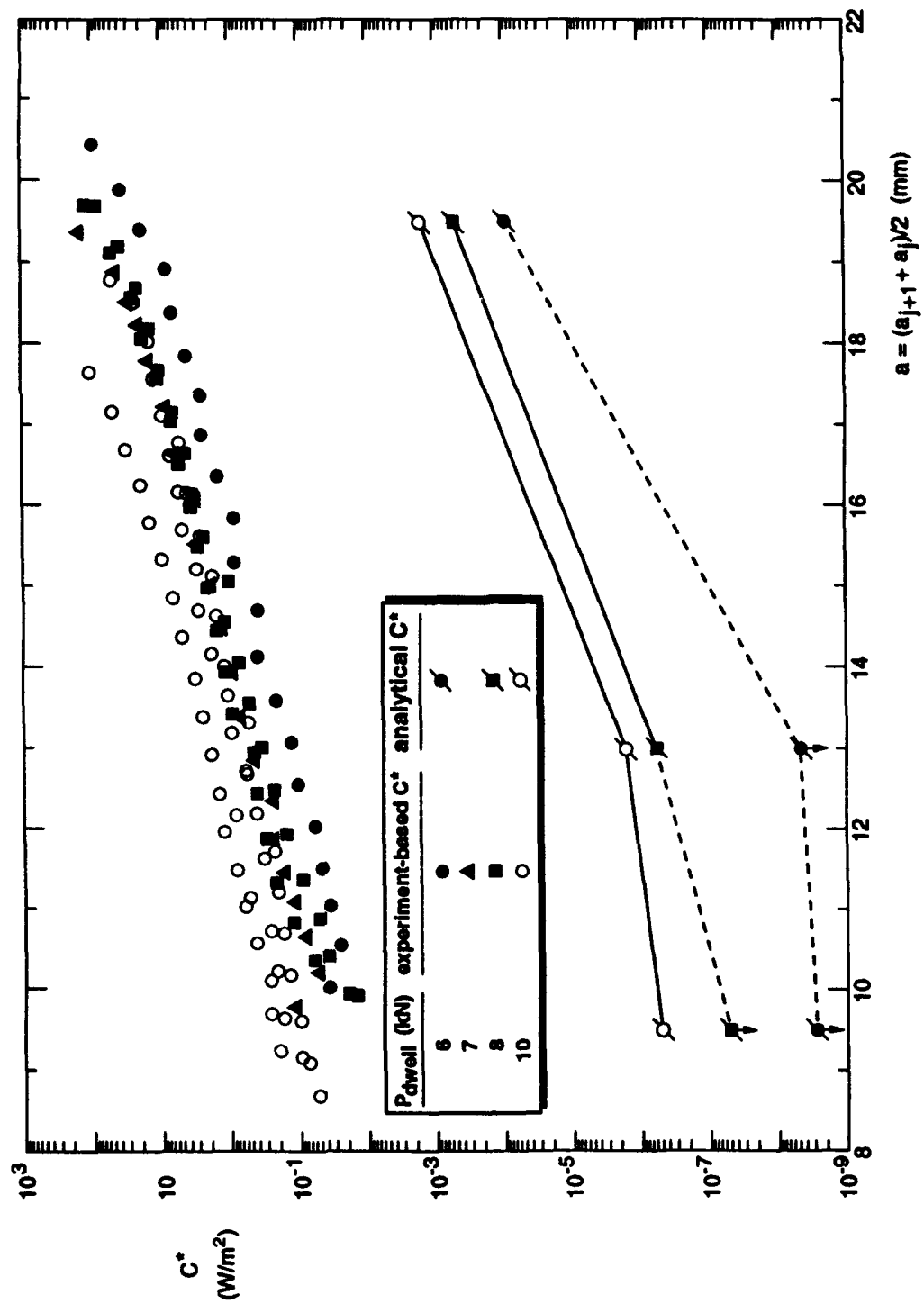


Fig. 37 Comparison of analytical and experiment-based C^* values as functions of P_{dwell} and crack length

**DAMAGE ASSESSMENT
IN
COMPOSITES
USING
THERMOELASTIC STRESS ANALYSIS (TSA) TECHNIQUES**

**D.H. NETHAWAY
DEC. 1, 1993**



MATERIALS ENGINEERING



FATIGUE DAMAGE ASSESSMENT FOR MMC'S

TSA Technique

Outline

- **Background**
- **Objectives**
- **Test approach**
- **Test results**
- **Summary**



BACKGROUND

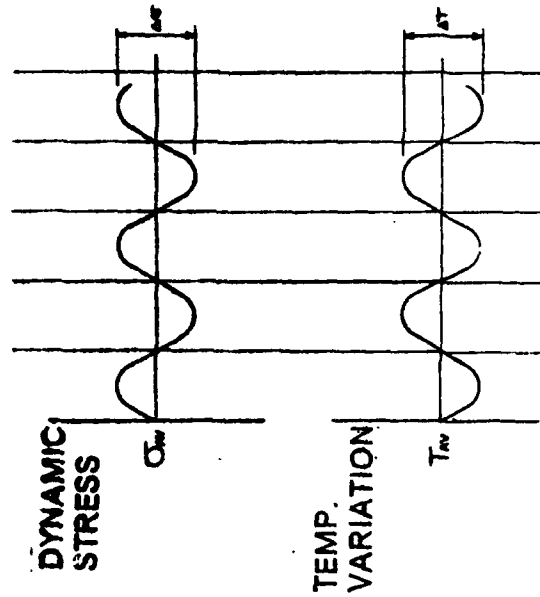
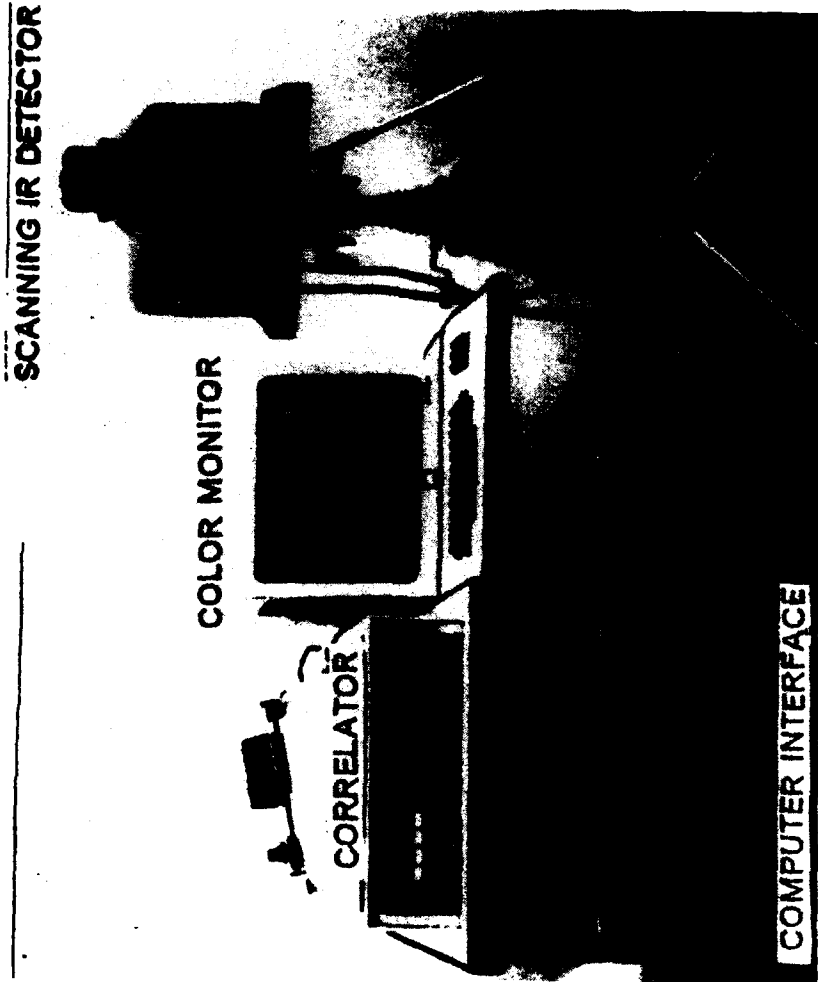
TSA (Thermographic Stress Analysis)

- Non-contacting
- Full field
- Analysis of structures under cyclic loading
- Broad frequency range (2 Hz to > 30 KHZ)
- High spatial resolution (20 Mil dia.)



BACKGROUND

SPATE 9000 System



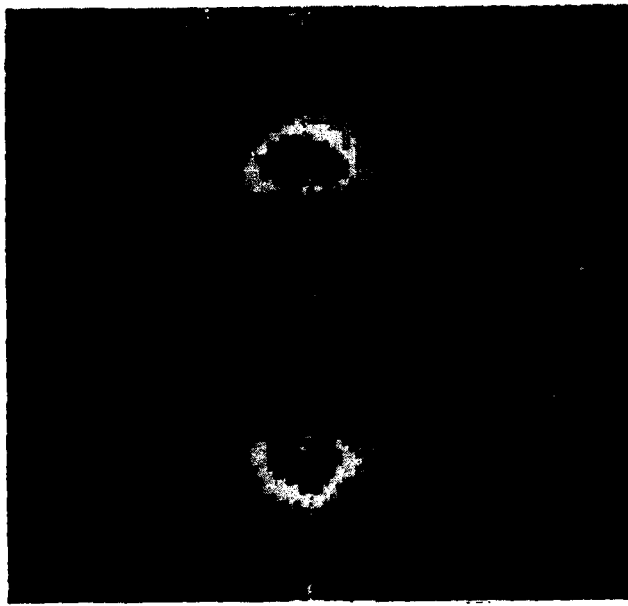
System detects instantaneous infra-red flux emitted from each point as a result of minute temp. fluctuations of a structure subjected to dynamic stress changes.



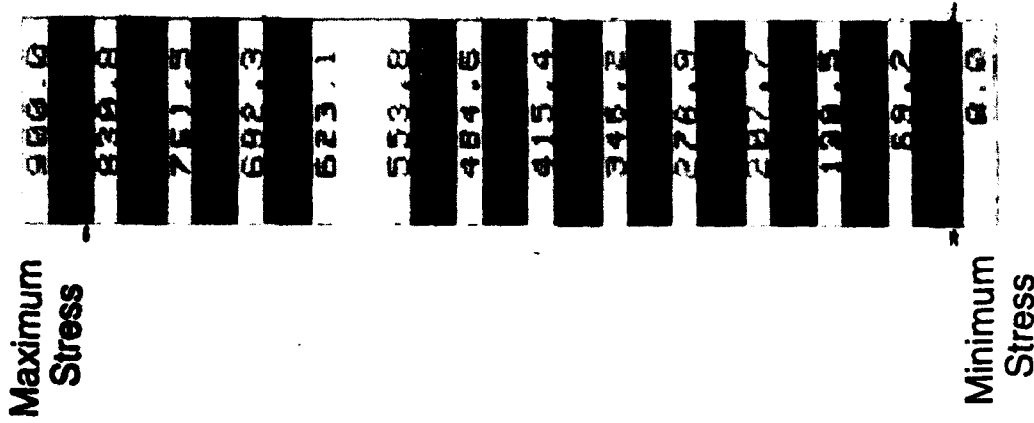
MATERIALS ENGINEERING

BACKGROUND

Typical TSA Patterns



Thermoelastic Emission
Scan of Specimen
with Stress Concentration



MATERIALS ENGINEERING

OBJECTIVE

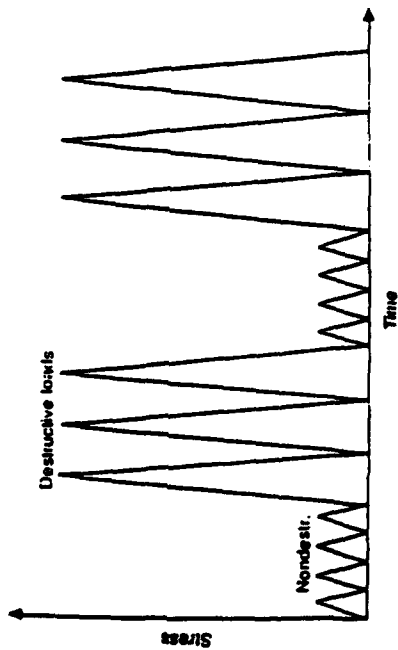
- Evaluate the capability of the Thermoelastic Stress Analysis (TSA) technique to monitor and evaluate the progression of damage in Titanium Matrix and Polymer Matrix Composites (TMC & PMC) tested at room temperature and elevated temperature.



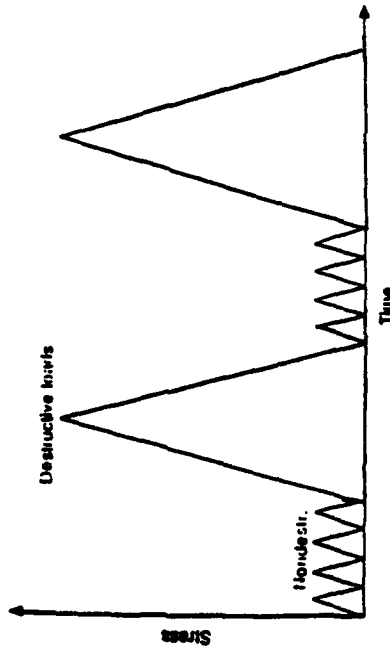
TEST APPROACH

TSA Damage Assessment Loading History For TMC Specimen And PMC Vanes

Ti Matrix Composites



Polymer Matrix Composites



1. Initially perform SPATE scan at nondestructive stress levels to establish baseline thermoelastic stress distribution and levels
2. Cycle at destructive stress level (typical at intervals \approx 10% estimated cyclic life)
3. Repeat SPATE scan at nondestructive stress levels to monitor changes in thermoelastic stress distribution and signal level

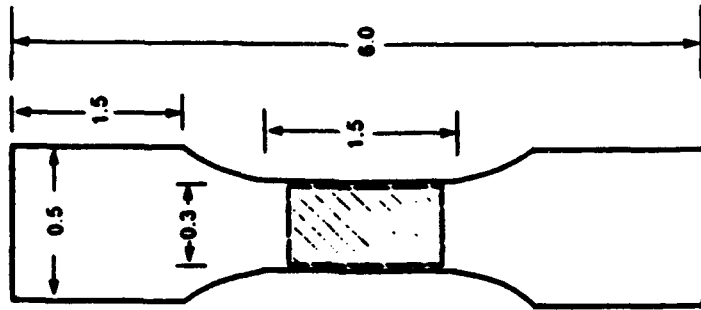


MATERIALS ENGINEERING

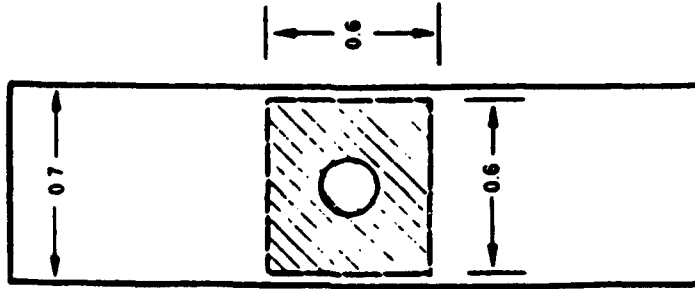
TEST APPROACH - TMC

TSA Damage Assessment Specimen Configurations

SCS₁/Ti-24-11
[0]_s



SCS₂/Beta Ti
[± 45/90/0]_s



(Area scanned for thermoelastic emissions)

MATERIALS ENGINEERING



TEST RESULTS - TMC

Fatigue Damage Observed With TSA Technique

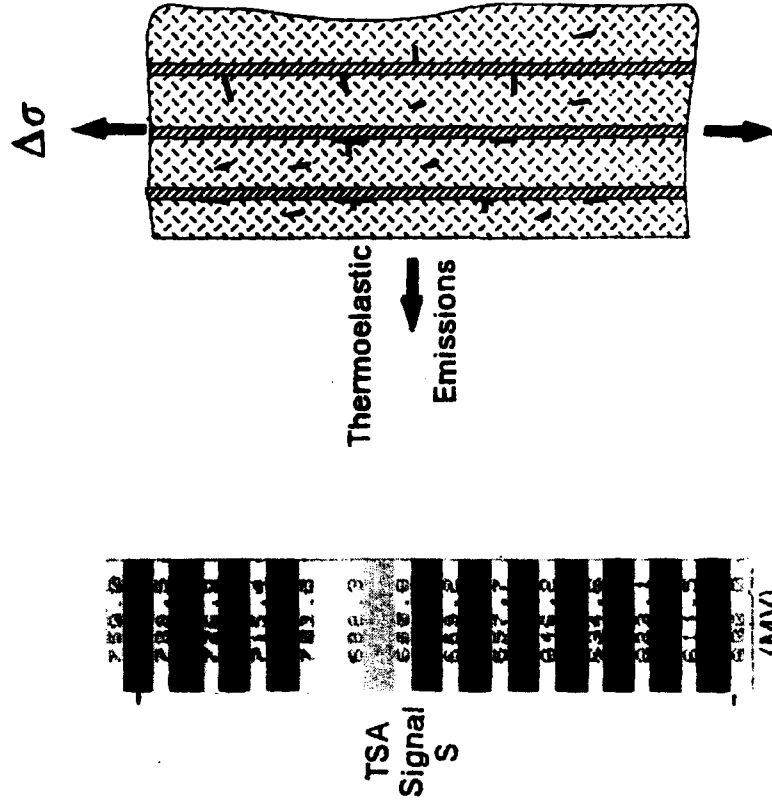
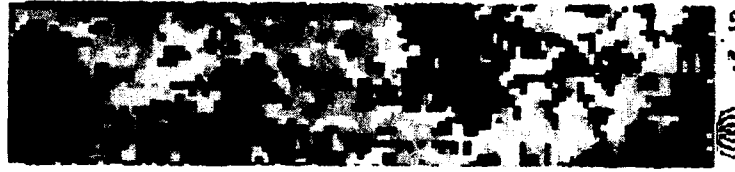
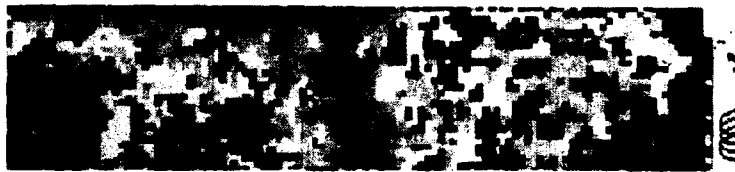
- **Dispersed damage**
 - Room temperature test - smooth SCS-6/Ti-24-11 TMC
 - Elevated temperature test - notched SCS-6/Beta Ti TMC
- **Localized damage**
 - Room temperature test - notched SCS-6/Beta Ti TMC



TEST RESULTS - TMC

TSA Scans Of Dispersed Damage Progression

- Damage state I



Smooth SCS-6/Ti-24-11 specimen - tested at room temperature

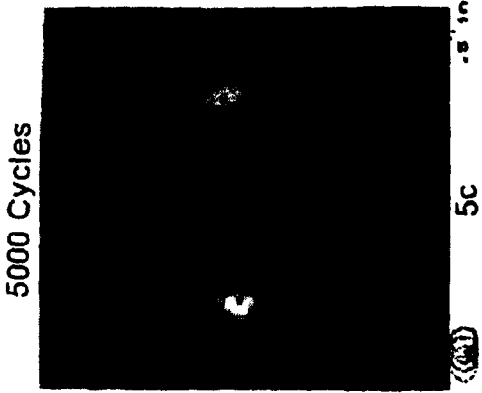
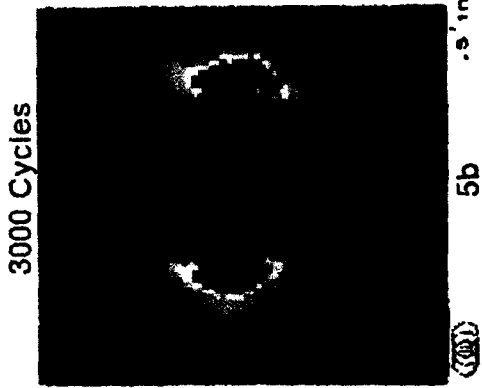
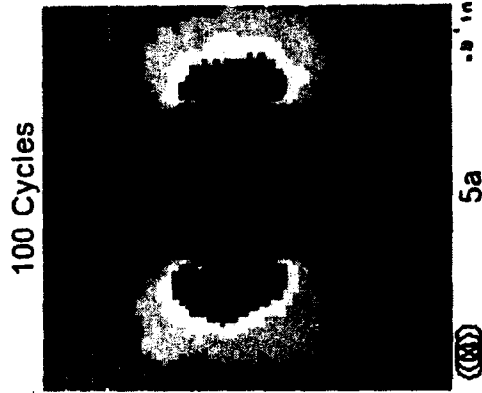


MATERIALS ENGINEERING

TEST RESULTS - TMC

Composite Damage Progression

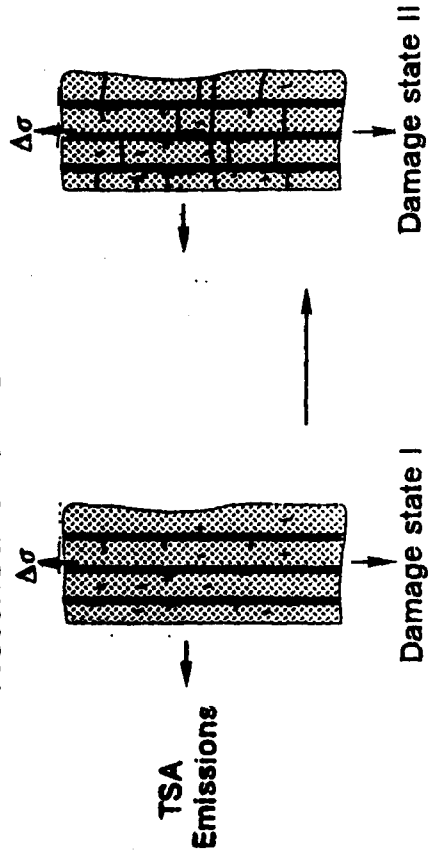
- Damage state II



TSA
Signal
S



Notched SCS-6/Beta Ti - tested at 800°F



MATERIALS ENGINEERING



TEST RESULTS - TMC

SEM Photographs Of Dispersed Damage



13X



25X

Notched SCS-6/Beta Ti - tested at 800°F

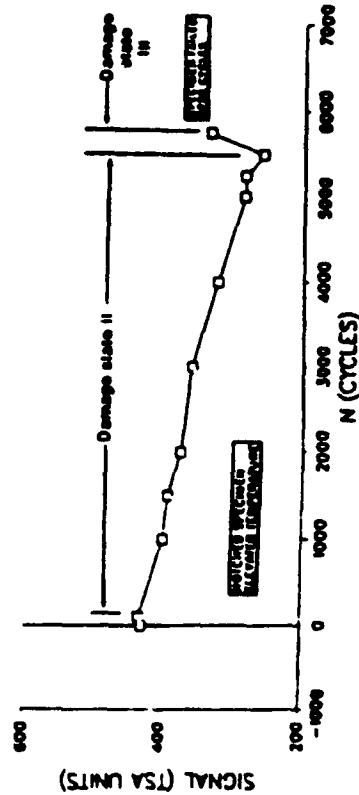
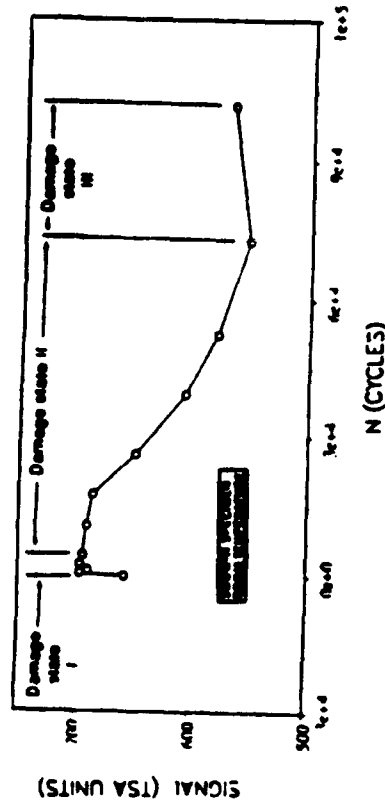
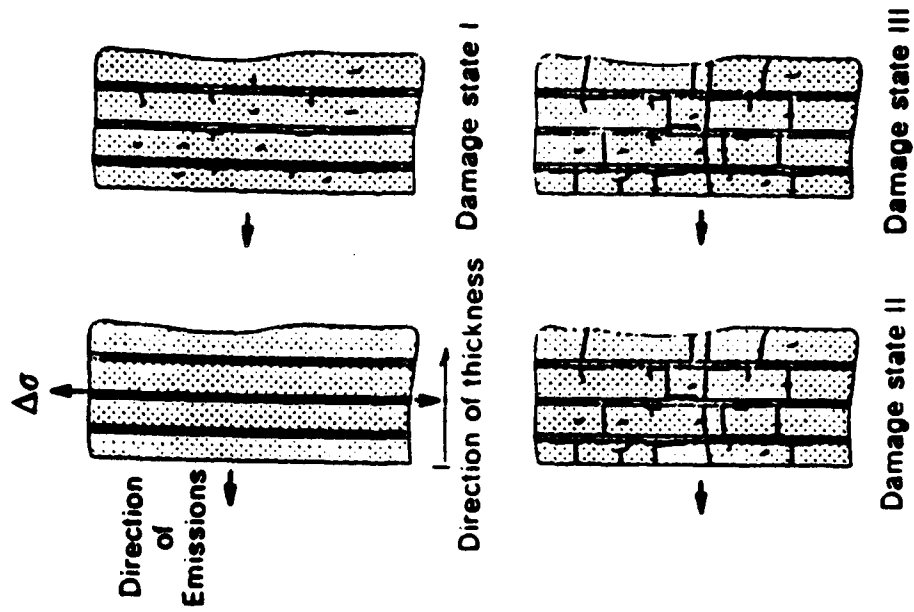


MATERIALS ENGINEERING

TEST RESULTS - TMC

TSA Fatigue Damage Assessment

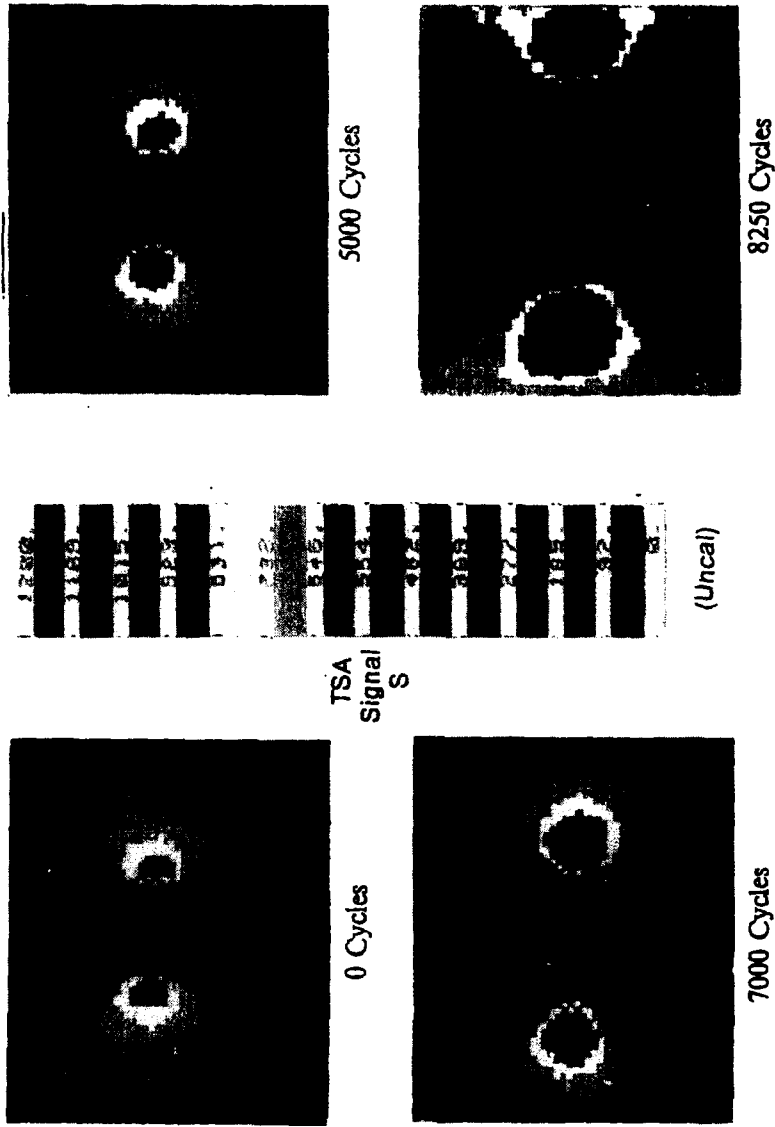
- Dispersed damage progression



MATERIALS ENGINEERING

TEST RESULTS - TMC

TSA Scans Of Localized Damage Progression



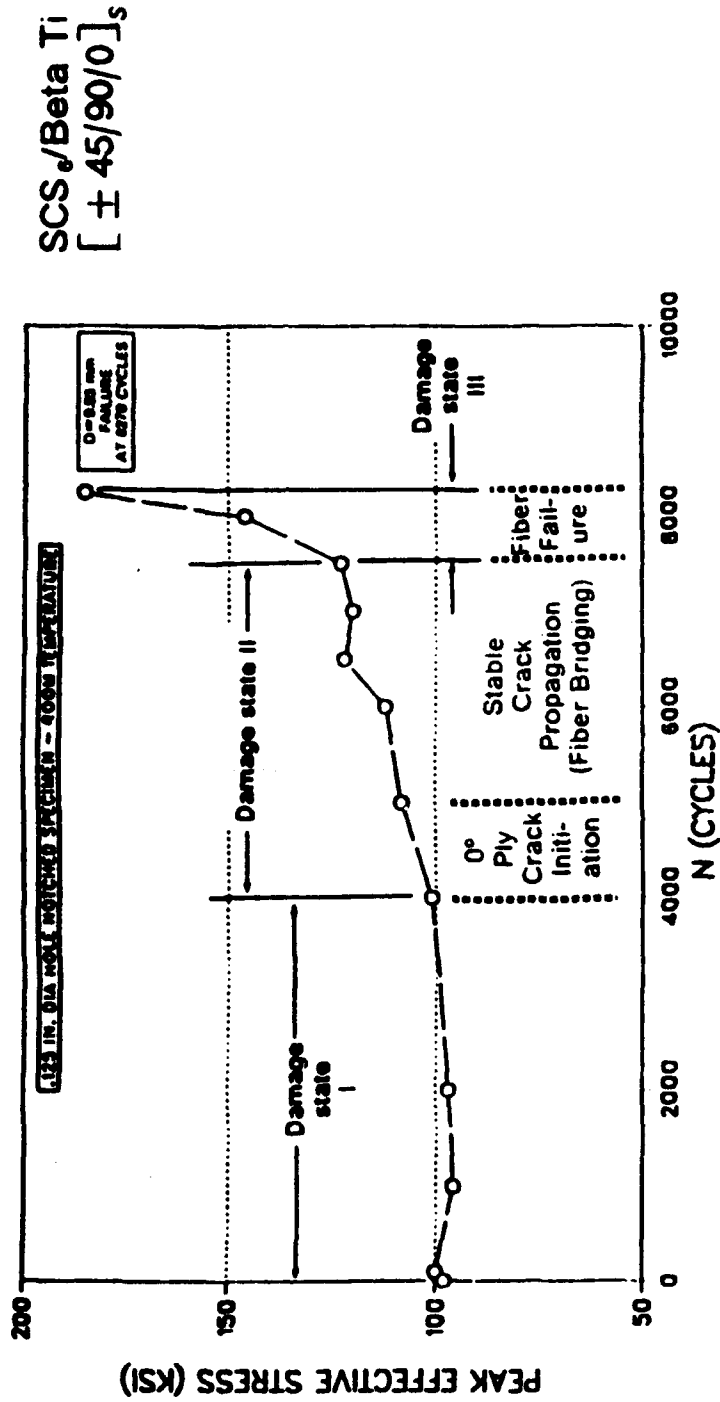
SCS-6/Beta Ti specimen - tested at room temperature

MATERIALS ENGINEERING



TEST RESULTS - TMC

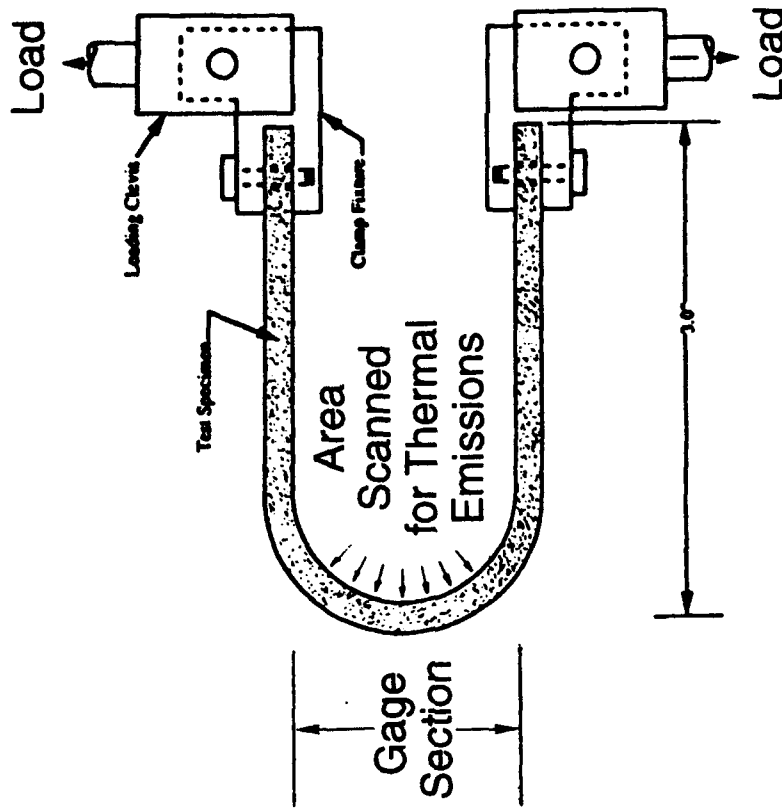
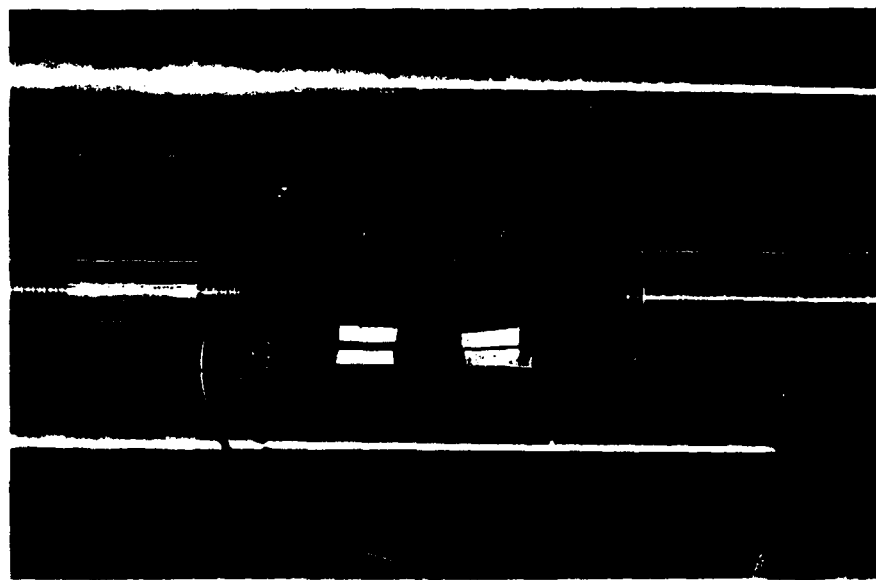
Fatigue Damage Assessment Using TSA Effective Stress Level In Vicinity Of Local Damage



MATERIALS ENGINEERING

TEST APPROACH - PMC

PMC Specimen Delamination In ID Radius Monitored With TSA Scans



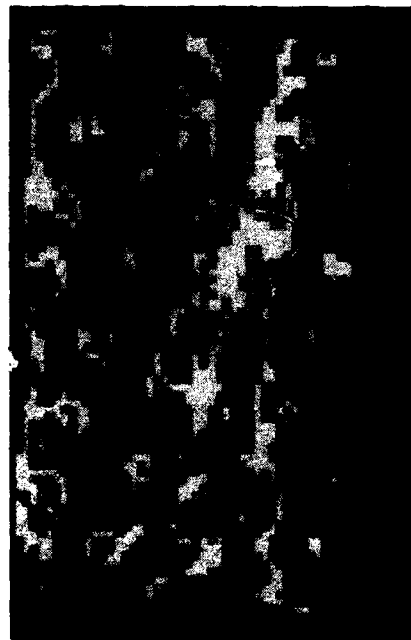
Specimen Test Arrangement

MATERIALS ENGINEERING

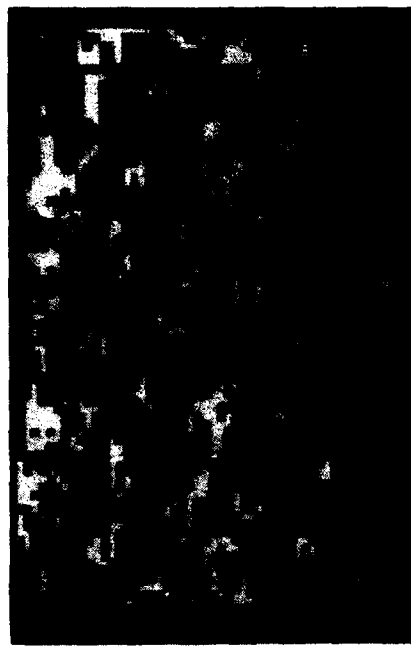


TEST RESULTS - PMC

Thermoelastic Emissions Used To Monitor Extent Of Delamination In Specimen C-Section



Baseline



After 100 Lbs Monotonic Load

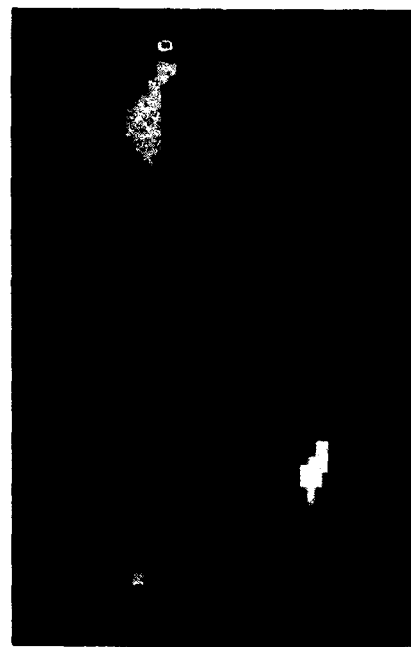


Bonded

Delaminated



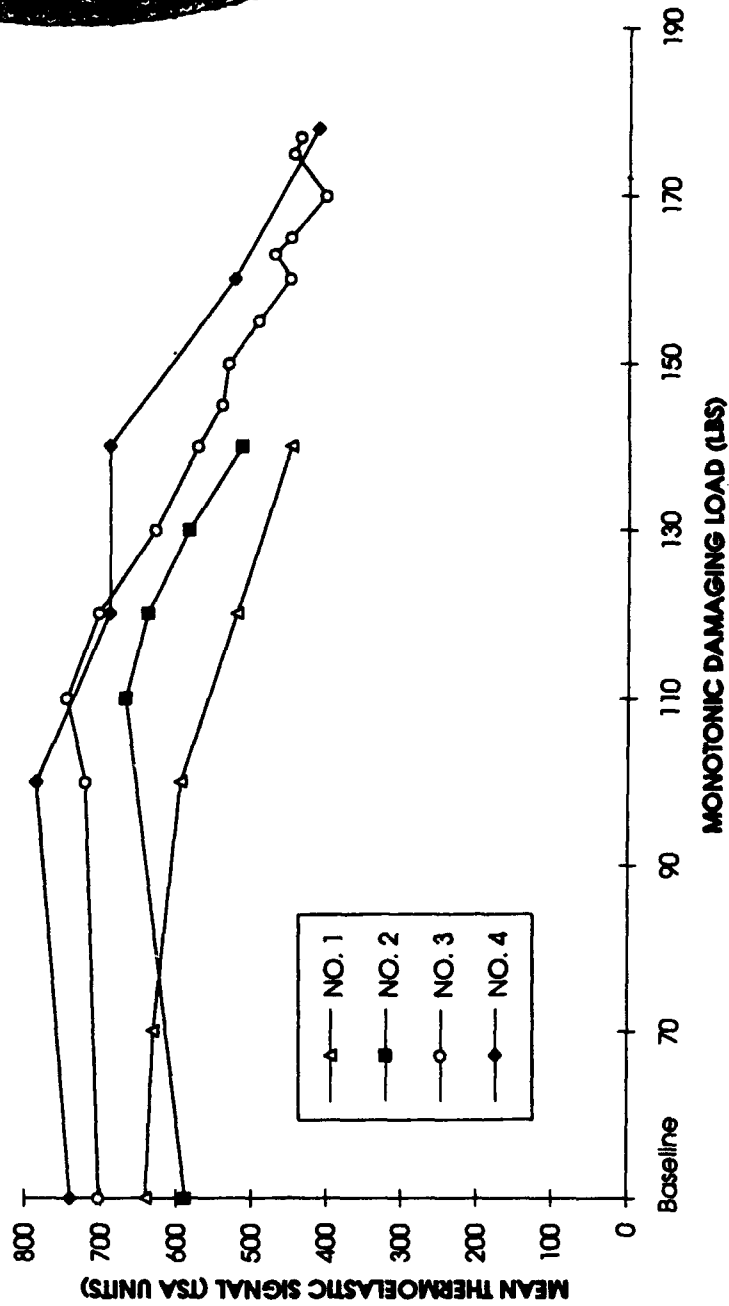
After 160 Lbs Monotonic Load



After 170 Lbs Monotonic Load

TEST RESULTS - PMC

Damage Assessment In Specimen Using Thermoelastic Signal Levels



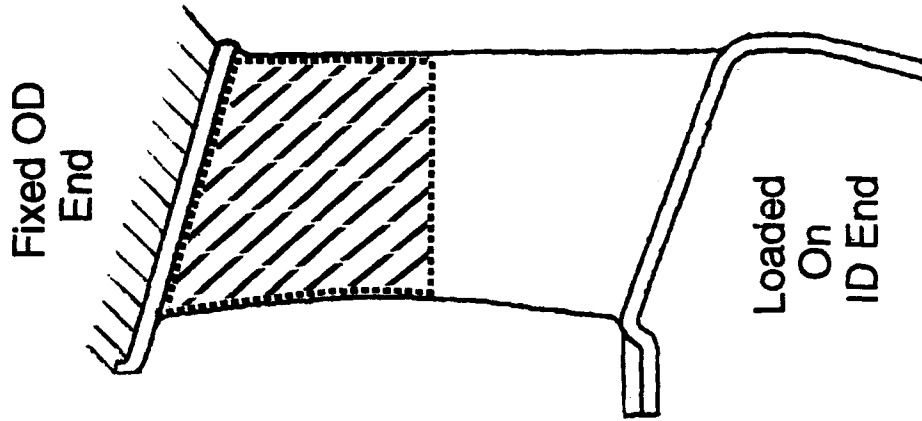
MATERIALS ENGINEERING

TEST APPROACH - PMC

Polymer Matrix Composite Stator Airfoil



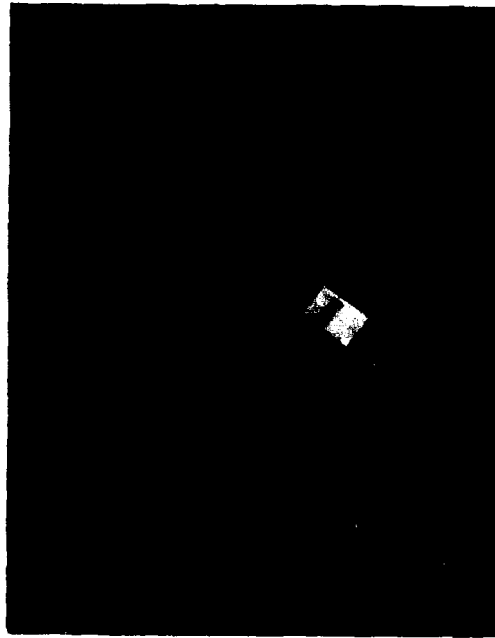
Stator Vane Test Arrangement



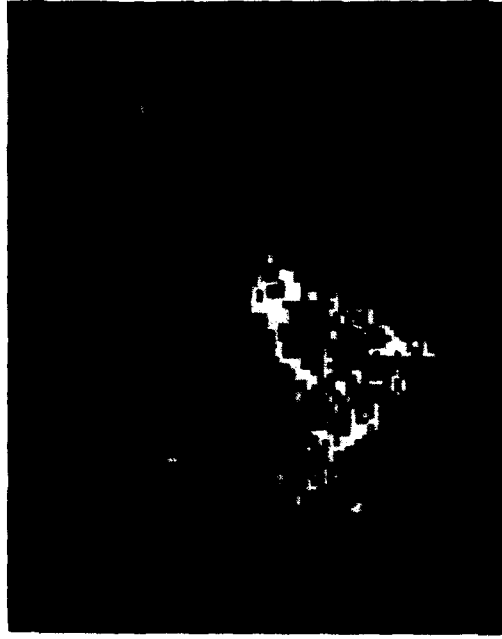
MATERIALS ENGINEERING

TEST RESULTS - PMC

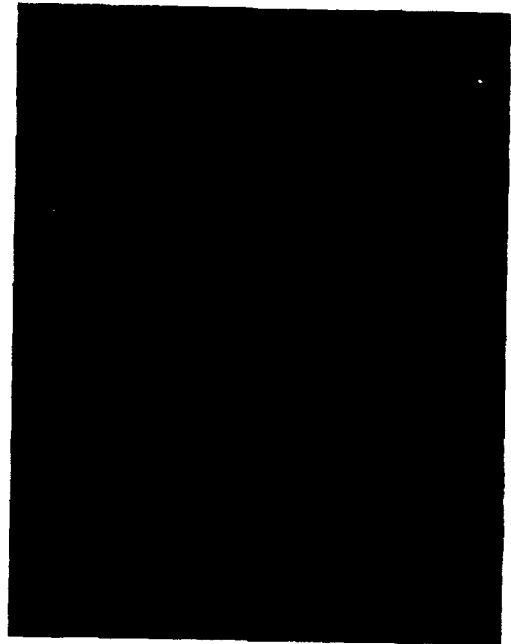
Thermoelastic Emissions Of Composite Stator Vane Monitor Extent Of Damage In Airfoil



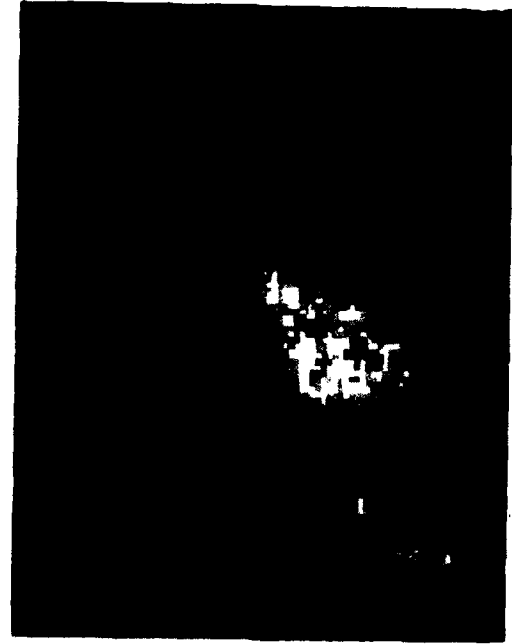
Baseline Scan - No Damage



TSA Scan After 35 Lb Load



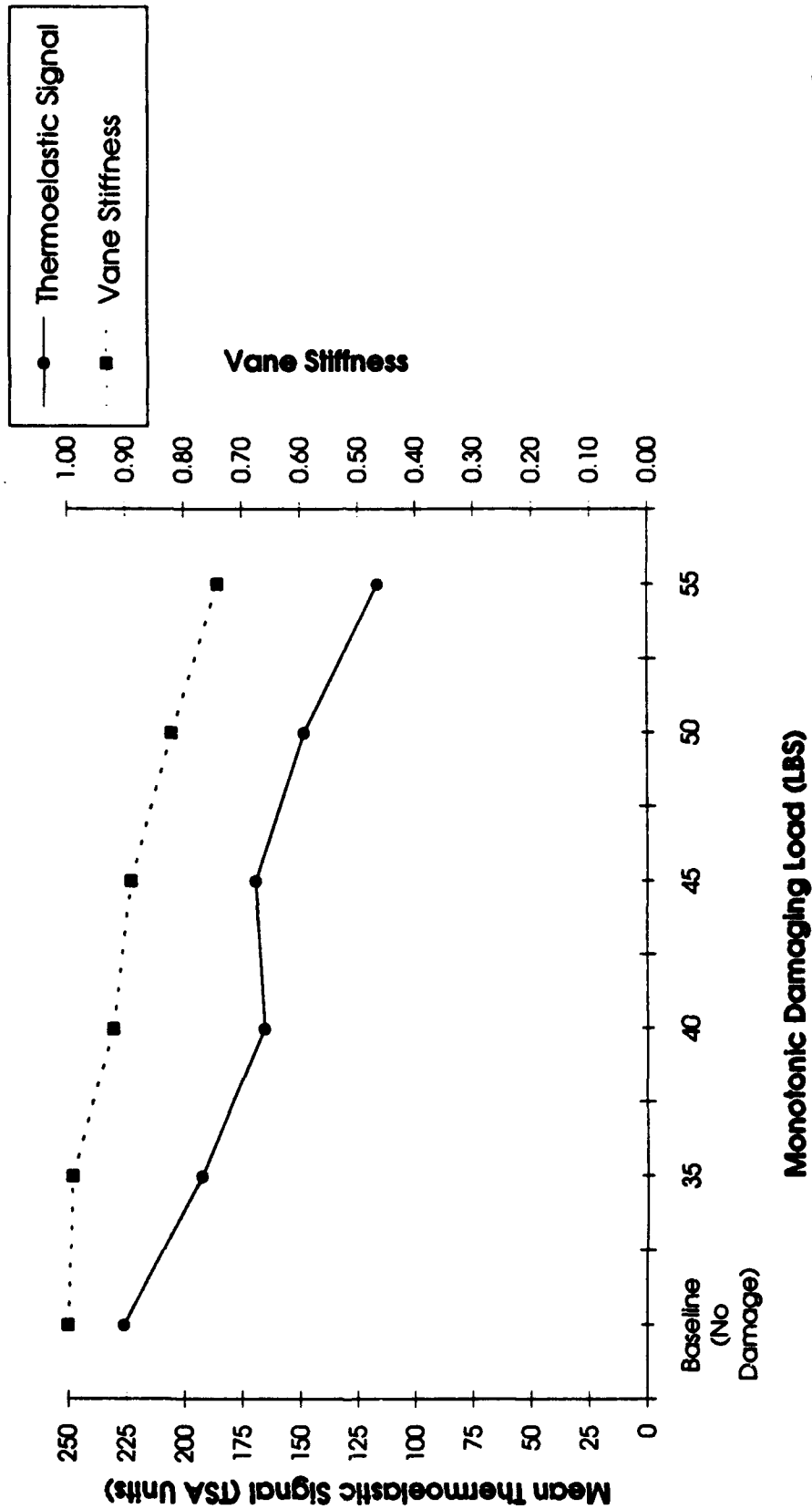
TSA Scan After 50 Lb Load



TSA Scan After 53 Lb Load

TEST RESULTS - PMC

Comparison Of TSA Emissions To Stator Vane Stiffness Loss



MATERIALS ENGINEERING

SUMMARY

Fatigue Damage Assessment In Composites Using TSA Technique

- Demonstrated capability to evaluate damage in TMC and PMC materials and components with either dispersed or localized damage progression
- Dispersed damage monitored primarily thru stiffness changes resulting from matrix micro cracking or ply delamination
- Localized damage monitored thru changes in stress intensity accompanying the progression of local cracking thru the ply's of the composite material
- Vane damage/stiffness changes directly related to thermoelastic signal
 - Technique shows potential for monitoring integrity of composite structures



The Influence of NDE in Assessing Aging Aircraft



1993 USAF Structural Integrity
Conference ... San Antonio, TX.
30 November - 2 December

Charles G. Annis, Jr., P.E.
Phone (407) 796-6565
FAX (407) 796-7454

Engines and Airframes are different ...

vis-à-vis NDE requirements.

	Engines	Airframes
cracks	small (0.005 in.)	large (0.100 in.)
crack number	one	many
accessibility	difficult	very difficult
materials (ECI)	Titaniums (difficult)	Aluminums (easier)
coatings (FPI)	easy	hard (painted surfaces)
corrosion	little	lots
cleaning	baked-on contaminants	enormous areas

Commercial Aviation Trails Military Aviation

... in field life management.

- Applied Fracture Mechanics used for two decades.
- Quantitative NDE applied since late 1970s.
- RFC implemented (cryo proof spin) in late 1985.

Retirement-for-Cause Methods ...

can be applied to the aging civil fleet.

- F/M recognizes the limitations of s-N
- Quantitative NDE measures $POD(a)$
- Probabilistics Life Analysis quantifies
Appropriate Risk.

Retirement-for-Cause ...

RFC is *not* a panacea.

- **Real risk accrues with age.**
- **NDE cannot undo the ravages of time.**

Definition of "Appropriate Risk" ...

- It won't happen to me.

"Appropriate Risk"

reconsidered:

- Risk is appropriate if the expected number^(*) of failures is less than one.

(*) number in operational lifetime

"Appropriate Risk"

... is *not* probability of failure:

- Probability of failure of 1 in 100 *may* be acceptable if you're only buying one.
- Probability of failure of 1 in 10,000 *may not* be acceptable if you're buying a million.

"Probability of Failure" (for an Engine) ...

depends on ...

- probability that a ^{ENGINE}critical defect exists, and
- probability of missing it during inspection.

so that ...

$$\begin{aligned}\text{"Probability of Failure"} &= p(\text{defect}) \times p(\text{miss}) \\ &= p(\text{defect}) \times (1 - POD)\end{aligned}$$

"Risk ..."

is *not* a probability:

- Risk is the expected number of failures:

$$\text{Risk} = p(\text{failure}) \times \text{Number}(\text{opportunities})$$

- Risk is appropriate if the expected number^(*) of failures is less than one.

(*) number in operational lifetime

"Probability of Failure" (for an Airframe) ...

depends on

- probability that a critical aggregate of defects^(*) exists, and
- probability of missing it during inspection.

so that ...

$$\text{"Probability of Failure"} = p(\text{aggregate}) \times p(\text{miss})$$

(*) also called "multiple-site damage."

Probability of Miss (POM)

depends on ...

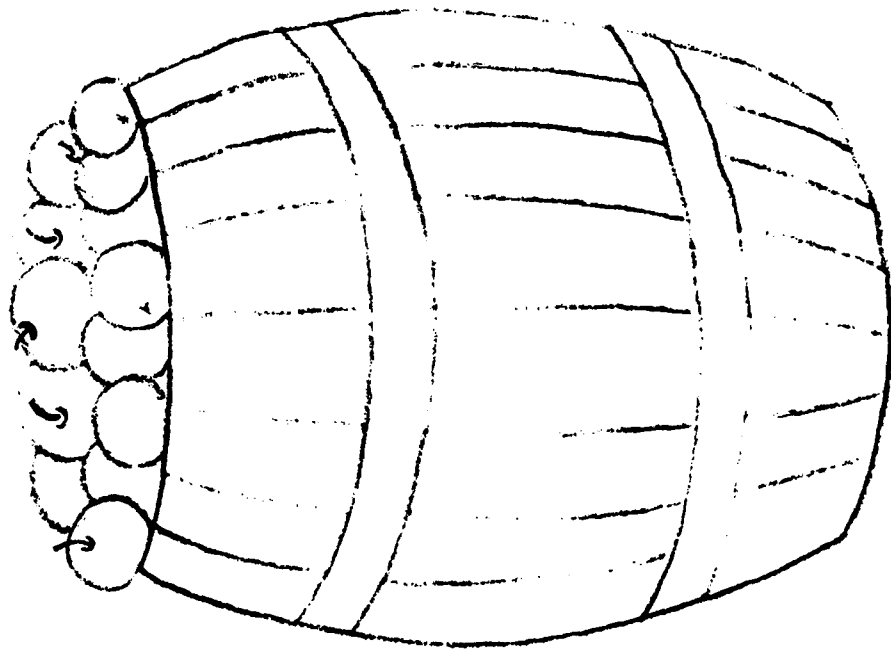
- POD : $POM = 1 - POD$, and
- correlation among inspections.

For uncorrelated inspections:

$$POM(n \text{ sites}) = \prod_{i=1}^n (1 - POD_i)$$

Small Samples Lie!

... more often than not.



What fraction
are red (green)
apples?

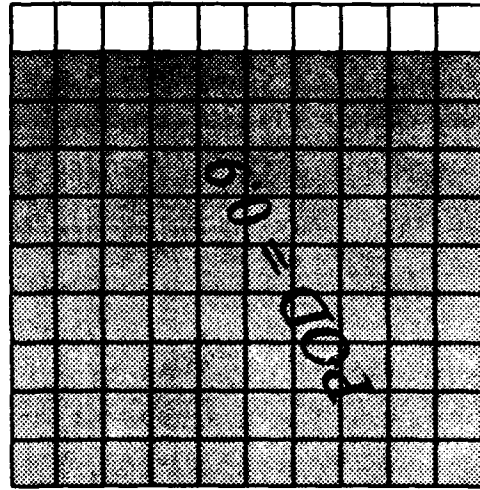
Repeat Inspections are NOT Uncorrelated

∴ but inspections of neighbors *may* be.

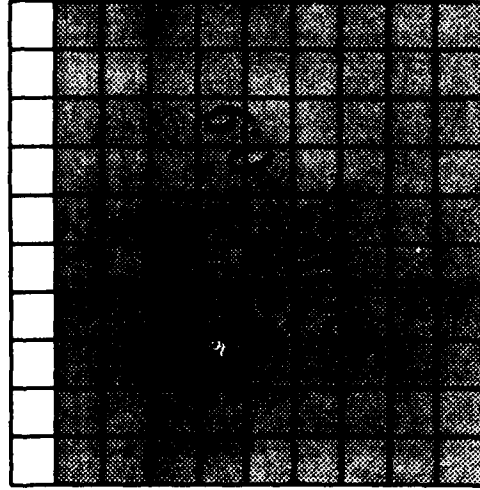
- For *uncorrelated* (eg: adjacent) inspections:

$$POD_{1 \text{ OR } 2} = POD_1 + POD_2 - POD_1 \cap POD_2$$

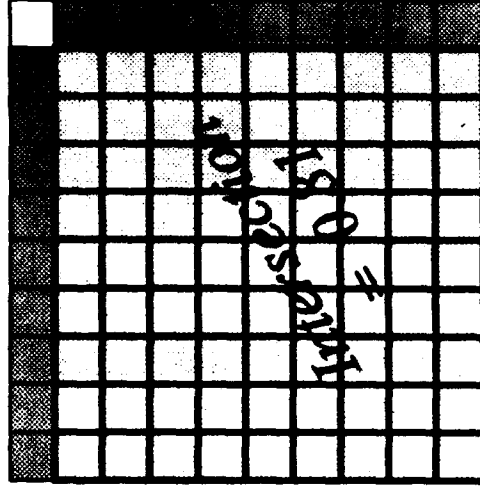
$$POD_{1 \text{ OR } 2} = 0.99$$



+



=

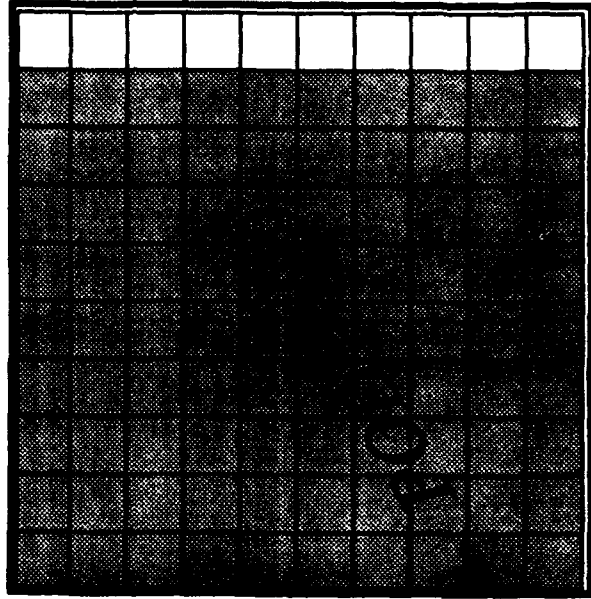


$$\text{Result: } POD_{1 \text{ OR } 2} = 1 - (1 - POD_1)^2 = 0.99$$

Repeat Inspections are NOT Uncorrelated

.. but inspections of neighbors *may* be.

- For 100% correlated (eg: repeat) inspections:
 $POD_{1 \text{ OR } 2} = POD_1 + POD_2 - POD_1 \cap POD_2$



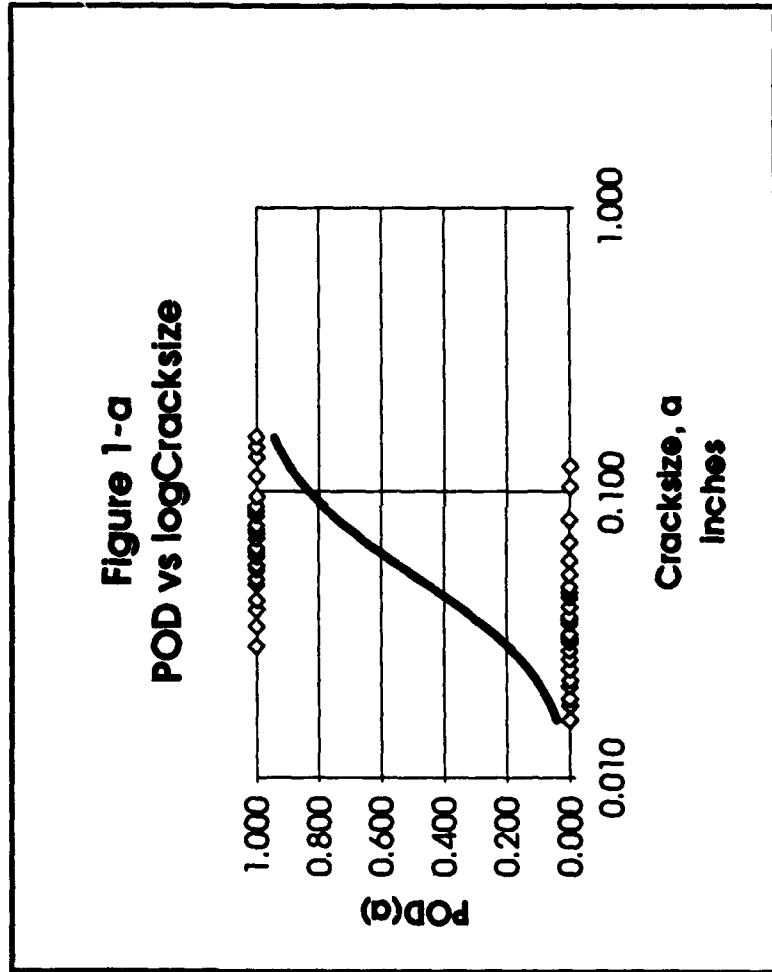
Result: $POD_n = POD_i$

Some Reasons to Reconsider Single-Point a_{90/95}

1. Is 90% POD good enough?
Would you submit to a blood transfusion if you were very confident that the test to determine the presence of HIV was at least 90% effective? (I wouldn't.)
2. Cracks nominally the same size often exhibit large differences in detectability.
"Unfair" specimens are often excluded because they're hard to find.
3. It is a practical impossibility to make cracked specimens where variations in cracksize can be ignored.
4. It's just as easy to do it right:
Model the entire *POD vs a* curve.

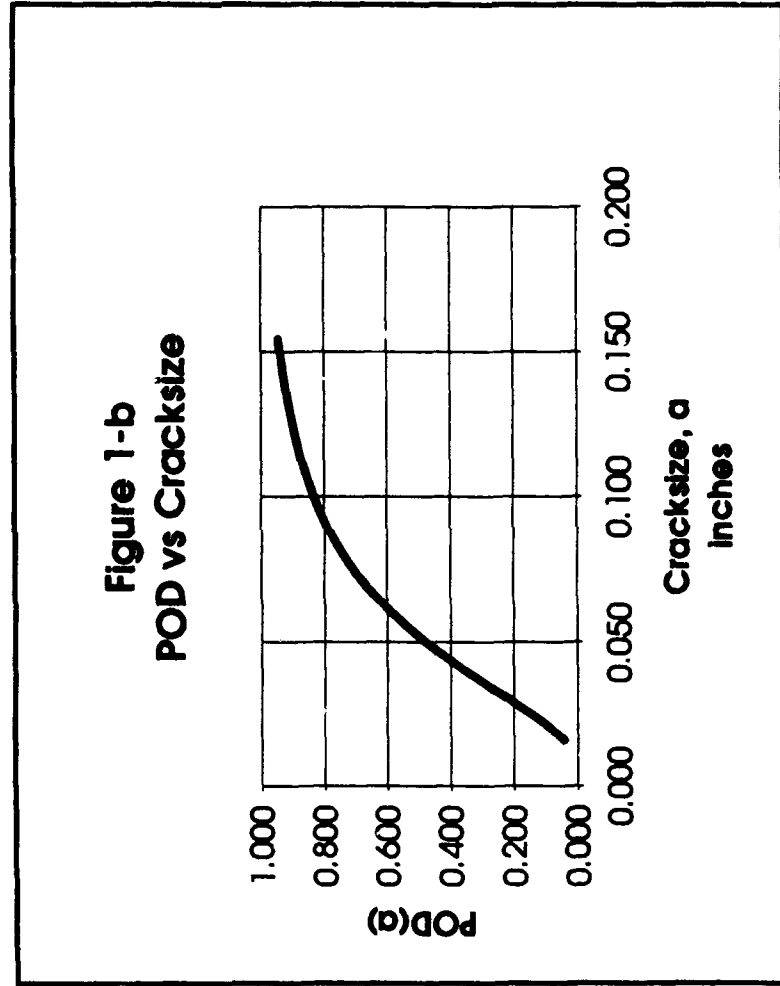
Hit / Miss Data

can be analyzed on a P/C spreadsheet



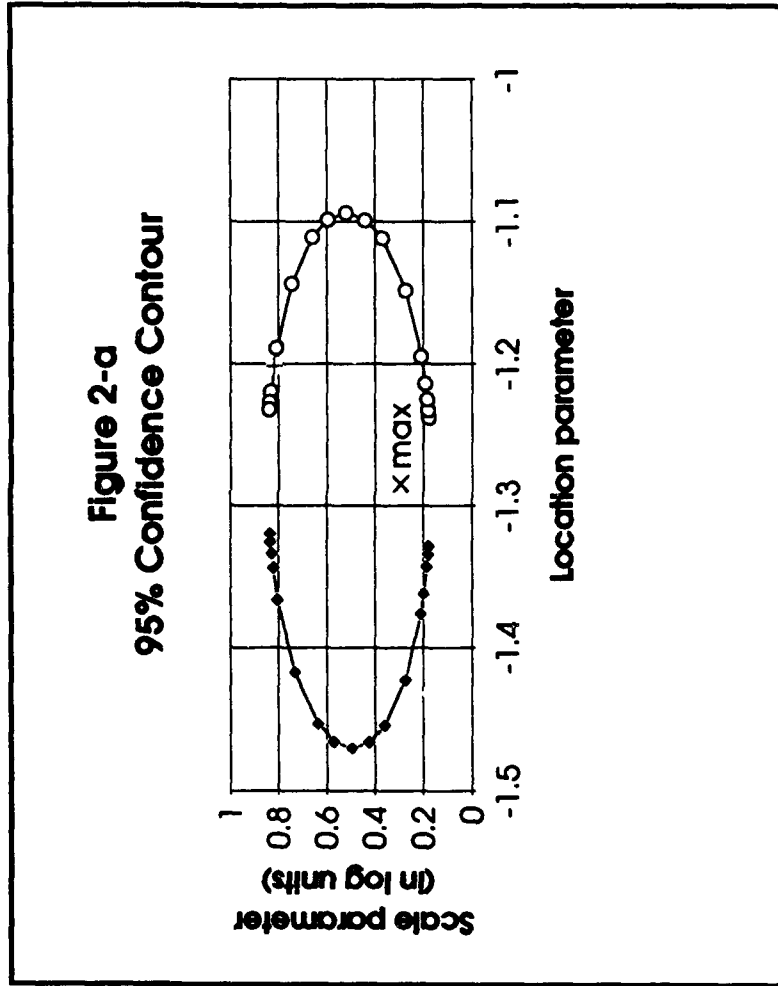
Hit / Miss Data

can be analyzed on a P/C spreadsheet



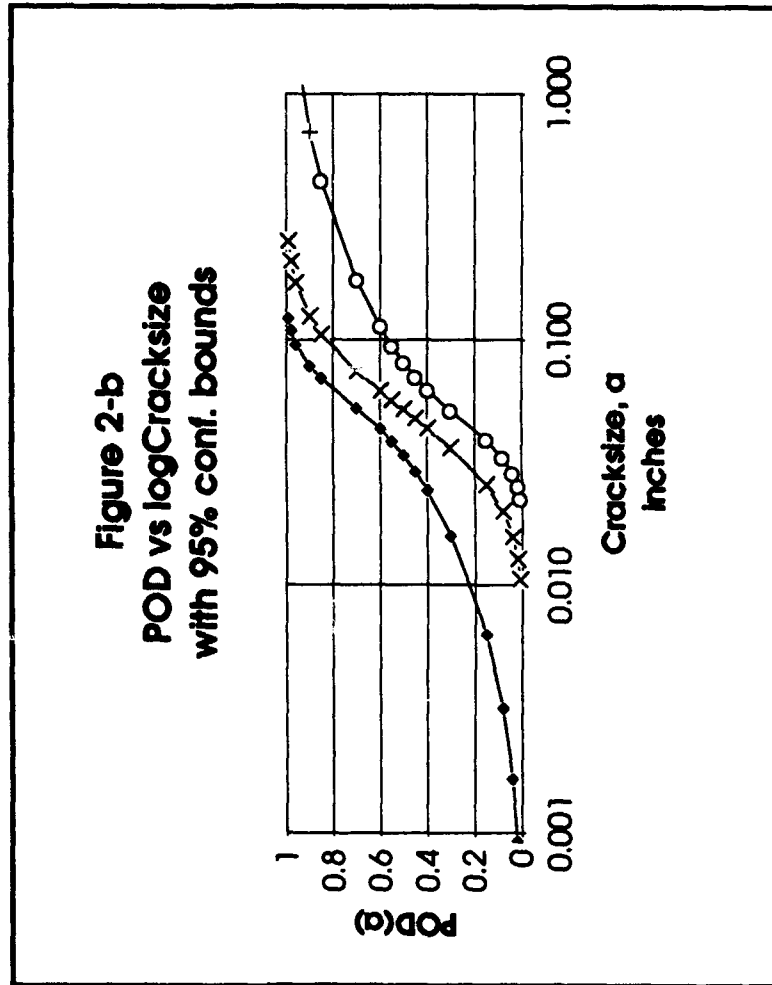
Confidence Region

contains "likely" combinations of Parameter Values



Confidence Bounds for POD

are determined from the Parameter Confidence Region



Generalized Linear Models on a P/C Spreadsheet

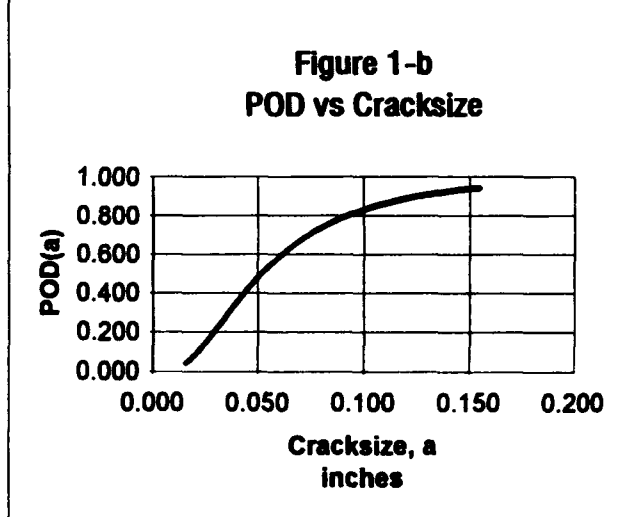
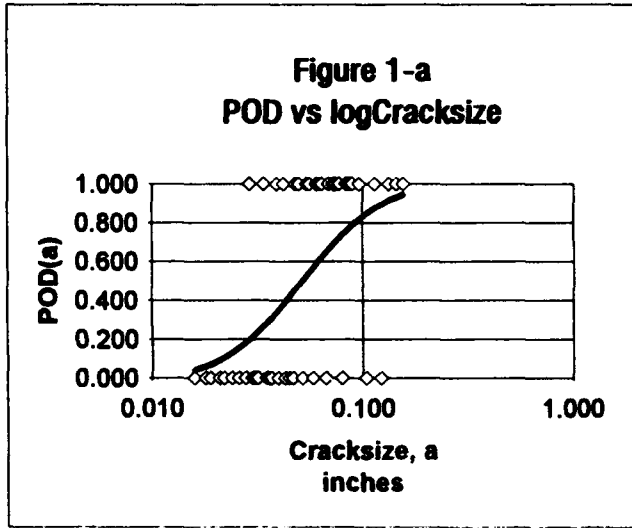
(EXCEL)

Page 1: Model Parameter Estimation, Evaluation, and Plotting

a	y	x=log(a)	(x-Loc)/S	LINK	lnlikelihood	Interim Results				
						Ones	location	scale	LAMBDA	
1	0.016	0	-1.79588	-1.723303	0.042	-0.0433427	23	-1.284589859	0.296691941	0
2	0.018	0	-1.74473	-1.550894	0.060	-0.0623687				
3	0.019	0	-1.72125	-1.471751	0.071	-0.0731560				
4	0.021	0	-1.67778	-1.325249	0.093	-0.0971105				
5	0.022	0	-1.65758	-1.257154	0.104	-0.1102045				
6	0.024	0	-1.61979	-1.129788	0.129	-0.1384382				
7	0.026	0	-1.58503	-1.012622	0.156	-0.1691531				
8	0.028	0	-1.55284	-0.904144	0.183	-0.2020667				
9	0.029	1	-1.5376	-0.852777	0.197	-1.6251031				
10	0.030	0	-1.52288	-0.803153	0.211	-0.2369170				
11	0.031	0	-1.50864	-0.755155	0.225	-0.2549927				
12	0.032	0	-1.49485	-0.708682	0.239	-0.2734648				
13	0.034	1	-1.46852	-0.619940	0.268	-1.3180805				
14	0.035	0	-1.45593	-0.577508	0.282	-0.3310044				
15	0.036	0	-1.4437	-0.536272	0.296	-0.3508139				
16	0.037	0	-1.4318	-0.496166	0.310	-0.3709024				
17	0.039	1	-1.40894	-0.419107	0.338	-1.0859848				
18	0.040	0	-1.39794	-0.382047	0.351	-0.4326515				
19	0.042	1	-1.37675	-0.310628	0.378	-0.9727506				
20	0.043	0	-1.36653	-0.276184	0.391	-0.4962709				
21	0.045	0	-1.34679	-0.209637	0.417	-0.5395261				
22	0.047	0	-1.3279	-0.145984	0.442	-0.5833371				
23	0.048	1	-1.31876	-0.115166	0.454	-0.7893132				
24	0.050	1	-1.30103	-0.055411	0.478	-0.7383428				
25	0.052	0	-1.284	0.001999	0.501	-0.6947437				
26	0.054	1	-1.26761	0.057243	0.523	-0.6485097				
27	0.056	1	-1.25181	0.110478	0.544	-0.6088339				
28	0.058	0	-1.23657	0.161844	0.564	-0.8307686				
29	0.060	1	-1.22185	0.211469	0.584	-0.5383009				
30	0.062	1	-1.20761	0.259466	0.602	-0.5068964				
31	0.064	1	-1.19382	0.305940	0.620	-0.4777542				
32	0.067	0	-1.17393	0.372995	0.645	-1.0368324				
33	0.069	1	-1.16115	0.416051	0.661	-0.4135271				
34	0.072	1	-1.14267	0.478349	0.684	-0.3800910				
35	0.074	1	-1.13077	0.518456	0.698	-0.3596368				
36	0.077	1	-1.11351	0.576627	0.718	-0.3314190				
37	0.080	0	-1.09691	0.632575	0.736	-1.3336806				
38	0.083	1	-1.08092	0.688463	0.754	-0.2826423				
39	0.086	1	-1.0655	0.738437	0.770	-0.2615263				
40	0.089	1	-1.05061	0.788629	0.785	-0.2422810				
41	0.096	1	-1.01773	0.899455	0.816	-0.2035923				
42	0.104	0	-0.98297	1.016621	0.845	-1.8664812				
43	0.113	1	-0.94692	1.138111	0.872	-0.1364352				
44	0.122	0	-0.91364	1.250286	0.894	-2.2481190				
45	0.132	1	-0.87943	1.365604	0.914	-0.0899593				
46	0.143	1	-0.84466	1.482770	0.931	-0.0715688				
47	0.155	1	-0.81103	1.596133	0.945	-0.0568133				

ln(likelihood) | -24.9157092
 ln(max likelihood) | -24.9157092
 LAMBDA | 0

critierion
 5.99



Note:
 Cell R4C3 generates a random 0 or 1 depending on the current values of the location and scale parameters (cells R5C9 and R5C10) and can be used to create a synthetic experience dataset.

Generalized Linear Models on a P/C Spreadsheet

(EXCEL)

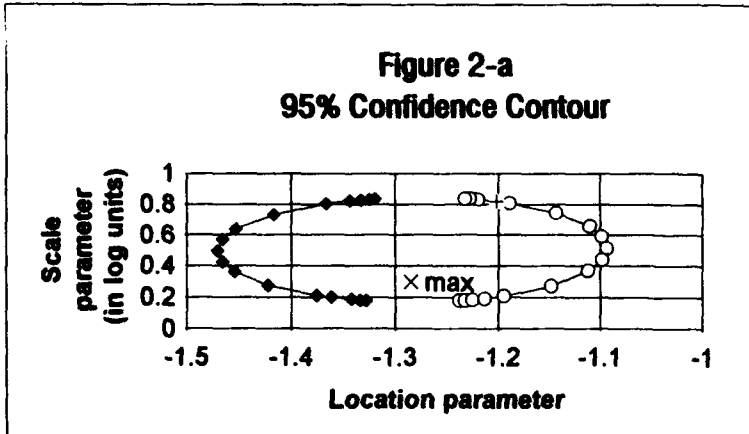
Page 2: Confidence Region Contour, left and right Confidence Limits

Model Evaluated at Max Likelihood

x=log(a)	POD	a	location	scale
-1.974797	0.01	0.011	-1.28459	0.296692
-1.893920	0.02	0.013	-1.28459	0.296692
-1.804004	0.04	0.016	-1.28459	0.296692
-1.701464	0.08	0.020	-1.28459	0.296692
-1.592091	0.15	0.026	-1.28459	0.296692
-1.440175	0.3	0.036	-1.28459	0.296692
-1.359756	0.4	0.044	-1.28459	0.296692
-1.321873	0.45	0.048	-1.28459	0.296692
-1.284590	0.5	0.052	-1.28459	0.296692
-1.247307	0.55	0.057	-1.28459	0.296692
-1.209424	0.6	0.062	-1.28459	0.296692
-1.129004	0.7	0.074	-1.28459	0.296692
-0.977089	0.85	0.105	-1.28459	0.296692
-0.904364	0.9	0.125	-1.28459	0.296692
-0.765175	0.96	0.172	-1.28459	0.296692
-0.675259	0.98	0.211	-1.28459	0.296692
-0.594383	0.99	0.254	-1.28459	0.296692

Right Confidence Contour

x=log(a)	POD	a	location	scale
-1.649406	0.01	0.022	-1.2376	0.177017
-1.600847	0.02	0.025	-1.23242	0.179395
-1.545930	0.04	0.028	-1.22502	0.183304
-1.481418	0.08	0.033	-1.21342	0.190734
-1.408602	0.15	0.039	-1.19474	0.206344
-1.290086	0.3	0.051	-1.14786	0.271225
-1.205000	0.4	0.062	-1.11173	0.368145
-1.153661	0.45	0.070	-1.09861	0.438067
-1.093719	0.5	0.081	-1.09372	0.516116
-1.024018	0.55	0.095	-1.09837	0.591685
-0.944196	0.6	0.114	-1.11041	0.656077
-0.753116	0.7	0.177	-1.14316	0.743789
-0.352964	0.85	0.444	-1.18843	0.806094
-0.153825	0.9	0.702	-1.20183	0.81776
0.232901	0.96	1.710	-1.21903	0.829351
0.484894	0.98	3.054	-1.22657	0.833335
0.712403	0.99	5.157	-1.23172	0.835698

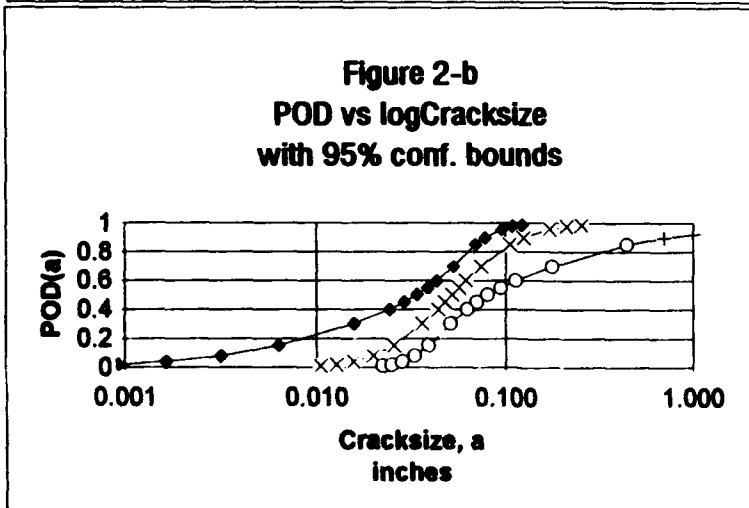


ITERATION WORKSPACE

x=log(a)	POD	row	location	scale
-1.974797	0.01	35	-1.28459	0.296692

GUESSES

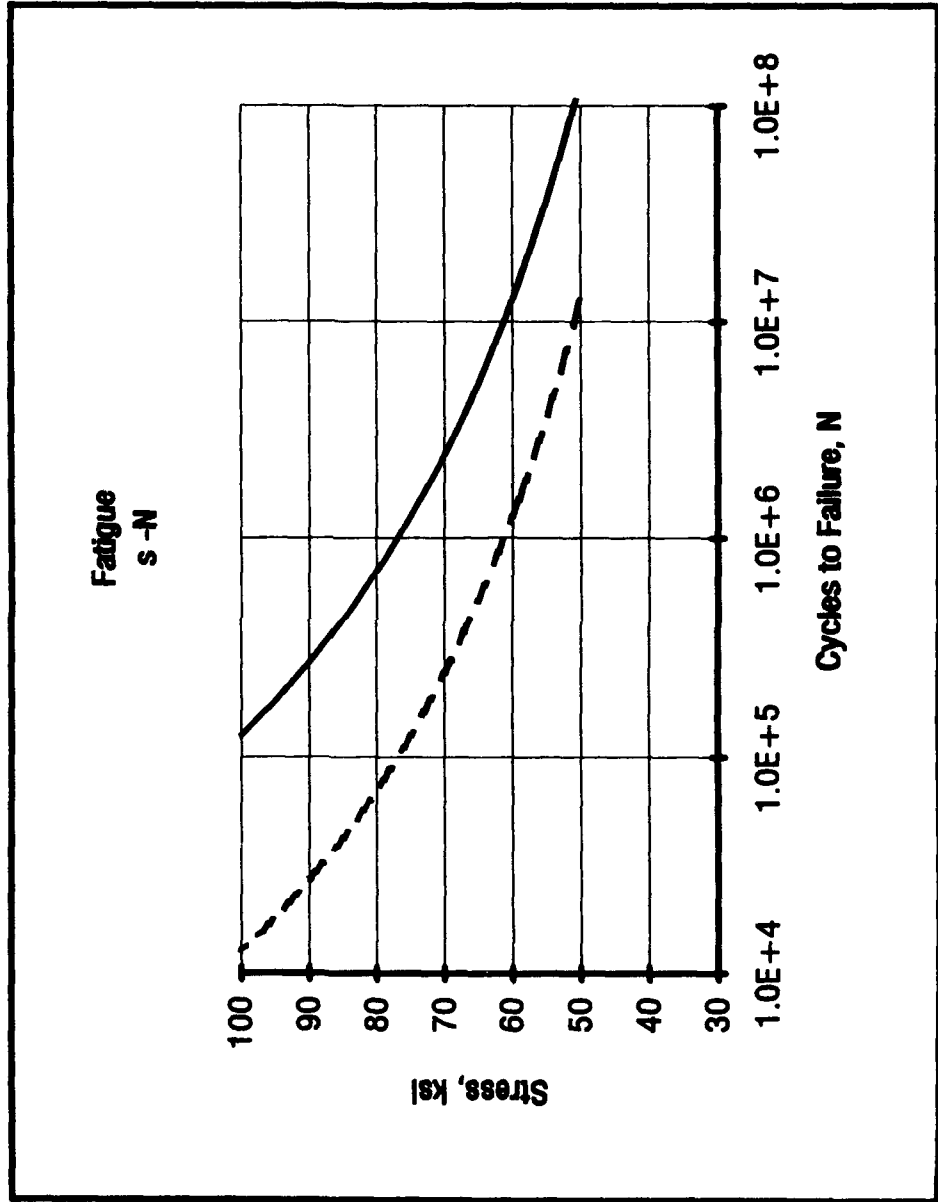
-1.32799	0.178012
----------	----------



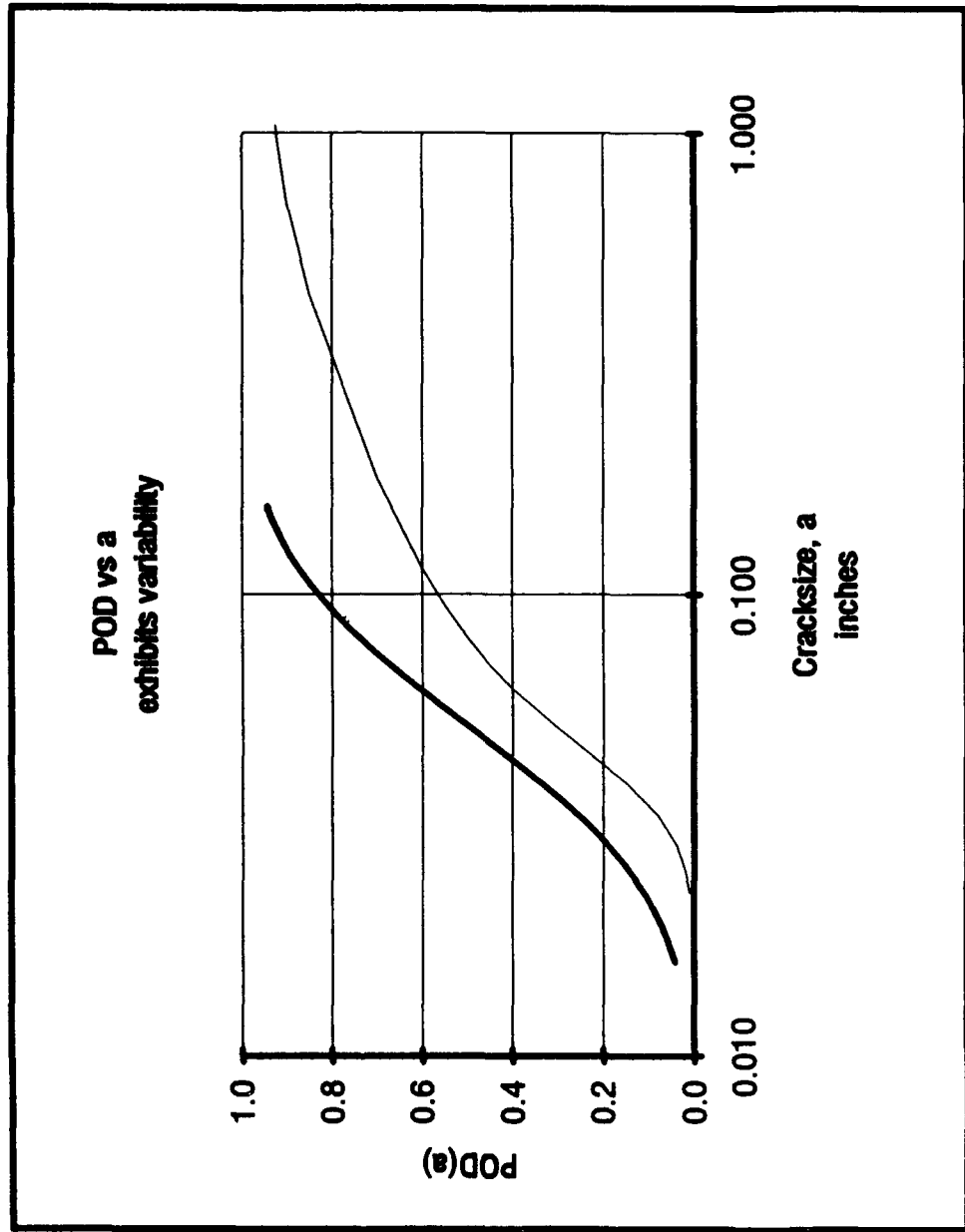
Left Confidence Contour

x=log(a)	POD	a	location	scale
-3.262656	0.01	0.001	-1.31933	0.835355
-3.035263	0.02	0.001	-1.32485	0.832827
-2.783462	0.04	0.002	-1.33299	0.828514
-2.498338	0.08	0.003	-1.34359	0.821841
-2.198724	0.15	0.006	-1.36633	0.803134
-1.801585	0.3	0.016	-1.41712	0.733155
-1.614546	0.4	0.024	-1.4533	0.636464
-1.537455	0.45	0.029	-1.46596	0.568953
-1.470588	0.5	0.034	-1.47059	0.494346
-1.413107	0.55	0.039	-1.46611	0.421789
-1.363328	0.6	0.043	-1.45453	0.359997
-1.278626	0.7	0.053	-1.42258	0.274503
-1.157641	0.85	0.070	-1.37603	0.210711
-1.107670	0.9	0.078	-1.36147	0.198045
-1.018184	0.96	0.096	-1.34232	0.185146
-0.962800	0.98	0.109	-1.33386	0.180673
-0.913940	0.99	0.122	-1.32794	0.17796

Materials Capabilities ... exhibit variability.



Materials Capabilities ... exhibit variability.



Things to Remember:

- Engines and Airframes have different problems.
- Acceptable POD depends on the consequences of a miss, and the probability of cracking.
- Repeat inspections won't help much.
(ineffective for single threat; too costly for multiple sites)
- NDE cannot undo the ravages of time:
(RFC cannot continue indefinitely.)
- Improper, optimistic estimates of POD do not impress Mother Nature.

Probabilistic Structural Analysis Methods for Engine Components

**Harry Millwater, Justin Wu, and Hal Burnside
Engineering and Materials Sciences Division
Structural Engineering Department
Southwest Research Institute**

Abstract

This paper discusses the advantages, development, and application of probabilistic structural analysis methods developed under the NASA contract "Probabilistic Structural Analysis Methods (PSAM) for Select Space Propulsion System Structural Components" funded through the NASA Lewis Research Center. The paper also describes a probabilistic structural analysis computer program NESSUS (Numerical Evaluation of Stochastic Structures Under Stress), which has been developed for probabilistic analysis of complex, time-consuming structural models. The methodology and NESSUS code are demonstrated by performing a failure analysis of a turbine blade subject to stress, creep and vibration failure modes. Future developments of the technology and code in the areas of fatigue and fracture mechanics, graphical user interface, interfaces with external analysis programs, and improved probabilistic algorithms are also discussed.

Presentation Overview

Uncertainties or variabilities typically exist in the analysis and design of structural components. The traditional approach to handle uncertainties is to use limit loads, minimum strength characteristics, extreme tolerances, etc. in order to ensure the structural integrity of structural components. A probabilistic approach, on the other hand, attempts to quantify the structural reliability and identify the important variables contributing to the failure by explicitly considering the variabilities. This information can be used to advantage in a number of areas. As examples, it can be used to indicate which failure modes and random variables to control for improved reliability, develop robust designs that are insensitive to input variations, develop designs with a consistent level of risk among components, reduce overconservatism, develop optimized risk-based inspection schedules, and perform probability-based decisions.

There are difficult issues that must be addressed; however, in adopting a probabilistic approach, such as, obtaining enough data to develop the input probability distributions, lack of confidence in the probability answers such as 10^{-6} , or 0.999999, and reluctance to quantify reliability, at least publicly, by companies. The probabilistic analysis itself can be very demanding in that it requires sophisticated computational tools which are not yet at maturity, multidisciplinary knowledge in probabilistic and deterministic methods by engineers, and can be very computationally demanding.

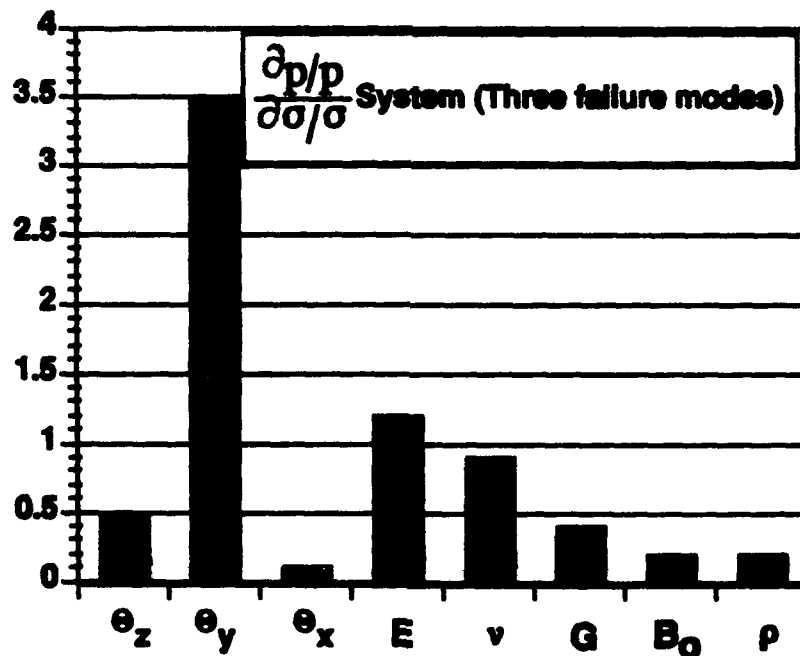
A very useful output of probabilistic analysis are the probabilistic sensitivity factors [1]. Three nondimensional probabilistic sensitivity factors are shown below.

$S_{\mu} = \frac{\partial p/p}{\partial \mu/\sigma}$ = sensitivity of probability to changes in the mean value of random variable X_i .

$S_{\sigma} = \frac{\partial p/p}{\partial \sigma/\sigma}$ = sensitivity of probability to changes in the standard deviation of random variable X_i .

$S_d = \frac{\Delta p}{p_{ref}}$ = change in probability with respect to changes in the distribution type of random variable X_i .

The probabilistic sensitivity factors indicate which random variables or parameters have the most effect on the probability. This information can be more useful than the computed probability number. For example, the graph below shows the effect each random variable has on the reliability of a turbine blade. The variation in the standard deviation of the y direction orientation of the anisotropic material (Θ_y) clearly affects the probability the most. Thus, if the standard deviation of this variable is highly uncertain due to limited data, further data collection is warranted. Modifications to reduce the standard deviation in this variable will have the greatest effect on reducing the probability of failure. These sensitivity factors can be computed during the probabilistic analysis without additional cost for some advanced probabilistic methods.



The NESSUS probabilistic structural analysis computer program has been developed to partially address the requirement for efficient, robust probabilistic algorithms. NESSUS contains finite element and boundary element methods for deterministic structural modeling integrated with advanced probabilistic methods.[2] Both component and system reliability capabilities are included. The focus of the program is on Space Shuttle Main Engine (SSME) components, however, the technology generated is general and is being applied to other analysis areas.

A significant amount of research in the PSAM program has focused on the development, implementation and application of efficient probabilistic methods.[3] The methods implemented in NESSUS are shown on the accompanying viewgraphs. The goal is to provide an accurate solution with a minimum number of calculations. The Monte Carlo method will always work but may require a very large number of computer runs. For example, for a probability of failure of 10^{-4} , Monte Carlo simulation requires 10^5 or 10^6 simulations. This is not feasible for many problems. Fast approximate methods such as the mean value first order and advanced mean value methods can be used. These methods often achieve accurate results with several orders of magnitude fewer computations than Monte Carlo simulation. However, these methods are not always guaranteed to work. The adaptive importance sampling method combines the benefits of sampling with the fast approximate methods.[4] For the adaptive importance sampling method, an approximate method is used to locate the high probability region. Then, sampling is initially performed locally only in this region. The sampling region is incrementally adjusted and new samples are obtained. The procedure continues until the probability converges within a user specified error tolerance and confidence.

NESSUS is demonstrated by computing a failure analysis of a turbine blade. The finite element model consists of 5946 degrees of freedom. Eight random variables are used; six affect all three failure modes, one affects creep only, and one affects vibration only. Failure of the blade was defined as failure due to a vibration, stress, or creep criteria. The failure modes are organized using a fault tree. The fault tree approach has the advantage in that correlation between the failure modes due to common random variables, i.e. the six common variables in this problem, can be accounted for automatically. The solution procedure was to use the advanced mean value method to compute polynomial approximations to the finite element models at high probability regions for each individual failure mode. 3.7 CPU hours on an HP 750 workstation were required for this step. The polynomial functions were then combined using the fault tree. The combined probability of failure, or system probability, was then computed using Monte Carlo sampling or adaptive importance sampling on the approximate functions. As a check, adaptive importance sampling was performed on the finite element models requiring 117 analyses and 25 CPU hours. The probability sensitivity factors for each individual failure mode and when all failure modes are combined are shown in the accompanying viewgraphs. The complete solution details for this problem can be found in reference [5].

The NESSUS program is still under development. Future developments will incorporate structural integrity models related to fatigue and fracture. Simple fatigue and fracture problems can already be solved with NESSUS; however, the infrastructure will be improved for more complicated problems.

Technology improvements in efficient probabilistic methods will continue to be explored. Improved robustness of the approximate methods and new probabilistic sensitivity measures are required.

External interfaces will be developed between NESSUS and other analysis programs, both small scale, e.g. user-developed codes, and large scale, e.g. ABAQUS, ANSYS, NASTRAN nonlinear finite element codes.

Graphical user interfaces for model development and output interpretation will be developed; both PC/Macintosh and X windows workstation versions. A scaled-down version of the NESSUS probabilistic module currently exists on a PC and Macintosh. This code will be used for education and training.

In summary, there are significant advantages to use probabilistic analysis methods. In particular, probabilistic sensitivity factors can be very effective in determining important variables affecting the structural reliability. The use of probabilistic sensitivity factors partially addresses the difficulties in obtaining input data and the lack of confidence in the absolute probability results.

Computational tools to perform probabilistic structural analysis have been developed and continue to be developed. The NESSUS computer code attempts to address the computational demands of probabilistic analysis by providing the engineer with an integrated probabilistic structural analysis tool with efficient algorithms. The NESSUS code was demonstrated by computed the reliability of a turbine blade subject to vibration, creep, and stress failure modes. Future enhancements to NESSUS will focus on fatigue and fracture, improved robust algorithms, interfaces to other deterministic codes, and a user-friendly graphical user interface.

References

- [1] Madsen, H. O., Krenk S. and N. C. Lind, Methods of Structural Safety, 1986, Prentice Hall, Inc., Englewood Cliffs, NJ.
- [2] Millwater, H. R., Wu, Y.-T., Tomg, Y., Thacker, B., Riha, D. and C. Leung, "Recent Developments of the NESSUS Probabilistic Structural analysis computer program," 33rd SDM conference, April 13-15, 1993, Dallas, TX, AIAA-92-2411.
- [3] Wu, Y.-T., H. R. Millwater, and T. A. Cruse, "Advanced Probabilistic Structural Analysis Method for Implicit Performance Functions," AIAA Journal, Vol. 28, No. 9, September 1990.
- [4] Wu, Y.-T., "An Adaptive Importance Sampling Method for Structural System Reliability Analysis," AD-Vol. 28, Reliability Technology, ASME 1992.
- [5] Millwater, H., and Y.-T. Wu, "Computational Structural Reliability Analysis of a Turbine Blade," International Gas Turbine and Aeroengine Congress and Exposition, Cincinnati, OH, May 24-27, 1993.



Probabilistic Structural Analysis Methods for Engine Components

**Harry Millwater, Justin Wu, and Hal Burnside
Engineering and Materials Sciences Division
Structural Engineering Department
Southwest Research Institute**

**1993 USAF Structural Integrity Program Conference
30 November - 2 December 1993
San Antonio, TX**



Overview of Presentation

Topics

- 1) Motivation for Probabilistic Methods
- 2) Development of NESSUS Probabilistic
Structural Analysis Computer Program
- 3) Application of NESSUS to Failure Analysis of
Turbine Blade
- 4) Future Developments
- 5) Summary and Conclusions



Motivation for Probabilistic Analysis

Advantages

- **Quantify reliability**
- **Identify important variables and failure modes**
- **Robust design - insensitive to input variations**
- **Reduce overconservatism**
- **Consistent level of risk among components**
- **Optimized inspection schedule**
- **Probability-based decision analysis**



Motivation for Probabilistic Analysis Methods

Difficult Issues

- **Data, data, data, ...**
- **Disbelief in the reality of probability numbers, e.g. 10^{-6} , 0.999999**
- **Reluctance to quantify reliability, at least publically -> lawsuits**
- **Multidisciplinary knowledge requirements**
- **Tools and Experience need maturing**
- **Computationally demanding**

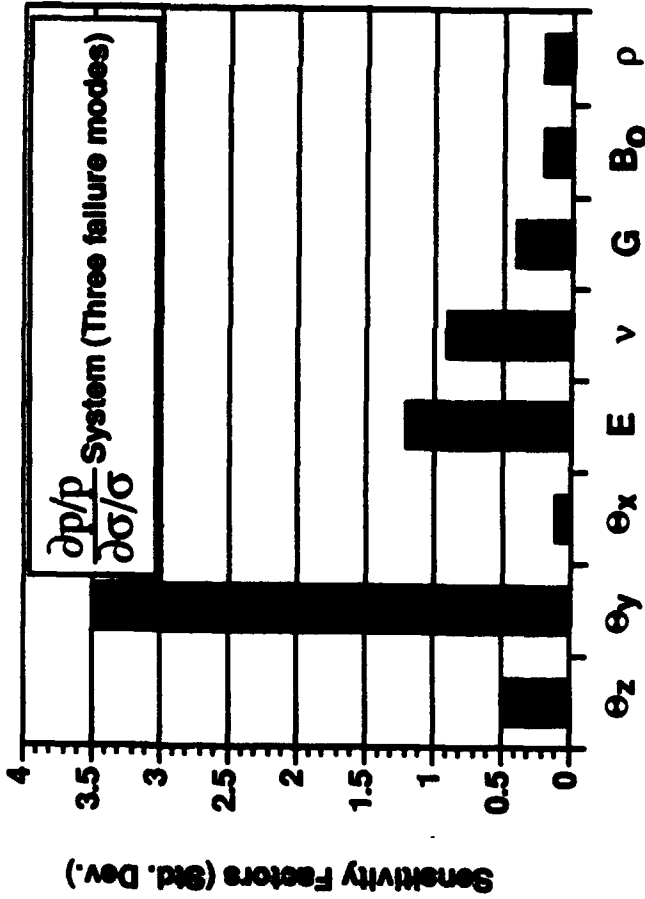


Probabilistic Sensitivity Factors

$$\frac{\partial p/p}{\partial \mu/\sigma}, \frac{\partial p/p}{\partial \sigma/\sigma}, \frac{\Delta p}{p}$$

Mean
Standard Deviation
Distribution Type

- Indicate sensitivity of probability to changes in input parameters, i.e. identify important variables



- Computed as by-product (no extra cost) for some methods
- Can be computed for system and component probability
- Can be used for "what-if" scenarios without reanalysis



Probabilistic Structural Analysis Methods (PSAM) Program

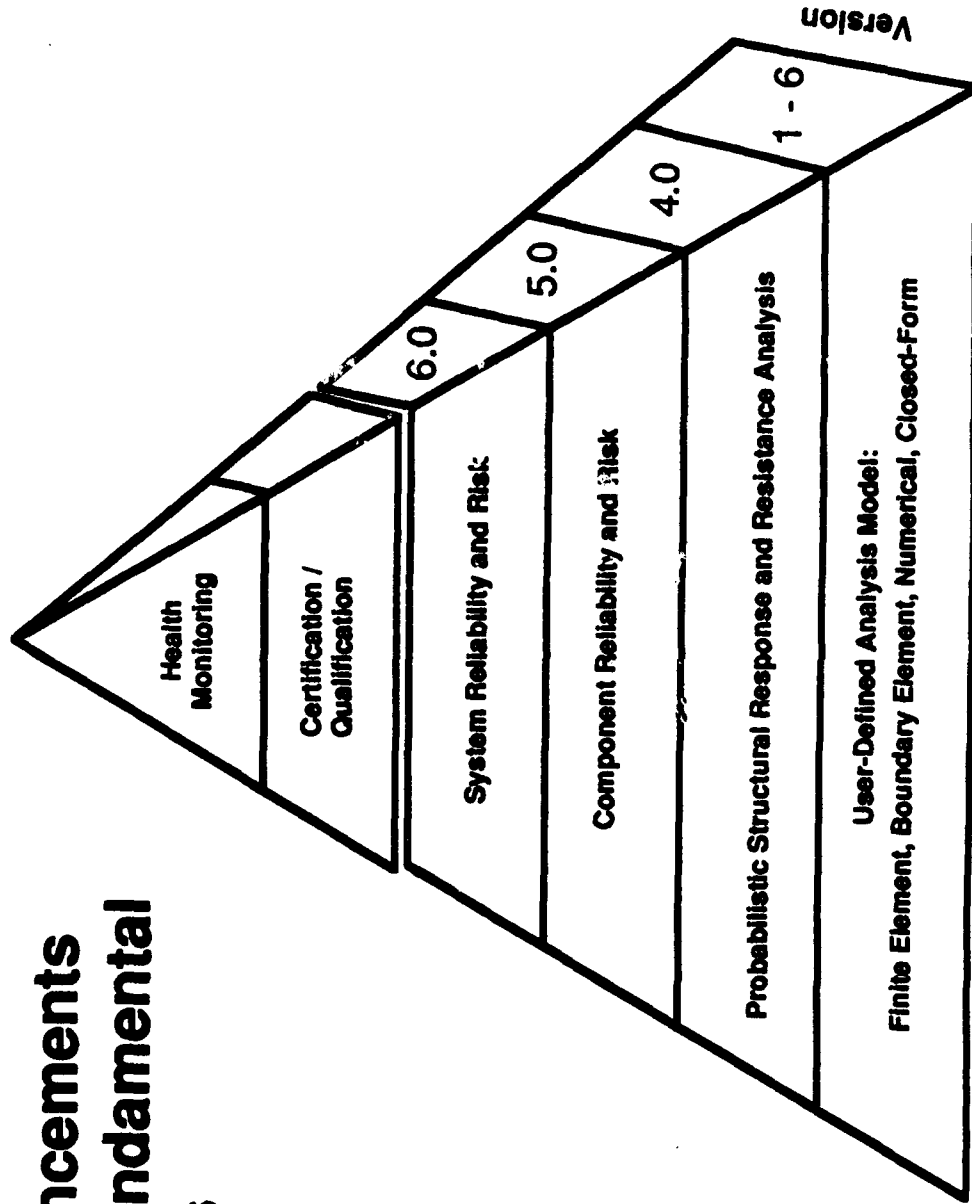
- **Ten-Year Research and Development Program**
 - **Phase 1: Probabilistic Structural Response Analyses of the Space Shuttle Main Engine Components (1984-1989)**
 - **Phase 2: Structural System Risk Assessment, Qualification, Certification, and Health Monitoring (1990-)**
- **Simulate Uncertainty/Variability in Loads, Material Properties, Geometries**
- **Computer Code NESSUS Integrates Reliability Methods with Structural Analysis Methods (FEM, BEM)**
- **PSAM Methodology and Code are General Structural Risk Assessment and Reliability Design Tools**

**Prime Contractor: Southwest Research Institute
Project Sponsor: NASA**



NESSUS Probabilistic Methodology Hierarchy

**Code Enhancements
Build on Fundamental
Capabilities**



NESSUS Probabilistic Structural Analysis Hierarchy

NESSUS Development History*

<u>Year</u>	<u>Version</u>	<u>New Capabilities</u>	<u>New Mechanics Models</u>	<u>New Probabilistic Methods</u>
1993-	7.0**	Certification Qualification Health Monitoring	Progressive Fracture	Event Tree Inspection Planning Reliability Updating
1992	6.0	System Reliability and Risk	Boundary Element	Fault Tree Adaptive Importance Samp. Latin Hypercube Sampling Probability Bounds
1991	5.0	Component Reliability and Risk	Resistance Models User-Defined Response and Resistance	Importance Sampling Fast Convolution (Second-Order)
1989	4.0	Probabilistic Structural Response	Finite Element	Advanced Mean Value (First-Order)

* NASA Contract NAS3-24389, SwRI Prime Contractor ** Under Development

Summary of NESSUS 6.0 Capability

Random Variables

Loads

- Forces
- Pressures
- Temperatures
- Vibrations (PSD)

Material properties

- Moduli
- Poisson's ratio
- Yield stress
- Hardening parameters
- Material orientation

Geometry

User-defined

Probabilistic Methods

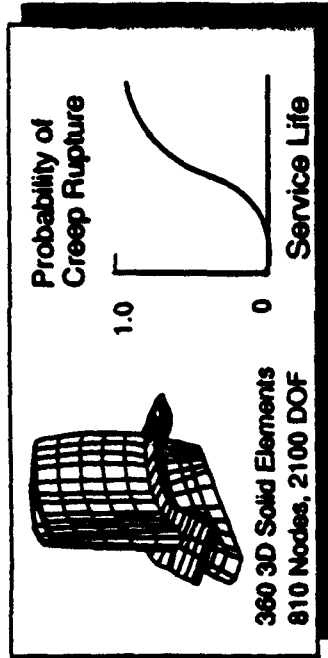
Fast Probability Analysis

- Advanced Mean-Value
- First and Second-Order
- Fast Convolution

Sampling

- Standard Monte Carlo
- Latin Hypercube
- Adaptive importance

Probabilistic Fault Tree



Analysis Types

- Static
- Transient dynamics
- Buckling
- Vibrations
- Nonlinearities
- Plasticity
- Large displacement

Probabilistic Analysis

- Full probability distribution
- Component reliability
- System/multi-failure-modes rel.
- Probabilistic sensitivities
- Probability-based risk/cost

Performance Functions

- Structural responses: stress, strain, disp., freq., etc.
- Fatigue and fracture life
- Creep rupture life
- User-defined subroutines
- External analysis programs (requires tailored interface)

Element Library

- Beam
- Plate
- Plane strain
- Plane stress
- Axisymmetric
- 3D solid
- Enhanced solids

Operating Systems

- Mainframes
- Workstations

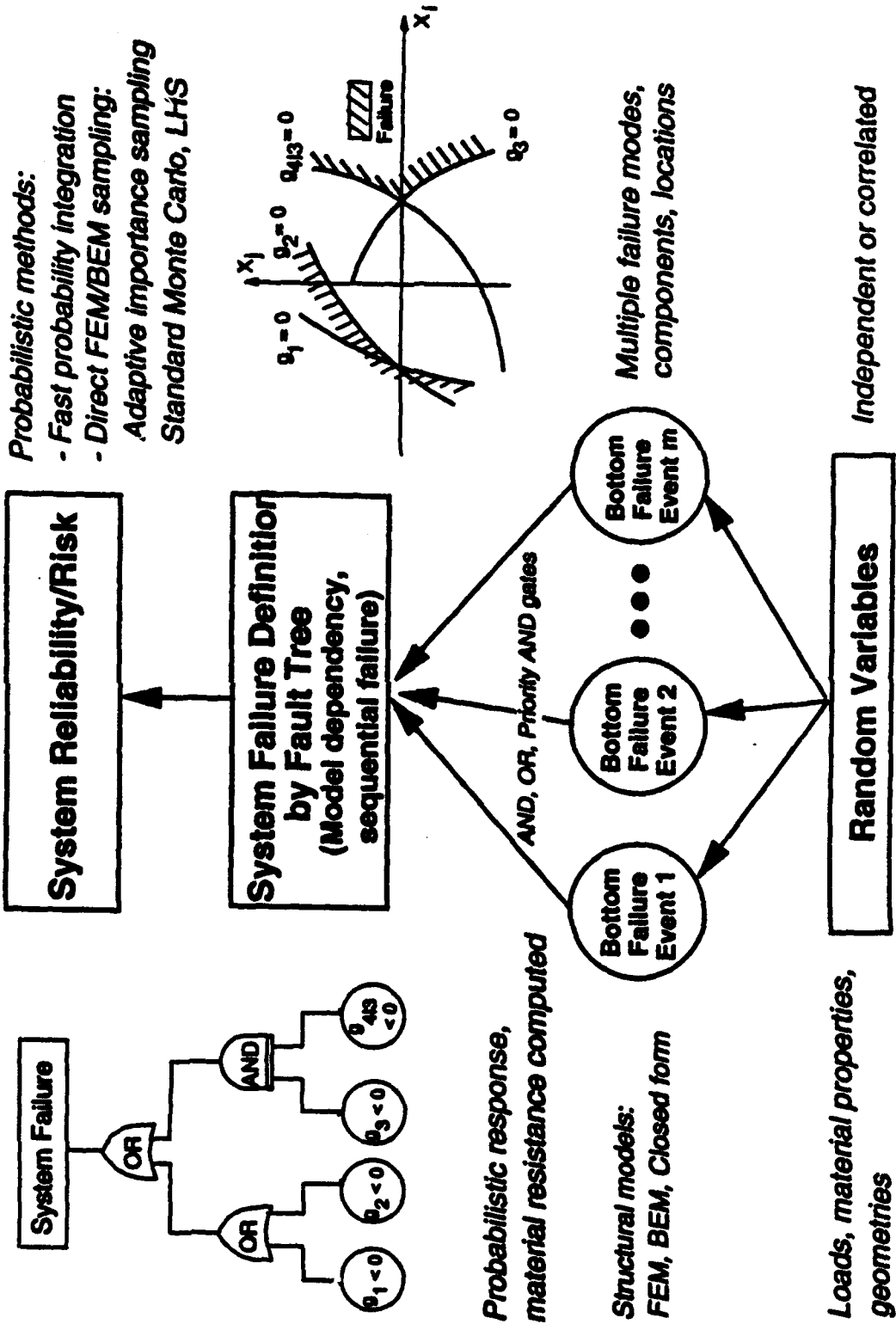
PROBABILISTIC STRUCTURAL ANALYSIS METHODS

Z = Performance Function, e.g. finite element model

Method	No. of Z-function calculations	Results	Remarks
Deterministic (Safety Factors)	1	"Bound" (Conservative)	<ul style="list-style-type: none"> No information on uncertainties
Standard Monte Carlo	$> 10^5$ (for prob. $< 10^{-3}$)	"Exact" prob. distribution	<ul style="list-style-type: none"> Typically used as a last resort
Latin Hypercube Sampling	4	"Exact" prob. distribution	<ul style="list-style-type: none"> More useful for mean and variance analysis than CDF or small probability analysis
Adap. Import. Sampling	$\approx 10^2 \sim 10^3$	"Exact" point probability	<ul style="list-style-type: none"> Can be used to supplement the AMV method
Mean-Value First-Order	$n + 1$	Mean and standard deviation	<ul style="list-style-type: none"> For quick estimate Good for small input standard deviations Useful to locate areas for more refined analyses
Advanced Mean Value (with iteration)	$= 3n$	"Accurate" prob. distribution	<ul style="list-style-type: none"> Shown to be applicable to nonlinear and non-monotonic functions Accuracy can be improved efficiently by adaptive sampling method

n = number of random variables

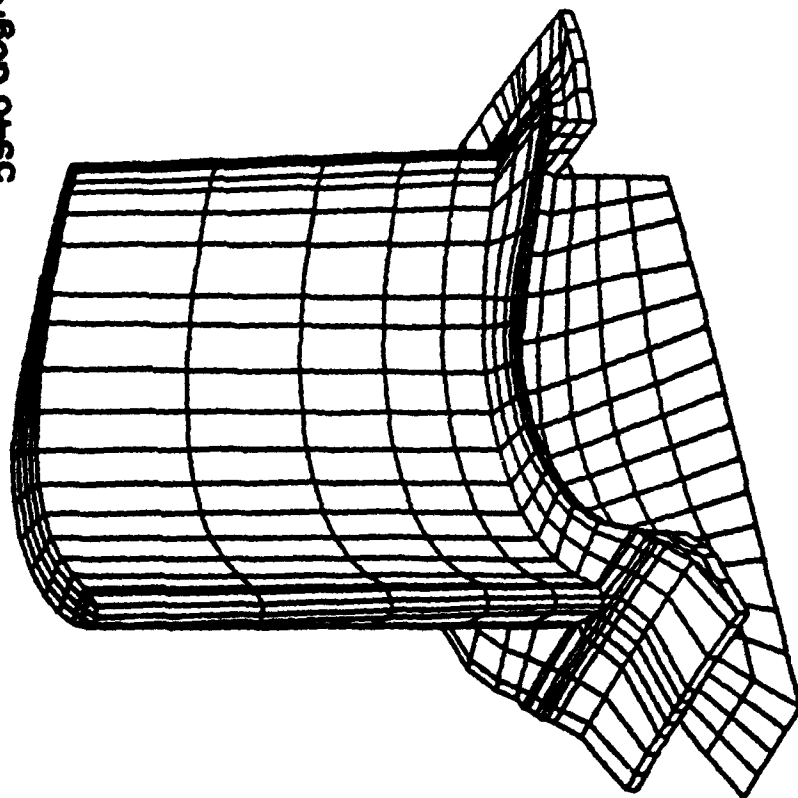
NESSUS 6.0 System Reliability/Risk Assessment



Turbine Blade Finite Element Model

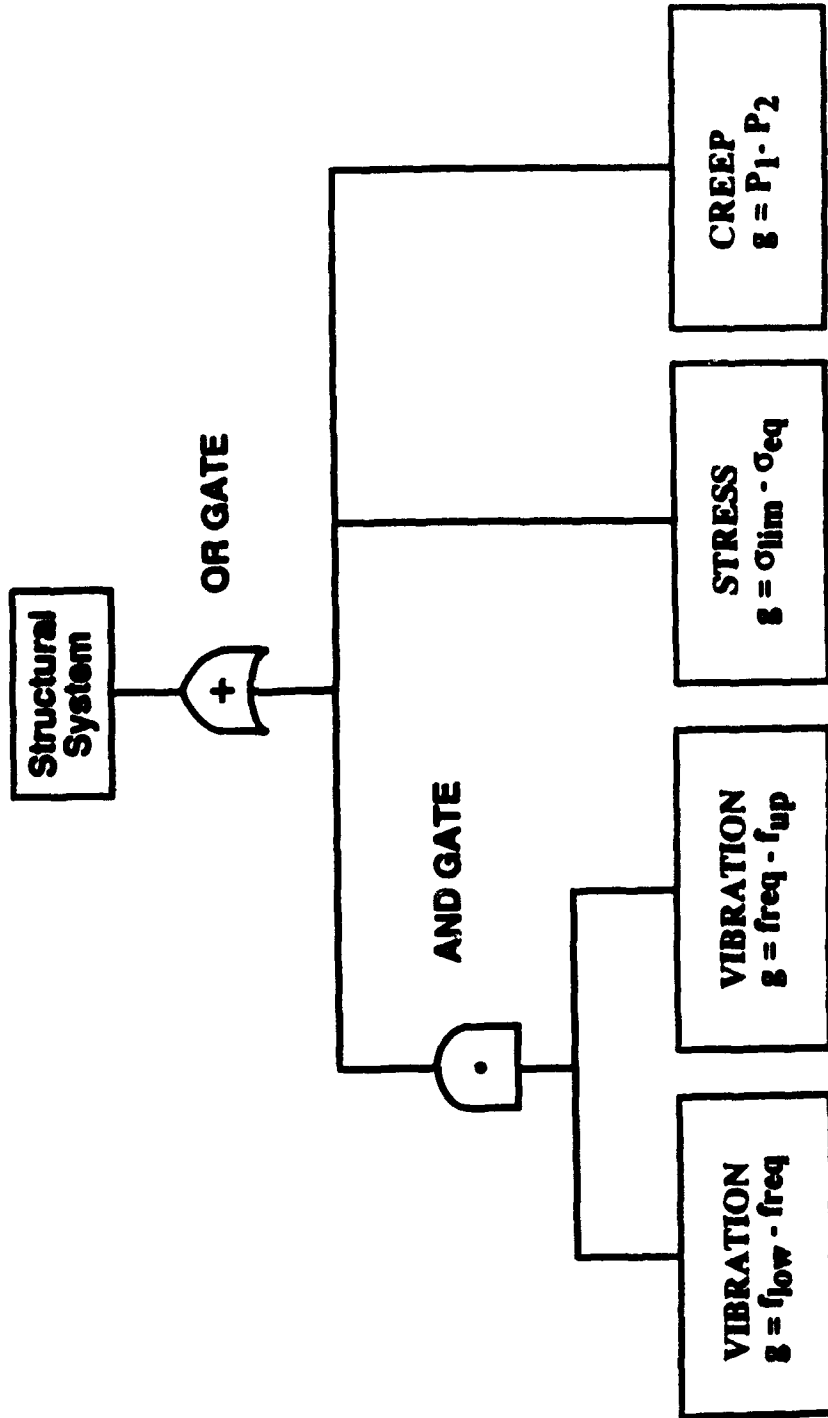


2519 Nodes
1456 3D Elements
5946 degrees-of-freedom





FAULT TREE REPRESENTATION OF STRUCTURAL SYSTEM FAILURE





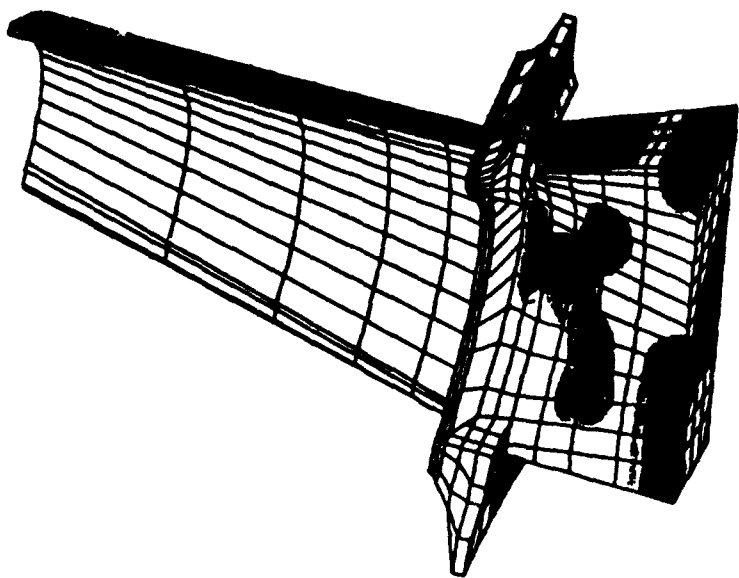
Random Variable Definitions

	Mean	Standard Deviation	Distribution	Bottom Event
Material Orientation θ_z	.05236°	0.067544	Normal	All
Material Orientation θ_y	-.03491°	0.067544	Normal	All
Material Orientation θ_x	.08727°	0.067544	Normal	All
Elastic Modulus E_0 +	18.36E6	.4595E6	Normal	All
Poisson's Ratio ν_0 +	.386	.00965	Normal	All
Shear Modulus G_0 +	18.63E6	.4657E6	Normal	All
Creep Equation Coefficient B_0	86.0	.086	Normal	Creep
Density ρ	.805E-3	.493E-5	Normal	Freq.

+ Defined at Room Temperature



PROBABILITY OF STRESS EXCEEDING 60 KSI





STRESS FAILURE MODE COMPUTATIONAL SUMMARY

Model	
Limit State	von Mises Stress at Node 2518 > 110 ksi
Finite Element Model	1456 8-Noded 3D Elements, 2519 Nodes, 5946 Degrees of Freedom
Memory	5.7 Million Single-Precision Words
Random Variables	6 Random Variables ($\theta_x, \theta_y, \theta_z, E, \nu, G$)
Perturbation Database	7.1 Megabytes

Computational Solution Times (cpu secs) *	
(1) Deterministic Solution	~150 secs
(1) Perturbed Solution	~67 secs
Total Sensitivity Calculation	~550 secs

Iteration Level	Prob. of Failure	Total CPU Time
Mean Value **	0.00238	550 secs 9.2 mins
Advanced Mean Value **	0.00198	850 secs 14.2 mins
1st Iteration **	0.00170	1400 secs 23.3 mins
2nd Iteration **	0.00227	1950 secs 32.5 mins
AIS (213/419) ***	0.00227	64,250 secs 17.8 hrs

+ All cpu times from an HP 750 workstation

** First order analysis

*** (# failures/# samples)



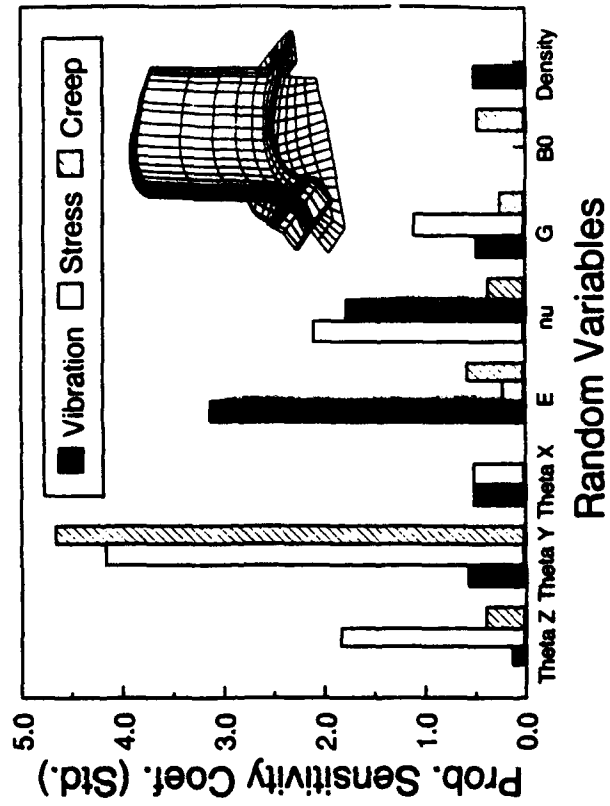
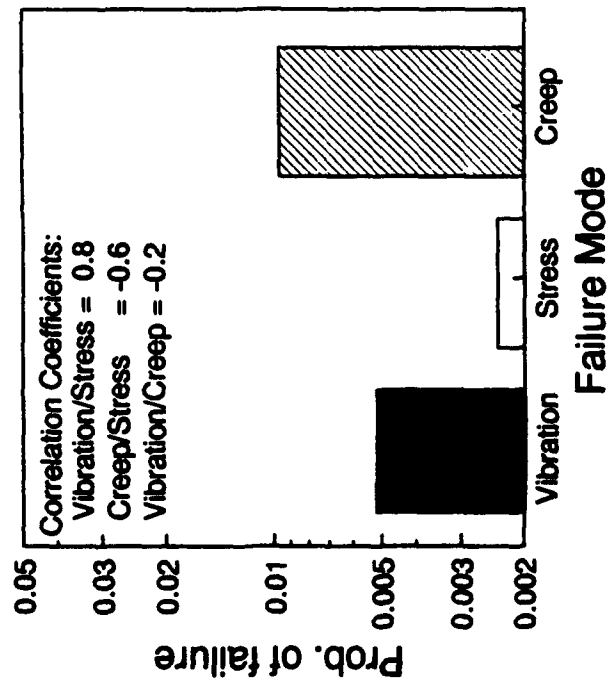
System Reliability Results

Analysis Type	Bottom Events	System Samples	Probability of Failure	Total CPU*
Monte Carlo	Approximate	1721/100000	0.0172	3.7 hrs
AIS	Approximate	70/83	0.0171	3.7 hrs
AIS	Finite Element	85/117	0.0222	25 hrs

+ Includes AMV + solution time

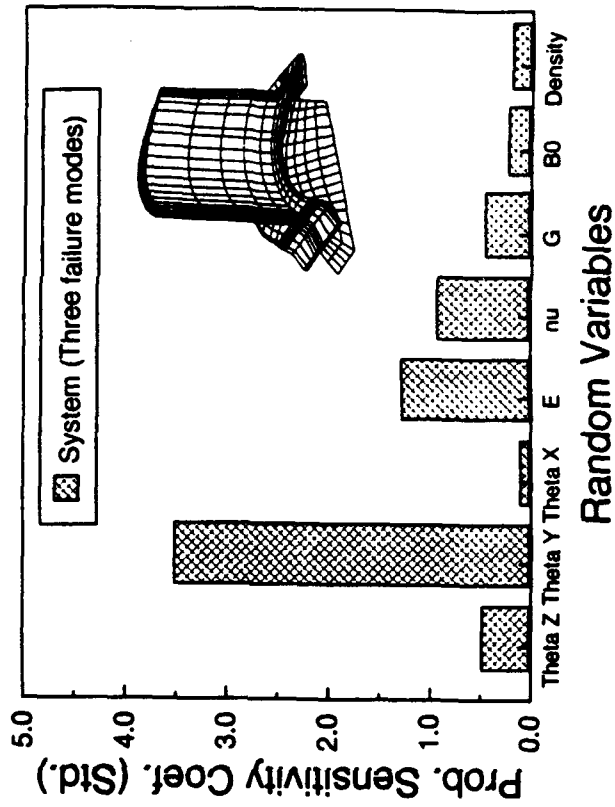
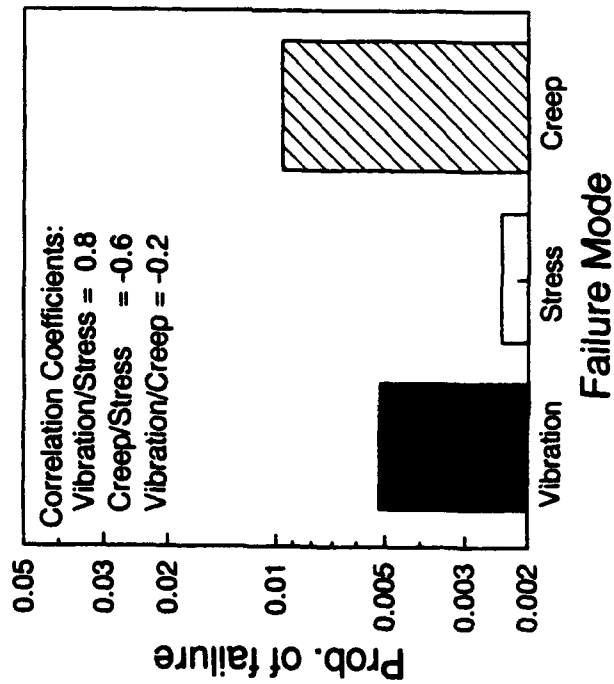


Failure Mode Reliability Sensitivity Analysis





System Reliability Sensitivity Analysis





NESSUS SSME Applications

- **Static stress analysis of turbine blade**
- **Natural frequency analysis of turbine blade**
- **Random vibration analysis of ducting system**
- **Plastic analysis of lox post**
- **Buckling analysis of transfer duct**
- **LCF & HCF damage analysis of lox post**

Performed by Rocketdyne

11/19/88



Future Directions

- Probabilistic structural integrity and life assessment
 - Fatigue and fracture crack growth, low cycle fatigue, probability of detection, multi-site damage
- Graphical User Interface (PC / X windows based)
- External Interfaces (simple programs and finite element programs, e.g. ABAQUS)
- Continued development of robust probabilistic algorithms
- Design oriented (improved sensitivities)



Summary and Conclusions

- **Probabilistic methods can assist in the management of variabilities**
- **Probabilistic sensitivity results are the key to the interpretation and use of probabilistic methods**
- **Technology and computer codes exist for probabilistic analysis of complex structures**
- **Continued development required:**
 - Probabilistic sensitivities
 - Adaptive, efficient probabilistic methods
 - Ease of use and interpretation
 - Education and training

FRACTURE ANALYSIS OF C-141 WEEP HOLE CRACKS

prepared by

**Satya N. Atluri, Georgia Institute of Technology
Padraic O'Donoghue, Georgia Institute of Technology
Brad Visser, Georgia Institute of Technology
Daniel C. Register, WR-ALC
Daniel S. Pipkins, Knowledge Systems Inc.**

**for presentation
at the
USAF Structural Integrity Program Conference
30 November - 2 December 1993
San Antonio, Texas**

1.0 INTRODUCTION

Fatigue cracks which initiate at weep holes located in the risers emanating from the lower wing surface panels have plagued the C-141 for some time. Such cracking was first observed in full-scale wing/fuselage durability tests. As a result of these observations, a rework procedure which consisted of reaming followed by low-interference cold working was developed for the weep holes. Despite the application of this rework procedure, weep hole cracking continues to adversely effect the structural integrity of the C-141 fleet.

The Air Force has recently begun using composite patches to repair lower wing panels in which weep hole cracks have been found. In support of this repair effort, a computational procedure has been developed which will allow engineers to perform rapid Damage Tolerance Analyses (DTA) of repaired and unrepaired lower wing panels. This procedure will allow for the efficient performance of residual strength and fatigue calculations of repaired and unrepaired lower wing panels containing part elliptical cracks. The procedure developed involves an extension of the Finite Element Alternating Method (FEAM) [1]. The details of this procedure are the subject of this report. Numerical results presented consist of a comparison of fatigue calculations performed on a model of an unrepaired weep hole with test data as well as repaired (generic) and unrepaired stress intensity factors of part elliptical weep hole cracks.

2.0 FINITE ELEMENT ALTERNATING METHOD (FEAM)

The Schwartz-Neumann alternating method is used to obtain the stress intensity factor solutions for a crack in a finite body. A detailed description of this procedure can be

found in [1]. Since a general closed form solution does not exist for a finite body which contains a crack and is subjected to arbitrary externally applied tractions, a numerical procedure is required to solve this problem. The Schwartz-Neumann alternating method is such a procedure. In the alternating method, two types of solutions are required.

Solution 1: A general analytical solution for an embedded elliptical crack in an infinite body subject to arbitrary crack face tractions.

Solution 2: A numerical scheme (finite or boundary elements for instance) capable of solving for the stresses in an uncracked finite body.

The needed analytical solution exists, the details of which can be found in [2]. In the present report, the finite element method will be used to solve for the stresses in the uncracked body. These two solutions are utilized in the following steps which make up the FEAM.

1. Solve the uncracked finite body under the given external loads using the finite element method. The uncracked body has the same geometry as in the given problem except for the crack. For example, when a crack emanates from a hole in a structure, the hole must still be analyzed in the uncracked structure.
2. Using the finite element solution of the uncracked body, compute the stresses at the crack location.
3. Compare these stresses calculated in step 2 with a permissible stress magnitude. If the stresses are less than the permissible stress magnitude, then stop.
4. The stresses at the crack location computed in step 2 are reversed to create the traction free crack faces as in the given problem.
5. The reversed stresses are applied to the infinite body problem and the analytical solution is obtained.
6. The stress intensity factors for the infinite body problem are computed analytically.
7. The stresses at the location of the external surfaces of the finite body are

determined from the analytical solution.

8. The stresses computed in step 7 are reversed and treated as externally applied tractions applied to the uncracked finite body.

9. Go to step 1, using the tractions computed in step 8 as the given external loading.

In practice, this process usually takes between three to five iterations to converge, depending upon factors such as the stress concentration present in the uncracked body at the crack location. The overall stress intensity factor solution is obtained by adding the stress intensity factor solutions for all iterations.

The advantages of utilizing FEAM to perform a DTA of structure containing elliptical or part elliptical cracks are many. However, they are all a result of the fact that only the uncracked structure is modeled with finite elements. The crack is specified simply by giving the major axis, minor axis and center coordinates of the ellipse which models the crack. As a consequence, FEAM is extremely efficient from both a computational and manpower point of view when performing parametric studies of crack size, shape and location because the finite element mesh remains the same. This property makes FEAM ideal for performing fatigue crack growth calculations of elliptical or part elliptical cracks.

2.1 Fatigue Crack Growth Algorithm

Exploiting the fact that the crack front does not need to be modeled explicitly in FEAM and thus only one finite element mesh is necessary to model various crack sizes and shapes, it is relatively straightforward to utilize FEAM to perform fatigue crack growth calculations. The steps involved in a fatigue crack growth calculation under constant amplitude loading are as follows.

1. Specify initial and final minor axis sizes and divide the interval into a number of subintervals (20 for the present work).
2. The number of cycles for minor axis crack growth in a given subinterval is calculated using a crack growth equation (Forman's for the present work) and the stress intensity factors (for the crack size and shape at the beginning of the subinterval) generated by a FEAM analysis.
3. The increment in major axis crack growth is determined by utilizing the number of cycles determined in step 2, the crack growth equation and the stress intensity factors (for the crack size and shape at the beginning of the subinterval) generated by a FEAM analysis.
4. If the minor axis size has reached the specified final size, then stop. Otherwise, go to step 2.

The analysis of fatigue crack growth from the C-141 weep hole requires the use of a variable amplitude loading spectrum. While it is possible to perform a cycle by cycle fatigue crack growth analysis using FEAM, this is not in general necessary. Rather, the present work has combined the software packages SAFEFLAW3D (which implements the FEAM) and NASA FLAGRO [3] for this purpose. NASA FLAGRO contains advanced features that can be used to consider fatigue crack growth under variable amplitude loading. Thus, by combining the efficient stress intensity factor calculation capability of SAFEFLAW3D with the fatigue crack growth capabilities of NASA FLAGRO, a powerful tool for performing fatigue crack growth analysis of elliptical and part elliptical cracks is created. Figure 1 illustrates this concept.

2.2 Composite Patch Algorithm

The FEAM, as presented to this point, is a powerful tool for generating stress intensity

factors for cracks in homogeneous bodies. However, its application to structure having adhesively bonded composite patches, such as the C-141 lower wing panels/risers, requires the introduction of a two step analysis procedure. This is because the analytical solution for an infinite body containing an elliptical crack, whose faces are subject to arbitrary tractions, is available only for certain homogeneous bodies. The two step analysis procedure used to generate stress intensity factors for structures repaired with adhesively bonded composite patches is as follows.

1. Perform a finite element analysis of the entire structure (i.e. original structure, adhesive and composite patch) under the given external loading. In this analysis, release the nodes at the location of the crack, but make no attempt to model the singular stress field which exists at the crack. Determine the equivalent nodal loads which exist at the interface of the adhesive and original structure.
2. Perform the previously described FEAM analysis of the original structure with the initial external loading consisting of the given loading and the equivalent nodal loads calculated in step 1.

Step 1 can in general be done using any finite element software which allows the user to model the original structure and adhesive with 3D solid elements and the composite patch with 3D solid elements or shell elements.

3.0 NUMERICAL RESULTS

The ability to model fatigue crack growth of a corner crack located at the weep hole in a C-141 lower wing panel/riser and to calculate the reduction in stress intensity factor due to the application of adhesively bonded composite patches is demonstrated in this section. The geometry and material parameters of the C-141 lower wing panel/riser are given in Figure 2. A critical stress intensity for a part elliptical crack in the riser was calculated to

be 57.6 ksi $\sqrt{\text{in}}$ using NASA FLAGRO. This number was based on a yield stress of 65 ksi, a plane strain fracture toughness of 27 ksi $\sqrt{\text{in}}$ and a riser thickness of 0.18 in. The limit stress for the lower wing panel/riser is 34 ksi. All applied loads in the analyses are uniformly distributed over the cross section of the panel/riser as shown in Figure 3. The mesh in Figure 3 consists of 597 20 node brick elements and is used in all analyses except as noted.

3.1 Fatigue Results

The fatigue crack growth calculations were done assuming a Forman model. The Forman relation is given by:

$$\frac{da}{dn} = \frac{C(\Delta K)^n}{\{(1-R)K_c - \Delta K\}}$$

where a is the crack length, n is the number of cycles, R is the ratio of K_{max} to K_{min} , and K_c is the critical stress intensity which was given previously. Experimental fatigue crack growth data for AL 7075-T651 was input into NASA FLAGRO, which determined the constants C and n to be 0.2112E-05 and 2.531, respectively. The crack was assumed to grow from a corner flaw above the weep hole as shown in Figure 4. The initial crack dimensions were 0.07 in. along the bore of the weep hole and 0.05 in. up the riser.

The variable amplitude spectrum used was comprised of peak-valley pairs representing six 504.5 flight hour passes or 3027 total flight hours. The number of peak-valley pairs is somewhat different for each pass in order to account for cycles that occur as little as once in 3027 flight hours and for an accumulation of fractional occurrences in the correct sequence. The data was filtered to remove stress differences of less than 2 ksi. The highest peak in the data was 17.89 ksi while negative loads were treated as zero in the

present analysis.

The fatigue crack growth results are presented in terms of major and minor axis growth in Figure 4. These results were produced using the previously outlined combination of NASA FLAGRO and SAFEFLAW3D. The results indicate that the crack would grow through the riser in approximately 1513 flight hours. The results were obtained in 1 hour on an HP 9000/735. Limited comparison was possible with weep hole fatigue test data performed for WR-ALC. Weep hole test specimen RN0002, which had an initial crack size very close to that of the numerical analysis, apparently propagated completely along the bore somewhere between 1475 and 3027 flight hours. While the 1513 flight hours predicted by analysis falls in this range, it appears that the test data indicates a somewhat higher time for the crack to propagate along the bore of the weep hole. There are several reasons which likely contribute to discrepancies that exist between the computational model and the test data. Firstly, the initial crack size along the bore of the weep hole was not known exactly. More precise measurements are needed to describe the progression of the crack in this direction. Also, the crack growth constants used in the fatigue calculation were not based on crack growth data of the Al 7075-T651 used in the tests. Finally, crack closure effects, which would reduce fatigue crack growth rates were not accounted for in the present computational model.

3.1 Composite Patch Results

Reductions in stress intensity factor due to adhesively bonded composite patch repairs of cracked panels/risers were studied for four separate cracking cases. The patch and adhesive geometry and material parameters are given in Figure 5 (These are generic in nature) The patch material properties are representative of an 8 ply, uni-directional

boron-epoxy. For each cracking case, two patching schemes are compared. Patch 1 models the riser patches only while Patch 2 models the riser patches as well a patch on the outer surface of the lower wing panel. This is done to study the effect that parasitic stiffening of the structure due to the patches has on stress intensity factors. The parasitic stiffening tends to induce local bending of the structure in the case of Patch 1 while this effect is lessened in the case of Patch 2.

Results for the four cracking cases are given in Figures 6-10. The stress intensity factors presented are for a 1 ksi unit load. The CPU time required for each run on a HP 9000/735 was about 11 minutes for the 597 element mesh. Results for case 1, which required an 868 element mesh due to the severe stress concentration (CPU time=25 minutes), indicate that while Patch 1 and Patch 2 significantly reduce the stress intensity factors, they do not restore sufficient residual strength to allow the structure to sustain the limit load of 34 ksi. Results for cases 2, 3 and 4 show significant reductions in stress intensity factors due to the composite patches. In all these cases, the Patch 2 scheme is superior to that of Patch 1. This is particularly true for cracks below the weep hole which tend to be affected to a greater extent by the local bending induced by the parasitic stiffening of Patch 1.

4.0 CONCLUSIONS

Methodology for performing a DTA of repaired and unrepaired C-141 weep holes containing part elliptical cracks has been presented. The techniques provide accurate solutions and are very efficient in terms of manpower and computational times. The methodologies are completely general and could easily be applied to other structural components.

REFERENCES

- [1] T. Nishioka and S.N. Atluri, Analytical Solution for Embedded Elliptical Cracks and Finite Element Alternating Method for Elliptical Surface Cracks Subjected to Arbitrary Loadings, *Eng. Fracture Mechanics*, Vol. 17 No. 3 (1983), pp. 247-268.
- [2] K. Vijaykumar and S.N. Atluri, An Embedded Elliptical Flaw in an Infinite Solid, Subject to Arbitrary Crack Face Traction, *J. of Applied Mechanics*, Vol. 48 (1981), pp. 88-96.
- [3] R.G. Forman, NASA/FLAGRO Version 2.0 Users Manual, January 1993 Draft.

FATIGUE CRACK GROWTH METHODOLOGY

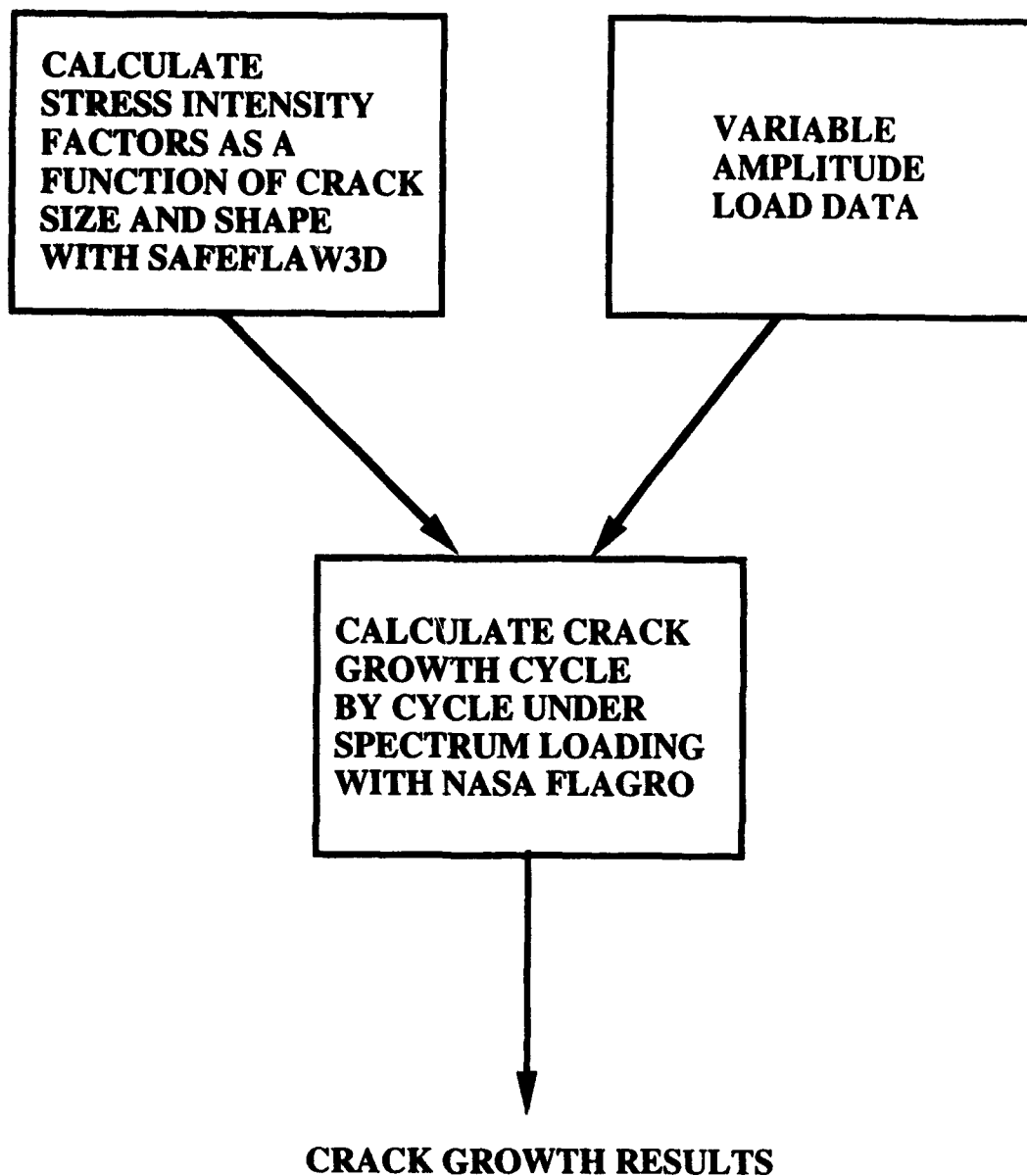
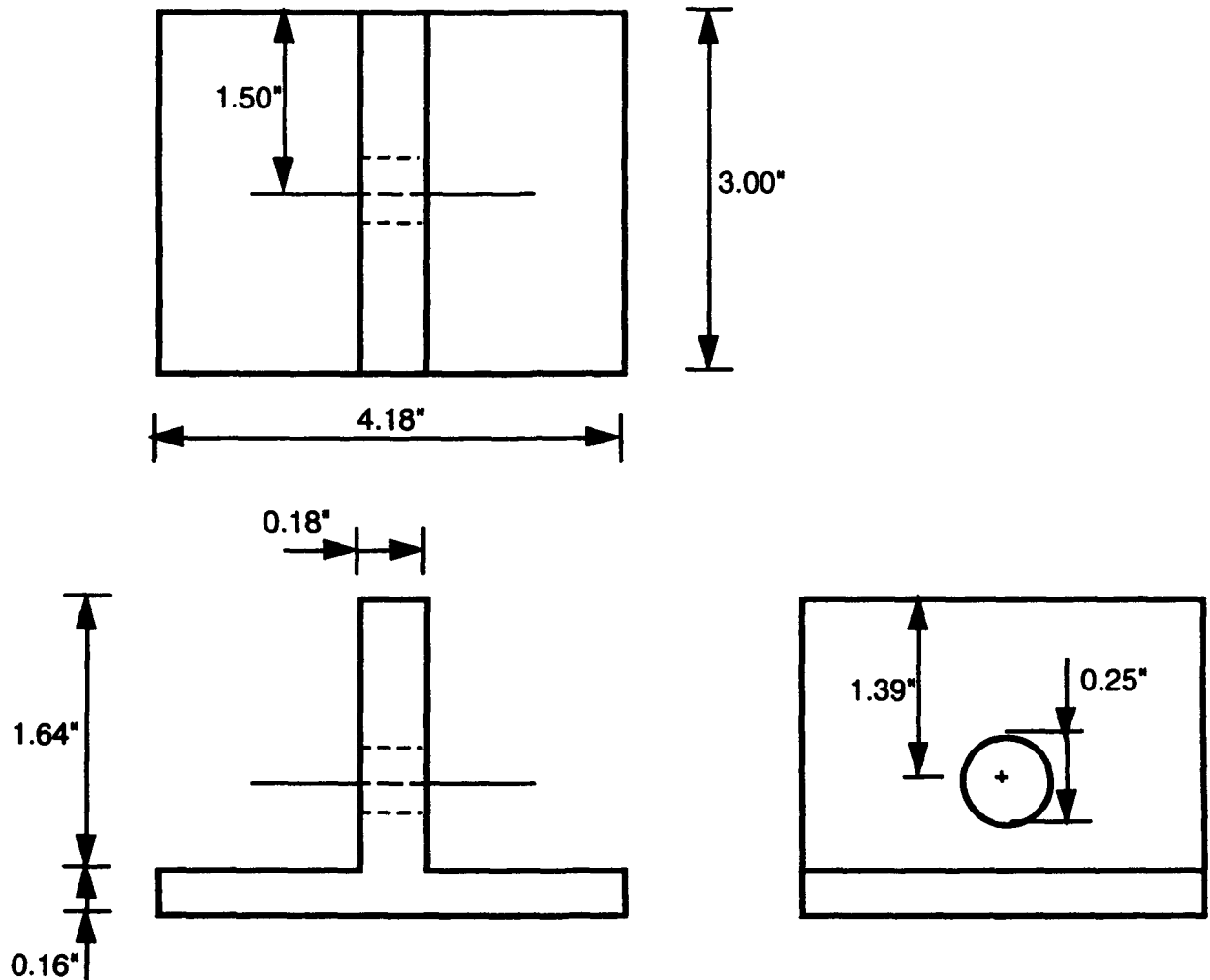


Figure 1

UNPATCHED MODEL GEOMETRY AND MATERIAL PARAMETERS



Material: AL 7075-T651
Young's Modulus: 10.3E+06
Shear Modulus: 3.9E+06
Poisson's Ratio: 0.33

Figure 2

SDRC I-DEAS VI.1(s): FE_Modeling_&_Analysis

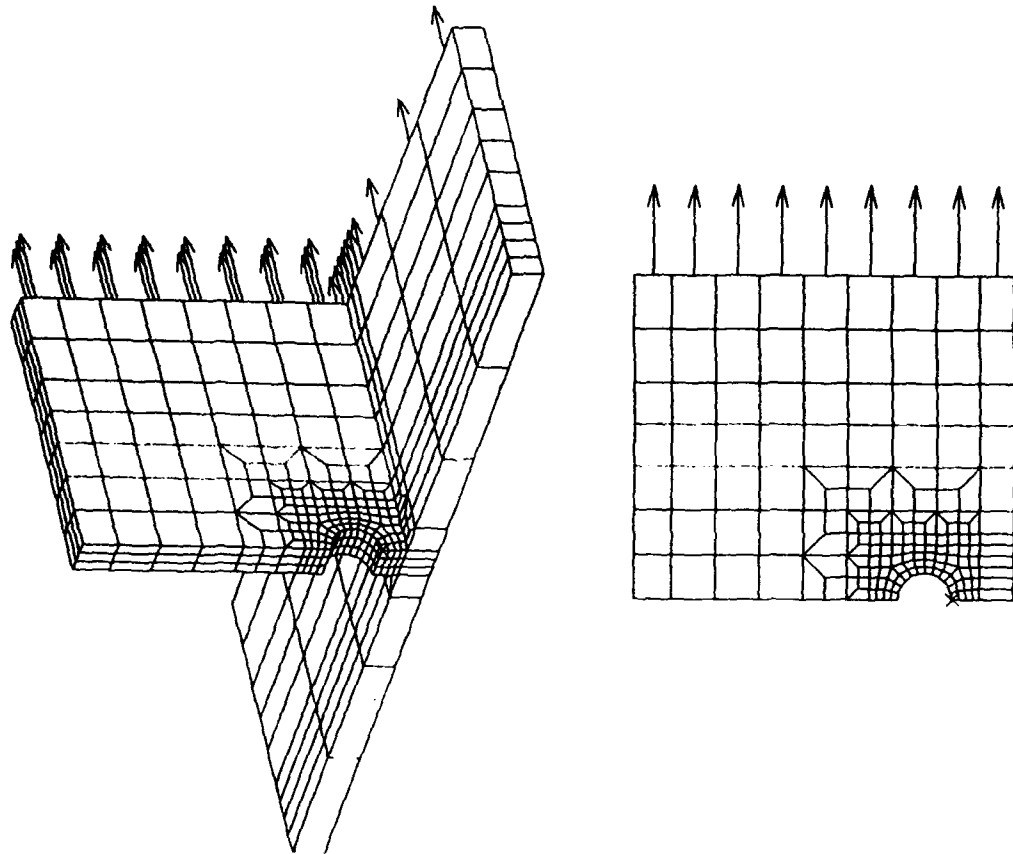
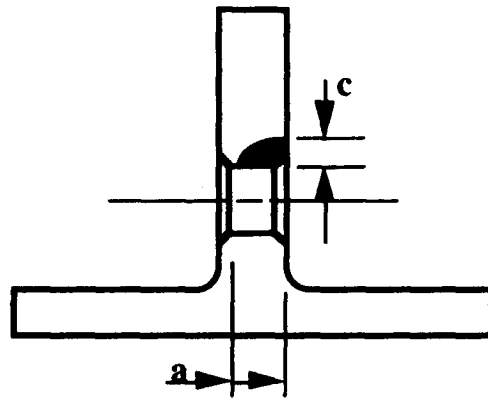


Figure 3



$a = 0.07''$ $c = 0.05''$

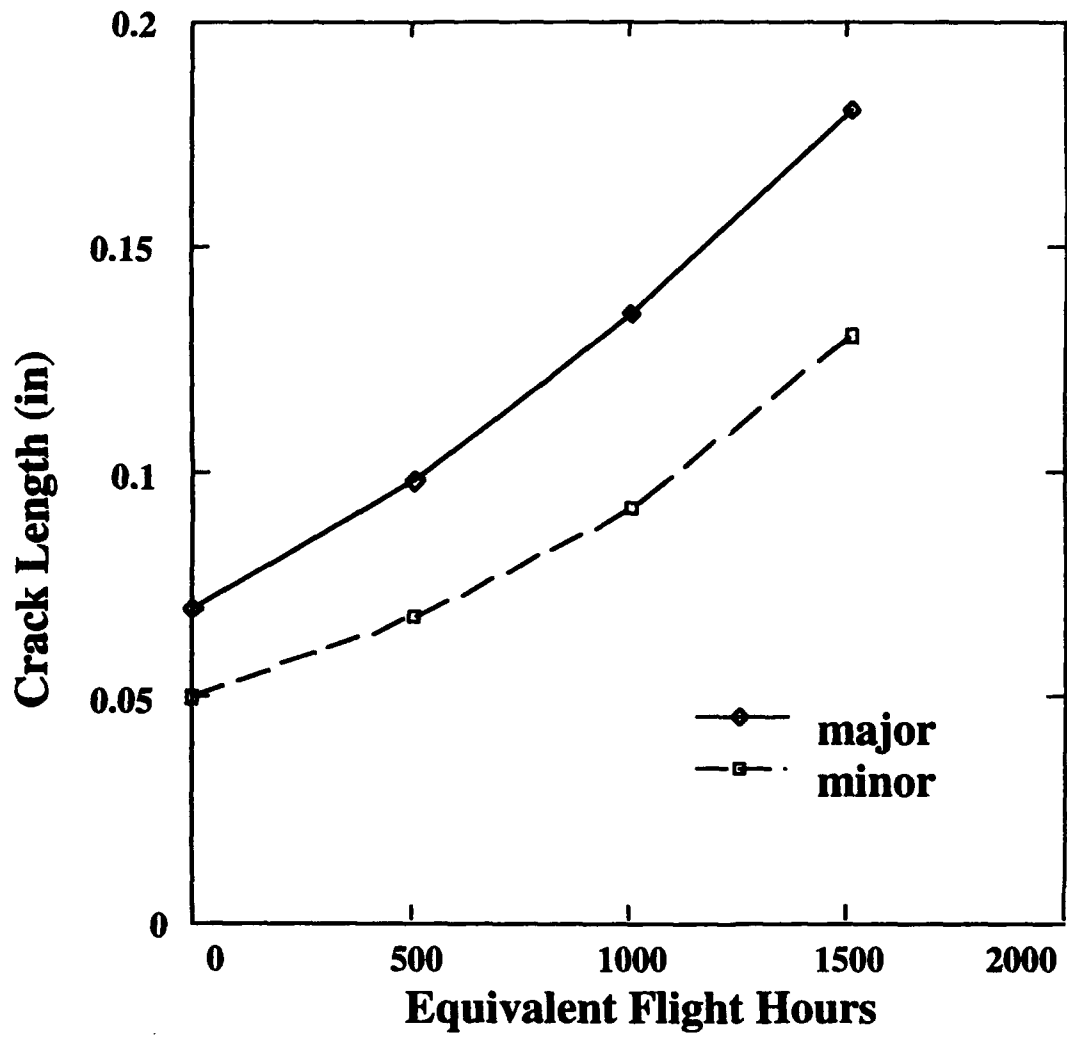
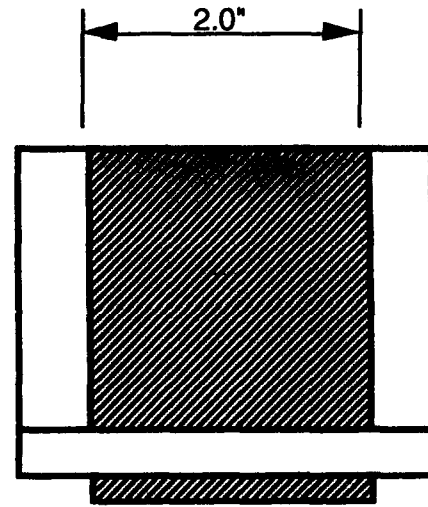
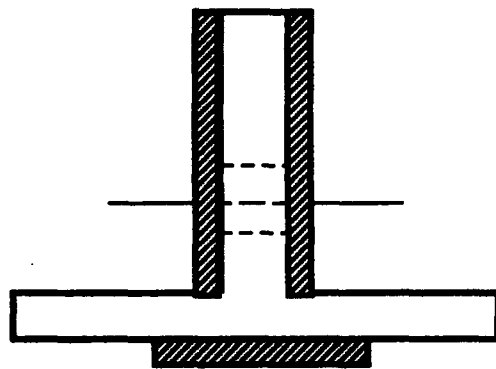
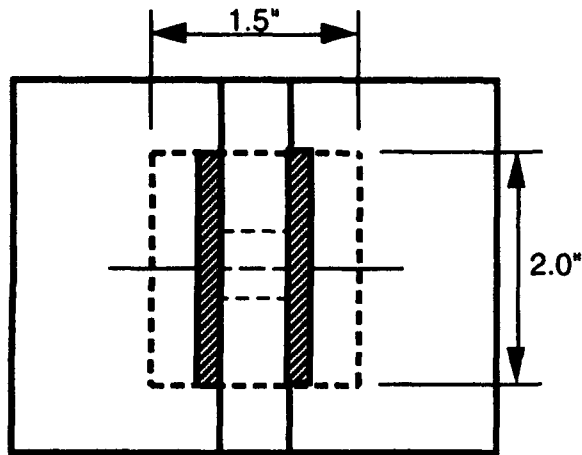


Figure 4

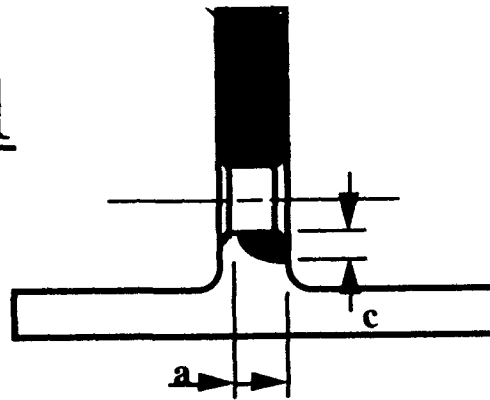


Material: Boron-Epoxy
Thickness: 0.04"
 E_x : 30.2E+06 psi
 E_y : 3.69E+06 psi
 G_{xy} : 1.05E+06 psi
 G_{xz} : 1.05E+06 psi
 G_{yz} : 0.716E+06 psi
 ν_{xy} : 0.1677

Material: Adhesive
Thickness: 0.004"
Young's Modulus: 0.31E+06 psi
Shear Modulus: 0.105E+06 psi
Poisson's Ratio: 0.48

Figure 5

CASE 1



$a = 0.10''$ $c = 0.08''$

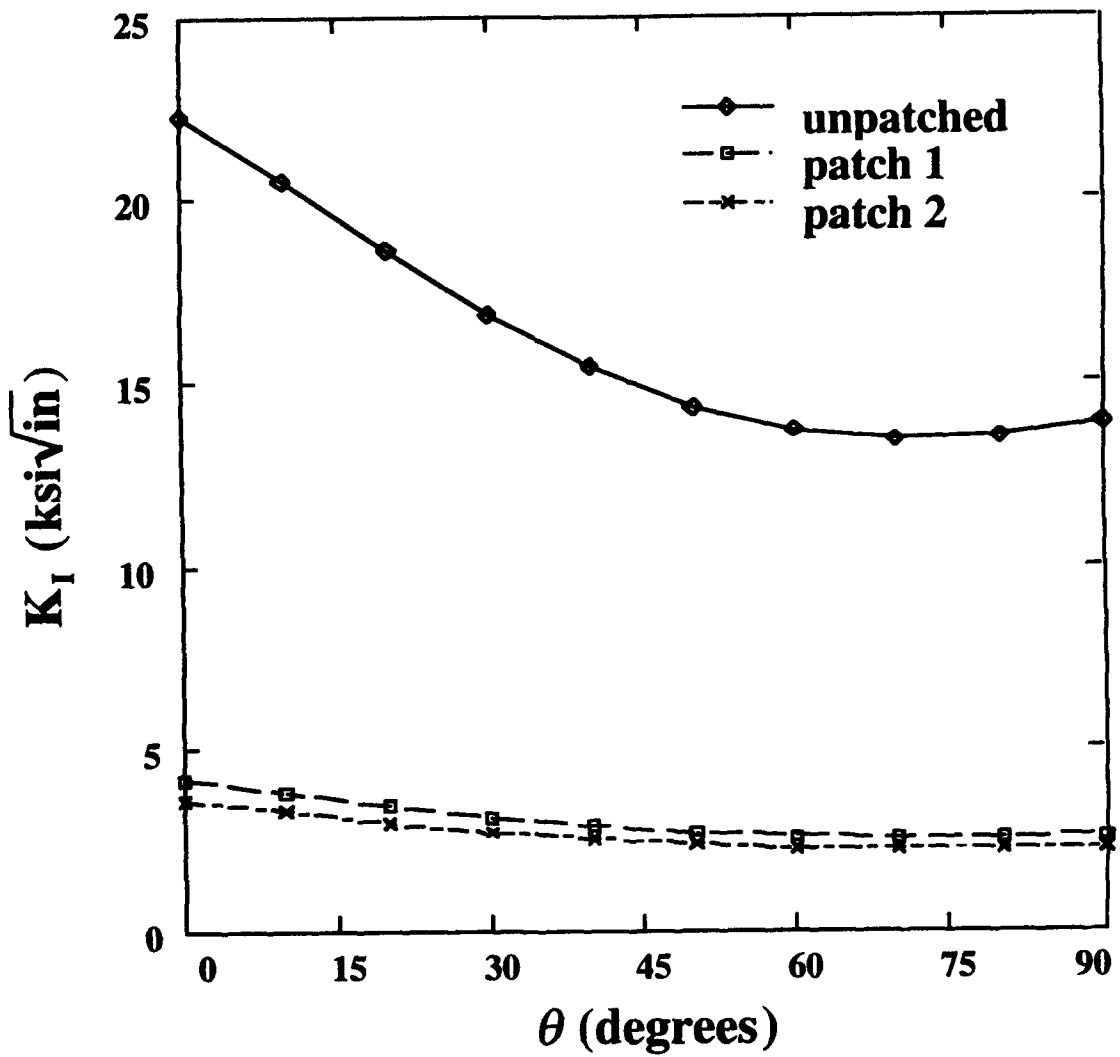
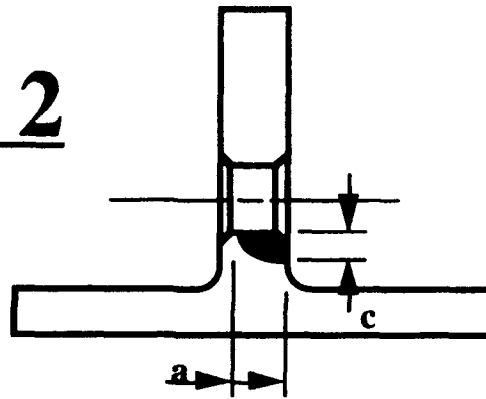


Figure 6

CASE 2



$$a = 0.10'' \quad c = 0.08''$$

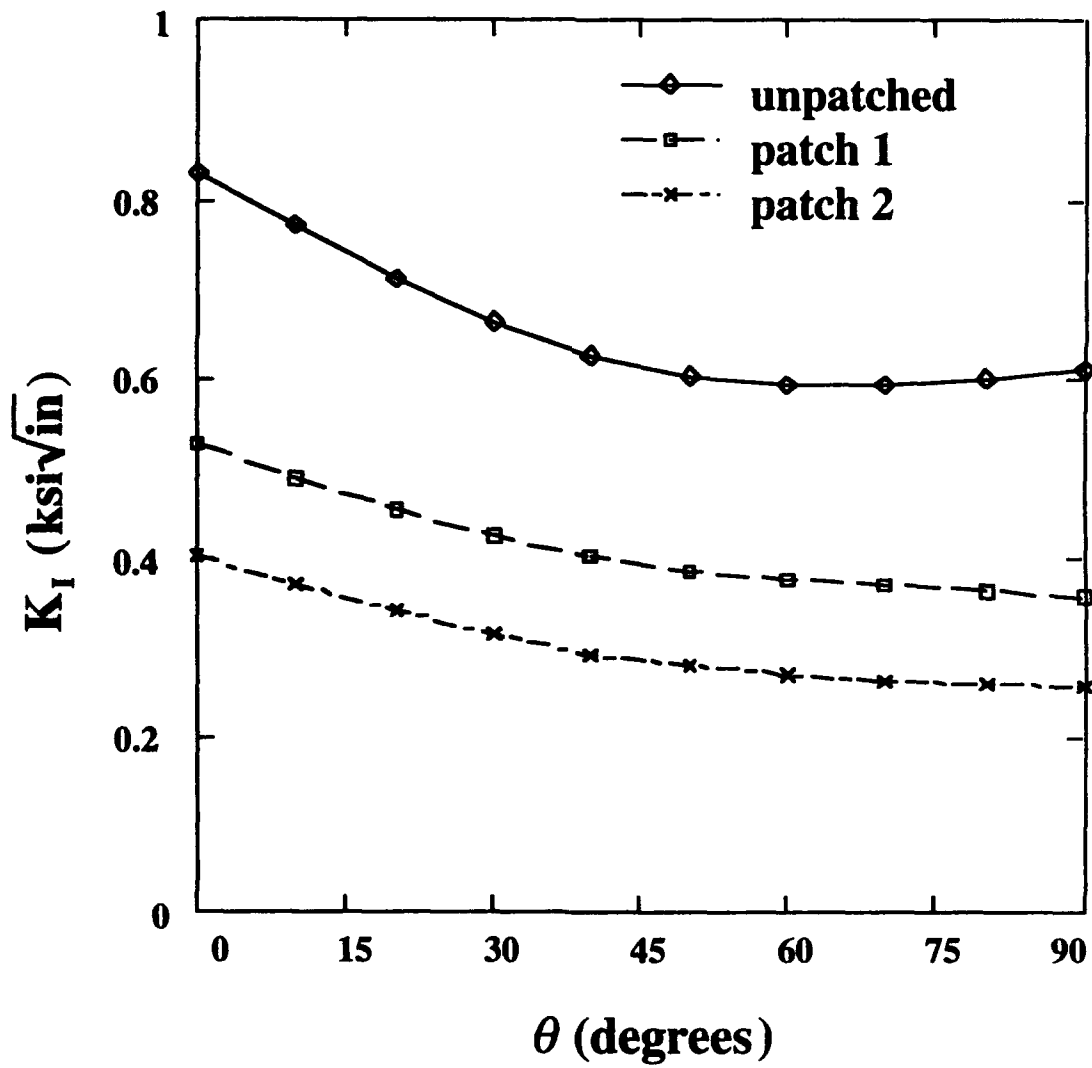
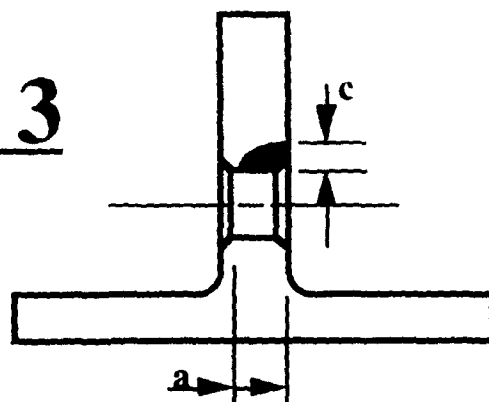


Figure 7

CASE 3



$$a = 0.10'' \quad c = 0.08''$$

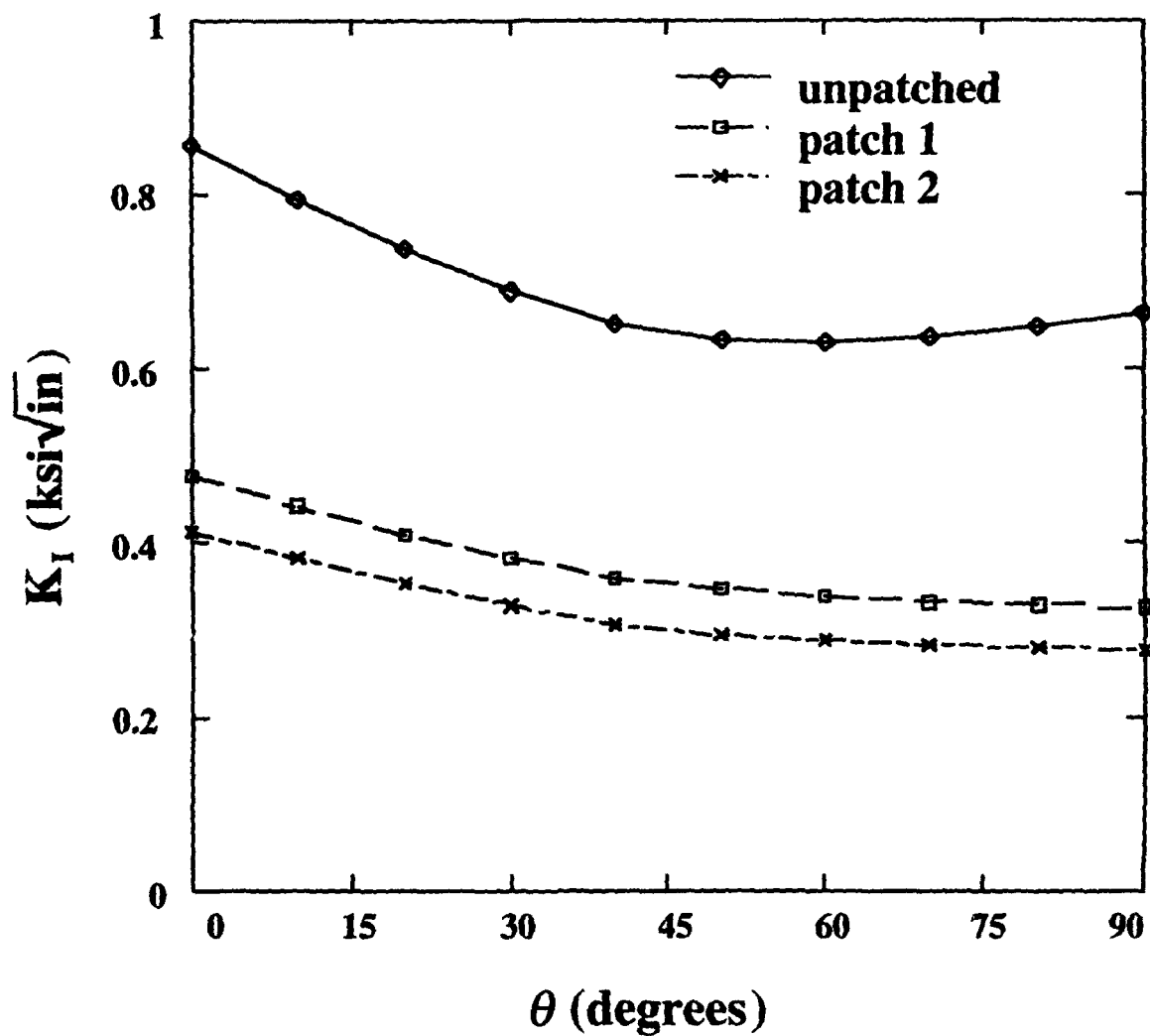
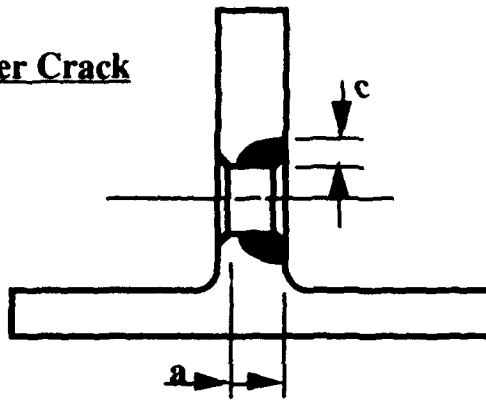


Figure 8

CASE 4: Upper Crack



$a = 0.10''$ $c = 0.08''$

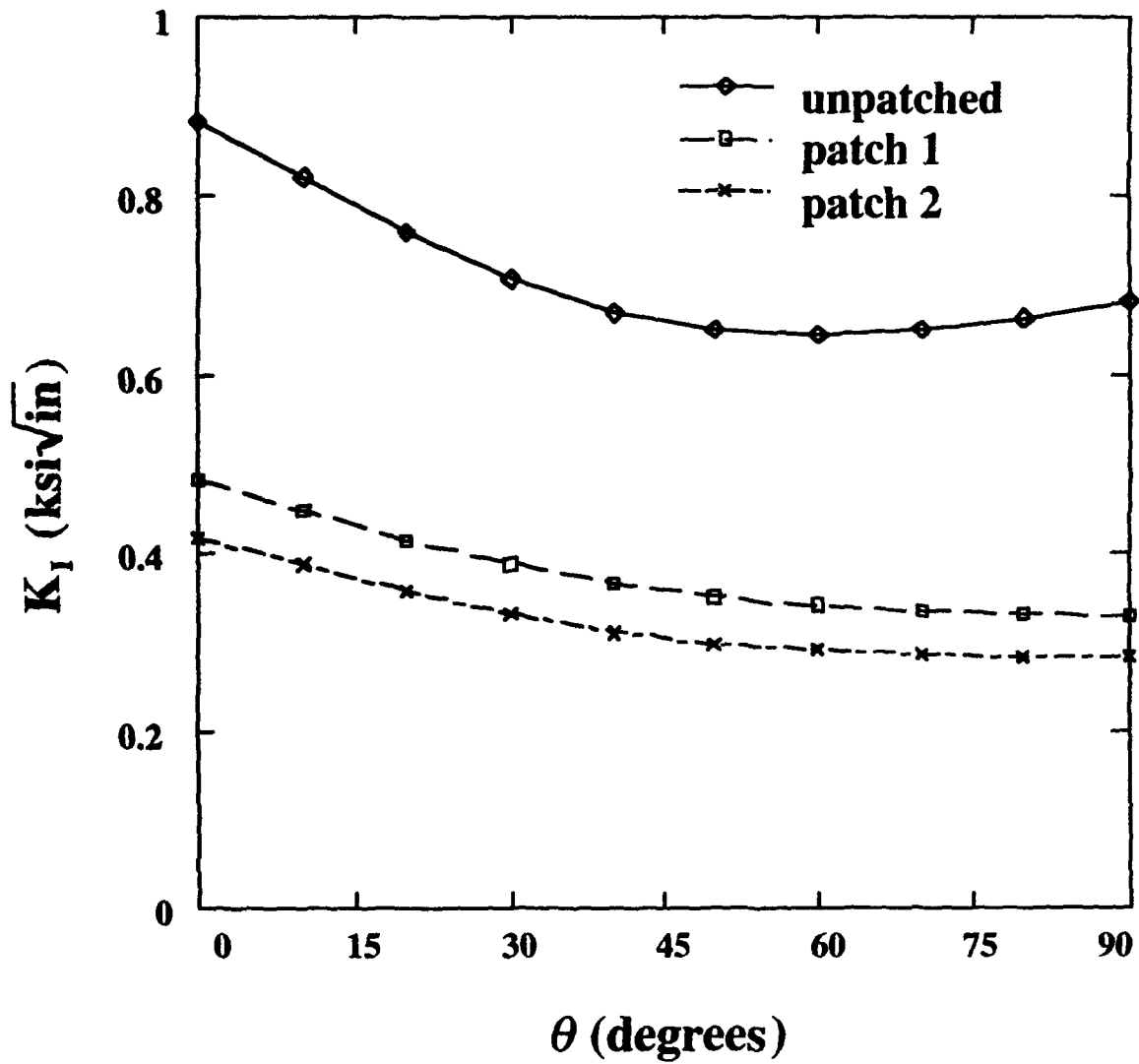
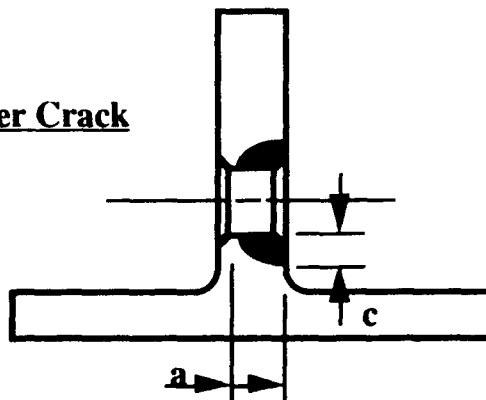


Figure 9

CASE 4: Lower Crack



$a = 0.10''$ $c = 0.08''$

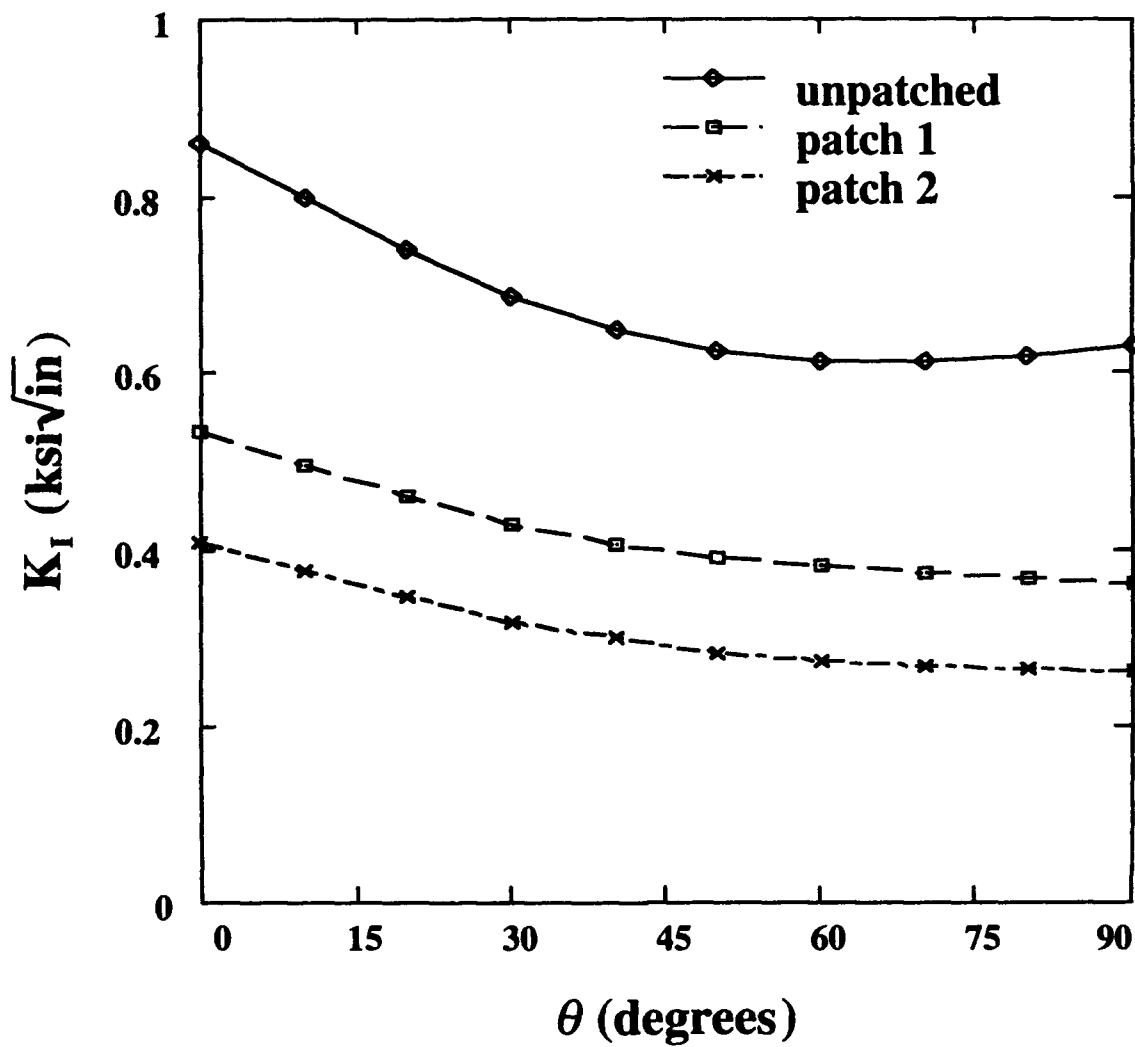


Figure 10

**Cold Expansion Rework
of Weep Holes in the Lower Wing Skin Structure
of C-141B Aircraft**

presented at

**1993 USAF Aircraft Structural Integrity Program Conference
November 30 - December 2, 1993
San Antonio, TX**

by

**Len Reid
Vice President, Engineering
Fatigue Technology Inc.
Seattle, WA • USA**

Approved for public release by Warner Robins Air ForceBase

COLD EXPANSION REWORK OF WEEP HOLES IN THE LOWER WING STRUCTURE OF C-141B AIRCRAFT

Len Reid¹

Antonio C. Rufin²

Eric T. Easterbrook³

Daniel C. Register⁴

ABSTRACT

The USAF C-141B aircraft are rapidly approaching an extended fatigue life of 45,000 flight hours. Fuel weep holes incorporated in design of the integral riser of lower wing panels have become a source of fatigue cracks. A program to correct the problem and further improve the fatigue life includes a mandrel-only coldworking process. This paper discusses a test program conducted to establish crack growth rates from pre-existing cracks in these weep holes in conjunction with the coldworking process. The evaluation included a comparison with an alternative split sleeve cold expansion process. The results show that both methods extend the crack growth life; however, the split sleeve cold expansion method arrested further growth from cracks up to 0.144 inches.

¹Vice President, Engineering, Fatigue Technology, Inc., Seattle, Washington

²Assistant Engineering Manager, Fatigue Technology, Inc., Seattle, Washington

³Engineering Manager, Fatigue Technology, Inc., Seattle, Washington

⁴WR-ALC/TIEDD, Robins AFB, Georgia

INTRODUCTION

The USAF's C-141B cargo aircraft have exceeded their original design lives of 30,000 flight hours and are rapidly approaching an extended life of 45,000 flight hours. Fatigue damage to the wings of these aircraft has been accelerated in varying degrees by severe mission requirements, including extended aerial refueling training and low level special mission flying. A mid-life modification to the aircraft provided for aerial refueling in order to extend the range of the aircraft. The original design of the wings incorporated 0.250 inch diameter weep holes drilled through integral risers of the lower wing panels to facilitate fuel transfer within the wings to achieve range requirements. The weep holes have now proven to be a source of fatigue cracks, especially in the more highly stressed areas of the lower wing panels.

As part of the C-141 design service life testing program, a structurally complete airframe with fuselage, wings, pylon and vertical stabilizer was tested. In 1977, some cracks were found in the weep holes. An initial inspection survey of four fleet aircraft found no cracks. In 1979, inspection of service aircraft was recommended at 21,000 hours followed by repeat inspections at 4,000 hour intervals. No cracks were found in the fleet at that time.

When additional cracks were found in 25 weep holes around wing station 77 of the fatigue test article in 1981, it was decided to coldwork the holes on the test wing using a sleeveless mandrel-only technique proposed by the Lockheed-Georgia Company. In 1983, Lockheed recommended coldwork of weep holes in the fleet aircraft at 30,000 flight hours. However, there remains a question as to the effectiveness of the program and its implementation since weep hole cracking has now been identified as a fleet wide problem.

As part of a program to further extend the service life of the C-141B fleet, the C-141 Management Directorate at Warner Robins Air Logistic Center (WR-ALC) has begun a program of oversize reaming and coldworking using the original Lockheed mandrel-only process. This method of coldworking, which expands the weep hole by up to 2.6 percent of its diameter, should theoretically extend fatigue life if no cracks remain in the reamed oversized hole. However, the effectiveness of the technique on holes, particularly with undetected cracks remaining, has never been tested.

This paper describes testing of coupons, machined from actual C-141B lower wing panels, to develop crack growth rates for weep holes coldworked in accordance with the current mandrel-only rework procedure. Similar crack growth data were also obtained for an alternative split sleeve cold expansion procedure developed by Fatigue Technology, Inc. (FTI) of Seattle, Washington. This alternative approach provides for higher expansion of the hole with an increase in the residual compressive stress zone. The tests were carried out at the FTI Materials Testing Facility in accordance with a WR-ALC statement of work [1].

WEEP HOLE COLDWORKING METHODS

The term "coldworking" usually applies to processes that improve strength and performance by cold-work hardening. This is not to be confused with the mechanism of expansion generally associated with coldworking of holes. Hole coldworking, or more preferably hole cold expansion, improves performance by pre-stressing the material adjacent to the hole. Usually, this type of process involves radially expanding the hole beyond the elastic limit of the material.

Sleeveless or Mandrel-Only Process

The sleeveless or mandrel-only process which is currently used in the C-141B weep holes uses a tapered mandrel to expand the hole. The oversized tapered mandrel is drawn or driven through the lubricated hole with an interference level such that the hole is expanded up to 2.6 percent of the hole diameter. A schematic of the mandrel-only process is shown in Figure 1. This technique does, however, suffer the following limitations:

- requires two sided access to the hole
- requires operator to lubricate both mandrel and hole using liquid lubricant
- seizing of mandrel and galling of hole can occur if lubrication is improperly applied
- has limited interference on the basis of lubrication and galling limitations
- requires a close-tolerance starting hole because of limited interference

After mandrel-only coldworking, the holes require extensive deburring to remove the large surface upset on the side the mandrel exits the weep hole. The surface upset results from the high frictional and contact forces between the mandrel and the hole, causing an axial plastic flow of material toward the mandrel exit side.

High Interference Split Sleeve Cold Expansion

The alternative split sleeve cold expansion process uses a solid-film pre-lubricated split sleeve that allows a one-sided limited-access operation at a considerably higher applied expansion level. It is therefore free from the limitations of the mandrel-only process described earlier. The tapered mandrel used with the split sleeve method has a large diameter sized to just pass through the starting hole. The split sleeve is fitted to the small diameter of the mandrel and then the mandrel/sleeve combination is placed in the hole. The sleeve is restrained in the hole by a nosecap assembly while the mandrel is pulled through the hole as shown in Figure 2. The lubricated sleeve protects the hole from damage and allows the tapered mandrel to radially expand and yield the material around the hole in a repeatable, controlled manner. Applied expansions for typical fastener hole diameters range from 3 to 6 percent.

The interference of the mandrel results in plastic yielding within a large diameter zone around the hole. After the mandrel passes through, the elastic material surrounding

the plastic zone forces the material within the zone into a compressive state. The depth and magnitude of the residual compressive tangential, or hoop, stress is proportional to the amount of applied expansion. For sleeve cold expansion, this zone typically extends up to one diameter around the hole.

A comparison of predicted hoop stress distributions around mandrel-only and sleeve cold expanded weep holes is shown in Figure 3. The mandrel-only process leaves considerably less compressive pre-stress around the hole. The stress distribution predictions were generated using an FTI proprietary elastic-plastic computer analysis program [2].

The greatest difference between the mandrel-only process and the sleeve cold expansion is the level of applied expansion. As shown in Figure 4, the resultant fatigue life improvement for the low interference mandrel-only process is much less and has a wide band of results for typical aluminum alloys. Sleeve cold expansion, on the other hand, produces consistently higher fatigue lives with a tighter variance. Small differences in tool wear and starting hole dimensions have a large impact on the effectiveness of these processes, particularly with the mandrel-only technique. Optimum fatigue performance is obtained using the high interference split sleeve cold expansion method.

The effectiveness of split sleeve cold expansion in extending fatigue and crack growth lives of open and filled fastener holes is well documented [3,4]. Typical life improvement factors are greater than 3 to 1. Of particular interest to the C-141B weep hole program was the ability of the split sleeve cold expansion process to arrest growth of pre-existing cracks under normal service loads. This effect was investigated under the WR-ALC sponsored test program which is discussed next.

TEST PROGRAM

The objective of the test program was to generate spectrum crack growth data for cracks emanating from weep holes in various conditions: no coldwork, mandrel-only (sleeveless) coldwork, and split-sleeve cold expansion.

Load Spectrum

The load spectrum was a modified flight-by-flight spectrum originally produced using Air Force provided software. Each spectrum pass contained 376,370 endpoints representing 3,027 flight hours. The peak gross stresses were 17.89 ksi (tension) and 14.93 ksi (compression). Spectrum endpoint occurrence and exceedence data are shown in Figure 5.

Test Specimens

WR-ALC prepared a total of 13 test specimens from existing wing panel structure from a tear-down aircraft. The end fittings, designed and manufactured by WR-ALC, were

intended to introduce a significant amount of tension into the riser with minimal bending.

Baseline Specimens

Three baseline specimens with no coldworking were used to establish baseline crack growth data. One of these specimens was strain gaged to verify that the specimens introduced loads into the riser in a manner consistent with aircraft wing structure loads. These specimens were precracked on the test frame.

Mandrel-Only Specimens

All weep holes in specimens designated for rework were processed using the same starting reamer, with a nominal diameter of 0.281 inches as specified in the current rework procedure. The mandrel-only coldwork specimens were processed at WR-ALC using the method described earlier in the paper. The holes were not reamed after processing.

Split Sleeve Cold Expansion Specimens

The weep holes were reamed to the same starting hole diameter that was used in the mandrel-only process. Split sleeve cold expansion was performed at FTI using tooling specifically designed for the weep holes. This special restricted-access tooling will permit split sleeve cold expansion of the risers in the actual aircraft structure, as shown in Figure 6. The holes in the test specimens were not reamed after processing.

Test Results

Baseline Specimens

The baseline specimens were precracked under constant amplitude loading to a 0.050-inch quarter circular flaw in the weep hole, running perpendicular to the riser edge. The crack growth rate tests were conducted under spectrum load conditions. Crack lengths were measured on each specimen at the end of every spectrum pass using a digital traveling microscope (DTM). On two of the specimens this was continued until the crack length was approximately half the riser height, about 0.450 inches from the edge of the hole.

In general, the cracks were placed on the riser side of the hole, except in one of the specimens, where a crack was intentionally oriented toward the skin. This specimen was used to investigate the effectiveness of the PRI Instrumentation Magneto-Optic Eddy Current Imaging (MOI) system for detecting, from outside the wing, cracks advancing toward the skin from the weep holes. Figure 7 shows the good degree of correlation attained between the flaw sizes estimated from MOI indications and the crack lengths measured with the DTM. The MOI technique successfully monitored crack growth through the riser until it became visible on the surface.

Coldworked Specimens

All specimens were cyclically tested until the crack was approximately half the riser height or until run-out was reached, at 45,000 equivalent flight hours. Crack lengths were measured using a DTM at the end of each spectrum pass.

The overall results are presented in Figure 8. For comparable initial crack lengths, the split-sleeve cold expanded holes met or exceeded the lives of the mandrel-only and non-coldworked specimens, as illustrated in Figure 9. Both mandrel-only coldworking and split sleeve cold expansion met the required 15,000 hour life goal after rework. However, the split sleeve cold expansion process was shown to meet this goal with cracks as large as 0.180 inches. For cracks of 0.144 inches or less, split sleeve cold expansion virtually arrested further crack growth during testing. The non-coldworked specimens showed crack growth rates consistent with those observed with in-service aircraft.

In general, for small cracks, the eddy current inspection measurements made before rework correlated well with the DTM measurements (allowing for the increase in diameter resulting from rework). However, for large cracks, there were significant discrepancies (Figure 10), which in some cases, were unconservative. This Figure shows that there is some uncertainty associated with measurement of pre-existing weep hole cracks using the present eddy current non-destructive inspection technique.

CONCLUSIONS

The non-coldworked baseline crack growth lives were comparable to recorded service life data. This would tend to confirm that the modified spectrum loading and configuration of the test specimen were reasonable representations of actual lower wing panel service conditions.

Crack growth life data for the mandrel-only and split sleeve cold expansion processes were also consistent with generally anticipated values. Mandrel-only coldworking of the weep holes with existing cracks of up to 0.064 inches, was successful in generating additional fatigue life when compared to equivalent flaw-size non-coldworked specimens. An acceptable maximum flaw-size for cracks emanating from the weep holes was not defined.

The split sleeve cold expansion process virtually contained any further crack growth on the specimens with initial flaw sizes up to 0.144 inches. The results clearly show that this process would achieve the required 15,000 hour additional life from the weep holes, even in the presence of large undetected flaws (up to 0.180 inches) prior to hole cold expansion. Furthermore, the quality controls inherent in the process ensure repeatability of results and optimization of process performance.

Acknowledgment

The authors would like to acknowledge the support given by WR-ALC/TIEDD personnel, and also the Fatigue Technology, Inc. personnel who completed the test program and tooling development and also assisted in preparing this paper and presentation material.

- [1] Warner Robins Air Logistics Center (WR-ALC/TIEDD), Statement of Work for contract No. F09603-93-C-1075, Aug. 1993.
- [2] Rufin, A.C., "Two-Dimensional Analysis of Cold Expansion Stresses and Strains Using the FTISTRS Version 2.1 Computer Program." FTI Report 37738, July 1993.
- [3] Phillips, J. L., "Sleeve Coldworking Fastener Holes", Vol. 1, Air Force Materials Laboratory Report AFML-TR-74-10.
- [4] Tiffany, C. F., Stewart, R. P., Moore, T. K., "Fatigue and Stress Corrosion Test of Selected Fastener/Hole Processes", Aeronautical Systems Division Report ASD-TR-72-111, January 1973.

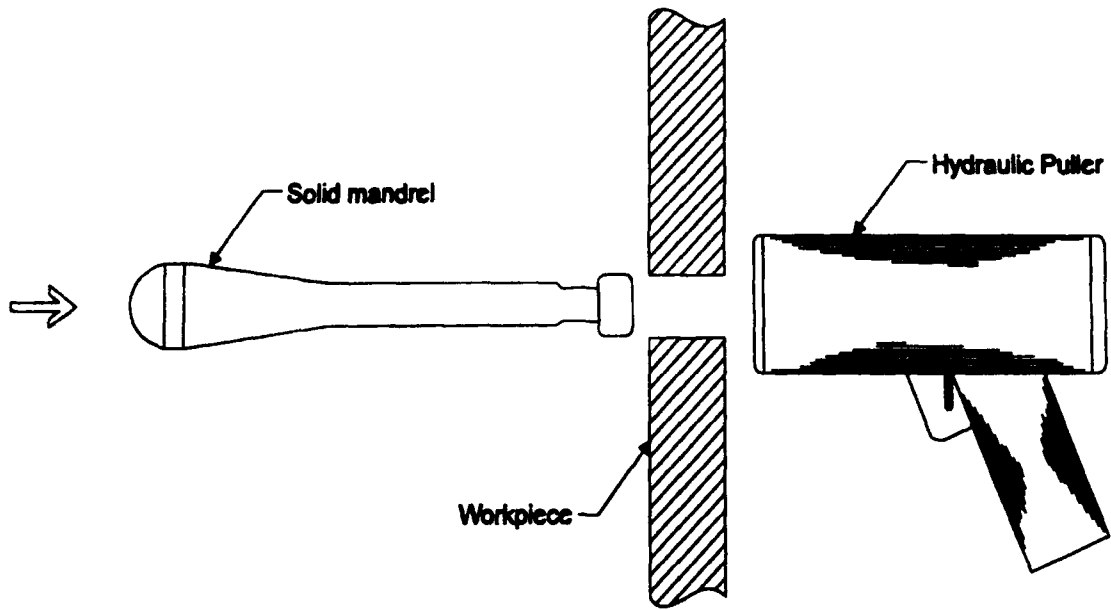


FIGURE 1

Schematic of Sleeveless Mandrel-Only Process

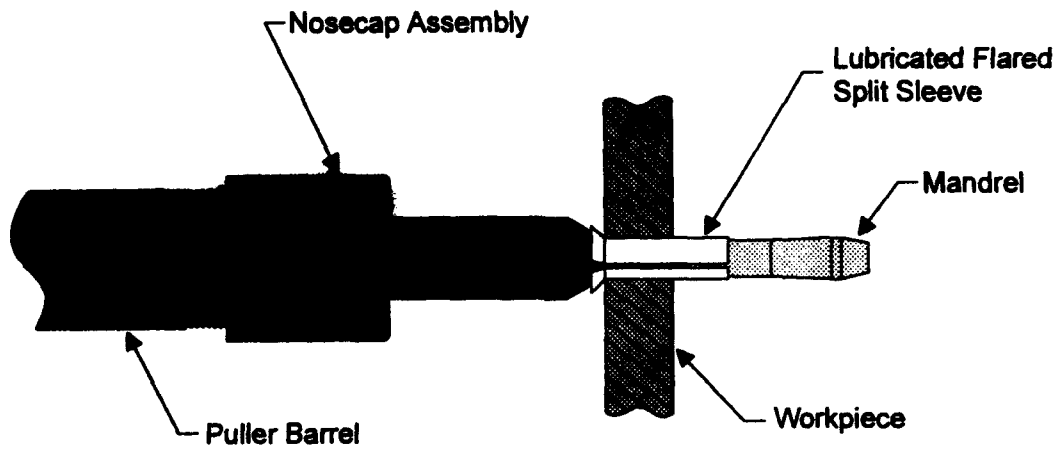


FIGURE 2

FTI's Split Sleeve Cold Expansion Process

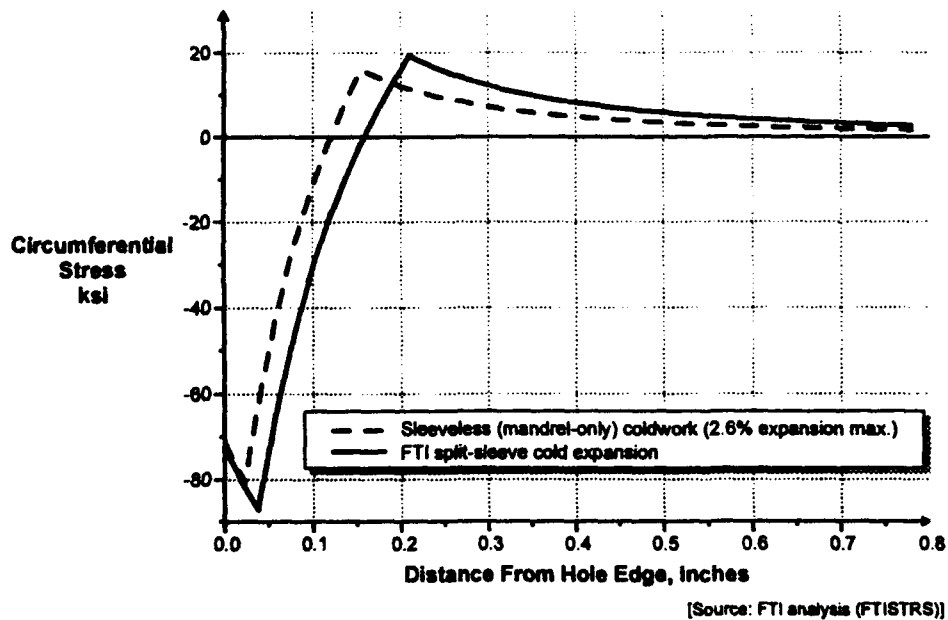


FIGURE 3

Effect of Applied Expansion Fatigue Life Improvement

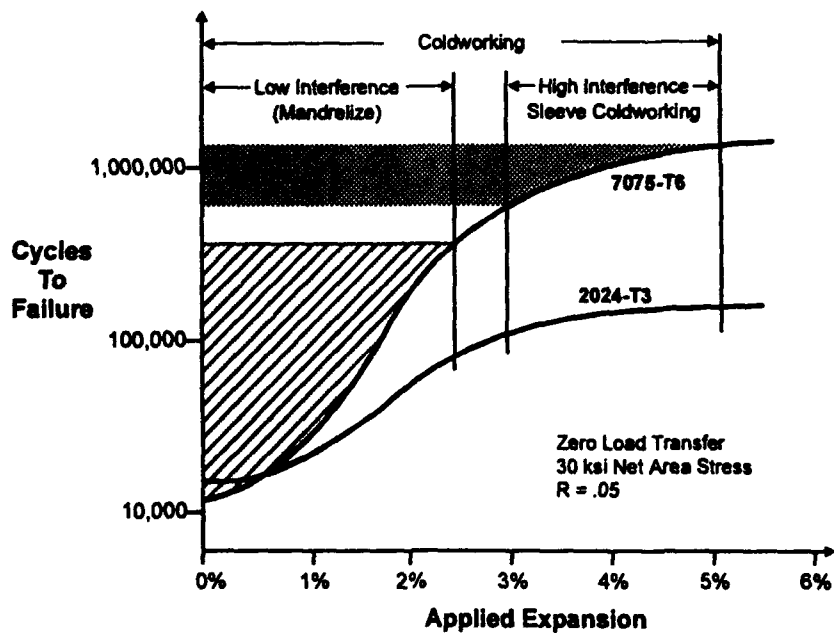


FIGURE 4

Residual Stress Distribution for Two Methods of Hole Cold Expansion, C-141B Weep Holes

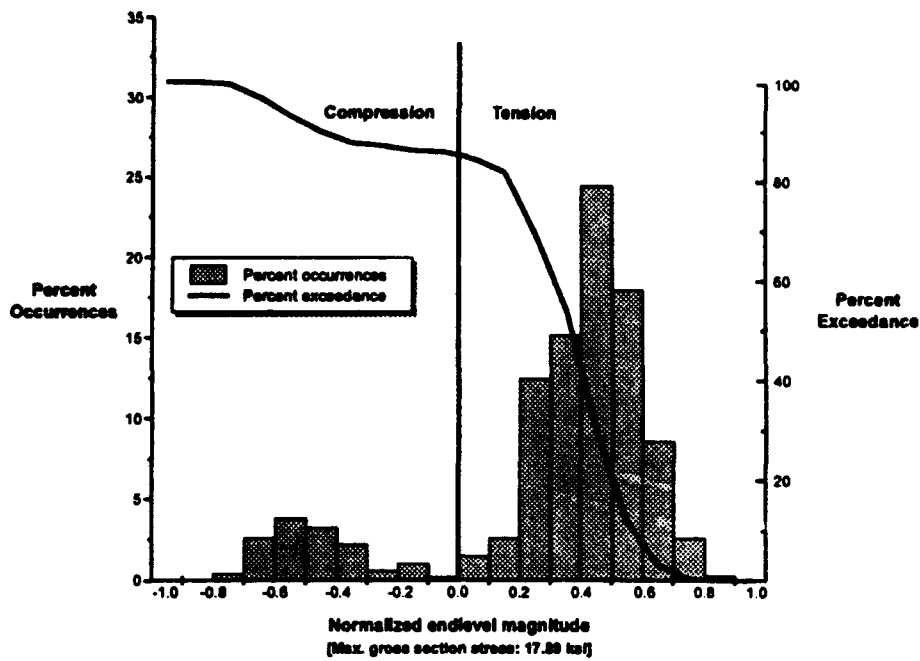


FIGURE 5

Modified USAF C-141B Flight-by-Flight Load Spectrum Statistics

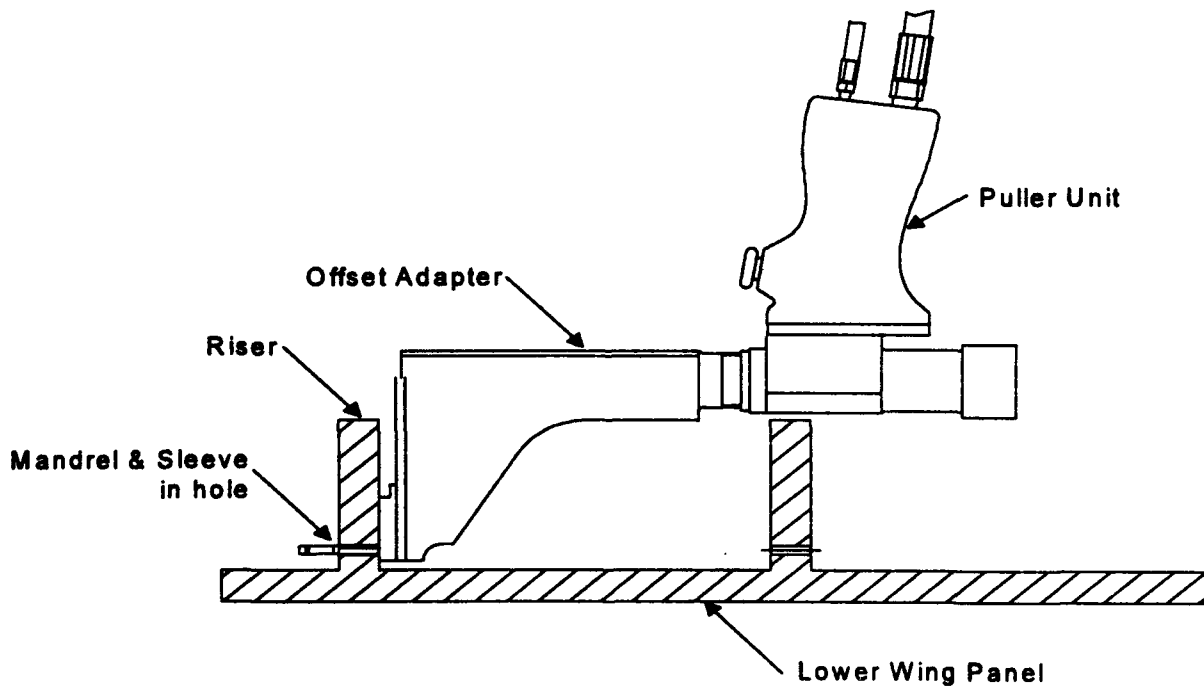


FIGURE 6

Tooling for Split Sleeve Cold Expansion of Weep Holes

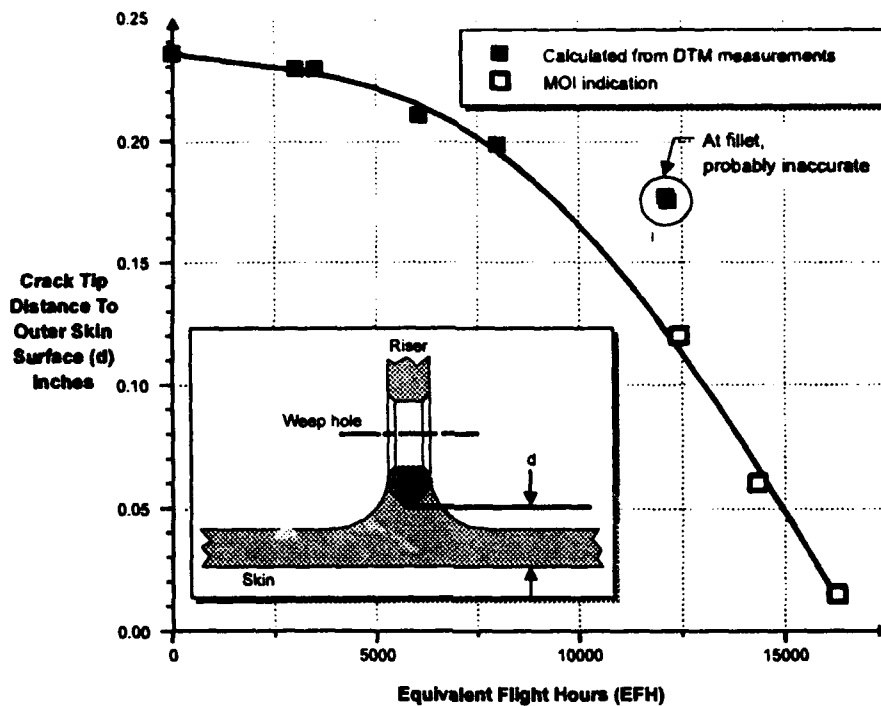


FIGURE 7

Magneto-Optic Inspection Measurements of Weep Hole Crack Growth
(Non-Coldworked Specimen)

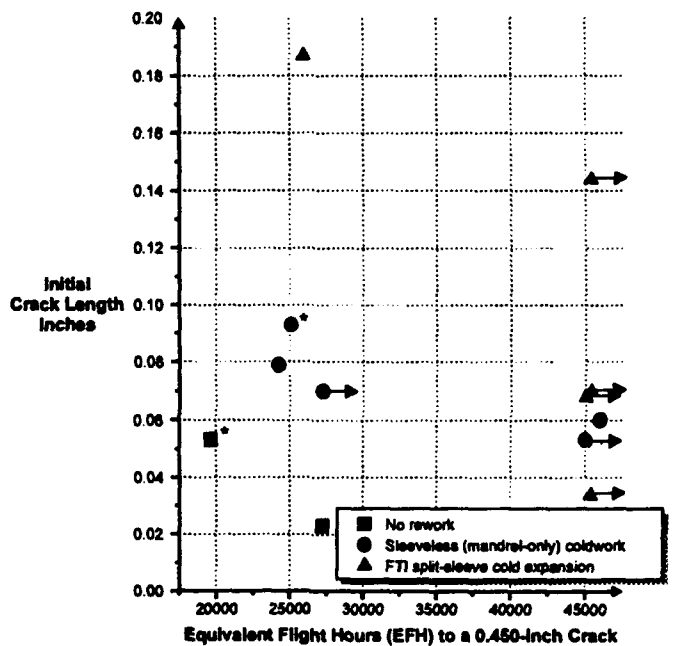


FIGURE 8

Summary of Total Crack Growth Lives

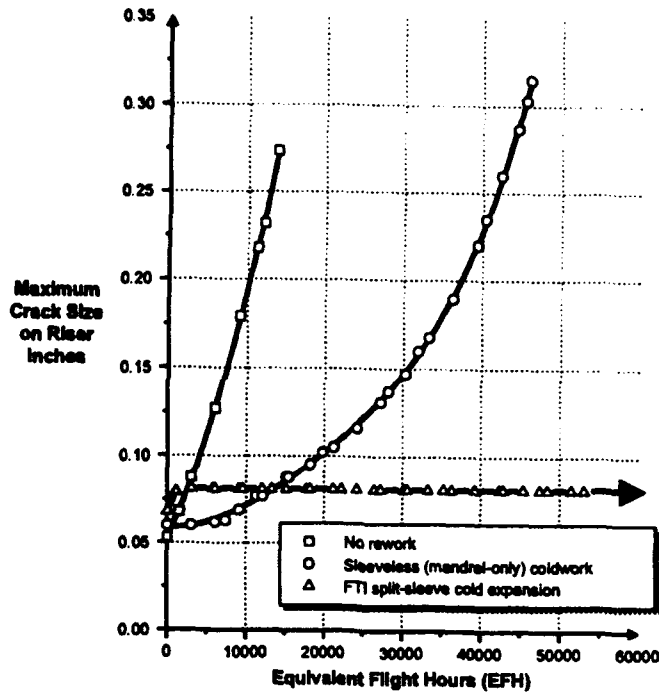


FIGURE 9

Typical Crack Growth Data

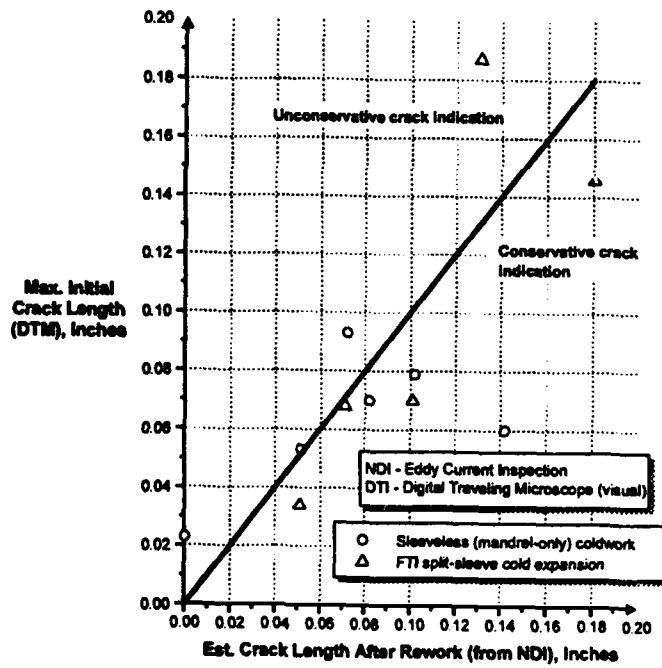


FIGURE 10

Eddy Current Crack Size Correlation to Visual Measurements

Split Mandrel Coldworking: A Manufacturing Solution for Automating a Critical Process

Geoffrey A. Rodman
West Coast Industries, Inc.
Seattle, Washington 98133

Matthew Creager
Structural Integrity Engineering
Chatsworth, California 91311

ABSTRACT—With an increasing requirement for automating manufacturing processes, the aerospace industry is closely examining automated processes for coldworking fastener holes in metal structures. One such system, an automated sleeveless coldworking system, is now being utilized in a robotics environment at Bristol Aerospace on their F-5 wing manufacture/re-manufacture repair programs and will have direct influence upon other new manufacture of metal structures which require the coldworking of a significant number of holes in an automated environment. The conclusions presented in this paper quantify the benefits (fatigue enhancement and cost savings) of automating a sleeveless coldworking system.

Introduction

Early processes used to coldwork fastener holes, such as mandrelizing, etc., were limited in the amount of applied expansion (E_a) induced into the hole. The lower level of E_a achieved, resulted in a lowered level of retained expansion (E_r), and produced levels of life improvement somewhat less than required. With the development of the split sleeve process [1-3], higher E_a levels (and the corresponding higher E_r levels) were achieved resulting in a tremendous increase in fatigue life over the levels previously achieved. While the split sleeve system provided the needed life improvement the aerospace community required, there was a downside. The requirement for a disposable split sleeve presented problems in attempts to minimize processing time, not to mention the high cost of a tool that is disposable after one use. In the early 1980's, Boeing's (BCA's) Materials Research & Development group

worked to develop a system which would indeed lower their perishable tooling costs while making the coldworking process much simpler to implement.

As sometimes occurs with any newly developing technology, the fatigue life benefits obtained during the developmental phase were somewhat disappointing. In 1983, an evaluation [6] was performed which compared the split sleeve process with the new sleeveless system, using an early developmental mandrel. The results of this program concluded that the sleeveless system, though cost effective, provided somewhat less fatigue life improvement (Figure 1) than that provided by the sleeve system. It was thought that "the higher retained expansion found in the holes coldworked with the sleeveless system may have been due to plastic flow into the mandrel slots" [6]. It is important to note that this test pro-



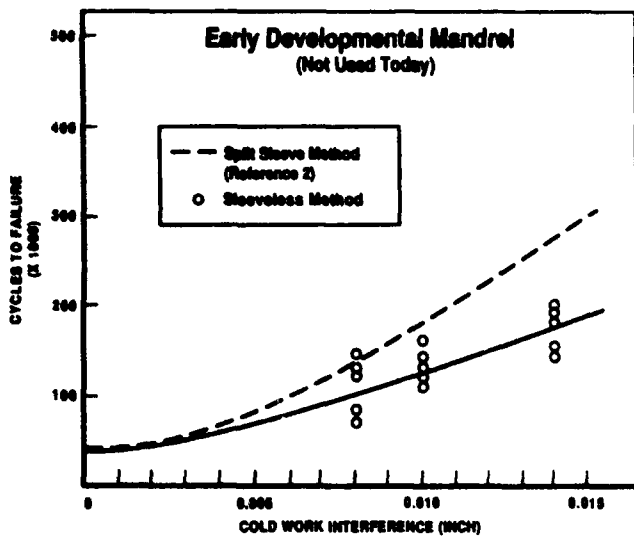


Figure 1—Test Results Using a Developmental Mandrel [6]

gram was conducted using tooling that was developmental, since the final tool configuration was not established until later. Despite the early disappointments, Boeing was able to eventually resolve the problems, with the results of their work becoming the sleeveless “split mandrel” system [4-5].

Process Description

The West Coast Industries’ patented split mandrel process utilizes a collapsible mandrel (Figure 2) with a sliding pilot shaft extending through the mandrel which serves to solidify the mandrel prior to coldworking a hole. With the pilot retracted, the mandrel becomes collapsible allowing insertion into the hole. The puller unit is then actuated, extending the pilot to solidify the mandrel, pulling the mandrel through the hole (Figure 3). Boelube, a Boeing developed lubricant, is used to lower the frictional forces resulting from the mandrel sliding against the hole during the coldworking process. The proper

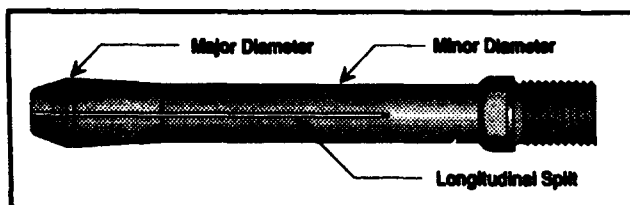


Figure 2—Split Mandrel

amount of lubrication (approximately one drop) is automatically applied to the mandrel after each cycle as it re-extends. As with other coldworking processes, the resulting fatigue life improvement is due to the introduction of a beneficial residual compressive stress.

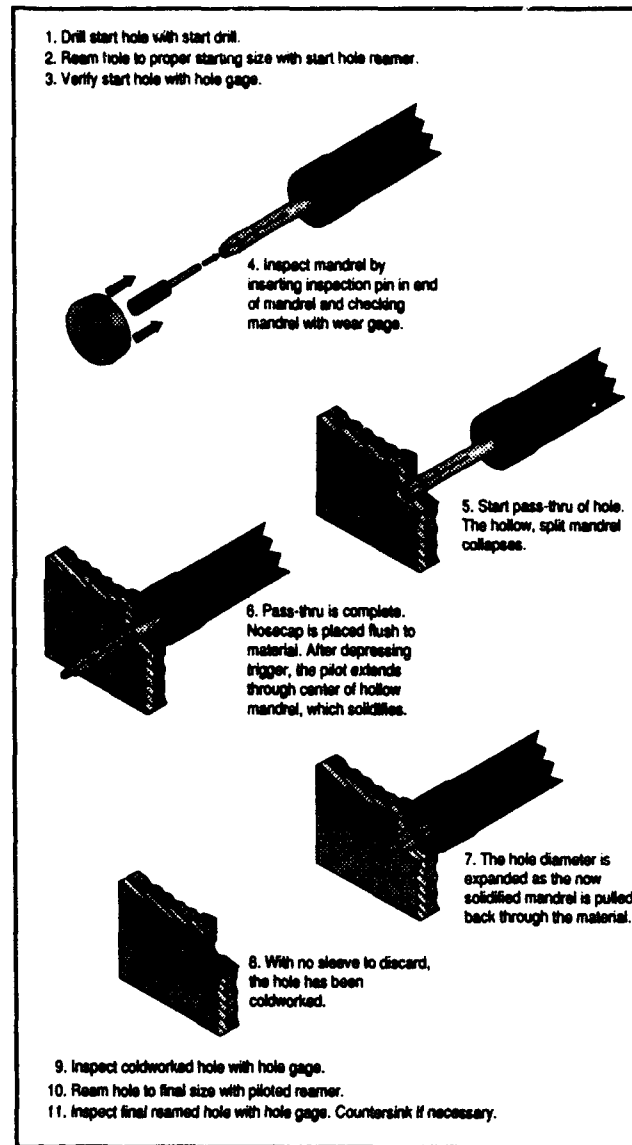


Figure 3—Split Mandrel Process Description

Test Program

In order to quantify the benefits of the Split Mandrel coldworking process (SpM) and facilitate a comparison of the benefits gained relative to the Split Sleeve process (SpSI), a series of fatigue tests for both split sleeve and split mandrel coldworked holes were performed. All tests were conducted under cyclic load control, with a gross stress level (σ_{max}) of 30 ksi at a stress ratio (R) of 0.1. The specimens (Figure 10, Page 9) were manufactured from 7075-T651 aluminum plate that was double disk ground to a material thickness of 0.250" with a surface finish of 63 rms. Four distinct hole sizes and corresponding tool sets were examined (Table I), with half of the specimens being coldworked at the specification maximum applied expansion level and half were coldworked at the specification minimum applied expansion level [2-5]. Non-coldworked specimens (NCw) were also tested for each hole size in order to provide a baseline reference. Additionally, a series of specimens were tested at various gross stress levels (S/N curve—Table II), in order to ascertain the fatigue life gain, for each of the processes, under various loading conditions.

Results and Discussion

Prior to performing an analysis of the collected data, it was decided that applied expansion values (E_a) are not the appropriate measure of what has been done to the metal around the hole, since the tooling absorbs some of the applied load during the coldworking process. This could be different for the various types of coldworking. For example, the split sleeve experiences a great deal of deformation during the coldworking process, rendering it unusable after working one hole. In addition to the deformation experienced by the split sleeve, mandrels (from either process) experience some deformation as well. It was concluded that the retained expansion value would indeed be a more accurate measure of what work has been performed on a hole. In either coldworking process, any desired retained expansion (E_r) level can be achieved by choosing an appropriate level of applied expansion. It should be noted, that the relationship between E_a and E_r could be different for each of the coldworking processes as well as various materials. In Figure 4, E_r vs. E_a is plotted for all of the coldworked specimens. The plotted data show that for the material, thickness, and sys-

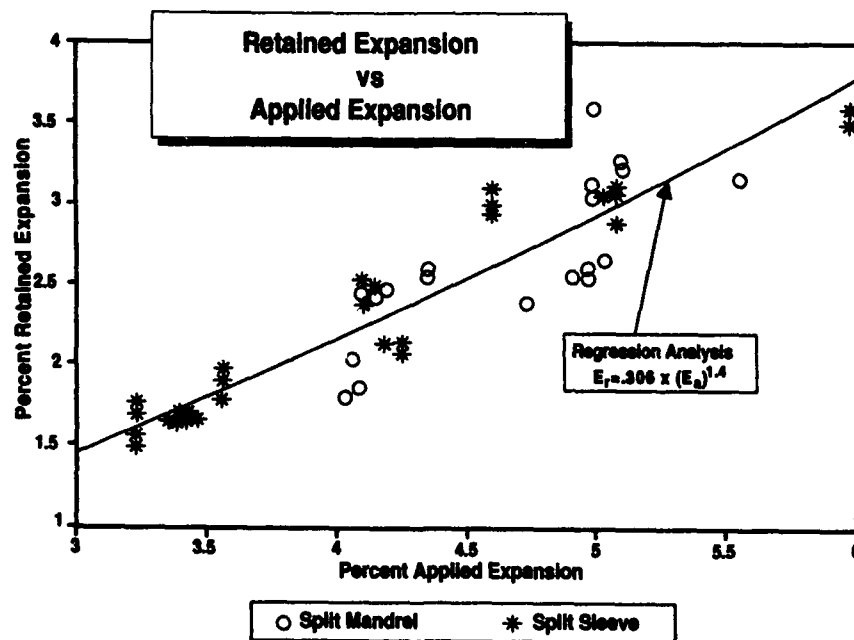


Figure 4—Retained vs Applied Expansion

tems tested, no significant difference existed in the relationship between E_r and E_n , for the two processes. Nevertheless, in order to assure a minimum of bias in the data analysis, all of the data analysis is based on the use of E_r as the coldwork parameter.

All of the data (Figure 5) clearly reflect the trends of longer fatigue life with increased retained expansion, and higher fatigue life for the split mandrel process, at corresponding values of retained expansion. The data further demonstrates that both coldwork processes consistently produce significantly longer

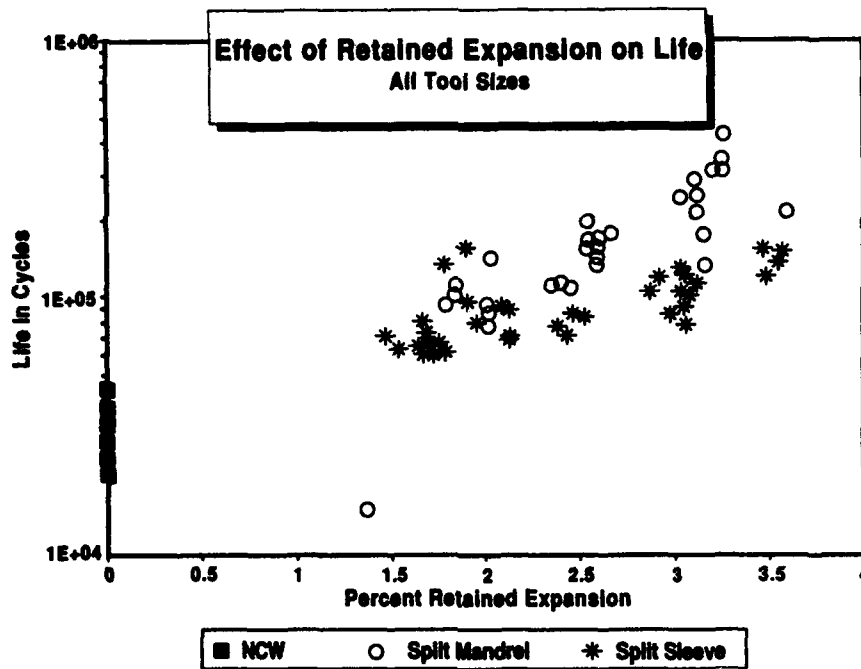


Figure 5—Effect of Retained Expansion

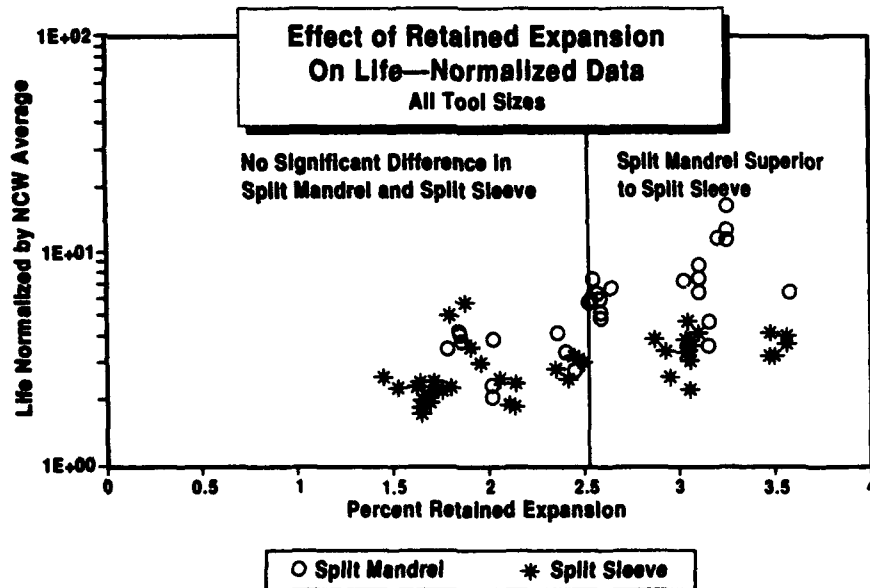


Figure 6—Normalized Data—Effect of Retained Expansion

lives than the non-coldworked (NCW) baseline specimens. It is useful to normalize the coldworked specimen life data by the average NCW life data at the corresponding hole diameter (Figure 6), which decreases any effect of hole size on observed data trends. Note that above a retained expansion level

of approximately 2.5%, that there is a clear discernible increase in life due to split mandrel coldworking over that due to split sleeve coldworking. Below 2.5% retained expansion that trend is not as clear. The effect is most probably present below 2.5% E_r , but is likely obscured by the basic scatter in fatigue

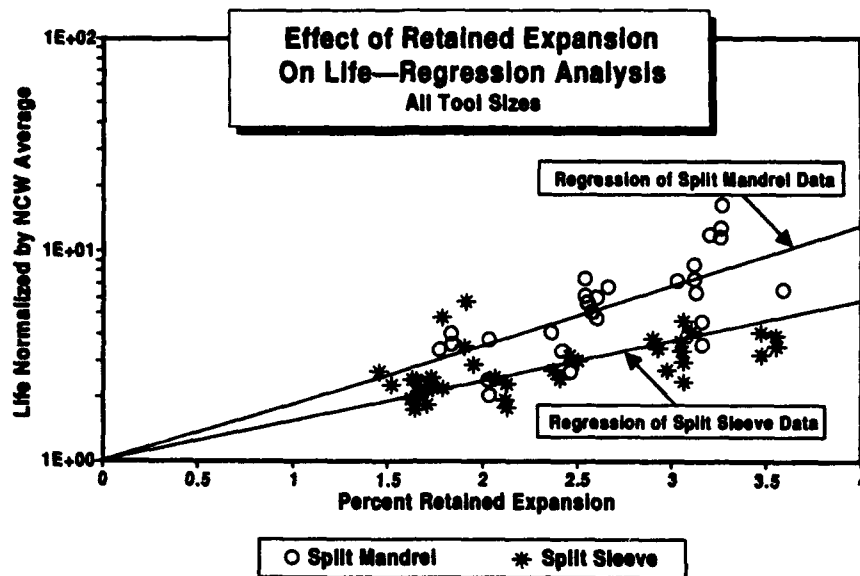


Figure 7—Regression Analysis—Effect of Retained Expansion

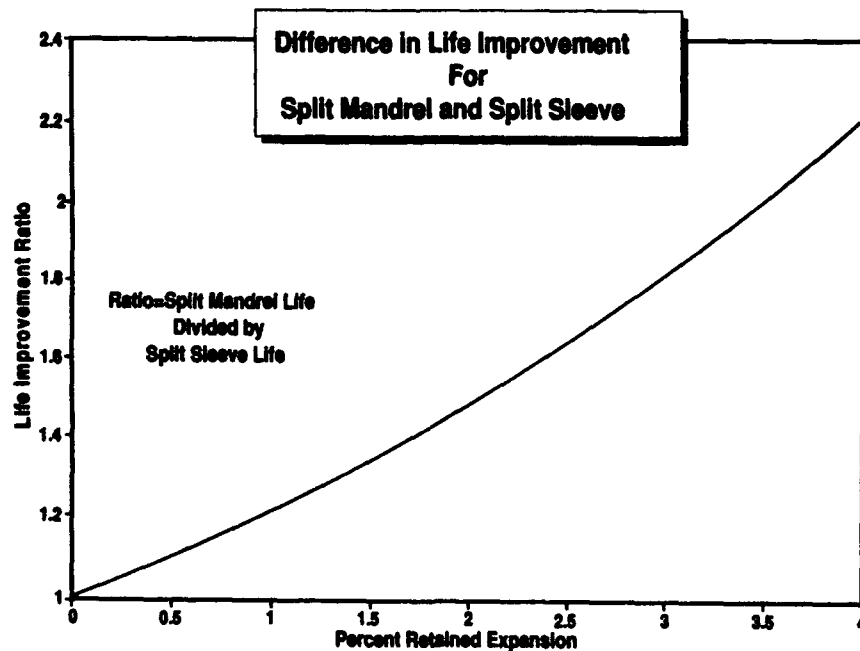


Figure 8—Life Improvement Differences Between the Split Mandrel and Split Sleeve

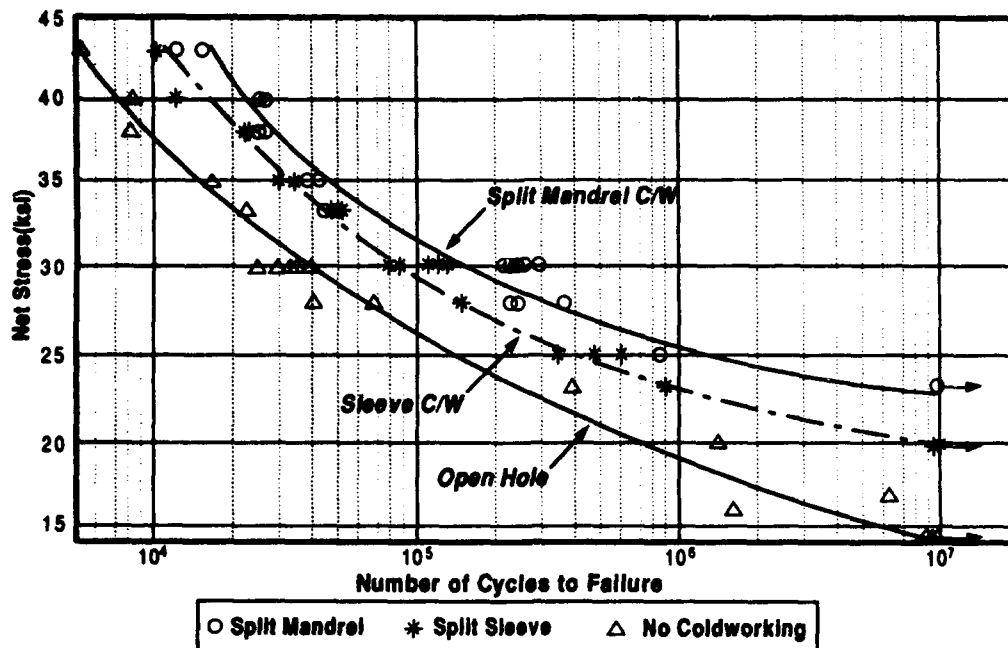


Figure 9—S/N Curves for 0.250 Inch Hole Diameter

data at low levels of E_r where the difference in the two processes is smaller. (Note: As the amount of E_r approaches zero, the effect of coldworking and the difference between any two coldworking processes must also approach zero.)

Figure 7 replots the data from figure 6 with linear regression lines (log life versus retained expansion) for the split mandrel and split sleeve coldworked processes. This allows quantification of the life improvement differences between the two coldworking processes (Figure 8).

At the start of the test program, it was expected that comparable retained expansion levels would result in comparable levels of life improvement. The increased efficacy of the split mandrel process as compared to the split sleeve process is surprising and is currently unexplainable. Until significantly more comparative data are generated, it would be prudent not to extrapolate this result to other geometries and alloys.

Additional tests were run at stress levels above and below 30 ksi for 0.250 inch diameter holes with the applied expansion levels at or near the maximum specification values. The test results are presented in Table II at the end of the paper. Figure 9 shows this test data and the corresponding data at 30 ksi along with regression analysis curves for the three data sets. Note that the increased effectiveness of the split mandrel as compared to the split sleeve process is observable at all stress levels for this test data.

Manufacturing Considerations

Once the fatigue enhancement questions have been sufficiently answered, the aerospace industry can turn to other areas of major interest. Boeing Commercial Aircraft Company has been using the split mandrel system in production since 1983. It is used in non-automated production, and was developed for an automated environment such as the new ASAT (Automated Spar Assembly Tool) machine for the manufacture of the new 777 wing. Bristol Aerospace has recently begun the manufacture of improved wing sets for the F-5 using automated split mandrel coldworking in order to respond to the fatigue problems found on such hardware systems.

The reason for interest in this system is one of simple economics. Both companies investigated the automation of the sleeve process, but found it impractical, and/or cost prohibitive, mainly due to the deceptively simple task of selecting, orienting, placing and removing the disposable sleeve in an automated environment.

The unit cost was another economic consideration driving the selection of the split mandrel system. The cost of coldworking a hole using the split sleeve system varies from 0.50¢ to \$17.00, depending upon sleeve size, length, etc. In deleting the sleeve cost, the split mandrel system will coldwork a hole at 0.05¢ per hole, without the burden of expensive supporting capital equipment. The only difference in the capital equipment between either process is the automatic lubricator utilized in the split mandrel system. Therefore, the capital equipment costs are virtually the same for either system. Additional cost savings are realized by cutting the amount of processing time required for each hole, taking roughly four seconds for a robot, or operator, to move from one hole to the next. With the split sleeve process, there is the additional processing time required for installing and disposing of the split sleeve (multiplying the time by a factor of 3).

Conclusions

The resulting test data collected in this research program readily support the conclusion that both the split sleeve and split mandrel coldworking processes do increase the fatigue life of holes significantly. The data also demonstrate (deemed valid only for this material and range of hole diameters) that the level of retained expansion can be related to the applied expansion through a simple single expression.

For equal levels of retained and applied expansion (due to the above noted relationship), fatigue life is extended significantly more by the Split Mandrel process than by the Split Sleeve process. In recognizing this fact of fatigue life improvement gain, many aerospace organizations are turning to the split mandrel system as a manufacturing solution to high perishable tooling costs and high manufacturing costs related to time consuming manufacturing steps.

References

1. J.L. Phillips, "Sleeve Coldworking of Fastener Holes," *AFML-TR-74-10, Vol. 1*, Air Force Materials Laboratory, Wright-Patterson AFB, February 1974.
2. "Sleeve Cold Working of Holes in Aluminum Structure," *BAC 5973*, Boeing Aircraft Co., Process Specification, 1975.
3. "Split Sleeve Coldworking—Holes (Aluminum, Steel & Titanium)," *Process Specification WCI-9201*, West Coast Industries, Inc., 1992.
4. "Mandrel Cold Working of Holes in Aluminum," *BAC 5768*, Boeing Aircraft Co., Process Specification, 1983.
5. "Split Mandrel Coldworking—Holes (Aluminum)," *Process Specification WCI-9202*, West Coast Industries, Inc., 1992.
6. M.W. Ozelton and T.G. Coyle, "Investigation of Fatigue Life Improvement By Cold Working Of Holes In Aircraft Materials," *NOR 83-191*, Northrop Corporation, 1983.
7. "Standard Practice for Conducting Constant Amplitude Axial Fatigue Tests of Metallic Materials," *ASTM E466-82, Vol. 03.01, Metals—Mechanical Testing*, 1982.
8. "Standard Practice for Statistical Analysis of Linear or Linearized Stress-Life (S/N) and Strain-Life (ϵ -N) Fatigue Data," *ASTM E739-91, Vol. 03.01, Metals—Mechanical Testing*, 1991.
9. G.A. Rodman and M. Creager, "Split Mandrel vs Split Sleeve Coldworking: A Comparison of Two Manufacturing Processes," *Laboratory Technical Report, LTR-9308*, West Coast Industries, 1993.

Table I [9]

5/32" Finished Hole Diameter						1/4" Finished Hole Diameter					
(NCw)						(NCw)					
AA001	31,219	30.02	0.1563	N/A	N/A	CC001	40,878	30.03	0.2504	N/A	N/A
AA002	27,934	30.02	0.1562	N/A	N/A	CC002	38,841	30.03	0.2505	N/A	N/A
AA003	34,528	30.02	0.1563	N/A	N/A	CC003	30,819	30.03	0.2505	N/A	N/A
AA004	31,082	30.02	0.1562	N/A	N/A	CC004	33,542	30.03	0.2505	N/A	N/A
AA005	36,727	30.03	0.1563	N/A	N/A	CC005	25,025	30.04	0.2510	N/A	N/A
(SpM Cw Min)						(SpM Cw Min)					
PP001	87,970	30.04	0.1562	2.027	4.054	II001	89883*	30.03	0.2503	2.453	4.188
PP002	77,884	30.03	0.1562	2.027	4.054	II002	113,965	30.03	0.2503	2.410	4.144
PP003	144,808	30.03	0.1563	2.027	4.054	II003	93,322	30.03	0.2502	2.452	4.144
PP004	92,189	30.04	0.1562	2.027	4.054	II004	21673*	30.03	0.2502	2.410	4.144
PP005	77,881	30.04	0.1563	2.027	4.054	II005	111,031	30.05	0.2503	2.453	4.188
(SpM Cw Max)						(SpM Cw Max)					
FF001	119,462	30.02	0.1562	2.056	5.552	JJ001	249,389	30.03	0.2505	3.026	4.987
FF002	140,063	30.02	0.1562	2.125	5.552	JJ002	219,589	30.03	0.2503	3.581	4.987
FF003	133,413	30.04	0.1562	3.153	5.552	JJ003	293,964	30.03	0.2504	3.112	4.987
FF004	176,917	30.27	0.1563	3.153	5.552	JJ004	221,081	30.03	0.2503	3.112	4.987
FF005	83,913	30.02	0.1562	3.018	5.624	JJ005	253,810	30.03	0.2503	3.112	4.987
(SpSI Cw Min)						(SpSI Cw Min)					
NN001	66,064	30.02	0.1562	1.985	4.107	SS001	66,909	30.04	0.2503	1.681	3.447
NN002	91,831	30.03	0.1563	2.055	4.247	SS002	72,203	30.04	0.2503	1.681	3.403
NN003	70,109	30.03	0.1563	2.123	4.247	SS003	80,223	30.04	0.2503	1.638	3.360
NN004	88,515	30.03	0.1562	2.122	4.175	SS004	65,926	30.03	0.2503	1.639	3.403
NN005	71,272	30.03	0.1562	2.122	4.175	SS005	60,185	30.03	0.2503	1.639	3.447
(SpSI Cw Max)						(SpSI Cw Max)					
DD001	120,886	30.03	0.1563	3.482	5.989	TT001	87,891	30.03	0.2504	2.975	4.590
DD002	155,863	30.04	0.1562	3.482	5.989	TT002	105,147	30.03	0.2504	3.060	4.590
DD003	140,162	30.03	0.1564	3.552	5.989	TT003	118,082	30.03	0.2504	2.932	4.590
DD004	188,103	30.03	0.1563	3.278	6.087	TT004	124,855	30.03	0.2504	3.060	4.590
DD005	151,218	30.03	0.1563	3.552	5.989	TT005	78,481	30.03	0.2504	3.060	4.590
3/16" Finished Hole Diameter						17/64" Finished Hole Size					
(NCw)						(NCw)					
GG001	20,341	30.03	0.1881	N/A	N/A	BB001	23,845	30.03	0.2657	N/A	N/A
GG002	34,837	30.03	0.1879	N/A	N/A	BB002	22,845	30.03	0.2658	N/A	N/A
GG003	24,212	30.03	0.1879	N/A	N/A	BB003	29,990	30.03	0.2658	N/A	N/A
GG004	33,343	30.03	0.1879	N/A	N/A	BB004	30,894	30.03	0.2657	N/A	N/A
GG005	20,203	30.03	0.1880	N/A	N/A	BB005	26,574	30.03	0.2658	N/A	N/A
(SpM Cw Min)						(SpM Cw Min)					
EE001	102,184	30.03	0.1880	1.847	4.085	KK001	139,581	30.04	0.2659	2.590	4.343
EE002	93,248	30.03	0.1880	1.790	4.027	KK002	134,888	30.03	0.2659	2.590	4.343
EE003	111,409	30.03	0.1880	1.847	4.085	KK003	188,880	30.03	0.2659	2.550	4.343
EE004	113,121	30.04	0.1880	1.847	4.085	KK004	140,598	30.03	0.2659	2.590	4.343
EE005	101,801	30.04	0.1880	1.847	4.085	KK005	187,410	30.04	0.2658	2.590	4.343
(SpSI Cw Max)						(SpSI Cw Max)					
HH001	199,866	30.07	0.1880	2.540	4.966	LL001	439,483	30.04	0.2659	3.250	5.096
HH002	163,515	30.03	0.1880	2.586	4.966	LL002	318172*	30.03	0.2659	3.250	5.096
HH003	112,854	30.03	0.1880	2.365	4.730	LL003	318,045	30.04	0.2659	3.250	5.096
HH004	182,079	30.05	0.1880	2.538	4.907	LL004	319,515	30.04	0.2659	3.210	5.096
HH005	181,087	30.03	0.1880	2.654	5.025	LL005	344,231	30.03	0.2659	3.250	5.096
(SpSI Cw Min)						(SpSI Cw Min)					
QQ001	80,227	30.03	0.1880	1.846	3.558	UU001	66,610	30.03	0.2659	1.655	3.231
QQ002	157,908	30.03	0.1880	1.890	3.558	UU002	60,562	30.04	0.2659	1.734	3.231
QQ003	60,857	30.04	0.1880	1.779	3.558	UU003	66,090	30.03	0.2659	1.734	3.231
QQ004	134,529	30.03	0.1880	1.779	3.558	UU004	62,475	30.04	0.2659	1.537	3.231
QQ005	96,476	30.03	0.1880	1.890	3.558	UU005	71,001	30.04	0.2659	1.458	3.231
(SpSI Cw Max)						(SpSI Cw Max)					
RR001	105,132	30.03	0.1880	3.046	5.076	VV001	87,778	30.03	0.2659	2.464	4.134
RR002	92,377	30.03	0.1880	3.046	5.076	VV002	89,152	30.03	0.2660	2.464	4.134
RR003	112,749	30.04	0.1880	3.102	5.076	VV003	76,497	30.03	0.2660	2.384	4.092
RR004	129,208	30.04	0.1880	3.044	5.017	VV004	70,870	30.03	0.2660	2.424	4.092
RR005	105,814	30.03	0.1880	2.876	5.076	VV005	86,063	30.03	0.2659	2.503	4.092

* Failed due to test frame error. Not used for analysis purposes

Table II [9]

Specimen #	Cycles To Failure	σ Max ksi
SpM Cw (Max)		
AB001	24,575	40.02
AB002	969,328	25.01
AB003	24,995	38.03
AB004	11,324	43.02
AB005	214,997	28.03
AB006	42,489	35.02
AB007	15,167	43.02
AB008	10,000,000	23.01
AB009	857,143	25.02
AB010	352,632	27.56
AB011	49,329	33.01
AB012	43,570	33.01
AB013	26,937	40.02
AB014	26,093	38.03
AB015	38,568	35.02
SpSI Cw (Max)		
AC001	340,355	25.02
AC002	33,279	35.02
AC003	30,187	35.02
AC004	489,432	25.02
AC005	10,000,000	20.02
AC006	900,712	23.03
AC007	10,000,000	20.16
AC008	39,268	33.01
AC009	12,782	40.2
AC010	43,027	33.01
AC011	21,982	38.02
AC012	140,154	28.03
AC013	540,320	25.02
AC014	22,468	38.02
AC015	10,314	43.02
NCw		
AD001	5,266	43.02
AD002	398,861	23.02
AD003	6,353,132	17.02
AD004	1,610,228	16.02
AD005	9,622,234	14.39
AD006	1,133,009	20.02
AD007	69,762	28.03
AD008	21,683	33.01
AD009	8,540	38.02
AD010	9,782,140	14.02
AD011	10,000,000	14.02
AD012	15,699	35.26
AD013	8,499	40.2
AD014	40,420	28.1
AD015	187,486	25.02

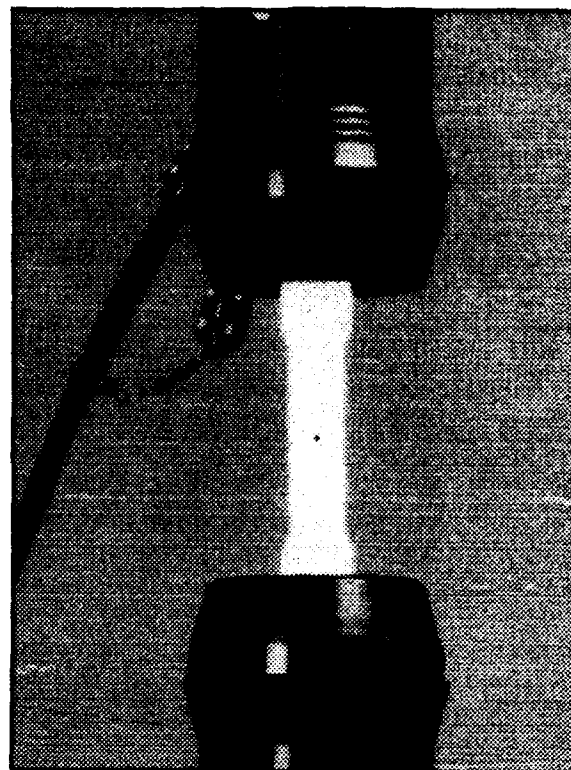


Figure 10—Test Specimen in Test Frame

Review of Boron/Epoxy Reinforcement of Aging Metallic Aircraft Structure

ABSTRACT

Boron, the original high strength fiber, in an epoxy matrix is a cost effective, high performance composite material for repair and structural enhancement of metallic aircraft components. Beginning with the F-111 wing pivot, it has been successfully used for over twenty years to reinforce steel, titanium and aluminum structure.

In comparison to current methodology, i.e. mechanical attachment of metallic reinforcement doublers, boron/epoxy reinforcements are:

- o Thinner and lighter due to the high specific strength and modulus of boron fiber.
- o More fatigue resistant with minimal stress risers because the reinforcement is fully adhered.
- o Effective at the crack tip because they are fully adhered, resulting in longer life extensions.
- o Conformable to complex contours and can be cured on the aircraft.
- o Tailorable for individual applications.
- o Inspectable using common techniques.

In addition, since boron is not conductive, there is no galvanic couple with metals, and since boron has a higher CTE than other high strength fibers it has better thermomechanical compatibility.

Currently boron/epoxy reinforcement technology is in development or implementation on many USAF planes, including the B-1, B-52, C-130, C-135, C-141, F-4, F-16 and F-111. The Australians have effectively used the technology for over fifteen years with thousands of reinforcements flying, and the Canadians are beginning to implement it on the F-5. In addition, the USAF currently has two PRAM programs to optimize the technology.

INTRODUCTION

Boron fiber, the original high strength fiber, was developed in the late 1960s and was first used to produce aircraft structural components in the early 1970s. Over 400,000 lbs have since been used to fabricate structural components for such aerospace applications as F-14, F-15, B-1, space shuttle and Black Hawk helicopters.

Beginning in 1971 with the F-111, Boron/Epoxy (B/E) has also been used as a bonded reinforcement for metallic aircraft structural

components. For the F-111 the B/E doubler was used to reinforce the D6AC steel wing pivot fitting after it failed catastrophically in a full-scale fatigue test. With few exceptions the reinforcement was applied to all F-111 aircraft. As of January, 1993 it "has been essentially trouble free in service."¹

Boron is not a yarn, like many high performance reinforcements, but a monofilament with a comparatively large diameter of 3,4 or 5.6 mils. It is produced by a chemical vapor deposition (CVD) of boron on a tungsten core (the tungsten is converted to borides of tungsten so it is no longer conductive).

BORON/EPOXY REINFORCEMENT TECHNOLOGY

The properties of Boron fiber and B/E composite materials are given in Table I. They have a unique combination of high tensile strength and modulus and very high compressive strength. In addition they have a relatively high CTE resulting in better thermomechanical compatibility with metals. A more extensive data base is available upon request.

To reinforce metallic structure B/E is bonded to the metal surface using a structural epoxy adhesive. Proper preparation of the metal surface (discussed below) is essential to proper and durable performance of bonded reinforcements. As such, B/E reinforcements have two (2) principal applications:

- o Repair of fatigued or corroded structure.
- o Structural enhancement of undamaged structure.

Numerous studies have shown that B/E reinforcements significantly increase the life of the underlying metal structure.²⁻¹¹ In many cases pre-existing cracks in the metal substrate do not continue to grow. For repair of corroded structure, the corrosion is removed, irregularities in the surface are filled in with epoxy and sufficient B/E is bonded to return the structure to its original strength. Structural enhancements, as in the case of the F-111 wing pivot fitting, delay or prevent the initiation of problems or increase the mechanical properties of undamaged structure.

Bonded B/E doublers is not new technology but rather a combination of existing technologies including; fracture mechanics, finite element analysis, composite design and processing, surface preparation of metals (including anodizing or the use of a coupling agent with aluminum), corrosion inhibiting primers and adhesive bonding. These technologies are combined to yield application specific designs and a general application process. Proper implementation requires training in the application process and precise process control during application.

An application process specification has been written by the USAF for C-141 applications and by the National Research Council of Canada¹² for F-5 applications (discussed below). A major U.S. aircraft

manufacturer is writing one for use on commercial aircraft under a Textron sponsored program. Training in the application process has been provided by Textron Specialty Materials and the Air Force Materials Lab.

Numerous studies^{2-11,13} have compared B/E reinforcement of metallic structure with existing technology, i.e. mechanically attached aluminum, titanium and steel doublers, and with Gr/E reinforcement. In virtually every application that has proceeded to flight evaluation B/E has been chosen. There are several reasons for this: In comparison to mechanically attached metal reinforcements B/E are thinner, lighter and more aerodynamic because of higher specific properties as shown in Table II. Simultaneous bonding and curing of B/E preforms (laid up and optionally B-staged in a lab) on a metal surface yield a fatigue resistant reinforcement with no fastener induced stress risers and exact conformation to surfaces with complex contours. Composite design procedures allow tailoring of mechanical properties to compensate for stresses in the metal. In comparison to Gr/E there is no galvanic couple and better thermo-mechanical compatibility with B/E. Finally eddy-current inspection techniques can be used right through B/E. (See below).

IMPLEMENTATION

As stated above proper implementation requires training in the application process and precise process control during application. The application process consists of three (3) steps: surface preparation, priming and adhesion (and optionally curing) of the doubler.

Surface preparation consists of removing all paints, primers and organic material, abraiding and anodizing or silane coupling of aluminum (acid etches have also been successfully employed). Grit blasting is the current preferred method for abrasion. Following abrasion any organic material (e.g. solvents, fingers) will contaminate the surface and destroy subsequent bonds. The USAF currently has a PRAM program at the materials lab at WPAFB^{15,16} to optimize silane coupling and phosphoric acid anodizing. They have chosen the PACS (Phosphoric-acid Anodizing Containment System) invented by Boeing for on aircraft anodizing of the repair area.

Current primers are solvent-based and contain chromate corrosion inhibitors. They are produced by adhesive companies to be compatible with specific structural adhesives. The WP/ML PRAM^{15,16} program is sponsoring the development of water-based corrosion inhibiting primers which do not contain chrome.

The adhesive and optionally the doubler are traditionally cured using a heating blanket. (The doubler can be precured in an autoclave for surfaces that are flat or for which a precise mold is available). Full vacuum is applied to remove volatiles during the heat-up ramp to the curing temperature. Curing is best accomplished at 15-18 in. Hg according to recent studies (results to be published).

Traditionally the epoxy matrix of the doubler and epoxy adhesive cure at 250°F for one (1) hour, however recent studies^{12, 13, 15} have shown equivalent cure at temperatures as low as 200°F for longer times. The B-52 Maintenance Engineering Office is sponsoring a program with Battelle through Boeing Military Aircraft to develop an ultrasonic curing process for the adhesive.¹⁷

Following cure the reinforcement is non-destructively tested (see below). It should then be sealed using, for example, a mil spec polysulfide sealant, primed and painted. Aluminum speed tape can be applied over the reinforcement before painting. Alternatively a protective cover ply of B/E or fiberglass could have been included during layup of the reinforcement.

Cost comparisons with mechanically attached metal doublers and component replacement have shown the bonded B/E reinforcement is no more expensive and can be considerably less expensive. The Australians claim to have saved millions of dollars using composite repairs.

NON-DESTRUCTIVE TESTING (NDI)

Traditional methods for crack detection can be used through B/E reinforcements to detect and measure cracks in the underlying metal. Studies at Textron Specialty Materials with eddy-current detection have resulted in the data in Figure III.¹⁸

The reinforcements and bondline should be checked for delaminations, voids or debonds using ultrasonic methods. A standard with known defects is required. Thermography and laser shearography can also be used for defect detection. Precured and B-staged reinforcements can be inspected ultrasonically for delaminations prior to adhesion.

BORON/EPOXY REINFORCEMENTS ON MILITARY AIRCRAFT

Table III lists current applications of B/E reinforcement of metallic structure on military aircraft. As discussed above, bonded reinforcement of the steel wing pivot of the F-111 was the first use of the technology. The technology was then picked up by the Australian Aeronautical Research Labs in the late 1970's, modified for use on aluminum surfaces and successfully employed for thousands of reinforcements.²⁻⁶

In the 1980's both the USAF ALC's at Warner Robins, Georgia and Oklahoma sponsored several programs to develop the technology. Lockheed developed reinforcements for the C-141 and C-130 for Warner Robins. 34 reinforcements in 16 different locations on the C-141 have been flying for up to 5 years. Tinker AFB has sponsored programs with Rockwell for the B-1, Boeing for the B-52 and E-Systems for the KC-135. In addition to the KC-135 E-Systems has applied demonstration doublers to a C-18 and over a crack on a C-130 landing gear door.

The B-1 and C-141 programs have begun fleetwide implementation of one repair each, at the 25° shoulder longeron and for weep holes in the integral wing stiffeners respectively. Crews have been specially trained in the application process at both locations.

Also in the 1980's the Canadian Air Force began a development effort for reinforcement of the upper wing skin golden triangle area of their F-5 trainer aircraft. This program too has progressed to the fleet implementation stage.

Recently the above mentioned PRAM program^{15,16} was initiated at the USAF materials labs at Wright Patterson AFB and a second PRAM program began at E-Systems. These programs will optimize and standardize the application process specification. New development programs have also been initiated at Kelly AFB for the T-38 and C-5 and at Hill AFB for the F-16 and F-4. The USAF has applied three (3) doublers over cracks emanating from the fuel vent hole in the lower wing skin of F-16's here and in the Netherlands.

APPLICATIONS OF B/E REPAIRS ON COMMERCIAL AIRCRAFT

Table IV lists the applications of B/E reinforcement to in-service commercial aircraft in the U.S., Australia, and Europe. These reinforcements are primarily "decals", in that the underlying structure is not damaged, to gain flight experience with commercial aircraft flight spectra. However, they generally carry about half of the load. The notable exceptions where doublers are repairing damaged structure are the Ansett 767 keel beam repair and the very thin doublers applied to Textron Lycoming steel engine cowlings on BAE aircraft that are now flying in the U.S. and Australia. The keel beam of the 767 was heavily corroded. The corrosion was removed and the beam was brought back to its original strength using a B/E doubler. This repair took 1.5 days as opposed to 20 days to replace the beam, the only alternative to B/E repair. The BAE 146 aircraft are approaching 2000h, in approximately 3000 flights over the past year, of problem-free service and a decision is imminent to implement the repair on all Lycoming ALF-502 engines.

Three of the doublers on the Federal Express 747-200F wing leading edges were applied over in-spec dents filled with epoxy resin. The doublers on these aircraft, shown in Figure II, were designed by a major U.S. airframe manufacturer and installed by Textron trained Federal Express composites technicians. All of these doublers are performing as intended.

A major U. S. airframe manufacturer is nearing completion of a Textron-funded program to collect the principal data necessary for design and approval of the use of B/E reinforcements on commercial aircraft. The data to be collected in this program are given in Table V. Included are 300 static ultimate and fatigue tension performance tests of B/E on precracked aluminum coupons. This program is also generating a detailed surface preparation and application specification. Results from this program will be available to the aerospace community in the Spring of 1994.

CONCLUSIONS

B/E composite reinforcement of metallic aircraft structure is a cost-effective technological advancement. Thousands of trouble-free reinforcements have been flying for over 20 years. The technology has been demonstrated to be thinner, lighter and more fatigue resistant than mechanically attached metal doublers in numerous programs.

REFERENCES

- 1) Sutherland, W. J. "Boron Reinforcement Modification of F-111 Wing Pivot Fittings, Status Report", Sacramento Air Logistics Center (1993)
- 2) Baker, A. A., "Fibre Composite Reinforcement of Cracked Aircraft Structure", ARL Tech. Memo Mat. 336 (1976)
- 3) Baker, A. A., "Boron Fiber Reinforced Plastic Patching for Cracked Aircraft Structures", Aircraft, pp. 30-35, (1981)
- 4) Davis, M.J., "Composite Repair for Metallic Structures: Understanding why Bonded Repairs are Better", 3rd Annual SAMPE Australian Symposium, Sydney (1990)
- 5) Baker, A. A., "Repair of Cracked or Defective Metallic Aircraft Components with Advanced Fibre Composites - An Overview of Australian work", Composite Structures 2, pp 153-181 (1984)
- 6) Baker, A. A. , "Fibre Composite Repair of Cracked Metallic Aircraft Components - Practical and Basic Aspects "Composites 18, pp. 293 - 308 (1987)
- 7) Sandow, F. A. and Cannon P. K., "Composite Repair of Cracked Aluminum Aircraft Structure", AFWAL-TR-87-3072, Air Force Wright Aeronautical Laboratories (1987)
- 8) Ong, C. L., and Shen, S., "Adhesive-Bonded Composite-Patching Repair of Cracked Aircraft Structure", 34th SAMPE Symposium, pp 1067 - 1078 (1989)
- 9) Kelly, L. G., "Composite Repair of Cracked Aluminum Structure", USAF Wright Aeronautical Laboratories, Aeronautical Systems Division (1987)
- 10) Bateman, G. R. and Zgela, M., "Composite Repairs to Metallic Structures: A Canadian Forces Experience", Canadian Aeronautics and Space Institute Sixth Symposium on Aerospace Structures and Materials (1992)
- 11) Bateman, G. R., "Composite Patch Repairs to Cracked Metal Sheets", Cranfield College of Aeronautics, MSC Thesis, (1990)
- 12) Raizenne, M. D., Heath, J. B. R, and Benak, T. J., "Processing Specification for CF-5 Upper Wing Skin Boron 5521/4 Fatigue Enhancement Doubler," National Research Council of Canada Report No. LTR-ST-1884 (1992)
- 13) Avery, S. S. , "Boron/Epoxy Repair of B-52 G/H Upper Wing Skin", Proceedings of the Second Workshop on Bonded Boron/Epoxy Reinforcement of Aging Military Aircraft Metallic Structure (1992)
- 14) Raizenne, M. D., Heath, J.B.R., and Benak, T, "TTCD PIP-4,

- Collaborative Test Program - Variable Amplitude Loading of Thin Metallic Materials Repaired with Composite Patches", National Research Council of Canada Report No. LTR - ST- 1662, (1992)
- 15) Mazza, J., Askins, R., Kubander, R., "Air Force Materials Lab/University of Dayton Research Institute PRAM Boron/Epoxy Repair and Structural Enhancement Program", Proceedings of the Third Workshop on Composite Repair of Metallic Aircraft Structures (1992)
 - 16) Mazza, J., "Overview of MLSE Sponsored PRAM Activities", Proceedings of the Second Workshop on Bonded Boron/Epoxy Reinforcement of Aging Military Aircraft Metallic Structure (1993)
 - 17) Senapati, N., Smith, S. and Moulder, R., "Ultrasonic Technique for Repair of Aircraft Structures with Bonded Composite Patches - Phase I - Proof of Concept" Battelle (1993)
 - 18) Shahood, T., "Detection of First Layer Cracks Beneath Boron/Epoxy Doublers", Textron Specialty Materials (1993)

TABLE I
PROPERTIES OF BORON FIBER AND BORON/EPOXY PREPREG

MATERIAL PROPERTY	BORON FIBER	5521 B/E 250 F CURE		5505 B/E 350 F CURE	
		R.T.	250 F	R.T.	350 F
Tensile Strength (ksi)	520	220	210	230	210
Tensile Modulus (ksi)	58	30	30	30	30
Compressive Strength (ksi)	1000	425	181	425	181
Compressive Modulus (msi)		30	30	30	30
Flex Strength (ksi)		260	250	300	265
Flex Modulus (msi)		28	25	28	25
Interlaminar Shear (ksi)		14.1	8.0	15.6	2.5
Coef. of Thermal Expansion (PPM/°F)	2.5	2.5	2.5	2.5	2.5
Density (lbm/in ³)	0.093	0.072	0.072	0.072	0.072

TABLE II
COMPARISON OF SPECIFIC TENSILE PROPERTIES

<u>MATERIAL</u>	<u>SPECIFIC STRENGTH</u> (IN)	<u>SPECIFIC MODULUS</u> (IN)
ALUMINUM	750	100
STEEL	640	110
TITANIUM	900	110
BORON/EPOXY	3060	420

TABLE III

BONDED B/E REINFORCEMENT OF METALLIC STRUCTURE ON MILITARY AIRCRAFT

<u>STATUS</u>	<u>AIRCRAFT</u>	<u>LOCATION</u>	<u>CONTRACTOR</u>	<u>APPLICATOR</u>	<u>APPLICATION DATES</u>
Fleet Implementation	F-111	Lower Wing Pivot	<u>USAF</u> G.D.	G.D./USAF	1970's
	B-1	Dorsal Longeron	Rockwell	Rockwell	'83--'86
	C-141	Fuselage	Rockwell	Rockwell	'92--'93
		Wing Weep Holes	Lockheed	Lockheed, USAF, CTI, Chrysler	'90--'93
Flight Test	F-5	Upper Wing Skin	<u>CANADA</u> National Res. Council	Canadian AF	'92--'93
	F-111	Upper Wing Pivot	<u>AUSTRALIA</u> ARL		1980's--'93
	C-130	Fuselage	ARL		1980's--'93
	Mirage 111	Wing Stiffeners Wing & Stabilizer	ARL ARL		1980's--'93
Ground Test Design	F-15, F-4	Various	<u>ISRAEL</u>		
	C-141	16 locations, 34 Aircraft	Lockheed	Lockheed	'85--'92
	KC-135	Fuselage Beam	E-Systems	E-Systems	'91
	C-18	Various	E-Systems	E-Systems	'91
	C-130	Landing Gear Door	E-Systems	E-Systems	'92
	F-16	Lower Wing Skin	Lockheed	USAF	'92
	C-130	Wing Stringers	Lockheed	Lockheed	'90
	B-52	Upper Wing Skin	Boeing	Boeing	'93
	F-4	Lower Wing Skin	McDonnell Douglas		
	T-38	Frames	E-Systems		
C-5	6 Locations	Lockheed			

TABLE IV

Commercial Bonded Boron/Epoxy Doubler Installations

OWNER	INSTALLER	AIRCRAFT	INSTALLATION	NUMBER OF AIRCRAFT	DOUBLERS PER AIRCRAFT	DATE
FRANCE						
Air Inter	Dassault	Mercure	Door Frames	11	9	~1974
AUSTRALIA						
Ansett	ARL	767	Build-Up thickness of corroded keel beam lower chord	1	2	1989
Australian Airlines	ARL	727	"Decals" on fuselage lap joint	1	1	1989
Qantas	ARL	747	"Decals" at various locations	1	9	1990
Ansett	Textron Lycoming	BAE 146	Repair of engine cowl cracks	1	4	11/92
UNITED STATES						
Air Wisconsin	Textron Lycoming	BAE 146	Repair of engine cowl cracks (Ref. Chart #7)	1	4	11/92
Federal Express	Federal Express	747-200F	"Decals" at various locations (Ref. Charts #11 through #15)	2	12 13	1/93 3/93

TEXTRON

Specialty Materials

TABLE V

LABORATORY TEST PROGRAM ON BONDED/EPOXY DOUBLERS

OVERVIEW

- Conducted By A Large US Airframe Manufacturer
- Funded By Textron Specialty Materials
- Performance Period: October '92 through March '94

OBJECTIVE

- Obtain The Core Body Of Substrating Data Required For FAA Approval

KEY EFFORTS

1) MATERIALS SPECIFICATION TESTS (AMS Spec. #3867/4A)

- Physical
- Mechanical
- Chemical
- Bond Strength

2) INSTALLATION PROCESS SPECIFICATION

- Surface Preparation
- Anodize (PAA)
- Primer
- Adhesive
- Curing Procedure
- NDI Procedures & Reference Standards
- Sensitivity Effects Of Process Deviations

3) PERFORMANCE TESTS

- ~160 Static Tension
 - ~153 Tension-Tension Fatigue
 - } • Boron/Epoxy Doublers Bonded To
7075-T6 With Pre-Induced Cracks
- GOAL: 300,000 Cycles Each

4) FEM STRUCTURAL DESIGN ANALYSIS/GUIDELINES FOR BONDED BORON DOUBLERS

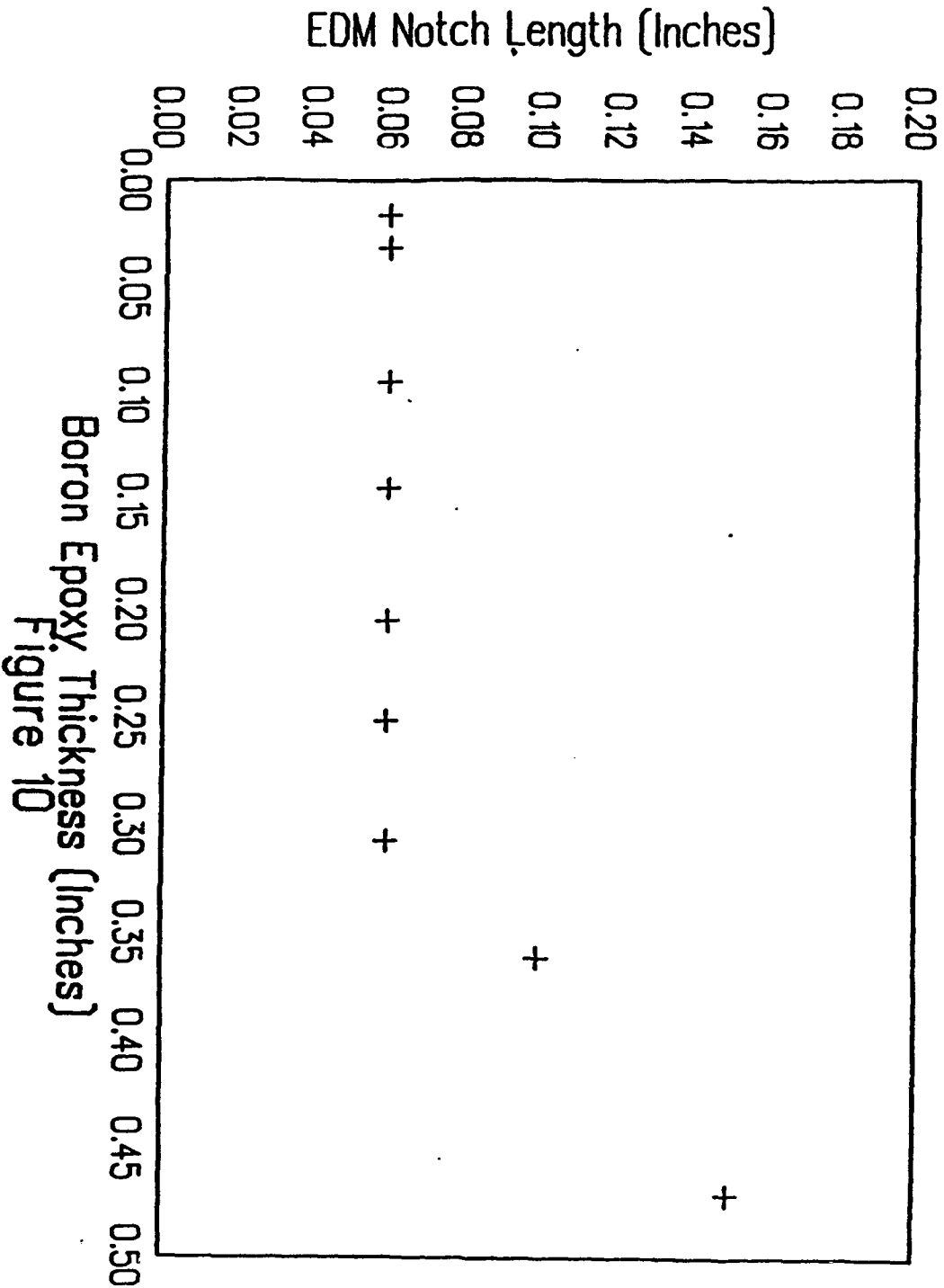
- Load Transfer
- Stress Concentrations
- Effects of Boundary Conditions (e.g. Underlying Ribs, etc.)
- Effects of Differential Coef. of Thermal Expansion (Aluminum vs. Boron/Epoxy)

TEXTRON

Specialty Materials

FIGURE III

MINIMUM NOTCH DETECTABILITY THROUGH BORON EPOXY



Boron Epoxy Thickness (Inches)
Figure 10

**AN INTEGRATED
DESIGN, FABRICATION, TESTING AND ANALYSIS
FOR THE
FATIGUE PERFORMANCE EVALUATION
OF
COMPOSITE PATCH REPAIRED
ALUMINUM AIRCRAFT STRUCTURE SAMPLES**

BY:

**T. P. SIVAM AND T. J. BEHRENS
CHRYSLER TECHNOLOGIES AIRBORNE SYSTEMS, INC.
WACO, TEXAS**

AND

**A. C. FAWCETT AND O. O. OCHOA
TEXAS A&M UNIVERSITY/VISTA ENGINEERING
COLLEGE STATION, TEXAS**

PRESENTED TO:

**1993 USAF STRUCTURAL INTEGRITY PROGRAM CONFERENCE
SAN ANTONIO, TEXAS
NOVEMBER 30 - DECEMBER 2, 1993**



WPMS607 -2

PRESENTATION OUTLINE

I TITLE

T. P. SIVAM - CTAS

II PROGRAM OVERVIEW

III TESTING AND ANALYSIS

A. C. FAWCETT - TAMU

IV CONCLUSION

OBJECTIVE(S)

- TO DEMONSTRATE AIRCRAFT REPAIRS THROUGH APPLICATION OF COMPOSITE PATCH REPAIR (CPR) TECHNIQUE AT CTAS IN AIRCRAFT MOD WORK
- TO DEMONSTRATE AIRCRAFT LIFE ENHANCEMENT OF "OLD" AIRCRAFT BY STRENGTHENING MOST CRITICALLY STRESSED STRUCTURAL PARTS THROUGH COMPOSITE PATCH ENHANCEMENT (CPE) TECHNIQUE
- TO DOCUMENT THE PROCESSES AND DESIGN GUIDELINES WITH SUPPORTING DATA AND ANALYSIS APPROACH FOR IMPLEMENTING THIS TECHNOLOGY WITHIN CTAS

BACKGROUND

- CHRYSLER TECHNOLOGIES AIRBORNE SYSTEMS, INC. (CTAS) MADE COMMITMENTS, IN THE FISCAL YEAR 1992, THROUGH AN IR&D PROGRAM (#1907) ON "COMPOSITE PATCH REPAIR", TO ESTABLISH THE ADVANCED COMPOSITE PATCH REPAIR TECHNOLOGY AT CTAS TO FACILITATE SYSTEM INTEGRATION AND MODIFICATION OF BOTH MILITARY AND COMMERCIAL AIRCRAFT, BECAUSE OF MANY ADVANTAGES OF COMPOSITE PATCH REPAIRS OVER THE CONVENTIONAL METAL REPAIRS.

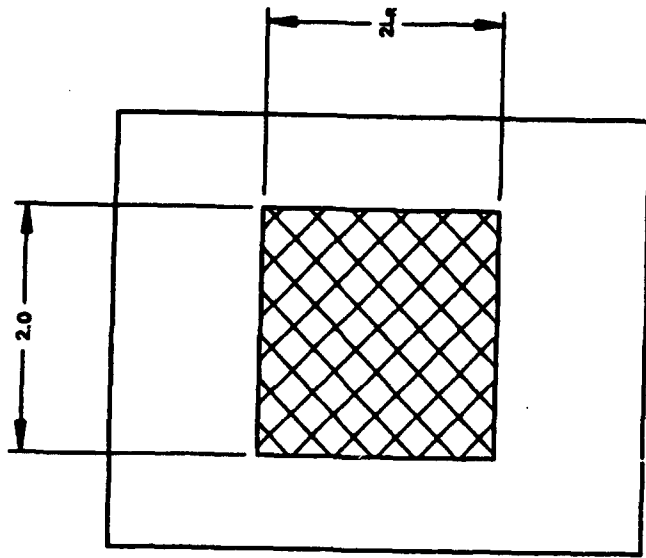
BACKGROUND - CONTINUED

PATCH DESIGN

- MINIMIZE ADHESIVE SHEAR STRESS

$$L_r = 6 \sqrt{\frac{T_a E_r T_r}{G_a (1+S)}}$$

$$S = E_r T_r / E_p T_p$$

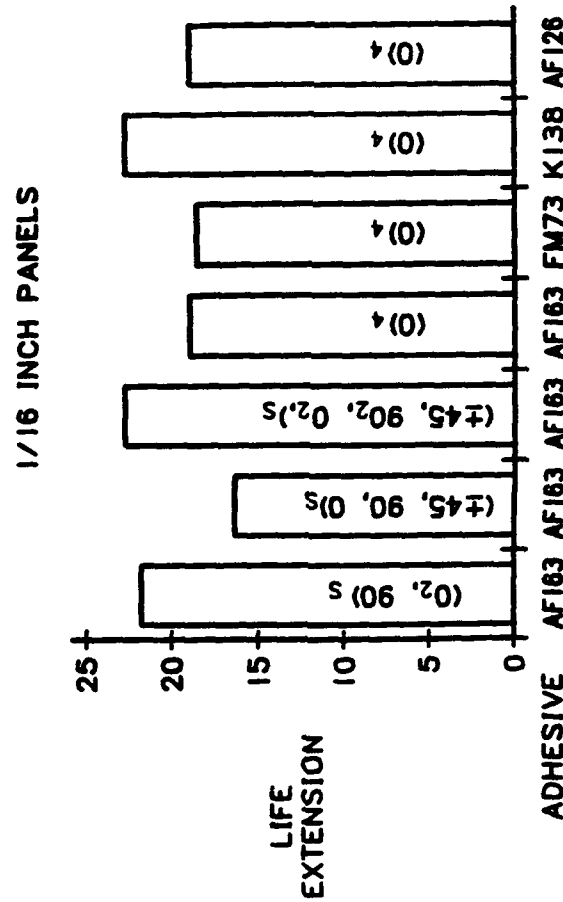
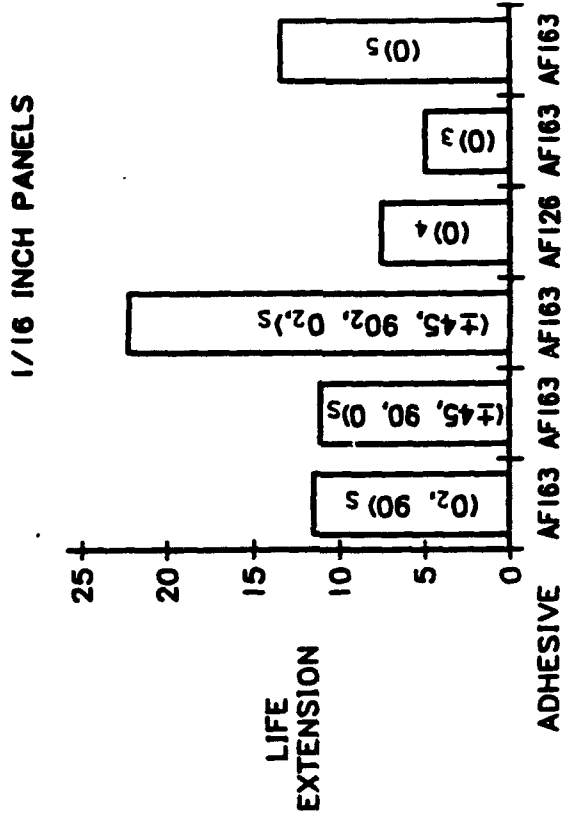


- ~ 2L_r ~ LENGTH OF PATCH
- ~ E_r ~ MODULUS OF THE SUBSTRATE SAMPLE
- ~ 2T_p ~ THICKNESS OF SUBSTRATE SAMPLE
- ~ E_r ~ MODULUS OF THE PATCH
- ~ T_r ~ THICKNESS OF THE PATCH
- ~ G_a ~ SHEAR MODULUS OF ADHESIVE
- ~ T_a ~ THICKNESS OF ADHESIVE



BACKGROUND - CONTINUED

PLY ORIENTATIONS



1/16-Inch-Thick Spectrum Tests

1/16-Inch-Thick Constant Amplitude Tests

Reference: Forest A. Sandow, and Raymond K. Cannon, "Composite Repair of Cracked Aluminum Alloy Aircraft Structure", AFWAL-TR-87-3072, September 1987.



CIAS APPROACH

- DOWN SELECTED 3-M SP-377 (GRAPHITE/EPOXY) AND TEXTRON 5521/4 (BORON/EPOXY) FOR PATCH REPAIR
- CONSTANT AMPLITUDE TESTING CONSISTED OF 15 SAMPLES (METHODOLOGY SAMPLES)
- SPECTRUM TESTING CONSISTED OF 12 SAMPLES (AIRCRAFT SAMPLES)
- PATCH DESIGN USED THE CONCEPT OF MINIMIZING SHEAR BETWEEN THE SUBSTRATE AND PATCH
- PLY ANGLES IN THE PATCH DESIGN CONSIDERED THREE DISTINCTLY DIFFERENT ORIENTATIONS
 1. QUASI-ISOTROPIC TYPE I DESIGN USING 0, 90 AND $\pm 45^\circ$ PLYS
 2. SPECIAL TYPE II DESIGN USING SPECIAL SET OF PLY ORIENTATIONS
 3. SPECIAL TYPE III DESIGN USING ANOTHER SET OF SPECIAL PLY ORIENTATIONS

ALL THREE (1, 2, AND 3) DESIGNS USED AS MANY AS 8, 12, AND 16 PLYS FOR THE PATCHES DEPENDING ON LOADS AND SUBSTRATE THICKNESSES

PATCH MATERIALS DIRECT AND INDIRECT

- 3-M SP-377 UNIDIRECTIONAL GRAPHITE/EPOXY SHEET
- TEXTRON 5521/4 UNIDIRECTIONAL BORON/EPOXY SHEET
- TYPE 120 GLASS FABRIC (BARRIER PLY)
- 3-M AF-163-2 (0.03 PSF) ADHESIVE
- 3-M EC-3960 ADHESIVE PRIMER
- 3-M 3911 DEGREASING PRIMER
- MEK, SANDPAPER, ALCOHOL, WIPING CLOTHS, ETC.

NOTE: 3-M SP-377 IS USER FRIENDLY

SUBSTRATE SURFACE PREPARATION

- CLEAN WITH MEK OR OTHER SUITABLE DEGREASER
- SAND WITH 180 OR 220 GRIT SILICON CARBIDE PAPER
- TREAT WITH 3-M 3911 DEGREASING PRIMER
- APPLY 3-M EC-3960 PRIMER
- CURE PRIMER AT ROOM TEMPERATURE FOR .5 HOUR AND AT 180°F FOR ONE HOUR
- KEEP EVERYTHING CLEAN. WIPE WITH ALCOHOL AS NEEDED

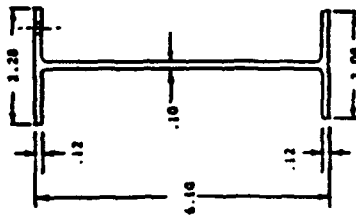
NOTE: 3-M 3911 PRIMER CONTAINS ORGANOSILANE

PATCH APPLICATION AND CURING

- APPLY ADHESIVE FILM 3-M TYPE AF-163-2
- USE GLASS FABRIC TYPE 120 (IF USING GRAPHITE/EPOXY PATCH)
- CURE GRAPHITE/EPOXY PATCHES AT 205°F FOR 3 HOURS
- CURE BORON/EPOXY (5521/4) PATCHES AT 205°F FOR 4 HOURS AND AT 250°F FOR ONE HOUR
- APPLY PATCH PLIES PER DESIGN AND FOLLOWING RECOMMENDED PROCEDURE FROM THE MANUFACTURER OF PREPREG

SAMPLE FABRICATION, TESTING AND ANALYSIS

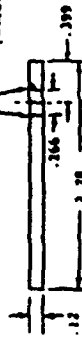
- CTAS DESIGNED AND FABRICATED ALL TEST SAMPLES
- ALL TESTING AND ANALYTICAL STUDIES WERE PERFORMED IN COLLABORATION WITH TEXAS A&M UNIVERSITY, COLLEGE STATION, TEXAS



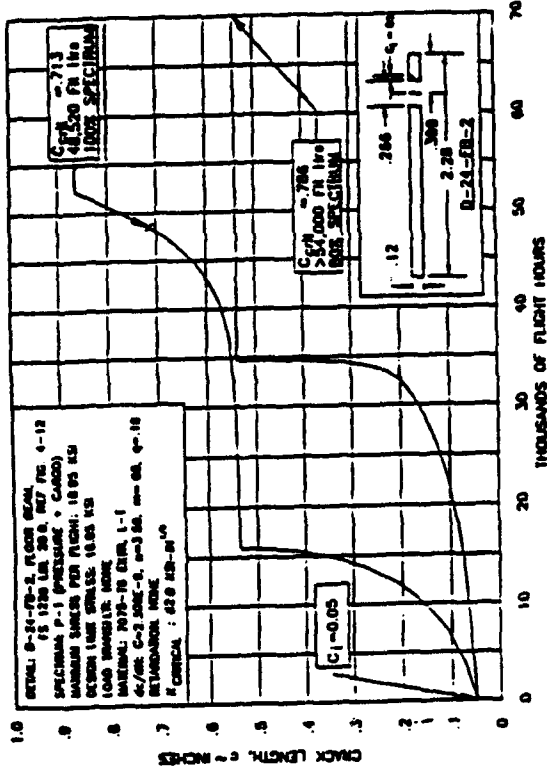
DETAIL D-24-FB-2
 MATERIAL 7075-T6 EXTRUSION
 $A = 1.1092 \text{ IN}^2$
 $\bar{y} = 3.1147 \text{ IN}$
 $I_{xx} = 6.3504 \text{ IN}^4$
 $I_{yy} = .2090 \text{ IN}^4$

FIGURE 4-13
 DETAIL D-24-FB-2 STRUCTURAL CONFIGURATION

.005 CONTINUING DAMAGE PLAN (CORNER)



SIMPLIFIED STRUCTURAL CONFIGURATION FOR ANALYSIS

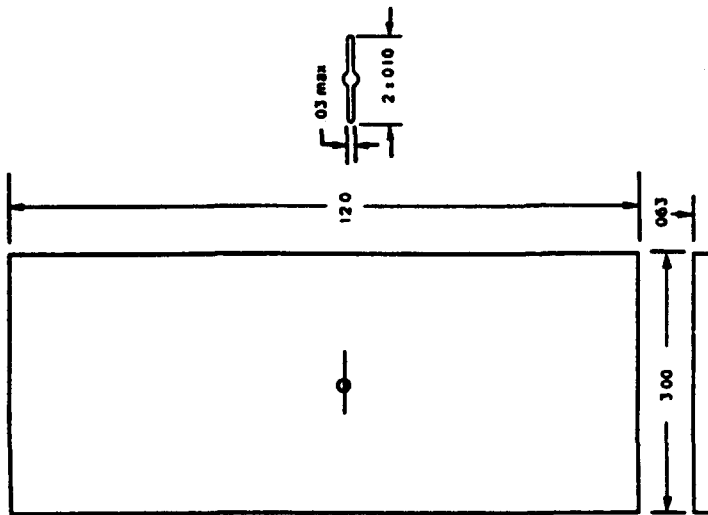


DETAIL D-24-FB-2, FLOOR BEAM
 IS 1270 LBS, REF FIG 4-12
 SPECIMEN P-1 (PRESSURE + CARDS)
 MAXIMUM STRESS PER FLIGHT: 18.95 KSI
 DESIGN LINE STRESS: 18.85 KSI
 LOAD WANDLER NONE
 MATERIAL: 7075-T6 EXTR. 1-1
 dc/da: C-2 JSMC-8, m=3.66, n=6.8, q=1.8
 RETARDATION NONE
 INITIAL CRACK: .020 IN-10

FIGURE 4-13
 CRACK GROWTH DIAGRAM, DETAIL D-24-FB-2

TYPICAL DETAIL AND DATA

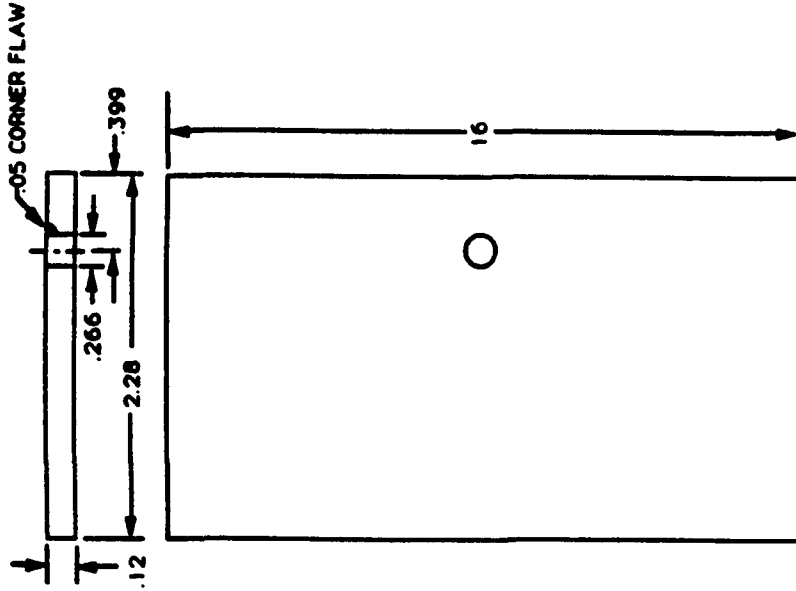
CENTER CRACK CLAD SHEET SPECIMENS



Sample ID:
 2S-CC-U-C
 2S-CC-B-C
 2S-CC-B-T
 7S-CC-U-C
 7S-CC-G-C
 7S-CC-G-T

R Value
 .4
 .4
 .4
 .7
 .7
 .7

**7075-T6 EXTRUSION, SINGLE STRAIGHT HOLE,
 CORNER FLAW SPECIMENS**

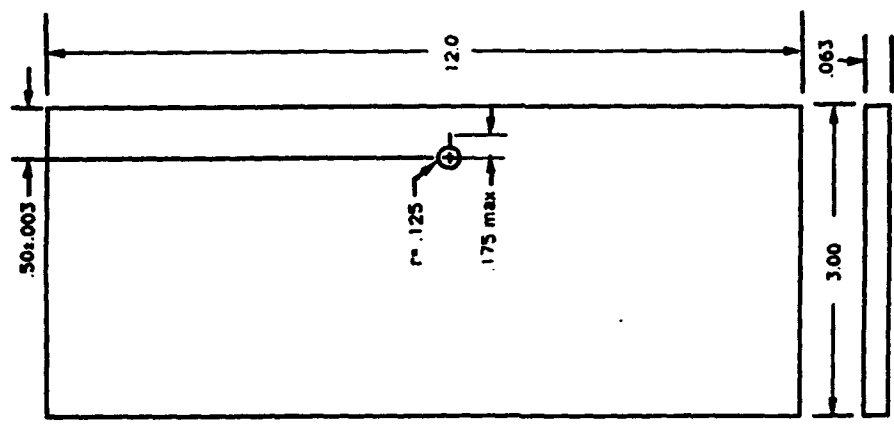


Sample ID:
 D-24-F3-2-BC3
 D-24-FB-2-GC3
 D-24-FB-2-BT4
 D-24-FB-2-GT4

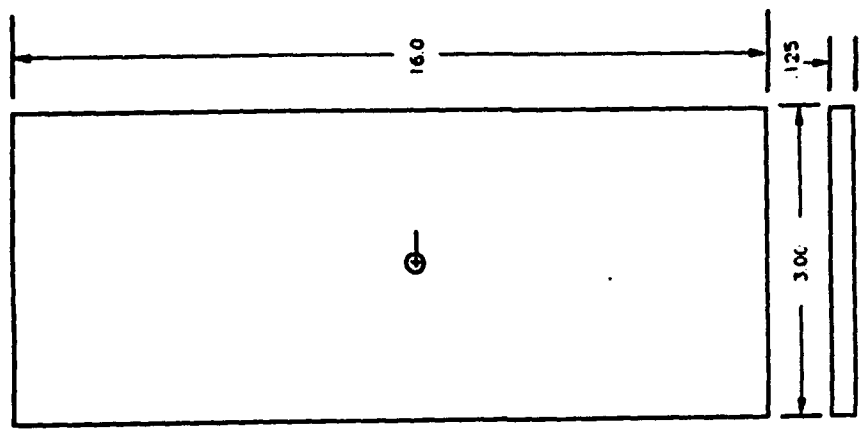


WPMS607-2

7075-T6 CLAD SHEET, ECCENTRIC HOLE CRACKED SPECIMENS 7075-T6 EXTRUSION, CENTER HOLE CRACKED SPECIMENS

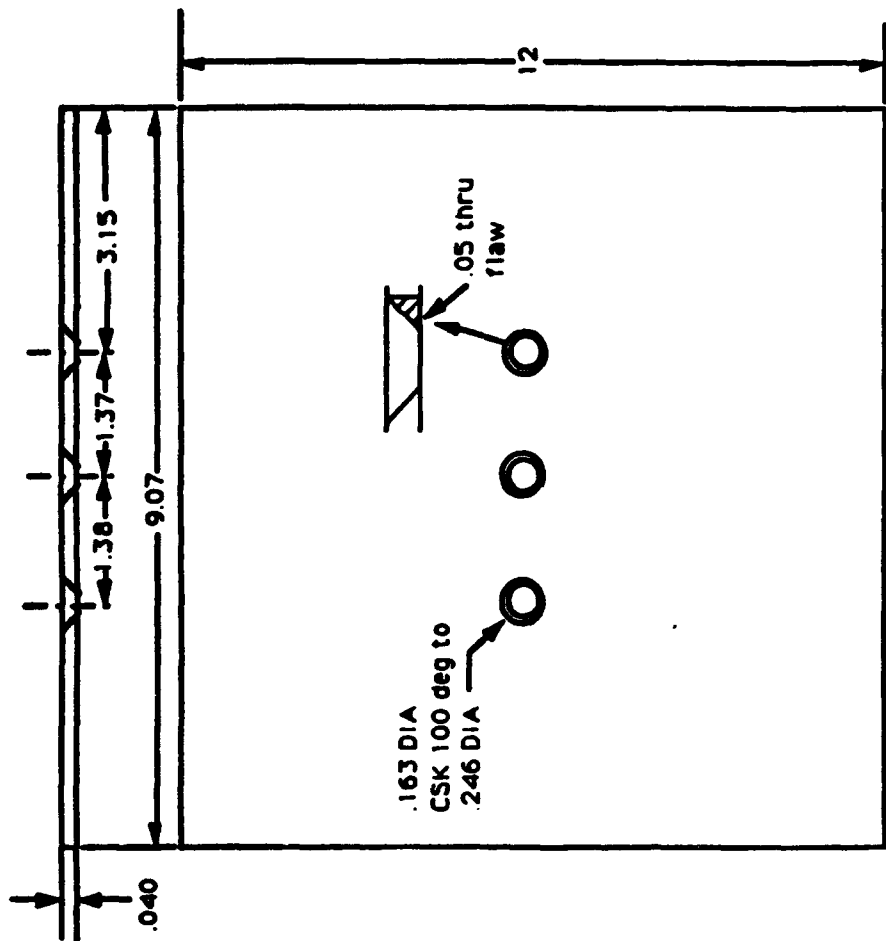


Sample ID:	R Value
7S-EH-U-C	.05
7S-EH-B-C	.05 ± .05
7S-EH-B-T	.4



Sample ID:	R Value
7E-CH-U-C	.2
7E-CH-B-C	.2 ± .2
7E-CH-B-T	.11 ± .2

2024-T4 CLAD SHEET, THREE HOLE, THRU FLAW SPECIMENS



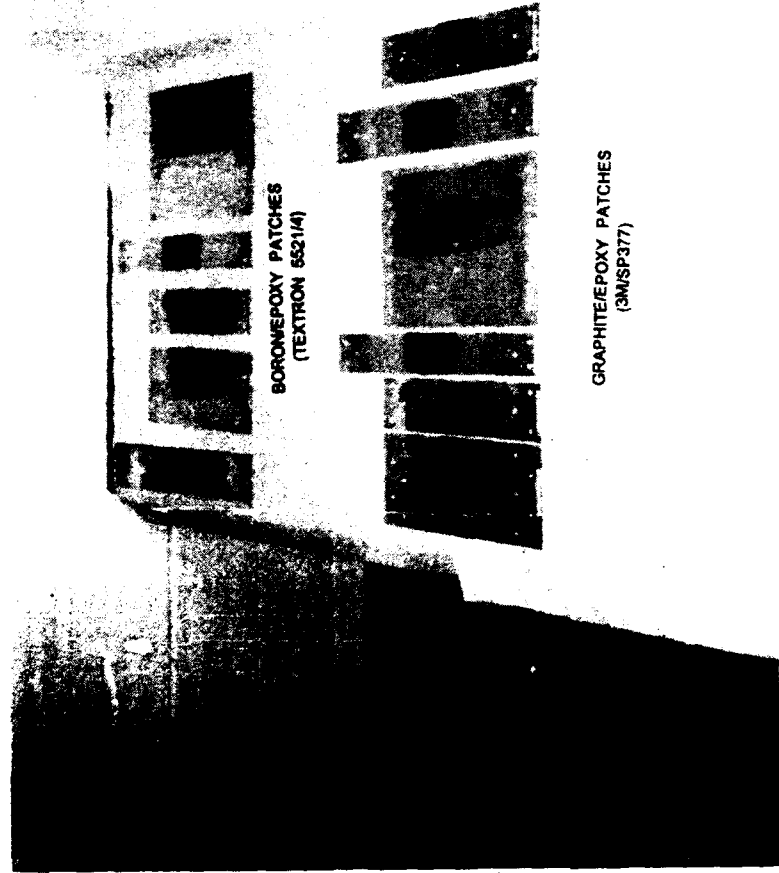
SAMPLE ID:
 A-27-S-2-BC5
 A-27-S-2-GC5
 A-27-S-2-GT6



WPMS607-2

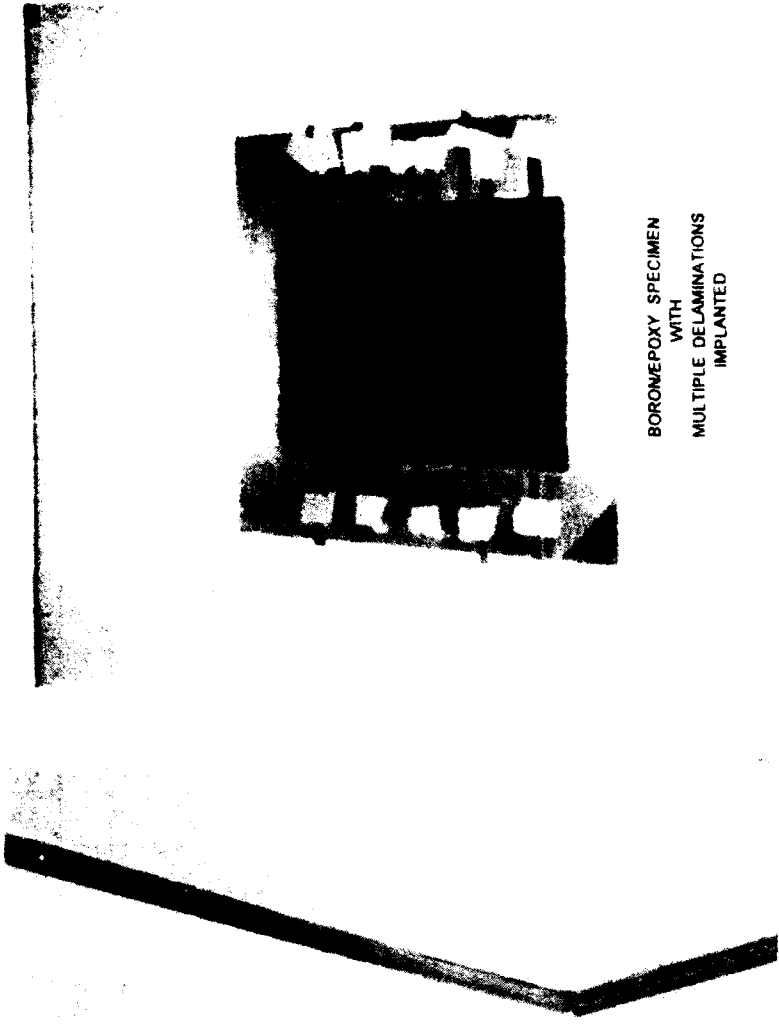
FATIGUE TEST SAMPLES

NON-DESTRUCTIVE INSPECTION (NDI) SAMPLE
WITH IMPLANTED DEFECTS



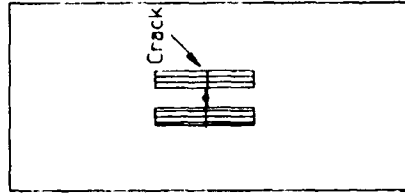
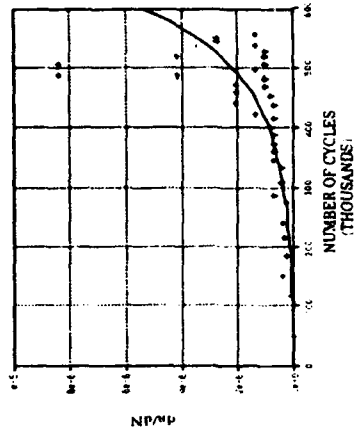
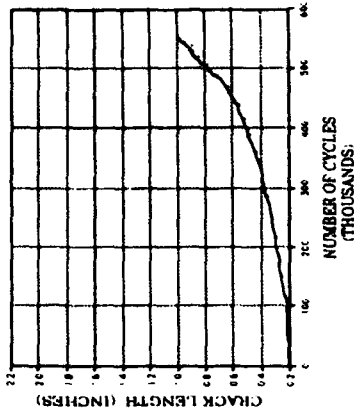
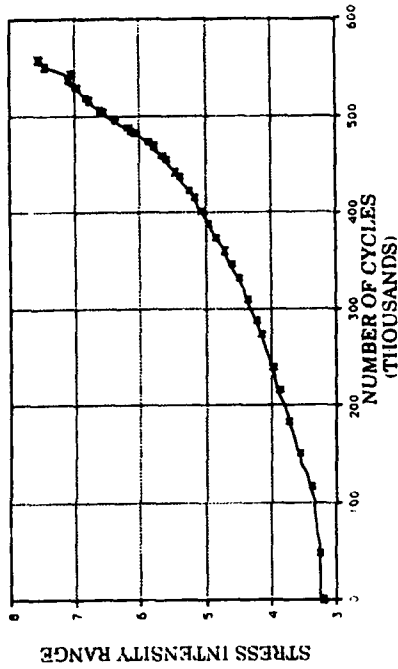
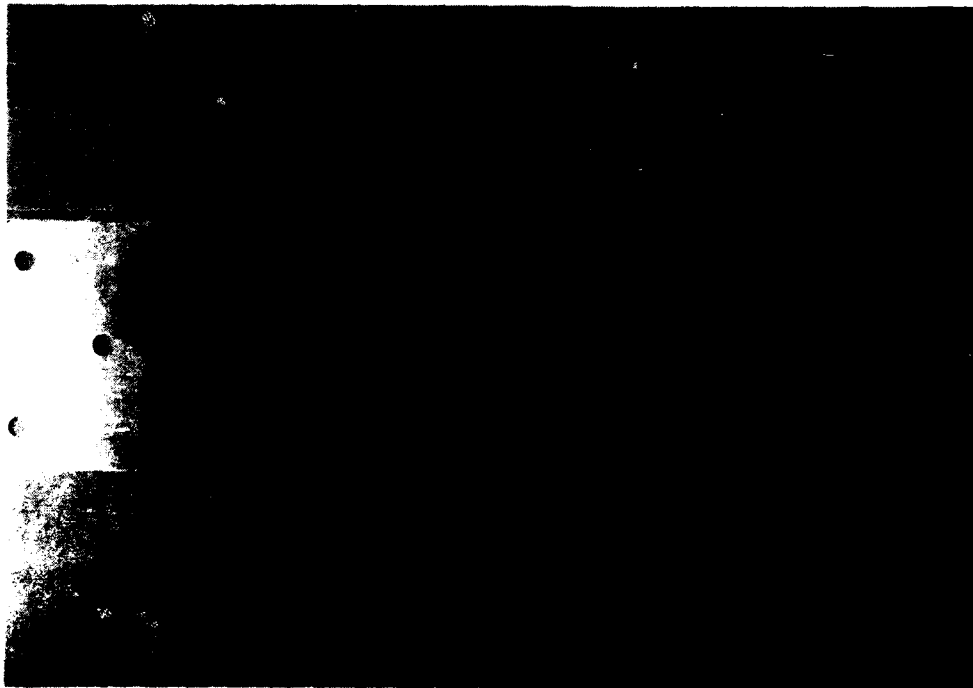
BORNEPOXY PATCHES
(TEXTRON 66214)

GRAPHITEPOXY PATCHES
(MSP377)



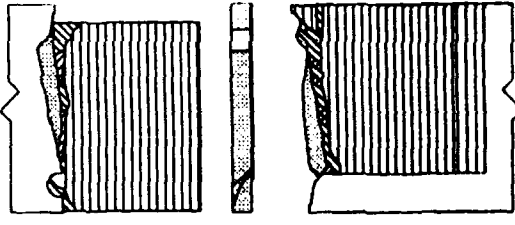
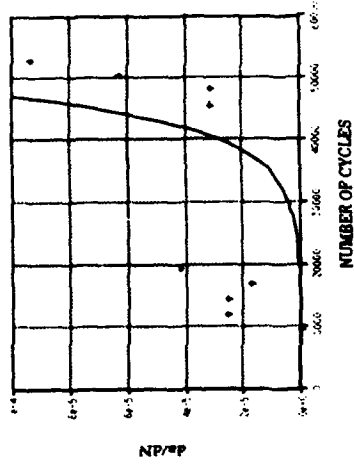
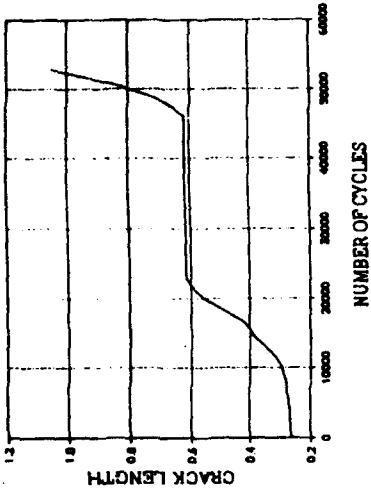
BORNEPOXY SPECIMEN
WITH
MULTIPLE DELAMINATIONS
IMPLANTED

7S-CC-G-C 7075-T6 CLAD SHEET

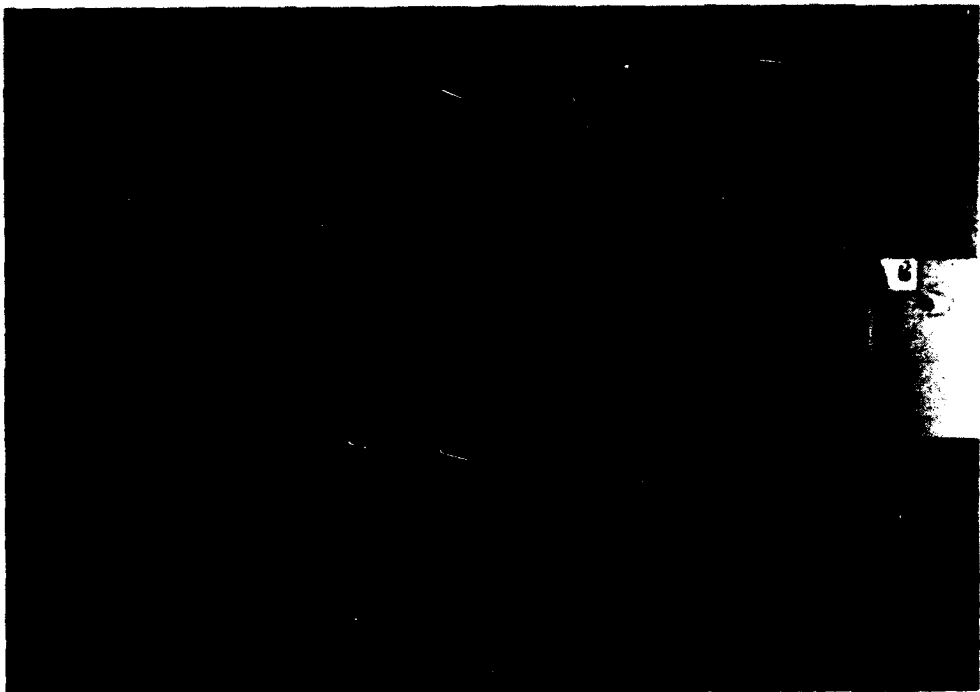


σ_{max} : 20 ksi
 σ_{min} : 14 ksi
 Cycles to Failure : stopped at 559200
 Patch Failures : none

D-24-FB-2-GC3



σ_{max} : 18.95 ksi
 σ_{min} : 2.085 ksi
 Cycles to Failure : 55200
 Patch Failures : 90 degree lamina. Loose fiber on surface



SUMMARY OF FATIGUE TESTS OF SPECIMENS WITH NOTCHES, CC, CH, EH

Serial #	Sample ID	Material	Patch	Notch	Stress (KSI)	R Value	Cycles to Failure	Comments
1	2S-CC-U-C	2024-T4 Clad Sheet	None	CC	16	0.4	206,400	
2	2S-CC-B-C	2024-T4 Clad Sheet	B/EP	CC	16	0.4	1,322,400	
3	2S-CC-B-T	2024-T4 Clad Sheet	B/EP	CC	16	0.4	1,636,800	
4	2E-CC-U-C	2024-T3511 Extrusion	None	CC	10	0.11	724,800	
5	2E-CC-G-C	2024-T3511 Extrusion	GR/EP	CC	10	0.11	808,800	
6	2E-CC-G-T	2024-T3511 Extrusion	GR/EP	CC	10	0.11	585,600	
7	7S-CC-U-C	7075-T6 Clad Sheet	None	CC	20	0.7	84,000	
8	7S-CC-G-C	7075-T6 Clad Sheet	GR/EP	CC	20	0.7	599,200	(Stopped at)
9	7S-CC-G-T	7075-T6 Clad Sheet	GR/EP	CC	20	0.7	1,238,400	
10	7E-CH-U-C	7075-T6 Extrusion	None	CH	7	0.2	3,000,000	No Crack
					8		1,533,600	
11	7E-CH-B-C	7075-T6 Extrusion	B/EP	CH	7	0.2	3,000,000	No Crack
					10		1,580,000	No Crack
					7	-0.2	3,000,000	No Crack
12	7E-CH-B-T	7075-T6 Extrusion	B/EP	CH	7	0.2	3,000,000	No Crack
*	7E-CH-B-T	7075-T6 Extrusion	B/EP	CH	10	0.11	3,000,000	Broke in Grips
13	7S-EH-U-C	7075-T6 Clad Sheet	None	EH	10	0.05	232,800	
14	7S-EH-B-T	7075-T6 Clad Sheet	B/EP	EH	16	0.4	1,024,800	
15	7S-EH-B-C	7075-T6 Clad Sheet	B/EP	EH	10	0.05	3,000,000	No Crack
*					10	-0.05		To be Tested

*Retest
 B/EP - Boron Epoxy
 GR/EP - Graphite Epoxy
 CC - Center Crsck
 CH - Center Hole
 EH - Eccentric Hole



SUMMARY OF FATIGUE TESTS OF SPECIMENS WITH SIMULATED FASTENER FLAWS

Serial #	Sample ID	Material	Flaw Type	Loading Spectrum	Cycles to Failure	Comments
1	A-28-ST-I-BCI	7075-T6 Clad Sheet	1	J	3,000,000	.721 in. crack
2	A-28-ST-I-BT2	7075-T6 Clad Sheet	1	J	3,000,000	No Crack Growth
3	D-24-FB-2-BC3	7075-T6 Extrusion	2	P-1	88,800	
4	D-24-FB-2-BT4	7075-T6 Extrusion	2	N-1 *		To be Tested
5	A-27-S-2-BC5	2024-T4 Clad Sheet	3	J	3,000,000	No Crack Growth
				C **	3,000,000	No Crack Growth
6	A-27-S-2-BT6	2024-T4 Clad Sheet	3	C **	3,000,000	No Crack Growth
7	A-28-ST-I-GC1	7075-T6 Clad Sheet	1	J	3,000,000	.796 in. crack
8	A-28-ST-I-GT2	7075-T6 Clad Sheet	1	C **	2,390,400	.416 - Broke in Grips
9	D-24-FB-2-GC3	7075-T6 Extrusion	2	P-1	55,200	
10	D-24-FB-2-GT4	7075-T6 Extrusion	2	P-1		Broke in Grips
	A-27-S-2-GC5	2024-T4 Clad Sheet	3	J	3,000,000	No Crack Growth
12	A-27-S-2-GT6	2024-T4 Clad Sheet	3	C **	3,000,000	No Crack Growth

- J: Spectrum loading
- P-1: Pressure and cargo load.
- N-1 *: Simulated Pressure and cargo load with negative amplitudes
- C **: Simulated spectrum with negative amplitudes
- (*): Retest
- 1 - Single countersunk hole, corner flaw
- 2 - Single hole, corner flaw
- 3 - Three countersunk holes, thru flaw on one



COMPARISON OF PATCH INFLUENCE

Sample ID	Patch	Cycles to Failure	N Patch N w/o Patch
2S-CC-U-C	None	206,400	
2S-CC-B-C	Q8	1,322,400	6.4
2S-CC-B-T	S8-III	1,636,800	7.9
2E-CC-U-C	None**	724,800	
2E-CC-G-C	Q16	808,800	1.1
2E-CC-G-T	S16-III	585,600	0.8
7S-CC-U-C	None	84,000	
7S-CC-G-C	Q8	Stopped at 599,200	
7S-CC-G-T	S8-II	1,238,400	14.7
7S-EH-U-C	None	232,800	
7S-EH-B-T	Q8	1,024,800	4.4
7S-EH-B-C	S8-II	3,000,000 NG	12.8
A-28-ST-1-BC1	Q8	3,000,000 .721 in. crack	
A-28-ST-1-BT2	S8-II	3,000,000 NG	□
D-24-FB-2-GC3	Q16	55,200	
D-24-FB-2-GT4	S16-II	52,800 Broke in grips	□

- Crack growth rate slower of the pair
- NG no crack growth
- ** Note that we consider this to be "BAD" data

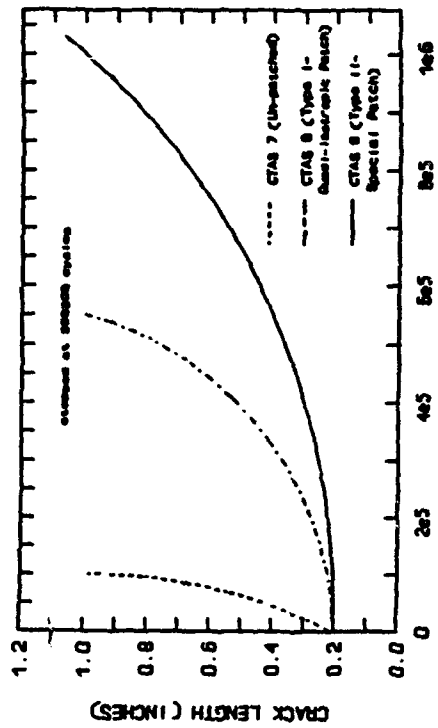


Figure 2a. Crack Length Comparison for 7075-T6 Clad Sheet

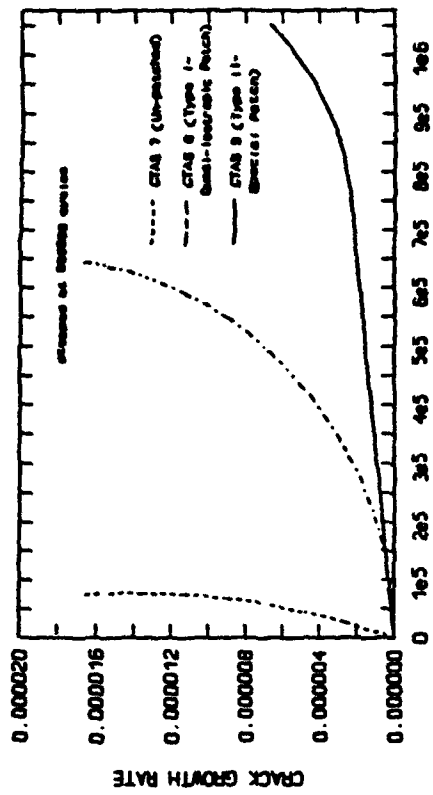


Figure 2b. Crack Growth Rate Comparison for 7075-T6 Clad Sheet

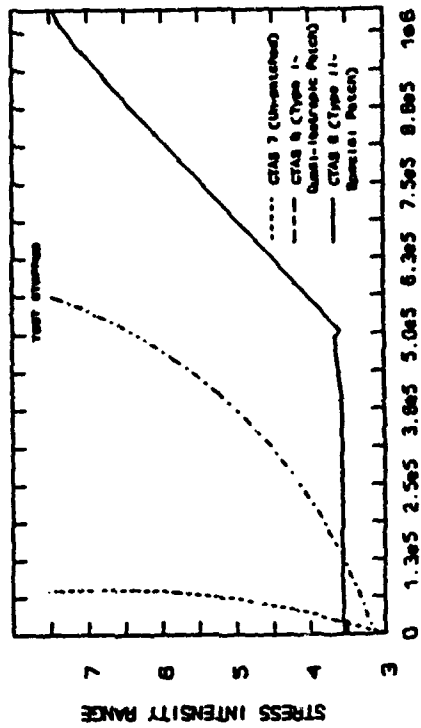
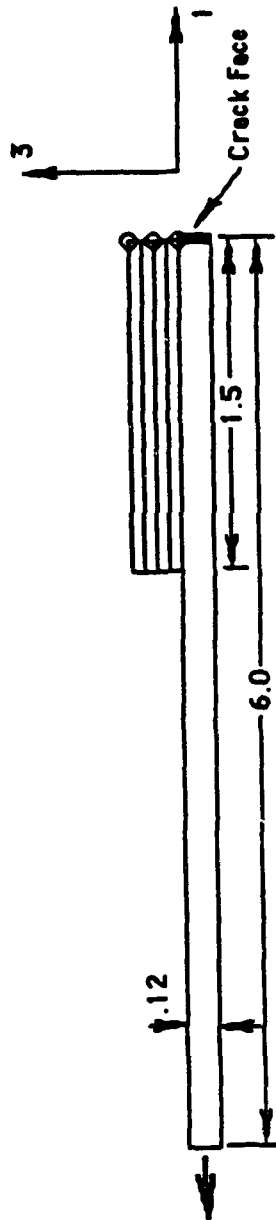
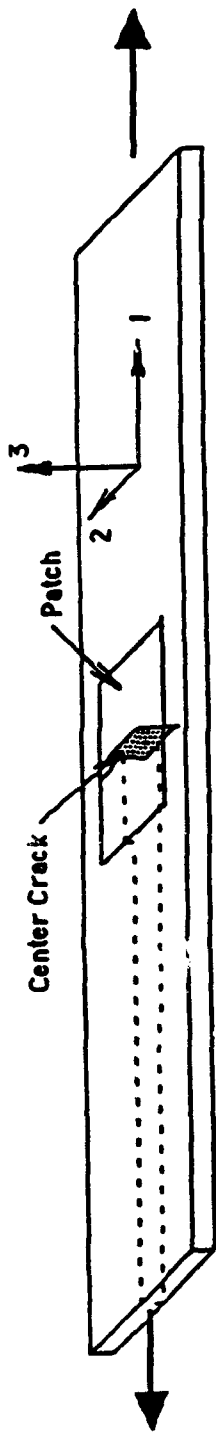
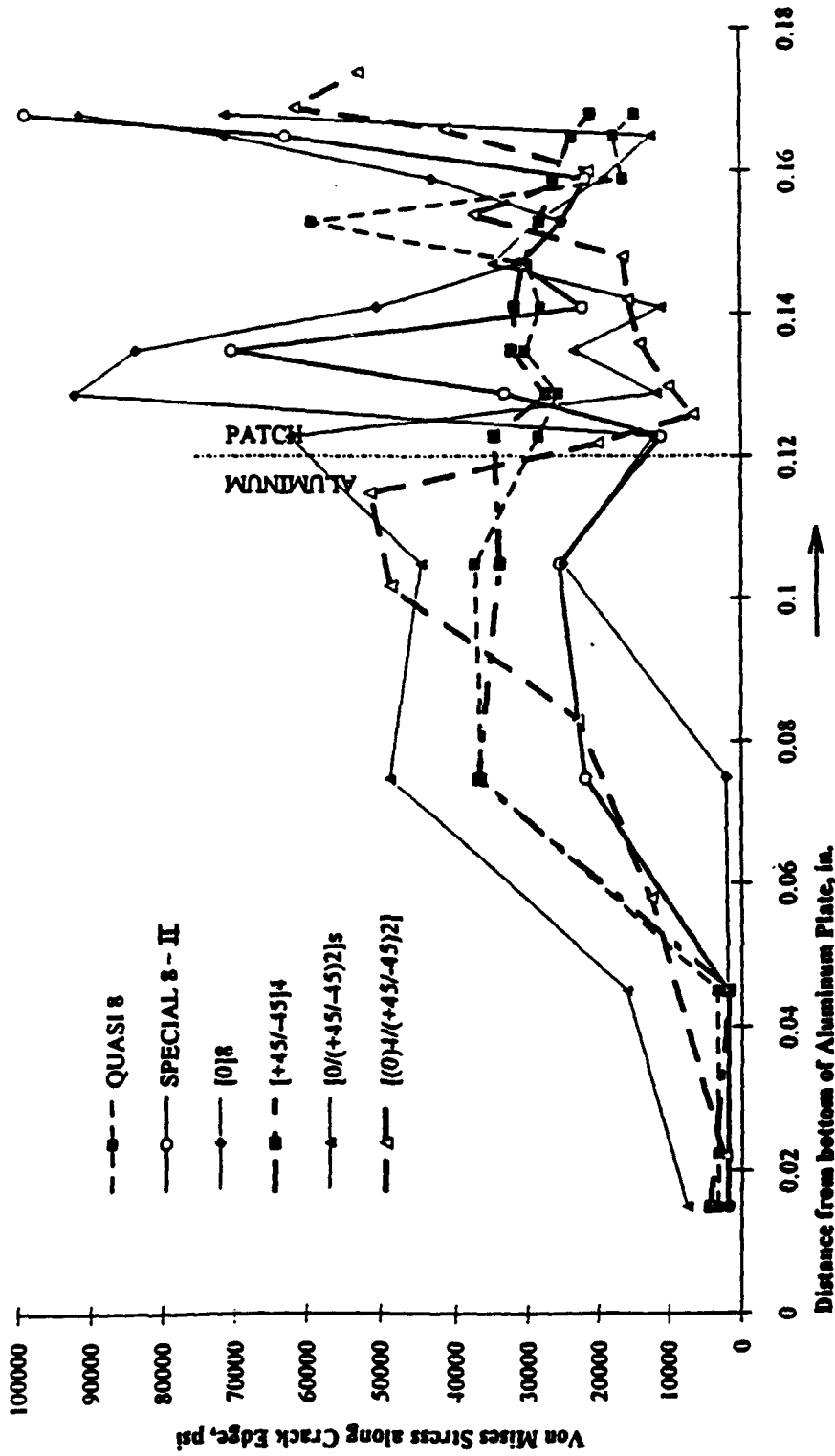


Figure 2c. Stress Intensity Range Comparison for 7075-T6 Clad Sheet



8 layer patch: 589 elements 945 nodes
 16 layer patch: 789 elements 1345 nodes

THROUGH-THE-THICKNESS MODEL



THROUGH-THE-THICKNESS MODEL, 8-LAYER PATCHES $t = .12$, $S = 10$ ksi

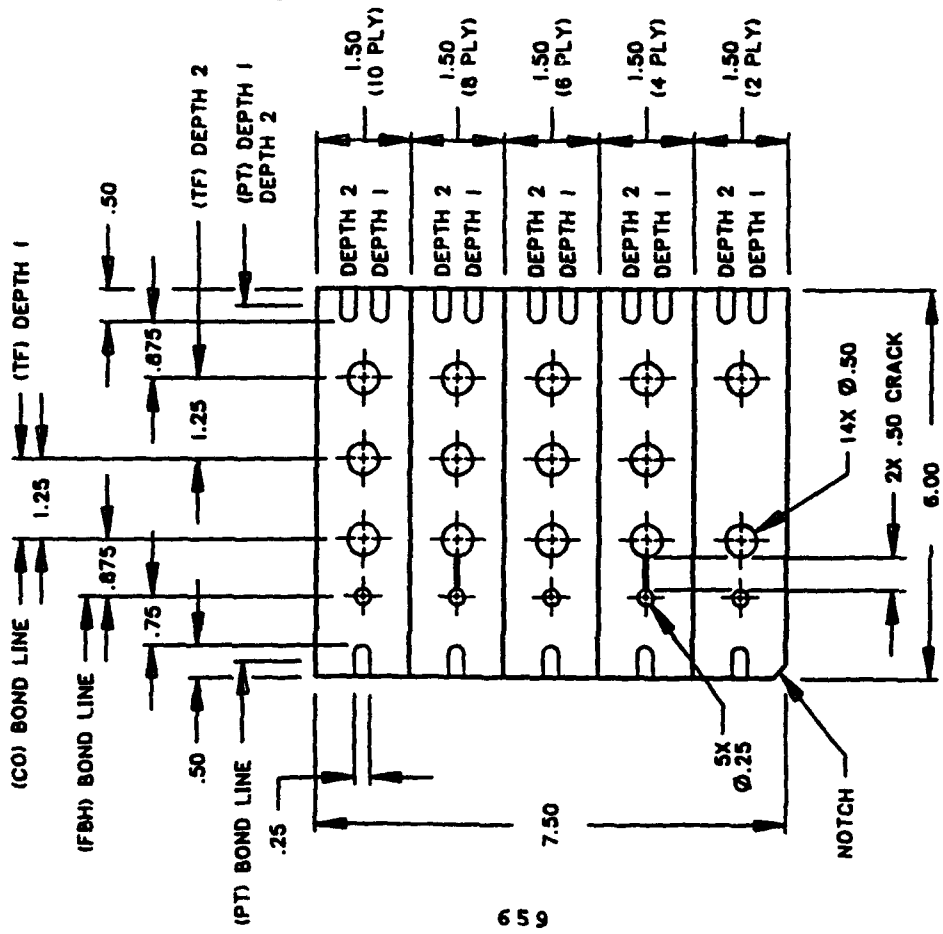


CURRENT DEVELOPMENTS

- NON-DESTRUCTIVE INSPECTION
- FABRICATED NDI TEST SPECIMEN WITH IMPLANTED DEFECTS
- IN-FIELD PATCH REPAIR

TABLE I

IMPLANTED FLAW LEGEND		IMPLANTED DELAMINATION DEPTHS		
CO	CUT-OUT	PLIES	DEPTH 1	DEPTH 2
PT	PULL TAB	2	1 - 2	N/A
FBH	FLAT BOTTOM HOLE	4	2 - 3	3 - 4
TF	TEFLON INSERT (2 PLYS OF 0.005 THICK TEFLON)	6	2 - 3	4 - 5
		8	3 - 4	5 - 6
		10	3 - 4	7 - 8



659

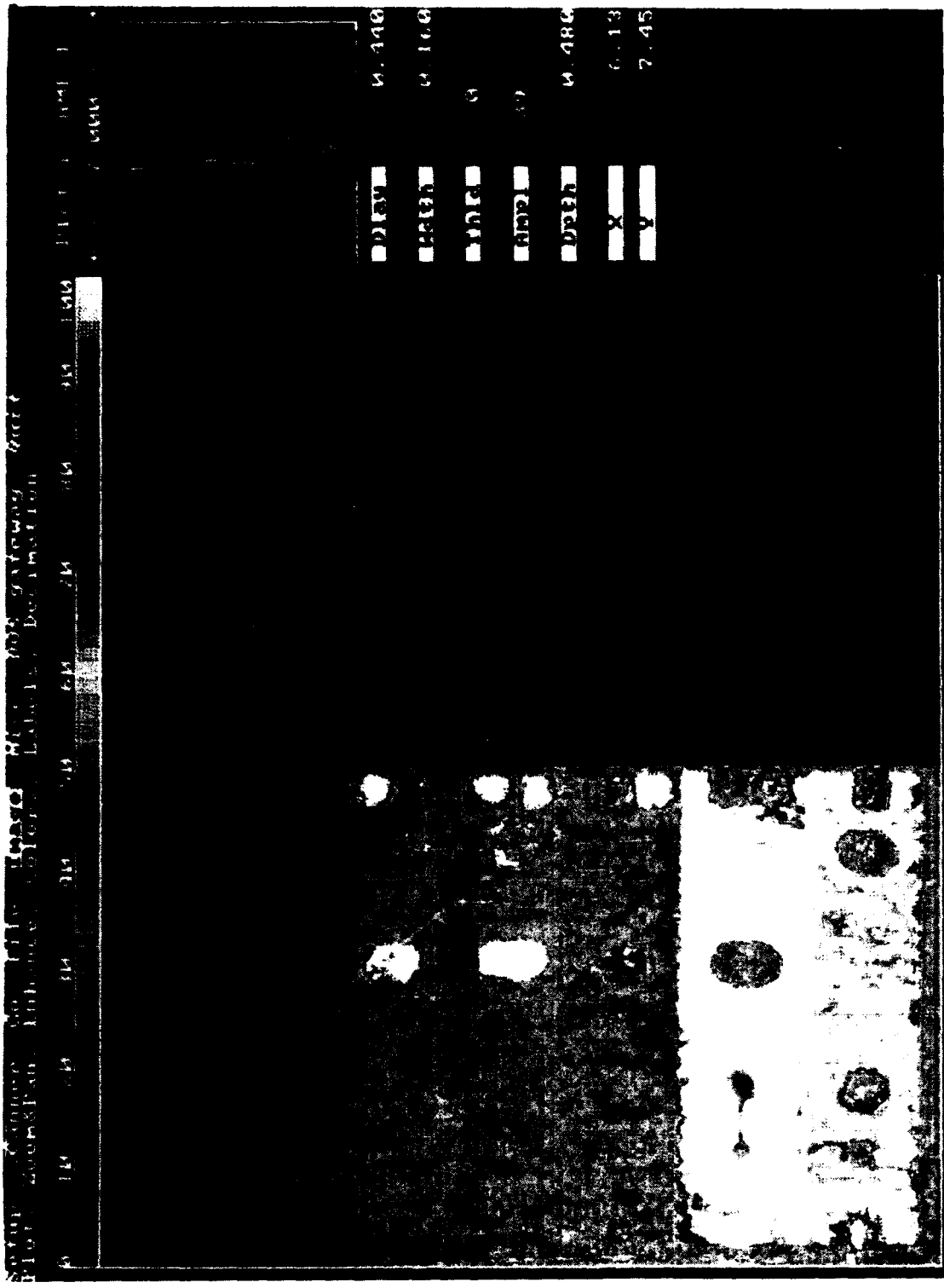
BORON/EPOXY DOUBLER ULTRASONIC REFERENCE STANDARD



ANALYSIS

● OBJECTIVES

- MINIMIZE STRESS INTENSITY AT CRACK TIP
- SMOOTH LOAD TRANSFER BETWEEN ALUMINUM AND PATCH
- PREVENT COMPOSITE PATCH FAILURE



C-SCAN MAP OF BORON EPOXY DOUBLER ULTRASONIC REFERENCE STAND
5MHZ IMMERSION SCAN

CHRYSLER TECHNOLOGIES
AIRBORNE SYSTEMS, INC.

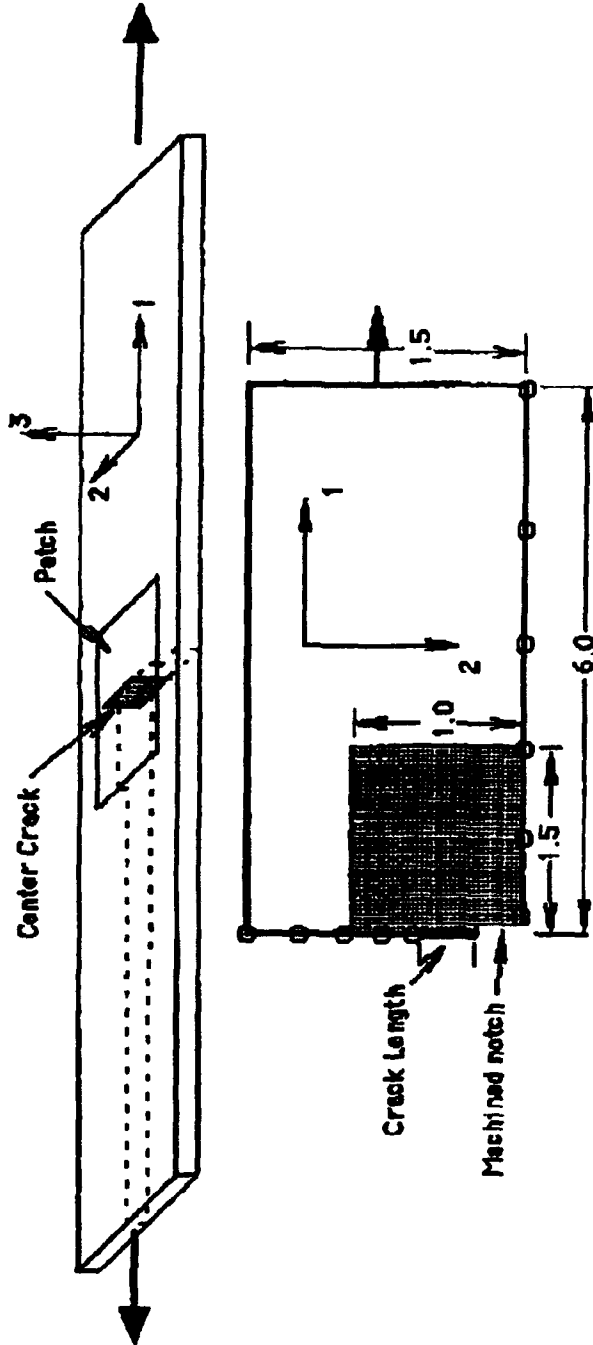
WPMS607-2

COMPUTATIONAL MODELS

(RESTRICTED TO SYMMETRIC, CENTER CRACK SPECIMEN)

6 3

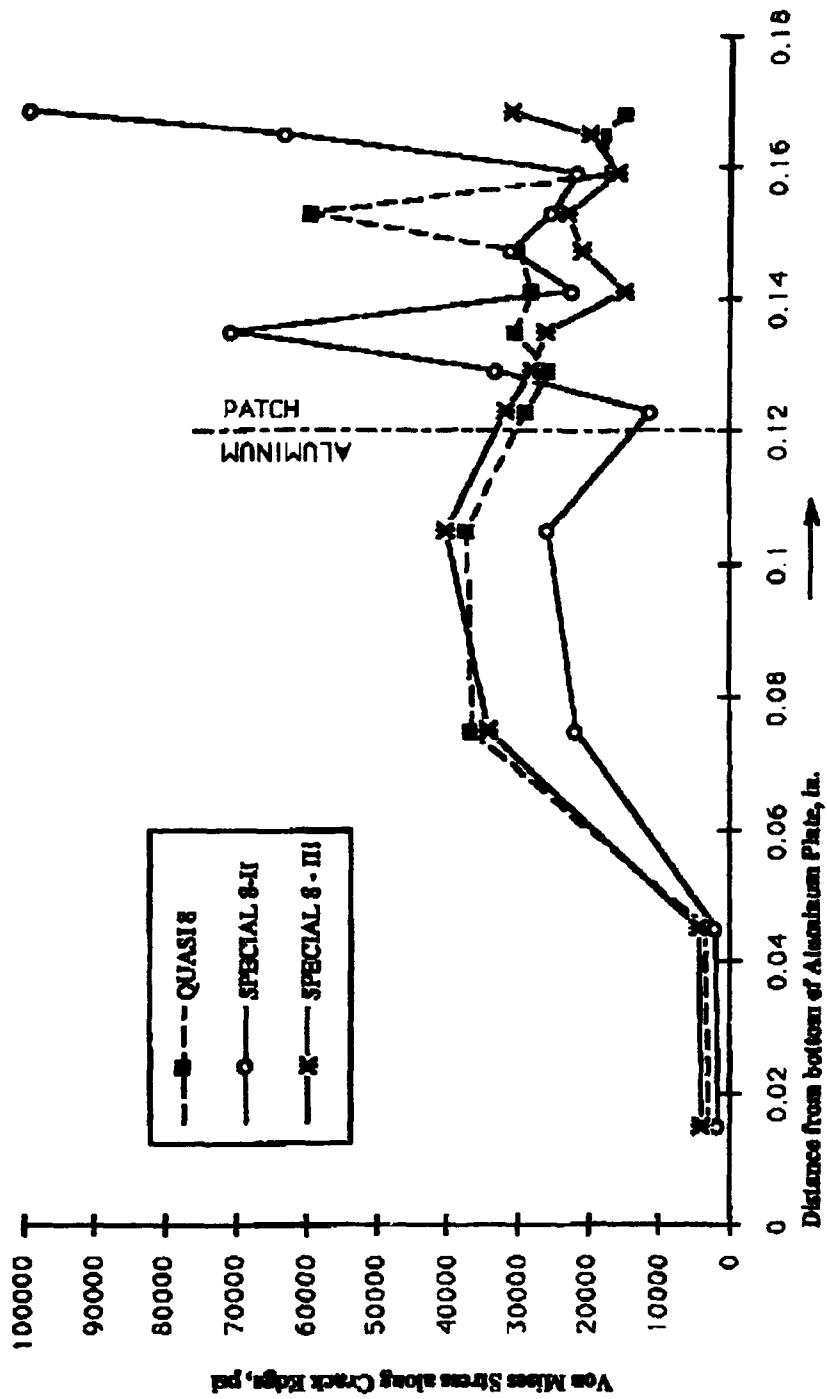
- USING PATRAN AND ABAQUS FINITE ELEMENT PACKAGES
- 2-D IN-PLANE MODEL
- 2-D THROUGH-THE-THICKNESS MODEL

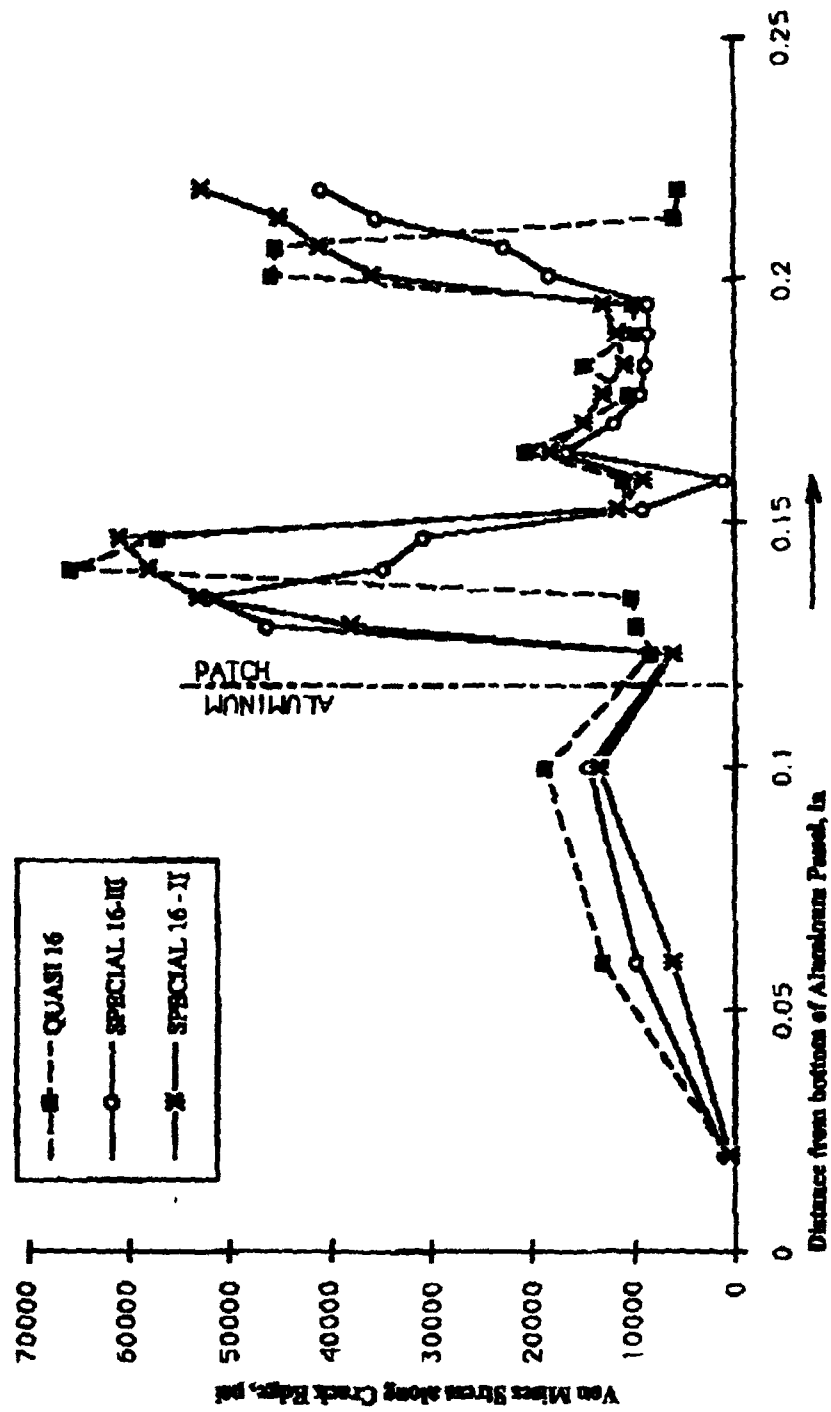


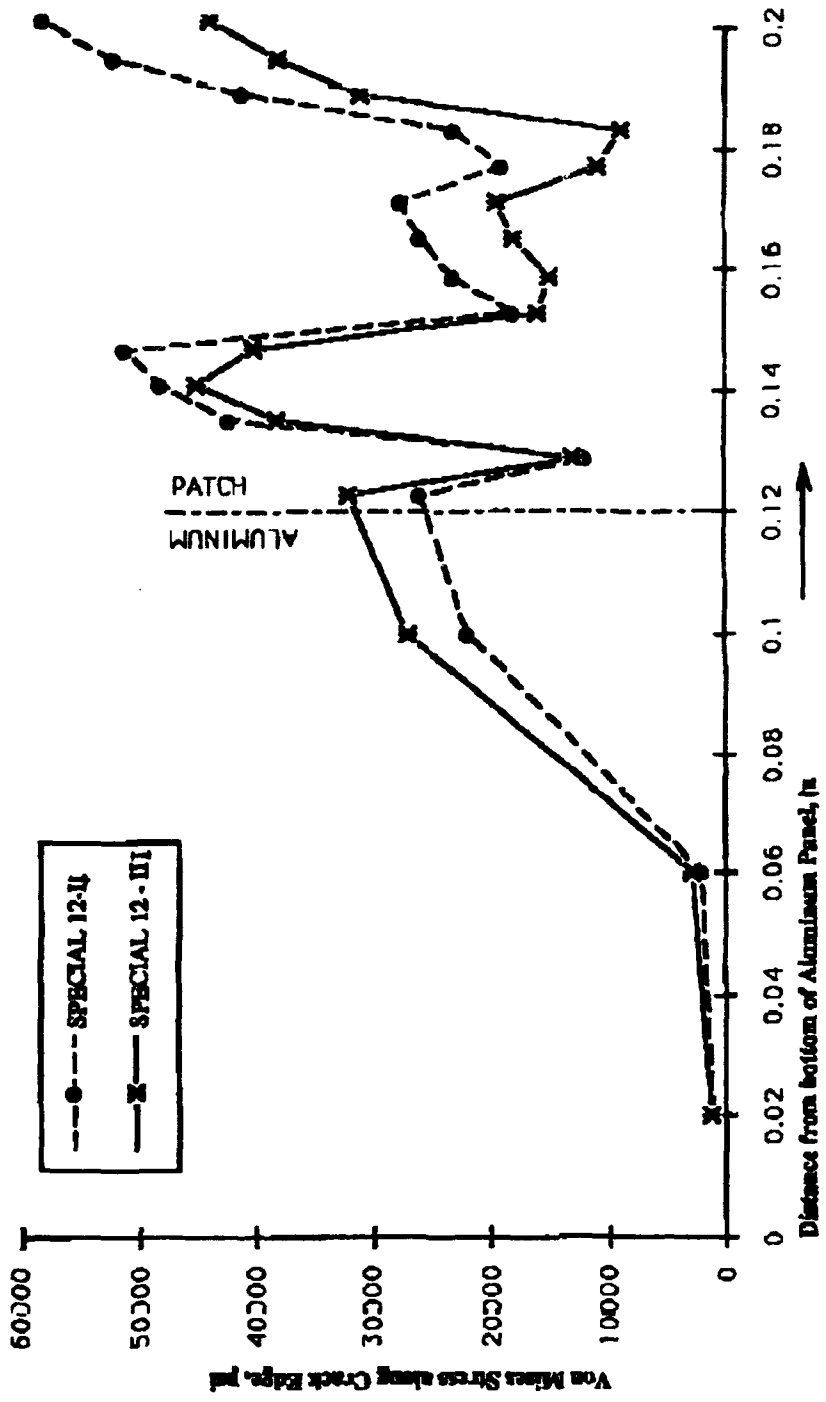
IN-PLANE MODEL

PATCH DESIGN

PATCH ID	E_p/E_{a1}
Q8	0.93
S8-II	1.50
S8-III	1.42
S12-II	1.72
S12-III	1.47
Q16	1.40
S16-II	1.87
S16-III	1.30







WPMS607-2



OBSERVATIONS

- TRADEOFF between PATCH STIFFNESS and THERMAL EXPANSION MISMATCH
- PATCH LAMINATE TAILORED TO LOAD DIRECTIONS
- PATCH NEVER FAILED

SUMMARY OF TESTING AND ANALYSIS EFFORT

- BOTH CONSTANT AMPLITUDE AND SPECTRUM LOADING TESTS DEMONSTRATED SUPERIOR PERFORMANCE OF SPECIAL PATCH DESIGNS (TYPE II AND TYPE III) COMPARED TO QUASI-ISOTROPIC PATCH DESIGN
- ANALYTICAL INVESTIGATIONS AND TEST DATA SUPPORTED THE REDUCTION OF STRESS INTENSITY FACTORS AT THE CRACK TIPS IN CASE OF PATCHED SPECIMEN(S). THE RELATIVE EFFECTS OF THE QUASI-ISOTROPIC PATCH DESIGNS OVER THE SPECIAL PATCH CONFIGURATIONS WERE ALSO DEMONSTRATED.
- CONFIDENCE ON THE PATCH QUALITY AND REPAIR PROCESS HAVE BEEN DEMONSTRATED
- THE R&D EFFORTS HAVE BEEN VERY USEFUL IN TRANSLATING AND TRANSFERRING THE TECHNIQUES OF PATCH WORK REPAIR AND PROCESS TO THE FIELD LEVEL REPAIRS



WPMS607-2

CONCLUSION

- PATCHES INCREASE FATIGUE LIFE

Soft Patches for Damage Tolerant Riveted Repair of Aluminum Fuselage Structures

Captain R. Fredell
Department of Engineering Mechanics
US Air Force Academy, CO 80840

M.E. Heerschap
Delft University of Technology
Faculty of Aerospace Engineering
P.O. Box 5058
2600 GB Delft, the Netherlands

B. van Wimersma
Structural Laminates Company
Kluyverweg 1
2629 HS Delft, the Netherlands

Abstract

Riveted repairs to pressurized aluminum alloy fuselage structures are common sources of fatigue "hot spots." Typical repair practices involve relatively thick aluminum sheets riveted in place over corrosion or incidental damage. Often in repair, design consideration is given to static residual strength, while fatigue concerns are generally ignored because the original structure is considered much older than the repair. However, as the average age of large transport aircraft continues to increase, repairs can suffer fatigue damage and present increased inspection requirements to operators. Certain techniques have been implemented in the past to reduce high stresses in the fatigue-critical first rivet row in skin repairs. These techniques generally involve tapering of the thickness of the patch, a process which requires machining or chemical milling. In the past, substitution of higher strength materials (e.g., titanium and stainless steels) has been avoided because of concerns about cost, corrosion, and increased patch stiffness.

The recently developed fiber metal laminate GLARE 3 provides a simple, damage-tolerant, light-weight alternative to highly tapered aluminum alloy patches. GLARE 3, an advanced sheet material developed for its excellent fatigue crack growth resistance, also offers higher tensile strength, lower elastic modulus and lower density than 2024-T3. The paper discusses the more efficient load transfer, enhanced fatigue life, extended inspection intervals, and easier repair installation achieved by the substitution of GLARE 3 for monolithic aluminum in the riveted repair of aluminum transport aircraft fuselages. The results of finite element calculations are presented and compared with strain gage data and results from extensive laboratory fatigue tests, including the effects of typical defects encountered in repair. This new approach, known as "soft patching," improves the fatigue life of riveted repairs by 50 to 200 percent.

Riveted Repairs

Riveted repairs make up the single largest type of repairs performed on metal-skinned aircraft structures. Riveted repairs possess many advantages over other techniques: They are quick

and easy to carry out on the aircraft and require little support equipment. Maintenance personnel often install riveted repairs with little or no engineering analysis.

The disadvantages of riveted repairs were summarized by Swift: "In general, any repair to an airframe structure can substantially degrade fatigue life if extreme care in detail design is not taken [1]." Most riveted repairs provide only for the restoration of equal or better static strength to the structure. Typically, repairers do not consider fatigue.

"Soft" Patches

A new approach to smoothing the load transfer into a riveted patch will be presented here. It involves the use of high-strength, moderate modulus fiber metal laminate GLARE 3 as patches to monolithic aluminum skins. Fiber metal laminates can be treated as aluminum sheets in the workshop: The same cutting, forming, drilling and riveting processes apply in almost all cases. The mechanical properties of GLARE 3 are listed in comparison with 2024-T3 in table 1. Using "soft" (i.e., low modulus) patches for the repair of multiple site damage in aluminum fuselage lap joints was first discussed in [2]. The current paper is excerpted from [3].

Table 1a. Mechanical, Physical Properties of 2024-T3 and GLARE 3. (SI)

Material	Lay-up	Thickness, mm	$E_{11}, E_{22},$ GPa	$\sigma_{0.2},$ MPa	$\sigma_{ult},$ MPa	$\sigma_{bluntnotch}$ MPa*
2024-T3	mono	variable	72	359	455	440
GLARE 3	2/1-0.3	0.85	60	315	662	452
GLARE 3	3/2-0.2	1.1	57	295	804	469
GLARE 3	3/2-0.3	1.4	58	305	717	456

*open hole, (hole diameter/panel width) = 0.25

Table 1b. Mechanical, Physical Properties of 2024-T3 and GLARE 3. (U.S.)

Material	Lay-up	Thickness, inches	$E_{11}, E_{22},$ Msi	$\sigma_{0.2},$ ksi	$\sigma_{ult},$ ksi	$\sigma_{bluntnotch}$ ksi*
2024-T3	mono	variable	10.4	52.1	66.0	63.8
GLARE 3	2/1-.012	0.034	8.7	45.7	96.0	65.6
GLARE 3	3/2-.008	0.044	8.3	42.8	117	68.0
GLARE 3	3/2-.012	0.056	8.4	44.2	104	66.1

*open hole, (hole diameter/panel width) = 0.25

Finite Element Analysis of Riveted Repairs

Specimen Geometry

A finite element model was built to represent a typical riveted patch repair to a fuselage skin shown in figure 1. The sketch shows a 50 mm (2 inch) diameter hole cut into a 600 by 300 mm (24 inch by 12 inch) sheet of 1.0 mm (.040 inch) thick 2024-T3 aluminum. The hole simulates the removal of corrosion or impact damage. The repair must accomplish two primary purposes: It provides an alternate load path in place of the removed material, and it acts as a pressure seal for the fuselage skin. The configuration is not intended to represent an optimized repair. Rather, it serves as a typical baseline for comparison of various patch concepts.

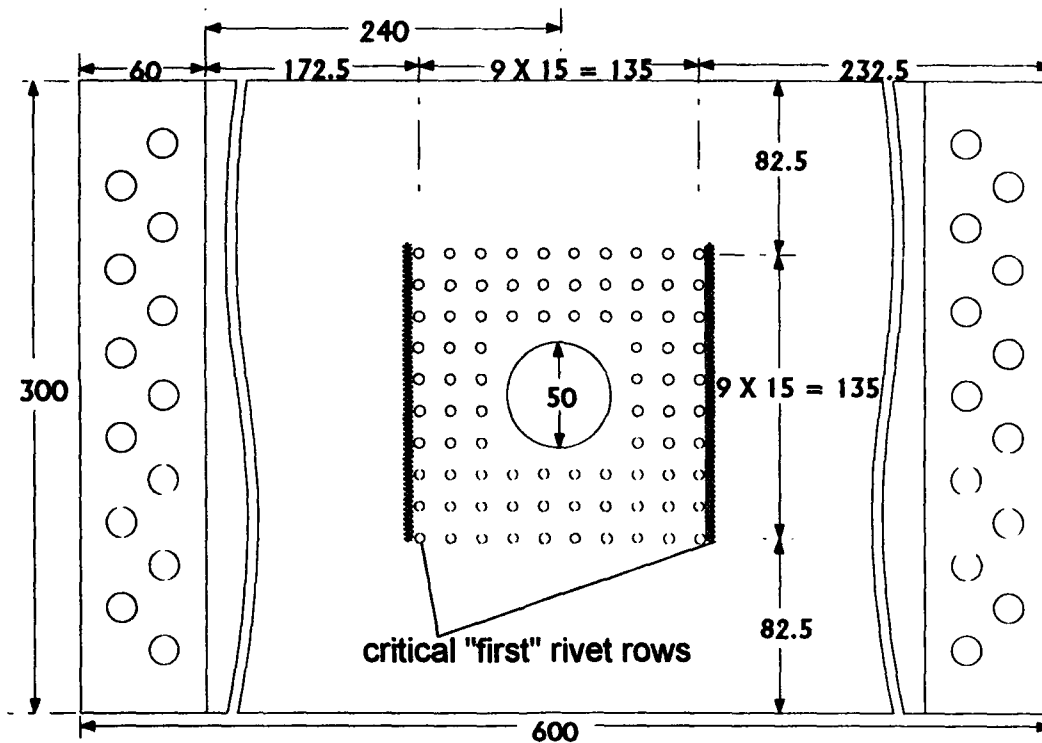


Figure 1. Riveted repair specimen used in this study. All dimensions mm.

Four different riveted patch types were modeled in the analysis: untapered 2024-T3 patches of 1.27 mm (.050 inch) and 1.0 mm (.040 inch) thickness, a 2024-T3 patch with thickness tapered from 1.27 to 0.7 mm (.050 to .028 inch), and an untapered GLARE 3 patch (2/1 lay-up) of thickness 0.85 mm (.034 inch). The patch thicknesses were chosen from standard sheet gauges to match or slightly exceed the static strength of the original 2024 skin. This resulted in a stiffness ratio (elastic modulus multiplied by thickness) of the GLARE patch to the untapered

1.27 mm (.050 inch) 2024 patch of approximately 0.56. All patches were attached with NAS1097AD countersunk rivets of 3.2 mm (1/8 inch) diameter.

Finite Element Modeling

Model pre- and post-processing was accomplished with PATRAN; finite element calculations were performed using ABAQUS version 4-9. The model was treated as a geometrically non-linear problem. Sheet rotation due to secondary bending was properly taken into account. Shear and normal deflection and rotation of the rivets were also modeled. The material response was treated as linear elastic.

The skin and patch were modeled as a series of 8-noded quadratic quadrilateral shell elements. The rivets were modeled as quadratic three-noded beam elements. The circular cross-section beam element used to represent the rivet allowed for bending, shear and extensional loading of the rivet. The beam diameter was chosen to match the actual rivet diameter.

Beams were used to make the skin-to-patch connection in the method discussed by Seegers [4] and Slagter [5]. The rivet holes were not explicitly modeled. This method of connecting beams to the shell elements has proven effective in modeling concentrated shear loads such as rivets. *It allows rivet flexibility to be modeled with good accuracy.*

The use of beams avoided the inflexible "hard points" of multi-point constraints or spot welds, which tend to overestimate the first rivet row loads. The connection of the beams at a single point in the shell element resulted in a stress singularity at that point and induced high local tensile stresses in the shell. These false tensile loads occur in addition to the compressive forces at the infinitely small nodal attachment point, resulting locally in very high stresses. These local disturbances damp out quickly, and overall model accuracy is very good, as will be shown in the following section. By not explicitly modeling the rivet holes, the output does not directly yield numerical values of the expected high stress concentrations known to exist at the rivet holes.

Load cases representing both uniaxial and biaxial tension were analyzed. The uniaxial model was 500 mm (20 inches) long by 300 mm (12 inches) wide, with 155 mm (6 inch) square patches. This geometry matched exactly the unclamped dimensions of the static and fatigue test articles. The biaxial model was modified to 500 mm square to give sufficient width for accurate distribution of secondary (longitudinal) loads. A biaxiality ratio ($\sigma_{long} / \sigma_{hoop}$) of 0.5

was chosen as representative of typical fuselage pressure loads. However, due to equipment limitations, the biaxial load case was not tested.

Validity of the model

The output of the convergent finite element calculations is compared in this section with measured and observed results from statically loaded specimens. Two riveted specimens identical to that shown in figure 1 were manufactured and instrumented with electrical resistance strain gages. The GLARE 3 and tapered 2024 patches were used. Strain gages were limited by practical considerations to the outside surfaces of the specimens; thus, comparison of the model predictions on the inner, more highly loaded surfaces is not possible.

The average difference between measured and predicted was 6.6 percent for the GLARE 3 patch specimen; for the tapered 2024 piece, an average difference of 8.1 percent was recorded. This slightly higher error in the tapered patch can be a result of the stepwise tapering used in modeling the patch, as opposed to the smooth machined taper milled into the test specimens. As expected, differences between the mathematical model and the measured strains were greatest in areas of high strain gradient. The measurements were especially suspect between rivets (within the two rivet diameter exclusion zone), where differences ranged up to 15 percent. This can be further attributed to strain gage placement and the averaging function of a finite size strain gage.

Some details are worthy of mention. The less stiff GLARE patch is loaded to a strain 42 percent higher than the relatively thick tapered 2024 patch. This was not anticipated to cause problems in the GLARE patch, which is stronger and more fatigue resistant than the monolithic material. However, the edge of the 2024 skin cut-out also has a higher strain with the more flexible patch: 2455 microstrains with the GLARE patch versus 1867 microstrains for the tapered patch, an increase of 31 percent.

The results of the strain comparison were considered adequate to proceed with confidence in the model. Areas not accessible to strain gages, especially the critical area on the inside surface of the skin near the outer rivet row, can be predicted with assurance that they accurately reflect the state of stress there.

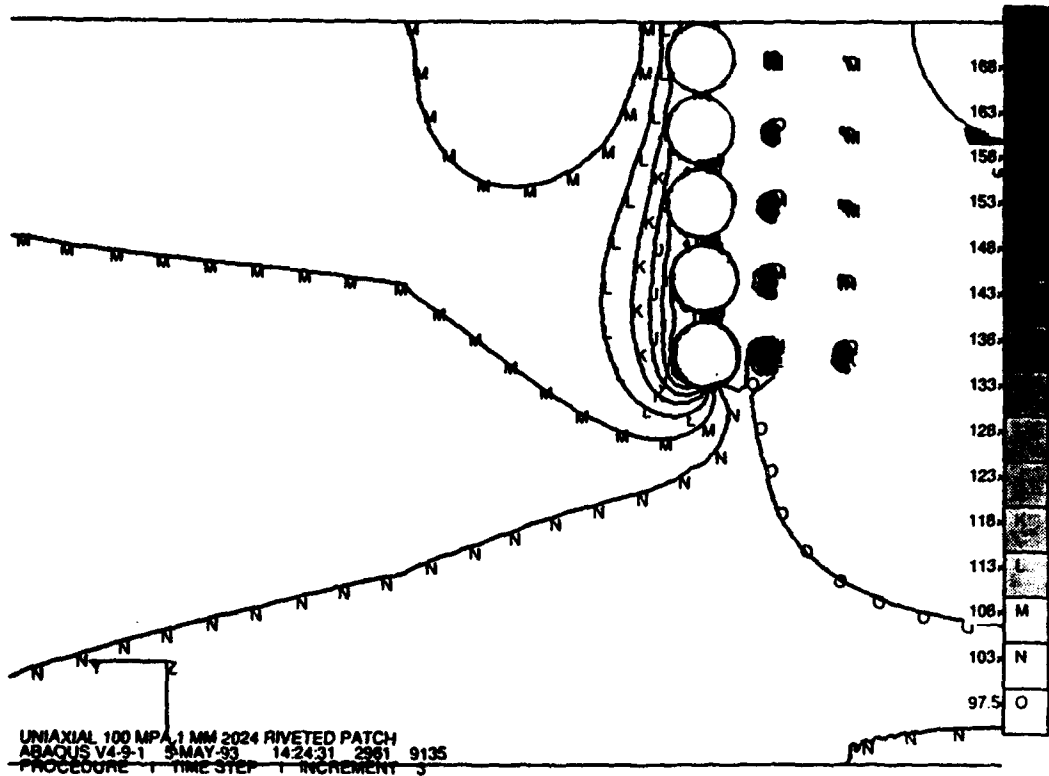
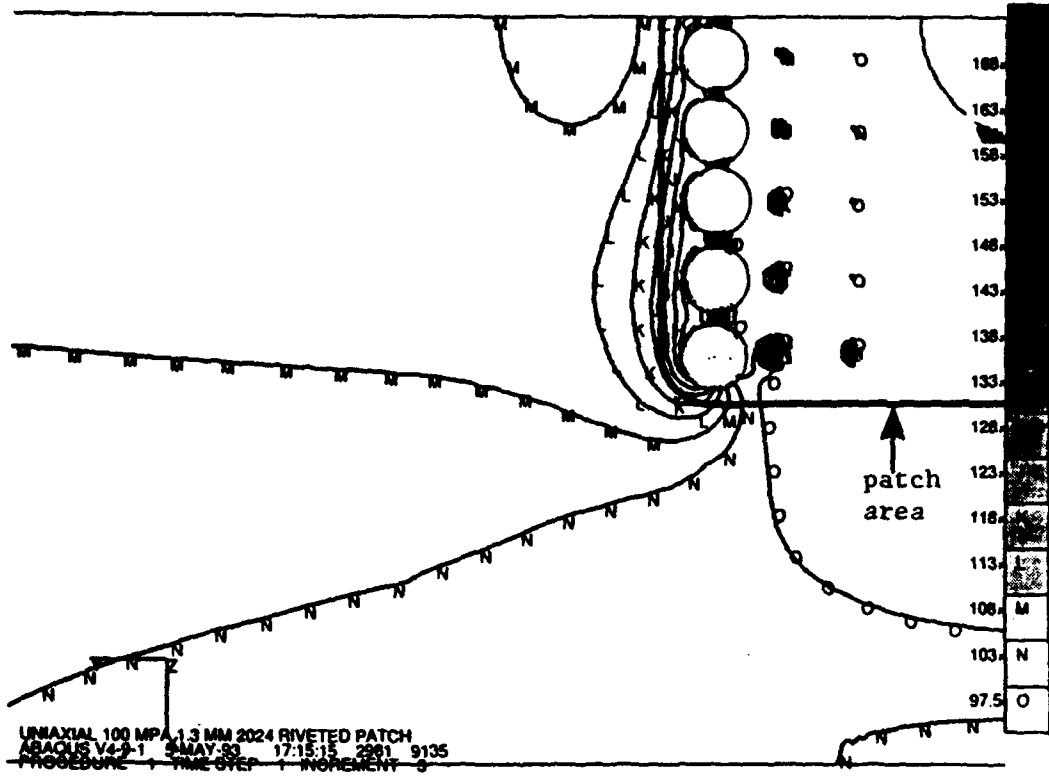
Finite Element Analysis Results

The analysis gives a fuller appreciation of the role of patch selection on the load transfer into and around the patch. Two factors dominate the response. The first is the patch *extensional stiffness*, which establishes the bearing load transfer and overall load attraction of the patched area. The patch *thickness* at the first rivet row affects the secondary bending stresses in the skin.

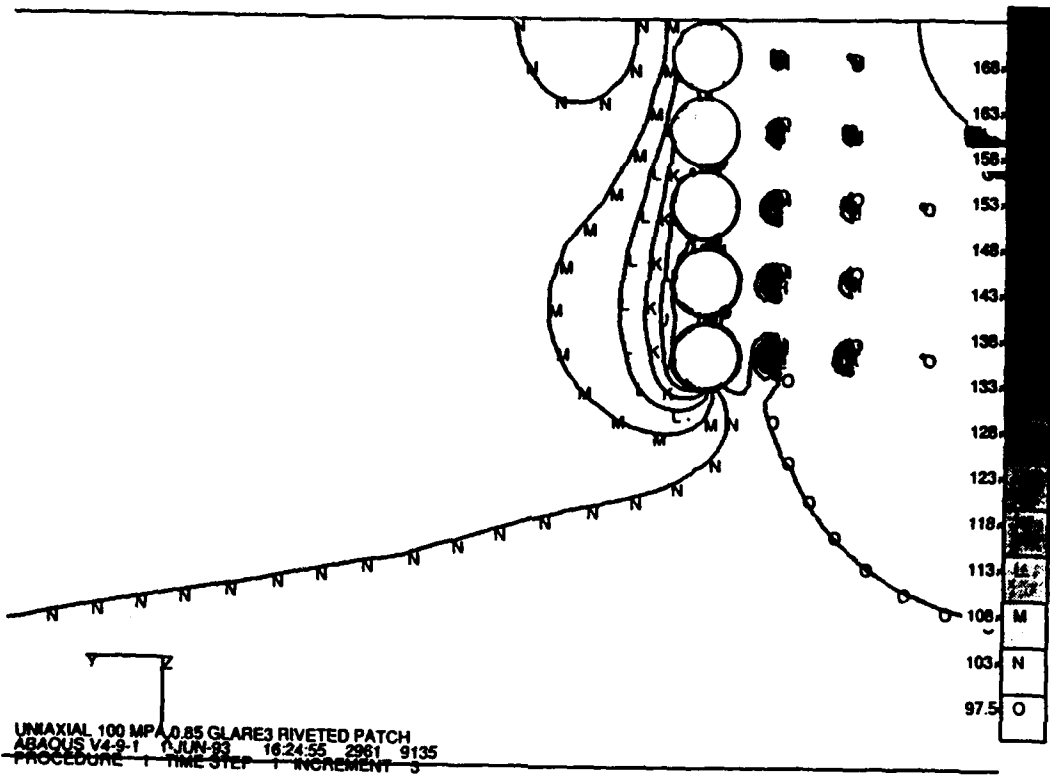
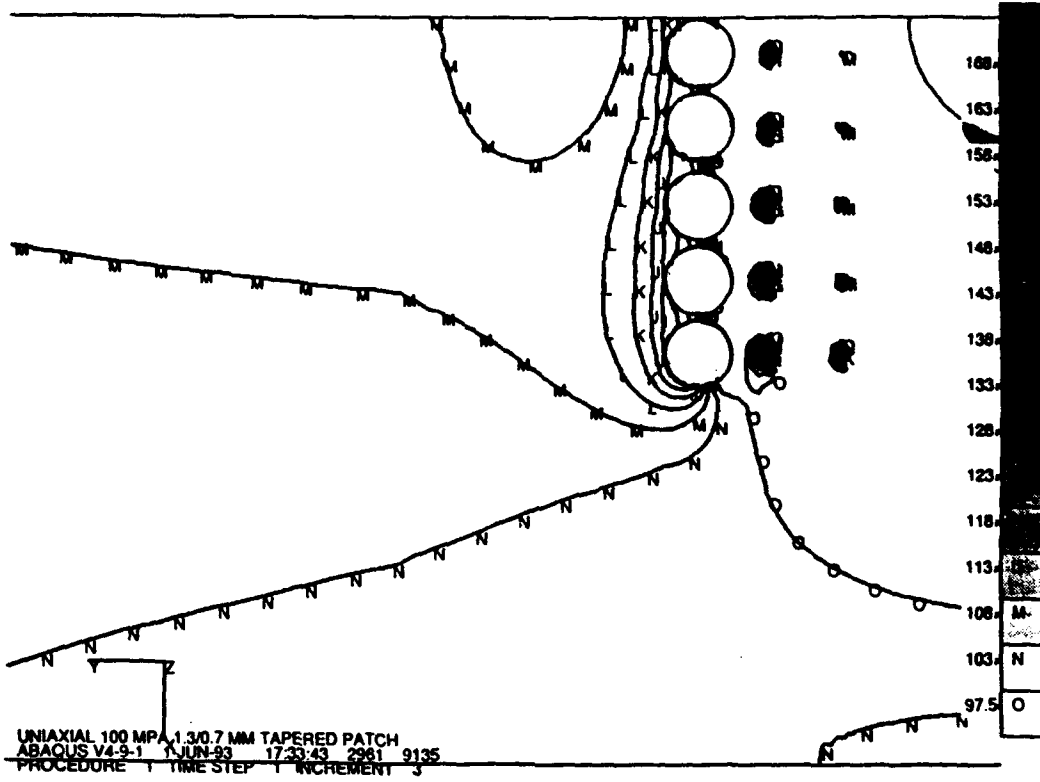
The very stiff doubled region attracts load into the area, which flows partly into the patch and relieves the stress concentration at the edge of the cut-out. An important function of the patch is to exert forces on the cut-out edges to prevent its deformation. In this sense, a stiff patch is desirable. However, the stiffness of the doubled region adversely affects the unreinforced skin at the edge of the patch by attracting additional loads. This can lead to early crack initiation and failure. This concept will be explained more fully in the following sections, where the results of the finite element model are presented in detail.

Four patch types were modeled. Figure 2 presents plots of the first principal stress for the four patch cases under 100 MPa (14.5 ksi) uniaxial tension. The primary load direction is oriented horizontally (along the y-axis) in the figures. One can see the large influence of patch selection on the overall stress pattern of the repaired sheet. (All plots show the inner surface of the repaired sheet which, due to bending effects, always experiences the highest stresses.) The outer surfaces were always loaded much less severely than the inner surfaces. This was primarily the effect of bending due to the step change in neutral axis at the outer rivet row.

A general impression can be gained by observing the size of the disturbed zone of the first principal stresses around the patches. From figure 2a (1.27 mm/.050 inch 2024 patch) to figure 2d (0.85 mm/.034 inch GLARE 3 patch), the disturbed area grows progressively smaller. A distinctive stress "hump" is visible around the doubler area. This illustrates how the doubler attracts load; again, the stiffest patch shows the largest disturbed area. It is interesting to note the relative similarity of the overall patterns of the 1.0 mm (.040 inch) and the tapered 1.27/0.7 mm (.050/.028 inch) aluminum patches (respectively, figures 2b and c). In all uniaxial cases, the second rivet was located in the center of the most highly loaded region. For the tapered patch, the corner and second rivets appeared to be about equally critical, though at distances more than several rivet diameters away, the larger disturbed zones tended to center on or nearest the second rivet. Beyond the first rivet row in the direction of the cut-out, the skin stresses decayed rapidly to below the nominal 100 MPa (14.5 ksi) level.



Figures 2a,b. First principal stresses of riveted patch designs, 100 MPa (14.5 ksi) uniaxial tension. The circles indicate areas near rivets considered to be inaccurate.



Figures 2c,d. First principal stresses of riveted patch designs, 100 MPa (14.5 ksi) uniaxial tension. The circles indicate areas near rivets considered to be inaccurate.

The lateral (Poisson) contraction should cause the higher corner rivet loads. Indeed, in the finite element analysis, the corner rivets consistently attracted about 15 percent higher section (bearing) loads than the other rivets in the same row. However, the stress plots appear to indicate that the second rivet is located in the area of highest stress. As will be discussed later, cracks usually initiated from the second rivet in the critical outer rivet row. Although the corner rivet consistently feels the highest resultant section force, the second rivet usually shows the highest stresses and/or the largest disturbed zone in the contour plots. The second rivet may feel the influence of its two stiff neighbors on either side. In other words, the stress field of each rivet extends into the disturbed zone of the adjacent rivets. This superposition of stresses gives the second rivet the highest stress concentration in the uniaxial cases. The corner rivet has a slightly smaller disturbed area because it has interaction with only one highly loaded rivet. For the biaxial load case, which was not presented here due to space limitations, the corner rivets were always in the region of highest stress.

Skin stresses at the edge of the cut-out were inversely proportional to the extensional stiffness of the repair patches. When a uniaxial gross skin stress of 100 MPa (14.5 ksi) was applied, measured skin stresses at the cut-out were 134 MPa (19.4 ksi) with the tapered 2024 patch, 177 MPa (25.7 ksi) with the GLARE 3 patch. The peak stresses in the patches were always much lower than in the skins.

Static and Fatigue Testing of Riveted Repairs to Unstiffened Sheets

A series of static strength and constant amplitude fatigue tests was performed on unstiffened 2024-T3 panels with central 50 mm (2 inch) diameter holes and riveted patches. The specimen configuration was shown previously in figure 1. Unless otherwise noted, the specimens represented a flush skin patch; that is, the fuselage skin was countersunk.

The configuration and test conditions matched as closely as possible the uniaxial finite element model. Specimen manufacturing conditions, especially rivet squeeze force, were closely controlled. Rivet lengths were milled to +/- 0.1 mm (.004 inch) tolerances. Riveting was accomplished on a force-controlled machine; squeeze forces were 8,500 +/- 50 N (1,870 +/- 10 lbs). In most cases, the only specimen variable was the patch material and thickness.

This close control of conditions admittedly is not feasible with repairs performed in the field. Nonetheless, it was implemented in these tests to reduce experimental scatter and focus on the

effect of patch selection on fatigue life. A small number of specimens purposely manufactured with known defects provided an indication of the sensitivity of the process to common errors made in fuselage structural repair.

Test Conditions

Tests were done at room temperature in laboratory air. Static tests were carried out under displacement control on a 100-ton MTS test frame. Constant amplitude fatigue tests were performed in load control on a servo-hydraulic six-ton test frame at a frequency of 10 Hz.

The fatigue stress ratio, R , ($\sigma_{\min} / \sigma_{\max}$) was 0.05. Maximum gross skin stresses varied from 105 to 140 MPa (15.2 to 20.3 ksi); however, as the results will show, none of the patch types were tested throughout the entire stress range. Stress levels for individual patch types were chosen to produce fatigue lives in the range from 150,000 to 600,000 cycles.

It was not the intent of these tests to establish precise "repair fatigue allowables." Rather, the goal was an investigation of the effect of patch selection and load transfer on fatigue quality. Many "real world" variables with strong influence on fatigue life such as riveting quality and operating environment will reduce the magnitude of the lives tested here. Thus, these lives cannot be applied directly to operational aircraft.

Test Results

Static tests were carried out on two repair configurations: the tapered aluminum patch and the GLARE 3 patch. Both specimens failed across the first rivet row in the skin at a gross stress of 330 MPa (48 ksi).

Figure 3 shows the results of the fatigue tests. The general "order of merit" of the fatigue tests matched the finite element results exactly. The relatively high stresses predicted by the model in the 1.27 mm (.050 inch) untapered patch consistently gave the lowest lives, followed in increasing lifetime by the 1.0 mm (.040 inch) untapered patch, the tapered patch and the GLARE 3 patch. The outcome of the tests is striking: the GLARE 3 patches far outperformed all aluminum patches in number of cycles to fatigue failure at all stress levels tested. For example, at a gross stress level of 120 MPa (17.4 ksi, corresponding to a stress range of 114 MPa, or 16.5 ksi), the GLARE patch outlived the untapered patches by almost 200%, and outlasted the tapered patch by about 55%.

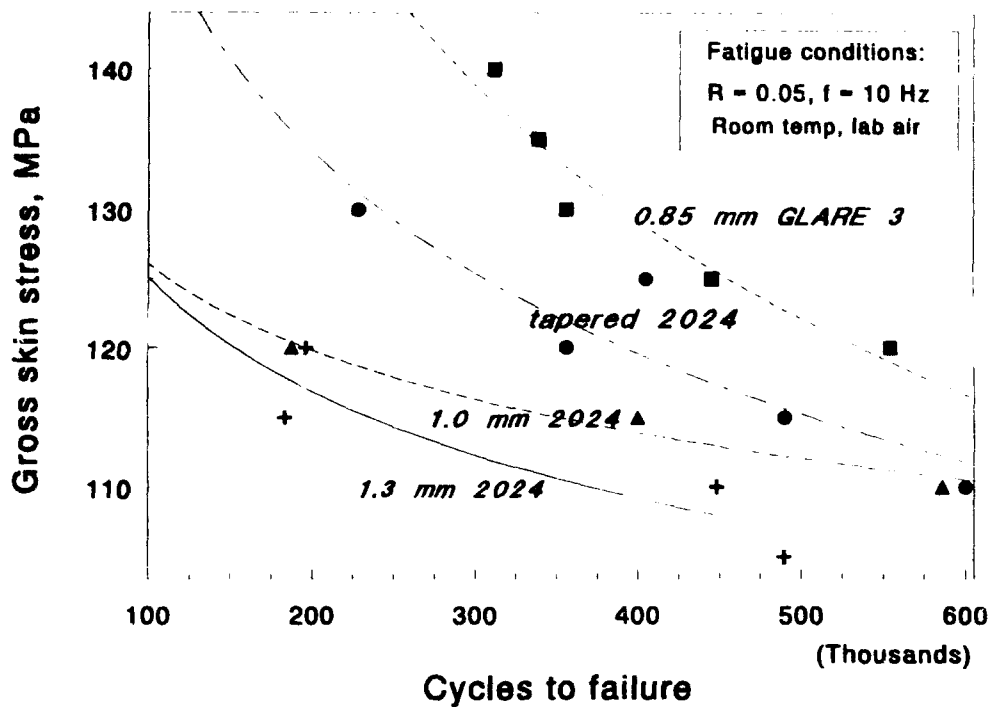


Figure 3. Constant amplitude fatigue performance of riveted repairs to 2024-T3 sheets. (All cracks and failures occurred in the 2024-T3 sheets.)

For all specimen types except the untapered 1.27 mm (.050 inch) 2024 patch, the results showed very little scatter. This may be attributed to the great care taken in specimen manufacturing, especially in the strict control of rivet squeeze forces, advocated in [6].

Two specimens were tested with countersinks in the patch rather than the sheet. The tapered patch specimen (tested at 6.5 to 130 MPa, or 0.9 to 18.9 ksi) failed after 131,000 cycles. The specimen repaired with a GLARE 3 patch was tested at the same stress level; failure occurred after 252,000 cycles, a 91 percent improvement. Both failures happened in the sheet at the critical rivet row.

All aluminum patch specimens failed by fatigue of the critical first rivet row in the skin. No damage was ever noted in any of the patches. In most instances where the initial skin crack was observed, it occurred at the second rivet hole of the first row. Some exceptions were noted with the tapered patches, where the first crack initiated from the corner rivet hole. When cracks were observed, failure followed rapidly. In the tapered patch specimen tested at a gross skin stress 130 MPa (18.9 ksi), for example, the first crack was observed visually at 220,000 cycles. Its length was 16 mm (0.63 inch). Complete failure occurred 8,400 cycles later, when

the crack had grown to an effective length of 85 mm (3.3 inches, including associated rivet holes).

The crack growth behavior of the GLARE 3 and tapered aluminum patches tested at 130 MPa (18.9 ksi) is illustrated in figure 4. Initiation times were quite similar, although at different locations, as mentioned previously. A striking feature is the extremely large number of cycles between initiation and failure in the skin repaired with the GLARE patch.

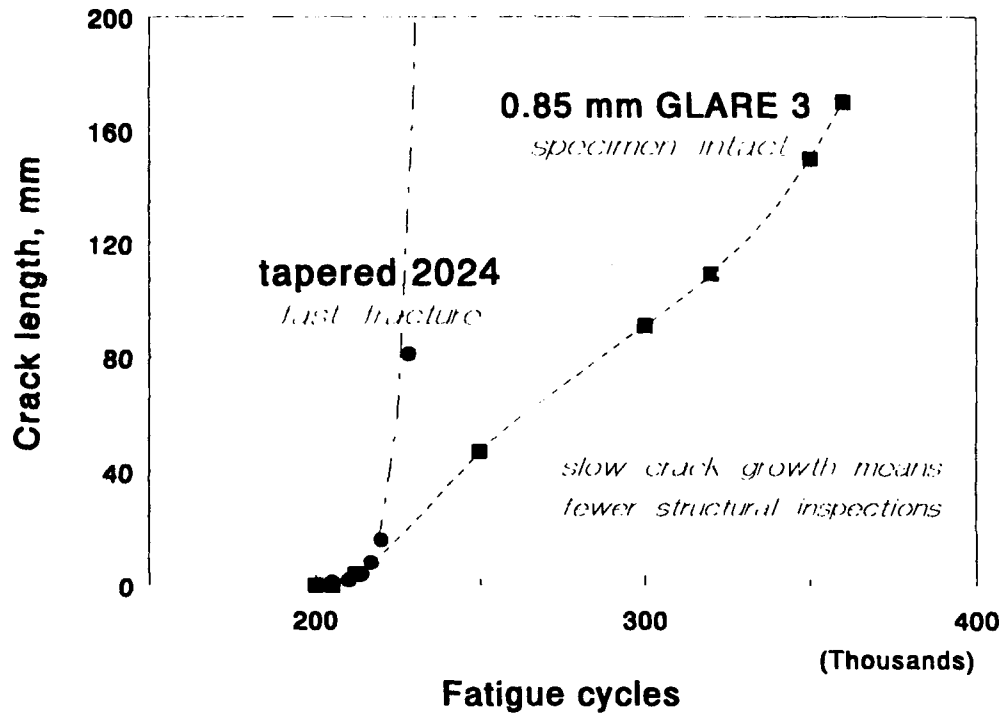


Figure 4. Comparison of crack growth behavior of 2024-T3 sheets repaired with GLARE 3 and tapered aluminum patches tested in constant ampl. fatigue at 6.5-130 MPa (0.9-18.9 ksi).

Most specimens patched with GLARE 3 failed differently from the test pieces employing aluminum patches. With GLARE 3 patches, cracks initiated at the cut-out in the skin, then grew relatively quickly until it lay between the nearest two rivets. Initiation was followed by a period of slow crack growth across both sides of the cut-out for more than 140,000 cycles. (This represents about a fifteen-fold increase in the time available to detect a crack compared with monolithic patch.) When the total crack exceeded the patch width by 10 to 20 millimeters, the crack growth rate increased considerably. Final failure occurred when the 2024 skin fractured, resulting in tensile overload of the GLARE patch.

Effect of Defects

Selected tests were repeated with an additional element added to represent typical mistakes made in repairs. Two defects were simulated: the knife edge condition, which results from too deep a countersink, and insufficient squeeze force, which can occur when access to both sides of the repair is restricted.

Knife edge countersinking is well-known for its drastic reduction of fatigue lives in riveted joints. According to Niu, the knife edge condition is said to exist when the total depth of the countersink exceeds about two-thirds of the skin thickness [7]. One can expect that the typical quality of riveting found in repairs is poor compared with newly manufactured aircraft because of the relative lack of control of the process.

In the first series, countersinks were made to approximately 80 percent of the sheet thickness, compared with about half the sheet thickness in the standard specimens. Table 2 shows the results.

Table 2. Effect of knife edge skin countersink on riveted repair fatigue lives.*

Patch Type	Nominal Sheet Stress, MPa (ksi)	Fatigue Life of Standard Countersink	Fatigue Life of Knife Edge Countersink	Life Reduction, %
GLARE 3	140 (20.3)	311,000	67,000	78
GLARE 3	130 (18.9)	356,000	293,000	18
Tapered 2024	130 (18.9)	228,000	75,300	67

*(*All failures initiated in the countersunk 2024-T3 sheet.)*

When the countersink depth was increased to the entire aluminum skin thickness (100% knife edge), the life reductions were even greater. At 130 MPa (18.9 ksi), the GLARE 3 specimen failed after 29,400 cycles (a 91 percent reduction). At the same stress level, the life of the tapered patch fell 92 percent, to 18,100 cycles.

Although the number of knife edge samples tested was small, the tendency toward reduced fatigue lives is clear. In addition to the considerable reduction in fatigue lives, a change in failure mode occurred in the specimens with GLARE 3 patches. Instead of the damage tolerant mode of cut-out cracking and slow growth observed in the nominally countersunk specimens, the knife edge condition shifted the failure location to the first rivet row, where the aluminum patch repair specimens also failed. However, the more efficient load transfer demonstrated in the analysis by the GLARE 3 patches apparently resulted in their continued longer lives for equivalent defects.

Another common defect in riveted repairs is improperly driven rivets. Table 3 illustrates the effect of insufficient squeeze force on the riveting operation on fatigue life. Clearly, a properly filled rivet hole is necessary for good fatigue performance. "To obtain substantial interference the rivet must be bucked (driven) squarely. Especially in field repairs where space may be [restricted], rivets are not bucked squarely." When this occurs, fatigue lives can be reduced by almost an order of magnitude [1].

Table 3. Effect of insufficient squeeze force on riveted repair fatigue lives.*

Patch Type	Nominal Sheet Stress, MPa (ksi)	Cycles to Failure, 8,500 N Squeeze Force	Cycles to Failure, 3,800 N Squeeze Force	Life Reduction %
GLARE 3	130 (18.9)	356,000	44,600	87
Tapered 2024	130 (18.9)	228,000	27,300	88

(*All failures initiated in the countersunk 2024-T3 sheet.)

These specimens were manufactured with 3,800 N (840 lbs) of squeeze force, instead of the 8,500 N (1,900 lbs) prescribed in the baseline tests. This resulted in a driven rivet head expansion of only about 10 percent, compared with 50 percent expansion for the baseline specimens. (The intent here was to simulate, in a controlled way, the effect of rivet clinching, which happens when the rivet is not driven squarely.)

The results portray the strong influence of poor hole filling on fatigue lives. Furthermore, the GLARE 3 patch specimens failed across the first rivet row instead of across the cut-out, as they had done in the nominal case. Nonetheless, the GLARE 3 patch repairs continued to outlast the tapered patches, which can be attributed to the more favorable load transfer.

Discussion

Finite element analysis performed on riveted patches showed that patch thickness and stiffness play dominant roles in the load redistribution in and around a typical repair configuration. Conventional aluminum alloy patches cause high stress concentrations at the first rivet row, which leads to early cracking in the corner rivet (biaxial load case) or the adjacent rivet (uniaxial load case). These corner cracks quickly grow out from under the patch, and reach a critical size after a few thousand flights.

This failure behavior involving riveted aluminum patch repairs casts doubt on the value of complex patch configurations like fingered patches for increased inspectability. Thickness tapering or fingering of patches, while increasing somewhat the overall life of a riveted repair, do

so at a high cost of time and labor. Furthermore, tapering only incrementally increases the amount of cycles during which a skin crack can be detected. This imposes a heavy inspection workload on operators.

The use of high-strength, moderate-modulus materials like GLARE 3 enables repairs to be made quickly and simply, without the need for thickness tapering. The high strength material allows a thinner patch to be used, which in turn reduces both secondary bending and first row rivet bearing loads, compared with a conventional aluminum patch. The lower overall extensional stiffness of the patch attracts less load into the repair area.

The fatigue life of 2024-T3 skins repaired with GLARE 3 riveted patches far exceeded any other riveted patch configuration tested. At equivalent stress levels, crack initiation times for tapered 2024 and untapered GLARE 3 were similar. However, uniaxially loaded skins repaired with the GLARE patch exhibited slow, stable crack growth periods more than 10 times greater than the tapered patch repairs.

The failure mode experienced with GLARE 3 patches (where cracks grew slowly from the cut-out) greatly enhances the damage tolerance of uniaxially loaded riveted repairs. An alternate load path exists through the patch, even when cracks extend well beyond the patch edges. This alternate load path results in a kind of macroscopic crack bridging by the GLARE patch, which retards crack growth in the aluminum skin until the cracking the skin exceeds the width of the patch. This very slow crack growth reduces the need for structural inspections of GLARE patches.

Typical defects found in riveted repairs (poor riveting and knife edge countersinking) reduced the fatigue lives of riveted repairs by factors of up to ten. When these defects occurred in aluminum skins patched with GLARE 3, the crack location changed from across the cut-out to the first rivet row. However, the GLARE 3 patch repairs retained their relatively better performance compared with monolithic patches with equivalent defects. The location of the countersink (in the skin or in the patch) had no affect on relative performance. In all cases, more efficient load transfer was the cause of the performance improvements.

In biaxial loading more typically encountered in pressurized fuselages, the corner rivets become more critical due to their location in two outer rows (hoop and longitudinal load directions). A change in failure location to the first row is anticipated. Regardless of failure location, it is expected that the more favorable load transfer in and around thin GLARE patches will continue to result in the highest fatigue lives possible for a riveted repair.

A simple rule of thumb can be applied in the substitution of GLARE 3 patches for repairing fuselage skins of 2024-T3. Repairers should choose a GLARE 3 patch thickness in the range from 85 to 100 percent of the skin being repaired to assure adequate static strength while maintaining a reasonably low patch extensional stiffness. Table 4 provides a simple look-up reference applicable to common fuselage skin thicknesses.

Table 4. Recommended GLARE 3 Patch Thickness for 2024-T3 Repairs.

Original skin thickness, mm (inches)	GLARE 3 patch thickness, mm (inches)	GLARE 3 patch lay-up (inches)
1.0 (0.040)	0.85 (0.034)	2/1-0.3 (0.012)
1.2 (0.047)	1.1 (0.044)	3/2-0.2 (0.008)
1.3 (0.050)	1.1 (0.044)	3/2-0.2 (0.008)
1.6 (0.063)	1.4 (0.056)	3/2-0.3 (0.012)
1.8 (0.070)	1.55 (0.062)	4/3-0.2 (0.008)
2.0 (0.080)	1.95 (0.078)	4/3-0.3 (0.012)

Elimination of the need for tapering the patch saves a substantial amount of time and cost from the repair process. A cost analysis presented in [2] indicated that the higher material cost of the GLARE patch is offset by these fabrication cost savings. Reduced inspections over the life of the repaired structure will result in a lower life cycle cost for GLARE patch repairs.

Riveted GLARE 3 repairs are best suited for patching of incidental damage and localized corrosion attack of monolithic aluminum fuselages. Conventional corrosion control practices (i.e., "wet" installation of fasteners and fay surface sealing with corrosion inhibiting sealant) should be applied.

Summary and Conclusions

Current methods of riveted repair of pressurized aluminum fuselage skins cause fatigue problems for operators. Besides their adverse affect on safety, conventional riveted repairs are accompanied by the unwanted economic burden of increased inspection requirements.

A new concept called "soft patching" has been introduced to improve the fatigue performance of riveted repairs to pressurized aluminum fuselage skins. Soft patching involves the use of thin, untapered patches of the high-strength, moderate-modulus fiber metal laminate GLARE 3 in place of thick tapered monolithic patches. This reduces load attraction to the repair zone, while diminishing bearing loads on the critical first rivet row and reducing secondary bending.

Soft patching with GLARE 3 improves the fatigue life of riveted repairs by 50 to 200 percent over various techniques involving monolithic aluminum patches. GLARE 3 patches simplify the repair task by eliminating the need for costly, time-consuming thickness tapering of patches. GLARE imposes no new training or equipment requirements on maintenance personnel. Inspection workloads are reduced while safety and damage tolerance are improved at a lower life cycle cost.

References

1. Swift, T., "Repairs to Damage Tolerant Aircraft," *Proc. Int. Symp. on Structural Integrity of Aging Airplanes*, Atlanta, Georgia, 20-22 March 1990.
2. Fredell, R. and J. Gunnink, "Fiber Metal Laminates for Improved Structural Integrity," *Proc. Int. Symp. on Structural Integrity of Aging Airplanes*, 31 March-2 April 1992, pp. 362-375.
3. Fredell, R., "Riveted Repairs", from *Damage Tolerant Repair Techniques for Pressurized Aircraft Fuselages*, Ph.D. dissertation, Delft University of Technology, Delft, the Netherlands, to be published in 1994.
4. Seegers, J.W.G., "Finite Element Calculations for a Stringer Reinforced Butt Joint," Master's Thesis, Delft University of Technology, Faculty of Aerospace Engineering, Delft, the Netherlands, June 1992.
5. Slagter, W.J., "Flexibility Parameters for a Monolithic Plate with Eccentrically Loaded Pin," *Computers and Structures*, **40**, 1991.
6. Müller, R.P.G., "Fatigue Crack Initiation in Riveted Lap Joints and in Pressurized Fuselages," *Proc. 1993 SAMPE European Conference*, Birmingham, England, October 1993.
7. Niu, M. C.-Y., *Airframe Structural Design*, Hong Kong: Conmilit Press Ltd., 1988, pp. 232-233.

B-1B Shoulder Longeron Repair

L.G. Hansen
Rockwell International
North American Aircraft Division

Abstract

Early in their service life, B-1B aircraft experienced cracking of the shoulder longerons, primary structural members of the B-1B fuselage. A highly efficient repair involving bonded doublers, both metallic and advanced composite, was developed and is presented in this paper. Analysis performed in support of the repair development included overall aircraft finite element models (FEM), detailed models of the repair, and the use of a p-element code to predict stress intensity factors for a complex geometry. Test configurations and results are presented for the element tests, full scale fatigue test, and flight verification tests that were conducted in support of the repair development. Since the final repair configuration used an elevated temperature cure adhesive, special tools and processes were developed to support the installation of the repair doublers. The special tools developed, the installation process, and some of the lessons learned are also presented.

Introduction.

Cracks were found in the B-1B shoulder longerons during one of the Analytical Condition Inspections (ACI) performed during February 1991 in support of the Aircraft Structural Integrity Program (ASIP). The cracks were determined to have been caused by a local stress concentration that was introduced during the production redesign after the completion of the full scale fatigue test. The shoulder longerons are located at 25° off the top dorsal longeron; the cracks occurred at the juncture of the forward intermediate fuselage and the wing

carry through structure (Ref. Fig. 1). The shoulder longerons are two of twelve longerons at that point, but together carry 30% of the total fuselage bending load. Actual aircraft usage has been higher than design values in both gross weight and load factors, and this also contributed to the early failures.

Repair Design

The shoulder longeron is made of 7075-T73 aluminum alloy forging material, is over 17 feet long, and attaches to the fuselage frames every 8 to 12 inches. The longeron cross sectional area is greater than 5 square inches. Furthermore, the longeron is part of the fuel tank close-out structure and therefore removal and replacement of the longeron would be a very expensive and time consuming process. It was

imperative that the longeron be repaired with a local doubler because the fuselage cross section is so large in the repair area that any reasonably sized doubler would have very little effect on the gross strains. The doubler had to be designed to reduce the local stress in the longeron below the crack growth threshold while maintaining low stresses in the doubler. Furthermore, load distribution changes caused by the doubler could not put other structure in the vicinity at risk.

A series of repair designs involving bolted and/or bonded configurations, both metallic and of advanced composites, were considered. The doubler to be installed over the cracked web would have to contend with a complex load path, complex geometry and existing bolt holes. The advanced composite versions would have required a cross plied lay-up to contend with the

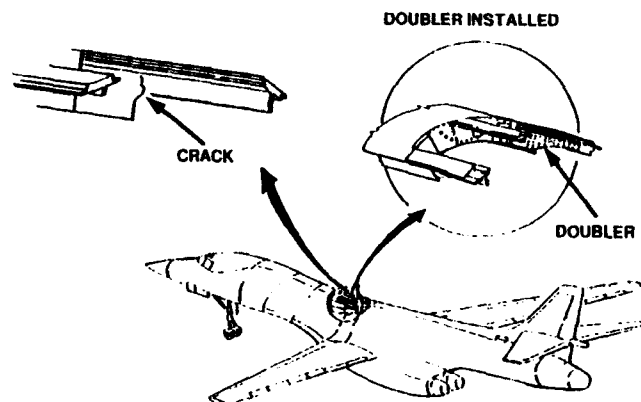


Figure 1. Longeron Crack Location

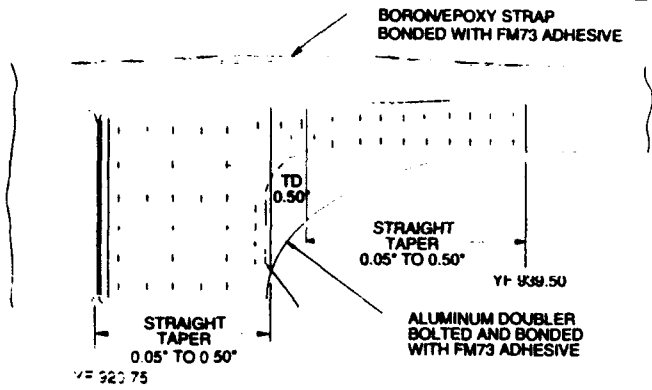


Figure 2. Final Repair Configuration

varying stress field and would have numerous bolt holes. The resulting strength would be no better than an aluminum doubler. Cocuring appeared to be impossible due to the complex geometry and limited access. For those reasons an aluminum doubler (7075-T7351 alloy) was selected instead of the advanced composite versions. The final configuration is bonded because a bonded joint is much stiffer than a bolted joint and therefore does better at holding the crack together.

To further reduce the stress level in the crack area, a bonded boron/epoxy strap doubler was added to the top of the cap also. Boron was selected in this case because it could be contoured to fit the outer moldline surface, its high modulus reduced the profile (important because the doubler is outside the aircraft moldline), and because the bonded approach

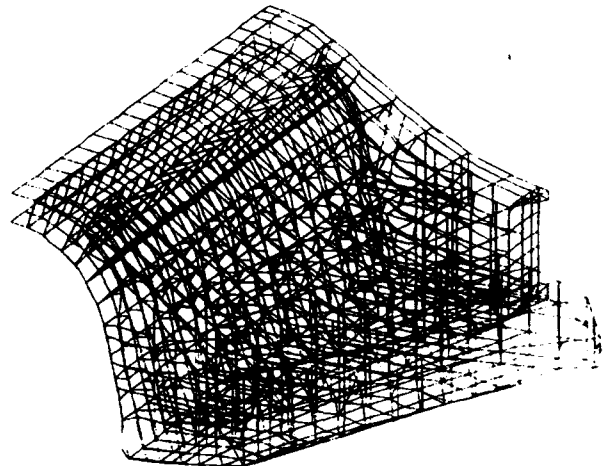


Figure 4. Fwd. Int. Fuselage FEM

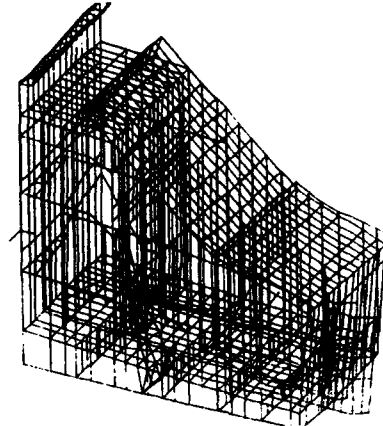


Figure 4. (cont.) Wing Carry Through FEM

avoided putting any fastener holes in the large mass of the longeron cap. The boron strap consists of 50 plies of boron epoxy, all aligned parallel to the longeron, with the strap tapering to two plies at each end of its 21 inch length. The final repair configuration is shown in Fig. 2.

Bonding of the boron strap results in an unfavorable pre-stress on the longeron due to the difference in thermal expansion coefficients. Fortunately however, the fuselage bending moment changes from tension to compression in the location of the repair as the aircraft is jacked off the gear using the fuselage jacks. This allowed the pre-load to be overcome by jacking the aircraft prior to repair. Fig. 3 shows the change in

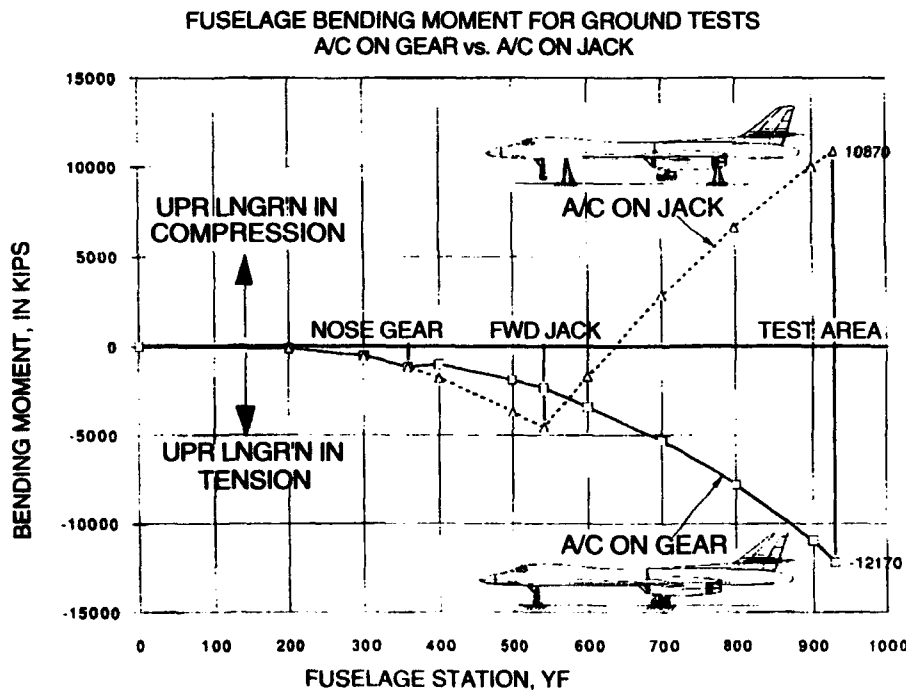


Figure 3 Fuselage Bending Moment Diagram

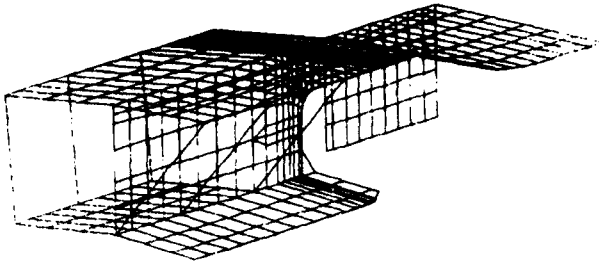


Figure 5. Local FEM of Longeron Crack Area

fuselage loads caused by jacking. This procedure also resulted in beneficial pre-stress on the aluminum doubler which reduces the stress at the crack location.

Analysis

An existing Nastran finite element model of the entire B-1B airframe was used to determine the loads in the longeron and to predict load changes with the doublers added. The model was modified to enhance the details in the area

Bondline Shear Stress (psi) for Aluminum Doubler
Piecewise Linear Solution @ Design Ultimate Load

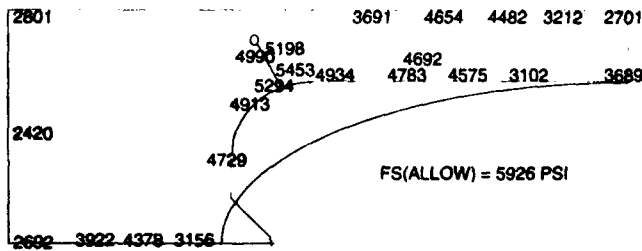


Figure 7. Bondline Stresses For Web Doubler

of the repair and to eliminate unnecessary substructures from the solution in order to reduce running costs. Model accuracy was verified by the available flight test strain gage data.

An even more detailed model was constructed of the local repair area using boundary loads extracted from the airframe model. The overall airframe model is shown in Fig. 4 and the more

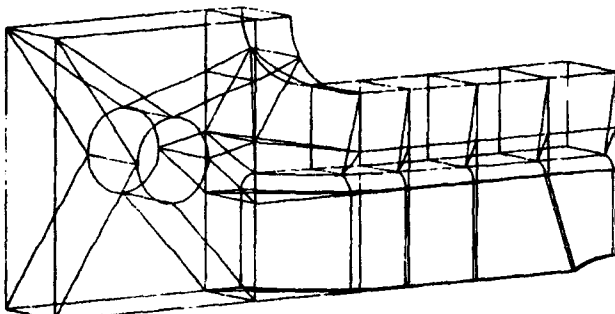


Figure 8. P-Element Model of Cap-Web Specimen

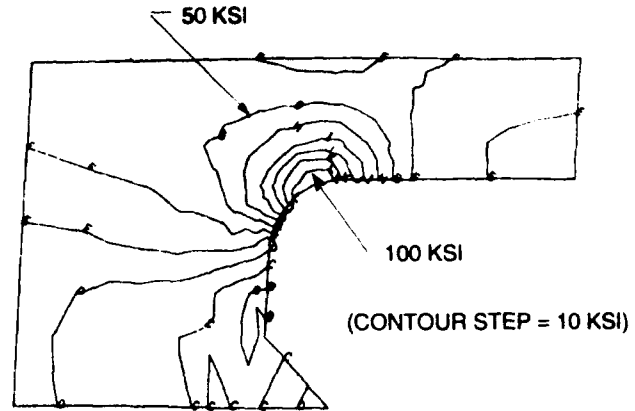


Figure 6. Shoulder Longeron Stresses at Crack Location

detailed finite element model is shown in Fig. 5. The detailed model was used to evaluate the various repair options and to support the optimization of sizing for the final selected configuration. Fig. 6 shows a typical stress distribution that was obtained from the detailed model. As will be shown in the following section on testing, the model gave very accurate predictions of the stress levels.

To assure the adequacy of the bonded joints a non-linear model was made of the doublers and bond joints. This is especially important for thick structures where the plasticity of the bond joint plays an important part in the success of the design. The non-linear models were used to help configure the tapers on the doublers and to evaluate variations in bond line thickness. This information was then used to set allowable tolerances on the bond joint assembly. Maximum bond line stresses as determined by the non-linear model of the web doubler are depicted in Fig. 7.

Determining the stress level at which the longeron web crack would no longer propagate

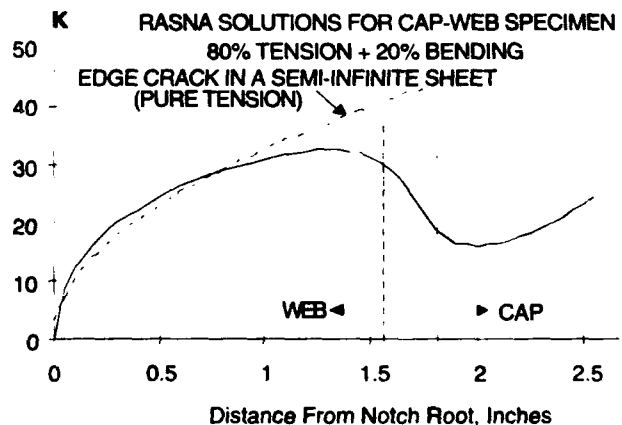


Figure 9. Stress Intensity Distribution as Predicted by P-Element Model



Figure 10. Element Test Specimen in Fatigue Machine

was a critical concern in the repair design. Due to the complex configuration of the cap-web intersection and the complex stress distribution, it was not possible to easily relate previous crack growth data to the longeron case. It was therefore decided to use available p-element codes to determine the stress intensity distribution and relate that to existing crack growth data. Rasna Corporation's "Mechanica" program was selected for the job of determining stress intensity factors.

The method was first tried by modeling geometry's with known stress intensity solutions and then modeling a test configuration similar to the actual longeron configuration. The p-element model of a cap-web test specimen and the resulting stress intensity distribution are shown in Fig. 8 and 9. Laboratory crack growth measurements (discussed in later section) were also conducted to validate this approach. A model was then constructed of the longeron with repair using the same approach and the doubler sizes were optimized to reduce the stresses below the crack growth threshold. This provided confidence going into the full scale fatigue test that the repair would be successful. For more detailed discussion on the p-element technique that was used, see Ref. 1.

Testing

Element Tests. A doubler element test specimen was designed to provide initial information on the capability of a doubler to

stop the crack growth and to evaluate the relative effectiveness of a bolted versus bolted and bonded repair. A bolt pattern already existed in the longeron at the location where the doubler was to be added, so a bonded only option was not viable. Since the repair had to be installed on the aircraft in an area that had large heat sinks and also was a fuel tank close-out structure, there was initial hope that room temperature cured adhesive could be used. For that reason, three separate doubler element test specimens were tested.

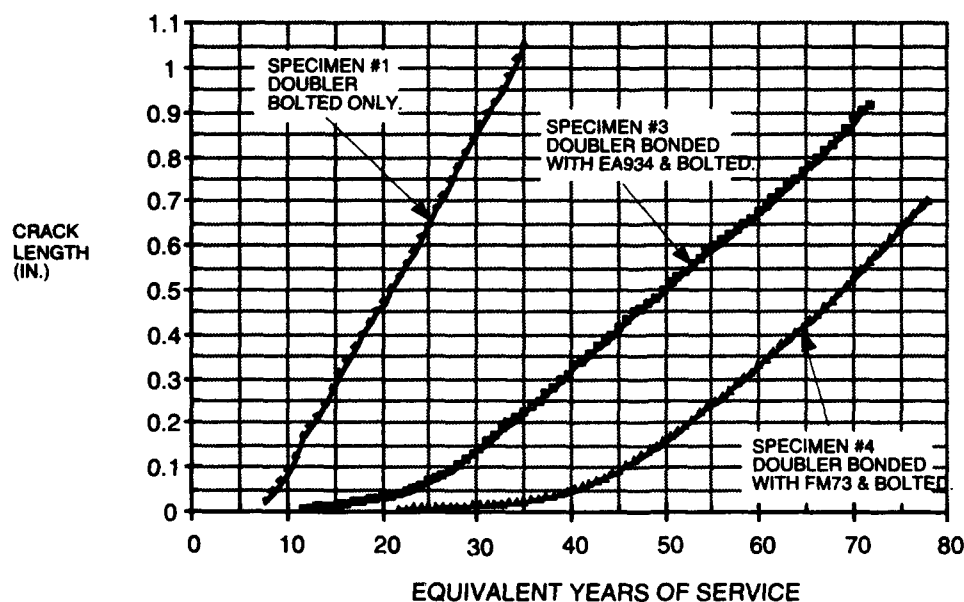


Figure 11. Crack Growth Comparison for Element Tests

A large plate with a cutout shaped like the longeron was mounted in the fatigue test machine and loaded to give the same stress as the longeron web at the critical corner. A 2 inch saw cut was made at the same location as the cracks on fleet aircraft. Then the doubler was installed (Ref. Fig. 10) and spectrum loading applied until the crack grew to 1.0" in length measured from the stop drill hole. Then the specimens were tested to failure to determine residual strength.

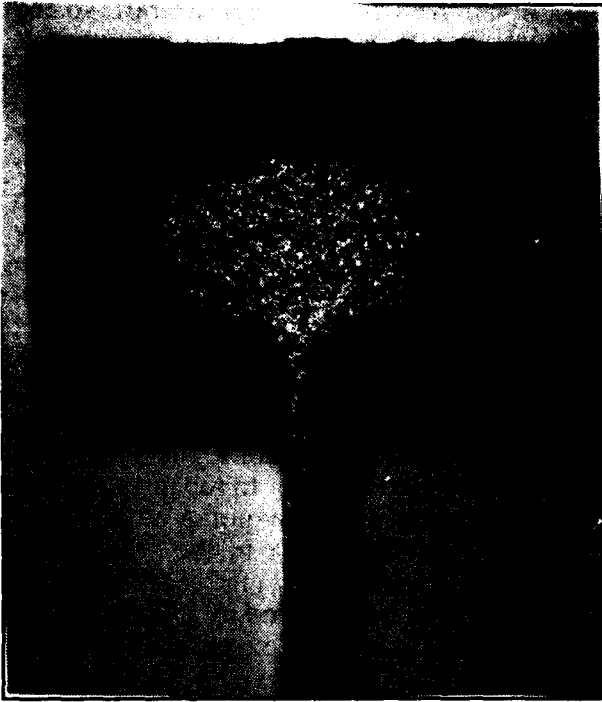


Figure 12. Failed Cross-Section of Cap-Web Specimen

As can be seen in Fig. 11, the bonded doublers had a distinctive advantage over the bolted only joint. Also evident was that the room temperature cure adhesive (EA934) was not as effective as the elevated temperature cure adhesive; this data led directly to the decision to proceed with American Cyanamid FM73



Figure 14 Cap- Web Specimen in Fatigue Machine

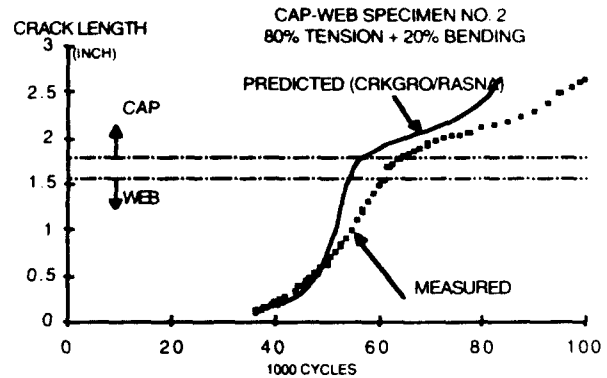


Figure 13. Cap-Web Crack Growth Comparison

adhesive for further development and verification testing.

Cap-Web Testing. All the cracks on the longerons originated in the relatively thin web that protruded downward from the large longeron cap. It was intuitively thought that the cap would act as a natural crack stopper for the web as the crack approached, but an analytical means was needed to determine how much the crack would be retarded by the mass of the cap and at what stress level would the crack growth be stopped. The p-element code mentioned earlier was the analytical method selected, but an empirical validation and calibration of that method was needed. A development test article was devised to grow a crack from a thin web into a thick cap with the same geometry and stress levels of the shoulder longeron. The failed specimen cross section is shown in Fig. 12.

Crack growth was predicted for the cap-web specimen using the p-code FEM as discussed in the earlier section and then compared to the test results. As can be seen in Fig. 13, the method gave very reasonable results and thus could be used to predict a stress level to stop the crack growth.

The third and final cap-web test specimen was also equipped with a bolted and bonded (FM73) aluminum doubler and also a boron strap doubler after a crack was initiated and thus served to give initial validation of the repair concept. The cap-web specimen with aluminum doubler and boron strap installed is shown in the fatigue test machine in Fig. 14. Both doublers successfully withstood 120 equivalent years of cycling without separation and stopped the crack growth. Smaller dog bone size specimens had been tested earlier to support the design of the boron strap in terms of the ply stackup, taper, and bond joint.

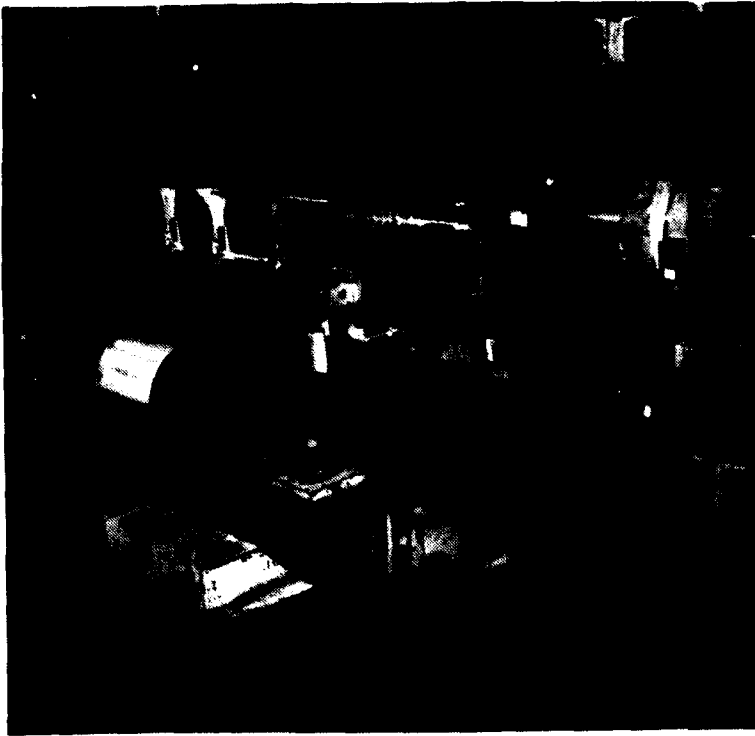


Figure 15. Full Scale Fatigue Test Article

Full Scale Fatigue Test. The availability of a residual production longeron made it possible to conduct a full scale fatigue test of the longeron and final repair design with high accuracy. Spectrum loading for the test specimen was derived from the ASIP strain gage that was located on the fuselage 80 inches forward of the crack area. Over 10,000 hours of flight data had

been analyzed for the fleet aircraft, so the actual aircraft usage was also known with high accuracy.

The specimen was mounted in a test fixture as shown in Figure 15 and loaded so as to match the stress distributions determined on the finite element model and confirmed by flight test strain gage data. The specimen was notched at the same location that cracks were being experienced on fleet aircraft and then cycled until a crack developed and grew to a length of 1.5", which was similar to cracks being found during aircraft inspections. A 90% load spectrum was used prior to repair to prevent the crack from suddenly going critical. The time to grow the crack to the 1.5" length was 3000 flight hours (10 years of B-1B service), which compared to 1500 hours for fleet aircraft which experienced 10% higher loads.

The crack was then repaired using the same repair that was to be applied to fleet aircraft.

A stop drill hole was drilled at the end of the crack both to retard more growth and also to provide an easy way to inspect for reinitiation of the crack using an eddy current probe. The aluminum doubler was first installed and a strain survey conducted and then the boron strap installed and the strain survey repeated. In this way the effectiveness of the boron strap to reduce overall longeron stress was confirmed. The 10-12% stress reduction matched

predictions and so the decision was made to include the boron strap in the final repair.

With the repair in place, the test article was cycled for the equivalent of 60 years of aircraft flying, which represents two lifetimes for the B-1B. At that point the crack had not grown at all, but the boron strap had started to disbond at the forward end. This was attributed to an incomplete cure caused by the large heat sink, discussed later. The boron strap was removed at this point and replaced using the improved process and tooling developed for field installations.

Shoulder Longeron Load vs. Exceedances

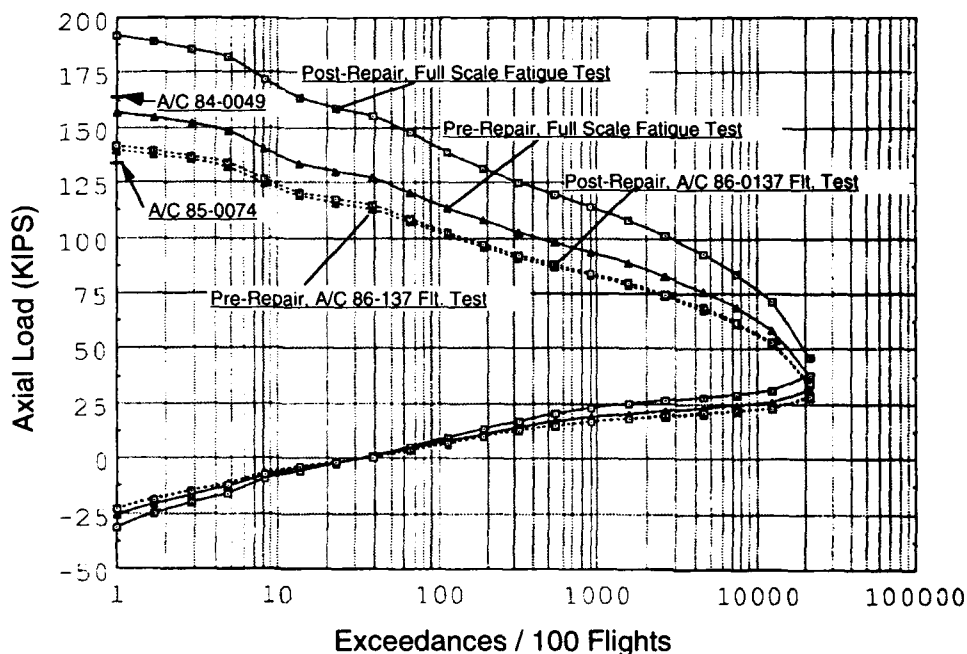


Figure 16. Exceedance Data for Full Scale Fatigue Test Loads

B-1B 25 LONGERON FLIGHT TEST DATA COMPARISON
ORIGINAL LONGERON VS. REINFORCED LONGERON

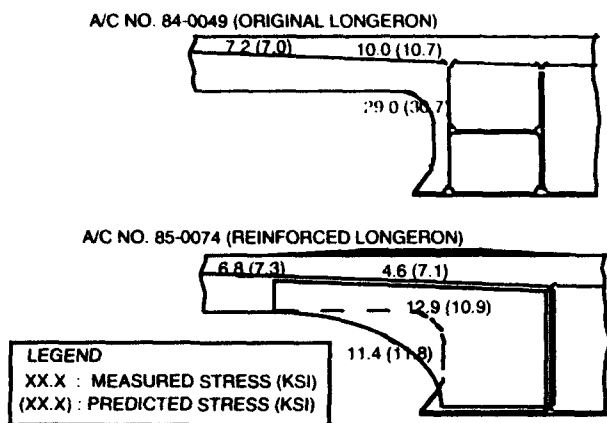


Figure 17. Measured vs. Predicted Stresses

Sharp notches were introduced to the specimen at this time using a jewelers saw at 3 critical locations, including the aluminum doubler, in order to conduct a damage tolerance test of the longeron and repair. Cycling was continued for another 60 aircraft years with no crack propagation at the original crack site or any of the other notches. Both the boron strap and aluminum doubler showed no indication of disbonds. The specimen was finally loaded to an ultimate load of 145% limit load to demonstrate residual strength. At that point the test article failed at a location away from the repair area and in the attachment to the test fixture.

The full scale fatigue test was conservative compared to fleet aircraft in three separate ways: (1) Longeron loads were increased by 10% over those determined analytically and confirmed by flight test. (2) The doubler for fleet aircraft is thicker than the fatigue test specimen because refined analysis showed a 10% stress improvement for the thicker doubler. (3) The stop drill hole on fleet aircraft was cold worked to further retard crack growth but the test article was conservatively left as-drilled.

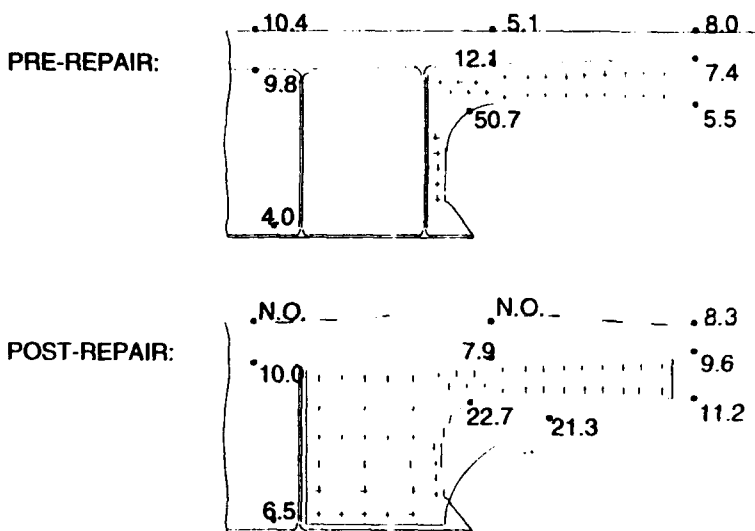
Figure 16 shows the conservatism in the test loads as compared to the

flight loads measured on the three flight test aircraft. Lower loads were applied to the test article prior to the doubler installation to avoid any sudden rupture of the specimen during the crack growth period.

Flight Test. Flight testing was performed on three different aircraft. Initially one of the B-1B flight test aircraft (A/C 84-0049) was instrumented to obtain stress levels in the critical region, to obtain longeron loads, and to verify the accuracy of the finite element model. At the same time that A/C 84-0049 was flight tested without a doubler, A/C 85-0074 was flight tested with a doubler. Later in the development program A/C 86-0137 was flown both with and without the repair doubler.

Test results on all three aircraft were similar in that the strain gage results confirmed that the finite element model accurately predicted the stress distributions. Figure 17 shows the predicted and measured stresses for forward wing sweep flight conditions flown on A/C 84-0049 without a repair doubler and on A/C 85-0074 with a repair doubler. The flight test also confirmed the large reduction in stress provided by the doubler and that the doubler stress also was not excessive (Ref. Fig. 18 for a flight condition with aft wing sweep). Several flight conditions were flown at different wing sweeps because the longeron load distribution varies considerably as the B-1B's wings are swept from

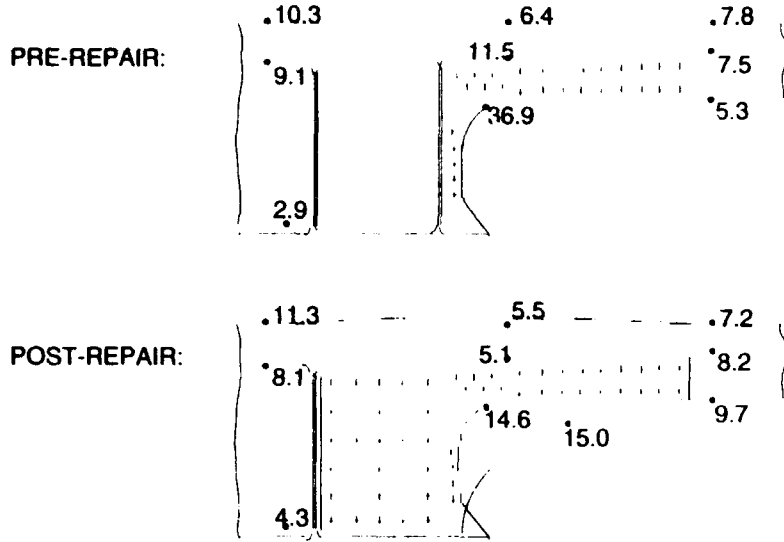
B-1B SHOULDER LONGERON REPAIR EVALUATION
A/C 86-0137 FLIGHT TEST RESULTS, 67.5° WING, 2.5G



STRESSES SHOWN ARE FROM GROUND REFERENCE TO FLIGHT STRESS.
NO. DENOTES NOT OPERATIONAL

Figure 18. Flight Test Measured Stresses

**B-1B SHOULDER LONGERON REPAIR EVALUATION
GROUND JACKING TEST RESULTS, A/C 86-0137 (A/C #97)**



(NOTE: NUMBERS SHOWN ARE DIFFERENCE IN STRESS (KSI) BETWEEN "ON GEAR" AND "ON JACK")

Figure 19. Longeron Stresses with Doubler

**FOREBODY BENDING ASIP GAGE STRESS vs. 25 ° LONGERON AXIAL LOAD
POST-REPAIR TEST, 67.5° WING MANEUVERS**

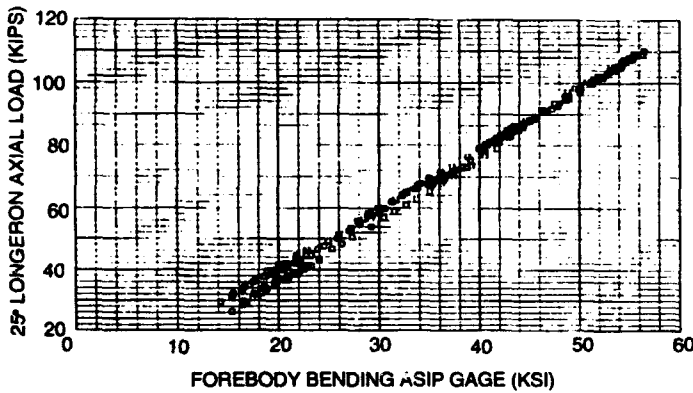


Figure 20. Relationship Between ASIP Gage and Longeron Load For Aft Wing Position

the 15° forward position to the 67° aft position. In addition, because the fuselage bending moment actually reverses at the critical crack location as the aircraft is jacked off the gear using the fuselage jacks, gages were monitored for the jacked and unjacked conditions. This provided a very accurate calibration of the strain gage because the fuselage bending moment was well known for these conditions. Results of this test are shown in Fig. 19.

Strain gages were strategically placed so that the total load in the longeron could be calculated before and after the doubler installation. This was important because the fatigue test loads for

the installed doubler were to be increased to match the aircraft load increase in the longeron due to increased stiffness with the doubler. Since the test spectrum was based on the ASIP strain gage, the longeron strain gage values from flight test were plotted versus the ASIP gage to determine the relationship (Ref. Fig. 20). This relationship was used to determine the proper load to apply to the full scale test article. Furthermore, the change in this relationship with the doubler installed showed that the longeron load only increased 3%. Therefore the 10% increase that had been applied to the test article was conservative, as expected.

Repair Installation.

Room temperature curing adhesive was selected for the initial prototype aluminum doubler installations because it was recognized that it would be very difficult to install a high temperature adhesive due to the considerable heat sink provided by the airframe. At the same time, a co-cure of the boron strap and adhesive was used in order to assure a good fit up to the longeron structure. The room temperature curing adhesive (Dexter / Hysol EA934NA) later was determined to be structurally insufficient for this application as further analysis was performed. Furthermore, co-curing of the boron strap proved to be very difficult due to the heat sink. Several of the early boron

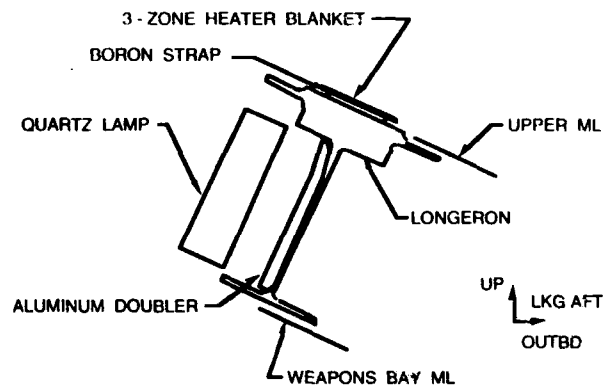


Figure 21. Heater Arrangement For Bonding

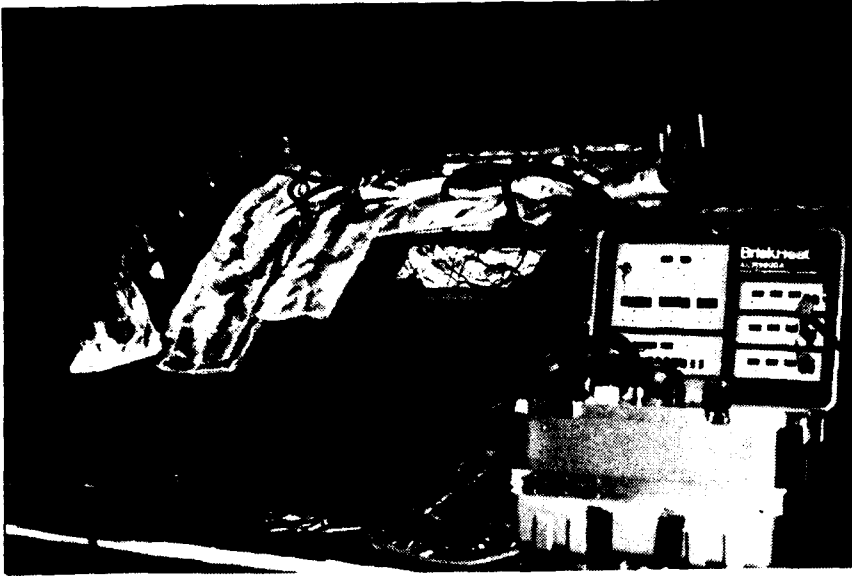


Figure 22. BriskHeat Unit With Heater Blanket During Boron Strap Bonding

straps delaminated or disbonded in service due to incomplete cure.

A bonding development task was initiated to resolve the bonding difficulties and several changes were initiated. Among the changes was a change to a pre-cured boron strap since there was found to be only very small variations in the machined longeron surface for bonding. It is felt that the boron strap could have been co-cured with the other changes that were made but this provided an opportunity to inspect a fully cured boron strap and reject bad ones prior to installation on the aircraft. Also, pre-curing allowed for a slightly lower bonding temperature and therefore less of a built in pre-stress condition. The adhesive system was changed to American Cyanamid FM73 which was cured at a minimum of 200°F for a minimum of 6 hours. Aluminum surfaces were primed with BR127 primer.

Other changes included the development of a more controllable heat source that allowed for complete heating of the longeron and doublers during the bonding process. A three zone heater blanket was placed on the boron strap atop the longeron while a quartz lamp heater was simultaneously heating the aluminum doubler in order to provide distributed heat to the longeron mass. (Ref. Fig. 21) The heater blanket was controlled using a BriskHeat ACR9000A control box which also provided the vacuum source for the boron bonding (Ref. Fig. 22). Thermocouples were placed strategically on the boron strap and on the aluminum longeron to assure that proper bonding temperature was

reached while at the same time assuring that longeron temperatures did not exceed allowable for the aluminum. The maximum temperature of the aluminum structure was kept at or below 260°F. Fuel tanks in the repair area were purged with nitrogen continuously during the heating process to remain safely below the lower explosion limit.

A special control box was built to control the quartz lamp box that was designed for placement inside the aircraft to heat the longeron web and aluminum doubler. (Ref. Fig. 23) Several thermal surveys were conducted prior to doubler bonding to refine the control box settings and the placement of custom fabricated insulation blankets.

To assure proper fit up of the doublers, Verifilm is used to determine gaps prior to each doubler installation and the heating apparatus is used to cure the Verifilm. This also provides a check of the heating process prior to the actual bonding step.



Figure 23. Heater Box With Control Unit Used For Aluminum Doubler Bonding

Pressure is provided to the boron strap atop the longeron by means of a vacuum bag which also covers test coupons at the same time. Because of the complex shape and location of the aluminum doubler, it would have been extremely difficult to use a vacuum bag for the curing operation. The existing fasteners were therefore used to provide the bonding pressure. Several development tests were conducted to determine the effect of fastener pre-load on bond strength. While consideration was given to spring loaded clecos to clamp the doubler, that method was discarded because of the difficulty in removing the clecos at the end of the bonding process. The final process calls for torquing the fasteners prior to and after bonding and then leaving them in place as a backup to the bond line in case of bond failure and to provide some anti-peel effect.

Training. Since the strength of a bond line is not determined by any NDI process, it is very important to assure that the bonding process is highly reliable. To achieve this, a very detailed step by step procedure was prepared for the B-1B longeron repair. The procedure (Reference 2) includes a complete description of all necessary tools and materials. Special inspection points were identified to assure that the process was being followed and bonding certification coupons used to validate materials, processes, and control settings.

In addition to the step by step procedure, a special training program was set up to provide instructions specific to this repair to all persons participating in the repair installation. This has become an important issue because the repair is being performed on-aircraft as a field repair and the repair crews change as time passes. The step by step procedure and the training program provide stability to the installation process.

Inspection. Provisions were made to allow for inspection of the doubler bond joints by manufacturing specimens with known defects to the same configurations as the repairs. Inspection processes were also developed to assure a high confidence in identifying defects. The defects include delaminations or cracks at any of the layers in the repair joint. Special inspection tools were purchased, including eddy current probes to view the back surface of the longeron through the stop drill hole and a back viewing boroscope. Ultrasonic inspection methods were developed to look through the thick aluminum doubler for indications of disbonds or cracks.

Summary.

B-1B shoulder longerons cracked because of local stress concentrations that were added to the design configuration after fatigue testing of the pre-production aircraft was complete. Extensive analysis and testing has resulted in a repair that has low weight impact, minimum cost impact, and high confidence of restoring the original design life. The complexity of the repair installation has been overcome by extensive development work and a complete set of tools and procedures that assure a successful installation. Provision has been made to provide for inspection capability both during the installation and after the repairs experience service loads.

Significant lessons were gained from this development task. First of all, the ability of a bonded repair joint to stop crack growth on a relatively heavy piece of structure with a large crack was demonstrated by this effort. Secondly, the special heating apparatus and the bonding process that enabled the repair to be accomplished on-aircraft as a field repair stands as an example to be used for repairing other heavy structure. Additionally, the use of a p-element FEM code to predict crack growth was demonstrated by this task. Also significant was the analytical value for the amount of crack growth retardation that occurs as the crack in a thin web grows towards a larger mass.

Final repair doublers have been installed on 24 aircraft as of Oct. 1, 1993. Another 18 aircraft have the prototype repair configuration that will eventually be replaced. The modification of the B-1B fleet is expected to be complete by Dec. 1994.

References.

1. Liu, A.F. and Gurbach, J.J., "Application of a P-version Finite Element Code to Analysis of Cracks", AIAA Paper No. 93-1450, AIAA/ASME/ASCE/AHS/ASC 34th Structures, Structural Dynamics and Materials Conference, La Jolla, California, April 19-21, 1993.
2. "B-1B Shoulder Longeron Standardized Repair Procedure", NA-92-1648 Rev. C, prepared by Structural Sciences Department, North American Aircraft Division, Rockwell International, June 18, 1993

AIRCRAFT ACCIDENT INCIDENT ANALYSIS USING ANIMATION TECHNIQUES

**BY: BOB KERR
USAF TINKER AFB, OK**

AND

**MIKE POOLE
CANADIAN TRANSPORTATION
SAFETY BOARD OTTAWA,CANADA**

INTRODUCTION:

1. ASIMIS CONNECTION:

The Mishap Analysis and Animation Facility has recently been added to the TILO Branch at Tinker AFB, Ok. The TILO Branch is better known to most of you as the Aircraft Structural Integrity Management Information System (ASIMIS). ASIMIS was established in 1972 to manage the ASIP data processing functions, and is currently processing ASIP data on 20 weapon systems and approximately 6,000 aircraft.

2. ASIMIS MISHAP SUPPORT:

For the past 20 years, ASIMIS has also processed whatever crash data survived from ASIP recorders for the accident review boards. Output was primarily listings and plots. However, without crash survivable data storage, most of this data was lost. But in January 1984 the AF contracted with the Lear Siegler Co. to develop a Crash Survivable Flight Data Recorder for the F-16C/D aircraft. In July 1988 the USAF contracted with Smiths Industries (Formally Lear Siegler Co.) to develop the Standard Flight Data Recorder (SFDR) for 12 other aircraft of which 5 would have CSMU/FDMU Crash Survivable Memory Units.

3. USAF POLICY :

In a recently revised Air Force Regulation titled "Investigating and Reporting USAF Mishaps", Air Force organic capability is required first "to promote investigation independence from sources other than the contractors involved in the design, manufacture, or maintenance of the aircraft." and secondly because "any processing based upon privileged information or involving board deliberation renders those portions non-releasable". The regulation states, "OC-ALC/TILO is the central Air Force activity for recovery, transcription, and analysis of FDR data in support of USAF mishap boards".

4. USAF SOLID STATE MISHAP MEMORY UNITS:

The Air Force currently has two types of Flight Data Recorders (FDR) with solid state crash survivable memory. The first is the Crash Survivable Flight Data Recorder developed by Smiths Industries, it is the self contained unit on the right. The second is the Crash Protected Memory Module on the left developed by Electrodynamics, it has crash protected memory boards inserted in the ASIP structural data collector. One of these memory modules recently survived the crash of a B-1B into the side of a solid rock cliff at .85 mach. Since the USAF crash survivable recorders utilize solid state "chip" memory, the first goal of these systems is to extract data from chip level. This means that in a smoking hole mishap, the Module itself is likely damaged or burned so that the module will need to be disassembled and the chips removed and installed on a jig or assembly board so that data can be extracted from those chips not damaged.

PROCESSING FLIGHT DATA RECORDER DATA

1. Two Systems Under Development:

To accomplish the goal of providing organic mishap analysis from chip level, MAAF has put under contract Smiths Industries and Ram Inc. We are also working with the Canadian Transportation Accident Investigation and Safety Board. Both systems will have the ability to provide lists and plots (2D) and animation(3D) analysis.

2. Silicon Graphics Computer System with Smiths Industries Software:

Smiths Industries had begun work on a Air Combat Training & Evaluation System (ACTES). Funds were awarded to this project in Dec 1991. However after buying a Silicon Graphics computer and developing some animation techniques, the funds were redirected in 1993 to support the development of the Mishap Analysis Lab at Tinker AFB. There are 12 weapon systems that will be supported with System 1. Five with 2D and 3D analysis, and seven with 2D analysis only. The current contract calls for delivery of SFDR assemblies for each aircraft configuration so chips can be removed from damaged memory modules and installed in special fixtures for data extraction. Smiths will also deliver extraction software to recover chip data including partial block data (last seconds) and PC decomp for decompressing (conversion & filling) the data. Smiths will also deliver animation software capable of including Defense Mapping Agency Terrain Elevation and Feature Analysis Data. The animation software will be capable of a Heads-Up-Display from the cockpit view and a generic instrument panel when selected. Out of the aircraft views are possible from any angle with selectable fast forward, reverse, slow motion and freeze modes. Animation can be recorded on a VHS-VCR tape. System delivery July 94.

3. Hewlett Packard System with Canadian Software:

A Joint services Process Action Team (JPAT) was established in 1993 by the Safety Center Chiefs in an attempt to standardize developments of Mishap Analysis systems within the various branches of the service. At the first meeting attended by the Army, Navy, Coast Guard, and USAF; The USAF was asked to take the lead in Configuration control during development of the joint services Mishap Analysis system. The NTSB was also in attendance at the JPAT meeting and gave high praise for the software system developed by their Canadian equivalent. During a demonstration of this software in Ottawa, Canada it became apparent this was a very good system. Funds were obtained from the B-1B System Program Director and we are including the Canadian software and its Hewlett Packard Hardware package as part of our facility. The B-2 aircraft will be added at a later date when funds are obtained. The Hewlett Packard System has been ordered with the new model 755 processor. The Canadian Data Analysis and Presentation System (RAPS) is scheduled to be installed next month (JAN 1994). In the Canadian software the raw data will first pass through the Front-End Processing System software which will handle problems such as partial loss of data stored on chips. Several algorithms exist which will "fix" the data before it is converted to engineering units. Any number of parameters can be analyzed and plotted with the RAPS software. The data then enters the Animation Graphics System software. During animation easily constructed instrument panels will display flight parameters around the edges of the screen. The viewer has complete control of his position around the fully shaded aircraft model with the use of a "knob box" and "button box". The viewer may be in the cockpit view, ground view, chase ground view, or chase plane view. Up to four simultaneous views may be seen by opening up additional "windows". System delivery is scheduled for this month (Dec 1993).

4. BENEFITS OF EACH SYSTEM:

The USAF intends to operate both systems. Bridge software programs will be written to move data between systems or Software delivered to the USAF will be modified to input various formats of data. Each system will have it's own special capability which exceeds the other and if possible the USAF will try to modify each system to incorporate the best of both systems. The Hewlett Packard System with the Canadian Software will provide the benefit of international cooperation and sharing of technical advances. The Silicon Graphics System with the Smith's Industries software will advance the state of the art in chip data extraction and the use of the Defense Mapping Agency Terrain Elevation and Features Data.

BENEFITS OF COMPUTER ANIMATION:

1. Fast resolution of mishaps or incidents can keep a fleet of aircraft from being grounded and improve military readiness.

2. Fast resolution of mishaps can reduce costs of system tests that otherwise might be required to resolve the reason for the mishap. The cost savings can be enormous, for example in the recent B-1B crash previously mentioned, the terrain following system was absolved by finding the real reason. The cost of testing the terrain following system could have been very large.

3. The ability to trace the flight path backwards to the point of system malfunction and look at the environmental conditions at that point in time is useful in human factors studies.

4. The training value of mishaps and near misses, can also be of great value to the USAF. Experience has shown that animated presentations of mishaps and the causes, make a very lasting impression on other pilots.

5. The facility is to have a good sized theater and conference room to accommodate mishap boards and investigators of aircraft incidents. Animation helps accident review boards to visualize vast amounts of data in a short period of time.

ADDITIONAL SPIN-OFF DEVELOPMENTS:

1. INTERFACE OF FDR DATA TO B-1B FLIGHT SIMULATOR:

First, A study is being conducted by Boeing thru the Ram Contract on Interface of the FDR output to the B-1B flight simulators, and to allow for manual over ride of control surface and switch position data. The purpose of this effort will be to train pilots for accident avoidance. A number of incidents occur each year which cause damage to aircraft, many of these incidents could be avoided.

2. JPAT TEAM COORDINATION:

Secondly, MAAF will keep other members of the JPAT team informed and involved in the development process so they will benefit from lessons learned by the Mishap Analysis and Animation Facility at Tinker AFB. The Navy is currently trying to buy a Hewlett Packard system and the Army is Testing a Smith's Flight Data Recorder. Both services are carefully watching our progress during the development of these two systems. A standardized mishap system would allow data to be processed at any of the DOD processing centers.

Flight Recorders and Animation

With the advent of modern electronic aircraft, the flight data recording system has advanced considerably over the past decade. It is now quite common to record several hundred parameters in crash protected memory. The advancement has not been in the recorder itself (although there has been some recorder advancements), but rather in the availability of the data on the aircraft with the use of digital data busses. Not too long ago, sensors had to be fitted on the aircraft for the purpose of flight data recording. On modern aircraft, the majority of the recorded data is already available on the aircraft's data buss and is needed for systems onboard the aircraft; there are few sensors onboard solely for use by the flight data recorder.

With this voluminous data on modern aircraft, investigators were confronted with a new problem. How do we handle all of this data following an accident. In 1990, the TSB was asked to analyze the flight recorders from the A320 that crashed in Bangalore, India. A print-out of the last five minutes of all of the data produced a document approximately one inch thick! We spent more time producing data than looking at data. At that time we were already working on software based tools to facilitate analysis of large amounts of data and we also had developed three-dimensional animation software, however substantial work was required to improve the user-interface to allow investigators to analyze the data in an interactive manner.

The software developed at the TSB is called RAPS (Recovery, Analysis and Presentation System). The system has been designed to provide *accident investigators* with tools to recover, analyze and present in three-dimensional animations, data from flight recorders. In the past, investigators had to rely on specialists and programmers to extract the data from recorders and their tools consisted of a print-out or data plot and a hand held calculator. This manual approach is no longer feasible for the modern accident investigator. This paper will focus on the animation portions of the system and how they are used in accident investigation.

Limitations of the data:

For routine flights with no severe or unusual attitudes, animations can be automated to the point that the user can watch the aircraft fly as the data is being decoded (or down-loaded) from the recorder. This is especially feasible when the parameter list and aircraft type is known well in advance. However, the TSB must be capable of quickly handling whatever appears on our doorstep so our animations tend to be custom designed using the tools within RAPS.

Often, in accident scenarios, flight data can not be directly animated as the flight path of the aircraft over the ground is not normally recorded and in cases where it has been, it is usually not to high resolution. For many accidents, the actual track over the ground is not of great importance. For landing occurrences, it is often extremely important to develop an accurate ground track. There are many ways to calculate a ground track and its accuracy is enhanced by the quantity and quality of data. For example, wind speed and direction from an inertial

reference system, latitude and longitude, radar data, ground speed, etc., will assist in calculating an accurate ground track. RAPS offers the user the tools necessary to calculate the ground track based on a variety of different inputs. In some cases where the ground track is known (lat/long. or radar data), the wind profile can actually be the output of the calculation. In some cases this technique has been used to demonstrate the existence of wind shear.

Other data such as roll, pitch, heading, etc., can also not always be directly animated, especially when the aircraft experiences violent manoeuvres, often the case just prior to an accident. In some cases, when an aircraft rolls or spins or is involved in other very dynamic behaviour, sampling rates, lags in inertial systems, pitot-static disturbances, inverse relationships in certain attitudes all require analysis to come up with the most reliable and probable animation of the sequence of events. It is important to note that the old adage 'garbage in garbage out' always applies. At the TSB, whenever we modify parameters based on analysis, we used defined, repeatable process and the software keeps a history of all the process that have been applied for future reference. While the process we choose may not always be the best, at least it can be duplicated by anyone else and then they can judge whether or not it was the correct thing to do.

A point that is often overlooked in the analysis of flight data is being aware of the limitations of the data. In order to have a good understanding of the quality of the data, one should be familiar with the sensor types, where they are actually located (are they recording aileron position or bell crank position where the bell crank connecting rod adjustment can change the aileron position without changing the bell crank position), resolution, sampling rate, buss transport delays, and the conversion relationship to yield engineering units. The conversion relationships are particularly important on some of the older aircraft due to their non-linear behaviour. I have seen unfortunate instances in the past where people have made conclusions from the data without being aware of the quality of the source data itself.

Realism of Flight Animations:

- Flight animation or flight reconstructions are becoming increasingly popular as an effective means of communicating a vast amount of information in a timely and meaningful manner while at the same time introducing the 'real time' component. It is sometimes easy to criticize a flight crew for a particular action, but when viewing the data in real time, the investigator develops a feel for the time frames in which decisions were made in the context of the particular operating environment. It is important to note that flight animations *are not the real world*, they are a representation of data, only as good as the source information and the processes that have been performed on the data. When looking at the data from the cockpit perspective, that is just what it is - the data from the cockpit perspective. It is not what the pilot saw or might have seen. Too many subjective variables come into play when one tries to make that extrapolation. Did he have his eyes open, where was he looking, did he have glasses on, window ergonomics combined with the accuracy of the aircraft's position in space, visibility over time, shadows, sunlight glare, clouds, fog, etc., all are difficult to define in a scientific and objective manner and often only one data point is available (ie: visibility 6 miles). While it might be useful to introduce some of this subjective and often speculative information into a reconstruction for

training purposes (a fictional training tape based on a true story) it is dangerous and potentially misleading to present it as official findings of the investigation. As a recent example, a reconstruction was done in which the aircraft was shown flying in a nice blue sky with a large dark cylinder representing a wind shear cloud. The video, to some extent, showed that the crew was not very alert because they flew their plane into the big dark cylinder when they should not have. In reality, the sky probably looked pretty ominous all around. This video was used in a court case to resolve liability. We can just begin to imagine what kind of psychology that was going on among the jurors when confronted with such a realistic video. The animation with aircraft colour scheme and detailed terrain surroundings was so realistic that it became reality to those who watched, regardless of its accuracy in depicting the sequence of events. TSB reconstructions contain the warning ~ 'Any conclusions based on this reconstruction should be thoroughly reviewed in light of the manner in which it was produced.' It is very important that people understand the limitations of the source information and that they be wary of any liberties the analyst has taken in generating the animation.

Flight Operational Quality Assurance:

An additional use for data analysis and flight animations is looking at flight data *before* there is an occurrence. Flight Operational Quality Assurance (FOQA) Programs are the new buzz words in the aviation industry. FOQA involves both performance monitoring and maintenance monitoring type programs. Monitoring routine flight data for defined events or combinations of events can be very useful in addressing flight safety issues before they develop into potential problems. An example of maintenance monitoring would be identifying hard landings so that maintenance could examine the undercarriage for structural damage. If you want to know why the hard landings are occurring and prevent them, you need to analyze more than just the event; you have to study all of the data leading up to the event. Since flight data is already on many aircraft by law, carriers are beginning to realize that it is advantageous to monitor and trend this data during routine operations to head off potential problems as well as improve the efficiency of their operations. Many 'near incidents' that are centered around Human Factors occur during routine flying and are not studied because no 'reportable event' happened. Furthermore, events which occur that are undetected by the air-crew or misinterpreted by the air-crew as to their significance can be readily studied through a FOQA program.

Most occurrences are the result of a chain of seemingly small events that build into an accident scenario on rare occasions. If operators have the ability to study the chains that are building in day to day operations and effectively *communicate* those studies back to flight crews and training managers, there is a reasonably good chance that the operator can reduce his occurrence rate and at the same time improve the efficiency of his operations. Flight animations are an excellent means of communicating such studies and events to flight crews. Many flight crews don't read occurrence reports, however animations have a certain fascination about them that encapsulates many pilots. In some cases, I have made animations in which people wanted to watch them over and over again. How many people want to read a report over and over again? Like any good movie, each time it is watched, the viewer sees things he didn't see before.

Powerful Presentation of the Facts:

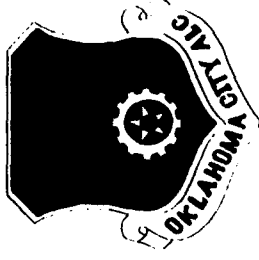
One last benefit of flight reconstructions worth mentioning is that they allow you to present the facts (or reasonably deduced facts) in a clear and understandable manner such that you do not have to spend a lot of time explaining what happened. The reconstruction shows clearly *what* happened and allows the viewers to focus on *why* it happened. I have been involved in investigations in which several months down the road I discovered that my perception of what happened and a colleagues perception of what happened were not the same. Flight reconstructions allow everyone on the investigation team to come up to speed on a dynamic and complex set of events in relatively short order. If we don't have a clear understanding of what happened, we have a long way to go to figure out the why. Furthermore, it is not necessarily important to correctly know why something happened; it is more important that it be prevented from happening again.

For example, I recently showed a reconstruction of an aircraft crashing on short final when the very experienced captain became disoriented during a missed approach in bad weather. The reconstruction was shown to a room of about 50 pilots. A very lively discussion ensued as to why this accident had happened. In the end, they wanted to know who was right about why it happened. The answer is ~ it doesn't matter who is right about why it happened. What matters is that none of the 50 pilots who saw it will let it happen to them. There are many fixes to this particular example and some fixes might be right for some operators and some pilots while other fixes are better for others. I am reasonably convinced that if any of the pilots who saw the reconstruction were in a similar situation in the future (missed approach in bad weather with all the pressures of continuing the flight) the animation would revisit their memories and they would think twice about each decision they made. Flight reconstructions are a powerful and persuasive tool in making others aware of the wealth of safety information available on today's flight recorders. We are in the information age; we are flooded with information and the focus is shifting away from data collection and more towards tools to utilize the data in a meaningful way.

Summary:

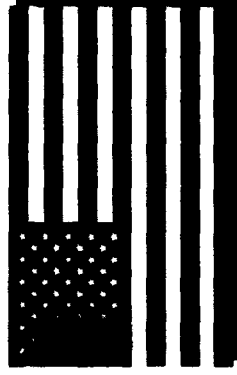
In summary, there are many uses for flight data to improve the safety and efficiency of aircraft operations, both in maintenance and human performance. The data is available on modern aircraft in large quantities and with today's technology there is no longer a problem to collect vast amounts of valuable information. The bigger problem facing the industry is knowing what to do with the data once collected, how to manage it, and how to extract the meaningful information that is embedded within it. Data analysis tools such as exceedence, event or trend monitoring as well as flight animations are beginning to play a major role in the routine operations of major airlines in the interests of improved efficiency and accident prevention.

**AIRCRAFT ACCIDENT / INCIDENT
ANALYSIS USING ANIMATION
TECHNIQUES**



BY

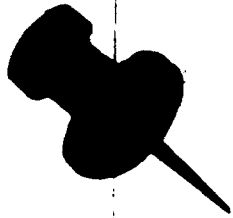
**BOB KERR, CHIEF
BOMBER STRUCTURAL SECTION
OC-ALC/TILO TINKER AFB, OK**



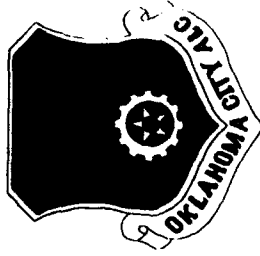
AND

**MIKE POOLE, SUPERINTENDENT
FLT RECORDERS, ENG. BRANCH
CANADIAN TRANSPORTATION
SAFETY BOARD, OTTAWA, CANADA**





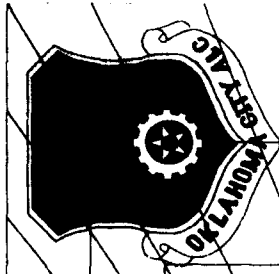
**U.S. AIR FORCE
POLICY ON MISHAP
INVESTIGATIONS:**



AFR 127-4

ORGANIC CAPABILITY AT OC-ALC/TILO

- 1. INVESTIGATION INDEPENDENCE**
- 2. SOME INFORMATION PRIVILEGED
AND NON-RELEASABLE**



**USAF MISHAP ANALYSIS AND
ANIMATION FACILITY (MAAF)**

1. ASIMIS CONNECTION

2. ASIMIS MISHAP SUPPORT





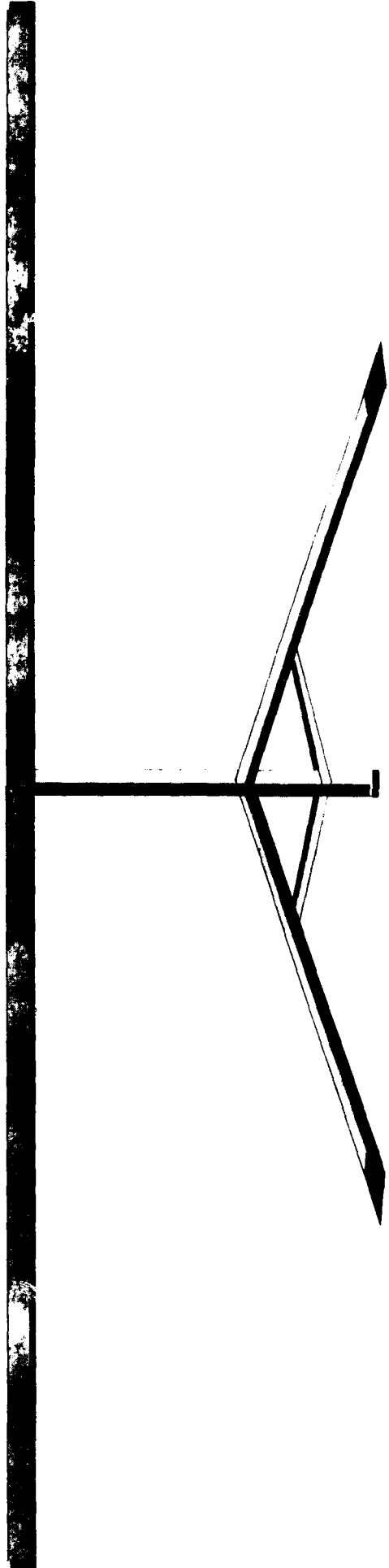
HISTORY OF CRASH SURVIVABLE MEMORY



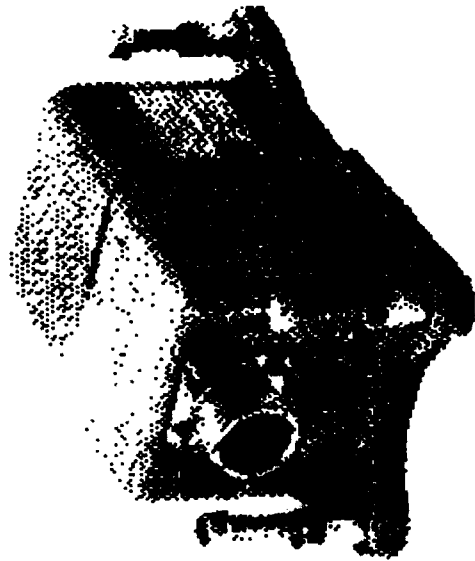
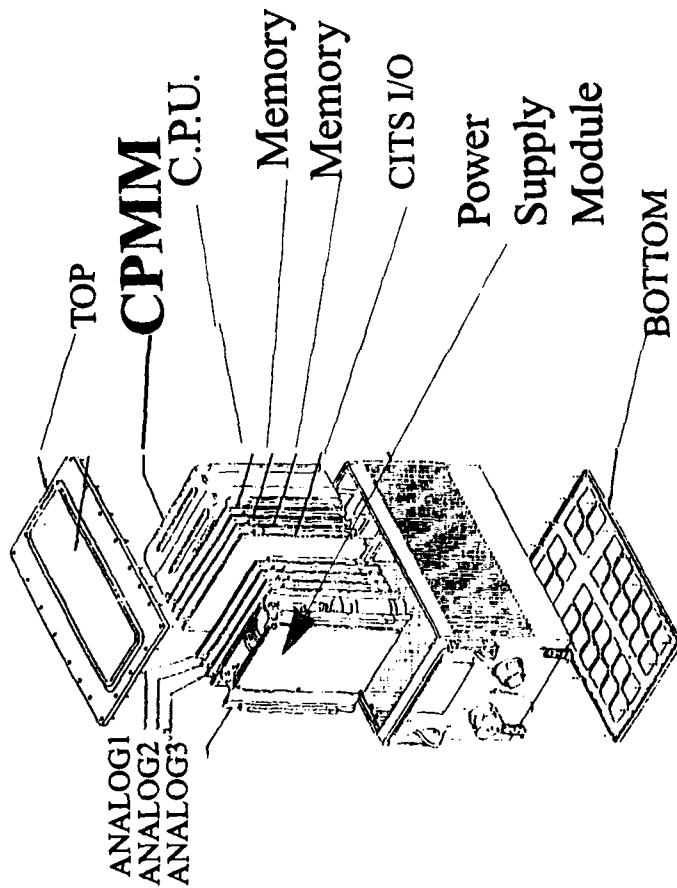
1981 - CPMM FOR B-1B

1984 - CSFDR WITH CSMU FOR F-16 C/D

1988 - SFDR WITH FDMU FOR OTHER A/C



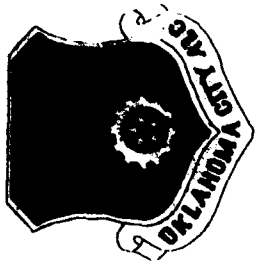
USAF SOLID STATE MISHAP MEMORY UNITS



**Smiths
Industries
Crash
Survivable
Memory
Module
(CSMU/FDMU)**

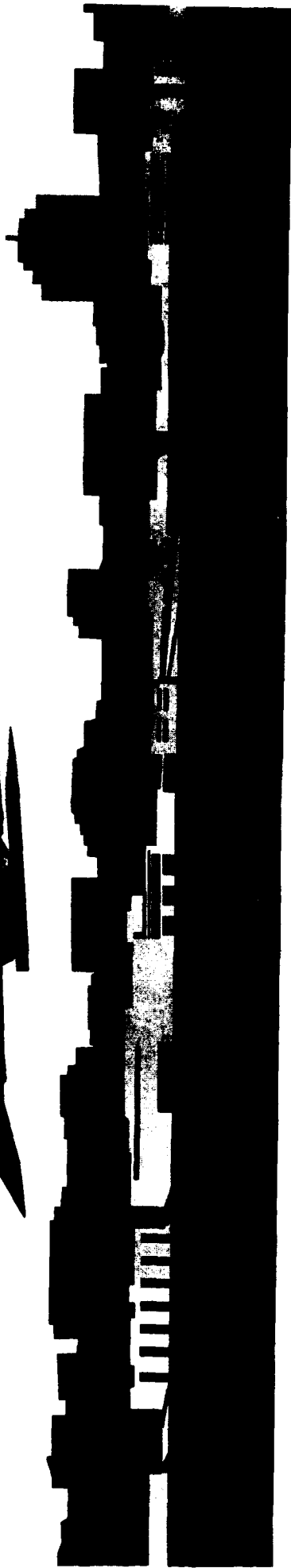
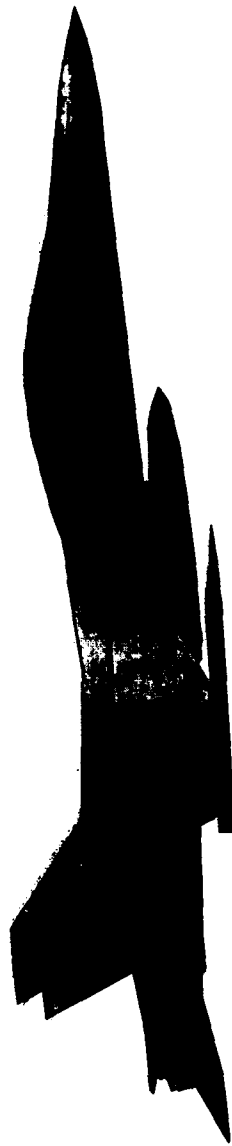
**Electrodynamics
Structural Data
Collector
Exploded View**

SYSTEM 1- SMITHS INDUSTRIES SILICON GRAPHICS SYSTEM



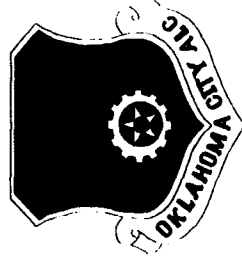
**MISHAP DATA (3D) CSMU/FDMU
(F-16, F-15, C-17, C-27A, T-1A)**

**STRUCTURAL DATA (2D) CSFDR /
SFDR (A/C ABOVE PLUS C-130, T-38,
C-141, E-3, F-111, B-52 AND C-135)**



**SILICON
GRAPHICS**

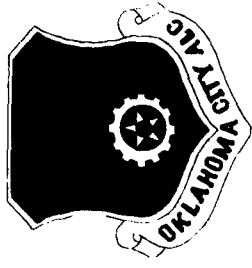
SMITHS IND



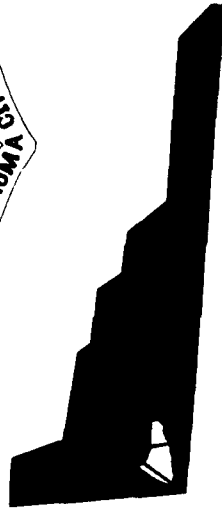
SYSTEM 1 - CAPABILITY

- 1. Reconstructing damaged CSMU/FDMU's**
- 2. Extracting crash data from CSMU/FDMU's**
- 3. Extracting Structural data from CSFDR/SFDR's**
- 4. Convert Compressed Data Files to engineering units**
- 5. List/Plot (2D) Analysis on PC LAN**
- 6. Animation (3D) Analysis on Silicon Graphics**
- 7. Create VHS/VCR tapes**

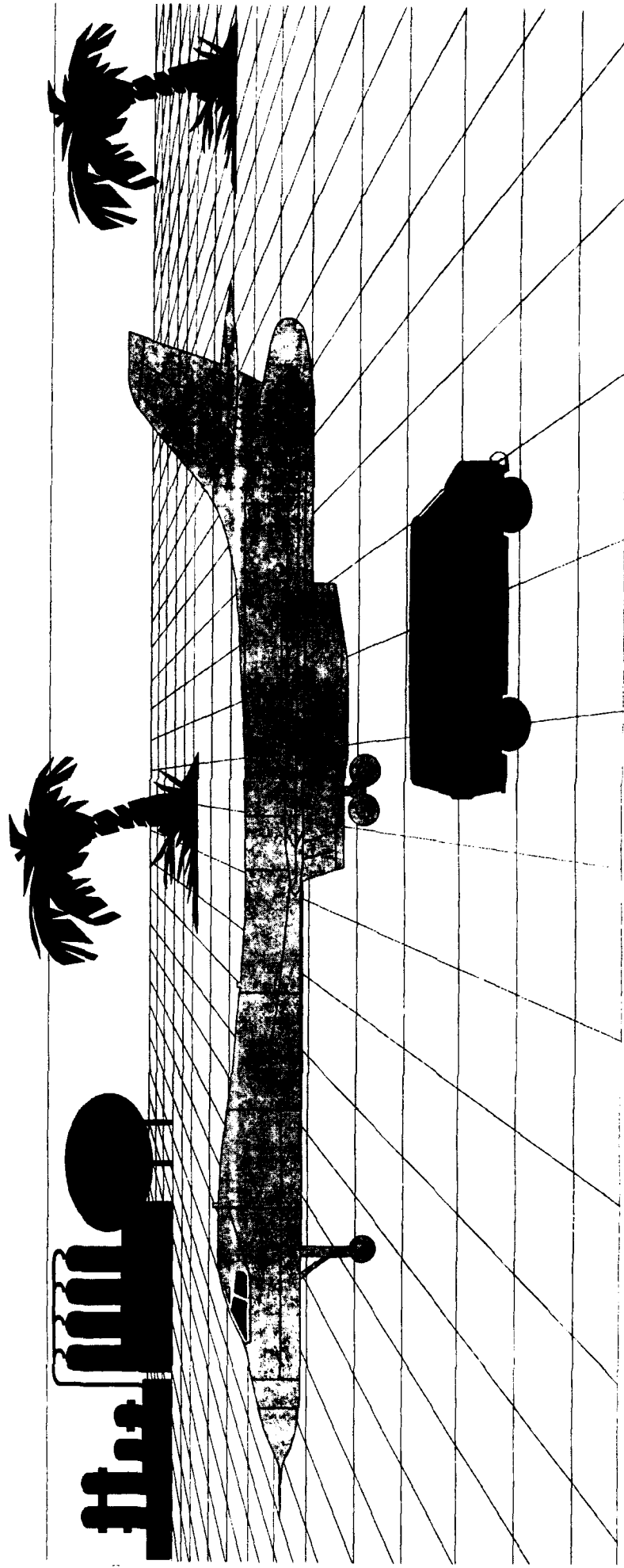
SYSTEM #2 - RAM, INC WITH CANADIAN DEVELOPED SOFTWARE



HEWLETT PACKARD COMPUTER SYSTEM



MISHAP DATA FROM THE CPMIM (B-1B, B-2)



RAM INC.

MIKE POOLE

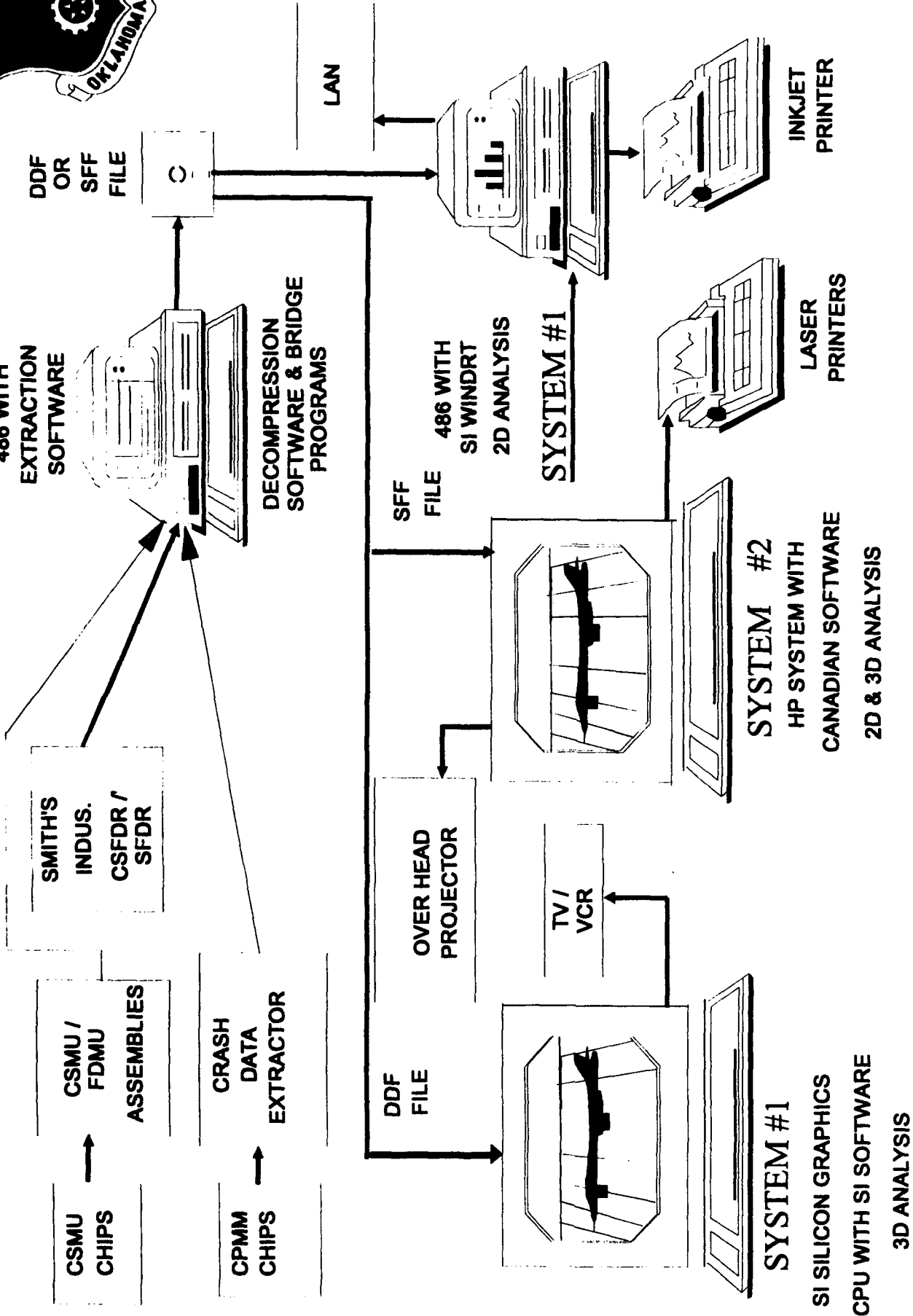
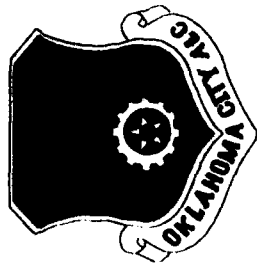
G.NEPERENY

SYSTEM 2 - CAPABILITY



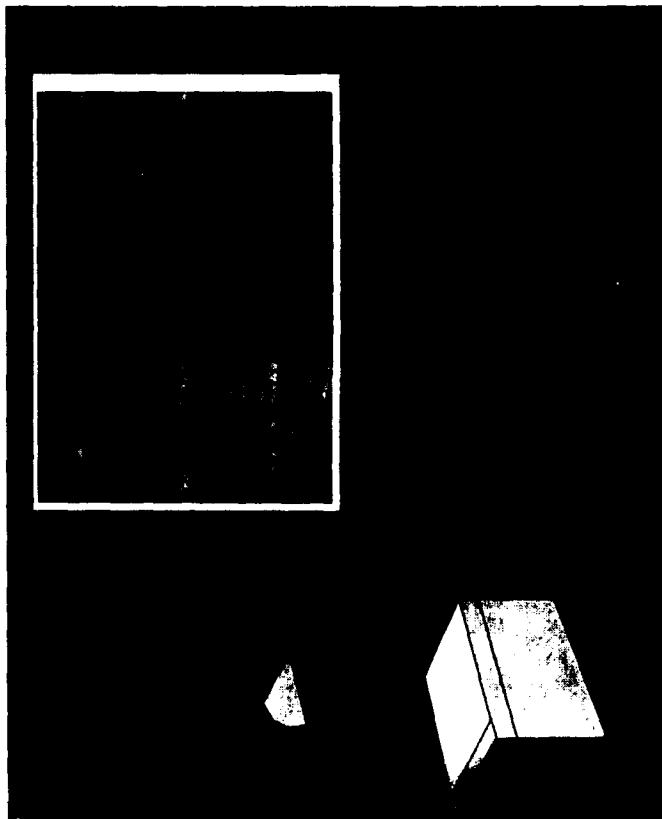
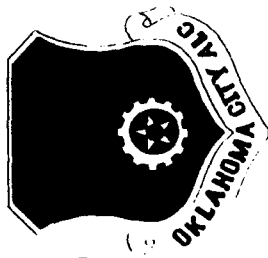
- 1. Reconstructing damaged B-1B CPM's.**
- 2. Extraction of data from Crash Data Extractor Jig.**
- 3. Decode serial bit stream using Canadian SW**
- 4. Conduct 2D analysis using Canadian SW**
- 5. Conduct 3D analysis using Canadian SW**

MAAF MAJOR COMPONENTS

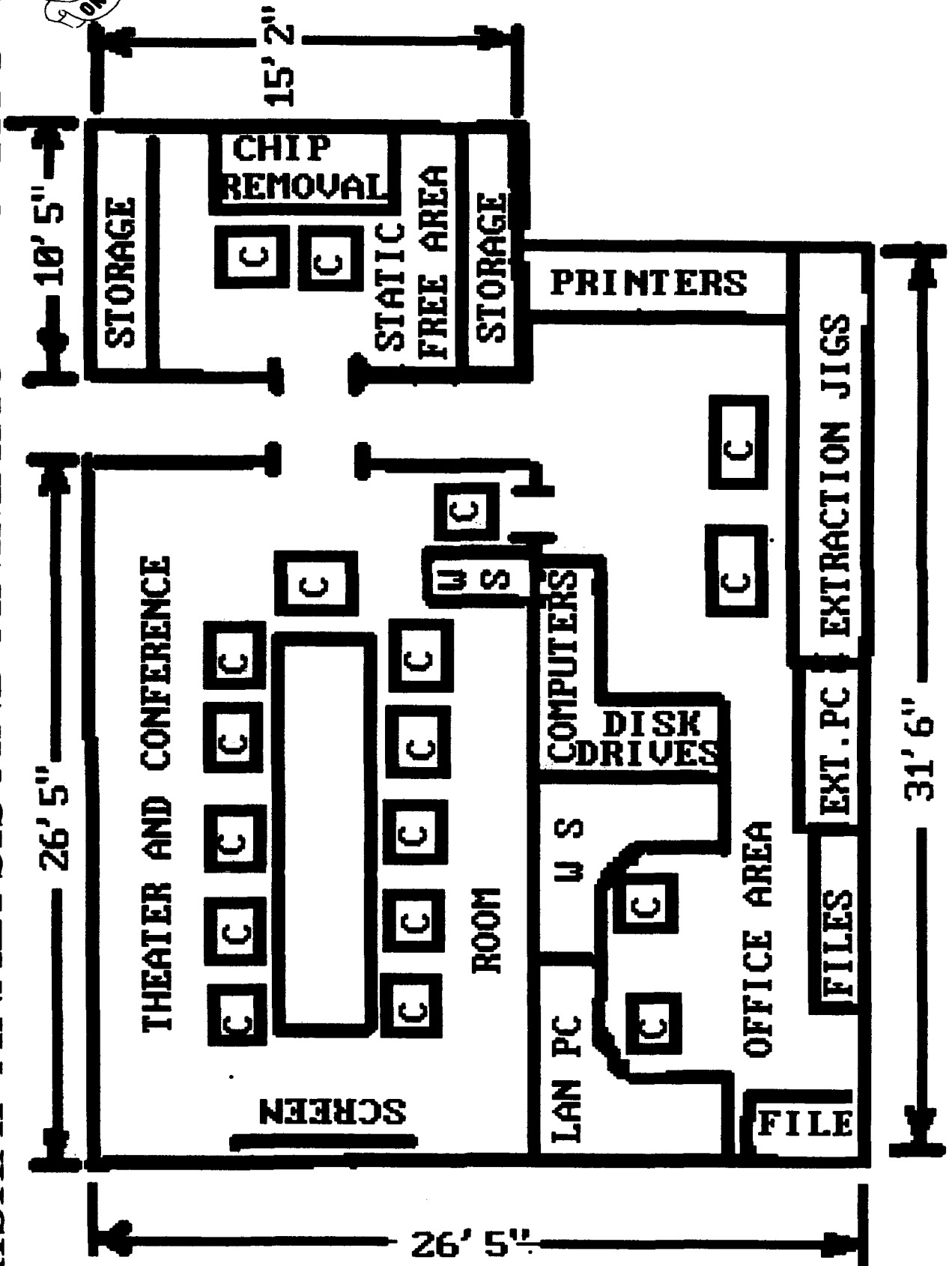
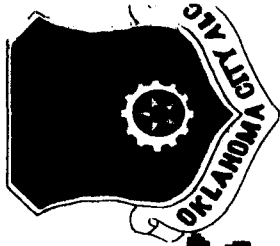


ANIMATION PRESENTATIONS

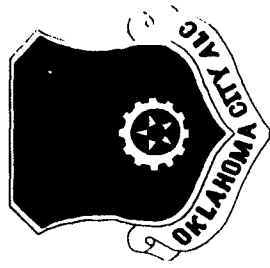
MAAF ANIMATIONS WILL BE PROJECTED IN
A THEATER TYPE FACILITY FOR MISHAP
BOARD DELIBERATIONS. VHS/VCR TAPES
CAN BE MADE AND SENT TO BASE LEVEL



MISHAP ANALYSIS AND ANIMATION FACILITY



BENEFITS OF ANIMATION:

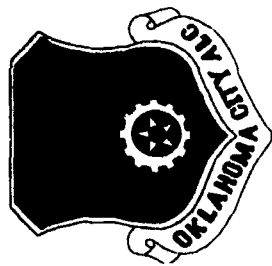


- 1. AIRCRAFT READINESS**
- 2. REDUCE OR ELIMINATE SYSTEMS TESTING**
- 3. ACCIDENT SCENARIO CHAIN OF EVENTS**
- 4. LASTING IMPRESSIONS FOR PILOT TRAINING**
- 5. SIMPLE DISPLAY OF LARGE AMOUNTS OF DATA**

B-1B FLIGHT SIMULATOR INTERFACE STUDY

**1. FDR DATA DRIVES FLIGHT
SIMULATOR**

**2. PILOT MANUAL OVER RIDE
AND WITH SAVE AND REPLAY**



**UNITED STATES AIR FORCE
STRUCTURAL INTEGRITY
CONFERENCE**

**THE CHALLENGES ASSOCIATED WITH THE
OPERATION OF LOADS MONITORING
EQUIPMENT FOR EFFICIENT STRUCTURAL LIFE
MANAGEMENT**

Co-Chairman:

Major M. B. Zgala
Manager, Structural Integrity
Fighter & Trainers
DAS Eng 93

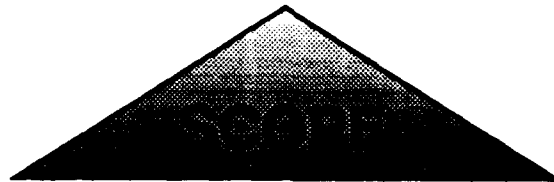
SAN ANTONIO, TEXAS
DECEMBER 1993

CONTENT

1. **INTRODUCTION**
 - "Challenges"
 - Scope
 - OLM/IAT Requirements
 - CF Service Life
 - History
2. **CURRENT SITUATION**
 - CF Loads Monitoring Effort
 - Typical Program Cost
 - Expected Fleet Management Benefits
 - Fatigue Life Management Process
3. **THE CHALLENGES**
 - Sensor Performance
 - Acquisition
 - Processing
 - Data Validation Process
 - System Integration
 - Fleet Management
4. **FUTURE SYSTEM CONCEPT**
 - Near Future System
 - System Algorithm
5. **CONCLUSION**

CONTENT

1. INTRODUCTION
2. CURRENT SITUATION
3. THE CHALLENGES
4. FUTURE SYSTEM CONCEPT
5. CONCLUSION



LOADS MONITORING EQUIPMENT:

ANY ELECTRONIC DEVICES WHICH MEASURE AND ACQUIRE RELEVANT STRUCTURAL PARAMETER DATA FOR THE PURPOSE OF QUANTIFYING STRUCTURAL FATIGUE ACCUMULATION



A CHALLENGE IS DEFINED AS...

**"SOMETHING WHICH TESTS A PERSON'S
ABILITY TO PERFORM A GIVEN TASK"**



LOADS MONITORING CHALLENGES

- * **SENSOR PERFORMANCE (ACCURACY, DURABILITY, COST)**
- * **DATA ACQUISITION (VOLUME OF DATA)**
- * **DATA PROCESSING (COST, ACCURACY)**
- * **DATA VALIDATION (ACCURACY, RELIABILITY)**
- * **SYSTEM INTEGRATION (MULTI FUNCTIONS)**
- * **FLEET MANAGEMENT**

**OLMAAT
REQUIREMENTS**

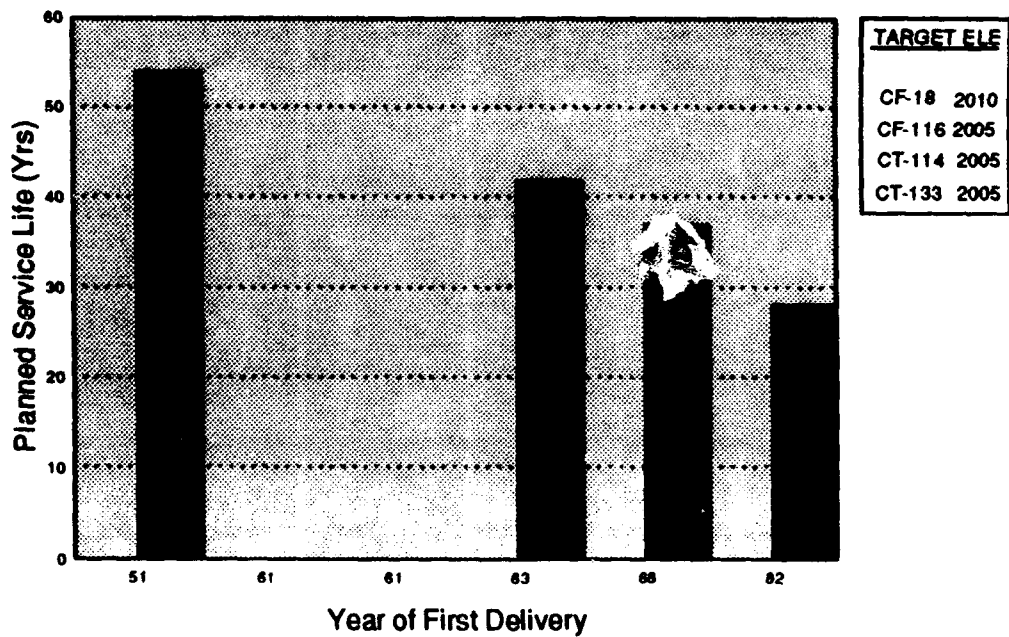
IMPROVED FLEET MANAGEMENT

- * TAILORED MAINTENANCE PROGRAM
- * OPTIMUM AIRCRAFT ROTATION
- * STRUCTURAL LIFE EXTENSION

IMPROVED SAFETY

- * RETIREMENT OF HIGHLY DAMAGED AC
- * PREDICTION OF STRUCTURAL FAILURE ONSET

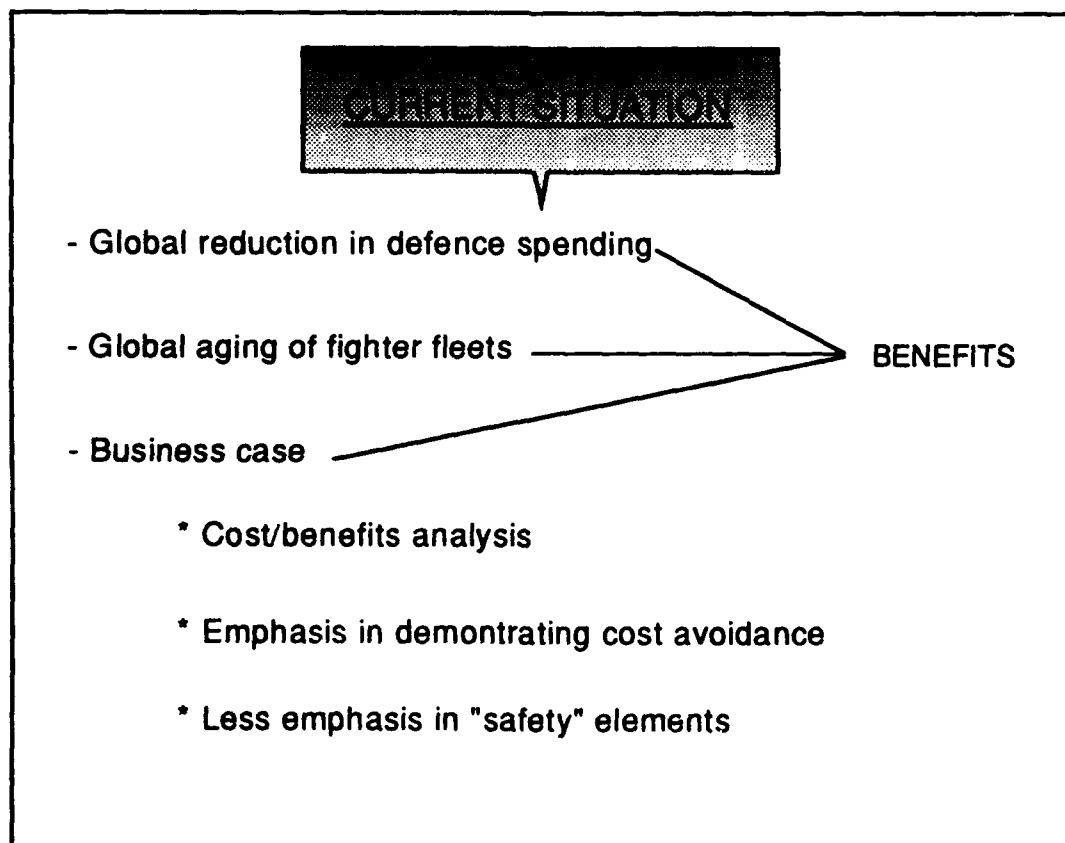
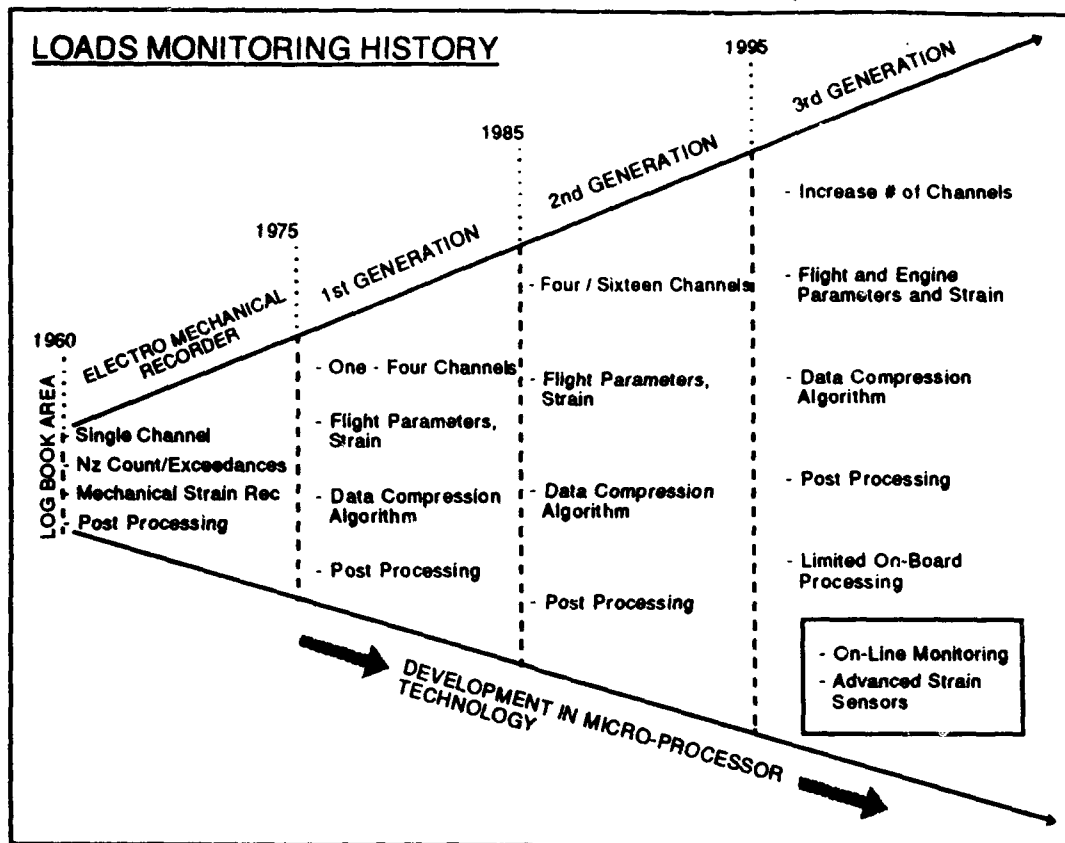
CF Service Life Requirements



TARGET ELE

CF-18	2010
CF-116	2005
CT-114	2005
CT-133	2005

Source:
 1. Canadian Military Aircraft, J.A. Grinn
 2. Canada's Airforce Today, Larry McHenry



CF LOADS MONITORING EFFORT

AIRCRAFT TYPE	FLEET FITMENT	PARTIAL FLEET	LESS	FLMP	PROGRAM COST (RCM)		COMMENTS
					N/R		
CF-18 (F/A-18)	X 126			X	U/K	450K	Implemented
CC-130 (Hercules)		X 31			10,000K	150	Being Implemented
CT-114 (Tutor)		X 46			4,500K	170K	Being Implemented
CC-144 (Challenger)	X 11			X	X,000K	150K	Being Implemented
CT-133 (T-Bird)		X 26	X 2		X,000K	150K	Under review
CF-118 (F/A-5)		X 15	X 4	X	X,000K	150K	Under review
				TOTAL	20,000K	1220K	

THRUST FOR LOADS MONITORING

* SAFETY

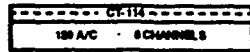
"EASY TO SELL / DEMONSTRATE"

* ECONOMICS

"NOT SO OBVIOUS"

CONCEPT

CONTROL SCENARIO



NON-SECURING

Rescuers
Sensors
Ground Support
Equipment



SECURING

20% System Maintenance
7% Data Processing
10% Software Updates

400k/year
20 yrs Service Life
0% Annual Growth



TOTAL LCC = 22.4M



EXPECTED FLEET MANAGEMENT BENEFITS

* SAFETY

- Prediction of Onset of Structural Failure
- Identify High Risk Airframe / Role

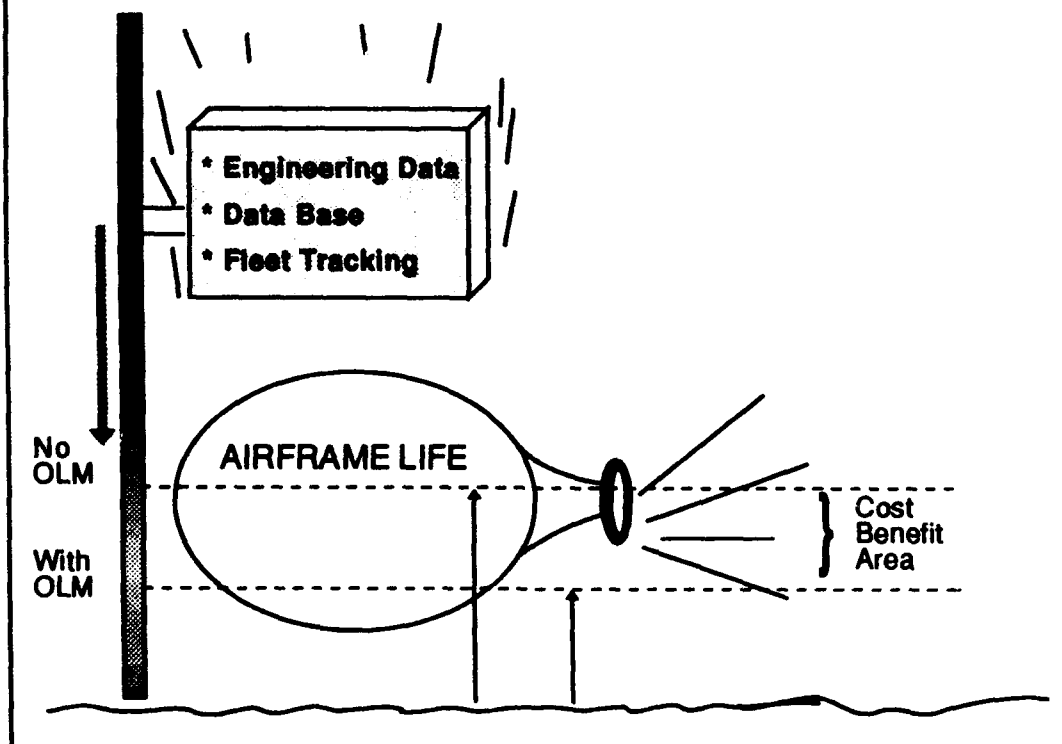
* COST

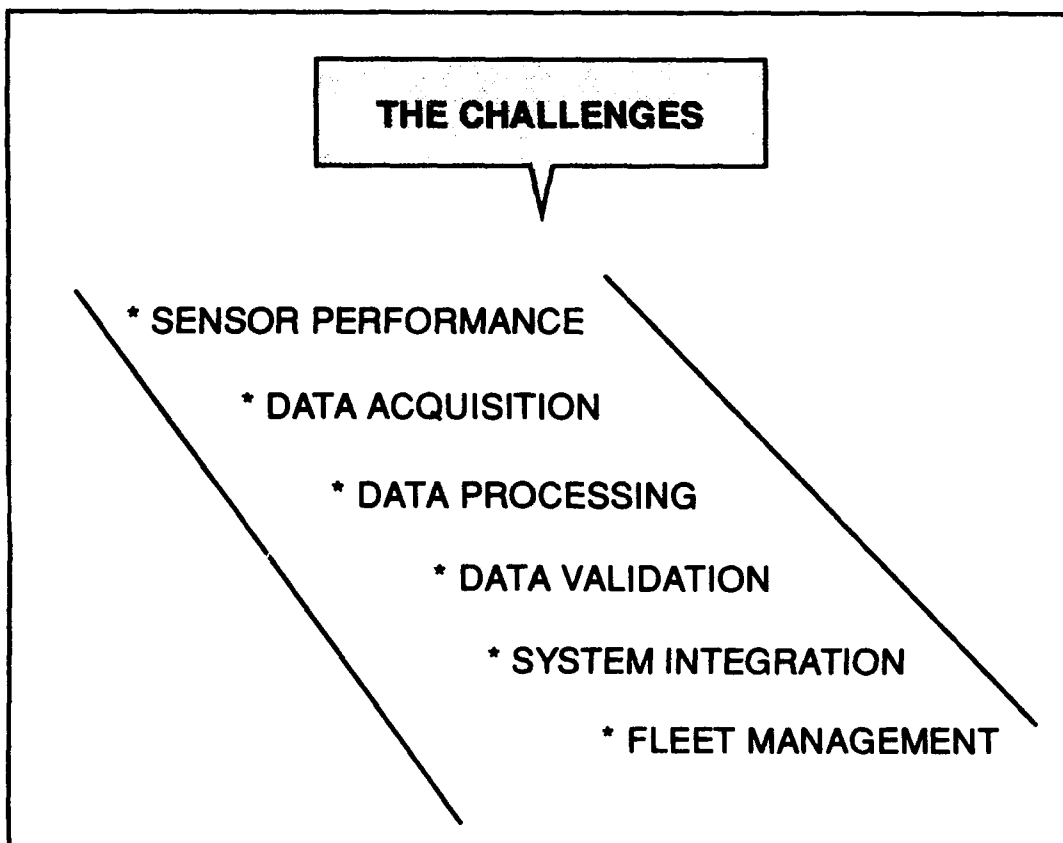
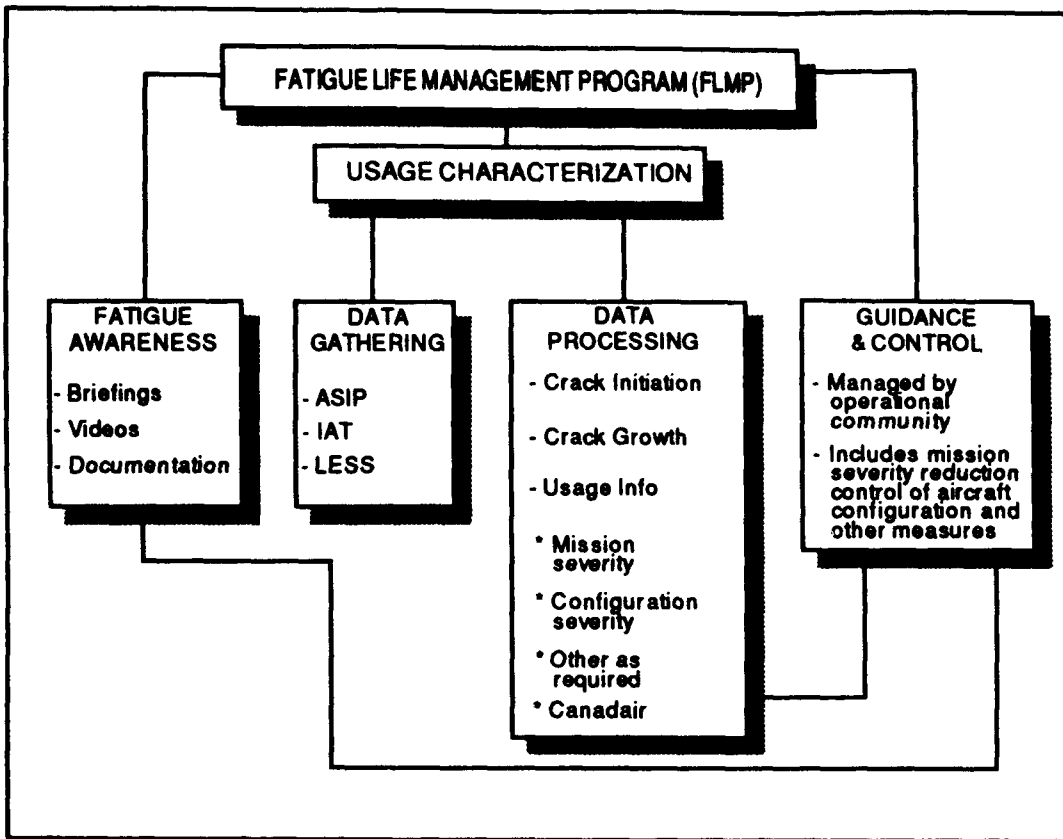
27,379K

- Avoid / Delay Potential Maintenance **
- Accurate Prediction of "Overstress"
- Potential for "Life Extension" **
- Fatigue Management Maximum Use of "Life Potential" **

** Large Cost Benefits but Difficult to Quantify

STRUCTURAL LIFE BALLOON







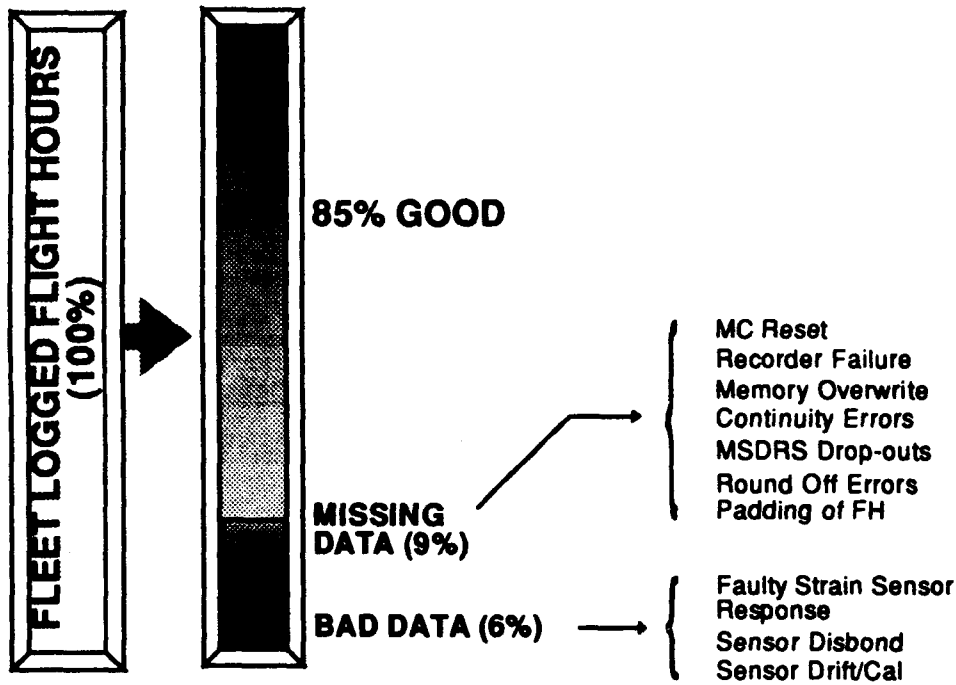
<u>FLIGHT PARAMETERS</u>	<u>PERFORMANCE ELEMENTS</u>	<u>STRAIN SENSORS</u>
Satisfactory	Accuracy	Satisfactory
Satisfactory	Sensitivity	Satisfactory
Periodic Calibration Required	Maintainability	Periodic Calibration Required
Satisfactory	Durability	Improvement Required
Satisfactory	Environmental Immunity	Satisfactory (Proper Installation)
Satisfactory	EMI / EMC	Satisfactory (Proper Design)
Improvement Required (\$1000 - \$3000)	Cost	Improvement Required (\$100 - \$500)

SENSOR PERFORMANCE IMPROVEMENTS

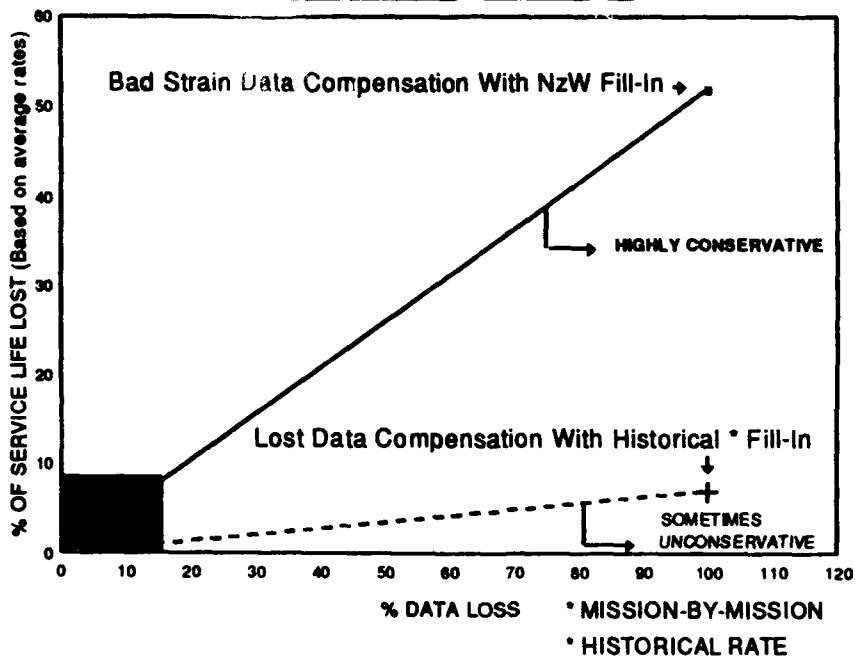
		<u>CURRENT</u>	<u>REQUIRED</u>
STRAIN SENSORS	DURABILITY	1500FH	6000FH
	MAINTAINABILITY *	1 / 1.5 yrs	25 / 30 yrs
	COST	\$100 / \$500	< \$100
FLIGHT PARAMETERS	MAINTAINABILITY *	2 / 3 yrs	25 / 30 yrs
	COST	\$1500 / \$3000	<\$1000

* CALIBRATION

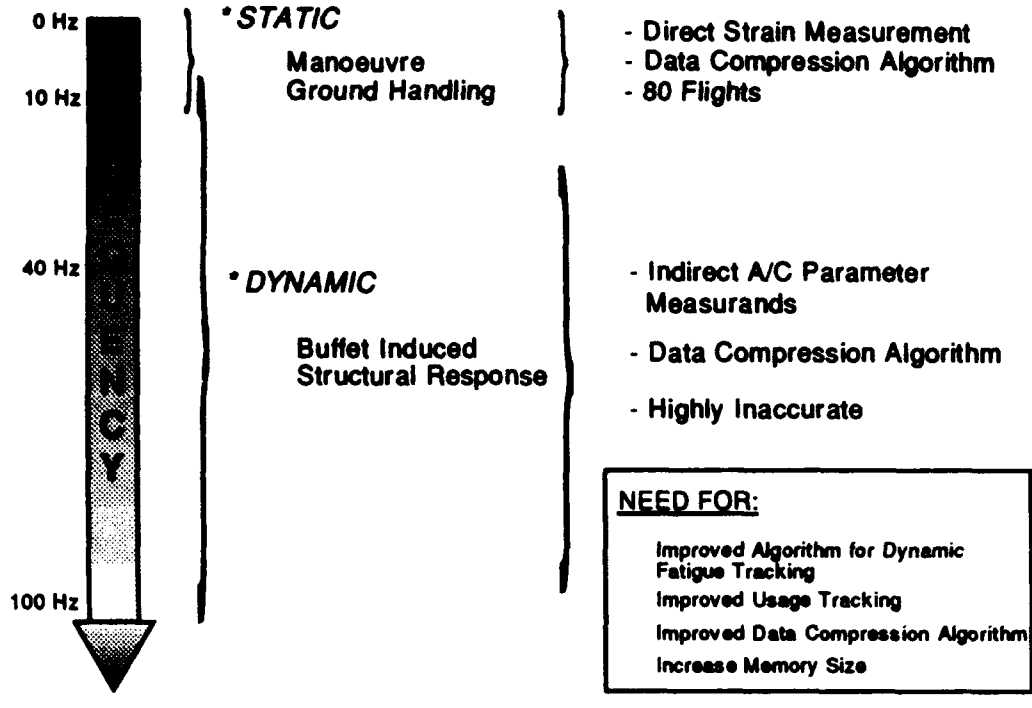
DATA ACQUISITION:



COST OF LOST DATA



DYNAMIC FATIGUE TRACKING



DATA PROCESSING REQUIREMENTS

MINIMUM COST

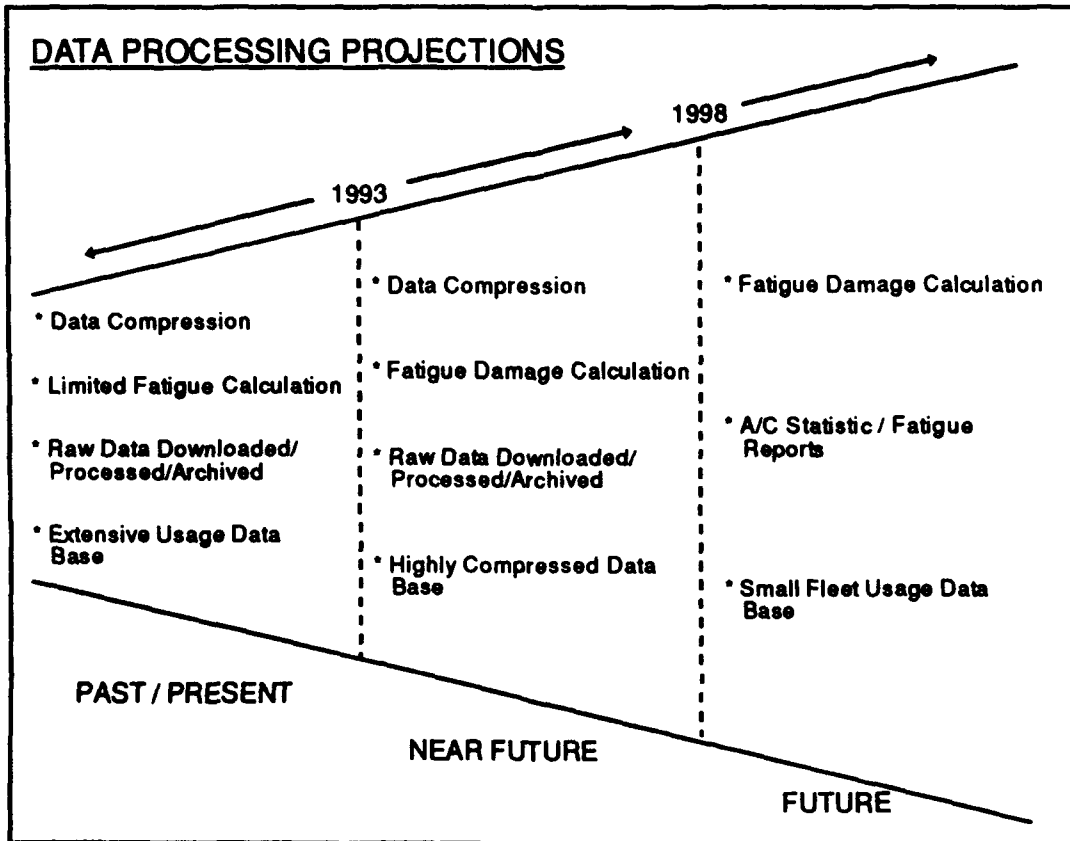
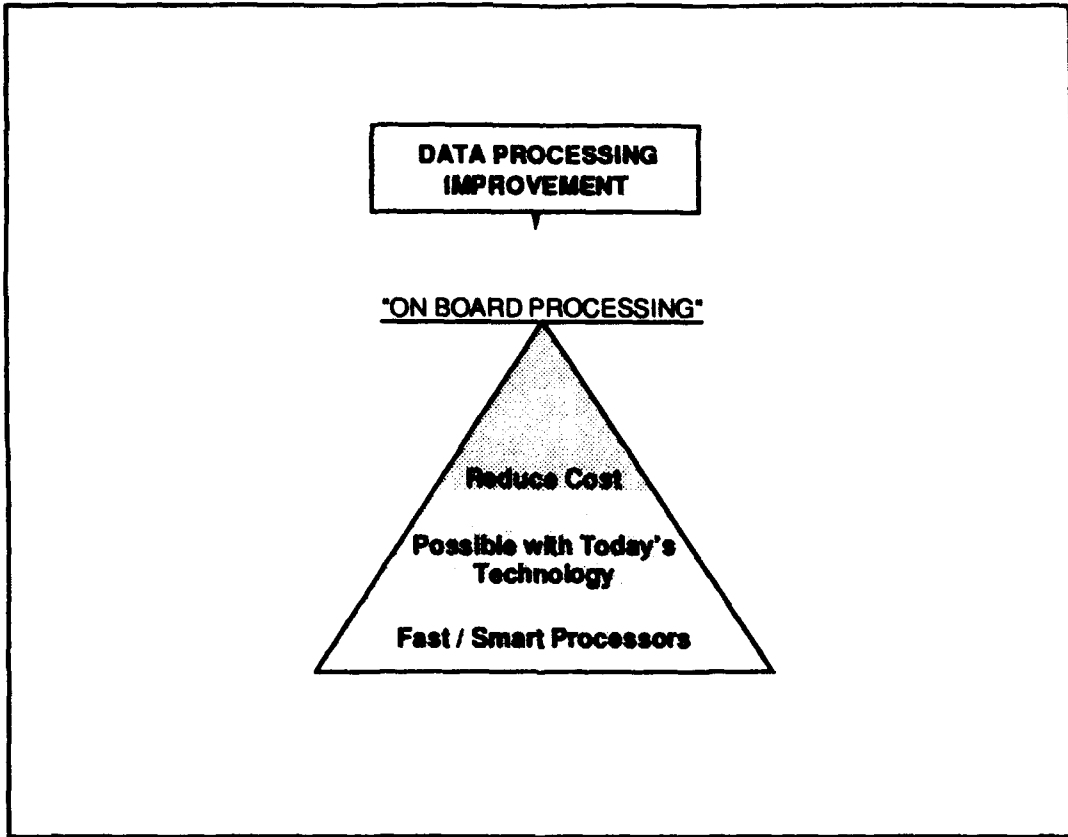
- 50% of System Life Cycle Cost
- Systematic Process / Minimum Operator Involvement

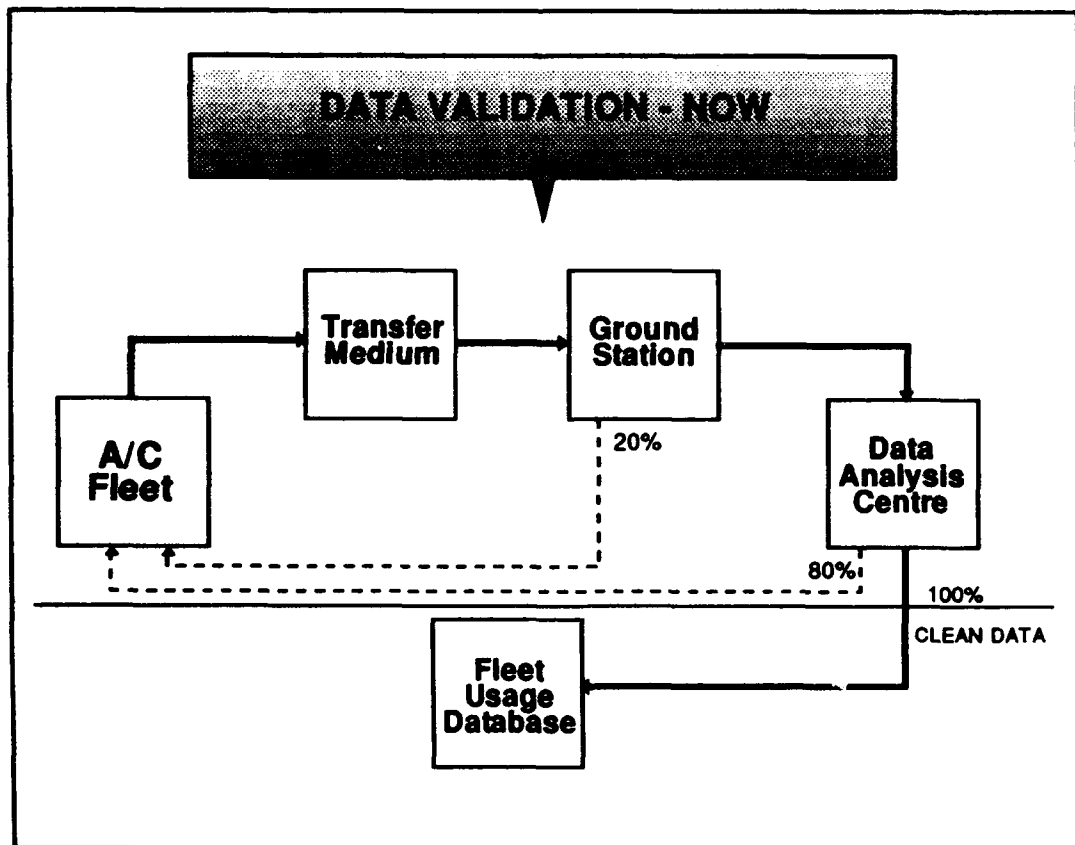
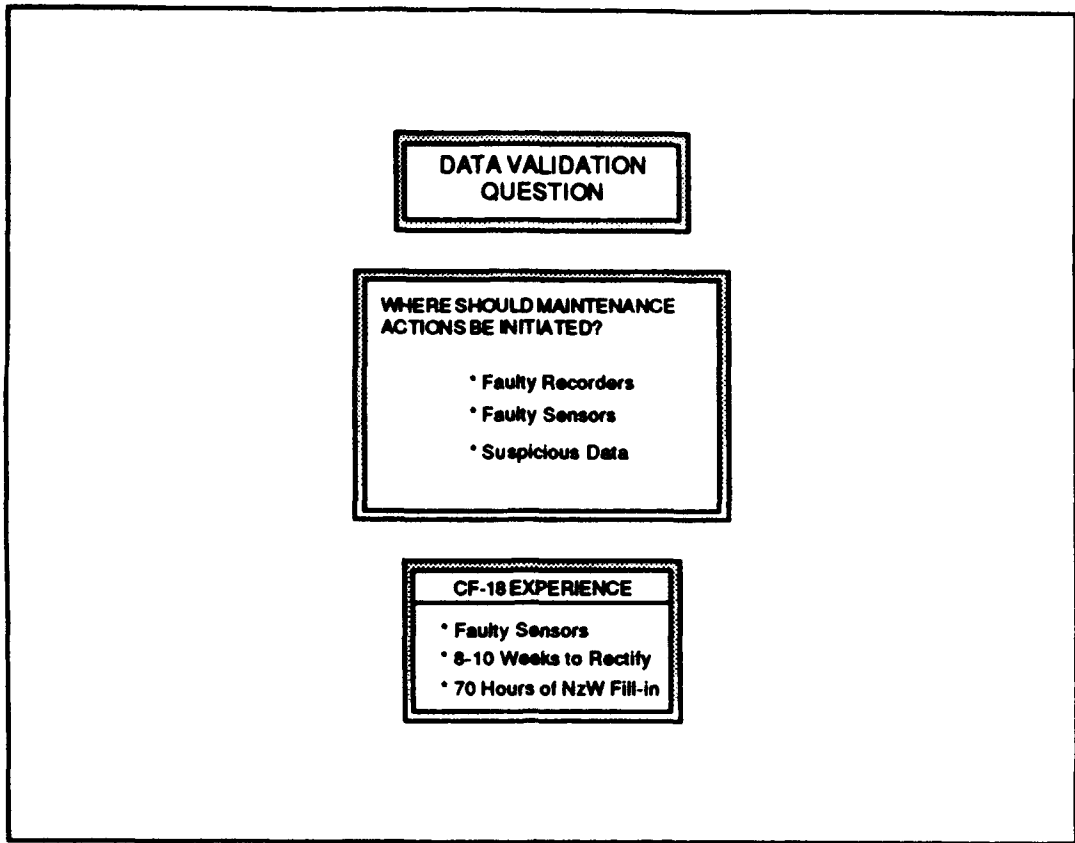
ACCURACY

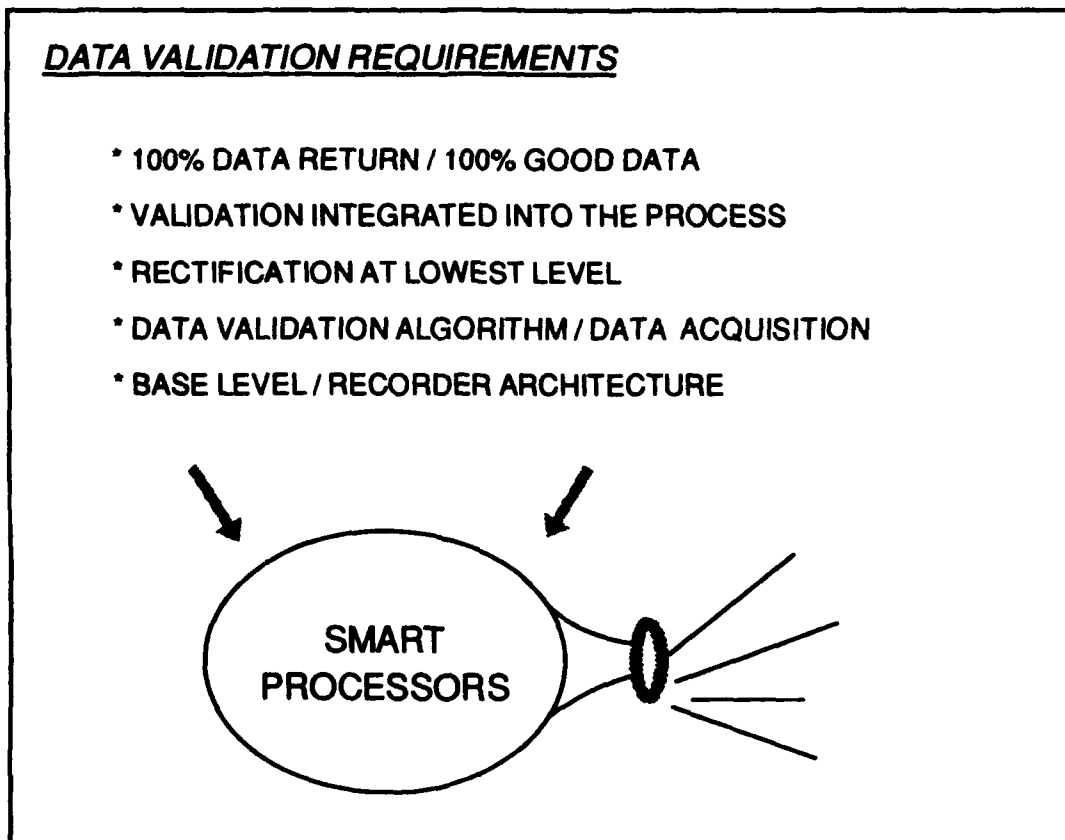
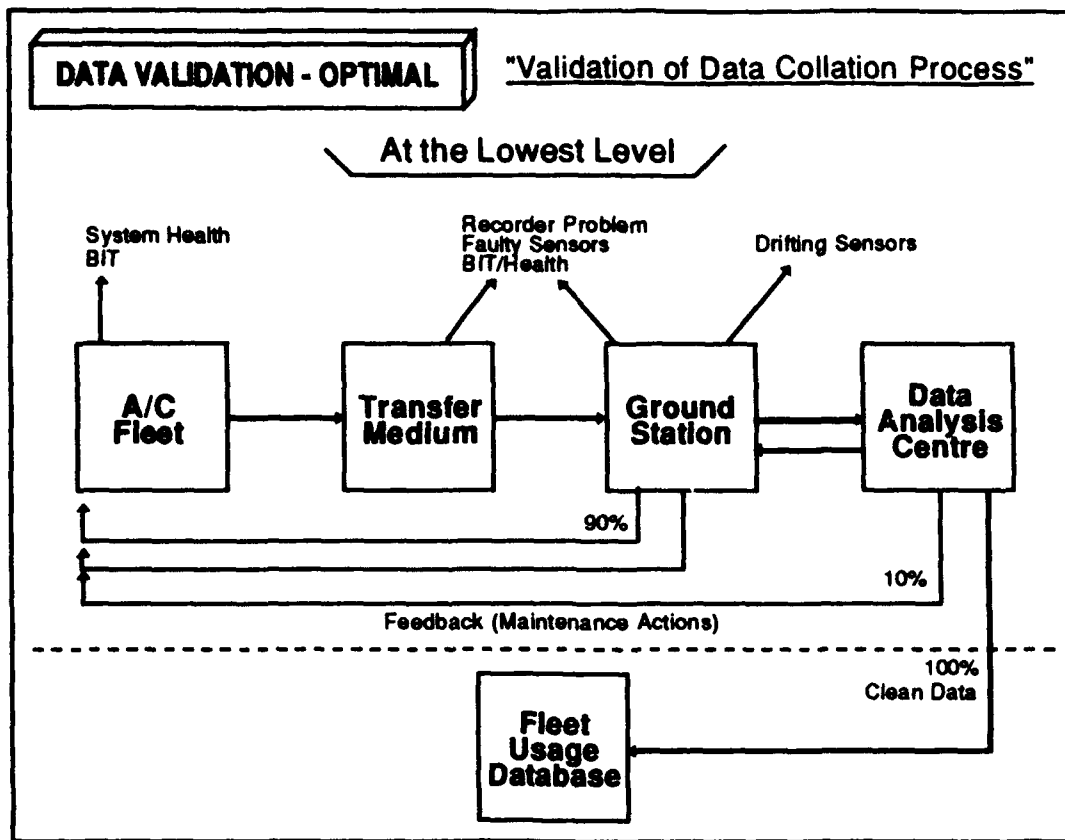
- Fatigue Calculation Algorithm must be validated by coupon / element tests
- Spectrum Sensitivity
- Periodic review

TIMING

- Monthly / Quarterly / Yearly
- On "Operator's Request"







INTEGRATION

OLD A/C DESIGN

- * OLM System not integrated
- * Space and Weight Penalties
- * Flexibility
 - software upgrades
 - system settings

NEW DESIGN

- * Fully Integrated into A/C Systems/ Mission Computers
- * Space and Weight Efficiency
- * No Flexibility
 - software upgrades
 - system settings

CF-18 EXPERIENCE

Takes Up to One Year To Implement Software Changes (Minor + Major Changes)

SYSTEM INTEGRATION FUTURE

- * System Integration Will Be Pursued
- * Addition Of On-Line Monitoring
- * New Software / Hardware Design to Make Loads Monitoring Function a NON MISSION CRITICAL ELEMENT in the Integrated System
- * Smart Structures / Processors Will Rely Extensively on Active Reaction to Maintain Stability, Safety Margin and Therefore Will Be Considered as "MISSION CRITICAL"

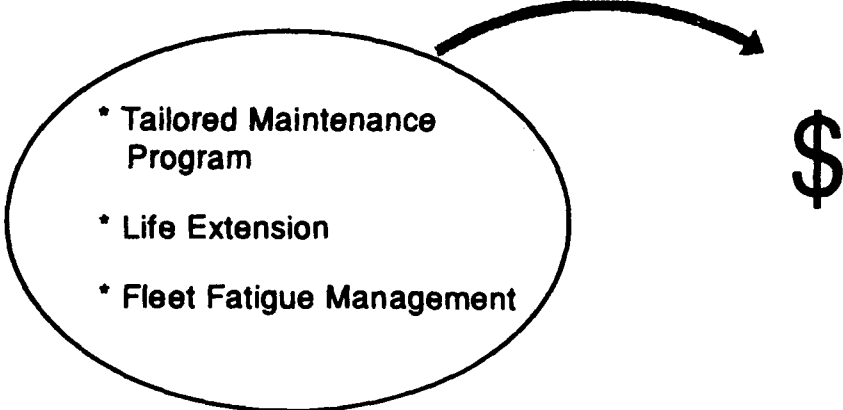
ON-LINE MONITORS

ON-LINE MONITORS

- Provide Real Time Feedback to Maintenance / Ground Crew
- On-Line Monitors System That Can Detect and Monitor
 - > crack initiation (AE)
 - > crack growth (ACPD Probe)
 - > disbond (AE/strain sensing)
- Integration of On-Line Monitors to "Classic" Loads Monitoring Recorders Is Required

FLEET MANAGEMENT

FLEET MANAGEMENT BENEFITS

- 
- The diagram features a large oval on the left containing three bullet points. A curved arrow points from the top of this oval to a large dollar sign (\$) on the right, indicating that the listed benefits result in cost savings.
- * Tailored Maintenance Program
 - * Life Extension
 - * Fleet Fatigue Management

**FLEET
MANAGEMENT
PREREQUISITES**

- * EFFICIENT USAGE DATABASES

- * ESTABLISH LINK BETWEEN:
 - Fleet Managers and Operators
 - Feedback to Maintenance Program ("Just In Time")

- * FLEET MANAGEMENT MODEL
 - Structural Reliability / Risk Assessment
 - "IF" Scenarios

**FUTURE SYSTEM
CONCEPT**

NEAR FUTURE

- * *Advanced Strain Sensors*
- * *Extensive On-Board Processing*
- * *Diagnostic / Self-Test Features*
- * *Base Level Sensor Performance Tracking*
- * *On-Line Monitors*

CONCLUSION

*** Near Future System Prerequisites to "Smart Structures"**

• Improvement to Actual Process

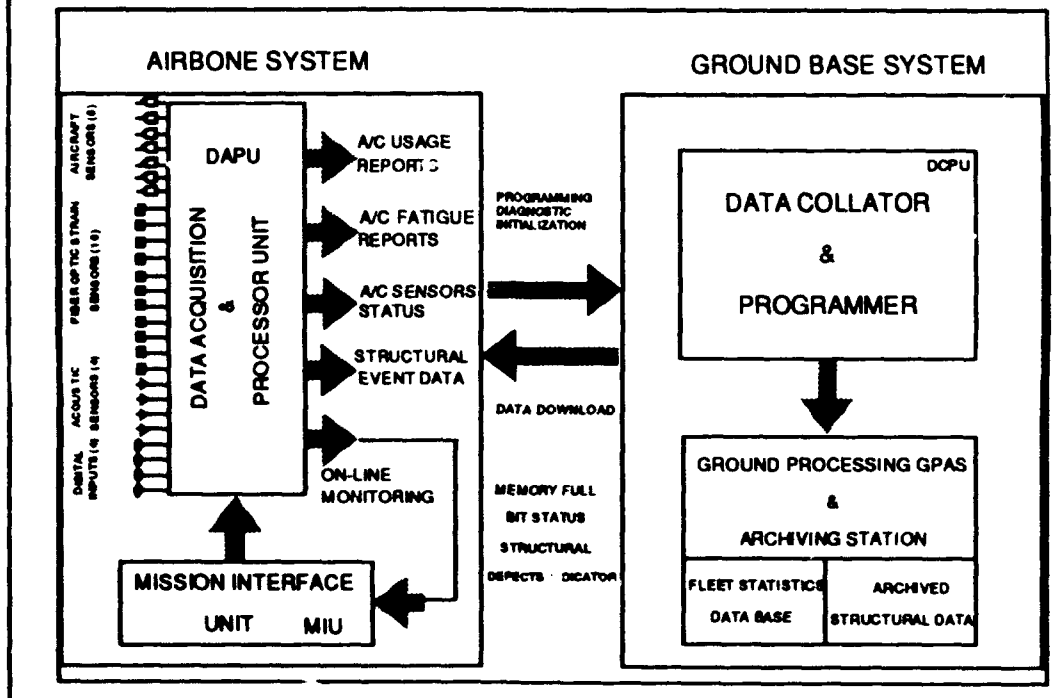
1. Push for More Reliable Strain Sensors
2. Move Towards On-Board Processing
3. Distributed Data Validation Algorithm
4. System Integration of On-Line Monitors
5. Better Integration of IAT to the Fleet Management Process

*** Technology / Know-how is Available**

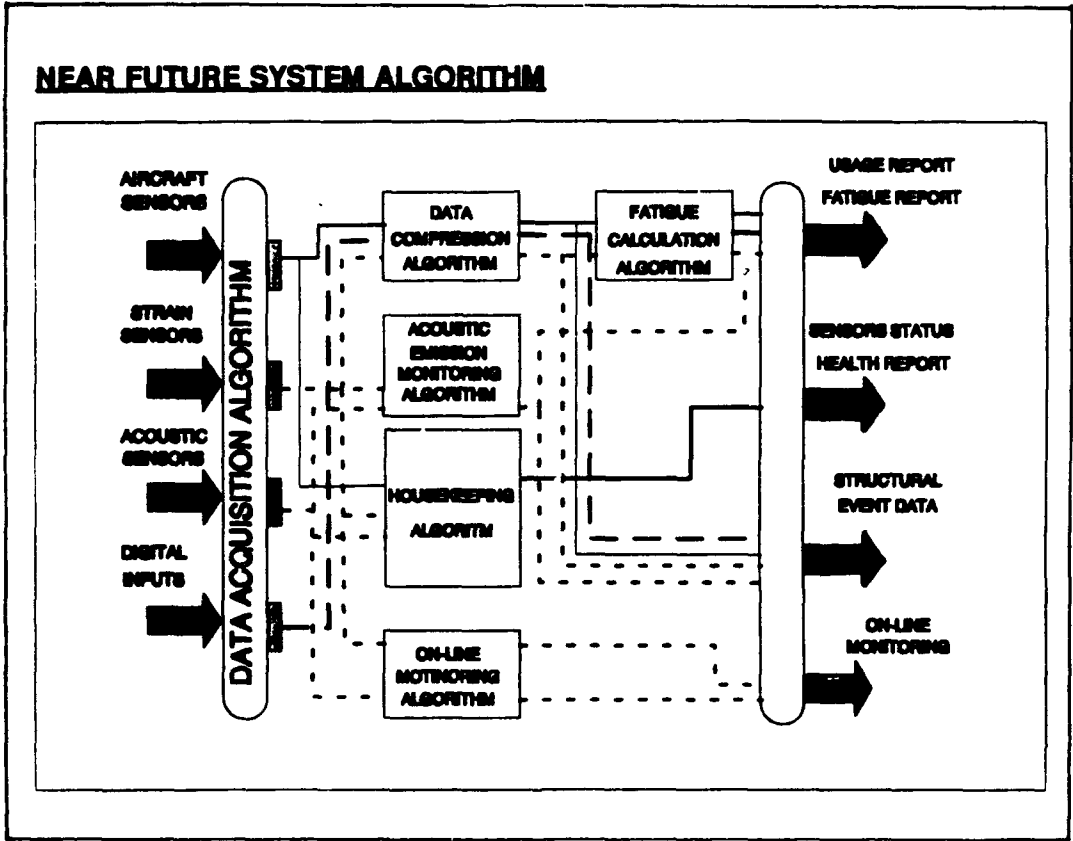
- Experience with AE (AEMs)
- Experience with FOSS (CMC)
- Fleet experience with loads recorder - (CF-18 MSORS and Esprit)
- On-line damage monitoring (ACPD)

*** Technology Integrator and \$\$**

NEAR FUTURE SYSTEM



NEAR FUTURE SYSTEM ALGORITHM



AN IMPROVED G-TRACKING METHOD FOR LARGE TRANSPORT AIRCRAFT

**1993 USAF STRUCTURAL INTEGRITY PROGRAM CONFERENCE
SAN ANTONIO, TEXAS
NOVEMBER 30 - DECEMBER 2, 1993**

**BRIAN MARTIN
C-141 OPERATIONAL LOADS
LOCKHEED AERONAUTICAL SYSTEMS CO.**

**RUSS ALFORD
C-141 ASIP MANAGER
WARNER-ROBINS AIR LOGISTICS CENTER**

THE STATE-OF THE ART IN AIRCRAFT REPEATED LOADS ANALYSIS AND RECORDER TECHNOLOGY HAS ADVANCED TO THE POINT WHERE INDIVIDUAL AIRCRAFT TRACKING LOADS MAY BE CALCULATED DIRECTLY FROM VERTICAL LOAD FACTOR (N_{zcg}) DATA, WITHOUT THE EXPENSE OR PROBLEMS INHERENT TO THE USE OF PAPER FORMS AND STRAIN GAGES. VARIOUS G-TRACKING METHODS ARE CURRENTLY IN USE ON MANY USAF AND NAVY WEAPONS SYSTEMS, AND WHILE SOME METHODS MAY ACCURATELY PREDICT LOAD MAGNITUDES BASED ON MEASURED N_{zcg} RESPONSE, THEY DO NOT ACCOUNT FOR DIFFERENCES IN THE CHARACTERISTIC FREQUENCY RESPONSE BETWEEN N_{zcg} AND THE STRUCTURAL TRACKING LOCATIONS DUE TO GUST ENCOUNTERS. NEAR THE AIRCRAFT CENTER OF GRAVITY, OR ON AIRCRAFT DESIGNED FOR HIGH-G MANEUVERS (e.g., FIGHTERS), THIS DIFFERENCE IS NOT A PROBLEM, SINCE THE RESPONSE RATIO CAN BE APPROXIMATELY ONE. HOWEVER, FOR LARGE TRANSPORT AIRCRAFT WITH FLEXIBLE WINGS, THE RATIO IS MUCH HIGHER. THIS PAPER WILL PRESENT A G-TRACKING METHOD FOR LARGE TRANSPORT AIRCRAFT THAT CAN PREDICT BOTH LOAD MAGNITUDES AND CHARACTERISTIC FREQUENCIES AT ANY STRUCTURAL TRACKING LOCATION, ON THE BASIS OF N_{zcg} MEASURED RESPONSE. THIS G-TRACKING METHOD IS SUITABLE FOR USE IN FOLLOW-ON FRACTURE MECHANICS ANALYSES (INSPECTION INTERVALS) OR FATIGUE ANALYSES (FATIGUE LIFE EXPENDED).

Overview of Tracking Methods for Large Transport Aircraft

Strain Gage Tracking

Strain Gage at Each Tracking Location on Each Aircraft in Fleet

Forms Tracking

Environmental Criteria

G-Tracking

Direct Conversion of Nzcg Peaks to Stress Peaks

Improved G-Tracking

Account for Differences in Characteristic Response Frequency

OVERVIEW

TO MAINTAIN THE STRUCTURAL INTEGRITY OF AN AIRCRAFT, REGULAR INSPECTIONS AT SPECIFIC INTERVALS DURING THE LIFE OF EACH AIRCRAFT ARE REQUIRED. SINCE STRUCTURAL LOADING MAY DIFFER SIGNIFICANTLY FROM ONE AIRCRAFT TO THE NEXT, STRUCTURAL DAMAGE MAY VARY AND THE INSPECTION INTERVALS SHOULD REFLECT THE DIFFERENCES. AIRCRAFT TRACKING PROGRAMS ARE IMPLEMENTED TO OBTAIN AIRCRAFT USAGE HISTORIES AND CONVERT THEM TO THE STRESS HISTORIES THAT DETERMINE EACH AIRCRAFT'S STRUCTURAL DAMAGE. SEVERAL METHODS EXIST FOR TRACKING AIRCRAFT DAMAGE, ALL OF WHICH REQUIRE SOME QUANTITY OF MEASURED STRUCTURAL RESPONSE DATA.

THE MOST ACCURATE METHOD FOR TRACKING AIRCRAFT STRUCTURAL DAMAGE IS TO ATTACH STRAIN GAGES AT OR NEAR EACH TRACKING LOCATION ON EACH AIRCRAFT IN THE FLEET. THIS METHOD IS ALSO THE MOST EXPENSIVE. IN ADDITION TO THE COST OF INSTALLING THE GAGES AND RECORDERS, THERE ARE HIGH DATA REDUCTION COSTS, AND THE RELIABILITY OF THE STRAIN GAGES IS LESS THAN 100%. THE COST OF THIS METHOD CAN BE REDUCED BY INSTRUMENTING ONLY A PERCENTAGE OF THE FLEET AND EXTRAPOLATING THE RESULTS, BUT THIS REDUCES THE ACCURACY OF THE STRESS HISTORIES FOR THE NON-INSTRUMENTED AIRCRAFT.

THE C-141 USES A TRACKING METHOD CALLED FORMS TRACKING. STRESS DATA IS OBTAINED USING A SET OF ENVIRONMENTAL CRITERIA DERIVED FROM A LARGE SAMPLE OF MEASURED N_{zcg} DATA, COUPLED WITH INDIVIDUAL AIRCRAFT USAGE (FUEL, CARGO, SPEED, ALTITUDE) FROM PAPER FORMS. THE ENVIRONMENTAL CRITERIA ARE APPLIED TO THE FORMS FROM EACH FLIGHT TO GET AN INDIVIDUAL AIRCRAFT'S STRESS HISTORY.

ANOTHER TRACKING METHOD IS G-TRACKING. G-TRACKING IS USED TO GENERATE STRESS HISTORIES FOR AIRCRAFT WITH RIGID STRUCTURE, OR NEAR THE CENTER OF GRAVITY (CG) ON AIRCRAFT WITH FLEXIBLE STRUCTURE. A RECORDER INSTALLED ON THE AIRCRAFT STORES USAGE PARAMETERS AND THE N_{zcg} PEAK HISTORY. N_{zcg} PEAKS ARE CONVERTED DIRECTLY TO STRESS PEAKS, WHICH ARE THEN USED TO DETERMINE STRUCTURAL DAMAGE.

IMPROVED G-TRACKING METHOD

BOTH FORMS TRACKING AND G-TRACKING HAVE ADVANTAGES AND DISADVANTAGES. FORMS TRACKING MAY BE USED TO DETERMINE STRUCTURAL DAMAGE AT ANY POINT ON THE AIRFRAME, THOUGH THE DAMAGE CALCULATIONS ARE NOT AS ACCURATE AS WITH G-TRACKING. G-TRACKING PROVIDES A MORE ACCURATE ASSESSMENT OF STRUCTURAL DAMAGE, BUT IT IS VALID ONLY IN AREAS WHERE THE RESPONSE FREQUENCY MATCHES THAT AT THE CG. THIS PRESENTATION WILL PRESENT AN IMPROVED G-TRACKING METHOD THAT COMBINES THE ADVANTAGES OF BOTH FORMS TRACKING AND G-TRACKING TO RESULT IN A MORE ACCURATE PICTURE OF STRUCTURAL DAMAGE AT ANY LOCATION ON A FLEXIBLE AIRFRAME.

Forms Tracking

Measured Data

Use VGH Recorder Program to Measure Large Sample of N_{zcg} Data

Analytical Data

Determine Analytical RMS G Response Data - \bar{A} , N_0

Using the Exceedance Equation, Determine Analytical Curve Fit Parameters for Measured VGH Data:

$$N(\Delta N_{zcg}) = N_0 T \left[P_1 e^{-\left(\frac{\Delta N_{zcg}}{b_1 A}\right)} + P_2 e^{-\left(\frac{\Delta N_{zcg}}{b_2 A}\right)} \right]$$

FORMS TRACKING

ANALYTICAL CURVE FIT PARAMETERS ARE DERIVED TO APPROXIMATE A LARGE SAMPLE OF MEASURED G RESPONSES. INDIVIDUAL FLIGHTS ARE RECORDED ON PAPER FORMS. THE CURVE FIT PARAMETERS ARE APPLIED TO THE RECORDED FLIGHTS TO DETERMINE THE STRESS HISTORY OF THAT FLIGHT.

MEASURED DATA

A VGH (VELOCITY, G, HEIGHT) RECORDER PROGRAM IS USED TO MEASURE A LARGE SAMPLE OF ACTUAL G PEAK OCCURRENCES. G PEAKS ARE SEPARATED INTO GUST AND MANEUVER PEAKS USING THE TWO-SECOND RULE.

ANALYTICAL DATA

DETERMINE ANALYTICAL ROOT MEAN SQUARED (RMS) G-RESPONSE DATA (\bar{A} , N_0 - ACCELERATION GRID) FOR POWER SPECTRAL DENSITY (PSD) GUST AND GROUND RESPONSE.

ANALYTICAL G UNIT RESPONSE DATA ARE USED TO FIT THE MEASURED VGH GUST AND GROUND DATA USING THE EXCEEDANCE EQUATION:

$$N(\Delta N_{zcg}) = N_0 T \left[P_1 e^{-\left(\frac{\Delta N_{zcg}}{b_1 \bar{A}}\right)} + P_2 e^{-\left(\frac{\Delta N_{zcg}}{b_2 \bar{A}}\right)} \right]$$

DETERMINATION OF P_1 , P_2 , b_1 , AND b_2 IS TRIAL AND ERROR, AND SUBJECTIVE.

RESULTING P_1 , P_2 , b_1 , AND b_2 ARE BASED ON TOTAL MEASURED GUST/GROUND G-OCCURRENCES.

MEASURED MANEUVER PEAKS ARE COMBINED INTO AN EXCEEDANCE CURVE TO GIVE THE NUMBER OF MANEUVER PEAK EXCEEDANCES PER UNIT TIME.

Forms Tracking Application

Determine Mean, Maneuver, and PSD Stress Response Data (\bar{A} , N_0 - Stress Grid)

Generate Stress Exceedance Curve for PSD Sources

$$N(\sigma) = N_0 T \left[P_1 e^{-\left(\frac{\sigma}{b_1 A}\right)} + P_2 e^{-\left(\frac{\sigma}{b_2 A}\right)} \right]$$

Add Mean Stress Plus Maneuver Occurrences

Determine Crack Growth

Generate Inspection Intervals

**This Method Accounts for both Magnitude and Frequency at the Tracking Location;
However, it is Based on Statistical Environmental Criteria**

FORMS TRACKING - APPLICATION

DETERMINE MEAN, MANEUVER, AND PSD STRESS RESPONSE DATA ($\bar{\sigma}$, N_0 - STRESS GRID FOR PSD GUST AND GRUND RESPONSE) AT THE TRACKING LOCATION - CREATE LOADS GRID, THEN CONVERT LOADS TO STRESSES.

GENERATE STRESS EXCEEDANCE CURVE AT THE TRACKING LOCATION.

FOR PSD SOURCES, USE GENERAL EXCEEDANCE EQUATION:

$$N_p(\sigma) = N_0 T \left[P_1 e^{-\left(\frac{\sigma}{b_1 A}\right)} + P_2 e^{-\left(\frac{\sigma}{b_2 A}\right)} \right]$$

P_1 , P_2 , b_1 , AND b_2 ARE THE SAME ENVIRONMENTAL PARAMETERS DERIVED FROM THE MEASURED VGH DATA FOR A GIVEN FLIGHT SEGMENT TYPE AND ALTITUDE.

MANEUVER OCCURRENCES AT THE TRACKING LOCATION ARE THE SAME AS THAT AT THE CG - ONE TO ONE CORRESPONDENCE. USE MANEUVER EXCEEDANCE CURVE TO DETERMINE PEAKS PER UNIT TIME.

MEAN STRESS IS ADDED TO PSD AND MANEUVER INCREMENTAL STRESS TO OBTAIN TOTAL STRESS.

COMPARE TO MEASURED STRESS EXCEEDANCE CURVE TO ENSURE ACCURACY.

BOTH STRESS MAGNITUDE AND CHARACTERISTIC FREQUENCY AT THE TRACKING LOCATION ARE ACCOUNTED FOR USING THIS METHOD. HOWEVER, THEY ARE BASED ON STATISTICALLY DETERMINED ENVIRONMENTAL CRITERIA PARAMETERS.

DETERMINE CRACK GROWTH FROM STRESS SPECTRA USING EXISTING DAMAGE TOLERANCE ANALYSIS (DTA) METHODS.

GENERATE INSPECTION INTERVALS ON THE BASIS OF CRACK GROWTH.

G-Tracking Measured Data

Data Recording

Usage Data

Aircraft Parameters

N_{zcg} Peak Time History

Data Processing

G-TRACKING

VGH AND BASIC USAGE RECORDER IS USED TO RECORD G-HISTORY OF EACH FLIGHT. INCREMENTAL G PEAKS ARE CONVERTED DIRECTLY TO INCREMENTAL STRESS PEAKS FOR TRACKING LOCATIONS NEAR THE CG. PAPER TRACKING FORMS ARE ELIMINATED. INSPECTION INTERVALS FOR THE TRACKING LOCATIONS ARE DERIVED FROM EACH AIRCRAFT'S UNIQUE G-EXPERIENCE, RATHER THAN ON PREVIOUSLY RECORDED FLEET AVERAGE G DATA (ENVIRONMENTAL CRITERIA).

MEASURED DATA - DATA RECORDING

TAKEOFF GROSS WEIGHT, TAKEOFF FUEL WEIGHT, LANDING FUEL WEIGHT, AIR REFUELING TIME AND FUEL WEIGHT TRANSFERRED, AND AIR DROP TIME AND CARGO WEIGHT DELIVERED.

SQUAT SWITCH (WEIGHT ON WHEELS), AIRSPEED, PRESSURE ALTITUDE, AND FLAP SETTING.

Nzcg TIME HISTORY - MEAN AND PEAK VALUES.

MEASURED DATA - DATA PROCESSING

DIVIDE FLIGHT DATA INTO SEGMENTS - GROUND, LANDING IMPACT, CLEAN FLIGHT, AND FLAPPED FLIGHT. USE RECORDED USAGE DATA - FLAP SETTING, SQUAT SWITCH, ALTITUDE, AIR REFUELING TIME, ETC. - TO DETERMINE SEGMENT BOUNDARIES. THE GOAL IS TO KNOW AS CLOSELY AS POSSIBLE THE VALUE OF FUEL WEIGHT, CARGO WEIGHT, MACH NUMBER, AND ALTITUDE AS A FUNCTION OF TIME.

CLASSIFY FLIGHT RECORDED PEAKS AS EITHER GUST-INDUCED OR MANEUVER-INDUCED.

SUBTRACT MEAN Nzcg FROM PEAK Nzcg TO OBTAIN INCREMENTAL Nzcg TIME HISTORY.

G-Tracking Analytical Data

Determine Analytical G Unit Response Data

Determine Analytical Loads Unit Response Data

Determine Stress Unit Response Data

G-TRACKING

ANALYTICAL DATA.

THE ANALYTICAL DATA DEVELOPED FOR THE FORMS TRACKING METHOD IS ALSO USED IN G-TRACKING.

DETERMINE ANALYTICAL G UNIT RESPONSE DATA (\ddot{A}_{Nzcg} - ACCELERATION GRID).

\ddot{A}_{Nzcg} IS THE INCREMENTAL RMS G RESPONSE AT THE AIRCRAFT CENTER OF GRAVITY TO A UNIT RMS INPUT EXCITATION.

FOR GUST RESPONSE, UNIT INPUT EXCITATION IS A GUST PSD FUNCTION WITH AN RMS VALUE OF ONE FOOT PER SECOND.

FOR GROUND RESPONSE, THE INPUT IS A RANDOM RUNWAY PROFILE GENERATED FROM A REFERENCE PSD LEVEL.

DETERMINE STRESS UNIT RESPONSE DATA (\ddot{A}_{Stress} - STRESS GRID) AT THE TRACKING LOCATION.

\ddot{A}_{Stress} FOR A GIVEN LOCATION ON THE AIRFRAME IS THE INCREMENTAL DYNAMIC STRUCTURAL STRESS AT THAT LOCATION TO A UNIT RMS INPUT EXCITATION.

OBTAIN STRESS TO LOAD RATIOS FOR DESIRED ANALYSIS POINT FROM FINITE ELEMENT MODEL (FEM).

MULTIPLY \ddot{A}_{Loads} BY STRESS/LOAD RATIOS TO OBTAIN \ddot{A}_{Stress} .

DETERMINE MEAN STRESS AND MANEUVER STRESS PER G AT THE TRACKING LOCATION.

G-Tracking Application

Convert Incremental N_{zcg} Peaks Directly to Incremental Stress Peaks

Multiply PSD Incremental N_{zcg} Peak Magnitude by $\bar{A}_{Stress} / \bar{A}_{Nzcg}$ to Obtain PSD Incremental Stress Peak Magnitude

Multiply Maneuver Incremental N_{zcg} Peak by Maneuver Stress/G Ratio to Obtain Maneuver Incremental Stress

Add Mean Stress to Incremental Stress to Obtain Total Stress

Use Stress Peak History to Determine Crack Growth

Crack Growth is now based on Aircraft's Unique G-History.

Method is Valid only for Tracking Locations whose Frequency of Response is near that of the CG.

G-TRACKING

APPLICATION.

CONVERT INCREMENTAL Nzcg PEAKS TO INCREMENTAL STRESS PEAKS AND USE TO DEVELOP CRACK GROWTH.

MULTIPLY PSD INCREMENTAL Nzcg PEAK MAGNITUDE BY $\bar{A}_{Stress}/\bar{A}_{Nzcg}$ TO OBTAIN THE PSD INCREMENTAL STRESS PEAK MAGNITUDE. $\bar{A}_{Stress}/\bar{A}_{Nzcg}$ IS A FUNCTION OF FUEL WEIGHT, CARGO WEIGHT, MACH NUMBER, AND ALTITUDE.

MULTIPLY MANEUVER INCREMENTAL Nzcg PEAK MAGNITUDE BY STRESS/G RATIO TO OBTAIN MANEUVER INCREMENTAL STRESS MAGNITUDE.

ADD MEAN STRESS TO INCREMENTAL STRESS TO OBTAIN TOTAL STRESS MAGNITUDE

USE STRESS PEAK HISTORY TO DEVELOP CRACK GROWTH USING EXISTING DTA PROGRAMS.

WITH G-TRACKING, CRACK GROWTH IS BASED ON EACH AIRCRAFT'S UNIQUE G-HISTORY, RATHER THAN FLEET STATISTICAL PARAMETERS (ENVIRONMENTAL CRITERIA).

THIS METHOD IS ONLY VALID IN AREAS WHERE THE CHARACTERISTIC RESPONSE FREQUENCY IS NEARLY THE SAME AS THAT AT THE CG (ONE TO ONE CORRESPONDENCE BETWEEN G PEAKS AND STRESS PEAKS). THIS METHOD IS NOT VALID FOR AREAS SUCH AS THE WING OF A C-141.

Improved G-Tracking

**Combine Forms Tracking Method With G-Tracking Method
to Provide Accurate Stress History at any
Location on the Aircraft Structure**

IMPROVED G-TRACKING

THE FORMS TRACKING METHOD ACCOUNTS FOR BOTH STRESS MAGNITUDE AND CHARACTERISTIC FREQUENCY. HOWEVER, STRESS EXCEEDANCE CURVES ARE BASED ON STATISTICALLY DETERMINED ENVIRONMENTAL CRITERIA PARAMETERS.

THE G-TRACKING METHOD IMPROVES ON THE FORMS TRACKING METHOD BY PROVIDING A STRESS PEAK HISTORY BASED ON AN AIRCRAFT'S MEASURED G-HISTORY. HOWEVER, THE METHOD DOES NOT ACCOUNT FOR DIFFERENCES IN THE CHARACTERISTIC FREQUENCY BETWEEN THE CG AND THE TRACKING LOCATION, AND IS THEREFORE VALID ONLY FOR STRUCTURAL LOCATIONS NEAR THE CG.

THE IMPROVED G-TRACKING METHOD COMBINES THE ADVANTAGES OF THE TWO PREVIOUS METHODS. USING THE AIRCRAFT'S UNIQUE G-HISTORY, IT PROVIDES A STRESS HISTORY AT ANY LOCATION ON THE AIRFRAME THAT ACCOUNTS FOR DIFFERENCES IN THE CHARACTERISTIC RESPONSE FREQUENCY. FOR A LARGE TRANSPORT AIRCRAFT SUCH AS THE C-141, THIS MEANS THAT STRESS HISTORIES MAY BE OBTAINED FOR TRACKING LOCATIONS WELL OUTBOARD ON THE WING USING ONLY THE N_{zcg} HISTORY.

Improved G-Tracking Procedures

Measured Data

Determine Acceleration Parameters - \bar{A} , N_0

Determine Load Parameters - \bar{A} , N_0 , Mean Load, Maneuver Load/G

Determine Stress Parameters - \bar{A} , N_0 , Mean Stress, Maneuver Stress/G

IMPROVED G-TRACKING

PROCEDURES

MEASURED DATA

COLLECT AND PROCESS DATA IN THE SAME MANNER AS WITH THE CURRENT G-TRACKING METHOD

RESPONSE PARAMETERS - \bar{A}_{Nzog} , N_{0Nzog} , \bar{A}_{Stress} , $N_{0Stress}$, MEAN STRESS, AND MANEUVER STRESS/G

DETERMINE IN THE SAME MANNER AS FOR THE FORMS TRACKING METHOD - ACCELERATION GRID, LOADS GRID, STRESS TO LOAD RATIOS, AND STRESS GRID.

N_0 IS A MEASURE OF THE CHARACTERISTIC RESPONSE FREQUENCY. THIS IS THE KEY PARAMETER FOR THE IMPROVED G-TRACKING METHOD.

Improved G-Tracking Procedures

Convert G-History to Stress-History

Peak by Peak

Exceedance Curves

Maneuver Response

Calculate Crack Growth Using Stress History

IMPROVED G-TRACKING - CONVERT G-HISTORY TO STRESS-HISTORY

PEAK BY PEAK - MULTIPLY PSD INCREMENTAL G PEAK MAGNITUDE BY $\bar{A}_{\text{stress}}/\bar{A}_{\text{Hzcg}}$ TO OBTAIN PSD INCREMENTAL STRESS PEAK MAGNITUDE

THE NUMBER OF PSD STRESS CYCLES AT THAT MAGNITUDE EQUALS $N_{\text{stress}}/N_{\text{Hzcg}}$

MULTIPLY MANEUVER INCREMENTAL G PEAK MAGNITUDE BY MANEUVER STRESS/G RATIO TO OBTAIN MANEUVER INCREMENTAL STRESS PEAK MAGNITUDE. THERE IS A ONE TO ONE CORRESPONDENCE BETWEEN MANEUVER N_{zcg} OCCURRENCES AND MANEUVER STRESS OCCURRENCES AT THE TRACKING LOCATION.

ADD MEAN STRESS TO INCREMENTAL STRESS TO OBTAIN TOTAL STRESS MAGNITUDE.

CRACK GROWTH PROGRAMS MUST BE ABLE TO HANDLE PARTIAL STRESS CYCLES

EXCEEDANCE CURVES - SEGMENT RECORDED DATA INTO GROUPS OF NEARLY CONSTANT FUEL WEIGHT, CARGO WEIGHT, MACH NUMBER, AND ALTITUDE

SORT, BAND, AND COUNT INCREMENTAL G DATA WITHIN EACH SEGMENT TO FORM G EXCEEDANCE CURVES FOR BOTH GUST/GROUND AND MANEUVER

FOR EACH BAND OF THE PSD INCREMENTAL G EXCEEDANCE CURVE, MULTIPLY THE MAGNITUDE OF THE BAND BY $\bar{A}_{\text{stress}}/\bar{A}_{\text{Hzcg}}$ TO OBTAIN THE INCREMENTAL STRESS BAND MAGNITUDE. MULTIPLY THE NUMBER OF G OCCURRENCES WITHIN EACH BAND BY $N_{\text{stress}}/N_{\text{Hzcg}}$ TO OBTAIN THE NUMBER OF STRESS OCCURRENCES. ADD MEAN STRESS AND PLOT AS STRESS EXCEEDANCE CURVE.

FOR EACH BAND OF THE MANEUVER INCREMENTAL EXCEEDANCE CURVE, MULTIPLY THE MAGNITUDE OF THE BAND BY THE MANEUVER STRESS/G RATIO TO OBTAIN THE STRESS BAND MAGNITUDE. THE NUMBER OF OCCURRENCES WITHIN THE BAND IS UNCHANGED. ADD THE MEAN STRESS AND PLOT AS MANEUVER STRESS EXCEEDANCE CURVE.

DECOMPOSE STRESS EXCEEDANCE CURVES INTO A STRESS HISTORY USING EXISTING METHODS

CALCULATE CRACK GROWTH USING STRESS HISTORY

Improved G-Tracking

Benefits

Crack Growth is based on Individual Aircraft's Actual G-Experience

Valid for Large Transport Aircraft with Flexible Structure

Inspection Intervals are More Accurately Tailored to Individual Aircraft

Eliminates Usage Form

IMPROVED G-TRACKING

BENEFITS OF IMPROVED METHOD.

ANALYTICAL CRACKS ARE GROWN SEGMENT BY SEGMENT, FLIGHT BY FLIGHT IN THE SEQUENCE THEY OCCURRED, BASED ON EACH AIRCRAFT'S UNIQUE G-EXPERIENCE.

VALID FOR LARGE TRANSPORT AIRCRAFT, SUCH AS THE C-141, WITH FLEXIBLE STRUCTURE

MORE ACCURATE KNOWLEDGE OF INDIVIDUAL AIRCRAFT CRACK GROWTH ALLOWS INSPECTION INTERVALS TO BE MORE ACCURATELY TAILORED TO INDIVIDUAL AIRCRAFT.

USAGE FORMS CAN BE ELIMINATED - USAGE DATA IS ACQUIRED BY THE RECORDER.

Improved G-Tracking Demonstration

C-141 L/ESS Recorded Data

Flight D3125F1, 4/16/93

Takeoff Fuel = 85000 Pounds

Takeoff Cargo = 4000 Pounds

C-141 MRS Loads System

C-141 Finite Element Model

IMPROVED G-TRACKING DEMONSTRATION

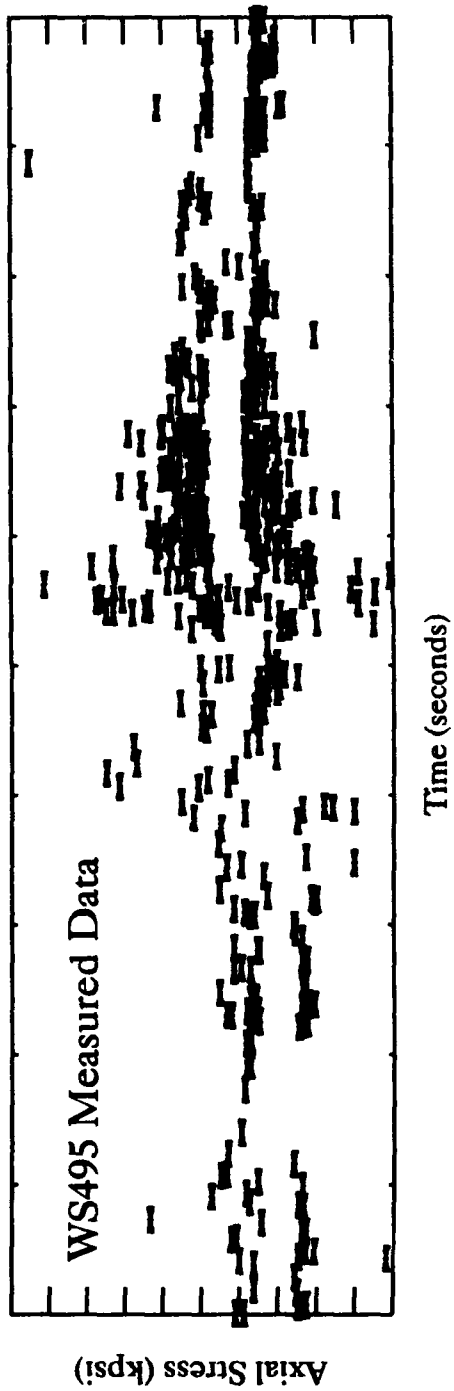
USING C-141 LOADS/ENVIRONMENT SPECTRA SURVEY (L/ESS) RECORDED GUST DATA, C-141 MULTIPLE REFERENCE STATION (MRS) LOADS SYSTEM, AND C-141 FEM, CONVERT MEASURED Nzcg PEAKS TO STRESS PEAKS AT A L/ESS STRAIN GAGE LOCATION AND COMPARE TO MEASURED STRAIN GAGE DATA.

C-141 L/ESS FLIGHT D3125F1, 4/16/93, TAKEOFF FUEL = 85000 POUNDS, TAKEOFF CARGO = 4000 POUNDS.

DEFINE TRACKING LOCATION AT WS 495 - COINCIDENT WITH L/ESS STRAIN GAGE FOR COMPARISON

Improved G-Tracking Demonstration

Measured Data



IMPROVED G-TRACKING DEMONSTRATION

EXAMPLE OF MEASURED L/ESS DATA - 1000 SECONDS

Nzcg DATA ON TOP, WS 495 STRAIN GAGE DATA ON BOTTOM

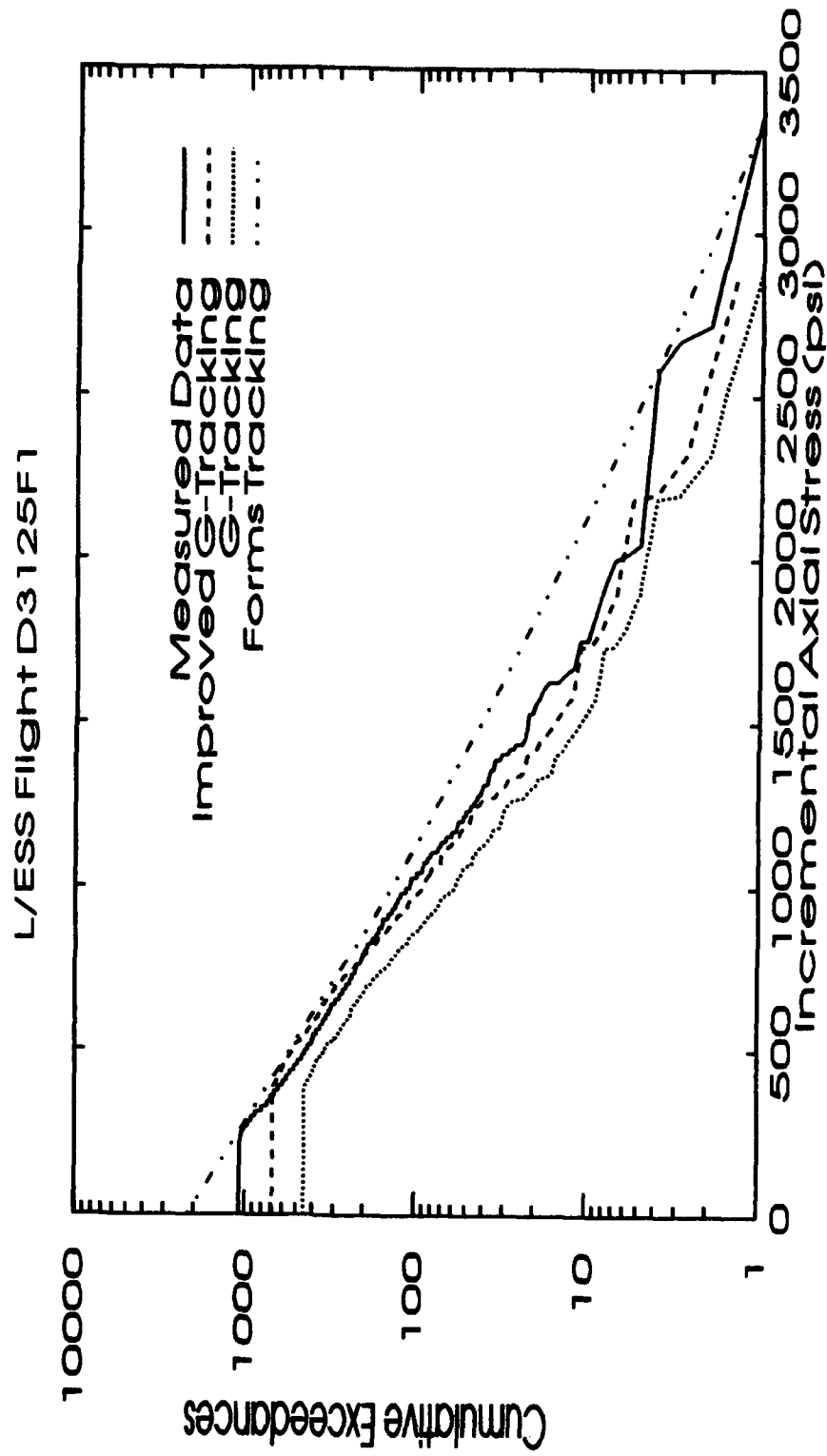
**GENERAL SHAPE OF THE RESPONSE IS THE SAME, THOUGH THERE ARE CLEARLY
MORE RECORDED PEAKS IN THE STRAIN GAGE DATA**

Improved G-Tracking Demonstration

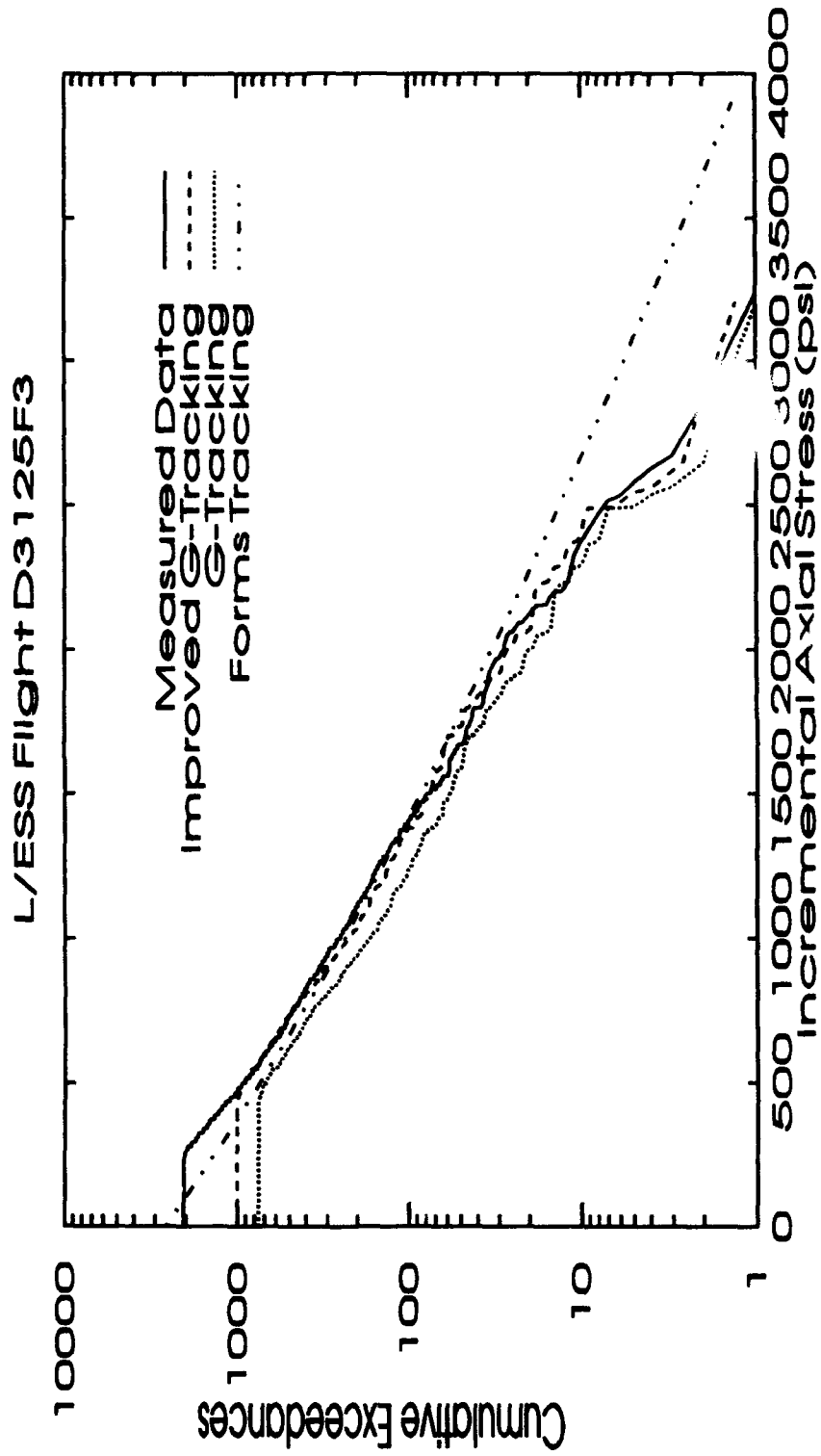
L/ESS Flight D3125F1 Mission Segments

Segment Type	Time	Fuel	Cargo	Mach	Altitude
1 CLIMB 0	2.00000	82364.0	4000.0	0.408	4166.7
2 CLIMB 0	3.00000	80975.6	4000.0	0.506	12500.0
3 CLIMB 0	5.00000	79399.2	4000.0	0.622	20833.3
4 CRUISE 0	32.86000	72823.6	4000.0	0.668	25000.0
5 DESCNT 0	2.81000	66964.7	4000.0	0.676	21750.0
6 DESCNT 0	3.75000	66715.2	4000.0	0.600	15250.0
7 CRUISE 0	2.13000	66133.2	4000.0	0.574	12000.0
8 DESCNT 0	4.73000	65545.6	4000.0	0.496	9375.0
9 DESCNT 0	4.73000	65249.1	4000.0	0.409	4125.0
10 TRAFFIC	2.45000	64550.4	4000.0	0.216	1500.0
11 APPROACH	3.60000	64000.0	4000.0	0.215	500.0

Improved G-Tracking Demonstration Measured Versus Analytical Data



Improved G-Tracking Demonstration Measured Versus Analytical Data



IMPROVED G-TRACKING DEMONSTRATION

C-141 L/ESS FLIGHT D3125F3 COMPARISON

TAKEOFF FUEL WEIGHT = 73,000 POUNDS

TAKEOFF CARGO WEIGHT = 29,000 POUNDS

TAKEOFF GROSS WEIGHT = 246,500 POUNDS

Improved G-Tracking Implementation

Hardware Requirements

Sensors

Data Recorder

Software Requirements

Flight Data Processing

N_{zcg} Processing

N_{zcg} to Stress Conversion

Data Collection Procedures

G-TRACKING IMPLEMENTATION.

HARDWARE REQUIREMENTS - ALL OFF-THE-SHELF.

SENSORS

Nzcg ACCELEROMETER

FLIGHT DATA INSTRUMENTS (AIRSPEED, PRESSURE ALTITUDE, ETC.)

DATA RECORDER

SOFTWARE REQUIREMENTS - MUCH OF THE SOFTWARE IS ALREADY WRITTEN FOR CURRENT TRACKING AND L/ESS PROGRAMS.

FLIGHT DATA PROCESSING - SEGMENTING, FILTERING, ETC.

Nzcg PROCESSING - SORTING, BANDING, AND COUNTING

Nzcg TO STRESS CONVERSION

\bar{A} AND N_0 RATIOS - LOADS SYSTEM AND FEM

MEAN STRESS AND MANEUVER STRESS/G - LOADS SYSTEM AND FEM

EXCEEDANCE CURVE CONVERSION

DATA COLLECTION PROCEDURES

Improved G-Tracking

Conclusions

Conversion of Measured N_{zcg} Occurrences Directly to Stress Occurrences on a Flight by Flight Basis Allows True Individual Aircraft Tracking.

Accurate Stress Histories can be Obtained for any Location on a Flexible Airframe, Without the use of Strain Gages.

Accurate Knowledge of an Individual Aircraft's Stress History Allows Inspection Intervals to be More Accurately set for Individual Aircraft.

Usage Data is Automatically Recorded as a part of G-Tracking, Eliminating the Need for and Expense of Paper Usage Tracking Forms.

NAVAL AIRCRAFT APPROACH

and

LANDING DATA ACQUISITION SYSTEM

(NAALDAS)

ACCEPTANCE TEST RESULTS

PRESENTED BY:

RICK MICKLOS
AEROSPACE ENGINEER
AERO STRUCTURES DIVISION
NAWC AD WARMINSTER PA.

INTRODUCTION:

The Naval Aircraft Approach and Landing Data Acquisition System (NAALDAS) was developed by the Naval Air Warfare Center, Aircraft Division, Warminster Pa. to modernize and automate the collection of aircraft landing parameters. NAALDAS replaces a 70 MM photographic system which had been used to collect this data, but required labor intensive data reduction and was becoming increasingly difficult to operate and maintain in a cost effective manner.

The last thirteen months have been highly significant time in the development of the NAALDAS. Operational testing of the system has been completed. The system has successfully demonstrated its capability and accuracy. Operational testing was performed in two phases

1. Land based testing was performed last November at the Naval Air Warfare Center, Aircraft Division, Patuxent River Maryland.
2. Last summer, NAALDAS was tested at sea on the aircraft carrier USS GEORGE WASHINGTON. We operated the system for over two weeks recording nearly 1600 carrier landings.

In addition, a modified version of NAALDAS designed to collect landing parameters of commercial jet aircraft will be demonstrated at the Federal Aviation Administration Technical Center in Atlantic City NJ. This system uses a series of video cameras to cover the wider dispersion of aircraft touchdown points associated with field landings.

BACKGROUND:

NAALDAS SYSTEM DESCRIPTION:

NAALDAS provides data on the following landing parameters:

- Engaging Speed (Closure speed)
- Approach Speed (Engaging Speed plus prevailing wind component)
- Sinking Speeds of the port, starboard and nose landing gear wheels
- Sinking Speed of the average position of the main wheels.
- Roll attitude and rate
- Pitch attitude and rate
- Off center Distance
- Ramp to Touchdown Distance
- Yaw angle at touchdown
- Flight Path Angle at touchdown
- Glide slope Angle (Instantaneous and Geometric)

NAALDAS CONSISTS OF TWO INDEPENDENT SUBSYSTEMS.

DATA ACQUISITION SUBSYSTEM :

This subsystem consists of a frame grab CCD video camera, laser disk video recorder, and portable computer to control and operate the system. The equipment runs on 110 volt current, weighs 500 pounds and is packaged in five shipping containers that can be fitted on two pallets. This contrasts with the 13,000 pounds of equipment and hardware accessories required to collect night landing data using the 70 mm film system.

The video camera is installed in the port catwalk of an aircraft carrier (edge of the flight deck landing area). The camera is located approximately 500 feet from the stern end of the flight deck and 75 ft off the center line of the landing area. The camera is aimed at the center of the target touchdown area and records the last 0.5 second of the aircraft's approach. The camera's aim is fixed, it does not track the aircraft.

The data recording equipment is located in an operating space below decks in the vicinity of the camera. The space must be air conditioned. The laser disk recorder has been installed in a shock mounted EMI enclosure and the computer has been ruggedized for use in the shipboard environment. All the interconnecting cabling and mounting hardware are installed by the survey team.

The system is calibrated by placing temporary targets at known locations in the camera field of view and recording these images as a calibration sequence. This sequence is processed to generate a transformation matrix to relate image measurements to the carrier flight deck, or for field operations, to the runway.

The video images are recorded on laser disks. Approximately 60 landings are stored on one disk. An identity number is assigned to the disk, and event numbers to each video sequence.

The video camera is remotely operated; there is no requirement to place operating personnel at the camera, as was necessary to change 70mm film magazines. There is no post processing required of the video disks. This eliminates film processing cost and the time required to perform it.

DATA REDUCTION AND ANALYSIS SUBSYSTEM :

This subsystem consists of a "Sun" computer work station with an image processing board installed, a laser disk player, computer monitor, high resolution monitor and associated power regulator and cables.

The combination of the laser disk recorder, image processing capability and high resolution monitor, along with the systems software, allows the operator to automatically track image features through a landing sequence. By positioning "windows" over the initial image feature in a track sequence, the operator sets up the system to track that feature through the entire sequence. Multiple image features can be tracked simultaneously using multiple windows. The operator has the capability of selection image threshold levels, various image enhancement formats and algorithms as well as the type of tracking (edge or centroid) being used. These selections allow the system to automatically track the image, eliminating the errors in data reduction inherent in the manual tracking procedures associated with 70 MM film. The centroid tracking algorithm enables the system to locate image features to sub-pixel accuracy.

Once the image sequence has been tracked, the software transforms the pixel information to a format compatible with the existing landing parameter analysis software. This software takes image position information, determines the change in image feature position of successive frames and generates position time curves for the feature. Currently, both linear and second order curve fit routines are used in the analysis. The second order curves are used for vertical positions which are effected by the motion of the carrier flight deck (ship pitch and roll) during recording.

NAALDAS SYSTEM TESTING

Land Based Testing

This testing was performed at the NAVAL AIR WARFARE CENTER, Aircraft Division, Patuxent River, Md. That facility has film cameras installed at a test site used to qualify carrier aircraft (and the equipment installed in them) for arrested carrier landings. Since the test site routinely photographs these test events and calculates landing parameters from that film data, it offered an excellent opportunity to evaluate the accuracy of NAALDAS prior to taking the system to sea. A sketch of the test site and camera locations is provided as figure 1.

The test site at Patuxent River has two camera locations. One in the runway center line and one perpendicular to the aircraft flight path at the arresting gear cable. Both the NAALDAS video camera and the Warminster 70 mm camera were installed along the edge of the runway pointed at a 14 degree angle toward the expected touchdown point, which was the runway center line at the arresting gear cable.

This was an extremely challenging test for NAALDAS. Because of the width of the runway at Patuxent River, and our desire to maintain the same geometric relationships existing on a carrier deck, the camera equipment was installed 100 ft further from the

touchdown point than on an aircraft carrier. The weather conditions were poor during the test period and light levels at the system's operational limit.

This testing involved the installation and calibration of NAALDAS at the test site, recording a series of arrested landings and comparing the NAALDAS results with those produced by the Patuxent River cameras. A comparison of the sink speed data from this test is included as figure 2, the results are tabulated in table 1. Engaging speed results are documented in figure 3 and table 2. It is particularly impressive to note that the values of sink speed reported by NAALDAS compare very favorably with the average value of sink speed calculated for the Patuxent River cameras.

We achieved excellent agreement with the Patuxent River cameras. The results of this testing proved we were ready to proceed with operational testing on an aircraft carrier.

Carrier Testing

Sixteen hundred carrier landings were recorded. The test landings were performed by fleet pilots, flying all the standard models of Navy carrier aircraft. A sketch of camera location and orientation on the carrier flight deck is included as figure 4. The data collected by NAALDAS was compared with the results from our 70 mm film system which photographed several hundred landings. The two data sets were processed and the comparison of the results indicate that we met our design goals. The NAALDAS camera and data collection equipment was installed during a five day period prior to the ship's departure. The equipment performed flawlessly despite being exposed to all the environmental hazards associated with operations at sea. (Electromagnetic interference, vibration, shock, salt spray, rain, and exposure to fire fighting foam and jet exhaust.) The NAVY considers this system to be operational and ready for use.

The results of these comparisons are presented in table 3, which lists statistical information on the distributions of landing parameters for the various types of aircraft covered by the survey. Comparisons between the average main wheel sinking speed determined by NAALDAS and the 70 MM film system are included as figures 5 for a fighter aircraft, figure 6 for a fighter/attack aircraft, figure 7 for an attack aircraft and figure 8 for an ASW aircraft. The same comparisons for engaging speed are included as figures 9 through 12.

The design of NAALDAS was driven by the size and landing speed of the Navy's fighter attack aircraft, which causes the greatest demands on system resolution. Examination of figures 6 and 10 show that we have successfully met these design goals.

LESSONS LEARNED:

NAALDAS technology meets our design goals.

A limited number of system refinements have been identified in our testing.

The prototype acquisition system does not include full remote capability. Remote lens focus and iris will be included. Since we manually adjust the 70mm camera, we adjust the video camera at the same time.

The automatic tracking routines have difficulty functioning in cluttered scenes. We occasionally lost track of aircraft wheels in a tree line during land based testing. At sea, aircraft parked on the opposite side of the landing area caused tracking problems. This problem is aggravated under poor lighting conditions. We are currently procuring a software upgrade to alleviate this problem. Remote lens control will also aid in this area.

FAA Demonstration:

A demonstration is scheduled this month (December 1993) which is intended as a dry run for a commercial landing loads survey scheduled this spring at John F. Kennedy International Airport in New York. Tentative approval for this survey has been granted by both the FAA and the NY Port Authority.

CONCLUSIONS

The design and development of NAALDAS has enhanced a unique and critical NAWC AD capability. These enhancements make the system more responsive and flexible while providing for significantly higher levels of operator safety.

The systems flexible design allows for collecting landing kinematic parameters on a wide variety of aircraft, from small private airplanes, through military fighter/attack models, to large commercial jet transports. This system meets all FAA safety and operational requirements.

NAALDAS is a valuable tool which monitors the structural effect of changes to aircraft landing procedures without impacting normal aircraft operations or requiring modifications or equipment installation on the aircraft. It monitors the effectiveness of various types of landing aids, the consequences of higher glide slope angles (caused by operational requirements and local topography) and the impact of special noise abatement procedures on the landing performance of aircraft and provides the information necessary for an accurate assessment of airframe structural life.

NAALDAS is a valuable tool which offers for the entire aviation community the opportunity to better define landing structural design requirements.

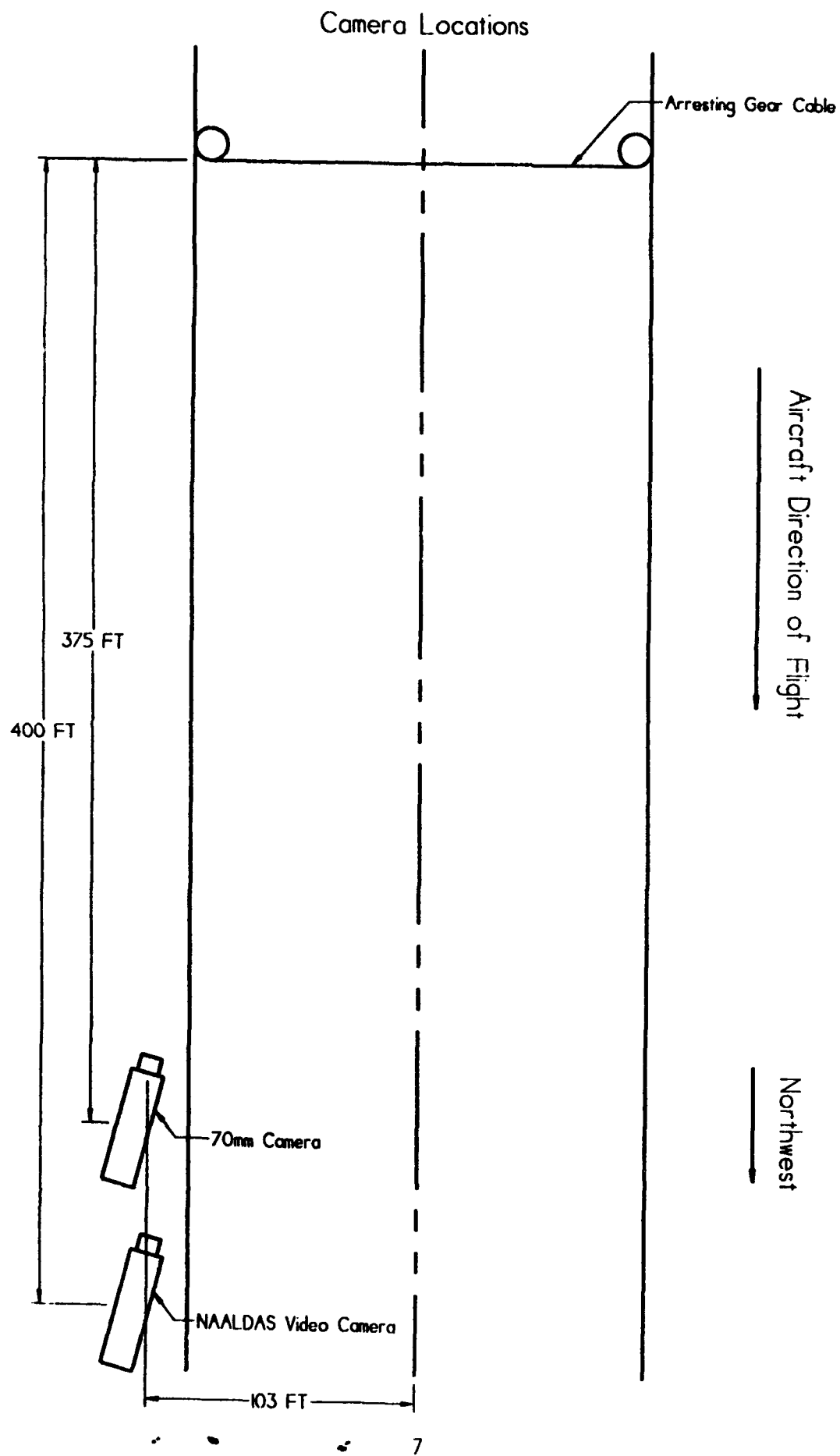


Figure 1

LAND BASED TESTING

NAALDAS RESULTS COMPARED WITH PATUXENT RIVER CAMERAS AND WARMINSTER 70MM CAMERA

	<i>PARAMETER</i>	<i>AVG. SINKING SPEED</i>	<i>(FT/SEC)</i>		
LANDING NUMBER	RECORDING SYSTEM	PATUXENT SIDE CAMERA	PATUXENT CENTER LINE	WARMINSTER FILM SYSTEM	NAALDAS VIDEO SYSTEM
1			11.6	11.7	11.8
2		14.9	13.6	15.0	14.1
3		14.9	13.4	13.9	14.5
4		16.1	14.8	15.7	15.4
5			14.5	15.6	15.1
6		17.7	16.0	16.7	16.5
7			17.5	18.4	18.4
8		18.3	16.9	17.4	17.5
9		19.7	18.4	18.9	19
10		21.6	19.5	20.4	20.2
11		19.5	17.7	18.0	18.5
12		19.8	18.2	19.3	18.7

TABLE 1

LAND BASED TESTING

NAALDAS RESULTS COMPARED WITH PATUXENT RIVER CAMERAS AND WARMINSTER 70MM CAMERA

	<i>PARAMETER</i>	<i>ENGAGING SPEED</i>	<i>(KNOTS)</i>		
LANDING NUMBER	RECORDING SYSTEM	PATUXENT SIDE CAMERA	PATUXENT CENTER LINE	WARMINSTER FILM SYSTEM	NAALDAS VIDEO SYSTEM
1			116.9	118.6	119.2
2		114.4	117.2	116.7	113.6
3		115.5	116.8	114.4	115.1
4		114.5	118.0	118.7	119.3
5			118.6	118.8	122.0
6		113.8	116.7	118.1	117.7
7			117.7	116.0	116.4
8		116.2	115.7	119.1	117.8
9		120.1	119.4	121.4	121.3
10		121.8	124.7	123.6	120.9
11		122.7	120.6	123.1	123.6
12		120.5	121.1	122.7	117.4

TABLE 2

NAALDAS TEST DATA COMPARISON

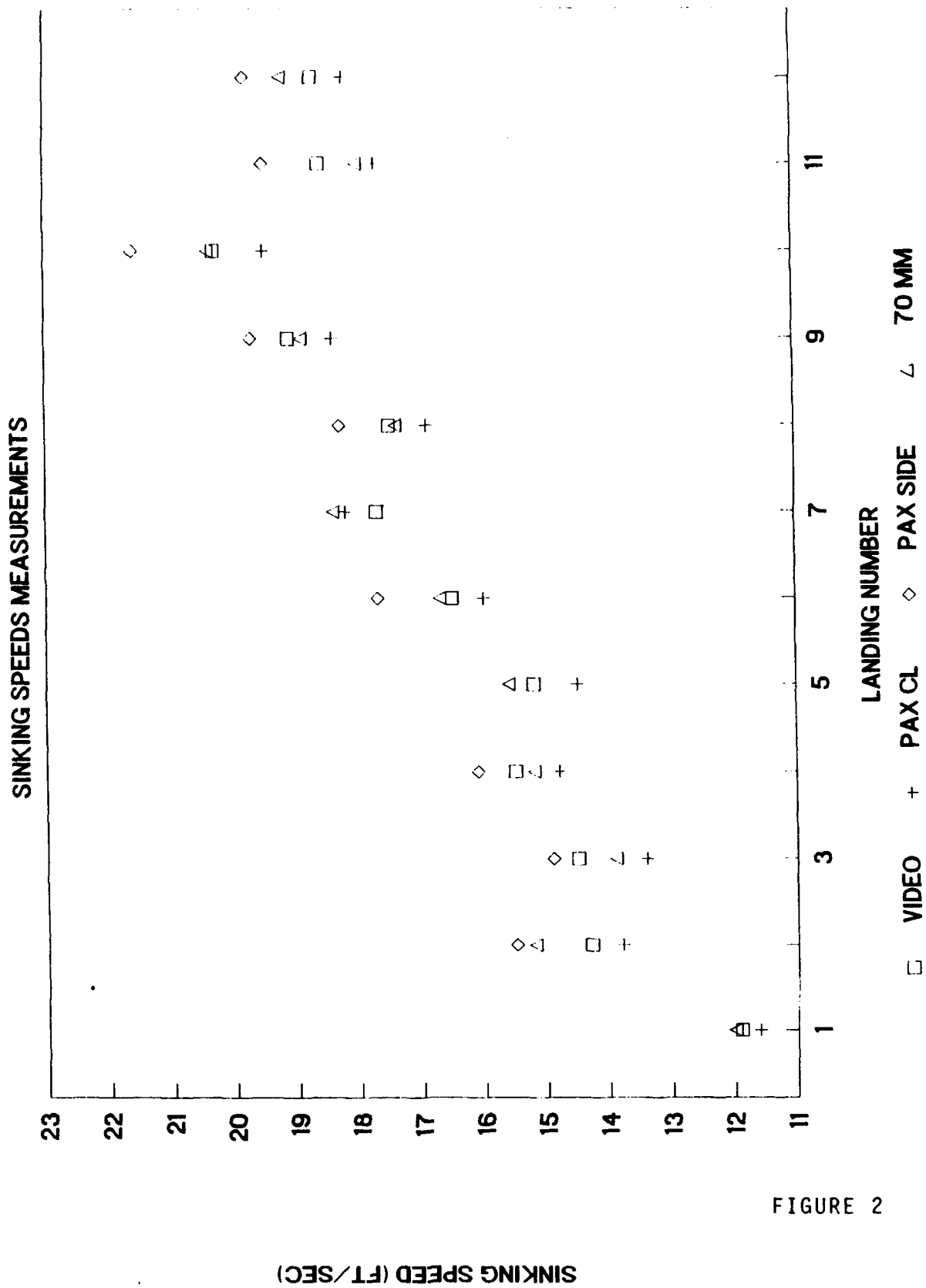


FIGURE 2

NAALDAS TEST DATA COMPARISON

ENGAGING SPEED MEASUREMENTS

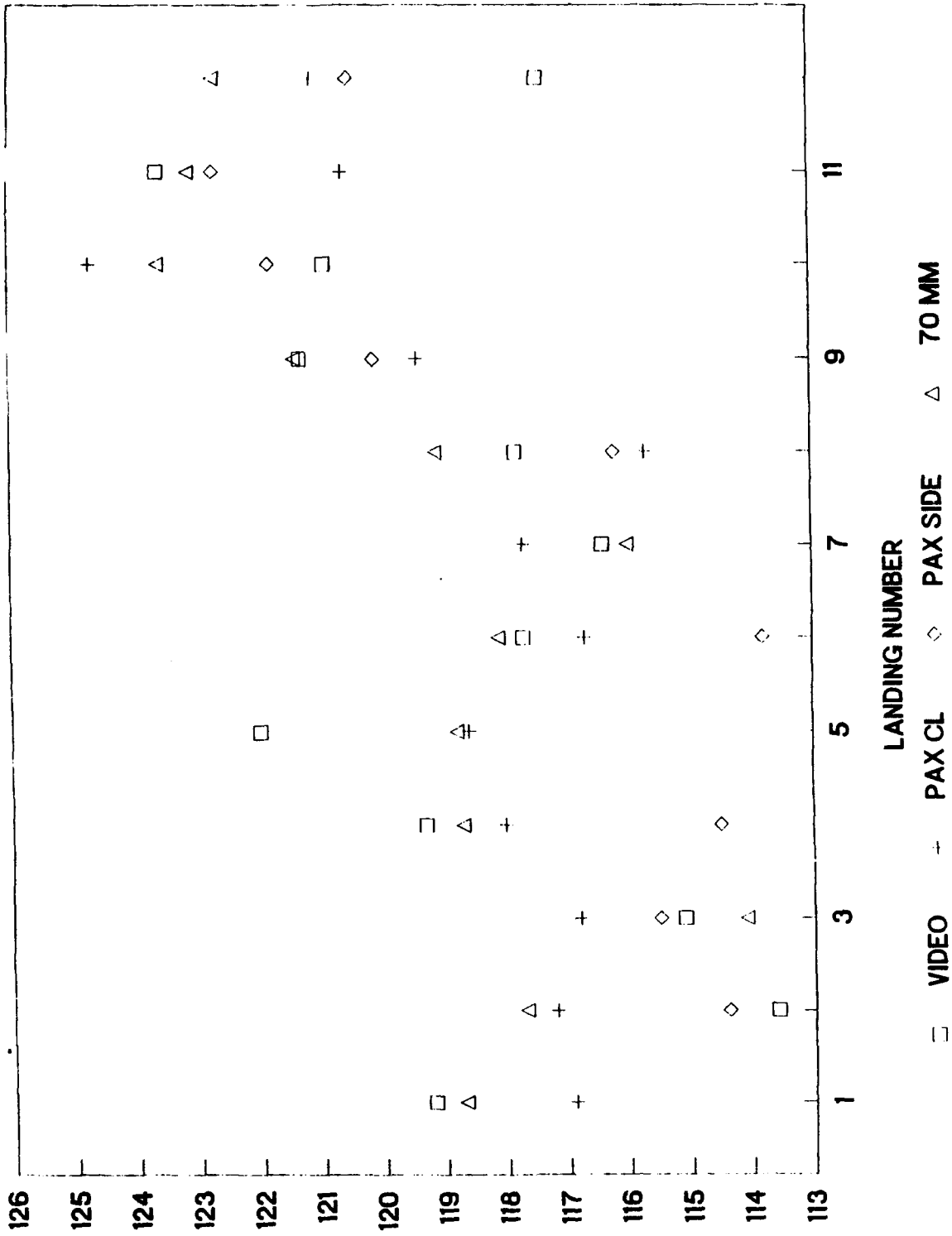


FIGURE 3

ENGAGING SPEED (KNOTS)

CARRIER DECK LAYOUT

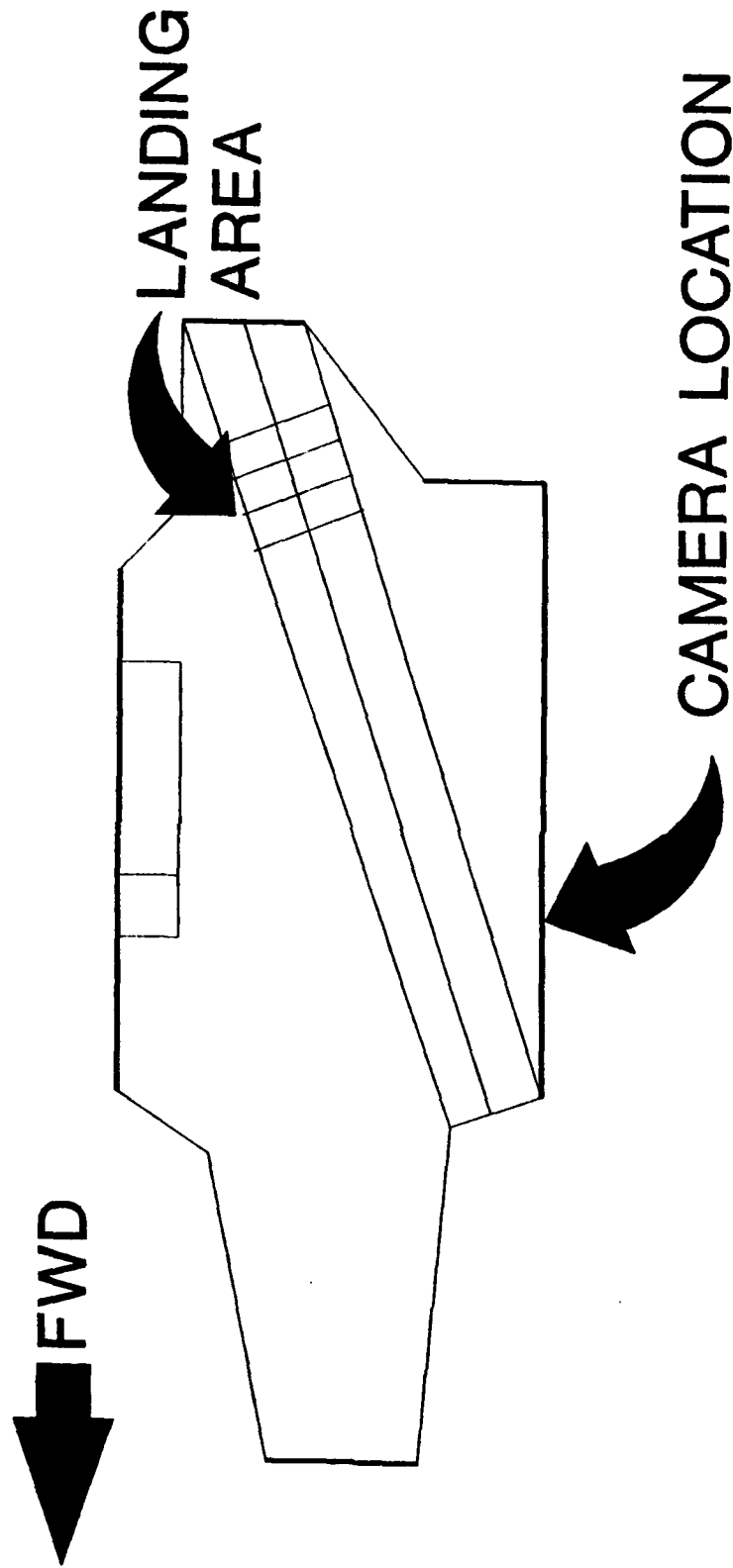


FIGURE 4

**CARRIER LANDING PARAMETER COMPARISON
NAALDAS vs 70 MM PHOTOGRAPHIC SYSTEM**

	AIRCRAFT TYPE	FIGHTER	FIGHTER ATTACK	ATTACK	ASW
PARAMETER	AVERAGE SINKING SPEED	FT/SEC	FT/SEC	FT/SEC	FT/SEC
NAALDAS	MEAN VALUE	12.3	11.7	10.1	9.5
	STANDARD DEVIATION	2.1	2.1	2.0	1.4
FILM SYSTEM	MEAN VALUE	12.0	11.7	10.2	9.2
	STANDARD DEVIATION	2.3	2.1	1.8	1.4
NUMBER OF LANDINGS		56	88	88	38

	AIRCRAFT TYPE	FIGHTER	FIGHTER ATTACK	ATTACK	ASW
PARAMETER	ENGAGING SPEED	KNOTS	KNOTS	KNOTS	KNOTS
NAALDAS	MEAN VALUE	119.6	131.3	114.4	103.0
	STANDARD DEVIATION	5.4	6.9	5.1	5.0
FILM SYSTEM	MEAN VALUE	118.1	129.0	109.7	100.5
	STANDARD DEVIATION	5.6	7.1	5.1	5.9
NUMBER OF LANDINGS		56	88	88	38

TABLE 3

NAALDAS/70MM FILM COMPARISON

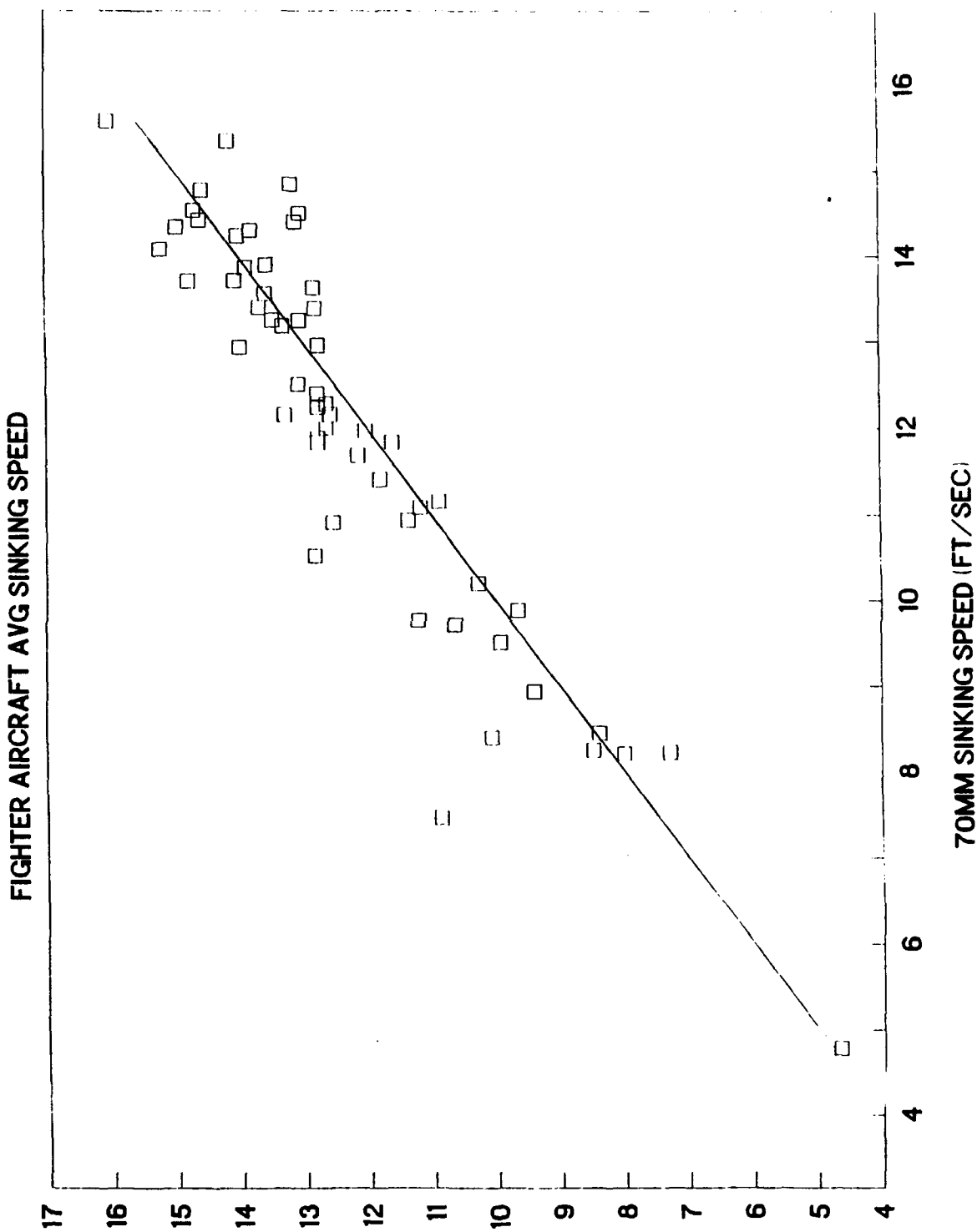


FIGURE 5

NAALDAS/70MM FILM COMPARISON

FIGHTER/ATTACK AIRCRAFT AVG SINK SPEED

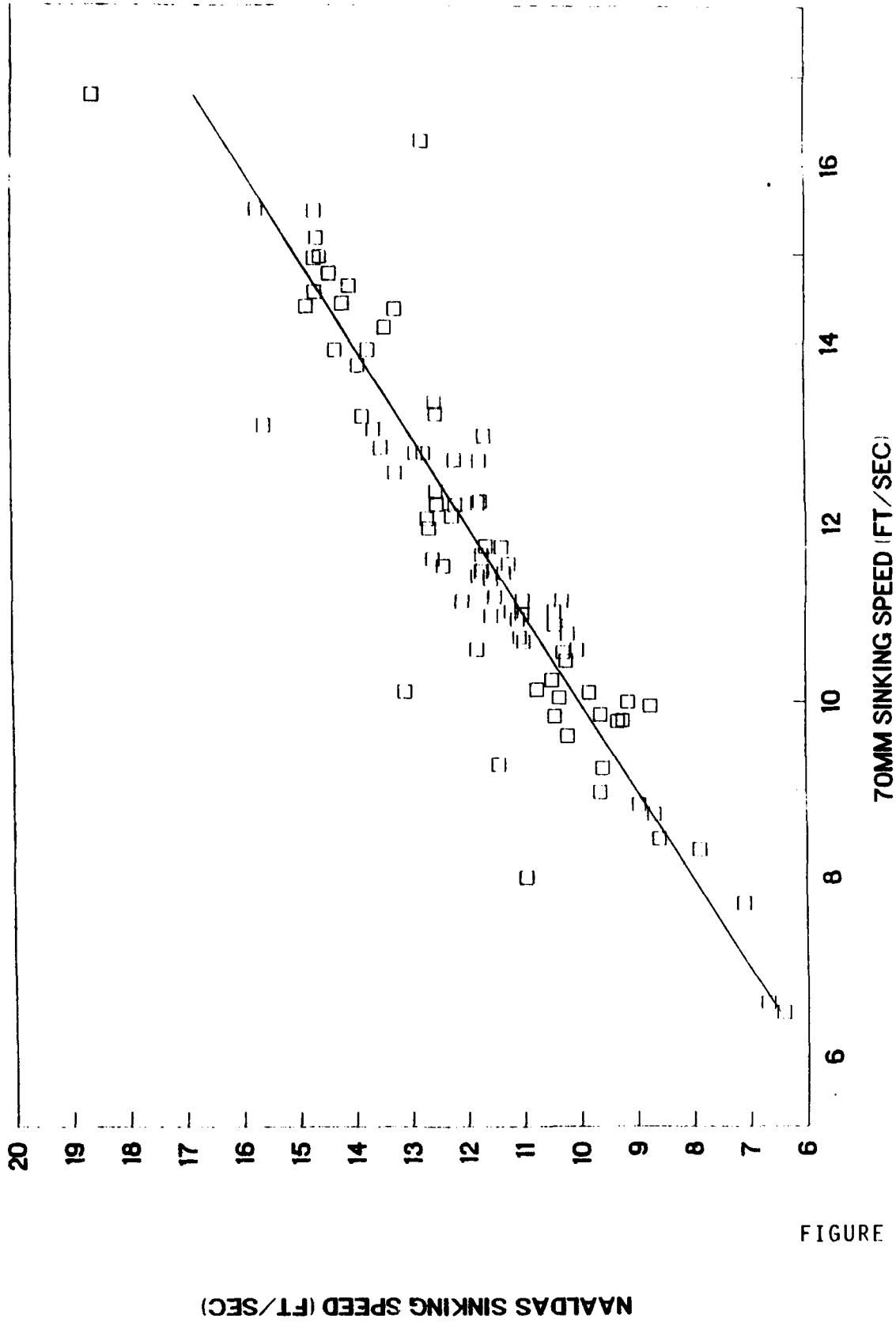


FIGURE 6

NAALDAS/70MM FILM COMPARISON

ATTACK AIRCRAFT AVG SINKING SPEED

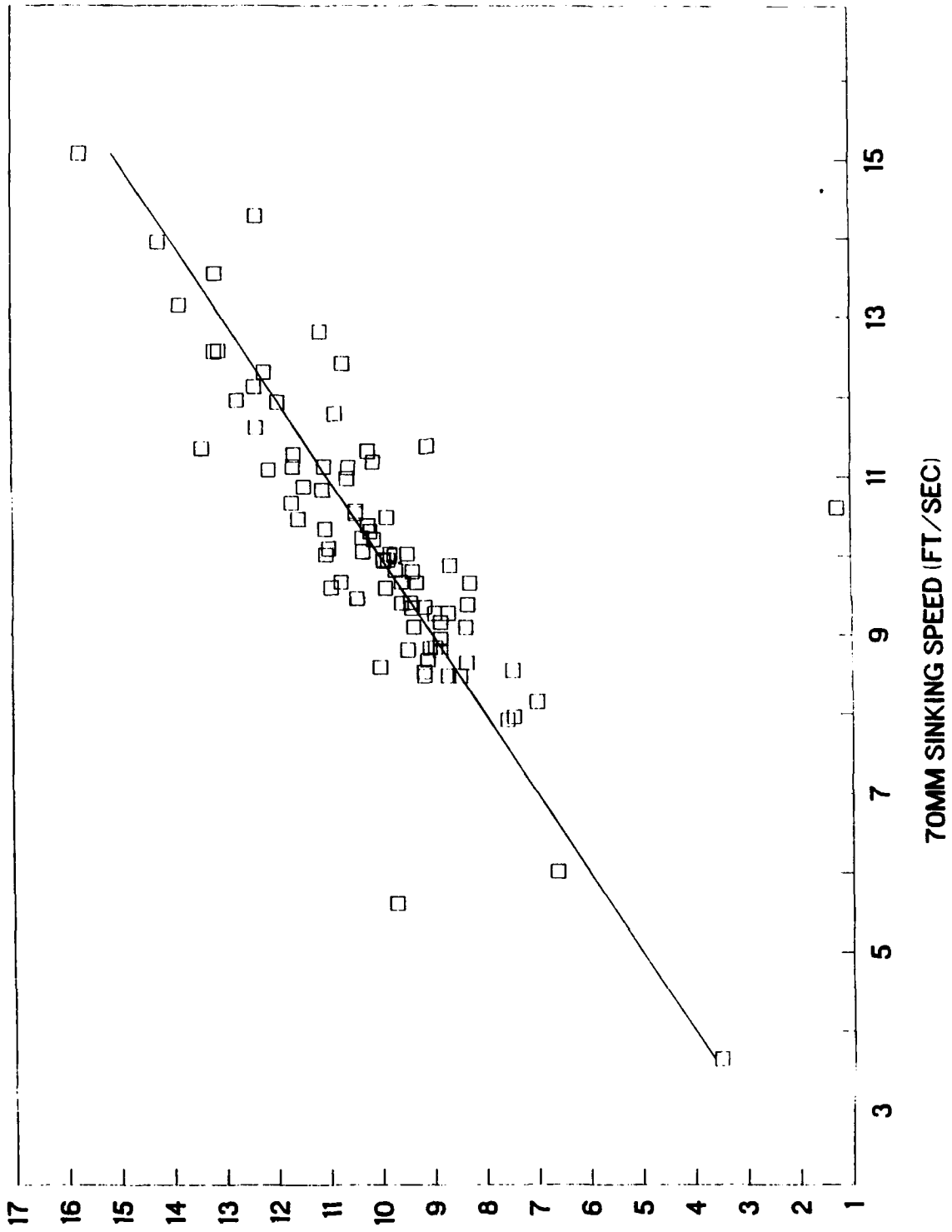


FIGURE 7

NAALDAS SINKING SPEED (FT/SEC)

NAALDAS/70MM FILM COMPARISON

ASW AIRCRAFT AVG MN WHEEL SINKING SPEED

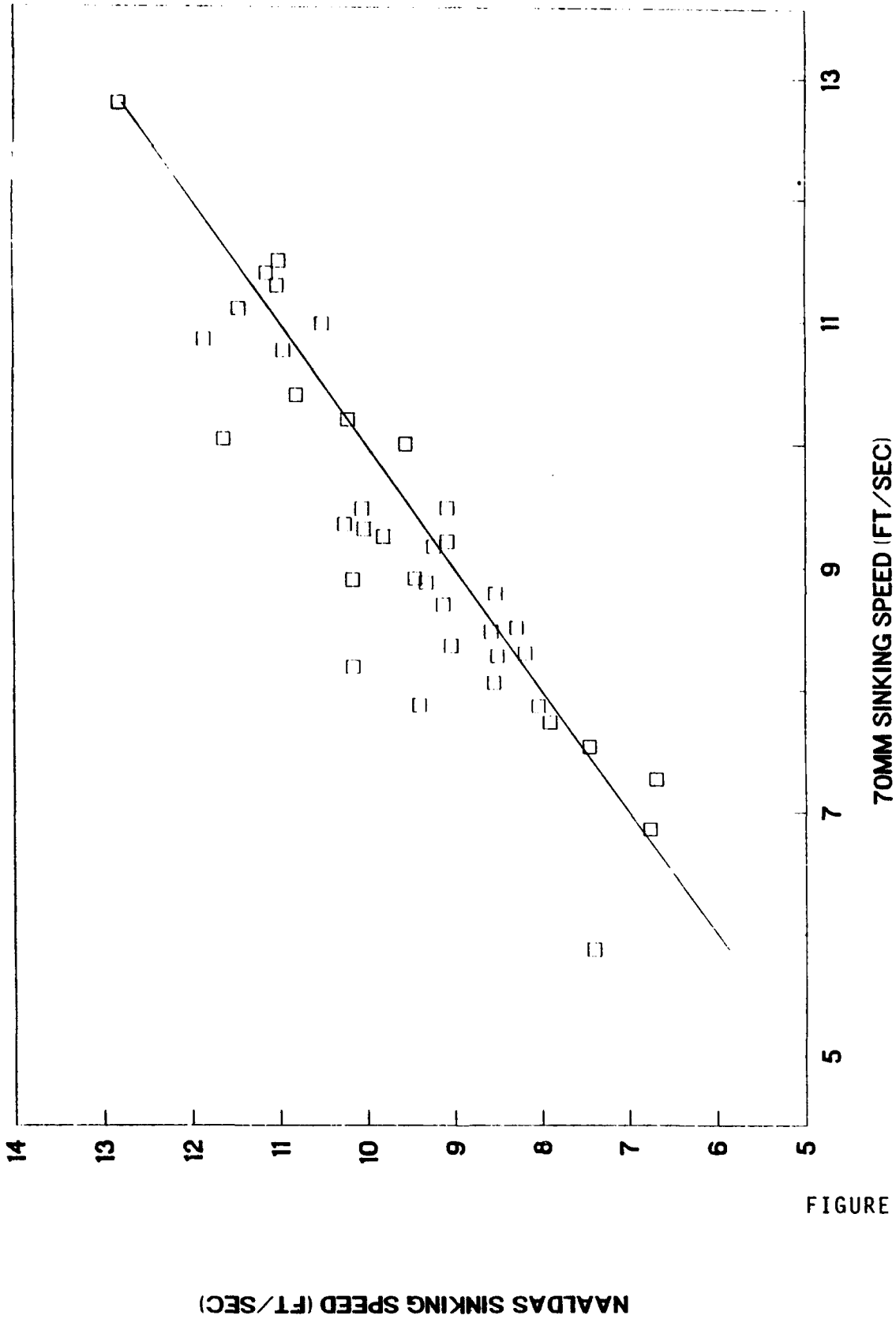


FIGURE 8

NAALDAS/70MM FILM COMPARISON

FIGHTER AIRCRAFT ENGAGING SPEED

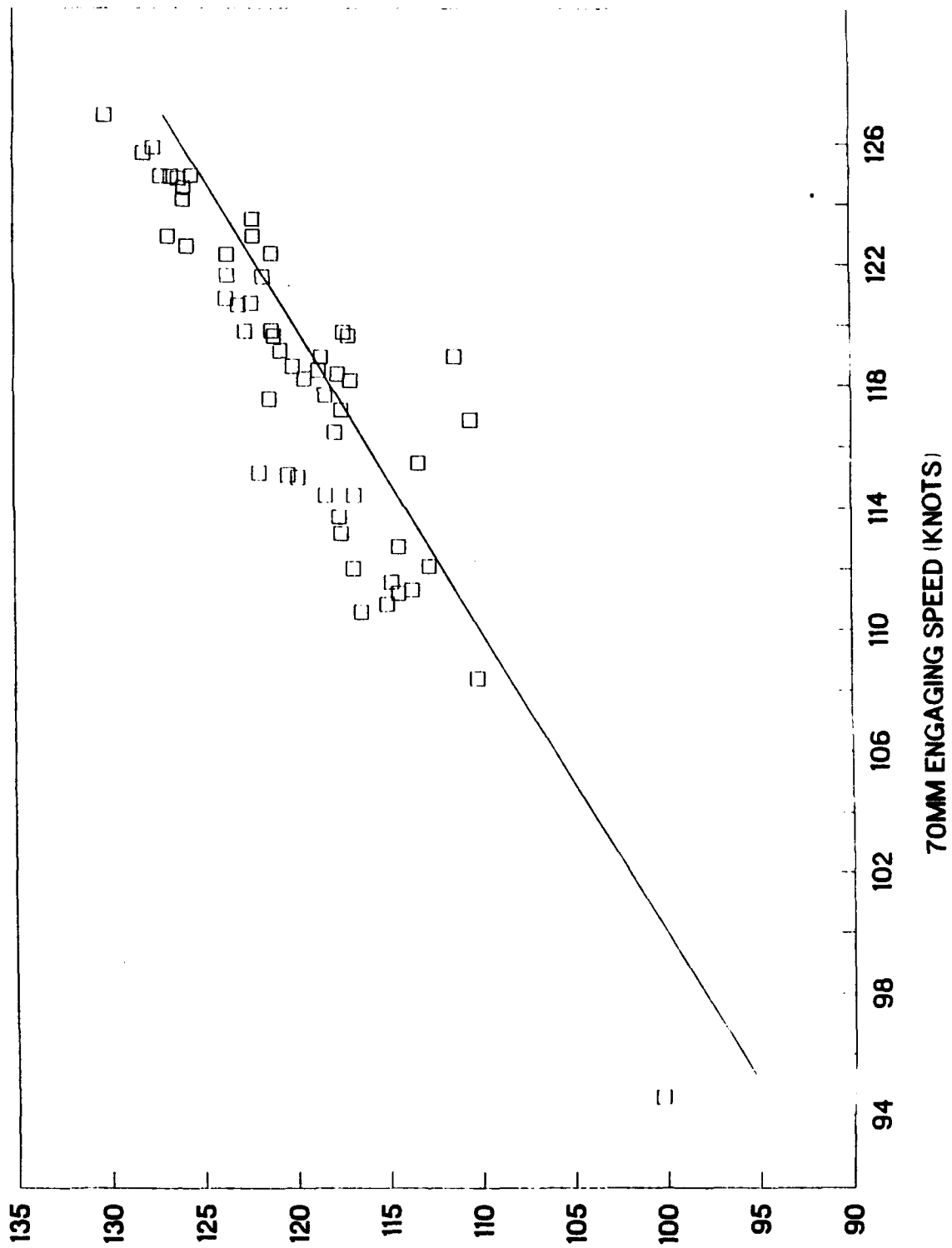


FIGURE 9

NAALDAS/70MM FILM COMPARISON

FIGHTER/ATTACK AIRCRAFT ENGAGING SPEED

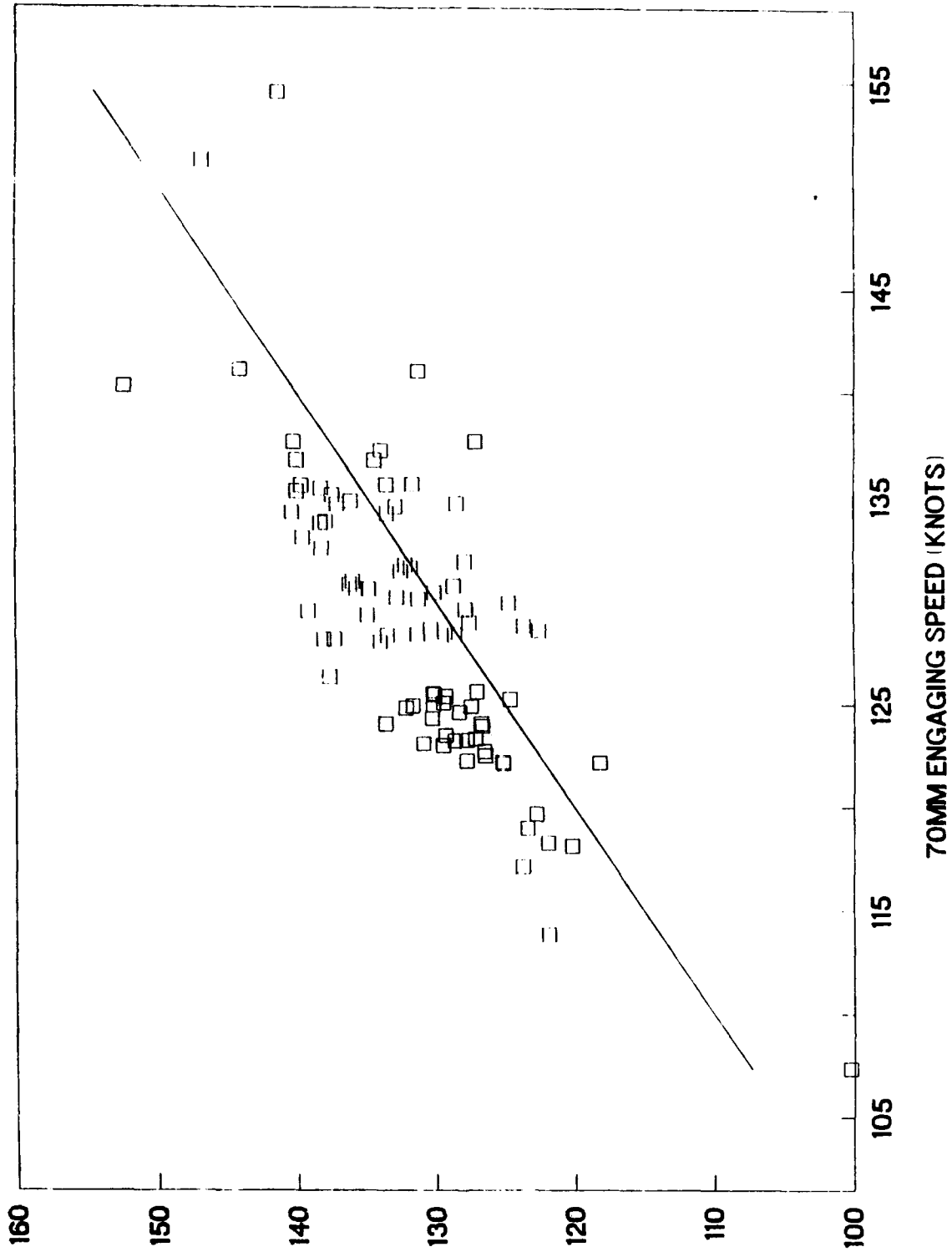
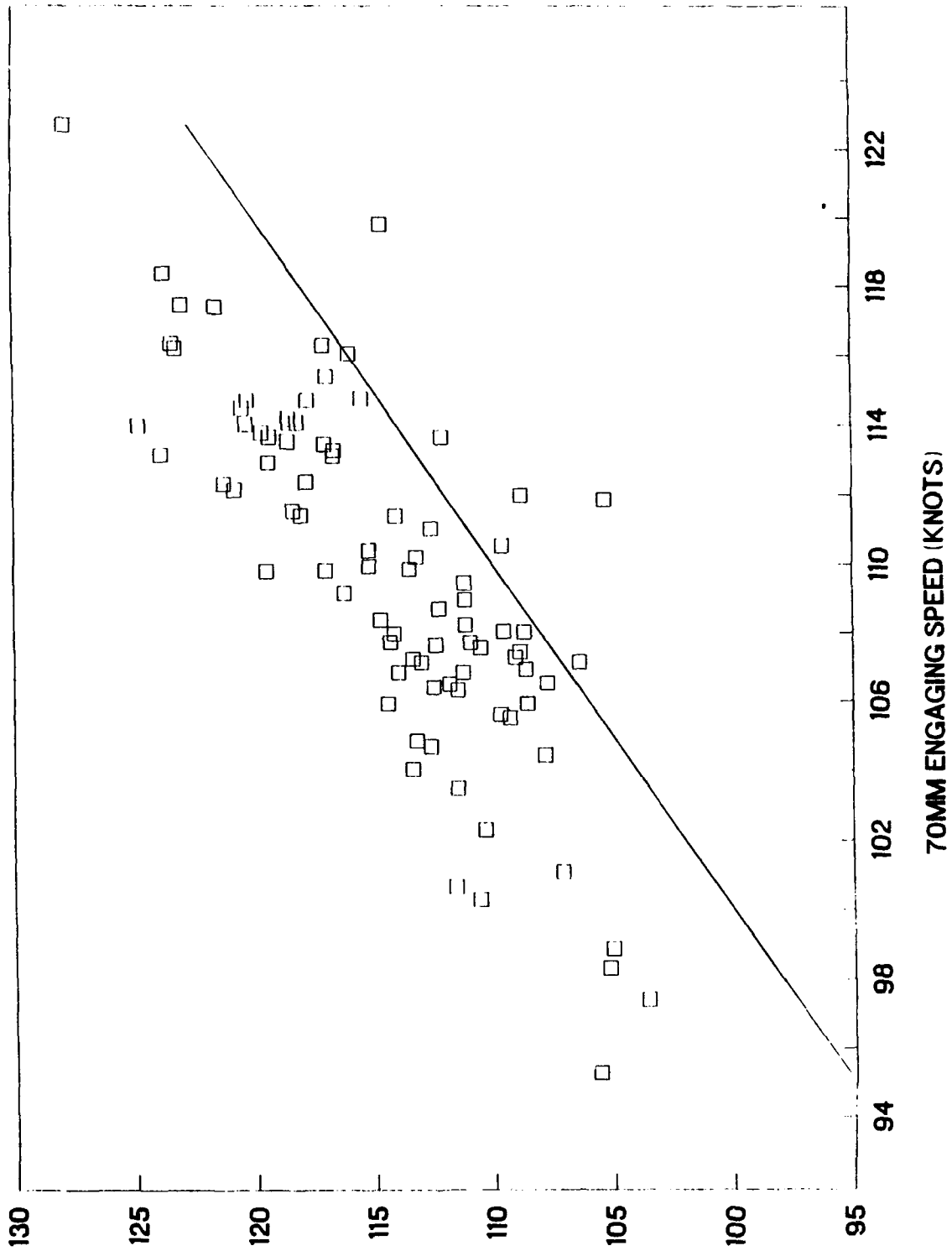


FIGURE 10

NAALDAS ENGAGING SPEED (KNOTS)

NAALDAS/70MM FILM COMPARISON

ATTACK AIRCRAFT ENGAGING SPEED



NAALDAS ENGAGING SPEED (KNOTS)

FIGURE 11

NAALDAS/70MM FILM COMPARISON

ASW AIRCRAFT ENGAGING SPEED

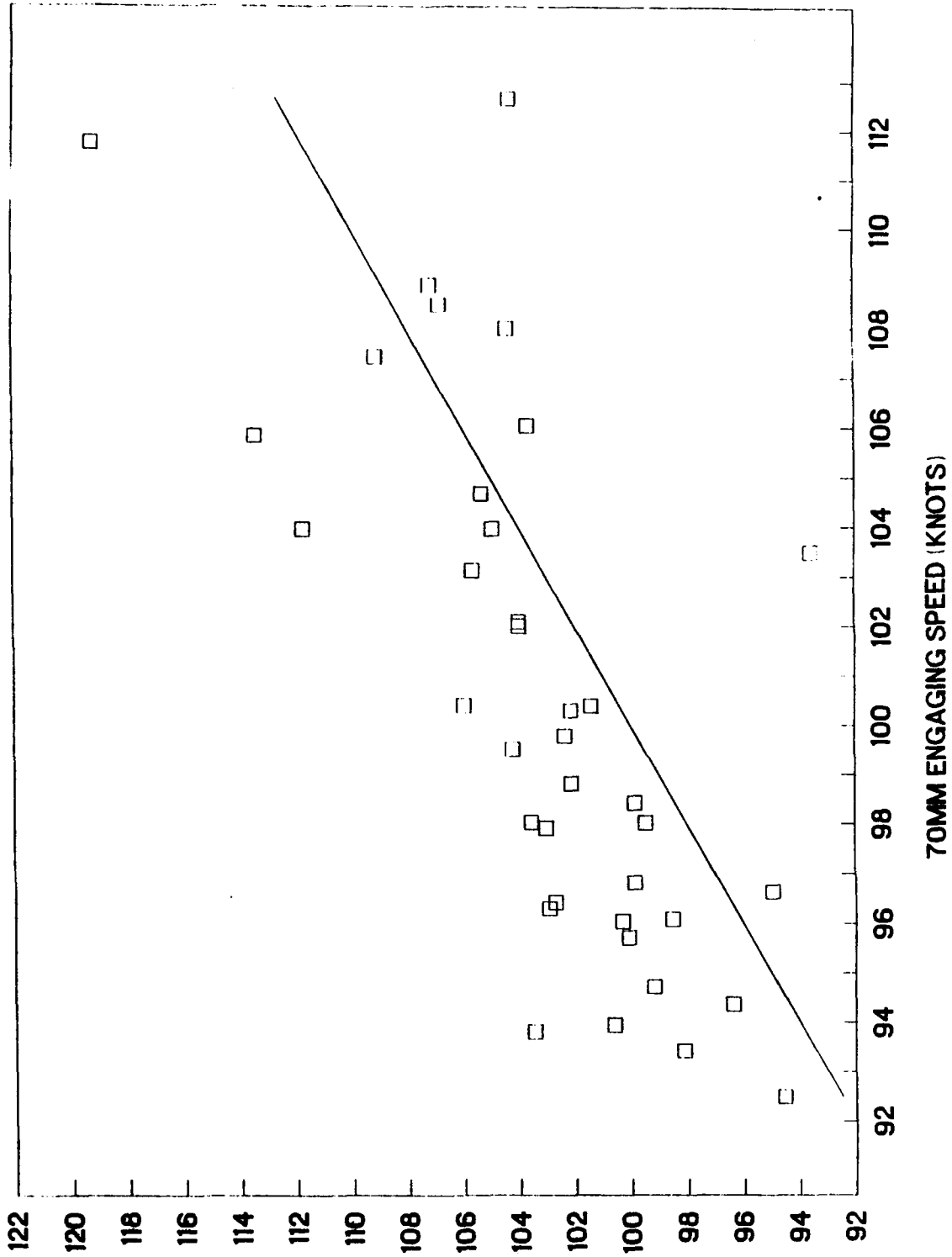


FIGURE 12

NAALDAS ENGAGING SPEED (KNOTS)

**STRUCTURAL UPGRADE OF THE F-16C/D BLOCK 40
AND RESULTS OF THE LOADS FLIGHT TEST**

Presented at

The 1993 Structural Integrity Program Conference

30 November - 2 December 1993

Presented by

Lt David Mack, USAF
F-16 Structural Loads Engineer

Structural Upgrade of the F-16C/D Block 40 and Results of the Loads Flight Test

Briefing Overview

Introduction

Structural Changes

Loads Flight Test

Further Analysis

Conclusion

Structural Upgrade of the F-16C/D Block 40 and Results of the Loads Flight Test

Briefing Overview

Introduction

Structural Changes

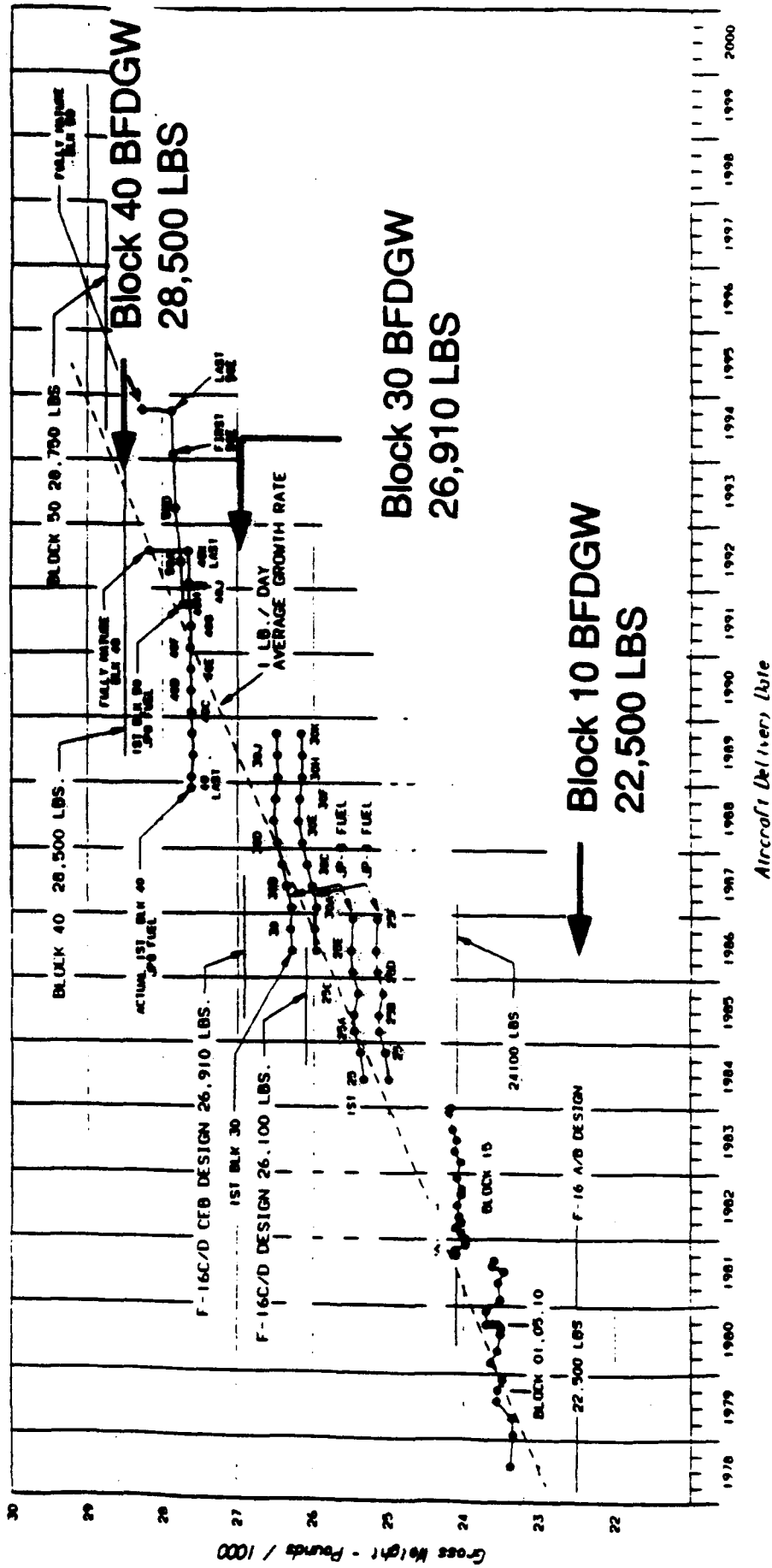
Loads Flight Test

Further Analysis

Conclusion

Structural Changes

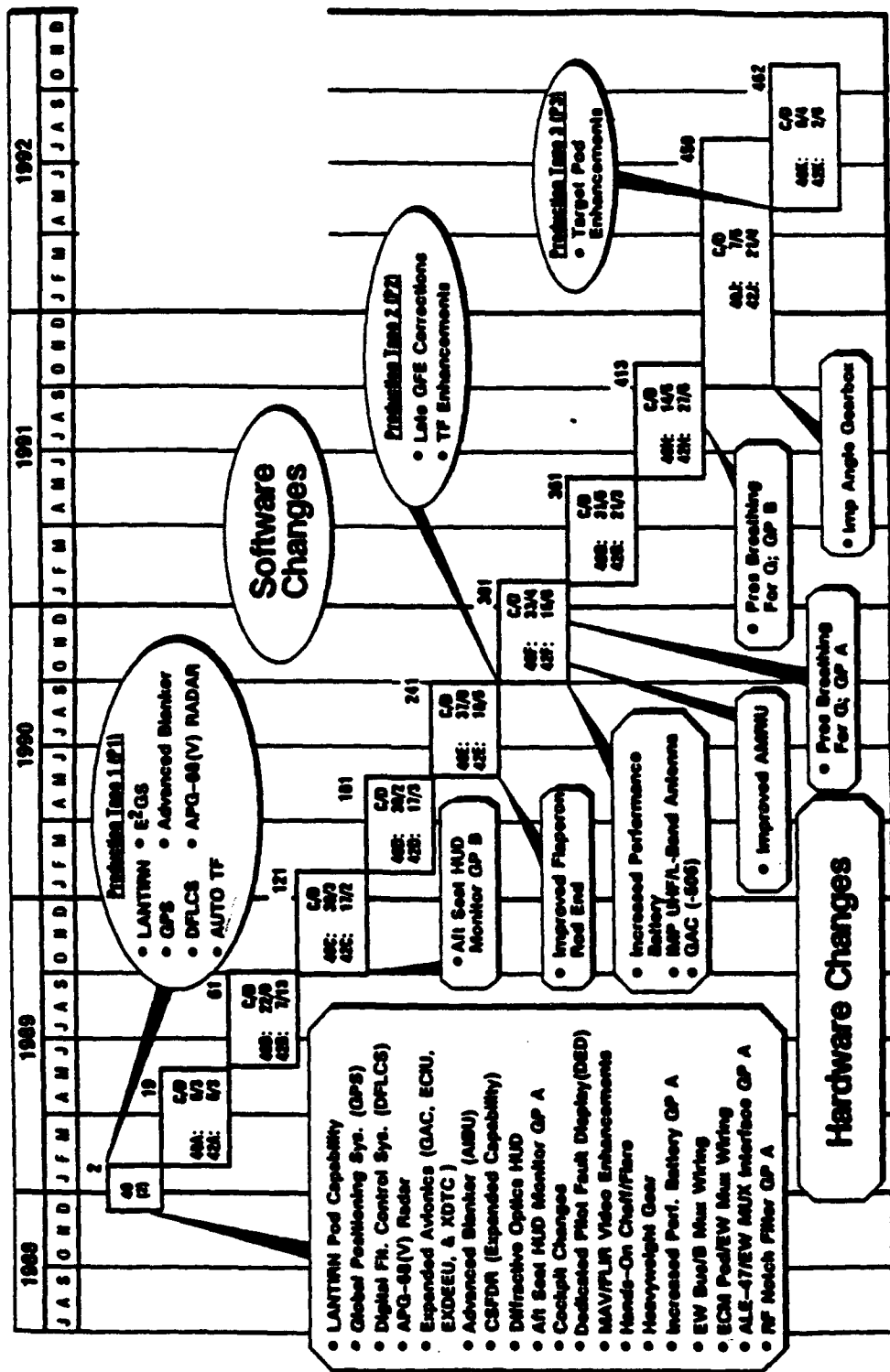
F-16 Weight Growth and Basic Flight Design Gross Weight



Source: Mass Properties Group, 20 October 1992

Structural Changes

USAF F-16 C/D Configuration Plan Block 40



Source: ASIP Master Plan, 16PP388, Vol I, Rev E

Structural Changes

Changes to design criteria for Bik 40

Item	C/D MODELS		
	A/B MODEL	Block 30	Block 40
Basic Flight Design Gross Weight	22, 500 lbs.	26, 910 lbs.	28, 500 lbs.
Max. Design Gross Weight	35, 400 lbs.	37, 500 lbs.	42, 300 lbs.
Landplane Landing Design Gross Weight	19, 500 lbs.	19, 500 lbs.	31, 000 lbs.
Max. Landing Design Gross Weight	27, 500 lbs.	27, 500 lbs.	42, 300 lbs.
8000 - hr Service Life	REQUIREMENT	GOAL	REQUIREMENT

Structural Changes

Reason for Block 40 structural upgrade changes

-To meet 9g Static Strength requirement

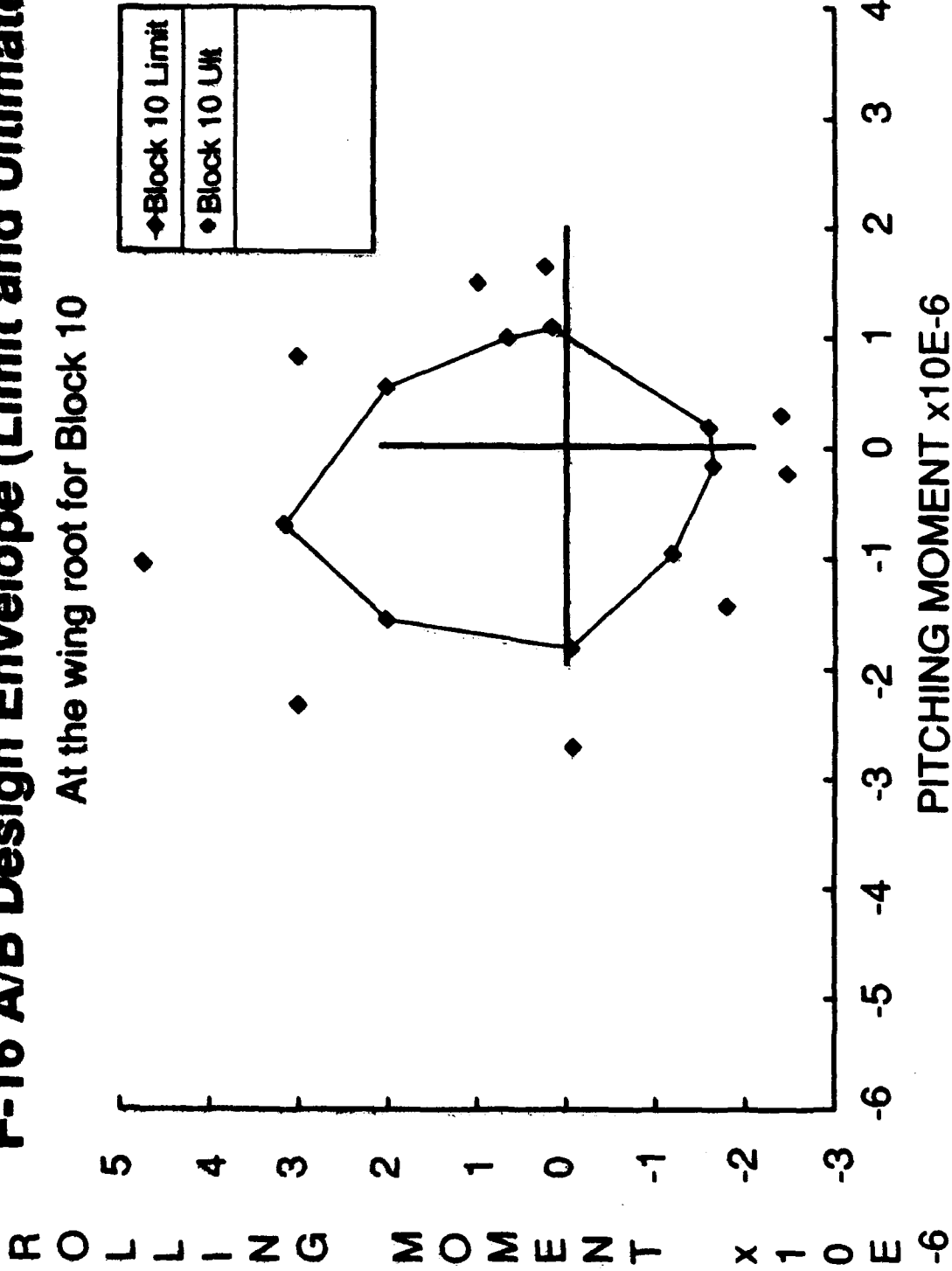
-To meet DADT requirements

due to significant weight growth

Structural Changes

F-16 A/B Design Envelope (Limit and Ultimate)

At the wing root for Block 10

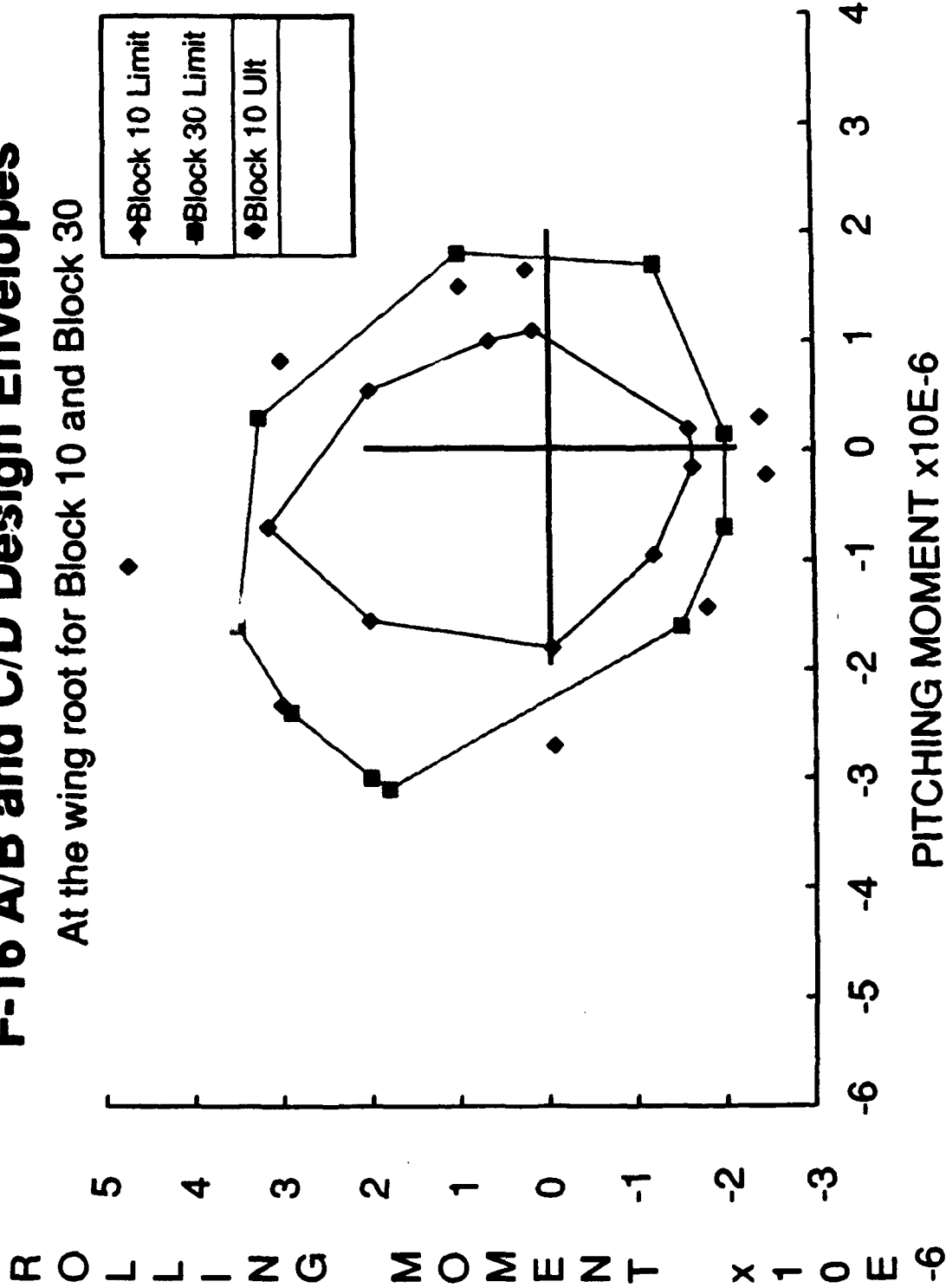


Source: F-16 A/B Strength Summary Report (16PR407 Rev B)

Structural Changes

F-16 A/B and C/D Design Envelopes

At the wing root for Block 10 and Block 30



PITCHING MOMENT x10E-6

Source: F-16 C/D Structural Loads Analysis (16PR3115)

Structural Changes

Changes to the major structural components from Block 30

-WING

-CENTER FUSELAGE

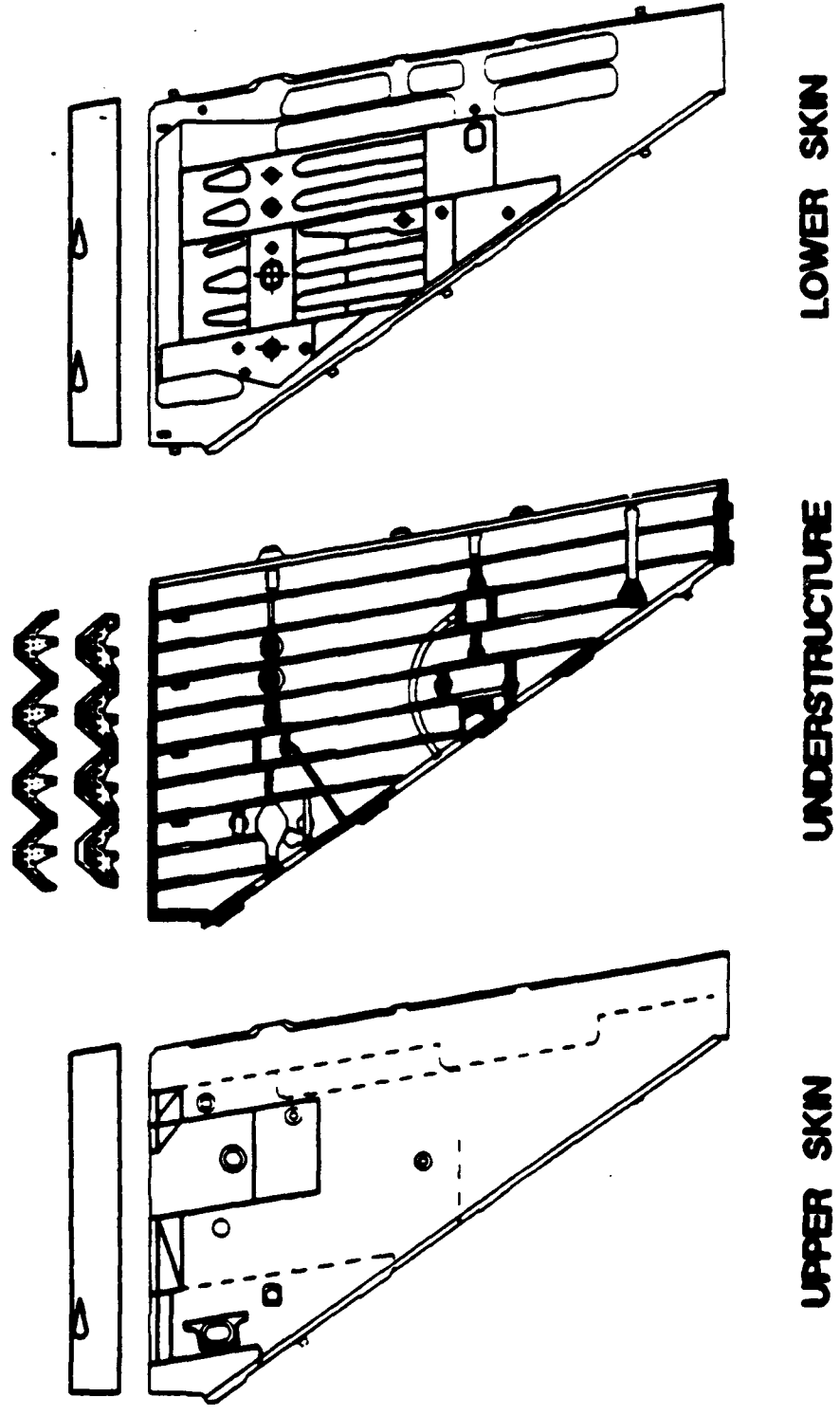
-AFT FUSELAGE

-VERTICAL TAIL

Landing Gear, LEF, Horizontal Tail, and Ventral Fin were also changed but are not pertinent to this briefing.

Structural Changes

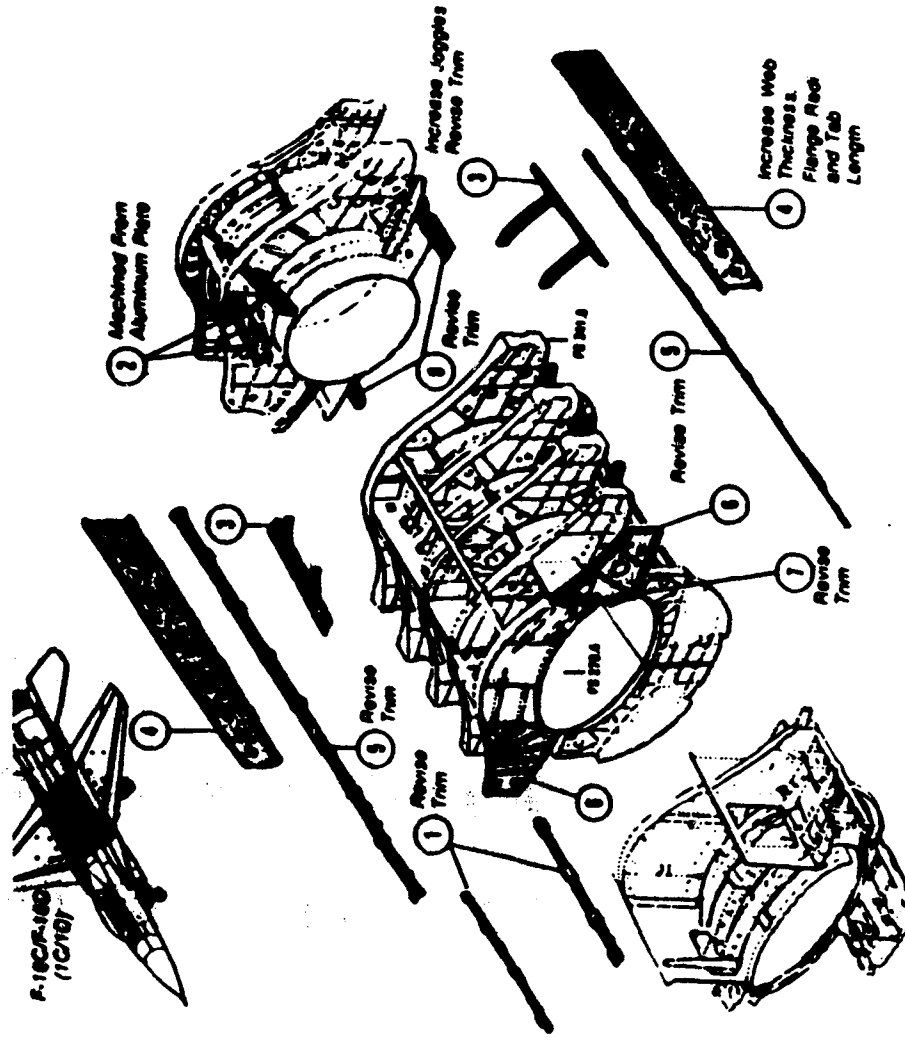
Block 40 wing changes



Source: "Block 40 Structural Changes", Briefing by G.D., 1989

Structural Changes

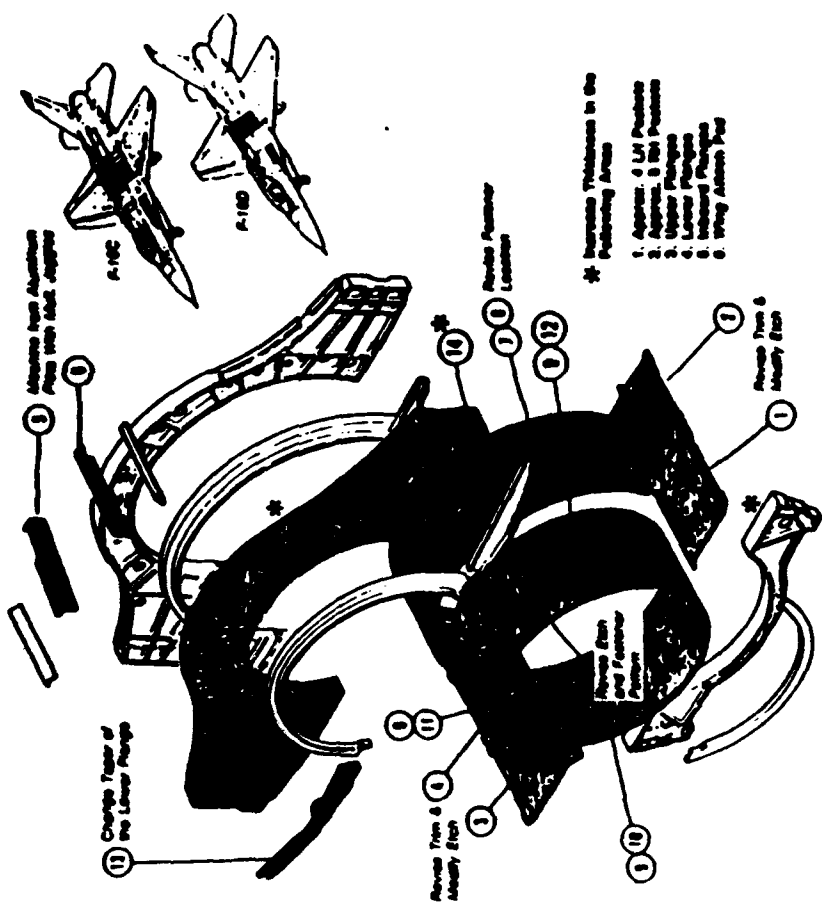
Block 40 center fuselage changes



Source: "ASIP Master Plan", 16PP388, Vol II, Rev A

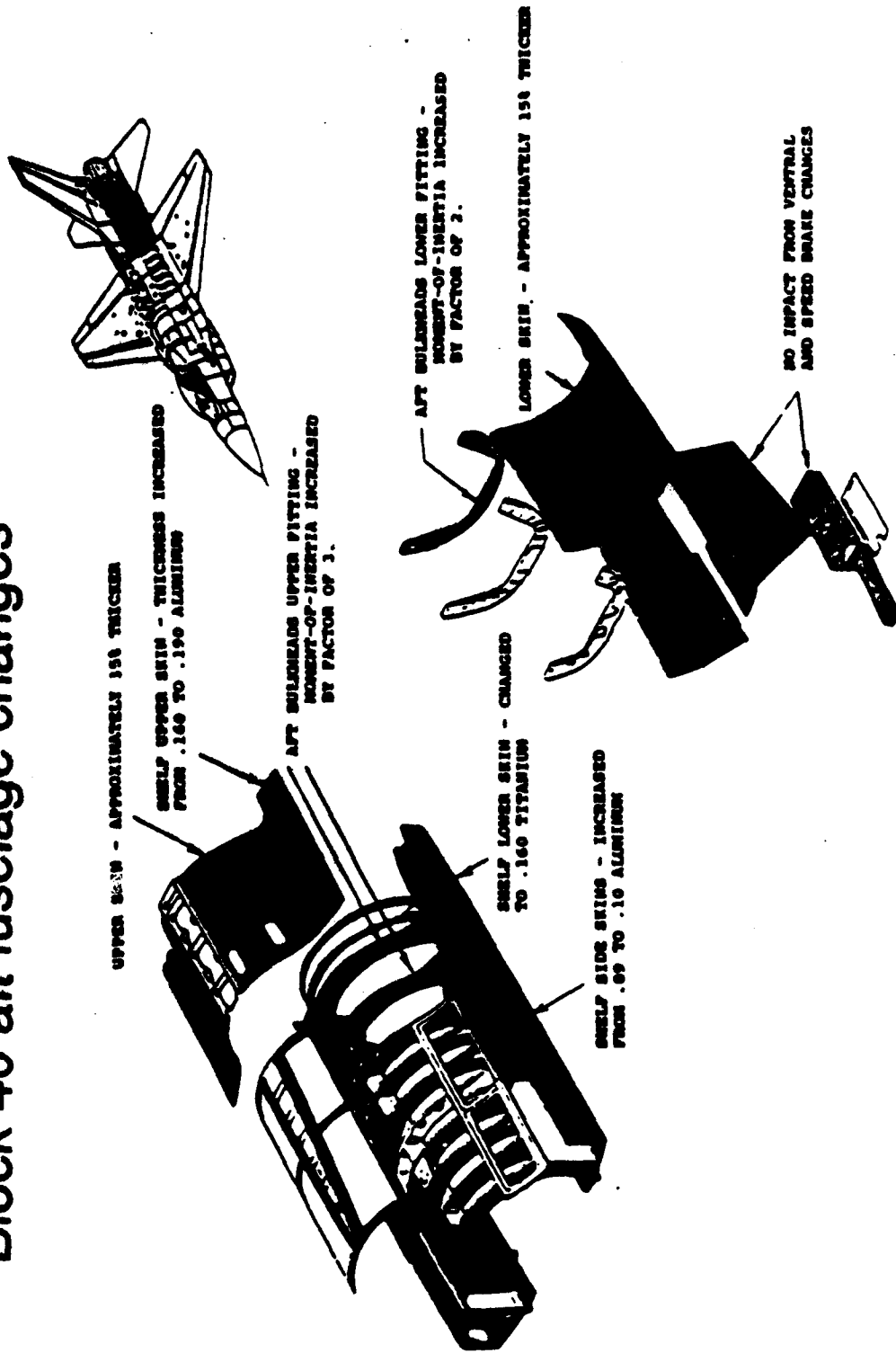
Structural Changes

Block 40 center fuselage changes



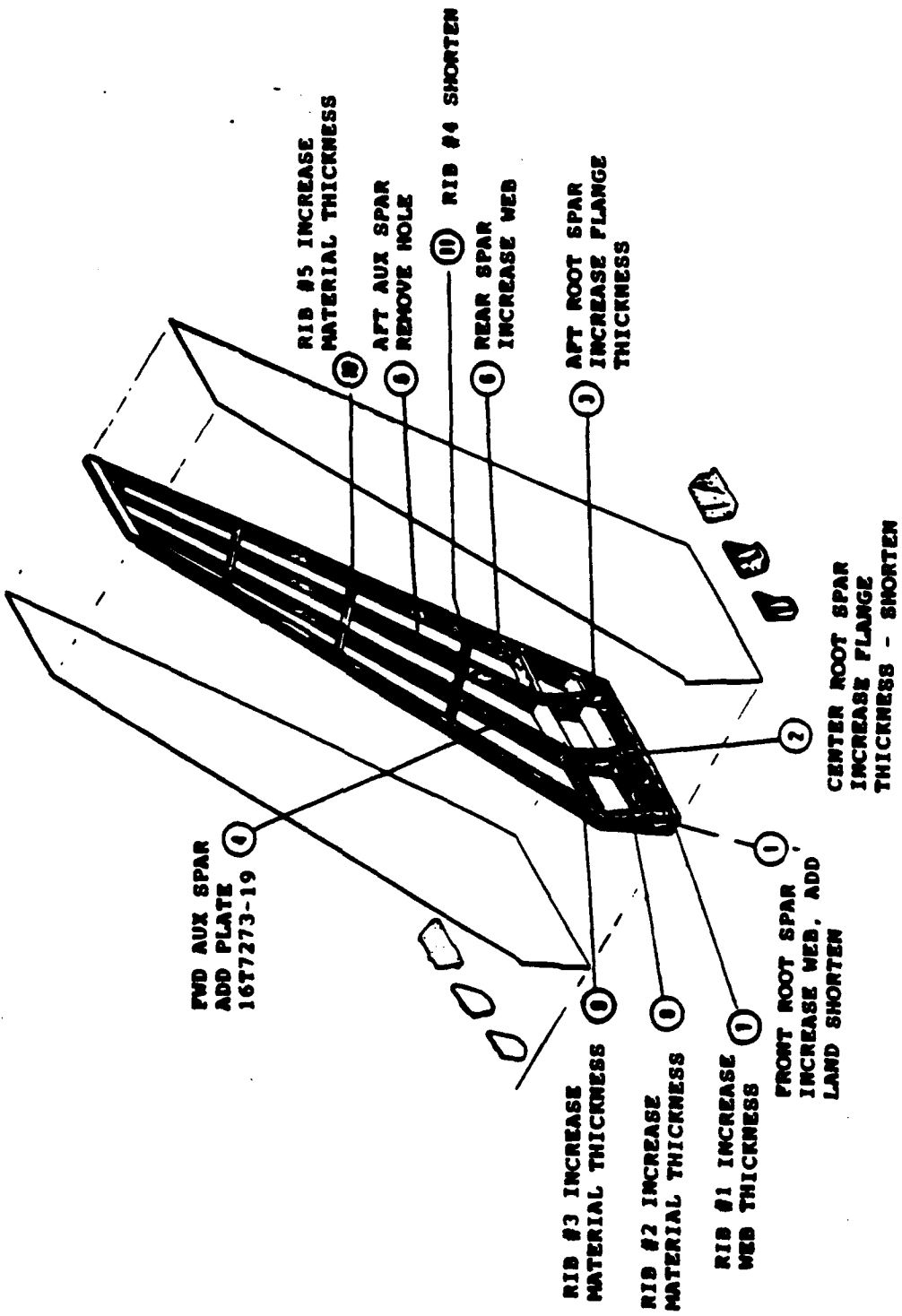
Structural Changes

Block 40 aft fuselage changes



Structural Changes

Block 40 vertical tail changes



Source: "Block 40 Structural Changes", Briefing by G.D., 1989

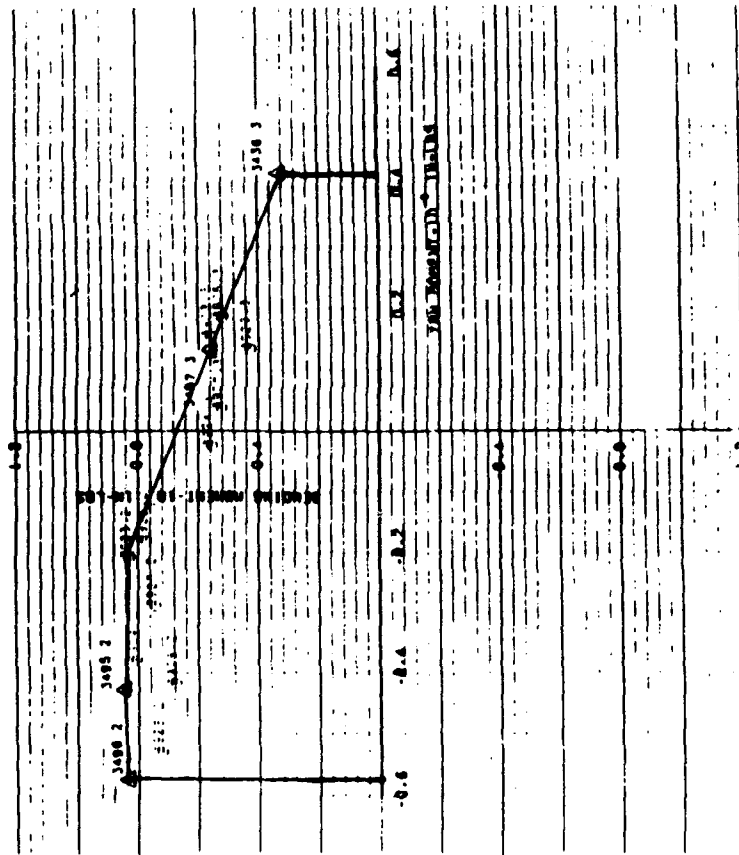
Structural Changes

Critical Conditions - use design loads envelope

- Each point - condition that proved to be analytically design critical for that structure
- Assumed no change in unit aerodynamic loads data base from other blocks.

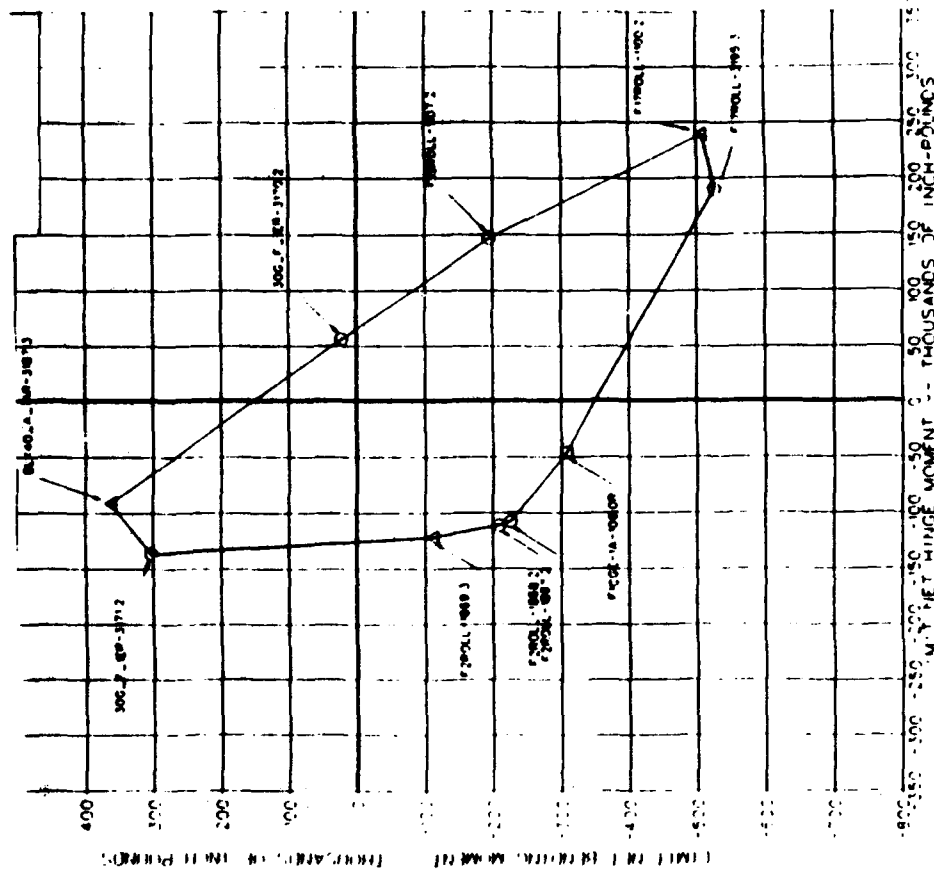
Structural Changes

Design loads envelope - vertical tail Bending Moment vs Yaw Moment



Structural Changes

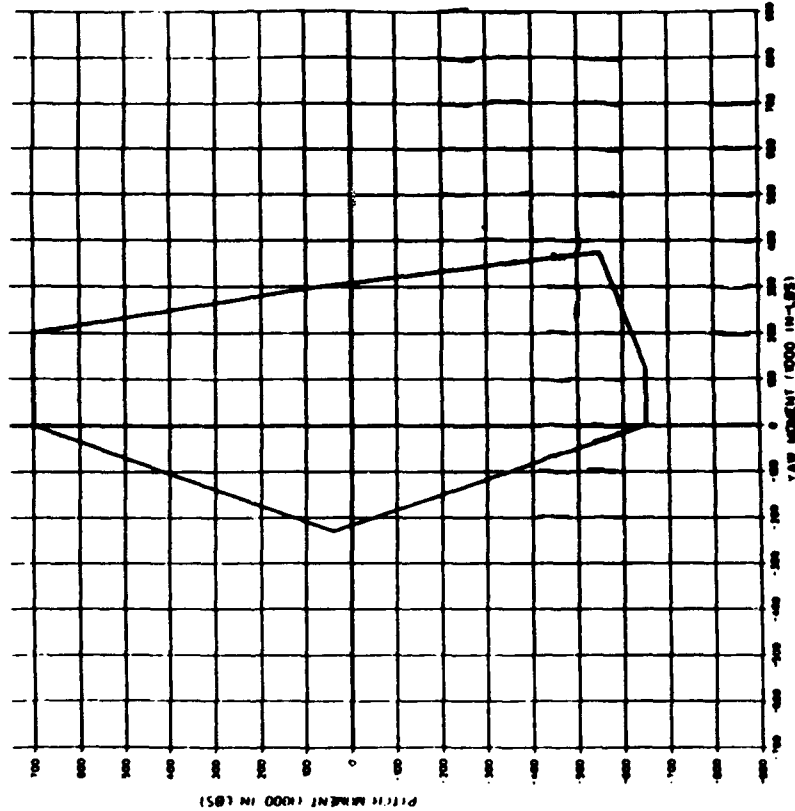
Design loads envelope - horizontal tail - BM vs HM



Source: "Block 40 Structural Design Loads", 16PR6658 Rev A

Structural Changes

Calculated limit strength envelope - 370 gallon tank wing hardpoint Pitch Moment vs Yaw Moment



Structural Upgrade of the F-16C/D Block 40 and Results of the Loads Flight Test

Briefing Overview

Introduction

Structural Changes

Loads Flight Test

Further Analysis

Conclusion

Loads Flight test

In General - I.A.W. MIL-A-8871

-Flight and Ground Operations Demonstration

- Demo points were planned and executed in a build up fashion**
 - Demo points based on design conditions - 100%**
- Instrumentation**
- Strain gauge method**
 - Calibrated and Validated**

Loads Flight test

Test objectives and rationale for test

- To evaluate analytical loads predictions**
- To demonstrate critical design loads for the F-16 C/D Block 40**
- Success criteria - when the data is obtained to satisfy the objective**

Loads Flight test

Test points for Block 40 certification

Loading type	Number of different configurations	
	considered	tested
Air-to-Air	33	9
Air-to-Ground	75	5
Total	108	14

Loads Flight test

Test point maneuvers

-rolls

--elevated G

--negative G

-wind up turns

-push overs

-abrupt pitch and check

-rudder maneuvers -steady sideslip with

--abrupt release

--rudder reversal

Loads Flight test

Preflight predictions

-Used to

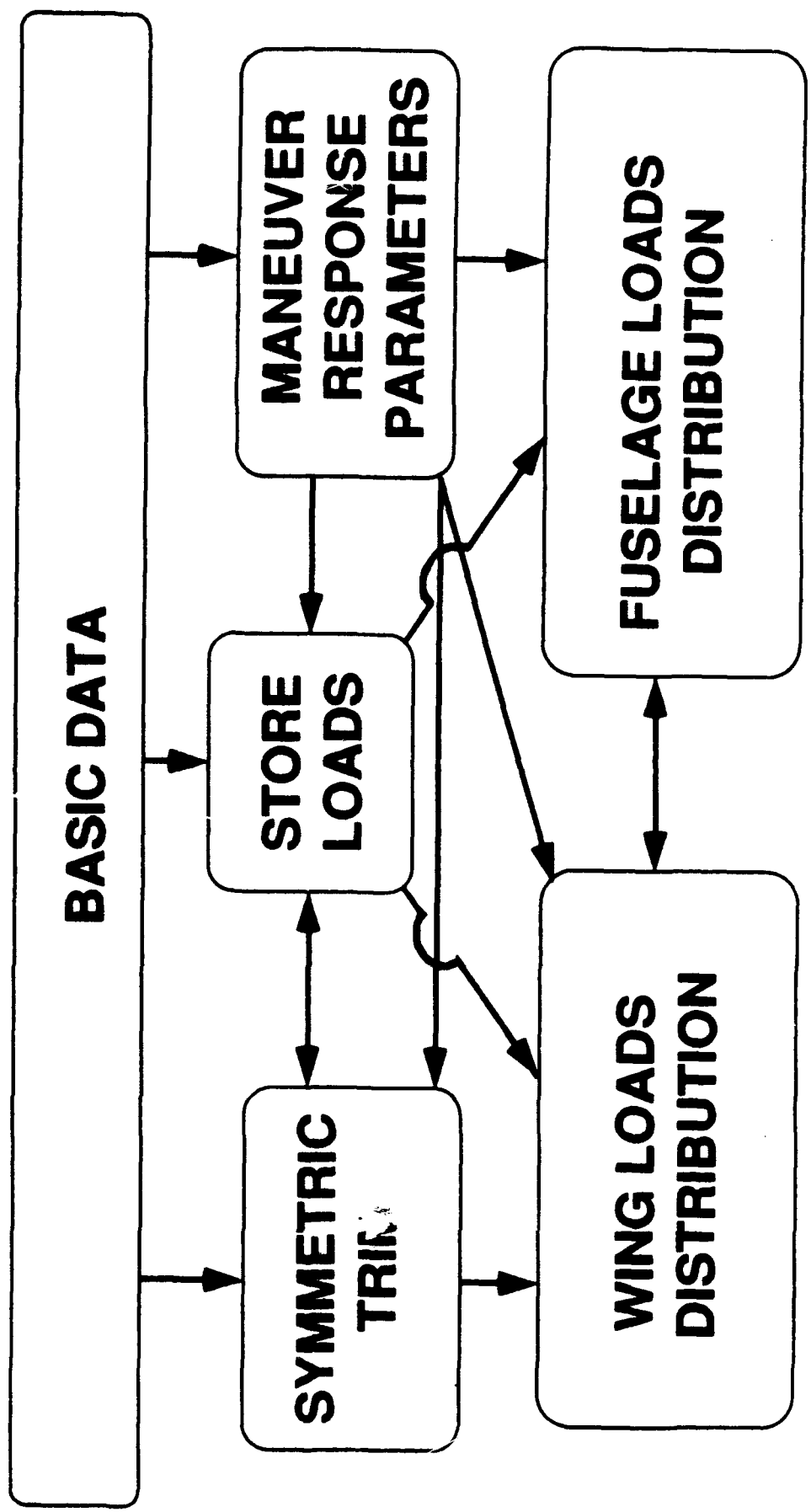
--Validate Analysis

--Perform safety review

-Brief description of procedure for predicting loads

Loads Flight test

Description of Loads Prediction Procedure



Loads Flight test

Unexpected results

-Vertical Tail

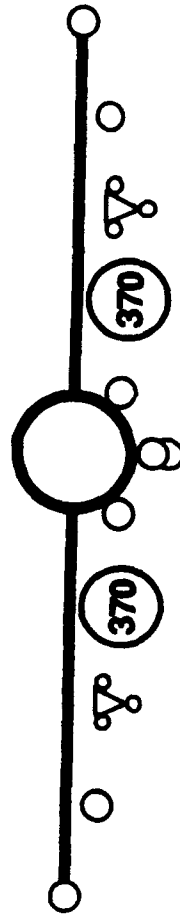
-Horizontal Tail

-370 Gallon Fuel Tank Pylon

Loads Flight test

Results - Vertical Tail

- Measured load - BM 105% Design Limit Load
- Conditions - Steady Slideslip with Abrupt Release and Rudder Reversal
- Configuration - 42,015 lbs



1 2 3 4 5L 5R 6 7 8 9

Loads Flight test

Results - Horizontal Tail

- Measured load - BM 108% Design Limit Load
- Condition - 360 Deg Overcheck Roll
- Configuration - 27,683 lbs

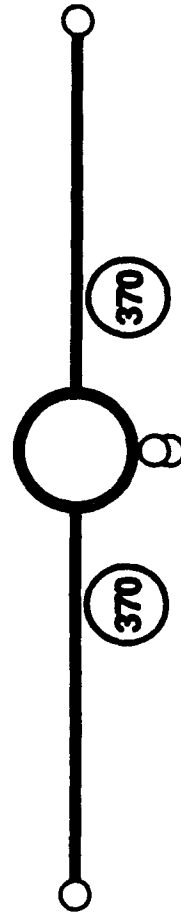


- 1 2 3 4 5L 5 5R 6 7 8 9

Loads Flight test

Results - 370 Gallon Fuel Tank Pylon

- Measured load - YM 106% Design Limit Load
- Condition - 360 Deg Check to Neutral Roll
- Configuration - 34,377 lbs



1 2 3 4 5L 5R 6 7 8 9

Structural Upgrade of the F-16C/D Block 40 and Results of the Loads Flight Test

Briefing Overview

Introduction

Structural Changes

Loads Flight Test

Further Analysis

Conclusion

Further Analysis

Explanations for unexpected results

Vertical tail

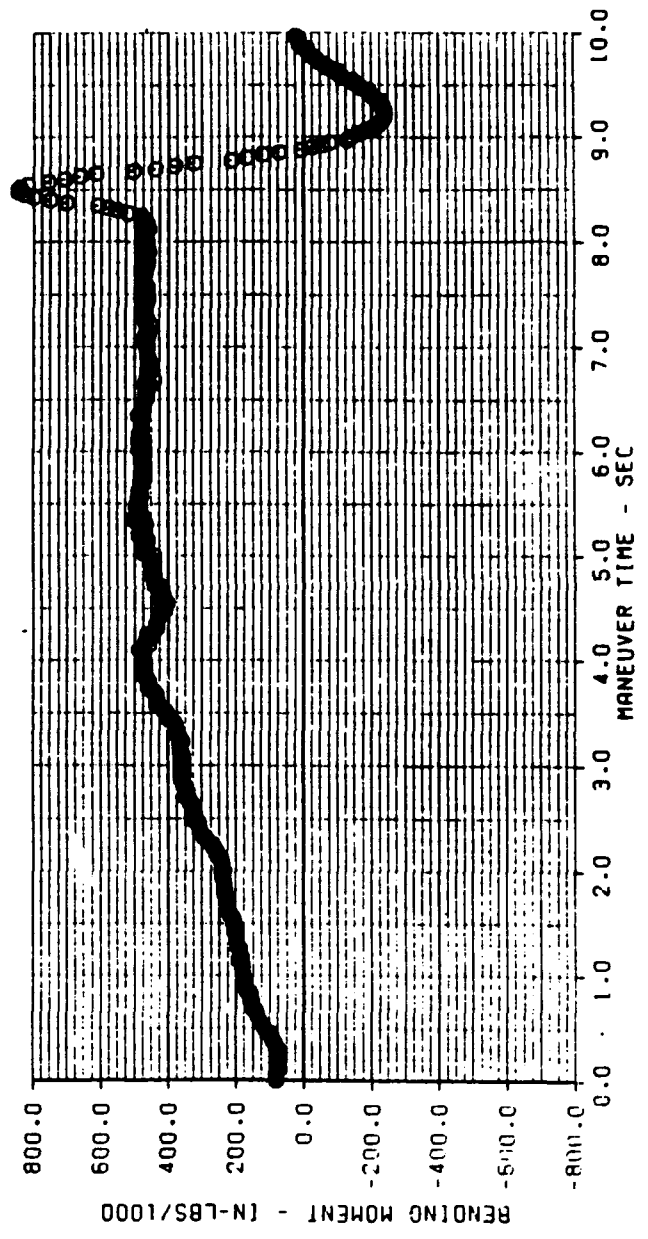
- The cause is a larger than predicted aerodynamic destabilizing effect of certain external stores
- Bending moment increase of 100% of steady value
- Destabilizing effect has been seen on other flight tests
- Destabilizing effect is more significant than inertial effects in accounting for the bending moment peak

Further Analysis

Block 40 measured data - .8M/2.5K 100% SS/AR

300 gallon tank - 370 gallon tank - LANTIRN

Vertical Tail - Bending Moment vs Time

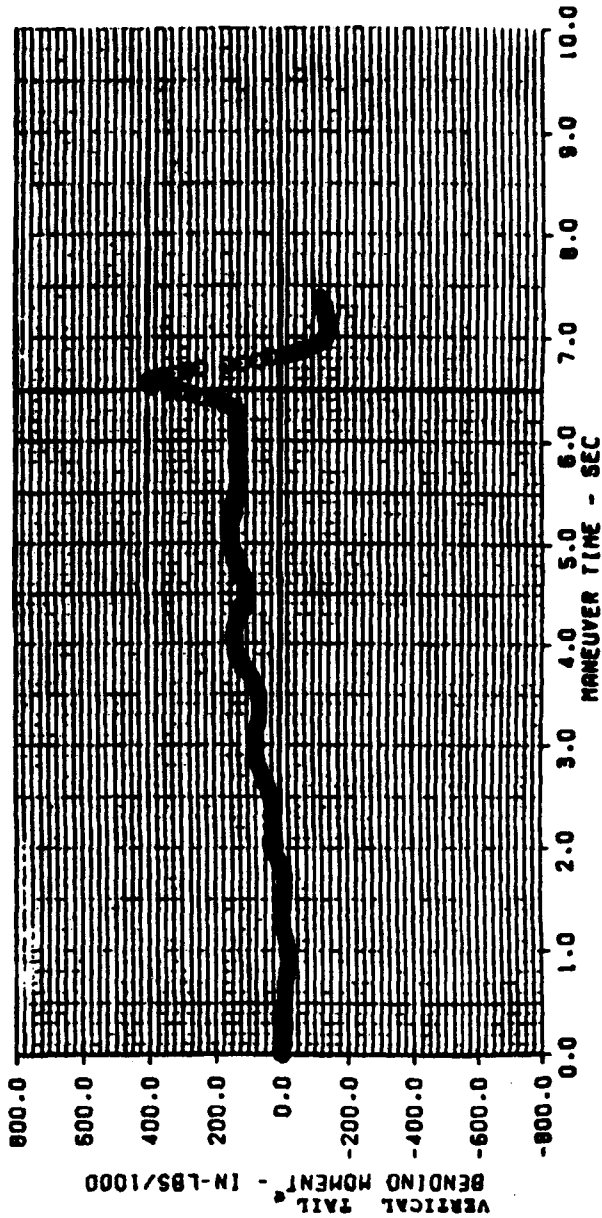


Further Analysis

Block 40 measured data - .8M/10K 100% SS/AR

Wing tip missiles

Vertical Tail - Bending Moment vs Time

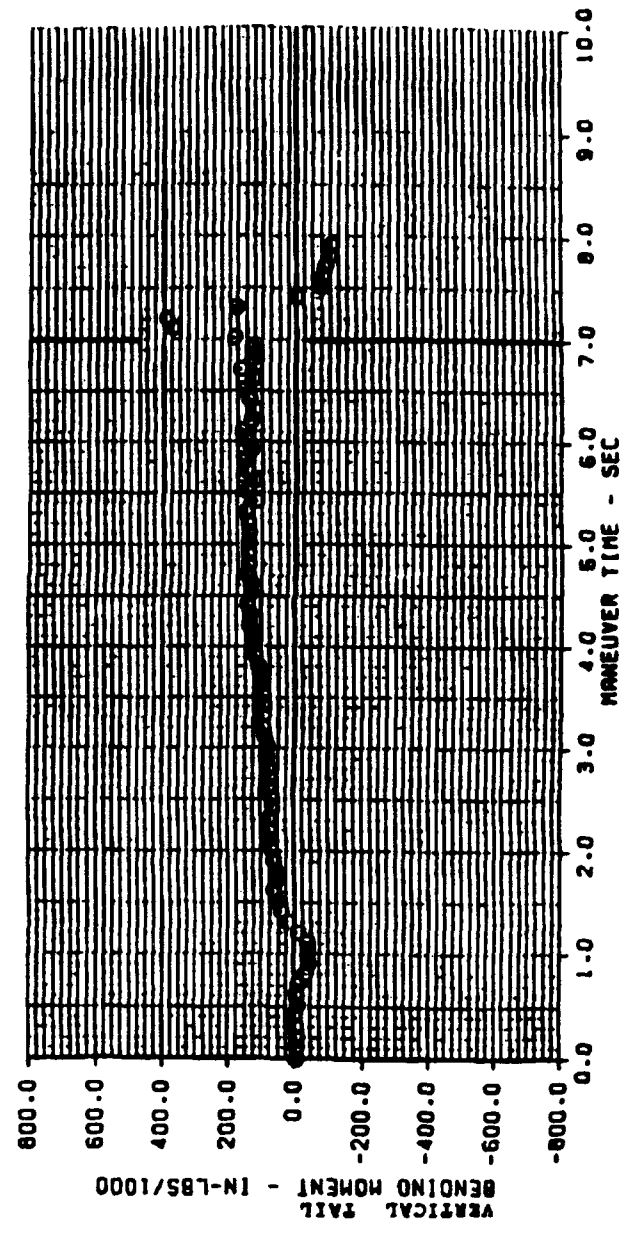


Further Analysis

Block 30 measured data - .8M/10K 100% SS/AR

Wing tip missiles

Vertical Tail - Bending Moment vs Time



Further Analysis

Explanations (continued)

Horizontal tail

- Rolls were not flown per design criteria - overcheck was held longer than specified**
- Holding overcheck rolls lead to roll reversal which significantly increases horizontal tail loads**
- Overcheck rolls difficult to perform without holding**

Further Analysis

Explanations (continued)

370 gallon fuel tank pylon

- Effect of fuselage mounted centerline store on the fuel tank aerodynamic yawing moment more significant than expected
- The condition that caused this was not flown in past loads tests
- Aerodynamic effect increases with Mach number

Further Analysis

Operational restrictions - do not significantly affect operational capability

Vertical Tail

rudder use restriction - SPO issued a restriction to prohibit rapid rudder release or reversal above 300 knots/0.6 Mach

832

Horizontal Tail

roll reversal restriction - SPO issued a restriction to prohibit abrupt roll reversals

370 Gallon Fuel Tank Pylon

roll rate limit - SPO issued a restriction to limit roll rate to 100 degrees per second when above .95 Mach with a centerline store and wet 370 gallon tanks

Structural Upgrade of the F-16C/D Block 40 and Results of the Loads Flight Test

Briefing Overview

Introduction

Structural Changes

Loads Flight Test

Further Analysis

Conclusion

Conclusion

Analysis

-for Static Strength Loads and

-for Service Loads as well

must be validated by testing

Any questions?

Integration of Smart Structures Concepts for Improved Structural Integrity Monitoring of the T-38 Aircraft.¹

C. B. Van Way, J. N. Kudva, and C. Marantidis

Northrop Corp.

One Northrop Ave. 3852/63

Hawthorne, California 90250

310/332-9639

1.0 Abstract

Smart structures concepts have the potential to improve the capabilities and extend the life of modern aircraft. The two concepts that show the most promise are active/adaptive structures and structural health monitoring systems (SHMS). In the health monitoring arena, advances in sensing systems and data processing hardware provide a means to dramatically improve capabilities in detecting structural damage and monitoring aircraft loads and environment. As further developments are made in smart structures technologies, methods for integration into aircraft fleets must be addressed. Incorporation of a SHMS will have a significant impact on current Air Force and Navy aircraft structural integrity program (ASIP and NASIP, respectively) requirements, and provide considerable savings in inspection and maintenance costs of military fleets.

This paper uses the Northrop T-38 aircraft to illustrate the impact of a SHMS on an existing military aircraft. Health monitoring benefits are addressed in addition to the affect of the system on current ASIP requirements (minimum flaw size, design service lifetime, loads tracking, etc.). Specific details are discussed on areas of ASIP which will be affected by the increased tracking capabilities of the SHMS. A prototype system design is presented with cost and installation data. A cost versus payoff assessment is made to determine the viability of fleet-wide retrofit of such a system.

¹ The work documented in this paper was performed under a government contract to Northrop Corp. entitled "Smart Metallic Structures (SMS)," F33615-92-C-3203. The contract monitors are Mr. Michael Ziegler of the Air Force Wright Laboratories and Dr. James Alper of the Naval Air Warfare Center.

2.0 Introduction

Recent restructuring of military resources has increased the emphasis on enhancing the capabilities of current systems. For modern military aircraft, one such method is improved loads and damage tracking. Current force management methods have proven to be time consuming and inefficient [1]. Some of the current Force Management problems are presented in Figure 1.

Data Capture & Validity Rates Very Low	<ul style="list-style-type: none">• Excessive Handling of Raw Data• ASIP Not Mission Critical• No Standard Methods• Outdated Equipment
Turnaround Time Too Long	<ul style="list-style-type: none">• Too Much Raw Data• No Local Validation/Preprocessing• Mainframe Cost Prohibitive
Data Collected and Not Used	<ul style="list-style-type: none">• System In-Place - No Users• Time Lag Prevents Useful Data
No Feedback of Maintenance Actions	<ul style="list-style-type: none">• IAT/FSMP Not Updated• Need Automated Reporting Method

Figure 1. Summary of Force Management Problem Areas

An automated, on-board SHMS designed to monitor aircraft loads and environment as well as determine structural reliability, would provide significant payoffs in terms of reduced inspections, reduced down time, improved tracking efficiency, and extended service life [2]. Recent advances in sensors, computer processors, and electronics miniaturization have significantly enhanced the potential for development of such a system.

A SHMS tracks the aircraft usage and environment (a detailed study of SHMS components and tracking parameters was performed under the "Smart Structures Concepts Requirements Definition (SSCORE)" program [3]). Individual sensors track strain, acceleration, temperature, corrosive environment, and damage. As currently envisioned, a SHMS will consist of acoustic emission sensors to detect structural damage, standard strain gages and fiber optic gages to monitor strain and temperature, and electro-chemical sensors to detect corrosion.

3.0 ASIP Impact

Incorporation of a SHMS will have significant effect on current ASIP procedures. The SHMS will benefit the Load/Environment Spectra Survey (L/ESS) program by providing improved monitoring of the structure with additional sensors. This will increase the accuracy of recorded loads and aircraft parameter data. Currently, structural loads are derived from measured usage parameters which correspond to known load conditions. More extensive direct monitoring of loads would provide the means for more accurate assessments of structural life. Instrumenting all fleet aircraft with a SHMS will provide improved fleet usage information.

Another significant area of change will be in the Individual Aircraft Tracking (IAT) program. The goal of IAT is to monitor the crack growth at critical structural locations (control points) due to operational loads. Standard methods for aircraft tracking assume an initial production flaw (typically a minimum detectable flaw size of 0.05 in.) at a critical structural location. The aircraft service life is then determined by the time to grow a critical flaw at the control location.

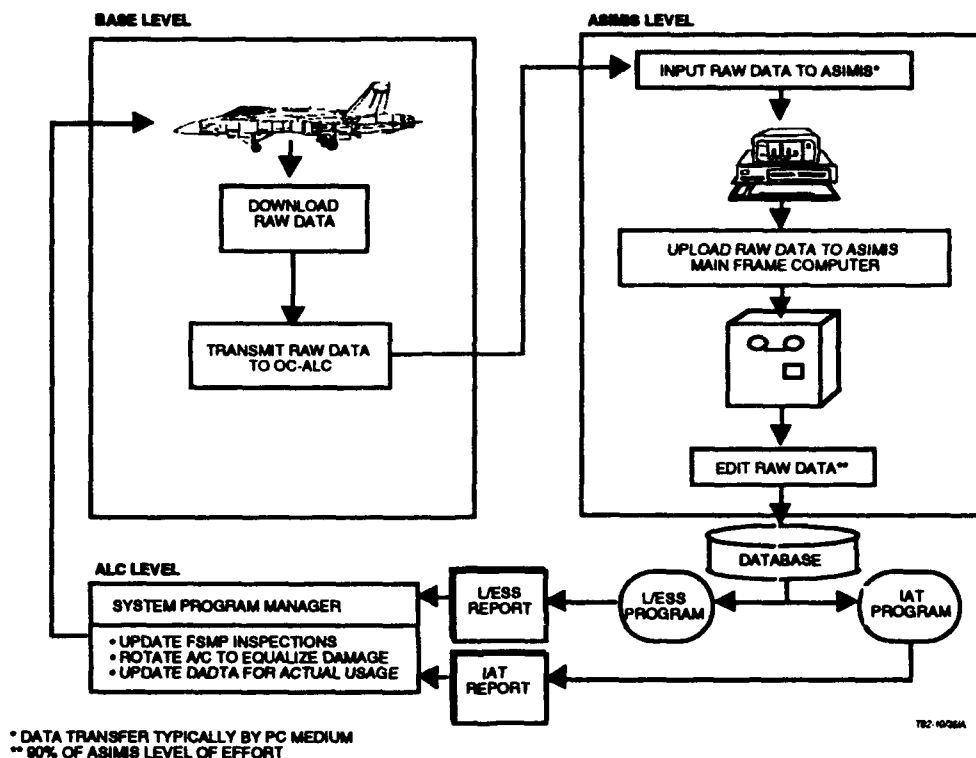


Figure 3. Current ASIP Data Reduction Loop.

An example of a current ASIP data loop appears in Figure 3. Much of the effort of current ASIP force management programs is spent in the processing of data through the loop from the bases to the Aircraft Structural Integrity Management Information System (ASIMIS) group at Oklahoma City Air Logistics Center (OC-ALC)[4]. The ASIMIS group is overwhelmed by the amount of data received from the bases. Much of the time lag in the data turnaround occurs at the ASIMIS level.

A SHMS capable of remote damage detection will obviate the need to base service life on assumed initial flaws and analytically predicted crack growth. If the SHMS can provide flaw size information, there will be no need for analytical tracking at all. If not, standard tracking methods can be started from time of detection, increasing the service life by a minimum of the interval from production to flaw detection. Thus, scheduled inspections will be essentially replaced by maintenance on demand (MOD). The minimum flaw size will no longer be regulated by standard NDE detection methods, but will be determined by the minimum detectable by the damage detection technique (possibly as small as 0.01 in. using acoustic emission methods [5]). In addition to the increase in service life, the accuracy of the methods used to predict the life will be enhanced by the actual aircraft usage spectra, as opposed to the standard method of using either a design spectra, or a fleet average usage.

After the usage and damage detection data have been collected and downloaded to a central fleet computer, the methods for processing, analyzing, and reporting will be significantly improved. A more streamlined ASIP loop is shown in Figure 4.

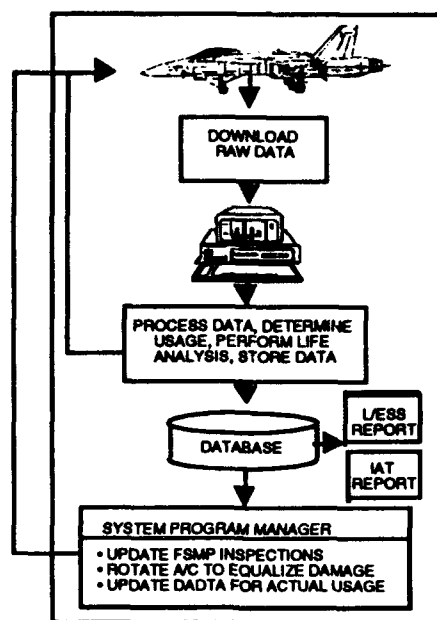


Figure 4. SHMS ASIP Processing.

By implementing a system whereby aircraft usage and damage data are taken directly from on-board storage and fed into a central processing system, the efficiency of ASIP will be greatly enhanced: changes in usage will be immediately apparent; ASIP managers will be able to take immediate action to rotate high- and low-time aircraft; maintenance personnel will benefit from having immediate access to detected damage information to perform inspection and maintenance on damaged parts; and by removing the transmittal to and processing of data by the ASIMIS group at Oklahoma City ALC, considerable time and cost will be saved by eliminating manual handling of information.

4.0 T-38 Health Monitoring

In order to assess the feasibility of incorporating a SHMS into an existing aircraft, a study was undertaken to develop a conceptual design of a system for the T-38 fleet to perform health monitoring of critical structural locations. The important issues for implementation of a SHMS are:

1. Monitoring Locations – which locations would provide cost savings through inspection elimination;
2. Sensors – type and location, sampling rates, cost, ruggedness, and parameter selection;
3. Hardware – central processors, local processors, communications, data storage, location, cost, and ruggedness;
4. Flight Qualification – cost, flight test procedures, system durability, failure rates;
5. Fleet Retrofit – cost and schedule for installation of the system on an existing aircraft; and
6. Cost – system cost versus payoffs.

4.1 Monitoring Locations

Studies of existing literature and discussions with T-38 personnel revealed a number of problem locations on the airframe. Review of past and present damage tolerance assessments (DTA), interviews with Air Force Air Logistics Center (ALC) personnel, and documented fleet failures produced a list of sixteen critical locations on the airframe which have historically been a source of inspection and maintenance activity. Table 1 presents a summary of these critical locations.

The majority of the identified locations are fatigue critical items, many of which were not identified through design or DTA analysis. These locations will provide the most payoff benefit due to the cost of both design and installation of a structural repair. A system installed during the design phase of aircraft development would detect this kind of damage during normal usage, removing any inspection requirements, and circumventing possible major structural failure.

Component	Failure	Structure	Source
Upper cockpit Longeron, 2-10301, @ FS 144	Fatigue	Fuselage	F-5E In-Service Cracking
Upper cockpit Longeron, 2-10301, canopy hookslot cutouts and side web	Fatigue	Fuselage	In-Service Cracking
Upper cockpit longeron, 2-10301, at avionics bay door	Fatigue	Fuselage	F-5F In-Service Cracking
Upper cockpit Longeron, 2-10301, upper longeron splice @ FS 284	Fatigue	Fuselage	Repair Area
Dorsal Longeron, 2-11413,	Analysis	Fuselage	DTA
Lower Wing Skin Fastener Holes	Fatigue	Wing	In-Service Cracking
Wing, 66% spar, 3-23282, aileron hinges, inboard and outboard	Fatigue	Wing	In-Service Cracking
Wing, 66% spar, 3-23282, upper and lower	Fatigue	Wing	In-Service Cracking
Wing, WS 125 wing-tip attach rib, 2-23221	Fatigue	Wing	In-Service Cracking
Upper fuselage skin, 2-11416, fuel cell access door cutout, FS 355	Fatigue	Fuselage	In-Service Cracking
Wing, lower wing skin, 3-23502, at nutplate holes aft of 44% Spar, between WS 84 and 92, land radius at WS 93	Analysis	Wing	SA-ALC/MMEOD
Wing, lower wing skin, 3-23502, land at WS 77 under aileron access panel (and repair)	Vibration Bearing	Wing	In-Service Wear
Wing, lower wing skin, 3-23502, reworked lands aft of 44% spar at MLG door.	Fatigue	Wing	Repair Area
Wing, lower wing skin, 3-23502, aft edge, land, WS 26.6 to 60	Fatigue	Wing	In-Service Cracking
Wing Skins	Fatigue	Wing	In-Service Cracking
Wing Skins	Fatigue	Wing	In-Service Cracking

Table 1. SHMS Critical Location Monitoring Locations.

4.2 Sensors and Hardware

Under the SSCORE contract (Reference 3) sensor technologies for a SHMS were investigated and acoustic emission (AE) sensors were determined to have the best potential for on-board damage detection. To perform damage detection functions and local load tracking, each monitored zone will be equipped with four acoustic emission sensors, two strain gages, and a corrosion sensor (additional strain and corrosion sensors will be used to track global aircraft loads and usage for L/ESS requirements). The sensors will be used to monitor fatigue damage, strain, and the corrosive environment of

the structure. The zone sensors will be controlled by a local processing unit which will contain a data acquisition board, a bus controller, and an AE processor. The local processors will perform the tasks of data collection, processing, and reduction before passing the data to the central processing unit. The central unit will consist of a system control processor, a health assessment processor, and a mass storage unit. It will perform the functions of system control, data storage, flaw location, usage tracking, and health assessment. The central processor will additionally be responsible for interrogating the central flight computer to collect pertinent aircraft usage parameters. Figure 5 shows a demonstration architecture for the system.

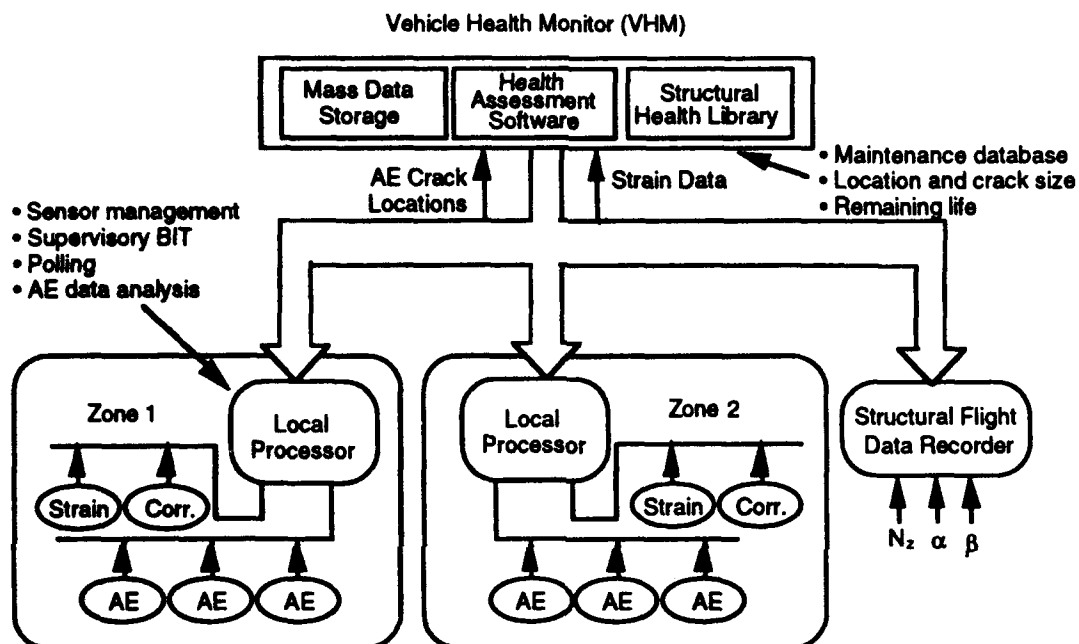


Figure 5. SHMS Architecture [6].

The system architecture is designed to be modular and highly adaptable. Raw sensor data is collected from each of the monitored zones and passed over the net to the local processors. The central processor interrogates each of the local processors in turn to extract the stored sensor data. The system communicates with the central flight computer over the network and stores flight parameters in the Standard Flight Data Recorder (SFDR). The system architecture work is documented in the SMS Task 1 report [7].

A number of identified monitoring locations have previously been instrumented with strain gage hardware during flight test studies on the T-38. The design of the SHMS will take advantage of this by using existing cabling routes to support the sensors and hardware.

4.3 Flight Qualification

Every component which is incorporated on an airframe must meet a series of military standards for flight qualification. Without performing the actual process of qualification, however, it is difficult to accurately assess the impact on system cost and final configuration. Of obvious importance to the SHMS is the effect of ruggedness requirements on the cost of computer processors. For the present study, it was assumed that the cost of flight qualification is small when averaged over the entire fleet, and would be balanced by the savings involved in full production of the system.

4.4 Fleet Retrofit

Installation of the system will be performed during regularly scheduled depot maintenance. It was found that the system installation could be performed within the time frame of regular maintenance (which requires 2-3 weeks for depot level maintenance), although it will require significant additional manpower. The study was based on estimates of the amount of time required to install strain gages and associated hardware on a production aircraft.

4.5 System Costs and Savings

The cost of the SHMS is based on monitoring 32 aircraft zones (16 zones each side). The initial cost estimates are based on a prototype system using off-the-shelf hardware. This provides a baseline for the cost of the SHMS upon which refinements can be made as further information becomes available. Two systems are current candidates for the final demonstration version of the SHMS under the Northrop Smart Metallic Structures (SMS) program: the VersaModule Eurocard (VME) computer architecture, and the Extended Industry Standard Architecture (EISA) computer architecture. Figure 6 presents the estimated costs of the current SHMS hardware. The VME and EISA architectures have been selected based on their applicable capabilities and current widespread industry usage. These architectures are currently being developed for the demonstration SHMS only, and other types of hardware may be considered for a flight qualified system.

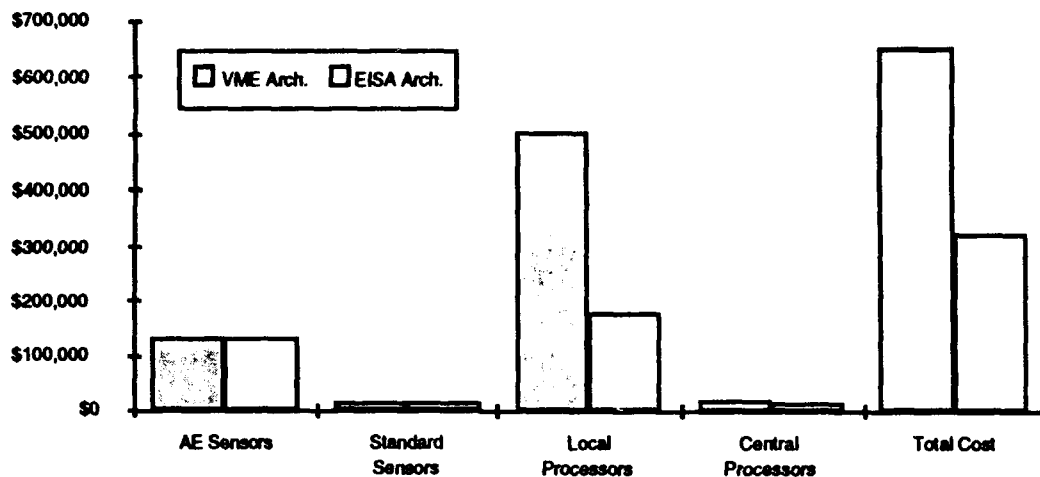


Figure 6. SHMS Computer Hardware Costs² [8, 9].

The cost figures were developed from quotes received from hardware vendors, sensor system integrators, and acoustic emission experts. The figures are based on off-the-shelf purchase prices for each of the components. There are 32 sets of sensors and local processors, 1 set of central processors, and some additional strain gages and corrosion sensors. As can be seen, the cost of a *prototype* SHMS is quite significant. The figures show that the EISA hardware is significantly less expensive than the corresponding VME hardware (the higher cost of the VME processors is evidenced by the difference in local processor costs). This is due to the higher market demand for the EISA hardware which drives the cost down due to volume manufacturing. Installing the SHMS on an entire fleet of aircraft would create a large demand, driving down costs. Mass production of

² Note: All hardware price information is based on price quotations received from Industrial Computer Source, Military and Aerospace Electronics, Digital Wave Corporation, and CyberResearch.

this kind of computer hardware can reduce the costs relative to the prototype system by a factor of 10 to 1 or even as high as 100 to 1 due to the ever decreasing costs of computer technology. The prototype SHMS is based on current (1993) state of the art processors and hardware. It would be possible and economical to design the system with older technology still capable of performing the functions of the SHMS with a small sacrifice in speed and power. Figure 7 shows the effects of technology and production cost decreases.

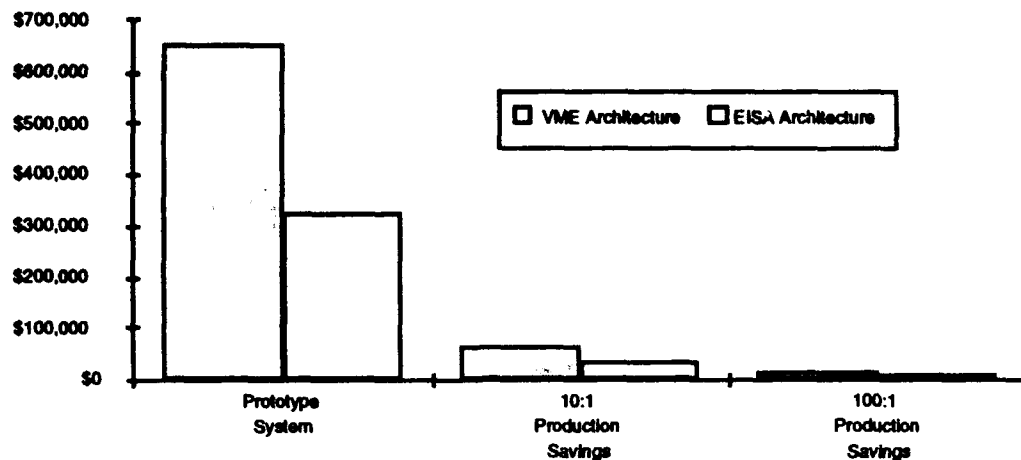


Figure 7. Cost Savings Due to Mass Production.

The use of specialized components for the system would also reduce the cost of the system hardware. The current prototype design makes use of off-the-shelf components which are purposely designed generically to meet a wide range of application requirements. A system specifically designed to perform the functions of a SHMS would provide cost savings through simplified electronics and fewer overall components. For instance, the hardware from the sensor to the data analysis input (including the sensor, preamplifier, and local processing) could be manufactured for a cost of less than \$1,000 [9]. Previous studies have additionally shown significant cost and performance benefits from the miniaturization and centralization of sensors and hardware [3].

In addition to the material costs of the system hardware are the associated installation costs. An installation study was based on estimates for installing strain gages in preparation for flight test. The estimate included manpower and dollar figures for installation of an aircraft strain monitoring system. Figure 8 presents the estimated installation cost of the system.

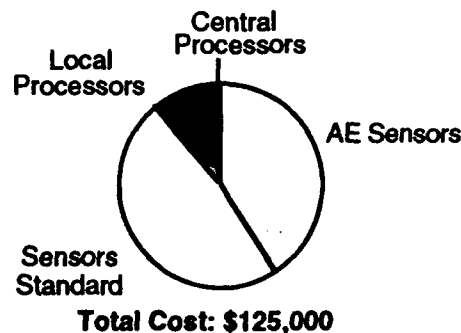
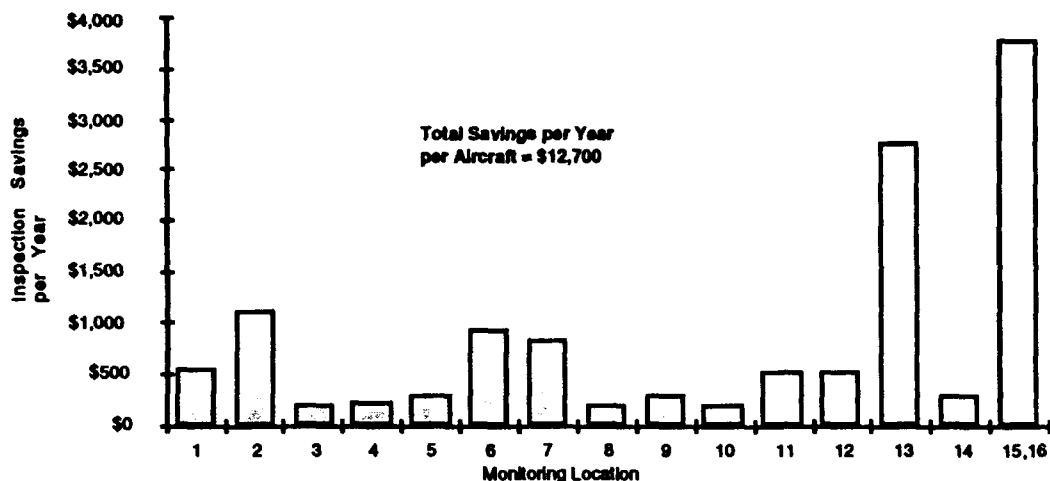


Figure 8. Installation Costs of an SHMS System.

Installation of the system was based on a one-time prototype installation, and thus are conservative. Production installation could reduce the cost by as much as 50%.

An SHMS would provide savings through elimination of structural inspections as discussed previously. Inspections are performed at a prescribed time interval and require not only the inspection of the part itself, but also any necessary teardown and installation. The figures presented for the time required per inspection are estimates of the total time required for teardown, preparation, inspection, and installation of the structure [10]. Figure 9 presents the inspection savings as a result of system integration.

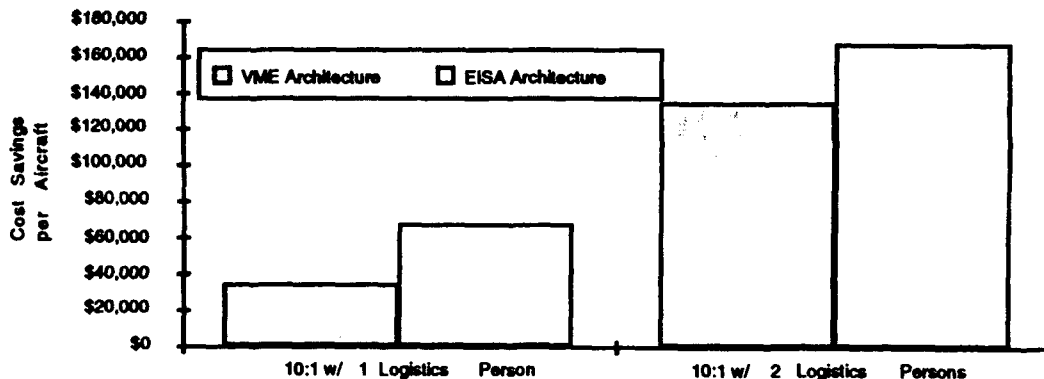


Notes:

1. Inspection savings based on fleet of 720 A/C, 420 average flight hours per A/C per year.
2. Savings calculated over ten year average to accommodate long inspection intervals.

Figure 9. Estimated Inspection Savings Resulting from SHMS [10, 11, 12, 13].

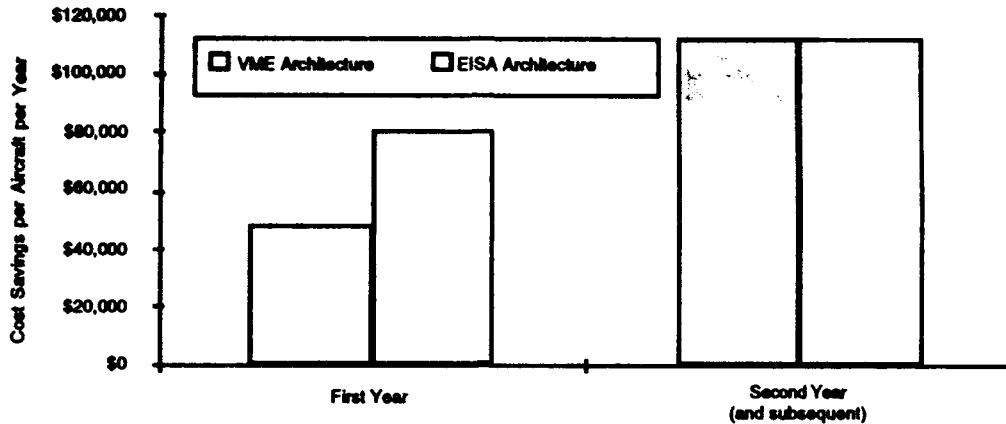
Each deployed aircraft is assigned a number of logistics and maintenance personnel who track and maintain aircraft usage, repair, and provisions. By eliminating the need for various maintenance and tracking operations, the SHMS would replace one or more of the personnel assigned to the aircraft. This represents an estimated savings of over \$100,000 per year per person. Figure 10 presents an estimate of the system cost savings due to a reduction in support personnel (also included are the effects of the savings on a production system).



Note: Figures include cost of system and savings due to reduction of logistics effort.

Figure 10. System Cost Savings with Logistics Personnel Reduction.

When the total cost of the system (hardware and installation) is compared with the total savings (inspections and logistics effort), the potential savings become quite significant (Figure 11).



Note:

1. Figures are based on a 10:1 reduction in cost for production system.
2. Assumed savings of one logistics person per aircraft per year.
3. First year savings include cost of system and installation.

Figure 11. Total System Savings per Aircraft per Year.

5.0 Conclusions

Smart structures technologies, especially health monitoring, have the capability to provide cost savings over the life of an aircraft, as well as reduce down time, increase safety of flight, and increase service life. While it is difficult to precisely quantify benefits versus costs, data accumulated through inspection personnel, DTA material, computer hardware manufacturers, and logistics personnel have provided an estimate of the costs associated with a prototype as well as a production version of a SHMS. The estimates resulted in a prototype cost of \$450,000 (including installation), and a conservative production cost of \$45,000. The projected savings, based on the elimination of structural inspections and reduction in logistics manpower, is in excess of \$200,000 per aircraft *per year*.

These numbers conservatively assume a 10 to 1 reduction in production costs for the system versus the prototype, and streamlining of the manufacturing and installation processes. It should be noted that the figures presented here were developed to retrofit an existing aircraft fleet. A system for a new aircraft could be designed integral with the aircraft control and ground support systems, eliminating the need for dedicated hardware and software. This would achieve unprecedented levels of structural efficiency by combining damage tolerance analysis, flight usage history, and maintenance procedures.

In addition, there is also the savings from the decrease in manual data handling by ASIP personnel (in particular the ASIMIS group at Oklahoma City ALC) which were not taken into account in the present study. Further, there is the consideration of the rare but plausible savings due to prevention of a catastrophic structural failure (failure resulting in loss of aircraft). The savings realized from the prevention of even one catastrophic failure would offset the cost of the SHMS for the entire fleet.

The transition from current processes to a fully automated health monitoring system will not be immediate. R&D efforts are required in the areas of damage detection, aircraft system integration, and ASIP automation. Significant developments are needed

particularly in the area of damage detection sensors. However, as has been demonstrated conceptually for the T-38, significant savings can be made by incorporating a SHMS. Immediate cost savings can be realized for an aircraft fleet simply by increasing the amount of automation of ASIP procedures. Savings can be made by reducing the amount of manual data handling and processing performed by the ASIMIS group. Additional savings can be accomplished by monitoring locations on the airframe which require frequent inspection, such as known fatigue areas or structural repairs. Work currently underway at Northrop addresses some of the issues pertaining to ASIP automation, damage detection, and system integration. In particular, a technology demonstration of a SHMS is planned on a large scale aircraft structural component subjected to fatigue loading. The testing will verify much of the conceptual work performed towards the goal of developing a prototype system.

References:

1. Gentry, J.D., Kudva, J.N., Van Way, C.B., "The Impact of Smart Structures on Aircraft Structural Integrity Programs", 1992 USAF Structural Integrity Program Conference, San Antonio, TX, December 1992.
2. Gentry, J.D., Van Way, C.B., Kudva, J.N., Marantidis, C., "Structural health assessment and review program (SHARP) - prototype of an on-board structural health monitoring system", 1993 SPIE Smart Structures Conference, Albuquerque, NM, February 1993.
3. Kudva, J.N., et. al., Smart Structures Concepts Requirements Definition (SSCORE) Interim Report, Northrop Corp., Contract No. F33615-89-C-3206, March, 1993.
4. Conversation with Bob Kerr, ASIP Manager, Oklahoma City ALC, Jan. 1, 1992.
5. Gorman, M. R., "Acoustic Emission for the 1990's", Naval Postgraduate School, Department of Aeronautics and Astronautics, Monterey, CA, Invited Talk, IEEE Ultrasonics, 1991.
6. Schoess, J. N., Honeywell, Inc., SMS Status Report, 5/93.
7. Kudva, J.N., et. al., Smart Metallic Structures (SMS) Interim Report, Northrop Corp., Contract No. F33615-92-C-3203, Nov., 1993 (in progress).
8. Conversations with Mr. Mark N. West, Mission Research Corp., 8/93-10/93.
9. Conversation with Michael R. Gorman, Digital Wave Corporation, on rough estimates of mass produced computer hardware, 10/93.
10. Conversation with SMSgt. Schwarting, NDI Operations, Randolph AFB, San Antonio, TX, 9/93.
11. T.O. 1T-38A-6 Inspection and Maintenance Requirements for the T-38A aircraft. Rev.: 1 March 1993
12. T.O. 1T-38A-2 Inspection Procedures for the T-38A Aircraft. Rev.: 1 February 1992.
13. Conversation with George Kuehn, Structures Branch, Kelly AFB, San Antonio Texas, 9/93.